IAEA-TECDOC-233

RESEARCH REACTOR CORE CONVERSION FROM THE USE OF HIGHLY ENRICHED URANIUM TO THE USE OF LOW ENRICHED URANIUM FUELS GUIDEBOOK

PREPARED BY A CONSULTANTS' GROUP,
COORDINATED AND EDITED BY THE
PHYSICS SECTION
INTERNATIONAL ATOMIC ENERGY AGENCY

A TECHNICAL DOCUMENT ISSUED BY THE
INTERNATIONAL ATOMIC ENERGY AGENCY, VIENNA, 1980

RESEARCH REACTOR CORE CONVERSION
FROM THE USE OF HIGHLY ENRICHED URANIUM
TO THE USE OF LOW ENRICHED URANIUM FUELS
GUIDEBOOK
IAEA, VIENNA, 1980

Printed by the IAEA in Austria
August 1980

Please be aware that all the Missing Pages
in this document were originally blank pages

FOREWORD

In view of the proliferation concerns caused by the use of highly enriched uranium (HEU) and in anticipation that the supply of HEU to research and test reactors will be more restricted in the future, this document has been prepared to assist reactor operators in determining whether conversion to the use of low enriched uranium (LEU) fuel designs is technically feasible for their specific reactor, and to assist in making a smooth transition to the use of LEU fuel designs where appropriate.

This book has been prepared and coordinated by the International Atomic Energy Agency, with contributions from different organizations. The experts from these organizations have participated in the Consultants' Meeting on Preparation of a Program on Research Reactor Core Conversions to use Low Enriched Uranium Instead of Highly Enriched Uranium, and have assisted in preparing this text.

CONTRIBUTING ORGANIZATIONS

Argonne National Laboratory	ANL	United States of America
Atomic Energy Research Establishment Harwell	AERE Harwell	United Kingdom
Commisión Nacional de Energía Atómica	CNEA	Argentina
Comissariat a l'Énergie Atomique	CEA	France
Compagnie Pour l'Étude et la Réalisation de Combustibles Atomiques	CERCA	France
Eidg. Institut für Reaktorforschung	EIR	Switzerland
General Atomic Company	GA	United States of America
General Electric Company Reactor Equipment Ltd.	GEC	United Kingdom
Internationale Atomreaktorbau GmbH	INTERATOM	Federal Republic of Germany
Japan Atomic Energy Research Institute	JAERI	Japan
Kernforschungszentrum Karlsruhe GmbH	KFK	Federal Republic of Germany
Kyoto University Research Reactor Institute	KURRI	Japan
NUKEM GmbH	NUKEM	Federal Republic of Germany
Österreichische Studiengesellschaft für Atomenergie	ÖSGAE	Austria

The IAEA is grateful for the contributions volunteered by these organizations and thanks their experts for preparing the detailed investigations and for evaluating and summarizing the results presented in this Guidebook.

SUMMARY

This Guidebook has been prepared to assist reactor operators and physicists in determining both the feasibility of converting their specific reactors from HEU to LEU fuel and the options available for implementation. A wide variety of information is presented on the physics, thermal-hydraulics, and fuels of light water moderated and cooled research and test reactors. Most of the methods discussed in this Guidebook can also be directly applied to the analysis of research reactors containing heavy water as moderator and/or coolant. However, in consideration of the special features of heavy water reactors, an addendum to this Guidebook is planned to address the feasibility of converting these reactors to LEU fuel and the options available for implementation.

The following is a brief outline of how the results were obtained, and how this Guidebook can be used most effectively.

1. Actions Needed For Conversion From HEU* Fuels to LEU* Fuels

Section 1.5 gives a summary of the type of studies that are needed to prepare for core conversion.

It is possible for these studies to be performed by the reactor operators/ physicists themselves, or with the aid of laboratories which have offered technical assistance. Appendix G lists the typical data needed for enrichment reduction conversion studies. Section 1.4.2, Chapter 3, and Appendix H contain information on the current status, development potential, and commercial availability of fuels with high uranium densities. Appendix I analyses the main economic aspects of core conversions to LEU fuel.

2. Generic Studies

Calculations have been performed by different laboratories for two generic MTR-type reactors with power levels of 2 MW and 10 MW to determine their potential for conversion. The results are summarized in Section 2 and include the uranium densities that would be required with different fuels and fuel element designs, the corresponding thermal-hydraulic safety margins, and the performance that would be expected from the converted core. Detailed information on the methods and procedures used and the results obtained for the various core conversion options are presented in Appendices A through D.

3. Specific Studies

The methods and results of core conversion studies for two specific reactors with power levels of 3.5 MW and 50 MW, respectively, are provided in Appendix E.

4. Benchmark Calculations

In order to compare the accuracy of calculation methods used in the different research centers, benchmark problems were defined and calculated with the different methods. The main core calculations using 93%, 45% and 20% enrichment are based on an idealized 6 x 5 element, plate-type core with a power of 10 MW reflected by single graphite rows on two sides, and surrounded by water. Results of the calculations, including cross section data, and descriptions of various burnup conditions are summarized in Section 2.4 and described in detail in Appendix F. As a first step in core conversion, it is recommended that reactor operators/physicists use their own methods and codes to calculate this benchmark problem, and to compare the results.

5. IAEA Assistance

The IAEA can be contacted, through official channels, to provide assistance for the core conversion of specific reactors. The IAEA can offer coordinating assistance between reactor organizations and those laboratories in the USA, the FRG, and France which have offered technical assistance (Section 1.3). If necessary, the IAEA can also provide fellowships to visit those laboratories for joint studies on core conversions. The preparation of a second guidebook addressing safety and licensing issues related to core conversions is planned under the auspices of the IAEA.

---

*For simplicity, the following definitions have been adopted for this publication:

HEU - Highly Enriched Uranium ($\geq$70 wt% ^{235}U)

MEU - Medium Enriched Uranium (45 wt% ^{235}U)

LEU - Low Enriched Uranium (<20 wt% ^{235}U)

REU - Reduced Enriched Uranium (includes MEU and LEU)

CONTENTS

APPENDICES

1. MAJOR CONSIDERATIONS IN REACTOR CONVERSIONS

1.1 INTRODUCTION

In the 1950s and 1960s, low power research reactors were built around the world which utilized MTR-type fuel elements containing <20% enriched uranium (LEU). This value was chosen because it was considered to be a limit for weapon usable material. However, the demand for higher specific power created a need for greater ^{235}U concentrations and led to the substitution of highly enriched uranium (HEU) in place of the LEU fuel previously utilized. HEU also yielded other benefits including longer core residence time, higher specific reactivity, and somewhat lower cost. HEU then became readily available and was used for high power reactors as well as low power reactors where LEU would have sufficed. The trend toward higher and higher specific power also led to the development of the dispersion type fuels which utilized HEU with a density of about 1.6 - 1.7 g/cm^3.

In the 1970s, however, concerns were again raised about the proliferation-resistance of fuels and fuel cycles, and since enrichment reduction to less than 20% is internationally recognized to be a fully adequate isotopic barrier to weapons usability certain Member States have moved to minimize the international trade in highly enriched uranium and have established Reduced Enrichment Research and Test Reactor (RERTR) Programs. The goal of these programs is to develop the technical means, such as design modifications and development of new fuels, to assist in implementing reactor conversions to LEU fuels with minimum penalties. These programs have been established in the U.S., France, the Federal Republic of Germany, and Japan. It is anticipated that through the continued efforts of these programs, and with IAEA coordination, many reactors currently utilizing fuel element materials and designs less advanced than currently feasible may soon be converted to the use of LEU fuel. For other reactors, whose conversion to the use of LEU fuel may be feasible only after significant fuel development, a temporary decrease of the enrichment to an intermediate range of 45% (MEU) would be a worthwhile improvement in proliferation resistance.

Concern has also been expressed about the presence of plutonium in spent fuel, especially when the fuel is irradiated in reactors utilizing very low enrichment and/or operating at high powers, and it is necessary to consider both the plutonium produced and the enriched uranium in the overall assessment of the proliferation potential of a particular reactor.

1.2 REASONS FOR REACTOR CONVERSIONS TO LEU

Operators of research and test reactors that use highly enriched uranium may consider converting their reactors to the use of low enriched uranium fuels for several closely related reasons. One could be the desire to reduce the proliferation potential of research reactor fuels. A second reason could be a desire to increase the assurance of continued fuel availability in the face of probable restrictions on the supply of highly enriched uranium. A third reason could be the possible reduction in requirements for physical security measures during fabrication, transportation, storage, and use. All these reasons are connected with each other and cannot be considered individually.

1.3 AGENCIES AND LABORATORIES AVAILABLE TO PROVIDE TECHNICAL ASSISTANCE FOR THE CONVERSIONS

The IAEA will provide technical assistance to reactor operators who wish to consider conversion of their reactor from the use of HEU fuel to the use of LEU fuel. A number of Member States including the USA, FRG, and France have offered to provide additional technical assistance services through the IAEA for such conversions. The programs in the areas of reduced enrichment fuels for research and test reactors which are in progress at laboratories in France, FRG, Japan, and the USA are summarized in Sections 1.3.1 to 1.3.4. The IAEA may be contacted through official channels by interested reactor operators to make necessary arrangements for assistance offered by these Member States.

1.3.1 The Reduced Enrichment Program of France

Considering the problem of highly enriched uranium and its nonproliferation concern for the use in test and research reactors, France has started since 1975 a general program of fuel development and of reactor studies. For already more than four years this program has been implemented in the different French laboratories and fabrication facilities.

The French program has been directed towards two purposes:

- to develop fuels with low enrichment, 20% ^{235}U and below, able to fulfill the main reactor requirements such as fuel cycle length and reactor flux performances. As a temporary solution an intermediate step of 45% ^{235}U enrichment is considered in some applications for which the 20% enrichment cannot be implemented in the near future.

- to evaluate the reactor performances, both thermal-hydraulics (flow rate, water velocity, pressure drop, heat flux and available power) and neutronics (fast and thermal fluxes in experimental positions). This is being done for cores using the above mentioned fuels; special consideration is given to the problems of existing reactors and to their adaptation to the new fuel supply conditions.

This program has already shown important and positive results, demonstrating the possibility for numerous existing reactors to go directly to enrichment below 20% ^{235}U (3% to 10% ^{235}U) with the CEA developed Caramel fuel.

These demonstrations have taken into account the results of core evaluation studies showing that in most cases the reactor performances would be kept in the same range.

The implementation of the fuel development program has followed two different ways, in the CEA with the Caramel fuel (UO_2-Zr plate type fuel element) and in CERCA with the classic MTR type fuel element (either UAl_x-Al or U_3O_8-Al).

The Commissariat à l'Énergie Atomique has been developing the Caramel fuel for five years. Based on a general program of fuels for low and medium power reactors used either in land based or merchant ship plants, this fuel specially designed for research reactors has been tested under irradiation on various scales (from elementary pellet samples to full scale fuel element) and various operation conditions. The Caramel fuel has been qualified since 1978 and is commercially available for use in low and medium power research reactors. For the use in the most severe conditions, the CEA has implemented a full scale demonstration in the Saclay OSIRIS reactor (70 MW). Two cores have already been fabricated: one for OSIRIS and one for the critical mock-up ISIS, in 1978 and

1979. The full power OSIRIS operation will show in 1980 the capability under a statistic scale of the Caramel fuel to fulfill the most severe operational requirements.

The Compagnie pour l'Étude et la Realisation des Combustibles Atomiques, CERCA, already involved in the manufacture of MTR UAl plate type fuels has undertaken for two years a special R and D effort to raise significantly the total uranium loading in the fuel meat both in UAl_x-Al and U_3O_8-Al dispersion. The results obtained are encouraging; densities up to 2.2 (UAl_x-Al) and 2.7 (U_3O_8-Al) are now well within technological possibilities with full size plates produced which meet all the required specifications. Irradiation qualification tests are planned in a near future in several reactors (ORR, Petten, SILOE).

In parallel to these fuel developments the CEA started generic studies of reactor performances for cores using these new fuels. They have included neutronics calculations to define cycle length and flux characteristics, as well as thermal-hydraulics calculations to evaluate the possible output power. When necessary, experimental work has been implemented in 1978 and 1979 such as the out of pile loop experiment run to determine the thermal-hydraulics correlations in a parameter range not yet covered and the critical mock-up experiment ISIS.

1.3.2 The Reduced Enrichment Program of the Federal Republic of Germany

As a contribution to the solution of the proliferation problem caused by the use of highly enriched uranium in research reactors the Federal Republic of Germany is implementing a 5 1/2 years program on enrichment reduction in research reactors. The main objective of the program is the development and testing of fuels and fuel elements which are essential for the conversion of reactors to reduced enrichment. With these fuels a continuous research reactor fuel element supply shall be possible when only reduced enriched uranium is available.

The fuel development program is supported by a program of generic reactor physics and thermodynamics calculations which has several purposes. It is guiding the fuel development program so that with a limited number of enrichment steps and fuel element types a wide coverage of reactors is achieved, which can smoothly be converted to reduced enrichment using these fuels. It helps in the decision for the conversion of a reactor to reduced enrichment by comparing different design options, their consequences and trade offs including optimization studies. It provides information on how to implement the conversion process.

In the frame of this program the design and calculation of a specific research reactor system is included which is projected to operate with 20% ^{235}U enriched fuel, fabricated under existing technologies and fuel densities. Neutron flux densities will reach 10^{14} n/cm^2 sec. A further developing step will be the using of advanced fuel elements with very high uranium densities which will result in a flux density up to $5 \cdot 10^{14}$ n/cm^2 for a core design adapted hereto. The developing program covers both the complete core and plant design including auxiliary systems, buildings, etc.

Independent of this program the Federal Republic of Germany offers specific consulting services to organizations which are considering enrichment reduction of their research reactors.

The fuel development program is divided into four subtasks:

A. Development and testing of fuel with which reactors presently using low density fuel can be converted to 45% enrichment without modification of the fuel element geometry (constant plate thickness and constant coolant channel width).

B. Development and testing of fuel with which reactors presently using low uranium loaded fuel can be converted to 20% enrichment when an increase of the meat thickness is possible.

C. Development and testing of fuel with which reactor presently using low uranium loaded fuel can be converted to 20% enrichment without fuel element geometry modification.

D. Development and testing of fuel with which reactors presently using high uranium loaded fuel can be converted to 45% enrichment without modification of the fuel element geometry.

Subtasks A and B shall be achieved with UAl_x-Al dispersion fuel and fuel element performance tests will be done which are sufficient for licensing and market introduction.

Subtasks C and D will be based on U_3O_8, UAl_2, and UO_2 plate type with new fuels such as U_3Si as a back-up solution. Irradiation of plates under different irradiation conditions will be followed by fuel element performance tests.

The new fuels will be developed to higher uranium concentration than are the limits of U_3O_8 in order to enlarge the range of convertible reactors.

Adaptation of the fuel element fabrication process including control and test procedures to the higher uranium loaded fuel forms an essential part of the program.

The program will be performed by NUKEM, a company especially involved with fabrication and development of research reactor fuel elements which is responsible for all activities related herewith and INTERATOM, a company with extensive accomplishments in the design, construction, and startup of research and test reactors which is responsible for the core and plant design of new research reactors as well as for the generic core studies supporting the fuel development within this programme. In the FRG there have been plates that are already fabricated, but not yet irradiated containing U_3O_8 with a density of >3.0 g U/cm^3. The irradiation tests necessary and the post irradiation examinations will be done by the research centres KFA-Jülich and GKSS Geesthacht.

1.3.3 The Reduced Enrichment Program of Japan

In order to contribute to the reduction of proliferation concerns, five year programs for the conversion to reduced enrichment uranium fuel in place of currently used highly enriched uranium fuel have started in the Japan Atomic Energy Research Institute (JAERI) for the JAERI's research and test reactors and the Kyoto University Research Reactor Institute (KURRI) for the KURRI's research reactors. These programs are promoted with close contact between the JAERI and the KURRI under coordination of the Japanese Government authorities.

The fundamental principles set up for guiding the reduced enrichment programs are:

A. The use of alternative fuel should not affect, even to small extent, research and development programs in nuclear utilization in Japan, and should not cause considerable degradation in reactor performance or long reactor shutdown for implementing fuel conversion.

B. In utilizing reduced enrichment fuel, the safety margin and fuel reliability should not be worse than for the present reactor with highly enriched fuel. The amount of fission product release from the fuel plate must satisfy the safety requirement.

C. The calculated critical mass and related parameters should be verified by experiments performed in critical facilities.

D. The fuel cycle cost for operating the reactor with alternative fuel, except for the R & D cost for such fuel, should be acceptable.

E. The fuel fabricator should be secured either inside or outside of Japan.

1.3.3.1 JAERI's Program

In JAERI's reactors, uranium loading density in its fuel meat of 1.6 gU/cm^3 (42 w/o) is to be used. No dimensional changes are to be made for the fuels used in the JRR-2, the JMTR and the JMTRC with MEU. For the JRR-4, utilization of LEU is planned with slight modification including both the volume of the fuel meat and the number of the fuel plates per element. Step by step approach to demonstrate the engineering feasibility of MEU fuels is inevitable to satisfy the safety requirements made by the Government authorities in Japan for changing fuel designs. Domestic data obtained through the demonstration program on irradiation behavior and mechanical strength will play the role of checking the validity of many foreign data which have been already reported to show the feasibility of the qualified fuel. Feasibility studies in the use of LEU in the JRR-2, the JMTR and the JMTRC are to be in progress in parallel with the utilization program of MEU. And some parts of this program will be promoted jointly under the JAERI - ANL Joint Study Program.

1. Core Design and Safety Analysis

These studies include reactor physics, thermal-hydraulic and structural analysis. Reactor physics study involves reactivity-lifetime and safety considerations such as control rod worth, and negative temperature and void coefficients.

2. Flow Tests

Flow tests are to be performed using dummy fuel elements for each reactor. The main objective of the flow tests, particularly for the JMTR, is to confirm that there is sufficient margin of fuel mechanical strength against exaggerated coolant flow. Drop impact tests, flow distribution and pressure drop measurements for those dummy fuels will be followed.

3. Critical Experiments

Critical experiments are to be carried out using the JMTRC to verify nuclear performances. Safety-related data such as temperature and void coefficients, etc., will be confirmed by the experiments.

4. Irradiation Tests

Several full-size fuel elements will be irradiated in the JRR-2, the JRR-4 and the JMTR at their rated powers. The average burnup obtained will be up to about 60% of initial ^{235}U. Post irradiation examinations will be followed.

5. Full Core Demonstration Tests

The full core demonstration test of alternative fuel in each reactor at both low power and rated power will be carried out in the middle of 1983.

1.3.3.2 KURRI's Program

The plate and core dimensions of the KUHFR (to be critical in 1982) will not be changed upon reducing HEU to MEU. This program is carried out as the ANL - KURRI Joint Study. After completion of the KUHFR, the existing KUR-1 will be converted to the TRIGA type core using LEU.

Phase A of ANL - KURRI Joint Study

1) Feasibility study of MEU fuel
2) Planning of critical experiment, burnup experiment and legal procedure for implementation of MEU fuel
3) Personnel exchange

Phase B of ANL - KURRI Joint Study

1) Detailed calculations of the KUHFR with MEU fuel
2) Technical and economical evaluations of MEU fuel and commercial considerations
3) Detailed planning for critical experiments in the KUCA(C) with MEU fuel
4) Application of safety review to Japanese Government for MEU fuel to be used in the KUCA(C)
5) Detailed planning and arrangements for burnup tests in the ORR and post irradiation examinations at the ORNL of MEU fuel fabricated in FRG, France and the USA
6) Performance and analysis of critical experiments with MEU in the KUCA(C) and of burnup tests with MEU in the ORR
7) Application of safety review to Japanese Government for MEU fuel in the KUHFR
8) Feasibility calculations for use of high-uranium-density fuels with LEU in the KUHFR
9) If LEU is feasible, the same test procedures will be followed
10) Personnel exchange

Phase C of ANL - KURRI Joint Study

1) Operational experience in the KUHFR with MEU fuel
2) If use of LEU fuel is feasible, all activities needed for the implementation of this fuel will be executed
3) Personnel exchange

1.3.4 The Reduced Enrichment Program of the United States

The U.S. Reduced Enrichement Research and Test Reactor (RERTR) Program includes six interacting technical elements. These are illustrated in Fig. 1-1 and described below.

1.3.4.1 Evaluation of HEU Export Requests

This activity provides the U.S. Executive Branch with a technical evaluation of every significant request for export of highly enriched uranium (HEU).

The technical and economic justification of need for HEU submitted with each Export License Application is reviewed by the Argonne National Laboratory (ANL) and a short lead-time technical evaluation is perfomed for the specific reactor(s) for which the application is made. Each evaluation addresses the potential of the reactor(s) for conversion to reduced-enrichment fuel and provides the Executive Branch with a technical analysis of the tradeoffs among experiment performance, core lifetime, economics and licensing issues.

1.3.4.2 Generic Reactor Analysis and Design

This activity provides generic core analysis and design (physics, safety, thermal-hydraulics, structures and fuels) and reactor-facility analysis and design (heat rejection, hydraulics) studies of the major types (U, U_3O_8, or UAl_x/H_2O, U-ZrH/H_2O, UO_2/H_2O, and U-Al/D_2O) of research and test reactors with reduced enrichment. Performance and fuel cycle cost implications, and the problems associated with plutonium production and fuel supply, are addressed. For each reactor type, in-depth redesign studies are undertaken for representative existing reactors to evaluate the potential for converting them from the use of highly-enriched uranium fuel to the use of reduced uranium enrichment. In-depth design studies are performed also for new research and test reactors in the design phase, to evaluate reduced-enrichment fuel alternatives. Collaborative studies with personnel from the reactor projects involved are carried out as appropriate.

1.3.4.3 Specific Reactor Technical Support

This activity is structured to expedite application of reduced enrichment replacement fuel to specific foreign and domestic reactors by providing technical support to the fuel element engineering design, component design, procurement specification preparation, and safety analysis revisions necessary to initiate fuel procurement. Wherever possible, the support work is carried out in close cooperation with the affected reactor operating organization and fuel manufacturers. If appropriate and contributory to expediting priority applications, drawings and other documents supporting the procurement specifications may also be provided by ANL to the reactor operating organization. Technical support during procurement negotiations and fuel fabrication are provided by ANL, if necessary.

1.3.4.4 Fuel Development

This activity is a long-term fuel development effort intended to yield fabrication techniques for research and test reactor fuels of high uranium density. The fuel development activity consists of four parallel fuel development efforts. Three of these efforts are concerned with development of plate-type UAl_x-Al fuel elements, plate-type U_3O_8-Al fuel elements, and rod-type U-ZrH_x (TRIGA) fuel elements with uranium loadings much greater than those currently available. These three efforts are further developments of fuels that are now utilized in research and test reactors. The fourth effort is the development of new research and test reactor fuels (such as U_3Si, U-Mo, UO_2) that accommodate very high uranium loadings beyond the development potential of current fuels.

Figure 1-1.- Work Breakdown Structure of Reduced-Enrichment Research and Test Reactor (RERTR) Program

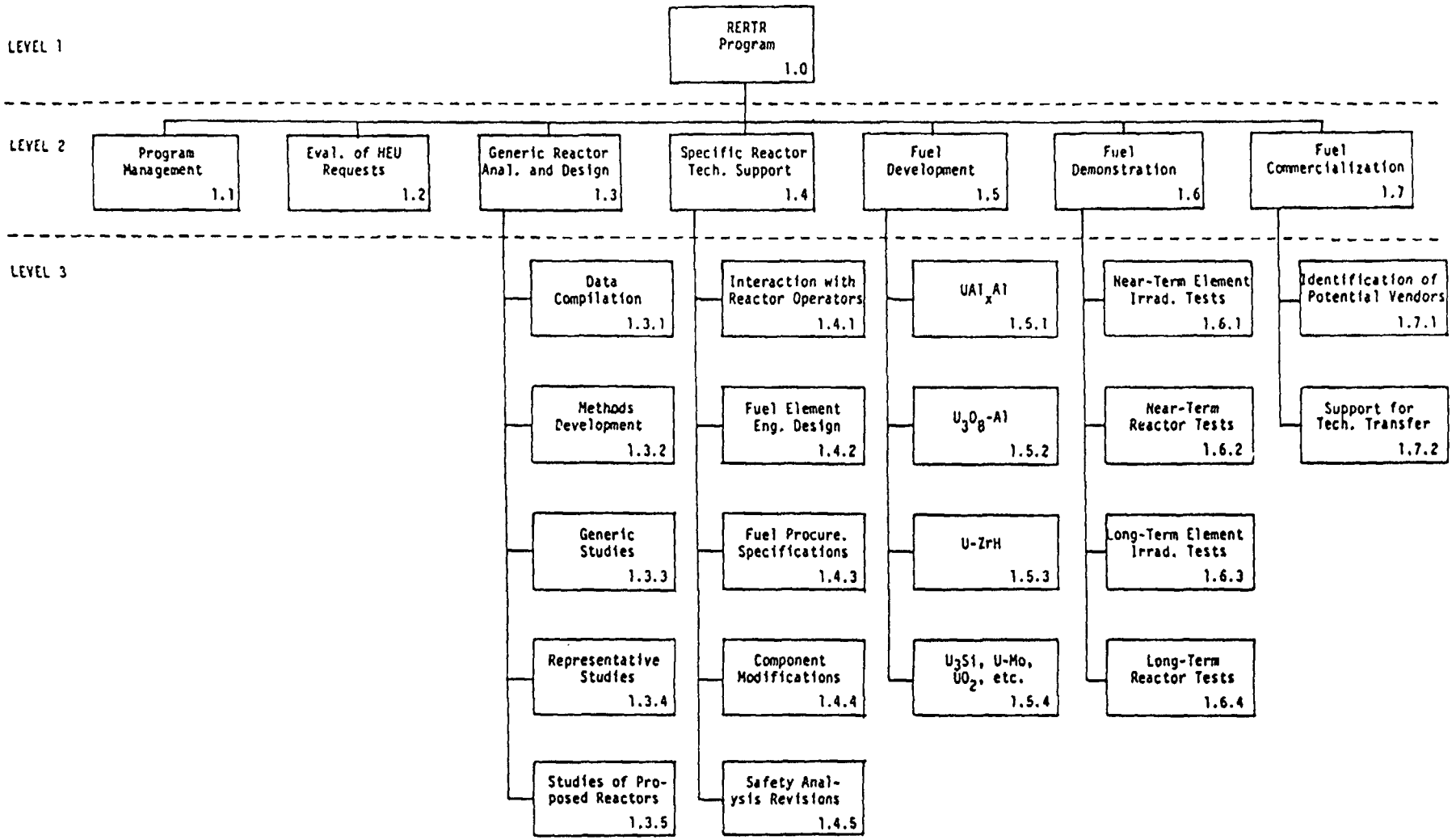

1.3.4.5 Fuel Demonstration

The objective of this activity is to demonstrate to the users and operators of research and test reactors that the operation of such reactors with reduced uranium enrichment fuels meets all the required criteria of reliability, performance, safety, core lifetime, and economics. The fuel demonstration activity includes three types of tests. The first test type consists in irradiating in a high-flux facility some elements of each relevant fuel type beyond their normal life burnup limit, and in verifying the ability of the fuel to stand such a test with acceptable metallurgical performance. The second test type consists of a whole-core demonstration in a reactor in which detailed physics measurements can be made to assess any change in the physics and safety characteristics of the core. The third test type consists of a whole-core demonstration in a reactor in which the burnup rate is sufficient to adequately study the physics/safety characteristics of the core throughout the entire fuel cycle. The fuel demonstration activity includes the planning of the tests, the procurement of the fuel elements/cores for the tests, the performance of the irradiations and experiments, post irradiation examinations, and analysis of data.

1.3.4.6 Fuel Commercialization

This activity is to provide the technical support to ensure that the fuel needed for the operation of all research and test reactors which can operate with reduced-enrichment fuel can become commercially available, on a worldwide basis, and without the need for significant government financial support. This part of the program includes: (1) identification of the potential commercial domestic and foreign suppliers of reduced-enrichment fuel for research and test reactors, (2) evaluation of their fabrication processes and capabilities, and (3) technical support and implementation for the transfer of technologies, wherever such transfer is appropriate and may contribute to the commercialization goal.

1.4 MAIN OPTIONS AVAILABLE FOR CONVERSION

1.4.1 General Technical Basis to Achieve Conversions Meeting Desired Criteria

In assessing the practical feasibility of utilizing lower enriched fuel in existing research reactors, the agreed criteria are that the safety margins and fuel reliability should not be lower than for the current design based on highly enriched uranium, major reactor modifications should not be required, and that preferably neither any loss in the overall reactor performance (e.g., flux-per-unit power) nor any increase in operation costs should be more than marginal. It is also recognized that the feasibility of reduced-enrichment use in each specific reactor must be objectively assessed on an individual basis taking into account all technical, programmatic, economic and licensing factors. However, it should be noted that there are specific applications requiring high flux reactor operation that can only be met with high enrichment fuel.

Enrichment reduction by simple substitution of lower enriched uranium in existing fuel designs has the immediate effect of reducing core performance and cannot meet the above criteria. Core reactivity is decreased, and therefore fuel burnup capability is decreased and fuel costs are increased, and/or core size is increased and therefore flux-per-unit power performance is decreased.

Enrichment reductions are feasible for most research and test reactor designs when the ^{235}U content in the fuel element can be kept approximately the same while the enrichment is decreased, or when it is increased, so that the reactivity loss due to the greater ^{238}U content is compensated to provide adequate lifetime.

Matching ^{235}U content (i.e., maintaining the same ^{235}U weight in each fuel element) would result in in-core flux-per-unit-power performance comparable to that of the unmodified reactor but, because of the poisoning effect of ^{238}U, would generally result in lower reactivity and reduced burnup potential. Burnup potential can be matched to that of the unmodified reactor by increasing the ^{235}U content in the reduced-enrichment core by some amount over that of the 93% enriched case at the expense of some decrease in in-core thermal-flux-per-unit-power performance. The importance of these flux effects is dependent on the particular reactor, the type of application, and conversion scheme adopted. For example, thermal flux decreases in the reflector and in flux traps are generally much less than in-core. Another possibility is to reduce costs by increasing the fuel cycle length. This could be accomplished by further increasing the ^{235}U content.

The increase of the overall uranium content per fuel element can be achieved by increasing the volume fraction of the fuel meat and/or by increasing the uranium concentration in the fuel meat.

Increasing the volume fraction of the fuel meat normally requires redesign of the fuel element. Three options are open: decreasing the clad thickness, decreasing the coolant volume fraction and/or decreasing the number of plates per element. The achievable reduction in the clad thickness may be limited by the minimum thickness needed for fission product retention. The achievable reduction in the coolant volume fraction may be limited by the need to avoid excessive pressure drop in the core and by the need to adequately moderate the neutron flux in the core. Otherwise the excess reactivity and cycle length would be significantly reduced. The reduction in the number of plates may be limited by the minimum heat transfer surface needed to prevent onset of nucleate boiling at a given reactor power.

These limitations may make it difficult to significantly increase the fuel meat volume fraction in some high-performance reactors that are designed very close to their thermal-hydraulic limit. In a majority of the research and test reactors in operation, however, and especially in those of low power, the volume fraction of the fuel meat can be increased above current values. Sometimes, a practicable way seems to consist in increasing the fuel meat thickness and coolant channel width by the same fraction, thereby reducing the number of fuel plates correspondingly. This is illustrated in Section 2 in more detail.

Increasing the uranium concentration in the fuel meat without changing the meat thickness has only negligible effects on the thermal-hydraulics properties of the core, and, therefore, it does not normally require redesign of the fuel element. (Only in some very rare cases might it be desirable to increase the coolant volume fraction to balance the hardening of the neutron spectrum caused by the increased uranium content). The only limitation to this approach is posed by the highest uranium concentration feasible with the most advanced fuel fabrication technology. This approach can be immediately applied to all those research and test reactors in which the uranium density in the fuel meat is less than currently qualified technology allows. Its application in reactors which already use the most advanced currently qualified fuel fabrication technology requires development of new fabrication techniques yielding even greater uranium densities in the fuel meat. Development of the new fabrication techniques is currently underway in the U.S. RERTR Program, in the French Reduced Enrichment Program, in the Reduced Enrichment Program of the Federal Republic of Germany, and also at the CNEA in Argentina, but it is anticipated that the desired fuel properties will be achieved only after several years.

For the rod-type $UZrH_x$ fuel, enrichment reduction is achieved by an increase in the uranium concentration in $UZrH_x$ alloy. The geometry of the fuel elements remain identical to the highly enriched version replaced.

The main properties of the currently qualified fuels and the status and development potential of the new fuels are summarized in the next section. More detailed information on the fuel development programs is provided in Section 3.

1.4.2 Status of Current, Near-Term, and Long-Term Fuel Technologies

Fuel meat materials currently qualified for use in research reactors are:

(1) U-Al Alloy, with uranium densities up to 1.1 g/cm^3.

(2) UAl_x-Al Dispersions, with uranium densities up to 1.7 g/cm^3.

(3) U_3O_8-Al Dispersions, with uranium densities up to 1.7 g/cm^3.

(4) U-ZrH_x, with uranium densities up to 1.3 g/cm^3.

Excellent burnup experience has been acquired on these fuels, albeit with uranium enrichment frequently greater than 20%. The enrichment is not expected to affect in any significant manner the metallurgical performance of the fuel, and tests already in progress are anticipated to prove conclusively that the experience gathered with these fuels does not depend on the fuel enrichment.

(5) UO_2 with density of 9.1 g U/cm^3 is currently used with rod cluster geometry. This fuel is qualified with plate-type geometry (Caramel) in low and medium power range and is under demonstration for high power reactors.

A high potential exists for increasing the maximum loading of many of these fuel types significantly above currently qualified values. In addition, greater uranium loadings can be achieved through the development of new fuel types, such as U_3Si and U-Mo. An overview of the development potential of the various fuel types is provided in Table 1-1, and the anticipated dates of commercial availability of suitably-qualified fuels are given in Table 1-2.

1.5 MAIN ACTIVITIES NEEDED IN PREPARATION FOR A TYPICAL CONVERSION

Several technical activities must be accomplished before a reactor conversion from the use of HEU fuel to the use of LEU fuel can be physically implemented. Because of their nature, a few of these activities are the exclusive responsibility of the organization to which the reactor to be converted belongs. Most of the activities may be shared, however, to a greater or lesser extent, with other organizations equipped with the needed expertise, resources, and willingness to assist in the conversion process. It is especially in this connection that the various national reduced enrichment programs can provide conversion assistance to the research and test reactor community, through IAEA coordination.

1.5.1 Characterization of Present Performance

Identification of key characteristics of reactor performance with the fuels currently utilized must be made. This, of course, must be responsibility of the reactor organization. This information is needed to identify any unique characteristics and special requirements of the reactor, and to establish a reference against which calculations with reduced enrichment may be compared. Needed information would include, for instance, the power distribution in the core, the neutron spectrum, the temperature coefficients of reactivity, the control rod worths, the thermal-hydraulic margins, the core lifetime, etc. Much of this information may be already available; however, collection and organization of the data in a form suitable for the intended purpose may be needed. In addition, experimental determinations may be needed in those cases in which the data are not available. Appendix G summarizes the reactor data normally needed as a basis for reduced enrichment conversion studies.

Table 1-1. Anticipated Uranium Densities, g/cm^3
(March 1980)

Fuel System	Manufacturer	Highest Density in Use[1] (Qualified)	Near-Term[2] Very Likely	Near-Term Some Uncertainty	Long-Term[3]
UAl_x-Al	NUKEM		2.2	2.4	2.6
	EG&G Idaho	1.7 (1.7)	2.4	2.6	2.8
	CERCA		2.2	2.4	2.5 - 2.8
	CNEA		1.8	2.2	
U_3O_8-Al	NUKEM		2.2	3.2	3.5
	ORNL	1.2 (1.7)	2.8	3.0	3.2
	CERCA		3.0	3.3	3.5 - 3.8
	CNEA		2.4	3.0	
U-ZrH_x	GA	1.3 (1.3)	3.7		
UO_2-plates	CEA	9.1 (9.1)			
	NUKEM			~9.0/4.5[4]	~9.0/4.5[4]
UO_2-rods	CEA	9.1 (9.1)			
U_3Si-Al	ANL			4.2 - 6.0	7.0 - 8.0
	NUKEM			~7.0	~8.0
U_3Si (bulk)	ANL				11 - 12
	NUKEM				~11

[1]For reactors with highest density in use, see Table 3-2.
[2]Near-Term : 1-3 years.
[3]Long-Term : 3-5 years.
[4]Two different fuel-types.

Table 1-2. Anticipated Dates of Commercial Availability of Suitably-Qualified REU Fuels

Fuel System	Uranium Density g/cm^3	Meat Thickness mm	Date of Availability
UAl_x-Al	2.6	0.5 - 1.5	1983
U_3O_8-Al	3.0	0.5 - 1.5	1983
	3.2 - 3.5	0.5 - 1.5	1985
UO_2-plates	9.1	$\geq$1.4	1980
	4.5	1.2	1983
UO_2-rods	9.1	8.2*	1980
U-ZrH_x	3.7	13.7*	1980
U_3Si-Al	4 - 8	0.5 - 0.8	1986

*Rod Diameter.

1.5.2 Performance Calculations with MEU and LEU

Before the conversion to reduced enrichment is studied in detail, the priority of design criteria for the conversion has to be specified. Possibilities include: minimum reactor core modification, minimum changes in operational characteristics and neutron flux values, minimum licensing problems, minimum fuel cycle costs, reoptimization for highest performance under certain boundary conditions (given maximum flow or power).

When the target is specified, the different options available should be compared which allow enrichment reduction to 20% or less. If no option satisfies the requirements, 45% enrichment would be considered.

This study will generally require calculations of the neutronic and thermal-hydraulic performance of the reactor with some parameter variations. The reactor data discussed in Section 1.5.1 must be calculated for the design variations considered to accompany the fuel enrichment change. Neutronics considerations include composition and thickness of the fuel meat, clad thickness, number of plates or rods per element, core size, fuel management strategy, etc.

Thermal-hydraulics considerations include heat transfer properties of the new fuels, coolant flow rates, pressure drops, margins to onset of nucleate boiling, to departure from nucleate boiling, and to flow instability, etc. The calculations may be normalized to the values measured in the core before the conversion. Neutronics and thermal-hydraulics methods and examples of applications to generic and specific reactors are described in Appendices A to E.

1.5.3 Engineering Studies

Although major modifications to the reactor to accomplish enrichment reduction are outside of the scope of the agreed criteria, several modifications in reactor components may be optionally considered by the reactor operator to improve the performance of the reactor when it is operating with the low enriched fuel. Such changes may include modifications of the control rods, instrumentation, fuel support plates, cooling system, etc. Engineering studies will be needed to evaluate the need, feasibility and performance of the system with these changes. It should be noted that changing to low enriched fuel may afford a suitable opportunity for maintenance or updating of reactor systems and components.

1.5.4 Safety Analysis Revisions and Licensing

The use of new fuel elements will require some revisions of the current safety analysis report to assess the new balance of safety factors. The amount of work needed will depend on the unique features of the reactor, on the changes caused by the conversion, on the details of the existing safety analysis document, and on the requirements of the licensing authority involved. Principal issues involved will include the effect of enrichment and fuel technology changes on temperature and void coefficients of reactivity, thermal-hydraulic safety criteria, fission product retention, and control system effectiveness. Also, the plutonium buildup in the fuel elements is a safety, safeguards, and licensing issue and must be included in the revision of the safety analysis (see Appendix A, Section A.6, and Benchmark Calculations, Section 2.4). As for any other issue related to safety, the primary responsibility for the safety analysis report must rest with the reactor organizations. A new guidebook is planned by the IAEA to address safety and licensing issues related to core conversions.

1.5.5 Effects on Utilization

It is important that the impact of the conversion on the planned utilization of the reactor be fully evaluated. For instance, it will be important to asssess for each individual conversion to what extent and in what manner planned reactor programs for irradiation, isotope production, and neutron beam research may be affected by the conversion. In this manner trade-offs may be identified and the conversion may be designed to match in the best possible way with existing plans.

1.5.6 Evaluation of Gradual Transition Feasibility

In general, a gradual transition to the reduced enrichment cycle would be expected. In many cases, it is anticipated that such gradual transition could minimize the costs, lead-time, and uncertainties associated with the conversion. The feasibility of operating the reactor in a mixed mode (i.e., part HEU and part LEU fuel) must be carefully evaluated, however. The safety analysis revision may need to consider operation of the reactor during the transition phase.

1.5.7 Detailed Technical Specifications

Detailed technical specifications must be prepared for the fuel and for any reactor component that needs to be modified in connection with the conversion.

1.5.8 Time and Cost Estimates

A detailed time schedule and a detailed cost plan must be prepared before the contracts leading to the conversion can be finalized. The choices of optimal fuel element designs for specific reactor conversions will depend on individual assessments of the trade-offs among economic, performance, safety, and licensing issues, consistent with the status of fuel development, demonstration, and commercial availability. Examples of analyses of the economic aspects of reactor core conversions are given in Appendix I.

2. DEMONSTRATION OF CONVERSION CALCULATIONS

2.1 OVERVIEW

In order to clarify the concepts and procedures discussed in other sections of this guidebook, it is useful to consider some examples of research reactors which may be converted to the use of reduced enrichment fuels, and to describe in detail the considerations, calculations, and results obtained for these particular examples. Two generic examples were chosen for this purpose, one for a 2 MW reactor and the other for a 10 MW reactor. These examples cannot, obviously, be directly applied to all the research reactors for which reduced enrichment may be considered. However, considerable effort was used to select their idealized design parameters so that the results obtained for these examples can be representative of many research reactors and illustrate the analytical procedure that can be followed in evaluating the effects of a conversion. Additional confirmation of the methods and procedures utilized can be obtained from the results of calculations for several specific examples.

The 2 MW reactor example is representative of low-power research reactors with low fissile loading in their elements and modest thermal-hydraulics requirements. Enrichment reduction in cores of this type can be successfully pursued using currently qualified technology by increasing both the uranium density in the fuel meat and by increasing the volume fraction of the fuel meat.

The 10 MW reactor example is representative of medium-power research reactors, with high fissile loadings and more demanding thermal-hydraulics requirements. The methodology for evaluating the conversion potential of this reactor type does not differ significantly from the methodology used for the 2 MW reactor, but the development and design changes needed to achieve successful conversion are significantly greater than for the 2 MW case.

The calculations and evaluations for the generic and specific examples were performed by several laboratories whose members participated in the different Consultants' Meetings (see Appendix J).

The independent calculations and evaluations performed by these groups provide (1) a broad overview of the methods and procedures that can be followed in evaluating a conversion, (2) an indication of the type of assistance which the groups could provide to reactors considering conversion, and (3) a check on the validity of the conclusions.

The calculations and evaluations performed for the 2 MW reactor example are summarized in Section 2.2 while those for the 10 MW reactor example are summarized in Section 2.3. Detailed descriptions of the calculations and of the methods used are provided in Appendices A through D for the generic examples and in Appendix E for the specific examples.

A set of "Benchmark" calculations for a simpler configuration have also been performed by the various laboratories. The purpose of these calculations is to check how closely the results obtained by the various laboratories compare when the calculations are run for identical conditions. The reactor specifications used in these calculations are not meant to be realistic, and the result should not be used to draw conclusions about actual reactor performance. Comparison of the results gives an indication, however, of the reliability of the methods and of possible biases. The results of the benchmark calculations are summarized in Section 2.4. Detailed descriptions of the calculations are provided in Appendix F.

The choices of optimal conversion strategy and optimal fuel element design for specific reactor conversions will depend on individual assessments of the trade-offs among economic, performance, safety and licensing issues. For example, the maximum uranium density that is available for conversions at a particular time will depend on the status (Section 3 and Appendix H) of fuel development, demonstration, and commercialization. Economic considerations in choosing a fuel element design and uranium density are discussed in Appendix I, where it is shown that the major cost components in the fuel cycle are uranium costs and fuel fabrication costs. Reprocessing and spent-fuel transportation charges tend to be balanced by uranium credits. REU fuels require a greater ^{235}U content than HEU fuels and fabrication costs are expected to be higher. An important aspect of choosing an optimal design may be the future that various designs hold for fully utilizing the potential of the high uranium density fuels currently under development. The safety and licensing aspects of core conversions are planned to be addressed in a new guidebook to be prepared under the auspices of the IAEA.

2.2 STUDIES OF GENERIC 2 MW REACTOR CONVERSION FROM HEU TO LEU FUEL

Generic studies of how a "typical" 2 MW research reactor could be converted from the use of HEU fuels to the use of LEU fuels have been conducted by several members of the Consultants' Meetings. The purpose of these studies was to provide an indication of (1) what type of reactor conversion could be feasible for reactors of this type either with current technology or with technology under development, (2) what performance and characteristics could be expected from the converted core, and (3) what methods could be followed to evaluate the conversion.

Several organizations took part in this effort, and their contributions are described in detail in Appendices A through D. Only an overall summary of their work and results is presented in this section.

A general description of the design parameters of the 2 MW reactor is provided in Table 2-1 and in Fig. 2-1. Briefly, the core is assumed to contain ~20 standard MTR elements and 4 control elements. Each standard element contains ~180 g of ^{235}U, distributed in 19 plates with 0.51 mm-thick meat. Each control element contains ~135 g of ^{235}U, distributed in 15 plates also with 0.51 mm-thick meat.

The studies summarized in Section 2.2.1 considered conversion of the reactor to LEU fuel with classical plate-type elements by increasing the uranium density in the fuel meat without redesign of the element geometry, and also by increasing both the volume fraction of the fuel meat and the uranium density with redesign of the element geometry. The studies summarized in Section 2.2.2 consider conversion of the reactor to LEU by using U-ZrH (TRIGA) rodded-type fuel, and the studies summarized in Section 2.2.3 consider conversion to LEU by using plate-type Caramel fuel.

Table 2-1. 2 MW Reactor - General Description of Design Parameters

Fuel Element: MTR-Type (76 x 80 x 600 mm)

Number of Fuel Plates in:

Standard Fuel Element: 19

Control Fuel Element: 15 + 2 Al Plates Assuming 2 Control Blades/Element

Plate Dimensions: Standard MTR-Plate

Plate Thickness: 1.27 mm

Meat Thickness: 0.51 mm

Shape of Plate: Straight

Fuel Loading: Standard Fuel Element: 180 g U-235

Control Fuel Element: 135 g U-235

Number of Fuel Elements in the Core: 24 $\pm$ 1

Standard Fuel Element: 20 $\pm$ 1

Control Fuel Element: 4

Reflector: Water

Core Geometry: 4 x 6 Arrangement

Grid Plate: 6 x 9 Positions

Desired Average Burnup of U-235 in the Fuel Element Discharged from the Core: 30%

Burnup-Status of the Core: Equilibrium Core

Fuel Shuffling: Introduction of New Fuel Elements into the Core Center

Thermo-Hydraulic Data: Coolant Flow Rate: 5000 l/min (300 m^3/h)

Core Inlet Temperature: 38°C

Figure 2-1.

2 MW Reactor - Standard[a] (19 Plates/Element) and Control[a,b] (13 Plates/Element) Fuel Elements.

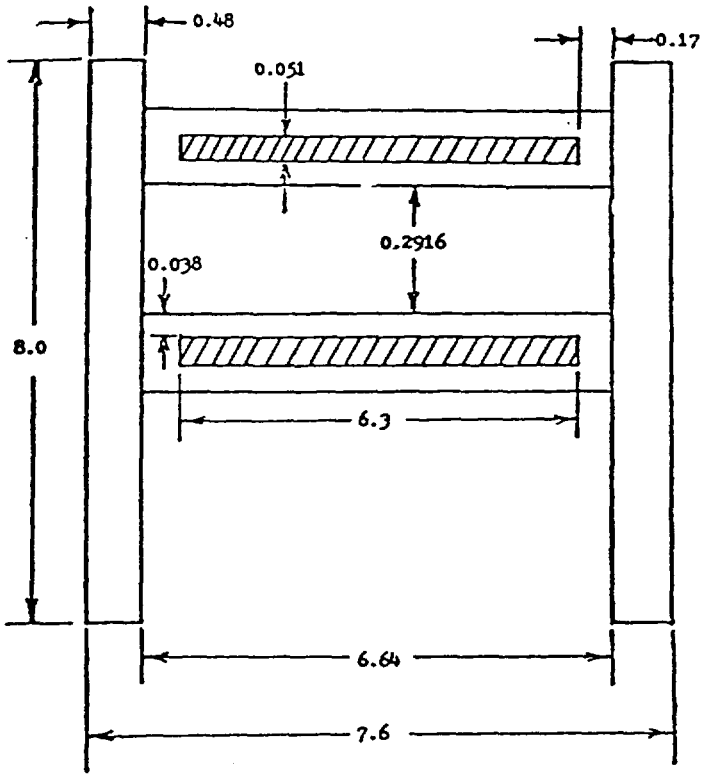

All dimensions in cm.

[a]The two outermost plates have a clad thickness of 0.0495 cm.

[b]Control fuel elements have two Al plates/ element assuming two fork-type absorber plates/element.

[c]Including a 0.5 mm water channel surrounding each element.

VOLUME FRACTIONS[c]

Standard Fuel Element		Control Fuel Element	
Fuel Meat	0.0979	Fuel Meat	0.0773
Aluminum	0.2870	Aluminum	0.2806
Water	0.6151	Water	0.6421

2.2.1 Conversion Studies Based on Classical Plate-Type Fuel

These studies were contributed by ANL-USA (Appendix A), by INTERATOM-FRG (Appendix C), and by CEA-France (Appendix D). Additional confirmation of the methods and results can be obtained from the specific examples (Appendix E) contributed by CNEA-Argentina and by JAERI-Japan.

Conversion Criteria and ^{235}U Loading Survey

The reference conversion criterion agreed upon during the Consultants' Meeting for identifying the options available for conversion to reduced enrichment fuels was a criterion based on matching the fuel cycle lengths of the REU and HEU cores at the end of their equilibrium cycles (EOC-criterion or cycle length matching criterion). Hence, most of the results described in this summary are based on the EOC-criterion. Several other conversion criteria were also considered, however. One of these assumed that the excess reactivities of the REU and HEU cores were matched at the beginning of the equilibrium cycle (BOC-criterion). Another criterion was based on data (Section 3) provided by fuel fabricators on the fuels that are expected to become available in the near-term and in the long-term (Fuel-Availability criterion). Yet another criterion assumed that the excess reactivities of the REU and HEU cores were matched for full-core loadings of fresh fuel.

The reference EOC-criterion and the BOC-criterion are the most realistic since most reactors are currently operating in an equilibrium cycle. Starting from the reference EOC-criterion and increasing the uranium density, there is a continuous range of conversion criteria that encompasses all the criteria mentioned above, and depends on the status of fuel development, demonstration, and commercial availability at a particular time.

To provide an overview of the ^{235}U loadings that might be expected with 45% and 20% enriched uranium fuels with no design changes, calculations were run using the EOC-criterion not only for the ^{235}U content of the elements for the "typical" 2 MW reactor (180 g/element), but also for a number of other ^{235}U contents between 180 and 600 g/element. These results (Table 2-2) have a more general application to water-moderated reactors using HEU with 0.51 mm thick fuel meat, and can be used to estimate the uranium densities required for conversion of many research reactors, regardless of their power level, if no design changes are made in the fuel elements. The calculations were done for an idealized reactor with 19 standard fuel elements, four control fuel elements, and 19 fuel plates per standard element, but approximate results for the impact of enrichment reduction on real reactors with different core size and numbers of fuel plates per element can be obtained by interpolation on the uranium density. For convenience, the uranium densities from Table 2-2 for LEU and MEU fuels have been plotted in Fig. 2-2 as a function of the uranium density for HEU fuel. Two comments on the results presented in Table 2-2 are appropriate: (1) The calculations were done for a core reflected by water on all four sides. If graphite or beryllium metal reflector elements are used in place of water, the required uranium densities are reduced considerably; (2) The table was prepared to illustrate what REU densities would be needed for different initial HEU densities. Some cycle lengths and burnups shown are not those that would actually be chosen for a practical 2 MW reactor. Normally, a reactor operator would select the core dimensions so that appropriate burnup results.

The limits or extremes of the conversion criteria mentioned above are represented by the EOC-criterion and by the criterion based on matching the excess reactivities of full-core loadings of fresh fuel. These limits were computed for a subset of the cases in Table 2-2, and are shown in Fig. 2-3, where the ratios of the ^{235}U densities with MEU and LEU fuels to the ^{235}U density with HEU fuel are plotted against ^{235}U loading per fresh HEU element for both conversion criteria. With increasing initial HEU loading, the EOC-criterion predicts a slightly decreasing ^{235}U density ratio, while the reactivity matching criterion for fresh fuel predicts increasingly larger ratios. Simple arguments based on one-group diffusion theory are presented in Appendix A to provide a qualitative basis for the divergent shapes of these curves. It is concluded that although core conversion calculations based on matching excess reactivities with fresh fuel loadings are simple to perform, these calculations predict uranium densities with MEU and LEU fuels that are unrealistically high and therefore should not be used in assessing the feasibility of core conversions to use of reduced enriched fuels.

Table 2-2. MTR Reactors with 19 Plates per Standard Element 0.51 mm Fuel Meat Thickness; 2.916 mm Water Channel Thickness ^{235}U Loading with Uranium Enrichments of 45% and 20% to Match Fuel Cycle Length of 93% Enriched Reference Core

	93% Enrichment, U-Al Alloy or UAl_x-Al						
Cycle Length, Days[a]	10.0	35.9	59.9	83.6	138.8	192.2	244.4
BOC k_{eff}	1.0058	1.0122	1.0174	1.0215	1.0293	1.0347	1.0387
EOC k_{eff}	0.9999	1.0000	1.0001	1.0000	1.0000	0.9999	1.0000
^{235}U Burned,[b] g	21.0	75.6	126.5	176.4	291.0	399.6	504.2
$H/^{235}U$[c]	334	273	231	200	150	120	100
ρ_{25},[d] g/cm^3	0.491	0.601	0.710	0.819	1.092	1.356	1.638
ρ_U, g/cm^3	0.528	0.646	0.763	0.881	1.174	1.468	1.761
wt.% U (5 v/o void)	17.5	20.7	23.7	26.5	32.9	38.4	43.3
^{235}U/Element, g	180	220	260	300	400.0	500.0	600.0
	45% Enrichment, UAl_x-Al						
Cycle Length, Days[a]	10.0	35.9	59.9	83.6			
BOC k_{eff}	1.0057	1.0110	1.0153	1.0187			
EOC k_{eff}	1.0001	1.0001	1.0003	1.0002			
^{235}U Burned,[b] g	21.2	76.0	126.6	176.5			
$H/^{235}U$[c]	303	249	212	184			
ρ_{25},[d] g/cm^3	0.541	0.657	0.773	0.889			
ρ_U, g/cm^3	1.203	1.460	1.718	1.977			
wt.% U (7 v/o void)	34.3	39.2	43.6	47.6			
^{235}U/Element, g	198.3	240.7	283.1	325.8			
	20% Enrichment, UAl_x-Al or U_3Si-Al						
Cycle Length, Days[a]	10.0	35.9	59.9	83.6	138.8	192.2	244.4
BOC k_{eff}	1.0052	1.0096	1.0135	1.0161	1.0202	1.0229	1.0253
EOC k_{eff}	1.0001	1.0001	1.0005	1.0005	1.0000	0.9998	1.0003
^{235}U Burned,[b] g	20.8	73.9	122.3	169.6	275.3	375.4	471.8
$H/^{235}U$[c]	281	234	200	174	134	109	91
ρ_{25},[d] g/cm^3	0.582	0.701	0.821	0.943	1.221	1.510	1.808
ρ_U, g/cm^3	2.912	3.505	4.103	4.719	6.103	7.552	9.038
wt.% U (7 v/o void)	58.7	64.6	69.3	79.4	79.2	84.6	88.7
^{235}U/Element, g	213.3	256.8	300.6	345.7	447.1	553.3	662.2
$\rho_{25}(45)/\rho_{25}(93)$	1.102	1.093	1.089	1.085	-	-	-
$\rho_{25}(20)/\rho_{25}(93)$	1.185	1.166	1.156	1.151	1.118	1.106	1.104

[a] Based on a power level of 2 MW.

[b] ^{235}U Burned in discharged fuel element.

[c] $H/^{235}U$ in fresh standard fuel element, including a 0.5 mm water channel surrounding each element.

[d] ρ_{25}, ρ_U, wt.% U, and ^{235}U content are for the fresh feed standard fuel element.

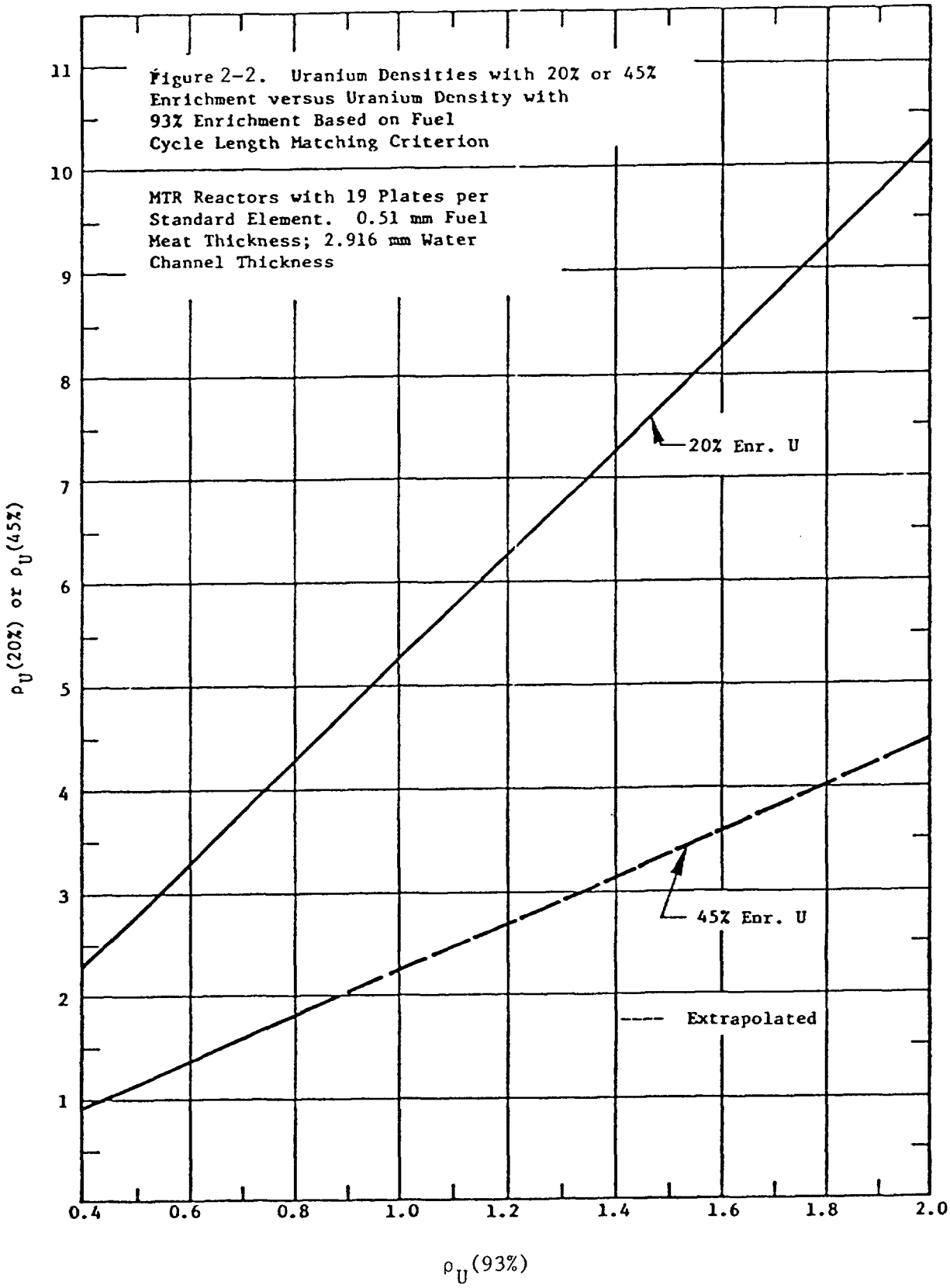
Figure 2-2. Uranium Densities with 20% or 45% Enrichment versus Uranium Density with 93% Enrichment Based on Fuel Cycle Length Matching Criterion
MTR Reactors with 19 Plates per Standard Element. 0.51 mm Fuel Meat Thickness; 2.916 mm Water Channel Thickness
20% Enr. U
45% Enr. U
Extrapolated
$\rho_U(20\%)$ or $\rho_U(45\%)$
$\rho_U(93\%)$
11
10
9
8
7
6
5
4
3
2
1
0.4
0.6
0.8
1.0
1.2
1.4
1.6
1.8
2.0

2 MW Reactor - Without Fuel Element Redesign

For the specific case of the 2 MW reactor with 180 g ^{235}U per fuel element, the uranium density required for conversion by simple substitution of a new fuel meat containing 45% enriched uranium was computed to be 1.2 g/cm^3. Fuel with this uranium density can be readily manufactured using current fuel fabrication technology, making the conversion to MEU fuel entirely feasible. Hence, little effort was spent on this alternative and the bulk of the calculations apply to enrichment reductions directly from 93% to 20%. The corresponding uranium density with LEU fuel was computed to be in the range of 2.83-2.91 g/cm^3 (207-213 g ^{235}U/element). One example of the determination of this loading is shown in Fig. 2-4. An example of the expected distributions of ^{235}U and Pu at the end of the equilibrium cycles with HEU and LEU fuels is shown in Fig. 2-5 based on an inside-out fuel management strategy with the order of element-insertion as indicated. Calculated flux ratios (across the core midplane) between MEU, LEU cases and the HEU case are shown in Fig. 2-6. In both cases, the thermal fluxes are reduced by less than 4% in the central irradiation channel and by less than 6% at the reflector peak. Fuel development programs (Section 3) in several countries are currently in progress to achieve uranium densities of about 3.0 g/cm^3 in the fuel meat. Conversion to 20% enrichment, without redesign of the element geometry and with no apparent changes in the thermal-hydraulics would be feasible when such fuels are developed, demonstrated, and commercially available.

2 MW Reactor - With Fuel Element Redesign

The uranium densities that are required for direct conversion of the 2 MW reactor from HEU to LEU fuel can be significantly reduced by increasing the fuel meat thickness and/or simultaneously decreasing the number of fuel plates per element. The ease with which such a conversion could be accomplished will depend on specific reactor operating conditions such as available excess pumping capacity and closeness to thermal-hydraulic safety margins.

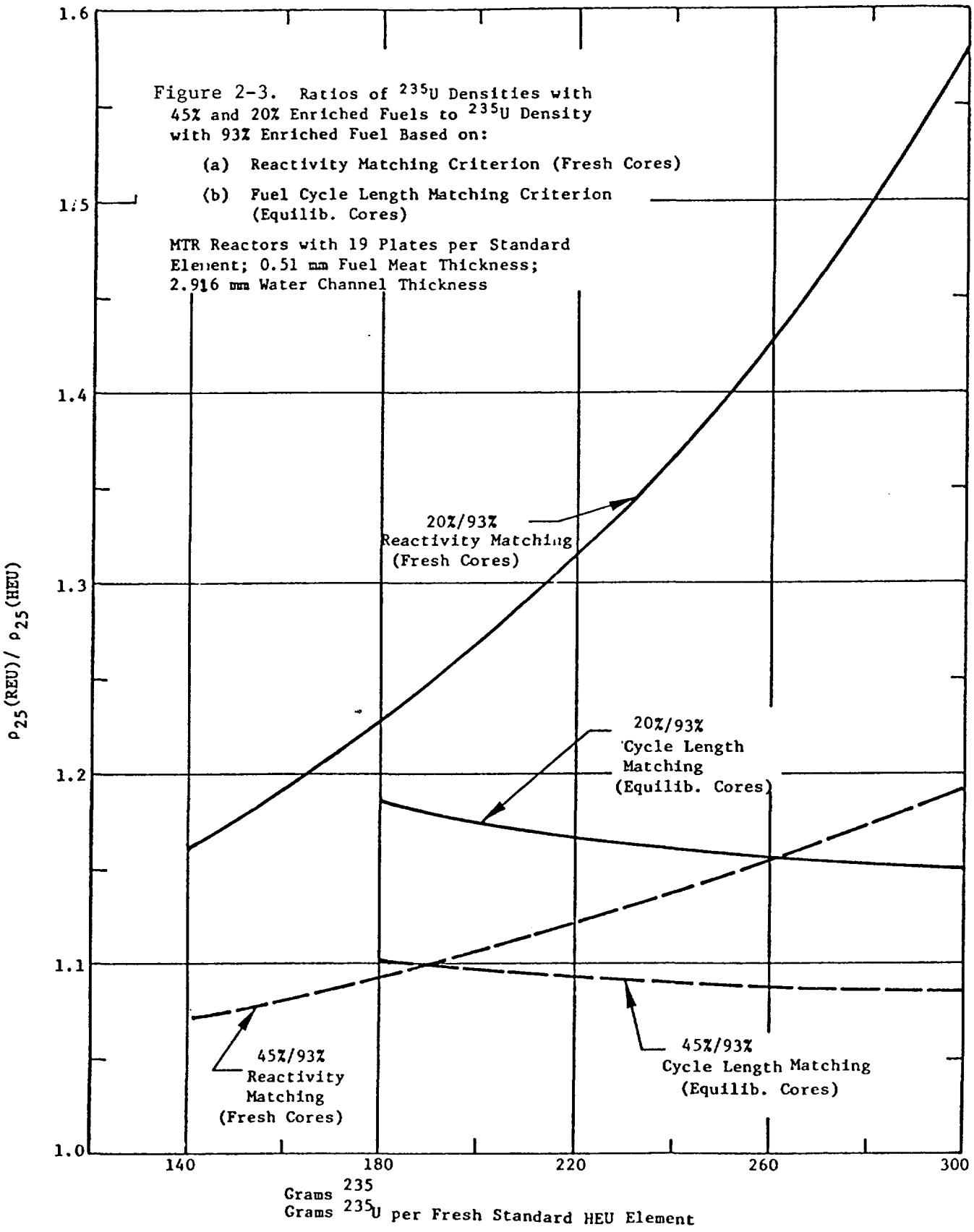

Figure 2-3. Ratios of ^{235}U Densities with 45% and 20% Enriched Fuels to ^{235}U Density with 93% Enriched Fuel Based on:

(a) Reactivity Matching Criterion (Fresh Cores)

(b) Fuel Cycle Length Matching Criterion (Equilib. Cores)

MTR Reactors with 19 Plates per Standard Element; 0.51 mm Fuel Meat Thickness; 2.916 mm Water Channel Thickness

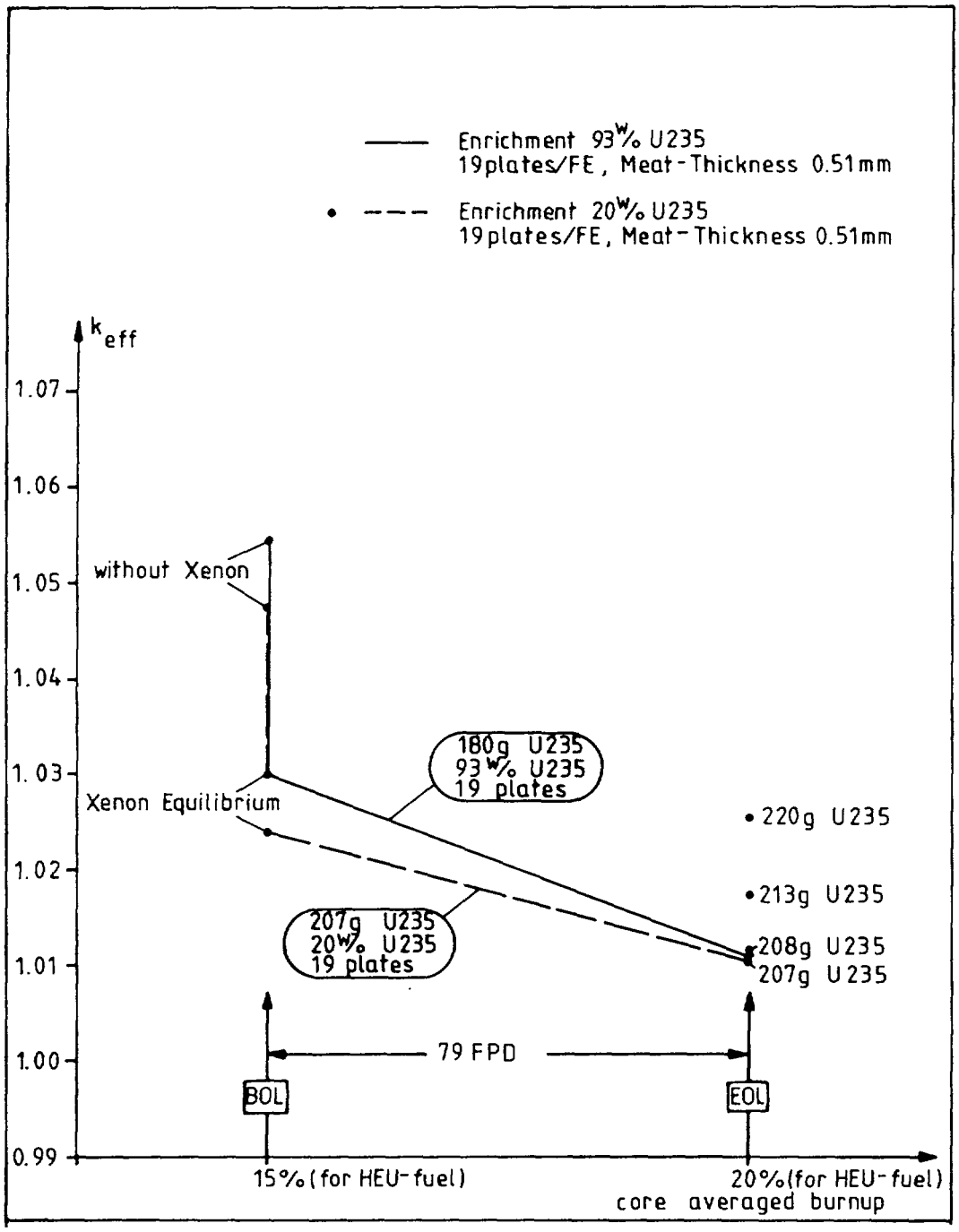

2 MW - Reactor Conversion EOL-Criterion
Determination of REU-Fuel with 20% U235 with no Fuel Element Redesign using the simplified RZ - Calculation

Fig. 2-4

Figure 2-5. 2 MW Reactor - HEU (93%) Fuel

End of Equilibrium Cycle Distribution of ^{235}U and Pu Based on Fuel Cycle Length Matching Criterion (0.51 mm Meat Thickness)

U Enrichment : 93%
U Density : 0.53 g/cm^3
Fresh Fuel Loading : 180 g ^{235}U

BOC k_{eff} : 1.0058
EOC k_{eff} : 0.9999
Cycle Length : 10.0 Days

END OF EQUILIBRIUM CYCLE

19 159.2 g ^{235}U 0.07 g Pu	8 169.5 0.03	9 168.3 0.04	10 167.0 0.04	11 165.9 0.05	12 165.1 0.05
18 159.9 0.06	CYE-1 131.3 0.03	1 178.3 g ^{235}U 0.01 g Pu	CYE-2 128.8 0.04	4 173.9 0.02	13 164.1 0.05
17 160.8 0.06	3 175.3 0.02	FLUX TRAP (H_2O)	2 176.6 0.01	CYE-3 130.6 0.04	14 163.1 0.05
16 161.7 0.06	CYE-4 133.9 0.02	7 170.5 0.03	6 171.7 0.03	5 172.9 0.02	15 162.3 0.06

2 MW Reactor - LEU (20%) Fuel

End of Equilibrium Cycle Distribution of ^{235}U and Pu Based on Fuel Cycle Length Matching Criterion (0.51 mm Meat Thickness)

U Enrichment : 20%
U Density : 2.91 g/cm^3
Fresh Fuel Loading : 213 g ^{235}U

BOC k_{eff} : 1.0052
EOC k_{eff} : 1.0001
Cycle Length : 10.0 Days

END OF EQUILIBRIUM CYCLE

19 192.5 g ^{235}U 1.40 g Pu	8 202.7 0.74	9 201.5 0.82	10 200.2 0.91	11 199.2 0.98	12 198.4 1.03
18 193.2 1.36	CYE-1 157.5 0.75	1 211.4 g ^{235}U 0.12 g Pu	CYE-2 155.1 0.91	4 207.1 0.44	13 197.4 1.10
17 194.1 1.30	3 208.4 0.33	FLUX TRAP (H_2O)	2 209.8 0.24	CYE-3 156.9 0.81	14 196.4 1.16
16 195.0 1.25	CYE-4 159.9 0.53	7 203.7 0.67	6 204.9 0.59	5 206.1 0.51	15 195.6 1.21

Figure 2-6. 2MW REACTOR FLUX RATIOS AT CORE MIDPLANE

180G U-235/ELEMENT REFERENCE

0.51 mm Fuel Meat Thickness; 2.916 mm Water Channel Thickness

Cycle Length Matching Criterion

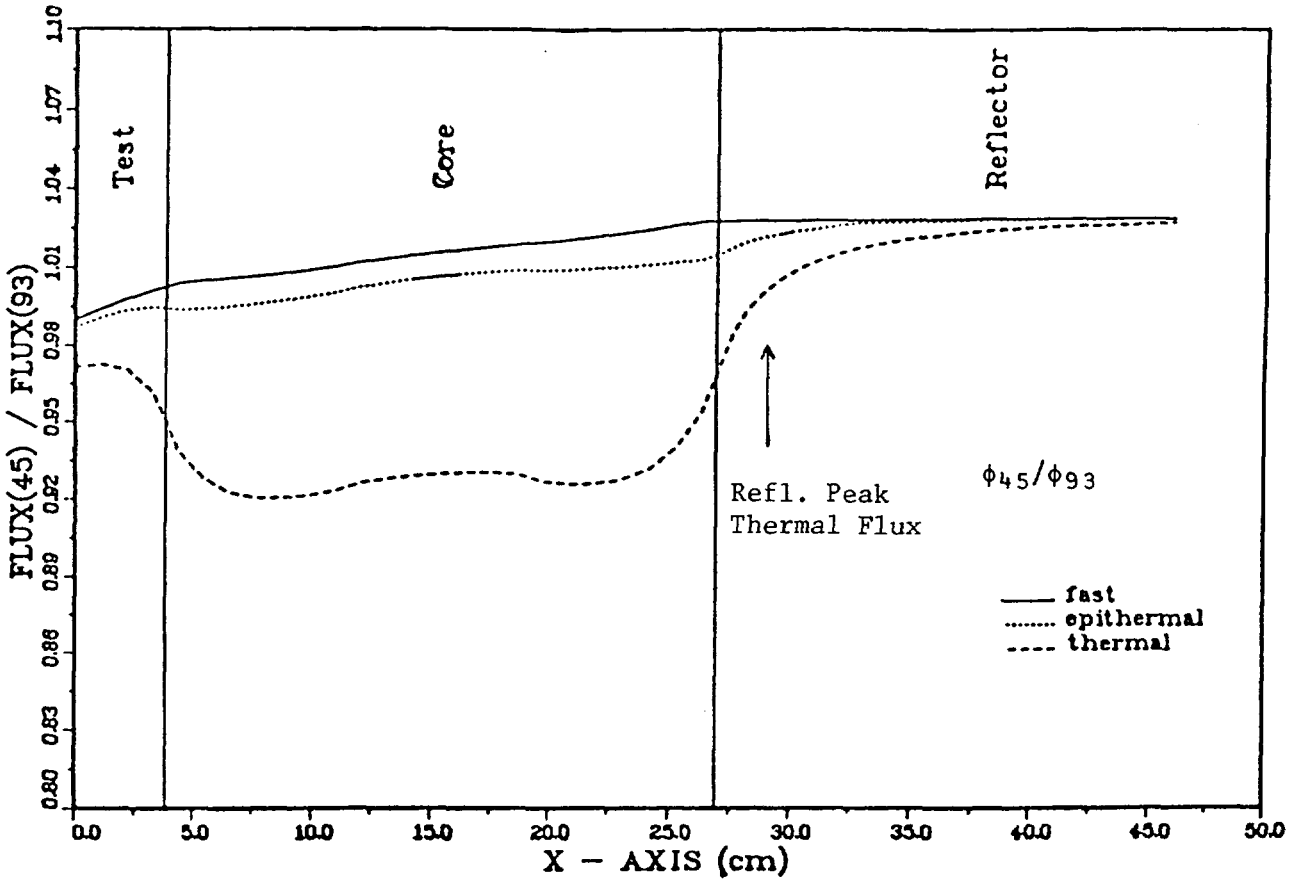

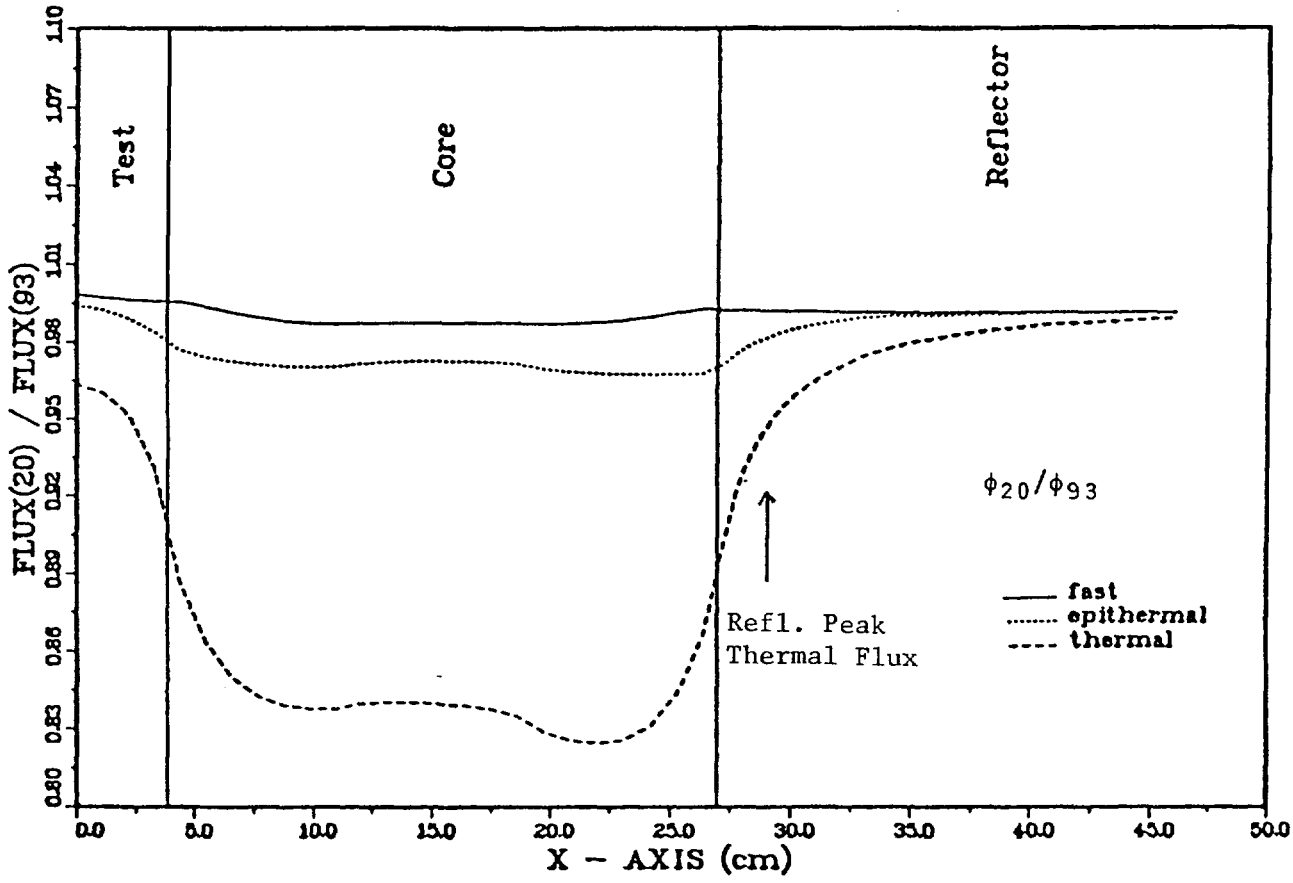

Table 2-3 presents the results of calculations for a number of fuel element design variations with different numbers of plates per element, fuel meat thicknesses, and water channel thicknesses. One example of how similar loadings were obtained is shown in Fig. 2-7. Thermal-hydraulic and safety margin data corresponding to the design variations in Table 2-3 are shown in Table 2-4 for steady-state operation. The safety margin data include the margin to onset of nucleate boiling (ONB), the margin to departure from nucleate boiling (DNB), and the margin to onset of instability due to a flow excursion. Detailed descriptions of the methods and procedures used by the various laboratories in calculating thermal-hydraulic and safety parameters can be found in Appendices A, C, and D.

Conclusions

In summarizing the results of the calculations, the following conclusions can be drawn:

1. Conversion from 93% enriched fuel to 45% enriched fuel can readily be achieved by simple substitution of a new meat manufactured using current fuel fabrication technology. Very modest flux changes were calculated in the experimental regions for this conversion making the conversion entirely feasible.

2. With an uranium density in the fuel meat of $\rho = 2.83 - 2.91$ g/cm^3 the reactor could be converted to 20% enrichment for a fuel cycle length equal to that of the highly enriched reactor without modification of the fuel meat thickness, or fuel element geometry. Thus, the thermo-hydraulic conditions would essentially be unaltered.

   The ^{235}U-mass would be increased by 15% to 18%. Therefore, the control rod worth would be reduced. On the other hand, the reactivity swing during burnup would also be smaller. Thus, no modification in the control system is expected to be necessary.

   The thermal neutron flux in the fueled regions is also reduced by about the same percentage as the ^{235}U-mass is increased (see Fig. 2-6). However, the thermal flux recovers rapidly in the reflector to its original value at the reflector peak, and has only a few percent depression in a typical beam hole or irradiation position inside or outside the core.

3. The reactor could be converted to 20% enrichment with equal fuel cycle length but lower uranium density requirements when the meat thickness is increased. This can be done by reducing the coolant channel width and/or the fuel plate number in the elements provided thermal-hydraulic conditions allow such reductions. Figure 2-8 shows on the basis of the calculations the relation between required uranium density and meat thickness with the plate number as a parameter. The curves correspond to an empirical fit of the numerical results with

Table 2-3. 2 MW Reactor - Fuel Element Design Variations With Equilibrium Core Using 20% Enriched Uranium Fuel. Fresh Fuel Loadings Required to Match the 10.0 Day Cycle Length of the HEU (93%) Reference Case With 180 g ^{235}U per Initial Standard Element

Number of Plates	Enrichment, %	$H/^{235}U$, Std. Element* (Fresh Fuel)	Thickness of Meat, mm	Thickness of Water Channel, mm	Volume of Meat, cm^3	Uranium Density, g/cm^3	^{235}U Density, g/cm^3	wt.% U**	^{235}U per Fresh Elmt. grams
19	93	334	0.510	2.916	366	0.53	0.492	17.5	180
19	20	282	0.510	2.916	366	2.91	0.582	59.0	213
19	20	140	1.238	2.188	889	1.83	0.367	45.4	326
18	20	279	0.588	3.071	400	2.68	0.535	56.6	214
18	20	265	0.665	2.994	446	2.48	0.496	53.8	221
18	20	250	0.743	2.916	506	2.25	0.451	51.5	228
18	20	118	1.471	2.188	1001	1.83	0.366	45.3	366
17	20	277	0.674	3.245	433	2.49	0.499	54.4	216
17	20	247	0.839	3.080	539	2.13	0.427	49.8	230
17	20	218	1.003	2.916	645	1.91	0.383	46.7	247
17	20	99	1.731	2.188	1112	1.87	0.373	45.9	415
16	20	188	1.295	2.916	783	1.73	0.346	43.8	271
15	20	159	1.626	2.916	922	1.64	0.328	42.2	302
14	20	131	2.005	2.916	1061	1.62	0.323	41.9	343
13	20	105	2.442	2.916	1200	1.67	0.333	42.7	400
12	20	81	2.952	2.916	1339	1.80	0.360	44.9	482

*Includes a 0.5 mm water channel surrounding each element.

**Porosity of 7 volume percent assumed with 20% Enriched UAl_x-Al Fuel.

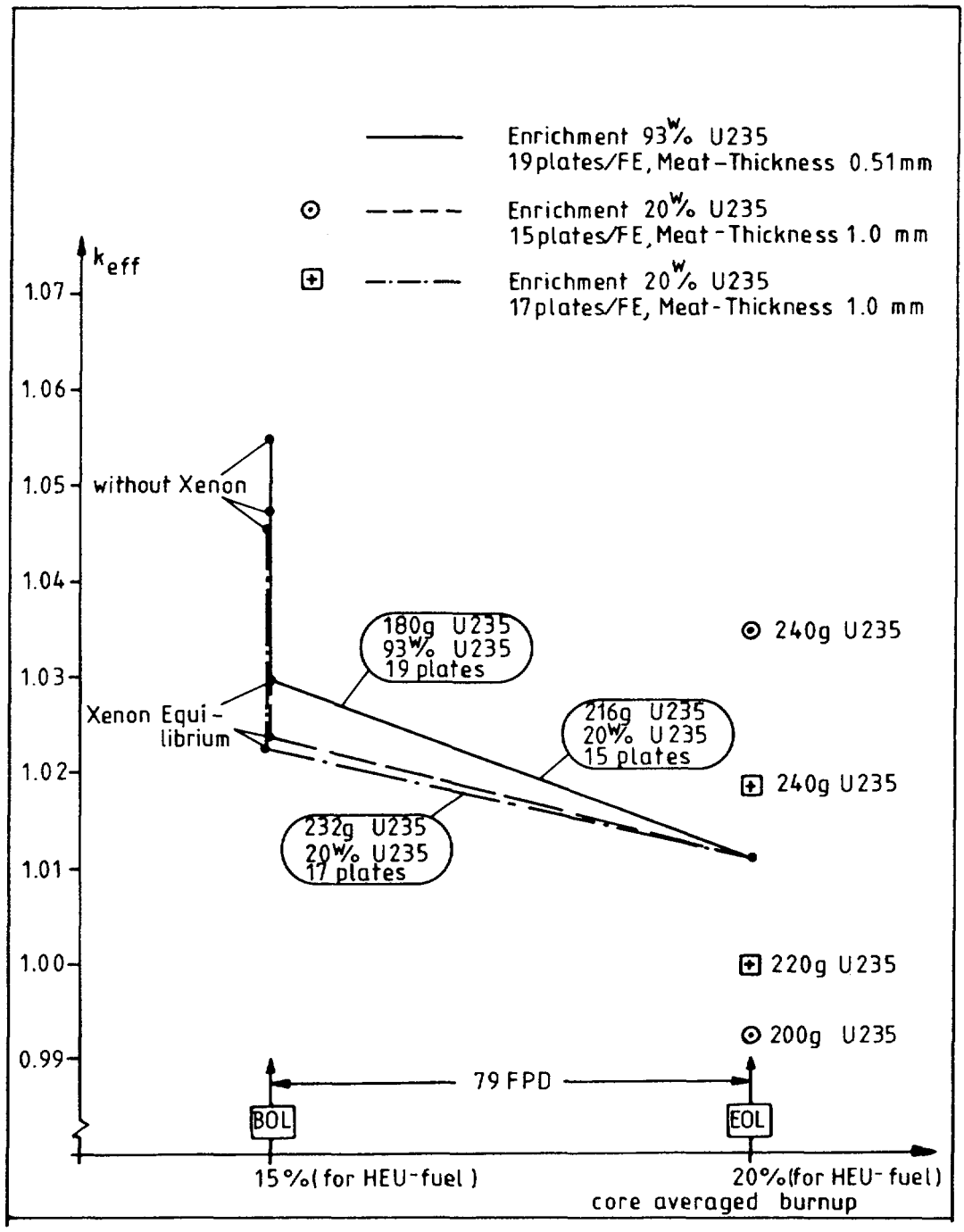

2 MW - Reactor Conversion EOL - Criterion
Determination of REU-Fuels with 20% U235 with Redesign of the Fuel Element Geometrie using the simplified RZ-Calculation

Fig. 2-7

TABLE 2-4. 2 MW Reactor
Thermal-Hydraulics
Fuel Element Design Variations
with 20% Enriched Uranium Fuel

Number of Plates	Thickness of Water Channel/Heat cm	Coolant Velocity m/s	Flow/ Element m^3/hr	Total Pressure Drop Across Channel bar	Avg.[b] Heat Flux W/cm^2	Avg. Heat[c] Flux at ONB W/cm^2	Burnout Heat Flux, W/cm^2		Limiting[f] Heat Flux at Onset of Flow Instability W/cm^2	Margin[g] to ONB	Margin[h] to DNB		Margin[i] to Onset of Flow Instability
							Labuntsov[d]	Mirshak[e]			Labuntsov	Mirshak	
19[a]	2.916/0.510	0.94	12.45	0.0186	5.80	11.4	231	231	102.2	1.94	12.6	12.6	5.58
19	2.916/0.510	0.99	13.08	0.0204	5.80	11.9	235	232	107.6	2.05	12.8	12.7	5.87
19	2.916/0.510	1.05	13.90	0.0266	5.80	12.6	240	233	114.1	2.17	13.1	12.7	6.23
19	2.188/1.238	0.94	9.34	0.0259	5.80	10.8	231	231	80.8	1.86	12.6	12.6	4.41
18	3.071/0.588	0.94	12.39	0.0177	6.12	11.5	231	231	106.5	1.88	11.9	11.9	5.51
18	2.994/0.665	0.94	12.09	0.0182	6.12	11.5	231	231	104.3	1.88	11.9	11.9	5.39
18	2.916/0.743	0.94	11.80	0.0188	6.12	11.4	231	231	102.2	1.86	11.9	11.9	5.28
18	2.916/0.743	0.99	12.44	0.0205	6.12	11.9	235	232	107.6	1.94	12.2	12.0	5.56
18	2.188/1.471	0.94	8.85	0.0260	6.12	10.8	231	231	80.8	1.76	11.9	11.9	4.18
17	3.245/0.674	0.94	12.39	0.0167	6.48	11.6	231	231	111.1	1.79	11.3	11.3	5.43
17	3.080/0.839	0.94	11.79	0.0177	6.48	11.5	231	231	106.7	1.77	11.3	11.3	5.21
17	2.916/1.003	0.94	11.15	0.0188	6.48	11.4	231	231	102.2	1.76	11.3	11.3	4.99
17	2.916/1.003	1.05	12.45	0.0229	6.48	12.6	240	233	114.1	1.94	11.7	11.4	5.57
17	2.188/1.731	0.94	8.36	0.0261	6.48	10.8	231	231	80.8	1.67	11.3	11.3	3.95
16	2.916/1.295	0.94	10.49	0.0189	6.89	11.4	231	231	102.2	1.65	10.6	10.6	4.69
15	2.916/1.626	0.94	9.83	0.0191	7.35	11.4	231	231	102.2	1.55	9.9	9.9	4.40
14	2.916/2.005	0.94	9.18	0.0192	7.87	11.4	231	231	102.2	1.45	9.3	9.3	4.11
13	2.916/2.442	0.94	8.52	0.0193	8.48	11.4	231	231	102.2	1.34	8.6	8.6	3.81
12	2.916/2.952	0.94	7.86	0.0195	9.19	11.4	231	231	102.2	1.24	8.0	8.0	3.52

[a]Reference HEU case and LEU case with no redesign.

[b]Peak Heat Flux = 1.58 x 2.0 x Avg. Heat Flux.

[c]The average heat flux at ONB is calculated with the conservative assumption that ONB occurs at the channel exit with peak heat flux, lowest pressure and saturation temperature, and highest coolant temperature rise.

[d]Burnout heat flux estimated using the Labuntsov correlation extrapolated with zero subcooling (see Section A.1.3.7 and Fig. A15).

[e]Burnout heat flux estimated using the Mirshak correlation extrapolated with zero subcooling (see Section A.1.3.7 and Fig. A15).

[f]Limiting heat flux at onset of instability due to flow excursion calculated with the Forgan correlation.

[g]Minimum ratio of local heat flux for ONB to actual heat flux.

[h]Minimum ratio of local heat flux for DNB using Labuntsov and Mirshak correlations to actual peak heat flux.

[i]Minimum ratio of local heat flux for onset of instability due to flow excursion to actual peak heat flux.

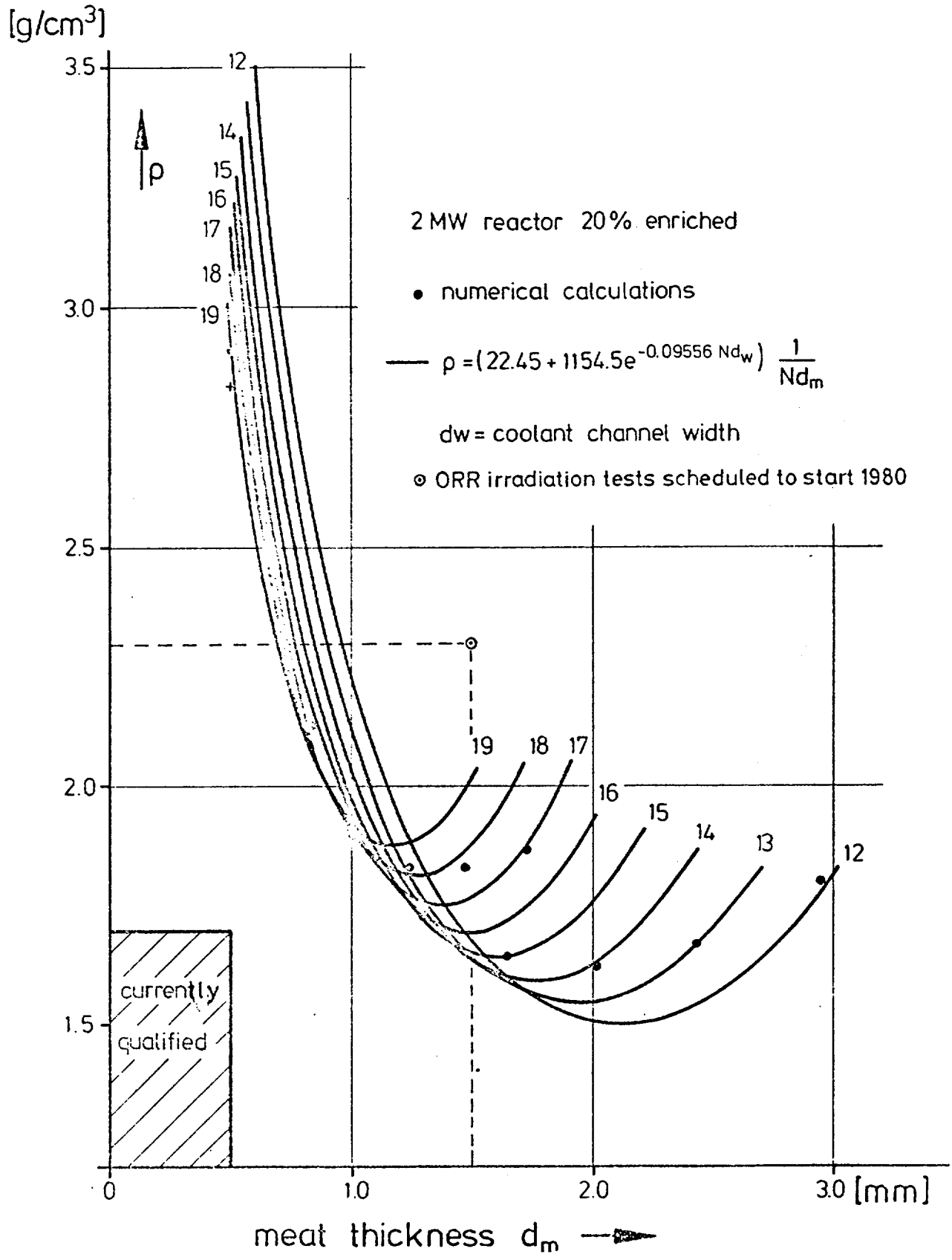

Fig. 2.8: Uranium density ρ vs. meath thickness d_m for equal cycle length number of fuel plates per element N as parameter.

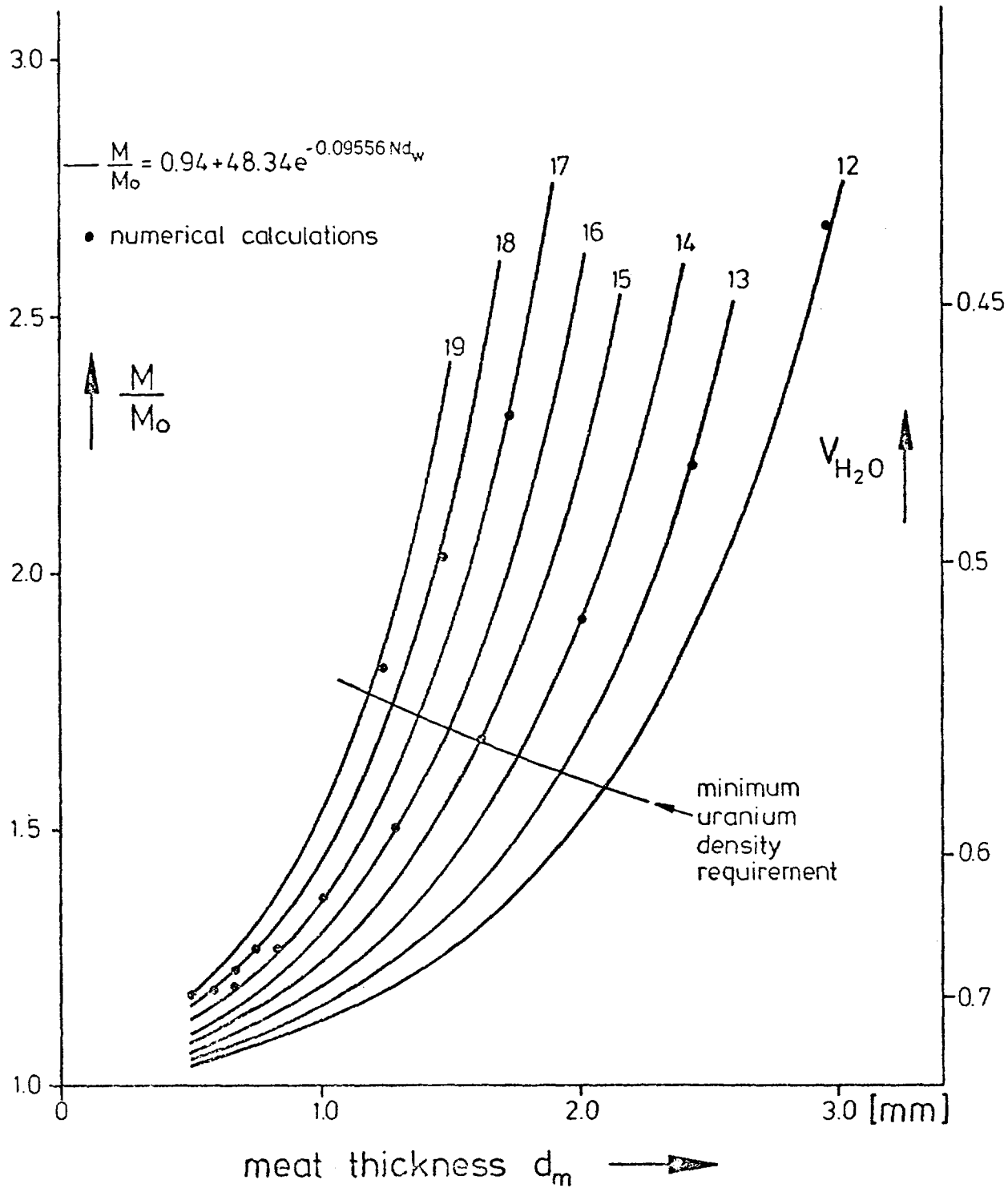

Fig. 2.9: Factor by which the ^{235}U-mass has to be increased compared to the 93% enriched case $\frac{M}{M_o}$ versus meat thickness plate number as parameter

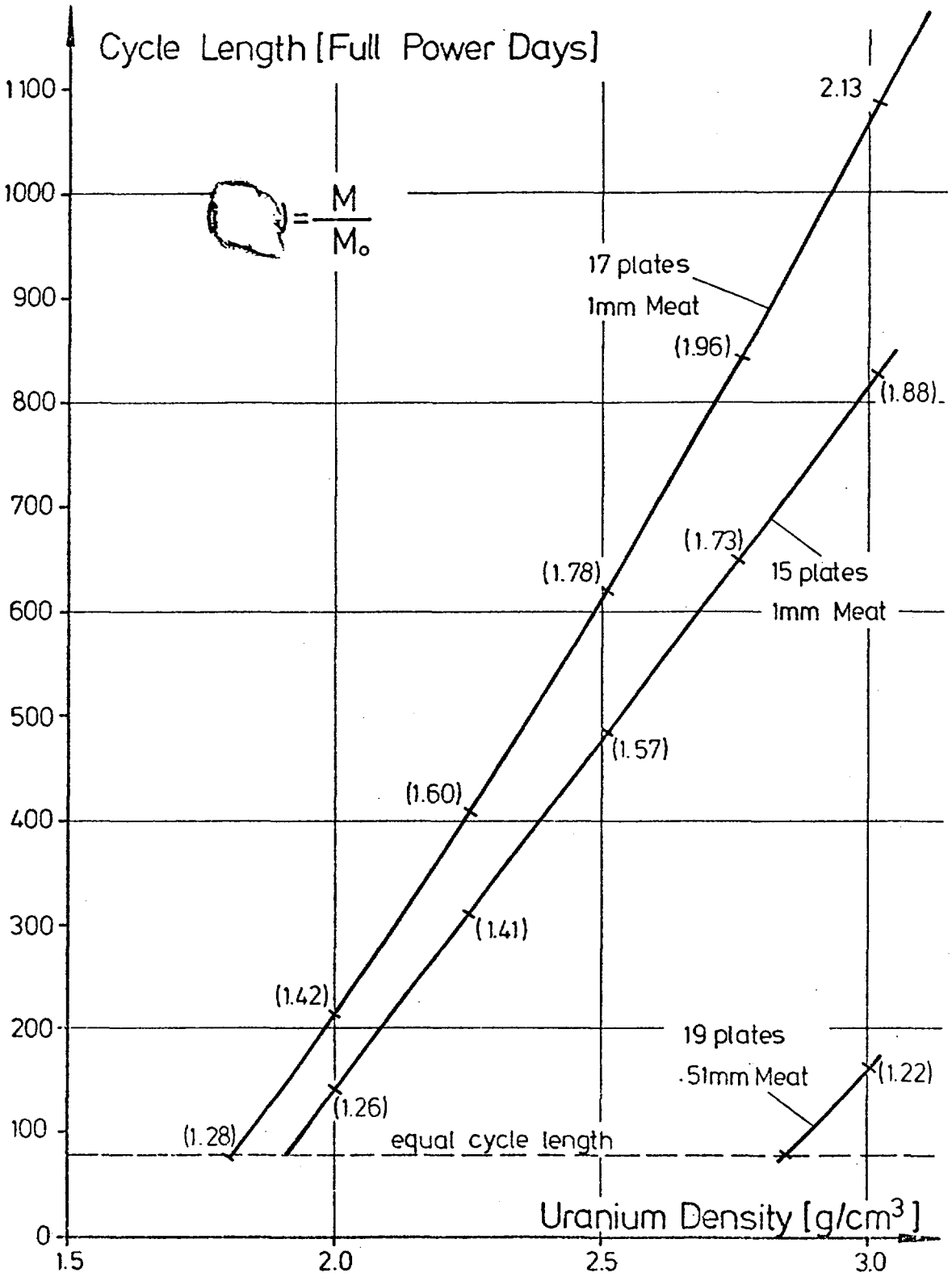

Fig. 2.10: 2 MW-Core **Cycle length versus uranium density**

$$\rho = (22.45 + 1154.5\ e^{-0.09556\ Nd_w})\ \frac{1}{Nd_m}$$

ρ = uranium density in fuel meat (g/cm^3)

N = number of fuel plates per element

d_w = coolant channel width (mm)

d_m = fuel meat thicknesss (mm)

The formula has no physical interpretation and other expressions can be found which fit the results as well. Some conclusions can be drawn, for instance:

- For a given plate number the uranium density requirement decreases rapidly with increasing meat thickness until $d_w \approx 1.8\ d_m$. Then it increases again since the reduced water content reduces the reactivity too much and has to be compensated by an increased ^{235}U-loading.

- Small increases in meat thickness can be very helpful in reducing the uranium density requirement. For instance, an increase in the meat thickness from 0.51 mm to 0.7 mm leads to a decrease in the uranium density from 2.9 g/cm^3 to 2.3 g/cm^3 for the 19 plate element.

- The larger meat thicknesses correspond to higher ^{235}U-requirements. Figure 2-9 shows the factor by which the ^{235}U-mass has to be increased compared to the highly enriched fuel versus meat thickness, with the plate number as a parameter. Included is the curve with the minimum uranium density requirements. One clearly would use only the range below the curve. Higher uranium loadings result in economic penalties without having any advantage.

- It seems to be feasible to convert the 2 MW reference reactor to 20% enrichment for equal cycle length with fuels that will be available in the near term. It could for instance be done with ρ = 1.9 g/cm^3 uranium density and d_m = 1.0 mm meat thickness. But there is a strong incentive to increase the uranium loading beyond that value in order to reduce the fuel cycle costs by increasing the cycle length. Figure 2-10 shows, for illustration, the full power days versus uranium density for 15 and 17 plates. A disadvantage of the high densities are the high ^{235}U-loadings which are written in brackets close to the curves. The large reactivity swing with burn up and the corresponding control requirements could also pose some problems.

2.2.2 Conversion Based on TRIGA Fuel

General Atomic Company has TRIGA LEU fuel available in shrouded clusters each containing four fuel rods designed for use in converting and upgrading MTR plate-type reactor cores and fueling new reactor facilities (Appendix B). The major design objective of this fuel is to provide a long-lifetime, readily-exportable fuel which considers both initial and operating costs to provide an attractive total fuel cycle cost.

The fuel rods used in the cluster are slightly reduced in diameter from the standard TRIGA fuel rods in use for over 20 years. The 3.24 cm (1.277 in.)-o.d. TRIGA fuel-moderator rods are clad with 3.35 cm (1.32 in.)-o.d. Incoloy 0.051 cm (0.020 in.)-thick and have an active fuel height of 50.8 cm

(20.0 in.). The bottom fitting in the aluminum shroud contains grid holes which determine the location and maintain the spacing of the fuel rods. The shroud also supports a top Inconel separator which maintains the spacing between fuel rods. The nominal shroud dimensions are: 7.257 cm (2.857 in.) square inside and 7.572 cm (2.981 in.) by 7.963 cm (3.125 in.) outside. These typical dimensions can change to some degree to accommodate the minor variations existing between the various MTR-type designs.

This TRIGA cluster is designed to operate at power levels of up to 3 MW; however, the achievable power level will be dependent on the cooling system available in the reactor facility. A coolant flow rate of about 3780 liters/min (1000 gpm) is needed for 2-MW operation.

The necessary U-235 content for long fuel life is achieved by using a somewhat higher uranium density than in past TRIGA fuels. The volume percent of uranium is still small, however, being about 7%. The fuel material (Er-U-ZrH) contains 1.3 g U/cm^3 (20 wt% U; 20% enriched, nominal), about 0.5 wt% erbium, and the hydrogen-to-zirconium ratio is 1.6. The small amount of erbium is included as a burnable poison and is a major contributor to the prompt negative temperature coefficient, the dominant safety feature of TRIGA fuel.

Core burnup calculations on reactors very similar to this 4-rod cluster TRIGA-LEU system have produced burnups of between about 1400 and 2000 MWd before the initial addition of reactivity is necessary to maintain the core at full power. The design condition established for the initial addition of reactivity is that the core has lost 2% in reactivity due to Sm buildup and fuel burnup (Δk aside from Xe). This reactivity loss is normally handled by the reactor control system. The average U-235 burnup is about 17% at the time of initial reactivity addition. It is estimated that the burnup will be about 30% in fuel clusters discharged from the core after an equilibrium fuel cycle condition has been established.

A few of the most pertinent estimated flux values for the 4-rod cluster TRIGA-LEU reactor are given in Table 2-5 for a power level of 2 MW.

Table 2-5. Estimated Peak Thermal (<0.625 eV) Flux at 2 MW 4-Rod Cluster TRIGA-LEU Reactor

Core	1.5×10^{13}
Core (central water hole)	7×10^{13}
Reflector (water)	2×10^{13}

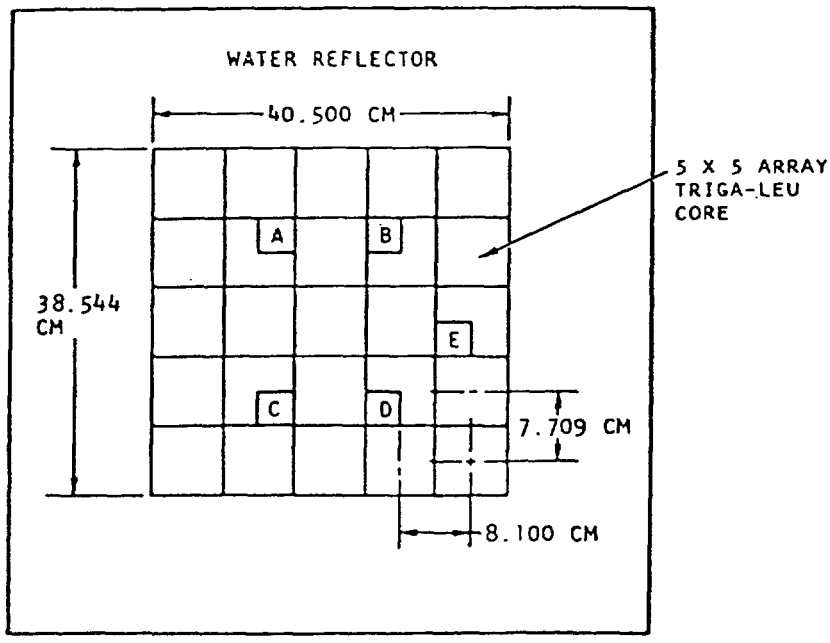

5 X 5 ARRAY OF 4-ROD CLUSTERS
SHOWING LOCATIONS OF 5 CONTROL
RODS (A — E)

Fig. 2-11. Water reflected configuration (rod locations for calculational purposes only)

TABLE 2-6.

SUMMARY OF CORE DESIGN PARAMETERS AND CHARACTERISTICS

Reactivity requirements, δk ($)		
Xenon (equilibrium)	∿1.9%	($2.71)
Samarium (equilibrium)	0.8%	($1.14)
Cold-to-hot reactivity change[a]	2.0-3.0%	($2.86-$4.29)
Total	∿4.7-5.7%	($6.71-$8.14)
Operational reactivity change[b]	∿3.9-4.9%	($5.57-$7.00)
β_{eff}(δk)	0.0070	
ℓ(microsec)	∿24 (beginning of life)	
Maximum fuel temperature	∿650°C	
Recommended excess reactivity at beginning of life, δk	>6.0%	($8.57)
Recommended control system worth, δk With maximum-worth rod stuck out	>6.5%	($9.29)

(a) Based on an average core temperature of 280°C

(b) Samarium not included

TABLE 2-7.

4-ROD CLUSTER TRIGA-LEU FUEL AND REACTOR DESCRIPTION SUMMARY

The parameters describing a 2 MW reactor utilizing the 4-rod cluster are as follows:

Fuel - cluster: TRIGA-LEU 20 wt-% U in UZrH (76 x 80 x 508 mm)

Fuel rods per cluster:
- Standard cluster: 4
- Control cluster: 3

Nominal fuel rod dimensions:
- Fuel O.D.: 32.4 mm
- Clad O.D.: 33.5 mm (incoloy)
- Fuel height: 508 mm

Fuel loading: 548 mm U (20% enriched)/rod
2.2 Kg U (20% enriched)/std cluster
440 gm U-235/std cluster
~0.5 wt-% Erbium as burnable absorber

Number of fuel clusters in the core: 26 ±1

- Standard clusters: 21
- Control clusters: 5 ±1

Reflector: Water

Core size (liters): 78 ±2

U-235 content/core (Kg): 10.6

Core geometry: 4 x 6 arrangement

Grid Plate: 6 x 9 positions (normal conversion)

Desired average burnup of U-235 in the fuel cluster discharged from the core: 30%

Burnup status of the core: equilibrium core

Average core burnup (%): ~20

Fuel shuffling: introduction of new fuel clusters into the core center

Thermal-hydraulic data:

Average power density (Kw/liter): 26
Coolant flow rate: 1000 GPM
227 m^3/hr (3.8 x 10^6 cc/min)
Core inlet temperature: 38°C

Figure 2-11 shows the general configuration of a typical water reflected core. The reactor shown has a core consisting of a 5 x 5 array containing 20 standard 4-rod clusters and 5 control clusters. The control clusters have three fuel rods with the fourth location containing a guide tube for a control rod. The guide tubes and control rods can be located in any fuel cluster.

Summaries of the TRIGA-LEU 4-rod cluster core design parameters and characteristics are given in Tables 2-6 and 2-7.

2.2.3 Conversion Studies Based on Caramel Fuel

The Caramel plate fuel is made of small squares of UO_2 separated by zircaloy spacers, and cladded between two zircaloy plates. Its use in research reactors offers several advantages: fuel operating at rather low temperature - fuel compartmented - negative Doppler effect in case of overpower transient - good chemical behavior in demineralized water which avoids the use of a hot layer.

Being similar in geometry to the currently used UAl elements of the flat or slightly curved MTR type, the Caramel assemblies are suitable for a wide range of research and test reactors. The high specific weight of this new fuel (about 10.3 g UO_2 per cm^3) can produce a weight of uranium per unit volume of core as high as 2 kg U/dm^3. This reduces the enrichment needed to as little as 3 to 10% ^{235}U, well below the currently recognized lowest weapons grade limit of 20% ^{235}U.

The calculations performed by the CEA show the feasibility of this solution in the cases considered to convert an HEU core directly to an LEU core. Particularly for the 2 MW core, such a conversion is not difficult. In this case the fuel economy being the main objective, the assembly is designed to provide the maximum reactivity for the smallest amount of uranium; i.e.,

- thick plates for self shielding of the ^{238}U and reduction of its absorption
- wide coolant channels to increase the moderation ratio, and hence the reactivity of the core.

From a neutronics point of view, one obtains a lifetime longer than with U-Al classic MTR type elements, for an enrichment around 4.5%. This is an attractive economy feature, and flux levels are also attractive from an experimental point of view.

From a thermal-hydraulics view point on the basis of the present safety criteria required by the French Regulation Authorities the conversion appears feasible in very good conditions, with about the same flow rate and pressure drop.

Table 2-8 summarizes the characteristics of both the original HEU core and the Caramel converted core.

TABLE 2-8. Summary of Characteristics of Original 2 MW HEU Core and Caramel Converted Core.

	93 % U_{235}	Caramel 4.5% U_{235}
fuel element dimensions (mm)	76 x 80	76 x 80
number of plates in standard fuel element	19	5
plate thickness (mm)	1.27	5
meat thickness (mm)	0.51	4
^{235}U weight by element (g)	180	250
uranium specific weight in meat (g/cm^3)	0.528	8.407
active height (mm)	600	500
average cycle length (days)	9.8	40
fast flux in central water hole(at the center) ϕ_1 < 0,9 MeV (averages height) ($n/s/cm^2$)	1.0 10^{13}	1.5 10^{13}
thermal flux in central water hole (at the center) ϕ_4 <0,625 eV (averages (averages height) ($n/s/cm^2$)	5.5 10^{13}	5.8 10^{13}
thermal flux in water reflector ϕ_4 < 0,625 eV (averages height)($n/s/cm^2$)	2.5 10^{13}	3.0 10^{13}

2.3 STUDIES OF GENERIC 10 MW REACTOR CONVERSION FROM HEU TO 45%-ENRICHED AND 20%-ENRICHED FUEL

Generic studies of how a "typical" 10 MW research reactor could be converted from the use of HEU fuels to the use of MEU and LEU fuels have been conducted by several members of the Consultants' Meetings (Appendix J). The purpose of these studies was to provide an indication of (1) what type of reactor conversion could be feasible for reactors of this type either with current technology or with technology under development, (2) what performance and characteristics could be expected from the converted reactor, and (3) what methods could be followed to evaluate the conversion.

Various organizations took part in this effort, and their contributions are described in detail in Appendices A through D. Only an overall summary of their work and results is presented in this section.

A general description of the design parameters of the 10 MW core considered in these studies is provided in Table 2-9 and in Fig. 2-12. Briefly, the core is assumed to contain 23 standard MTR elements and 5 control elements. Each fresh standard element with 93% enrichment contains 280 g of ^{235}U, distributed in 23 plates with 0.51 mm-thick meat. Each control element contains 207 g of ^{235}U distribution in 17 plates, also with 0.51 mm-thick meat.

The studies summarized in Section 2.3.1 considered conversion of the reactor to MEU and LEU fuel with classical plate-type elements by increasing the uranium density in the fuel meat without redesign of the element geometry, and also by increasing both the volume fraction of the fuel meat and the uranium

density with redesign of the element geometry. The studies summarized in Section 2.3.2 consider conversion of the reactor to LEU by using U-ZrH (TRIGA) rodded-type fuel, and the studies summarized in Section 2.3.3 consider conversion to LEU by using plate-type Caramel fuel.

2.3.1 Conversion Studies Based on Classical Plate-Type Fuel

These studies were contributed by the ANL-USA (Appendix A), by INTERATOM-FRG (Appendix C), and by CEA-France (Appendix D). Additional confirmation of the methods and results can be obtained from the specific examples (Appendix E) contributed by CNEA-Argentina and by JAERI-Japan.

Conversion Criteria and Fuel Management Strategies

As for the conversion studies of the 2 MW reactor, the conversion criterion used as a reference for identifying the options available for conversion of the 10 MW reactor to reduced enrichment fuels was based on matching the fuel cycle lengths of the REU and HEU cores at the end of their equilibrium cycles (EOC-criterion or Fuel Cycle Length Matching criterion). Most of the results described in this summary are based on the EOC-criterion, but the other criteria described for the 2 MW reactor were also considered in some of the calculations.

The EOC-criterion was used to calculate the uranium density in the fuel meat that would allow conversion to MEU fuel without redesign of the fuel element and conversion to LEU fuel both with and without redesign. Different organizations chose different fuel management strategies in their calculations. In the calculations with MEU fuel, an outside-in strategy was used in which five fresh elements were added to outer core positions at the beginning of each operational cycle. In the calculations with LEU fuel, an inside-out strategy was used in which one fresh element was added near the center of the core at the beginning of each cycle. However, each organization used a consistent strategy for calculation of both the HEU and REU cases. Thus, the cycle lengths and reactivity swings during burnup for the reference HEU core that were computed by the different organizations are not inconsistent.

MEU Case [58.7 Full Power Days (FPD); Five Elements; Outside-In Strategy]

For the MEU case with no redesign, the uranium density needed to match the cycle length (58.7 FPD) of the HEU design was computed to be 1.50 g/cm^3, corresponding to a ^{235}U loading of 295 g per fresh fuel element. An example of the determination of this loading is shown in Fig. 2-13. The BOL and EOL burnup distributions in the core are shown in Fig. 2-14 for fresh fuel loaded into the outer core positions. The calculated effects on the neutron flux can be summarized as follows. Fast and epithermal fluxes are essentially unchanged. The peak thermal flux at the irradiation position in the core center is reduced by ~1.8%; the average thermal flux decreases by ~10% in the fueled core regions; and the peak of the thermal flux in the radial reflector is reduced by ~3%. Since fuel with a uranium density of 1.5 g/cm^3 can be readily manufactured using current fuel fabrication technology, conversion to MEU fuel is entirely feasible with only minor losses in neutron flux at the experimental positions.

If the reactivity of the MEU and HEU cores are matched at the beginning of the equilibrium cycle (BOC-criterion), a uranium density of about 1.55 g/cm^3 is needed. This uranium density yields a cycle length of 73.1 FPD, an increase of ~25% over that of the EOC-criterion. An even longer cycle length (121.9 FPD - 108% greater than for the EOC-criterion) is obtained with a uranium density of 1.7 g/cm^3.

Table 2-9. 10 MW Reactor - General Description of Design Parameters

Fuel Element: MTR-Type Element (76 x 80 x 600 mm)

Number of Fuel Plates in:

Standard Fuel Element: 23

Control Fuel Element: 17 Fuel + 4 Al Plates
(Fork Type Absorber Blades)

Plate Dimensions: Standard MTR-Plate

Shape of Plate: Straight

Fuel Loading: Standard Fuel Element: 280 g U-235

Control Fuel Element: 207 g U-235
(without burnable poison)

Core Size: 28 Fuel Elements

Standard Fuel Elements: 23

Control Fuel Elements: 5

Core Geometry: 5 x 6 Arrangement

1 Irradiation Channel in the Core Center

1 Irradiation Channel at the Core Edge

Absorber Plates: Thin Fork Type Absorber Blades

Grid Plate: 6 (8) x 9

Reflector: Water 2 Core Sides Reflected by Graphite and Water (76 mm)

Desired Average Burnup of U-235 in the Fuel Element Discharged from the Core: 50%

Burnup Status of the Core: Equilibrium Core

Fuel Shuffling: New Fuel Elements into Core Edge or Core Center

Thermo-Hydraulic Data: Coolant Flow Rate: 1000 m^3/h (16666 dm^3/min)

Core Inlet Temperature: 38°C

Figure 2-12.

10 MW Reactor - Standard[a] (23 Plates/Element) and Control[a,b] (17 Plates/Element) Fuel Elements.

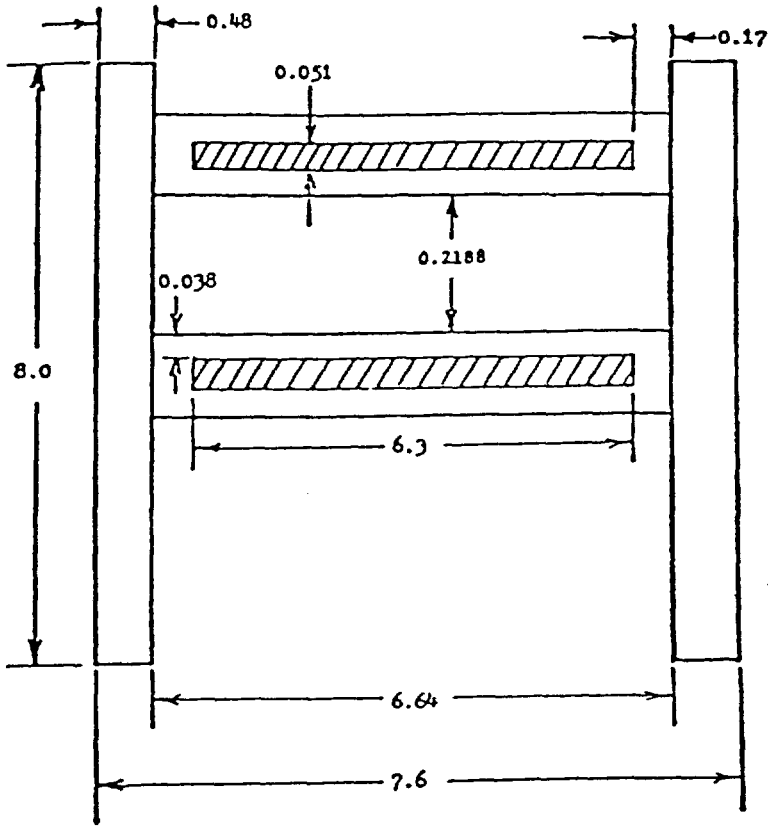

All dimensions in cm.

[a]The two outermost plates have a clad thickness of 0.0495 cm.

[b]Control fuel elements have four Al plates/ element, assuming two fork-type absorber plates/element.

[c]Including a 0.5 mm water channel surrounding each element.

VOLUME FRACTIONS[c]

Standard Fuel Element		Control Fuel Element	
Fuel Meat	0.1185	Fuel Meat	0.0876
Aluminum	0.3205	Aluminum	0.3244
Water	0.5610	Water	0.5880

LEU Case [16.7 FPD; One Element; Inside-Out Strategy]

For the LEU case with no redesign, the uranium density in the fuel meat needed to match the cycle length (16.7 FPD) of the HEU core was computed to be 3.59 g/cm^3. Since this uranium density exceeds the probable development potential (Section 3) of U_3O_8-Al and UAl_x-Al fuels, redesign of the fuel element geometry needs to be considered to achieve conversion to LEU with these fuel-types.

Uranium densities in the fuel meat using LEU are shown in Table 2-10 for several combinations of plates per element, fuel meat thickness, and water channel thickness. A case with 19 plates per element was studied extensively.

Figure 2-15 shows the relation between uranium density requirement and meat thickness with the plate number as a parameter. The curves correspond to an empirical fit with

$$\rho = (35.65 + 2977\ e^{-0.1232\ Nd_w})\ \frac{1}{Nd_m}\ .$$

Table 2-10.

10 MW Reactor - Cycle Length Matching Criterion (16.7 Days)
Fuel Element Design Variations With 20% Enriched Uranium Fuel[a]

Number of Plates	Enrichment, %	H/^{235}U, Std. Element[b]	Thickness of meat, mm	Thickness of Water Channel, mm	Volume of Meat cm^3/Element	Uranium Density, g/cm^3	^{235}U Density, g/cm^3	wt.% U[c]	^{235}U per Element, grams
23	93	196	0.51	2.188	443	0.68	0.632	22	280
23	20	172	0.51	2.188	443	3.59	0.718	66.3	318
21	20	145	0.839	2.188	666	2.60	0.523	56.6	346
19	20	207	0.51	2.916	366	3.96	0.792	69.2	290
19	20	184	0.70	2.726	503	3.05	0.610	61.4	307
19	20	171	0.80	2.626	575	2.77	0.554	58.6	319
19	20	158	0.90	2.526	646	2.56	0.512	56.2	331
19	20	145	1.00	2.426	718	2.42	0.483	54.4	347
19[a]	20	113	1.238	2.188	889	2.27	0.453	52.6	403
18	20	97	1.471	2.188	1001	2.23	0.445	52.1	446
17	20	83	1.731	2.188	1112	2.24	0.448	52.2	498

[a]All calculations in the table were done with microscopic cross sections corresponding to the fuel element with average burnup in the core. To investigate changes in cycle length and uranium density in the fresh feed elements due to cross section variation with burnup, the calculations for both the reference 93% enriched case and the 19 plate case with 1.238 mm thick fuel meat were repeated for extreme values of the cross sections. With microscopic cross sections corresponding to slightly-burned (i.e., at equilibrium Xe and Sm) fresh elements, the cycle length in both the 93% and the 20% enriched cases was 15.9 days, and the uranium density in the fresh feed elements of the 20% enriched case was 2.26 g/cm^3. With microscopic cross sections corresponding to elements with the discharge burnup, the cycle length in both the 93% and 20% enriched cases was 17.4 days, and the uranium density in the fresh feed elements of the 20% enriched case was 2.24 g/cm^3.

[b]Includes a 1 mm water channel surrounding each element.

[c]Porosity of 10 volume percent assumed with 20% enriched UAl_x-Al fuel.

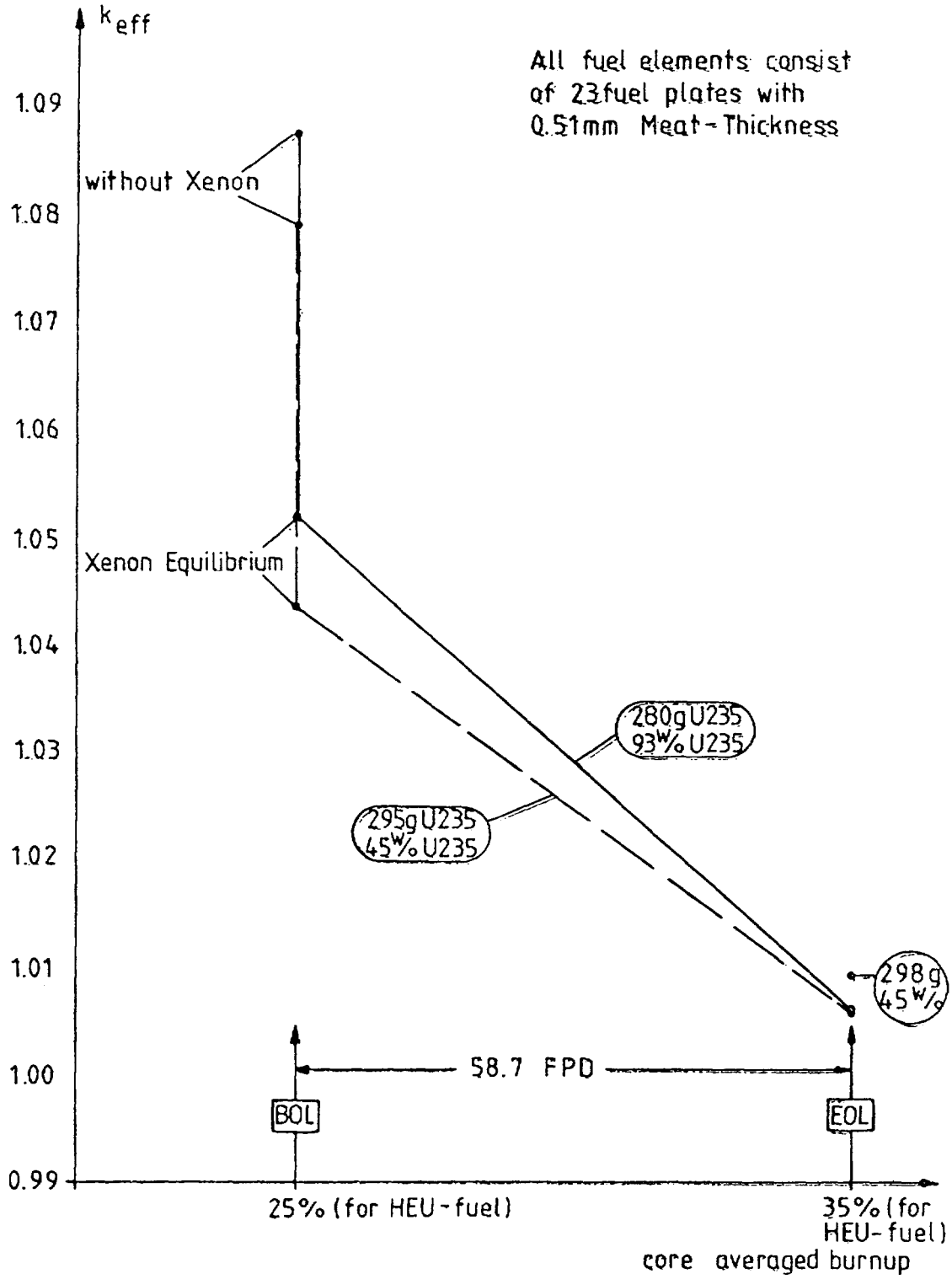

10 MW - Reactor Conversion EOL-Criterion
Determination of REU-Fuel with 45% U235 using the XY-Calculation Modell

Fig. 2-13

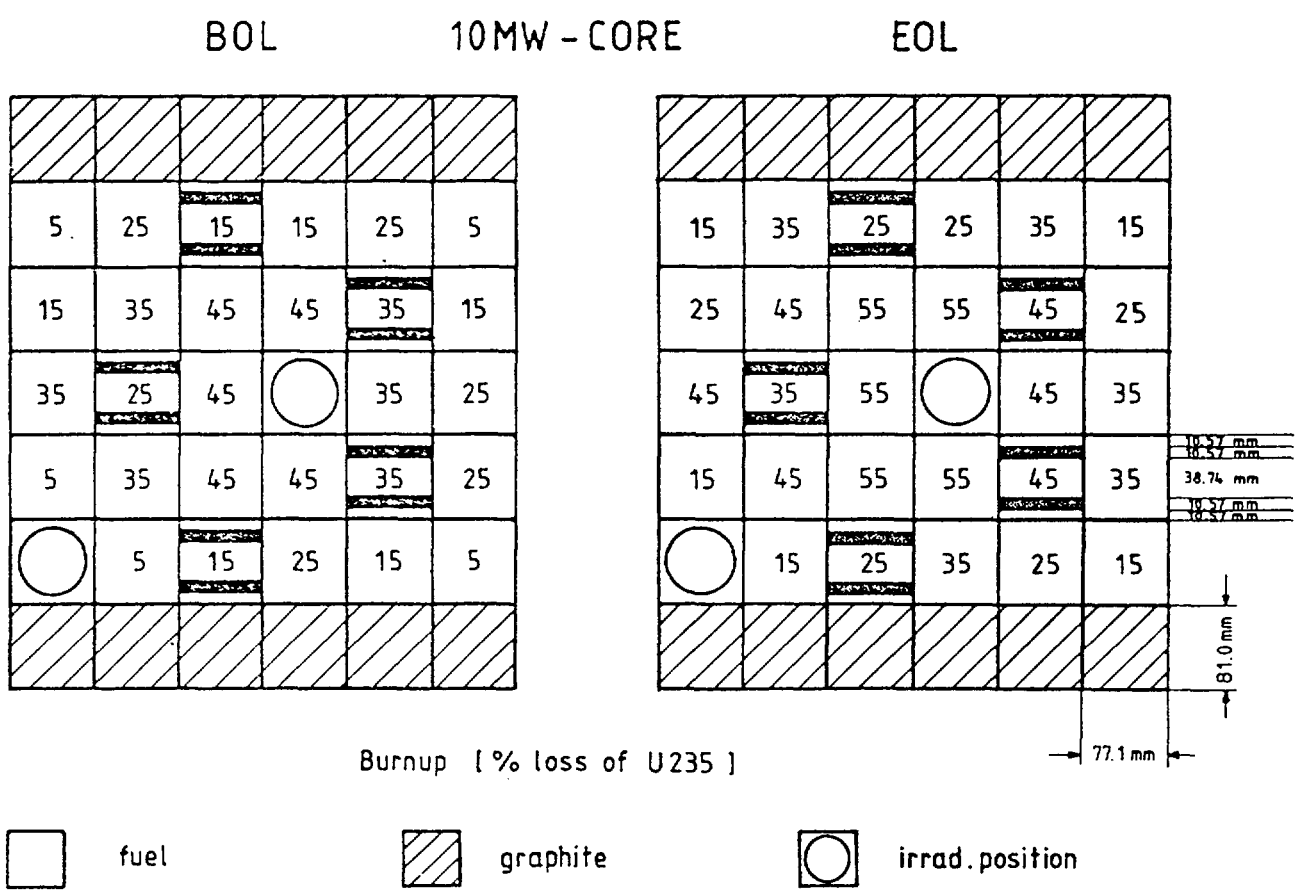

10MW - GENERIC STUDIES
XY - MODEL FOR DIFFUSION CALCULATIONS

Fig. 2-14

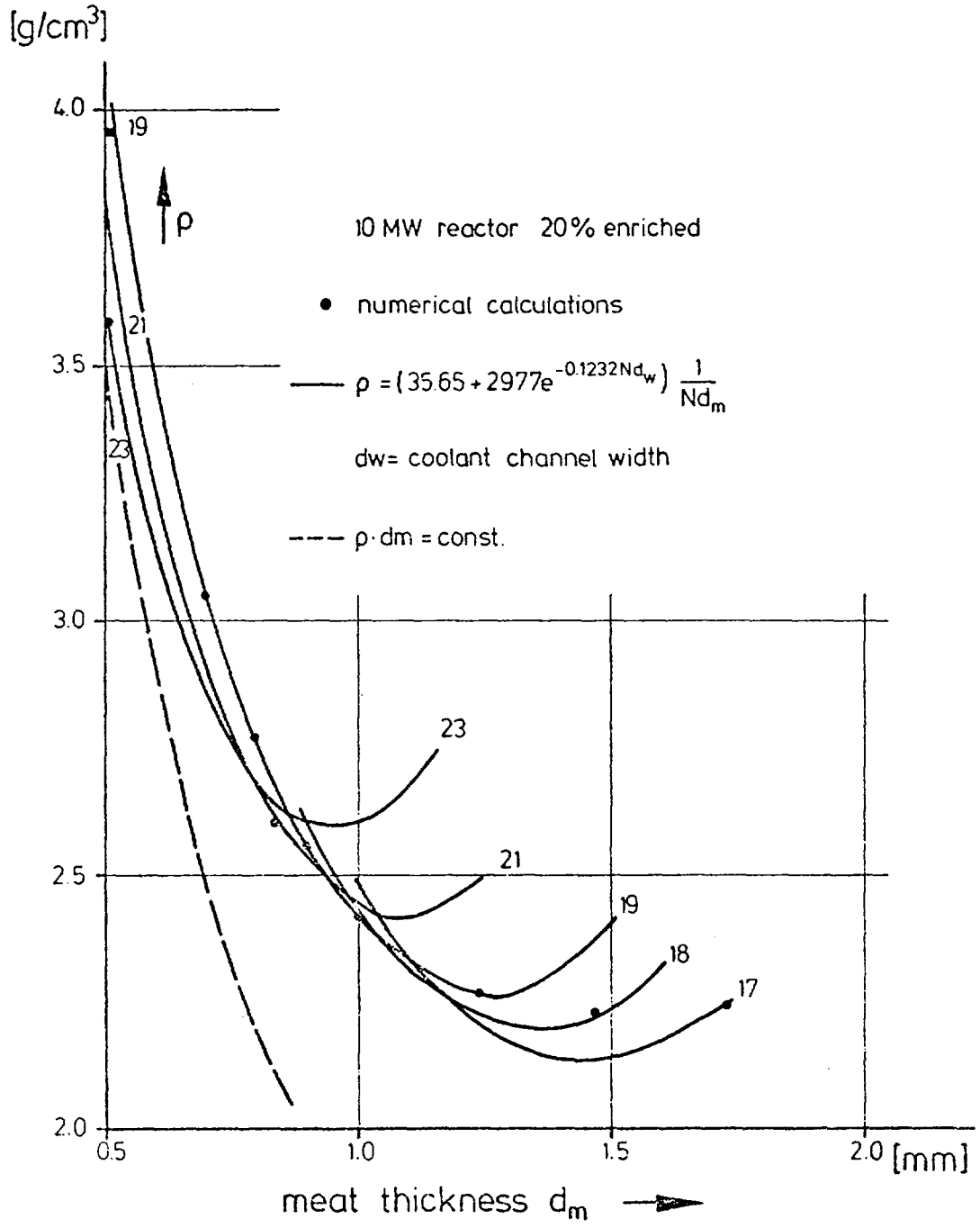

Fig. 2.15: Uranium density ρ vs. meat thickness d_m for equal cycle length number of fuel plates per element N as parameter

The situation is similar to the 2 MW case (Fig. 2-8) and essentially the same conclusions can be drawn. The dotted curve in Fig. 2-15 corresponds to a constant ^{235}U-loading of the core. The deviation from such a behavior results from the reactivity loss, due to undermoderation and increased leakage, which has to be compensated by an increased uranium loading. Reducing the number of plates improves the moderation. However, for each case, there is a maximum meat thickness beyond which the moderation is inadequate.

Figure 2-16 shows for the 2 MW and the 10 MW reactors the factor M/M_o by which the ^{235}U-mass has to be increased compared with the HEU case for equal cycle length as a function of the water volume fraction (V_{H_2O}) in the core. Obviously, clear correlations exist between M and V_{H_2O} for both the 2 MW and 10 MW cases. However, the correlations are different for the two reactors.

Correlation of the results becomes simpler if one notes that the dependence of M on V_{H_2O} results primarily from an increasing neutron leakage with decreasing water content in the core. Therefore, a more meaningful variable than V_{H_2O} is B^2/V_{H_2O}, which is approximately proportional to the leakage term DB^2. Using this variable, it is possible to correlate with a single expression all the results listed in Tables 2-2, 2-3, and 2-10. This expression provides a recipe which can be used to determine the uranium density in the fuel meat required for a core conversion to a different enrichment (and, in particular, from 93% to 20%) with plate-type fuel, water moderator, and equal cycle length.

According to this recipe, and with the following definitions:

ρ = uranium density in the fuel meat (g/cm^3)

d_m = meat thickness (cm)

d_w = water channel width (cm)

d_p = plate thickness (cm)

N = number of plates per element

ε = enrichment (wt% ^{235}U)

M = ^{235}U-loading of one element (g)

B^2 = geometric core buckling (cm^{-2})

$V_{H_2O} = (d_w + d_p)/d_w$ = water volume fraction,

the ^{235}U loading of one element is determined by the condition that the expression

$$\frac{M\ (1 + 0.348\ \varepsilon - 0.096\ \varepsilon^2)}{1 + 0.208\ e^{158\ B^2/V_{H_2O}}}$$

remain invariant in the conversion. The required uranium density in the fuel meat is determined by

$$\rho = \frac{M}{N d_m \varepsilon}\ .$$

This recipe provides accurate results for all the cases which were considered in its derivation, if all reflector savings are assumed to be 8 cm long. In view of its empirical nature, however, great caution should be used when attempting to use the same recipe for different reactor configurations or with parameters outside the ranges which were considered in its derivation.

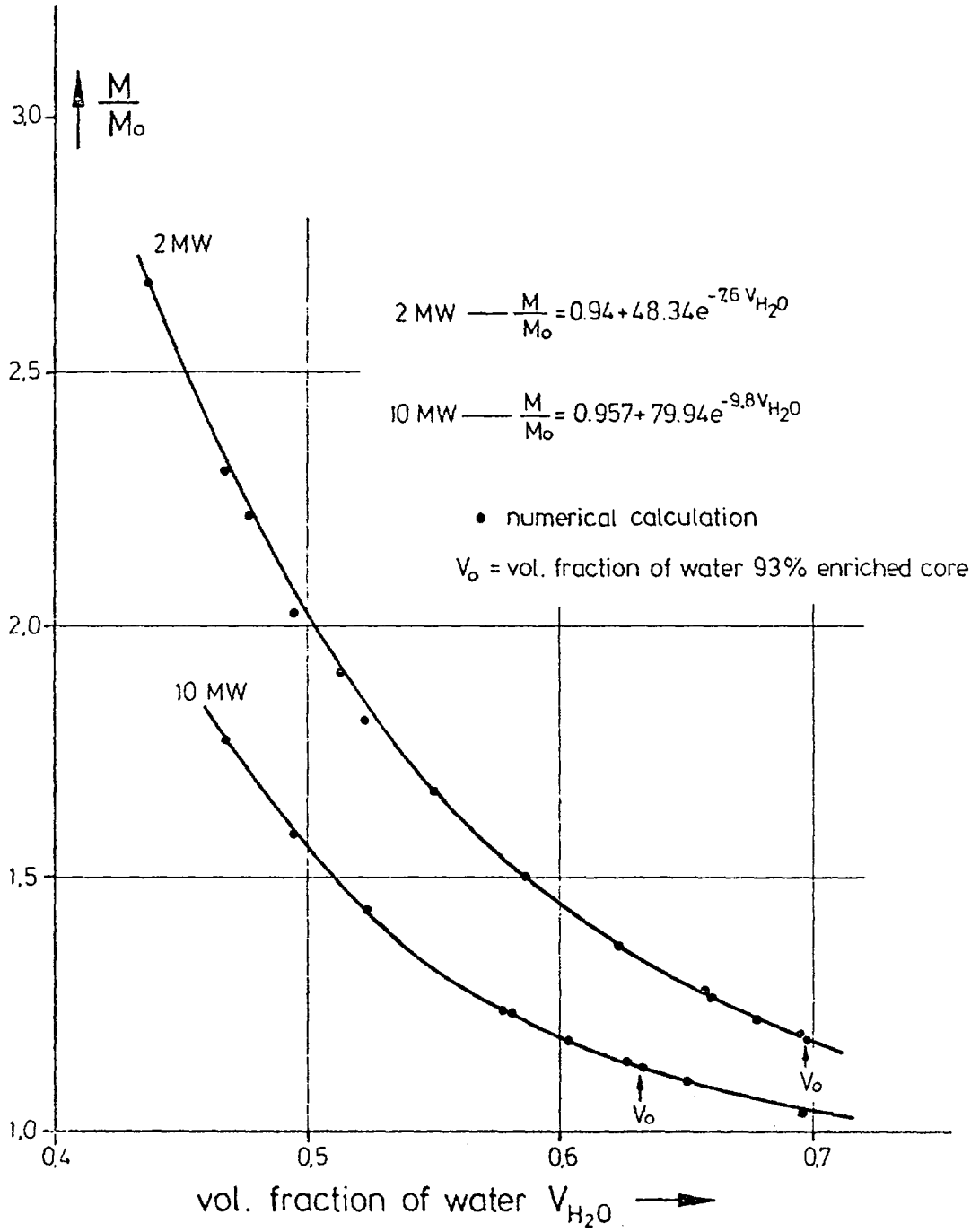

Fig. 2.16: Factor $\frac{M}{M_o}$ by which the ^{235}U-mass has to be increased compared with the 93% enriched case versus vol. fraction of water

The optimum fuel meat thickness for practical conversion will depend upon the fabricability and qualification of fuel with a particular uranium density and meat thickness, as well as on safety margin, thermal-hydraulic, backfitting, and licensing considerations. The ^{235}U and Pu content in each fuel element at the end of equilibrium cycle are shown in Fig. 2-17 for both the 23 plate reference case using HEU and the 19 plate case (1.238 mm fuel meat thickness) with LEU that requires the minimum uranium density of 2.27 g/cm^3. Figure 2-18 shows the ratios of the average fast, epithermal, and thermal fluxes between this LEU design and the reference HEU case in each fuel element and peak fluxes in the central and edge irradiation channels at beginning and end of equilibrium cycle. In the core, fast fluxes are increased by 1-27%, and thermal fluxes are reduced by 40-45% because of the higher ^{235}U content (403 g ^{235}U/element) in the LEU case.

Typical thermal-hydraulic and safety margin data corresponding to the design variations in Table 2-10 are shown in Table 2-11 for steady-state operation. The safety margin data include the margin to onset of nucleate boiling (ONB), the margin to departure from nucleate boiling (DNB), and the margin to onset of instability due to a flow excursion. Detailed descriptions of the methods and procedures used by the various laboratories in calculating thermal-hydraulic and safety parameters can be found in Appendices A, C, and D.

Conclusions

The calculations performed to study the conversion potential of the "typical" 10 MW research reactor considered in this study to REU classical plate-type fuel can be summarized as follows:

1) The reactor can be converted to the use of MEU fuel with no fuel element redesign, no significant performance penalties, and using currently-qualified fuel fabrication technology.

   Use of the most advanced currently-qualified fuel fabrication technology (1.7 g U/cm^3) can approximately double the lifetime of the core resulting from such conversion, compared to the HEU core.

2) Use of fuels with very high uranium densities, (2.3 - 3.0 g/cm^3), currently unavailable but well within the goals of fuel development programs in several countries, combined with fuel element redesign can allow conversion of the reactor to the use of LEU fuel with acceptable lifetime and performance characteristics.

Figure 2-17. 10 MW Reactor - HEU (93%) Fuel

End of Equilibrium Cycle Distribution of ^{235}U and Pu Based on Fuel Cycle Length Matching Criterion (0.51 mm Fuel Meat Thickness)

U Enrichment : 93%
U Density : 0.68 g/cm^3
Fresh Fuel Loading : 280 g ^{235}U

BOC k_{eff} : 1.0210
EOC k_{eff} : 1.0000
Cycle Length : 16.7 Days

END OF EQUILIBRIUM CYCLE

GRAPHITE	23 101.6 g ^{235}U 0.57 g Pu	13 151.1 0.48	6 207.3 0.31	CFE-2 121.1 0.26	8 191.6 0.36	H_2O	GRAPHITE
	22 105.2 0.57	CFE-1 110.4 0.31	3 242.0 0.18	1 266.5 g ^{235}U 0.06 g Pu	10 176.3 0.41	16 133.3 0.52	
	21 110.0 0.56	11 166.7 0.45	5 216.0 0.29	H_2O	12 157.4 0.47	CFE-3 130.1 0.25	
	19 118.9 0.55	CFE-5 110.0 0.31	2 254.0 0.13	4 229.7 0.23	14 144.0 0.50	18 124.1 0.54	
	17 128.9 0.53	9 184.3 0.38	7 198.8 0.35	CFE-4 119.9 0.26	15 138.5 0.51	20 115.3 0.55	

10 MW Reactor - LEU (20%) Fuel

End of Equilibrium Cycle Distribution of ^{235}U and Pu Based on Fuel Cycle Length Matching Criterion (1.238 mm Fuel Meat Thickness, 19 Plates)

U Enrichment : 20%
U Density : 2.27 g/cm^3
Fresh Fuel Loading : 403 g ^{235}U

BOC k_{eff} : 1.0108
EOC k_{eff} : 1.0002
Cycle Length : 16.7 Days

END OF EQUILIBRIUM CYCLE

GRAPHITE	23 232.5 g ^{235}U 13.83 g Pu	13 286.5 10.27	6 340.0 6.06	CFE-2 234.0 6.17	8 324.9 7.18	H_2O	GRAPHITE
	22 236.9 13.64	CFE-1 227.5 7.63	3 371.1 3.36	1 391.4 g ^{235}U 1.14 g Pu	10 310.7 8.40	16 268.0 11.58	
	21 242.2 13.28	11 302.1 9.22	5 347.9 5.40	H_2O	12 292.8 9.83	CFE-3 242.8 6.10	
	19 252.3 12.64	CFE-5 227.0 7.71	2 381.1 2.28	4 360.1 4.34	14 279.6 10.87	18 257.9 12.23	
	17 263.1 11.84	9 318.0 7.72	7 332.0 6.72	CFE-4 231.9 6.23	15 273.8 11.24	20 248.0 12.84	

Figure 2-18. 10 MW Reactor

20% : 19 Plates per Std. Element; 1.238 mm Fuel Meat Thickness

93% : 23 Plates per Std. Element; 0.51 mm Fuel Meat Thickness

Ratios of Average Fast, Epithermal, and Thermal Fluxes with LEU and HEU Fuel in Each Fuel Element and Peak Fluxes in Central and Edge Flux Traps at Beginning and End of Equilibrium Cycle Based on Cycle Length Matching Criterion.

EPITHERMAL (0.625 eV < E < 5.53 keV)

GRAPHITE							GRAPHITE
	23	13	6	CFE-2	8	H_2O	
	1.173 1.167	1.071 1.064	1.005 0.997	1.014 1.007	1.035 1.027	1.096 1.088	
	22	CFE-1	3	1	10	16	
	1.139 1.133	1.052 1.046	0.973 0.966	0.972 0.965	1.016 1.009	1.093 1.085	
	21	11	5	H_2O	12	CFE-3	
	1.117 1.110	1.028 1.020	0.977 0.968	0.999 0.993	1.045 1.037	1.113 1.104	
	19	CFE-5	2	4	14	18	
	1.117 1.109	1.046 1.036	0.983 0.971	1.002 0.990	1.058 1.047	1.128 1.117	
	17	9	7	CFE-4	15	20	
	1.129 1.117	1.053 1.041	1.017 1.004	1.036 1.043	1.104 1.092	1.174 1.161	

FAST (>5.53 keV)

GRAPHITE							GRAPHITE
	23	13	6	CFE-2	8	H_2O	
	1.274 1.269	1.133 1.126	1.043 1.010	1.061 1.054	1.087 1.078	1.121 1.112	
	22	CFE-1	3	1	10	16	
	1.228 1.224	1.102 1.097	1.008 1.000	1.003 0.997	1.069 1.061	1.169 1.160	
	21	11	5	H_2O	12	CFE-3	
	1.200 1.194	1.076 1.070	1.016 1.007	1.009 1.001	1.102 1.095	1.165 1.156	
	19	CFE-5	2	4	14	18	
	1.197 1.189	1.095 1.086	1.015 1.003	1.040 1.028	1.121 1.110	1.207 1.196	
	17	9	7	CFE-4	15	20	
	1.210 1.198	1.104 1.091	1.062 1.048	1.105 1.092	1.175 1.162	1.270 1.257	

THERMAL (<0.625 eV)

GRAPHITE							GRAPHITE
	23	13	6	CFE-2	8	H_2O	
	0.600 0.591	0.587 0.575	0.619 0.604	0.608 0.596	0.653 0.640	0.990 0.977	
	22	CFE-1	3	1	10	16	
	0.545 0.534	0.551 0.537	0.601 0.582	0.657 0.638	0.570 0.555	0.612 0.600	
	21	11	5	H_2O	12	CFE-3	
	0.544 0.531	0.543 0.526	0.626 0.605	0.941 0.929	0.596 0.580	0.620 0.606	
	19	CFE-5	2	4	14	18	
	0.553 0.540	0.553 0.537	0.613 0.591	0.637 0.616	0.546 0.530	0.571 0.558	
	17	9	7	CFE-4	15	20	
	0.618 0.605	0.615 0.598	0.625 0.606	0.621 0.604	0.589 0.575	0.620 0.608	

TABLE 2-11. 10 MW Reactor
Thermal-Hydraulics
Fuel Element Design Variations
with 20% Enriched Uranium Fuel

Number of Plates	Thickness of Water Channel/Meat cm	Coolant Velocity m/s	Flow/ Element m^3/hr	Total Pressure Drop Across Channel bar	Avg.[b] Heat Flux W/cm^2	Avg. Heat[c] Flux at ONB W/cm^2	Burnout Heat Flux, W/cm^2		Limiting[f] Heat Flux at Onset of Flow Instability W/cm^2	Margin[g] to ONB	Margin[h] to DNB		Margin[i] to Onset of Flow Instability
							Labuntsov[d]	Mirshak[e]			Labuntsov	Mirshak	
23[a]	2.188/0.510	2.97	35.7	0.193	20.54	35.9	353	266	208.8	1.75	6.90	5.20	4.08
23	2.188/0.510	3.24	39.0	0.226	20.54	38.9	368	272	227.8	1.89	7.19	5.31	4.45
23	2.188/0.510	3.59	43.2	0.272	20.54	42.8	387	(288)	252.4	2.08	7.56	5.63	4.93
23	2.188/0.510	3.80	45.7	0.300	20.54	45.0	398	(298)	267.1	2.19	7.77	5.82	5.22
21	2.188/0.839	2.97	32.6	0.195	22.50	35.9	353	266	208.8	1.59	6.30	4.74	3.72
21	2.188/0.839	3.24	35.6	0.228	22.50	38.9	368	272	227.8	1.73	6.56	4.85	4.06
21	2.227/0.700	2.97	33.2	0.191	22.50	36.1	353	261	211.9	1.60	6.30	4.65	3.78
21	2.227/0.700	3.19	35.6	0.217	22.50	38.5	365	271	227.6	1.71	6.51	4.83	4.06
19	2.916/0.510	2.97	39.3	0.243	24.86	37.6	353	(289)	264.1	1.51	5.70	4.66	4.26
19	2.726/0.700	2.97	36.8	0.154	24.86	37.3	353	(282)	250.2	1.50	5.70	4.55	4.04
19	2.626/0.800	2.97	35.4	0.160	24.86	37.1	353	(278)	242.7	1.49	5.70	4.49	3.92
19	2.526/0.900	2.97	34.1	0.167	24.86	36.9	353	(274)	235.2	1.48	5.70	4.42	3.80
19	2.426/1.000	2.97	32.7	0.175	24.86	36.6	353	(270)	227.5	1.47	5.70	4.36	3.67
19	2.188/1.238	2.97	29.5	0.197	24.86	35.9	353	266	208.8	1.44	5.70	4.29	3.37
19	2.188/1.238	3.59	35.7	0.277	24.86	42.8	387	(288)	252.4	1.72	6.24	4.65	4.07
18	2.188/1.471	2.97	27.9	0.198	26.25	35.9	353	266	208.8	1.37	5.40	4.07	3.19
18	2.188/1.471	3.80	35.7	0.308	26.25	45.0	398	(298)	267.1	1.71	6.08	4.56	4.08
18	2.789/0.870	2.97	35.6	0.151	26.25	37.4	353	(284)	254.8	1.43	5.40	4.34	3.90
17	2.188/1.731	2.97	26.4	0.199	27.79	35.9	353	266	208.8	1.29	5.10	3.84	3.02

[a]Reference HEU case and LEU case with no redesign.

[b]Peak Heat Flux = 1.4 x 1.78 x Avg. Heat Flux.

[c]The average heat flux at ONB is calculated with the conservative assumption that ONB occurs at the channel exit with peak heat flux, lowest pressure and saturation temperature, and highest coolant temperature rise.

[d]Burnout heat flux estimated using the Labuntsov correlation extrapolated with zero subcooling (see Section A.1.3.7).

[e]Burnout heat flux calculated using the Mirshak correlation, which is strictly applicable for positive subcooling (cases in parentheses). Other cases were estimated based on extrapolation with zero subcooling.

[f]Limiting heat flux at onset of instability due to flow excursion calculated with the Forgan correlation.

[g]Minimum ratio of local heat flux for ONB to actual heat flux.

[h]Minimum ratio of local heat flux for DNB using Labuntsov and Mirshak correlations to actual peak heat flux.

[i]Minimum ratio of local heat flux for onset of instability due to flow excursion to actual peak heat flux.

2.3.2 Conversion Based on TRIGA Fuel

General Atomic Company has TRIGA LEU fuel available in shrouded clusters each containing 16 fuel rods designed for use in converting and upgrading MTR plate-type reactor cores and fueling new reactor facilities (Appendix B). The major design objective of this fuel is to provide a long-lifetime, readily-exportable fuel which considers both initial and operating costs to provide an attractive total fuel cycle cost.

The major technical design objectives for the 16-rod TRIGA fuel cluster were: to use the identical fuel rod and coolant channel geometry used for the 14-MW TRIGA core (using 25-rod clusters); to be able to achieve 10-MW operation with coolant flow rates in the range of 18,900 to 22,700 liters/min (5000 to 6000 gpm); and to achieve a core burnup lifetime similar to the design using HEU (highly enriched uranium) fuel. Operation at about 5 MW was also to be achievable with a flow rate of 8300 liters/min (2200 gpm). These design objectives were achieved with a 30-cluster core size.

The fuel rods used in the conversion cluster are identical in size to the fuel rods used in the 14-MW TRIGA core built for the Romanian Institute for Nuclear Technologies. The 1.295 cm (0.510 in.)-o.d. TRIGA fuel-moderator rods are clad with 1.377 cm (0.542 in.)-o.d. Incoloy 0.041 cm (0.016 in.) thick and have an active fuel height of 55.88 cm (22.0 in.). Fuel rod spacing within the cluster is identical to that of the 14-MW TRIGA design, with 0.254 cm (0.100 in.) between fuel rods and between rods and the cluster shroud. Two intermediate Inconel spacers are used within the cluster to maintain clearances along the length of the fuel rods.

The necessary U-235 content for long fuel life is achieved by using a higher uranium density than in past TRIGA fuels. The volume percent of uranium is still modest, however, being about 20%. The fuel material (Er-U-ZrH) contains 3.7 g U/cm^3 (45 wt% U; 20% enriched, nominal), about 0.8 wt% erbium, and the hydrogen-to-zirconium ratio is 1.6. The small amount of erbium is included as a burnable poison and is a major contributor to the prompt negative temperature coefficient, the dominant safety feature of TRIGA fuel.

Figure 2-19 shows the general layout of the fuel cluster. It consists of 16 fuel rods arranged in a 4 by 4 square array. The cluster is contained within a rectangular aluminum shroud with inner dimensions forming a 6.805-cm (2.679-in.) square. The typical outside dimensions shown can change to some degree to accommodate the minor variations existing between the various MTR-type designs.

Shown in Fig. 2-20 is a general layout of the reactor configuration used for the nuclear analysis of the 10-MW TRIGA. Calculations for the TRIGA-LEU core used water reflection of all four sides.

Flux distributions in the core and reflector were determined from two-dimensional, x-y, full-core, diffusion theory calculations for an operating power of 10 MW. Plots are given in Fig. 2-21 of the flux for a mid-plane traverse through the center of fuel in row 3. Figure 2-22 shows the same traverse for a core containing a water-filled flux trap in position C3.

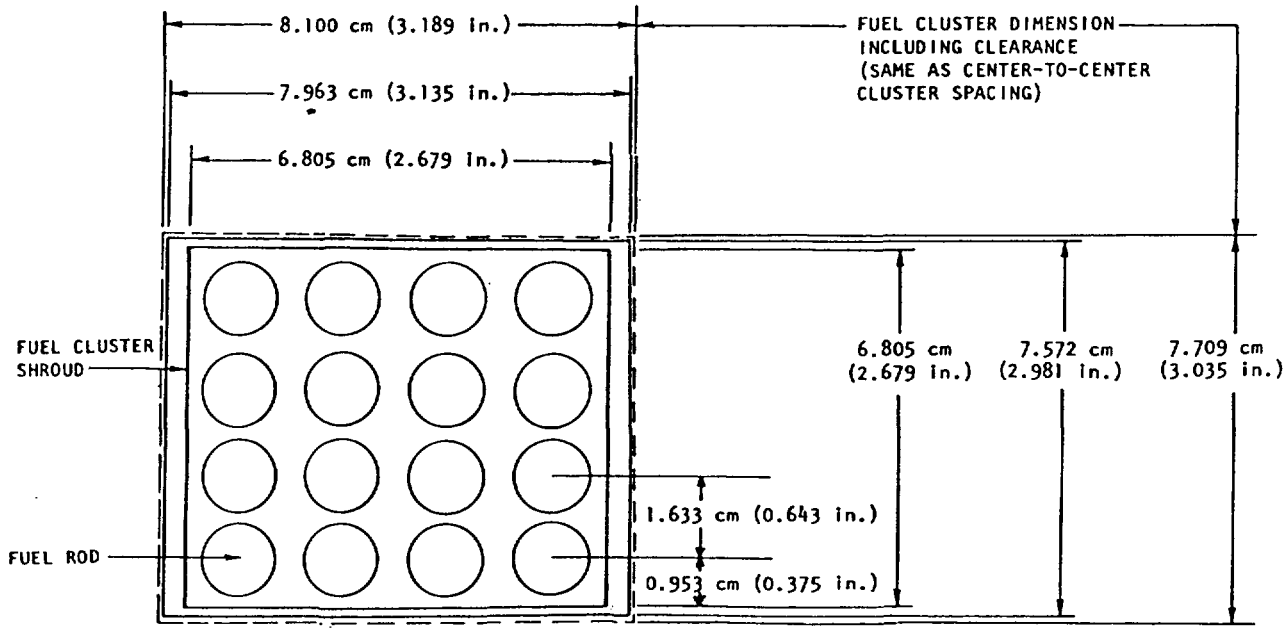

Fig. 2-19. **General layout of 16-rod fuel cluster**

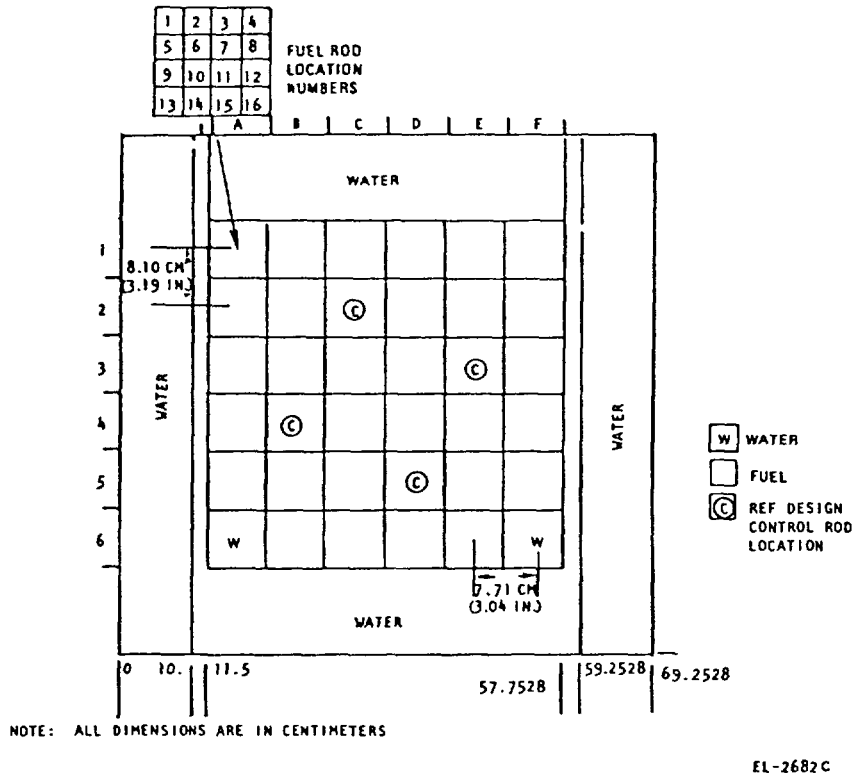

Fig. 2-20. Grid locations and typical dimensions for 10-MW TRIGA geometry

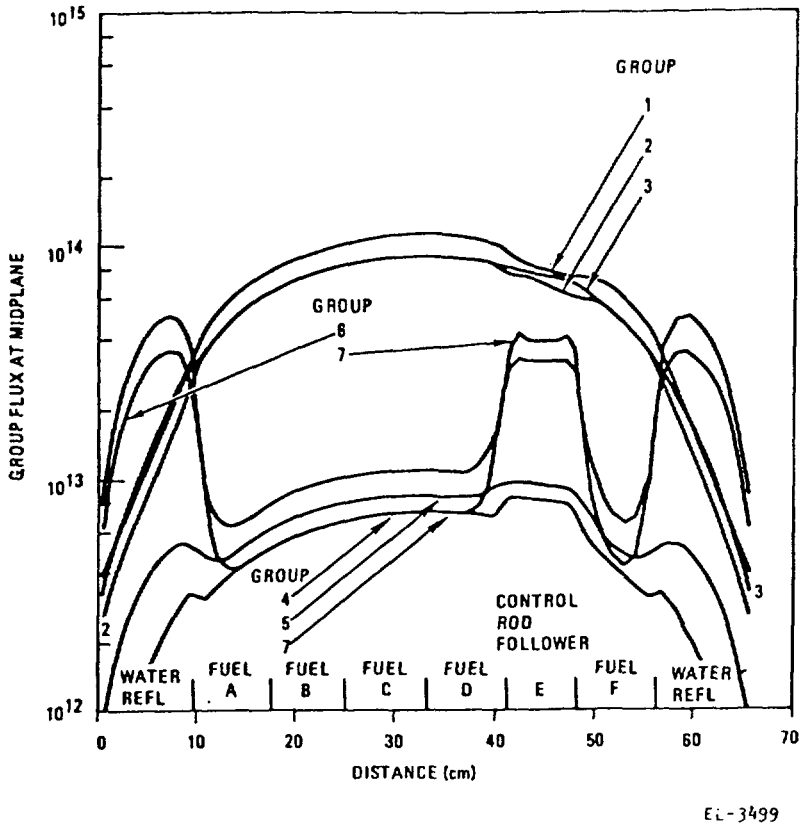

Fig. 2-21. Mid-plane flux at 10-MW; flux traverse through center of row 3 fuel (core has water reflector on all sides

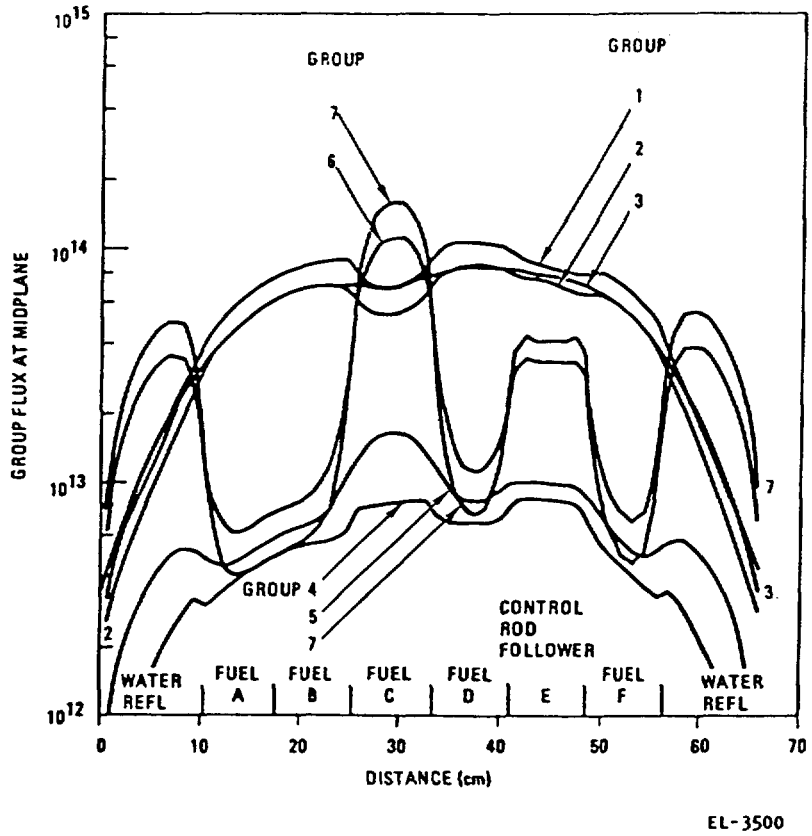

Fig. 2-22. Mid-plane flux at 10-MW; Flux traverse through center of row 3 fuel, water in C3 position (core has water reflector on all sides)

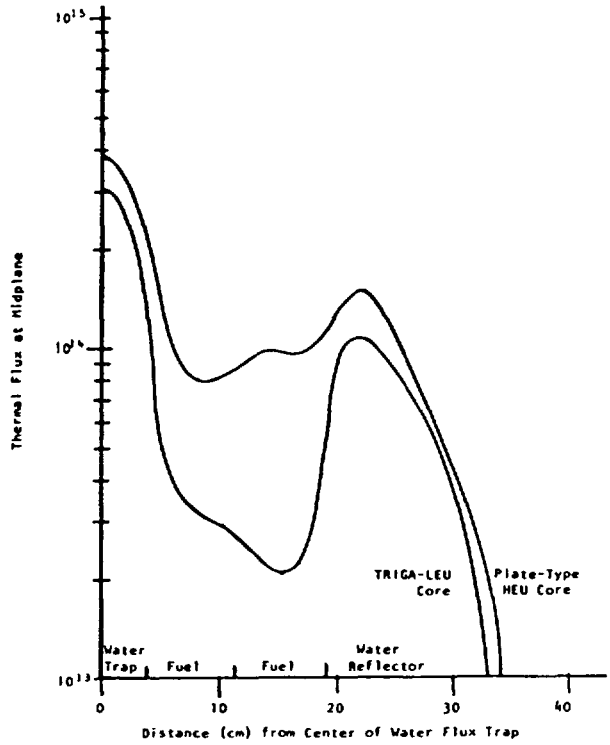

Fig. 2-23. Mid-plane thermal flux (<0.62 eV) at 10-MW for reactors with TRIGA-LEU fuel and plate-type HEU fuel

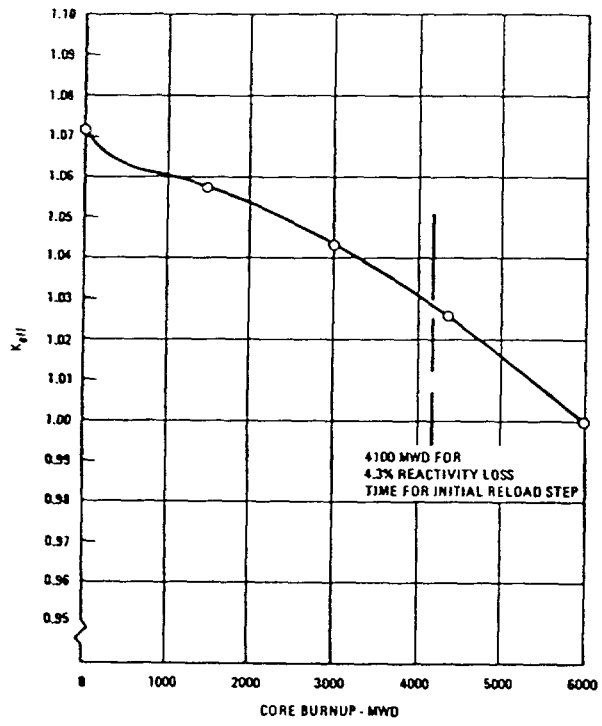

Fig. 2-24. K_{eff} as a function of core burnup for reference design

TABLE 2-12.
SUMMARY OF CORE DESIGN PARAMETERS AND CHARACTERISTICS

Reactivity requirements, δk ($)		
Xenon (equilibrium)	∿2.8%	($4.00)
Samarium (equilibrium)	0.8%	($1.14)
Cold-to-hot reactivity change[a]	0.8-1.3%	($1.14-$1.86)
Total	∿4.4-4.9%	($6.29-$7.00)
Operational reactivity change[b]	∿3.6-4.1%	($5.14-$5.86)
β_{eff} (δk)	0.0070	
ℓ (microsec)	∿25 (beginning of life) ∿32 (end of life)	
Maximum fuel temperature	640°C	
Recommended excess reactivity at beginning of life, δk	>6.0%	($8.57)
Recommended control system worth, δk		
With maximum-worth rod stuck out	>6.5%[c]	($9.29)

[a] Based on a peak fuel temperature of 640°C and an average core temperature of 255°C

[b] Samarium not included

[c] It is possible to use an existing control system when converting a core. General Atomic has a control system designed for use with this core having a worth of about 8% with the maximum worth rod stuck out.

TABLE 2-13.

10 MW TRIGA-LEU FUEL AND REACTOR DESIGN DESCRIPTION SUMMARY

The parameter describing a 10 MW TRIGA-LEU reactor which uses the 16-rod UZrH fuel cluster is described as follows:

Fuel - Cluster: TRIGA-LEU 45 wt-% U in UZrH (76 x 80 x 559 mm)

Fuel rods per cluster:

Standard cluster: 16

Nominal fuel rod dimensions:

Fuel O.D.: 13.0 mm

Clad O.D.: 13.7 mm (Incoloy)

Fuel height: 559 mm

Fuel loading: 274 gm U (20% enriched)/rod

4.38 Kg U (20% enriched)/cluster

877 gm U-235/cluster

~0.8 wt-% Erbium as burnable absorber

Number of fuel clusters in the core: 30

Number of control rods: 4 or 5

Reflector: Water

Core size (liters): 105

U-235 Content/core (Kg): 26.3

Core Geometry: 6 x 6 arrangement

Grid plate: 6 x 9 positions (normal conversion)

Desired average burnup of U-235 in the fuel cluster discharged from the core: >40%

Burnup status of the core: equilibrium core

Average core burnup (%): ~25

Fuel shuffling: introduction of new fuel clusters into the core center

Thermal-hydraulic data:

Average power density (Kw/liter): 95

Coolant flow rate: 5000 GPM, 1135 M^3/hr (1.9×10^7 cc/min)

Core inlet temperature: 38^0C

Figure 2-23 shows the thermal flux (<0.625 eV) distribution for both a TRIGA-LEU core and the generic, 10 MW, plate-type HEU core discussed in Section 2.3. Both cores have a flux trap, but not located at exactly the same position. The TRIGA core has all fresh fuel, and 29 TRIGA-LEU clusters containing 25.4 Kg of U-235. The plate-type HEU core has the equilibrium cycle burnup distribution given in Fig. 2-17. The TRIGA-LEU core was totally water reflected and the plate-type HEU core had a row of graphite (~7.6 cm thick) followed by water on two opposite core faces and water reflection on the other two core faces. The flux distributions shown are for traverses into the water reflected faces. Figure 2-23 shows the peak thermal fluxes to be higher for the equilibrium cycle, plate-type HEU core in both the water-filled flux trap, and at the peak in the water reflector. The flux traverse for the plate-type HEU core was provided by ANL.

Figure 2-24 gives the calculated k_{eff} as a function of core burnup for the 10 MW TRIGA-LEU fuel. These data indicate a burnup of ~4100 MWd before the initial reloading of the core needs to begin. The initial reloading point is defined as the time at which a reactivity loss of 4.3% has occurred from an initial reactivity being defined as k_{eff} at t = 0, with equilibrium xenon. This is a reactivity decrease used with the control system designed by General Atomic.

It is emphasized that the 4100 MWd mentioned above, and representing a U-235 burnup of about 21%, is the point at which the initial core needs additional reactivity to remain operational at full power. It is estimated that when an equilibrium reload condition has been reached, the fuel removed from the core will have a U-235 burnup of about 40%.

Summaries of the TRIGA-LEU 16-rod cluster core design parameters and characteristics are given in Tables 2-12 and 2-13.

2.3.3 Conversion Studies Based on Caramel Fuel

As already described above, the Caramel fuel plate takes the form of two thin sheets of zircaloy, enclosing a regular array of rectangular pieces of UO_2, separated by small pieces of zircaloy. These plates are assembled in parallel between two side plates to which they are welded, and equipped with a foot and a handling head to form the fuel element.

It results from this description that these Caramel fuel elements are quite similar in geometry to the currently used UAl elements of the flat or slightly curved MTR type. Therefore, the Caramel assemblies can fit very easily with a wide range of research and test reactors. Especially for the 10 MW reactor under consideration there is no difficulty in implementing such a conversion.

Caramel fuel has strong nonproliferation characteristics due to the high specific weight of the UO_2 fuel (10.3 g/cm^3); it can lead to a core with a volumetric uranium weight as high as 2 kg U/dm^3 and thus to an enrichment in the range as low as 3% to 10% ^{235}U. The calculations performed by the CEA have confirmed the feasibility of this solution for converting HEU cores directly to LEU cores in most cases. Furthermore the Caramel has several specific advantages:

- fuel compartmented and operated at a rather low temperature
- negative Doppler coefficient in case of power excursion
- good chemical behavior in demineralized water which suppresses the necessity of a hot layer at the pool surface (this can be a great advantage in countries with hot and wet summers).

In the case of this 10 MW reactor one must find the optimum design in balancing neutronic and thermal-hydraulic aspects. For such a power range one has to increase the heat surface area, and therefore to divide the lattice with rather numerous thin fuel plates and thin channels adjusted to keep a reasonable moderation ratio and a good reactivity. These evaluations have been performed for the OSIRIS reactor conversion; they have resulted in the following data used as convenient for this 10 MW reactor:

fuel plate thickness	2.25 mm
oxide thickness	1.45 mm
coolant channel thickness	2.6 mm
plate number per assembly	16
active plate length	60 cm
uranium weight per assembly	7.65 kg U

From a neutronics point of view, the enrichment has been determined to reach the same cycle length as the HEU design. This is a low value of the enrichment, and the fluxes are similar to those achieved with the HEU.

From a thermal-hydraulics viewpoint, on the basis of the present safety criteria required by the French Regulation Authorities, the conversion appears feasible in very good conditions.

Table 2-14 summarizes the characteristics of both the original HEU core and the Caramel converted one.

Table 2-14. Summary of Characteristics of Original 10 MW HEU Core and Caramel Converted Core.

		93 % U_{235}	Caramel 6.5% U_{235}
fuel element dimensions	(mm)	76 x 80	76 x 80
number of plates in standard fuel element		23	16
water gap	(mm)	2.1	2.75
plate thickness	"	1.27	2.25
meat thickness	"	0.51	1.45
^{235}U weight by element	(g)	280	500
active height	(mm)	600	600
average cycle length	(days)	16.4	16.4
fast flux in central water hole(at the center) $\phi_1 > 0,9$ MeV (averages height)	(n/s/cm^2)	5.40 10^{13}	5.81 10^{13}
thermal flux in central water hole (at the center) $\phi_4 < 0,625$ eV (averages height	(n/s/cm^2)	2.8 10^{14}	2.6 10^{14}
thermal flux in water reflector $\phi_4 < 0,625$ eV (averages height)	(n/s/cm^2)	1.0 10^{14}	1.0 10^{14}
water velocity	(m/s)	1.8	2
flow rate	(m^3/h)	600	630

2.4 "BENCHMARK" CALCULATIONS

2.4.1 Definitions and Aims

In order to compare reactor physics methods used in various research centers, benchmark problems were calculated by seven international centers for well defined reactor conditions. Since the emphasis of these calculations is on the comparison of the results, rather than on their absolute values, the reactor configurations were idealized and simplified as much as possible. Thus, these calculations may not correspond to realistic conditions and conclusion about actual reactor performance with REU fuels should not be drawn from them, even though some results are very similar to the results of the generic studies.

The specifications of the benchmark problems are provided in Table 2-15 and in Fig. 2-25. Briefly, they correspond to a 10 MW, 6 x 5 element core reflected by a graphite row on two opposite sides, and surrounded by water. The standard MTR-elements contain 23 fuel plates. The enrichments considered are 93%, 45%, and 20%, and each of these correspond to a ^{235}U content of 280, 320, and 390 grams per element, respectively. The calculations were to be carried out with Xe-equilibrium and for various burnup conditions. The main data to be calculated were the absolute reactivities k_{eff} as well as the subsequent reactivity differences and the flux distributions.

Some ambiguity was caused by the fact that the burnup states were specified in terms of % (i.e., percentage loss of the number of ^{235}U atoms). Cores of different enrichments contain different amounts of ^{235}U, and their burnup in MWd is very different when they have the same burnup in %. Since it is the burnup in MWd that is more significant, some technical groups assumed that the % burnup of the specifications applied only to the 93% enriched case, and used the corresponding MWd burnup for all other cases. Other groups used the % burnup in all cases. Results for both choices are used in this summary.

2.4.2 Results

The results of the seven contributors can be divided into two parts, i.e., absolute reactivities plus reactivity steps and absolute fluxes plus flux ratios for different enrichments.

The starting point for the comparison of the reactivities is the k_∞-behaviour for the three enrichments. The great number of results forces to plot the infinite reactivity versus burnup in percentage loss of U-235 for each enrichment separately (Fig. 2-26 - 2-28). The overall impression of these three figures is a good agreement within the majority of the contributors. Deviations exist for the JAERI-calculations* and some small deviations for the EIR-results.

Based on this agreement the effective reactivities for the core calculations as given by Table 2-16 show similarly small deviations below 1% $\Delta\rho$ from each other (with only one exception) as may be seen from Table 2-17. The INTERATOM results are an arbitrary choice of a basis. These reactivities are backed by another interesting k_{eff} comparison which was obtained by ANL by running detailed 3-D, continuous energy Monte Carlo calculations, and comparing their results with those of diffusion-theory calculations. The results are listed in Table 2-18.

*For the reasons see Appendix F-6, Section 1.3.

Table 2-15. Specifications for the Methodical Benchmark-Problem

Aims: Comparison of the different calculation methods and cross-section data sets used in different laboratories, limited conclusions for real conversion problems.

Data and Specifications Agreed Upon:

Active Core Height 600 mm
Extrapolation Length 80 mm (in 80 mm distance from the core, the cosine-shaped flux goes to zero)
X-Y Calculations only

Space at the grid plate per fuel element 77 mm x 81 mm

Fuel element cross-section
76 mm x 80.5 mm including support plate
76 mm x 80.0 mm without support plate

Meat dimensions
63 mm x 0.51 mm x 600 mm

Aluminum-canning with $\rho_{Al} = 2.7\ g \cdot cm^{-3}$

Thickness of support plate 4.75 mm; $\rho_{Al} = 2.7\ g \cdot cm^{-3}$

Number of fuel plates per fuel element:
23 identical plates, each 1.27 mm thick

Number of fuel plates per control element:
17 identical plates, each 1.27 mm thick

Identification of the remaining plate positions of the control element:
4 plates of pure aluminum $\rho_{Al} = 2.7\ g \cdot cm^{-3}$, each 1.27 mm thick in the position of the first, the third, the twenty-first, and the twenty-third standard plate position; water gaps between the two sets of aluminum plates.

Specifications of the different fuels (UAl_x-Al Fuel) for HEU, MEU, LEU corresponding to the previous definitions:

HEU:
- Enrichment 93 w/o (weight %) U-235
- 280 g U-235 per fuel element, which corresponds to 12.174 g U-235 per each fuel plate
- 21 w/o of uranium in the UAl_x-Al
- only U-235 and U-238 in the fresh fuel

MEU:
- Enrichment 45 w/o U-235
- 320 g U-235 per fuel element (23 plates)
- 40 w/o of uranium in the UAl_x-Al
- only U-235 and U-238 in the fresh fuel

LEU:
- Enrichment 20 w/o U-235
- 390 g U-235 per fuel element (23 plates)
- 72 w/o of uranium in the UAl_x-Al
- only U-235 and U-238 in the fresh fuel

Total power: 10 MW_{th} (power buildup by 3.1×10^{10} fission/Joule)

Thermal hydraulic data:
Water temperature 20°C
Fuel temperature 20°C
Pressure at core height 1.7 bar

Xenon-State:
Homogeneous Xenon content corresponding to average-power-density

Results

k_{eff}; fluxes and flux ratios along the two symmetry-axes of the core in three groups and for beginning of cycle (BOL) and end of cycle (EOL), respectively.

$\phi_{thermal}$ with $0\ eV < E_n < 0.625\ eV$

$\phi_{epithermal}$ with $0.625\ eV < E_n < 5.531\ keV$

ϕ_{fast} with $E_n > 5.531\ keV$

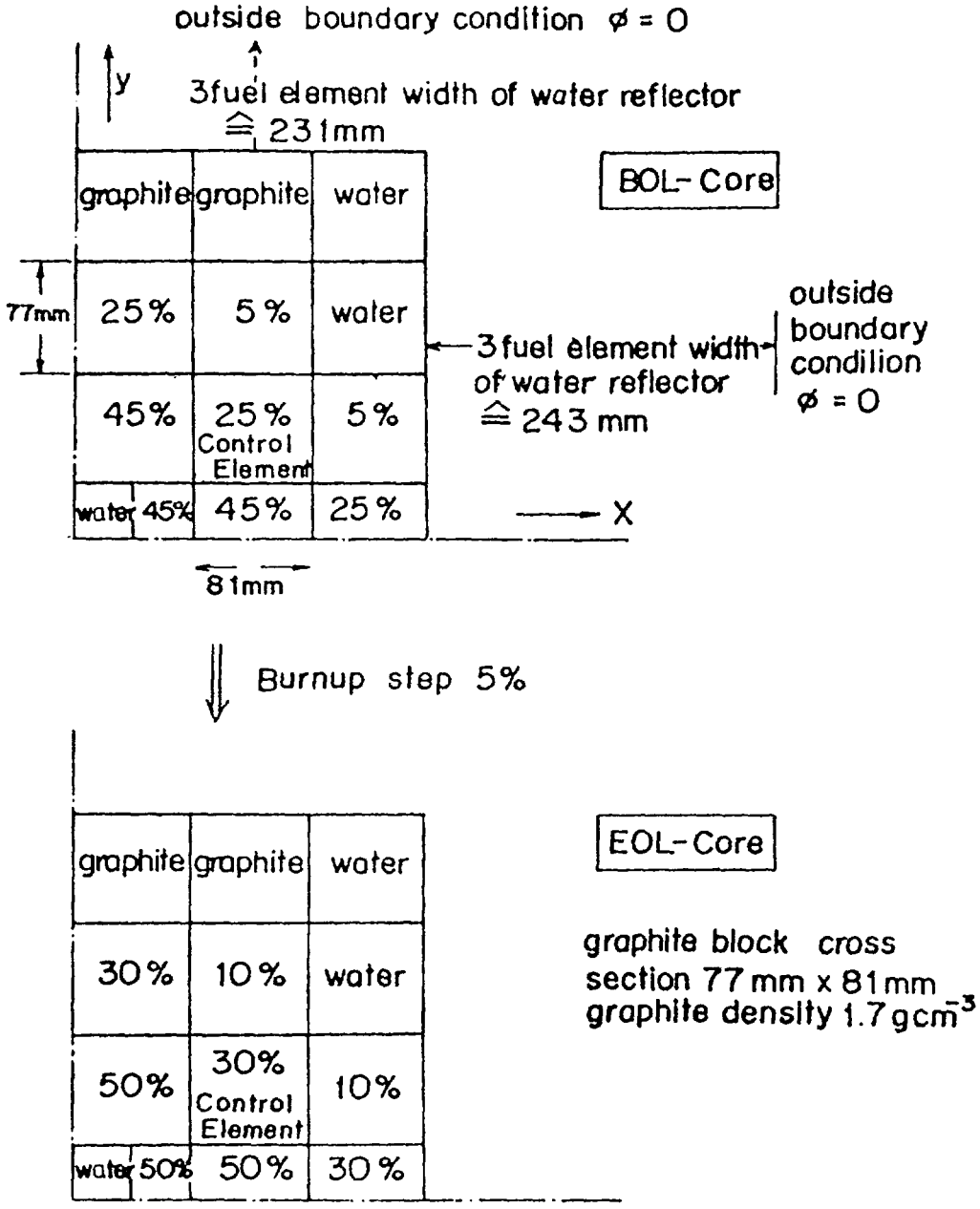

Burnup definition : (%) means the percentage of loss of the number of U 235 - Atoms

METHODICAL BENCHMARK
10 MW CASE
CORE CROSS SECTION

FIG. 2-25

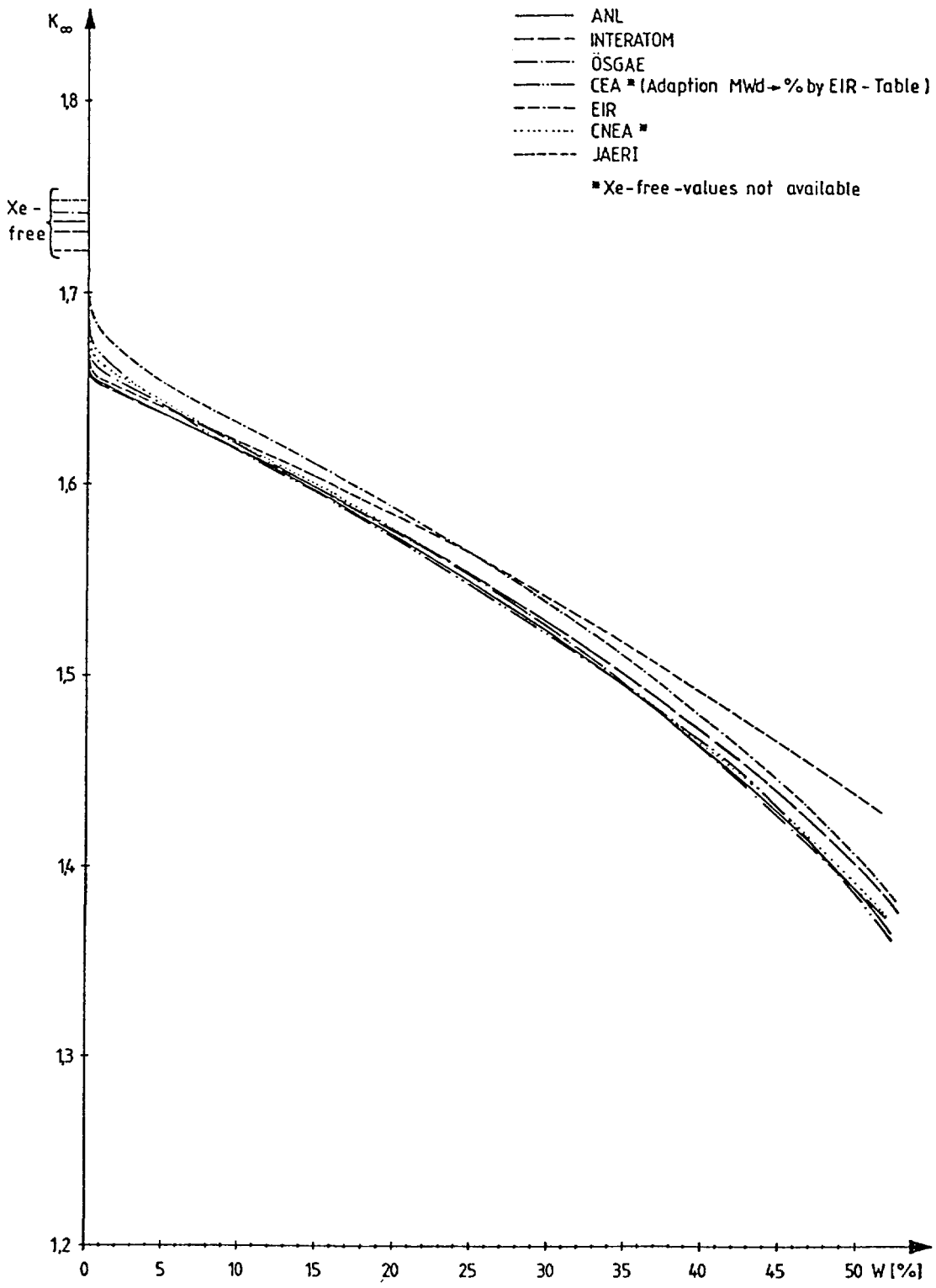

10 MW - BENCHMARK
K∞ FOR 93% ENRICHMENT AS A FUNCTION OF THE BURNUP W [%]

fig. 2-26

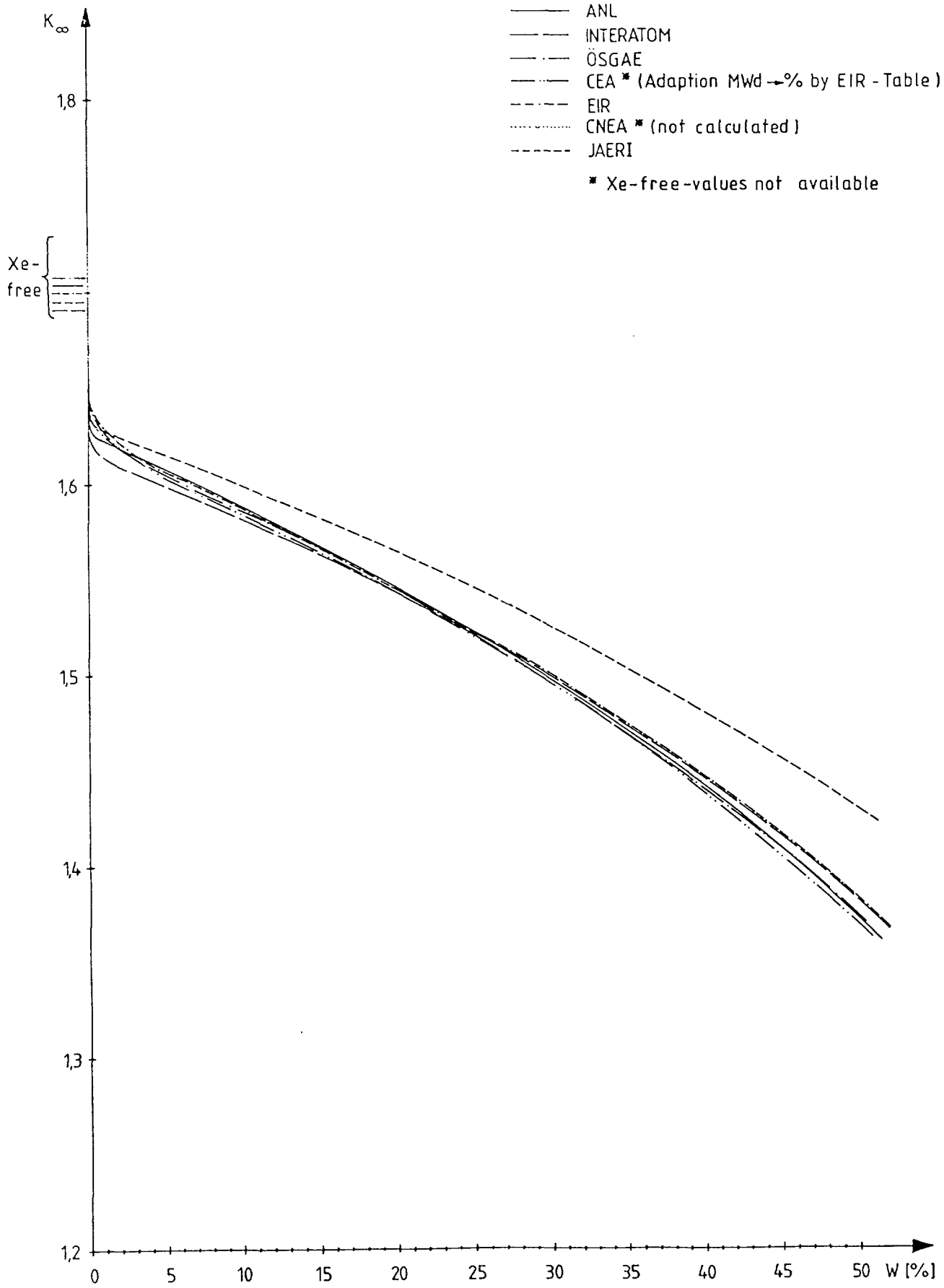

10 MW - BENCHMARK
K_∞ FOR 45 % ENRICHMENT AS A FUNCTION OF THE BURNUP W [%]

fig. 2-27

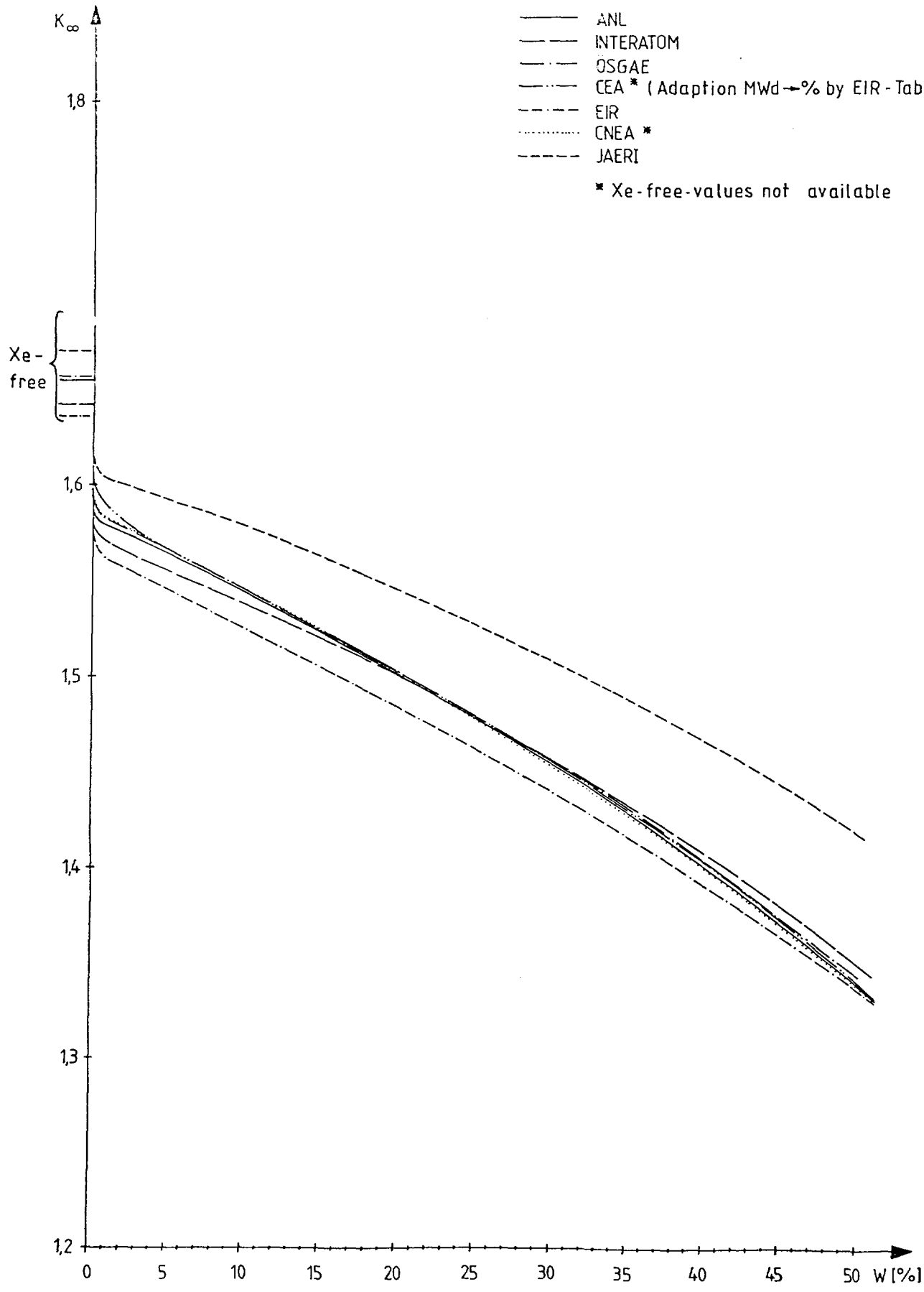

10 MW - BENCHMARK
K∞ FOR 20 % ENRICHMENT AS A FUNCTION OF THE BURNUP W [%]

fig. 2-28

TABLE 2-16: REACTIVITY LEVEL (K_{EFF})

ENRICH-MENT	CORE	GERMANY (INTERATOM)	USA (ANL)	SWITZERL. (EIR)	AUSTRIA (ÖSGAE)	FRANCE (CEA)	ARGENTINA (CNEA)	JAPAN (JAERI)
93	BOL	1.0328	1.0233	1.0368	1.0320	1.0404	1.0377	1.0420
93	EOL	1.0101	1.0004	1.0138	1.0090	1.0170	1.0143	1.0220
93	FRESH	1.1888	1.1834	1.1939	1.1966	1.202	1.2002	1.1810
45	BOL (MWD)	1.0474	1.0410					
45	EOL (MWD)	1.0309	1.0238					
45	BOL (%)	1.0311	1.0247	1.0306	1.0334	1.0408		1.0489
45	EOL (%)	1.0108	1.0033	1.0099	1.0116	1.0190		1.0306
45	FRESH	1.1790	1.1782	1.1791	1.1896	1.195		1.1811
20	BOL (MWD)	1.0599	1.0540					
20	EOL (MWD)	1.0485	1.0419					
20	BOL (%)	1.0278	1.0213	1.0178	1.0320	1.0394	1.0332	1.0578
20	EOL (%)	1.0091	1.0014	1.0000	1.0120	1.0191	1.0130	1.0412
20	FRESH	1.1683	1.1683	1.1594	1.1813	1.187	1.1815	1.1834

TABLE 2-17: COMPARISON OF REACTIVITY LEVEL FROM THE 10 MW-BENCHMARK

ENRICH-MENT	CORE STATE	GERMAN RESULTS (INTERATOM)	DEVIATIONS ($\Delta\varrho$) FROM ANL USA	EIR-SWITZERL.	ÖSGAE AUSTRIA	CEA FRANCE	CNEA ARGENTINA	JAERI JAPAN
93	BOL	1.0328	- .90 %	+ .37 %	- 0.08 %	+ .71 %	- 0.45 %	+ 0.85 %
93	EOL	1.0101	- .96 %	+ .36 %	- 0.11 %	+ .68 %	- 0.41 %	+ 1.15 %
93	FRESH	1.1888	- .38 %	+ .36 %	+ 0.55 %	+ .92 %	- 0.41 %	- 0.55 %
45	BOL (MWD)	1.0474	- .59 %					
45	EOL (MWD)	1.0309	- .67 %					
45	BOL (%)	1.0311	- .61 %	- .05 %	+ 0.22 %	+ .90 %		+ 1.65 %
45	EOL (%)	1.0108	- .73 %	- .09 %	+ 0.08 %	+ .80 %		+ 1.90 %
45	FRESH	1.1790	- .57 %	+ .01 %	+ 0.76 %	+ 1.14 %		+ 1.85 %
20	BOL (MWD)	1.0599	- .53 %					
20	EOL (MWD)	1.0485	- .61 %					
20	BOL (%)	1.0278	- .63 %	- .96 %	+ 0.40 %	+ 1.08 %	- 0.5 %	+ 2.75 %
20	EOL (%)	1.0091	- .76 %	- .90 %	+ 0.28 %	+ 0.98 %	- 0.38 %	+ 3.06 %
20	FRESH	1.1683	.00 %	- .66 %	+ 0.94 %	+ 1.35 %	- 0.96 %	+ 1.09 %

TABLE 2-18: ANL-RESULTS, COMPARISON OF MONTE CARLO* AND DIFFUSION THEORY EIGENVALUES

CORE	MONTE CARLO $K_{MC} \pm \sigma$	DIFFUSION K_D	$K_{MC} - K_D$	$(K_{MC} - K_D)/\sigma$
93 % FRESH	1.189 ± .0033	1.18343	+ .006	1.82
20 % FRESH	1.168 ± .0033	1.16830	.0	0.
93 % EOL**	1.045 ± .0036	1.03366	+ .011	3.06
20 % EOL**	1.048 ± .0034	1.03934	+ .009	2.65
20 % EQ MWD**	1.072 ± .0027	1.06847	+ .004	1.48

* 100,000 HISTORIES PER CALCULATION
** THESE CALCULATIONS DID NOT INCLUDE LUMPED FISSION PRODUCTS

TABLE 2-19: COMPARISON OF REACTIVITY-LOSS ($\Delta\varrho$) BY BURNUP

ENRICH-MENT	EQUAL BURNUP IN	USA (ANL)	GERMANY (INTER-ATOM)	AUSTRIA (ÖSGAE)	SWITZL. (EIR)	FRANCE (CEA)	JAPAN (JAERI)	ARGENTINA (CNEA)
93 W/O	MWD	2.24 %	2.18 %	2.21 %	2.19 %	2.21 %	1.88 %	2.22 %
	%							
45 W/O	MWD	1.61 %	1.53 %					
	%	2.08 %	1.92 %	2.09 %	1.99 %	2.06 %	1.70 %	
20 W/O	MWD	1.10 %	1.03 %					
	%	1.94 %	1.81 %	1.92 %	1.75 %	1.91 %	1.51 %	1.93 %

As the main purpose of this check of methods is the comparison of the reactivity differences for given burnup-steps at the different enrichments as well as for the reactivity differences caused by the enrichment reduction these results are compiled within the Tables 2-19 and 2-20, respectively. These differences are of great importance for the determination of the U-235-loading necessary when reducing the enrichment. With one exception all reactivity differences are in good agreement as far as the loss by burnup is concerned. Table 2-20 shows some relatively great deviations which supply the extreme figures far away from each other. Nevertheless the majority of the contributors are fairly close together.

To compare the different flux distributions of the contributors flux ratios were plotted for three cases (Figs. 2-29, -30, -31). All comparisons were carried out for the core state BOL with Xenon-equilibrium and along the x-axis only. For the fast flux the ratio of the LEU-case to the HEU-case was plotted only (Fig. 2-29) which delivers excellent agreement in two sets of results which must be distinguished. With equal burnups in % loss of U-235 for both enrichments all ratios end at 1.0 in the reflector with very small differences inside the core area except the ÖSGAE-results. With equal burnups in MWd for both enrichments there exists a clear difference of 5% loss of fast flux in the reflector area as well as a somewhat different behavior inside the core.

For the ratios of thermal fluxes the comparisons were carried out for both reductions under consideration, i.e., to MEU-fuel (Fig. 2-30) as well as to LEU-fuel (Fig. 2-31). The differences between the two sets of burnups (equal percentage loss of U-235 and equal MWd, respectively) are found again. Within these sets there exists excellent agreement. Only the ÖSGAE-results are to be found within the gap between the two sets in the reflector area whereas the two sets are clearly separated for the other contributors.

From the figures one can get the rough values for the reduction of the thermal flux caused by the enrichment reduction as

- 14-17% in case of MEU
- 31-38% in case of LEU

in the fuel area

and

- 0-2% in case of MEU
- 0-4% in case of LEU

in the reflector area

for equal burnup in MWd only. Using the equal %-loss of U-235 these small reductions in the reflector are reduced to zero. But it must be emphasized that at the position of the thermal flux peak in the reflector ($x \sim 27$ cm) there exists a clear reduction of the thermal flux. A similar comparison for the y-direction with somewhat different results due to the graphite reflector elements used there may be carried out by interested users on basis of the various results of the different laboratories.

A last aspect worth mentioning from a proliferation point of view is the plutonium content of the burned fuel. The data on ^{239}Pu content shown in Table 2-21 were compiled from the results of cell calculations at 50% burnup for the three enrichments. They are intended only for comparing results obtained at the various laboratories. More accurate data for real reactors can be obtained from the results of the generic studies (see, for example, Appendix A, Section A.6).

TABLE 2-20: COMPARISON OF REACTIVITY-DIFFERENCES ($\Delta\rho$) BY ENRICHMENT REDUCTION (10 MW-BENCHMARK)

		AUSTRIA (ÖSGAE)	FRANCE (CEA)	GERMANY (INTER-ATOM)	JAPAN (JAERI)	SWITZERL. (EIR)	USA (ANL)	ARGENTINA (CNEA)
93 W/O	FRESH FUEL	- 0.49 %	- 0.49 %	- 0.70 %	0.00 %	- 1.05 %	- 0.38 %	
	%	+ 0.13 %	+ 0.03 %	- 0.16 %	+ 0.63 %	- 0.58 %	+ 0.13 %	
	BOL							
	MWD			+ 1.35 %			+ 1.65 %	
	%	+ 0.25 %	+ 0.19 %	+ 0.06 %	+ 0.82 %	- 0.38 %	+ 0.29 %	
45 W/O	EOL							
	MWD			+ 2.00 %			+ 2.29 %	
93 W/O	FRESH FUEL	- 1.08 %	- 1.05 %	- 1.47 %	+ 0.17 %	- 2.49 %	- 1.09 %	- 1.32 %
	%	+ 0.00 %	- 0.09 %	- 0.47 %	+ 1.44 %	- 1.80 %	- 0.20 %	- 0.42 %
	BOL							
	MWD			+ 2.48 %			+ 2.84 %	
	%	+ 0.29 %	+ 0.20 %	- 0.10 %	+ 1.81 %	- 1.36 %	+ 0.10 %	- 0.12 %
20 W/O	EOL							
	MWD			+ 3.63 %			+ 3.98 %	

Table 2-21. Pu-239-Content at 50% Burnup in Grams per Fuel Assembly (Obtained from Cell Calculations)

	ÖSGAE	ANL	INTERATOM	EIR	JAERI	CNEA
93 w/o U^{235}	0.42	0.44	0.42	0.45	0.37	0.43
45 w/o U^{235}	4.34	4.24	4.41	5.50	3.32	/
20 w/o U^{235}	12.30	12.17	11.92	14.80	9.13	12.71

In conclusion, all the comparisons which have been performed as part of the benchmark studies, including k_∞, k_{eff}, $\Delta\rho$, and flux-distributions as a function of burnup and enrichment indicate that the calculations carried out at the different laboratories and companies are in good agreement with each other. Some minor exceptions may bring these contributors to a recheck of their methods and calculations to find the reasons for the deviations.

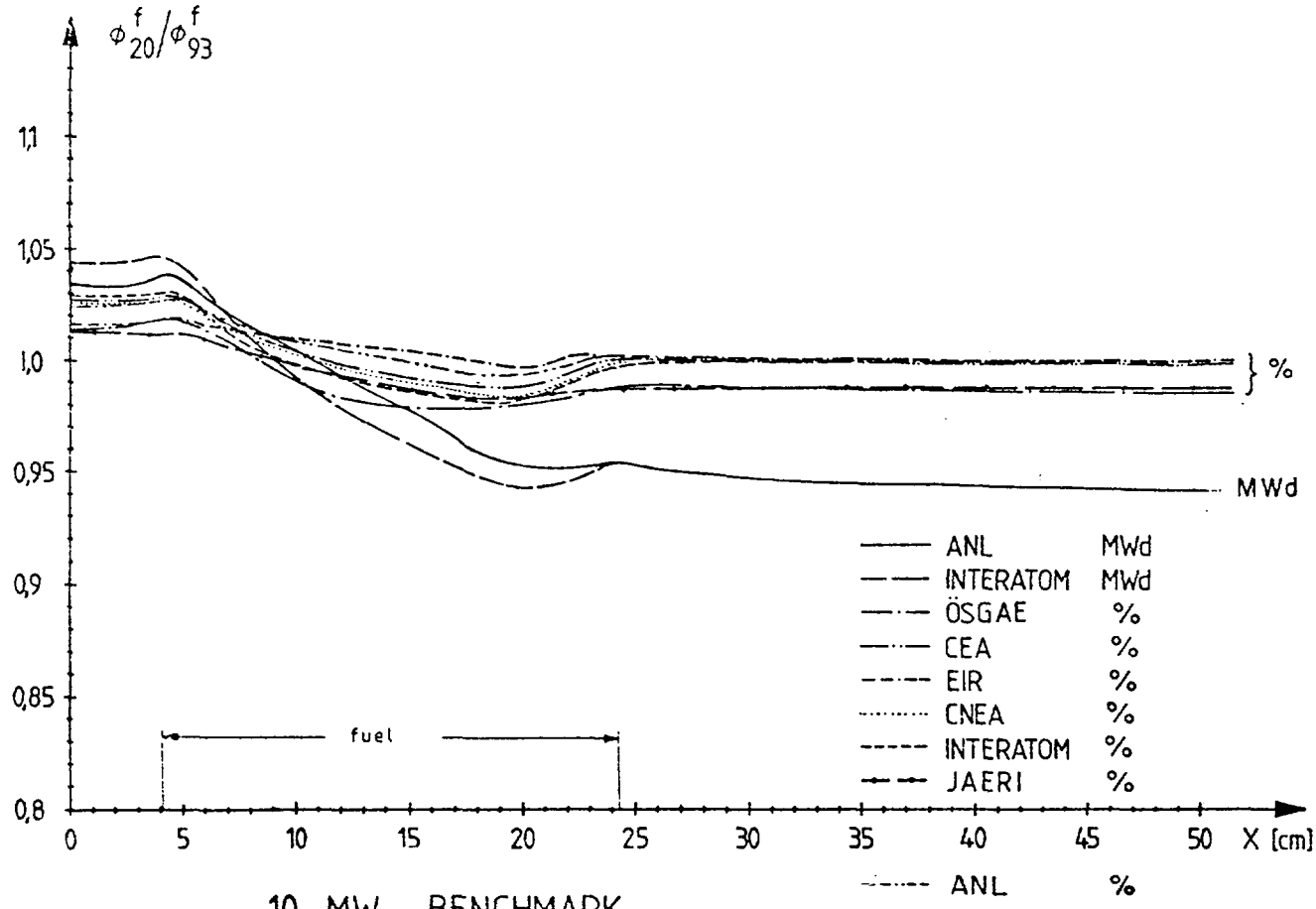

10 MW - BENCHMARK
Flux Ratios ($\phi^{fast}_{20}/\phi^{fast}_{93}$) vs. X - Distance
Core State: BOL, Xe - Equil.

FIG 2-29

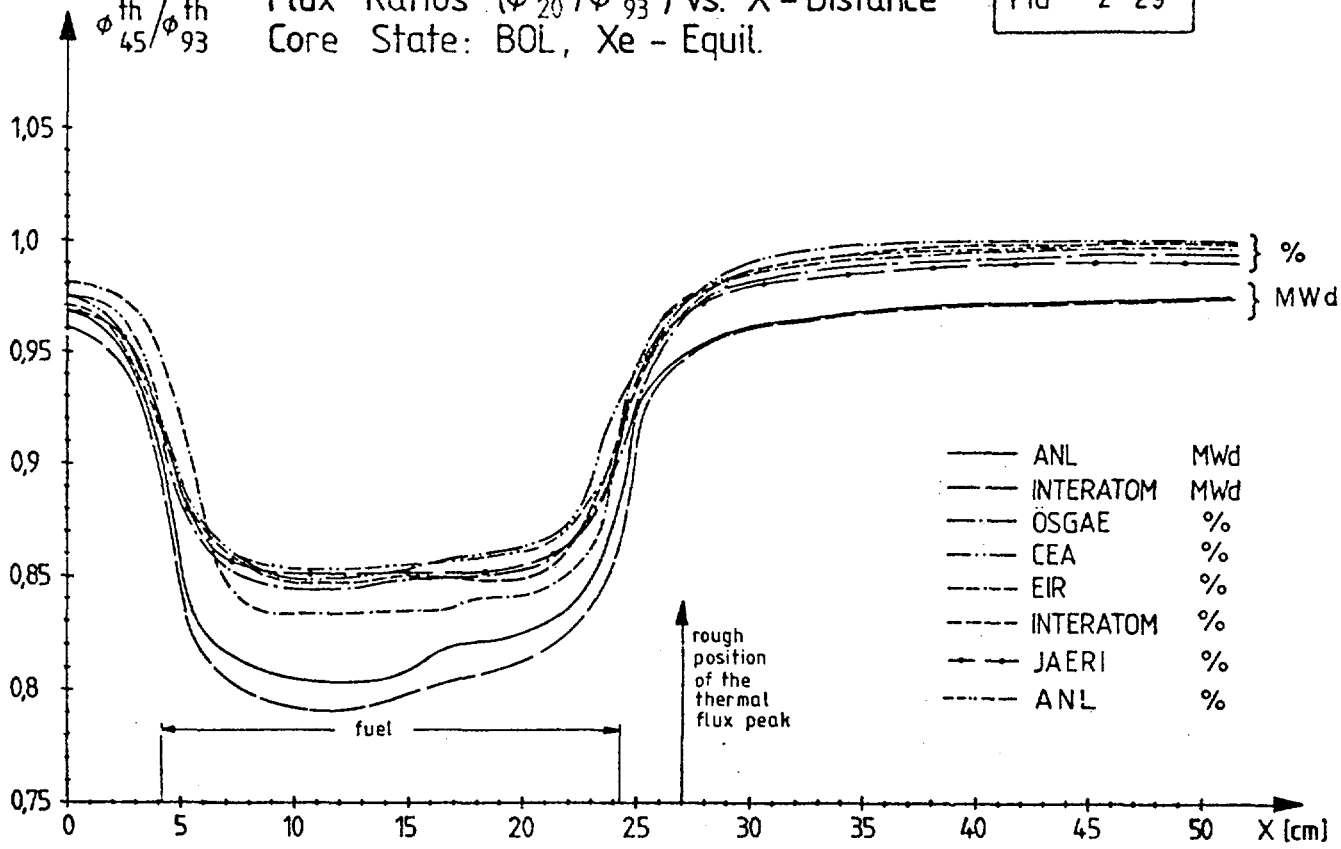

10 MW - BENCHMARK
Flux Ratio ($\phi^{th}_{45}/\phi^{th}_{93}$) vs. X - Distance
Core State: BOL, Xe - Equil.

FIG 2-30

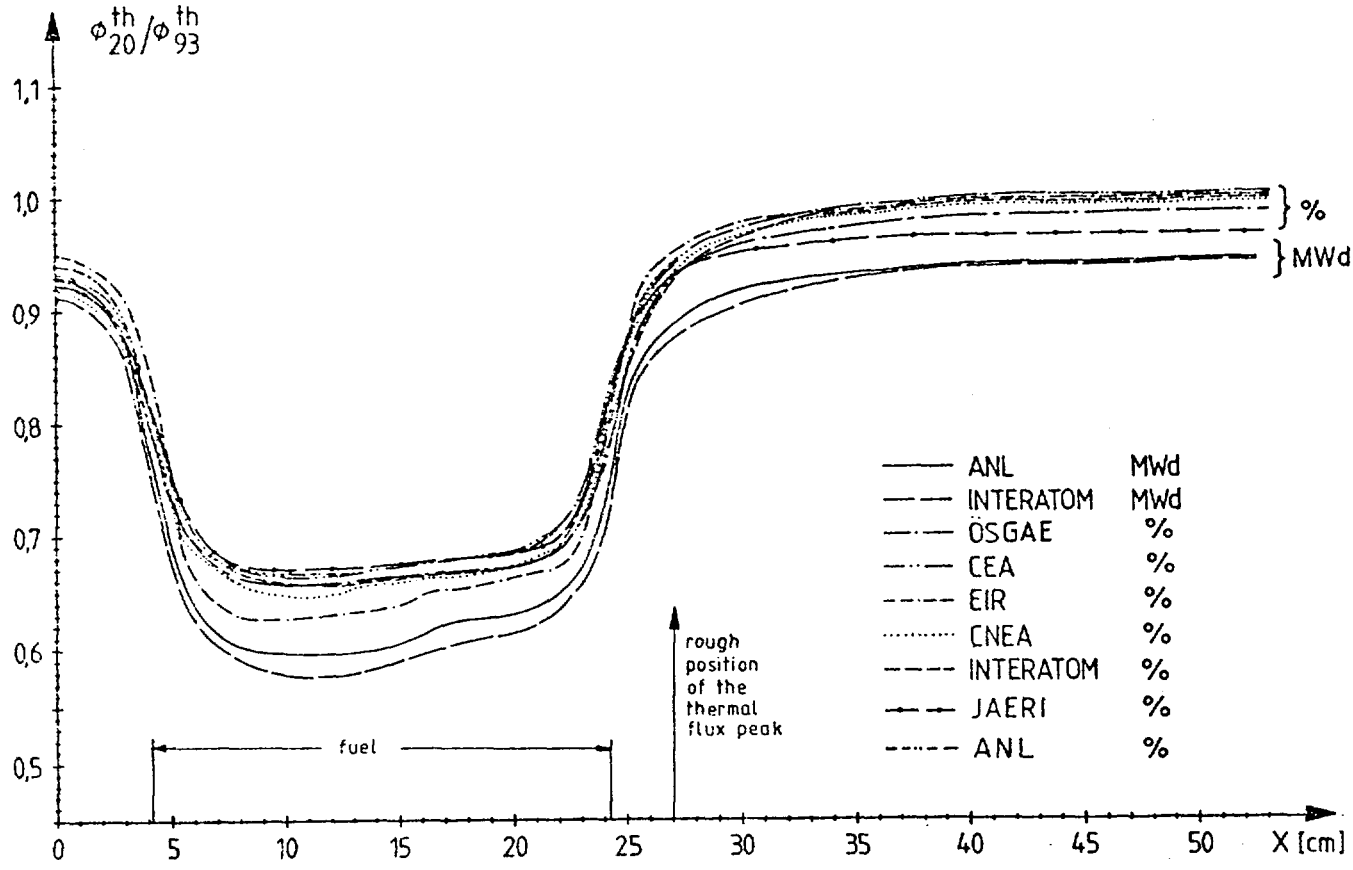

10 MW - BENCHMARK
Flux Ratio ($\phi^{th}_{20}/\phi^{th}_{93}$) vs. X-Distance
Core State: BOL, Xe - Equil.

FIG 2-31

3.0 STATUS AND DEVELOPMENT POTENTIAL OF RESEARCH AND TEST REACTOR FUELS

3.1 OVERVIEW

Table 3-1 summarizes the status, as of March 1980, of reduced enrichment fuel availability from commercial research reactor fuel suppliers. Further data on the availability and development potential of these fuels can be obtained from Tables 1-1 and 1-2 in Section 1 and from Appendix H.

3.2 STATUS OF PLATE-TYPE FUEL TECHNOLOGY

Development of high density fuels for high flux/power research reactors has already led to considerable fabrication and irradiation experience with high uranium density plate-type fuels (see Table 3-2). At the moment the highest uranium densities routinely used are in the range 1.1 - 1.7 g/cm^3 (ATR, HFIR, BR-2, RHF, ORPHEE).

In recent years, with the prospect of enrichment reductions to 45% and 20% instead of 93%, important research and development work has been started in Europe by the companies CERCA and NUKEM, in Argentina by the CNEA, and in the United States by the Department of Energy (DOE) under the Reduced Enrichment

Table 3-1

ESTIMATED SCHEDULE OF TESTS ON REDUCED ENRICHMENT FUELS FOR RESEARCH REACTORS
(Status of March 1980)

Fuel Type	Element Configuration	Uranium Density in Fuel Meat g/cm^3	79	80		81	
U-ZrH	rod	$\leq$0.75	D				
		1.3	C		D		
		2.2		C			
		3.7		C			
U-Al alloy	plate	1.1	C				
UAl_x-Al	plate	1.6-1.7	C		D		
		2.0		A	B		C
		2.2/2.8		A	B		C
U_3O_8-Al	plate	1.7	C		D		
		2.1-2.5		A	B		C
		~3.0		A	B		
UO_2	plate	4.5			A		
	plate	~9	C	D			
	rod	~9	C	D			
U_3Si-Al	plate	4-8		A	B		

LEGEND:

A Beginning of small-sample irradiation tests.

B Results from small-sample irradiation tests available.

C Results from full-size element irradiation tests available.

D Results from full core demonstration with LEU available.

Table 3-2. Reactors Currently Using Fuels With High Uranium Density

Reactor	Country	Power, MW	Fuel Type	Uranium Density g/cm^3	Specific Power MW/kg ^{235}U	Ave. Power Density MW/ℓ	Heat Flux,* W/cm^2 Max. (Ave.)	Discharge Burnup, % Max. (Ave.)
GETR	USA	50	U-Al Alloy	1.1	5.1	0.35	347 (101)	50 (-)
ATR	USA	250	UAl_x-Al	1.6-1.7	5.8	0.92	703 (185)	56 (35)
MURR	USA	10	UAl_x-Al	~1.6	1.6	0.30	113 (57)	50 (25)
BR-2	Belgium	100	UAl_x-Al	1.3	6.5	0.35	470 (200)	70 (57)
RHF Grenoble	France	57	UAl_x-Al	~1.3	6.0	1.14	500 (174)	70 (36)
ORPHEE	France	14	UAl_x-Al	~1.3	2.4	0.25	120 (61)	70 (40)
HFIR	USA	100	U_3O_8-Al	1.2	10.6	1.96	387 (245)	65 (31)
HFBR	USA	40	U_3O_8-Al	1.1	4.9	0.40	418 (120)	49 (37)
OSIRIS	France	70	UO_2 (plate)	9.1	2.6	0.38	310 (125)	70 (40)
PHEBUS	France	40	UO_2 (rod)	9.1	2.5	0.20	203 (107)	Few %
SSR	Romania	14	U-ZrH	0.6	0.5	0.11	204 (80)	70 (38)
TRR-1/M1	Thailand	2	U-ZrH	1.3	0.2	0.034	72 (46)	30 (17)

*Without hot channel factors.

Research and Test Reactor (RERTR) Program managed by Argonne National Laboratory. The objective of the above programs is twofold: firstly to increase the uranium content of existing plate-type fuels, e.g. alloy, and aluminide and U_3O_8 dispersions; and secondly to examine and develop newer high density fuels, such as U_3Si. At the same time, fabrication development is underway to produce thicker fuel meats for those reactors which can accept them.

CERCA, with more than 170,000 plates delivered up to now, has already fabricated (in 1972) for the French CEA UAl_x-Al prototype elements with a uranium density of 1.7 g/cm^3, which were qualified with very good results at burnups of 58% (mean value, maximum attained-70%). Plates made of U_3O_8-Al dispersions with a uranium density of 1.7 g/cm^3 were also tested with satisfactory results.

NUKEM, with a capacity of 20,000 plates per year, has delivered up to now almost 200,000 fuel plates within 18 years of MTR fuel program. In this period more than 2 1/2 tons of HEU in the form of UF_6 and additional amounts of recoverable scraps have been converted to uranium metal. Using this metal, UAl-alloy and UAl_x-Al fuel elements have been fabricated for various research and test reactors, mainly in Europe and the U.S. Different core conversions in European research reactors have been done with NUKEM advanced type fuels in order to increase power and neutron flux. For this purpose dispersed fuels (aluminides and oxides) and dead burned U_3O_8, partly mixed with burnable poisons, have been developed and successfully tested.

In the U.S., both Texas Instruments (TI) and Atomics International (AI) operate plate-fuel fabrication lines for the DOE. These facilities together fabricate about 20,000 plates per year for U.S. reactors, principally the ATR and HFIR, with some elements also supplied to U.S. universities, under a DOE university assistance program.

3.2.1 UAl_x-Al Fuel

In the course of the development program, CERCA is preparing this year two elements with 45% enriched uranium and a uranium density of about 1.7 g/cm^3 for irradiation in the ORR reactor. With this same enrichment of 45%, CERCA will also fabricate 300 plates with a uranium density of 1.6 g/cm^3 in the fuel meat for the Kyoto University Critical Assembly (KUCA) in Japan. The next step is to increase the uranium density to about 2.1 g/cm^3 in thin (1.3 mm) or thick plates (2.2 mm). An irradiation experiment with two elements is planned in the EURATOM reactor at Petten (The Netherlands) within the scope of a cooperative agreement between ANL, CERCA, NUKEM, and the European Community. The technology for uranium densities up to 2.2 - 2.3 g/cm^3 is presently well mastered with UAl_x-Al, so that irradiation of elements with 20% enriched uranium are planned in the ORR reactor for 1980.

At NUKEM, prototype fuel elements, with UAl_x-Al fuel and a uranium density of up to 2.2 g/cm^3 in the fuel meat, without changing the geometry of fuel plates and number of plates per element, will be delivered to several reactors in Europe in 1980. In connection with the national R & D program in Germany for using reduced enriched fuels, NUKEM is going to insert prototype fuel elements with up to 2.6 g U/cm^3 in the fuel meat in the ORR and European research reactors for examination of irradiation behaviour, life time, core physics, reactivity studies, etc. This is planned step by step starting soon and within the following 12 to 15 months.

CNEA-Argentina has obtained good results in fabricating miniplates with 2.2 g U/cm^3 in the fuel meat using natural uranium. Plans are being made for irradiation testing of miniplates in the ORR and a prototype fuel element in the RA-3 reactor.

The U.S. effort for UAl_x-Al is divided into two areas: fuel development and irradiation testing at EG&G, Idaho; and full-scale element fabrication development at Atomics International. Fuel development is underway with the irradiation of mini plates containing up to 2.6 g U/cm^3 beginning early in 1980 in the ORR. Fabricability tests already completed at AI have indicated that full scale plates containing at least 2.2 g U/cm^3 in the fuel meat can be fabricated easily.

3.2.2 U_3O_8-Al Fuel

CERCA is also developing the technology of U_3O_8-Al dispersions, as it appears that UAl_x-Al fuel plates may be limited in the future, from technical and economical reasons, to uranium densities in the range 2.5 - 2.8 g/cm^3. Now the U_3O_8-Al technology is at hand for 3.0 g U/cm^3 in the meat, and irradiation experiments are planned in ORR. Uranium densities in the range 3.3 - 3.8 g/cm^3 are expected to be reached in the near future.

NUKEM has set up and scheduled a similar program for U_3O_8-Al dispersion fuel. Irradiation experiments will be conducted in the ORR and in European research reactors with fuels containing up to 3.2 g U/cm^3 in the fuel meat.

The CNEA-Argentina fuel development program for U_3O_8-Al fuel is similar to that for its UAl_x-Al fuel. Irradiation tests on miniplates in the ORR and prototype elements in the RA-3 are being planned with uranium densities in the range 2.4 - 3.0 g/cm^3.

The U.S. effort on U_3O_8-Al follows the same plan as that for UAl_x-Al. Oak Ridge National Laboratory is performing fuel development and irradiation testing, while Texas Instruments will perform the full scale fabrication develoment. Irradiation testing of mini plates will begin in early 1980 in the ORR. The fuel development effort has shown that a uranium density of 3.0 g/cm^3 is the maximum possible with the materials and processing methods currently used at ORNL.

3.2.3 U_3Si Fuel

U_3Si was the primary choice of Argonne National Laboratory for a new, much higher uranium density fuel. Fabrication development of U_3Si and aluminum-modified U_3Si in aluminum dispersion is underway. Miniplate irradiation testing of U_3Si-Al fuel with uranium densities of 4.2 and 6.0 g/cm^3 is scheduled early in 1980 in the ORR. NUKEM will also be evaluating U_3Si fuel.

3.2.4 Summary

In summary, based on the present status and near-term expected improvements of the plate-type Al fuels it is possible to conclude that nearly all MTR reactors which may be expected to undergo a reduction of uranium enrichment over the next few years will be assured of the option of continued operation with the same type of fuel plate elements without special investments for modifying the reactor. An adaptation of the fuel element's internal geometry (i.e., number and thickness of plates) might be required to accommodate the desired enrichment reduction of the reactor.

3.3 STATUS OF UZrH RODDED FUEL TECHNOLOGY

3.3.1 Up to 1.3 g U/cm^3 (20 wt% U)

Sixty TRIGA reactors have been sold and the earliest of these are now passing twenty years of operation. All of these reactors use the uranium-zirconium hydride fuel (UZrH) which provides certain unique advantages arising out of its large prompt negative temperature coefficient, very low fission product release, and high temperature capability. With only a few exceptions, TRIGA reactors have always used low-enriched uranium (LEU) fuel with an enrichment of 19.9%. The original standard TRIGA fuel has a uranium density of 0.5 g/cm^3 (8.5 wt% U) and is 20% enriched (nominal). Experience with TRIGA fuel includes over 650 reactor years of successful operation. TRIGA fuel with a uranium density of 0.75 g/cm^3 (12 wt% U) has been proved through successful reactor operation for over a decade. Previous work on UZrH fuels during the Space Nuclear Auxiliary Program (SNAP) had developed the technology up to 1.3 g U/cm^3 (20 wt% U) and found no indication of this being a limit. Burnup of U-235 reached values of about 80% in SNAP program tests. The LEU development program at General Atomic has also included extensive tests with 1.3 g U/cm^3. Tests have shown fuel with greater than 1.3 g U/cm^3 to have essentially the same fission product retentivity as TRIGA fuel with 0.5 g U/cm^3. On-going in-core tests with 1.3 g U/cm^3 fuel, started in April 1978, have been an unqualified success during pulsing and steady-state operation including over 1500 thermal cycles where the reactor has gone from shutdown to powers of 1 to 1.5 MW with 1.3 g U/cm^3 fuel.

3.3.2 Up to 3.7 g U/cm^3 (45 wt% U)

General Atomic undertook an LEU development program in early 1976. Laboratory and production tests of fuels containing up to 3.7 g U/cm^3 (45 wt% U) are complete. In-core tests of production elements for thermal cycling and pulsing tests have been under way since April of 1978. The extensive metallographic, electron microprobe and X-ray diffraction examinations have shown that the more highly loaded alloys contain no significant differences in structural characteristics when compared with the standard 0.5 and 0.75 g U/cm^3 fuels. The phase distribution and homogeneity are excellent and these factors, coupled with the grain structure observed, support expectation of excellent long-term irradiation behavior. The measured fission product release and physical properties show very suitable characteristics up to 3.7 g U/cm^3. The fission product release experiments were conducted to temperatures up to 1100°C and showed very low release fractions, characteristic of the standard TRIGA fuels, where the temperature independent value to about 300°C is 1.5 x 10^{-5}. Test results on samples quenched from up to 1200°C can be characterized as showing remarkably benign response. Some minor cracking, volume shrinkage, loss of hydrogen and surface oxidation occurred. Out-of-pile thermal cycling tests show that the ZrH matrix stabilizes the fuel material such that it is dimensionally stable when repeatedly cycled through the uranium phase change temperature of about 680°C. Reactor testing of production elements includes 1.3 and 3.7 g U/cm^3 fuels being tested in the TRIGA Mark F reactor at General Atomic both in the steady state and pulsing modes. The principal objective of these tests is to demonstrate the fuel stability for thermal cycling from ambient to operating temperatures. Nearly 2000 in-core cycles have been completed to date and no adverse conditions noted. An irradiation test of a standard 16-rod cluster configuration has been in progress in the 30 MW ORR since December 1979.

3.4 STATUS OF THE UO_2 PLATE-TYPE FUEL

Type of Fuel

Zircaloy-clad UO_2 (CARAMEL).

Configuration

The fuel consists of rectangular or square sintered UO_2 platelets. The flat platelets are mounted into a Zircaloy grid which isolates them from their neighbors and from the environment. The grid and the platelets, sealed by a zircaloy cladding form the element plate. The plates are assembled in parallel in bundles which make up the fuel element.

These fuel elements have the same outside dimensions as the MTR-type UAl elements and can replace the latter (see Fig. 3-1: case of the OSIRIS reactor).

Currently feasible dimensions of the various parts of a Caramel fuel element (the extreme combinations are not all possible).

	Length (mm)	Width (mm)	Thickness (mm)
Platelet	12 - 26	12 - 26	1.4 - 4
Plate	600 - 1800	65 - 200	2.2 - 5
Assembly	600 - 1800	65 - 200	-

Power Level

Critical experiments and low-power reactors: zero to several hundred kilowatts.

Research reactors: up to 70 MW.

Operational Performance

The data supplied relate to fuel with 1.45 mm oxide thickness, which is suitable for the most severe operating conditions. Thicker fuel can be used under less demanding conditions; in particular, the fuel with 4-mm oxide thickness is suitable for critical experiments or low-power reactors.

Prototype elements have been irradiated under the following conditions: mean (maximum) specific power of 2000 (3400) W/cm^3 of UO_2; mean (maximum) heat flux per unit surface of 190 (248) W/cm^2; and mean (maximum) burnup of 19,000 (32,000) MWd/t. The start-up core of OSIRIS has: a mean specific power of 1730 W/cm^3 of UO_2; a maximum specific power of 4400 W/cm^3 at an average burnup of 9000 MWd/t at the hot point; a mean heat flux per unit surface of 124 W/cm^2; and a maximum heat flux per unit surface of 310 W/cm^2 at an average burnup of 9000 MWd/t.

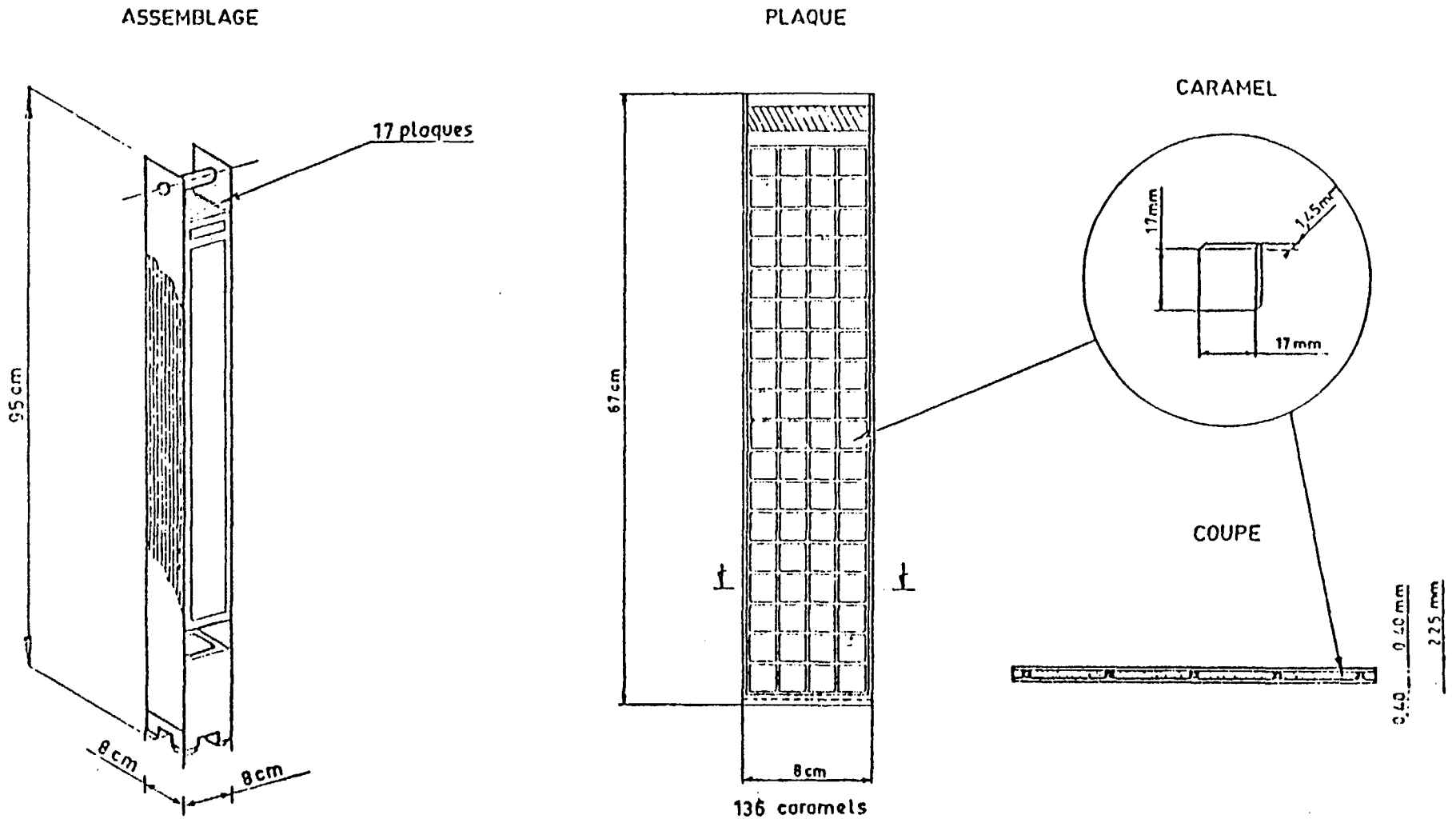

Fig. 3-1. ÉLÉMENT COMBUSTIBLE CARAMEL "OSIRIS"

Uranium Content

Example: standard OSIRIS fuel element: 594 g of UO_2 per plate, or 523 g of uranium, or 7.86 g per cm^3 of plate.

Burnable Poisons

The CARAMEL fuel is well adapted for the introduction of burnable poisons (gadolinium oxide in the UO_2, ZrB alloy in the edge plates). Experimental irradiation of platelets containing mixed Gd_2O_3-UO_2 oxide has already shown satisfactory behaviour.

Experiment

Three Caramel OSIRIS precursor elements of 17 platelets, i.e., 51 plates irradiated over a period of six months in the UAl core. Experience of the irradiation of a complete core for OSIRIS will have been gained by the end of 1979.

Short-term Developments

Operation of the OSIRIS reactor with a CARAMEL-type core.

3.5 STATUS OF UO_2 RODDED FUEL

UO_2 rod type fuel is already available from experience gained in the production of fuel elements for power reactors (LWR and FBR). Research reactors like CABRI in France, FR_2 and KNK (sodium cooled) in Germany and the PULSTAR reactors in the U.S. are using this type of fuel in various geometries and enrichments.

APPENDIX A

U.S. Generic Enrichment Reduction Calculations for Plate-Type and Rodded-Type Reactors

Performed by the

Reduced Enrichment Research and Test Reactor
(RERTR) Program

Argonne National Laboratory
9700 South Cass Avenue
Argonne, Illinois 60439
U.S.A.

ABSTRACT

Neutronics and thermal-hydraulics methods applicable to research and test reactors are described in detail and compared with experimental data.

Systematic studies are presented for conversion of two generic MTR-type reactors from HEU to LEU fuels:

(1) Conversion of a 2 MW reactor to use of classical, plate-type dispersion fuel (UAl_x-Al or U_3O_8-Al) and

(2) Conversion of a 10 MW reactor to use of classical, plate-type dispersion fuel, to plate-type Caramel fuel (UO_2-Zr4), and to rodded-type UZrH fuel.

Detailed results include burnup performance, neutron flux performance, and thermal-hydraulic safety margins for each of the reactors, fuel-types, and fuel element geometries. A number of design variations are considered with classical dispersion fuel.

APPENDIX A

TABLE OF CONTENTS

TABLE OF CONTENTS (Cont.)

TABLE OF CONTENTS (Cont.)

A.1 METHODS AND CODES AT ANL

A.1.1 Computer Codes

The computer codes available at ANL for analysis of the feasibility and implementation of research and test reactor conversions from HEU to LEU fuel designs are listed in Table A1.

The EPRI-CELL[1] code is used to generate few-group, collapsed cross sections for use with the various diffusion[6-8] and transport[9-11] codes. EPRI-CELL combines a GAM-1[2] resonance treatment in the epithermal energy range with a THERMOS,[3] heterogenous, integral-transport treatment in the thermal energy range. The 68-group epi-thermal, GAM, library data are generated using the integral transport option of the MC^2-2 Code [4] to accurately account for resonance self-shielding, and the 35-group thermal, THERMOS, library data are generated using the AMPX[5] code system.

VIM[12] is a continuous energy Monte Carlo code that is used for cross section comparison and validation, and for reactor calculations for which deterministic codes are inadequate.

The data base for both VIM and EPRI-CELL is ENDF/B. The current VIM library is entirely version IV data. Since the original EPRI-CELL intermediate group libraries contained a collection of different versions of earlier ENDF/B data, these libraries were expanded by ANL to include version IV data for the isotopes ^{235}U, ^{238}U, ^{239}Pu, and hydrogen.

The REBUS-2[15] code, originally developed for fast reactor applications, and the PDQ-7[16] code, developed for thermal reactor applications, are used for fuel cycle analysis. The MIT version of COBRA3C[17] and the MACABRE[18] codes are used for thermal-hydraulic calculations. Various kinetic codes[14] and RELAP-4[19] are available for transient analyses.

TABLE A1. Computer Codes Available at ANL for Analysis of Research and Test Reactor Conversions to LEU Fuel Designs

	Comments		Comments
Cross Section Generation		**Monte Carlo Codes**	
EPRI-CELL[1,2,3]	GAM-1 - Resonance, THERMOS - Thermal	VIM[12]	Continuous Energy
		MORSE[13]	Multigroup
MC^2-2[4]	Rigorous Slowing-down		
AMPX[5]	Nordheim - Resonance, FLANGE - Thermal	**Kinetics Codes**	
		Point Kinetics	Various Codes
		FX-2[14]	1,2 D
Diffusion Codes		**Fuel Cycle Codes**	
DIF3D[6]	1,2,3 D	REBUS-2[15]	1,2 D
DIF2D[7]	2 D	PDQ-7[16]	1,2,3 D
DIF1D[8]	1 D		
Perturbations[7,8]	1,2 D	**Thermal-Hydraulics Codes**	
Transport Codes		COBRA-3C/RERTR[17]	Plate, Pin Gecmetries
DIF3D[6]	2 D	MACABRE[18]	Plate Geometries
TWOTRAN-II[9]	2 D	RELAP-4[19]	System Transients
DOT-III[10]	2 D		
ANISN[11]	1 D		

A.1.2 Methods-Neutronics

Benchmark Calculations of the TRX Uranium Metal Lattices

A.1.2.1 Introduction

In order to partially validate the EPRI-CELL cross section generation code and the thermal capability of the VIM Monte Carlo code, calculations were performed on four TRX uranium-metal-lattice critical experiments.[20] Four measured reaction rate ratios are compared with those calculated with EPRI-CELL, VIM, and the Bettis Atomic Power Laboratory (BAPL) Monte Carlo code RCP01.[21]

Designated TRX-1 through TRX-4 by the U.S. Cross Section Evaluation Working Group (CSEWG), the thermal lattices are also refereed to respectively as the 2.35/1, 4.02/1, 1.00/1 and 8.11/1 lattices in BAPL nomenclature. The numbers indicate the ratio of moderator-to-fuel volume. TRX-1 and TRX-2 were single region hexagonal pitch critical lattices composed of 1.3% uranium metal rods clad in aluminum and moderated by water. TRX-3 and TRX-4 were central zone metal lattices surrounded by a uranium oxide driver zone. The two full lattices had asymptotic spectra and the zoned lattices had nearly asymptotic spectra. A more detailed description of the lattices is given in Table A2.

Enriched and depleted, bare and cadmium-covered foils were activated in the core center and the following reaction rate ratios were measured:

ρ^{28} - ratio of epithermal-to-thermal U-238 capture

δ^{25} - ratio of epithermal-to-thermal U-235 fission

δ^{28} - ratio of U-238 fission -to-U-235 fission

CR* - ratio of U-238 capture-to-U-235 fission

The foil activities were adjusted for an epithermal-thermal boundary of 0.625 eV. Experimental values reported here and in Ref. 21 have been corrected for systematic errors by Sher and Fiarman.[22] The measured values are compared to results for RCP01,[21] an improved version of the BAPL multigroup Monte Carlo code RECAP.

EPRI-CELL was also used to calculate the oxide driver lattice properties and is compared to similar EPRI-CELL benchmarking presented by Eich and Kennedy.[23]

A.1.2.2 Calculations

The RCP01 calculation was performed by Hardy[21] for a zero leakage hexagonal cell using ENDF/B-IV version cross sections. For each lattice, 225,000 histories were accumulated. Leakage corrections to the reaction rates were obtained by a pair of multigroup calculations, one at zero leakage and one using the measured total buckling. Leakage correction factors, which typically deviated less than 7% from unity, were multiplied by the RCP01 zero leakage reaction rate ratios to obtain the final results. Full core Monte Carlo calculations were done on the two full lattices. A further description of the calculations can be found in Ref. 21.

The VIM calculations were similar to the RCP01 cell calculations for the four metal lattices. The basic difference in the two codes is that VIM is a continuous energy Monte Carlo treatment while RCP01 is a multigroup treatment. The VIM cell calculation was done using hexagonal geometry periodic boundary conditions with ENDF/B-IV version data. For each cell calculation, 50,000 histories were accumulated. The VIM cell results are compared to experiment by using the same leakage correction factors that were applied to RCP01. Full core calculations were not performed with VIM.

TABLE A2. Summary of TRX Lattice Properties

A. Fuel

1. Atomic number

Density ($\times 10^{-24}$ cm^{-3})		TRX Metal	TRX UO_2	Natural Slab
Fuel:	U^{238}	0.0472050	0.0231270	0.0474830
	U^{235}	0.0006253	0.0003112	0.0003401
	O^{16}	—	0.0469460	—
Clad:	Al^{27}	0.0602500	0.0602500	—

2. Dimensions, cm

Fuel radius	0.4915	0.4864	
Clad inner radius	0.5042	0.5042	
Clad outer radius	0.5753	0.5753	
Fuel rod length	122	122	—
Slab thickness	—	—	2.5400
Slab thickness x width	—	—	61 x 61

B. Cell

1. Atomic number density (x 10-24 cm-3)

Moderator:	H^1	0.06676
	O^{16}	0.03338

2. Dimensions

	Vol Mod/Vol Fuel	d, cm
TRX metal	1.00	1.4412
TRX metal	2.35	1.8060
TRX metal	4.02	2.1740
TRX metal	8.11	2.8824
TRX UO_2	2.40	1.8060
Mat slab	1.09	2.7686
	0.50	1.2700
	0.16	0.4064

d = rod center-to-center spacing, triangular pitch, for TRX lattice
= moderator thickness, for slab lattices

The 1.00/1 and 8.11/1 TRX lattices were surrounded by driver regions of 2.40/1 TRX UO_2.

TABLE A2 (Cont'd.)

C. Lattice Configurations

1.00/1 TRX Inner Lattice

A hexagonal array of 169 rods was removed from the center of the TRX UO_2 lattice (W/F = 2.40) leaving 1432 rods with an approximately cylindrical outer boundary and a thick water reflector. An inner lattice plate was inserted to center a hexagonal array of 217 TRX metal rods (W/F = 1.00) in the resulting space. $B^2_{axial} = 0.000526$ cm^{-2}.

8.11/1 TRX Inner Lattice

Every other metal rod of the 1.00/1 TRX inner lattice was removed to leave a hexagonal array of 61 rods with W/F = 8.11. 1809 UO_2 rods were now required in the outer lattice. $B^2_{axial} = 0.000526$ cm^{-2}.

2.35/1 TRX Full Lattice

764 metal rods, fully reflected radially. $B^2_{axial} = 0.000526$ cm^{-2}, $B^2_{total} = 0.0057 \pm 0.0001$ cm^{-2}.

4.02/1 TRX Full Lattice

578 metal rods, fully reflected radially. $B^2_{axial} = 0.000526$ cm^{-2}, $B^2_{total} = 0.005469 \pm 0.000036$ cm^{-2}.

Natural Slab Cores

The 1.09/1 and 0.5/1 natural slab cores contained 11 fuel slabs, with a highly enriched driver region at each end. Each driver consisted of 20 aluminum fuel boxes arranged in two rows of 10 boxes each, with an aluminum control rod scabbard between the rows. The highly enriched uranium fuel was in the form of 6.3 w/o U-Zr plates. This type of driver was depicted in the dry lattice experiment report (Reference 2). The measured buckling, applicable in the asymptotic regions were:

W/U = 1.09 $B^2_{trans} = +0.00367 \pm 0.00006$ cm^{-2}; $B^2_{total} = -0.0013 + 0.0001$ cm^{-2}

W/U = 0.5 $B^2_{trans} = +0.00367 \pm 0.00006$ cm^{-2}, $B^2_{total} = -0.0037 + 0.0003$ cm^{-2}

(B^2_{trans} refers to directions parallel to slab faces.)

The 0.16/1 core contained 12 fuel slabs between the drivers. There was no asymptotic region in this case.

EPRI-CELL was used to generate 5 group cell-averaged cross sections and fluxes with an imposed buckling such that k = 1. Because the spectra were considered asymptotic, the reaction rate ratios were calculated using these spectra. The ANL version of EPRI-CELL uses an ENDF-IV based cross section library[24] created at ANL, and requires pin shielding factors in the epithermal range. The shielding factors were generated with the MC^2-2 code. Sauer's method was used to approximate a Dancoff factor, C, with an EPRI-recommended Σ_T = 1.484 cm^{-1} for the moderator. Some uncertainty in the value of C was introduced by having two formulations for the value of τ, the geometric factor, presented in the EPRI-documentation.[1] The Dancoff factors resulting from the two formulations are presented in Table A3 along with Dancoff factors calculated by the RECAP code.[20] Because of this uncertainty in C, the lattice parameters were calculated for several values of C and the sensitiities of the lattice parameters to C were determined.

TABLE A3. Dancoff Factors

Lattice	Sauer's Method[a] 1	Sauer's Method[b] 2	RECAP[c]
1.00 (TRX-3)	0.337	0.360	0.376 ± 0.004
2.35 (TRX-1)	0.148	0.160	0.143 ± 0.002
4.02 (TRX-2)	0.0790	0.0853	0.0611 ± 0.001
8.11 (TRX-4)	0.0349	0.0380	0.0142 ± 0.0008

[a] Ref. 1, Eq. 5-34, p. 5.14.
[b] Ref. 1, p. 5-76.
[c] Ref. 21.

For all EPRI-CELL calculations, the heterogeneous fast effect correction option of the code was applied. Analytic isotropic boundary conditions were used. For the two full lattices and the driver oxide lattice, the EPRI-CELL broad group cross sections were input to a 5 group two dimensional, diffusion eigenvalue calculation. The critical experiment for the oxide lattice is documented in Ref. 25. The diffusion calculation was performed using the DIF2D[7] code.

A.1.2.3 Results

The assumption of asymptotic spectra for the two full cores is verified by the results of the DIF2D R-Z calculation for the TRX-1 (2.35/1) lattice. Figure A1 plots group flux ratios as a function of radius for TRX-1 and the ratios are within 1% of the asymptotic values at about 7 cm from the core-reflector boundary. The radii of the two partial zones was about 11 cm, and the spectra were therefore taken to be asymptotic.

Sensitivities of some lattice parameters to the Dancoff factor are given for the TRX-1 lattice in Fig. A2. In the other lattices, the sensitivities of the parameters are similar, the main variation being decreased sensitivity with increased lattice spacing.

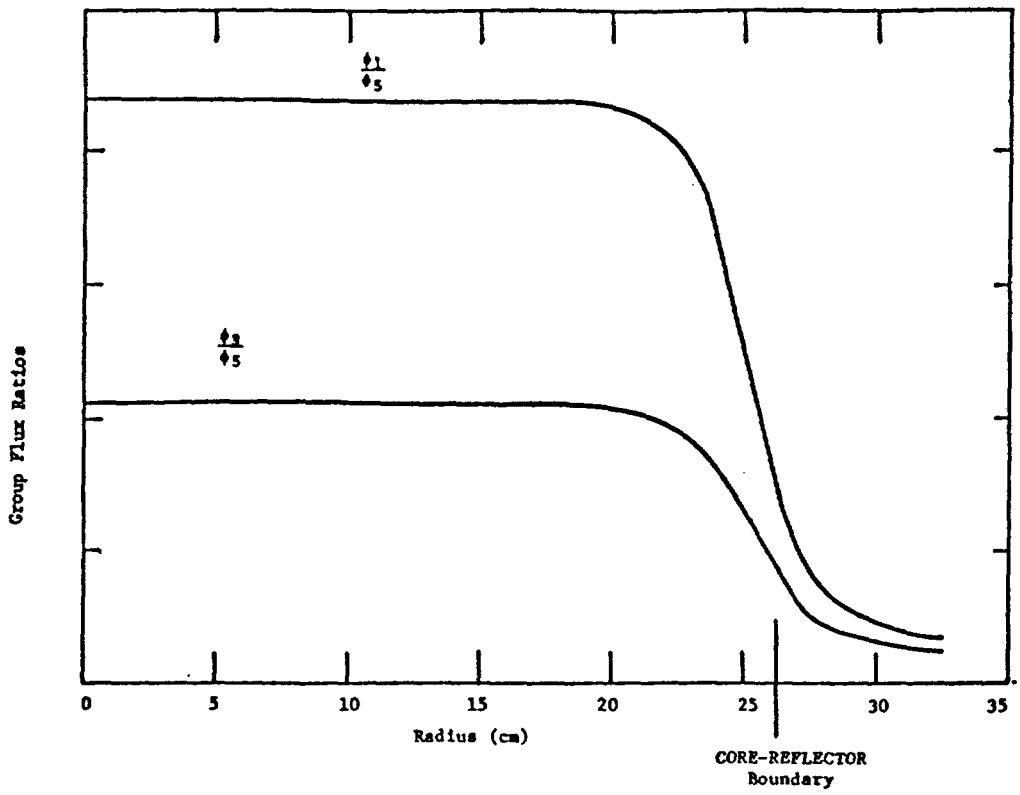

Figure A1. Group Flux Ratios as a Function of Radius for TRX-1 (V_{mod}/V_{fuel} = 2.35) Uranium Metal Lattice. Energy Group Upper Boundaries; 1-10.0 MeV, 2 - 0.821 MeV, 3 - 5.53 keV, 4 - 1.855eV, 5 - 0.625 eV.

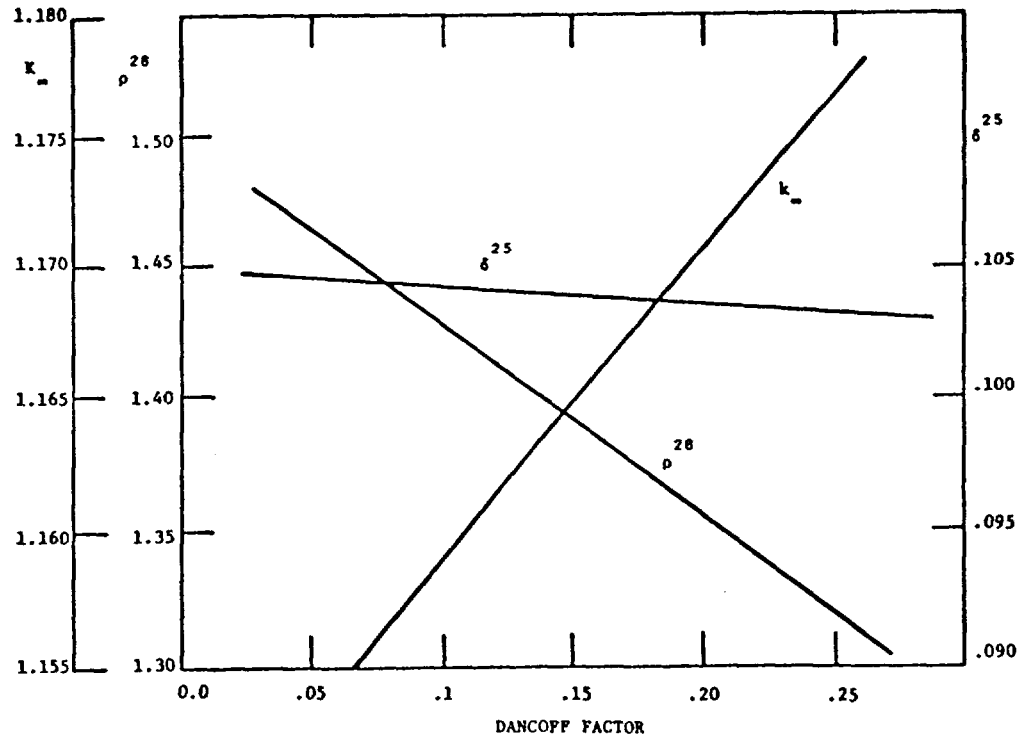

Figure A2. Sensitivity of ρ^{28}, δ^{25}, and k_∞ to Dancoff Factor for TRX-1 (V_{mod}/V_{fuel} = 2.35) Uranium Metal Lattice.

For the purpose of comparison with experimental values and also in keeping with EPRI methods, the calculational results are reported for Dancoff factors derived using Sauer's method 2 of Table A3. The uncertainty in k and ρ^{28} due to the uncertainty in C has been crudely estimated by computing the parameters with C derived by Sauer's method and by RECAP, and subtracting. The uncertainties have been tabulated for ρ^{28} in Table A4 and for k_∞ in Table A5.

The results of RCP01, VIM, EPRI-CELL, and experiment are given for ρ^{28}, δ^{25}, δ^{28}, and CR* in Table A4 and for k_∞ and k_{eff} in Table A5. Calculated-to-experimental ratios, (C/E), are given in Table A6. Uncertainties assigned to the C/E's are the quadrature sums of experimental and calculational uncertainties. For the EPRI-CELL C/E's, the uncertainty is attributed to experiment alone. RCP01 and VIM Monte Carlo calculations are also compared in Table A6. The average RCP01-to-VIM calculated ratio over the four lattices is tabulated for each of the four spectral indices. Agreement between the two Monte Carlo codes is generally within statistics. However, comparison of the δ^{28} results indicates that there may be some systematic difference between the two. Reaction rate ratios calculated by RCP01 full core calculations of TRX-1 and TRX-2 agree very well with RCP01 leakage-corrected results with the exception of δ^{28}, where 0.8% and 1.7% higher values were found for the full core calculations. Agreement of the Monte Carlo codes with experiment is also generally good. The two most significant quantities of disagreement are the ρ^{28} values and the eigenvalues. The disagreement between experiment and RCP01 have been explored in Ref. 21, and the general conclusion is that a strong correlation exists between the two parameters such that a small decrease in the resonance capture cross section of ^{238}U would improve agreement with experiment for both quantities. The effect of using alternative ^{238}U cross sections in the calculation has been investigted in Ref. 21.

In general, EPRI-CELL results agree with Monte Carlo results within a few percent. A small but systematic bias exists for δ^{28}. The oxide lattice results are presented in Table A7. The calculations of Eich and Kennedy[23] were performed with modified ENDF/B-I ^{238}U cross sections and, presumably, modified ENDF/B-I cross sections for all other isotopes. For comparison, the lattice was also calculated here with the EPRI-library cross sections which are essentially ENDF/B-I version cross sections. Agreement is good between the two version I calculations. The small difference in eigenvalues is attributable to different treatments of the reflector cross sections. Using version IV data increased ρ^{28} about 5% and decreased the eigenvalue by 0.5%. The effect of version I vs. version IV uranium data was investigated, for one metal lattice, TRX-1. The results are shown in Table A8. A 6% increase in ρ^{28} and a 1% decrease in eigenvalue was observed.

A.1.2.4 Summary and Conclusions

RCP01 multigroup Monte Carlo and VIM continuous energy Monte Carlo gave consistent results for all measured parameters with the possible exception of δ^{28} where VIM calculated 1.4% $\pm$ 0.6% lower values averaged over the four lattices. Agreement with experiment was generally good. ρ^{28} was consistently overpredicted by about 5% and the eigenvalue underpredictd by about 1%. The disagreements can be reduced by a decrease in the U-238 resonance capture cross section.

EPRI-CELL results using ENDF/B-IV uranium data generally paralleled the VIM results. EPRI-CELL results for δ^{28} were approximately 5% lower than the Monte Carlo values.

TABLE A4. Results of RCP01, VIM, and EPRI-CELL Calculations of ρ^{28}, δ^{25}, δ^{28}, and CR*

Lattice	Experiment	RCP01[a]	VIM[a]	EPRI-CELL
		ρ^{28}		
1.00 (TRX-3)	3.03 ± 0.05	3.18 ± 0.01	3.19 ± 0.03	3.1724 ± 0.04[b]
2.35 (TRX-1)	1.320 ± 0.021	1.396 ± 0.004	1.375 ± 0.015	1.386 ± 0.013
4.02 (TRX-2)	0.837 ± 0.016	0.867 ± 0.004	0.868 ± 0.009	0.8582 ± 0.011
8.11 (TRX-4)	0.481 ± 0.011	0.507 ± 0.003	0.501 ± 0.008	0.4958 ± 0.006
		δ^{25}		
1.00 (TRX-3)	0.231 ± 0.003	0.241 ± 0.001	0.243 ± 0.002	0.2421
2.35 (TRX-1)	0.0987 ± 0.0010	0.1009 ± 0.0004	0.1005 ± 0.0009	0.0995
4.02 (TRX-2)	0.0614 ± 0.0008	0.0614 ± 0.0003	0.0609 ± 0.0005	0.0599
8.11 (TRX-4)	0.0358 ± 0.0005	0.0352 ± 0.0002	0.0359 ± 0.0004	0.0349
		δ^{28}		
1.00 (TRX-3)	0.167 ± 0.008	0.179 ± 0.0002	0.178 ± 0.002	0.1614
2.35 (TRX-1)	0.0946 ± 0.0041	0.0964 ± 0.0003	0.0941 ± 0.0009	0.0918
4.02 (TRX-2)	0.0693 ± 0.0035	0.0686 ± 0.0003	0.0679 ± 0.0006	0.0654
8.11 (TRX-4)	0.0482 ± 0.0020	0.0483 ± 0.0002	0.0476 ± 0.0004	0.0464
		CR*		
1.00 (TRX-3)	1.255 ± 0.011	1.282 ± 0.002	1.285 ± 0.010	1.2770
2.35 (TRX-1)	0.797 ± 0.008	0.809 ± 0.001	0.820 ± 0.006	0.8062
4.02 (TRX-2)	0.647 ± 0.006	0.648 ± 0.001	0.650 ± 0.005	0.6458
8.11 (TRX-4)	0.531 ± 0.004	0.533 ± 0.001	0.5317 ± 0.004	0.5291

[a] RCP01 and VIM results are leakage corrected results of zero buckling, infinite lattice calculations.

[b] Estimated uncertainties in ρ^{28} due to the uncertainty in the Dancoff factor (see text).

TABLE A5. K_∞ and K_{eff} Calculations by RCP01, VIM and EPRI-CELL

	K_∞			K_{eff}		
Lattice	RCP01	VIM	EPRI-CELL[a]	RCP01	VIM[b]	EPRI-CELL
1.00 (TRX-3)	1.0532 ± 0.0010	1.0517 ± 0.0031	1.043 ± 0.004			
2.35 (TRX-1)	1.1696 ± 0.0008	1.1724 ± 0.0040	1.165 ± 0.002	0.9837 ± 0.0010	0.98606 ± 0.0034	0.9787
4.02 (TRX-2)	1.1586 ± 0.0013	1.1601 ± 0.0043	1.156 ± 0.002	0.9894 ± 0.0013	0.9907 ± 0.0037	0.9817
8.11 (TRX-4)	1.0156 ± 0.0016	1.0183 ± 0.0036	1.018 ± 0.001			

[a] The K_∞ calculation was done with zero leakage. Uncertainty estimates are due to the uncertainty in the Dancoff factor (see text).

[b] $K_{eff}^{VIM} = K_\infty^{VIM} \; (K_{eff}/K_\infty)^{RCP01}$

TABLE A6. Calculated-to-Experimental Ratios (C/E) for ρ^{28}, δ^{25}, δ^{28}, CR*, and Average Values of RCP01/VIM Calculations

Lattice	RCP01	VIM	EPRI-CELL
		ρ^{28} C/E	
1.00	1.050 ± 0.017	1.053 ± 0.019	1.047 ± 0.016
2.35	1.058 ± 0.016	1.042 ± 0.019	1.050 ± 0.016
4.02	1.036 ± 0.020	1.037 ± 0.023	1.025 ± 0.020
8.11	1.054 ± 0.025	1.041 ± 0.029	1.031 ± 0.025
		δ^{25} C/E	
1.00	1.043 ± 0.014	1.052 ± 0.015	1.048 ± 0.014
2.35	1.022 ± 0.011	1.018 ± 0.014	1.008 ± 0.011
4.02	1.000 ± 0.014	0.992 ± 0.015	0.976 ± 0.013
8.11	0.983 ± 0.015	1.003 ± 0.018	0.973 ± 0.014
		δ^{28} C/E	
1.00	1.072 ± 0.052	1.066 ± 0.052	0.966 ± 0.045
2.35	1.019 ± 0.044	0.995 ± 0.044	0.970 ± 0.042
4.02	0.990 ± 0.050	0.980 ± 0.050	0.944 ± 0.048
8.11	1.002 ± 0.042	0.987 ± 0.042	0.962 ± 0.040
		CR* C/E	
1.00	1.022 ± 0.009	1.024 ± 0.012	1.017 ± 0.008
2.35	1.015 ± 0.010	1.029 ± 0.013	1.011 ± 0.010
4.02	1.002 ± 0.009	1.005 ± 0.012	0.998 ± 0.009
8.11	1.004 ± 0.008	1.001 ± 0.011	0.996 ± 0.008

Variable	Average RCP01/VIM Result
ρ^{28}	1.006 ± 0.006
δ^{25}	0.996 ± 0.005
δ^{28}	1.014 ± 0.006
CR*	0.996 ± 0.004

TABLE A7. Results of EPRI-CELL Calculations for the 2.40/1 Oxide Lattice

	Experiment	EPRI-CELL Ref.	EPRI-CELL ENDF/B-I	EPRI-CELL ENDF/B-IV
ρ^{28}	0.906 ± 0.01	0.90	0.900	0.946
δ^{25}	0.052 ± 0.001	0.054	0.0537	0.0526
k	1.000	0.9999	0.9924	0.9874

[a] Taken from Ref. 23.

TABLE A8. Results of EPRI-CELL Calculations for the 2.35/1 (TRX-1) Lattice Using ENDF/B-I and ENDF/B-IV Data

	Experiment	ENDF/B-I	ENDF/B-IV
ρ^{28}	1.320 ± 0.021	1.328	1.386
δ^{25}	0.0987 ± 0.010	0.1014	0.0995
CR*	0.797 ± 0.008	0.799	0.806
δ^{28}	0.0946 ± 0.0041	0.0895	0.918
k	1.000	0.9867	0.9787

A.1.3 Methods - Thermal-Hydraulics

The design of a plate-type fuel element requires basic thermal-hydraulic information such as: the heat transfer regime at which onset of nucleate boiling (ONB) will occur, the pressure drop and flow rate through the fuel element, the departure from nucleate boiling (DNB), the conditions for flow instability, and the critical velocity beyond which the fuel plates will collapse. This section outlines the approaches and correlations used to obtain this information. Symbols and units used in this section are defined in Table A9.

A.1.3.1 Fuel Element Dimensions

In the redesign of a fuel element, one of the constraints is to maintain the same overall element dimensions (width and thickness). For a given number of fuel plates (N_f) and clad thicknesses (t_{ci}, t_{co}), the element thickness (t_e) provides a constraint between the water channel thickness (t_w) and the fuel meat thickness (t_m). Assuming that the plates are uniformly spaced (Fig. A15), the constraint between t_w and t_m is given by:

$$(N_f - 2)\ (t_m + 2t_{ci}) + 2(t_m + 2t_{co}) + N_f t_w = t_e$$

or

$$t_w + t_m = (t_e - 4[t_{co} - t_{ci}])/N_f - 2t_{ci} \qquad (1)$$

The area ratio (A_c/A_o) used to calculate the pressure loss at the channel exit can be written as:

$$\frac{A_c}{A_o} = \frac{(N_f - 1)\ t_w}{t_e - t_w - 2t_m - 4t_{co}} \qquad (2)$$

The volumetric flow rate through an element given by:

$$Q = 0.36\ N_f\ U\ W\ t_w \qquad (3)$$

A.1.3.2 Pressure Drop Across Fuel Plates

The total pressure drop across a fuel element consists of losses in the upper and lower end boxes of the element and the pressure drop across the fuel plates themselves. Depending on the flow rate and the geometries and dimensions of the end boxes, the sum of the first two losses is about 1/4 to 1/3 of the total pressure drop.

The pressure drop across the fuel plates includes the pressure loss at the entrance to the fuel channel (ΔP_{en}), the friction loss in the fuel channel ΔP_f, and the pressure loss at the exit of the fuel channel (ΔP_{ex}). That is:

$$\Delta P_F = \Delta P_{en} + \Delta P_f + \Delta P_{ex} \qquad (4)$$

TABLE A9. Definitions of Thermal-Hydraulics Variables

Symbol	Definition	Unit
A_c	Total water channel cross-sectional area in an element	cm^2
A_o	The cross-sectional area of the end box immediately beyond the channel exit	cm^2
C_p	Specific heat of water	KJ/kg°C
D_e	Equivalent hydraulic diameter = $2t_w/(1+t_w/w)$	cm
E	Young's modulus of elasticity	bar
f	Fraction factor	(dimensionless)
f_a	Axial peak-to-average heat flux ratio	(dimensionless)
f_r	Radial peak-to-average power ratio	(dimensionless)
G	Mass flux = ρu	kg/m^2s
h	Film heat transfer coefficient	$w/cm^2°C$
H_{co}	Effective fuel plate length for heat transfer	cm
k	Heat conductivity of water	w/m°C
K	Entrance pressure loss coefficient	(dimensionless)
L_c	Length of fuel plates (coolant channels)	cm
N_f	Number of fueled plates	(dimensionless)
P	Pressure at channel exit	bar abs
P_c	Critical pressure of coolant	bar abs
ΔP_{en}	Pressure loss at channel entrance	bar
ΔP_{ex}	Pressure loss at channel exit	bar
ΔP_f	Pressure loss through channel due to friction	bar
ΔP_p	Pressure loss across fuel	bar
Pr	Prandtl number	(dimensionless)
q	Local heat flux	w/cm^2

TABLE A9.(Contd). Definitions of Thermal-Hydraulics Variables

Symbol	Definition	Unit
q_a	Axial average heat flux along plate	w/cm2
q_c	Critical (burnout) heat flux	w/cm2
Q	Volumetric flow rate through the element	m3/hr
Re	Reynolds number	(dimensionless)
ΔT_c	Water temperature rise in coolant channel	°C
T_{in}	Core entrance water temperature	°C
T_{sat}	Saturation temperature of water at pressure P	°C
T_s	Clad surface temperature	°C
ΔT_{sub}	Water subcooling i.e., °C below saturation	°C
T_{co}	Clad thickness of inside fuel plate	cm
t_{ci}	Clad thickness of outside fuel plate	cm
t_e	Thickness of an element	cm
t_m	Fuel meat thickness	cm
t_p	Fuel plate thickness	cm
t_w	Water channel thickness	cm
u	Water velocity in channel	m/s
u_o	Water velocity just beyond channel exit	m/s
V_{crit}	Critical flow velocity	m/s
w	Water channel width	cm
W_h	Effective fuel plate width for heat transfer	cm
z	Axial location	cm
λ	Heat of vaporization	KJ/kg
μ	Viscosity of water	Pascal-sec
ρ	Density of water	kg/m3
ν	Poisson's ratio	(dimensionless)
X	Average flowing steam fraction or quality at position of burnout	(dimensionless)

Most plate-type research reactors were designed for subcooled core flow under normal operation. The entrance, friction, and exit pressure losses for single-phase flow can be calculated from the following standard formulae,[26]

$$\Delta P_{en} = \frac{K\rho U^2}{2} \times 10^{-5} \tag{5}$$

$$\Delta P_f = \frac{4f\ L_c \rho U^2}{2\ D_e} \times 10^{-5} \tag{6}$$

$$\Delta P_{ex} = \frac{\rho(U - U_o)^2}{2} \times 10^{-5} \tag{7}$$

A conservative value for the entrance loss coefficient is K = 0.5. For turbulent flow in smooth channels, the friction factor[27] can be expressed as:

$$f = 0.0791/R_e^{0.25} \text{ for } 5000 < R_e < 51094$$

$$= 0.0460/R_e^{0.20} \text{ for } 51094 < R_e \tag{8}$$

Assuming constant coolant density, then

$$\frac{U_o}{U} = \frac{A_c}{A_o} \tag{9}$$

where A_c is the total water channel cross-sectional area in the fuel element and A_o is the cross-sectional area of the end box immediately beyond the channel exit.

Combining Eqs. (5) through (7) and Eq. (9) gives an expression for the pressure losses across the fuel plates:

$$\Delta P_F = \frac{\rho U^2}{2} \left\{ K + \frac{4fL_c}{D_e} + \left(1 - \frac{A_c}{A_o}\right)^2 \right\} \times 10^{-5} \tag{10}$$

A.1.3.3 Critical Flow Velocity

It has been shown that a critical flow velocity exists for a given plate assembly. At this critical velocity, the plates become unstable and large deflections of the plates can occur. These plate deflections can cause local overheating of the fuel plates and possibly a complete blockage of the coolant flow.

Miller[28] has derived a formula for the critical velocity based on the interaction between the changes in channel cross-sectional areas, coolant velocities, and pressures in two adjacent channels. For design purposes, Ref. 29 recommends that the coolant velocity be limited to 2/3 of the critical velocity given by Miller, i.e.,

$$V_{crit} = \frac{2}{3}\left[\frac{15 \times 10^5 E(t_p^3 - t_m^3)\, t_w}{\rho\, W^4\, (1 - \nu^2)}\right]^{1/2} \tag{11}$$

A.1.3.4 Onset of Nucleate Boiling (ONB)

The ONB is not a limiting criterion in the design of a fuel element. However, it is a heat transfer regime which should be identified for proper hydraulic and heat transfer considerations, i.e., single-phase flow versus two-phase flow.

Under ONB conditions, the clad surface temperature over which nucleate boiling will occur for a given local coolant pressure and surface heat flux can be expressed by the correlation developed by Bergles and Rohsenow[30]:

$$T_s = T_{sat} + \frac{5}{9}\left(\frac{9.23\, q}{p^{1.156}}\right)^{\left(\frac{p^{0.0234}}{2.16}\right)} \tag{12}$$

This correlation is widely used and is applicable down to the low pressures characteristic of research and test reactors.

The local clad surface temperature can be calculated from the coolant temperature and heat flux as follows:

$$T_s = T_{in} + \frac{20 W_h \int_0^z q\, dz}{W\, G\, t_w\, C_p} + \frac{q}{h}\,. \tag{13}$$

The second term on the right hand side of Eq. (13) is the coolant temperature rise from the channel entrance to the axial location z. The third term is the film temperature difference between the clad surface and the coolant.

By equating Eqs. (12) and (13), an expression that relates heat flux, water channel thickness, and mass flux (or coolant velocity through the channel) is obtained. This relationship enables calculation of the maximum allowable surface heat flux without local boiling for a given channel thickness and flow condition.

The actual axial location at which ONB will occur depends upon the axial heat flux distribution, the coolant velocity, and the pressure drop along the channel. Typically, ONB occurs at about 20 cm upstream of the channel exit for plate-type fuels. Using a trial and error procedure, the exact ONB location can be found. For simplicity, the heat flux for ONB can be calculatd conservatively by using the worst combination of parameters, i.e., ONB occurs at the channel exit with peak heat flux, lowest pressure and saturation temperature, and highest coolant temperature rise. With these assumptions, the resulting expression for Eqs. (12) and (13) becomes:

$$T_{sat} + \frac{5}{9}\left(\frac{9.23\, f_a f_r q_a}{p1.156}\right)\left(\frac{p0.0234}{2.16}\right) = T_{in} + \frac{20 f_r q_a H_{co} W_h}{G\, t_w C_p W} + \frac{f_a f_r q_a}{h} \qquad (14)$$

With the conservative assumptions used, the heat flux at ONB calculated from Eq. (14) will be about 15% lower (see Fig. A4) than that calculated from Eqs. (12) and (13) using an iterative procedure for the exact ONB location.

The heat transfer coefficient (h) depends upon the mass flux (G) through the channel and the channel hydraulic diameter (D_e). It can be derived by using the Boelter correlation:[31]

$$h = 0.023 \frac{k}{100\, D_e} R_e^{0.8} P_r^{0.3} \qquad (15)$$

where

$$R_e = \frac{G\, D_e}{100\, \mu} \quad \text{(Reynolds Number)} \qquad (16)$$

$$P_r = \frac{\mu\, C_p}{k} \times 10^3 \quad \text{(Prandtl Number)} \qquad (17)$$

A.1.3.5 Comparison of the ONB Correlation with Experiment

A boiling experiment[32] was performed in the Oak Ridge Research Reactor (ORR) in which the coolant temperature at two axial locations near the channel exit was measured. Boiling was observed to occur at a power level of 5.6 MW and a coolant velocity of 0.57 m/s (1.88 ft/s). Under the same conditions, the Bergles and Rohsenow correlation[30] predicts that ONB will occur when the clad surface temperature is higher than 121.3°C (250.3°F). The thermal-hydraulic conditions in this case were modelled and the coolant and clad surface temperatures were calculated by using COBRA-3C/RERTR,[17] a modified version of the computer code COBRA-3C/MIT.[17] As shown in Fig. A3, the calculated coolant temperatures agree very well with measured values and those calculated in Ref. 32. The peak clad surface temperature of 124.7°C (256.7°F), calculated using COBRA-3C/RERTR, shows that boiling will occur, in agreement with the experiment.

From the results of a similar series of boiling experiments[32] conducted in the ORR, a curve of the power level at which boiling begins versus coolant flow rate was developed. The boiling power level of these tests ranged from 3.5 MW to 12 MW. By using Eqs. (12) and (13), the power level at which boiling commences under the test thermal-hydraulic conditions can be calculated. As shown in Fig. A4, the predicted power level is about 5-6% lower than the measured values. Results calculated by using Eq. (14), which has built-in conservative assumptions (peak heat flux, lowest pressure and saturation temperature, and highest coolant temperature rise at the ONB location) are also shown in Fig. A4. The conservative assumptions employed in Eq. (14) result in an under-prediction of heat flux at ONB by about 15%, as compared with results calculated by Eqs. (12) and (13).

Figure A3. Comparison of Axial Coolant Temperture Distribution Calculated Versus Measured in the Oak Ridge Research Reactor

——— (---) Coolant (Clad) temperature calculated in Ref. 32.

▲ (+) Coolant (Clad) temperature calculated by COBRA-3C/RERTR.

● Coolant temperature measured during boiling test (Ref. 32).

—•— -- —•— Lowest clad temperature for nucleate boiling calculated in Ref. 32.

— — — Lowest clad temperature for nucleate boiling calculated by the Bergles and Rohsenow correlation.[30]

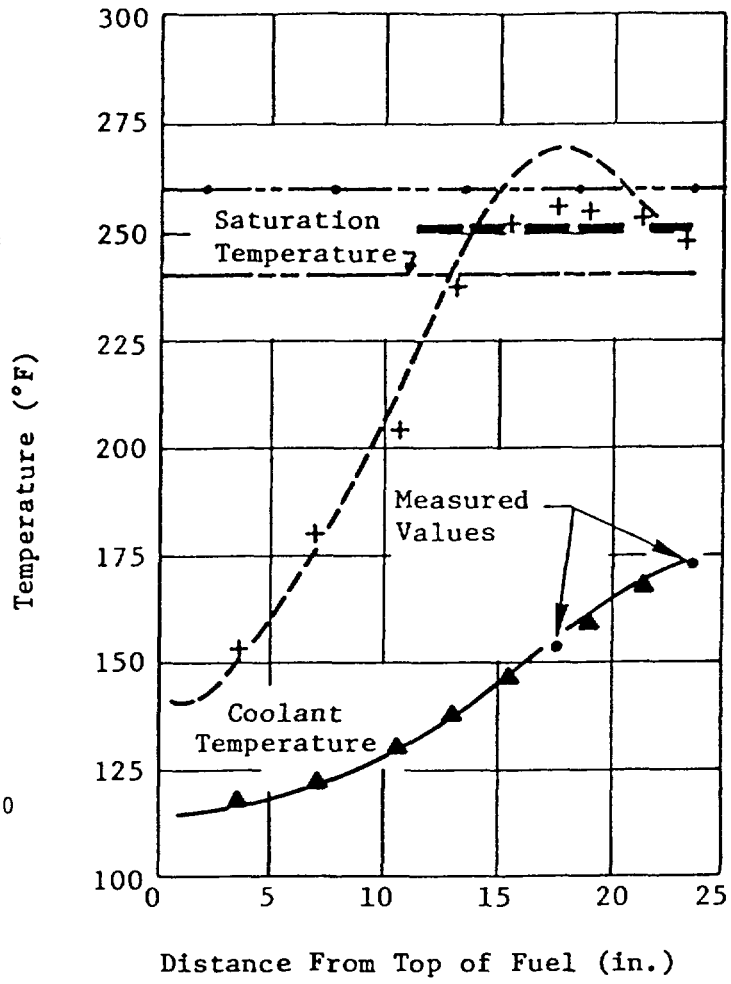

Figure A4. Comparison of Calculated and Measured Power Level vs. Flow at Which Boiling Commences in the Oak Ridge Research Reactor

\+ Power level estimated using Eqs. (12) and (13)

▲ Power level estimated using Eq. (14)

Line Data from boiling experiment (Ref. 32)

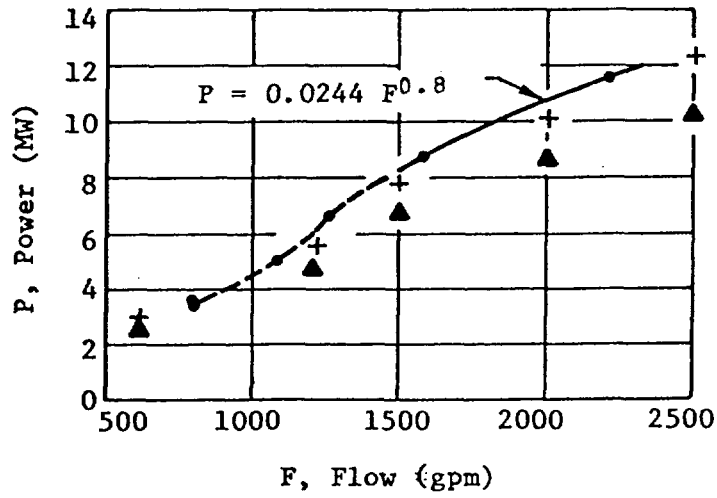

A.1.3.6 Flow Instability

This section was contributed jointly by ANL (USA), AERE Harwell (UK), GEC (UK), and EIR (Switzerland).

Flow instabilities are undesirable in heated channels because flow oscillations affect the local heat transfer characteristics and may induce premature burnout.

For a low-pressure subcooled boiling system,[33,34] flow excursions leading to burnout were observed. The burnout heat flux occuring under unstable flow conditions was well below the burnout heat flux for the same channel under stable flow conditions. For practical plate-type fuel design purposes, the critical heat flux that leads to the onset of flow instability may be more limiting than that of stable burnout.

A.1.3.6.1 Flow Excursion and Density Wave Oscillation Types of Flow Instabilities

The most common flow instabilities encountered in heated channels with forced convection are the flow excursion and density wave oscillation types.

The flow excursion or Ledinegg instability occurs when the slope of the channel demand pressure drop-flow rate curve becomes algebraically smaller than or equal to the slope of the loop supply pressure drop-flow rate curve. The typical demand pressure drop-flow rate curves for subcooled boiling of water are shown in Fig. A5 (from Ref. 34). With channel power input S_2, operation at point d is stable, while operation at point b is unstable since a slight decrease in flow rate will cause a spontaneous shift to point a.

For a given system, there is a channel power input S_c (Fig. A5) such that the demand curve is tangent to the supply curve. The conditions at the tangent point c correspond to the threshold conditions for the flow excursive instability: any slight increase in power input or decrease in flow rate will cause the operating point to spontaneously shift from point c to point a, and the flow rate drops abruptly from M to M_c.

For research and test reactors using plate-type fuel, each channel is surrounded by many channels in parallel. The supply characteristic with respect to flow perturbations in a channel (say, the peak power channel) is essentially horizontal, and independent of the pump characteristics. Thus, the criterion of zero slope of the channel demand pressure drop-flow curve is a good approximation for assessing the onset of the excursive flow instability, i.e.,

$$\frac{\partial(\Delta P)_{\text{channel}}}{\partial G} = 0 \qquad (18)$$

Functionally, the channel pressure drop-flow curve depends on the channel geometry, inlet and exit resistances, flow direction, subcooled vapor void fraction, and heat flux distribution along the channel.

FIGURE A5

Typical pressure drop curves in heated channel (from Reference 34)

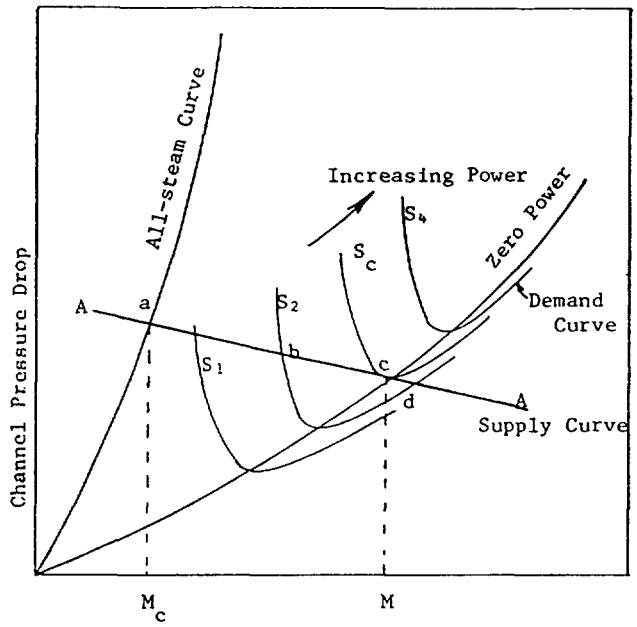

FIGURE A6

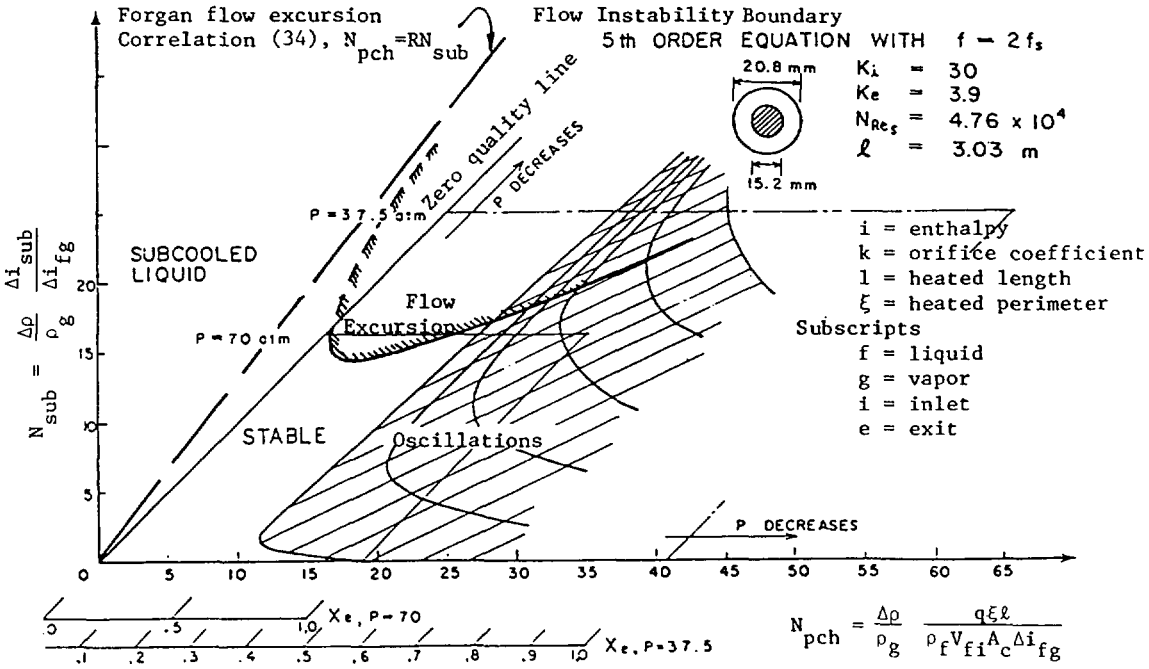

Density wave oscillations are low-frequency oscillations in which the period is approximately the order of magnitude of the time required for a density wave to travel through the channel. Inlet flow perturbations in a heated channel will result in delayed mixture-density changes throughout the channel. These disturbances in the mixture-density affect the local mixture velocity and the pressure drop in a channel. Under certain conditions, the inlet flow perturbations satisfy a self-exciting relation such that sustained oscillations with considerable amplitudes appear in the system.

By applying a small perturbation on the inlet velocity, Ishii[35,36] solved the linearized system equations for the stability boundary and reported results that are in good agreement with experimental data. A typical flow instability boundary from Ref. 35 is shown in Fig. A6. A similiar flow instability diagram is also reported in Ref. 37.

In Ishii's model, the dynamic effects of the system pressure are characterized by the density ratio (η /η_g), and it has been concluded that the extent of the system pressure effects in the stability plane is quite limited.

As shown in Fig. A6, there is a critical value for the inlet subcooling ($N_{sub} \approx 14$ for the system in Fig. A6) below which flow instability is due to the density wave oscillations only, and no flow excursion will occur. For a high pressure system, this critical subcooling value corresponds to a very low inlet temperature. However, for a low pressure system, this critical subcooling value corresponds to a high inlet temperature (e.g., about 95°C at 1 atm) very close to the saturation temperature.

For most research and test reactors, the steady-state operating system pressure is low and the inlet coolant temperature is much lower than the saturation temperature. It can be concluded from the stability boundary diagram (Fig. A6) that, (1) flow excursion will occur for a given flow rate at a high enough heat flux, and (2) density wave oscillations will not occur under normal operating conditions.

A.1.3.6.2 Prediction of Flow Excursion

The criterion for the onset of flow excursion is given by Eq. 18. The pressure drop across the channel depends on the flow rate, inlet and exit resistances, flow direction, subcooled vapor fraction, and heat flux distribution. Analytical modelling of the flow excursion requires knowledge of the pressure drop dependence on subcooled void fraction as well as the heat transfer coefficient for subcooled boiling. The accuracy of the prediction of flow excursion based on Eq. 18 therefore depends on the accuracy of the correlations (subcooled void fraction, pressure drop, and heat transfer coefficient) applicable to the given system pressure and channel geometry. Equation 18 can be applied either analytically or empirically. The analytical approach models the variables making up pressure and mass flow rate using experimentally determined correlations which were developed for general use. Since these correlations (usually high pressure) may not be as accurate when applied to research reactor conditions, and since their accuracy suffers further upon differentiation, highly accurate analytical models for prediction of the onset of flow instability cannot be expected at the present time. The empirical approach simply measures pressure and mass flow parameters and locates the Eq. 18 condition directly.

Empirical Correlations

Whittle and Forgan [34] measured the mass flow, exit temperature, and pressure drop corresponding to the minima in the pressure drop versus flow rate curves for subcooled water flowing (upward and downward) in narrow heated channels (width 2.54 cm, thickness 0.14 to 0.32 cm, length 40 to 61 cm) under the following conditions:

$$17 < P_{exit} < 25 \text{ psia}$$

$$83 < \frac{L_H}{D_H} < 190$$

where

L_H = heated length of channel

D_H = heated equivalent diameter of channel

$$= 4 \times \frac{\text{Channel Flow Area}}{\text{Channel Heated Perimeter}} = 2\, t_w\, W/(t_w + W_H)$$

Based on these measurements the following correlation was proposed:

$$R = \frac{T_{out}-T_{in}}{T_{sat}-T_{in}} = \frac{1}{1+\eta \frac{D_H}{L_H}} \qquad (19)$$

A value of $\eta = 25$ was determined as a best fit to their data. Further discussion of η is provided in the next subsection on bubble detachment and flow instability. The average heat flux at onset of flow instability can be expressed in terms of velocity, channel geometry, temperatures, and fluid properties:

$$\bar{q}_c = R\, \rho\, C_p \frac{W\, t_w}{W_H\, L_H} U\, (T_{sat} - T_{in}) \qquad (20)$$

The peak critical heat flux can be obtained by multiplying $\bar{q}_c$ by the axial peak-to-average factor, f_a.

In order to clarify the use of Eq. 19, we note the following:

1. The effect of channel entrance losses, which is a strong stabilizing factor[35] for the system, is not included in the correlation. Thus, the system could be more stable than the correlation predicts.
2. Since pressure drop characteristics are not required, the accuracy of the prediction does not depend on two-phase correlations (subcooled void fraction, pressure drop, and heat transfer coefficient). All two-phase effects are included in the parameter η.
3. The phenomenon is sensitive to system pressure through the saturation temperature, T_{sat}.
4. The scatter in the Maulbetch and Griffith data[33] used by Forgan and Whittle to extend their correlation to lower ratios of L_H/D_H increases to about ± 30% at $L_H/D_H \sim 25$.

As an example of how flow instability data can be specialized, Winkler[38] examined data by Forgan and Whittle[39] and burnout experiments on an MTR fuel mockup by Fried, Hofmann and Peterson.[40] Equation 21 is Winkler's expression for the average heat flux at onset of flow instability. It is applicable over a limited range: U(0.5 - 6 m/s), T_{in}(10 - 65°C), for exit pressures from 1.2 to 1.5 bar absolute.

$$\bar{q}_c = - 29.35 + (128.15 - 1.104\ T_{in})\ U^{0.8} \qquad (21)$$

The experimental data and fits[38] using Eq. 21 are shown in Fig. A7. As suggested by Allen,[41] this data can be reduced further based on the form of Eq. 20 if the average heat flux is plotted against $U(T_{sat} - T_{in})$. The result is shown in Fig. A8 for a saturation temperature of 108°C, which corresponds to an exit pressure of 1.35 bar absolute.

It is also interesting to note that the Forgan correlation (Eq. 19) can be expressed in terms of the non-dimensional parameters used in Ref. 35. The result is a straight line in the stability plane and is shown in Fig. A6 for illustrative comparison.

Bubble Detachment and Flow Instability

Flow instability cannot occur in single-phase flow except through flow-induced vibrations or deformations. In two-phase flow, the presence of saturated water vapor in the form of bubbles provides a new mechanism which affects the flow rate-pressure drop relationship in a complex manner. Slip flow indicates the existence of different velocities associated with the liquid and vapor phases.

As the power supplied to a coolant channel is increased, bubbles will be formed (sub-cooled boiling) first as small bubbles, then of larger sizes. The larger bubbles eventually restrict the channel cross-section, and force the liquid phase to accelerate in order to maintain the same mass flux down the channel. This acceleration, in turn, leads to an increased pressure drop - which restricts flow further, enhancing the flow blockage. These phenomena are divergent and oscillatory under appropriate conditions, and associate bubble size or void fraction with the onset of flow instability. Whittle and Forgan[34,39] were the first to explore this connection. In Eq. 19, η is their bubble detachment parameter. A literature survey by Essler and Kreyger[42] reported values for η ranging from 12 to 37. Figure A9, adapted from Ref. 42, shows experimental test data, together with predictions of R for various η values. Selection of the value of η requires engineering judgement.

Axial Heat Flux Distributions

Flow instability is intimately related to pressure drop. The pressure drop depends on the local water quality, which follows from the axial heat flux distribution. Consequently some dependence on the axial heat flux distribution may be expected, despite the fact that the exit quality will be the same for a given power input. Investigations of this relationship have been carried out both experimentally and theoretically.

The influence of the axial heat flux distribution on the onset of flow excursion was investigated experimentally by Forgan,[34] Croft,[43] Waters,[44] and Courtand et al.[48] The axial heat flux distributions tested included uniform, chopped cosine, and ramp at the channel exit. It was reported that the possible effects are small and within the range of the experimental data.

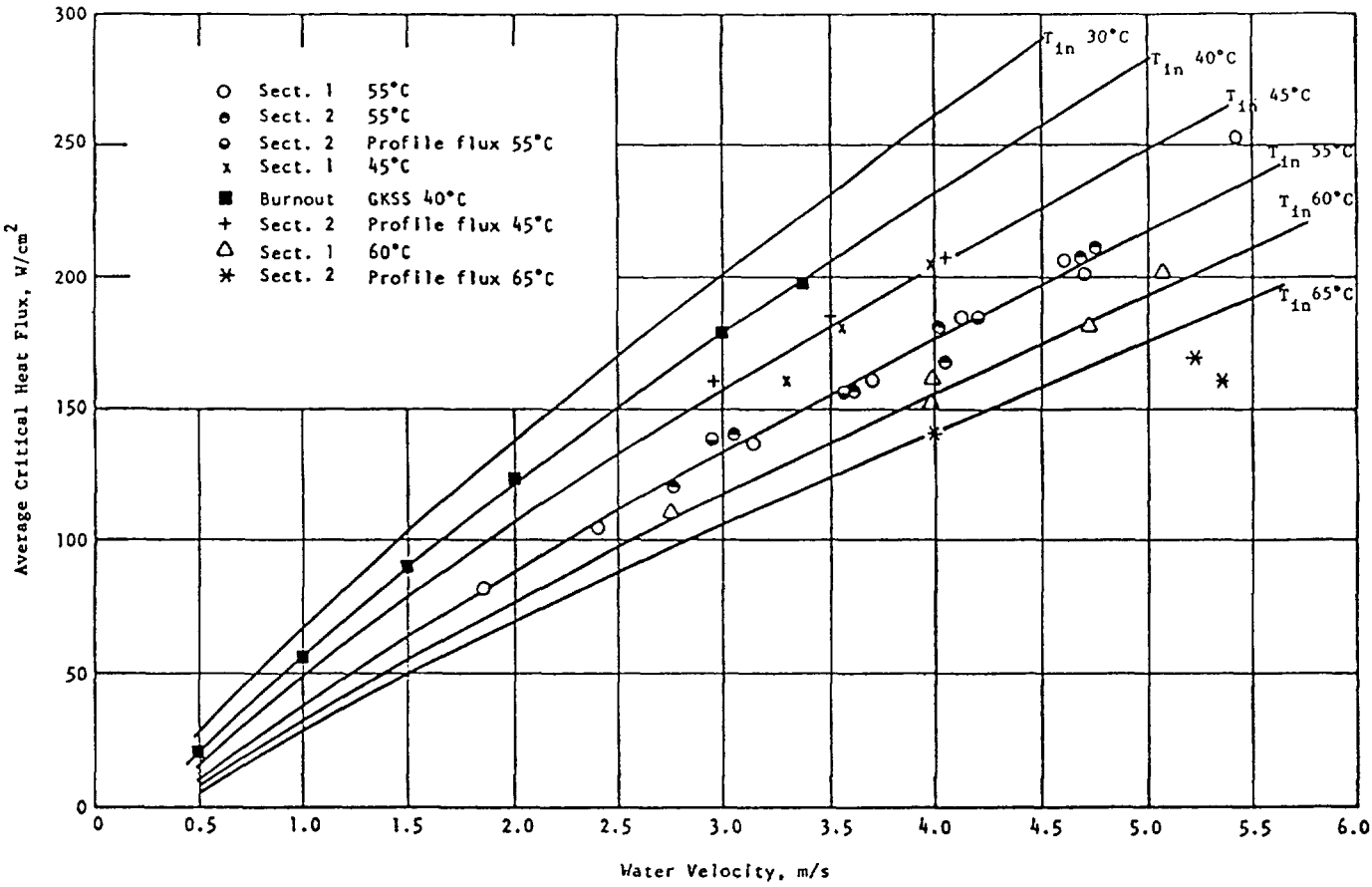

Figure A7. Average Critical Heat Flux at Onset of Flow Instability versus Water Velocity (from Ref. 38). The Channel Geometry of Sections 1 and 2 is 61 cm Long x 2.54 cm Wide x 0.323 cm Thick.

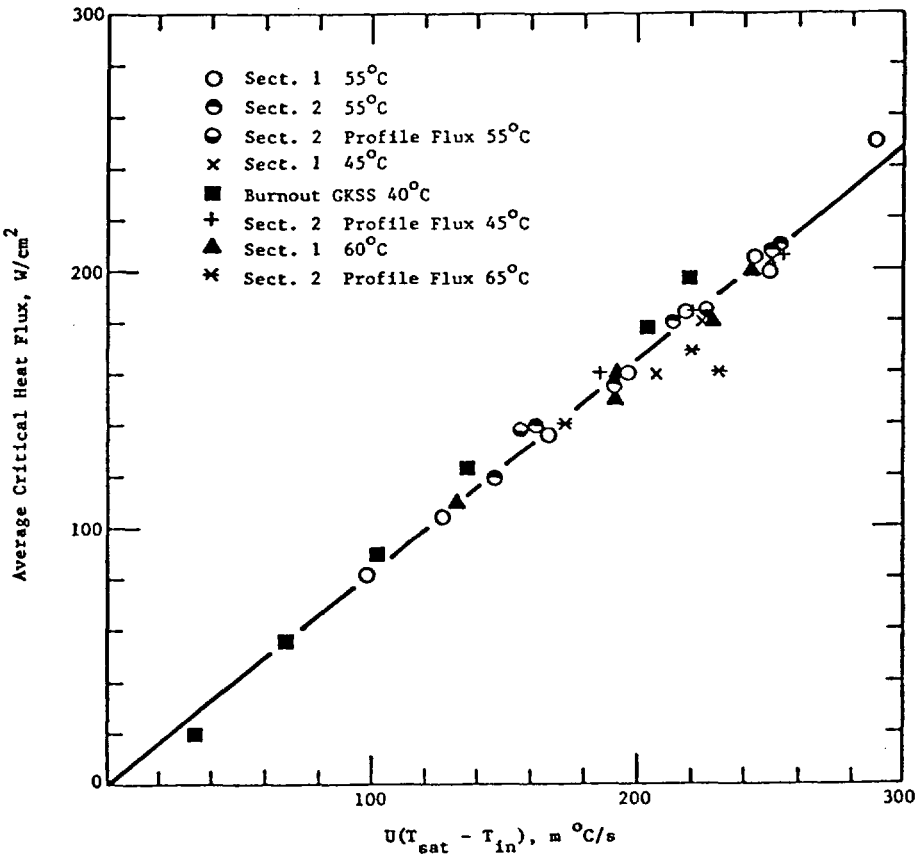

Figure A8. Average Critical Heat Flux at Onset of Flow Instability vs. $U(T_{sat}-T_{in})$ (Ref. 41). The Data Plotted are those of Fig. A7.

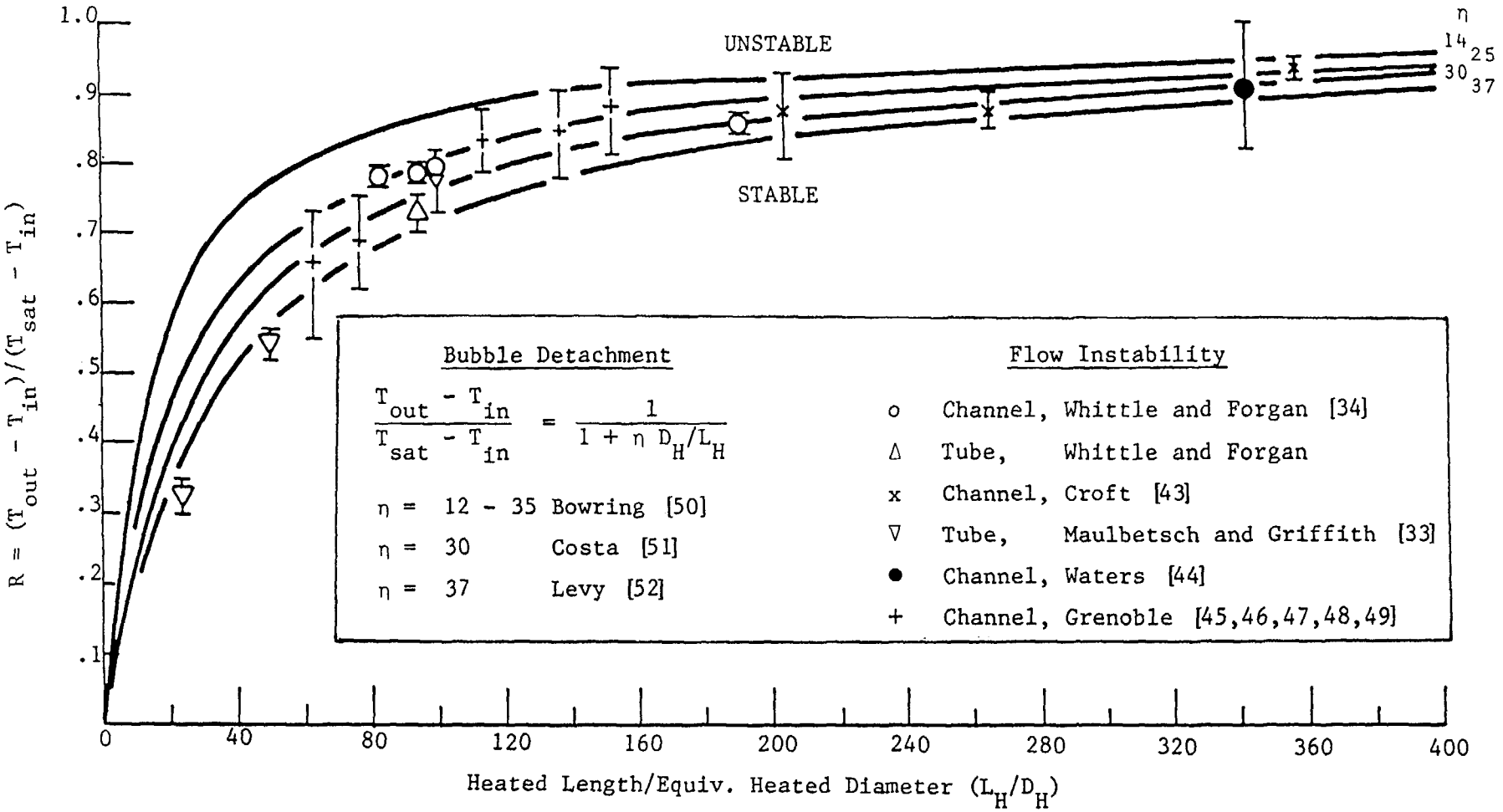

Figure A9. Correlation for Flow Instability and Bubble Detachment

For a heat flux profile which is skewed towards the exit and has a local value at the exit higher than the average, Essler and Kreyger[42] studied the effects theoretically using the criterion for bubble detachment. The limiting heat load so calculated is lower than that calculated using Eq. 20. The difference depends on the ratio of the local heat flux at the exit to the average heat flux and is about 10% for a ratio of 1.4. However, for a normal chopped cosine distribution, the limiting heat load calculated by this approach will be about 8 to 10% higher than that from Eq. 20.

A.1.3.7 A Review of DNB Correlations Applicable to Research and Test Reactor Conditions

For reactor design purposes, acceptable data on burnout heat flux are needed since departure from nucleate boiling (DNB) is potentially a limiting design constraint. Optimization of core cooling against other neutronic, economic, and materials constraints can best be accomplished by judicious use of standard, experimentally-deduced DNB correlations. The purpose of this review of critical heat flux measurements and DNB correlations is to provide a basis for analysis of thermal-hydraulic design constraints and to compare some of the correlations applicable to research and test reactors.

A literature survey of DNB correlations applicable to low pressure plate-type research and test reactors found that DNB data for rectangular channel flow in the low pressure range are very limited. Five round tube DNB correlations (Lowdermilk,[53] Macbeth,[54,55] Labuntsov,[56] Thorgerson,[57] and Katto[59,60]) and one narrow channel DNB correlation (Mirshak[61]) applicable in the low pressure range are reviewed. These correlations, together with their ranges of applicability, are summarized in Fig. A10.

The DNB Correlations

The Lowdermilk correlation[53] covers a wide range of inlet velocities and ratios of channel length to diameter. However, it is applicable only for atmospheric exit pressure and an inlet water temperature of 24°C. Test results[53] showed that the burnout heat flux was decreased by as much as 20% for an increase in inlet water temperature from 21°C to 100°C, and increased by approximately 15% for an increase in exit pressure from atmospheric pressure to 7 bars.

The Macbeth correlations[54,55] are divided into low-velocity and high-velocity burnout regimes. The boundary between these regimes depends on the system pressure and the L/D ratio. For research and test reactor conditions (P = 1-4 bar absolute, L_H/D_H = 75-150), the regime boundary in terms of coolant velocity is approximately 0.06 to 0.11 m/s. In the low-velocity regime, a correlation was derived based on burnout heat fluxes for a wide range of pressures. In the high velocity-regime, separate correlations were derived for each of eight distinct pressure groups (1.03, 17.2, 38.6, 70.0, 86.2, 106.9, 124.1, and 138.0 bar absolute) since the effect of pressure on burnout heat flux is complex. Data in the high pressure groups are more extensive than those in the low pressure groups. The high-velocity correlation for the data group at 1.03 bar absolute, which is the most applicable correlation for research reactor conditions, was developed using 65 data points from experiments performed by Lowdermilk and Weiland[62] and 23 points from other experiments. In a later experiment by Lowdermilk, Lanzo, and Siegel[53], it was found that the data of Ref. 62 were probably influenced by the presence of nitrogen dissolved in the test water and the arrangement of the apparatus, and are about 25-85% lower than the data of Ref. 53.

Figure A10. Five Round Tube DNB Correlations (a-e) and One Narrow Channel DNB Correlation (f) Applicable to Research and Test Reactor Conditions

a.) The Lowdermilk et al Correlation[53]

Low-Velocity High-Quality Region

$$1 < \frac{737.3\ G}{(L/D)^2} < 150^{*} : q_c = \frac{46.2\ G^{0.85}}{D^{0.2}\ (L/D)^{0.85}}$$

High-Velocity Low-Quality Region

$$150 < \frac{737.3\ G}{(L/D)^2} < 10{,}000 : q_c = \frac{23.75\ G^{0.5}}{D^{0.2}\ (L/D)^{0.15}}$$

* L = channel length, cm D = diameter, cm

Parameter Ranges

Steam Quality	:	positive
Diameter	:	0.130 - 0.478 cm
L/D	:	25 - 250
Velocity	:	0.03 - 30 m/s
Pressure	:	atmospheric
Inlet Water Temp.	:	~24°C
q_c	:	284 - 4164 W/cm^2

b.) The Macbeth Correlation[54,55]

Low-Velocity Regime

$$q_c = \frac{0.1\ G\ (\lambda + \Delta hi)}{4.2\ D^{0.1}\ G^{0.49} + 4(L/D)}\ ^{**}$$

Parameter Ranges

Steam Quality	:	positive
Diameter	:	0.3 - 1.0 cm
Length	:	15 - 312 cm
Mass Flux	:	13.6 - 841 kg/m^{2}s
Pressure	:	1 - 138 bar absolute
Δhi	:	65 -1400 kJ/kg

** Δhi = subcooled enthalpy at channel inlet, kJ/kg

High-Velocity Regime

$$q_c = \frac{5.953\ D^{1.19}\ G^{1.37} + 0.00984\ DG\ \Delta hi}{0.1394\ D^{1.4}\ G^{1.05} + 0.3937\ L}$$

Parameter Ranges

Steam Quality	:	positive
Diameter	:	0.1 - 2.39 cm
Length	:	2.54 - 86 cm
L/D	:	8.5 - 50
Mass Flux	:	14 - 5750 kg/m^{2}s
Pressure	:	1.03 bar absolute

c.) The Labuntsov Correlation[56]

$$q_c = 145.4\ \theta(P)\ [1 + 2.5\ U^2/\theta(P)]^{1/4}$$
$$(1 + 15.1\ C_p\ \Delta T_{sub}/\lambda P^{1/2})$$
$$\theta(P) = 0.99531\ P^{1/3}\ (1 - P/P_c)^{4/3}$$
$$\Delta T_{sub} = T_{sat} - T_{in} - \Delta T_c$$

Parameter Ranges

Steam Quality	:	negative - 0
Velocity	:	0.7 - 45 m/s
Pressure	:	1 - 200 bar absolute
Subcooling (ΔT_{sub})	:	0 - 240°C
q_c	:	116 - 5234 W/cm^2

d.) The Thorgerson et al Correlation[57]

$$q_c = 0.05\ \frac{7.413}{R_e^{0.545}}\ \rho\ C_p\ U\ (T_w - T_b)$$

The wall temperature T_w is calculated by the Weatherhead correlation[58]

$$T_w = T_{sat} + 0.133\ (47.7 - 0.127\ T_{sat})\ q_c^{1/4}$$

T_b = bulk coolant temperature, °C

Parameter Ranges

Steam Quality	:	negative
Velocity	:	3.05 - 18.3 m/s
Pressure	:	1.7 - 13.3 bar absolute
Subcooling	:	greater than 25°C

Figure A10. Five Round Tube DNB Correlations (a-e) and One Narrow Channel DNB Correlation (f) Applicable to Research and Test Reactor Conditions (Cont.)

e.) The Katto Correlation[59,60]

The following non-dimensional group are defined here and used in the correlation:

$$C_1 = \frac{q_{co}}{0.1\ G\lambda} \qquad C_3 = \frac{\rho_v}{\rho_\ell}$$

$$C_2 = \frac{\sigma\ \rho_\ell}{0.01\ G^2 L} \qquad C_4 = \frac{L}{D}$$

q_{co} = critical heat flux for $\Delta hi = 0$, W/cm^2

σ = surface tension, N/m

ρ_ℓ = density of liquid, kg/m^3

ρ_v = density of vapor, kg/m^3

Prediction of Critical Heat Flux q_{co} at $\Delta hi = 0$

L - Regime

$$C_1 = C C_2^{0.043}\ \frac{1}{C_4}$$

$C = 0.25$ for $C_2 > 5 \times 10^{-4}$

$C = 0.34$ for $C_2 < 5 \times 10^{-4}$

H - Regime

$$C_1 = 0.1\ C_2^{0.333}\ C_3^{0.133}\ \frac{1}{1 + 0.0031\ C_4}$$

N - Regime

$$C_1 = 0.098\ C_2^{0.433}\ C_3^{0.133}\ \frac{C_4^{0.27}}{1 + 0.0031\ C_4}$$

HP - Regime

$$C_1 = 8.2\ C_2^{0.453}\ C_3^{0.65}\ \frac{1}{1 + 107\ C_2^{0.54}\ C_4}$$

Boundaries of Each Regime

L - and H - Regime

$$\frac{L}{D} = \frac{1}{0.1\ C_3^{0.133}\ C_2^{0.29}/C - 0.0031}$$

H - and N - Regime

$$\frac{L}{D} = \frac{0.77}{C_2^{0.37}}$$

H - and HP - Regime

$$\frac{L}{D} = \frac{82\ C_3^{0.517} - C_2^{-0.12}}{107\ C_2^{0.42} - 0.254\ C_3^{0.517}}$$

Prediction of Critical Heat Flux q_c for $\Delta hi > 0$

For L -, H -, and HP - Regime, q_c can be predicted by

$$q_c = q_{co}\ (1 + \kappa \frac{\Delta\ hi}{\lambda})$$

κ in L - Regime : $\kappa_L = 1$

κ in H - Regime :

$$\kappa_H = 1.8\ (\frac{130}{C_4})^{5C_3} \text{ for } C_2 < 3 \times 10^{-6}$$

$$\kappa_H = 0.075\ (\frac{130}{C_4})^{5C_3}\ C_2^{-0.25} \text{ for } C_2 > 3 \times 10^{-6}$$

κ in HP - Regime :

$$\kappa_{HP} = 0.664\ C_3^{-0.6} \text{ for } C_2 < 4 \times 10^{-8}$$

$$\kappa_{HP} = 3.08\ C_2^{0.09}\ C_3^{-0.6} \text{ for } C_2 > 4 \times 10^{-8}$$

Parameter Ranges

Steam Quality : negative - positive

L/D : 26 - 500

Pressure : 1 - 200 bar absolute

f.) The Mirshak Correlation[61]

$$q_c = 151.\ (1 + 0.1198\ U)\ (1 + 0.00914\ \Delta T_{sub})\ (1 + 0.19\ P)$$

q_c = critical heat flux, W/cm^2

U = coolant velocity, m/s

ΔT_{sub} = exit water subcooling, °C

P = pressure, bar absolute

Parameter Ranges

Steam Quality	: negative
Velocity	: 1.5 - 13.7 m/s
Subcooling (ΔT_{sub})	: 5 - 75°C
Pressure	: 1.72 - 5.86 bar absolute
Equivalent Diameter	: 0.53 - 1.17 cm
q_c	: 284 - 1022 W/cm^2

The Labuntsov correlation[56] is based on experimental data from several sources. These data cover a wide range of velocity and pressure, but all have positive subcooling at the channel exit. Labuntsov observed that the burnout heat fluxes are determined by the pressure, coolant velocity, and the magnitude of subcooling at exit and that these fluxes are virtually independent of the length, diameter, and configuration of the operating channel. The effect of channel dimensions becomes pronounced only for diameters that are less than 2 mm.

The Thorgerson et al correlation[57] was developed by using the Reynolds analogy, which relates the heat transfer coefficient and the friction factor, and a friction factor correlation based on pressure drop measurements at burnout. The reported agreement between the predicted and measured burnout heat fluxes on round tubes cooled by forced downward flow of water is generally within $\pm$ 20 percent. This DNB correlation is not applicable for exit subcooling less than 25°C, where the acceleration effects due to significant void formation become more important and the friction factor correlation is outside the range of nominal applicability.

The Katto correlation,[59,60] developed with the aid of vectorial dimensional analysis, correlates experimental data obtained from the literature for seven fluids over a wide range of test conditions. Katto[59] reported that the data of Lowdermilk, Lanzo, and Siegel[53] agree well with the predictions of his correlation.

The Mirshak correlation[61] is based on data from annular channels (with heated tube diameters of 1.27 cm and 2.03 cm) and rectangular channels (with channel width of 6.40 cm, heated strip width of 5.08 cm, channel thickness from 0.3 to 0.58 cm). For both test sections, only one side of the channel was heated. All data correlated have positive subcooling at the channel exit.

Brief Remarks on the Correlations

Except for the Labuntsov correlation, which is independent of channel geometry, the round tube correlations have an explicit dependence on tube diameter (D). When applying these correlations to rectangular channels, the burnout heat fluxes can be estimated by substituting a heated equivalent diameter (4 x flow area/heated perimeter) for the tube diameter (for lack of a better alternative). This approach has been tested by Macbeth,[55] who compared his high-pressure, high-velocity, round tube correlation (not shown in Fig. A10) at 138 bar absolute (2000 psia) with rectangular channel DNB data and found a root-mean-square error of 18.5%. A comparable test using data at low pressures has not been found.

All of the DNB correlations reviewed above are based on data from uniformly heated channels. In a reactor situation, however, the heat flux varies along the length of a channel. One result of nonuniform heating is that burnout does not always occur at the channel exit as it does with uniform heating, provided instabilities are avoided. For high pressure data (38.6 - 138 bar absolute), the burnout heat flux for any heat flux profile can be related to that for a uniform profile under the same conditions by using the empirical method summarized in Ref. 63. However, a corresponding set of empirical values are not available for lower pressures. For lack of a better alternative, one can conservatively assume that the burnout heat flux predicted by the uniform-profile correlations is equal to the peak (maximum) heat flux in a channel with a non-uniform profile. For correlations which depend on water subcooling (i.e., lower burnout heat flux for lower subcooling), one can further conservatively assume that DNB occurs at the channel exit, where the water subcooling is the lowest.

In both the Labuntsov and Mirshak correlations, the burnout heat flux depends on the water subcooling. From an energy balance for a rectangular channel, the water subcooling can be expressed as a function of channel heat flux, channel geometry, coolant velocity, and coolant properties:

$$\Delta T_{sub} = T_{sat} - T_{in} - \Delta T_c$$

$$= (T_{sat} - T_{in}) - \frac{20\ H_{co}\ W_H\ q_c}{\rho\ C_p\ t_w\ W\ f_a\ U} \quad .$$

By substituting this expression into the Labuntsov and Mirshak correlations, the burnout heat flux can be derived as a function of coolant velocity for a given inlet water temperature, system pressure, and channel geometry.

The literature reviewed here indicates that DNB is a complex phenomenon even for a simple channel geometry. The burnout heat flux depends on a number of variables, such as pressure, channel geometry, coolant velocity, and coolant inlet or exit conditions. The experimental data from which the above correlations were developed are scattered in the space of DNB dependent variables. For example, some data are in the positive subcooling region while others are in the positive steam quality region; some data are limited to only one system pressure and/or one inlet water temperature. So far, a complete data set, which is applicable to plate-type fuel channels and covers the low pressure range and exit conditions from positive subcooling to positive steam quality, has not been found. Consequently, engineering judgement and caution are required in using the above DNB correlations to estimate the burnout heat flux in plate-type fuel channels, especially when the applied conditions are outside the ranges of nominal applicability of the correlations.

Comparison of Round Tube DNB Correlations

To study the physical trend of burnout heat flux predictions using the different round tube correlations, burnout heat fluxes versus inlet coolant velocity were calculated using these correlations for an exit pressure of 1.66 bar absolute, an inlet water temperature of 48.8°C, a channel length of 61 cm, and tube diameters ranging from 0.508 cm to 1.27 cm. The round tubes were uniformly heated. The results of the calculations are shown in Figs. A11 to A14.

As shown in these figures, the burnout heat flux calculated using the Macbeth high-velocity correlation decreases as the tube diameter increases. This trend appears to be incorrect because it contradicts the effect of tube diameter on the burnout heat flux[54] at high pressures. This poor prediction can be attributed to the questionable data base from which the Macbeth high-velocity correlation at 1.03 bar absolute was derived, as pointed out earlier. The predictions using the Lowdermilk correlation also decrease slightly with increasing tube diameter. This effect could be due to the large extrapolation of the applicable inlet water temperature of 24°C to 48.8°C.

The burnout heat flux predicted by the Katto correlation increases consistently with the tube diameter, as expected in the case of high pressure burnout data. For tube diameters less than 0.762 cm, predictions by the Katto correlation are about 4% (low velocities) to 50% (high velocities) lower than those by the Macbeth and Lowdermilk correlations.

Figure All to A14. Comparison of Peak Critical Heat Fluxes versus Coolant Velocity from Different Round Tube DNB Correlations for Various Tube Diameters (D) and L = 61 cm, T_{in} = 48.8°C, P = 1.66 bar absolute.

Figure All. D = 0.508 cm

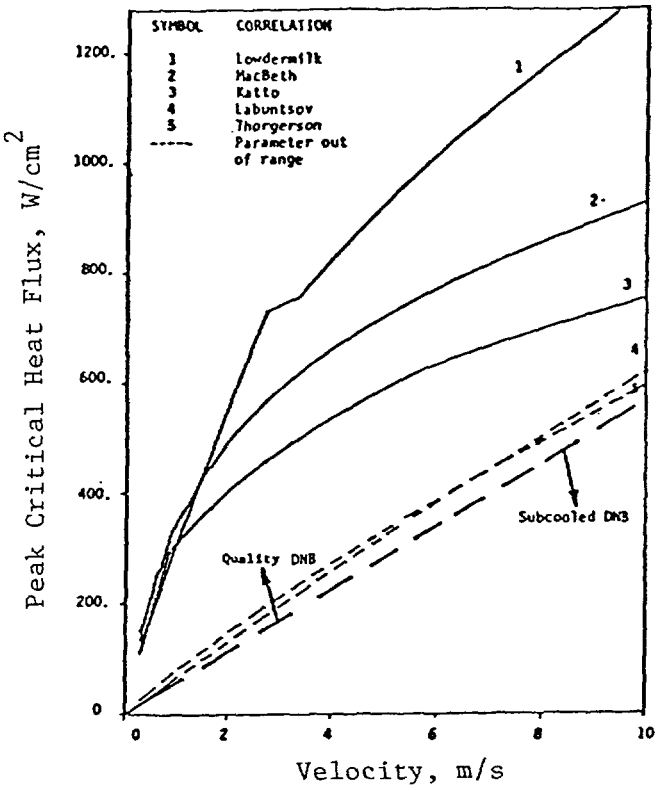

Figure A12. D = 0.762 cm

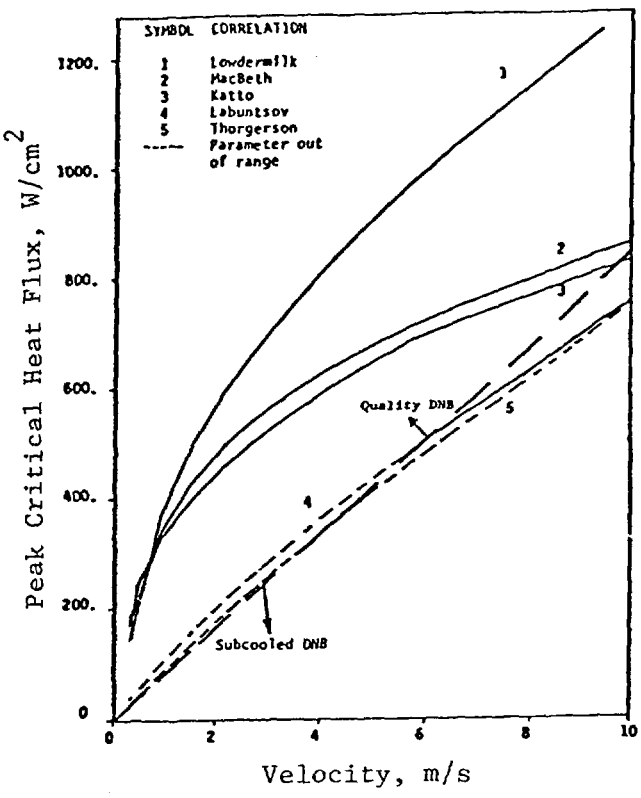

Figure A13. D = 1.016 cm

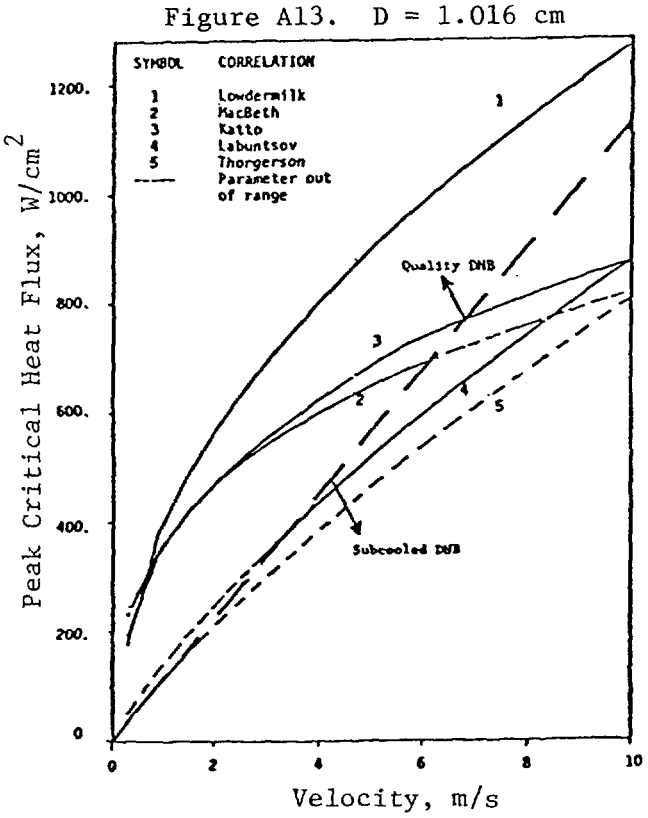

Figure A14. D = 1.27 cm

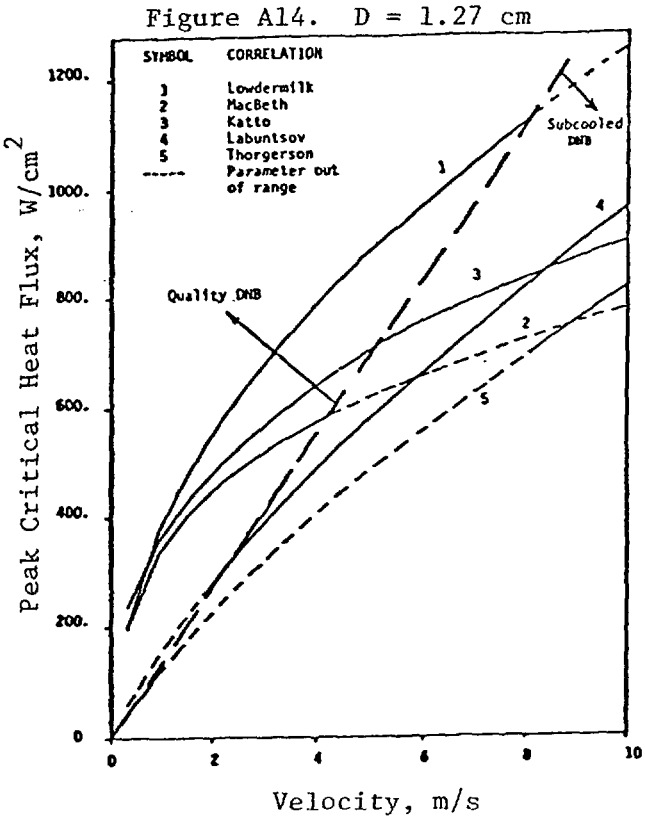

For a tube diameter of 0.508 cm, both the Labuntsov and the Thorgerson correlations are not strictly applicable for the range of coolant velocities shown in Fig. A11, because the calculated heat fluxes indicate that the coolant temperature at the burnout location is not below the local saturation temperature.

For larger tube diameters of 0.762 and 1.016 cm and velocities higher than 4.6 m/s, the Labuntsov and the Thorgerson correlations predict burnout heat fluxes at subcooled conditions. The results using these two correlations are in farily good agreement, as shown in Figs. A12 and A13. However, a close look at the bulk coolant temperature at the burnout location found that the subcooling predicted by the Thorgerson correlation was smaller than the applicable lower limit of 25°C. This indicates that the burnout heat fluxes calculated using the Thorgerson correlation for these conditions are extrapolations beyond the proper range of applicability.

For a tube diameter of 1.27 cm, the Thorgerson correlation predicts a subcooling in excess of 20°C for velocities greater than 8.2 m/s. For this velocity range the critical heat flux calculated using the Katto correlation is intermediate between those calculated using the Thorgerson and Labuntsov correlations. All three predictions are shown in Fig. A14 and agree to within 20%.

From the comparisons shown in Figs. A11 to A14, it appears that the Labuntsov correlation yields a much lower estimate of the burnout heat flux than is given by the other round tube correlations for the range of conditions of interest in research reactors. Further detailed comparisons of the Labuntsov and the Mirshak correlations are given in the next section and in Fig. A15.

Comparison of the Mirshak and Labuntsov DNB Correlations

The physical trends of the burnout heat fluxes predicted by the Mirshak (narrow channel) correlation and the Labuntsov correlation were investigated by using these correlations to calculate burnout heat fluxes versus inlet coolant velocity for a plate-type fuel channel with t_w = 0.2916 cm, P = 1.961 bar absolute pressure, and f_a = 1.58 (reference values for the 2 MW reactor to be discussed in Section A.2; other parameters are listed in Table A21).

Results of these calculations are shown in Fig. A15. At coolant velocities between 3 m/s and 5 m/s, where exit subcoolings are positive, the burnout heat fluxes predicted using the Mirshak correlation are about 20 to 25% lower than those predicted using the Labuntsov correlation. The difference becomes smaller at lower coolant velocities.

As shown in Fig. A15, the degree of subcooling decreases as the coolant velocity decreases. For this case, calculations using the Labuntsov and Mirshak correlations show that negative subcooling starts to occur at a coolant velocity of 2.52 m/s for the Labuntsov correlation and 1.86 m/s for the Mirshak correlation. Strictly speaking, these correlations are not applicable when the coolant velocity is less than the value corresponding to negative subcooling.

Figure A15. Comparison of Peak Critical Heat Fluxes from Different Correlations for Reserach Reactor Conditions

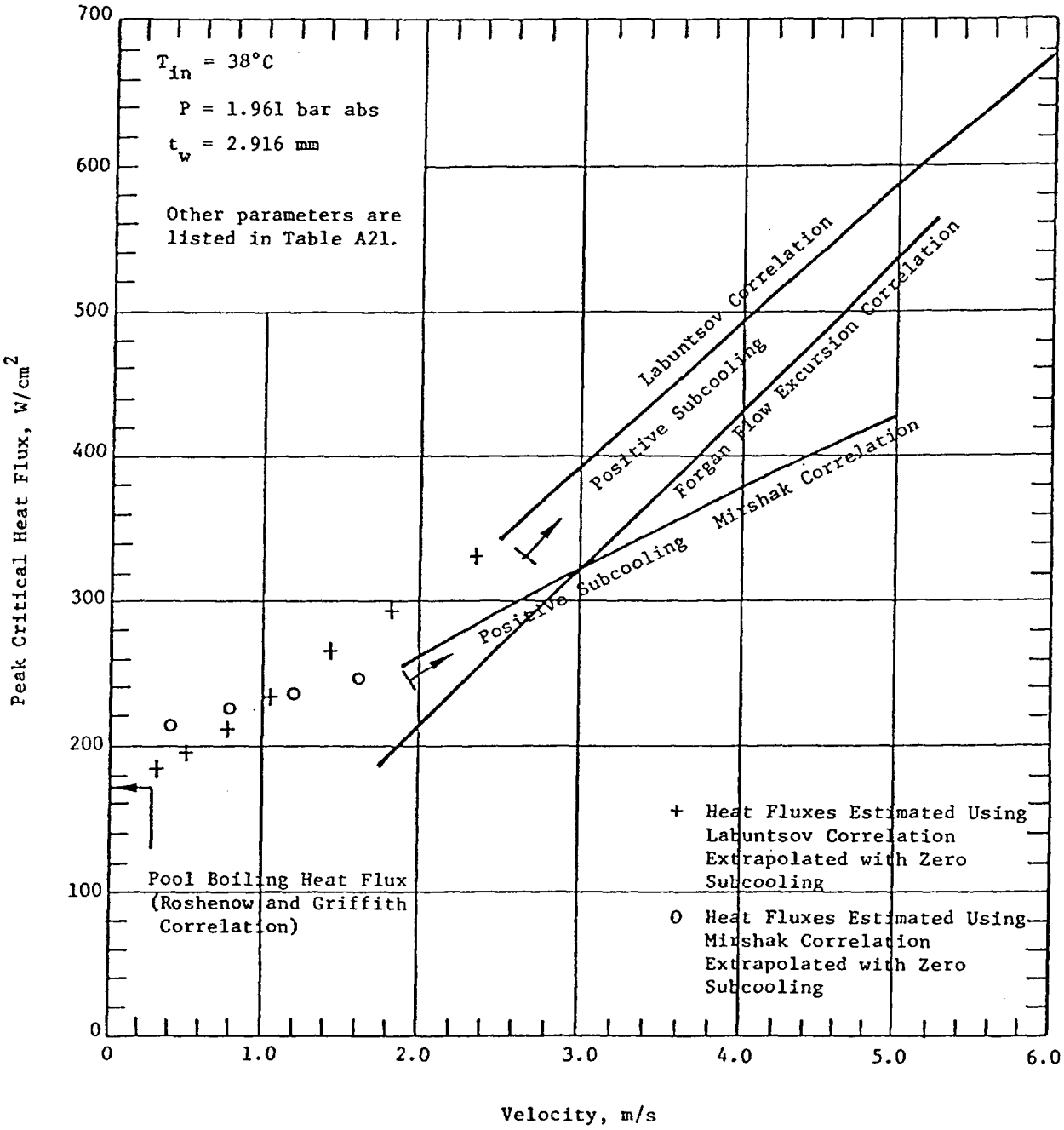

Extrapolation of the Labuntsov and Mirshak Correlations with Zero Subcooling at Low Velocities

For very low coolent velocities, the lower limit of burnout heat flux can be estimated from the pool boiling case. The pool boiling peak heat flux, as given by the Rohsenow and Griffith correlation,[64] is as follows:

$$q_{c,\text{pool boiling}} = 1.21 \times 10^{-3}\ \rho_v \lambda \left(\frac{\rho_\ell - \rho_v}{\rho_v} \right)^{0.6} \quad (23)$$

where ρ_ℓ and ρ_v are the liquid and steam densities, respectively, and λ is the heat of vaporization.

For P = 1.961 bar absolute, the pool boiling peak heat flux is estimated to be 169 W/cm^2.

For the low coolant velocity region at which subcooling is negative, the burnout heat flux can be estimated by using the Labuntsov and Mirshak correlations extrapolated with zero subcooling. Results of these extrapolations are shown in Fig. A15, where the lower limits of the burnout heat fluxes agree well with that of pool boiling.

Based on this comparison, it can be concluded that at the low coolant velocities for which the exit subcooling is negative, burnout heat fluxes can be reasonably estimated by using the Labuntsov and the Mirshak correlations extrapolated with zero subcooling.

A.1.3.8 Comparison of the Burnout Correlations and the Flow Instability Correlation with Experiment

The limiting heat fluxes at onset of flow instability were calculated using the Forgan correlation for the same conditions as for the plate-type fuel channel shown in Fig. A15. These results are also shown in Fig. A15 for comparison. At velocities less than 2 m/s, the limiting heat flux predicted by the Forgan correlation is generally much lower than the burnout heat fluxes estimated using the Labuntsov and the Mirshak DNB correlations.

However, for velocities greater than 3 m/s, the burnout heat flux predicted by the Mirshak correlation is lower than the limiting heat flux predicted by the Forgan flow excursion correlation. This is not a general conclusion, of course, since initial heat fluxes depend on channel geometry, exit pressure, inlet temperature, and coolant velocity. Thus, the location of the intersection of these curves will depend on these parameters. As an example, for P = 1.2 bar absolute pressure and T_{in} = 55°C (with other parameters being the same as those used in Fig. A15), the curves will intersect at a coolant velocity of 4.75 m/s.

Further comparisons between the Mirshak correlation and the Whittle and Forgan experimental data[34] are shown in Figs. A16 and A17. The pressure drop versus flow rate curves were obtained by reducing the flow rate step by step while holding the power input constant. The flow rate was never reduced below that corresponding to net boiling at the test section outlet or when a hot-spot was detected. In other words, for a given heat flux, burnout was not observed in the flow rate ranges shown in these figures. However, using the Mirshak correlation, burnout is predicted at a flow rate of 5.5 gal/min (4.2 m/s) at 250 W/cm^2 for the No. 1 Test Section and at a flow rate of 4.1 gal/min (5.0 m/s) at 276 W/cm^2 for the No. 3 Test Section. These contradictory results suggest that:

FIGURE A16

Comparison of burnout prediction by the Mirshak correlation with the Forgan data (Ref. 34).

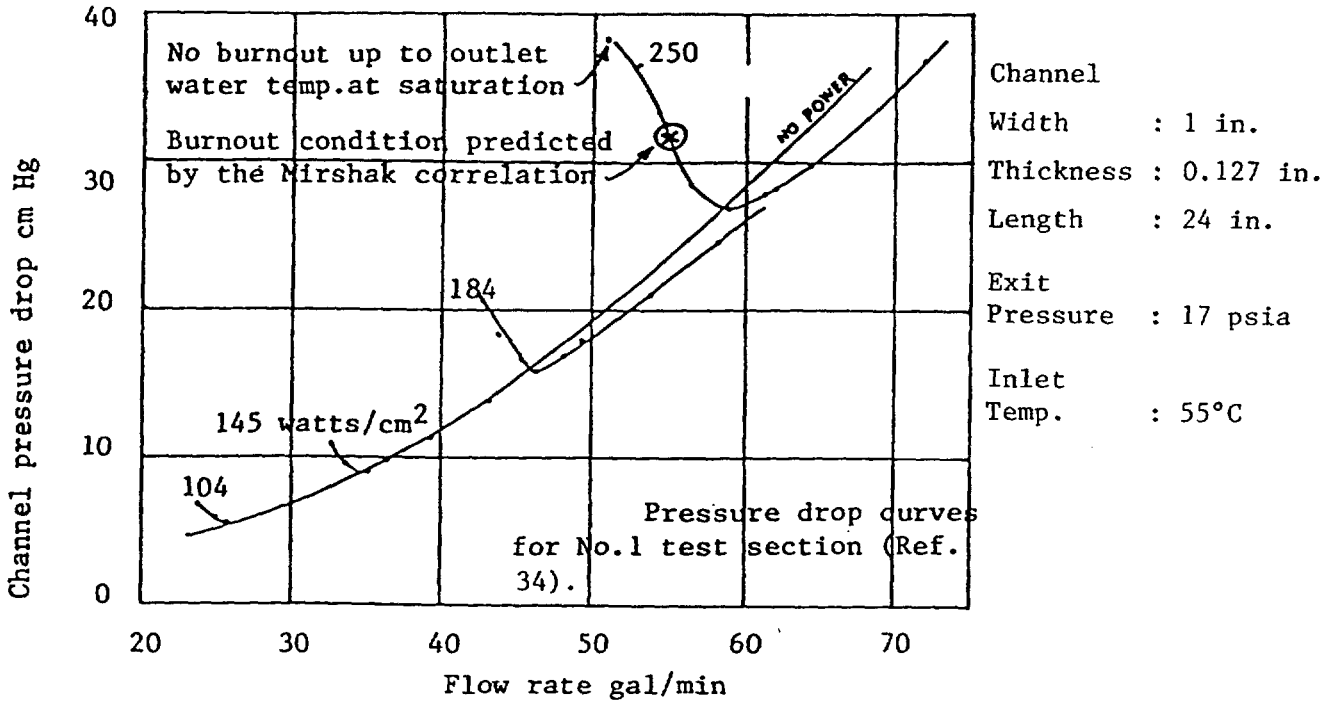

FIGURE A17

Comparison of burnout prediction by the Mirshak correlation with the Forgan data (Ref. 34).

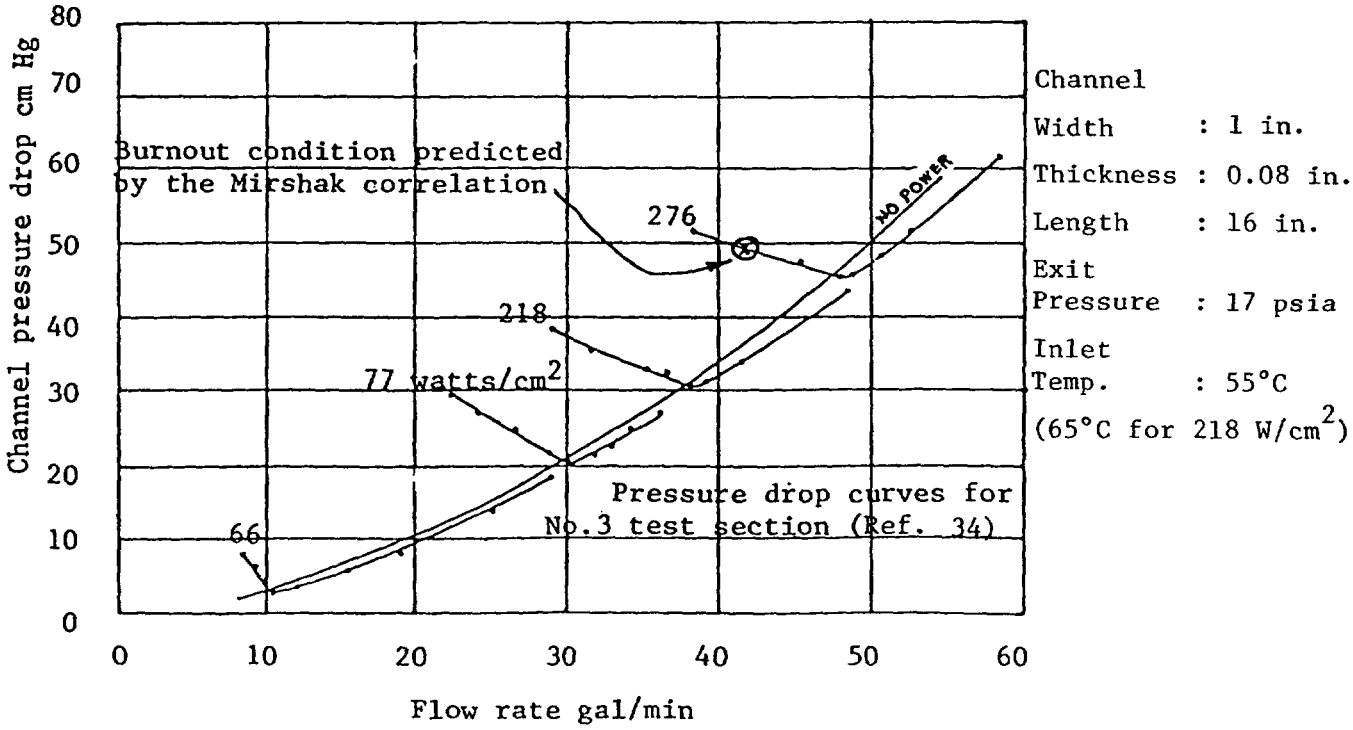

(1) the extrapolation of the one-side heated Mirshak burnout correlation to a two-sided heated channel is questionable, or

(2) the Mirshak data could be affected by unstable flow conditions.

Generally, it can be concluded that critical heat fluxes predicted by the Forgan flow excursion correlation are more limiting than those for stable burnout, and that critical heat fluxes predicted by the Mirshak correlation could be very conservative.

General Remarks

A specific, single correlation cannot be recommended as "best" for all research and test reactors. Instead, each potentially applicable correlation must be considered to see how it performs at conditions of interest, and to see how well the original data base supports the correlation under those conditions. Uncertainties in thermal-hydraulic correlations usually are large for general-purpose correlations. Improved accuracy ultimately depends upon specific tests in the geometry of interest, in mockups, or through in-plant tests.

A.2 APPLICATION TO THE 2 MW REACTOR BASED ON CLASSICAL PLATE-TYPE FUEL

A.2.1 Introduction

General design specifications agreed upon at the Consultants' Meeting for a typical 2 MW research reactor are shown in Table A10. The specific design descriptions for the reactor and the fuel elements that were used in the ANL calculations are shown in Table A11.

Neutronics and thermal-hydraulics results are presented for a range of alternatives for conversion to fuels with reduced uranium enrichment.

Two conversion criteria are studied in a general survey, based on the 2 MW reactor design, of the ^{235}U loadings that might be expected with uranium enrichments of 45% and 20% for initial ^{235}U loadings between 140 g and 300 g per standard element with HEU fuels. The first criterion is simple and conservative, and is based on matching the initial excss reactivity of the fresh HEU core using fuels with reduced enrichment. The second criterion is more complicated, but also more realistic, and is based on matching the fuel cycle length of an equilibrium core of the HEU design using fuels with reduced enrichment. The two criteria yield divergent results for the increase in ^{235}U loading that is required to compensate for a larger ^{238}U content, especially for reactors with higher initial HEU loadings. Simple arguments based on one-group diffusion theory are formulated to provide a qualitative explanation for these differences. In addition, the survey also includes results for three advanced fuel-types: U_3Si-Al, bulk U_3Si, and U-10 Mo.

Systematic burnup studies are then presented for the 2 MW reactor with an initial fissile (HEU) loading of 180 g ^{235}U per element. These calculations are based on matching the fuel cycle length of the reference HEU core for a variety of fuel element geometries. The results indicate several promising alternatives for direct conversion to LEU fuel using current fuel fabrication technology, or technology that will be available in the near-term.

A.2.2 Neutronics

A.2.2.1 Calculational Model

Five group microscopic cross sections were prepared using the EPRI-CELL code[1] with the methods described in Section A.1.2. The design details of the physical fuel element are shown in Fig. A18. The geometry of the unit cell used for cross section preparaton is shown in Fig. A19. Individual cross sections sets were prepared for uranium enrichments of 93%, 45%, 20%, and for each fuel meat and water channel thickness to be reported.

The ZR and XY models used in the two-dimension diffusion theory calculations for the ^{235}U loading survey based on matching the initial excess reactivities of the HEU and reduced enrichment cores are shown in Figs. A20 and A21. All results are reported for the XY model. The purpose of the ZR calculations was to determine extrapolation lengths for use in the XY case. Separate ZR calculations were done for each change in reactor parameters, e.g., a change in uranium enrichment, uranium density, fuel meat thickness, and/or water channel thickness.

The XY model used in the burnup studies (using the REBUS-2[15] fuel cycle analysis code) based on matching the fuel cycle length of the reference HEU design is shown in Fig. A22. Fresh fuel is inserted near the center of the reactor (position 1), and the remaining standard fuel elements are rotated sequentially

TABLE A10. 2 MW Reactor - General Description of Design Parameters

Fuel Element: MTR-Type (76 x 80 x 600 mm)

Number of Fuel Plates in:

Standard Fuel Element: 16 (19)

Control Fuel Element: 12 (15) + 2 Al Plates Assuming 2 Control Blades/Element

Plate Dimensions: Standard MTR-Plate

Plate Thickness: 1.27 mm

Meat Thickness: 0.51 mm

Shape of Plate: Straight

Fuel Loading: Standard Fuel Element: 140-180 g U-235

Control Fuel Element: 105-135 g U-235

Number of Fuel Elements in the Core: 24 ± 1

Standard Fuel Element: 20 ± 1

Control Fuel Element: 4

Reflector: Water

Core Geometry: 4 x 6 Arrangement

Grid Plate: 6 x 9 Positions

Desired Average Burnup of U-235 in the Fuel Element Discharged from the Core: 30%

Burnup-Status of the Core: Equilibrium Core

Fuel Shuffling: Introduction of New Fuel Elements into the Core Center

Thermo-Hydraulic Data: Coolant Flow Rate: 5000 l/min, 300 m^3/h

Core Inlet Temperature: 38°C

TABLE A11. 2 MW Reactor - Description of Design Parameters Used in USA/ANL Calculations

Reactor Design Description

Reactor Type	Pool-Type MTR
Steady-State Power Level	2 MW
Number of Standard Fuel Elements	19
Number of Control Fuel Elements	4
Irradiation Channels	1 at Core Center
Core Geometry	4 x 6 Arrangement
Grid Plate	6 x 9 Positions
^{235}U Content/Core	3988 g
Active Core Volume	86 l
Average Volumetric Power Density	23.3 kW/l
Average Linear Power Density	0.08 kW/cm
Specific Power	502 kW/kg ^{235}U
Moderator, Coolant	Water
Reflector	Water on All Four Sides

Fuel Element Design Description

Type	MTR, Straight Plates
Uranium Enrichment	93%
Lattice Pitch	77 x 81 mm
Fuel Element Dimensions	76 x 80 x 600 mm
Plate Thickness	1.27 mm (Inner Plates) 1.50 mm (Outer Plates)
Water Channel Thickness	2.916 mm
Plates/Standard Fuel Element	19
Plates/Control Fuel Element	15 Fueled and 2 Al Plates
Fuel Meat	UAl_x-Al (17.5 wt.% U)
Meat Dimensions	0.51 x 63 x 600 mm
Clad Thickness (Al)	0.38 mm (Inner Plates) 0.495 mm (Outer Plates)
^{235}U Density in Fuel Meat	0.4914 g/cm^3
^{235}U/Standard Fuel Element	180 g
^{235}U/Control Fuel Element	142 g
Coolant Flow Rate	300 m^3/h
Core Inlet Temperature	38°C
Burnup Status of Core	Equilibrium Core

after each cycle. Standard fuel elements are discharged from position 19 after 19 operational cycles. The control fuel elements are fixed, but 1/19 of the fuel in each control element is replaced with fresh fuel after each operational cycle. With this fuel shuffling pattern, the REBUS-2 code was used to search for the equilibrium burnup distribution at the beginning and end of each operational cycle. Computed cycle lengths represent an average cycle length, with the average taken over replacement of nineteen standard fuel elements and four control fuel elements. The criteria and procedures used in the calculations are discussed further in Section A.2.2.3. This fuel shuffling pattern is intended to be illustrative, and not necessarily practical or optimal. Further studies are planned with different shuffling patterns.

Figure A18. 2 MW Reactor - Standard[a] (19 Plates/Element) and Control[a,b] (15 Plates/Element) Fuel Elements.

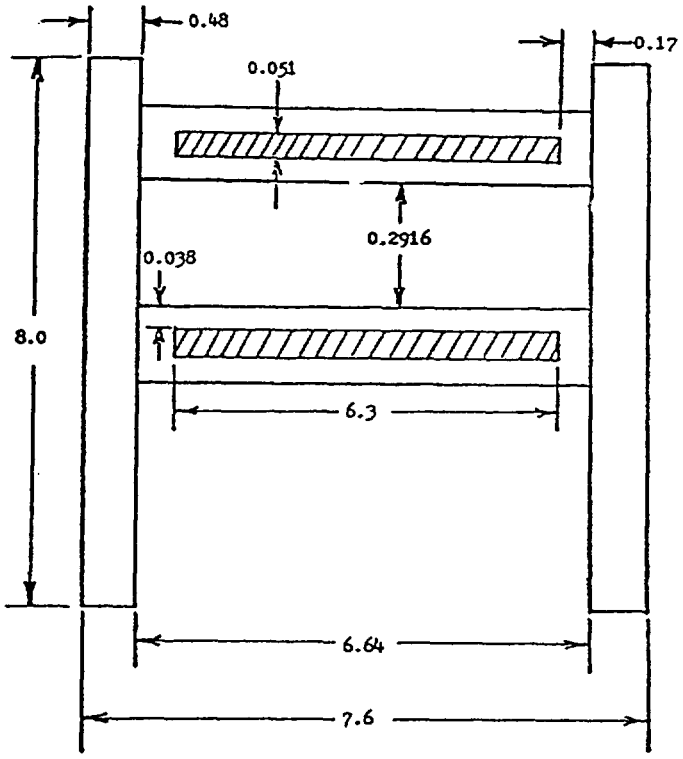

All dimensions in cm.

[a]The two outermost plates have a clad thickness of 0.0495 cm.

[b]Control fuel elements have two Al plates/ elements, assuming two fork-type absorber plates/element.

[c]Including a 0.5 mm water channel surrounding each element.

VOLUME FRACTIONS[c]

Standard Fuel Element		Control Fuel Element	
Fuel Meat	0.0979	Fuel Meat	0.0773
Aluminum	0.2870	Aluminum	0.2806
Water	0.6151	Water	0.6421

Figure A19. 2 MW Reactor - Geometry of Unit Cell for EPRI-CELL Calculation of Reference Core Cross Sections (All Dimensions in cm).

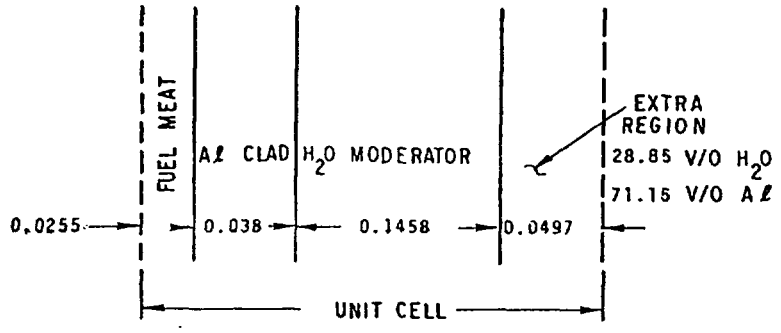

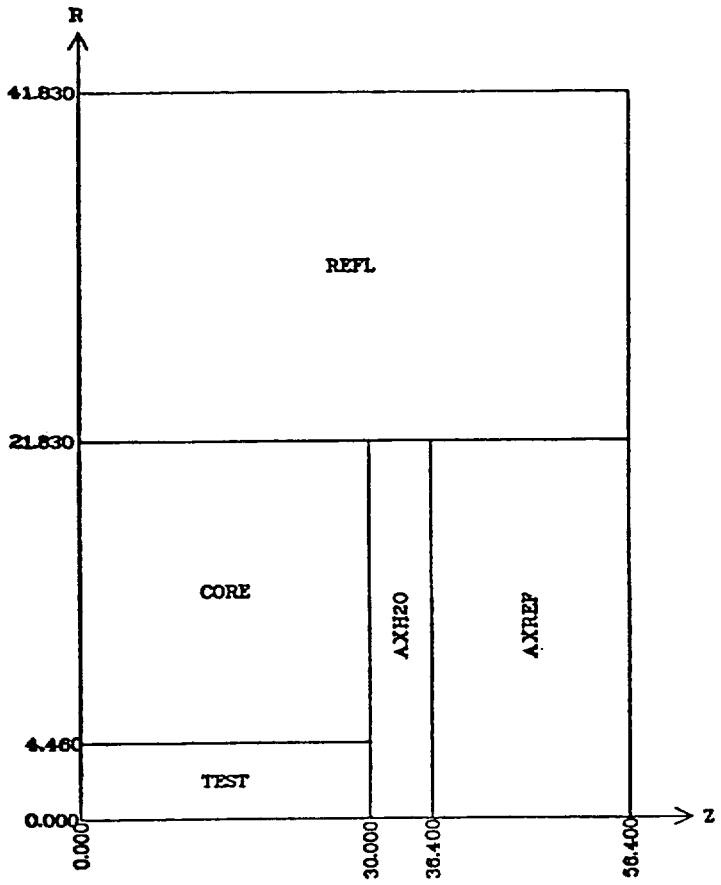

Figure A20.

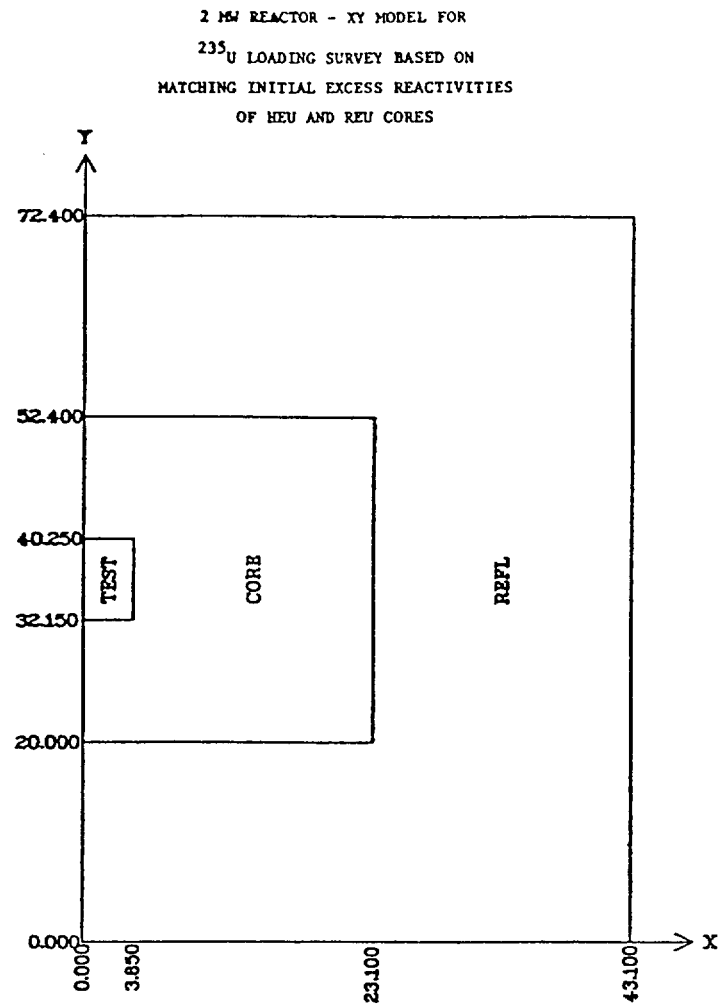

Figure A21.

Fresh Fuel is Inserted into Position 1. All Standard Elements Are Rotated Sequentially After Each Cycle. Standard Elements Are Discharged From Position 19 After 19 Operational Cycles. The Control Fuel Elements Are Fixed.

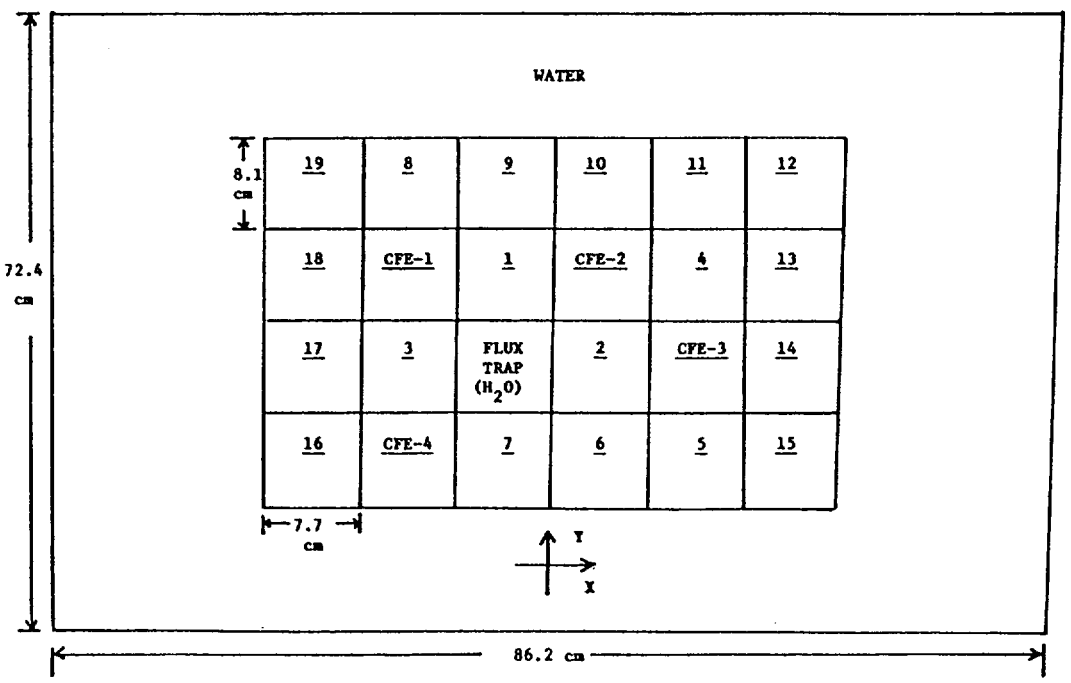

Figure A22. XY Model for Burnup Studies of 2 MW Reactor

A.2.2.2 Survey of ^{235}U Loadings and Comparison of Conversion Criteria

To provide an overview of the ^{235}U loadings that might be expected with 45% and 20% enriched uranium fuels, neutronics calculations have been done for reactors with 19 (15) plates per standard (control) fuel elements and initial HEU (93%) loadings between 140 g and 300 g ^{235}U per element. For comparison purposes, these calculations have been repeated using both the reactivity matching and fuel cycle length matching criteria. In all cases, fuel meat and water channel thicknesses of 0.51 mm and 2.916 mm, respectively, have been used in the reactor models described in Section A.2.2.1.

The results of the ^{235}U loading survey are shown in Table A12 for the reactivity matching criterion and in Table A13 for the fuel cycle length matching criterion. In the latter calculations, a search was first done on the average burnup of discharged fuel elements for each initial HEU loading such that the reactor was just critical at the end of equilibrium cycle (EOC). The computed cycle length for each case with HEU fuel was then fixed. Another search was then performed using uranium enrichments of 45% and 20%, to determine the uranium density in the fuel meat of the fresh fuel element such that the cycle length of the equilibrium core (EOC k_{eff} = 1.0) with reduced enrichment fuel matched that of the HEU core.

Plotted in Fig. A23 are the ratios of the ^{235}U densities with 45% and 20% enriched uranium fuels to the ^{235}U density with 93% enriched uranium fuel for both conversion criteria. With increasing initial ^{235}U loading using HEU fuel, the cycle length matching criterion predicts a slightly decreasing ^{235}U density ratio, while the reactivity matching criterion predicts increasingly larger ^{235}U density ratios to compensate for the greater ^{238}U content with reduced uranium enrichment.

Simple arguments based on one-group diffusion theory are formulated below to provide a qualitative basis for the divergent shapes of the ^{235}U density ratio curves computed with the two conversion criteria. The intention of these simple considerations is to provide general insights into the shapes of these curves, and not necessarily to predict accurate numerical values.

In one-group diffusion theory, the eigenvalue can be written

$$k^{\varepsilon} = \frac{\nu\sigma_{f5}^{\varepsilon}\,(N_{i5}^{\varepsilon} - N_{b5}^{\varepsilon})}{\sigma_{a5}^{\varepsilon}\,(N_{i5}^{\varepsilon} - N_{b5}^{\varepsilon}) + \sigma_{a8}^{\varepsilon}N_{8}^{\varepsilon} + \Sigma_{0}^{\varepsilon}} \qquad (24)$$

where

ε = uranium enrichment

N_{i5}^{ε} = initial atoms of ^{235}U

N_{b5}^{ε} = atoms of ^{235}U burned

$\sigma_{a}^{\varepsilon}(\sigma_{f}^{\varepsilon})$ = microscopic absorption (fission) cross sections of ^{235}U and ^{238}U

Σ_{0}^{ε} = effective absorption cross section for losses other than absorption in ^{235}U and ^{238}U

$= \Sigma_{H_2O}^{\varepsilon} + \Sigma_{Al}^{\varepsilon} + \Sigma_{fiss.prod}^{\varepsilon} + Leakage^{\varepsilon}$

TABLE A12. MTR Reactors
with 19 Plates per Standard Element
0.51 mm Meat Thickness; 2.916 mm Water Channel Thickness

^{235}U Loading with Uranium Enrichments
of 45% and 20% to Match Initial Excess
Reactivity of 93% Enriched Reference Core (Fresh Cores)

^{235}U/Element, g	140	180	220	260	300
93% Enrichment, U-Al Alloy					
k_{eff}	0.9869	1.0521	1.0983	1.1327	1.1592
$H/^{235}U$*	429	333	273	231	200
ρ_{25}, g/cm^3	0.382	0.491	0.601	0.710	0.819
ρ_U, g/cm^3	0.411	0.528	0.646	0.763	0.881
wt.% U (5 v/o void)	14.1	17.5	20.7	23.7	26.5
^{235}U/Element, g	140	180	220	260	300
45% Enrichment, UAl_x-Al					
k_{eff}	0.9869	1.0521	1.0983	1.1327	1.1592
$H/^{235}U$*	401	305	243	200	168
ρ_{25}, g/cm^3	0.409	0.538	0.674	0.820	0.976
ρ_U, g/cm^3	0.908	1.196	1.498	1.822	2.169
wt.% U (7 v/o void)	27.8	34.1	39.9	45.3	50.3
^{235}U/Element, g	150	197	247	300	357
20% Enrichment, UAl_x-Al					
k_{eff}	0.9869	1.0521	1.0983	1.1327	1.1592
$H/^{235}U$*	370	271	208	162	127
ρ_{25}, g/cm^3	0.444	0.604	0.790	1.013	1.296
ρ_U, g/cm^3	2.220	3.020	3.950	5.065	6.480
wt.% U (7 v/o void)	50.9	60.1	68.1	75.3	82.0
^{235}U/Element, g	163	221	289	371	475
$\rho_{25}(45)/\rho_{25}(93)$	1.071	1.096	1.121	1.155	1.192
$\rho_{25}(20)/\rho_{25}(93)$	1.162	1.230	1.314	1.427	1.582

*Hydrogen to ^{235}U ratio in standard fuel element, including a 0.5 mm water channel surrounding element.

Table A13. MTR Reactors
with 19 Plates per Standard Element
0.51 mm Fuel Meat Thickness; 2.916 mm Water Channel Thickness

^{235}U Loading with Uranium Enrichments
of 45% and 20% to Match Fuel Cycle Length
of 93% Enriched Reference Core

93% Enrichment, U-Al Alloy				
Cycle Length, Days[a]	10.0	35.9	59.9	83.6
BOC k_{eff}	1.0058	1.0122	1.0174	1.0215
EOC k_{eff}	0.9999	1.0000	1.0001	1.0000
^{235}U Burned,[b] g	21.0	75.6	126.5	176.4
$H/^{235}U$[c]	334	273	231	200
ρ_{25},[d] g/cm^3	0.491	0.601	0.710	0.819
ρ_U, g/cm^3	0.528	0.646	0.763	0.881
wt.% U (5 v/o void)	17.5	20.7	23.7	26.5
^{235}U/Element, g	180	220	260	300
45% Enrichment, UAl_x-Al				
Cycle Length, Days[a]	10.0	35.9	59.9	83.6
BOC k_{eff}	1.0057	1.0110	1.0153	1.0187
EOC k_{eff}	1.0001	1.0001	1.0003	1.0002
^{235}U Burned,[b] g	21.2	76.0	126.6	176.5
$H/^{235}U$[c]	303	249	212	184
ρ_{25},[d] g/cm^3	0.541	0.657	0.773	0.889
ρ_U, g/cm^3	1.203	1.460	1.718	1.977
wt.% U (7 v/o void)	34.3	39.2	43.6	47.6
^{235}U/Element, g	198.3	240.7	283.1	325.8
20% Enrichment UAl_x-Al				
Cycle Length, Days[a]	10.0	35.9	59.9	83.6
BOC k_{eff}	1.0052	1.0096	1.0135	1.0161
EOC k_{eff}	1.0001	1.0001	1.0005	1.0005
^{235}U Burned,[b] g	20.8	73.9	122.3	169.6
$H/^{235}U$[c]	281	234	200	174
ρ_{25},[d] g/cm^3	0.582	0.701	0.821	0.943
ρ_U, g/cm^3	2.912	3.505	4.103	4.719
wt.% U (7 v/o void)	58.7	64.6	69.3	79.4[e]
^{235}U/Element, g	213.3	256.8	300.6	345.7
$\rho_{25}(45)/\rho_{25}(93)$	1.102	1.093	1.089	1.085
$\rho_{25}(20)/\rho_{25}(93)$	1.185	1.166	1.156	1.151

[a] Based on a power level of 2 MW.

[b] ^{235}U Burned in discharged fuel element.

[c] $H/^{235}U$ in fresh standard fuel element, including a $\frac{0.5}{2}$ mm water channel surrounding each element.

[d] ρ_{25}, ρ_U, wt.% U, and ^{235}U content are for the fresh feed standard fuel element.

[e] U/UAl_x was assumed to be 0.8 to perform this calculation. All other data are based on $U/UAl_x = 0.7$.

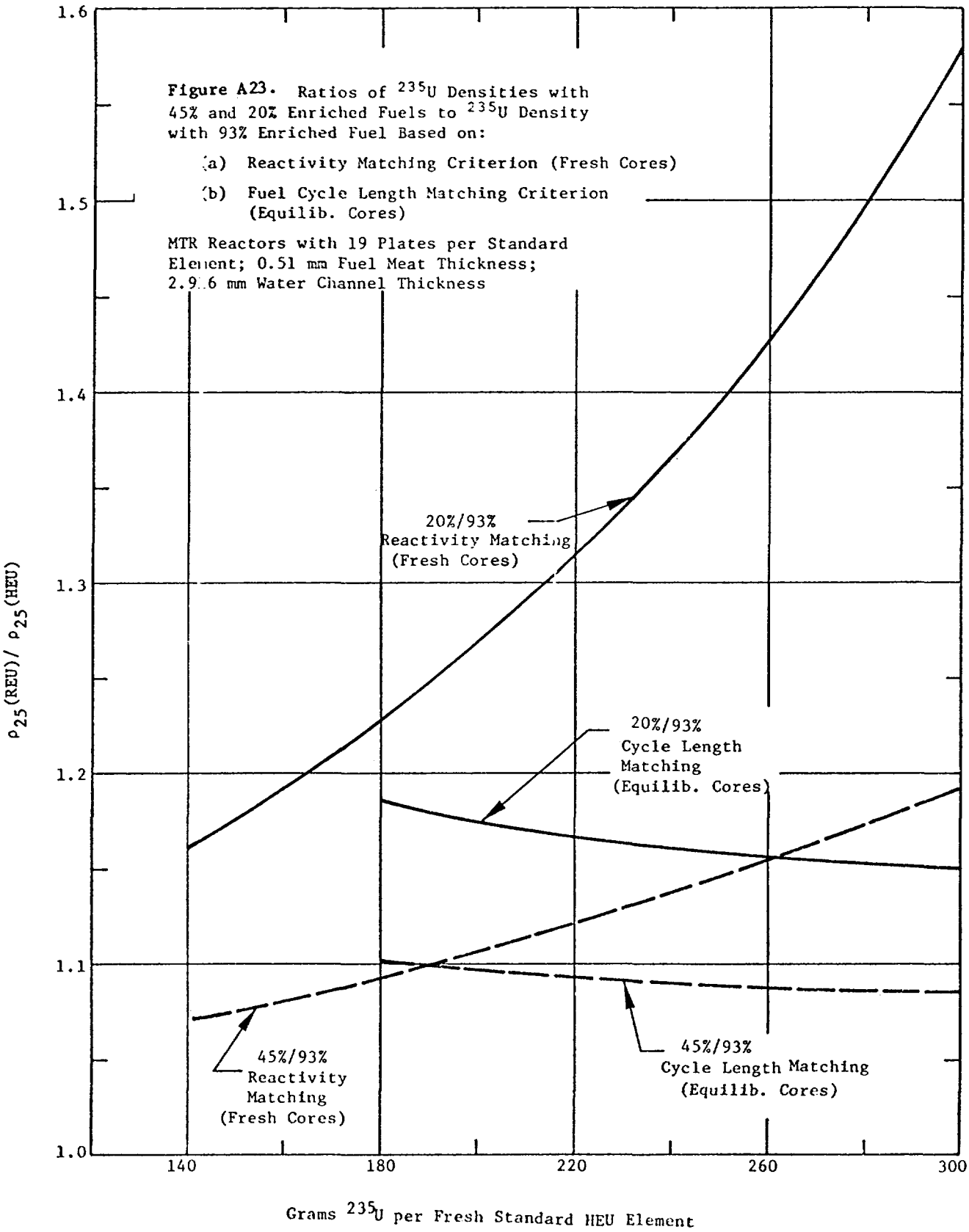

Figure A23. Ratios of ^{235}U Densities with 45% and 20% Enriched Fuels to ^{235}U Density with 93% Enriched Fuel Based on:

(a) Reactivity Matching Criterion (Fresh Cores)

(b) Fuel Cycle Length Matching Criterion (Equilib. Cores)

MTR Reactors with 19 Plates per Standard Element; 0.51 mm Fuel Meat Thickness; 2.96 mm Water Channel Thickness

For simplicity, assume that the microscopic cross sections of ^{235}U and ^{238}U and the other absorption losses (Σ_0) are independent of enrichment. Equation (24) then becomes

$$k^{\varepsilon} = \frac{\nu\sigma_{f5}(N_{i5}^{\varepsilon} - N_{b5}^{\varepsilon})}{\sigma_{a5}(N_{i5}^{\varepsilon} - N_{b5}^{\varepsilon}) + \sigma_{a8}N_8^{\varepsilon} + \Sigma_0} \tag{25}$$

Matching Reactivities of Fresh Cores

In this case, $k^{93} = k^{20}$ and $N_{b5} = 0$. Equating the k's and solving for N_{i5}^{20}/N_{i5}^{93}, with $N_8/N_{i5} = 1-\varepsilon/\varepsilon$, yields

$$\frac{N_{i5}^{20}}{N_{i5}^{93}} = \frac{1}{1 - N_{i5}^{93}\left[\frac{3.925 \cdot \sigma_{a8}}{\Sigma_0}\right]} . \tag{26}$$

If σ_{a8} and Σ_0 are relatively constant, the right hand side of Equation (26) has a strong dependence on the initial 93%-enriched ^{235}U loading. The shape of the ^{235}U density ratio curve predicted by Eq. (26) is qualitatively similar to the curve shown in Fig. A23 for the reactivity matching criterion with 20% enriched fuel.

Equation (26) predicts a singularity in the ^{235}U density ratio if $N_{i5}^{93} = \Sigma_0/3.925\ \sigma_{a8}$. This value of N_{i5}^{93} corresponds to a ^{235}U loading of the fully enriched core which is so high that the value of k_{eff} to which it corresponds equals the maximum value of k_∞ which can be achieved with 20% enriched fuel. Therefore, only an infinite ^{235}U concentration in the 20% enriched core can yield the same reactivity as the HEU core for this value of N_{i5}^{93}.

Match Fuel Cycle Length of Cores with Equal Burnup

If $k^{\varepsilon} = 1.0$ at end of cycle and both cores have equal cycle length, approximately N_{b5} atoms of ^{235}U will have been burned, independent of uranium enrichment. Solving Eq. (25) for N_{b5} with $k^{\varepsilon} = 1.0$, and setting $N_{b5}^{93} = N_{b5}^{20}$, we obtain

$$N_{i5}^{93}(\sigma_{a5} - \nu\sigma_{f5}) + N_8^{93}\sigma_{a8} = N_{i5}^{20}(\sigma_{a5} - \nu\sigma_{f5}) + N_8^{20}\sigma_{a8} \tag{27}$$

Since $N_8/N_{i5} = 1-\varepsilon/\varepsilon$, solving Eq. (27) for N_{i5}^{20}/N_{i5}^{93} gives

$$\frac{N_{i5}^{20}}{N_{i5}^{93}} = \frac{1 - 0.075\,\frac{\sigma_{a8}}{\nu\sigma_{f5} - \sigma_{a5}}}{1 - 4.0\,\frac{\sigma_{a8}}{\nu\sigma_{f5} - \sigma_{a5}}} . \tag{28}$$

Since the right hand side of Eq. (28) is independent of the initial HEU loading, a flat ^{235}U density ratio is predicted, similar to the curve shown in Fig. A23 for the cycle length matching criterion with 20% enriched fuel. With some minor adjustments of the constants, these results also apply for 45% enriched uranium fuel.

The condition that the reactivity matching and cycle length matching criteria yield equal increases in the ^{235}U density required with reduced enrichment fuels can be found from Eqs. (25), (26), and (28). Equating the N_{i5}^{20}/N_{i5}^{93} ratios from Eqs. (26) and (28), and solving for N_{i5}^{93} (min),

$$N_{i5}^{93}\ (\text{min}) = \frac{\Sigma_0}{\nu\sigma_{f5} - \sigma_{a5} - 0.075\ \sigma_{a8}} \quad .$$

If this expression is inserted into Eq. (25) with $N_{b5}^{\epsilon} = 0$, a value of $k^{93} = 1.0$ is obtained. This result is not surprising since it corresponds to a reactor whose fresh ^{235}U loading is just sufficient to make the reactor critical. The equilibrium cycle loading is the fresh fuel loading and the cycle length is zero. Referring to the data in Table A12 for 93% enriched fuel, interpolation yields $k_{eff} = 1.0$ for an initial ^{235}U loading of about 145 g per element. Only at or around this initial HEU loading should the two conversion criteria result in equal ^{235}U density ratios. The ^{235}U density increase with 145 g ^{235}U per fresh element is about 2.268 with 20% enriched fuel and about 1.074 with 45% enriched fuel.

The data in Fig. A23 based on the two conversion criteria are not entirely consistent due to small differences in the initial reactivities of the fresh cores computed with slightly different calculational models for the reactor. For example, the computed k_{eff} for a fresh HEU core with an initial loading of 180 g ^{235}U per element based on the reactor model (Fig. A14) for reactivity matching was 1.0541, and the corresponding eigenvalue based on the reactor model (Fig. A15) for cycle length matching was 1.0549. This corresponds to a reactivity differene of 0.25% $\Delta k/k$. Thus, extrapolating the data in Fig. A16 based on cycle length matching to initial ^{235}U loadings less than 180 g may result in apparent minor inconsistencies.

Reflector Materials

The 2 MW reference reactor with 180 g ^{235}U per fresh standard fuel element is reflected by water on all four sides. To achieve the same fuel cycle length as the HEU design with 20% enrichment, a uranium density of 2.91 g/cm^3 was computed. One option for reducing the required uranium density without redesign of the fuel elements is to replace the row of water reflector elements (20 elements) immediately surrounding the core by either graphite (1.7 g/cm^3) or beryllium metal (1.84 g/cm^3) reflector elements. The results in Table A14 indicate that the uranium density with 20% enrichent needed to match the cycle length of the reference HEU design is 2.23 g/cm^3 with a graphite reflector and 1.76 g/cm^3 with a beryllium metal reflector.

Few operating reactors are totally reflected by water, but many are currently reflected with graphite or beryllium metal elements. To provide further indications of the effects of these reflector materials, calculations were run on the 2 MW reference reactor using graphite and beryllium metal reflector elements in both the 93% and 20% enriched cases. The results shown in Table A15 indicate that the uranium densities needed to match the cycle lengths of the reference HEU designs with graphite and beryllium metal reflector elements are 2.74 and 2.61 g/cm^3, respectively, instead of the 2.91 gU/cm^3 with water reflection.

Table A14. Reflector Materials
MTR Reactors with 19 Plates per Standard Element
0.51 mm Fuel Meat Thickness; 2.916 mm Water Channel Thickness

^{235}U Loading Using 20% Enriched Uranium
with Radial Reflectors of Water, Graphite,* and Beryllium*
to Match Fuel Cycle Length of 93% Enriched Reference Core (Water Reflected)

93% Enrichment, U-Al Alloy

Reflector Material	Water
Cycle Length, Days[a]	10.0
BOC k_{eff}	1.0058
EOC k_{eff}	0.9999
^{235}U Burned,[b] g	21.0
$H/^{235}U$[c]	334
ρ_{25},[d] g/cm^3	0.491
ρ_U, g/cm^3	0.528
wt% U (5 v/o void)	17.5
^{235}U/Element, g	180

20% Enrichment, UAl_x-Al

Reflector Material	Water	Graphite	Beryllium
Cycle Length, Days[a]	10.0	10.0	10.0
BOC k_{eff}	1.0052	1.0055	1.0058
EOC k_{eff}	1.0001	0.9998	0.9996
^{235}U Burned,[b] g	20.8	20.7	20.8
$H/^{235}U$[c]	281	371	466
ρ_{25},[d] g/cm^3	0.582	0.4466	0.352
ρ_U, g/cm^3	2.912	2.231	1.760
wt% U (7 v/o void)	58.7	51.1	44.3
^{235}U/Element, g	213.3	163.4	128.9

*20 C or Be reflector elements surrounding core. Remainder of reflector was H_2O.

[a]Based on a power level of 2 MW.

[b]^{235}U Burned in discharged fuel element.

[c]$H/^{235}U$ in fresh standard fuel element, including a 0.5 mm water channel surrounding each element.

[d]ρ_{25}, ρ_U, wt% U, and ^{235}U content are for fresh standard fuel element.

Table A15. Reflector Materials
MTR Reactors with 19 Plates per Standard Element
0.51 mm Fuel Meat Thickness; 2.916 mm Water Channel Thickness

^{235}U Loading Using 20% Enriched Uranium
to Match Fuel Cycle Length of 93% Enriched Reference Core
with Radial Reflectors of Water, Graphite,* and Beryllium*

93% Enrichment, U-Al Alloy

Reflector Material	Water	Graphite	Beryllium
Cycle Length, Days[a]	10.0	32.9	50.1
BOC k_{eff}	1.0058	1.0142	1.0232
EOC k_{eff}	0.9999	1.0001	1.0001
^{235}U Burned,[b] g	21.0	69.3	105.9
$H/^{235}U$	334	334	334
ρ_{25}, g/cm^3	0.491	0.491	0.491
ρ_U, g/cm^3	0.528	0.528	0.528
wt% U (5 v/o void)	17.5	17.5	17.5
^{235}U/Element, g	180.0	180.0	180.0

20% Enrichment, UAl_x-Al

Reflector Material	Water	Graphite	Beryllium
Cycle Length, Days[a]	10.0	32.9	50.1
BOC k_{eff}	1.0052	1.0113	1.0176
EOC k_{eff}	1.0001	1.0002	0.9997
^{235}U Burned,[b] g	20.8	67.5	102.0
$H/^{235}U$[c]	281	299	314
ρ_{25},[d] g/cm^3	0.582	0.549	0.521
ρ_U, g/cm^3	2.912	2.744	2.606
wt% U (7 v/o void)	58.7	57.3	55.7
^{235}U/Element, g	213.3	201.0	190.9

*20 C or Be reflector elements surrounding core. Remainder of reflector was H_2O.

[a]Based on a power level of 2 MW.

[b]^{235}U Burned in discharged fuel element.

[c]$H/^{235}U$ in fresh standard fuel element, including a 0.5 mm water channel surrounding each element.

[d]ρ_{25}, ρ_U, wt% U, and ^{235}U content are for fuel standard fuel elements.

Advanced Fuels

Calculations have been performed for three advanced fuel-types (U_3Si-Al, bulk U_3Si, and U-10Mo) with very high uranium densities to determine their potential for conversion of reactors with currently-high HEU densities to use of LEU fuel.

Fabrication development of U_3Si-Al dispersion fuel is currently underway at ANL. Irradiation in the ORR of mini-plates with uranium densities of 4.2 and 6.0 g/cm^3 is scheduled for early 1980. Higher uranium densities will be evaluated concurrently with the first irradiation tests. Table A16 contains results for the uranium densities required with 20% enriched U_3Si-Al fuel to match the cycle length of 2 MW reactor with initial HEU loadings between 400 g and 600 g ^{235}U per element (1.17 to 1.76 g U/cm^3). For these cases, the LEU densities range between 6.1 and 9.0 g/cm^3. The maximum uranium density that can be achieved with U_3Si-Al dispersion fuel is estimated to be about 8 g/cm^3. If development, demonstration, and commercialization of this fuel with ~8 g U/cm^3 is successful, nearly all reactors currently using HEU have a potential for conversion to LEU fuel.

Bulk U_3Si and U-10Mo (10 w/o Mo, 90 w/o U) are also candidate advanced fuels with very high uranium densities. The maximum density of bulk U_3Si for practical use is estimated to be about 12.0 g/cm^3 (11.5 g U/cm^3), and the uranium density in U-10Mo fuel is about 14.2 g/cm^3. In Table A17, the reference fuels for the 2 MW reactor were taken to be bulk U_3Si and U-10Mo with 20% enrichment. After the cycle lengths were computed with these LEU fuels, searches were done using UAl_x-Al fuel with 93% enrichment to determine the maximum HEU loadings for which conversion to these LEU fuels may be feasible. For bulk U_3Si, this HEU density was computed to be 2.25 g/cm^3. Since the cladding and structural materials for use with U-10Mo fuel require further evaluation, calculations were done with both aluminum and zircaloy-2 cladding and side plates. The maximum HEU densities were computed to be 2.33 and 2.45 g/cm^3 with aluminum and zircaloy-2 structurals, respectively.

Conclusions - ^{235}U Loading Survey

All conclusions are based on the fuel cycle length matching criterion.

Reactors currently using 19 plates per fuel element with up to about 260 g ^{235}U can be converted to use of 45% enriched uranium, without changes in the thermal-hydraulics, simply by substituting a new high uranium density fuel meat fabricated with current technology for the low uranium density fuels that are presently in use. For reactors with 300 g ^{235}U and 19 plates per element, a small extension of current fuel fabrication technology is needed for conversion via direct fuel meat substitution.

The data for the 20% enriched case indicate that high uranium densities are desirable for reactor conversions via direct fuel meat substitution. These data are summarized in Fig. A24, where the required uranium densities with 20% or 45% enrichment are plotted against the uranium density with 93% enrichment. Fuel development and demonstration programs in several countries are currently in progress to achieve these high uranium densities and to demonstrate their use.

High uranium loadings can also be achieved in many reactors which are not currently operating at their thermal-hydraulic limits by increasing the thickness of the fuel meat, and/or simultaneously decreasing the number of fuel plates per

Table A16. U_3Si-Al Dispersion Fuel
MTR Reactors with 19 Plates per Standard Element
0.51 mm Fuel Meat Thickness; 2.916 mm Water Channel Thickness
^{235}U Loading with 20% Enriched U_3Si-Al Fuel
to Match Fuel Cycle Length of
93% Enriched Reference Core

93% Enrichment, U-Al Alloy			
Cycle Length, Days[a]	138.8	192.2	244.4
BOC k_{eff}	1.0293	1.0347	1.0387
EOC k_{eff}	1.0000	0.9999	1.0000
^{235}U Burned,[b] g	291.0	399.6	504.2
$H/^{235}U$[c]	150	120	100
$\bar{\rho}_{25}$,[d] g/cm^3	1.092	1.356	1.638
ρ_u, g/cm^3	1.174	1.468	1.761
wt.% U (5 v/o void)	32.9	38.4	43.3
^{235}U/Element, g	400.0	500.0	600.0
20% Enrichment, U_3Si-Al			
Cycle Length, Days[a]	138.8	192.2	244.4
BOC k_{eff}	1.0202	1.0229	1.0253
EOC k_{eff}	1.0000	0.9998	1.0003
^{235}U Burned,[b] g	275.3	375.4	471.8
$U/^{235}U$[c]	134	109	91
ρ_{25},[d] g/cm	1.221	1.510	1.808
ρ_u, g/cm^3	6.103	7.552	9.038
wt.% U (7 v/o void)	79.2	84.6	88.7
^{235}U/Element, g	447.1	553.3	662.2
$\rho_{25}(20)/\rho_{25}(93)$	1.118	1.106	1.104

[a] Based on a power level of 2 MW.

[b] ^{235}U Burned in discharged fuel element.

[c] $H/^{235}U$ in fresh standard fuel element, including a $\frac{0.5}{2}$ mm water channel surrounding each element.

[d] ρ_{25}, ρ_u, wt.% U, and ^{235}U content are for the fresh feed standard fuel element.

Table A17. Bulk U_3Si and U-10 Mo Fuel
MTR Reactors with 19 Plates per Standard Element
0.51 mm Fuel Meat Thickness; 2.916 mm Water Channel Thickness
^{235}U Loading with 93% Enriched UAl_x-Al Fuel
to Match Fuel Cycle Lengths of Reference Core with *
20% Enriched Bulk U_3Si (12.0 g/cc) and U-10 Mo Fuels

20% Enrichment			
Fuel Meat	U_3Si (Bulk)	U-10 Mo	U-10 Mo
Clad	Al	Zircaloy-2	Al
Cycle Length, Days[a]	329.6	395.0	374.0
BOC k_{eff}	1.0267	1.0262	1.0237
EOC k_{eff}	1.0001	1.0000	1.0001
^{235}U Burned,[b] g	626.7	746.6	714.7
$H/^{235}U$[c]	71	58	58
ρ_{25},[d] g/cm^3	2.309	2.839	2.839
ρ_U, g/cm^3	11.544	14.193	14.193
wt.% U	96.2	90.0	90.0
^{235}U/Element, g	845.9	1039.7	1039.7
93% Enrichment			
Fuel Meat	UAl_x-Al	UAl_x-Al	UAl_x-Al
Clad	Al	Al	Al
Cycle Length, Days[a]	329.6	395.0	374.0
BOC k_{eff}	1.0430	1.0454	1.0448
EOC k_{eff}	1.0000	1.0000	1.0001
^{235}U Burned,[b] g	673.3	802.6	761.1
$H/^{235}U$[c]	78	67	70
ρ_{25},[d] g/cm^3	2.092	2.448	2.333
ρ_U, g/cm^3	2.250	2.632	2.509
wt.% U	51.3	56.0	54.6
^{235}U/Element, g	766.3	896.7	854.6
$\rho_{25}(20)/\rho_{25}(93)$	1.104	1.160	1.217

* In this table, the reference fuels were taken to be 20% enriched bulk U_3Si (12.0 g/cm^3) and U-10 Mo (90 wt.% U). The uranium density with 93% enriched UAl_x-Al fuel was then found in order to match the cycle length of the 20% enriched case.

[a] Based on a power level of 2 MW.

[b] ^{235}U Burned in discharged fuel element.

[c] $H/^{235}U$ in fresh standard fuel element, including a $\frac{0.5}{2}$ mm water channel surrounding each element.

[d] ρ_{25}, ρ_U, wt.% U, and ^{235}U content are for the fresh feed standard fuel element.

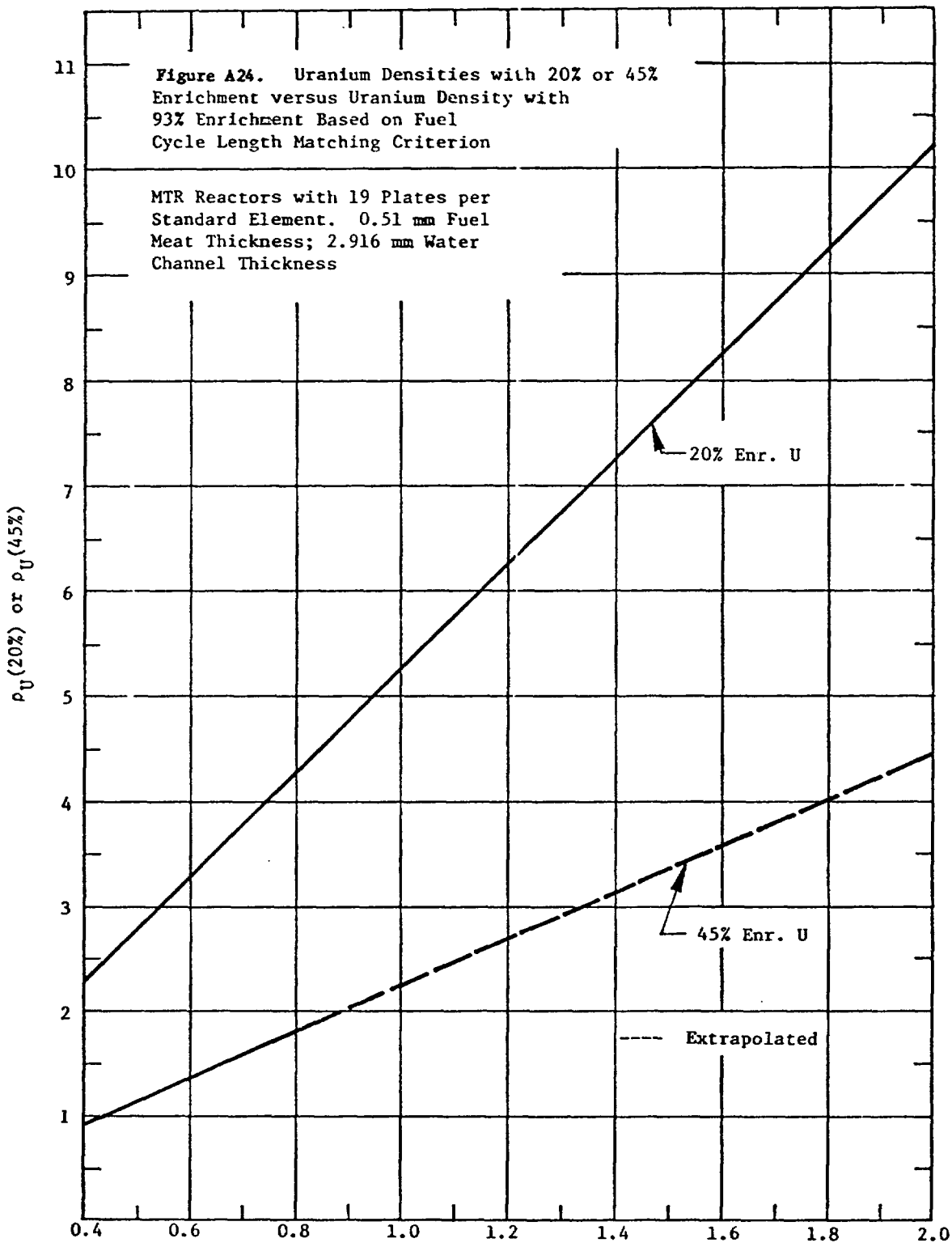
Figure A24. Uranium Densities with 20% or 45% Enrichment versus Uranium Density with 93% Enrichment Based on Fuel Cycle Length Matching Criterion
MTR Reactors with 19 Plates per Standard Element. 0.51 mm Fuel Meat Thickness; 2.916 mm Water Channel Thickness
20% Enr. U
45% Enr. U
Extrapolated
$\rho_U(20\%)$ or $\rho_U(45\%)$
11
10
9
8
7
6
5
4
3
2
1
0.4
0.6
0.8
1.0
1.2
1.4
1.6
1.8
2.0

element. Neutronics and thermal-hydraulics calculations for alternative fuel element designs with various fuel meat thicknesses, water channel thicknesses, and numbers of plates per element for an initial ^{235}U loading of 180 (280) g ^{235}U per element are discussed in Section A.2.2.3 (A.3.2.3) for the 2 (10) MW reactor.

Neutron flux ratios between the reduced enrichment cases and the HEU reference case are shown in Figs. A25 and A26 for the cases (based on matching the fuel cycle length) in Table A13 with 180 g ^{235}U per fresh standard element. For convenience, numerical flux ratios are also provided in Table A18 at key locations in the reactor. With both 45% and 20% enriched uranium fuels, the peak fast and epithermal fluxes in the center irradiation channel and in the reflector are virtually identical. The thermal flux in these locations is reduced by about 2% with 45% enriched fuel and by 4-5% with 20% enriched fuel. With the reduced enrichment fuels, the fast flux averaged over the core is also nearly identical with the 93% enriched case. The core-average epithermal flux is reduced by about 1% with 45% enriched fuel and by about 3% with 20% enriched fuel. The core average thermal fluxes are reduced by about 8% and 17% with 45% and 20% enriched fuels, respectively.

Table A18. 2 MW Reactor - 180 g ^{235}U (93%) per Standard Element Flux Ratios in Central Irradiation Channel, Core, and Radial Reflector due to Use of Fuels with 45% and 20% Enriched Uranium Instead of 93% Enriched Uranium Based on Fuel Cycle Matching Criterion

Enrichment	Region	ϕ_E/ϕ_{93} (Fast)*	ϕ_E/ϕ_{93} (Epithermal)*	ϕ_E/ϕ_{93} (Thermal)*	ϕ_E/ϕ_{93} (Total)
45%	Central Irradiation Channel** (Peak)	0.990	0.987	0.971	0.978
	Core (Average)	0.997	0.987	0.933	0.975
	Reflector (Peak)	1.028	1.022	1.001	1.010
20%	Central Irradiation Channel (Peak)	0.998	0.994	0.963	0.975
	Core (Average)	0.996	0.975	0.847	0.944
	Reflector (Peak)	0.989	0.977	0.942	0.958

*Energy Ranges

Fast: 10.0 MeV - 0.553 MeV
Epithermal: 0.553 MeV - 0.625 eV
Thermal: 0.625 eV - 0.0 eV

**Central fuel element filled with water.

2MW REACTOR FLUX RATIOS AT CORE MIDPLANE

180G U-235/ELEMENT REFERENCE

0.51 mm Fuel Meat Thickness; 2.916 mm Water Channel Thickness

Cycle Length Matching Criterion

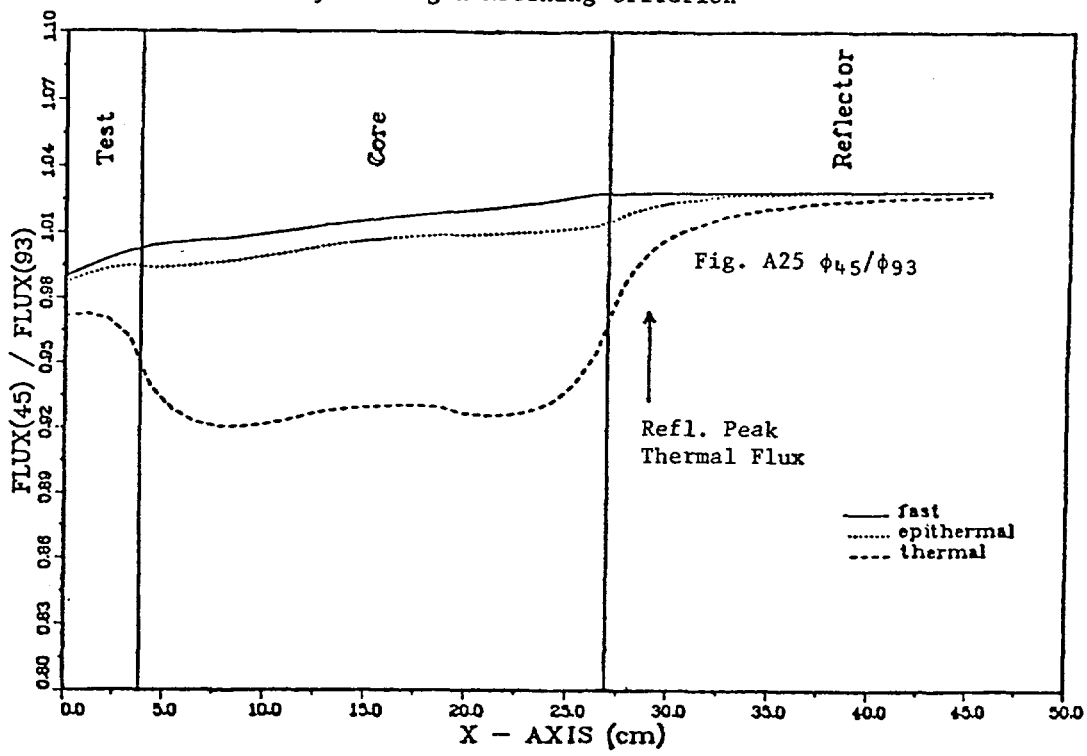

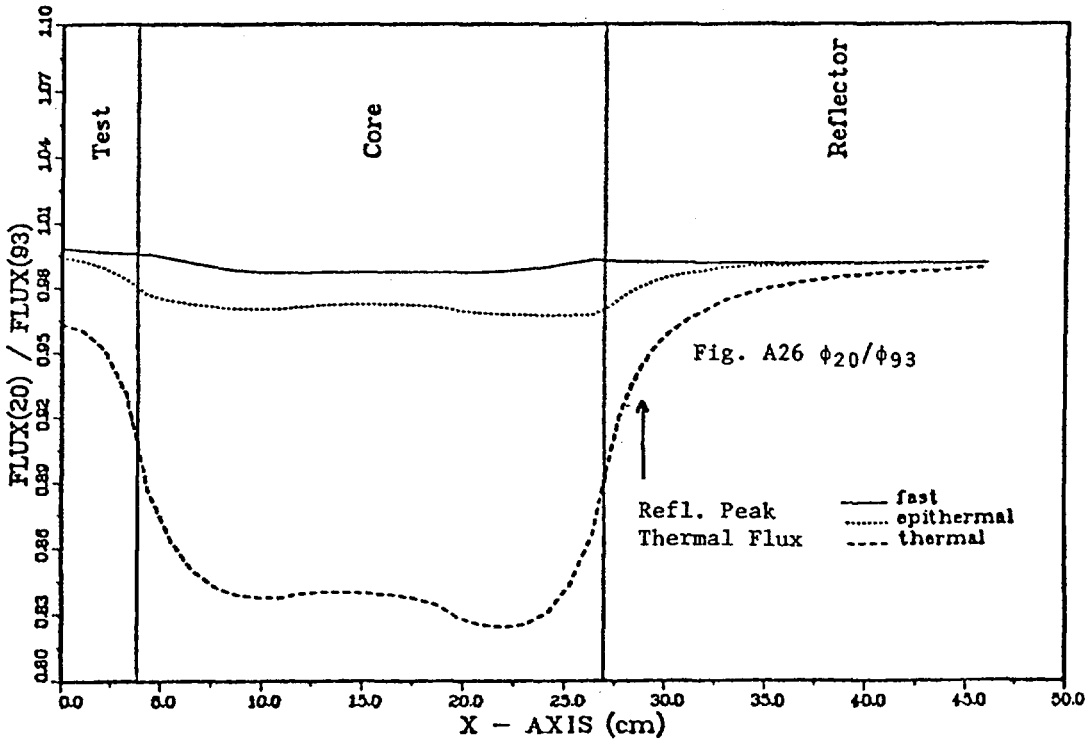

A.2.2.3 Burnup Studies - Fuel Element Design Variations

The higher uranium loadings that are required for reactor conversions from HEU (93%) to LEU (<20%) fuels can be achieved by increasing the fuel meat thickness and/or simultaneously decreasing the number of fuel plates per element in those reactors that are not currently operating at their thermal-hydraulic limits. Results presented in this section are based on matching the fuel cycle length of the HEU design using LEU fuel.

Table A19 contains a matrix of burnup calculations for the 2 MW reactor, initially with 19 plates and 180 g ^{235}U per standard element, for various numbers of plates, fuel meat thicknesses, and water channel thicknesses. Only fuels with 20% enriched uranium are considered. Fuel plates were successively removed from the 19 plate standard element and the additional space was utilized to thicken the fuel meat in the remaining plates. The clad thicknesses of 0.38 mm and 0.495 mm on the inner and the outer fuel plates were preserved. Fuel plates were also successively removed from the control fuel elements. The minimum water channel thickness (2.188 mm) considered here is that of a fuel element initially containing 23 fuel plates. This is not necessarily the minimum thickness. A water channel thickness of 2.916 mm preserves the water channel geometry of the 19 plate, HEU fuel element design. The results of thermal-hydraulic calculations for these fuel element design variations are discussed in Section A.2.3.

Individual cross section sets were prepared for each case to assure that spatial and resonance self-shielding of the ^{235}U and ^{238}U isotopes are properly accounted for.

Using the REBUS-2 fuel cycle analysis code and the fuel shuffling pattern shown in Fig. A22, a search was done on the average burnup of discharged fuel elements in the HEU reference case such that the reactor was just critical at the end of equilibrium cycle (EOC). The beginning of equilibrium cycle (BOC) k_{eff} was 1.0058, and the fuel cycle length was 10.0 days. No attempt was made in this generic study to provide excess reactivity for xenon override or for experimental loads since these parameters vary from reactor to reactor. Most reactors operating in this power range contain about 30 standard fuel elements instead of the 19 standard elements specified for these studies. The computed EOC ^{235}U and Pu content in each fuel element of the reference equilibrium core containing HEU are shown in Fig. A27.

For the fuel element design variations shown in Table A19, the fuel cycle length was fixed at 10.0 days, and a search was performed on the LEU density in the fuel meat of the fresh feed element such that the EOC equilibrium core was just critical.

With this procedure, a ^{235}U loading of 213 g per fresh fuel element (ρ_u = 2.9 g/cm in the fuel meat) was found if no changes are made in the geometry of the HEU element design. For comparison, a ^{235}U loading of 221 g per fresh element was required (Table A12) with the conservative reactivity matching criterion. The computed EOC ^{235}U and Pu content in each LEU fuel element of the equilibrium core are shown in Fig. A28. Ratios of the average fast, epithermal,and thermal fluxes with LEU and HEU fuel in each fuel element and peak fluxes in the central irradiation channel and reflector at beginning and end of equilibrium cycle are shown in Fig. A29. Fast fluxes throughout the reactor and epithermal fluxes in the central irradiation channel are virtually identical for the HEU and LEU cases. In the LEU core, epithermal fluxes are reduced by less than 2% at the reflector peak and by 2-3% in the active core. Thermal fluxes are reduced by about 4% in the central irradiation channel, by about 6% in the reflector, and by about 15% in the active core.

Table A19. 2 MW Reactor - Fuel Element Design Variations With Equilibrium Core Using 20% Enriched Uranium Fuel. Fresh Fuel Loadings Required to Match the 10.0 Day Cycle Length of the HEU (93%) Reference Case With 180 g ^{235}U per Initial Standard Element

Number of Plates	Enrichment, %	H/^{235}U, Std. Element* (Fresh Fuel)	Thickness of Meat, mm	Thickness of Water Channel, mm	Volume of Meat, cm^3	Uranium Density, g/cm^3	^{235}U Density, g/cm^3	wt.% U**	^{235}U per Fresh Elmt. grams
19	93	334	0.510	2.916	366	0.53	0.492	17.5	180
19	20	282	0.510	2.916	366	2.91	0.582	59.0	213
19	20	140	1.238	2.188	889	1.83	0.367	45.4	326
18	20	279	0.588	3.071	400	2.68	0.535	56.6	214
18	20	265	0.665	2.994	446	2.48	0.496	53.8	221
18	20	250	0.743	2.916	506	2.25	0.451	51.5	228
18	20	118	1.471	2.188	1001	1.83	0.366	45.3	366
17	20	277	0.674	3.245	433	2.49	0.499	54.4	216
17	20	247	0.839	3.080	539	2.13	0.427	49.8	230
17	20	218	1.003	2.916	645	1.91	0.383	46.7	247
17	20	99	1.731	2.188	1112	1.87	0.373	45.9	415
16	20	188	1.295	2.916	783	1.73	0.346	43.8	271
15	20	159	1.626	2.916	922	1.64	0.328	42.2	302
14	20	131	2.005	2.916	1061	1.62	0.323	41.9	343
13	20	105	2.442	2.916	1200	1.67	0.333	42.7	400
12	20	81	2.952	2.916	1339	1.80	0.360	44.9	482

*Includes a 1 mm water channel surrounding each element.

**Porosity of 7 volume percent assumed with 20% Enriched UAl_x-Al Fuel.

Figure A27. 2 MW Reactor - HEU (93%) Fuel
End of Equilibrium Cycle Distribution of ^{235}U and Pu Based on Fuel Cycle Length Matching Criterion (0.51 mm Meat Thickness)

U Enrichment : 93%
U Density : 0.53 g/cm^3
Fresh Fuel Loading : 180 g ^{235}U

BOC k_{eff} : 1.0058
EOC k_{eff} : 0.9999
Cycle Length : 10.0 Days

END OF EQUILIBRIUM CYCLE

19 159.2 g ^{235}U 0.07 g Pu	8 169.5 0.03	9 168.3 0.04	10 167.0 0.04	11 165.9 0.05	12 165.1 0.05
18 159.9 0.06	CFE-1 131.3 0.03	1 178.3 g ^{235}U 0.01 g Pu	CFE-2 128.8 0.04	4 173.9 0.02	13 164.1 0.05
17 160.8 0.06	3 175.3 0.02	FLUX TRAP (H_2O)	2 176.6 0.01	CFE-3 130.6 0.04	14 163.1 0.05
16 161.7 0.06	CFE-4 133.9 0.02	7 170.5 0.03	6 171.7 0.03	5 172.9 0.02	15 162.3 0.06

Figure A28. 2 MW Reactor - LEU (20%) Fuel
End of Equilibrium Cycle Distribution of ^{235}U and Pu Based on Fuel Cycle Length Matching Criterion (0.51 mm Meat Thickness)

U Enrichment : 20%
U Density : 2.91 g/cm^3
Fresh Fuel Loading : 213 g ^{235}U

BOC k_{eff} : 1.0052
EOC k_{eff} : 1.0001
Cycle Length : 10.0 Days

END OF EQUILIBRIUM CYCLE

19 192.5 g ^{235}U 1.46 g Pu	8 202.7 0.76	9 201.5 0.85	10 200.2 0.93	11 199.2 1.01	12 198.4 1.06
18 193.2 1.42	CFE-1 157.5 0.78	1 211.4 g ^{235}U 0.12 g Pu	CFE-2 155.1 0.95	4 207.1 0.45	13 197.4 1.14
17 194.1 1.36	3 208.4 0.34	FLUX TRAP (H_2O)	2 209.8 0.24	CFE-3 156.9 0.84	14 196.4 1.21
16 195.0 1.30	CFE-4 159.9 0.54	7 203.7 0.69	6 204.9 0.61	5 206.1 0.52	15 195.6 1.26

Figure A29. 2 MW Reactor - 180 g ^{235}U (93%) per Fresh Standard Element Ratios of Average Fast, Epithermal, Thermal, and Total fluxes with LEU and HEU Fuel in Each Fuel Element and Peak Fluxes in Flux Trap and Reflector at Beginning and End of Equilibrium Cycle Based on Fuel Cycle Matching Criterion (0.51 mm Meat Thickness).

FAST (>5.53 keV).

19 1.007 1.005	8 0.997 0.996	9 0.992 0.992	10 0.990 0.989	11 0.987 0.987	12 0.989 0.989	
18 1.006 1.004	CFE-1 1.000 0.999	1 0.994 0.994	CFE-2 0.991 0.991	4 0.984 0.984	13 0.987 0.987	
17 1.009 1.007	3 1.005 1.004	FLUX TRAP 0.999 0.998	2 0.993 0.993	CFE-3 0.989 0.989	14 0.990 0.990	REFL. 0.989 0.989
16 1.016 1.014	CFE-4 1.012 1.010	7 1.008 1.006	6 0.996 0.995	5 0.990 0.990	15 0.994 0.994	

EPITHERMAL (0.625 eV < E < 5.53 keV)

19 0.982 0.980	8 0.976 0.975	9 0.971 0.970	10 0.969 0.968	11 0.965 0.965	12 0.965 0.965	
18 0.984 0.982	CFE-1 0.984 0.983	1 0.976 0.976	CFE-2 0.975 0.975	4 0.966 0.966	13 0.965 0.965	
17 0.986 0.984	3 0.987 0.985	FLUX TRAP 0.995 0.994	2 0.975 0.974	CFE-3 0.973 0.973	14 0.968 0.968	REFL. 0.977 0.977
16 0.992 0.989	CFE-4 0.994 0.993	7 0.986 0.985	6 0.974 0.974	5 0.970 0.970	15 0.970 0.970	

THERMAL (<0.625 eV)

19 0.852 0.850	8 0.847 0.845	9 0.844 0.842	10 0.840 0.838	11 0.836 0.835	12 0.842 0.842	
18 0.847 0.844	CFE-1 0.852 0.850	1 0.856 0.854	CFE-2 0.843 0.842	4 0.833 0.832	13 0.835 0.834	
17 0.850 0.847	3 0.864 0.862	FLUX TRAP 0.964 0.963	2 0.855 0.853	CFE-3 0.841 0.839	14 0.836 0.835	REFL. 0.942 0.942
16 0.863 0.860	CFE-4 0.871 0.868	7 0.869 0.867	6 0.851 0.849	5 0.845 0.844	15 0.845 0.844	

Reactivity worths of fission product poisons at beginning of equilibrium cycle in the HEU and LEU cores with 0.51 mm thick fuel meat are shown in Table A20. These fission product worths are very similar in the two cases.

Table A20. Reactivity Worths of Fission Product Poisions at Beginning of Equilibrium Cycle in HEU and LEU Cores With 0.51 mm Thick Fuel Meat (^{235}U Loadings Based on Equal Fuel Cycle Lengths)

	δ k/k (%) for 93% Fuel	δ k/k (%) for 20% Fuel
No ^{135}Xe	2.34	2.23
No ^{149}Sm	0.57	0.58
No Lumped Fission Product Residuals	0.42	0.38

The remaining fuel element design variations in Table A19 must be considered in conjunction with thermal-hydraulic parameters and safety margins (see Table A22, Section A.2.3). Table A19 contains several potential alternatives for direct conversion to LEU fuel using current fuel fabrication technology, or technology that will be available in the near-term. One case, for example, considers a standard fuel element with 19 plates, a fuel meat thickness of 1.238 mm, and a water channel thickness of 2.188 mm. The uranium density in the fuel meat needed to match the 10.0 day cycle length of the HEU design was computed to be 1.8 g/cm^3, instead of the 2.9 g U/cm^3 value needed if no geometrical changes are made in the fuel element. Another possible alternative with 17 fuel plates per standard element, a fuel meat thickness of 1.0 mm, and a water channel thickness of 2.916 mm (no change from the reference HEU element) requires a uranium density of about 1.9 g/cm^3 to match the cycle length of the HEU design.

Table A19 also contains a systematic survey to determine the neutronic limits of fuel meat thickness for efficient utilization of fissile fuel with an initial ^{235}U (93%) loading of 180 g per element. The limiting neutronic variable is probably the hydrogen-to-^{235}U ratio in a standard fuel element since it is primarily this moderating ratio that determines the hardness of the neutron spectrum. Figure A30 shows the LEU density that is required to match the cycle length of the HEU design with different numbers of fuel plates, fuel meat thicknesses and H/^{235}U ratios, for a constant water channel thickness of 2.916 mm. Initially, the slope of this uranium density versus moderating ratio curve is very steep. For H/^{235}U less than about 150, increasing the fuel meat volume does not result in significantly lower uranium densities since the lattice is too under-moderated. Using this result, the approximate maximum fuel meat thickness that will result in the minimum uranium density can be found.

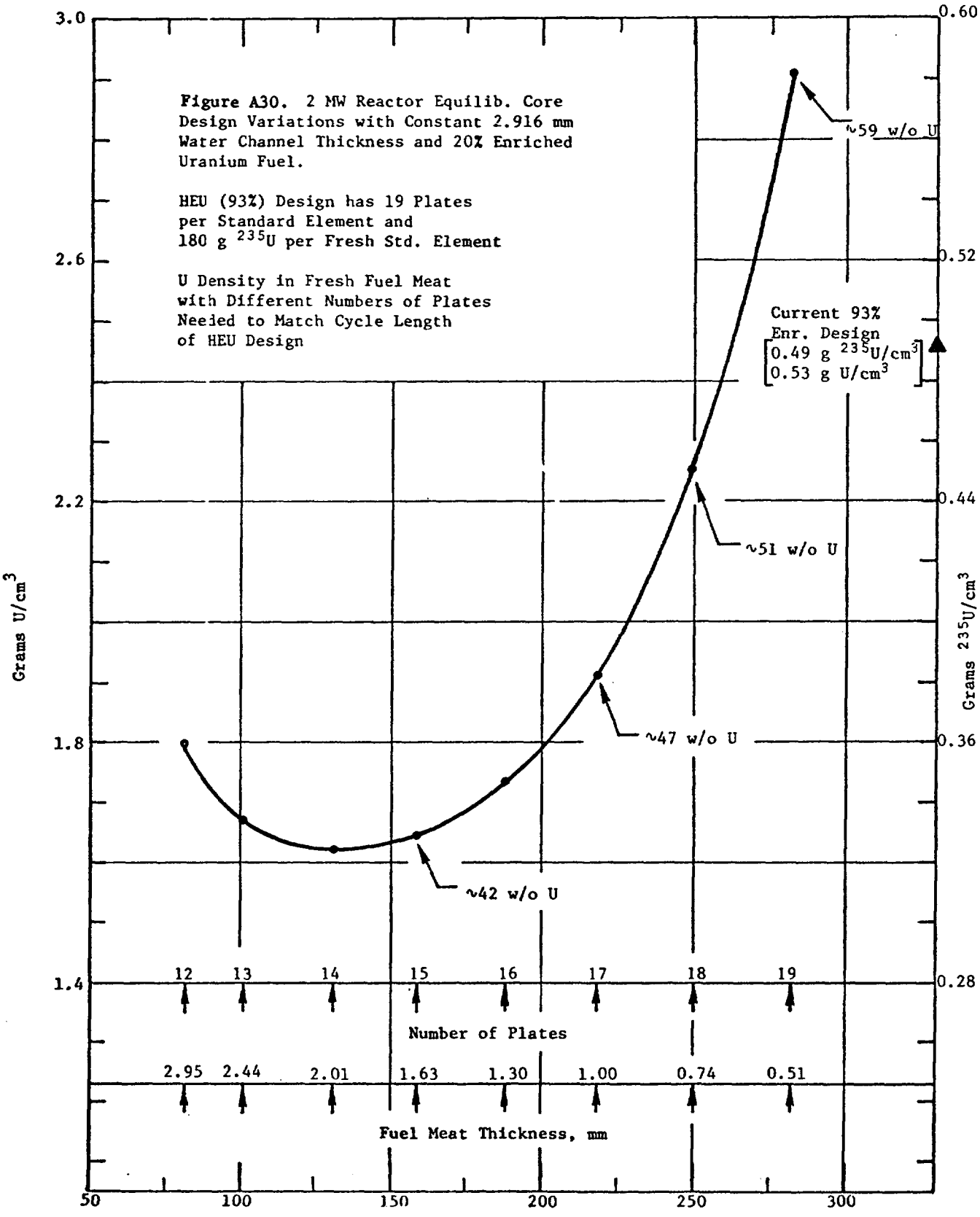
Figure A30. 2 MW Reactor Equilib. Core Design Variations with Constant 2.916 mm Water Channel Thickness and 20% Enriched Uranium Fuel.
HEU (93%) Design has 19 Plates per Standard Element and 180 g 235U per Fresh Std. Element
U Density in Fresh Fuel Meat with Different Numbers of Plates Needed to Match Cycle Length of HEU Design
Current 93% Enr. Design
[0.49 g 235U/cm3
0.53 g U/cm3]
~59 w/o U
~51 w/o U
~47 w/o U
~42 w/o U
Grams U/cm3
Grams 235U/cm3
3.0
2.6
2.2
1.8
1.4
0.60
0.52
0.44
0.36
0.28
12 13 14 15 16 17 18 19
Number of Plates
2.95 2.44 2.01 1.63 1.30 1.00 0.74 0.51
Fuel Meat Thickness, mm
50 100 150 200 250 300

A.2.3 Thermal-Hydraulics

The thermal-hydraulic aspects of the 2 MW plate-type reactor were studied by using the methods outlined in Section A.1.3. The results of these studies are summarized in the following four sub-sections. The input parameters used in the calculations are shown in TAble A21.

Table A21. Input Values Used in the Thermal-Hydraulic Calculation for the IAEA 2 MW Reactor

Parameter	Value Used	Parameter	Value Used
W (cm)	6.64	λ (kJ/Kg)	2203.2
W_h (cm)	6.30	E (Bar)	0.7306×10^6
H_{co} (cm)	60.0	ν	0.33
L_c (cm)	62.5	K	0.5
t_e (cm)	8.0	f_a	1.58
t_{co} (cm)	0.0495	f_r	2.0
t_{ci} (cm)	0.0381	ρ (kg/m^3)	990.2*
T_{in} (C)	38.0	μ (Pascal-Sec)	6.0507×10^{-4}
P (bar abs)	1.961	k (W/mK)	0.640
T_{sat} (C)	119.6	C_p (kJ/KgK)	4.176

*Water properties are assumed to be constant and evaluated at mean coolant temperature. For 2 MW these are evaluated at 45°C.

A.2.3.1 Average Heat Flux at ONB and Friction Loss in Channel

For a given constant value of average heat flux at ONB (q_a), the water channel thickness can be derived as a function of coolant velocity by using Eqs. (14) and (15). Similarly, the water channel thickness versus coolant velocity can be derived from Eq. (6) for a given constant value of friction pressure loss (ΔP_f) in channel. These parametric curves of constant q_a at ONB and constant ΔP_f are plotted in Fig. A31.

As an example, at the reference design point of the 2 MW reactor (0.2916 cm water channel thickness and 0.94 m/s coolant velocity), Fig. A31 shows that ONB will not occur when the reactor is operated at average heat fluxes below 11.4 W/cm^2. At this design point, the friction pressure drop in the channel is about 0.019 bar. For the same water channel thickness, if the coolant velocity is increased to 1.1 m/s, the heat flux at ONB will increase to 13 W/cm^2 and the corresponding friction pressure drop will be 0.02 bar.

For a given water channel thickness, the average heat flux at ONB as a function of coolant velocity can also be derived using Eq. (14). Results for the 2 MW reactor are presented in Fig. A32. As shown in this figure, for the same coolant velocity, a thicker water channel allows a higher heat flux at ONB.

Figure A31. 2 MW Reactor

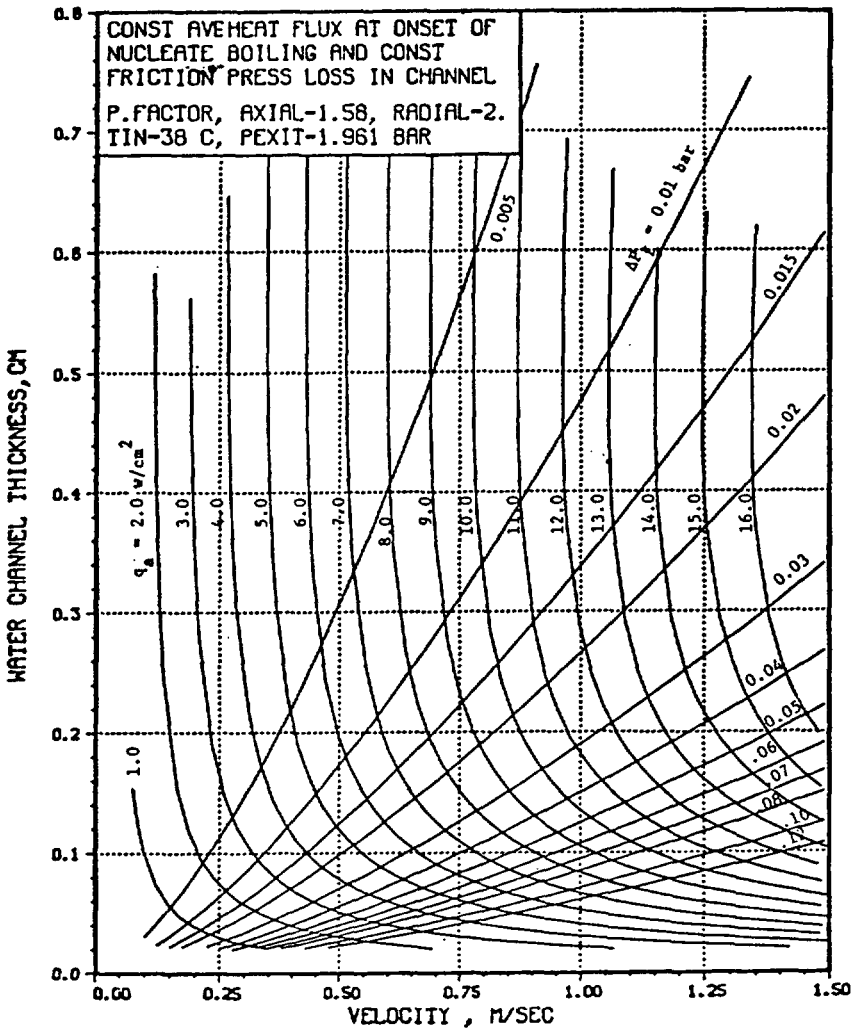

Figure A32. 2 MW Reactor

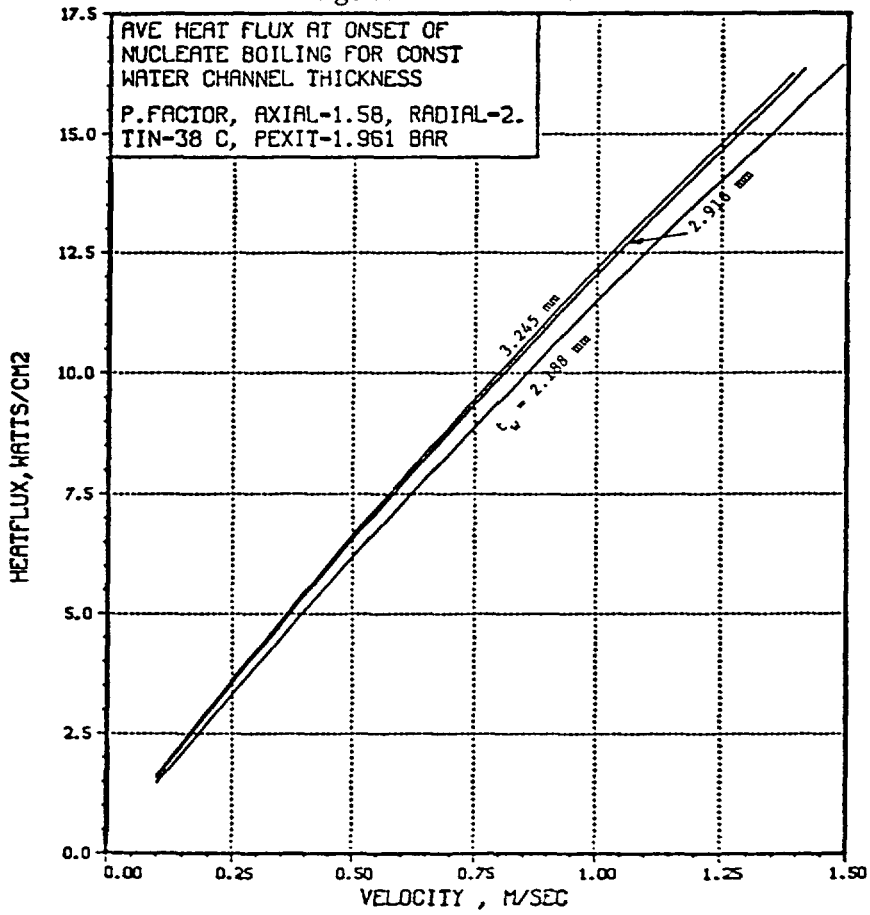

A.2.3.2 Total Pressure Drop and Flow Through an Element

For a given water channel thickness and number of plates per element, the friction pressure loss in channel (ΔP_f), total pressure drop across the fuel channel (ΔP_F) and volumetric flow rate (Q) through an element can be derived as functions of coolant velocity from Eqs. (6), (10), and (3), respectively. Figures A33 and A34 present the results for the 2 MW reactor. As shown in Fig. A33, a thicker water channel requires a lower pressure drop for the same coolant velocity. At the same coolant velocity and water channel thickness, using fewer plates per element results in thicker plates and smaller cross-sectional flow area, which causes a higher total pressure drop across the fuel channel. Figure A34 shows that at the same coolant velocity, using a thicker channel and more (thinner) plates per element results in a larger flow through the element.

A.2.3.3 Critical Flow Velocity

For a given number of plates and fixed element dimensions, the critical flow velocity can be derived as a function of water channel thickness by using Eqs. (1) and (11). Results for the 2 MW reactor are presented in Fig. A35. As shown in this figure, for the same water channel thickness, fewer plates in the element corresponds to thicker, more rigid plates, and therefore, a higher critical velocity. The calculated critical flow velocity is generally about 10 times larger than the nominal channel velocity in the 2 MW reactor.

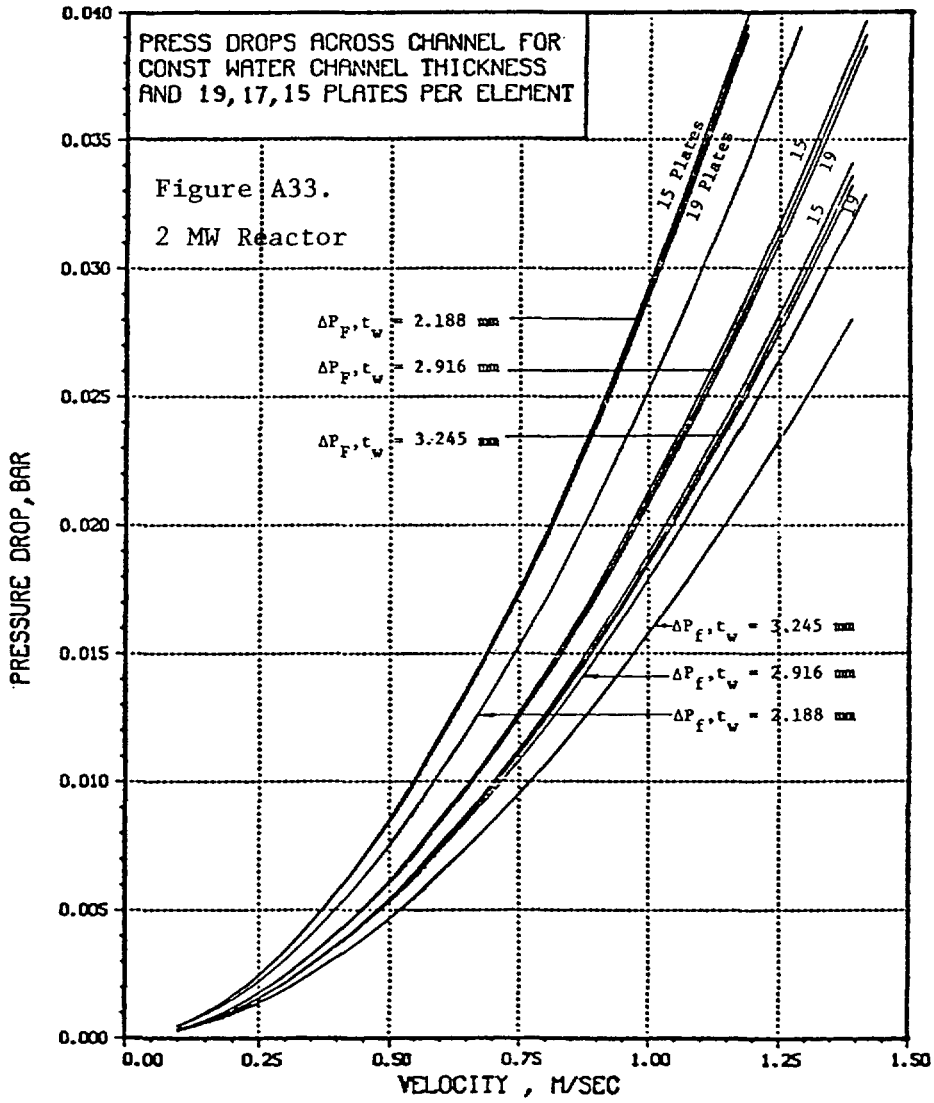

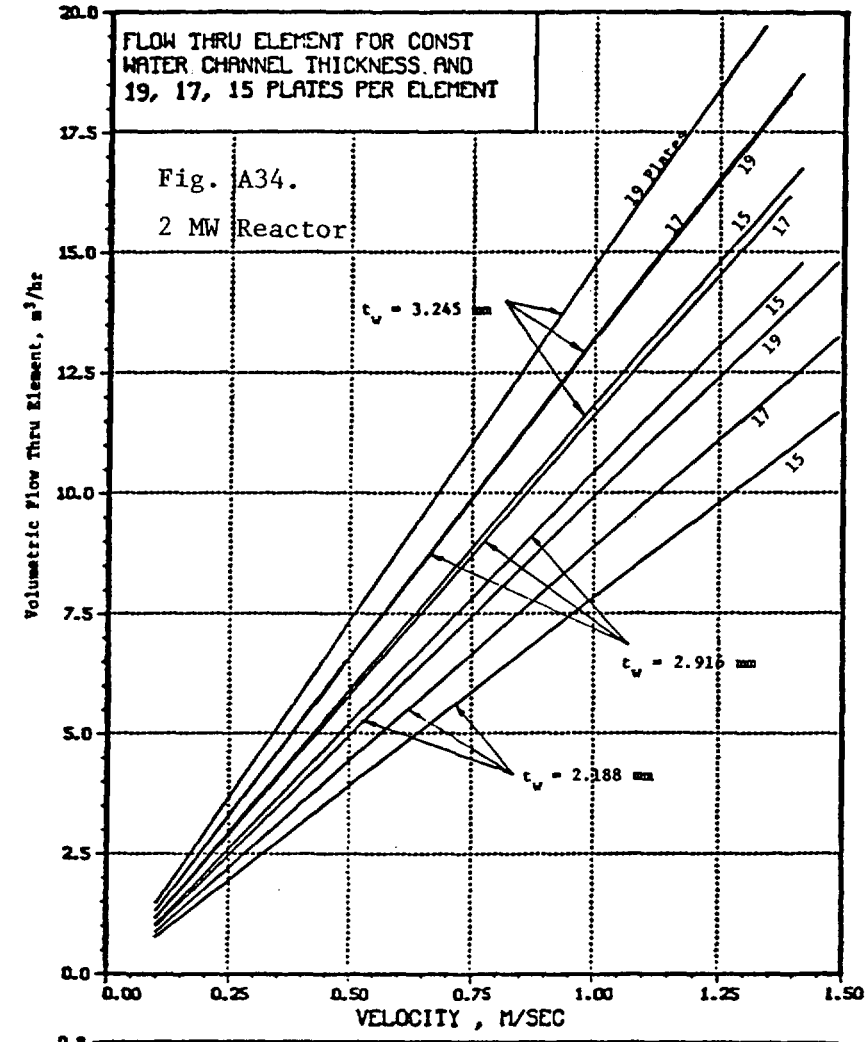

Fig. A34.
2 MW Reactor

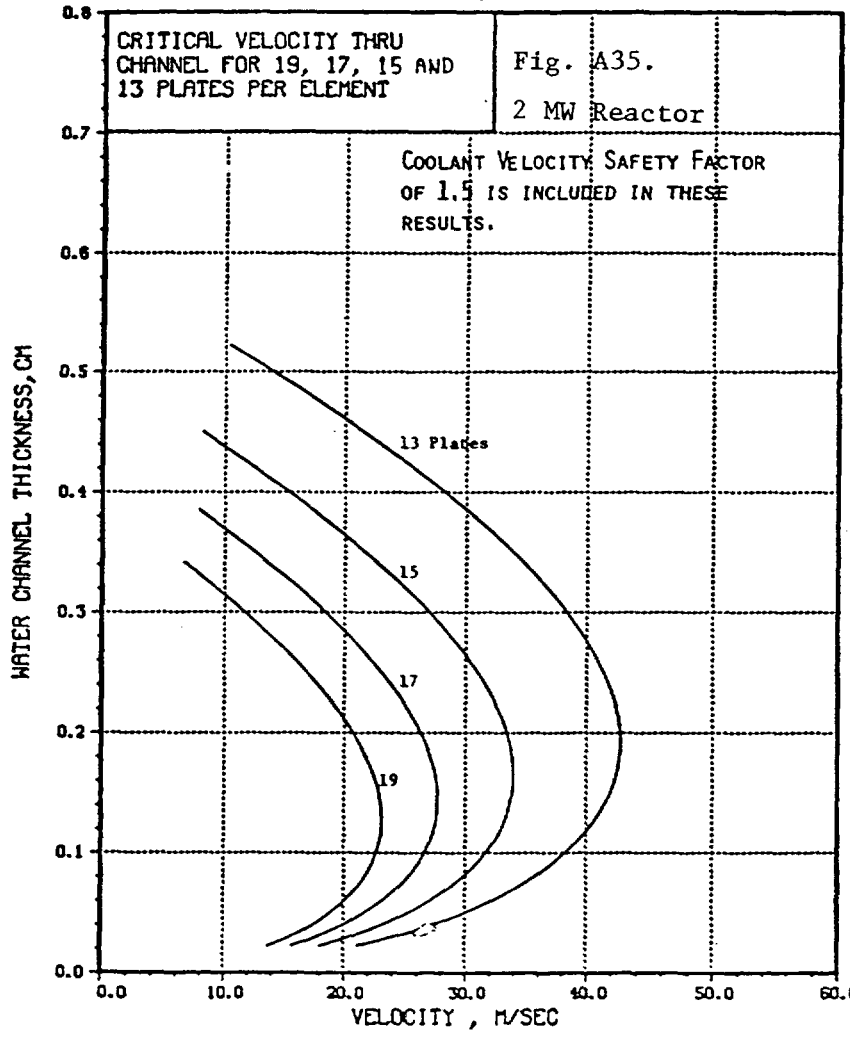

Fig. A35.
2 MW Reactor

A.2.3.4 Heat Fluxes at Onset of Flow Instability and Burnout

The limiting heat flux at onset of flow instability was calculated using the Forgan correlation (Eqs. 19 and 20, with η = 25). For a given system pressure and inlet coolant temperature, this heat flux is proportional to the coolant velocity and channel thickness.

The Labuntsov and the Mirshak correlations (Fig. A10) were used to calculate the burnout heat flux because they yield more conservative results in comparison with the other DNB correlations. Results of the calculations show that the exit subcooling is negative for the range of coolant velocities considered in the 2MW reactor. Under this condition, which is outside the range of applicability of these two correlations, the burnout heat flux was estimated using these correlations extrapolated with zero subcooling (see Section A.1.3.7). In general, the estimated burnout heat flux increases as the coolant velocity increases.

A.2.3.5 Fuel Element Design Variations - Thermal-Hydraulics

Table A22 presents some of the thermal-hydraulic design variations for the 2 MW reactor. These cases correspond to those considered in the burnup studies (Table A19). Numbers in the first row of Table A22 are data for the reference HEU case described in Table A10, and for the LEU case without fuel element redesign.

From this table, a few interesting points can be summarized:

(a) Fpr the same power level (i.e., average heat flux x number of plates = constant), a design with fewer plates will have higher average heat flux.
(b) For the same water channel thickness, a design with higher coolant velocity (at the cost of higher pressure drop) will have higher heat fluxes at ONB, at onset of flow instability, and at burnout.
(c) For the same coolant velocity, a design with a thicker water channel has a smaller pressure drop and higher heat fluxes at ONB and at onset of flow instability.
(d) For the same water channel thickness and coolant velocity, a design with fewer plates per element will have a slightly higher pressure drop across the fuel channel and a lower flow rate through the element due to the smaller cross sectional flow area.
(e) The volumetric flow rate is proportional to the number of plates per element, and the coolant temperature rise is inversely proportional to the flow rate. For a constant coolant inlet temperature, maintaining the same coolant temperature rise requires maintaining the same flow rate.
(f) For the design variations studied here, the increase in pressure drop is very small (less than 0.008 bar) compared with the reference HEU case. Thus, the pumping capability (see Section A.7.5) of the current HEU design is likely to be adequate.
(g) For the cases studied here, the margin to ONB is larger than 1.24; the margin to onset of flow instability ranges from 3.5 to 6.2; and the margin to DNB using both the Labuntsov and the Mirshak correlations ranges from 8 to 13.

From a thermal-hydraulic point of view, the results presented in Table A22 indicate that there are comfortable safety margins, with no major engineering difficulties, for these fuel element design variations.

TABLE A22. 2 MW Reactor
Thermal-Hydraulics
Fuel Element Design Variations
with 20% Enriched Uranium Fuel

Number of Plates	Thickness of Water Channel/Meat mm	Coolant Velocity m/s	Flow/ Element m^3/hr	Total Pressure Drop Across Channel bar	Avg.[b] Heat Flux W/cm^2	Avg. Heat[c] Flux at ONB W/cm^2	Burnout Heat Flux, W/cm^2		Limiting[f] Heat Flux at Onset of Flow Instability W/cm^2	Margin[g] to ONB	Margin[h] to DNB		Margin[i] to Onset of Flow Instability
							Labuntsov[d]	Mirshak[e]			Labuntsov	Mirshak	
19[a]	2.916/0.510	0.94	12.45	0.0186	5.80	11.4	231	231	102.2	1.94	12.6	12.6	5.58
19	2.916/0.510	0.99	13.08	0.0204	5.80	11.9	235	232	107.6	2.05	12.8	12.7	5.87
19	2.916/0.510	1.05	13.90	0.0266	5.80	12.6	240	233	114.1	2.17	13.1	12.7	6.23
19	2.188/1.238	0.94	9.34	0.0259	5.80	10.8	231	231	80.8	1.86	12.6	12.6	4.41
18	3.071/0.588	0.94	12.39	0.0177	6.12	11.5	231	231	106.5	1.88	11.9	11.9	5.51
18	2.994/0.665	0.94	12.09	0.0182	6.12	11.5	231	231	104.3	1.88	11.9	11.9	5.39
18	2.916/0.743	0.94	11.80	0.0188	6.12	11.4	231	231	102.2	1.86	11.9	11.9	5.28
18	2.916/0.743	0.99	12.44	0.0205	6.12	11.9	235	232	107.6	1.94	12.2	12.0	5.56
18	2.188/1.471	0.94	8.85	0.0260	6.12	10.8	231	231	80.8	1.76	11.9	11.9	4.18
17	3.245/0.674	0.94	12.39	0.0167	6.48	11.6	231	231	111.1	1.79	11.3	11.3	5.43
17	3.080/0.839	0.94	11.79	0.0177	6.48	11.5	231	231	106.7	1.77	11.3	11.3	5.21
17	2.916/1.003	0.94	11.15	0.0188	6.48	11.4	231	231	102.2	1.76	11.3	11.3	4.99
17	2.916/1.003	1.05	12.45	0.0229	6.48	12.6	240	233	114.1	1.94	11.7	11.4	5.57
17	2.188/1.731	0.94	8.36	0.0261	6.48	10.8	231	231	80.8	1.67	11.3	11.3	3.95
16	2.916/1.295	0.94	10.49	0.0189	6.89	11.4	231	231	102.2	1.65	10.6	10.6	4.69
15	2.916/1.626	0.94	9.83	0.0191	7.35	11.4	231	231	102.2	1.55	9.9	9.9	4.40
14	2.916/2.005	0.94	9.18	0.0192	7.87	11.4	231	231	102.2	1.45	9.3	9.3	4.11
13	2.916/2.442	0.94	8.52	0.0193	8.48	11.4	231	231	102.2	1.34	8.6	8.6	3.81
12	2.916/2.952	0.94	7.86	0.0195	9.19	11.4	231	231	102.2	1.24	8.0	8.0	3.52

[a]Reference HEU case and LEU case with no redesign.

[b]Peak Heat Flux = 1.58 x 2.0 x Avg. Heat Flux.

[c]The average heat flux at ONB is calculated with the conservative assumption that ONB occurs at the channel exit with peak heat flux, lowest pressure and saturation temperature, and highest coolant temperature rise.

[d]Burnout heat flux estimated using the Labuntsov correlation extrapolated with zero subcooling (see Section A.1.3.7 and Fig. A15).

[e]Burnout heat flux estimated using the Mirshak correlation extrapolated with zero subcooling (see Section A.1.3.7 and Fig. A15).

[f]Limiting heat flux at onset of instability due to flow excursion calculated with the Forgan correlation.

[g]Minimum ratio of local heat flux for ONB to actual heat flux.

[h]Minimum ratio of local heat flux for DNB using Labuntsov and Mirshak correlations to actual peak heat flux.

[i]Minimum ratio of local heat flux for onset of instability due to flow excurstion to actual peak heat flux.

A.3 APPLICATION TO THE 10 MW REACTOR BASED ON CLASSICAL PLATE-TYPE FUEL

A.3.1 Introduction

General design specifications agreed upon at the Consultants' Meeting for a typical 10 MW research reactor are shown in Table A23. The initial conditions were not completely specified and the input data was only selected within a limited range. The specific design descriptions for the reactor and the fuel elements that were used in the ANL calculations are shown in Table A24.

Neutronics and thermal-hydraulics results based on matching the fuel cycle length of the HEU design are presented for a range of alternatives for conversion to fuels with reduced uranium enrichment. Based on the discussion in Section A.2.2 of the differences in ^{235}U loadings with LEU fuel calculated using the cycle length and reactivity matching criteria, only the cycle length matching criterion is considered for conversion of the 10 MW reactor.

The 10 MW reactor can be converted to use 45% enriched uranium fuel, without change in the fuel element geometry and without change in the core thermal-hydraulics, by simple substitution of a new fuel meat with a uranium density of about 1.48 g/cm^3. Since fuel with this uranium density can be readily manufactured with currently-qualified fuel fabrication technology (1.6 - 1.7 g U/cm^3), no further effort has been expended on this alternative.

The data reported here consider enrichment reductions directly from 93% to <20% with various fuel element geometries. Several options with thicker fuel meat and fewer than 23 plates per standard element are identified for which the cycle length of the HEU core can be matched with LEU densities in the 2.3 - 3.0 g U/cm^3 range. Fuel development programs in several countries are currently in progress to achieve uranium densities in this range with UAl_x-Al and U_3O_8-Al cermet fuels.

A.3.2 Neutronics

A.3.2.1 Calculational Model

Five-group microscopic cross sections were prepared using the EPRI-CELL code[1] with the methods described in Section A.1.2. The design details of the physical fuel element are shown in Fig. A36. The geometry of the unit cell used for cross section preparation is shown in Fig. A37. Individual cross sections sets were prepared for uranium enrichments of 93% and 20% for each fuel meat and water channel thickness to be reported.

The ZR and XY models used in the two-dimension diffusion theory calculations based on matching the fuel cycle length of the HEU and LEU equilibrium cores are shown in Figs. A38 and A39, respectively. All results are reported for the XY model. The purpose of the ZR calculations was to determine extrapolation lengths for use in the XY cases. Separate ZR calculations were done for each change in reactor parameters, e.g., a change in uranium enrichment, uranium density, fuel meat thickness, and/or water channel thickness.

In the burnup studies (using the REBUS-2[15] fuel cycle analysis code), fresh fuel is inserted near the center of the reactor (position 1), and the remaining standard fuel elements are rotated sequentially after each cycle. Standard fuel elements are discharged from position 23 after 23 operational cycles. The control fuel elements are fixed (see comments in Section A.2.2). With this fuel shuffling pattern, the REBUS-2 code was used to search for the equilibrium burnup distribution at the beginning and end of each operational cycle. The procedures used in the calculations are discussed further in Section A.3.2.2. This fuel shuffling pattern is intended to be illustrative, and not necessarily practical or optimal.

Table A23. 10 MW Reactor - General Description of Design Parameters

Fuel Element: MTR-Type Element (76 x 80 x 600 mm)

Number of Fuel Plates in:

Standard Fuel Element: 23

Control Fuel Element: 17 Fuel + 4 Al Plates (Fork Type Absorber Blades)

Plate Dimensions: Standard MTR-Plate

Plate Thickness: 1.27 mm

Meat Thickness: 0.51 mm

Shape of Plate: Straight

Fuel Loading: Standard Fuel Element: 280 g U-235

Control Fuel Element: 207 g U-235 (without burnable poison)

Core Size: 28 Fuel Elements

Standard Fuel Elements: 23

Control Fuel Elements: 5

Core Geometry: 5 x 6 Arrangement

1 Irradiation Channel in the Core Center

1 Irradiation Channel at the Core Edge

Absorber Plates: Thin Fork Type Absorber Blades

Grid Plate: 6 (8) x 9

Reflector: Water 2 Core Sides Reflected by Graphite and Water (76 mm)

Desired Average Burnup of U-235 in the Fuel Element Discharged from the Core: 50%

Burnup Status of the Core: Equilibrium Core

Fuel Shuffling: New Fuel Elements into Core Edge

Thermo-Hydraulic Data: Coolant Flow rate: 1000 m^3/h (16666 dm^3/min)

Core Inlet Temperature: 38°C

Table A24. 10 MW Reactor - Description of Design Parameters Used in USA/ANL Calculations

Reactor Design Description

Reactor Type	Pool Type MTR
Steady-State Power Level	10 MW
Number of Standard Fuel Elements	23
Number of Control Fuel Elements	5
Irradiation Channels	1 at Core Center 1 at Core Edge
Core Geometry	5 x 6 Arrangement
Grid Plate	8 x 9 Positions
^{235}U Content/Core	7475 g
Active Core Volume	105 ℓ
Average Volumetric Power Density	95.2 kW/ℓ
Average Linear Power Density	0.27 kW/cm
Specific Power	1338 kW/kg ^{235}U
Moderator, Coolant	Water
Reflectors	Graphite on Two Sides Water on Two Sides

Fuel Assembly Design Description

Type	MTR, Straight Plates
Uranium Enrichment	93%
Lattice Pitch	77 x 81 mm
Fuel Element Dimensions	76 x 80 x 600 mm
Plate Thickness	1.27 mm (Inner Plates) 1.50 mm (Outer Plates)
Water Channel Thickness	2.188 mm
Plates/Standard Fuel Element	23
Plates/Control Fuel Element	17 + 4 Al Plates
Fuel Meat	UAl_x-Al (21 wt.% U)
Meat Dimensions	0.51 x 63 x 600 mm
Clad Thickness (Al)	0.38 mm (Inner Plates) 0.495 mm (Outer Plates)
^{235}U Density in Fuel Meat	0.6315 g/cm^3
^{235}U/Standard Fuel Element	280 g
^{235}U/Control Fuel Element	207 g
Coolant Flow Rate	1000 m^3/h
Core Inlet Temperature	38°C
Burnup Status of Core	Fresh Loading and Equilibrium Core

Figure A36. 10 MW Reactor - Standard[a] (23 Plates/Element) and Control[a,b] (17 Plates/Element) Fuel Elements.

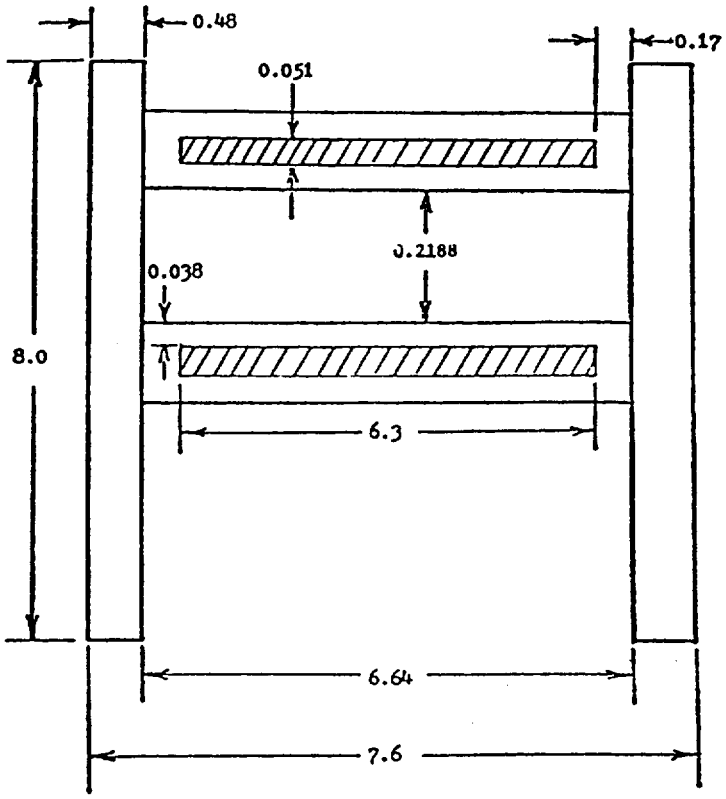

All dimensions in cm.

[a]The two outermost plates have a clad thickness of 0.0495 cm.

[b]Control fuel elements have four Al plates/ element, assuming two fork-type absorber plates/element.

[c]Including a 0.5 mm water channel surrounding each element.

VOLUME FRACTIONS[c]

Standard Fuel Element		Control Fuel Element	
Fuel Meat	0.1185	Fuel Meat	0.0876
Aluminum	0.3205	Aluminum	0.3244
Water	0.5610	Water	0.5880

Figure A37. 10 MW Reactor - Geometry of Unit Cell for EPRI-CELL Calculation of Reference Core Cross Sections (All Dimensions in cm).

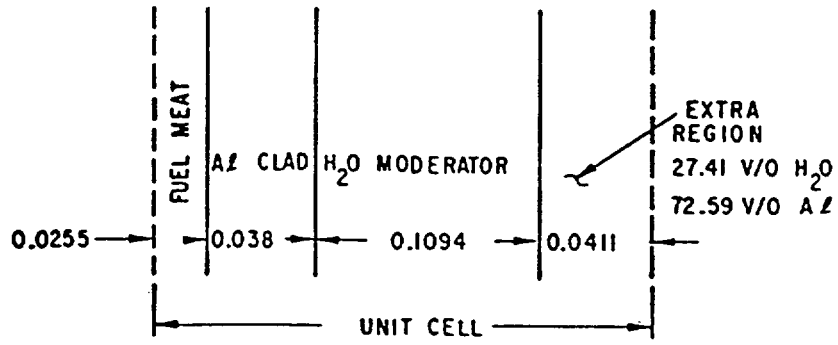

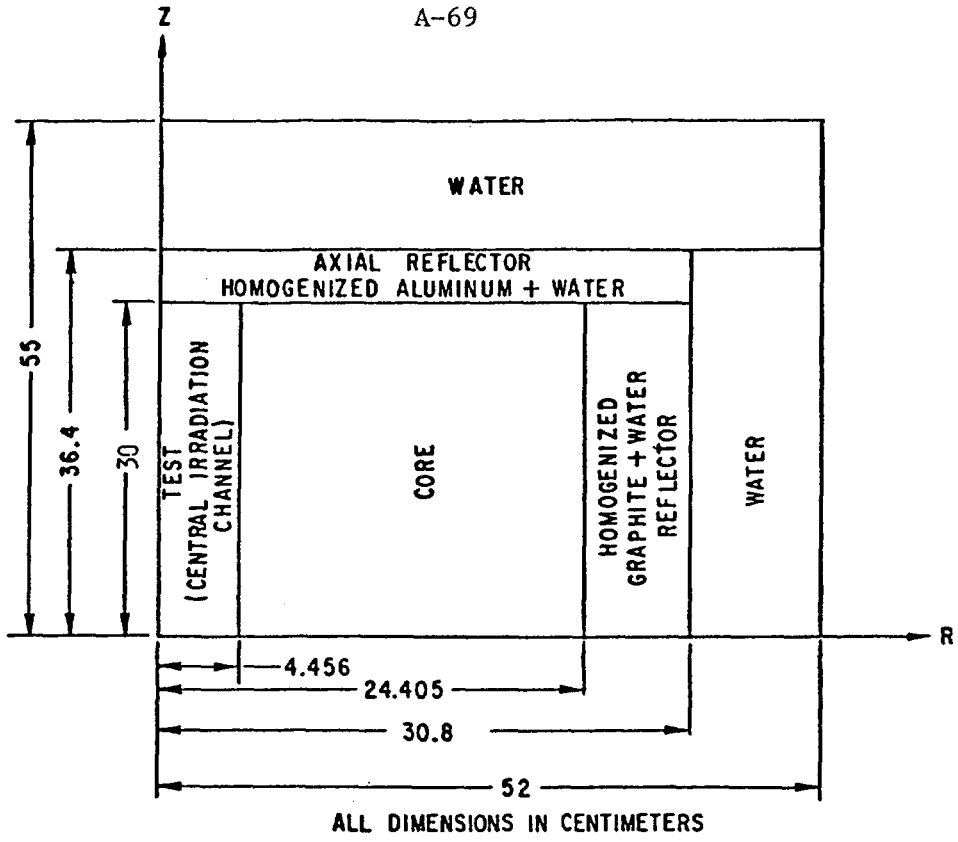

Figure A38. ZR Model for 10 MW Reactor

Fresh Fuel is Inserted into Position 1. All Standard Elements Are Rotated Sequentially After Each Cycle. Standard Elements Are Discharged From Position 23 After 23 Operational Cycles. The Control Fuel Elements Are Fixed

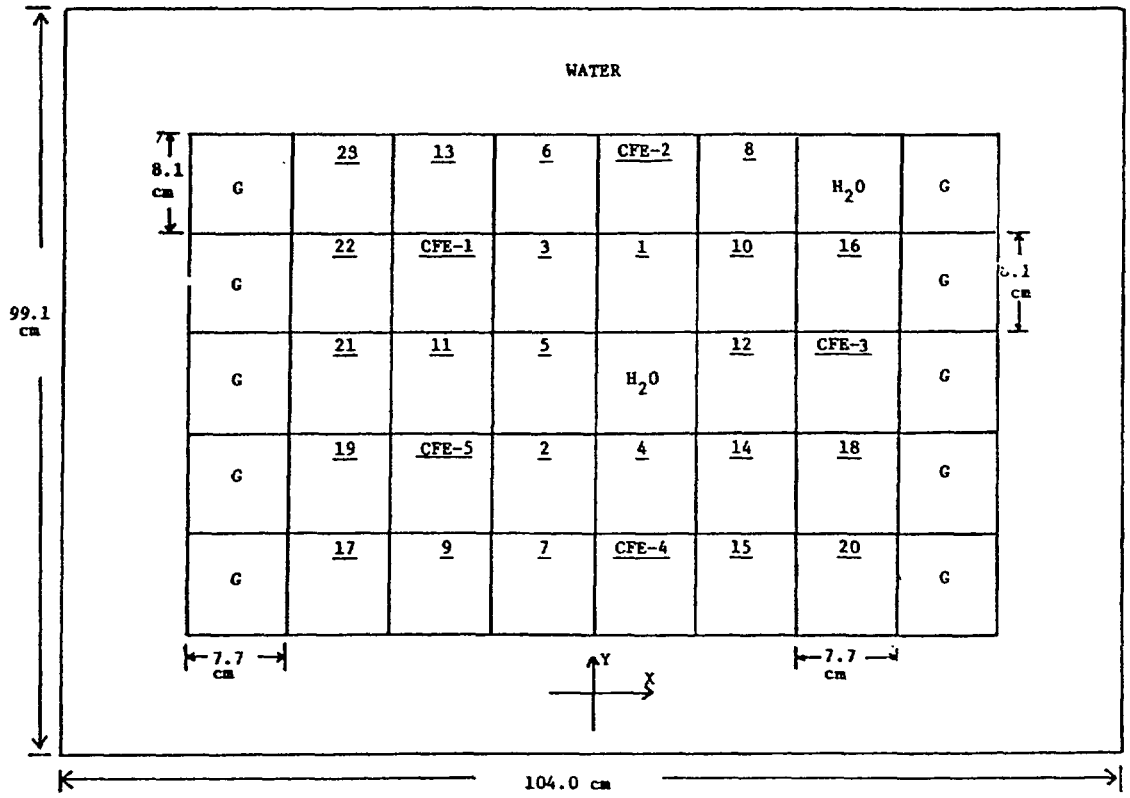

Figure A39. XY Model for Burnup Studies of 10 MW Reactor Based on Matching Cycle Lengths of HEU and LEU Cores

A.3.2.2 Burnup Studies - Fuel Element Design Variations

The results of burnup calculations are presented for the uranium density in the fuel meat that is required to match the cycle length of the 10 MW HEU (93%) core using LEU (20%) fuel with various fuel element geometries. One design variation with 19 fuel plates per standard element is studied extensively. The results of thermal-hydraulic calculations for all geometries studied are discussed in Section A.3.3. Individual cross section sets were prepared for each case.

Using the REBUS-2 fuel cycle analysis code and the fuel shuffling pattern shown in Fig. A39, a search was performed on the average burnup of discharged fuel elements in the HEU (93%) reference case such that the reactor was just critical at the end of equilibrium cycle (EOC). The beginning of equilibrium cycle (BOC) k_{eff} was 1.0210; the average discharge burnup was 63.7%, and the average fuel cycle length was 16.7 days. No attempt was made in this generic study to provide excess reactivity for xenon override or for experimental loads since these parameters vary from reactor to reactor. The computed EOC ^{235}U and Pu content in each fuel element of the reference equilibrium core containing HEU are shown in Fig. A40.

With the same fuel element geometry (23 fuel plates per standard element, 0.51 mm fuel meat thickness) as the HEU (93%) case and with a fixed cycle length of 16.7 days, a search was performed on the LEU (20%) density in the fuel meat of the fresh feed element such that the EOC equilibrium core was just critical. The resulting uranium density was found to be 3.59 g/cm^3, as compared with 5.91 g/cm^3 obtained using the reactivity matching criterion. The computed EOC ^{235}U and Pu content in each LEU fuel element of the equilibrium core are shown in Figure A41.

Ratios of the average fast, epithermal,and thermal fluxes with LEU and HEU fuel in each fuel element and peak fluxes in the central and edge irradiation channels at beginning and end of equilibrium cycle are shown in Fig. A42 for the cases with 23 plates and 0.51 mm fuel meat thickness. These ratios vary throughout the core, depending upon core position and residence time. Generally, the fast and epithermal fluxes in the active core with LEU fuel were computed to be equal to or greater than those with HEU fuel. Thermal flux reductions in the active core ranged from 10% to 25%. The thermal flux was reduced by about 4% in the central irradiation channel and by about 10% in the edge irradiation channel.

Table A25 contains a matrix of burnup calculations for the 10 MW reactor based on matching the average fuel cycle length (16.7 days) of the HEU (93%) design for different numbers of plates, fuel meat thicknesses, and water channel thicknesses per standard element. Only fuels with 20% enriched uranium are considered. The procedure for fuel element geometry changes is identical with that described in Section A.2.2.3 for the 2 MW reactor.

A standard element with 19 fuel plates was studied extensively. As expected, increasing the fuel meat volume decreases the uranium density required in the fresh feed elements. The required uranium densities vary from 3.96 g/cm^3 for 0.51 mm fuel meat thickness to 2.27 g/cm^3 for 1.238 mm fuel meat thickness. The effect is not linear, through, due to increasing undermoderation of the neutron spectrum for smaller $H/^{235}U$. The optimum fuel meat thickness for practical conversions will depend upon the fabricability and qualification of fuel with a particular uranium density, as well as on safety margin, thermal-hydraulic, and backfitting considerations.

Figure A40. 10 MW Reactor - HEU (93%) Fuel
End of Equilibrium Cycle Distribution of ^{235}U and Pu Based on
Fuel Cycle Length Matching Criterion (0.51 mm Fuel Meat Thickness)

U Enrichment : 93%
U Density : 0.68 g/cm^3
Fresh Fuel Loading : 280 g ^{235}U

BOC k_{eff} : 1.0210
EOC k_{eff} : 1.0000
Cycle Length : 16.7 Days

END OF EQUILIBRIUM CYCLE

GRAPHITE							GRAPHITE
	23 101.6 g ^{235}U 0.57 g Pu	13 151.1 0.48	6 207.3 0.32	CFE-2 121.1 0.26	8 191.6 0.36	H_2O	
	22 105.2 0.57	CFE-1 110.4 0.31	3 242.0 0.18	1 266.5 g ^{235}U 0.06 g Pu	10 176.3 0.41	16 133.3 0.52	
	21 110.0 0.56	11 166.7 0.45	5 216.0 0.29	H_2O	12 157.4 0.47	CFE-3 130.1 0.25	
	19 118.9 0.55	CFE-5 110.0 0.31	2 254.0 0.13	4 229.7 0.23	14 144.0 0.50	18 124.1 0.54	
	17 128.9 0.53	9 184.3 0.38	7 198.8 0.35	CFE-4 119.9 0.26	15 138.5 0.51	20 115.3 0.55	

Figure A41. 10 MW Reactor - LEU (20%) Fuel
End of Equilibrium Cycle Distribution of ^{235}U and Pu Based on
Fuel Cycle Length Matching Criterion (0.51 mm Fuel Meat Thickness, 23 Plates)

U Enrichment : 20%
U Density : 3.59 g/cm^3
Fresh Fuel Loading : 318 g ^{235}U

BOC k_{eff} : 1.0145
EOC k_{eff} : 1.0003
Cycle Length : 16.7 Days

END OF EQUILIBRIUM CYCLE

GRAPHITE							GRAPHITE
	23 148.2 g ^{235}U 11.61 g Pu	13 198.0 9.04	6 251.3 5.56	CFE-2 154.3 5.06	8 236.5 6.51	H_2O	
	22 152.0 11.49	CFE-1 144.7 6.10	3 283.6 3.15	1 305.9 g ^{235}U 1.06 g Pu	10 221.1 7.53	16 180.5 10.03	
	21 156.9 11.25	11 213.1 8.21	5 259.4 4.98	H_2O	12 204.1 8.70	CFE-3 163.3 4.84	
	19 166.0 10.80	CFE-5 144.2 6.17	2 294.6 2.14	4 272.2 4.03	14 191.2 9.51	18 171.3 10.50	
	17 176.1 10.22	9 229.6 6.96	7 243.3 6.13	CFE-4 153.0 5.05	15 185.7 9.78	20 162.3 10.94	

Figure A42. 10 MW Reactor

20% : 23 Plates per Std. Element; 0.51 mm Fuel Meat Thickness

93% : 23 Plates per Std. Element; 0.51 mm Fuel Meat Thickness

Ratios of Average Fast, Epithermal, and Thermal Fluxes with LEU and HEU Fuel in Each Fuel Element and Peak Fluxes in Central and Edge Flux Traps at Beginning and End of Equilibrium Cycle Based on Cycle Length Matching Criterion.

EPITHERMAL (0.625 eV < E < 5.53 keV)

GRAPHITE							GRAPHITE
	23 1.021 1.020	13 0.979 0.976	6 0.948 0.943	CFE-2 0.951 0.945	8 0.954 0.948	H_2O 0.979 0.973	
	22 1.014 1.012	CFE-1 0.980 0.977	3 0.942 0.937	1 0.940 0.934	10 0.956 0.951	16 0.980 0.975	
	21 1.004 1.002	11 0.969 0.965	5 0.945 0.939	H_2O 0.952 0.946	12 0.971 0.967	CFE-3 0.994 0.990	
	19 1.003 0.999	CFE-5 0.977 0.972	2 0.946 0.940	4 0.953 0.947	14 0.977 0.972	18 1.000 0.996	
	17 0.999 0.995	9 0.970 0.964	7 0.953 0.947	CFE-4 0.971 0.964	15 0.990 0.985	20 1.014 1.010	

Fast (>5.53 keV)

GRAPHITE							GRAPHITE
	23 1.084 1.082	13 1.017 1.014	6 0.974 0.969	CFE-2 0.976 0.970	8 0.985 0.979	H_2O 1.002 0.997	
	22 1.069 1.068	CFE-1 1.007 1.004	3 0.961 0.956	1 0.957 0.951	10 0.985 0.980	16 1.025 1.020	
	21 1.057 1.055	11 0.998 0.996	5 0.968 0.962	H_2O 0.963 0.957	12 1.005 1.000	CFE-3 1.022 1.018	
	19 1.052 1.049	CFE-5 1.003 0.999	2 0.964 0.958	4 0.975 0.968	14 1.013 1.008	18 1.047 1.043	
	17 1.049 1.045	9 1.001 0.995	7 0.980 0.973	CFE-4 0.997 0.991	15 1.032 1.027	20 1.072 1.067	

THERMAL (<0.625 eV)

GRAPHITE							GRAPHITE
	23 0.743 0.737	13 0.758 0.748	6 0.790 0.777	CFE-2 0.792 0.779	8 0.791 0.780	H_2O 0.922 0.915	
	22 0.729 0.721	CFE-1 0.771 0.758	3 0.807 0.790	1 0.833 0.816	10 0.763 0.749	16 0.761 0.751	
	21 0.731 0.720	11 0.756 0.741	5 0.808 0.791	H_2O 0.937 0.929	12 0.771 0.757	CFE-3 0.794 0.783	
	19 0.737 0.727	CFE-5 0.774 0.760	2 0.815 0.797	4 0.814 0.797	14 0.744 0.730	18 0.745 0.735	
	17 0.760 0.751	9 0.781 0.768	7 0.793 0.779	CFE-4 0.797 0.784	15 0.752 0.741	20 0.753 0.745	

Table A25.

10 MW Reactor - Cycle Length Matching Criterion (16.7 Days)
Fuel Element Design Variations With 20% Enriched Uranium Fuel[a]

Number of Plates	Enrichment, %	H/^{235}U, Std. Element[b]	Thickness of meat, mm	Thickness of Water Channel, mm	Volume of Meat cm^3/Element	Uranium Density, g/cm^3	^{235}U Density, g/cm^3	wt.% U[c]	^{235}U per Element, grams
23	93	196	0.51	2.188	443	0.68	0.632	22	280
23	20	172	0.51	2.188	443	3.59	0.718	66.3	318
21	20	145	0.839	2.188	666	2.60	0.523	56.6	346
19	20	207	0.51	2.916	366	3.96	0.792	69.2	290
19	20	184	0.70	2.726	503	3.05	0.610	61.4	307
19	20	171	0.80	2.626	575	2.77	0.554	58.6	319
19	20	158	0.90	2.526	646	2.56	0.512	56.2	331
19	20	145	1.00	2.426	718	2.42	0.483	54.4	347
19[a]	20	113	1.238	2.188	889	2.27	0.453	52.6	403
18	20	97	1.471	2.188	1001	2.23	0.445	52.1	446
17	20	83	1.731	2.188	1112	2.24	0.448	52.2	498

[a]All calculations in the table were done with microscopic cross sections corresponding to the fuel element with average burnup in the core. To investigate changes in cycle length and uranium density in the fresh feed elements due to cross section variation with burnup, the calculations for both the reference 93% enriched case and the 19 plate case with 1.238 mm thick fuel meat were repeated for extreme values of the cross sections. With microscopic cross sections corresponding to slightly-burned (i.e., at equilibrium Xe and Sm) fresh elements, the cycle length in both the 93% and the 20% enriched cases was 15.9 days, and the uranium density in the fresh feed elements of the 20% enriched case was 2.26 g/cm^3. With microscopic cross sections corresponding to elements with the discharge burnup, the cycle length in both the 93% and 20% enriched cases was 17.4 days, and the uranium density in the fresh feed elements of the 20% enriched case was 2.24 g/cm^3.

[b]Includes a 1 mm water channel surrounding each element.

[c]Porosity of 10 volume percent assumed with 20% enriched UAl_x-Al fuel.

For the 19 plate case with the same water channel thickness (2.188 mm) as the 23 plate element, a uranium density of only 2.27 g/cm^3 is required in the fresh fuel meat to obtain a cycle length of 16.7 days. For this case (1.238 mm thick fuel meat), the computed EOC ^{235}U and Pu content in each fuel element are shown in Fig. A43. Ratios of the various fluxes between this LEU case and the HEU reference case are shown in Fig. A44. In the core, fast fluxes are increased by 1-27%, and thermal fluxes are reduced by 40-45% because of the high ^{235}U loading. Peak thermal fluxes in the H2O flux traps are reduced by a maximum of about 7%.

Figure A43. 10 MW Reactor - LEU (20%) Fuel

End of Equilibrium Cycle Distribution of ^{235}U and Pu Based on Fuel Cycle Length Matching Criterion (1.238 mm Fuel Meat Thickness, 19 Plates)

U Enrichment : 20%
U Density : 2.27 g/cm^3
Fresh Fuel Loading : 403 g ^{235}U

BOC k_{eff} : 1.0108
EOC k_{eff} : 1.0002
Cycle Length : 16.7 Days

END OF EQUILIBRIUM CYCLE

GRAPHITE							GRAPHITE
	23 232.5 g ^{235}U 13.83 g Pu	13 286.5 10.27	6 340.0 6.06	CFE-2 234.0 6.17	8 324.9 7.18	H_2O	
	22 236.9 13.64	CFE-1 227.5 7.63	3 371.1 3.36	1 391.4 g ^{235}U 1.14 g Pu	10 310.7 8.40	16 268.0 11.58	
	21 242.2 13.28	11 302.1 9.22	5 347.9 5.40	H_2O	12 292.8 9.83	CFE-3 242.8 6.10	
	19 252.3 12.64	CFE-5 227.0 7.71	2 381.1 2.28	4 360.1 4.34	14 279.6 10.87	18 257.9 12.23	
	17 263.1 11.84	9 318.0 7.72	7 332.0 6.72	CFE-4 231.9 6.23	15 273.8 11.24	20 248.0 12.84	

Figure A45 shows the LEU density in the fresh feed element that is required to match the fuel cycle length of the HEU design for a constant water channel thickness of 2.188 mm and the corresponding maximum fuel meat thickness for different numbers of plates. Initially, the required uranium density decreases in approximate proportion to the increase in fuel meat volume. The curve becomes nonlinear for H/^{235}U < 150 and reaches a minimum for H/^{235}U ~ 100. For H/^{235}U < 100, further increases in the fuel meat volume result in about the same or larger uranium densities in the fresh feed elements due to the severe undermoderation of the neutron spectrum. For fewer than 17 plates per element and larger fuel meat thicknesses than 1.73 mm, the required uranium density is expected to increase substantially.

The neutronic limit of H/^{235}U $\sim$ 100 is also expected to hold approximately if the number of fuel plates is fixed and the fuel meat thickness is varied until the minimum uranium density is obtained. This result is apparent for the design variations in Table A25 for 19 plates per standard element.

Figure A44. 10 MW Reactor

20% : 19 Plates per Std. Element; 1.238 mm Fuel Meat Thickness

93% : 23 Plates per Std. Element; 0.51 mm Fuel Meat Thickness

Ratios of Average Fast, Epithermal, and Thermal Fluxes with LEU and HEU Fuel in Each Fuel Element and Peak Fluxes in Central and Edge Flux Traps at Beginning and End of Equilibrium Cycle Based on Cycle Length Matching Criterion.

EPITHERMAL (0.625 eV < E < 5.53 keV)

GRAPHITE							GRAPHITE
	23	13	6	CFE-2	8	H_2O	
	1.173 1.167	1.071 1.064	1.005 0.997	1.014 1.007	1.035 1.027	1.096 1.088	
	22	CFE-1	3	1	10	16	
	1.139 1.133	1.052 1.046	0.973 0.966	0.972 0.965	1.016 1.009	1.093 1.085	
	21	11	5	H_2O	12	CFE-3	
	1.117 1.110	1.028 1.020	0.977 0.968	0.999 0.993	1.043 1.037	1.113 1.104	
	19	CFE-5	2	4	14	18	
	1.117 1.109	1.046 1.036	0.983 0.971	1.002 0.990	1.058 1.047	1.128 1.117	
	17	9	7	CFE-4	15	20	
	1.129 1.117	1.053 1.041	1.017 1.004	1.056 1.043	1.104 1.092	1.174 1.161	

FAST (>5.53 keV)

GRAPHITE							GRAPHITE
	23	13	6	CFE-2	8	H_2O	
	1.274 1.269	1.133 1.126	1.043 1.010	1.061 1.054	1.087 1.078	1.121 1.112	
	22	CFE-1	3	1	10	16	
	1.228 1.224	1.102 1.097	1.008 1.000	1.003 0.997	1.069 1.061	1.169 1.160	
	21	11	5	H_2O	12	CFE-3	
	1.200 1.194	1.076 1.070	1.016 1.007	1.009 1.001	1.102 1.095	1.165 1.156	
	19	CFE-5	2	4	14	18	
	1.197 1.189	1.095 1.086	1.015 1.003	1.040 1.028	1.121 1.110	1.207 1.196	
	17	9	7	CFE-4	15	20	
	1.210 1.198	1.104 1.091	1.062 1.048	1.105 1.092	1.175 1.162	1.270 1.257	

THERMAL (<0.625 eV)

GRAPHITE							GRAPHITE
	23	13	6	CFE-2	8	H_2O	
	0.600 0.591	0.587 0.575	0.619 0.604	0.608 0.596	0.653 0.640	0.990 0.977	
	22	CFE-1	3	1	10	16	
	0.545 0.534	0.551 0.537	0.601 0.582	0.657 0.638	0.570 0.555	0.612 0.600	
	21	11	5	H_2O	12	CFE-3	
	0.544 0.531	0.543 0.526	0.626 0.605	0.941 0.929	0.596 0.580	0.620 0.606	
	19	CFE-5	2	4	14	18	
	0.553 0.540	0.553 0.537	0.613 0.591	0.637 0.616	0.546 0.530	0.571 0.558	
	17	9	7	CFE-4	15	20	
	0.618 0.605	0.615 0.598	0.625 0.606	0.621 0.604	0.589 0.575	0.620 0.608	

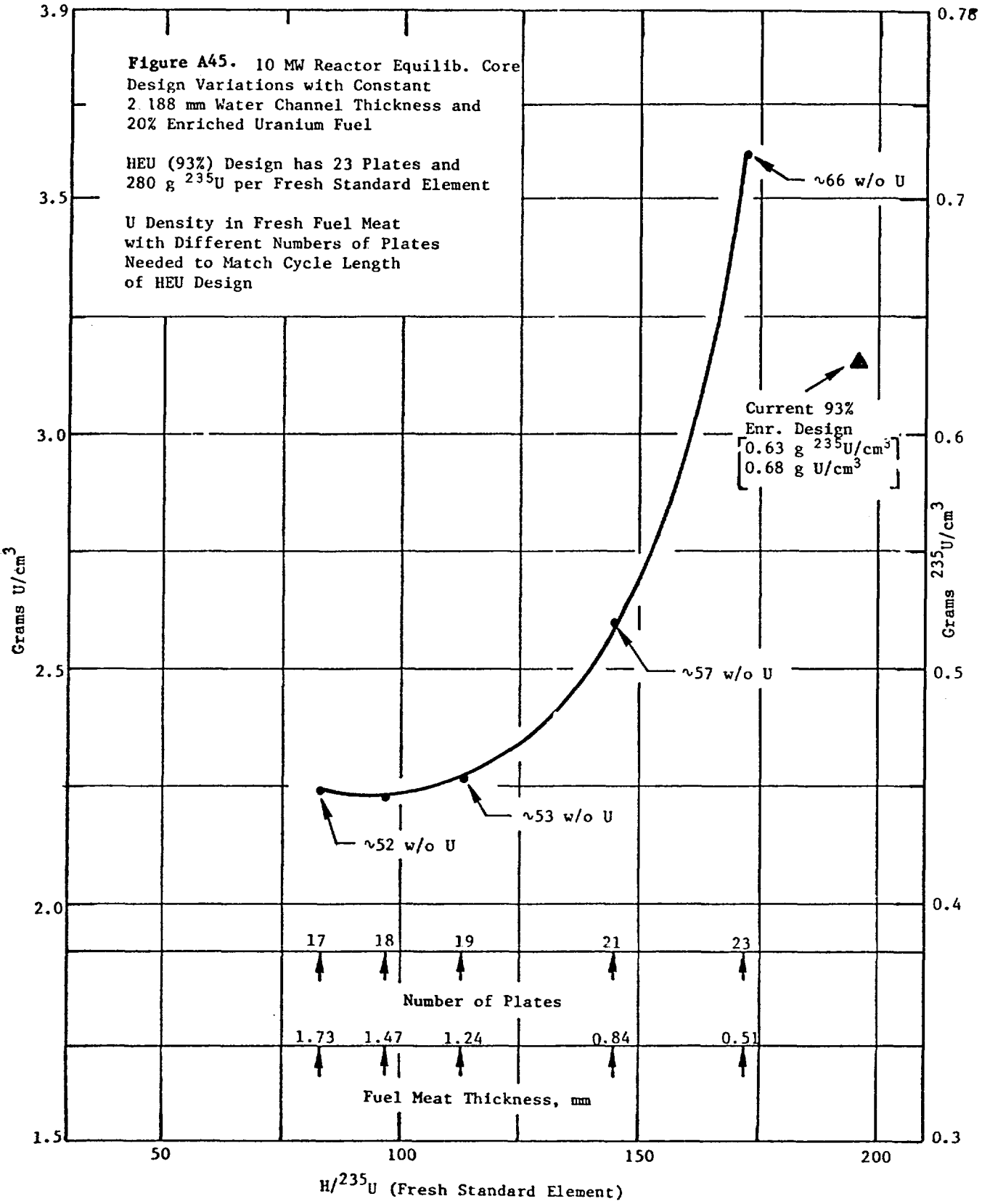
Figure A45. 10 MW Reactor Equilib. Core Design Variations with Constant 2.188 mm Water Channel Thickness and 20% Enriched Uranium Fuel
HEU (93%) Design has 23 Plates and 280 g 235U per Fresh Standard Element
U Density in Fresh Fuel Meat with Different Numbers of Plates Needed to Match Cycle Length of HEU Design
~66 w/o U
Current 93% Enr. Design
0.63 g 235U/cm3
0.68 g U/cm3
~57 w/o U
~53 w/o U
~52 w/o U
17
18
19
21
23
Number of Plates
1.73
1.47
1.24
0.84
0.51
Fuel Meat Thickness, mm
Grams U/cm3
Grams 235U/cm3
H/235U (Fresh Standard Element)
3.9
3.5
3.0
2.5
2.0
1.5
0.78
0.7
0.6
0.5
0.4
0.3
50
100
150
200

A.3.3 Thermal-Hydraulics

The thermal-hydraulic aspects of the 10 MW reactor using classical plate-type fuel were studied with the methods outlined in Section A.1.3. The results of these studies are summarized in the following four sub-sections. The input parameters used in the calculations are shown in Table A26.

Table A26. Input Values Used in the Thermal-Hydraulic Calculation for the IAEA 10 MW Reactor

Parameter	Value Used	Parameter	Value Used
W (cm)	6.64	λ (kJ/Kg)	2222.7
W_h (cm)	6.30	E (Bar)	0.7306×10^6
H_{co} (cm)	60.0	ν	0.33
L_c (cm)	62.5	K	0.5
t_e (cm)	8.0	f_a	1.4
t_{co} (cm)	0.0495	f_r	1.78
t_{ci} (cm)	0.0381	ρ (kg/m^3)	998.04*
T_{in} (C)	38.0	μ (Pascal-Sec)	5.551×10^{-4}
P (bar abs)	1.566	k (W/mK)	0.647
T_{sat} (C)	112.7	C_p (kJ/KgK)	4.178

*Water properties are assumed to be constant and evaluated at mean coolant temperature. For 10 MW these are evaluated at 48°C.

A.3.3.1 Average Heat Flux at ONB and Friction Loss in Channel

As discussed for the 2 MW reactor in Section A.2.3.1, parametric curves of water channel thickness versus coolant velocity are derived using Eqs. (6), (14), and (15) for constant average heat flux at ONB and for constant ΔP_f. Results for the 10 MW reactor are shown in Fig. A46. At the reference design point (0.2188 cm water channel thickness and 2.97 m/s coolant velocity), Fig. A46 shows that ONB will not occur when the reactor is operated at an average heat flux below 36 W/cm^2. At this design point, the friction pressure drop in the channel is about 0.17 bar. For the same water channel thickness, the heat flux at ONB will increase to 40 W/cm^2 and the corresponding friction pressure drop will be 0.2 bar if the coolant velocity is increased to 3.3 m/s.

The average heat flux at ONB is also derived as a function of coolant velocity for constant water channel thickness using Eq. (14). The results are plotted in Fig. A47. For the same coolant velocity, thicker water channels allow a higher heat flux at ONB.

Figure A46.

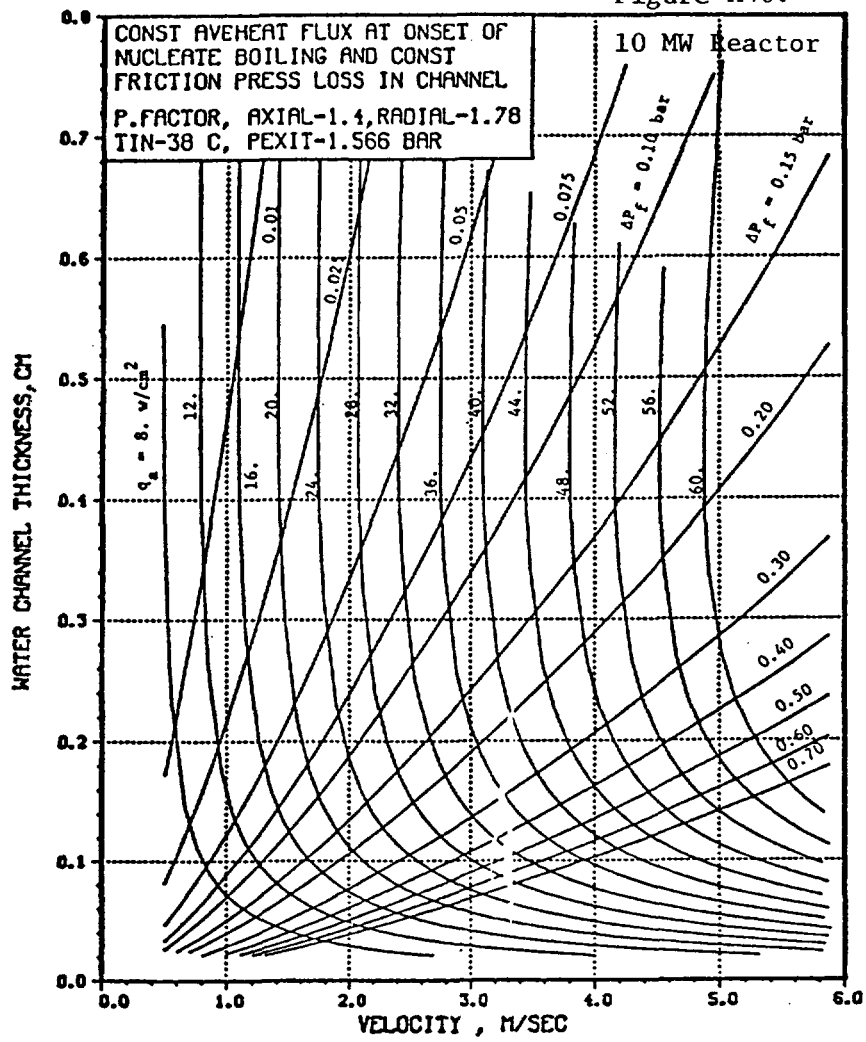

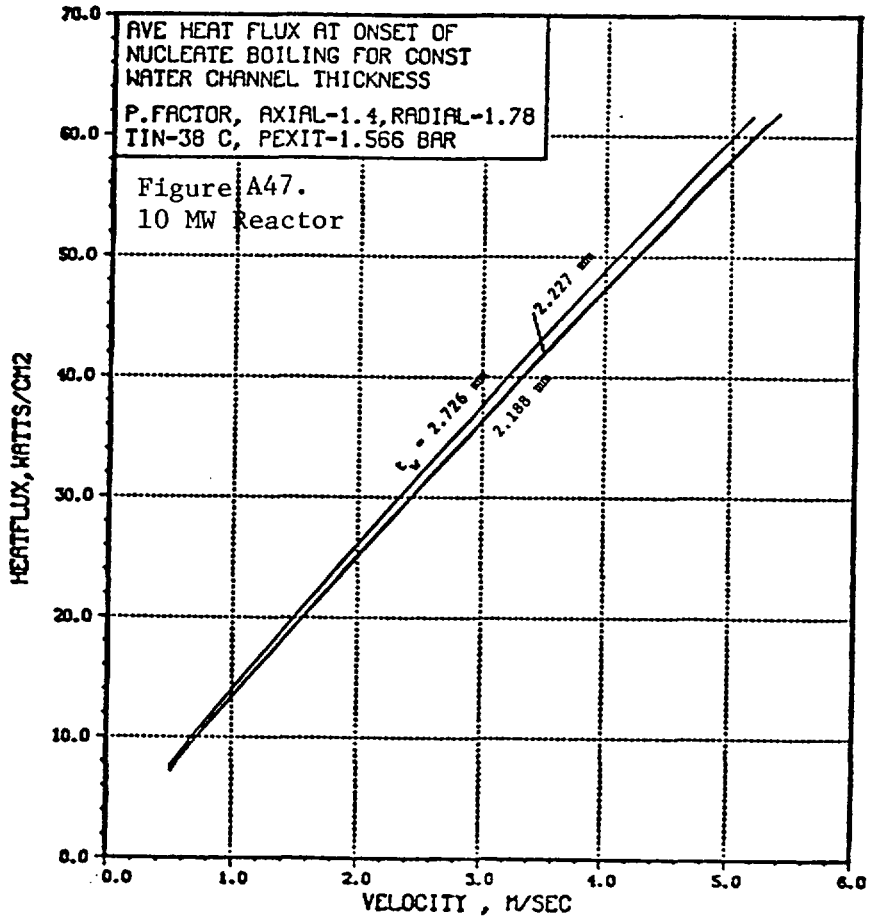

Figure A47.
10 MW Reactor

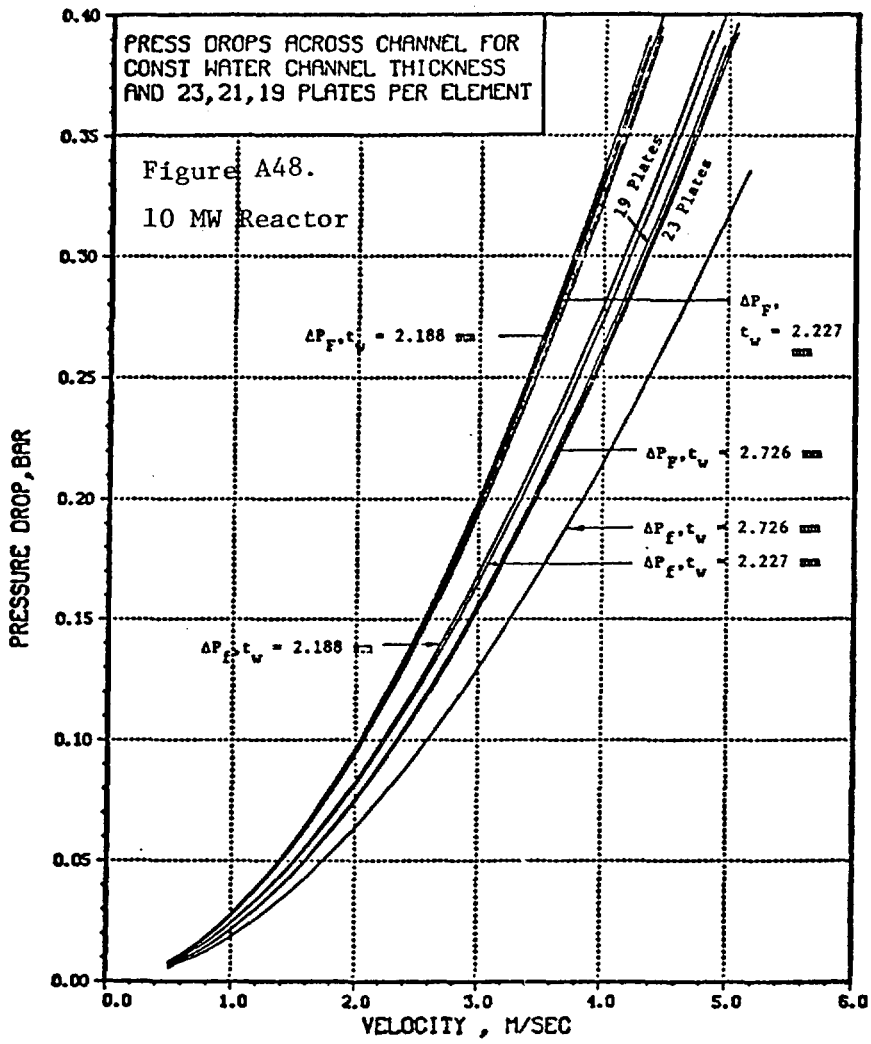

Figure A48.

10 MW Reactor

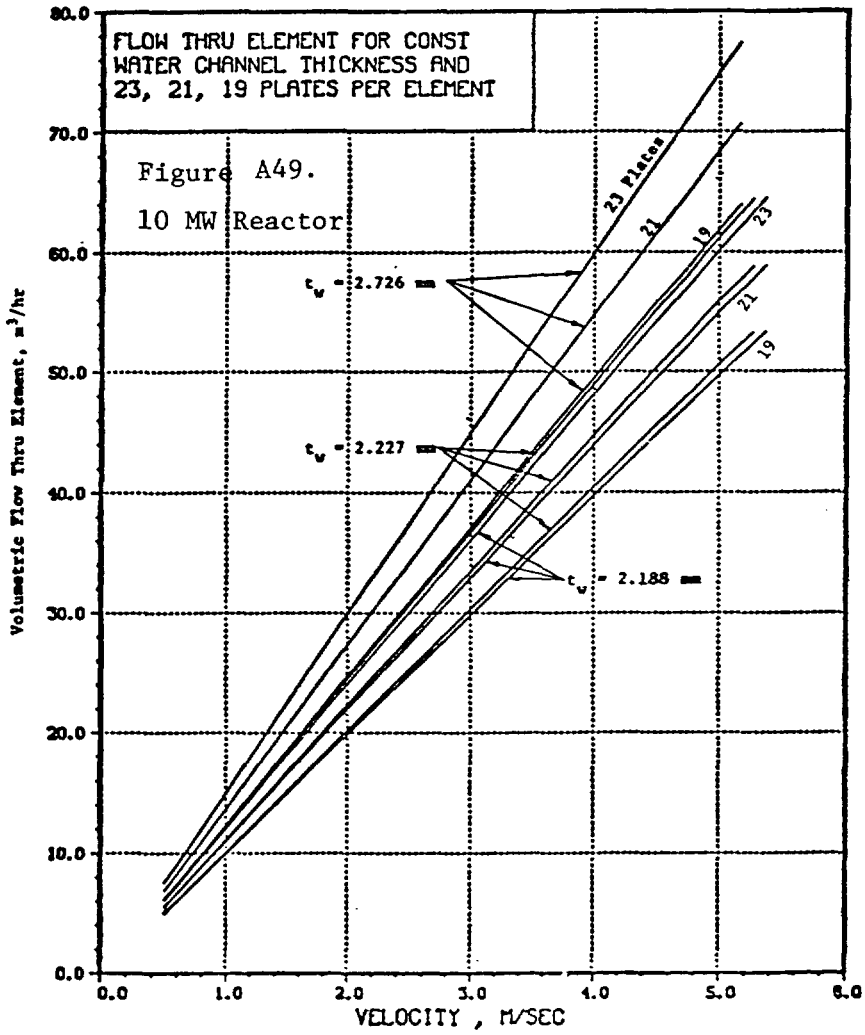

Figure A49.

10 MW Reactor

A.3.3.2 Total Pressure Drop and Flow Through an Element

The friction pressure loss in a channel (ΔP_f), the total pressure drop across a fuel channel (ΔP_F), and the volumetric flow rate (Q) through an element are derived as functions of coolant velocity for constant water channel thickness using Eqs. (6), (10), and (3), respectively. Results are presented in Figs. A48 and A49. As shown in Fig. A48, a thicker water channel requires a lower pressure drop for the same coolant velocity. At the same coolant velocity and water channel thickness, using fewer plates per element results in thicker plates and smaller cross-sectional flow area, which causes a higher total pressure drop across the fuel channel. Fig. A49 shows that at the same coolant velocity, using a thicker channel and more (thinner) plates per element results in a larger flow through the element.

A.3.3.3 Critical Flow Velocity

The critical flow velocity is derived as a function of water channel thickness for a given number of plates and fixed element dimensions, by using Eqs. (1) and (11). Results for the 10 MW reactor are presented in Fig. A50. As shown in this figure, the calculated critical flow velocity is generally about 5 times larger than the nominal channel velocity.

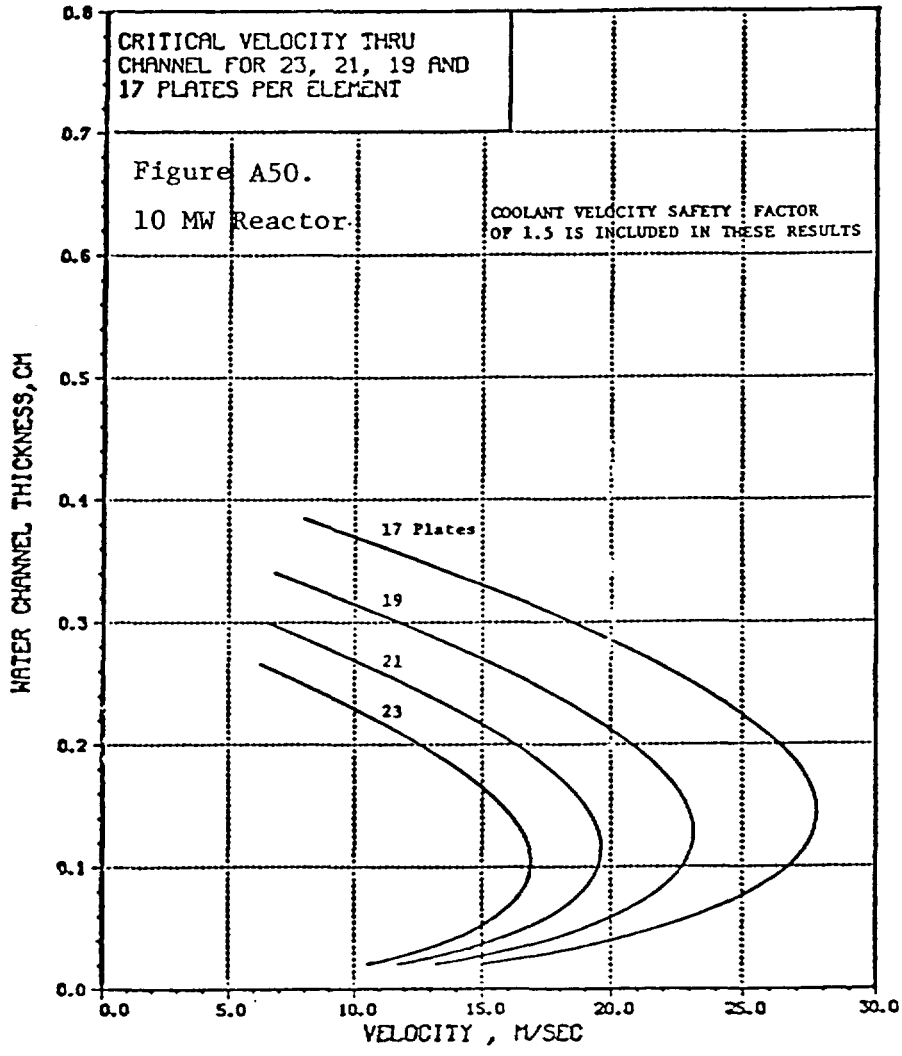

Figure A50.
10 MW Reactor

A.3.3.4 Heat Fluxes at Onset of Flow Instability and Burnout

The limiting heat flux at onset of flow instability was calculated using the Forgan correlation (Eqs. 19 and 20 with $n = 25$). For a given system pressure and inlet coolant temperature, this heat flux is proportional to the coolant velocity and water channel thickness.

The Labuntsov and the Mirshak correlations (Fig. A10) were used to calculate the burnout heat flux because they yield more conservative results in comparison with the other DNB correlations. Results of the calculations using the Labuntsov correlation show that the exit subcooling is negative for the range of coolant velocities considered for the 10 MW reactor. Using the Mirshak correlation, the exit subcooling is positive in some cases and negative in others. When the exit subcooling is negative, which is outside the range of applicability of these two correlations, the burnout heat flux was estimated using these correlations extrapolated with zero subcooling (see Section A.1.3.7). In general, the estimated burnout heat flux increases as the coolant velocity increases.

A.3.3.5 Fuel Element Design Variations - Thermal-Hydraulics

Table A27 presents some of the thermal-hydraulic design variations for the 10 MW reactor. These cases correspond to those considered in the burnup studies (Table A25). Numbers in the first row of Table A27 are data for the reference HEU case described in Table A23, and for the LEU case without fuel element redesign. From this table, a few interesting points can be summarized:

(a) For the same power level (i.e., average heat flux x number of plates = constant), a design with fewer plates will have higher average heat flux.
(b) For the same water channel thickness, a design with higher coolant velocity (at the cost of higher pressure drop) will have higher heat fluxes at ONB, at onset of flow instability, and at burnout.
(c) For the same coolant velocity, a design with a thicker water channel has a smaller pressure drop and higher heat fluxes at ONB and at onset of flow instability.
(d) For the same water channel thickness and coolant velocity, a design with fewer plates per element will have a slightly higher pressure drop across the fuel channel and a lower flow rate through the element due to the smaller cross-sectional flow area.
(e) The volumetric flow rate is proportional to the number of plates per element and the coolant temperature rise is inversely proportional to the flow rate. For a constant coolant inlet temperature, maintaining the same coolant temperature rise requires maintaining the same flow rate.
(f) For the design variations studied here, the increase in pressure drop is less than 0.12 bar compared with the reference HEU case. For this increased pressure drop, the pumping capability (see Section A.7.5) of many current HEU designs may be adequate.
(g) For the cases studied here, the margin to ONB is larger than 1.29; the margin to onset of flow instability ranges from 3.0 to 5.2; and the margin to DNB using both the Labuntsov and the Mirshak correlations is larger than 3.8.

From a thermal-hydraulic point of view, the results presented in Table A27 indicate that there are comfortable safety margins, with no major engineering difficulties, for these fuel element design variations.

TABLE A27. 10 MW Reactor
Thermal-Hydraulics
Fuel Element Design Variations
with 20% Enriched Uranium Fuel

Number of Plates	Thickness of Water Channel/Meat mm	Coolant Velocity m/s	Flow/ Element m^3/hr	Total Pressure Drop Across Channel bar	Avg.[b] Heat Flux W/cm^2	Avg. Heat[c] Flux at ONB W/cm^2	Burnout Heat Flux, W/cm^2		Limiting[f] Heat Flux at Onset of Flow Instability W/cm^2	Margin[g] to ONB	Margin[h] to DNB		Margin[i] to Onset of Flow Instability
							Labuntsov[d]	Mirshak[e]			Labuntsov	Mirshak	
23[a]	2.188/0.510	2.97	35.7	0.193	20.54	35.9	353	266	208.8	1.75	6.90	5.20	4.08
23	2.188/0.510	3.24	39.0	0.226	20.54	38.9	368	272	227.8	1.89	7.19	5.31	4.45
23	2.188/0.510	3.59	43.2	0.272	20.54	42.8	387	(288)	252.4	2.08	7.56	5.63	4.93
23	2.188/0.510	3.80	45.7	0.300	20.54	45.0	398	(298)	267.1	2.19	7.77	5.82	5.22
21	2.188/0.839	2.97	32.6	0.195	22.50	35.9	353	266	208.8	1.59	6.30	4.74	3.72
21	2.188/0.839	3.24	35.6	0.228	22.50	38.9	368	272	227.8	1.73	6.56	4.85	4.06
21	2.227/0.700	2.97	33.2	0.191	22.50	36.1	353	261	211.9	1.60	6.30	4.65	3.78
21	2.227/0.700	3.19	35.6	0.217	22.50	38.5	365	271	227.6	1.71	6.51	4.83	4.06
19	2.916/0.510	2.97	39.3	0.143	24.86	37.6	353	(289)	264.1	1.51	5.70	4.66	4.26
19	2.726/0.700	2.97	36.8	0.154	24.86	37.3	353	(282)	250.2	1.50	5.70	4.55	4.04
19	2.626/0.800	2.97	35.4	0.160	24.86	37.1	353	(278)	242.7	1.49	5.70	4.49	3.92
19	2.526/0.900	2.97	34.1	0.167	24.86	36.9	353	(274)	235.2	1.48	5.70	4.42	3.80
19	2.426/1.000	2.97	32.7	0.175	24.86	36.6	353	(270)	227.5	1.47	5.70	4.36	3.67
19	2.188/1.238	2.97	29.5	0.197	24.86	35.9	353	266	208.8	1.44	5.70	4.29	3.37
19	2.188/1.238	3.59	35.7	0.277	24.86	42.8	387	(288)	252.4	1.72	6.24	4.65	4.07
18	2.188/1.471	2.97	27.9	0.198	26.25	35.9	353	266	208.8	1.37	5.40	4.07	3.19
18	2.188/1.471	3.80	35.7	0.308	26.25	45.0	398	(298)	267.1	1.71	6.08	4.56	4.08
18	2.789/0.870	2.97	35.6	0.151	26.25	37.4	353	(284)	254.8	1.43	5.40	4.34	3.90
17	2.188/1.731	2.97	26.4	0.199	27.79	35.9	353	266	208.8	1.29	5.10	3.84	3.02

[a]Reference HEU case and LEU case with no redesign.

[b]Peak Heat Flux = 1.4 x 1.78 x Avg. Heat Flux.

[c]The average heat flux at ONB is calculated with the conservative assumption that ONB occurs at the channel exit with peak heat flux, lowest pressure and saturation temperature, and highest coolant temperature rise.

[d]Burnout heat flux estimated using the Labuntsov correlation extrapolated with zero subcooling (see Section A.1.3.7).

[e]Burnout heat flux calculated using the Mirshak correlation, which is strictly applicable for positive subcooling (cases in parentheses). Other cases were estimated based on extrapolation with zero subcooling.

[f]Limiting heat flux at onset of instability due to flow excursion calculated with the Forgan correlation.

[g]Minimum ratio of local heat flux for ONB to actual heat flux.

[h]Minimum ratio of local heat flux for DNB using Labuntsov and Mirshak correlations to actual peak heat flux.

[i]Minimum ratio of local heat flux for onset of instability due to flow excursion to actual peak heat flux.

A.4 APPLICATION TO THE 10 MW REACTOR BASED ON CARAMEL FUEL

A.4.1 Introduction

The results of neutronics and thermal-hydraulics calculations are presented for the potential conversion of the 10 MW reactor to a fuel element design using Caramel fuel with uranium enrichments of 7.5% and 6.5%. These results include comparisons with the HEU reference design of neutron flux performance, average cycle length, ^{235}U and Pu loading distributions of the equilibrium cores, and thermal-hydraulic safety margins to onset of nucleate boiling and to onset of flow instability for several core flow rates.

The design specifications used in the ANL calculations for the 10 MW reactor using Caramel fuel with uranium enrichments of 7.5% and 6.5% are shown in Table A28. These specifications were provided by CEA (see Appendix D). For convenience, the design specifications for the HEU reference core using classical, plate-type, aluminide fuel (Table A24) are also repeated in Table A28.

A.4.2 Neutronics

A.4.2.1 Calculational Model

Five-group microscopic cross sections were prepared using the EPRI-CELL code[1] with the methods described in Section A.1.2. For purposes of comparing fluxes with the reference HEU design, this five-group structure was reduced to the fast (10.0 MeV - 0.821 MeV), epithermal (0.821 MeV - 5.53 keV), and thermal (0.625 eV - 0.0 eV) groups that were used in Section A.3 and for the benchmark calculations described in Appendix F.1. The design of the standard fuel element and a description of the control fuel element are provided in Fig. A52. The geometry of the unit cell used for cross section preparation is shown in Fig. A53. The physical heterogeneous assembly of a Caramel fuel plate was modeled by homogenizing the zircaloy-4 separators between individual caramels of UO_2 to form a UO_2-Zr4 fuel meat, which was then clad in zircaloy-4 in the standard manner.

The XY model and the fuel shuffling pattern used in the burnup calculations (using the REBUS-2 code[15]) with two-dimensional diffusion theory are the same as those shown in Fig. A39 and described in Section A.3.2.1. In this shuffling pattern, the control fuel elements are fixed, but 1/23 of the fuel in each control element is replaced with fresh fuel after each operational cycle. Computed cycle lengths thus represent an average cycle lengths, with the average being 1/23 of the operation time required to replace 23 standard fuel elements and 5 control fuel elements. The ZR model shown in Fig. A38 was used to compute the axial extrapolation length for use in the XY cases. The axial peak-to-average power density ratios were 1.292 using Caramel fuel and 1.311 using aluminide fuel.

The one difference between the methods used by ANL in the calculations with Caramel fuel and with aluminide fuel was the values chosen for the end of equilibrium cycle reactivity. Cross sections used by CEA (Appendix D) for Caramel fuel had an effective uranium temperature of 170°C, while those used by ANL for aluminide fuel (Section A.3) and for Caramel fuel had an effective uranium temperature of 20°C. To compensate for this 150°C temperature difference, the ANL calculations with Caramel fuel were done with an EOC k_{eff} of 1.0053. This value was based on an estimated reactivity worth (provided by CEA) of 3.5×10^{-5} $\Delta k/k/°C$ for changes in effective uranium temperature in Caramel fuel. However, the results presented would not be significantly different if a uranium temperature of 170°C were used and the k_{eff} at EOC were 1.0 since the k_{eff} at BOC would change as well.

Table A28. 10 MW Reactor - Description of Design Parameters Used in the ANL Calculations

Reactor Design Description

Reactor Type	Pool-Type MTR
Steady-State Power Level,MW	10
Number of Standard Fuel Elements	23
Number of Control Fuel Elements	5
Irradiation Channels	1 at Core Center 1 at Core Edge
Core Geometry	5 x 6 Arrangement
Lattice Pitch,mm^2	77 x 81
Active Core Volume,ℓ	105
Core Average Volumetric Power Density,kW/ℓ	95.2
Average Linear Power Density,W/cm	385
Moderator, Coolant	Water
Reflectors	Graphite Two Sides Water on Two Sides
Burnup Status of Core	Equilibrium Core

Fuel Element Design Description

Fuel Type (Straight Plates)		Aluminide	Caramel	Caramel
Uranium Enrichment,%		93	7.5	6.5
Fuel Element Cross Section, mm^2		76 x 80	76 x 80	76 x 80
Plate Thickness,mm		1.27	2.25	2.25
Water Channel Thickness,mm		2.188	2.75	2.75
Plates/Standard Fuel Element		23	16	16
Plates/Control Fuel Element		17	13	13
Fuel Meat Material		UAl_x-Al	UO_2 with Zr-4 Separators	UO_2 with Zr-4 Separators
Fuel Meat Dimensions,mm^3		0.51 x 63 x 600	1.45 x 65.4 x 600	1.45 x 65.4 x 600
Clad Material		Al	Zr-4	Zr-4
Clad Thickness,mm		0.38	0.40	0.40
Side Plate Material		Al	Zr-4	Zr-4
Side Plate Thickness,mm		4.75	3.0	3.0
Densities in Aluminide Fuel Meat, g/cm^3	UAl_x-Al	3.075		
	U	0.679		
	Al	2.399		
	^{235}U	0.632		
Densities in UO_2-Zr4 Fuel Meat, g/cm^3	UO_2-Zr4		9.961	9.961
	UO_2		9.542	9.542
	Zr-4		0.419	0.419
	U		8.407	8.407
	^{235}U		0.631	0.547
^{235}U/Standard Fuel Element,g		280	574.0	497.5
^{235}U/Control Fuel Element,g		207	466.4	404.2
^{235}U Content/Core, kg		7.475	15.534	13.464
U Content/Core, kg		8.037	207.1	207.1
Effective Uranium Tempeature,°C		20	20	20
Water Temperature,°C, for Neutronics Calculations		20	20	20
Inlet Water Temp., °C, for Thermal-Hydraulics Calculations		38	38	38

Figure A52. 10 MW Reactor - Caramel Fuel Design of Standard Fuel Element[a] (16 Plates/Element)

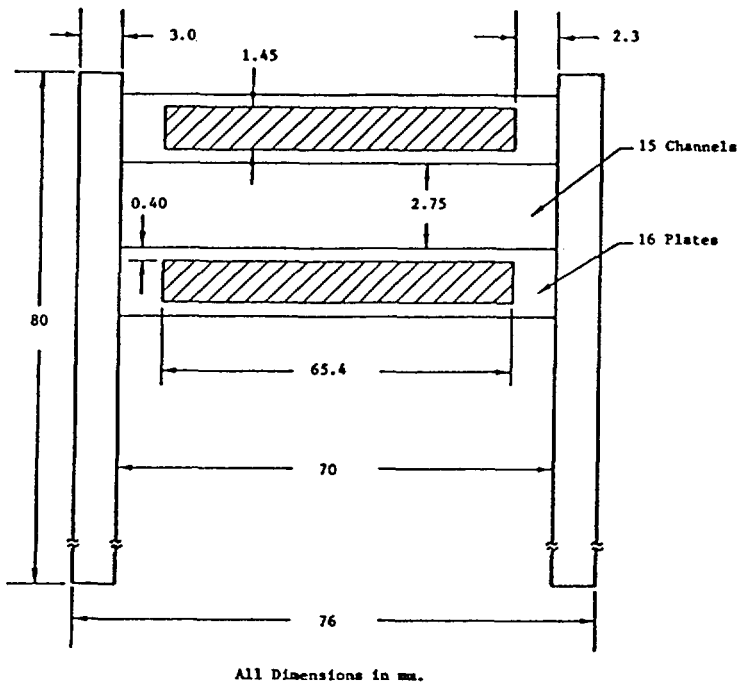

[a]The control fuel elements have 13 fuel plates with a thickness of 2.25 mm, ten interior water channels with a thickness of 2.75 mm, and two water channels with a thickness of 10.25 mm near the outsides of the element for fork-type absorber blades.

[b]Including a 0.5 mm water channel surrounding each element.

VOLUME FRACTIONS[b]

Standard Fuel Element		Control Fuel Element	
Fuel Meat	0.2433	Fuel Meat	0.1977
Zircaloy-4	0.2377	Zircaloy-4	0.2075
Water	0.5190	Water	0.5948

Figure A53. 10 MW Reactor-Caramel Fuel. Geometry of Unit Cell for Calculation of Core Cross Sections

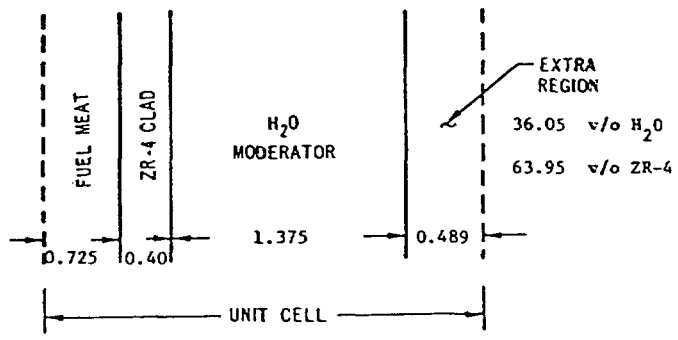

A.4.2.2 Burnup Performance and Flux Performance Results

The beginning of equilibrium cycle (BOC) and end of equilibrium cycle (EOC) distributions of ^{235}U and the EOC distribution of Pu for the Caramel fuel cases with uranium enrichments of 7.5% and 6.5% are shown in Figs. A54 and A55, respectively. The corresponding data for the HEU reference case are shown in Fig. A40. Fissile uranium loadings in the fresh standard elements, average cycle lengths, fissile materials burned in the discharged elements, and average discharge burnups for the three cases are compared in Table A29.

Table A29. Comparison of Burnup Data for the HEU Reference Case and Cases with Carmel Fuel

Fuel-Type and Enrichment	^{235}U in Fresh Std. Element, g	Average Cycle Length, Days	Grams Fissile Burned in Discharge Element		Average Discharge Burnup	
			^{235}U	$^{239}Pu+^{241}Pu$	% ^{235}U	MWd*
Aluminide, 93%	280	16.7	178.4	~0	63.7	142.7
Caramel, 6.5%	497.5	22.5	206.2	33.4	41.5	186.5
Caramel, 7.5%	574.0	31.5	284.7	52.8	49.6	261.8

* Energy production is based on burnup of 1.25 g ^{235}U/MWd and 1.55 g ($^{239}Pu+^{241}Pu$)/MWd.

Since the ^{235}U loadings with Caramel fuel are much higher than the ^{235}U loading of the HEU reference case, the average cycle lengths and average discharge burnups (in MWd) are also significantly higher with Caramel fuel.

Fast, epithermal, and thermal fluxes for each of the three fuels are compared in Figs. A56, A57, and A58, respectively, for a midplane traverse (along the y-axis) through the central irradiation channel and through the water-reflected faces of the core. The asymmetry in the fluxes about the central irradiation channel is due to the asymmetry in the equilibrium burnup distribution with the fuel shuffling pattern that was used. A similar comparison is shown in Figs. A59, A60, and A61 for a midplane traverse (along the x-axis) through the central irradiation channel and through the graphite-reflected faces.

For convenience, numerical ratios of average (both planar and axial) fast, epithermal, and thermal fluxes between each case with Caramel fuel and the HEU reference case are shown in Figs. A62 and A63 for each standard and control fuel element in the core. Ratios of peak planar fluxes at the core midplane are provided in the in-core irradiation positions and in the water reflectors. Peak fluxes outside the graphite reflectors occur in the water just beyond the graphite. Axially-averaged flux ratios at the peaks in the irradiation channels and reflectors can be obtained by utilizing the ratio of peak-to-average factors for Caramel and aluminide fuel given in Section A.4.2.1.

Figure A54. 10 MW Reactor - Caramel Fuel, 7.5% Enrichment

Beginning and End of Equilibrium Cycle Distribution of ^{235}U and End of Equilibrium Cycle Distribution of Pu

U Enrichment : 7.5%
U Density : 8.407 g/cm^3
Fresh Fuel Loading : 574 g ^{235}U

BOC k_{eff} : 1.0187
EOC k_{eff} : 1.0053
Average Cycle Length : 31.5 Days

^{235}U (BOC) ^{235}U (EOC) Pu (EOC)	23 295.2 289.3 53.8	13 376.9 367.3 41.6	6 468.7 455.2 25.9	CFE-2 323.5 312.1 25.6	8 441.8 430.5 42.8	H_2O	
	22 302.7 295.2 53.2	CFE-1 309.8 297.5 31.3	3 531.4 512.1 14.8	1 574.0 551.4 5.1	10 419.5 407.2 34.7	16 347.8 339.3 46.3	
GRAPHITE	21 311.1 302.7 52.0	11 407.2 392.5 37.8	5 491.7 468.7 23.3	H_2O	12 392.5 376.9 40.1	CFE-3 342.5 332.4 24.5	GRAPHITE
	19 325.0 316.8 49.8	CFE-5 308.4 296.0 31.6	2 551.4 531.4 10.1	4 512.1 491.7 18.9	14 367.3 356.4 43.9	18 332.5 325.0 48.4	
	17 339.3 332.5 47.1	9 430.5 419.5 32.0	7 455.2 441.8 28.4	CFE-4 323.1 311.6 25.6	15 356.4 347.8 45.1	20 316.8 311.1 50.5	

Figure A55. 10 MW Reactor - Caramel Fuel, 6.5% Enrichment

Beginning and End of Equilibrium Cycle Distribution of ^{235}U and End of Equilibrium Cycle Distribution of Pu

U Enrichment : 6.5%
U Density : 8.407 g/cm^3
Fresh Fuel Loading : 497.5 g ^{235}U

BOC k_{eff} : 1.0161
EOC k_{eff} : 1.0053
Average Cycle Length : 22.5 Days

^{235}U (BOC) ^{235}U (EOC) Pu (EOC)	23 295.9 291.3 44.1	13 358.2 351.0 32.9	6 424.5 414.9 19.8	CFE-2 304.5 296.3 20.3	8 405.4 397.3 23.2	H_2O	
	22 301.8 295.9 43.4	CFE-1 292.3 283.2 25.4	3 468.3 454.9 11.1	1 497.5 482.1 3.8	10 389.3 380.4 27.0	16 336.4 330.0 37.0	
GRAPHITE	21 308.3 301.8 42.3	11 380.4 369.6 29.6	5 440.6 424.5 17.7	H_2O	12 369.6 358.2 31.6	CFE-3 316.9 309.6 19.5	GRAPHITE
	19 319.0 312.7 40.3	CFE-5 291.2 282.1 25.7	2 482.1 468.3 7.5	4 454.9 440.6 14.2	14 351.0 342.8 34.8	18 324.8 319.0 39.0	
	17 330.0 324.8 37.8	9 397.3 389.3 24.8	7 414.9 405.4 21.8	CFE-4 303.2 294.9 20.5	15 342.8 336.4 36.0	20 312.8 308.3 40.9	

Figures A56 and A57. Comparison of Fast and Epithermal Fluxes at EOC Between the HEU Reference Case and the Caramel Fuel Cases For a Midplane Traverse Along the Y-Axis Through the Central Irradiation Channel and the Water-Reflected Faces.

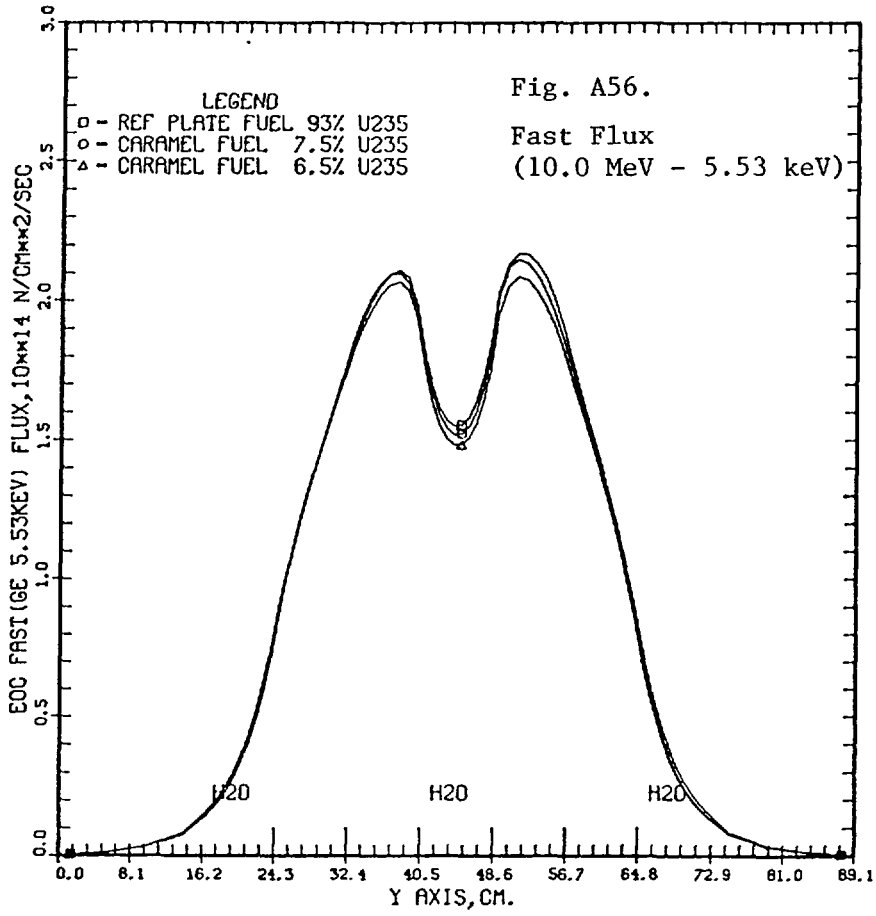

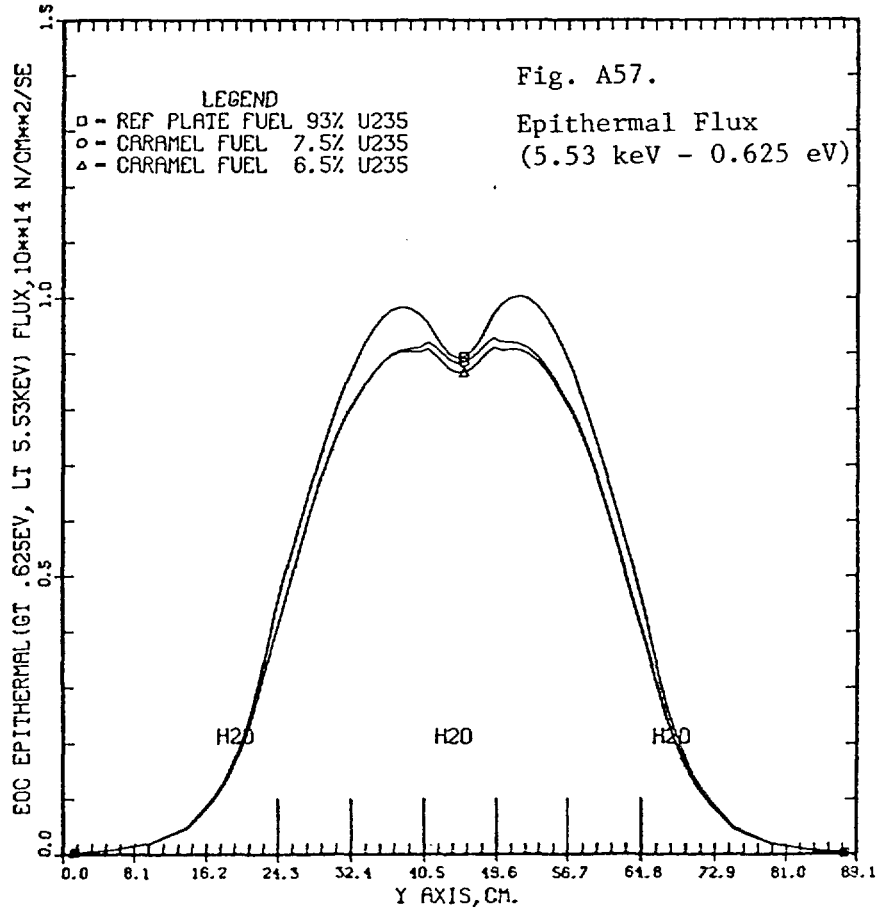

Figure A58. Comparison of Thermal Fluxes at EOC Between the HEU Reference Case and the Caramel Fuel Cases For A Midplane Traverse Along the Y-Axis Through the Central Irradiation Channel and the Water-Reflected Faces.

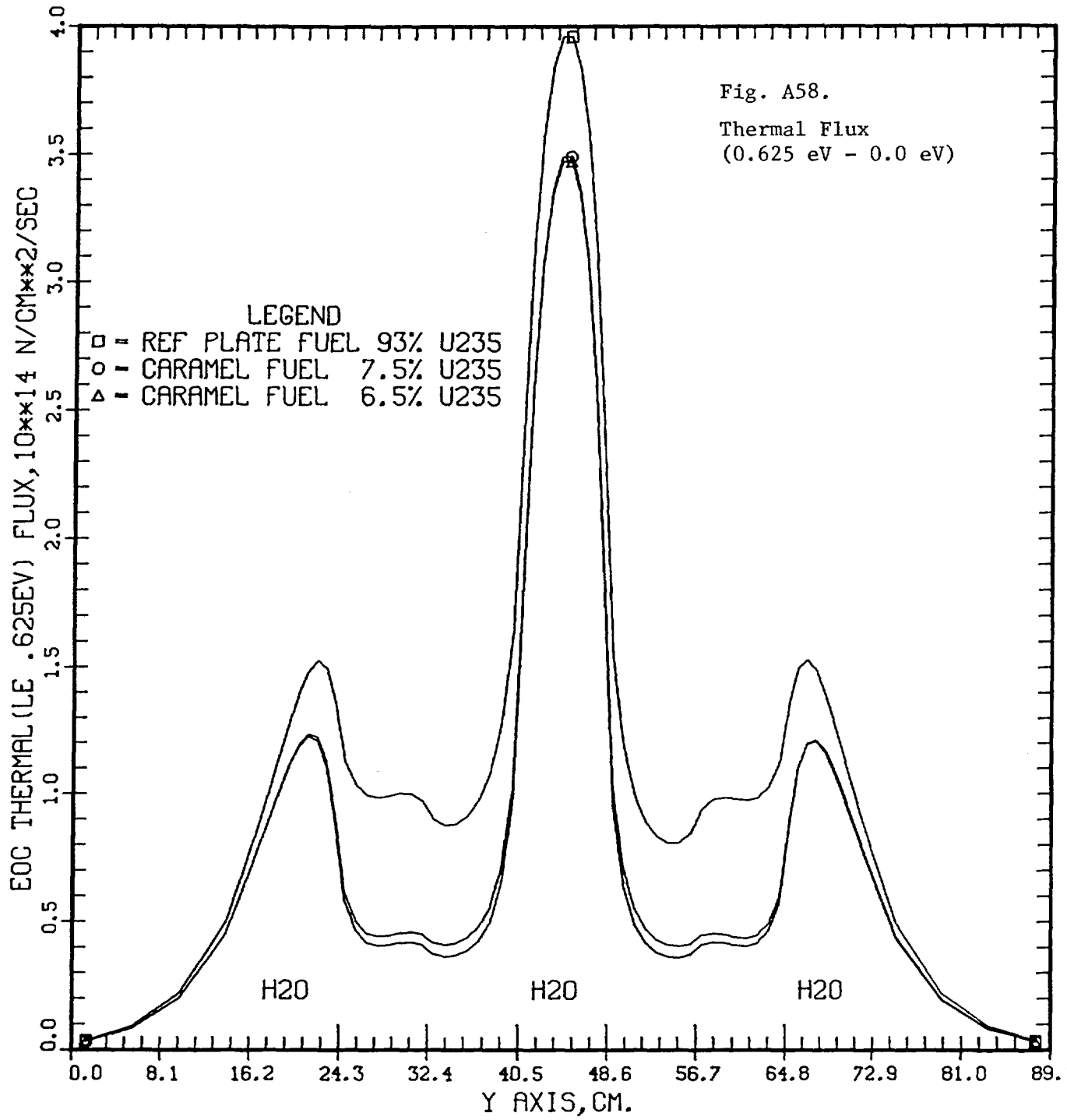

Figures A59 and A60. Comparison of Fast and Epithermal Fluxes at EOC Between the HEU Reference Case and the Caramel Fuel Cases For a Midplane Traverse Along the X-Axis Through the Central Irradiation Channel and the Graphite-Reflected Faces.

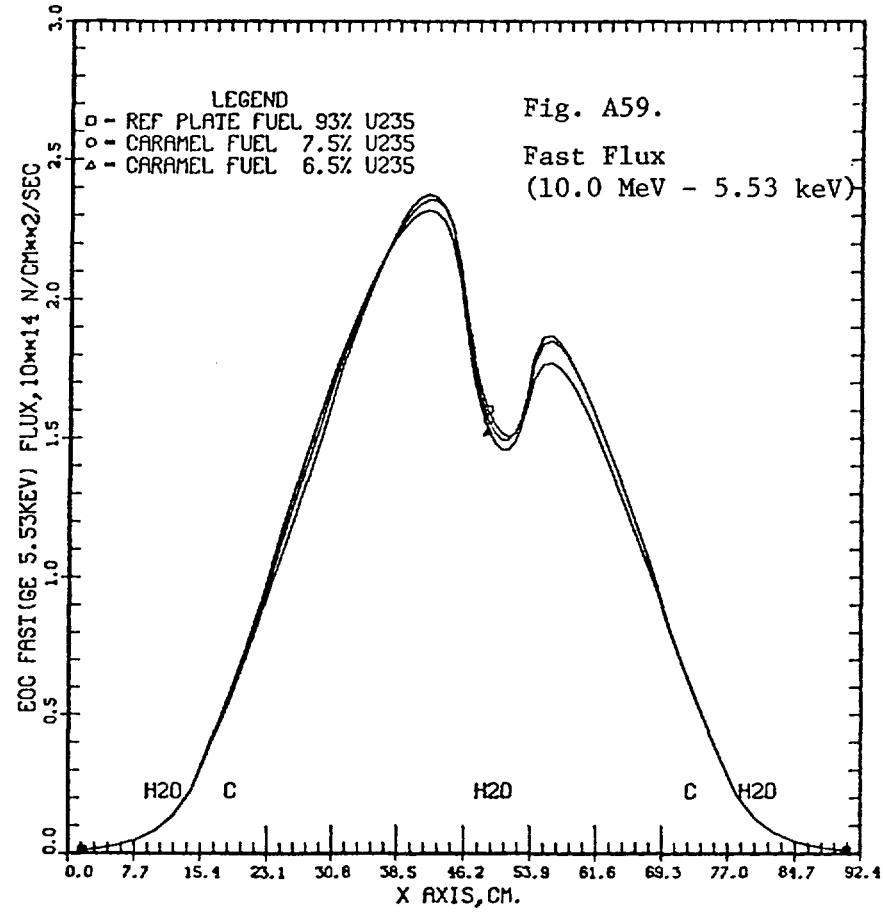

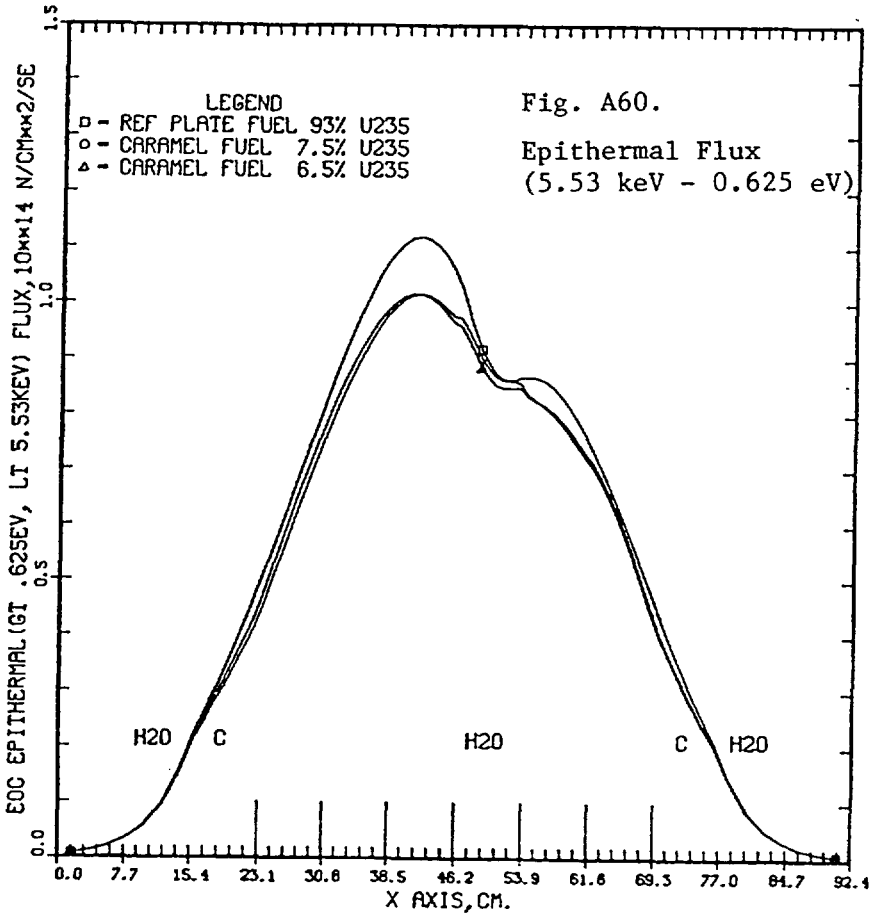

Figure A61. Comparison of Thermal Fluxes at EOC Between the HEU Reference Case and the Caramel Fuel Cases For a Midplane Traverse Along the X-Axis Through the Central Irradiation Channel and the Graphite-Reflected Faces.

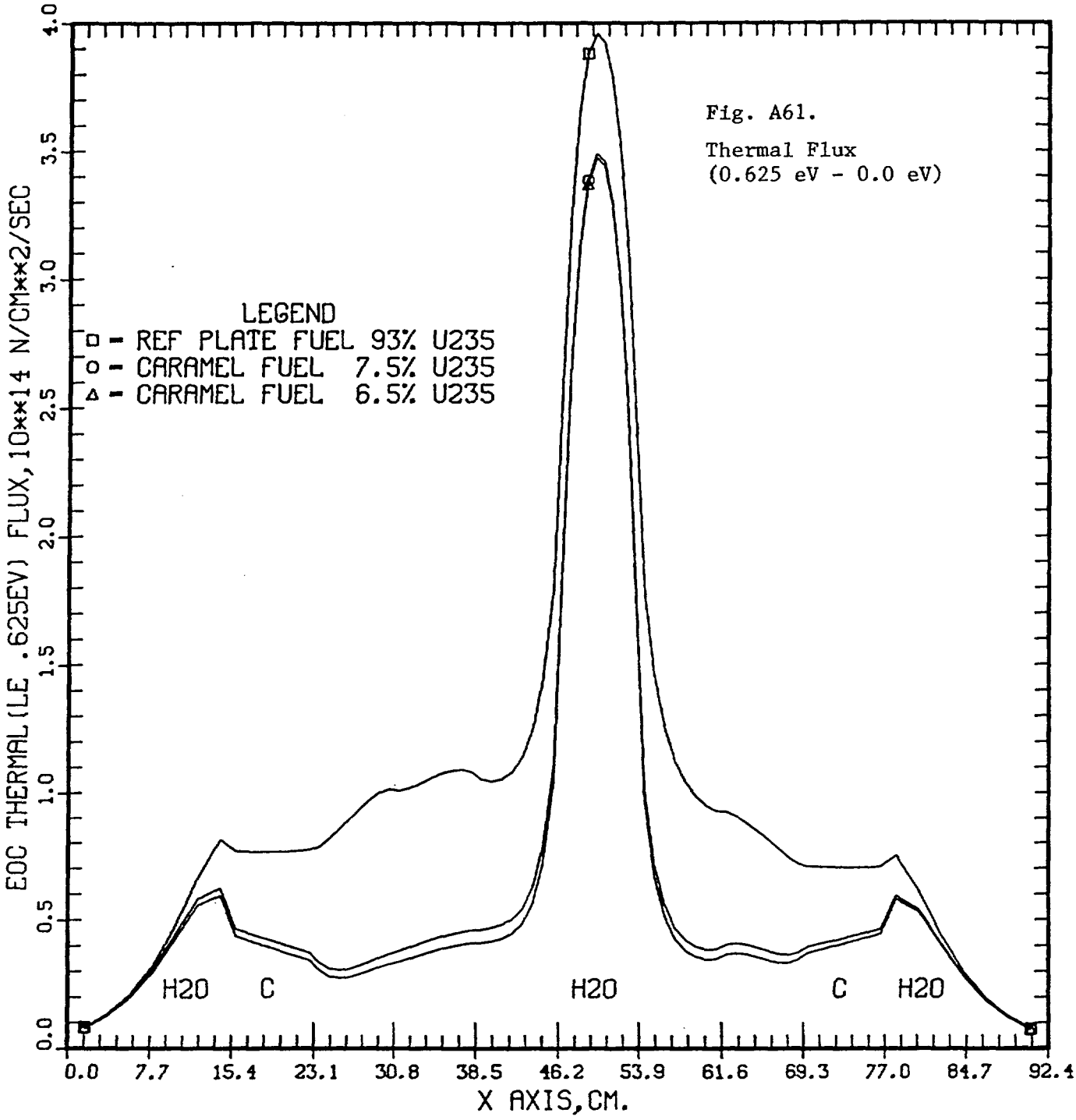

Figures A62 and A63. Ratios of Average Fast, Epithermal, and Thermal Fluxes Between the Caramel Fuel Cases and the HEU Reference Case in Each Fuel and Control Element. Peak Flux Ratios at the Axial Midplane are Shown in the In-Core Irradiation Positions and in the Reflectors.

Fig. A62. Caramel 7.5%/HEU Ref.

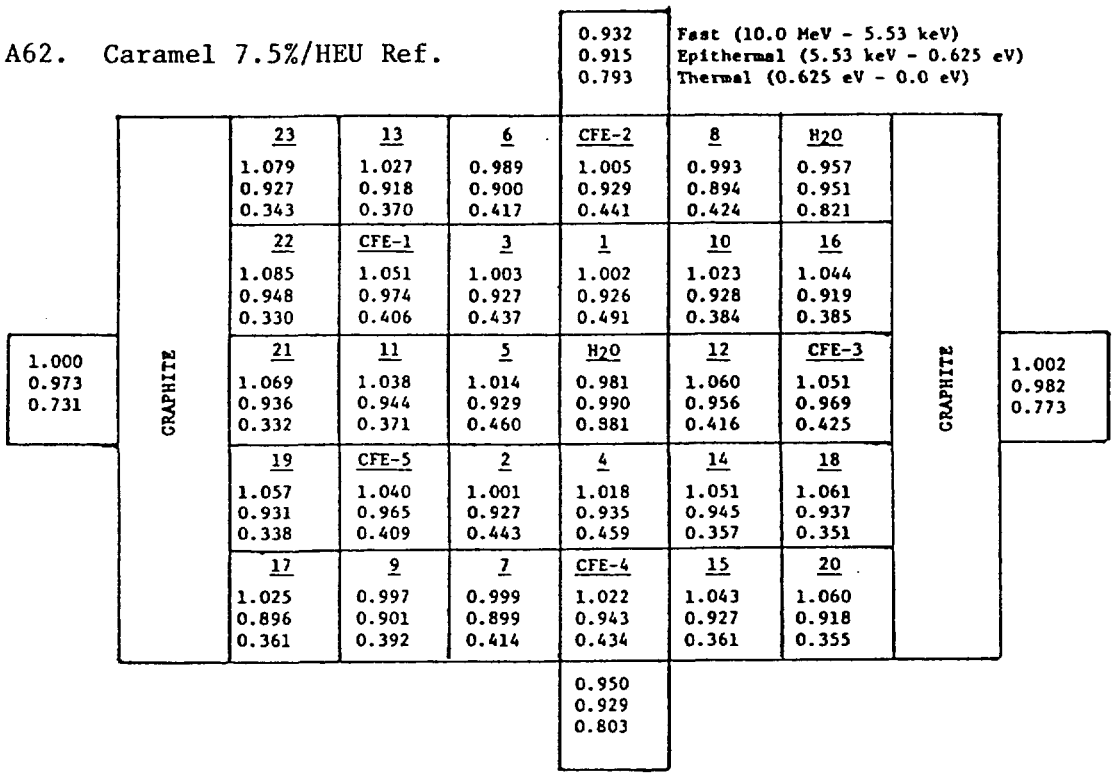

Fig. A63. Caramel 6.5%/HEU Ref.

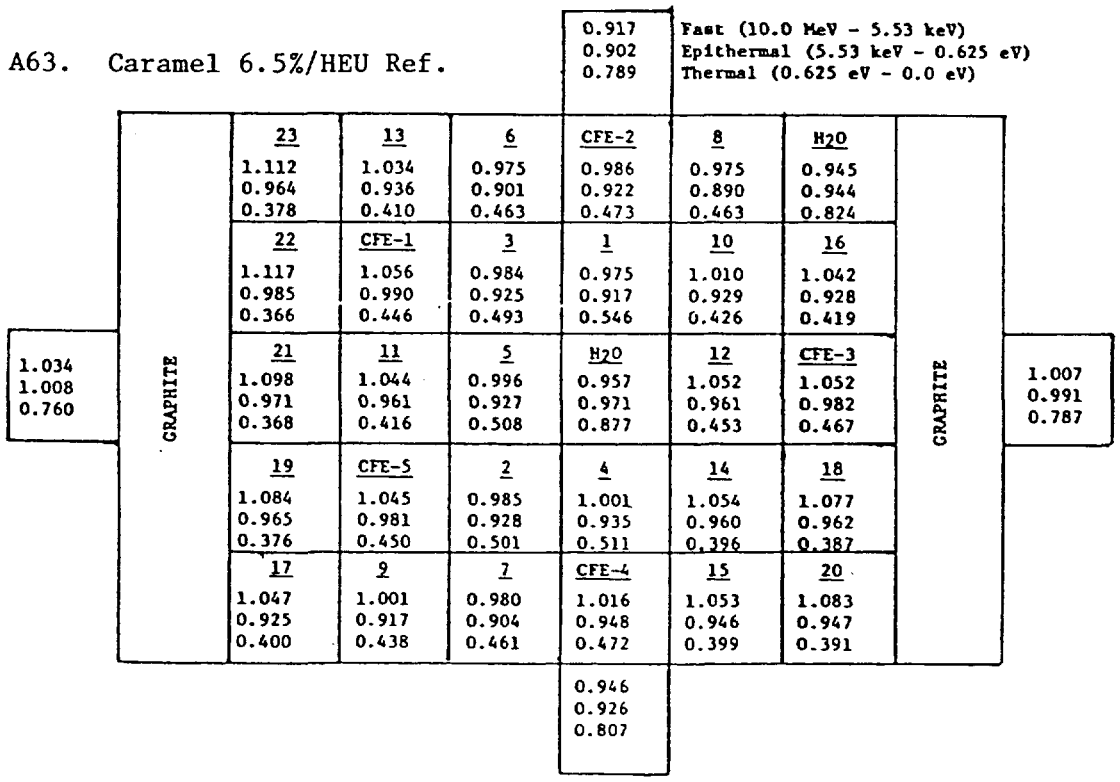

A.4.3 Thermal-Hydraulics

The thermal-hydraulic aspects of the 10 MW reactor using Caramel fuel and the reference HEU core using aluminide fuel were studied with the methods outlined in Section A.1.3. The geometries of the Caramel (aluminide) standard and control fuel elements are summarized in Fig. A52 (Fig. A36). Other physical parameters (such as water properties, pressure, and power peaking factors) used in the calculations are the same as those in Table A26. No attempt was made here to account for the effects on the thermal-hydraulic variables of the physical heterogeneity of the Caramel fuel plates. As in the neutronics calculations, the fuel meat (clad in zircaloy-4), was assumed to be a homogeneous mixture of the UO_2 and the zircaloy-4 separators.

A.4.3.1 Margins to ONB

As discussed in Section A.1.3.4, the average heat flux at ONB depends on the axial location at which ONB occurs. For the cases studied here, heat fluxes at ONB were calculated in two ways: (1) conservatively assuming that ONB occurs at the channel exit with peak heat flux, lowest pressure and saturation temperature, and highest coolant temperature rise; and (2) more realistically assuming that ONB occurs with the peak heat flux at 40 cm from the channel entrance. The results of these calculations are summarized in Table A30.

For the cases with Caramel fuel, the heat fluxes at ONB calculated by assuming that ONB occurs at the channel exit are about 10% lower than those calculated by assuming that ONB occurs at 40 cm from the channel entrance. The limiting coolant velocity below which ONB will occur was calculated to be about 2.02 m/s (for a core flow rate of 630 m^3/hr). At a coolant velocity of 2.97 m/s (nominal coolant velocity for the reference HEU case with a core flow rate of 1000 m^3/hr), the margin to ONB is larger than 1.28.

For the HEU reference case with aluminide fuel, the heat fluxes at ONB calculated with the conservative method are about 13% lower than those calculated with the more realistic method. The margins to ONB for coolant velocities between 1.78 m/s and 2.97 m/s (core flow rates between 600 m^3/hr and 1000 m^3/hr) range from 1.05 to 1.67 using the conservative approach.

A.4.3.2 Margins to Onset of Flow Instability

Limiting heat fluxes at onset of flow instability were calculated using the Forgan correlation (Eqs. 19 and 20, with $\eta = 25$). With given thermal-hydraulic conditions in Eq. (20), this limiting heat flux is proportional to the coolant velocity. The results of the calculations are shown in Table A30. For the cases with Caramel fuel, the margins to onset of flow instability were computed to be 2.35 and 3.45 for coolant velocities of 2.02 m/s and 2.97 m/s, respectively. In the reference HEU cases, this margin ranges linearly from 2.33 to 3.89 for coolant velocities between 1.78 m/s and 2.97 m/s.

Table A30. Comparison of Thermal-Hydraulic Parameters for Cases with Caramel Fuel and HEU Reference Case with Aluminide Fuel

Fuel Type	Number of Plates/Element Std. (Control)	Thickness of Water Channel/Meat mm	Inlet Water Temp. °C	Coolant Velocity m/s	Core[a] Flow Rate m^3/hr	Ave.[b] Heat Flux W/cm^2	Ave. Heat Flux at ONB W/cm^2	Limiting[e] Heat Flux at Onset of Flow Instability W/cm^2	Margin[f] to ONB	Margin[g] to Onset of Flow Instability
Caramel	16 (13)	2.75/1.45	38	2.02	630	29.4	26.6[c] (29.4)[d]	171.9	0.90[c] (1.00)[d]	2.35
Caramel	16 (13)	2.75/1.45	38	2.97	926	29.4	37.5 (41.3)	252.8	1.28 (1.40)	3.45
Aluminide	23 (17)	2.188/0.51	38	1.78	600	21.5	22.5 (25.6)	125.1	1.05 (1.19)	2.33
Aluminide	23 (17)	2.188/0.51	38	1.87	630	21.5	23.6 (26.8)	131.5	1.10 (1.25)	2.45
Aluminide	23 (17)	2.188/0.51	38	2.02	680	21.5	25.3 (28.7)	142.0	1.18 (1.33)	2.65
Aluminide[a]	23 (17)	2.188/0.51	38	2.97	1000	21.5	35.9 (40.5)	208.8	1.67 (1.88)	3.89

[a]Reference HEU case.

[b]Peak Heat Flux = 1.4 x 1.78 x Ave. Heat Flux.

[c]Conservatively assuming that ONB occurs at the channel exit with peak heat flux, lowest pressure and saturation temperature, and highest coolant temperature rise.

[d]Assuming that ONB occurs at 40 cm from the channel entrance.

[e]Calculated using the Forgan correlation with $\eta = 25$.

[f]Minimum ratio of local heat flux at ONB to actual heat flux.

[g]Minimum ratio of local heat flux at onset of flow instability to actual peak heat flux.

A.5 APPLICATION TO THE 10 MW REACTOR BASED ON UZR-H FUEL

A.5.1 Introduction

The results of neutronics and thermal-hydraulics calculations are presented for potential conversion of the 10 MW reactor using classical, plate-type aluminide fuel with HEU to the use of rodded-type, UZr-H fuel with LEU and a uranium density of 3.7 g/cm^3 (45 wt% U). The design specifications (provided by GA, Appendix B) used in the ANL calculations using UZr-H fuel elements with 16 fuel rods per cluster are shown in Table A31. The design specifications for the HEU reference case using plate-type, aluminide fuel are given in Table A24.

Burnup calculations were performed for two cores: (1) a 30 element initial core reflected by water on all four faces, and (2) a 30 element equilibrium core reflected by graphite on two faces and by water on two faces. The initial core is identical with that discussed by General Atomic in Appendix B. The equilibrium core is similar to that described in Section A.3 for conversion of the reference HEU core to use of classical, plate-type, aluminide fuel with LEU and in Section A.4 for conversion of the HEU reference core to use of Caramel fuel.

For the initial UZr-H core, the results include curves of reactivity, versus burnup for three values of the erbium burnable poison, flux distributions with and without a flux-trap near the center of the fresh core, and a comparison of thermal flux distributions between the UZr-H fueled core just before initial reload is required and the reference HEU core at the end of an equilibrium cycle. For the equilibrium core calculations with UZr-H fuel, average cycle lengths, ^{235}U and Pu loading distributions at EOC, and neutron flux distributions are compared with those of the reference HEU plate-type design.

The thermal-hydraulics results for UZr-H rodded-type fuel include determinations of maximum reactor power based on limiting conditions defined by maximum fuel temperture and by departure from nucleate boiling (DNB). For DNB, results using several critical heat flux correlations are compared. For maximum fuel temperture, results using heat transfer correlations for single-phase and two-phase flow are discussed and compared. Parametric results are also provided for the maximum fuel temperature expected at a power level of 10 MW as functions of gap conductance and fuel conductivity.

A.5.2 Neutronics

A.5.2.1 Calculational Models

Ten-group microscopic cross sections were prepared using the EPRI-CELL code[1] with the methods described in Section A.1.2. The upper energy boundaries of the neutron groups used in the calculations and those used for plotting fluxes are given in Table A32. The design of a standard UZr-H fuel element containing 16 fuel rods is shown in Fig. A64 (provided by General Atomic, Appendix B). The geometry of the unit cell used for cross section preparation is shown in Fig. A65. For the results presented on the initial cores, cross sections were prepared with the following temperatures: 291°C for Er, ^{238}U. and ^{235}U, 227°C for H in UZr-H, and 20°C for H_2O. For the results presented on the equilibrium cores, all cross sections were prepared at 20°C, but one case with the same temperatures as for the initial core was run as a check. The results were found to be very similar. For example, the average cycle length was 40.8 days with cross section prepared at 20°C and 40.3 days with cross sections at the same temperatures as for the initial core.

TABLE A31. 10 MW Reactor - UZrH 16-Rod Clusters

Description of Design Parameters Used in the ANL Calculations
for the Initial and the Equilibrium Cores

Reactor Design Descriptions

	Initial Core	Equilibrium Core
Reactor Type	Pool	Pool
Steady-State Power Level, MW	10	10
Number of Standard Fuel Elements	30	30
Number of Control Fuel Elements	0	0
Number of Control Rods	4	4
Irradiation Channels	1 at Core Center 1 at Core Edge	1 at Core Center 1 at Core Edge
Core Geometry	6 × 6 Arrangment	6 × 6 Arrangement
Lattice Pitch, mm^2	77 × 81	77 × 81
^{235}U/Core, kg	26.3	26.3
Active Core Volume, ℓ	105	105
Core Average Volumetric Power Density, kW/ℓ	95.2	95.2
Average Linear Power Density, W/cm	373	373
Moderator, Coolant	Water	Water
Reflectors	Water on 4 Sides	Graphite on 2 Sides Water on 2 Sides
Burnup Status of Core	Initial Core	Equilibrium Core

Fuel Element Description

Fuel Geometry	Rods
Fuel Rods/Standard Element	16
Fuel Material	UZrH
Uranium Enrichment, %	20
Uranium Density, g/cm^3	3.72 (45 wt% U)
Fuel Rod Outer Diameter (Unclad), mm	12.95
Fuel Rod Active Length, mm	558.8
Clad Material	Incoloy 800
Clad Outer Diameter, mm	13.77
Clad Thickness, mm	0.41
Shroud Material	Aluminum
Shroud Side Dimensions, mm^2	7.572 × 7.963
Shroud Thickness, mm	3.84 and 5.79
Rod Center-to-Center Spacing, mm	16.33
Rod-Rod Clearance, mm	2.57
Rod-Shroud Clearance, mm	2.64
Clearance Between Shrouds, mm	1.37
Fuel Rod Loadings, g	
Uranium	274
^{235}U	54.8
^{166}Er	1.571 (0.80 wt% Er)
	1.311 (0.67 wt% Er)
^{167}Er	1.085 (0.80 wt% Er)
	0.905 (0.67 wt% Er)
Fuel Cluster Loadings, g	
Uranium	4384
^{235}U	876.8
^{166}Er	25.14 (0.80 wt% Er)
	20.97 (0.67 wt% Er)
^{167}Er	17.36 (0.80 wt% Er)
	14.48 (0.67 wt% Er).

Table A32. Neutron Energy Group Structures for Calculations and for Flux Plots Using UZR-H Fuel

For Calculations		For Flux Plots	
Group	Upper Boundary of Energy Interval (eV)	Group	Upper Boundary of Energy Interval (eV)
1	10.0×10^6	1	10.0×10^6
2	6.08×10^5	2	5.53×10^3
3	9.12×10^3	3	0.625
4	5.53×10^3		
5	1.855		
6	1.125		
7	0.625		
8	0.420		
9	0.140		
10	0.050		

Table A33. Core Axial Buckling - UZrH Fuel - 16 Rod Cluster

Group	B_g^2(Core)	Group	B_g^2(Core)
1	0.002921	6	0.000239
2	0.002774	7	-0.000862
3	0.002210	8	0.000050
4	0.001745	9	-0.010104
5	0.000519	10	-0.030449
		$\overline{B^2}$	0.002388

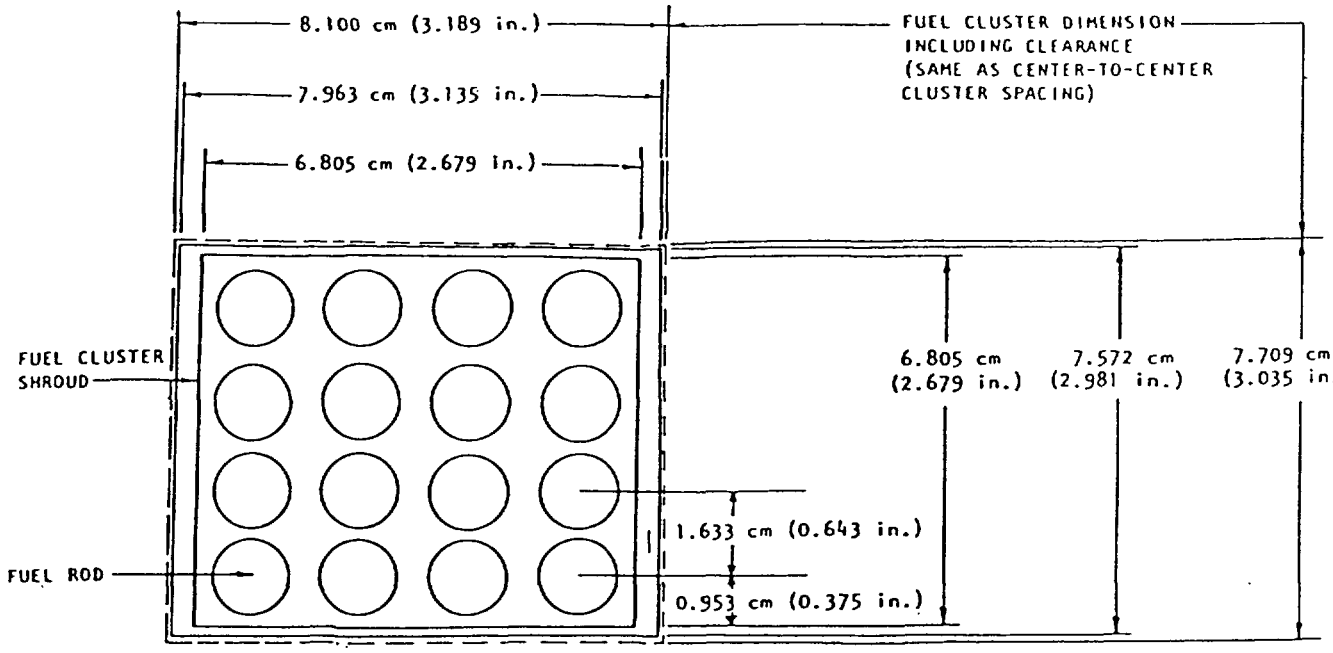

Fig. A64. General layout of 16-rod fuel cluster
(Provided by GA, Appendix B)

Figure A65. 10 MW Reactor - UZr-H 16-Rod Cluster. Geometry of Unit Cell for Calculation of Core Cross Sections

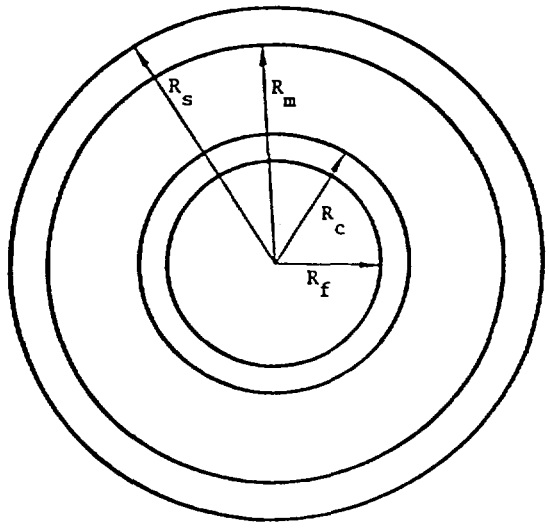

Radii, cm		Volume Fractions	
R_f	0.6475	Fuel	0.3378
R_c	0.6885	Clad	0.0442
R_m	0.9817	Moderator	0.3946
R_s	1.1140	Shroud	0.2234

The XY and the RZ models (provided by GA, Appendix B) used in the calculations of the water-reflected, initial core are shown in Figs. A66 and A67, respectively. The RZ model was used to compute the core, group-dependent bucklings shown in Table A33 for use in the XY calculations. The average buckling was used in the water reflector regions. The axial peak-to-average power density ratio at the center of this core was 1.338.

The XY model constructed by ANL for burnup studies of an equilibrium core using UZr-H fuel is shown in Fig. A68. This configuration is based on the XY model of the HEU reference core (twenty-three standard fuel elements, five control fuel elements, reflection by graphite on two faces and by water on two faces) shown in Fig. A39, and on the XY model shown in Fig. A66. Since the UZr-H core designed by GA for operation at 10 MW has 30 standard fuel elements an additional row of fuel elements was added to the 5 x 6 arrangement of the HEU reference core. In addition, the five control fuel elements of the reference core were replaced with four control rods (containing no fuel) in the UZr-H equilibrium core (see Fig. A66 for comparison). Both cores contain one water-filled flux trap near the center and one near the edge. The positions of the four control rods in the UZr-H core were modified slightly from those of the HEU reference core so that flux traverses through the central flux trap would pass through fueled regions in both cases.

The fuel shuffling pattern shown in Fig. A68 was chosen to be similiar to that of the HEU reference case in order to compare the two cores on as nearly an equal basis as possible. Fresh fuel is inserted near the center of the core (position 1) and the remaining fuel elements are rotated sequentially after each operational cycle. Fuel elements are discharged from position 30 after 30 cycles. This model is intended only for illustration and does not necessarily represent either the core configuration or the fuel shuffling pattern that might be chosen for actual conversion of an HEU plate-type core to use of UZr-H fuel.

The REBUS-2 fuel cycle analysis code,[15] using the group-dependent bucklings shown in Table A33 and cross sections for fresh fuel at the indicated temperatures, was used for all burnup calculations. Further refinements in calculational techniques, such as utilization of burnup-dependent microscopic cross sections, may result in higher burnups than those presented here. An 8 x 8 mesh was used to describe each fuel element in calculations of the initial core and a 4 x 4 mesh was used for those on the equilibrium core. In both XY models with UZr-H fuel, the control rods were fully-withdrawn and consist of an aluminum follower rod with a radius of 2.54 cm inside an aluminum shroud filled with water.

A.5.2.2 Burnup Performance and Flux Performance of the Initial Core

Using the data described above, the water-reflected initial core shown in Fig. A66 with fresh fuel and an erbium content of 0.8 wt% had a k_{eff} of 1.0835 calculated with diffusion theory. Fast, epithermal, and thermal fluxes (with the energy group structure defined in Table A32) are shown in Fig. A69 for a midplane traverse along the y-axis through position C3 and through two of the water-reflected faces. If the fresh fuel in position C3 is replaced with a water-filled flux trap, the fast, epithermal, and thermal fluxes shown in Fig. A70 are found for the same traverse.

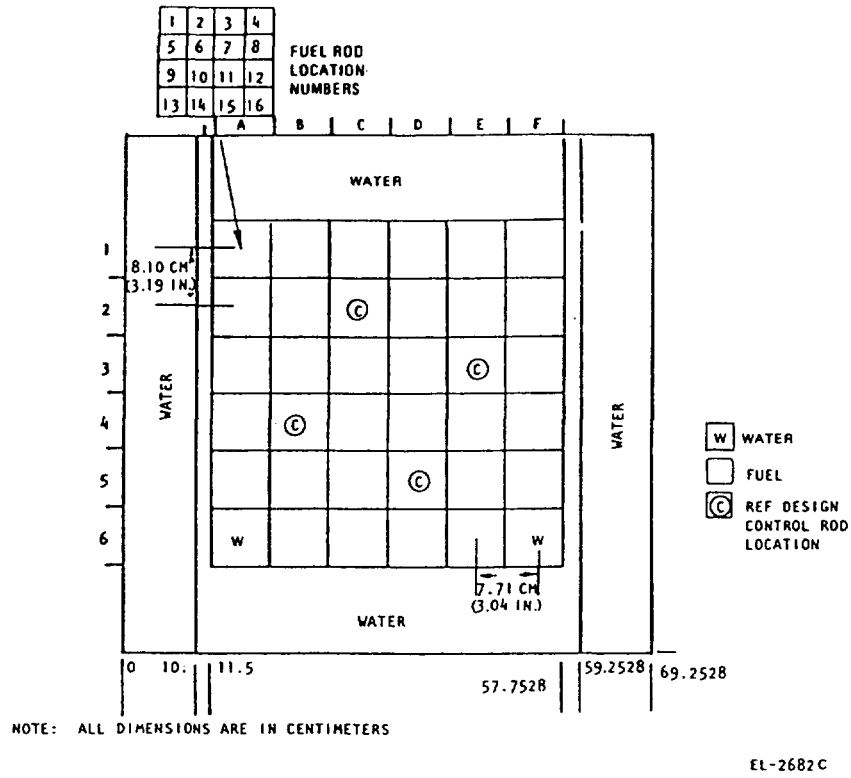

Fig. A66. Grid locations and typical dimensions for 10-MW TRIGA geometry (Provided by GA, Appendix B)

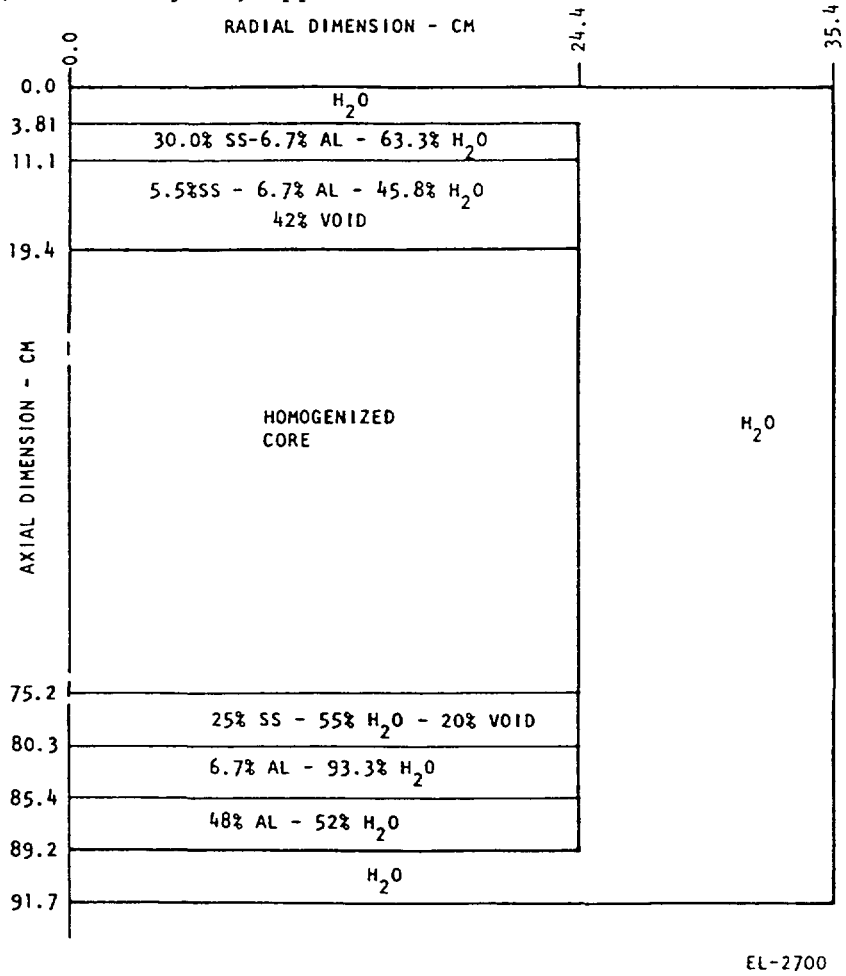

Fig. A67. R-Z calculational model (Provided by GA, Appendix B)

Fresh Fuel Is Inserted into Position 1. All Fuel Elements Are Rotated Sequentially After Each Cycle, And Are Discharged From Position 30 After 30 Operational Cycles. The Control Rods, Which Contain No Fuel, Are Fully-Withdrawn (See Text).

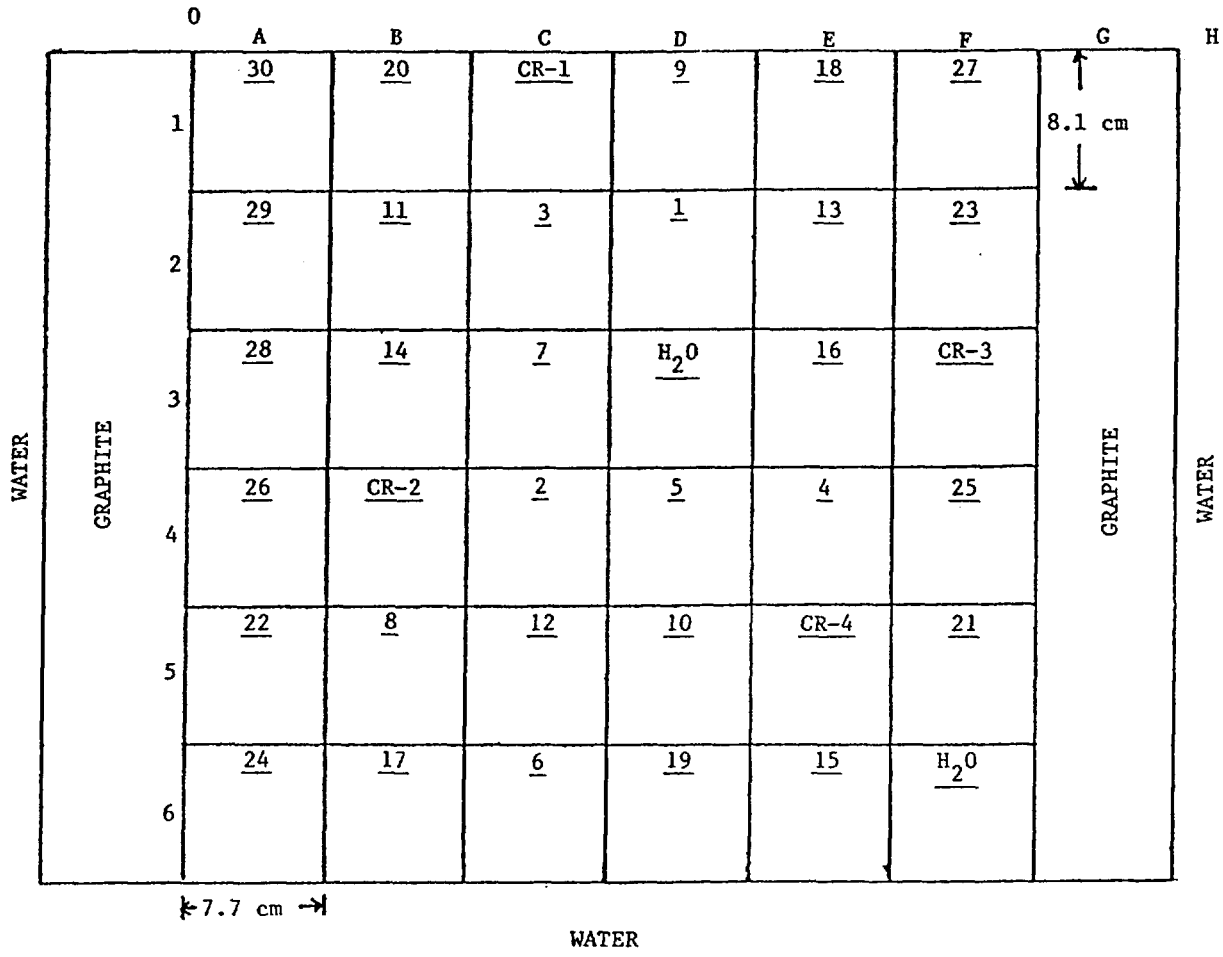

Figure A68. XY Model for Equilibrium - Core Burnup Studies on 10 MW Reactor Using UZr-H LEU Fuel.

Figure A69. Fluxes in Initial UZr-H Fresh Core (Fig. A66). Midplane Traverse Through C3 Fuel.

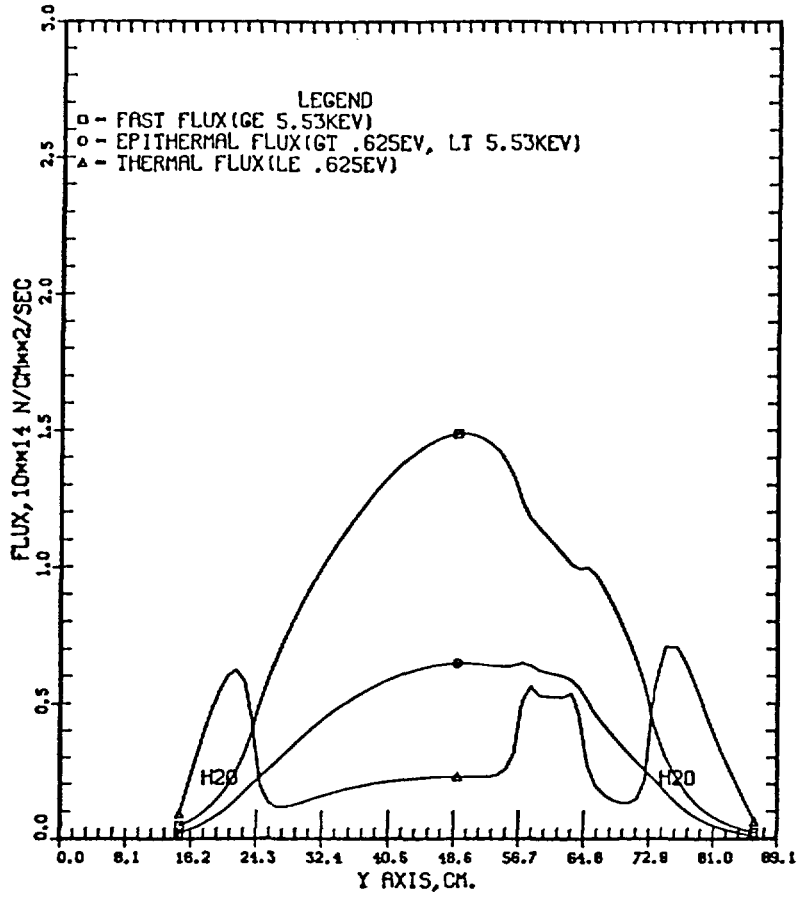

Figure A70. Fluxes in Initial UZr-H Fresh Core (Fig. A66). Midplane Traverse Through C3 Filled with Water.

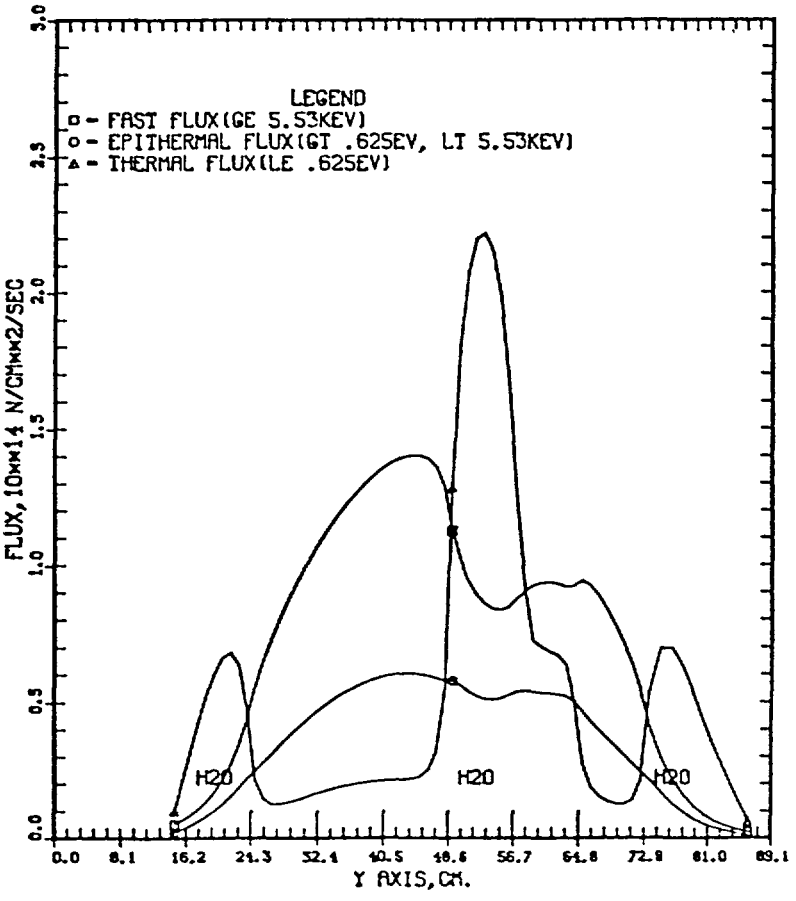

Figure A71 shows the reactivity change as a function of burnup for an initial erbium content of 0.8 wt%. The equilibrium concentration of xenon is normally reached after about 100 hours of operation. The change in k_{eff} due to this xenon poison was 0.027. No attempt is made here to define a core lifetime since this value will depend on the reactivity worth of experiments, the excess reactivity desired for xenon-override, and the design of the control system in individual cases. However, for orientation purposes, the burnup at a k_{eff} of 1.0 was computed to be about 4550 MWd.

Two additional curves of reactivity versus burnup are also shown in Fig. A71 to provide an indication of the burnup that could be expected for different initial values of the erbium burnable poison. Key data from this figure are shown in Table A34.

Table A34. Reactivity and Burnup Data for Initial UZr-H Core with Different Initial Values of Erbium Burnable Poison

Initial Erbium Content, Wt%	k_{eff} at t=0	k_{eff} at Equilib. Xe t=100 hrs	Δk_{eff} Due to Xe Buildup	Burnup at k_{eff} = 1.0, MWd
0.80	1.0835	1.0563	0.0272	4550
0.67	1.0991	1.0711	0.0280	4900
0.0	1.1864	1.1544	0.0320	6150

The choice of the initial erbium loading is essentially determined by the reactivity shutdown margin required in the most reactive state of the core for a given control system effectiveness. In one of the cases, the initial erbium content of the fresh core was adjusted to 0.67 wt% to yield a k_{eff} of 1.0991. The value of k_{eff} at equilibrium xenon was computed as 1.0711, and the burnup at a k_{eff} of 1.0 was found to be about 4900 MWd. A third burnup curve, without erbium, is also shown only to indicate the maximum burnup (~6150 MWd) that might be expected. This case is probably not realistic since the fresh core had a k_{eff} of 1.1864, and the control system is probably not designed for this high initial excess reactivity.

For a burnup of 4550 MWd and 0.8 wt% Er content, a comparison of the thermal flux distribution with the reference, HEU, plate-type equilibrium core is shown in Fig. A72 for a midplane tranverse along the y-axis through position C3 (with a water-filled flux trap) and through two of the water reflected faces. One of the reflector peaks is displaced by approximately one fuel element in the UZr-H case due to the different sizes of the cores. The ratios of the peak thermal fluxes between the UZr-H case and the reference HEU case in are 0.81 at the center of the flux trap, 0.83 for the reflector peaks at about 77 cm, and 0.62 for the displaced reflector peaks. The average thermal flux ratio in the core is much smaller (~0.33), principally because of the much higher initial ^{235}U loading of the UZr-H core, and also partly because of the relative burnup states of the two cores.

Fig. A71. K_{eff} Vs. Burnup for Water-Reflected Initial UZ_r-H Core (Fig. A66) with Initial Erbium Contents of 0.8, 0.67, and 0.0 wt%.

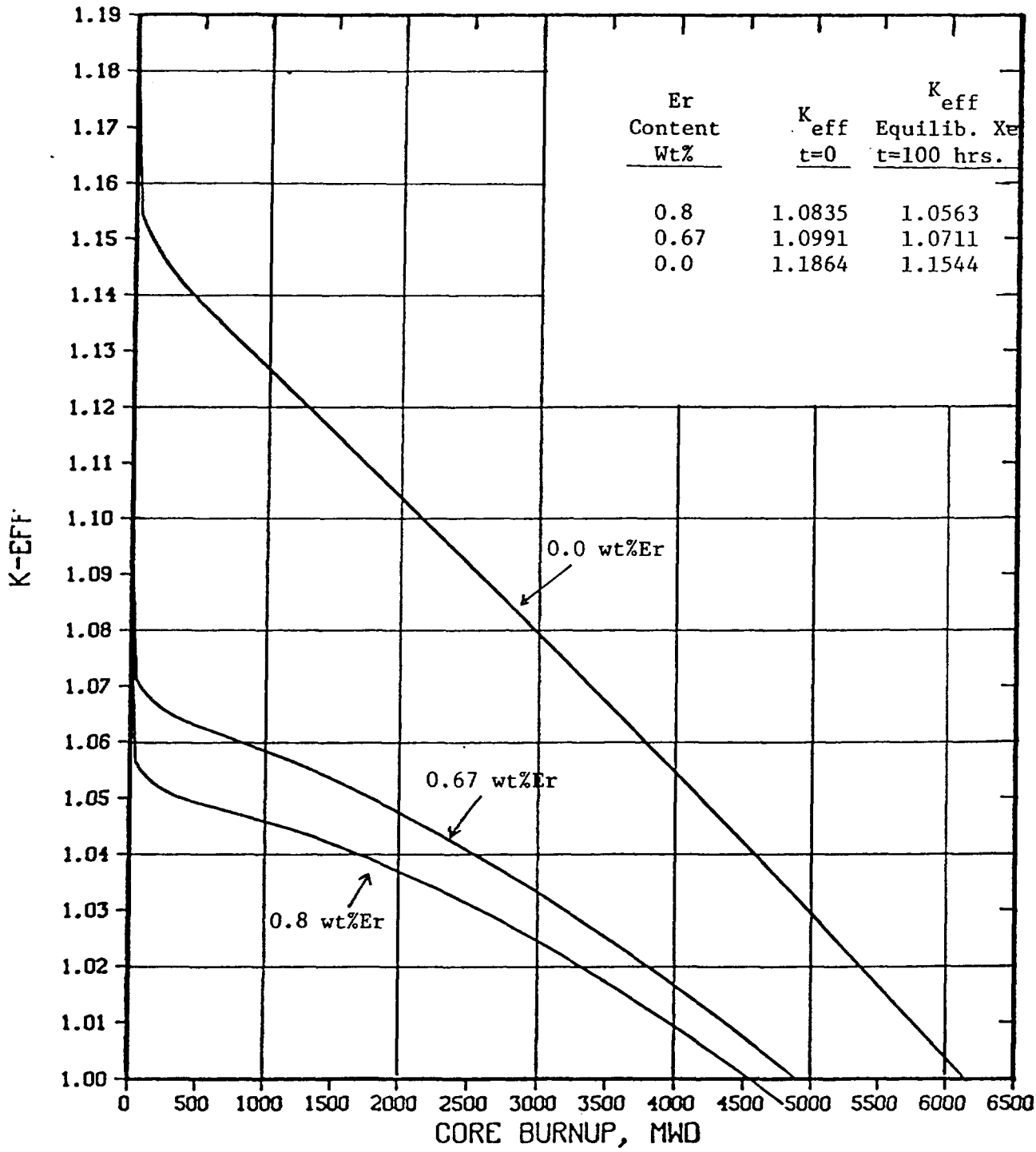

Fig. A72. Comparison of Thermal Fluxes Between Initial UZ_r-H Core (Fig. A66) with Burnup of 4550 MWd and Position C3 Filled with Water and Reference HEU Equilibrium Core Flux Trap (Fig. A40) for a Midplane Traverse Along Y-Axis Through Water-Reflected Faces.

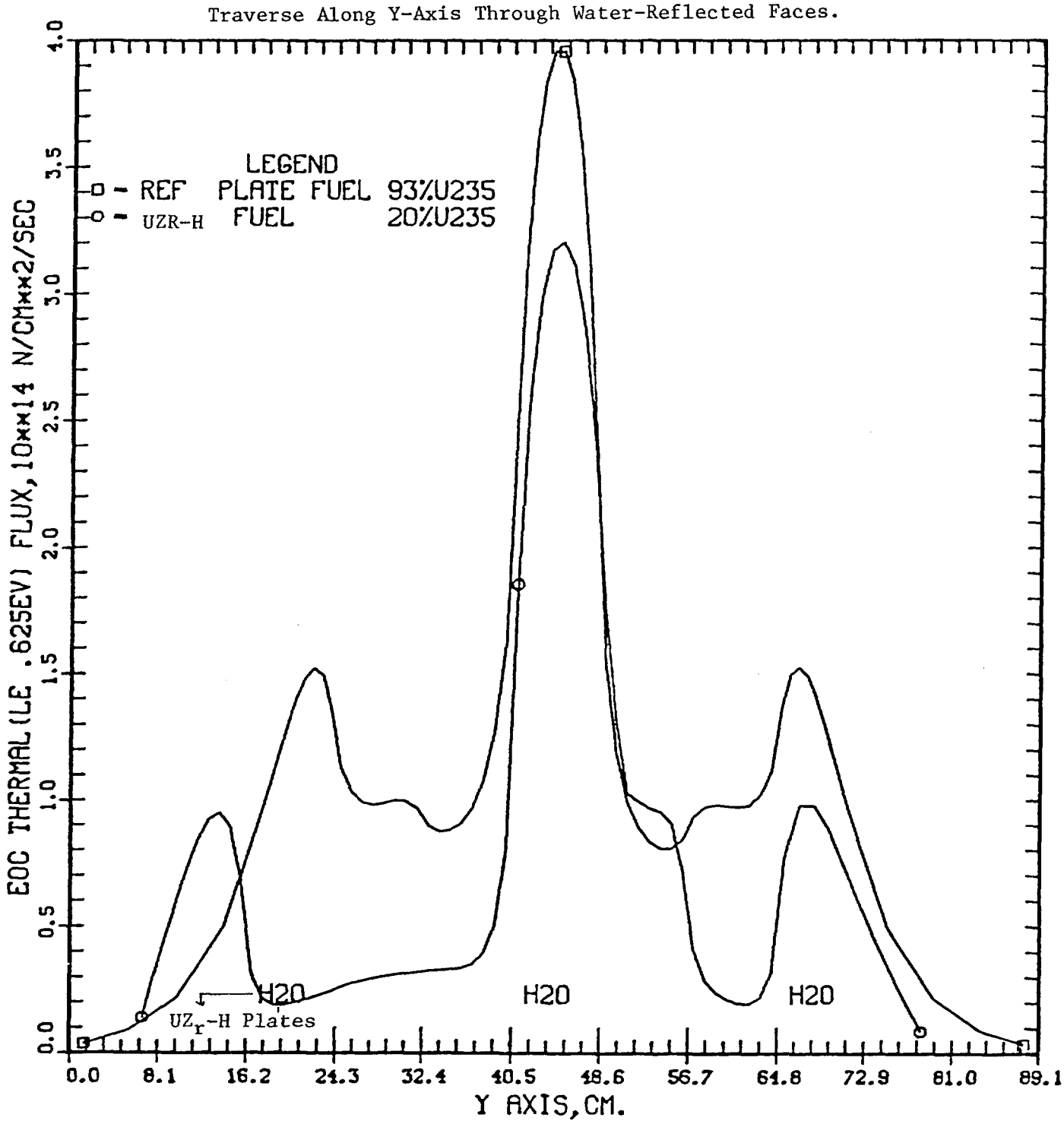

A.5.2.3 Burnup Performance and Flux Performance of the Equilibrium Core

The beginning of equilibrium cycle (BOC) and end of equilibrium cycle (EOC) distributions of ^{235}U and the EOC distribution of Pu for the UZr-H LEU fuel cases with initial erbium contents of 0.8 wt% and 0.67 wt% are shown in Figs. A73 and A74, respectively. Fissile uranium loadings in the fresh standard elements, average cycle lengths, fissile materials burned in the discharged elements, and average discharge burnups for the reference HEU case and the two UZr-H cases are compared in Table A35.

Table A35. Comparison of Burnup Data for the HEU Reference Case and the Cases with UZr-H LEU Fuel

Fuel-Type and Erbium Content	^{235}U in Fresh Std. Element, g	Average Cycle Length, Days	Grams Fissile Burned in Discharge Element		Average Discharge Burnup	
			^{235}U	$^{239}Pu+^{241}Pu$	% ^{235}U	MWd*
Aluminide,-	280	16.7	178.4	~0	63.7	142.7
UZr-H, 0.8 wt%	876.8	40.8	477.5	56.0	54.5	418.1
UZr-H, 0.67 wt%	876.8	43.2	502.2	62.6	57.3	442.2

* Energy production is based on burnup of 1.25 g ^{235}U/MWd and 1.55 g (^{239}Pu + ^{241}Pu)/MWd.

Since the ^{235}U loading with UZr-H fuel is much higher than that of the reference HEU case, the cycle lengths and average discharge burnups (in MWd) are also much higher with UZr-H fuel. As pointed out in Section A.5.2.1, cross sections for the equilibrium core calculations with UZr-H fuel were prepared at 20°C. As a check, the case in Table A35 with 0.8 wt% erbium was recomputed with cross sections prepared at the same temperatures (~290°C) as for the initial core calculations. The average cycle length and average discharge burnup of ^{235}U were computed as 40.3 days and 53.8%, respectively, instead of the 40.8 days and 54.5% values with the 20°C cross sections.

Fast, epithermal, and thermal fluxes at EOC for the reference HEU plate-type core and the UZr-H LEU rodded-type core with an erbium content of 0.8 wt% are shown in Figs. A75, A76, and A77 for a midplane traverse (along the y-axis) through the central flux-trap and through the water-reflected faces of the cores. The asymmetries in the fluxes about the central flux trap are due to the different core sizes and to the asymmetries in the equilibrium burnup distributions with the fuel shuffling patterns that were used. The flux peaks in the water on one side of the cores are displaced since the core with UZr-H fuel has an additional row of fuel elements. A similar comparison is shown in Figs. A78, A79, and A80 for a midplane traverse (along the x-axis) through the central flux trap and through the graphite-reflected faces. Fluxes for the UZr-H fuel case with 0.67 wt% erbium have not been plotted in these figures since the thermal flux at the peak in the central flux trap is only 1.5% higher than that for the case with 0.8 wt% erbium. This flux difference is much smaller at other core locations.

Fig. A73. 10 MW Reactor - UZr-H Fuel - 0.8 wt% Erbium

Beginning and End of Equilibrium Cycle Distributions of ^{235}U
and End of Equilibrium Cycle Distribution of Pu

U Enrichment: 20%
U Density: 3.72 g/cm^3 BOC k_{eff}: 1.0084
Erbium Content: 0.8 wt% EOC k_{eff}: 0.9999
Fresh Fuel Loading: 876.8 g ^{235}U Average Cycle Length: 40.8 Days

	A	B	C	D	E	F	G	H
	30	20	CR-1	9	18	27		
^{235}U(BOC)	405.7	507.5		681.2	529.5	432.0		
^{235}U(EOC)	399.3	496.8		666.5	519.9	425.6		
Pu(EOC)	46.8	40.9		25.6	39.3	45.2		
2	29	11	3	1	13	23		
	414.6	645.6	821.1	876.8	609.5	474.4		
	405.6	629.3	798.4	850.8	594.7	464.3		
	46.6	29.8	10.7	3.4	33.7	43.0		
3	28	14	7	H_2O	16	CR-3		
	425.7	594.7	730.3		561.8			
	414.6	574.6	701.4		541.2			
	46.0	35.6	21.9		37.7			
4	26	CR-2	2	5	4	25		
	445.0		850.8	776.0	798.4	456.3		
	432.0		821.1	746.8	775.9	445.0		
	44.9		7.6	16.9	13.6	44.1		
5	22	8	12	10	CR-4	21		
	485.2	701.5	629.3	666.5		496.8		
	474.4	681.2	609.4	645.5		485.2		
	42.4	24.2	32.1	27.9		41.5		
6	24	17	6	19	15	H_2O		
	464.4	541.2	746.8	519.9	574.6			
	456.3	529.5	730.2	507.4	561.8			
	43.4	38.6	18.8	40.3	36.3			

GRAPHITE (left) GRAPHITE (right)

Fig. A74. 10 MW Reactor - UZr-H Fuel - 0.67 wt% Erbium

Beginning and End of Equilibrium Cycle Distributions of ^{235}U
and End of Equilibrium Cycle Distribution of Pu

U Enrichment: 20%
U Density: 3.72 g/cm^3 BOC k_{eff}: 1.0099
Erbium Content: 0.67 wt% EOC k_{eff}: 1.0000
Fresh Fuel Loading: 876.8 g ^{235}U Average Cycle Length: 43.2 Days

	A	B	C	D	E	F	G	H
	30	20	CR-1	9	18	27		
^{235}U(BOC)	380.9	484.8		666.8	507.6	407.7		
^{235}U(EOC)	374.6	473.8		651.2	497.6	401.1		
Pu(EOC)	47.9	42.3		27.0	40.8	46.4		
2	29	11	3	1	13	23		
	390.0	629.0	816.5	876.8	591.1	450.8		
	380.9	612.0	791.9	848.6	575.5	440.5		
	47.7	31.3	11.4	3.6	35.2	44.3		
3	28	14	7	H_2O	16	CR-3		
	401.2	575.6	719.0		541.3			
	390.0	554.5	688.1		519.7			
	47.1	37.2	23.1		39.2			
4	26	CR-2	2	5	4	25		
	420.8		848.6	767.9	792.0	432.4		
	407.6		816.5	736.5	767.9	420.8		
	46.2		8.1	18.0	14.5	45.4		
5	22	8	12	10	CR-4	21		
	461.9	688.2	612.0	651.2		473.8		
	450.8	666.8	591.0	629.0		461.8		
	43.7	25.5	33.7	29.4		42.9		
6	24	17	6	19	15	H_2O		
	440.5	519.7	736.6	497.6	554.6			
	432.4	507.6	718.9	484.7	541.2			
	44.7	40.1	20.0	41.7	37.9			

GRAPHITE (left) GRAPHITE (right)

Figs. A75 and A76. Comparison of Fast and Epithermal Fluxes at EOC in Rodded-Type UZr-H LEU and Reference Plate-Type HEU Equilibrium Cores for a Midplane Traverse Along the Y-Axis Through the Central Flux Trap and the Water-Reflected Faces.

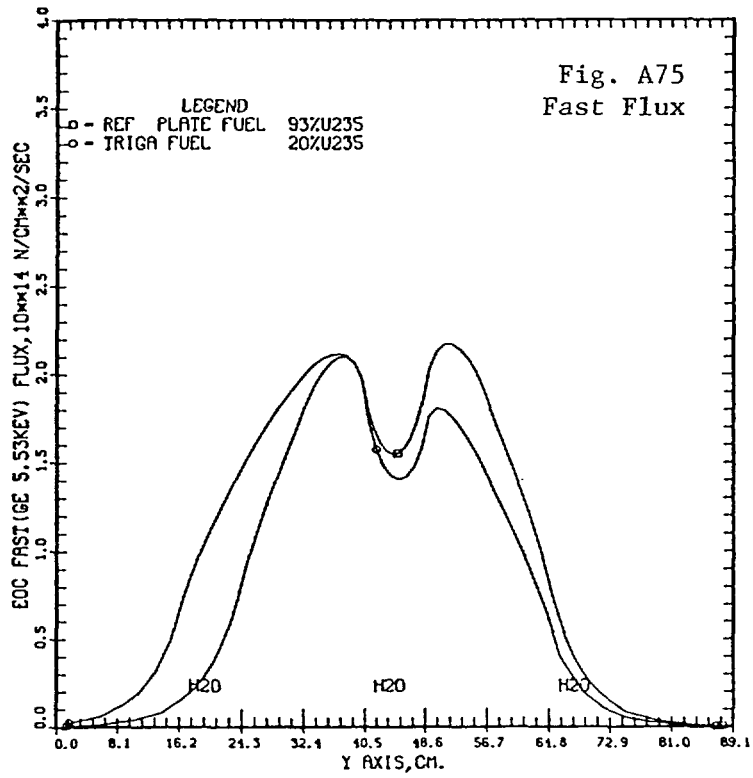

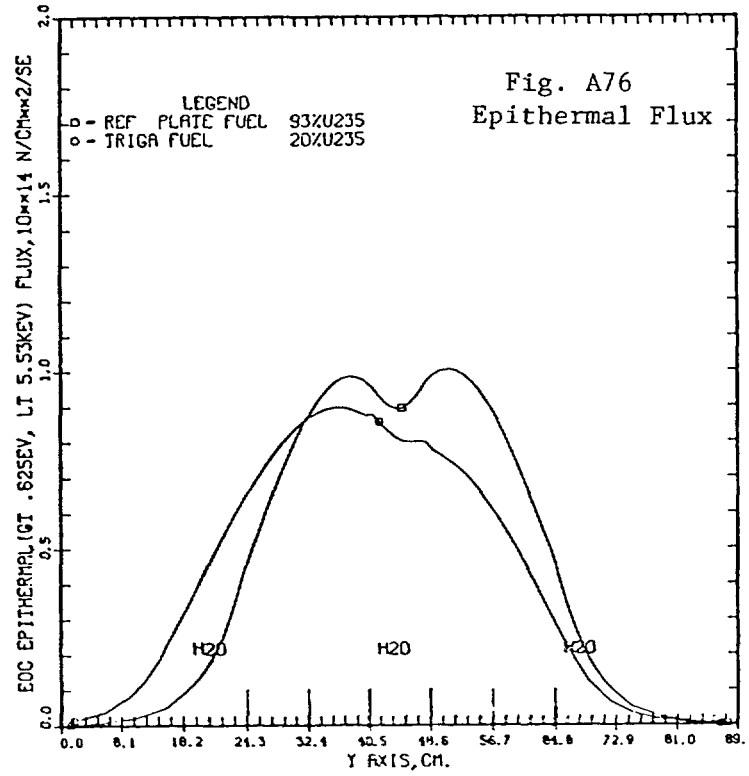

Fig. A77. Comparison of Thermal Fluxes at EOC in Rodded-Type UZr-H LEU and Reference Plate-Type HEU Equilibrium Cores for a Midplane Traverse Along the Y-Axis Through the Central Flux Trap and the Water-Reflected Faces.

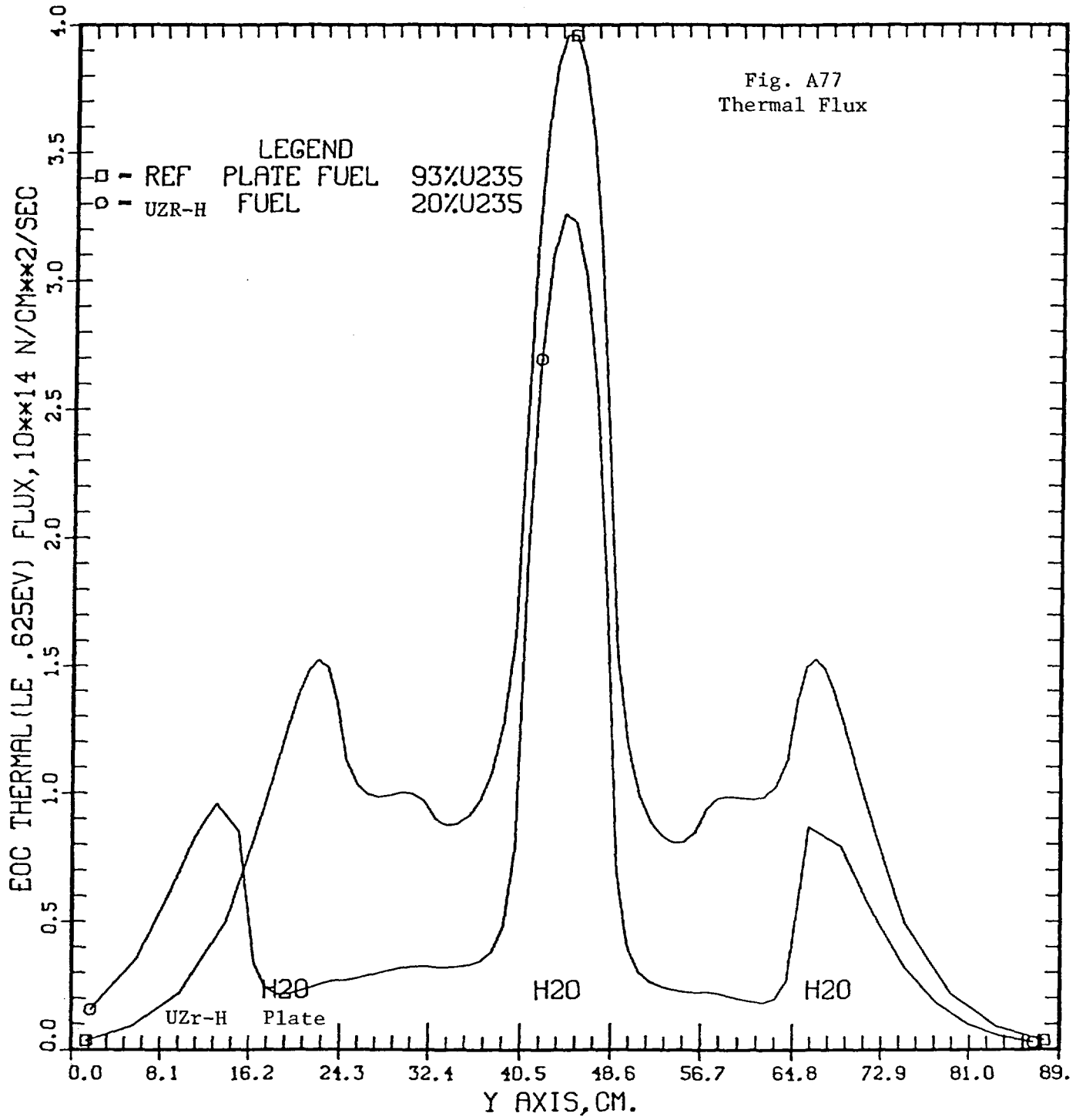

Figs. A78 and A79. Comparison of Fast and Epithermal Fluxes at EOC in Rodded-Type UZr-H LEU and Reference Plate-Type HEU Equilibrium Cores for a Midplane Traverse Along the X-Axis Through the Central Flux Traps and the Graphite-Reflected Faces.

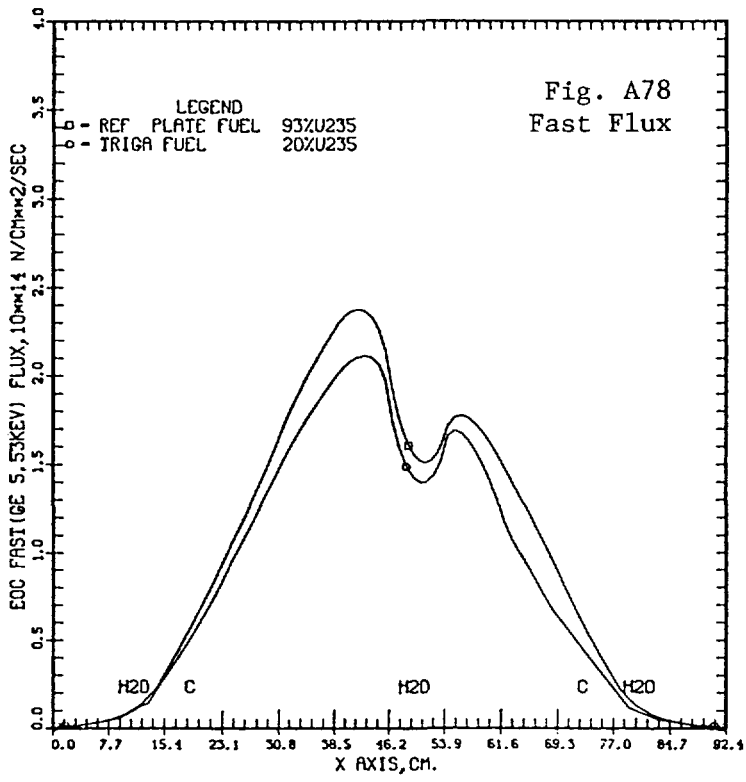

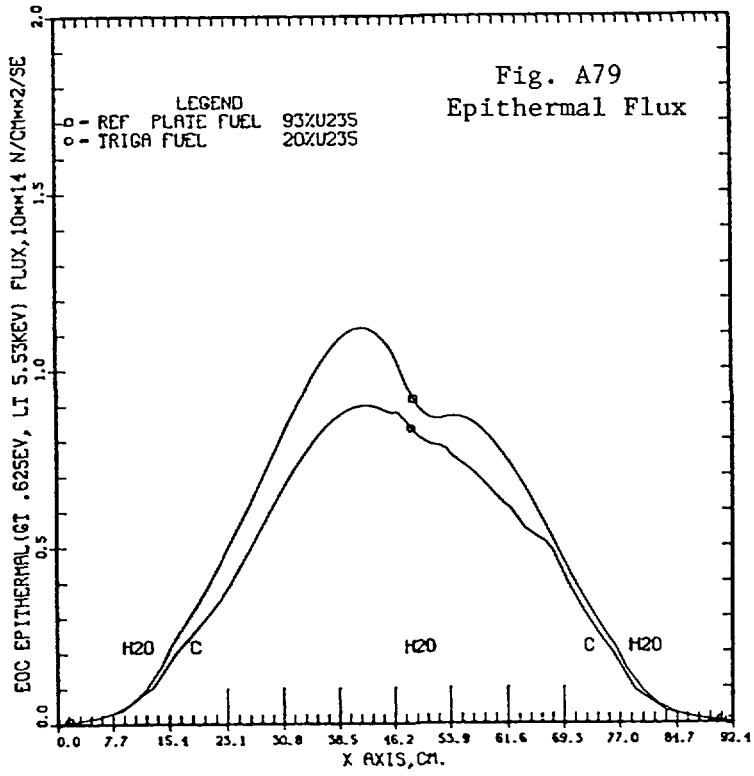

Fig. A80. Comparison of Thermal Fluxes at EOC in Rodded-Type UZr-H LEU and Reference Plate-Type HEU Equilibrium Cores for a Midplane Traverse Along the X-Axis Through the Central Flux Trap and the Graphite-Reflected Faces.

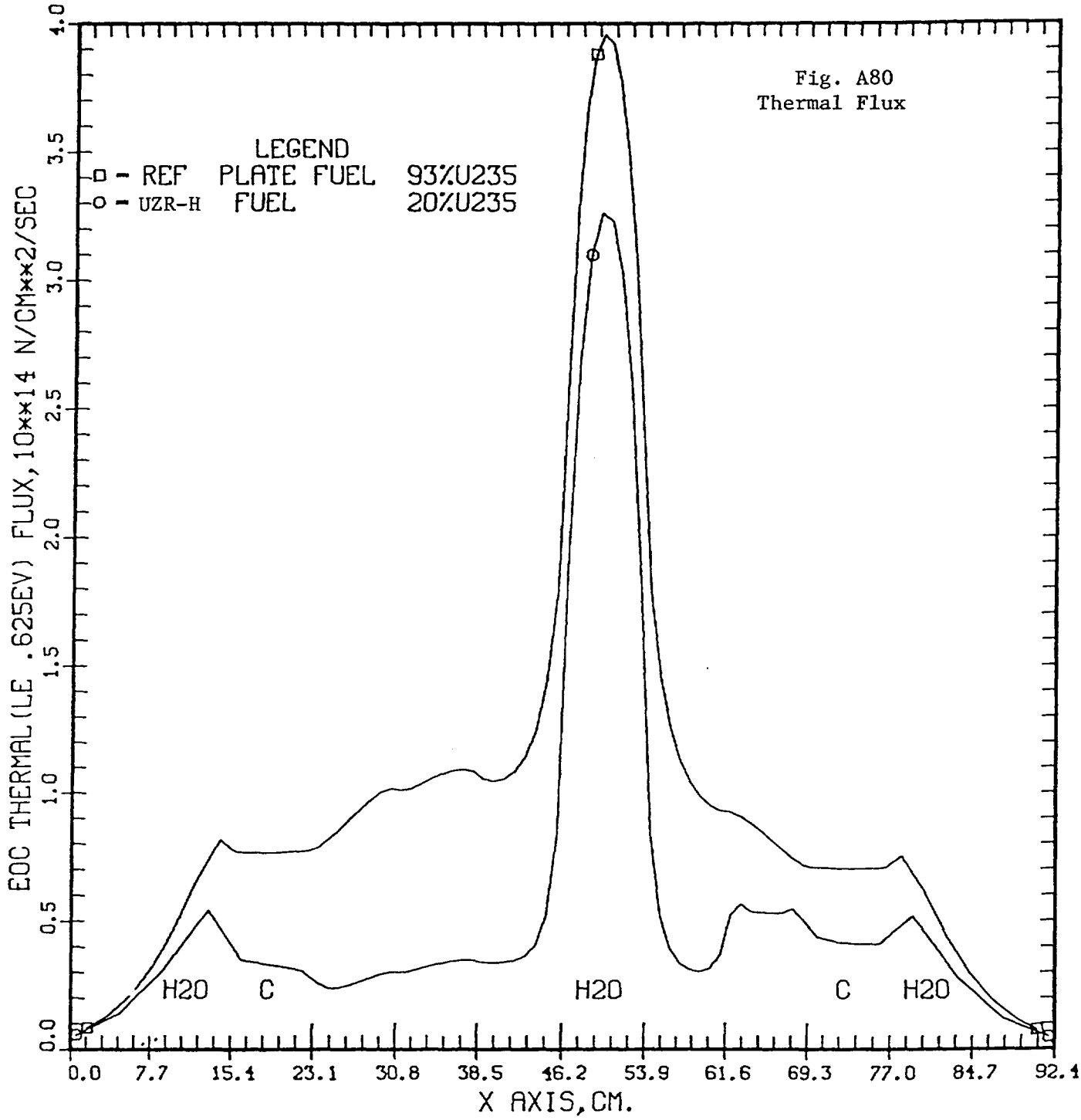

Because of the different core sizes and the different compositions and locations of the control elements, a consistent core map of numerical flux ratios between the case with UZr-H LEU fuel (0.8 wt% Er) and the reference case with HEU aluminide fuel cannot be constructed. However, for convenience, flux ratios are listed in Table A36 at selected positions that the cores shown in Figs. A68 and A39 have in common. In addition to the central flux trap and water reflectors, these positions are: the position (D2) at which fresh fuel is inserted, the position (A1) at which fuel is discharged from the reactor, and the position (E3) corresponding to about one-half the residence time of the discharge element. Row and column identifiers identical to those shown in Fig. A68 can be used in Fig. A39. Ratios of average (over the entire element) fluxes are shown in the fueled regions, and ratios of peak fluxes at the core midplane are shown in the central flux trap and in the water reflectors. Peak fluxes outside the graphite reflectors occur in the water just beyond the graphite.

Table A36. Ratios of Average Fast, Epithermal, and Thermal Fluxes at EOC Between the UZr-H (0.8 wt% Er) LEU Case and the HEU Reference Case for Selected Fuel Elements and Peak Flux Ratios at the Midplane in the Central Flux Trap and in the Water Reflectors. The Energy Group Boundaries Are Those Defined in Table A32 for Flux Plots.

Core Position (in Figs. A68 and A39)	Ratios of Fluxes		
	Fast	Epithermal	Thermal
Central Flux Trap (D3)	0.923	0.875	0.824
Water Reflector (D0)	0.523	0.522	0.569
Water Reflector (Opposite D0)	0.670	0.635	0.629
Water Reflector (H3)	0.555	0.616	0.729
Water Reflector (Opposite H3)	0.643	0.641	0.666
D2	0.792	0.717	0.320
E3	0.894	0.815	0.336
A1	0.731	0.636	0.237

A.5.3 Thermal-Hydraulic Analysis

The thermal-hydraulic analysis done at ANL on the performance of the 10 MW reactor using UZr-H fuel in 16-rod clusters is summarized in this section. The purpose of the analysis is to determine the power limits for the reactor under various coolant flow conditions.

The maximum steady-state power is limited by the smaller value of the power determined either by the maximum fuel temperature or by the minimum DNB ratio (MDNBR). The maximum power in a fuel rod is limited by the peak fuel temperature because long-term fuel growth is a function of fuel temperature. Extensive fuel growth will cause high stress in the clad, for which the yield stress decreases as the temperature increases. The power level can also be limited by the minimum DNB ratio. Experiencing DNB causes excessive temperatures in the fuel and clad, which lead to excessive internal pressure, degradation of the clad mechanical properties, and rod failure. Consequently, a safe margin to DNB must be maintained under all conditions.

In order to study these limiting conditions, both single-phase and two-phase heat transfer are considered for the maximum fuel temperature and several CHF correlations are compared for MDNBR. Parametric results are also provided for the maximum fuel temperature expected at a power level of 10 MW as functions of gap conductance and fuel conductivity.

A.5.3.1 Computer Codes

COBRA-3C/RERTR[17], developed for the RERTR program at ANL, is an improved version of the COBRA-3C/MIT[17] thermal-hydraulic subchannel analysis code. COBRA-3C/RERTR calculates pressure drops along the coolant channels, cross flows, fuel temperatures, clad temperatures, and DNB ratios as a function of axial position for all of the fuel rods (or plates), and identifies the location where the minimum DNB ratio occurs.

HEATING5[65] is a heat conduction code that is used to calculate temperature distribtions in one-, two-, or three-dimensions. The heat generation and the thermal properties may be both spatial and temperature dependent. HEATING5 is used iteratively with COBRA-3C/RERTR to solve for the temperature profile corresponding to a skewed heat generation profile in the hottest rod.

A.5.3.2 Critical Heat Flux (CHF) Correlations

Several low-pressure CHF correlations, by Macbeth,[54,55] Labuntsov,[56] Mirshak,[61] Bernath,[66] and Lund[67] have been implemented in COBRA-3C/RERTR. The Macbeth, Labuntsov, and Mirshak correlations have been discussed in Section A.1.3.7 and are summarized in Fig. A10. The Bernath and the Lund correlations are given in Fig. A81.

The Lund correlation is based on experiments performed with a 25-rod-cluster geometry and is used here for DNBR calculations because the geometries of the 16- and 25-rod clusters are similar. However, a comparison is also made among the Bernath, Mirshak, and Lund correlations at several coolant velocities. Figure A82 shows the calculated minimum DNB ratios using the three correlations at a reactor power of 10 MW. For coolant velocities between 3.8 m/s and 5.5 m/s, the minimum DNB ratios calculated with the the Lund correlation are between those calculated with the Bernath and Mirshak correlations. For coolant velocities less than 3.8 m/s, the MNDBR ratios using the Lund correlation are smaller than those using the other correlations.

Figure A81. The Bernath and the Lund Critical Heat Flux Correlations

The Bernath Correlation[66]

$$q_c = h_c(T_w - T_b)$$

$$h_c = 6.7 \left(\frac{D_e}{D_e + D_i}\right) + 0.0065 \frac{U}{D_e^{0.6}}$$

$$T_w = 57 \ln (14.5\ P) - 54 \left(\frac{P}{P + 1.0345}\right) - \frac{U}{122}$$

where

q_c = Critical Heat Flux, W/cm^2
h_c = Heat Transfer Coefficient, W/cm^2-°C
T_w = Wall Temperture, °C
T_b = Bulk Coolant Temperature, °C
D_e = Hydraulic Diameter, cm
D_i = Heated Diamter ≡ Heated Perimeter/π, cm
U = Coolant Velocity, m/s
P = Pressure, bar absolute

Parameter Ranges

Velocity : 1.22 - 16.5 m/s
Pressure : 1.59 - 206.9 bar absolute
Hydraulic Diameter : 0.363 - 1.68 cm

The Lund Correlation[67]

$$q_c = 50\ f_c\ \rho\ C_p\ V_g\ (T_c - T_o)$$

$$T_c = T_{sat}\ (1 + 6\ \sqrt{\theta_c})$$

$$\theta_c = q_c\ \sigma_{sat}/P\mu_{sat}\ h_{fg}$$

$$f_c = 0.55\ R_{e_g}^{-0.37}$$

$$R_{e_g} = 2\ \rho\ V_g\ D_r\ (S - 1)/\mu_{sat}$$

$$V_g = U\ (1 - 0.98\ e^{-2.2\ (S-1)})$$

where

q_c = Critical Heat Flux, W/cm^2
T_c = Critical Wall Temperture, °C
T_o = Temperture at Outlet of Coolant Channel, °C
T_{sat} = Saturation Temperature, °C
f_c = Friction Factor for Channel Between Fuel Rods
ρ = Density, kg/m^3
C_p = Specific Heat at Constant Pressure, J/kg°C
V_g = Interrod Channel Velocity, m/s
U = Coolant Velocity, m/s
σ_{sat} = Saturation Surface Tension, N/m
P = Pressure, bar absolute
μ_{sat} = Viscosity at Saturation Temperature, Pa·s
h_{fg} = Heat of Vaporization, kJ/kg
R_{e_g} = Reynolds Number for the Interrod Channel
D_r = Rod Diameter, cm
S = Pitch to Diameter Ratio

Parameter Ranges

Coolant Velocity : 2.4 - 6.4 m/s
Pressure : 0.94 - 13.7 bar absolute
Subcooling : 40 - 80 °C
q_c : 135.5 - 335.1 W/cm^2

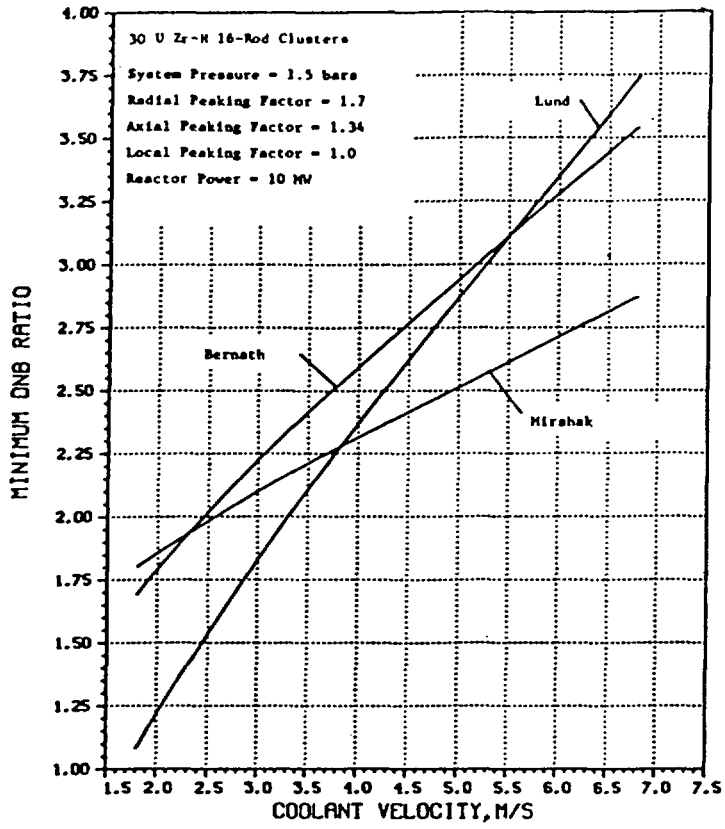

Figure A82. A Comparison Among the Bernath, Mirshak, and Lund Correlations.

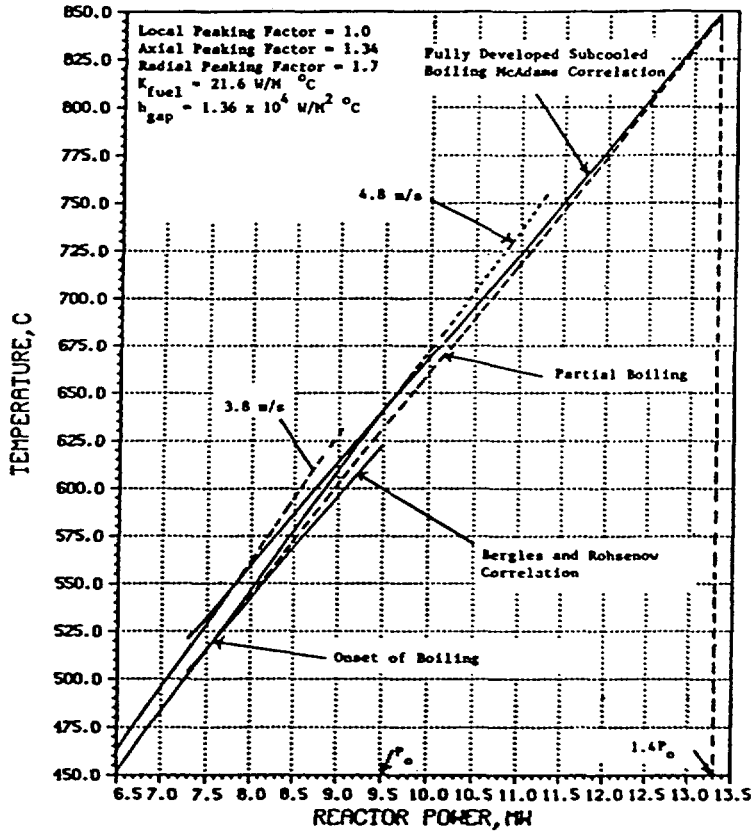

Figure A83. The Maximum Fuel Temperature vs. Reactor Power Using Different Heat Transfer Correlations.

A.5.3.3. Single-Phase and Two-Phase Heat Transfer Correlations

The Boelter correlation[31] is used for the single-phase heat transfer coefficient in the single-phase regime which occurs at relatively low reactor powers and high flow rates. The Bergles and Rohsenow correlation[30] is used to determine the onset of subcooled boiling. The McAdams correlation[68] is used for subcooled flow in a fully-developed boiling condition, which occurs at relatively high powers and relatively low flow rates. The Boelter correlation and the Bergles and Rohsenow correlation were discussed in Section A.1.3.4. The McAdams correlation is written as:

$$q_{sb} = 2.26 \times 10^{-4} (\Delta T_s)^{3.86}$$

where

q_{sb} = surface heat flux in the subcooled boiling region (in W/cm^2)

ΔT_s = wall super-heat in °C; i.e., $T_w - T_s$, where T_w is the wall temperature, and T_s is the saturation temperature.

Five curves for the maximum fuel temperature as a function of reactor power are shown in Fig. A83. Two curves are based on single-phase flow for coolant velocities of 3.8 m/s and 4.8 m/s. The other three curves are based on the two-phase correlations and include the onset of boiling curve , the fully-developed boiling curve, and a partial boiling curve based on an interpolation between the previous two curves. The partial boiling curve, interpolated between reactor powers of P_o and 1.4 P_o, is discussed here only to illustrate the existence of the partial boiling regime. The value of P_o (9.5 MW) is taken as the intersection of the single-phase curve and the McAdams two-phase curve. The value of 1.4 P_o is based[69] on pool boiling data (which may not be applicable to boiling flow), and was chosen to indicate the end of partial boiling and the beginning of fully-developed subcooled boiling. However, the maximum fuel temperature predicted by the partial boiling curve is close to that predicted by the single-phase curve for reactor power less than P_o, and close to that predicted by the McAdams curve for reactor power greater that P_o. Thus, only the single-phase correlation and the McAdams two-phase correlation are utilized for temperature predictions in this analysis.

Figure A83 also illustrates the use of the single-phase and the two-phase heat transfer correlations to determine the maximum reactor power by specifying a limit on the maximum fuel temperature. If the maximum fuel temperature is taken as 750°C, the maximum reactor power is predicted as 11.5 MW using the McAdams two-phase curve and as 11.25 MW using the single-phase curve for a coolant velocity of 4.8 m/s (5000 gpm flow rate in a core with 30 fuel elements). The maximum reactor power would be 11.5 MW. Although this difference is not significant here, it illustrates that the McAdams two-phase curve provides an envelope above which the single-phase curves are not applicable.

A.5.3.4 Power Peaking Factors

Figure A84 shows the subchannel model used in COBRA-3C/RERTR for a 16-rod fuel cluster and the radial rod power peaking factors computed by ANL for the limiting fuel element in the 10 MW reactor (position C3 in Fig. A66) with fresh fuel. For the hottest rod, the radial power peaking factor (average power in the hottest rod relative to the average power in the core) is 1.71, and the axial power peaking factor is 1.34.

The heat generation in fuel rods will be skewed at interfaces where fuel elements adjoin regions of higher moderating power (e.g. flux traps and control rod follower regions). However, the maximum temperature in a fuel rod with a skewed power profile has a value close to that with a uniform power profile. This is essentially because the maximum fuel temperature is proportional to the square of the heat conduction length and to the heat generation rate. Although the peak value of the heat generation rate with a skewed profile can be two or three times that with a uniform power profile, the location of the peak value is usually near the surface of the rod, and its heat conduction length is near zero. Thus, the peak heat generation rate has little influence on the maximum fuel temperature, and a local power peaking factor is not needed to determine the maximum steady-state reactor power based on maximum fuel temperature. The total power peaking factor in this case is then:

Total Power Peaking Factor = (Radial Peaking Factor) x (Axial Peaking Factor) (For Max. Fuel Temperature)

Since DNB is a surface phenomenon, a skewed power profile has a strong influence on the azimuthal distribution of the surface heat flux. Therefore, a local power peaking factor is required in this case to account for the azimuthal variation of the surface heat flux. The local power peaking factor is defined as the local maximum surface heat flux in the hottest rod at the location of the axial power peak, divided by the average surface heat flux in the same rod at the same axial location. The peak surface heat flux at the hot spot in the reactor is then:

Peak Surface Heat Flux = (Core Average Heat Flux) x (Axial Peaking Factor) x (Radial Rod Peaking Factor) x (Local Peaking Factor).

In this analysis, HEATING5 and COBRA-3C/RERTR were used iteratively in a two-loop scheme to calculate the two-dimensional temperature profile in a radial plane for a skewed heat generation profile[70] in the hottest rod adjacent to a water-filled flux trap. This temperature profile was then used to calculate the azimuthal distribution of the surface heat flux at the location of the axial power peak. The local power peaking factor obtained by taking the ratio of the maximum surface heat flux to the average surface heat flux was found to be 1.29. Again, for steady-state operation, this local power peaking factor is applicable only to calculation of the MDNBR.

A.5.3.5 Results and Discussion

A radial temperature profile across the hottest rod (see Fig. A84) at the peak of the axial power distribution in a 30 element core operating at 10 MW is shown in Fig. A85. A uniform heat generation profile and a coolant velocity of 4.8 m/s (corresponding to 5000 gpm) were used. The radial and axial power peaking factors were 1.71 and 1.34, respectively. The gap conductance was 1.36×10^4 W/m^2/°C, and the fuel conductivity was 21.6 W/m/°C. The maximum fuel temperature shown in Fig. A85 is 670°C.

Figure A86 shows the maximum fuel temperature as a function of reactor power for various coolant velocities. If the maximum fuel temperature is taken as 750°C based on the consideration of fuel growth from temperature-dependent irradiation effects, the limiting reactor power is 11.5 MW for coolant velocities less than 5.8 m/s, and 11.75 MW for a coolant velocity of 6.8 m/s. Thus, the limiting reactor power based on a maximum fuel temperature of 750°C is nearly independent of coolant velocity, since boiling heat transfer is nearly independent of coolant velocity.

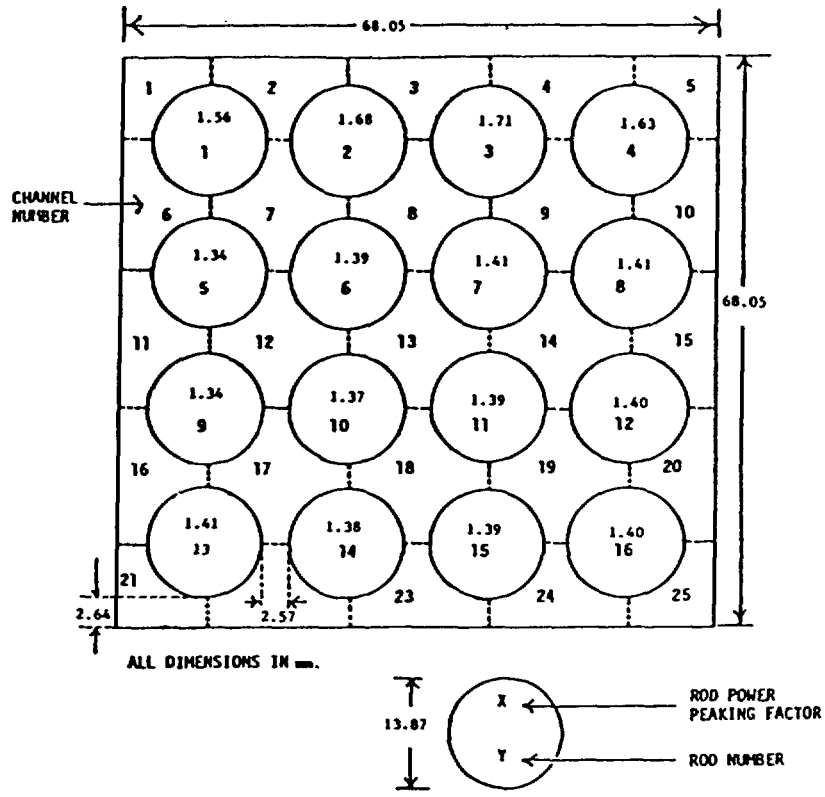

Figure A84. Subchannel Modelling and Radial Power Peaking Factors for Fuel Element (Position C3, Fig. A66) with Hottest Rod.

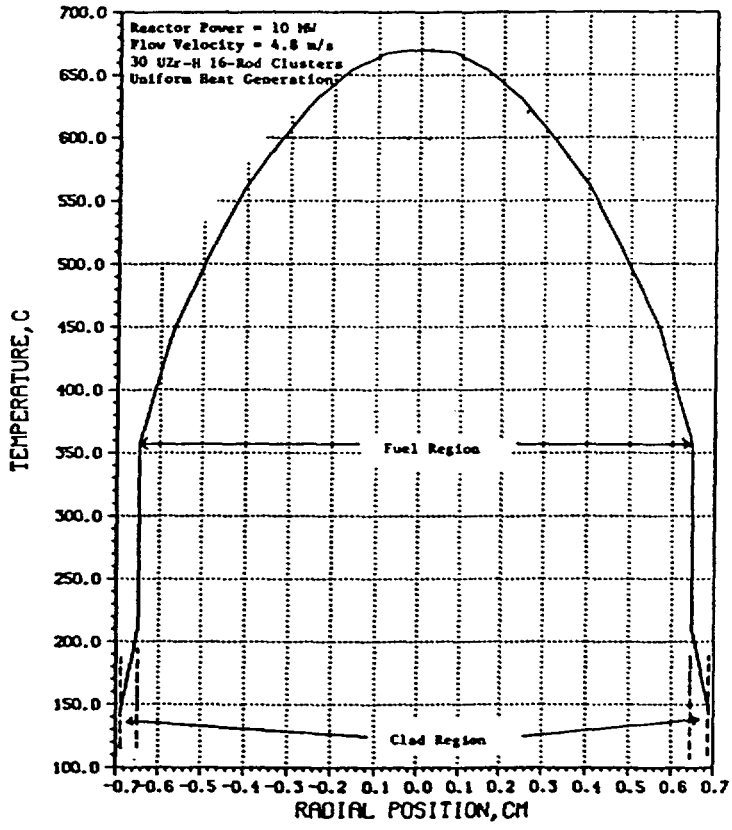

Figure A85. A Radial Temperature Profile for the Hot Rod at Reactor Power of 10 MW.

Figure A87 shows minimum DNB ratios based on the Lund correlation as a function of reactor power for various coolant velocities. At a reactor power of 10 MW and coolant velocities of 2.8, 3.8, 4.8, and 5.8 m/s, the minimum DNB ratios are about 1.22, 1.66, 2.05, and 2.43, respectively. The coolant velocity is thus closely related to the degree of conservatism desired in the MDNBR.

This relationship between coolant velocity and maximum reactor power based on maximum fuel temperature and on minimum DNB ratio is further illustrated in Fig. A88. For given design conditions, both limits must be considered.

By appropriate scaling, Figs. A86 and A87 can also be used to find the maximum reactor power if the number of fuel elements in the core is different from 30. Of the power peaking factors, the radial rod factor is the most sensitive to core size, and affects the maximum power directly. For example, if a core had 28 fuel elements and a radial peaking factor of 1.8, the reactor power of 11.5 MW at a maximum fuel temperature of 750°C in Fig. A86 would be scaled down by a factor of (28 x 1.7)/(30 x 1.8) to a new maximum power of 10.1 MW. The same procedure can be applied in Fig. A87 to find the maximum reactor power based on the MDNBR for various coolant velocities.

The thermal conductivities of the fuel and the Incoloy clad[71] used in this analysis are 21.6 W/m/°C and 14.9 W/m/°C, respectively. Actually, the fuel conductivity is a function of fuel temperature. For UZr-H fuel containing HEU, the conductivity[72] is given by: $K_f = 18 + 7.67 \times 10^{-3} T$, where K_f is in W/m/°C and T is the fuel temperature in °C. The thermal conductivity of UZr-H fuel containing LEU is expected to be slightly lower than that using HEU.

The gap conductance is a sensitive function of the width of the gap between the fuel rod and the clad, which depends upon manufacturing tolerances. The gap width at a given power level depends on the temperatures of both the fuel and the clad because of the difference between their thermal expansion coefficients. Thus, the gap conductance is also a function of the fuel temperature. The value of the gap conductance used here was 1.36×10^4 W/m^2/°C. Analytical modelling of gap conductance is difficult, and large discrepancies usually result in comparison with experimental data.[73]

For reference purposes, the variation of the maximum fuel temperature with fuel thermal conductivity and with gap conductance are shown in Figs. A89 and A90, respectively, for a wide range of values. However, typical values for these parameters are expected to be close to those used in this analysis.

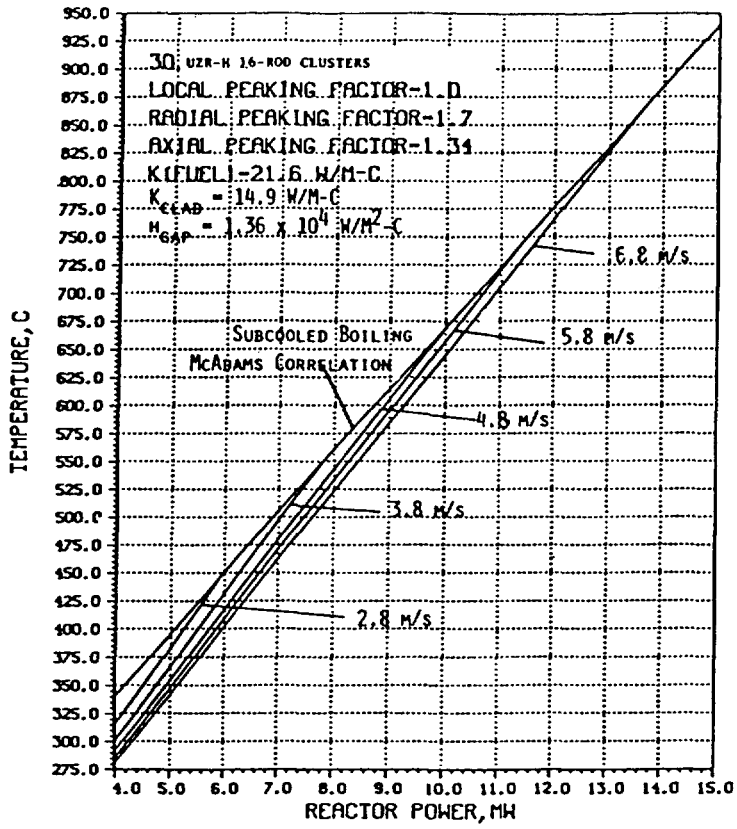

Figure A86. The Maximum Fuel Temperature vs. Reactor Power for Various Coolant Velocities.

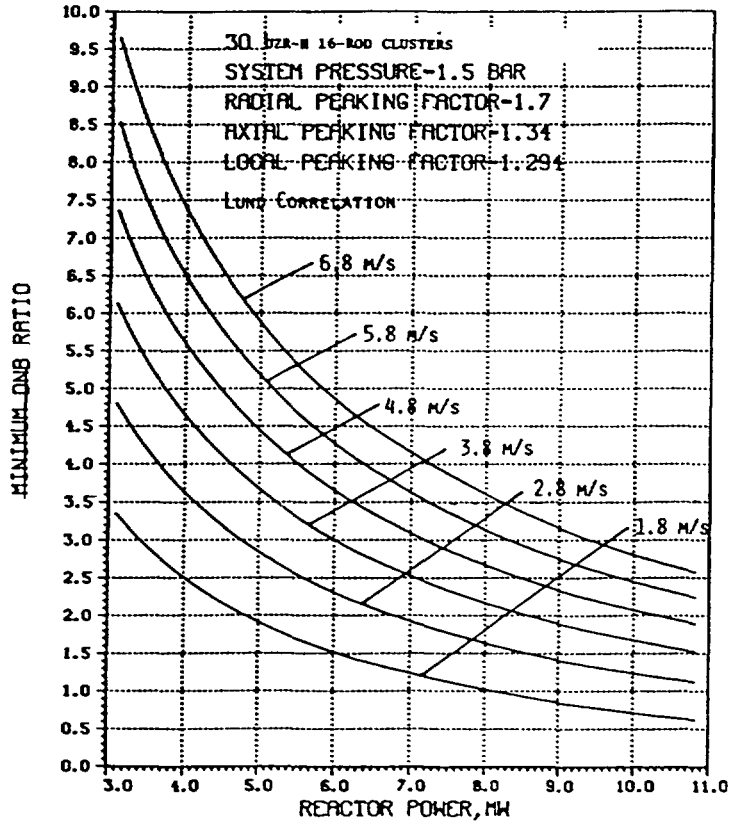

Figure A87. Minimum DNB Ratios Based on the Lund Correlation vs. Reactor Power for Various Coolant Velocities.

Fig. A88. Maximum Reactor Power Based on Maximum Fuel Temperature and on MDNBR (Lund Correlation) as a Function of Coolant Velocity.

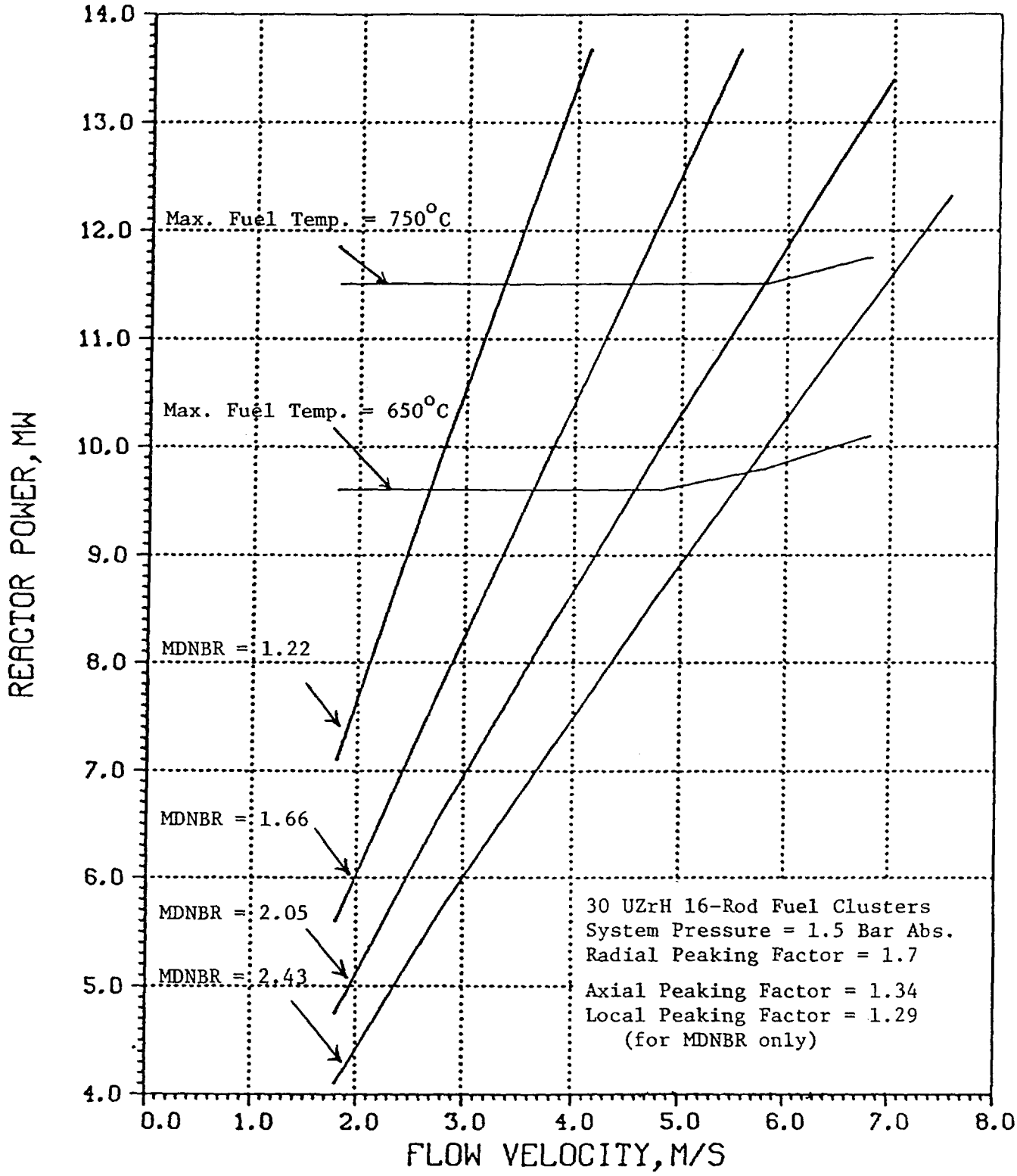

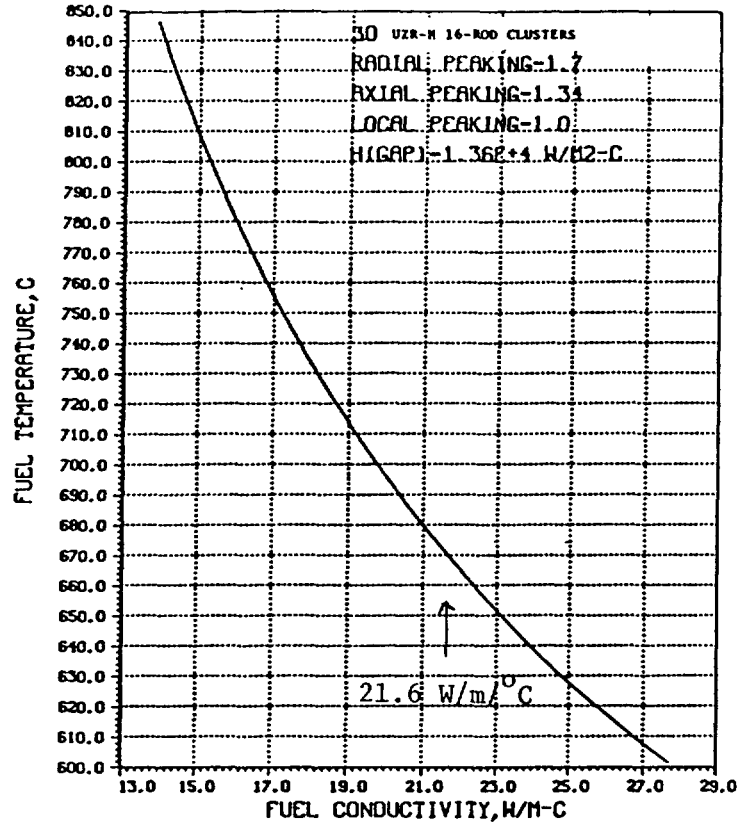

Figure A89. Sensitivity of the Maximum Fuel Temperature to the Fuel Thermal Conductivity at a Power of 10 MW.

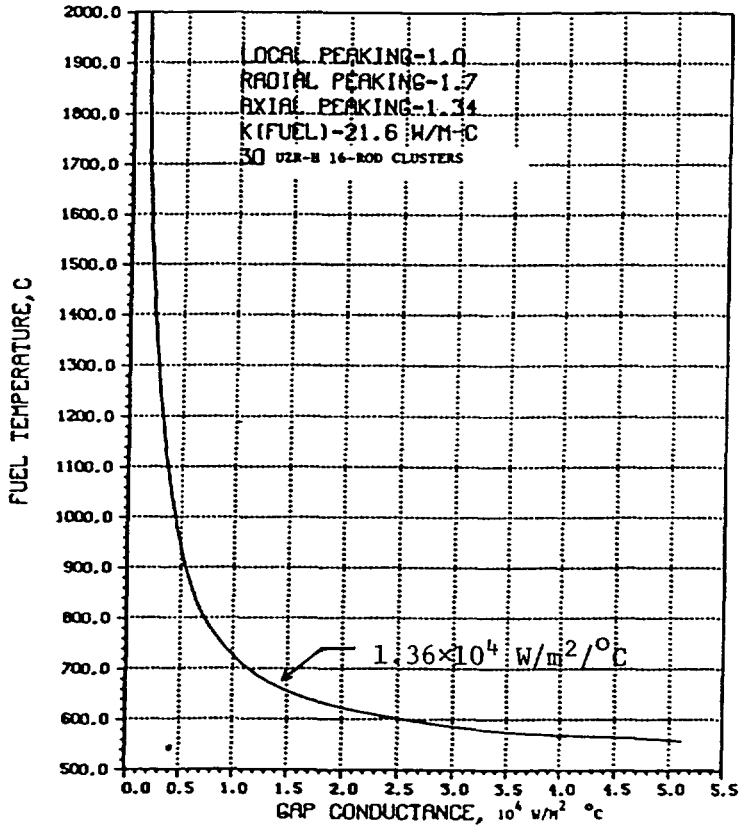

Figure A90. Sensitivity of the Maximum Fuel Temperature to the Gap Conductance at a Power of 10 MW.

A.6 COMPARATIVE PERFORMANCE OF 10 MW REACTOR WITH DIFFERENT FUELS AND PLUTONIUM PRODUCTION DATA

This section compares burnup and flux performance data for selected cases which were separately presented in Sections A.3, A.4, and A.5 to discuss the potential for conversion of the 10 MW HEU reference core to the use of LEU in classical dispersion fuels (UAl_x-Al or U_3O_8-Al), Caramel fuel (UO_2-Zr4), and UZrH fuel. Total plutonium and ^{239}Pu content of discharged fuel elements as a function of uranium enrichment are also summarized for the various fuels.

A.6.1 Comparative Burnup and Flux Performance

Burnup and flux performance are compared for the following fuels:

(1) HEU reference case: Plate-type aluminide fuel with a uranium density of 0.68 g/cm^3 in 0.51 mm thick fuel meat; 23 plates and 280 g ^{235}U per fresh standard element.

(2) Plate-type aluminide fuel with a uranium enrichment of 20% and a uranium density of 2.27 g/cm^3 in 1.238 mm thick fuel meat; 19 plates and 403 g ^{235}U per fresh standard element.

(3) Plate-type Caramel fuel (UO_2-Zr4) with a uranium enrichment of 6.5% and a uranium density of 8.41 g/cm^3 in 1.45 mm thick fuel meat; 16 plates and 498 g ^{235}U fresh standard element.

(4) Rodded-type UZrH fuel with a uranium enrichment of 20%, a uranium density of 3.72 g/cm^3, and an erbium content of 0.8 wt% in 12.95 mm outer diameter fuel meat; 16 rods and 877 g ^{235}U per fresh standard element.

Burnup data for these cases are sumarized in Table A37.

Table A37. Comparison of Burnup Data for the HEU Reference Case and Cases with LEU Fuels.

Fuel-Type and Enrichment	Uranium Density Fuel Meat, g/cm^3	^{235}U in Fresh Std. Element, g	Average Cycle Length, Days	Grams Fissile Burned in Discharge Element ^{235}U	Grams Fissile Burned in Discharge Element $^{239}Pu+^{241}Pu$	Average Discharge Burnup % ^{235}U	Average Discharge Burnup MWd*
Aluminide, 93%	0.68	280.0	16.7	178.4	~0	63.7	142.7
Aluminide, 20%	2.27	403.0	16.7	170.5	10.7	42.3	143.3
Caramel, 6.5%	8.41	497.5	22.5	206.2	33.4	41.5	186.5
UZrH, 20%	3.72	876.8	40.8	477.5	56.0	54.5	418.1

*Energy production is based on burnup of 1.25 g ^{235}U/MWd and 1.55 g (^{239}Pu + ^{241}Pu)/MWd.

Fast, epithermal, and thermal fluxes at EOC for the reference HEU case and for the three LEU cases are shown in Figs. A91, A92, and A93, respectively, for a midplane traverse (along the y-axis of each core) through the central irradiation channel and the water-reflected faces. One of the thermal flux peaks for the UZr-H fuel case is displaced by about one fuel element since the size of the core is larger by one row. The asymmetries in the fluxes about the central irradiation channel are mainly due to the asymmetries in the equilibrium burnup distributions with the shuffling patterns that were used. A similar comparison of fluxes is shown in Figs. A94, A95, and A96 for a midplane traverse (along the x-axis of each core) through the central irradiation channel and the graphite-reflected faces. Numerical flux ratios between each LEU case and the HEU reference case are shown in Table A38 for several key locations in the cores.

The behavior of the flux performance for the various cores, illustrated in Figs. A92 through A96 and in Table A38, indicates some simple and predictable trends.

1) The main differences among the four cases considered are closely related to the ^{235}U loading of a fresh fuel element in the various cores. In order of increasing ^{235}U element loading, the cores are so ordered: HEU, Aluminide, Caramel, and UZrH.

2) Thermal neutron fluxes in fresh fuel elements are very nearly inversely proportional to the ^{235}U loading of the elements. This is due, of course, to the fact that for the same core volume and total power, the power of a given element must be approximately the same in each core.

3) Fast and epithermal fluxes in fresh fuel elements also show a decreasing trend with increasing ^{235}U loading of the elements. However, the magnitudes of these flux reductions are much smaller than for the thermal fluxes.

4) Thermal fluxes in the central irradiation channel decrease with increasing ^{235}U loading, but by much less than the thermal fluxes in the fuel elements. An empirical fit shows that they are approximately inversely proportional to the 0.174 power of the ^{235}U loading.

5) Neutron fluxes in the reflectors show a behavior similar to that in the central irradiation channel, with some significant deviations due to differences in core configurations and neutron spectra. In several cases, the LEU fast and epithermal fluxes in the reflectors exceed the HEU fluxes at the same locations.

6) Neutron fluxes in irradiatiated fuel elements follow the same general trend as those in fresh fuel elements, with some significant deviations due to differences in neutron spectra, average cycle lengths, and burnable poison content.

7) The average cycle lengths increase significantly (up to 2-3 times) with the increasing ^{235}U loading for the cases considered. However, in general, the average cycle length will also depend on the water volume fraction in the fuel elements and on the core geometric buckling.

Figures A91 and A92. Comparison of Fast and Epithermal Fluxes at EOC Between the HEU Reference Case and Cases with Different LEU Fuels for a Midplane Traverse Along the Y-Axis Through the Central Irradiation Channel and the Water-Reflected Faces.

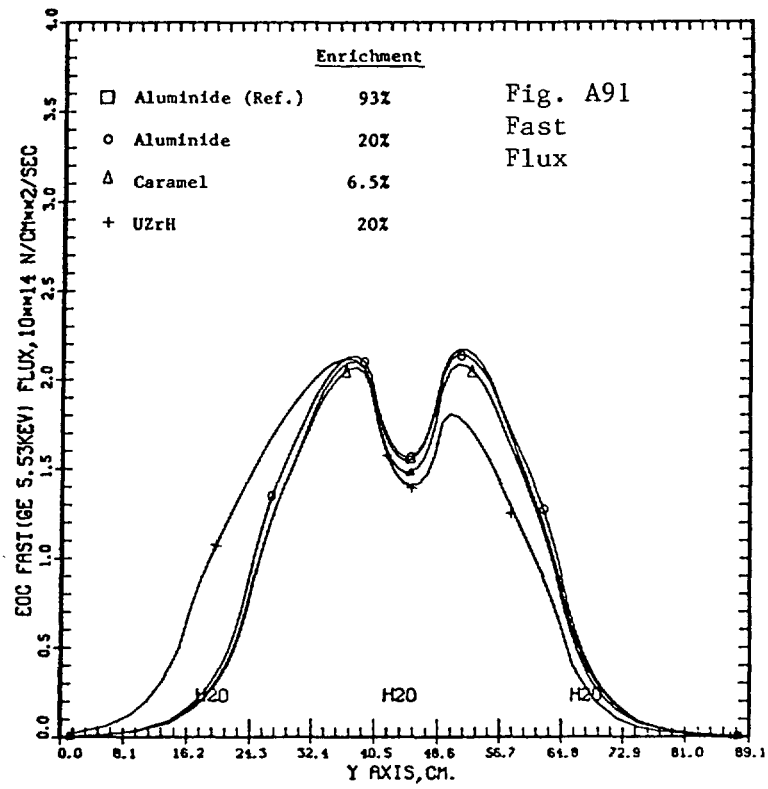

Fig. A91
Fast
Flux

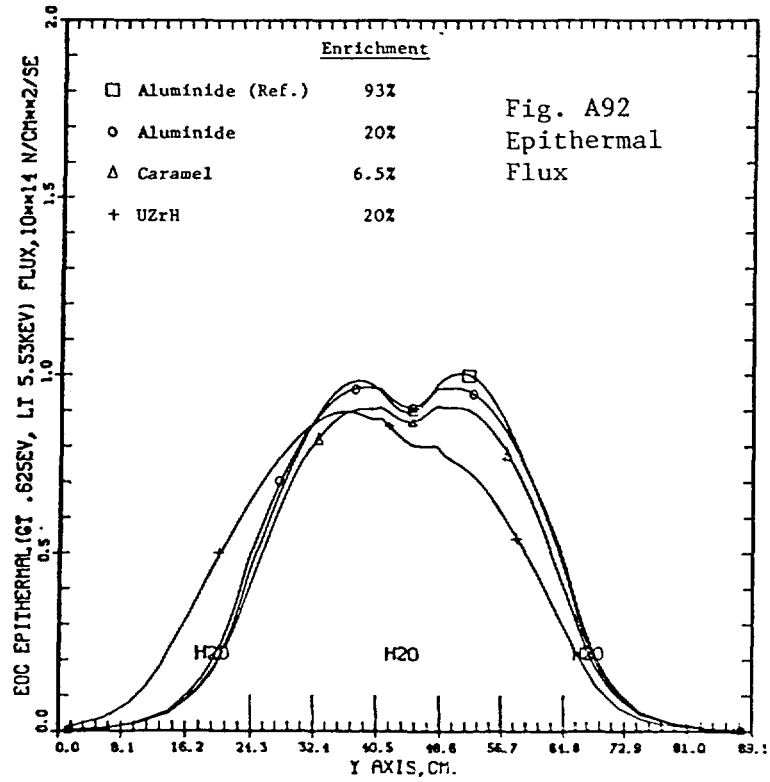

Fig. A92
Epithermal
Flux

Fig. A93. Comparison of Thermal Fluxes at EOC Between the HEU Reference Core and Cases with Different LEU Fuels for a Midplane Traverse Along the Y-Axis Through the Central Irradiation Channel and the Water-Reflected Faces.

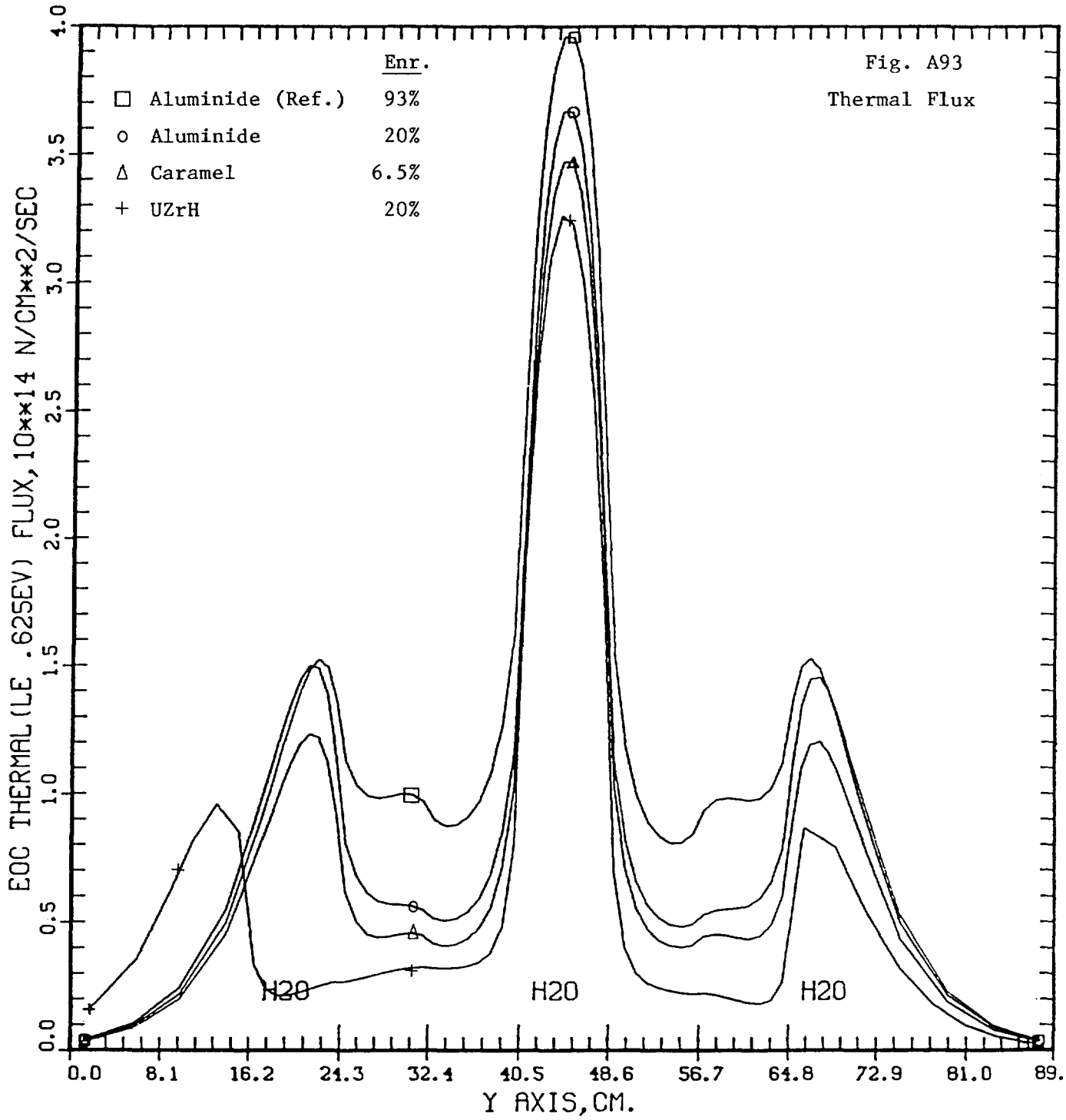

Figures A94 and A95. Comparison of Fast and Epithermal Fluxes at EOC Between the HEU Reference Case and Cases with Different LEU Fuels for a Midplane Traverse Along the X-Axis Through the Central Irradiation Channel and the Graphite-Reflected Faces.

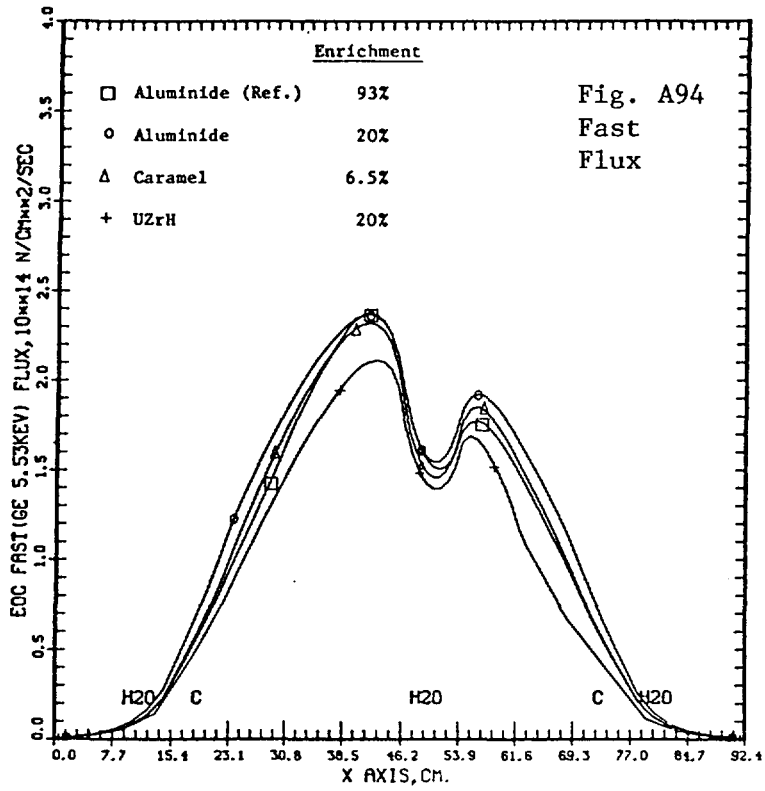

Fig. A94
Fast
Flux

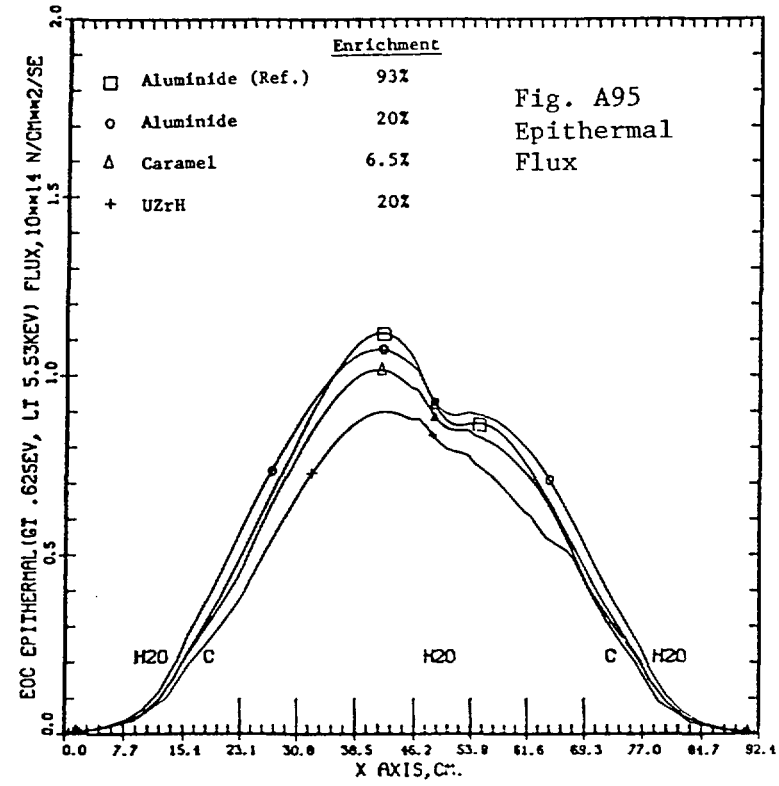

Fig. A95
Epithermal
Flux

Fig. A96. Comparison of Thermal Fluxes at EOC Between the HEU Reference Case and Cases with Different LEU Fuels for a Midplane Traverse Along the X-Axis Through the Central Irradiation Channel and the Graphite-Reflected Faces.

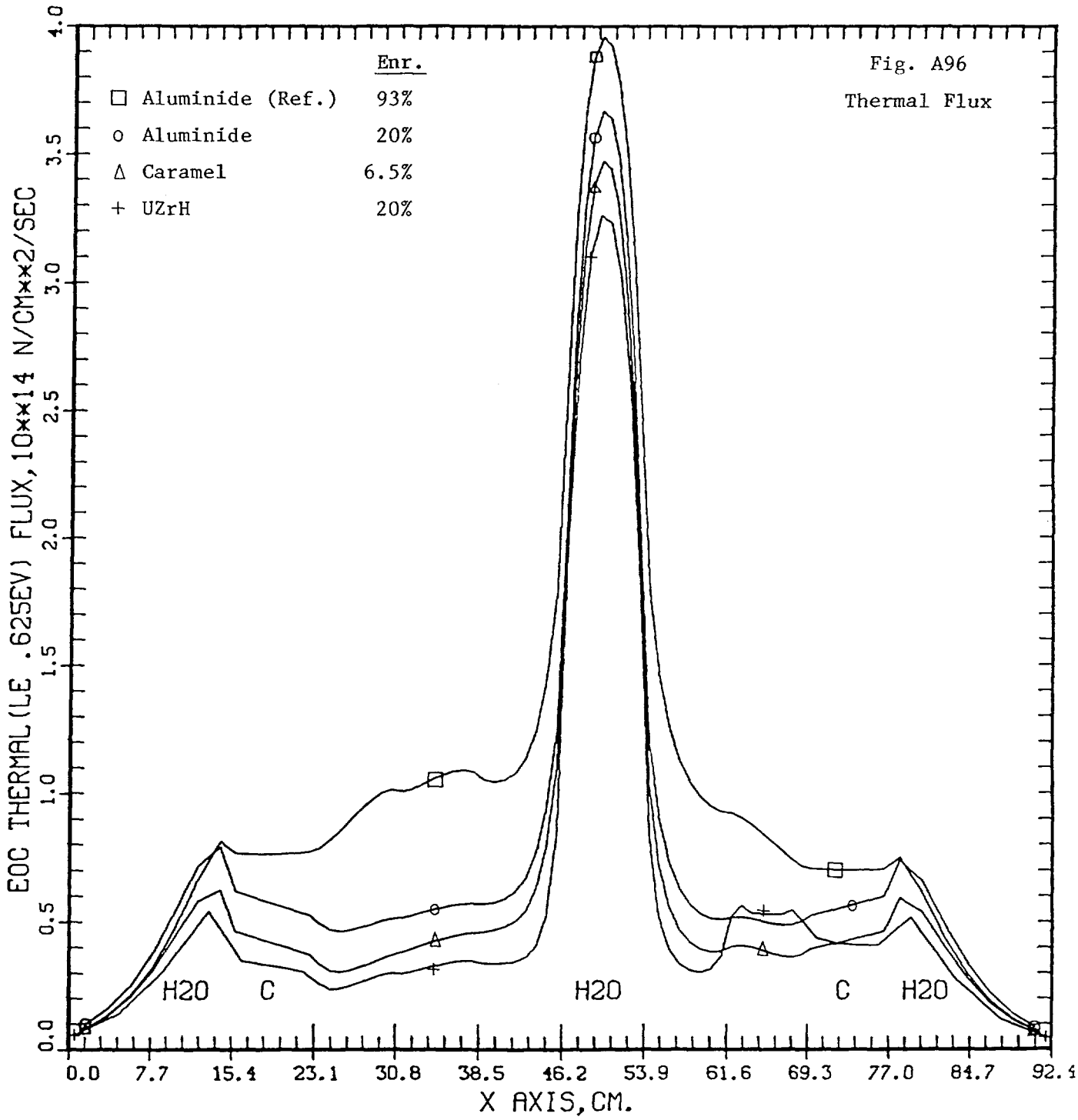

TABLE A38. Ratios of Fast, Epithermal, and Thermal Fluxes at EOC Between Each LEU Case and the HEU Reference Case at Selected Core and Reflector Positions

		Aluminide	Caramel	UZrH
Central Irradiation Channel (Peak)				
	Fast:	1.00	0.96	0.92
	Epithermal:	0.99	0.97	0.88
	Thermal:	0.93	0.88	0.82
Reflector Peak at ~ 68 cm in Figs. A91-A93		1.01	0.92	0.52
		1.02	0.90	0.52
		0.95	0.79	0.57
Reflector Peaks at ~ 21 cm for Aluminide LEU and Caramel and at ~ 13 cm for UZrH in Figs. A91-A93		1.12	0.95	0.67
		1.12	0.93	0.64
		0.98	0.81	0.63
Water Just Outside Graphite Reflector at ~ 77 cm in Figs. A94-A96		1.19	1.01	0.56
		1.20	0.99	0.62
		0.99	0.79	0.73
Water Just Outside Graphite Reflector at ~ 15 cm in Figs. A94-A96		1.23	1.03	0.64
		1.23	1.01	0.64
		0.97	0.76	0.67
Fresh Inserted Element at EOC (Ratio of Average Fluxes)		1.00	0.98	0.79
		0.97	0.92	0.72
		0.64	0.55	0.32
Fuel Element with About One Half the Residence Time of the Discharge Element (Ratio of Average Fluxes)		1.10	1.05	0.89
		1.04	0.96	0.82
		0.58	0.45	0.34
Discharge Fuel Element (Ratio of Average Fluxes)		1.27	1.11	0.73
		1.17	0.96	0.64
		0.59	0.38	0.24

The advantages and disadvantages of the various cores must be carefully considered, keeping in mind these general trends and the special requirements of individual research reactors. In particular, the better neutron flux performance of the fuel elements with lower ^{235}U loading may be more than compensated, in some cases, but the economical advantage due to the increased burnup (in MWd) of the elements with larger ^{235}U loadings (see Appendix I).

A.6.2 Plutonium Production Data

The total plutonium content in g/MWd as a function of uranium enrichment that can be expected in each fuel element discharged from a research and test reactor that is moderated and cooled by light water is shown in Fig. A97. Calculations using the 2 MW reference reactor (180 g ^{235}U/standard element with HEU) were done to obtain the uranium density in a fresh standard element that is needed to match the 10.0 day average cycle length of the HEU design with uranium of various enrichmnts in uranium-silicide fuels. The geometry of the standard element (19 plates, a fuel meat thickness of 0.51 mm, and a water volume fraction of 0.615) was unchanged in all the calculations. Bulk U_3Si and U_3Si-Al dispersion fuels were used since the maximum uranium densities expected with these fuels are about 12.0 g/cm^3 and 8.0 g/cm^3, respectively. The average discharge burnup in the calculation for each enrichment was about 16.7 MWd. The results of these calculations are shown by the solid curve in Fig. A97.

Table A39 summarizes the data on fuel element geometry, fresh fuel loading, burnup of fissile materials in the discharged fuel elements, and total Pu and ^{239}Pu content in the discharged fuel elements for all cases studied for the 10 MW reactor. Selected data from Table A39 are also shown in Fig. A97.

The data for the 2 MW and 10 MW reactors are in good agreement in cases for which the volume fraction of water in their standard elements is approximately the same. The hardness of the neutron spectrum in the fuel depends on the volume fraction of water in an element, on the ^{235}U loading, and on content of burnable poison. Since the bulk of neutron absorption in ^{238}U occurs in the epithermal energy range, a harder neutron spectrum will result in a larger plutonium content per MWd in the discharged element. This effect is shown in Fig. A97 and Table A39 for the cases with a uranium enrichment of 20%.

The ^{239}Pu/Total Pu ratio as a function of per cent ^{235}U burnup in the discharge fuel elements is shown in Fig. A98 (solid curves) to be nearly independent of uranium enrichment and ^{235}U loading. These curves were obtained from cell calculations with different ^{235}U loadings for the same enrichment and with different enrichments for the same ^{235}U loading. Cell calculations characteristically yield higher Pu contents than reactor calculations and the same trend also holds for the ^{239}Pu/Total Pu ratio. The dashed curve in Fig. A98 has been drawn through data points obtained from Table A39, and should provide a better estimate for this ratio.

Fig. A97. Total Plutonium Content (in g/MWd) in Discharge Fuel Element vs Uranium Enrichment.

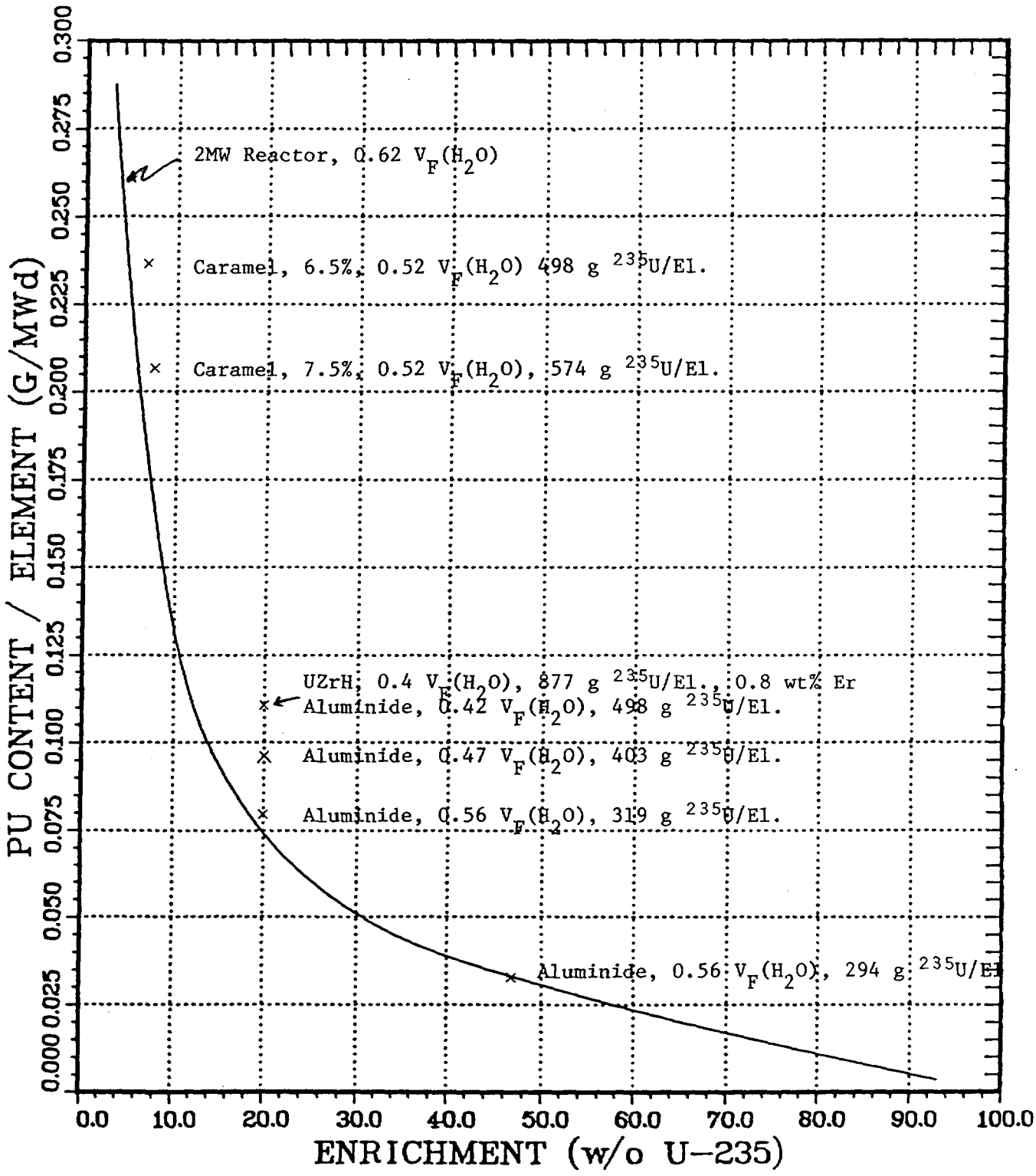

TABLE A39. Comparison of Burnup Data and Plutonium Contents of Discharged Fuel Elements for the 10 MW Reactor

Fuel Type and Enrichment	Plates or Rods per Std. Element	Fuel Meat Thickness mm	Water[d] Volume Fraction Std. El.	^{235}U in Fresh Std. Element, g	Average Cycle Length, Days	Grams Fissile Burned in Discharge Element		Average Discharge Burnup		Total $Pu/^{239}Pu$ Content Discharge Element, g	Total Pu Content of Discharge Element/MWd
						^{235}U	$^{239}Pu+^{241}Pu$	% ^{235}U	MWd[e]		
Aluminide, 93%	23	0.51	0.561	280.0	16.7	178.4	~0	63.7	142.7	0.6/0.4	0.004
Aluminide, 45%	23	0.51	0.561	293.8	16.7	175.3	5.8	59.7	144.0	5.0/3.5	0.035
Aluminide, 20%	23	0.51	0.561	318.5	16.7	170.1	11.4	53.4	143.4	11.4/8.6	0.080
Aluminide, 20%	21	0.839	0.515	346.3	16.7	168.9	11.1	48.8	142.3	12.6/9.5	0.089
Aluminide, 20%	19	0.51	0.615	290.2	16.7	168.5	10.6	58.1	141.6	10.5/7.5	0.074
Aluminide, 20%	19	0.70	0.577	306.5	16.7	168.5	11.2	55.0	142.0	11.1/8.0	0.078
Aluminide, 20%	19	0.80	0.556	318.6	16.7	169.0	11.1	53.0	142.4	11.5/8.4	0.081
Aluminide, 20%	19	0.90	0.536	330.9	16.7	169.2	11.0	51.1	142.5	11.9/8.8	0.084
Aluminide, 20%	19	1.00	0.516	347.0	16.7	169.5	11.0	48.8	142.7	12.3/9.2	0.086
Aluminide, 20%	19	1.238	0.468	403.0	16.7	170.5	10.7	42.3	143.3	13.8/10.7	0.096
Aluminide, 20%	18	1.471	0.444	445.5	16.7	171.4	10.5	38.5	143.9	14.8/11.6	0.103
Aluminide, 20%	17	1.731	0.421	498.2	16.7	172.3	10.2	34.6	144.4	16.4/13.2	0.114
UZrH,[a] 20%	16	12.95[c]	0.395	876.8	40.8	477.5	56.0	54.5	418.1	46.8/33.0	0.112
UZrH,[b] 20%	16	12.95[c]	0.395	876.8	43.2	502.2	62.6	57.3	442.2	47.9/33.1	0.108
Caramel, 7.5%	16	1.45	0.519	574.0	31.5	284.7	52.8	49.6	261.8	53.8/39.1	0.206
Caramel, 6.5%	16	1.45	0.519	497.5	22.5	206.2	33.4	41.5	186.5	44.1/34.0	0.237

[a]0.8 wt% Erbium
[b]0.67 wt% Erbium
[c]Fuel Outer Diameter
[d]Water Volume Fraction is standard element of 2MW reference core is 0.6151.
[e]Energy production based on fission of 1.25 g ^{235}U/MWd and 1.55 g ($^{239}Pu+^{241}Pu$)/MWd.

Fig. A98. ^{239}Pu/Total Pu Ratio in Discharge Element as a Function of Per Cent ^{235}U Burnup.

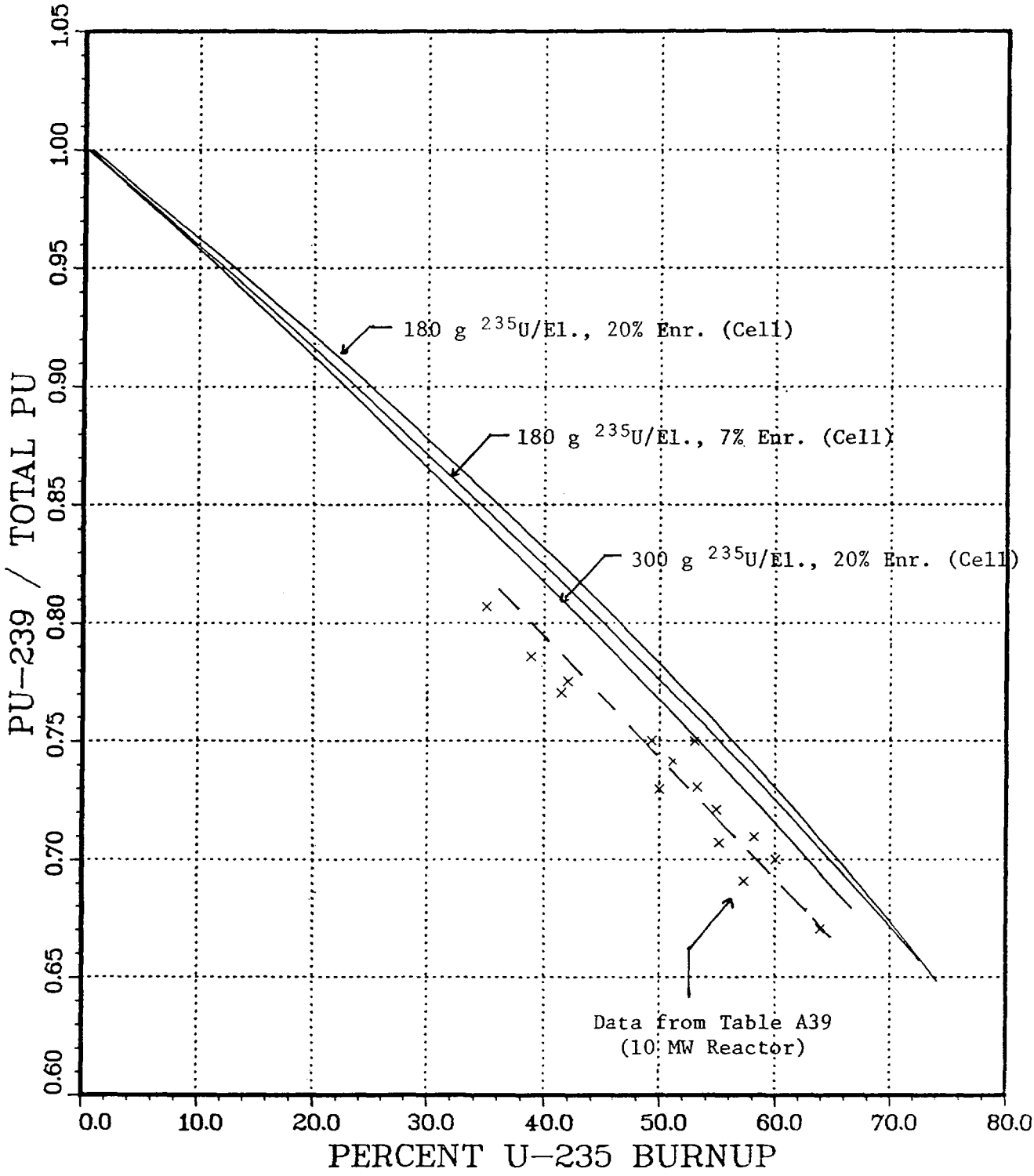

A.7 PRIMARY COOLANT PUMP STUDY

A.7.1 Introduction

One of the principal objectives of the RERTR Program is to make revisions to existing test reactors as simple as possible. Modification to fuel element hardware would be minimized and efforts focussed on maintaining the original power output levels. In general terms, there will be higher coolant mass flow rates and consequently an increased pressure drop across the cores.

To accommodate a higher pressure drop the coolant pump discharge pressure must be increased in those reactors having closed loop pressurized cooling systems. The reactors with gravity flow of coolant will require other measures to increase system pressure, or to reduce other parasitic pressure losses. The purpose of this investigation is to establish the design criteria and performce envelopes of existing coolant pumps to determine the feasibility of modifying these pumps, or the flow and pressure controls, or both, in order to accommodate new fuel designs.

A.7.2 Reactor Data

In order to determine flow rates, pressures and other design parameters of coolant pumps now in use on research and test reactors, a tabulation of data was made. This helped to establish some broad categories of the various reactor types and thereby define some of the problems evolving from the proposed conversion to reduced-enrichment fuels.

A.7.2.1 Size and Type

Table A40 is a compilation of pertinent primary coolant flow data for twelve experimental reactors that could be candidates for the reduced-enrichment fuels. The data was taken from information provided by reactor operators in response to the questionnaire sent out by ANL and the American Nuclear Society and from the IAEA Directory of Nuclear Reactors

A.7.2.2 Categories of Primary Coolant Systems

The reactors being considered here are in three power classifications: low (1 MW through 4 MW), medium (5 MW through 10 MW), and high (11 MW and up). The low power range and some of the medium range are pool-type reactors with gravity flow of coolant through the core. The tank-type reactors in the medium power range have pressurized upward flows. The high power reactors are all pressurized tank-type with downward flows.

Three general categories of primary coolant systems are suggested by Table A40.

1. Gravity Flow
2. Upward Forced Flow
3. Presurized Closed Loop

Gravity flow of coolant through the core is dependent on the static head of the water above the core and the flow control valves downstream from the core. Upward forced flow is a function of the coolant pump head, the flow control valves and the static head of the elevation of the core in relation to the pumps. The pressurized closed loop has coolant circulated under pressure in the entire system including the reactor.

Table A40.

REACTOR PRIMARY COOLING SYSTEM DATA

REACTOR	FLOW RATE TOTAL (ℓ/Min)	VELOCITY (m/sec)	CORE COOLANT PRESS. (Bar) GAGE INLET	CORE COOLANT PRESS. (Bar) GAGE OUTLET	CORE COOLANT TEMP. °C INLET	CORE COOLANT TEMP. °C ΔT	FLOW DIRECTION	REACTOR TYPE
			LOW POWER RANGE REACTORS					
FNR 2MW	3,785	0.6	Pool Static Head	—	28.8	3.4	Down H_2O	Pool
HOR 2MW	3,667	0.5	Pool Static Head	1.6	30.0	8.0	Down H_2O	Pool
FRM 4MW	6,600	0.8	Pool Static Head	—	25.0	10.0	Down H_2O	Pool
RINSC 2MW	5,678	0.76	Pool Static Head	0.9	43.3	5.1	Down H_2O	Pool
			MEDIUM POWER RANGE REACTORS					
ASTRA 8MW	11,340	2.7	Pool Static Head	0.55	38	8	Down H_2O	Pool
JRR-2 10MW	22,716	3.9	6.16*	1.14	45	5.3	Up D_2O	Tank
MITR-II 5MW	7,960	2.6	1.62	0.3	40	8.8	Up H_2O	Tank
FRG-1 5MW	12,667	1.5	Pool Static Head	1.59	45	5.7	Down H_2O	Pool
			HIGH POWER RANGE REACTORS					
HFR-PETTEN 50MW	71,122	7.1	2.5	2.0	40 winter 50 summer	10	Down H_2O	Tank
JMTR 50MW	99,240	10.0	14.1	10.7	42	7.2	Down H_2O	Tank
ORR 30MW	66,490	9.14	2.67	0.91	48.8	6.2	Down H_2O	Tank
FRJ-2 15MW	26,249	4.1	6.48*	1.2	58	11.3	Up D_2O	Tank

*Estimated

A.7.2.3 Pumping Rates and Pressures

Primary coolant pumping rates in the reactor as they are now operated vary from 400 to 600 gpm per megawatt of power, the variations being due to the core and fuel element design. With one exception the system pressure increase is a relatively simple matter. Piping controls and similar accessories will probably be adequate since the new system pressure will still fall within the lowest rating in which the present equipment was initially selected. More detailed information on the primary coolant system components will be required regardless of the approach taken to increase system pressure.

A.7.3 Primary Coolant Pump Technology

The key element in the primary cooling system is the pump. The types used, their vital design parameters and how they are applied are an important part of this investigation.

A.7.3.1 Specifications

High-volume flow and low output head characterize the primary coolant pump on this type of reactor. There are a few exceptions. The general characteristics are similar to a quality commercial certrifugal pump with the additional requirement of the seismic rating. This feature is present in the heavier casing and increased rating of the connecting flanges. Special seals are also employed, usually graphite or metal materials. Generally two seals are used with leakage being collected between the seals and returned to the low pressure side of the system. When zero leakage is a requirement a canned, gas-seal, or submerged pump may be used. Generally these are very expensive and are not widely applied.

A.7.3.2 Pump Manufacturers

Eight suppliers of pumps for nuclear applications were contacted in reference to the modification of existing pumps in the primary coolant system. Some of the suppliers no longer make pumps for these applications. Generally, the suppliers concur that it is practical to increase the impeller size. This would provide the additional head required to meet the higher pressure required with the modified fuel element designs. It would be unusual if pumps were purchased without some margin for increasing the head.

A.7.3.3 Constraints to Modifying Existing Coolant Pumps

The prime areas to investigate when considering the modification of these pumps are:

1. Technical
2. Institutional
3. Economic

Technical - The information from pump suppliers is that the existing pumps probably can be fitted with large-diameter impellers. They do caution that pump serial numbers must be provided so that positive identification can be made and the records can be checked to determine what size the original impellers were and if the casings will take larger impellers.

Any pump that is modified would have to be examined for wear and deterioration and appropriate parts replaced. Depending on age and amount of use some of the pumps may have lost 20% of their initial head through deterioration of the impeller and wear rings.

Institutional - Some of the coolant pumps that have been in place for a long time may have to be completely reanalyzed for conformance to new or revised licensing requirements. This would be necessitated by the rebuilding of the pump.

Economic - The decision to change to larger impellers has to be weighed against the possibility of a new pump and the related advantages. New parts can be accurately priced but the labor costs can be uncertain and variable unless firm quotations can be obtained.

The advantage may be a shorter delivery time if only components such as impellers and wear rings are involved. New pumps may have delivery times of six months. However, the new pump would offer better reliability against the uncertainty of a retrofit on an older pump, and the advantages of the improvements in the state of the art.

The approximate cost of a horizontally split case pump in the 1360 m^3/hr (6,000 gpm) range is $7,500 plus $3,400 for a 200 kw motor. This size pump with a nuclear "N" stamp rating would cost 9 to 10 times more. The new impeller and wear rings, required to increase the performance of such an existing pump, would cost $3,000 to $4,000.

A.7.4 Options and Alternatives to Pump Revisions

Since no single universal solution exists for increasing pressure in the coolant systems for all reactors, other alternatives must be considered. Increasing coolant pump pressure on gravity flow systems will not provide the required pressure increase through the core; therefore, some other approach is needed in these instances. Upward flow systems and the closed loop pressurized systems can benefit from increased pump pressures, but the entire system should be reviewed for adequacy of other components.

Listed below are the options available for each of the three categories of core coolant systems.

Gravity Flow (Pool only)

1. Decrease decay tank pressure
2. Enclose and pressurize core
3. Alternate coolant
4. Increase pool static head
5. Flow control adjustment (outlet side)
6. Add suction pump on outlet side

Upward Forced Flow (Pool or Tank)

1. Flow control adjustment
2. Increase pump impeller size or speed
3. Addition of booster pumps
4. Reduce system pressure losses
5. Alternate coolant
6. Reduced static head

Pressurized Closed Loop (Tank Type)

1. Flow control adjustment
2. Increase coolant pump pressure
3. Addition of booster pumps
4. Reduce pressure losses in coolant system
5. Alternate coolant

A.7.5 Increasing Primary Coolant System Pressure

The following section discusses the options that appear to be the most practical to increase the primary coolant system pressure. The reactors actually fall into two broad types; gravity flow coolant systems or pressurized coolant systems. This is the most convenient way to discuss the available options because of the overlapping of the type of coolant systems when considering the reactors in terms of power ranges.

A.7.5.1 Gravity Flow Coolant Systems

A.7.5.1.1 Flow Control Adjustment-Pool Type Reactors

The gravity flow, primary coolant system is used in the majority of the low-power, and in some of the medium-power range reactors. This coolant system is characterized as an open tank reactor with about 8 to 10 meters of water above the core. The water flows by gravity downward through the core, core plenum, flow control valve (FCV) and associated piping into a decay tank, if used. Recirculating pumps take suction from the Decay Tank and discharge back to the reactor pool through a heat exchanger.

A schematic of a representative 8 MW primary cooling system is shown in Fig. A100. The pressure drop through the core is shown in Fig. A101, plotted in relation to the square of the coolant flow.

The estimated pressure drop characteristics between the Reactor Tank and Decay Tank are shown in Fig. A102. This figure is based on data from Figs. A100 and A101 with the following assumptions:

1. The data points at 220 $(m^3/min)^2$ represents maximum flow (Fig. A101).

2. Pressure drop through the butterfly FVC is 1.54 meters H_2O at maximum flow. This pressure drop corresponds to a typical 25.4 cm, (10 inch) butterfly FVC and modified disc to approximate equal percentage flow characteristics.

This curve indicates 50% of the available pressure drop is absorbed by the FCV for control at design flow (681 m^3/hr), and the valve requires 13.5% of available pressure drop at maximum flow i.e., wide open.

A 10% or 30% increase in core pressure drop would not affect the control capabilities of the FCV at design flow and the maximum flow would be reduced by only 12 m^3/hr and 31 m^3/hr, respectively.

A.7.5.1.1 Booster Pump - Pool Type Reactor

Pressure drops through the reactor core, above that available from gravity flow alone, can be obtained by the use of a booster pump. The pump would be installed between the core and the Decay Tank or existing recirculation pump. This high specific speed pump (Fig. A116) would partially compensate for the pressure drop in the core discharge piping. Thus additional pressure drop would be made available for use in the core.

The additional pressure drop made available could amount to approximately 4 meters of water in the core of a typical reactor. This would allow retaining the present maximum coolant flow, which will otherwise be reduced due to any increase in core pressure drop (Fig. A102) and insure the operation of the flow control valve in its best control range. The possibility exists that a variable speed booster could also act as the coolant flow control element.

Figure A100.

Representative 8 MW
Primary Coolant System

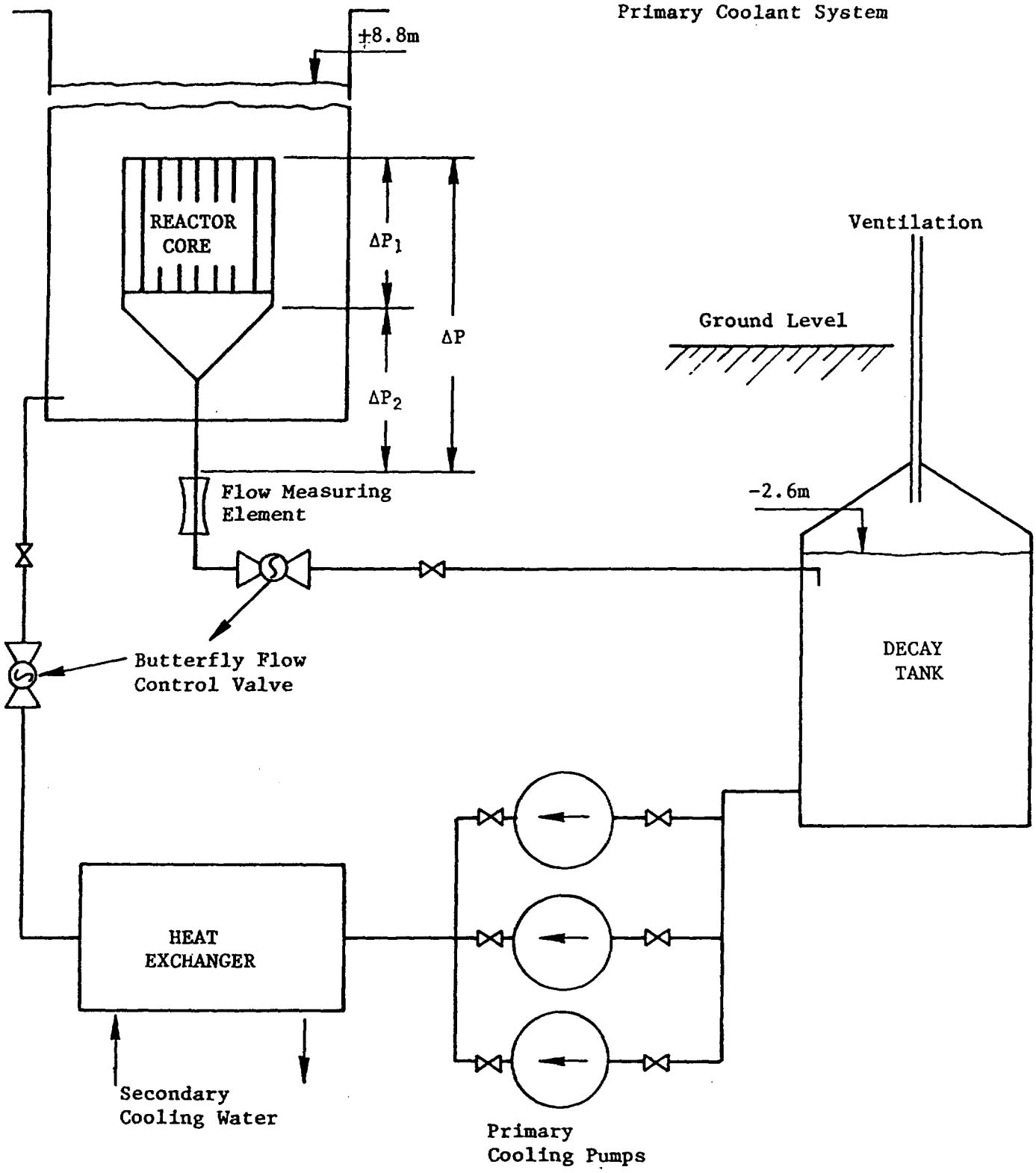

Figure A101.

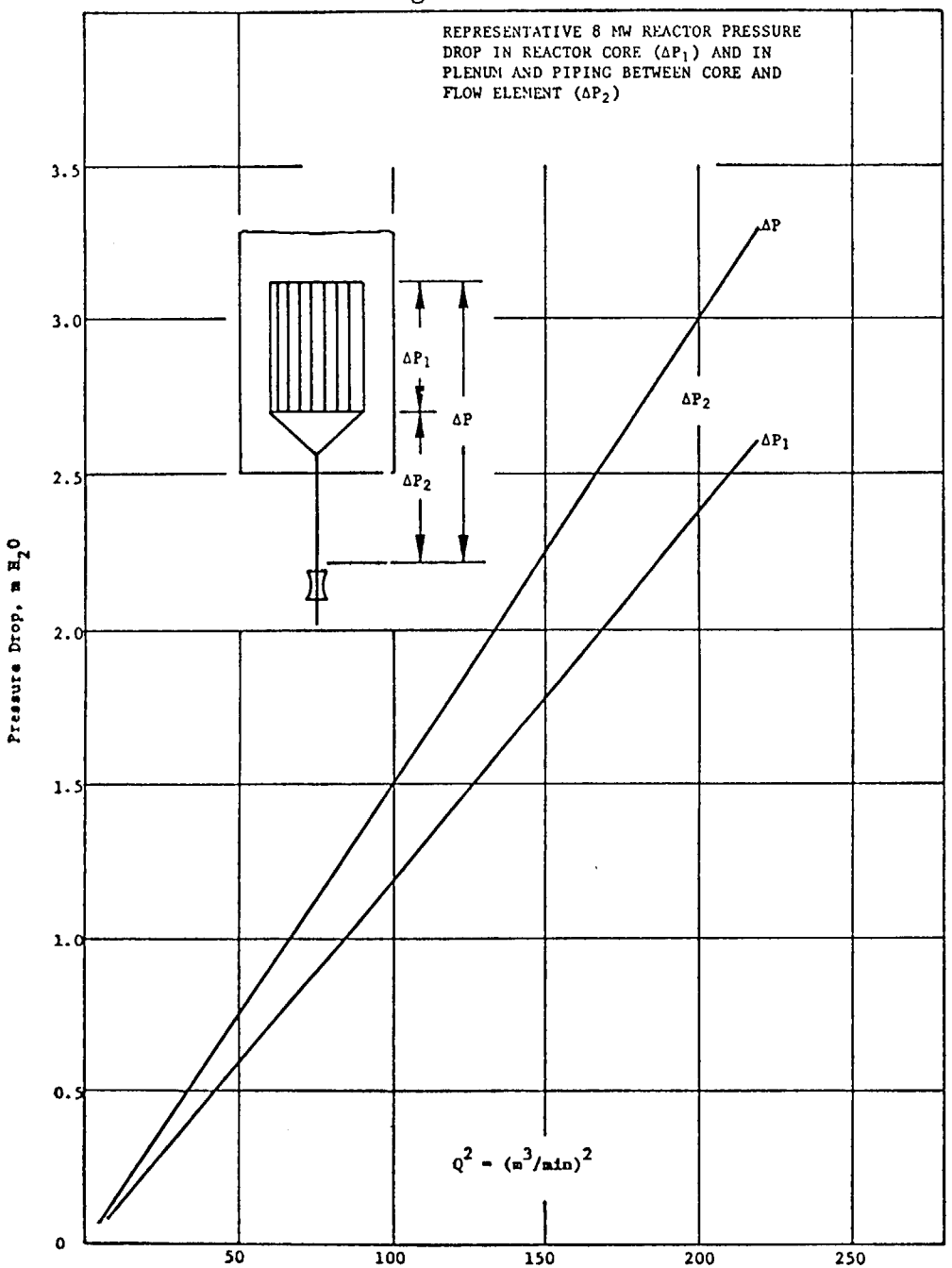

Figure A102.

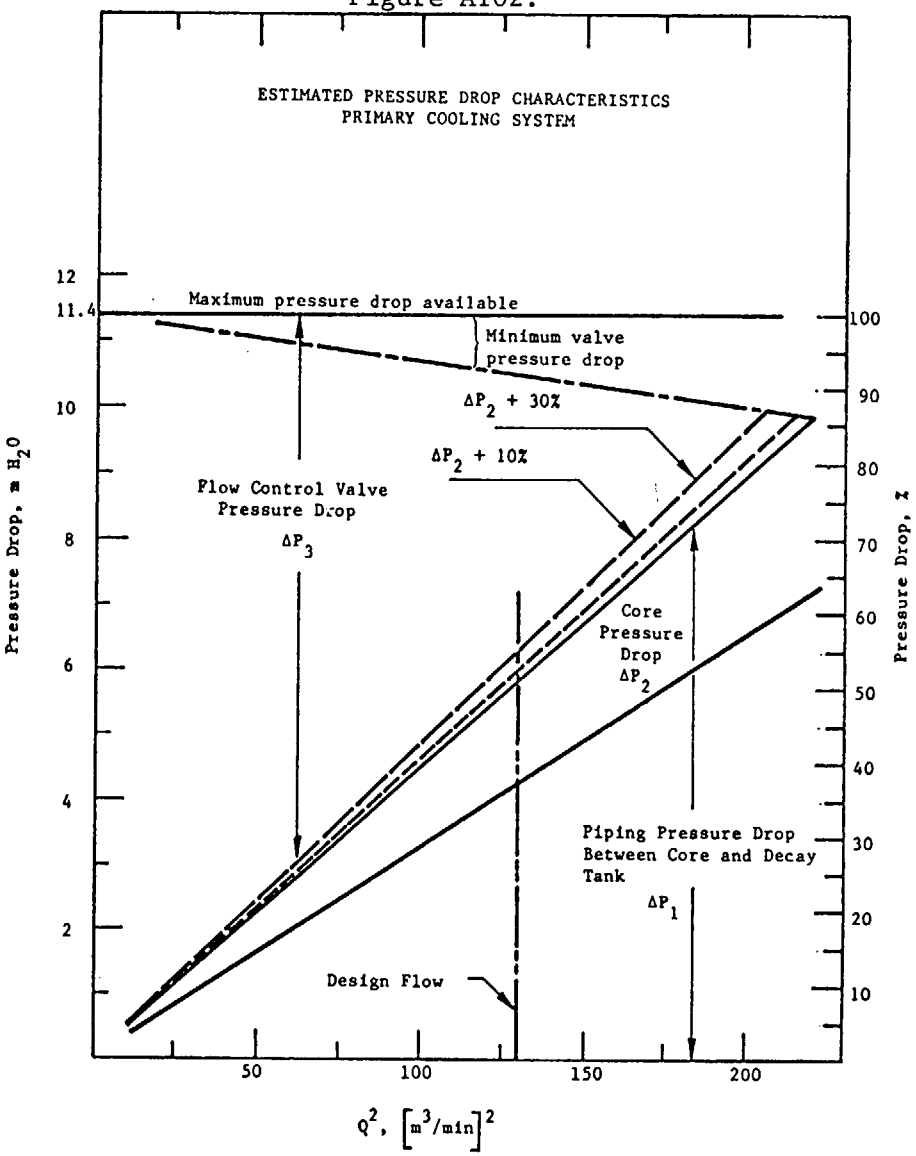

The addition of a booster pump in a gravity flow coolant system requires investigation of the potential for cavitation.

Cavitation occurs when the pressure at any point in the flowing water drops below the vapor pressure of the water, which varies with temperature. The relationship which produces cavitation is between vapor pressure, barometric pressure and net positive suction head (NPSH) on the inlet side of the pump or other object through which the water is flowing.

Unless there is sufficient positive head at the inlet of an object, to exceed the entrance losses, cavitation will occur. This is the condition whereby some of the fluid is vaporized and bubbles are formed and carried downstream. These bubbles collapse violently at some point downstream of the inlet and produce very sharp crackling noises, frequently accompanied by physical damage of adjacent metal surfaces. In the case of a centrifugal pump this usually occurs inside the impeller.

When cavitation occurs at the entrance of a pump, there is also loss of efficiency and overspeeding of the impeller in addition to the long-term effects of impeller damage.

Axial flow or propeller pumps are also subject to cavitation with much the same net results. Blade erosion is the most serious physical damage and at times can become severe enough to cause blades to be replaced. Cavitation occurs on the face or on the back of the blade. Face cavitation does not materially affect performance, but this cavitation can be controlled by alterations to the blade cross section This is not true of the back surface, however. Therefore, the tip speed becomes the controlling parameter in this specialized pump design if the available NPSH is fixed, as is usually the case for the reactors considered here.

Fig. A103 illustates critical propeller tip speeds as a function of pumping head. The figure can be used to assist in selecting an axial flow pump for use as a booster in an existing coolant system.

A.7.5.1.3 Reduce Entrance Losses

Reduction of presure losses in gravity flow can be accomplished by improving the entrance flow conditions at the core. The head loss can be determined from the expression:

$$h = \frac{KU^2}{2g}$$

The only variable for a given situation would be the coefficient K which is affected by the geometry of the entrance configuration.

Typically, gravity flow core coolant systems draw the coolant from the reactor pool through the core into an outlet pipe. This can be compared to a classic inward projecting outlet pipe as shown in Fig. A104. A detailed investigation would require an adjustment of the K-factor to account for the difference in cross sections of the core assemblies; cylindrical versus rectangular, etc. However, approximations can be made even from the gross assumptions made here.

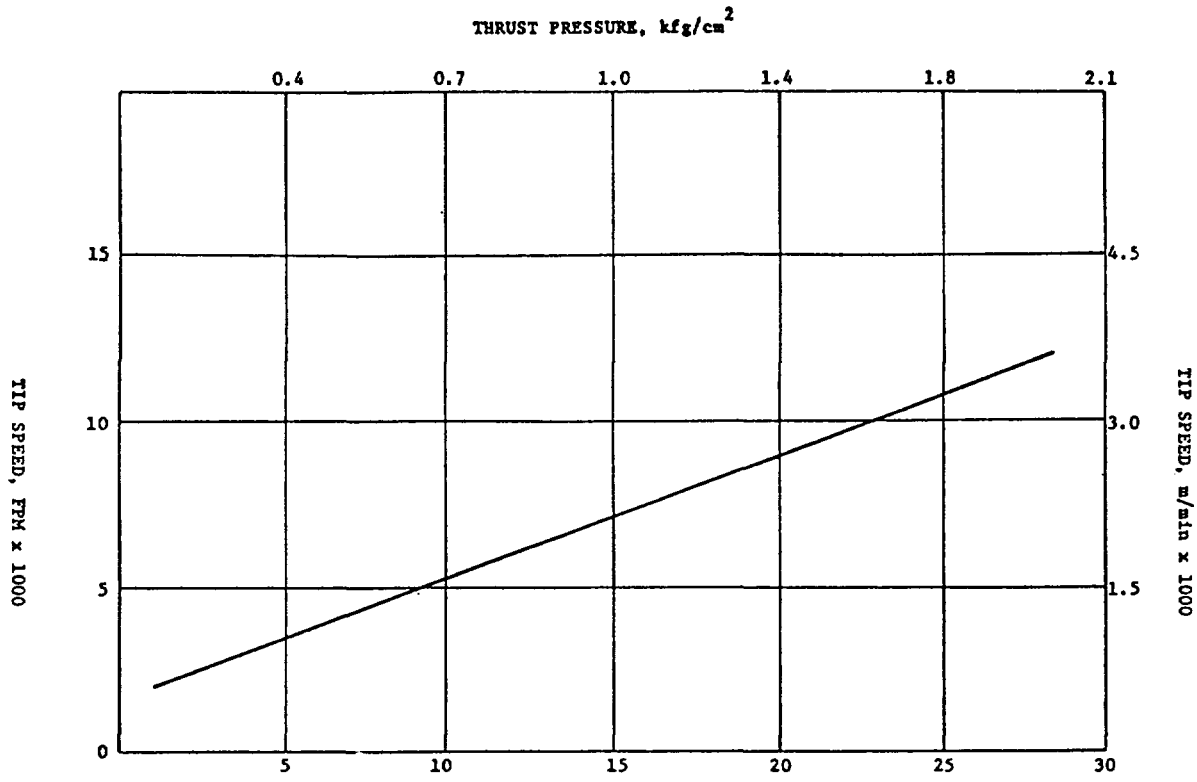

Figure A103. THRUST PRESSURE, PSIG
CRITICAL CAVITATION PARAMETERS FOR AXIAL FLOW PUMPS

*Baumiester and Marks, Standard Handbook for Mechanical Engineers, Seventh Edition; McGraw-Hill

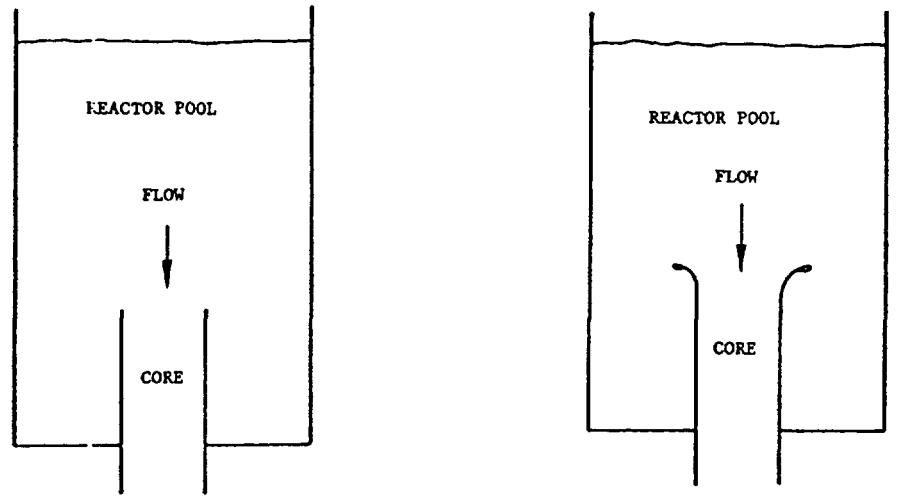

SHARP EDGED OUTLET, K = 0.78

IMPROVED (SHROUDED) OUTLET, K = 0.05

Figure A104.

Without an entrance shroud, the coefficient is 0.78*, adding a well rounded shroud, the coefficient is reduced to 0.05*. This assumes that the flow is stagnated below the top of the core and therefore coefficients are applicable.

A typical example has 0.6 m/sec coolant velocity through the core. There would be a 93% reduction in head loss by improving the entrance conditions with a cowling.

$$h = \frac{K(0.6\ m/sec)^2}{2(9.8\ m/sec)^2} = K(.018m)$$

This shows that for most gravity flow systems the shroud would give only minor improvements. However as the velociy of the coolant increases, improving the entrance conditions of the fluid entering the core can be worthwhile.

A.7.5.1.4 Increased Static Head on the Reactor Pool

This option could be implemented in several different ways depending on the design of the reactor pool. The objective is to simply increase the height of the water level in the reactor pool, thereby increasing the static head acting on the core. This is most easily done by building up the sides of the pool containment as shown in Fig. A105. The example is a typical gravity flow reactor pool with a fuel manipulator above the pool.

Aluminum plate can be formed to match the periphery of the pool and would be properly supported. In this instance additional structural steel is used to span the pool to support the movable bridge. A water-tight interface would be used between the new aluminum extension and the existing concrete side to prevent leakage. If properly designed and constructed, this could be an inexpensive method of increasing the useful static head in a gravity flow core coolant system.

If the reactor pool is very small, an alternate approach to increase the head on the pool is to enclose and pressurize the top of the pool. A preformed aluminum or steel enclosure, such as spun tankheads, could be used with pools up to ~2.5 m diameter. This type of structure minimizes field construction and optimizes the required thickness of material. If control rods are located at the top of the pool, provisions would have to be made for their penetration through the dome of the enclosure. Anticipated pressure increases are nominal, on the order of 5 to 7 psig, so heavy enclosures are not needed. Reactor refueling down time and access to experiments both would be adversely affected.

* Baumiester and Marks, Standard Handbook for Mechanical Engineers, Seventh Edition, McGraw Hill.

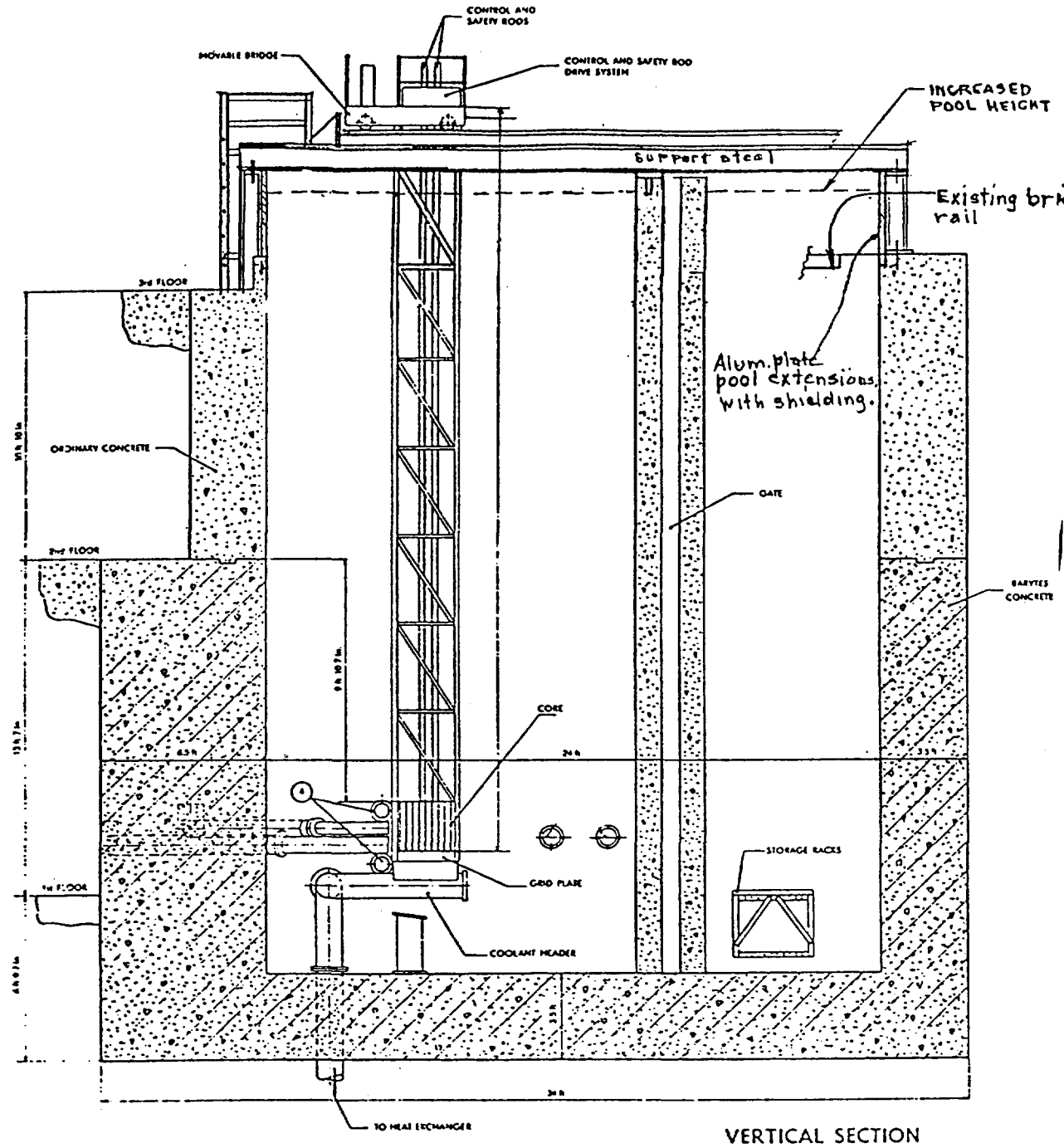

EXTENDED REACTOR POOL HEAD
FIGURE A105.

A.7.5.1.5 Reduced Pressure in Decay Tanks

This would increase the pressure differential through the core for gravity flows. The limit of the pressure would be the sum of the static head due to the pool elevation above the core and atmospheric pressure. Structurally, the decay tanks would have to be reinforced to prevent collapse when the negative pressure is pulled. The complexity and cost of this modification depends on the size, shape and accessability of the tank. Probably, standard structural steel shapes and plate can be used for reinforcing and largely shop-fabricated to minimize field work. Mechanically, the primary coolant loop would have to be investigated for the adaptability of the existing flow controls and the pumps for their ability to generate the required suction head.

A.7.5.2 Pressurized Coolant Systems

A.7.5.2.1 Increase the Performance of the Existing Pumps

The effect of changes in operating conditions for certrifugal pumps may be summarized by the affinity laws. The affinity laws express the mathematical relationship between the several variables involved in pump performance. They apply to all types of certrifugal and axial flow pumps. They are as follows:

1. With speed, N held constant

   A. $\frac{Q_1}{Q_2} = \frac{D_1}{D_2}$

   B. $\frac{H_1}{H_2} = \left(\frac{D_1}{D_2}\right)^2$

   C. $\frac{P_1}{P_2} = \left(\frac{D_1}{D_2}\right)^3$

2. With impeller diameter, D held constant

   A. $\frac{Q_1}{Q_2} = \frac{N_1}{N_2}$

   B. $\frac{H_1}{H_2} = \left(\frac{N_1}{N_2}\right)^2$

   C. $\frac{P_1}{P_2} = \left(\frac{N_1}{N_2}\right)^3$

where Q = Capacity (m^3/min)

H = Total Head (in water)

P = Power (kw)

N = Pump Speed (rpm)

When the performance (Q_1, H_1 and P_1) is known at some particular diameter (D_1) or speed (N_1), the formulas can be used to estimate the performance (Q_2, H_2 and P_2) at some other diameter (D_2) or speed (N_2). The efficiency remains nearly constant for speed changes and for small changes in impeller diameter (approximately 10%).

A.7.5.2.2 Increase Impeller Diameter

The performance characteristics of a particular pump at 1770 rpm with various impeller diameters are shown in Fig. A106. The present head capacity requirements of the cooling system may be 409 m^3/hr (1800 gpm) at 40 m (130 ft) total head. These conditions would dictate the use of a 30.5 cm (12 in) diameter impeller (point 1 on curve) having an efficiency of 74%, and require a 75 kw motor. To prevent cavitation in the pump, a net positive suction head of 3.4 m (11 ft) is required (point 2).

A change in the core design may change the cooling system head-capacity curve such as to require a 10% increase in head capability from the pump at the same flow rate, i.e., 44 m @ 409 m^3/hr (143 ft @ 1800 gpm). This new condition can be met by the installation of a larger diameter impeller. The pump used as the example (Fig. A106) can handle an impeller of up to 33 cm diameter (13 in) within the same casing.

The size of the required impeller can be obtained by the use of the affinity laws as they apply with the speed held constant. To find the correct impeller diameter it is necessary to calculate portions of the new head capacity curves which would result for different, larger, impeller diameters and select the diameter whose curve satisfies the new system head capacity requirements. This has been done using the existing 30.48 cm impeller curve data and calculating points on the curves for various diameters (Table A41). The resultant curves are superimposed on the pump characteristic curves (Fig. A107).

The performance curve for the 31.75 cm (12.5 in) diameter impeller matches the new system requirements (point 3).

The complete impeller curve can be constructed using the same technique. In this way the head produced at shut-off can be determined and the head-capacity point where the existing 75 kw motor is no longer adequate can be determined.

A.7.5.2.3 Increase Pump Rotational Speed

For a given impeller diameter, the greater the rotational speed, the greater the head and capacity of the pump. The pump curves of Fig. A108 are used to illustrate the use of affinity laws as they apply to increasing the rpm of the pump. The curves show the performance of a particular pump at 1750 rpm and 1150 rpm with various impeller diameters. This performance data has been determined by actual tests by the manufacturer. Assume the pump has a 14 1/2 inch (37 cm) maximum diameter impeller and the speed is to be increased by the use of a belt drive to 1850 rpm.

The affinity laws, as they apply with the impeller diameter held constant, will be used to determine the new performance with N_1 = 1750 rpm and N_2 = 1850 rpm. The head and capacity are read at several points along the 14 1/2 inch diameter curve and converted from the existing 1750 rpm to 1850 rpm. For example, one point may be at the 83% efficiency point where capacity is 2750 gpm (625 m^3/hr) at 183 ft. (56 m) head and requires a 200 horsepower motor. A 150 HP motor would be overloaded.

$$\frac{3750}{Q_2} = \frac{1750}{1850} \qquad Q_2 = 2907 \text{ gpm}$$

$$\frac{183}{H_2} = \frac{1750}{1850} \qquad H_2 = 204 \text{ ft.}$$

This will then be the 83% efficiency point on the new 1850 rpm curve.

E-34 METERS^3/HR.

CURVE: 761432-2

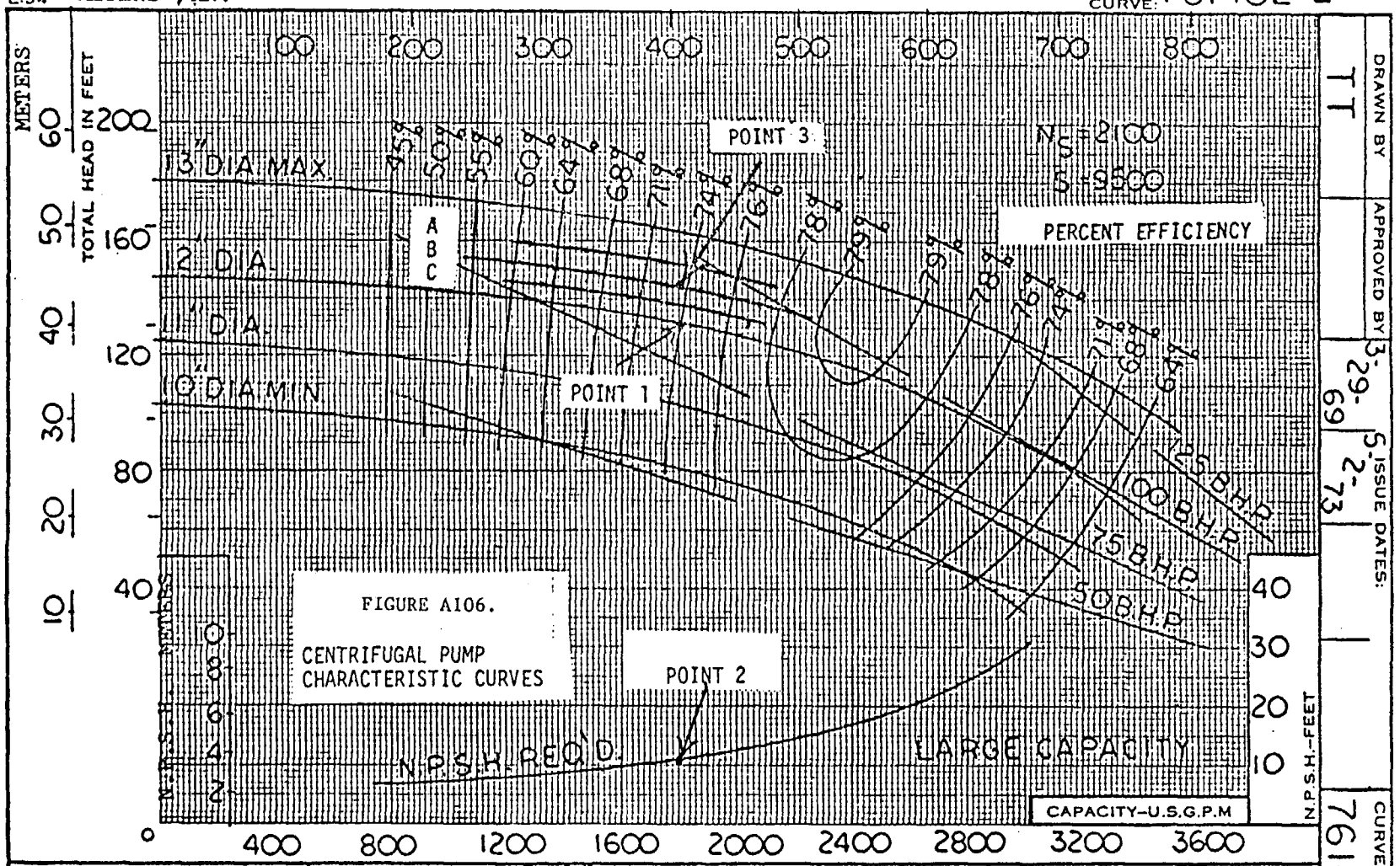

FIGURE A106.

CENTRIFUGAL PUMP CHARACTERISTIC CURVES

WEAR-RING DIAMETER: 9.125 MAX.	IMPELLER:	PUMP SIZE & TYPE	DRAWN BY: TT
STANDARD RING CLEARANCE: .020-.022 ON DIA.	805-C-1834	6x8x13 HH	APPROVED BY:
MAX. SPHERE THAT WILL PASS THRU IMPELLER: 1-3/4" DIA.	EYE AREA:		ISSUE DATES: 3-29-69, 5-2-73
SERVICE CONDITION	50.0	1770 RPM	CURVE NO.: 761432-2
CAPACITY ____ G.P.M. HEAD ____ FT.			

TABLE A41.

CALCULATED HEAD-CAPACITY POINTS
FOR INCREASED IMPELLER DIAMETERS
6X8X13 1770 RPM

$H_2 = H_1 (D_2/D_1)^2$ $Q_2 = Q_1 (D_2/D_1)$

Pump Operating Points 12 inch Diameter Impeller (D_1)		Calculated Operating Points Points A D_2 = 12 1/4 Inch		Points B D_2 = 12 1/2 Inch		Points C D_2 = 12 3/4 Inch	
Q	H	Q	H	Q	H	Q	H
(gpm)	(ft)	(gpm)	(ft)	(gpm)	(ft)	(gpm)	(ft)
1200	141	1230	146	1250	153	1280	159
1600	135	1630	140	1670	146	1700	153
2000	127	2040	132	2080	138	2130	145
D_1 = 30.48cm		D_2 = 31.11cm		D_2 = 31.75cm		D_2 = 32.39cm	
m^3/hr	m	m^3/hr	m	m^3/hr	m	m^3/hr	m
273	43	279	45	284	47	291	49
363	41	370	43	379	45	386	47
454	39	463	40	472	42	484	44

60 Hz Performance Curves

Customer _____ Inquiry No. _____ Date _____
Service _____ Item No. _____ P.O. No. _____ Date _____
F.O. No. _____ ; _____ GPM; _____ TDH; _____ RPM; _____ % Eff.; CDS No. _____

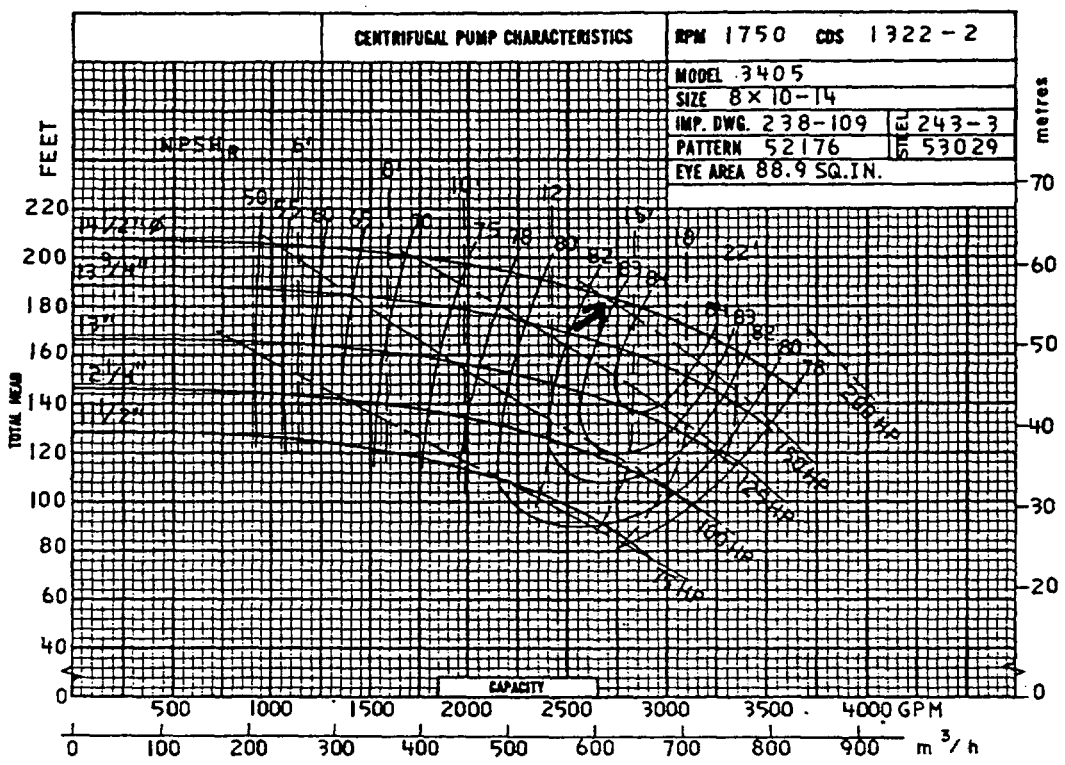

1750 R.P.M.

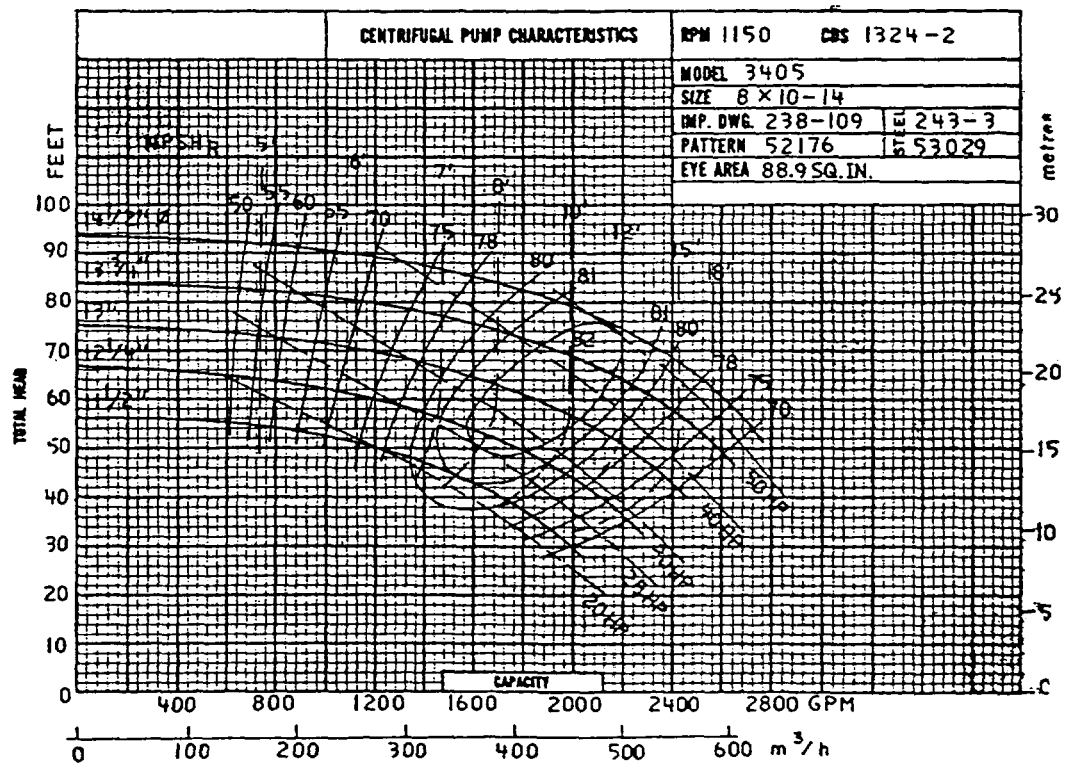

1150 R.P.M.

FIGURE A107. CENTRIFUGAL PUMP CHARACTERISTICS AT 1750 and 1150 RPM

Figure A108.

Approximate Characteristic Curves
Centifugal Pump

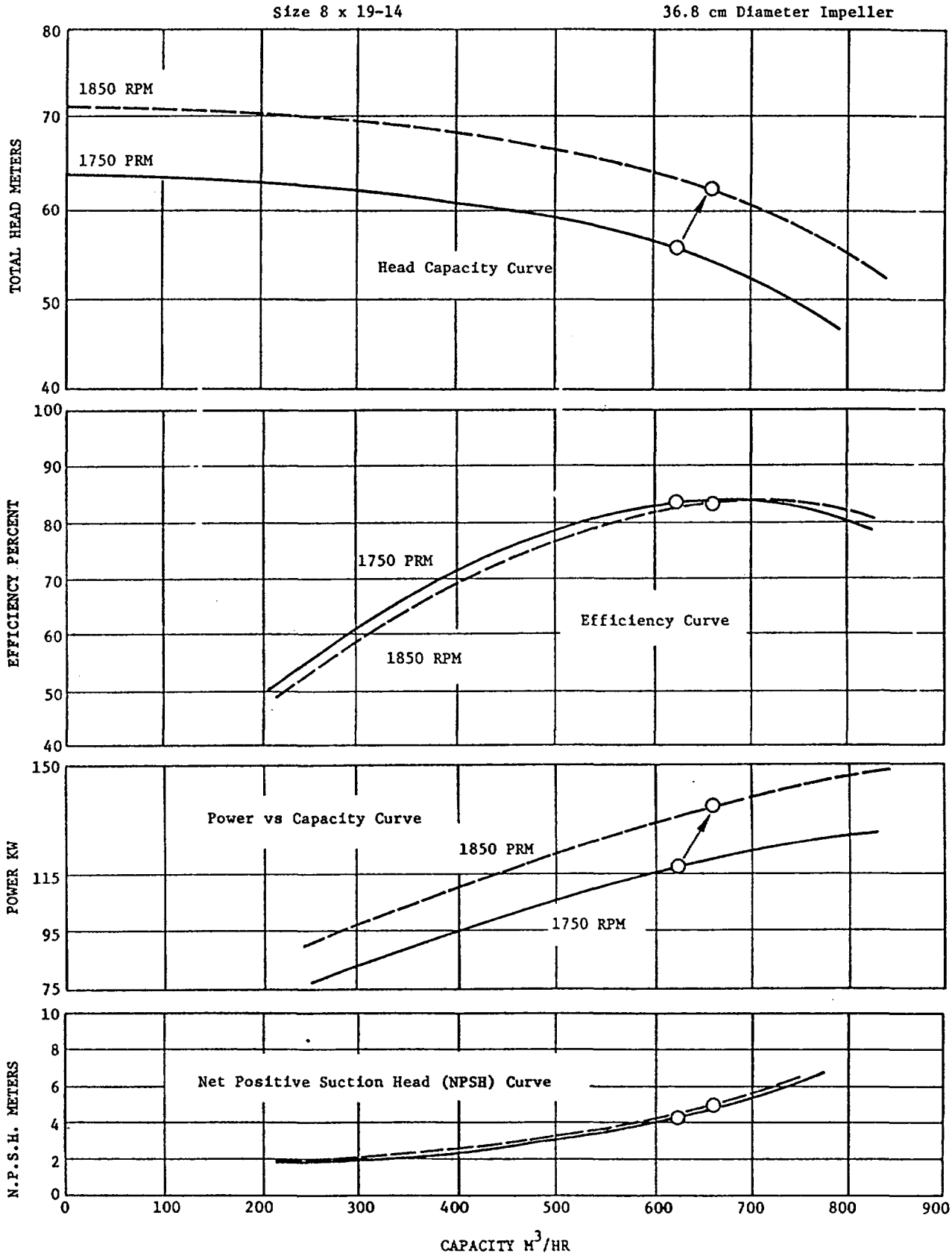

By performing the same calculation for several other points, a new curve can be drawn which will approximate the pump performance at 1850 rpm. This new performance curve is shown in Fig. A108. The manufacturer's data for the 14 1/2 inch impeller at 1750 rpm is shown as solid lines and the dotted lines represent the corresponding 1850 rpm characteristics.

The power requirements for the increased rpm can be obtained from the manufacturer's curve and the affinity laws, i.e., power changes with the cube of the speed change ratio, or calculated using head-capacity and efficiency points from the curves.

$$BHP = \frac{H \times Q \times \text{Sp. Gr.}}{3960 \times \text{Pump Efficiency}}$$

Sp. Gr. = specific gravity

$$3960 = \frac{33{,}000 \text{ ft-lb/HP}}{8.33 \text{ lb/gallon water}}$$

The Net Positive Suction Head Required (NPSHR) by the pump to prevent cavitation will vary with the square of the speed ratio, resulting in a very small increase in suction head requirements:

$$\frac{14.5}{NPSHR_2} = \left(\frac{1750}{1850}\right)^2 \qquad NPSHR_2 = 16.2 \text{ feet}$$

This speed increase provides an increase in excess of 10% in the head capability of the existing pump and motor up to 795 m^3/hr (3500 gpm). Above this flow the 150 kw motor would be overloaded. The possibility of rapid wear on the bearings and the ability of the pump casing to withstand the increased pressure should be investigated by the manufacturer.

A.7.5.2.4 Increase Pump Impeller Size - Paralleled Pumps

A typical reactor primary coolant system will circulate approximately 1360 m^3/hr (6000 gpm) using two pumps operating in parallel at 30 to 38 meters (100 to 125 ft) total head. These pumps may be of the double suction, orizontal split case type (Fig. A114).

The specific speed, Ns, required for the head and flow requirements places the impeller characteristics mid-way between the radial and mixed flow classes (Francis Vane Impeller). The horsepower requirements rise only slightly as flow increases above the design point (Fig. A109).

FIGURE A109

FRANCIS VANE IMPELLER

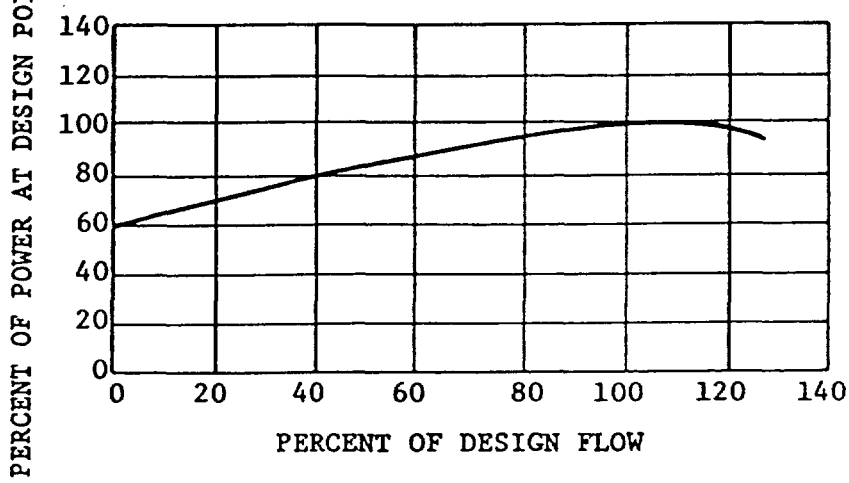

Therefore, overloading of the pump motor is less likely as the system pressure requirements are lowered during one pump operation.

A system head curve is shown in Fig. A110 based on 1360 m^3/hr (6000 gpm) at 37 meters (120 ft) head. Two 29.2 cm (11 1/2 inch) impeller pumps operating in parallel satisfy the requirements. Each will delivery 1190 m^3/hr (5250 gpm) when operating alone and require less than 115 kw (150 hp).

Figure A110.

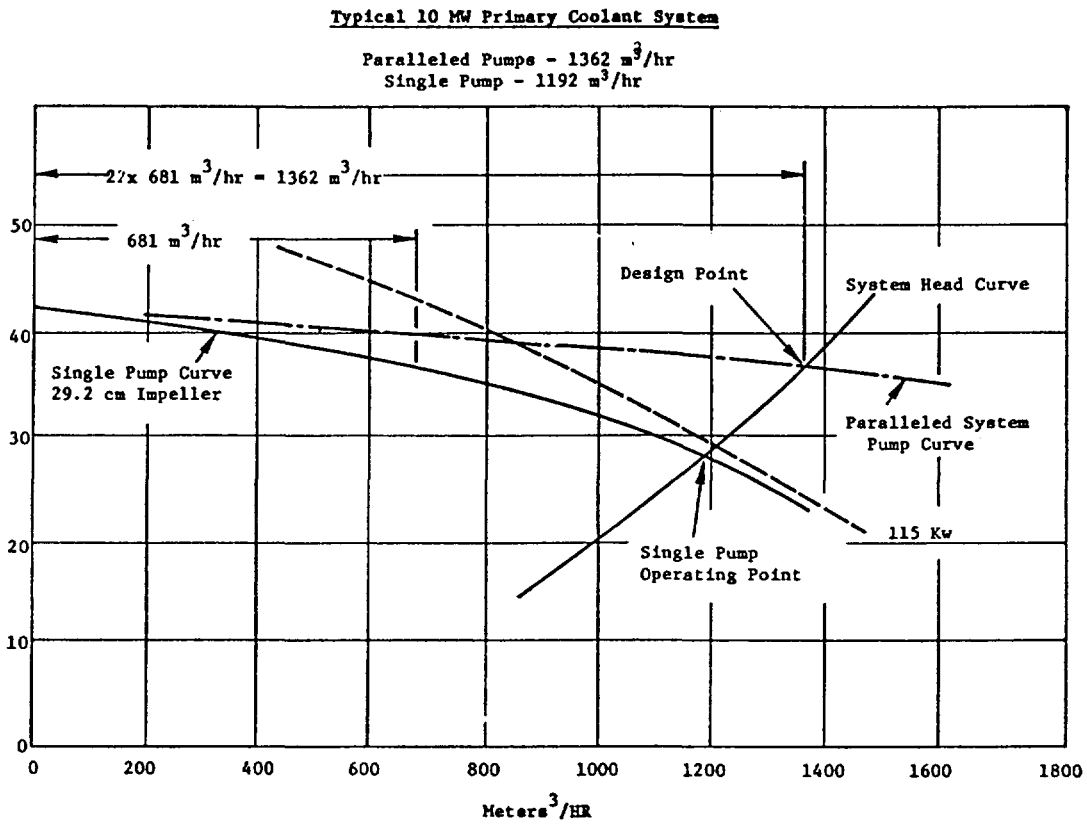

The system head curve in Fig. A111 shows the effect of a 10% increase in system head to be expectd from a redesigned reactor core.

Figure A111.

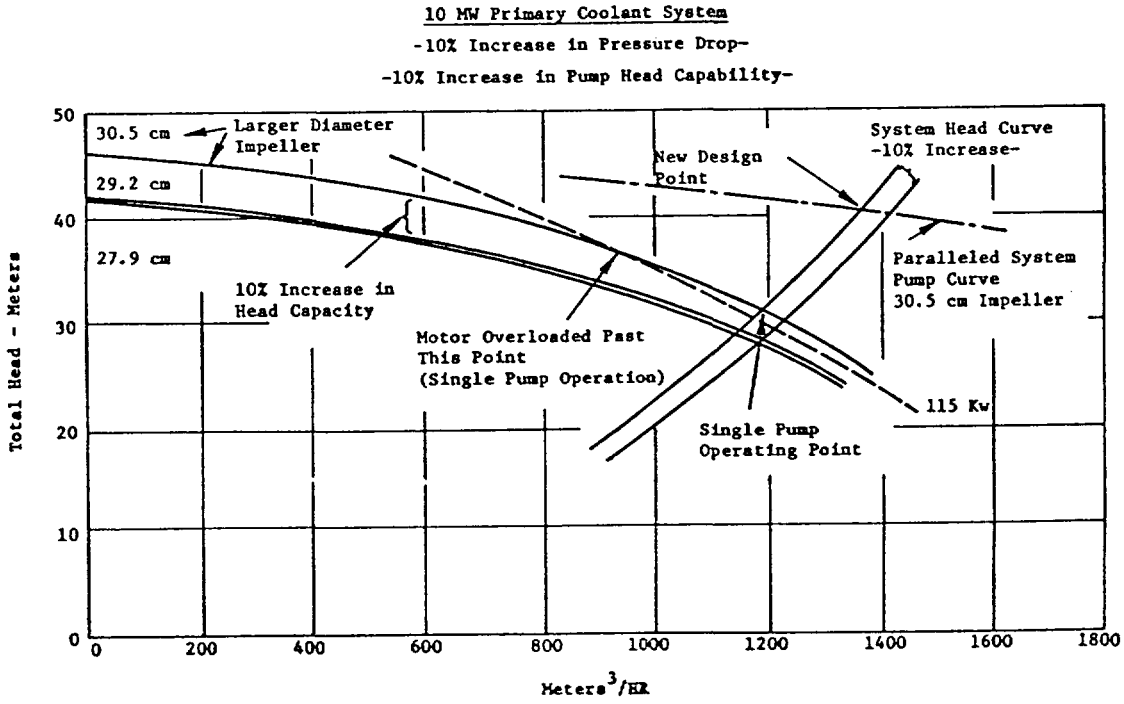

The centrifugal pump affinity laws indicate the same pump casing with a larger impeller 30.5 cm (12 inch) will satisfy the new system head curve requirements. The same 115 kw motor is more than adequate for the paralleled pumping system at the higher head requirements.

The 115 kw motor will, however, become overloaded when a single pump is operated at flows above 910 m^3/hr (4000 gpm), which will be the immediate case if one pump failed.

A larger motor is therefore required for the eventuality of one pump shutting down. This is also true of any emergency auxiliary drives.

For upward flow and pressurized coolant systems the addition of a booster pump(s) may be the simplest approach to increasing system discharge pressure. The booster pump would increase the discharge pressure by increasing the suction-side pressure. A pump imparts a set amount of energy to the system; therefore when a booster pump is placed in a system, the original pump discharge pressure is increased.

The booster is placed in series and upstream of the primary coolant pump, so that the pressure on the suction side is increased. The characteristics of the booster pump would require the volume flow to be equal to that of the existing system but the increase in pressure would only be equal to the required system increase. Paragraph A.7.5.1.2 discusses some details pertinent to application of a booster pump in a core coolant system.

A.7.5.2.5 Reduce Reactor Pool Static Head

A number of reactors in the medium power range have upward flow of coolant through the core. The required pumping head is the total of the piping system pressure loss plus core pressure drop plus the static head of the height of the reactor pool above the core. This static head will vary with different reactors, but lowering the pool level is a means of reducing the required pumping head.

As an illustration, lowering the reactor pool surface one meter reduces the static heat by 0.1 kg/cm^2. Reducing the depth of the pool can usually be accomplished by lowering the overflow pipe, but it cannot be lowered below the level of the outlet for the coolant return.

This may not be a practical procedure if the reactor pool is open and the depth of the water is acting as a radiation shield for operators working above. However, many reactors of the upward flow coolant circulation type have covered pools. These covers could be used to support the necessary radiation shielding.

If the existing pool level is a safety requirement, an elevated reservoir can be added to the system to return the pool level to its proper height in an emergency. Many of these reactors already have redundant spray cooling systems for emergency core cooling.

The reduction of the reactor pool level could be an inexpensive way to reduce the required pumping head for this type of system. It may be adequate in itself to produce the necessary reduction in head or it may be one of several related moves.

A.7.5.2.6 Reduce System Pressure Losses

Major system components, such as the primary heat exchanger, contribute significant pressure drops to the system. Since the pressure drop in any system is a direct function of the velocity of the fluid, reducing the fluid velocity through the primary heat exchanger will reduce the pressure drop of this component This can be done by adding another heat exchanger, of similar size, in parallel to the existing ones.

An illustration is a primary coolant system with two heat exchangers and a 2000 gpm total flow. The current ΔP from pump discharge to the heat exchanger exit is (Fig. A112) 6 psig through each line. The pipe from the pump to heat exchangers is 6" diameter, which results in a fluid velocity of 11.1 fps. Adding a third heat exchanger in paralel to the existing one will reduce the fluid velocity to about 670 gpm for a resulting velocity of 7.3 fps, assuming that 6" pipe is used for the new line. The pressure drop across each heat exchanger is now:

$$\Delta P = 6 \text{ psig} \left(\frac{7.30}{11.10}\right)^2 = 2.59 \text{ psig } (0.18 \text{kg/cm}^2)$$

$$\text{or a } \frac{(6-2.59) \text{ psig}}{32 \text{ psig}} \times 100 = 10.6\% \text{ reduction}$$

in the pressure drop on the discharge side of the pump.

In this example a heat exchanger equal in size to the existing unit is used to illustrate the point. A smaller heat exchanger might be used if a smaller pressure drop is adequate.

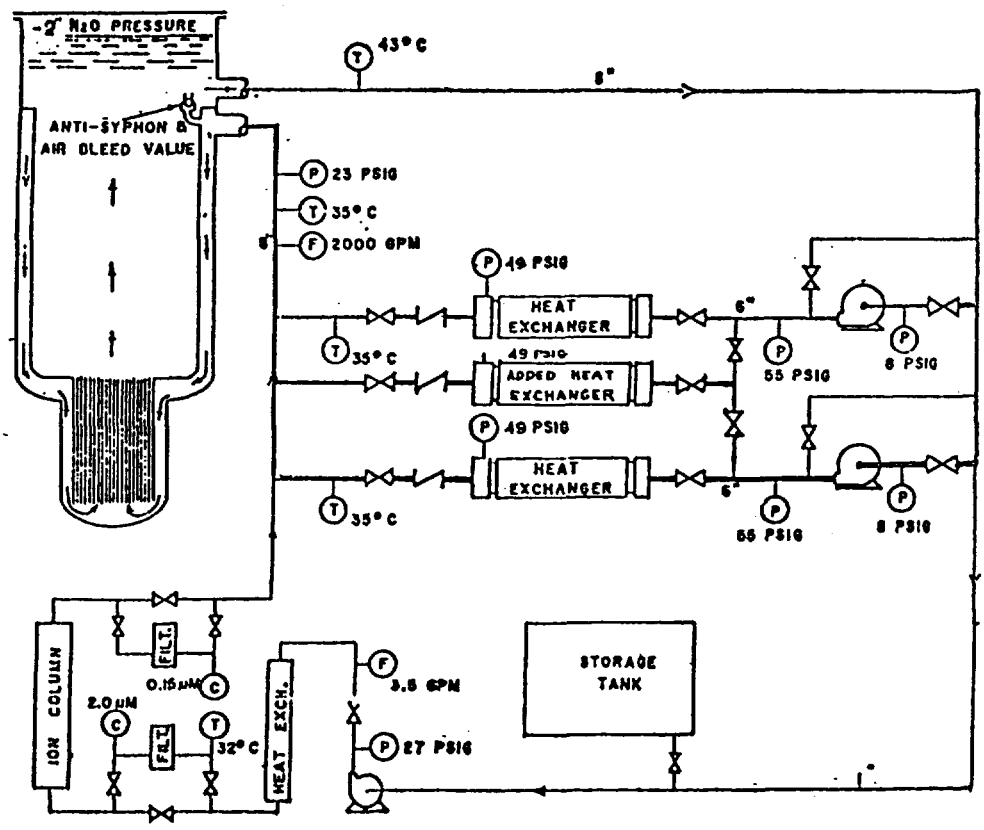

Figure A112.

A.7.5.2.7 Low Power Range Pressurized Coolant Systems (11 MW)

In general, these reactors circulate approximately 230 m^3/hr (1000 gpm) in the primary coolant loop. This flow is obtained by two pumps operating in parallel, each capable of 140 to 180 m^3/hr (600 to 800 gpm) in the case of a single pump failure.

The flow rate is controlled by flow control valves on a signal from a flow measuring instrument. The FCV puts added resistance in the coolant loop to match the system pressure drop to the combined head-capacity curve of the paralleled pumps.

Thus, for the tank-type reactor, an increase in core pressure drop can be offset by further opening of the FCV. The pumps see the same discharge head so they operate at the same point on the combined pump curve.

The characteristics of the FCV must be investigated relative to the system head curve to assure stable operation with the FCV supplying a lower percentage of the system pressure drop.

The individual pump performance curves must be checked to insure that the pump drive motor is not overloaded at the lower system head caused by one pump shutting down and the FCV not responding. The lower system head will allow the operating pump flow to exceed its design point.

The specific speed range of these pumps indicate they would be of the radial-flow type. With radial flow impellers the power required increases to a maximum with maximum flow. This may cause overloading of the existing motor if one pump shuts down (Figs. A113 and A115).

FIGURE A113.

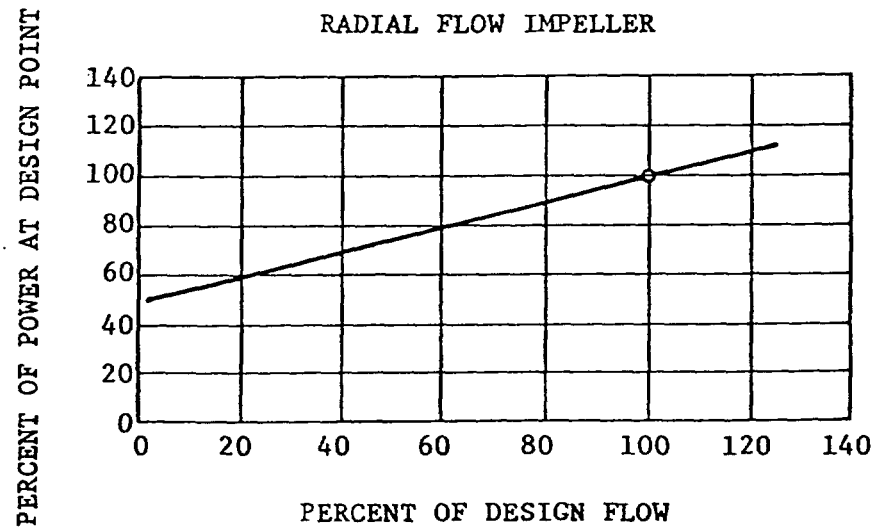

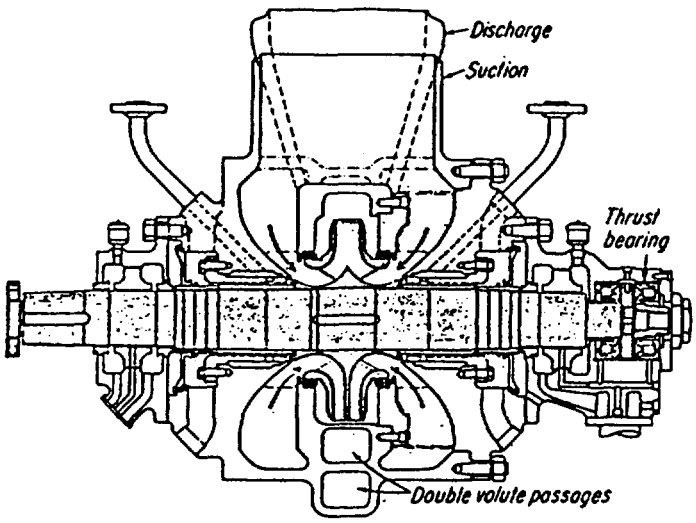

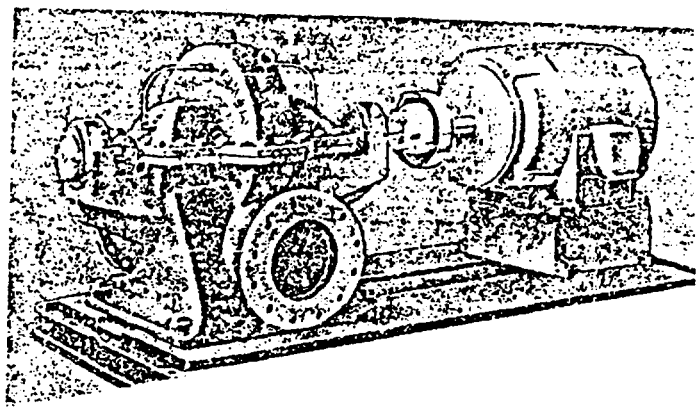

Figure A114.
Single stage, double suction, horizontally split case pump

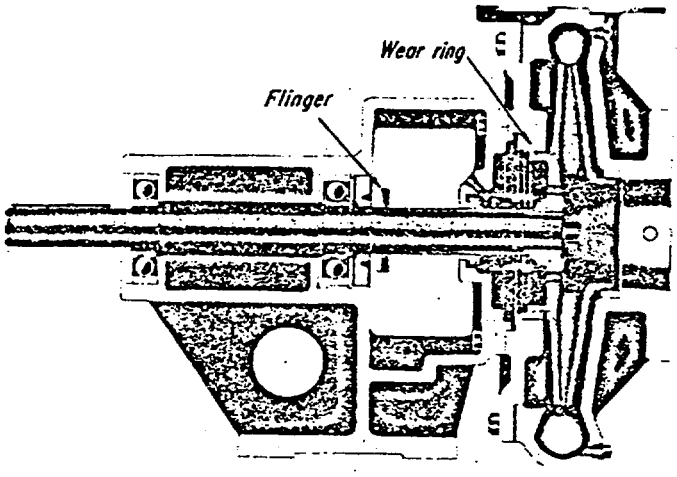

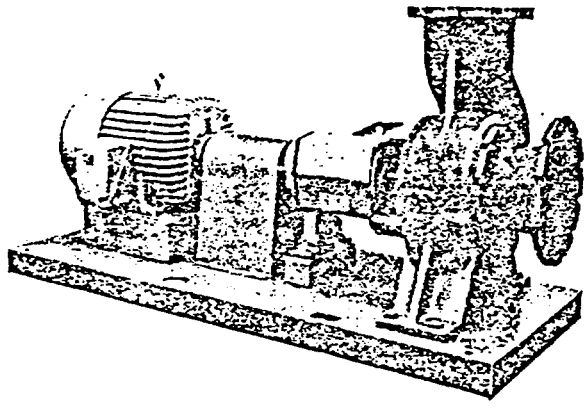

Figure A115.
Single stage, end suction, overhung impeller pump

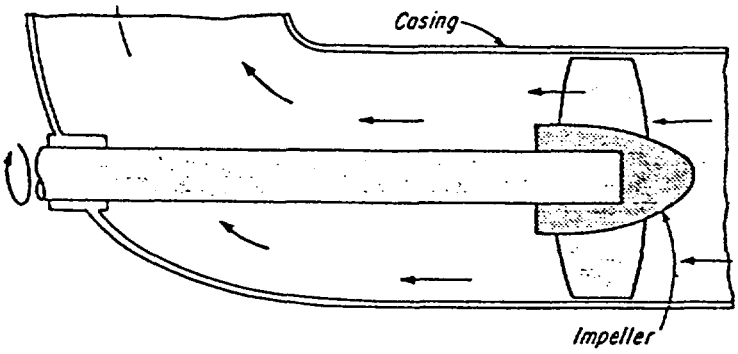

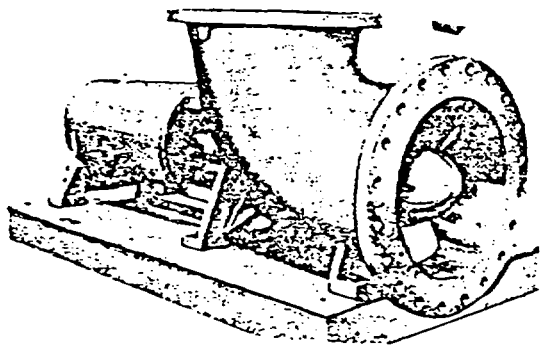

Figure A116.
Horizontal axial flow propeller pump

APPENDIX A

REFERENCES

1. B. A. Zolotar, et al., "EPRI-CELL Code Description," Advanced Recycle Methodology Program System Documentation, Part II, Chapter 5 (Oct. 1975).
2. G. D. Joanu and J. S. Dudek, "GAM-1: A Consistent P_1 Multigroup Code for the Calculation of Fast Neutron Spectra and Multigroup Constants," GA-1850 (1961).
3. H. C. Honeck, "THERMOS, A Thermalization Transport Theory Code for Reactor Lattice Calculations," BNL 5826 (1961).
4. H. Henryson II, B. J. Toppel and C. G. Stenberg, "MC^2-2: A Code to Calculate Fast Neutron Spectra and Multigroup Cross Sections," ANL-8144 (1976).
5. N. M. Greene, et al., "AMPX: A Modular Code System For Generating Coupled Multigroup Neutron-Gamma Libraries from ENDF/B," ORNL/TM-3706 (1976).
6. D. R. Ferguson and K. L. Derstine, "Optimized Iteration Strategies and Data Management Considerations for Fast-Reactor Finite-Difference Diffusion Theory Codes," Nuc. Sci. Eng. 64, pp. 593-604 (1977).
7. T. A. Daly, G. K. Leaf and A. S. Kennedy, "The ARC System TWO-Dimensional Diffusion Theory Capability, DARC2D," ANL-7716, May 1972.
8. D. E. Neal, G. K. Leaf, and A. S. Kennedy, "The ARC System One-Dimensional Diffusion Theory Capability, DARC1D," ANL-7715 (1971).
9. K. D. Lathrop and F. W. Brinkley, "TWOTRAN-II: An Interfaced, Exportable Version of the TWOTRAN Code for Two-Dimensional Transport," LA-4848-MS (1973).
10. W. A. Rhodes and F. R. Mynatt, "The DOT III Two-Dimensional Discrete Ordinates Transport Code," ORNL-TM-4280 (1973).
11. W. Engle, "ANISN - A One-Dimensional Discrete Ordinates Transport Code with Anisotropic Scattering," ORNL Radiation Shielding Information Center Code Package CCC-82 (1973).
12. E. M. Gelbard and R. E. Prael, "Monte Carlo Work at Argonne National Laboratory," in Proc. NEACRP Mtg. Monte Carlo Study Group, July 1-3, 1974, Argonne, Illinois, ANL-75-2 (NEA-CRP-L-118), Argonne National Laboratory (1975), p. 201.
13. M. B. Emmett, "The MORSE Monte Carlo Radiation Transport Code System," ORNL-4972 (1975).
14. D. A. Meneley, G. K. Leaf, A. J. Linderman, T. A. Daly, and W. T. Sha, "A Kinetics Model for Fast Reactor Analysis in Two Dimensions," Dynamics of Nuclear Systems, pp. 483-500, The University of Arizona Press, Tucson, Arizona (1972).
15. R. B. Hosteny, "The ARC System Fuel Cycle Analysis Capability, REBUS-2," ANL-7721 (1978)
16. W. R. Cadwell, "PDQ-7 Reference Manual," WAPD-TM-678 (1967).
17. MEKIN: MIT-EPRI Nuclear Reactor Core Kinetics Code, Thermal-Hydraulics part: COBRA-3C/MIT, EPRI-RP-227, September 1975; J. Chao, Y. K. Cheung, and A. P. Olson, "COBRA-3C/RERTR, A Subchannel Code for Research and Test Reactors," to be published in Trans. Am. Nucl. Soc., June 1980.

REFERENCES (Cont.)

18. M. L. Griebenow and K. D. Richert, "MACABRE II," Report No. IN-1107, Idaho Nuclear Co., September 1969; "MACABRE III," EG&G Idaho, private communication, January 1979.

19. "REPAP4/MOD 6, A Computer Program for Transient Thermal-Hydraulic Analysis of Nuclear Reactors and Related Systems," CDAP-TR-78-003, Idaho National Engineering Laboratory, January 1978.

20. J. Hardy, Jr., D. Klein and J. J. Volpe, "A Study of Physics Parameters in Several Water Moderated Lattices of Slightly Enriched and Natural Uranium," WAPD-TM-931, March 1970.

21. J. Hardy, Jr. "Monte Carlo Analyses of TRX Slightly Enriched Uranium-H_2O Critical Experiments With ENDF/B-IV and Related Data Sets," WAPD-TM-1307, December 1977.

22. R. Sher and S. Fiarman, "Studies of Thermal Reactor Benchmark Data Interpretation: Experimental Corrections," EPRI NP-209, October 1976.

23. W. J. Eich and M. L. Kennedy, "EPRI-CELL Criticals Benchmarking," Advanced Recycle Methodology Program System Documentation, Part I, Chapter 2, July 1976.

24. R. N. Hwang and D. J. Malloy, Applied Physics Division, Argonne National Laboratory, Private Communication, May 1979.

25. J. R. Brown, et al., "Kinetic and Buckling Measurements on Lattices of Slightly Enriched Uranium or UO_2 Rods in Light Water," WARD-176 (1958).

26. W. H. McAdams, Heat Transmission, 3rd Ed., McGraw-Hill Book Company, New York (1954).

27. W. M. Rohsenow and H. Y. Choi, Heat, Mass, and Momentum Transfer, Prentice-Hall, Englewood Cliffs (1961).

28. D. R. Miller, "Critical Flow Velocities for Collapse of Reactor Parallel-Plate Fuel Assemblies," KAPL-1954, August 1958.

29. S. McLain and J. H. Martens, Reactor Handbook, Vol. IV, Interscience Publishers (1964).

30. A. E. Bergles and W. M. Rohsenow, "The Determination of Forced-Convection Surface-Boiling Heat Transfers," Transactions of the ASME 86 (Series C - Journal of Heat Transfer), pp. 365-371 (August 1964).

31. J. P. Holman, Heat Transfer, 4th Ed., McGraw-Hill Book Company, New York (1976).

32. F. T. Binford, "The Oak Ridge Research Reactor - Safety Analysis," Oak Ridge National Laboratory, ORNL-4196, Vol. 2 (1978).

33. J. S. Maulbetsch and P. Griffith, "A Study of System - Induced Instabilities in Forced-Convection Flows With Subcooled Boiling," MIT Engineering Projects Lab Report 5382-35 (1965).

34. R. H. Whittle and R. Forgan, "A Correlation for the Minima in the Pressure Drop Versus Flow-Rate Curves for Subcooled Water Flowing in Narrow Heated Channels," Nuclear Engineering and Design, Vol. 6, (1967) pp. 89-99.

35. M. Ishii, "Thermally Induced Flow Instabilities in Two-Phase Mixtures in Thermal Equilibrium," Ph.D. thesis, Georgia Inst. of Tech., Atlanta (1971).

36. M. Ishii and N. Zuber, "Thermally Induced Flow Instabilities in Two Phase Mixtures," 4th Int. Heat Transfer Conf., Paris (1970).

REFERENCES (Cont.)

37. J. A. Bowre, "The Oscillatory Behavior of Heat Channels," Part I and II, French Report CEA-R 3049, Grenoble (1966).

38. H. Winkler, "Thermische Belastung der Brennelemente," EIR Internal Report TM-SR-106, December 1976.

39. R. Forgan and R. H. Whittle, "Pressure-drop Characteristics for the Flow of Subcooled Water at Atmospheric Pressure in Narrow Heated Channels," Part I, AERE-M-1739, May 1966.

40. S. Fried, K. Hofmann, G. Peterson, "Burnout-experimente in Beheizten Rechteckkanälen unter FRG-Bedingungen," GKSS 72/E/30.

41. F. R. Allen, Research Reactors Division, AERE Harwell, United Kingdom, Private Communication, April 1980.

42. W. A. Essler and P. J. Kregyer, "Flow Instability in HFR Fuel Element Cooling Channels," Internal EURATOM Report PET-398 (also, RCN-Int-69-108), October 1968.

43. M. W. Croft, "Advanced Test Reactor Burn-out Heat Transfer Tests," ATR-FE-102, January 1964.

44. E. D. Waters, "Heat Transfer Experiments for Advanced Test Reactor," BNWL-216, UC-80 (TID-4500), May 1966.

45. Ph. Vernier, Compte Rendu d'Essais, ORIRIS - Etude de Sûreté, "Détermination expérimentale des courbes en S et des conditions de redistribution de débit," C.E.N. Grenoble, TT/65-19-B/PV, December 1965.

46. M. Courtaud, G. Coulon, and F. Mazzili, Compte Rendu d'Essais, Boucle CASIMIR, "Trace de courbes en S (canal de 900 mm), Essais de dépressurisation," C.E.N. Grenoble, TT/66-7-B/MC-GC-FM, March 1966.

47. K. Schleisiek and J. C. Dumaine, Compte Rendu d'Essais, Essais préliminiares pour RHF, "Détermination expérimentale des conditions de redistribution de débit a des pressions comprises entre 4 et 5 kg/cm^2 abs pour un canal rectangulaire de 2 mm d'épaisseur et de 60 cm de longueur," C.E.N. Grenoble, TT/66-10-B/KS-JCD, April 1966.

48. M. Courtaud, G. Coulon, and F. Mazzili, Compte Rendu d'Essais, Boucle CASIMIR, "Trace de courbes en S sur des canaux a flux non uniforme," C.E.N. Grenoble, TT/66-14-B/MC-GC-FM, June 1966.

49. M. Courtaud, K. Schleisiek, G. Coulon, and F. Mazzili, Compte Rendu d'Essais, "Pertes de charge et redistribution de débit sur des canaux rectangulaires de 1.8 mm d'entrefer (type R.H.F.)," C.E.N. Grenoble, TT/67-7/B/MC-KS-GC-FM, June 1967.

50. R. W. Bowring, "Physical Model, based on Bubble Detachment and Calculation of Voidage in the Subcooled Region of a Heated Channel," HPR 10, 1962.

51. J. Costa, "Mesure de la perte de pression par acceleration, Etude de l'apparition de taux de vide en ébullition locale a basse pression," Communication présentée au Meeting de Groupe Européen Double-Phase, Winfrith, 1967.

52. S. Levy, "Forced Convection Subcooled Boiling. Prediction of Vapour Volumetric Fraction," GEAP-5157, April 1966.

53. W. H. Lowdermilk, C. D. Lanzo, and B. L. Siegel, "Investigation of Boiling and Flow Stability for Water Flowing in Tubes," NACA TN-4382 (1958).

REFERENCES (Con't.)

54. R. V. Macbeth, "The Burnout Phenomenon in Forced-Convection Boiling," Advances in Chemical Engineering, Vol. 7, (1968).

55. R. V. Macbeth, "Burnout Analysis. Part 4: Application of a Local Conditions Hypothesis to World Data for Uniformly Heated Round Tubes and Rectangular Channels," AEEW-R267, August 1963.

56. D. A. Labunstov, "Critical Thermal Loads in Forced Motion of Water which is Heated to a Temperature Below the Saturation Temperature," Soviet Journal of Atomic Energy (English Translation) 10, 516-18, November 1961.

57. E. J. Thorgerson, D. H. Knoebel, and J. H. Gibbons, "A Model to Predict Convective Subcooled Critical Heat Flux," J. Heat Transfer 96, pp. 79-82 (1974).

58. R. J. Weatherhead, "Nucleate Boiling Characteristics and the Critical Heat Flux Occurrence in Subcooled Axial-Flow Water System," USAEC Report, ANL-6675 (1962).

59. Y. Katto, "A Generalized Correlation of Critical Heat Flux for the Forced Convection Boiling in Vertical Uniformly Heated Round Tubes," Int. J. Heat Mass Transfer, Vol. 21, pp. 1527-1592 (1978).

60. Y. Katto, "A Generalized Correlation of Critical Heat Flux for the Forced Convection Boiling in Vertical Uniformly Heated Round Tubes--A Supplementary Report," Int. J. Heat Mass Transfer, Vol. 22, pp. 783-794 (1979).

61. S. Mirshak, W. D. Durant and R. H. Towell, "Heat Flux at Burnout," DuPont, DP-355, February 1959.

62. W. H. Lowdermilk and W. F. Weiland, "Some Measurements of Boiling Burn-Out," NACA RM E54K10 (1955)

63. J. G. Collier, Convective Boiling and Condensation, McGraw Hill Book Company, London (1972).

64. W. Rohsenow and P. Griffith, "Correlations of Maximum Heat Transfer Data for Boiling of Saturated Liquids," Chem. Eng. Prog. Symp. 52 (1956).

65. W. D. Turner, et. al., "HEATING5, An IBM-360 Heat Conduction Program", ORNL/CSD/TM-15, Oak Ridge National Laboratory.

66. L. A. Bernath, "A Theory of Local Boiling Burnout," Heat Trans. Symp. A.I.Ch.E. National Meeting, Louisville, Kentucky, 1955.

67. K. O. Lund, "Critical Heat Flux in A Subcooled, Low-Pressure Rod-Bundle with Various Rod Spacings," ASME Publication 75-HT49, 1975 (Reprinted as GA-13331, October 1979).

68. W. H. McAdams, et al., "Heat Transfer at High Rate to Water with Surface Boiling," Ind. Eng. Chem. 41, 1945-1959, (1949).

69. K. Forster and R. Greif, "Heat Transfer to a Boiling Liquid; Mechanism and Correlations," Tran. ASME. Ser. C., J. Heat Transfer 81, 43-53, (1959).

70. K. Almenas, University of Maryland, USA, Private Communication, December 1979.

71. "Engineering Properties of Incoloy Alloy 800", The International Nickel Company, Inc., Huntington Alloy Products Division, Huntington, West Virginia.

72. M. T. Simnad, "The U-ZrH_x Alloy: Its Properties and Use in TRIGA Fuel", General Atomic Company, E-117-833, February 1980.

73. R. A. Deen, "Thermal Contact Conductance Between UO_2 and Zircoloy 2," Westinghouse Electric Corporation, CVNA-127 (1962).

APPENDIX B

GENERIC ENRICHMENT REDUCTION CALCULATIONS FOR ROD-TYPE REACTORS

Provided by

General Atomic Company

TRIGA REACTOR DIVISION

P. O. Box 81608

San Diego, California 92138

U.S.A.

ABSTRACT

Reactor cores using rodded UZrH LEU fuel in place of current HEU fuel and the corresponding performance parameters are described for reactor powers of 2 MW and 10 MW.

INTRODUCTION

General Atomic Company has developed shrouded 4-rod and 16-rod clusters utilizing the TRIGA low-enriched uranium zirconium hydride (UZrH) fuel for use in converting and upgrading existing MTR plate-type reactors and also for fueling new TRIGA reactors. The use of low-enriched uranium is in keeping with non-proliferation policies and is readily exportable. The 4-rod cluster is designed to operate at power levels up to 3 MW and the 16-rod cluster is designed for power levels up to 10 MW in existing reactor core structures.

Both types of clusters use fuel-moderator rods which contain the well proven UZrH fuel in an Incoloy cladding. The rod diameter in the 4-rod cluster (3.24 cm) is only slightly smaller than that used in standard TRIGA fuel for more than 20 years. The 16-rod cluster uses a rod of 1.295 cm diameter and is identical in design to the fuel rods used in the 14 MW TRIGA now in operation at the Romanian Institute for Nuclear Technology. The fuel alloy used in the 4-rod cluster contains 20 wt-% uranium and in the 16-rod cluster 45 wt-% uranium. This provides a very high U-235 content with low enrichment, i.e., 440 grams U-235 in the 4-rod cluster and 880 grams U-235 in the 16-rod cluster. A small amount of erbium is included as a burnable poison and is a major contributor to the prompt negative temperature coefficient, the dominant safety feature of the TRIGA fuel. The high uranium loading combined with the burnable poison result in a very long burnup lifetime and favorable fuel cycle economics.

This Appendix is divided into two parts: B.1, which describes a 2 MW reactor using the 4-rod cluster and B.2, which describes a 10 MW reactor using the 16-rod cluster.

B.1 4-ROD CLUSTER TRIGA-LEU FUEL AND REACTOR DESCRIPTION

1. SUMMARY

The parameters describing a 2 MW reactor utilizing the 4-rod cluster are as follows:

Fuel - cluster: TRIGA-LEU 20 wt-% U in UZrH (76 x 80 x 508 mm)

Fuel rods per cluster:
Standard cluster: 4
Control cluster: 3

Nominal fuel rod dimensions:
Fuel O.D.: 32.4 mm
Clad O.D.: 33.5 mm (incoloy)
Fuel height: 508 mm

Fuel loading: 548 mm U (20% enriched)/rod
2.2 Kg U (20% enriched)/std cluster
440 gm U-235/std cluster
$\sim$0.5 wt-% Erbium as burnable absorber

Number of fuel clusters in the core: 26 ±1

Standard clusters: 21
Control clusters: 5 ±1

Reflector: Water

Core size (liters): 78 ±2

U-235 content/core (Kg): 10.6

Core geometry: 4 x 6 arrangement

Grid Plate: 6 x 9 positions (normal conversion)

Desired average burnup of U-235 in the fuel cluster discharged from the core: 30%

Burnup status of the core: equilibrium core

Average core burnup (%): $\sim$20

Fuel shuffling: introduction of new fuel clusters into the core center

Thermal-hydraulic data:

Average power density (Kw/liter): 26
Coolant flow rate: 1000 GPM
227 m^3/hr (3.8 x 10^6 cc/min)
Core inlet temperature: 38°C

2. DESIGN OBJECTIVE

The major design objective for the 4-rod cluster TRIGA-LEU fuel is to provide a long-lifetime, readily-exportable fuel which considers both initial and operating costs to provide a relatively low and attractive total fuel cycle cost. The cluster is designed to replace fuel in existing plate-type cores

and can, of course, also be used to fuel new reactor facilities. The design steady-state power level is up to 3 MW, depending upon available cooling system capabilities. A coolant flow rate of about 3780 liters/min (1000 gpm) is needed for 2-MW operation with a core containing about 26 clusters. Pulsing operation is possible with the core, but dependent upon the overall operating requirements of the facility. If maximized steady-state capabilities are required, the pulsing option should not be utilized.

The fuel uses low enriched uranium (LEU). The necessary U-235 content for long fuel life is achieved by using a somewhat higher percentage by weight of uranium than in past TRIGA fuels. The volume percent of uranium is still small, however, being about 7%. The fuel material (U-ZrH-Er) contains 20 wt-% uranium (20% enriched, nominal) about 0.5 wt-% erbium, and the hydrogen-to-zirconium ratio is 1.6.

More extensive details concerning the nuclear design procedures used for TRIGA reactors and a descriptive, in-depth example of the thermal-hydraulic design procedures used for TRIGA cores can be obtained from General Atomic Company.

3. FUEL DESIGN DESCRIPTION

The TRIGA fuel uses a uranium-zirconium hydride fuel material in which the hydrogen moderator is homogeneously contained within the fuel material. It is this feature which leads to the large prompt negative temperature coefficient of reactivity and the inherent safety of TRIGA reactors. Although each fuel rod is actually a fuel-moderator rod, they will be referred to simply as fuel rods throughout this report.

Figure 1 shows the general layout of the fuel rod and the fuel cluster. The fuel cluster consists of 4 fuel rods arranged in a square array. The individual fuel rods are designed so that any signle rod can be removed from its fuel cluster at any time. The cluster is contained within a rectangular aluminum shroud with inner dimensions forming a 2.857 in. square. The shroud serves two principal functions:

1. It provides structural support and protection.

2. It confines the coolant flow for each array to a fixed channel, making it unnecessary to provide a cooling flow shroud around the complete core and thus allowing greater flexibility to the core size and shape.

The shroud is attached to an aluminum bottom fitting which fits into the reactor grid plate. The top surface of the bottom fitting contains grid holes which determine the location and maintain the spacing of the fuel rods. The shroud also supports a top separator of Inconel which maintains the spacing between fuel rods. Four circular holes are located in the shroud wall near the top which provide an alternate flow path for coolant in the unlikely event that the top of the fuel cluster is blocked by some foreign object. The holes are also used for handling the cluster.

The fuel rods are 1.32 in. in diameter and approximately 30 in. long, with a fueled length of 20 in. Each fuel rod is clad with a 0.020-in. thickness of Incoloy 800. Stainless steel end fittings are heliarc welded to both ends

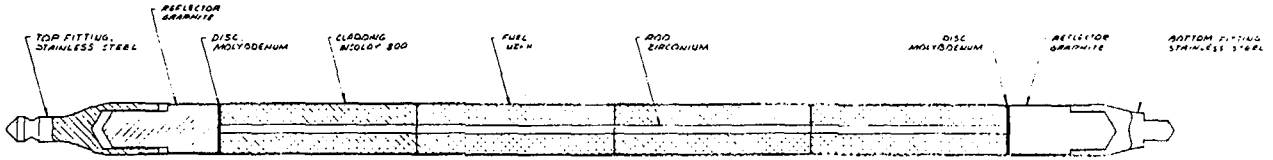

FUEL ROD ASSEMBLY

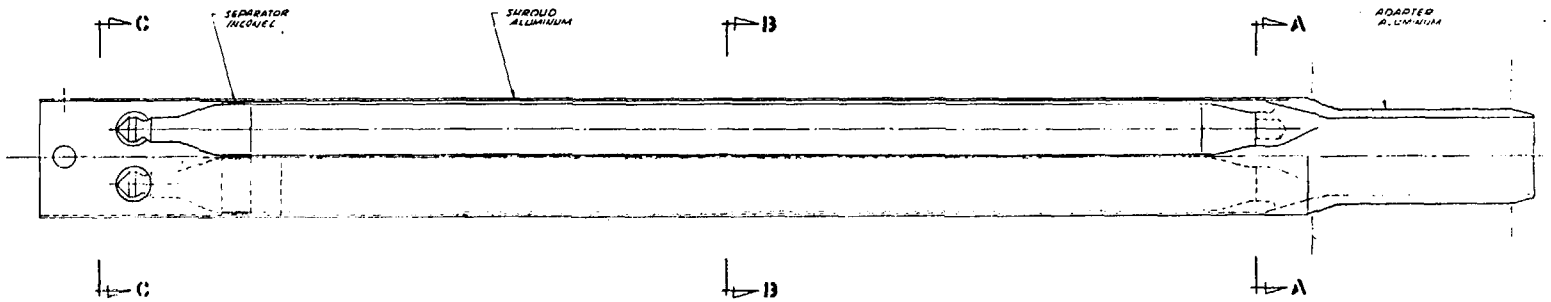

4 ROD FUEL CLUSTER ASSEMBLY

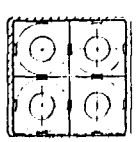

SECT C C

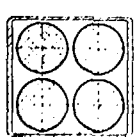

SECT B B

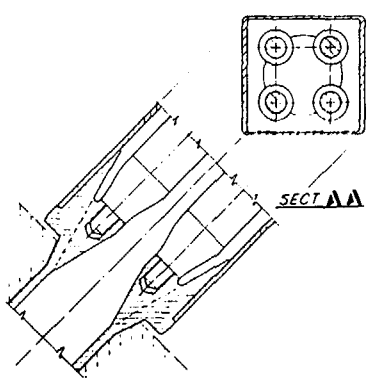

SECT A A

Fig. 1. 4 rod fuel cluster shrouded

of the cladding. The top end fitting is designed to fit into the fuel rod handling tool and the bottom end fitting is designed to fit into the fuel cluster grid. The fuel rod specifications are summarized in Table 1.

TABLE 1

NOMINAL FUEL SPECIFICATIONS FOR A SINGLE FUEL ROD

Overall length	30.0 in.	(76.2 cm)
Outside clad diameter	1.32 in.	(3.35 cm)
Overall weight	∿7.5 lb	(∿3.4 Kg)
Fuel outside diameter	1.277 in.	(3.24 cm)
Fuel length	20.0 in.	(50.8 cm)
Fuel composition	U-Zr-Er	
Weight of U-235	110 g	
Uranium content	20 wt-%	
Uranium-235 enrichment	20% (nominal)	
Hydrogen-to-zirconium ratio	∿1.6	
Cladding material	Incoloy 800	
Cladding thickness	0.020 in.	(0.051 cm)
Erbium	∿0.5 wt-%	

The fuel is a solid, homogeneous mixture of erbium-uranium-zirconium hydride alloy containing about 20% by weight of uranium enriched to 20% in U-235 and about 0.5% by weight of erbium. The hydrogen-to-zirconium atom ratio is approximately 1.6. The fuel material is divided into four equal-length pieces in each rod. The fuel pieces are ground to a high polish and exact tolerances in order to fit closely into the cladding.

Instrumented fuel rods have three thermocouples inserted in the fuel. The sensing tips of the thermocouples are located on the axial centerline of the fuel section and spaced about 1.0 in. below the core horizontal midplane. The thermocouple leadout wires pass through a seal contained in the stainless steel top end fitting and through another seal in the upper section of a tube welded to the top end fitting. This tube projects about 18.0 in. above the top end fitting and is extended by additional lengths of tubing connected by unions to provide a watertight conduit carrying the leadout wires above the water surface in the reactor pool. In other respects the instrumented fuel rod is identical to the standard rod.

4. NUCLEAR DESIGN AND CHARACTERISTICS

4.1 REACTIVITY REQUIREMENTS

Table 2 summarizes many of the core design parameters and characteristics. On initial startup of the core, it is estimated that about 5% to 6% excess reactivity is necessary to compensate for equilibrium xenon, the reactivity loss due to heating of the fuel, and the buildup of Sm-149 during the initial few weeks of full-power operation. Since the samarium loss results from a stable isotope, it builds up to an equilibrium value (rather quickly) and

remains at that value during core life. Thus, the reactivity change in going from zero to full power does not include the reactivity loss due to Sm-149.

TABLE 2

SUMMARY OF CORE DESIGN PARAMETERS AND CHARACTERISTICS

Reactivity requirements, δk ($)		
Xenon (equilibrium)	∿1.9%	($2.71)
Samarium (equilibrium)	0.8%	($1.14)
Cold-to-hot reactivity change[a]	2.0-3.0%	($2.86-$4.29)
Total	∿4.7-5.7%	($6.71-$8.14)
Operational reactivity change[b]	∿3.9-4.9%	($5.57-$7.00)
$\beta_{eff}(\delta k)$	0.0070	
ℓ(microsec)	∿24 (beginning of life)	
Maximum fuel temperature	∿650°C	
Recommended excess reactivity at beginning of life, δk	>6.0%	($8.57)
Recommended control system worth, δk With maximum-worth rod stuck out	>6.5%	($9.29)

[a] Based on an average core temperature of 280°C

[b] Samarium not included

4.2 GEOMETRICAL DESCRIPTION

Figure 2 shows the general configuration of a typical water reflected core used for design calculations. The reactor shown has a core consisting of a 5 by 5 array containing 20 standard 4-rod clusters and 5 control clusters. The control clusters have 3 fuel rods with the fourth location containing a guide tube for a control rod. The guide tubes and control rods can be located in any fuel cluster. Water passage around the control rod is provided by a large number of holes evenly distributed over the length of the tube. The guide tube assembly is anodized to increase resistance to wear and corrosion. The reactor core considered for the design described in this report consists of 26 fuel clusters, 4 to 6 of which are 3-rod control clusters. The core arrangement is a 4 by 6 array with the additional fuel above 24 clusters being placed on a single face of the core.

4.3 CALCULATIONAL METHODS

Neutron cross sections used in the analyses are generated for seven neutron energy groups. The lethargy and the energy for each of the seven broad groups are given in Table 3.

TABLE 3

NEUTRON ENERGY GROUP STRUCTURE

Group	Lethargy Interval	Energy Interval (eV)
1	-0.4 - 2.8	14.9×10^6 - 6.08×10^5
2	2.8 - 7.0	6.08×10^5 - 9.12×10^3
3	7.0 - 16.0	9.12×10^3 - 1.125
4	16.0 - 16.98	1.125 - 0.420
5	16.98 - 18.08	0.420 - 0.140
6	18.08 - 19.11	0.140 - 0.050
7	19.11 -	0.050 - 0.002

All neutron cross sections for energies above thermal (>1.125 eV) are generated using the GGC-5 code where fine-group (approximately 100-group) cross sections, stored on tape for all commonly used isotopes, are averaged over a spatially independent flux derived by solution of the B-1 equations for each discrete reactor design composition. This code and its related cross section library predict the age of each of the common moderating materials to within a few percent of the experimentally determined values. The resonance integral method of Nordheim is used to generate cross sections for resonance materials.

The core thermal cross sections are generated using the miltigroup cross section code GTF. GTF computes the spatially dependent thermal spectra at each mesh point in the cell, using the discrete ordinates method and the fine-group (58-point) cross section data contained in the thermal portion of the GGC-5 code.

Scattering kernels are used to describe properly the interactions of the neutrons with the chemically bound moderator atoms. The bound hydrogen kernels for hydrogen in water were generated by the THERMIDOR code, while those for hydrogen in zirconium hydride were generated by SUMMIT. These scattering models have been used to predict adequately the water and hydride (temperature-dependent) spectra as measured at the General Atomic linear accelerator.

Two-dimensional calculations are done using both diffusion and transport theory codes. In general, diffusion theory is used for the design calculations since it has given adequate results for systems of this kind and since the two-dimensional transport theory code requires an excessive amount of computer time. The transport theory code is used primarily for the determination of axial buckling in the radial reflectors.

The diffusion theory code used is GAMBLE-5, a multigroup code which solves the neutron diffusion equations with arbitrary group scattering.

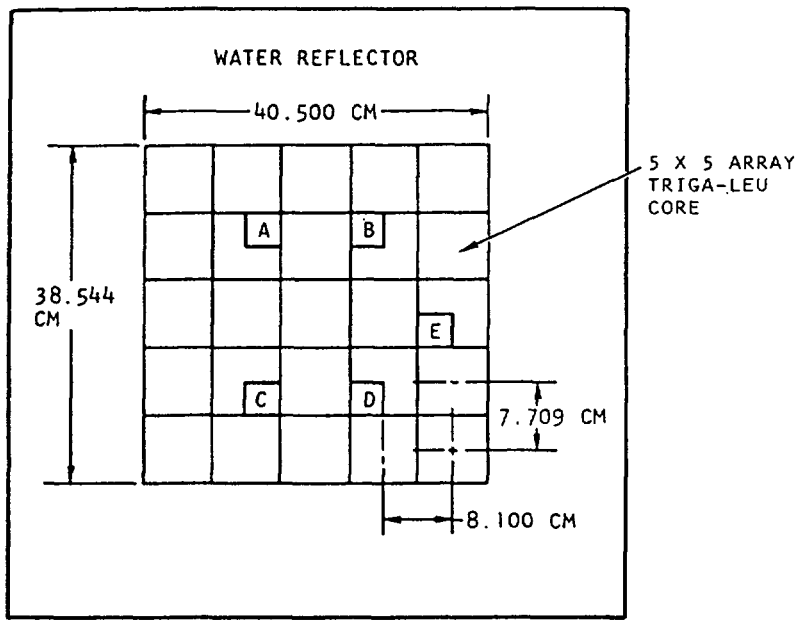

5 X 5 ARRAY OF 4-ROD CLUSTERS
SHOWING LOCATIONS OF 5 CONTROL
RODS (A — E)

Fig. 2. Water reflected configuration (rod locations for calculational purposes only)

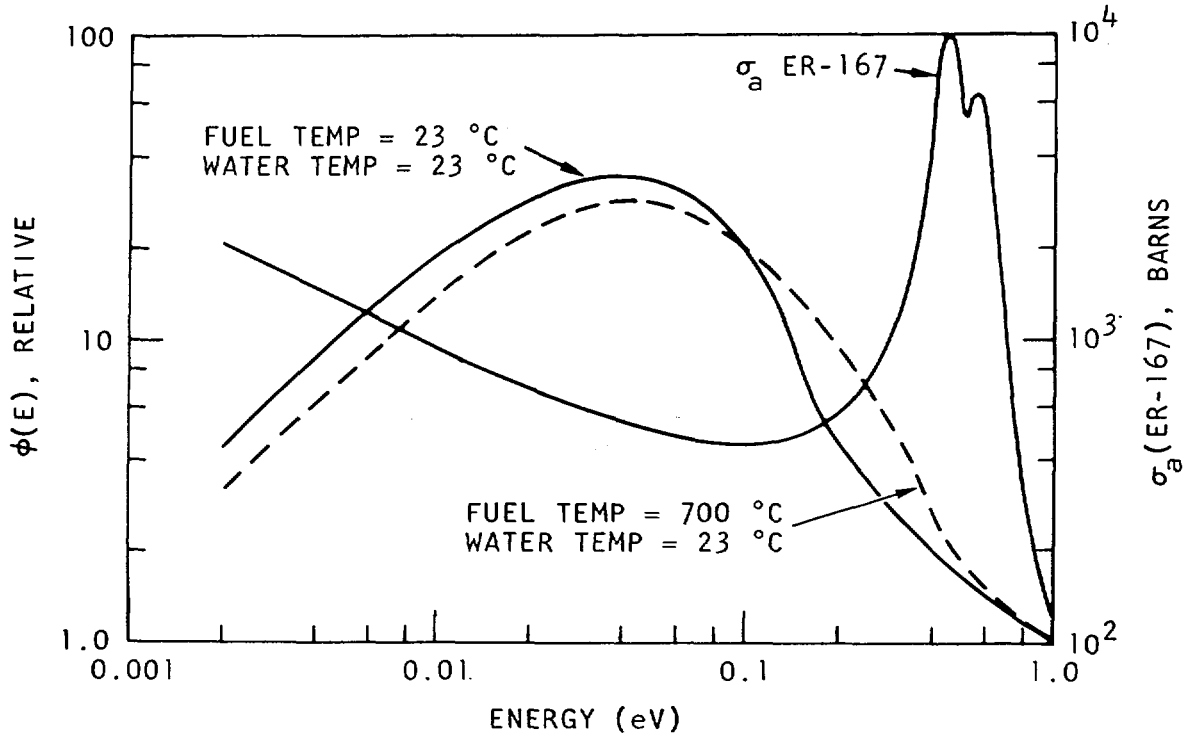

Fig. 3. Thermal neutron spectra versus fuel temperature relative to σ_a versus energy for Er-167

The transport theory code used is TWOTRAN, a multigroup code which solves the transport equation by the method of discrete ordinates. An S_4 approximation for the flux anisotropy and a modified P_0 approximation for the scattering anisotropy are used. The modified P_0 approximation is a diagonal transport approximation in which the total cross section for each group is replaced by the transport cross section and a correction for anisotropic scatter is applied to the P_0 self-scatter term. This approximation is used to reduce the excessive computer time and to provide for a larger mesh description. One-dimensional calculations have shown that modified P_0 calculations give reactivities within approximately 0.5% of the P_1 calculations.

The two-dimensional burnup code used is BUG, which solves the multi-group neutron diffusion theory equations for x-y and r-z geometry to obtain the multiplication factor and the spatial flux and power distribution. The depletion scheme of all burnable nuclides is specified, and a regionwide depletion scheme is used. Complete reactor life histories with partial refueling at a number of reload points can be calculated.

One-dimensional calculations are also done using both diffusion and transport theory codes. In general, one-dimensional calculations are used only for preliminary or survey type analyses, since the high-power cores are usually not easily mocked up in one dimension because of asymmetric fuel arrangements caused by experiment or control rod locations.

The diffusion theory code used is GAZE, a one-space dimensional multi-group code which allows scatter-transfer of neutrons between all neutron energy groups.

The transport theory code used is IDFX, a multigroup code which solves the transport equation by the method of discrete ordinates. An S_4 approximation for the flux anisotropy and a P_1 approximation for the scattering anisotropy are usually used.

The burnup code used is FEVER, a one-dimensional neutron diffusion-depletion code which calculates the spatial distribution of the neutron flux, the effective multiplication factor, and the spatial composition of a reactor for specified periods of time and reactor operating conditions.

4.4 POWER PEAKING

Power peaking in the core is analyzed on the basis of the following component values:

1. $\overline{P}_{rod}/\overline{P}_{core}$: rod power factor, the power generation in a fuel rod relative to the core average power generation
2. $(\hat{P}/\overline{P})$ axial: axial peak-to-average power ratio
3. $(\hat{P}_{rod}/\overline{P}_{rod})$ radial: rod-peaking factor, the peak-to-average power on a radial plane within a fuel rod

Since maximum fuel temperature is the limiting operational parameter for the core, the peaking factor of greatest importance is $\bar{P}_{rod}/\bar{P}_{core}$. The maximum value of this factor, the hot-rod factor $[(\bar{P}_{rod}/\bar{P}_{core})_{max} \equiv$ hot-rod factor], determines the power generation in the hottest fuel rod. When combined with the axial power distribution, the hot-rod factor is used in the thermal analysis for determination of the maximum fuel temperature. (The radial power distribution within the rod has a small effect on the peak temperature.)

The rod peaking factor $(\hat{P}_{rod}/\bar{P}_{rod})$ radial, is of importance in the transient analysis for calculating maximum fuel temperatures in the time range where heat transfer is not yet significant. It is used in the safety analysis where the product of the three peaking factors is used to calculate the peak fuel temperature under adiabatic conditions where the temperature distribution is the same as the power distribution.

The axial peak-to-average power is obtained from an r-z diffusion theory calculation. The top and bottom axial reflectors are mocked up such as to represent as nearly as possible the structure in the water reflectors.

Peaking factors calculated for a TRIGA-LEU core very similar to this 4-rod cluster system are shown in Table 4. The axial power distribution is relatively independent of radial position in the core. Analyses for other TRIGA cores have also shown that the shape of the axial power distribution changes significantly adjacent to a partially inserted control rod, but the peak power value is essentially equal to the unrodded value.

TABLE 4

PEAKING FACTORS

Type of Peaking	$\hat{P}/\bar{P}$
Core radial	1.57
Core axial	1.36
1D Cell (23°C)	1.48
1D Cell (310°C)	1.52
1D Cell (700°C)	1.61

The final component of the total peaking factor composite consists of the detailed power distribution within the fuel rod. Two-dimensional analysis is required because of the varying water thickness around a rod in a square array, and also because the hot-rod factors occur in regions where the rod environment is not symmetric.

Previous analyses of the rod peaking factor for other TRIGA reactors have shown this parameter to be somewhat temperature-dependent. The cell peaking factors shown in Table 4 can be used to investigate this effect. These cell peaking factors are from one-dimensional transport theory cell calculations. It is seen that the power peaking at 23°C is lower than the value at 310°C by about 3 and lower than the 700°C value by about 8%.

4.5 PROMPT NEGATIVE TEMPERATURE COEFFICIENT

The basic parameter which provides the great degree of safety in the operation of a TRIGA reactor system is the prompt negative temperature coefficient. This temperature coefficient (α) allows great freedom in steady-state operation, since the effect of accidental reactivity changes occurring from experimental devices in the core is minimized.

The prompt negative temperature coefficient for the TRIGA-LEU core is based on the same core spectrum hardening characteristic that occurs in a standard* TRIGA core. The spectrum hardening is caused by heating of the fuel-moderator elements. The rise in temperature of the hydride increases the probability that a thermal neutron in the fuel element will gain energy from an excited state of an oscillating hydrogen atom in the lattice. As the neutrons gain energy from the ZrH, the thermal neutron spectrum in the fuel element shifts to a higher average energy (the spectrum is hardened), and the mean free path for neutrons in the element is increased appreciably. For a standard TRIGA element, the average chord length is comparable to a mean free path, and the probability of escape from the element before being captured is significantly increased as the fuel temperature is raised. In the water the neutrons are rapidly rethermalized so that the capture and escape probabilities are relatively insensitive to the energy with which the neutron enters the water. The heating of the moderator mixed with the fuel in a standard TRIGA element thus causes the spectrum to harden more in the fuel than in the water. As a result, there is a temperature-dependent disadvantage factor for the unit cell in which the ratio of absorptions in the fuel to total cell absorptions decreases as fuel element temperature is increased. This brings about a shift in the core neutron balance, giving a loss of reactivity.

In the 4-rod cluster TRIGA-LEU fuel, the temperature-hardened spectrum is used to decrease reactivity through its interaction with a low-energy resonance material. Thus, erbium, with its double resonance at $\sim$0.5 eV, is used in the TRIGA-LEU fuel both as a burnable poision and as a material to enhance the prompt negative temperature coefficient. The ratio of the absorption probability to the neutron leakage probability is increased for the 4-rod cluster TRIGA-LEU fuel relative to the standard TRIGA fuel because the U-235 density in the fuel rod is about 2.5 times greater and also because of the use of erbium. When the fuel-moderator material is heated, the neutron spectrum is hardened, and the neutrons have an increasing probability of being captured by the low-energy resonances in erbium. This increased parasitic absorption with temperature causes the reactivity to decrease as the fuel temperature increases. The neutron spectrum shift, pushing more of the thermal neutrons into the Er-167 resonance as the fuel temperature increases, is illustrated in Fig. 3 where cold and hot neutron spectra are plotted along with the energy dependent absorption cross section for ER-167. As with a standard TRIGA core, the temperature coefficient is prompt because the fuel is intimately mixed with a large portion of the moderator; thus, fuel and solid moderator temperatures rise sumultaneously, producing the temperature-dependent spectrum shift.

*A standard TRIGA core contains U-ZrH fuel with no erbium. The uranium enrichment is 20%, and the fuel element (rod) diameter is about 3.8 cm (1.5 in.) with a core water volume fraction of about 0.33.

For the reasons just discussed, more than 50% of the temperature coefficient for a standard TRIGA core comes from the temperature-dependent disadvantage factor, or cell effect, and ∿20% each from Doppler broadening of the U-238 resonances and temperature-dependent leakage from the core. These effects produce a temperature coefficient of ∿-9.5 x 10-5°C, which is essentially constant with temperature. On the other hand, for the 4-rod cluster TRIGA-LEU core, the effect of cell structure on the temperature coefficient is smaller. Over the temperature range from 23° to 700°C, about 70% of the coefficient comes from temperature-dependent changes in nf within the core, and more than half of this effect is independent of the cell structure. Almost all of the remaining part of the prompt negative temperature coefficient is contributed by Doppler broadening of the U-238 resonances. Over the temperature range from 23°C to 700°C, the temperature coefficient for the 4-rod cluster TRIGA-LEU fuel is about -1.0 x 10-4/°C, thus being somewhat greater than the value for standard TRIGA fuel. It is also temperature dependent.

The calculation of the temperature coefficient for standard TRIGA and TRIGA-LEU cores requires a knowledge of the differential slow neutron energy transfer cross section in water and zirconium hydride, the energy dependence of the transport cross section of hydrogen as bound in water and zirconium hydride, the energy dependence of the capture and fission cross sections of all relevant materials, and a multigroup transport theory reactor description which allows for the coupling of groups by speeding up as well as by slowing down.

Qualitatively, the scattering of slow neutrons by zirconium hydride can be described by a model in which the hydrogen atom motion is treated as an isotropic harmonic oscillator with energy transfer quantized in multiples of ∿0.14 eV. More precisely, the SUMMIT model uses a frequency spectrum with two branches: one for the optical modes for energy transfer with the bound proton, and the other for the acoustical modes for energy transfer with the lattice as a whole. The optical modes are represented as a broad frequency band centered at 0.14 eV and whose width is adjusted to fit the cross-section data of Woods. The low-frequency acoustical modes are assumed to have a Debye spectrum with a cutoff of 0.02 eV and a weight determined by an effective mass of 360.

This structure then allows a neutron to thermalize by transition in energy units of ∿0.14 eV so long as its energy is above 0.14 eV. Below 0.14 eV, the neutron can still lose energy by the inefficient process of exciting acoustic Debye-type modes in which the hydrogen atoms move in phase with one another. These modes therefore correspond to the motion of a group of atoms whose mass is much greater than that of hydrogen, and indeed even greater than the mass of zirconium. Because of the large ineffective mass, these modes are very inefficient for thermalizing neutrons; but for neutron energies below 0.14 eV, they provide the only mechanism for neutron slowing down. (In a TRIGA core, the water provides for ample neutron thermalization below 0.14 eV). In addition, in the ZrH it is possible for a neutron to gain one or more energy units of ∿0.14 eV in one or several scatterings from excited Einstein oscillators. Since the number of excited oscillators present in a ZrH lattice increases with temperature, this process of neutron speeding up is strongly temperature-dependent and plays an important role in the behavior of ZrH-moderated reactors.

The temperature coefficient at the beginning of life for a 4-rod cluster TRIGA-LEU core increases as a function of fuel temperature because of the steadily increasing number of thermal neutrons being pushed into the Er-167 resonance. This temperature-dependent character of the temperature coefficient of a TRIGA core containing erbium is advantageous in that a minimum reactivity loss is incurred in reaching normal operating temperatures, but any sizeable increase in the average core temperature results in a sizably increased prompt negative temperature coefficient to act as a shutdown mechanism. The calculated temperature coefficient, depicting the approximate shape, is shown in Fig. 4.

4.6 CORE BURNUP LIFETIME

Core burnup calculations on reactors very similar to this 4-rod cluster TRIGA-LEU system have produced burnups of between about 1400 and 2000 MWd before the initial addition of reactivity is necessary to maintain the core at full power. The design condition established for the initial addition of reactivity is that the core has lost 2% in reactivity due to Sm buildup and fuel burnup (∇k aside from Xe). This reactivity loss is normally handled by the reactor control system. The average U-235 burnup is about 17% at the time of initial reactivity addition. It is estimated that the burnup will be about 30% in fuel clusters discharged from the core after an equilibrium fuel cycle condition has been established.

4.7 NEUTRON FLUX VALUES

A few of the most pertinent estimated flux values for the 4-rod cluster TRIGA-LEU reactor are given in Table 5 for a power level of 2 MW.

TABLE 5
ESTIMATED PEAK THERMAL FLUX AT 2 MW
4-ROD CLUSTER TRIGA-LEU REACTOR

Core	1.5×10^{13}
Core (central water hole)	7×10^{13}
Reflector (water)	2×10^{13}

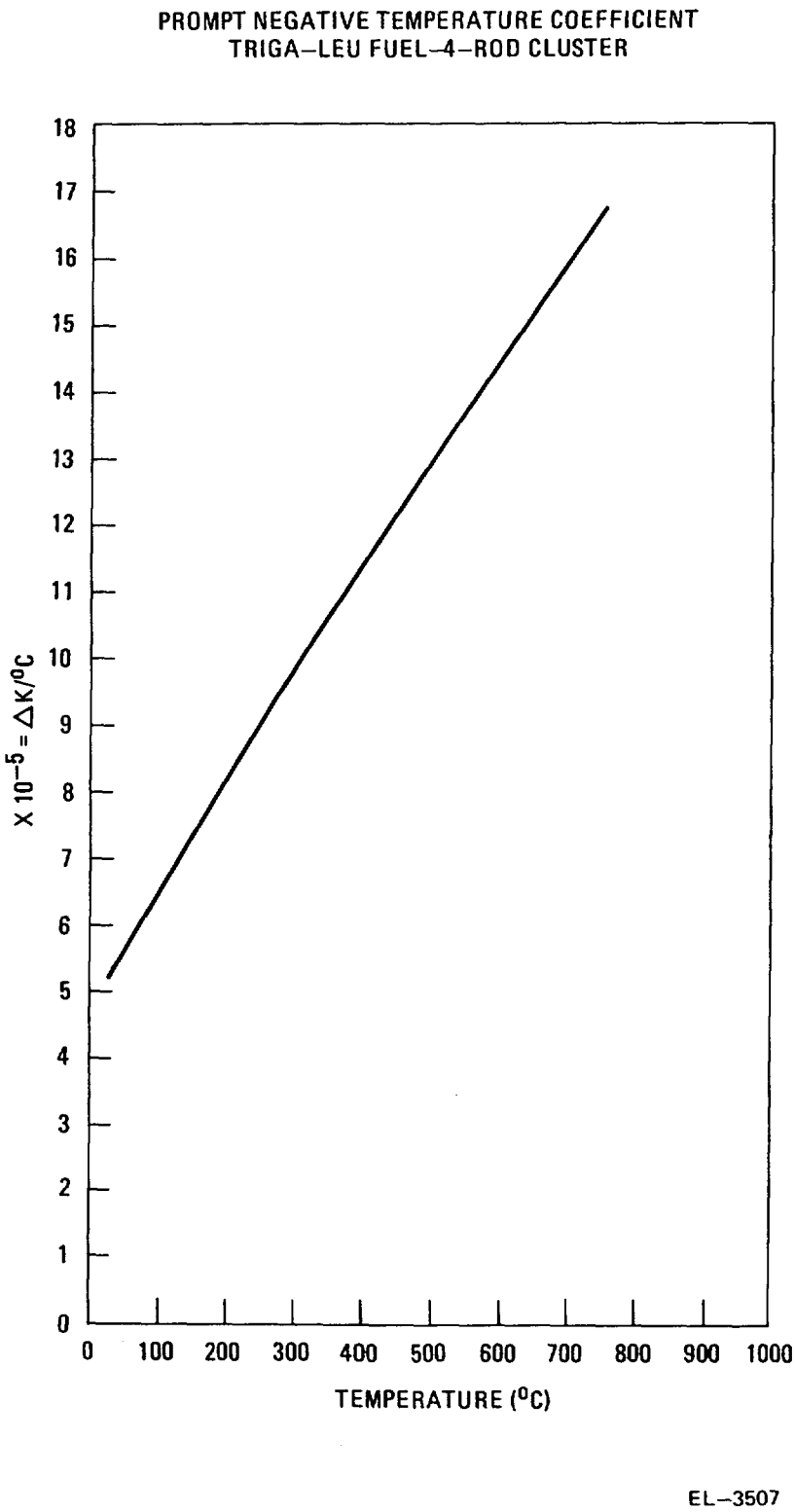

Fig. 4. Relative temperature coefficient as a function of temperature for beginning of life

B.2 10 MW TRIGA-LEU FUEL AND REACTOR DESIGN DESCRIPTION

1. SUMMARY

The parameter describing a 10 MW TRIGA-LEU reactor which uses the 16-rod UZrH fuel cluster is described as follows:

Fuel - Cluster: TRIGA-LEU 45 wt-% U in UZrH (76 x 80 x 559 mm)

Fuel rods per cluster:

Standard cluster: 16

Nominal fuel rod dimensions:

Fuel O.D.: 13.0 mm

Clad O.D.: 13.7 mm (Incoloy)

Fuel height: 559 mm

Fuel loading: 274 gm U (20% enriched)/rod

4.38 Kg U (20% enriched)/cluster

877 gm U-235/cluster

∿0.8 wt-% Erbium as burnable absorber

Number of fuel clusters in the core: 30

Number of control rods: 4 or 5

Reflector: Water

Core size (liters): 105

U-235 Content/core (Kg): 26.3

Core Geometry: 6 x 6 arrangement

Grid plate: 6 x 9 positions (normal conversion)

Desired average burnup of U-235 in the fuel cluster discharged from the core: >40%

Burnup status of the core: equilibrium core

Average core burnup (%): ~25

Fuel shuffling: introduction of new fuel clusters into the core center

Thermal-hydraulic data:

Average power density (Kw/liter): 95

Coolant flow rate: 5000 GPM, 1135 M^3/hr (1.9×10^7 cc/min)

Core inlet temperature: 38^0C

2. DESIGN OBJECTIVES

The major design objective for the 16-rod TRIGA fuel cluster was to use the identical fuel rod and coolant channel geometry used for the 14-MW TRIGA core (using 25-rod clusters) and to be able to achieve 10-MW operation with coolant flow rates in the range of 18,900 to 22,700 liters/min (5000 to 6000 gpm). Operation at about 5 MW was also achievable with a flow rate of 8300 liters/min (220°gpm). These design objectives were achieved with a 30-cluster core size and a design maximum fuel temperature of 750°C as summarzied in Table 1.

TABLE 1
MAJOR DESIGN OBJECTIVES FOR 16-ROD CONVERSION CLUSTERS

Use basic fuel rod developed for the 14-MW TRIGA to produce:	
Reactor power	10 MW
Core size	∿30 clusters
Maximum operational fuel temperature	750°C
Active core length	55.88 cm (22.0 in.)

Maintaining the fuel rod and coolant channel geometry of the 14-MW design enables maximum utilization of the existing nuclear, thermal, and mechanical design information in developing the 16-rod cluster design.

The fuel uses low enriched uranium (LEU). The necessary U-235 content for long fuel life is achieved by using a higher percentage by weight of uranium than in past TRIGA fuels. The volume percent of uranium is still modest, however, being about 20%. The fuel material (U-ZrH-Er) contains 45 wt-% uranium (20% enriched), about 0.8 wt-% erbium, and the hydrogen-to-zirconium ratio is 1.6.

3. FUEL DESIGN DESCRIPTION

The TRIGA fuel uses a uranium-zirconium hydride fuel material in which the hydrogen moderator is homogeneously contained within the fuel material. It is this feature which leads to the large prompt negative temperature coefficient of reactivity and the inherent safety of TRIGA reactors. Although each fuel rod is actually a fuel-moderator rod, they will be referred to simply as fuel rods throughout this report.

Figures 1, 2, and Engineering Drawing T4C 210E205 show the general layout of the fuel rod and the 16-rod fuel cluster. The fuel cluster consists of 16 fuel rods arranged in a 4 by 4 square array. The cluster is contained within a rectangular aluminum shroud with inner dimensions forming a 6.805-cm (2.679-in.) square. The shroud serves two principal functions:

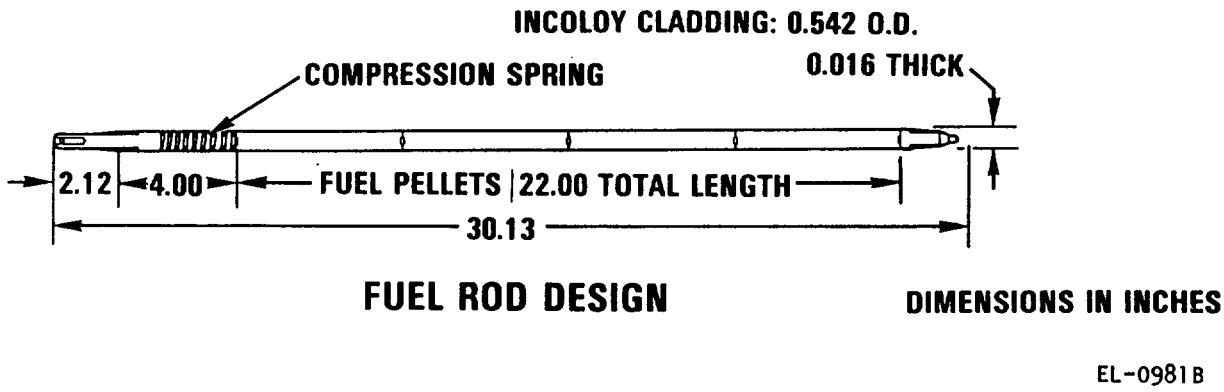

Fig. 1. TRIGA fuel rod for 16-rod cluster

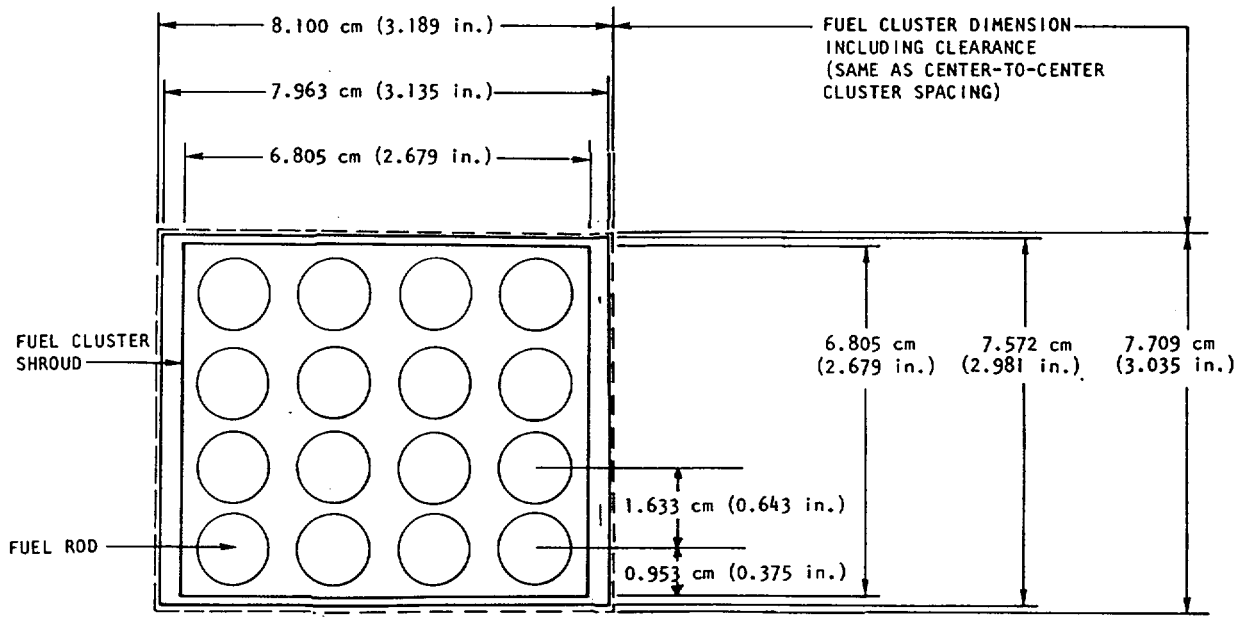

Fig. 2. General layout of 16-rod fuel cluster

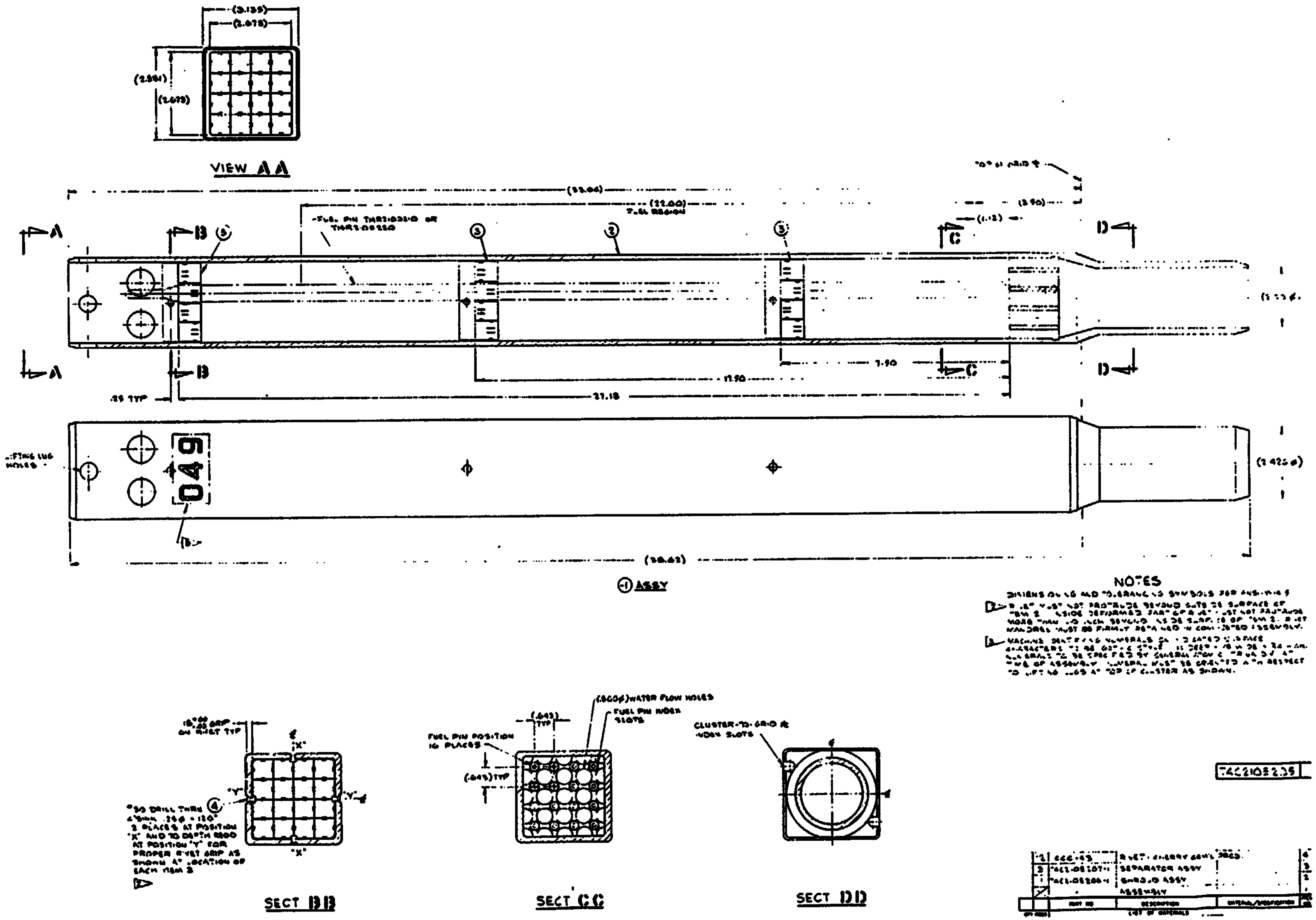
VIEW AA
(3.139)
(2.675)
(2.991)
(2.675)
(33.04)
(22.00)
FUEL REGION
(3.50)
(1.13)
A
B
C
D
7.50
17.50
21.18
.25 TYP
049
(2.425 ⌀)
(38.62)
-1 ASSY
NOTES
(.500⌀) WATER FLOW HOLES
FUEL PIN INDEX SLOTS
FUEL PIN POSITION 16 PLACES
(.643) TYP
CLUSTER-TO-GRID & INDEX SLOTS
SECT BB
SECT CC
SECT DD
SEPARATOR ASSY
SHROUD ASSY
ASSEMBLY
DESCRIPTION
LIST OF MATERIALS

1. It provides structural support and protection.

2. It confines the coolant flow for each array to a fixed channel, making it unnecessary to provide a cooling flow shroud around the complete core and thus allowing greater flexibility to the core size and shape.

The shroud is attached to an aluminum bottom fitting which fits into the reactor grid plate. The top surface of the bottom fitting contains grid holes which determine the location and maintain the spacing of the fuel rods. Each of the grid holes contains a keying arrangement which fixes the orientation of each fuel rod in relation to other fuel rods and the cluster. The fitting contains flow holes to provide sufficient area for cooling water flow. The shroud also supports a top separator and two intermediate separators which maintain the spacing between fuel rods. Two circular holes are located in the shroud wall near the top of the shroud which are used for handling the cluster. Rectangular holes are located in the shroud wall near the top of the fuel rods to provide an alternate flow path for coolant in the unlikely event that the top of the fuel cluster is blocked by some foreign object.

The fuel rods are 1.377 cm (0.542 in.) in diameter and approximately 76.2 cm (30.0 in.) long, with a fueled length of 55.88 cm (22.0 in.). Each fuel rod is clad with a 0.041-cm (0.016-in.)-thickness of Incoloy 800. There is an ∿10-cm (4-in.) section at the top of each fuel rod which is included as a flow-straightening section for the coolant and allows free differential expansion of the fuel and cladding. A spring is installed to ensure that the fuel pieces remain in position. Stainless steel and fittings are heliarc welded to both ends of the cladding. The top end fitting is designed to fit into the fuel rod handling tool and the bottom end fitting is designed to fit into the fuel cluster grid. The fuel rod specifications are summarized in Table 2.

TABLE 2
NOMINAL FUEL SPECIFICATIONS FOR A SINGLE FUEL ROD

Overall length	76.2 cm (30.0 in.)
Outside clad diameter	1.377 cm (0.542 in.)
Overall weight	438 g (0.97 lb.)
Fuel outside diameter	1.295 cm (0.510 in.)
Fuel length	55.88 cm (22.0 in.)
Fuel composition	U-ZrH-Er
Weight of U-235	∿55 g
Uranium content	45 wt-%
Uranium-235 enrichment	20% (nominal)
Hydrogen-to-zirconium ratio	∿1.6
Cladding material	Incoloy 800
Cladding thickness	16 mils
Erbium	∿0.8 wt-%

The active fuel length of each fuel rod is 55.88 cm (22.0 in.), with a diameter of 1.295 cm (0.510 in.). The fuel length is made up of four equal-length pieces. The fuel is a solid, homogeneous mixture of erbium-uranium-zirconium hydride alloy containing about 45% by weight of uranium enriched to 20% in U-235 and about 0.8% by weight of erbium. The hydrogen-to-zirconium atom ratio is approximately 1.6. The fuel pieces are ground to a high polish and exact tolerances in order to fit closely into the cladding. During final assembly, the clearance area between the fuel rod and the cladding will be filled with helium at about 1/10th of atmospheric pressure before final welding. The close tolerances and helium backfill increase the heat transfer across the fuel-clad interface and result in lower fuel centerline temperature.

Instrumented fuel rods have three thermocouples inserted in the fuel. The sensing tips of the thermocouples are located on the axial centerline of the fuel section and spaced about 2.54 cm (1.0 in.) below the core horizontal midplane. The thermocouple leadout wires pass through a seal contained in the stainless steel top end fitting and through another seal in the upper section of a tube welded to the top end fitting. This tube projects about 45.72 cm (18.0 in.) above the top end fitting and is extended by additional lengths of tubing connected by unions to provide a watertight conduit carrying the leadout wires above the water surface in the reactor pool. In other respects the instrumented fuel rod is identical to the standard rod.

The individual fuel rods are designed so that any single rod can be removed from its fuel cluster at any time.

4. NUCLEAR DESIGN AND CHARACTERISTICS

4.1. REACTIVITY REQUIREMENTS

Table 3 summarizes many of the core design parameters and characteristics. On inital startup of the core, it is estimated that about 4% to 5% excess reactivity is necessary to compensate for equilibrium xenon, the reactivity loss due to heating of the fuel and the buildup of Sm-149 during the initial few weeks of full-power operation. Since the samarium loss results from a stable isotope, it builds up to an equilibrium value (rather quickly) and remains at that value during core life. Thus, the reactivity change in going from zero to full power does not include the reactivity loss due to Sm-149.

TABLE 3
SUMMARY OF CORE DESIGN PARAMETERS AND CHARACTERISTICS

Reactivity requirements, δk ($)		
Xenon (equilibrium)	∿2.8%	($4.00)
Samarium (equilibrium)	0.8%	($1.14)
Cold-to-hot reactivity change[a]	0.8-1.3%	($1.14-$1.86)
Total	∿4.4-4.9%	($6.29-$7.00)
Operational reactivity change[b]	∿3.6-4.1%	($5.14-$5.86)
β_{eff} (δk)	0.0070	
ℓ (microsec)	∿25 (beginning of life) ∿32 (end of life)	
Maximum fuel temperature	640°C	

TABLE 3 (Continued)

Recommended excess reactivity at beginning of life, δk	>6.0%	($8.57)
Recommended control system worth, δk		
With maximum-worth rod stuck out	>6.5%[c]	($9.29)

[a] Based on a peak fuel temperature of 640°C and an average core temperature of 255°C

[b] Samarium not included

[c] It is possible to use an existing control system when converting a core. General Atomic has a control system designed for use with this core having a worth of about 8% with the maximum worth rod stuck out.

4.2. GEOMETRICAL DESCRIPTION

Table 4 shows the detailed geometrical descriptions for the 16-rod fuel cluster.

TABLE 4
DESIGN DATA FOR THE 16-ROD FUEL CLUSTER

Dimensions	Nominal Design Value
Fuel rod o.d. (unclad)	1.295 cm (0.510 in.)
Clad thickness	0.041 cm (0.016 in.)
Clad o.d.	1.377 cm (0.542 in.)
Rod-rod clearance	0.257 cm (0.101 in.)
Rod-shroud clearance	0.264 cm (0.104 in.)
Shroud thickness	0.384 cm (0.151 in.) and 0.579 cm (0.228 in.)
Clearance between shrouds	0.137 cm (0.054 in.)
Shroud side dimensions	7.572 cm (2.981 in.) x 7.963 cm (3.135 in.)
Fuel cluster spacing (center-to-center)	7.709 cm (3.035 in.) x 8.100 cm (3.189 in.)
Cross-sectional areas of:	
Unclad fuel rod	1.318 cm^2 (0.2043 $in.^2$)

TABLE 4 (Continued)

Dimensions	Nominal Design Value
Clad	0.170 cm^2 (0.0264 $in.^2$)
Clad fuel rod	1.488 cm^2 (0.2307 $in.^2$)
Unclad fuel inside shroud	21.089 cm^2 (3.2688 $in.^2$)
Clad inside shroud	2.725 cm^2 (0.4224 $in.^2$)
Water inside shroud	22.489 cm^2 (3.4858 $in.^2$)
Water in shroud clearance	2.150 cm^2 (0.3332 $in.^2$)
Shroud	13.990 cm^2 (2.1684 $in.^2$)
Volume fractions for 16-rod fuel cluster (including clearance dimensions)	
Unclad fuel	0.3378
Clad	0.0436
Shroud	0.2240
Water inside shroud	0.3602 } 0.3946
Water in shroud clearance	0.0344 }
Fuel length	55.88 cm (22.0 in.)
Fuel rod volume (unclad)	73.647 cm^3
Fuel rod loadings[(a)]	
Uranium	274 g
U-235	54.8 g
Erbium	~4.6 g
Er-167	~1.1 g
Fuel cluster loadings	
Uranium	4.38 kg
U-235	0.877 kg
Erbium	~74 g
Er-167	~17 g

[(a)] Based on U-ZrH-Er with 45 wt-% U (20% enriched) and ~0.8 wt-% Er

Shown in Fig. 3 is a general layout of the grid plate encompassing a calculational model used for previous nuclear analyses of a 10-MW TRIGA. Each of the grid locations is indexed for reference. It must be emphasized that the grid nomenclature designates a location and not a rod or cluster. The nomenclature can validly be used to describe any location in the grid regardless of whether the location does or does not contain fuel.

Each fuel cluster was described by an 8 x 8 mesh array for calculations done with this geometry.

4.3 CALCULATIONAL METHODS

Neutron Cross Sections - Neutron cross sections used in the analyses are generated for seven neutron energy groups. The lethargy and the energy for each of the seven broad groups are given in Table 5.

TABLE 5
NEUTRON ENERGY GROUP STRUCTURE

Group	Lethargy Interval	Energy Interval (eV)
1	-0.4 - 2.8	$14.9 \times 10^6 - 6.08 \times 10^5$
2	2.8 - 7.0	$6.08 \times 10^5 - 9.12 \times 10^3$
3	7.0 - 16.0	$9.12 \times 10^3 - 1.125$
4	16.0 - 16.98	1.125 - 0.420
5	16.98 - 18.08	0.420 - 0.140
6	18.08 - 19.11	0.140 - 0.050
7	19.11 -	0.050 - 0.002

All neutron cross sections for energies above thermal (>1.125 eV) are generated using the GGC-5 code where fine-group (approximately 100-group) cross sections, stored on tape for all commonly used isotopes, are averaged over a spatially independent flux derived by solution of the B-1 equations for each discrete reactor region composition. This code and its related cross section library predict the age of each of the common moderating materials to within a few percent of the experimentally determined values. The resonance integral method of Nordheim is used to generate cross sections for resonance materials.

The core thermal cross sections are generated using the multigroup cross section code GTF. GTF computes the spatially dependent thermal spectra at each mesh point in the cell, using the discrete ordinates method and the fine-group (58-point) cross section data contained in the thermal portion of the GGC-5 code.

Scattering kernels are used to describe properly the interactions of the neutrons with the chemically bound moderator atoms. The bound hydrogen kernels for hydrogen in water were generated by the THERMIDOR code, while those for hydrogen in zirconium hydride were generated by SUMMIT. These scattering models have been used to predict adequately the water and hydride (temperature-dependent) spectra as measured at the General Atomic linear accelerator.

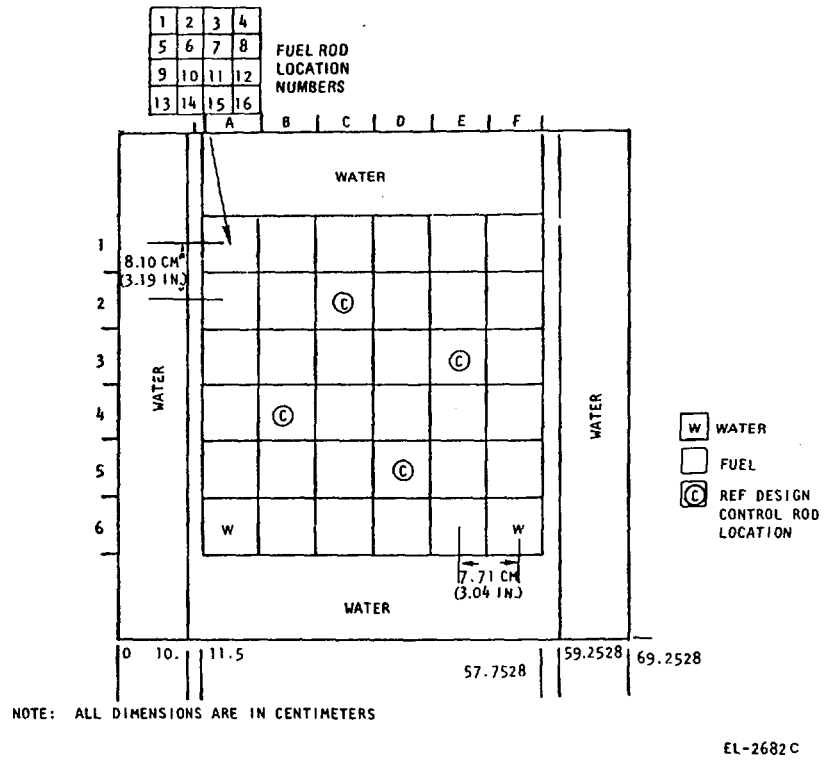

Fig. 3. Grid locations and typical dimensions for 10-MW TRIGA geometry

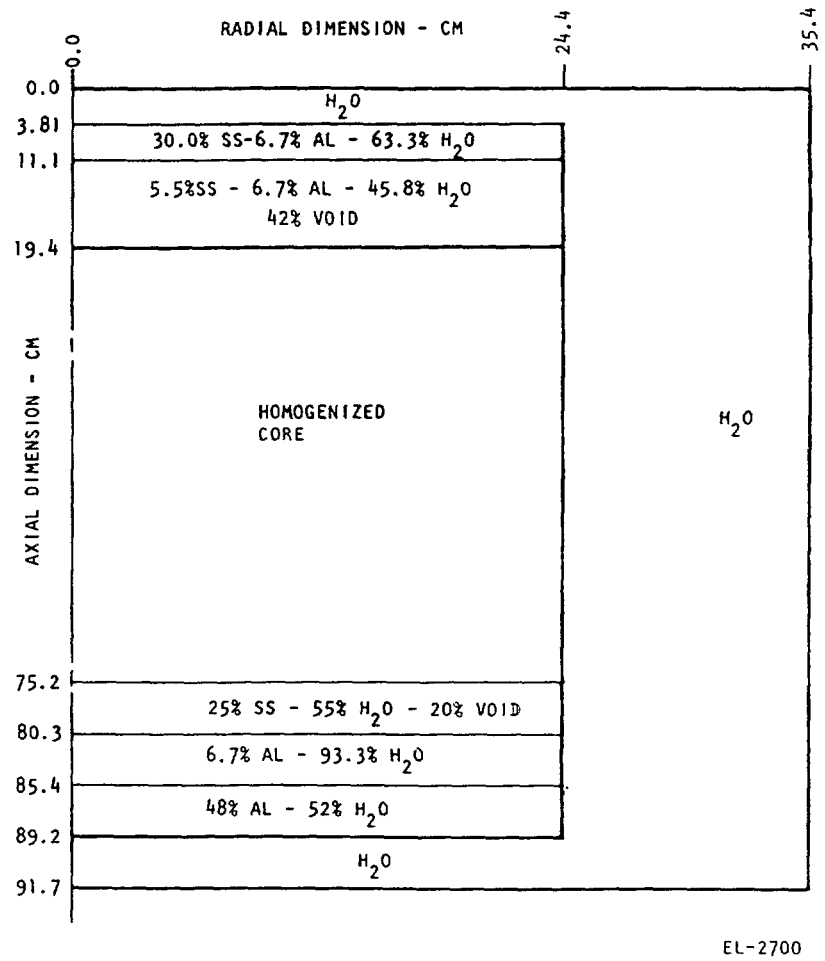

Fig. 4. R-Z calculational model

The unit cell description used in the generation of the thermal cross sections for the core is given in Table 6. The fuel and clad dimensions represent the rod exactly, but the water dimension has been specified such that it represents 1/16 of the water associated with a fuel cluster (including the shroud clearance). The aluminum shroud will not affect the spectrum so is not included in the calculation.

The epithermal core spectrum was calculated using the homogenized fuel cluster atom densities as given in Table 7.

Two-Dimensional Codes - Two-dimensional calculations are done using both diffusion and transport theory codes. In general, diffusion theory is used for the design calculations since it has given adequate results for systems of this kind and since the two-dimensional transport theory code requires an excessive amount of computer time. The transport theory code is used primarily for the determination of axial buckling in the radial reflectors.

The diffusion theory code used is GAMBLE-5, a multigroup code which solves the neutron diffusion equations with arbitrary group scattering.

The transport theory code used is TWOTRAN, a multigroup code which solves the transport equation by the method of discrete ordinates. An S_4 approximation for the flux anisotropy and a modified P_0 approximation for the scattering anisotropy are used. The modified P_0 approximation is a diagonal transport approximation in which the total cross section for each group is replaced by the transport cross section and a correction for anisotropic scatter is applied to the P_0 self-scatter term. This approximation is used to reduce the excessive computer time and to provide for a larger mesh description. One-dimensional calculations have shown that modified P_0 calculations give reactivities within approximately 0.5% of the P_1 calculations.

The two-dimensional burnup code used is BUG, which solves the multigroup neutron diffusion theory equations for x-y and r-z geometry to obtain the multiplication factor and the spatial flux and power distribution. The depletion scheme of all burnable nuclides is specified, and a regionwide depletion scheme is used. Complete reactor life histories with partial refueling at a number of reload points can be calculated.

One-Dimensional Codes- One-dimensional calculations are also done using both diffusion and transport theory codes. In general, one-dimensional calculations are used only for preliminary or survey type analyses, since the high-power cores are usually not easily mocked up in one dimension because of asymmetric fuel arrangements caused by experiment or control rod locations.

The diffusion theory code used is GAZE, a one-space dimensional multigroup code which allows scatter-transfer of neutrons between all neutron energy groups.

TABLE 6
UNIT CELL DESCRIPTION

Region	Radius (cm)	Nuclide	N (Atoms/b-cm)
Er-U-$ZrH_{1.6}$	0.6475	H	0.044004[b]
		Zr	0.029282[b]
		Er-166	7.747×10^{-5}
		Er-167	5.319×10^{-5}
		U-235	0.001885
		U-238	0.007539
Incoloy clad[a]	0.6885	SS	0.0969
Water	0.98195	H	0.0668
		Oxy	0.0334

[a] Composition assumed to be 20 wt-% Cr, 2 wt-% Mn, 68 wt-% Fe, and 10 wt-% Ni (stainless steel) with stainless steel atomic density (0.0843 atoms/b-cm) increased by 15% to give thermal neutron absorption equivalent to incoloy.

[b] $N_H/N_{Zr} \neq 1.6$ because some Zr combines with carbon impurity to form ZrC and some H combines with Er to form $ErH_{1.6}$ or ErH_2.

TABLE 7
HOMOGENIZED FUEL CLUSTER DESCRIPTION

Region	Volume Fraction	Nuclide	N (Atoms/b-cm)
Er-U-$ZrH_{1.6}$	0.3378	H	0.01486
		Zr	0.009892
		Er-166	2.617×10^{-5}
		Er-167	1.797×10^{-5}
		U-235	6.366×10^{-4}
		U-238	2.547×10^{-3}
Incoloy clad	0.0436	SS	0.00422
Water	0.3946	H	0.02636
		Oxy	0.01318
Al shroud	0.2240	Al	0.01351

The transport theory code used is IDFX, a multigroup code which solves the transport equation by the method of discrete ordinates. An S_4 approximation for the flux anisotropy and a P_1 approximation for the scattering anisotropy are usually used.

The burnup code used is FEVER, a one-dimensional neutron diffusion-depletion code which calculates the spatial distribution of the neutron flux, the effective multiplication factor, and the spatial composition of a reactor for specified periods of time and reactor operating conditions.

Determination of Axial Buckling - The axial buckling values for the homogenized fuel cluster, to be used in one-dimensional and two-dimensional (x-y) calculations, were obtained from one-dimensional diffusion theory calculations by iterating axially and radially.* The radial model assumed a homogenized core containing 30 fuel clusters surrounded by a water reflector. The axial model assumed a homogenized core with the top and bottom reflectors mocked up to represent the structural material in the water reflector (see Fig. 4).

The axial B_g^2 values for the homogenized core, obtained from these one-dimensional calculations, are given in Table 8. Previous calculations have shown the axial buckling valves to be essentially independent of core temperature, at least in the temperature range of interest for this design. This is due to the fact that the temperature effects are more significant in the lower energy ranges and the leakage effects are more significant in the higher energy ranges.

The core average value was used for axial buckling in the water reflector.

Calculational Result - Using the methods and information presented in the previous pages, and the additional atomic densities given in Table 9, a completely water reflected core was calculated using the BUG code. The core contained 30 fuel clusters and 4 control rod followers as shown in the core layout in Fig. 3. Locations A6 and F6 (in Fig. 3) contained water. The core cross sections were for a fuel rod temperature of 280°C. The calculated reactivity was 1.0849.

4.4 POWER PEAKING

Power peaking in the core is analyzed on the basis of the following component values:

1. $\bar{P}_{rod}/\bar{P}_{core}$: rod power factor, the power generation in a fuel rod relative to the core average power generation.
2. $(\hat{P}/\bar{P})$ axial: axial peak-to-average power ratio
3. $(\hat{P}_{rod}/\bar{P}_{rod})$ radial: rod-peaking factor, the peak-to-average power on a radial plane within a fuel rod

*B_g^2, obtained from this method, has been shown to give essentially the same k and flux as a B_g^2 obtained from an r-z calculation. This method is considerably more economical than the r-z model and is generally used for obtaining B_g^2 for the core.

TABLE 8
CORE AXIAL BUCKLING

Group	B_g^2 (core)
1	0.00306
2	0.00275
3	0.00192
4	0.000034
5	0.00231
6	-0.00796
7	-0.03188
$\overline{B}^2$	0.00255

TABLE 9
ADDITIONAL ATOM DENSITIES USED IN THE
X-Y CALCULATIONS (ATOMS/b-cm)

Nuclide	H_2O	Water & Shroud Around Follower	Al Follower[a]
H (H_2O)	0.0668	0.0368	
Oxy	0.0334	0.0184	
Al		0.0242	0.0687
B^2	0.00255	0.00171	0.00118

[a]Follower is an aluminum rod of radius 2.54 cm.

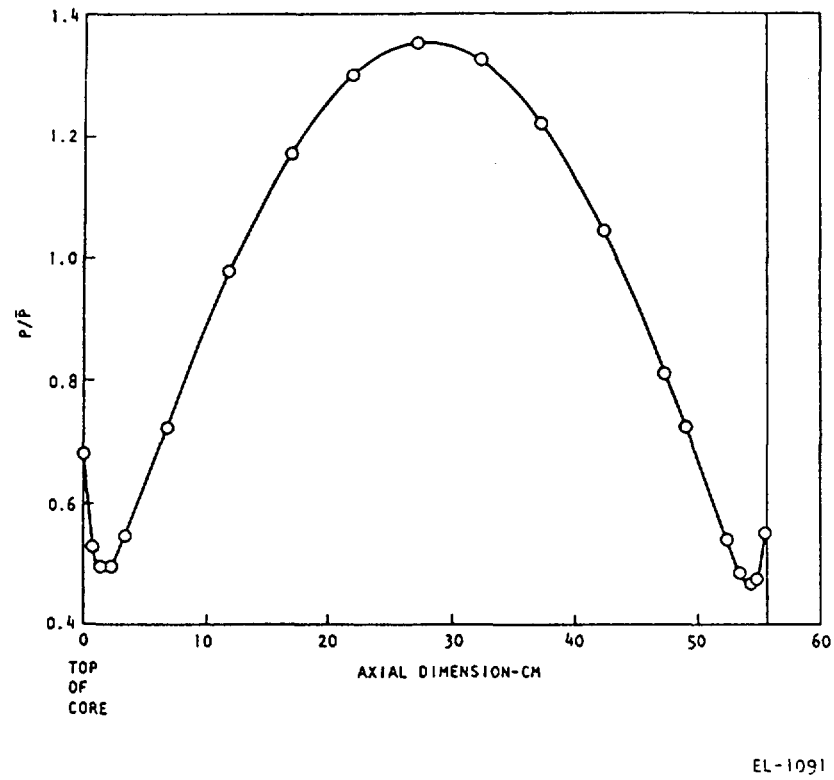

Fig. 5. Relative axial power distribution (400°C)

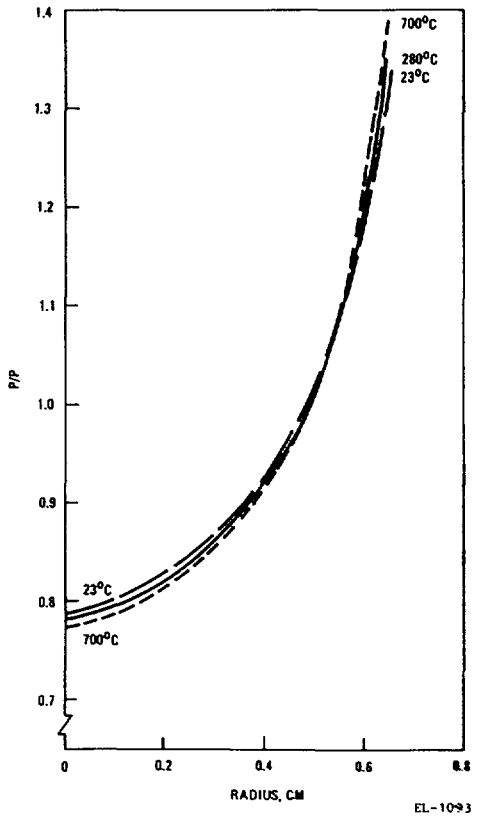

Fig. 6. Relative radial power distribution in fuel rod at various temperatures

Since maximum fuel temperature is the limiting operational parameter for the core, the peaking factor of greatest importance is P_{rod}/P_{core}. The maximum value of this factor, the hot-rod factor [$(P_{rod}/P_{core})_{max}$ = hot-rod factor], determines the power generation in the hottest fuel rod. When combined with the axial power distribution, the hot-rod factor is used in the thermal analysis for determination of the maximum fuel temperature. (The radial power distribution within the rod has a small effect on the peak temperature.) Results of the thermal analysis show that, for nominal design conditions, hot-rod factors can be as high as about 2.3 before the design maximum operational fuel temperature of 750°C is reached.

The rod peaking factor, $(P_{rod}/P_{rod})_{radial}$, is of importance in the transient analysis for calculating maximum fuel temperatures in the time range where heat transfer is not yet significant. It is used in the safety analysis where the product of the three peaking factors is used to calculate the peak fuel temperature under adiabatic conditions where the temperature distribution is the same as the power distribution.

The axial peak-to-average power is obtained from the r-z diffusion theory calculation. The top and bottom axial reflectors are mocked up such as to represent as nearly as possible the structure in the water reflectors.

The axial relative power distribution at the core centerline is given in Fig. 5. This distribution is nonsymmetric because of the differences in structural materials in the top and bottom reflectors. These data are normalized to an average of 1.0 such that the axial peak-to-average power of 1.35 can be read directly from the curve. The axial power distribution is relatively independent of radial position in the core. Analyses for other TRIGA cores have also shown that the shape of the axial power distribution changes significantly adjacent to a partially inserted control rod, but the peak power value is essentially equal to the unrodded value.

The final component of the total peaking factor composite consists of the detailed power distribution within the fuel rod. Two-dimensional analysis is required because of the varying water thickness around a rod in a square array, and also because the hot-rod factors occur in regions where the rod environment is not symmetric.

Previous analyses of the rod peaking factor for other TRIGA reactors have shown this parameter to be somewhat temperature-dependent. To investigate this effect, a series of one-dimensional, transport theory cell calculations was done for the fuel rod using fuel temperatures of 23°C, 280°C, and 700°C. These results are given in Fig. 6. It is seen that the power peaking at 23°C is lower than the value at 280°C by about 1%.

4.5 PROMPT NEGATIVE TEMPERATURE COEFFICIENT

The basic parameter which provides the great degree of safety in the operation of a TRIGA reactor system is the prompt negative temperature coefficient. This temperature coefficient (α) allows great freedom in steady-state operation, since the effect of accidental reactivity changes occurring from experimental devices in the core is minimized.

The prompt negative temperature coefficient for the 10-MW-TRIGA-LEU core is based on the same core spectrum hardening characteristic that occurs in a standard* TRIGA core. The spectrum hardening is caused by heating of the fuel-moderator elements. The rise in temperature of the hydride increases the probability that a thermal neutron in the fuel element will gain energy from an excited state of an oscillating hydrogen atom in the lattice. As the neutrons gain energy from the ZrH, the thermal neutron spectrum in the fuel element shifts to a higher average energy (the spectrum is hardened), and the mean free path for neutrons in the element is increased appreciably. For a standard TRIGA element, the average chord length is comparable to a mean free path, and the probability of escape from the element before being captured is significantly increased as the fuel temperature is raised. In the water the neutrons are rapidly re-thermalized so that the capture and escape probabilities are relatively insensitive to the energy with which the neutron enters the water. The heating of the moderator mixed with the fuel in a standard TRIGA element thus causes the spectrum to harden more in the fuel than in the water. As a result, there is a temperature-dependent disadvantage factor for the unit cell in which the ratio of absorptions in the fuel to total cell absorptions decreases as fuel element temperature is increased. This brings about a shift in the core neutron balance, giving a loss of reactivity.

In the 10-MW TRIGA-LEU fuel, the temperature-hardened spectrum is used to decrease reactivity through its interaction with a low-energy resonance material. Thus, erbium, with its double resonance at $\sim$0.5 eV, is used in the 10-MW TRIGA-LEU fuel both as a burnable poison and as a material to enhance the prompt negative temperature coefficient. With the smaller diameter used in the 10 MW-TRIGA, the ratio of the absorption probability to the neutron leakage probability is greatly increased relative to the standard TRIGA fuel because the U-235 density in the fuel rod is about seven times greater and also because of the use of erbium. When the fuel-moderator material is heated, the neutron spectrum is hardened, and the neutrons have an increasing probability of being captured by the low-energy resonances in erbium. This increased parasitic absorption with temperature causes the reactivity to decrease as the fuel temperature increases. The neutron spectrum shift, pushing more of the thermal neutrons into the Er-167 resonance as the fuel temperature increases, is illustrated in Fig. 7 where cold and hot neutron spectra are plotted along with the energy-dependent absorption cross section for Er-167. As with a standard TRIGA core, the temperature coefficient is prompt because the fuel is intimately mixed with a large portion of the moderator; thus, fuel and solid moderator temperatures rise simultaneously, producing the temperature-dependent spectrum shift.

For the reasons just discussed, more than 50% of the temperature coefficient for a standard TRIGA core comes from the temperature-dependent disadvantage factor, or cell effect, and $\sim$20% each from Doppler broadening of the U-238 resonances and temperature-dependent leakage from the core.

*A standard TRIGA core contains U-ZrH fuel with no erbium. The uranium enrichment is 20%, and the fuel element (rod) diameter is about 3.8 cm (1.3 in.) with a core water volume fraction of about 0.33.

These effects produce a temperature coefficient of $\sim -9.5 \times 10^{-5}/^{\circ}C$, which is essentially constant with temperature. On the other hand, for the 10-MW TRIGA-LEU core, the effect of cell structure on the temperature coefficient is small. Over the temperature range from 23°C to 700°C, slightly more than half of the coefficient comes from temperature-dependent changes in nf within the core, and ~90% of this effect is independent of the cell structure. Almost all of the remaining part of the prompt negative temperature coefficient is contributed by Doppler broadening of the U-238 resonances.

The calculation of the temperature coefficient for standard TRIGA and 10-MW TRIGA-LEU cores requires a knowledge of the differential slow neutron energy transfer cross section in water and zirconium hydride, the energy dependence of the transport cross section of hydrogen as bound in water and zirconium hydride, the energy dependence of the capture and fission cross sections of all relevant materials, and a multigroup transport theory reactor description which allows for the coupling of groups by speeding up as well as by slowing down.

Qualitatively, the scattering of slow neutrons by zirconium hydride can be described by a model in which the hydrogen atom motion is treated as an isotropic harmonic oscillator with energy transfer quantized in multiples of ~0.14 eV. More precisely, the SUMMIT model uses a frequency spectrum with two branches: one for the optical modes for energy transfer with the bound proton, and the other for the acoustical modes for energy transfer with the lattice as a whole. The optical modes are represented as a broad frequency band centered at 0.14 eV and whose width is adjusted to fit the cross-section data of Woods. The low-frequency acoustical modes are assumed to have a Debye spectrum with a cutoff of 0.02 eV and a weight determined by an effective mass of 360.

This structure then allows a neutron to thermalize by transition in energy units of ~0.14 eV so long as its energy is above 0.14 eV. Below 0.14 eV, the neutron can still lose energy by the inefficient process of exciting acoustic Debye-type modes in which the hydrogen atoms move in phase with one another. These modes therefore correspond to the motion of a group of atoms whose mass is much greater than that of hydrogen, and indeed even greater than the mass of zirconium. Because of the large effective mass, these modes are very inefficient for thermalizing neutrons; but for neutron energies below 0.14 eV, they provide the only mechanism for neutron slowing down. (In a TRIGA core, the water provides for ample neutron thermalization below 0.14 eV.) In addition, in the ZrH it is possible for a neutron to gain one or more energy units of ~0.14 eV in one or several scatterings from excited Einstein oscillators. Since the number of excited oscillators present in a ZrH lattice increases with temperature, this process of neutron speeding up is strongly temperature-dependent and plays an important role in the behavior of ZrH-moderated reactors.

The temperature coefficient at the beginning of life for the 10-MW TRIGA-LEU core increases as a function of fuel temperature because of the steadily increasing number of thermal neutrons being pushed into the Er-167 resonance. This temperature-dependent character of the temperature coefficient of a TRIGA core containing erbium is advantageous in that a minimum reactivity loss is incurred in reaching normal operating temperatures,

but any sizeable increase in the average core temperature results in a sizably increased prompt negative temperature coefficient to act as a shutdown mechanism. The end-of-life coefficient is less temperature-dependent than the beginning-of-life coefficient because of the sizable loss of Er-167 and the resulting increased transparency of the approximate 0.5-eV resonance region to thermal neutrons. Temperature coefficient values are shown in Fig. 8, which depicts the approximate shape and relationship of the beginning-of-life and end-of-life curves.

4.6 NEUTRON FLUX DISTRIBUTIONS

Flux distributions for a core with water reflection on all four sides were determined from two-dimensional, x-y, full-core, diffusion-theory calculations. Plots are given in Fig. 9 of the flux for a mid-plane traverse through the center of fuel in row 3. Figure 10 shows the same traverse for a core containing a water-filled flux trap in position C3. In-core flux traps provide a very effective means of producing very high thermal flux levels that are nearly independent of the fuel loading in the core.

Figure 11 shows the thermal flux (<0.625 eV) distribution for both a TRIGA-LEU core (880 gm U-235/cluster, new) and a plate-type HEU core (280 gm U-235/cluster, new). Both cores have a flux trap. The curve for the TRIGA core is for 4500 MW days of burnup (approximate point for initial reload step) and that for the plate-type core is representative of the end of an equilibrium cycle. Both cores have 29 elements but five of the plate-type core are partially loaded control elements. The TRIGA-LEU core was totally water reflected and configured in a 6 x 6 array (Fig. 3) while the plate-type HEU core was in a 5 x 6 array and had a row of graphite ($\sim$7.6 cm thick) followed by water on two opposite core faces and water reflection on the other two core faces. The flux distributions shown are for a traverse from the center of the flux trap, through two fuel elements and water reflected face.

The thermal flux for the lightly-loaded HEU plate-core is higher as expected, particularly in the fueled region. However, the effect on the flux in the experimental positions (central hole and reflector) in going to a highly loaded, low enriched, UZrH fuel is small. The flux traverse for the plate-type HEU core was taken from a curve supplied by Argonne National Laboratory (reference core, Fig. A33, Appendix A).

4.7 CORE BURNUP LIFETIME

Burnup analyses were done using BUG, a two-dimensional diffusion theory burnup code. The calculation uses cross sections generated for beginning-of-life concentrations at a fuel temperature of 280°C.

The core is assumed to burn for 600 days at 10 MW using 150-day-burnup time steps. (One-dimensional burnup studies have shown the adequacy of this burnup time step.) The final reactivity calculation, therefore, corresponds to a core burnup of 6000 MWd. In all cases the control rods are fully withdrawn.

Figure 12 gives the calculated k_{eff} as a function of core burnup. It should also be noted that the time steps used for the burnup calculations were large compared with the time for burn-in of Sm-149. Thus, the initial reactivity loss due to this effect is not shown on the curves but is accounted for in the longer-term reactivity values. Additional evaluations have indicated other refinements in the analysis are needed which could affect the results shown for this specific case.

These data indicate a burnup of about 4000 MWd before addition of any new fuel is required. The initial reloading point is defined as the time at which a reactivity loss of 4.3% has occurred from an initial reactivity being defined as k_{eff} at t = 0, with equilibrium xenon. This is a reactivity decrease used with the control system designed by General Atomic. This burnup of about 4000 MWd represents a U-235 burnup of about 20%, and is the point at which the initial core needs additional reactivity to remain operational at full power with an assumed margin of 2.8% for experiments. It is estimated that when an equilibrium reload condition has been reached, the fuel removed from the core can have a U-235 burnup of 40 to 60%.

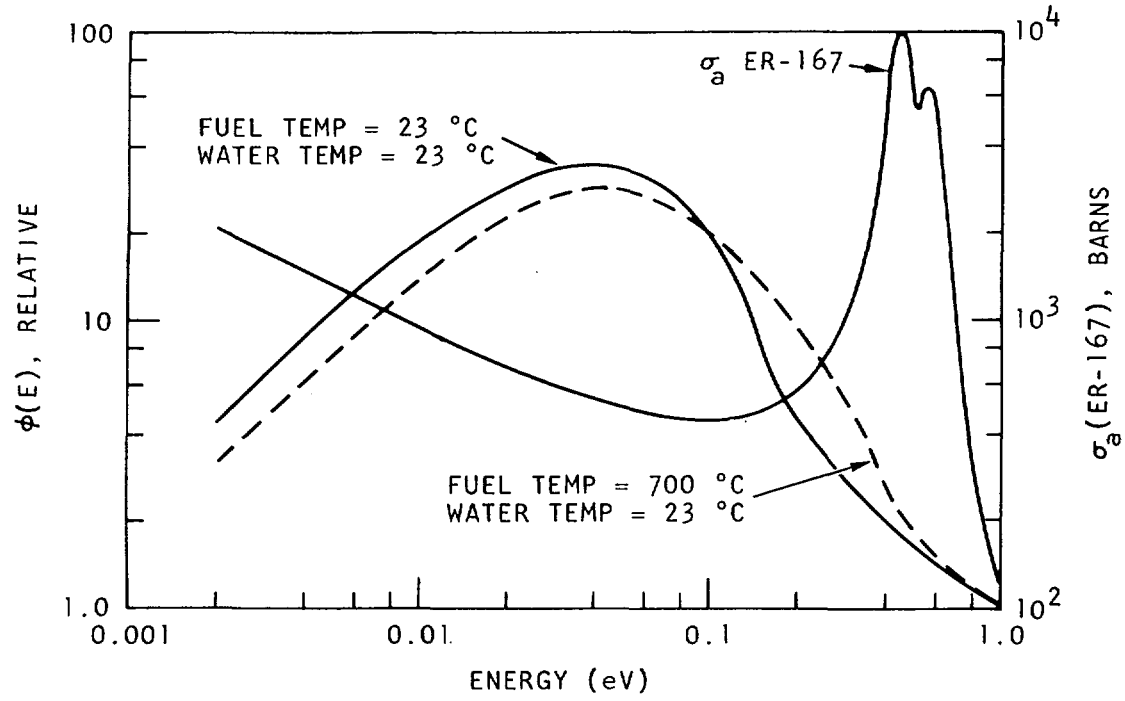

Fig. 7. Thermal neutron spectra versus fuel temperature relative to σ_a versus energy for Er-167

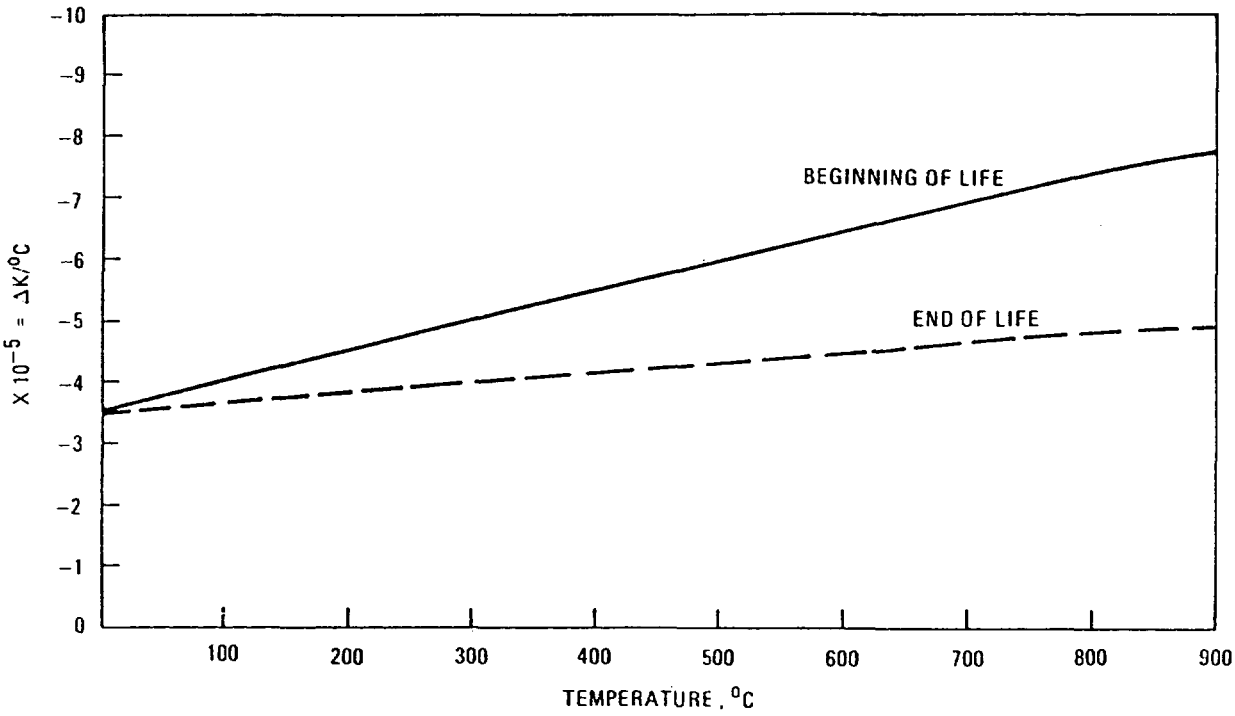

Fig. 8. Relative temperature coefficient as a function of temperature for beginning life and end of life

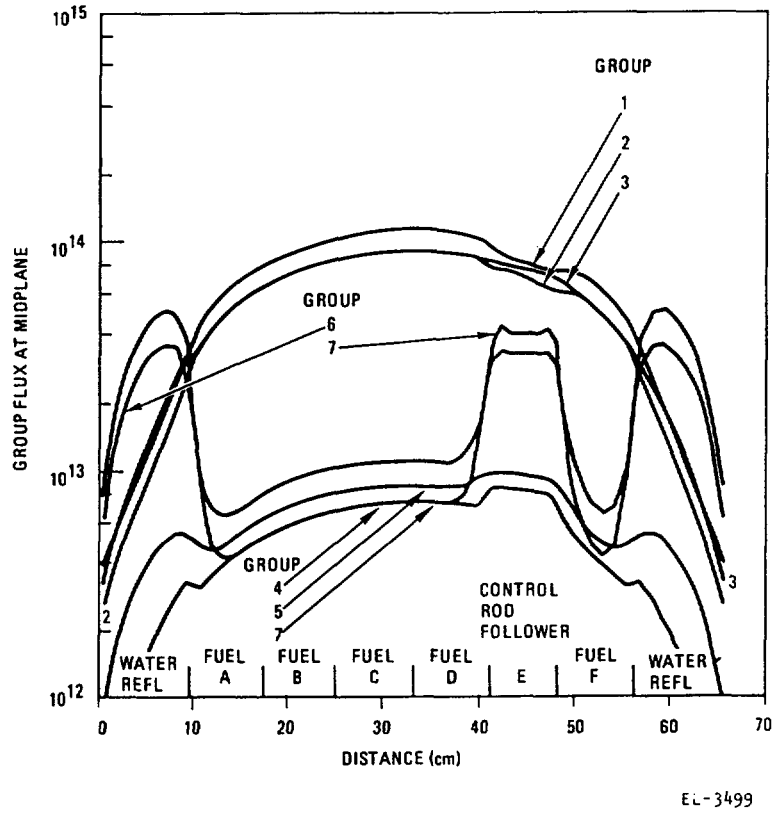

Fig. 9. Mid-plane flux at 10-MW; flux traverse through center of row 3 fuel (core has water reflector on all sides

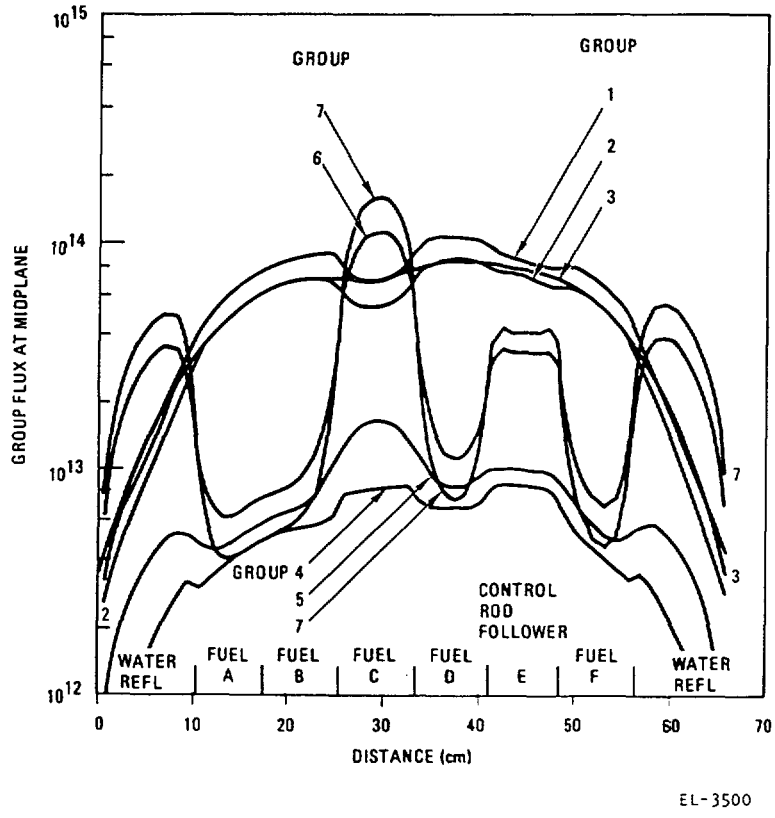

Fig. 10. Mid-plane flux at 10-MW; Flux traverse through center of row 3 fuel, water in C3 position (core has water reflector on all sides)

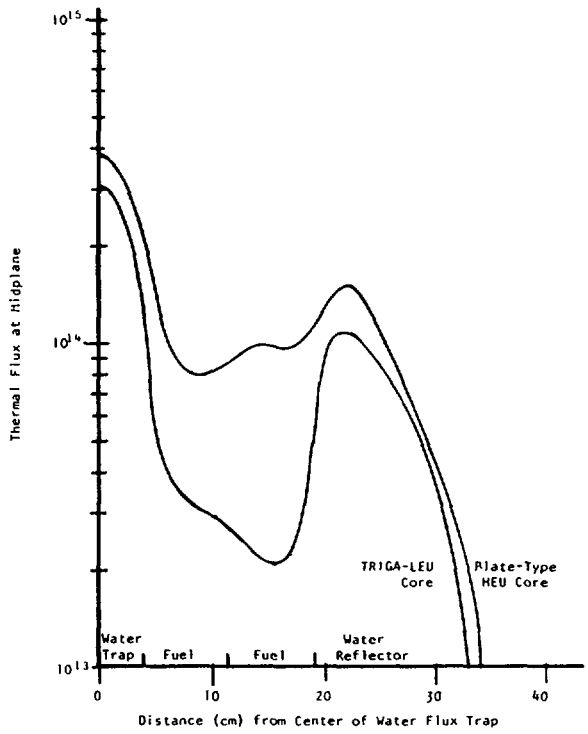

Fig. 11. Mid-plane thermal flux (<0.62 eV) at 10-MW for reactors with TRIGA-LEU fuel and plate-type HEU fuel

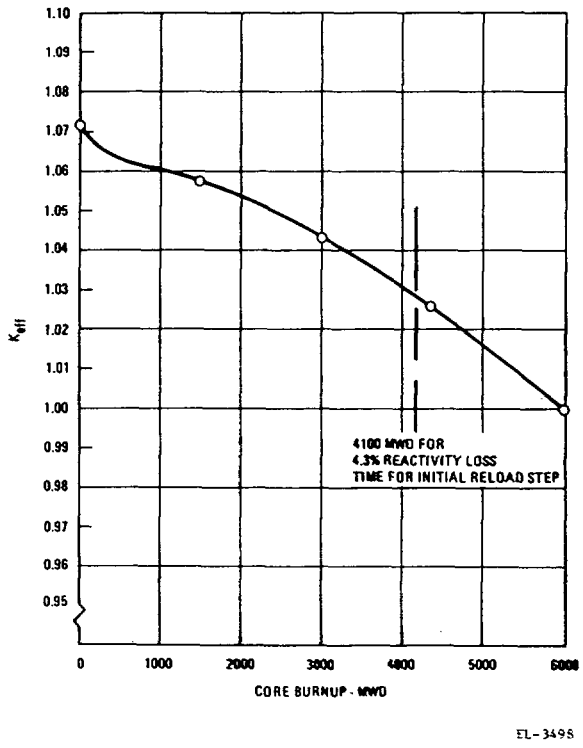

Fig. 12. K_{eff} as a function of core burnup for reference design

5. HEAT TRANSFER ANALYSIS

The heat transfer analysis established the range of operating parameters in the core which would meet the criteria of:

1. Fuel temperature below 750°C
2. Reasonably high DNB* ratio
3. Fluid flow rates giving reasonable pressure drops through the core

The analysis was broken down into two parts:

1. Conduction of heat in the fuel rods
2. Convection of heat from the surface of the fuel rods

The heat generated in the fuel is conducted through the fuel, across the fuel-cladding interface, and through the cladding to the coolant. Although most of the temperature drop from the center of the fuel rod to the coolant takes place in the fuel, a significant drop occurs in the fuel-cladding interface. Special attention was given, therefore, to this fuel-cladding interface in the design of the fuel rod.

The TIGER computer code was used to perform the thermal-hydraulic analysis of the steady-state reactor core. This code was originally developed by Westinghouse for the analysis of pressurized water reactors; hence, correlations applicable to 10 MW TRIGA conditions were added to the code. The TIGER code is a finite difference solution of the one-dimensional momentum and energy transport equations. The output from the code includes the axial variations of flow rate, velocity, pressure drop, bulk coolant and surface temperatures, and DNB ratio.

The forced convection heat transfer coefficient h was determined with the Dittus-Boelter correlation as recommended by Tong and Weisman:

$$Nu = 0.023\ Re^{0.8}\ Pr^{0.4} \quad , \tag{1}$$

where Nu, Re, and Pr are the Nusselt, Reynolds, and Prandtl numbers, respectively, based on the bulk water properties. Various refinements to Eq. 1 are possible by considering film properties; however, these were not considered necessary and Eq. 1 was used, although it is somewhat conservative. Similarly, the pressure loss calculations were based on bulk properties, which also is conservative. Although Eq. 1 was derived from experiments in tubes, it has been shown, as discussed by Tong, that it is valid for fuel cluster geometries provided the equivalent hydraulic diameters of the subchannels are used. In fact, for the fuel rod pitch-to-diameter ratios in the 10 MW TRIGA, the leading coefficient in Eq. 1 is actually smaller than some published values, and hence conservative. In forced convection the heat flux and the wall and bulk temperatures are related by

$$q_{fc} = h\ (T_w - T_b) \quad , \tag{2}$$

where q_{fc} = forced convection heat flux (Btu/hr-ft^2),

h = forced convection heat transfer coefficient (Btu/hr-ft^2-°F),

T_w = wall temperature (°F)

T_b = coolant bulk temperature (°F)

*Departure from nucleate boiling (ratio of critical heat flux to calculated heat flux).

At certain pressure and temperature conditions an incipient heat flux, q_i, exists at which isolated vapor nucleations occur on the cladding surface. The correlation used with the Dittus-Boelter relationship (Eq. 1) to predict q_i was reported by Bergles and Rohsenow as follows:

$$q_i = 15.60\ p^{1.156} \Delta T_s^{\alpha} \quad , \qquad \alpha = 2.30\ p^{-0.0234} \quad , \tag{3}$$

where p = absolute pressure (psia)
T_s = degree of superheat (°F) (the surface temperature minus the saturation temperature),
q_i = incipient heat flux (Btu/hr-ft^2).

At heat fluxes above q_i more nucleation sites are created on the cladding surface so that the heat is removed partly by forced convection and partly by local, subcooled nucleate boiling. Eventually, at still higher heat fluxes, the surface is uniformly covered by a dynamic bubble-layer and the heat is removed by fully developed, subcooled nucleate boiling. The correlation used for this mode of heat transfer is due to McAdams et al:

$$q_{fd} = 0.074\ \Delta T_s^{3.86} \quad , \tag{4}$$

where q_{fd} is the heat flux for fully developed, subcooled nucleate boiling (Btu/hr-ft^2). In the transition region, between forced convection and fully developed, subcooled nucleate boiling, Eqs. 2 and 4 were interpolated by a scheme due to Bergles and Rohsenow. Since the heat flux is specified for the TRIGA fuel rod, Eqs. 1 to 4 and the interpolation scheme can determine the surface temperature. This is done in TIGER.

In the fully developed nucleate boiling regime it is possible to increase the heat flux further without an appreciable change in the surface temperature, until the bubble motion on the surface becomes so violent that a hydrodynamic crisis occurs with the formation of a continuous vapor film on the surface. This is termed departure from nucleate boiling (DNB) and the heat flux is the critical heat flux (CHF). The ratio of the CHF to the actual heat flux is the DNB ratio. In subcooled boiling the CHF is a function of the coolant velocity, the degree of subcooling, and the pressure. The correlation used to predict CHF is due to Lund which was developed from empirical data gathered from an experiment conducted on a test assembly that conformed to the actual fuel bundle in terms of dimension, flow, and heat flux. The critical heat flux is given by

$$q_c = 0.5\ f_c\ \rho\ V_g\ C_p\ (T_c - T_o) \quad , \tag{5}$$

where f_c = friction factor for the channel between fuel rods
$= 0.55\ Re_g^{-0.37}$
Re_g = Reynolds number for the interrod channel
$= 2\rho V_g D_r\ (S-1)/\mu_{sat}$
V_g = interrod channel velocity
$= V\ \left[1.0 - 0.98\ e^{-2.2(S-1)}\right]$
S = pitch-to-diameter ratio
D_r = rod diameter, ft
V = average velocity, ft/hr
ρ = density, lb/ft^3

μ_{sat} = viscosity at saturation temperature, lb/ft. hr.

C_p = constant pressure specific heat, Btu/lb°F

T_o = temperature at outlet of cooling channel, °F

T_c = critical wall temperature, °F

The critical wall temperature is given by

$$T_c = T_{sat} (1 + 6 \sqrt{\theta_c})$$

where

T_{sat} = saturation temperature

$\theta_c = q_c \sigma_{sat} / p \mu_{sat} h_{fg}$

σ_{sat} = saturation surface tension, lb/ft

p = absolute pressure, lb/ft^2

and h_{fg} = heat of vaporization, Btu/lb

The design flow rate has a lower limit determined by the value of the CHF at that flow rate; the larger the flow rate the larger will be the CHF and hence the safety margin. The flow rate also has an upper limit which is determined by the maximum allowable pressure drop through the bundle to avoid cavitation in the flow system. In TIGER, pressure losses are calculated using the friction perimeter and area of the cluster with the standard Blasius formula for turbulent pipe flow. In addition, there are provisions for head loss coefficients along the flow channel to account for the presence of spacer grids. The values used in TIGER for the head loss coefficients were derived from measured pressure drops through a fuel element cluster that was hydraulically equivalent to the 10 MW TRIGA fuel cluster. In the 10 MW TRIGA design there is a large range of feasible flow rates between the upper and lower limits.

The contact pressure or the interface gap between the fuel rod and the clad are computed by TIGER, given the temperature distribution and the initial (cold) gap. Assuming a parabolic temperature distribution, which closely approximates the temperatures in the fuel, the expansion of the fuel material is calculated as a nonlinear function of the temperature. The cladding expansion is proportional to the average cladding temperature. When the power generation in the fuel increases, a temperature distribution is reached where the fuel expands more than the cladding, narrowing the initial interface gap until contact occurs between the fuel and cladding. At this point the fuel and cladding may interact and develop a contact pressure between the fuel and cladding which can increase until the yield stress of the cladding is reached, beyond which no further increase in pressure occurs.

The results of the thermal-hydraulic analyses, using the design conditions in Table 10, are summarized in Fig. 13. The abscissa is the axial distance from top to bottom of the heated length of the cluster. The ordinates are heat flux, fuel temperature, cladding temperature, and water temperature. The results are shown for the hot channel with a hot-rod factor of ∿1.8.

As can be seen from Fig. 13, the peak heat flux occurs at the horizontal mid-plane of the core, and the DNB ratio is a minimum at this location. Only a small amount of local subcooled nucleate boiling is predicted for the hottest rods, and this may occur over the central region between the two spacers.

As discussed earlier, the largest temperature increase is in the fuel and at the fuel-cladding interface. At the horizontal mid-plane of the individual fuel rod, the beginning-of-life (BOL) radial gap between the fuel and cladding is 0.0005 in. and the gap is filled with helium. This results in an interface conductance of approximately 2400 Btu/hr-ft^2. As the fuel burns up, radiation-induced swelling will cause this gap to close, and this will reduce the peak fuel temperature. The calculated peak fuel temperature at BOL is 640°C, which is well below the design maximum of 750°C.

Figure 14 shows the variation in temperature within a fuel rod as a function of rod power density.

The effects of design variables and off-standard conditions have been evaluated to determine the amount of margin existing in the design point selected for the steady-state reactor core. The results of the thermal-hydraulic tests correlating critical heat flux and flow rate for minimum clearance between rods have been used in the design analysis summarized in Fig. 15. For the limiting design conditions described in Fig. 15, including fuel rods bent to give only a 0.0762-cm (0.030-in.) clearance, the critical heat flux is a factor of 1.3 greater than the operational heat flux at 10 MW [coolant flow rate of 18,900 liters/min (5000 gpm), hot-rod factor of 2.0]. It is also seen from Fig. 15 that a flow rate of about 8300 liters/min (2200 gpm) will allow 5 MW operation with a critical heat flux about 1.4 times the operational heat flux. Thus, existing reactor systems with the lower flow rate can be upgraded to TRIGA fuel and can operate at about 5 MW until additional cooling capability is installed to permit 10 MW operation.

TABLE 10
DESIGN CONDITIONS USED FOR THERMAL ANALYSIS OF THE 10-MW TRIGA REACTOR

Fuel pellet diameter, cm (in.)	1.29 (0.508)
Cladding outside diameter, cm (in.)	1.37 (0.540)
Heated length, cm (in.)	55.9 (22.0)
Inlet temperature, °C (°F)	37 (98.6)
Bulk coolant temperature rise @ 5000 gpm, °C (°F)	7.7 (13.8)
Inlet pressure, kPa (psia)	174 (25.2)
Core pressure drop @ 5000 gpm, kPa (psi)	68.9 (10)
Cluster flow area per rod, cm^2 ($in.^2$)	1.37 (0.213)
Cluster hydraulic diameter, cm (in.)	0.91 (0.36)
Cluster mass velocity, kg/sec-m^2 [lb (mass)/hr-ft^2] (equivalent to 5000 gpm per 30 clusters)	4780 (3.526×10^6)
Inlet pressure loss coefficient (converting one velocity head)	3.2
Spacer pressure loss coefficient (each)	0.4
Outlet pressure loss coefficient (converting one velocity head)	0.8
Hot rod factor	1.8
Core average heat flux, W/cm^2 [Btu/hr-ft^2]	86.4 ±4.4 [(2.74 ±0.14) x 10^5]
Initial fuel-cladding radial gap, μ (in)	22.2 ±9.5 (0.00087 ±.00037)
Fuel-cladding surface roughness, μ (μin.)	0.813 ±0.203 (32 ±8.0)
Cladding thermal conductivity, W/m °C (Btu/hr-ft-°F)	16.8 ±0.7 (9.7 ±0.4)
Fuel thermal conductivity @ 1000 °F W/m °C (Btu/hr-ft-°F)	21.6 ±2.6 (12.5 ±1.5)
Fuel-cladding gap helium gas conductivity, W/m °C (Btu/hr-ft-°F)	0.199 ±0.026 (0.115 ±0.015)
Fuel-cladding gap helium gas partial pressure, kPa (psia)	10.1 (1.47)
Cladding thermal expansion coefficient, $°C^{-1}$ ($°F^{-1}$)	(17.2 ±0.5) x 10^{-6} [(9.53 ±0.28) x 10^{-6}]

TABLE 10 (continued)

Cladding hardness to yield stress ratio	6.4 ±0.6
Fuel linear thermal expansion coefficient, $°C^{-1}$ ($°F^{-1}$)	$(4.18 \pm 0.22) \times 10^{-6}$ [$(2.32 \pm 0.12) \times 10^{-6}$]
Fuel second-order thermal expansion coefficient, $°C^{-2}$ ($°F^{-2}$)	19.2×10^{-9} (5.94×10^{-9})
Cladding yield strength, MPa (ksi)	251.5 (36.5)
Cladding elasticity modulus, MPa (ksi)	188,000 (27,400)
Fuel elasticity modulus, MPa (ksi)	75,900 (11,000)

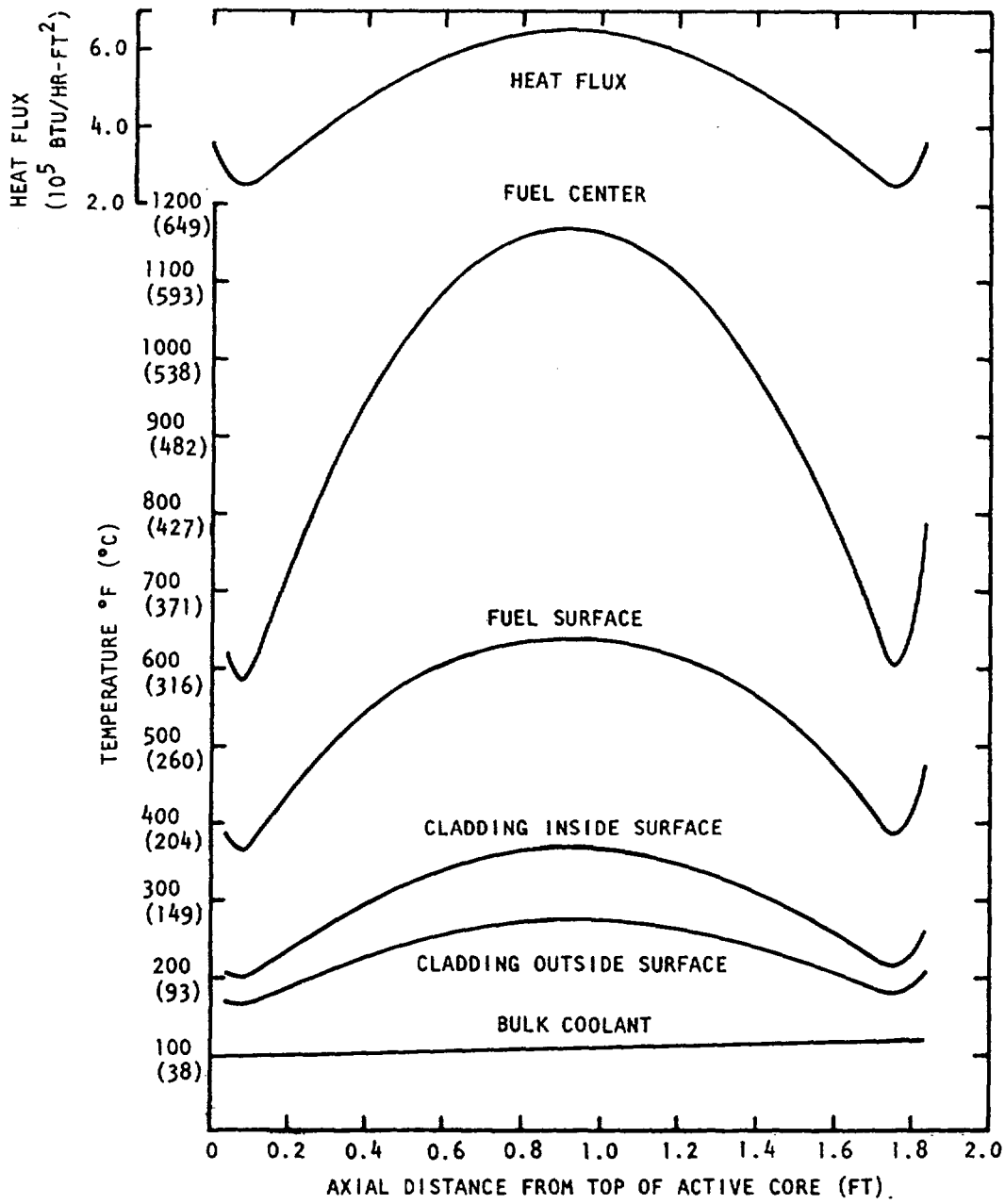

Fig. 13. Axial temperature profiles of the 10-MW TRIGA-LEU design (hot channel, hot-rod factor ∿1.8)

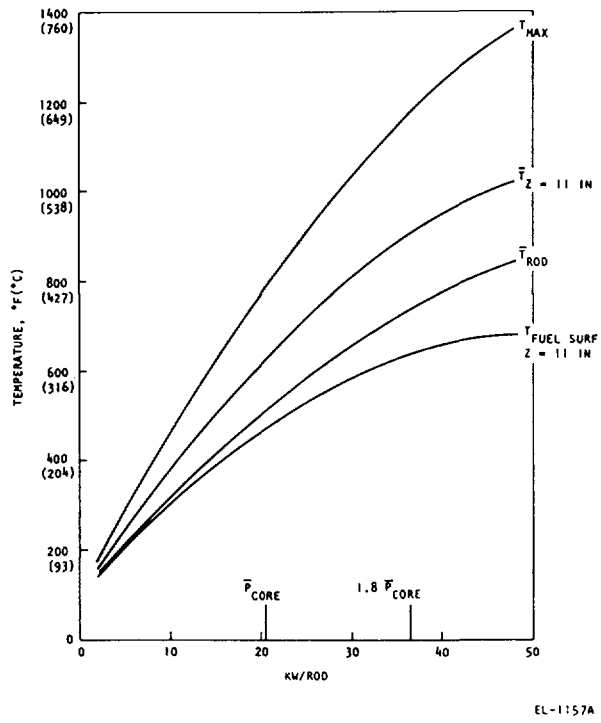

Fig. 14. Temperature as a function of kW/rod

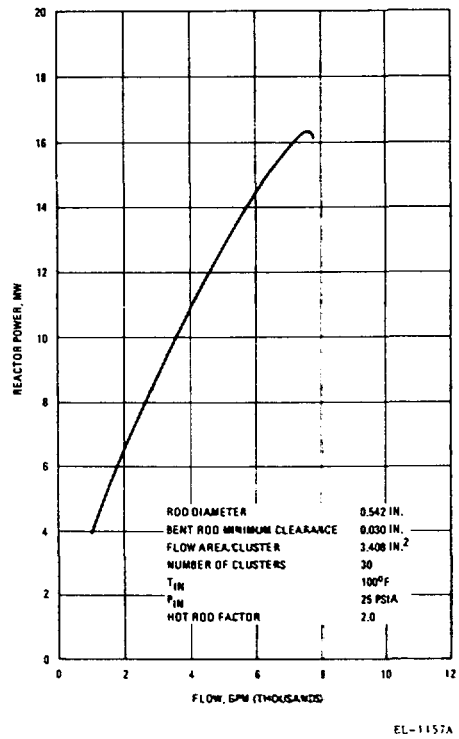

Fig. 15. Critical heat flux power versus flow for 16-rod clusters

APPENDIX C

FRG Generic Enrichment Reduction Calculations

Performed by

INTERATOM

Internationale Atomreaktorbau GmbH
9120 Kernauslegung Therm. Reaktoren
Postfach
5060 Bergisch Gladbach 1
Federal Republic of Germany

ABSTRACT

The conversions of a generic 10 MW core to MEU fuel and a generic 2 MW core to LEU fuel were investigated.

The investigations used different criteria such as cycle length-, excess reactivity at beginning of cycle-, and fuel availability-criterion. Simplified RZ-models are tested against detailed XY-models. Detailed flux distributions before and after conversion are presented for comparison. For the 2 MW-core different ways of redesign of the fuel element are taken into account including their influence to safety margins by thermal-hydraulic assessment.

Introduction

This paper is the contribution of the consultants of the Federal Republic of Germany to "IAEA-Guidebook on Research Reactor Conversions from the Use of high enriched Uranium to the Use of low enriched Uranium". The contribution is prepared by INTERATOM, Internationale Atomreaktorbau GmbH, Bergisch Gladbach 1 on behalf of the Minister of Research and Technology of the Federal Republic of Germany. The paper describes the different calculations and investigations done. The results will enable reactor users willing to convert their reactor to assess their specific problem. They also show what are the differences after converting the cores. Therefore the paper deals with two typical cases:

- the conversion of a 10 MW-core with HEU-fuel to fuel with reduced enriched uranium (REU-fuel), here with 45 weight % U235 (part 2.1)

- the conversion of a 2 MW-core with HEU fuel to fuel with reduced enriched uranium (REU-fuel), here with 20 weight % U235 (part 2.2)

These are the two examples agreed upon after discussions at the different meetings at the IAEA.

Moreover the methods of calculation are described in a separate chapter (part 2.3).

The results are mainly shown in graphs and tables. Thereby interpolations and extrapolations by the different users for their specific problems and given specifications such as fuel, power level, burnup, cooling conditions etc. will be simplified. Informations concerning further aspects such as dynamic behaviour, safety related problems, cost, shutdown reactivity etc. are not presented here. They will be part of the case by case studies of real cores. Furthermore we are willing to assist every user in solving his specific problems by specific calculations.

2 Conversions Examples

2.0 Principle Aspects of Calculations

2.01 Overview over the Different Fuels

In the following the calculations and results for the two typical core conversions are presented. It must be emphasized here, that all calculations within this paper are done for MTR-fuel only; other alternative fuels such as TRIGA-fuel and CARAMEL-fuel are not covered by this contribution.

First, to give an overview of all the different fuels calculated within this contribution, a plot of the different U235-loadings versus the uranium density necessary for these loadings is put ahead of (fig. 2.01). Parameters of this plot are the different number of fuel plates per fuel element*, the different enrichments used (93 weight %, 45 weight %, 20 weight %), and the different meat thicknesses of the fuel plates. Very helpful in this context is the figure 2.02 which shows the uranium weight percentage in the meat as a function of the uranium density based on the specifications of the German NUKEM-company and used in this contribution throughout.

2.02 Constant Parameters

Constant parameters for all the different fuels are

- the grid space per fuel element in the core (8.1 cm x 7.71 cm)
- the active length of the fuel used (60 cm)
- the kind of fuel (UAl_x- Al-cermet)
- the density of the coolant (water of density 0.9924 g/cm^3)
- the cladding and supporting material of the fuel elements (pure aluminium)
- the composition of the top and the bottom part of the fuel elements.

---

* same meaning as fuel assembly

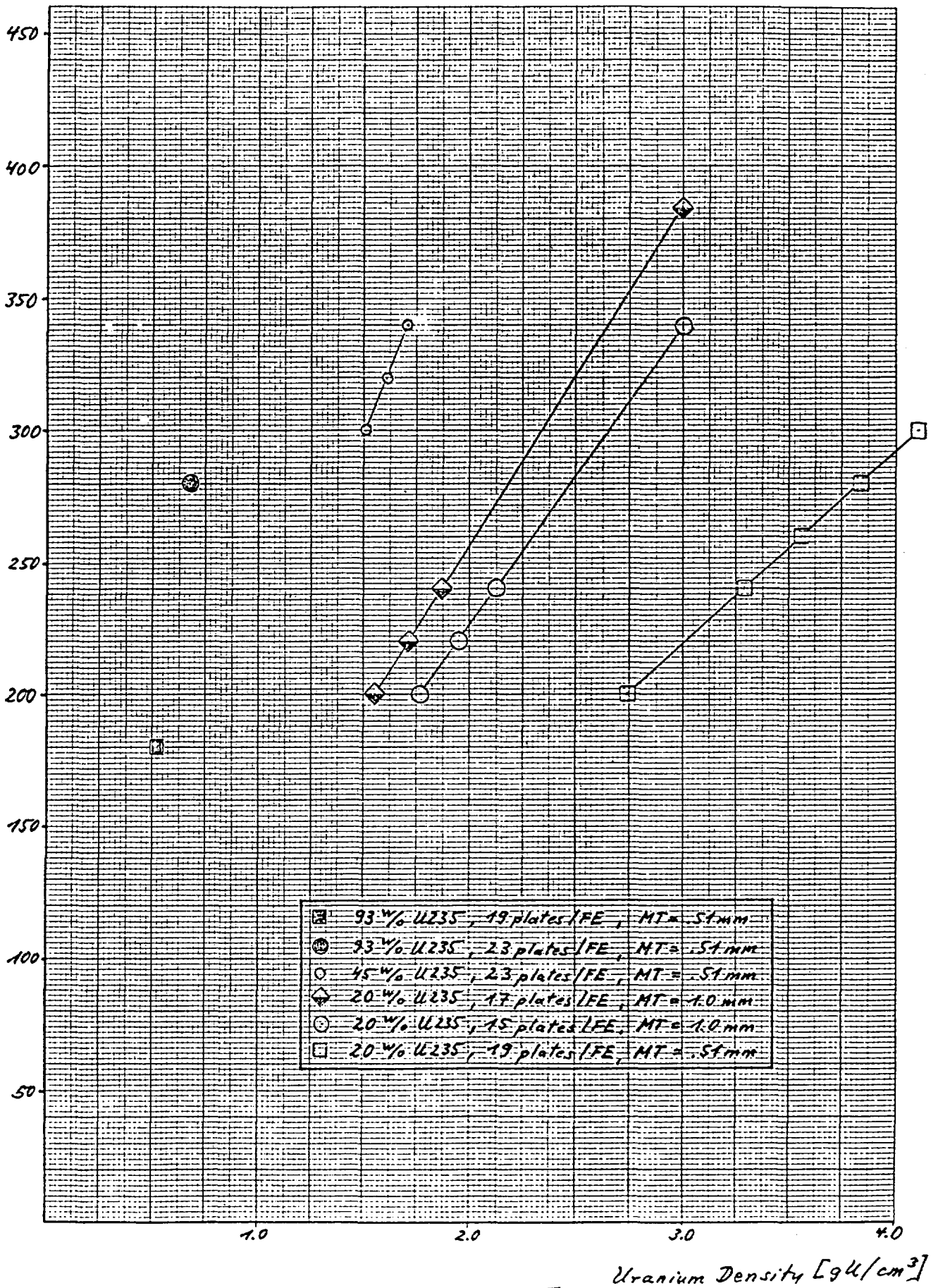

Uranium Loading [g U235/Fuel Element] versus Uranium Density [g U / cm³ Meat] for the different fuels used for calculations

2.0.1

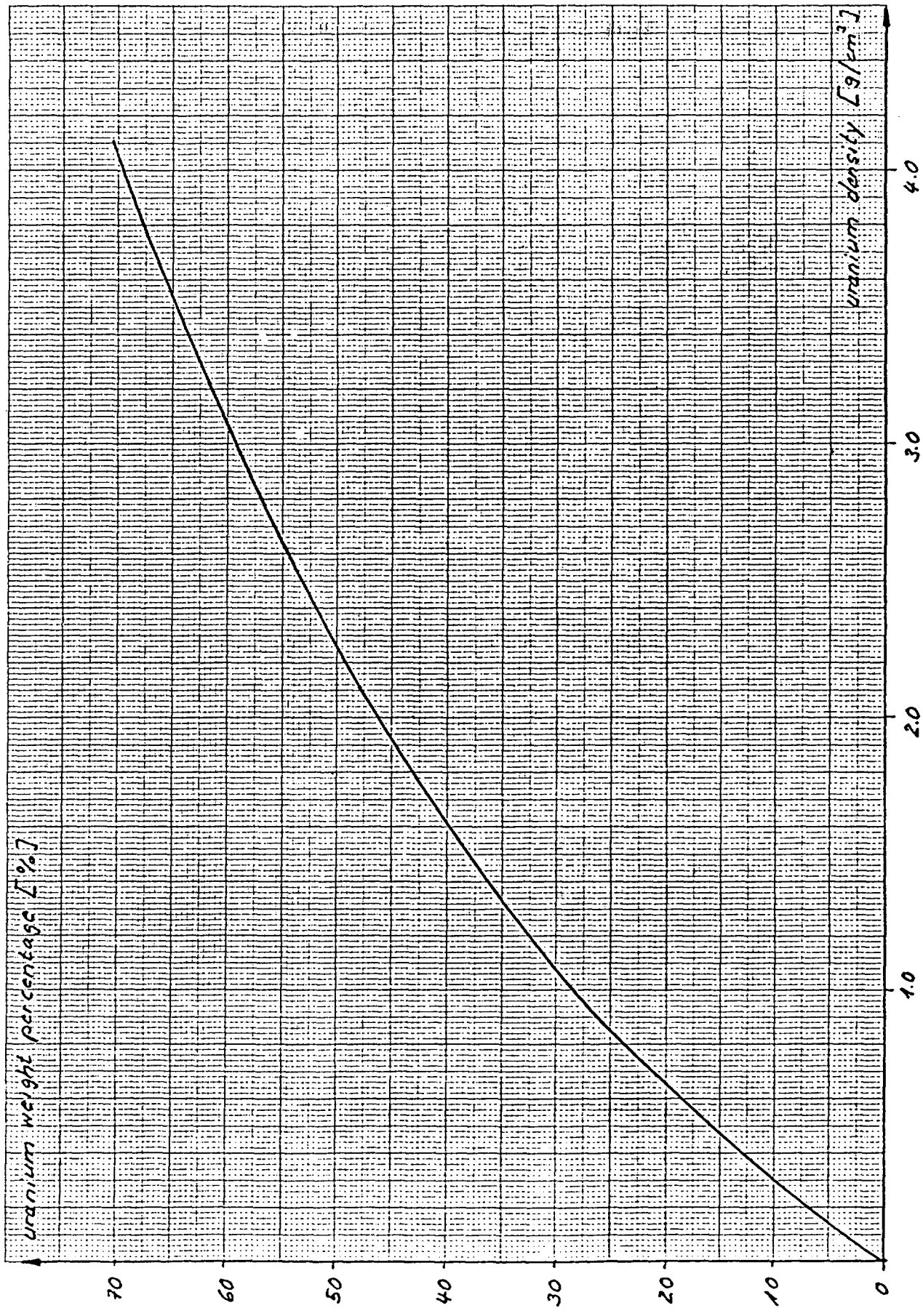

Uranium weight percentage versus Uranium density based on NUKEM-specifications

2.0.2

All these parameters are either of nearly no influence to the results within the range they are in use in the different MTR-fuel elements of the different manufacturers and/or for different users or are common parameters for all MTR-fuel elements worldwide.

2.03 Cross Section Calculation Results

The starting point of all core calculations was the preparation of cross sections for the different fuels including their dependency from the burnup. Most of the research reactor users express the burnup in percentage, which means the percentage loss of U235 during irradiation.

The so defined burnup-values depend on the enrichment and the U235-loading of the fuel. So, if one wants to compare different fuels (different U235-loadings and different enrichments) under the aspect of their burnup behaviour it might be better to use the MWd (Mega Watt days) or alternatively the FPD (Full Power days) as a measure of burnup. To demonstrate the different fuels in use here fig. 2.03 to fig. 2.06 show the infinite reactivity k_∞ as a function of the different burnup-descriptions for all fuels under discussion within this contribution. Specifically, looking at these figures, one can assess the loss of reactivity by parasitic absorption. This absorption is caused by the increase of U238-content when reducing the enrichment.

2.04 Criteria for the Determination of REU-Fuels

Starting from this basis of cross sections there are several ways to define and/or to calculate a REU-fuel that is appropriate to exchange the HEU-fuel. In a very early stage fo the discussions on this subject a simple reduction of the enrichment of the research rector fuel was under discussion without any change in the U235-loading per fuel element. This simple criterion is by no means appropriate to get a suitable REU-fuel as will be shown later. Therefore three criteria were stated to define a REU-fuel provided that the number of fuel elements in a typical working core * is kept unchanged:

---

* The two working cores (see fig. 2.1.17 and 2.2.18) used in the calculations throughout are typical examples of real cores only which are nevertheless appropriate to demonstrate the problems of the conversions even if a great number of different working cores is imaginable.

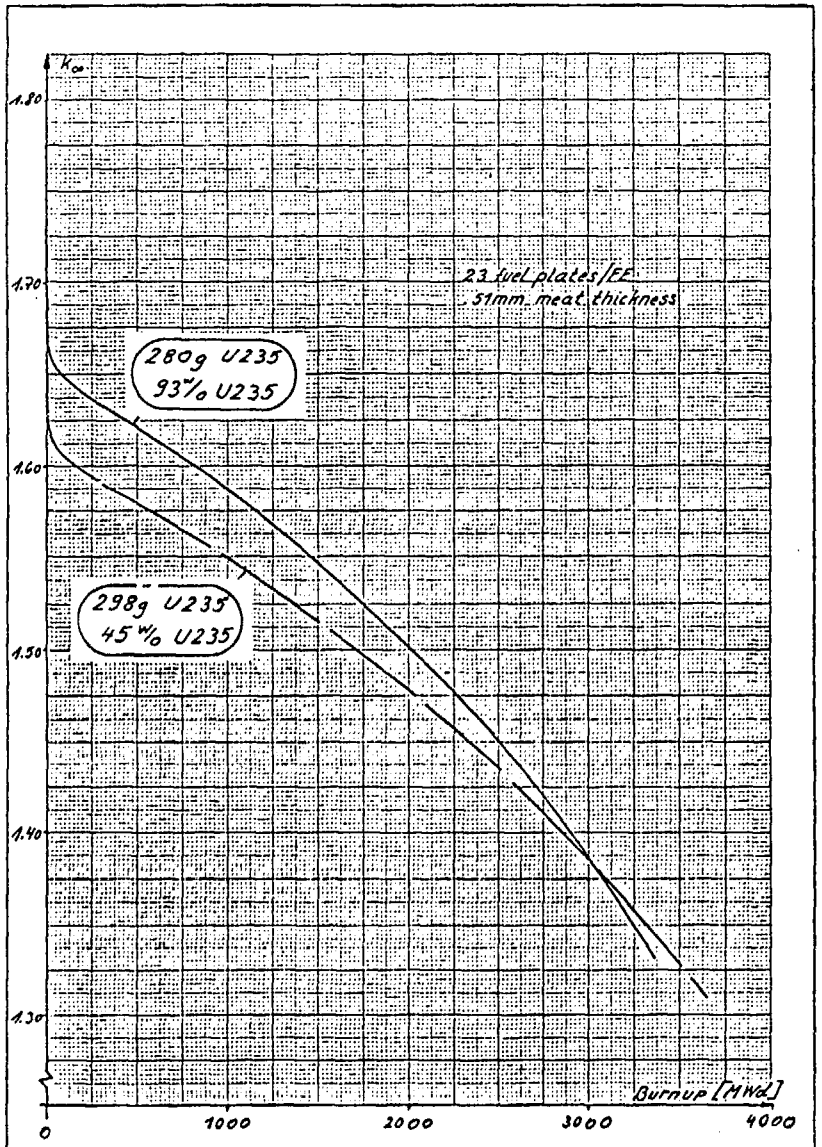

10 MW - Case Fuels

Reactivity (k_∞) vs. Burnup [MWd]

2.0.3

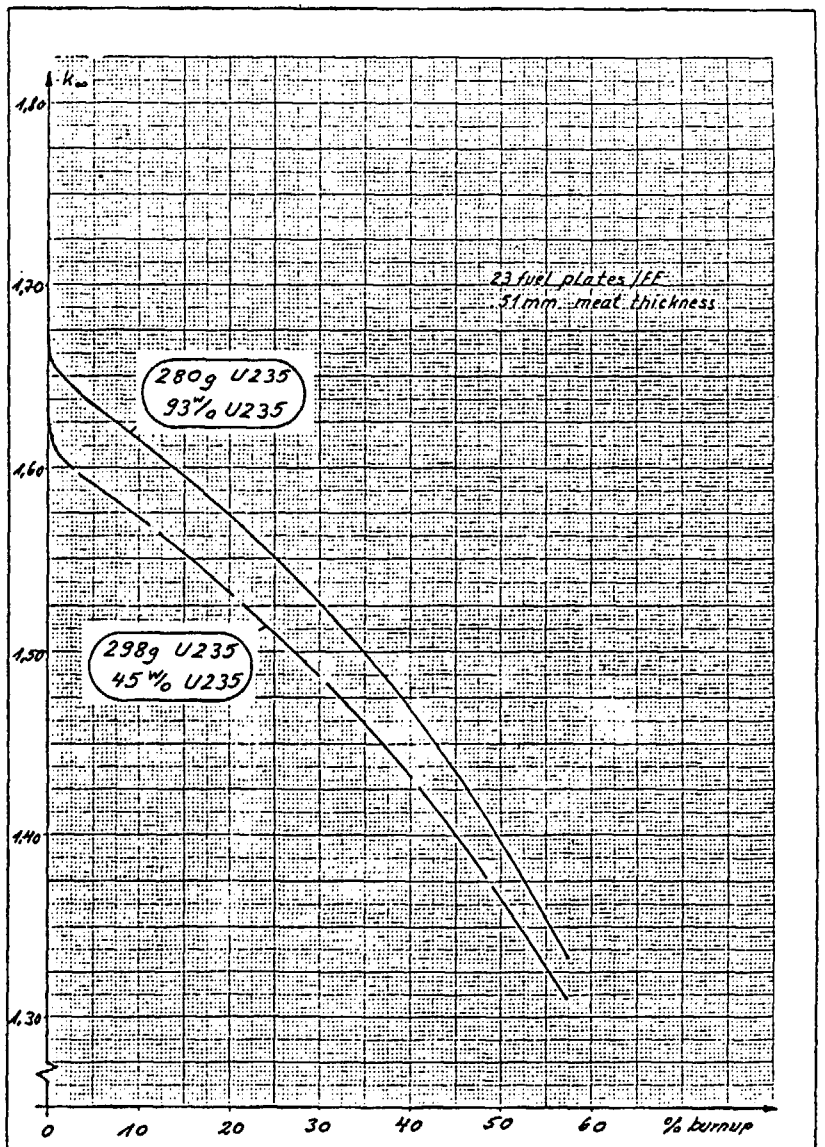

10 MW - Case Fuels

Reactivity (k_∞) vs. Burnup measured in loss of U235-content [%]

2.0.4

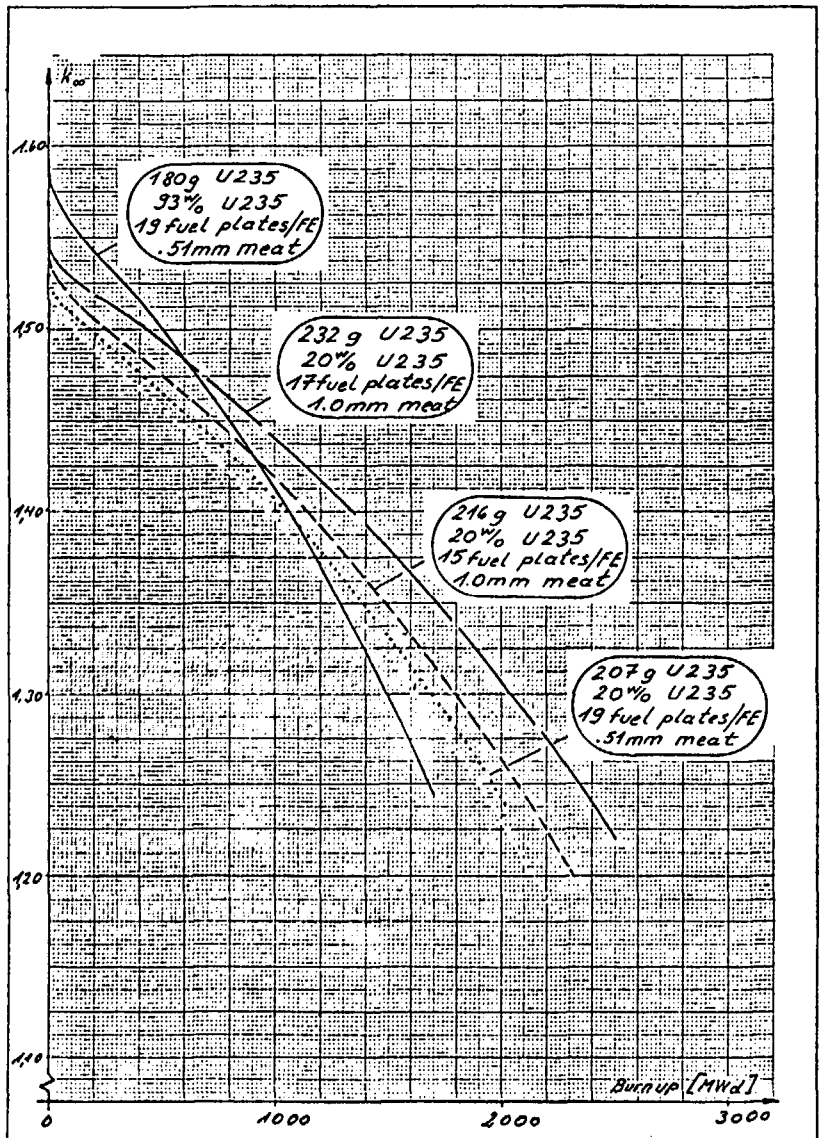

2 MW-Case Fuels

Reactivity (k_∞) vs. Burnup [MWd]

2.0.5

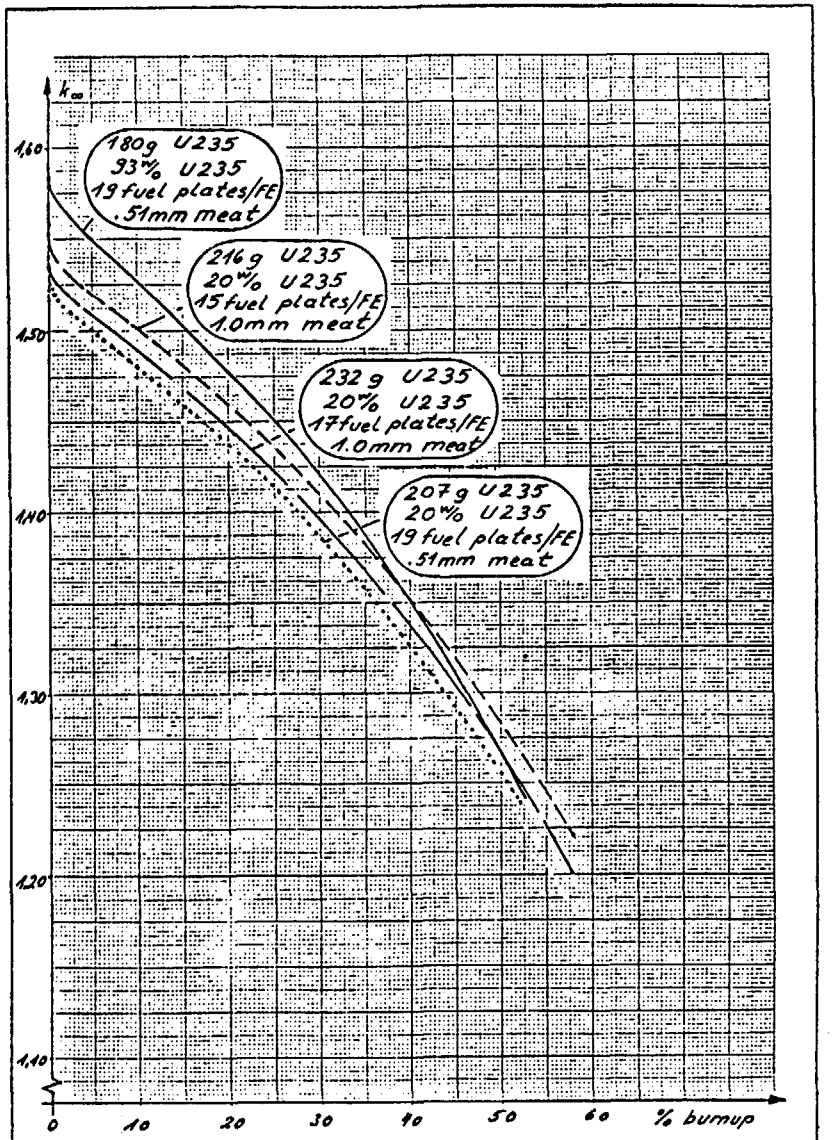

2 MW-Case Fuels

Reactivity (k_∞) vs. Burnup measured in loss of U235-content [%]

2.0.6

- from our point of view the user of a specific research reactor should be interested to get a REU-fuel, that produces the same excess reactivity at the core-state "End of Life" (EOL) as the HEU-fuel does. I. e. at the end of the same burnup-period measured in full power days the same reactivity binding by experiments and the same flexibility for changes of power levels is to be provided. It must be stated here, that as a consequence of this criterion the excess reactivity of the core build up from REU-fuel is reduced at the core-state "Begin of Life" (BOL).

  But this is by no means a disadvantage. Normally a higher part of the excess reactivity at BOL must be compensated by control rods. So a reduction of the excess reactivity at BOL only without any reduction at EOL seems to be a slight advantage. In the discussions following we call this criterion the EOL-excess reactivity matching criterion or, more shortened the EOL-criterion.*

- on the other hand it is stated very often that the REU-fuels should provide no disadvantage and in consequence it is demanded to stay with the same excess reactivity at BOL, sometimes even for the totally fresh core (first core). If one starts with this criterion at least for a typical working core there are two main consequences: the burnup-period of this core will increase - a desirable aspect - and caused by a slight reduction of the shutdown reactivity of the unchanged number and kind of control rods - the reactivity binding at BOL will be more problematic. These facts will sometimes even prevent from going this way. But of course it is possible to use a fuel matching this criterion only in principle. To outflank the problems of reactivity compensation one has to shorten the irradiation period in a way that the BOL-excess reactivity can be compensated by the specific control mechanism at the reactor. Then the total burnup attainable is still enlarged in comparison to the HEU-fuel. This criterion we call the BOL excess reactivity matching criterion or more shortened the BOL-criterion.

---

* This criterion is called the cycle length criterion in parallel contributions.

- a third kind of criterion we want to use in our discussion faces the feasibility of fuel fabrication here limited to the UAl_x-Al-fuel. If one tries to use the maximum uranium density feasible to find out what improvements are possible in changing from the HEU-fuel to the fuel with reduced enrichment, one has to look at the table within part 3, wherein the different fabricators of fuel have fixed their limits.
  In the discussion of this contribution we use the limits given by the German NUKEM-company, which are in agreement with the German fuel development program. There we have a near-term availability of uranium density of 1.7 g/cm^3. For long term availability the corresponding figure is 3.0 g/cm^3.
  In discussions this criterion is called the fuel availability criterion.

In the meetings of the participants the EOL-criterion was determined as the basic criterion to define the REU-fuel. So this criterion is used at first.

2.05 Core Calculation Models

As mentioned above there are many ways of calculating the cores, too. Typical calculation models are 2-dimensional RZ- or XY-geometry diffusion calculations in 4 energy groups. Differences also result from the different way of dealing with the burnup and xenon-distributions over the core cross sections, the distribution of areas free of fuel (irradiation positions, control rod areas), the xenon state (xenon-free, xenon-equilibrium, xenon-override) etc. To simplify the calculations necessary the participants have agreed to use a simple RZ-model with a constant burnup averaged for the whole core as a first step.

In extension other models and details should check the validity of the results of this first step.
So this contribution starts with RZ-diffusion calculations and than adds a lot of other details and proves to this first step for both cores under consideration.

2.1 The 10 MW -Reactor

2.1.1 Prerequisites

The case of the conversion of the core of a 10 MW-reactor is chosen first because in this case it is in a way simpler to demonstrate how the conversion may work. This is caused mainly by the prerequisites resulting from the higher power level. Taking into account the cooling conditions of most of the reactors in question for a conversion it is advisable not to reduce the number of fuel plates. Otherwise the specific power per fuel plate will grow up and the heat dissipation will become more problematic, i. e., the safety margins of the onset of nucleate boiling and of the departure of nucleate boiling will be reduced.

2.1.2 Fuel Element

So, for this specific 10 MW-case we kept the fuel element geometry unchanged. The main data of this specification are presented in table 2.1.1 together with the different fuels used for the conversions described later. In addition figure 2.1.1 shows a detailed drawing of the fuel element used for all the calculations in connection with the 10 MW reactor conversion.

2.1.3 REU-Fuel Determination by RZ-Calculations

The cross section sets made available for the core calculations are presented by their k_∞ versus burnup-behaviour in fig. 2.03 and 2.04 resp. They are used in the simplified RZ-model shown in fig. 2.1.2 to get the reactivity and flux distributions

- for the state BOL without xenon
- for the state BOL with xenon equilibrium
- for the state EOL with xenon equilibrium

First we made this calculation for the basic fuel (280 g U235 per fuel element with 93 weight % U235) and afterwards we tried to find the U235-loading of the enrichment reduced fuel (45 weight % U235) as shown in fig. 2.1.3 using the EOL-criterion. The specifications of this REU-fuel are given within table 2.1.1. With this U235-loading from the intersection in fig. 2.1.3 we calculated the two BOL-states for this REU-fuel. The result of this method was

298 g U235-loading at 45 w/o-U235.

Table 2.1.1: Fuel specifications / 10 MW-case

	HEU-fuel	REU-fuels		
		EOL reactivity matching basis	BOL reactivity matching basis	Uranium density 1,7 g/cm³ *
number of fuel plates	23	23	23	23
meat volume/FE	441.635 cm³	441.635 cm³	441.635	441.635 cm³
inner water gap width	0.223 cm	0.223 cm	0.223 cm	0.223 cm
grid space per FE	8.1cmx7.71cmx60.0cm	8.1cmx7.71cmx60.0cm	8.1cmx7.71cmx60.0cm	8.1cmx7.71cmx60.0cm
meat thickness	0.051 cm	0.051 cm	0.051 cm	0.051 cm
U235 loading/FE	280 g U235	298+ g U235	307 g U235	338 g U235
enrichment	93 w/o U235	45 w/o U235	45 w/o U235	45 w/o U235
uranium loading/ fuel plate	13.090 g U	28.792 g U	29.662 g U	32.657 g U
Uranium density	.682 gU/cm³	1.50 gU/cm³	1.545 gU/cm³	1.70 gU/cm³
Weight percentage/ meat	20.85 w/o U	37.9 w/o U	38.7 w/o U	41.3 w/o U
moderation ratio at BOL averaged burnup (25 % for HEU-fuel)	261	240	231	205

* this value was chosen because it is a near term gain of the German Fuel Development Program

\+ result of RZ-calculations; XY-calculations show 295 g U235 instead of the 298 g U235

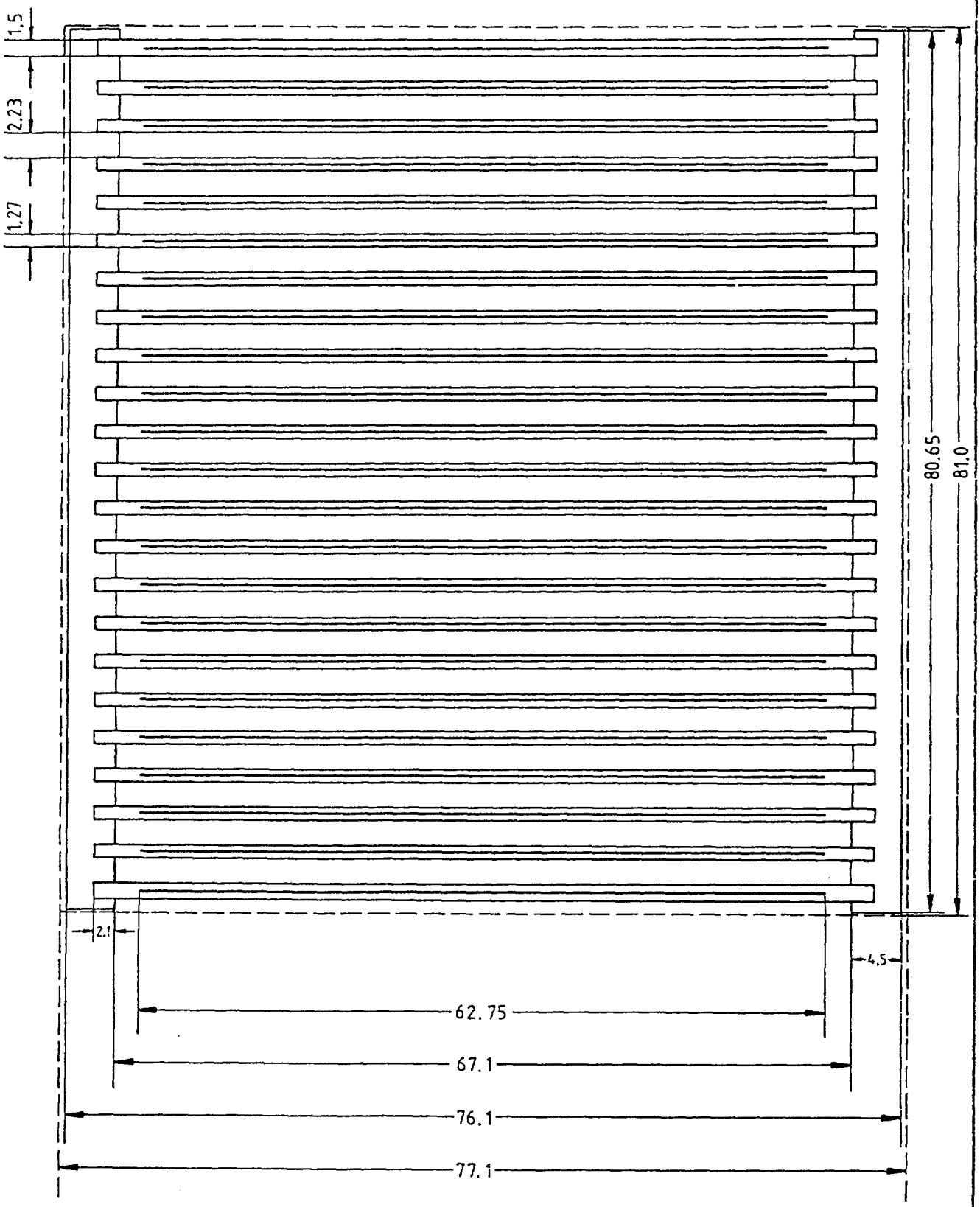

all dimensions in mm

10 MW - CORE
FUEL ELEMENT GEOMETRY
(HORIZONTAL CROSS SECTION)

2 : 1 . 1

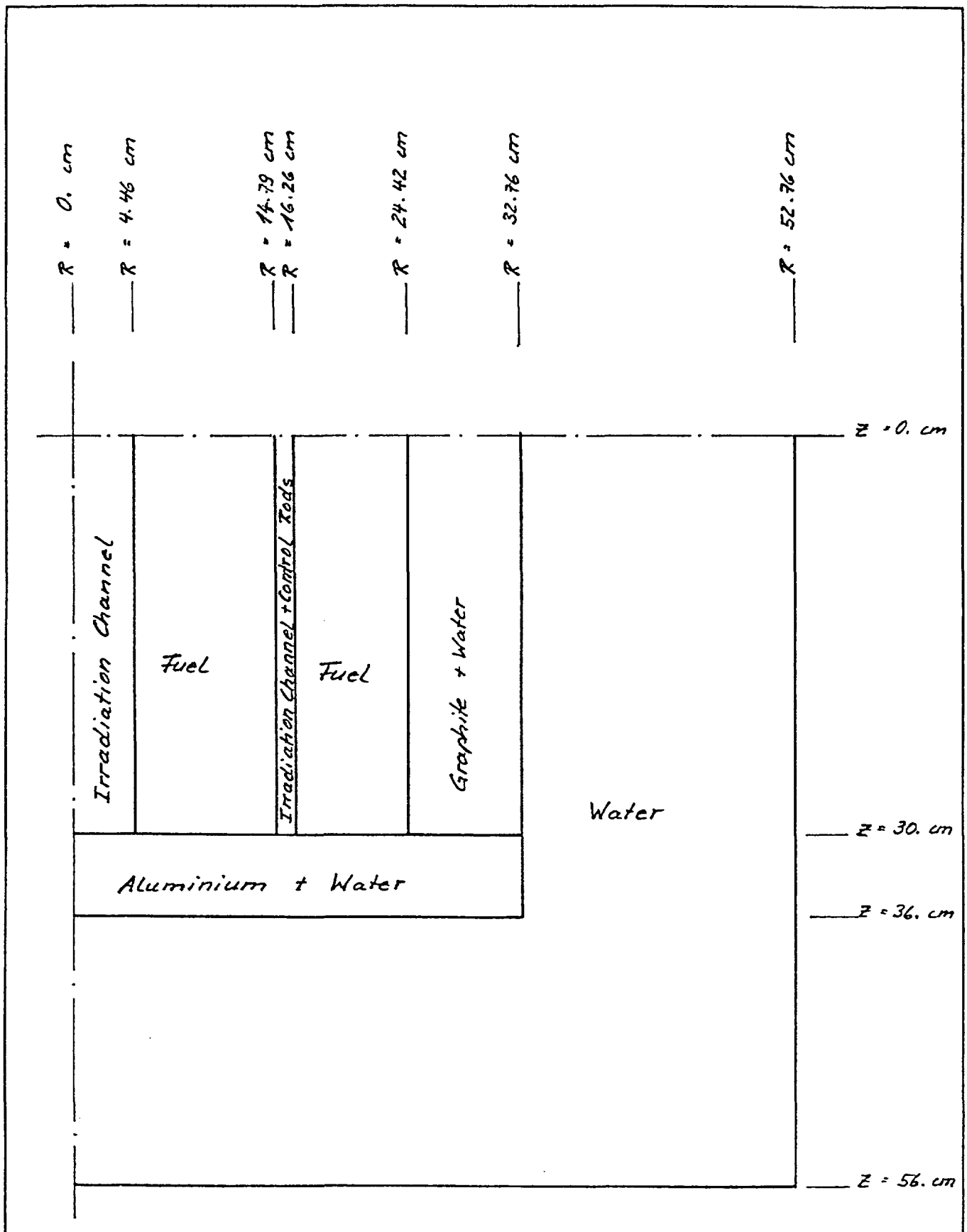

10 MW - Core
RZ - Model for Diffusion Calculation

2.1.2

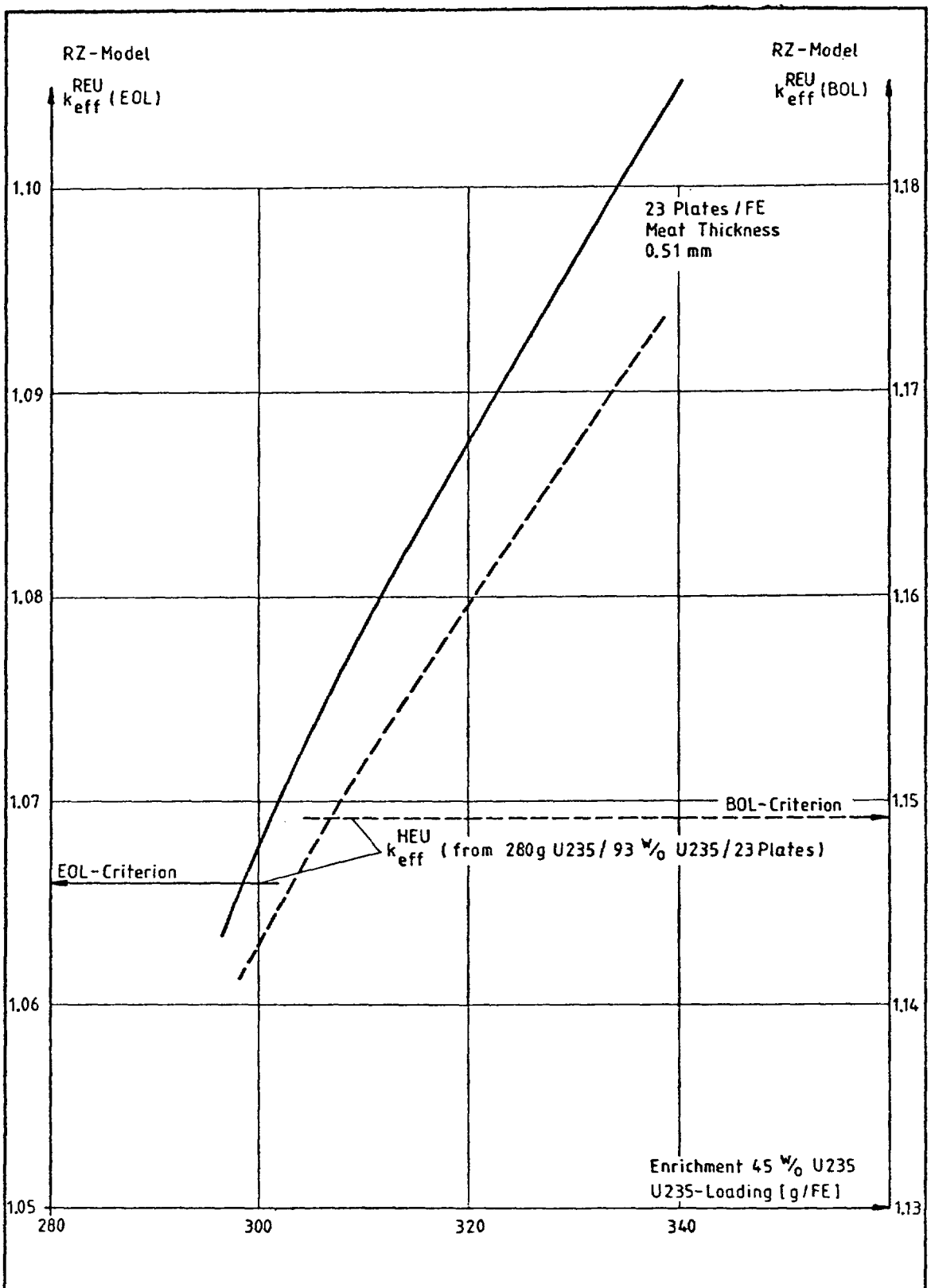

10 MW-CORE-CONVERSION
BURNUP [FPD] MATCHING BASIS WITH
EQUAL EXCESS REACTIVITY
DETERMINATION OF U-LOADING FOR CONVERSION

2.1.3

The results are put together in fig. 2.1.4 in the way of plotting k_{eff} versus burnup.

The values of burnup in percentage are correct only for the HEU-fuel. So the abscissa scaling is somewhat voluntary, only the burnup step from BOL to EOL with 58.7 full power days is correct for both fuels under consideration.

The results in fig. 2.1.4 show the typical reduction of excess reactivity at BOL of $\Delta\rho \approx 6$ o/oo.
It must be mentioned here that all the reactivities given in the figures and tables are pure calculation values. On the other hand we learned from comparing the calculations for the benchmark, that the absolute reactivities are in good agreement to the figures of other contributors.

Moreover this affects the results in view to the determination of the REU-fuel under the different criterions by no means. The somewhat flattened burnup behaviour of the reactivity is a typical effect of the fuel with higher uranium content, too. It gives some advantage in the reactivity binding measures during the irradiation period.

One of the main purposes of this calculations was to find out the loss in flux level within the core, the irradiation positions, and the reflector. To show the influence of the REU-fuel the differences in flux are to compare within 3 energy groups (fast flux, epithermal flux, thermal flux).
A detailed nomenclature of the flux figures is given separately by table 2.1.2.

It seems to be suitable at this point to discuss this EOL-criterion in another direction. From fig. 2.1.7 one gets a reduction of ca. 10 % for the thermal flux at the control rod positions. This reduction corresponds to an approximately equal reduction in the effectiveness of the control system. Since on the other hand the excess reactivity at BOL is reduced by ca. 8 % $\Delta\rho$ the main part of the reduction in effectiveness is compensated by the reduction in control demand. This rough estimate demonstrates that there is only a small gap remaining.
Nevertheless it must be stated clearly that a recalculation of the control rod effectiveness is necessary in a case by case study.

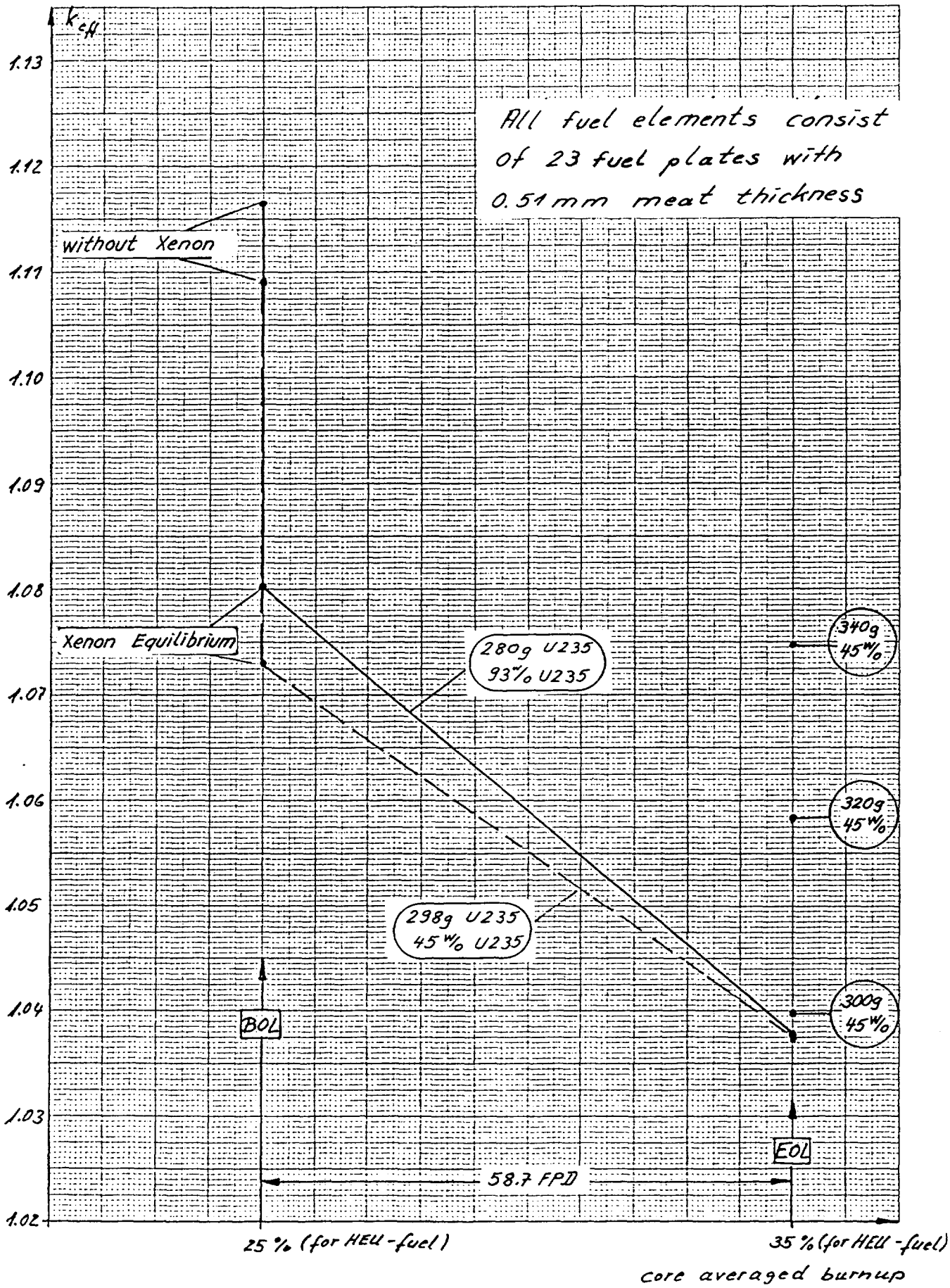

1o MW - Reactor Conversion EOL-Criterion
Determination of REU-Fuel with 45 w/o U235 using the simplified RZ-Calculation

2.1.4

Table 2.1.2
Nomenclature of Flux Figures

The flux figures show flux traverses (FLUSS-VERTEILUNG) of neutron fluxes in different energy groups.

These groups (Gruppen) are marked by numbers:

- 1. GRUPPE 10 MeV > E_n > 5.531 keV (fast flux) (this is a summing up of the 1. and 2. group calculated)
- 3. GRUPPE 5.531 keV > E_n > .625 eV (epithermal flux)
- 4. GRUPPE .625 eV > E_n (thermal flux)

All fluxes are given in absolute values based on a total power for the specified core (10 MW or 2 MW). For XY-calculations the axial averaged flux is plotted.

The core state is described by

- Power of the Core (10 MW, 2 MW)
- End of Life or Begin of Life (EOL or BOL)
- Xenon-State (NO-XE = No Xenon, XE-EQUILIBRIUM= Xenon Equilibrium)
- Enrichment of the fuel (20 w/o-U235 = 20 W/%-U5)

The model used is described by

- RZ 2 dimensional diffusion calculation in RZ-geometry
- XY 2 dimensional diffusion calculation in XY-geometry

The section plotted is described by

- ZEILE 1 horizontal traverse through the core center in RZ
- SPALTE 1 vertical traverse through the core center in RZ
- ZEILE i, SPALTE j horizontal traverses perpendicular to each other in XY

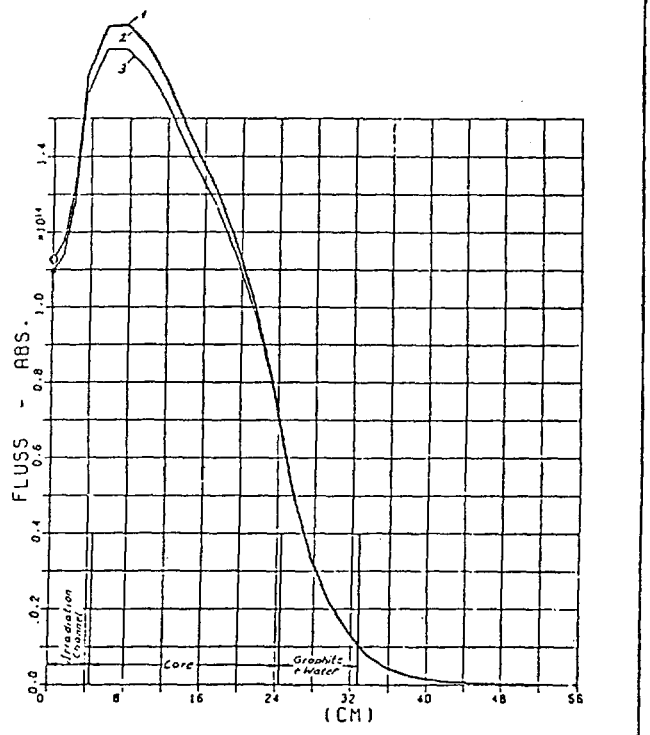

1 = HEU - fuel 280g U235/FE, 93 % U235
2 = REU - fuel 298g U235/FE, 45 % U235
3 = alternative REU - fuel 338g U235/FE, 45 % U235

10MW-RZ-MODEL BOL XE-EQUILIBRIUM
FLUSS - VERTEILUNG 1.GRUPPE
ZEILE 1

ABB 2.1.5

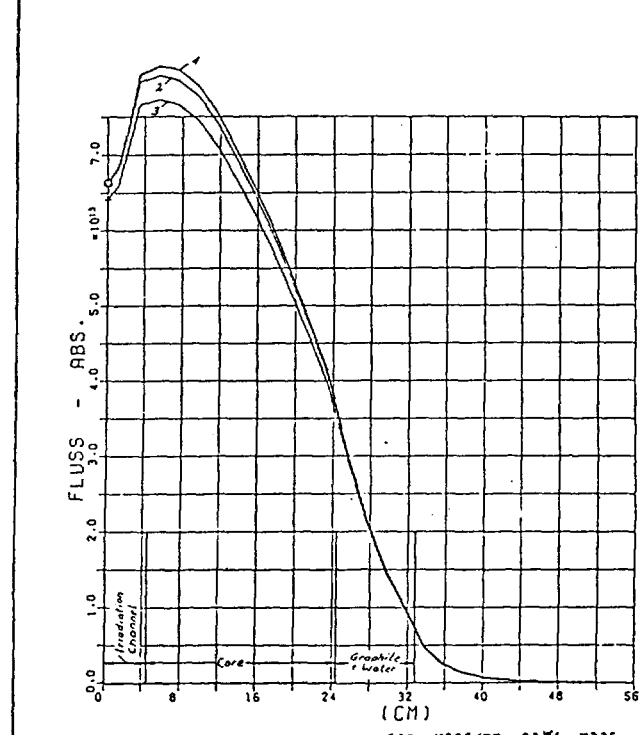

1 = HEU - fuel 280g U235/FE, 93 % U235
2 = REU - fuel 298g U235/FE, 45 % U235
3 = alternative REU - fuel 338g U235/FE, 45 % U235

10MW-RZ-MODEL BOL XE-EQUILIBRIUM
FLUSS - VERTEILUNG 3.GRUPPE
ZEILE 1

ABB 2.1.6

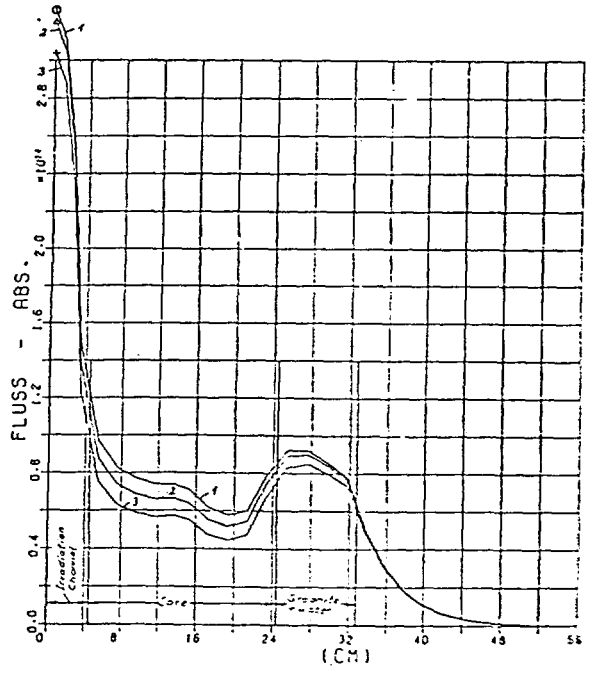

1 = HEU - fuel 280g U235/FE, 93 % U235
2 = REU - fuel 298g U235/FE, 45 % U235
3 = alternative REU - fuel 338g U235/FE, 45 % U235

10MW-RZ-MODEL BOL XE-EQUILIBRIUM
FLUSS - VERTEILUNG 4.GRUPPE
ZEILE 1

ABB 2.1.7

The figures 2.1.5 to 2.1.16 show the different fluxes at traverses horizontally and vertically through the centre of the core. Each figure compares the flux produced by the HEU-fuel and by the REU-fuel resulting from the simplified RZ-calculation (the results of the alternative REU-fuel within these figures will be discussed later).

Whereas the fast fluxes differ scarcely for the two fuels under consideration, the epithermal flux is reduced by ca. 1.5 % at its maximum value. The most interesting flux is the thermal flux. Here we find from fig. 2.1.7 for example a reduction of

- ca. 1.8 % at the irradiation position in the core center
- ca. 10 % at the fuel area
- ca. 3 % at the reflector peak (mixture out of graphite and water)

caused by the use of the REU-fuel.

2.1.4 Prove of the RZ-Results by XY-Calculations

The simplifications used at the RZ model may affect the results in view of the U235-loading of the spare fuel as well as the different flux levels resulting. Therefore a XY-model for a diffusion calculation was set up for a prove of the previous results.

This model is presented at fig. 2.1.17 and is in agreement with the prerequisites found by the Vienna-meeting, 29. Nov. to 2. Dec. 78.

The presented working cores of fig. 2.1.17 corresponds in its averaged burnup to the burnup used in the RZ-calculation; the burnup distribution is chosen so that the fresh fuel is loaded into the outer core positions.

What was found out by the XY-calculations is

- the U235-loading of the RZ-calculated REU-fuel and of the XY-calculated REU-fuel differ only by 3 g U235 (298 g U235 per fuel element by RZ to 295 g U235 per fuel element by XY).

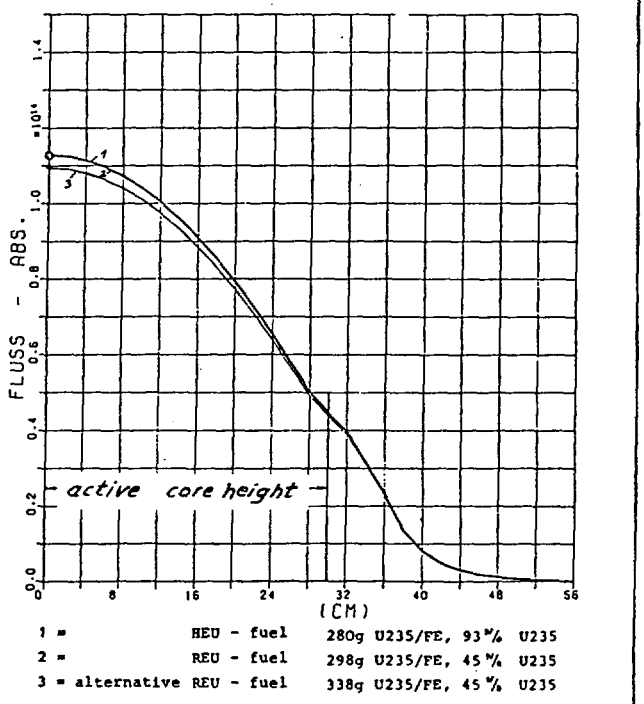

10MW-RZ-MODEL BOL XE-EQUILIBRIUM
FLUSS - VERTEILUNG 1.GRUPPE
SPALTE 1 (IRRADIATION CHANNEL)

ABB 2.1.8

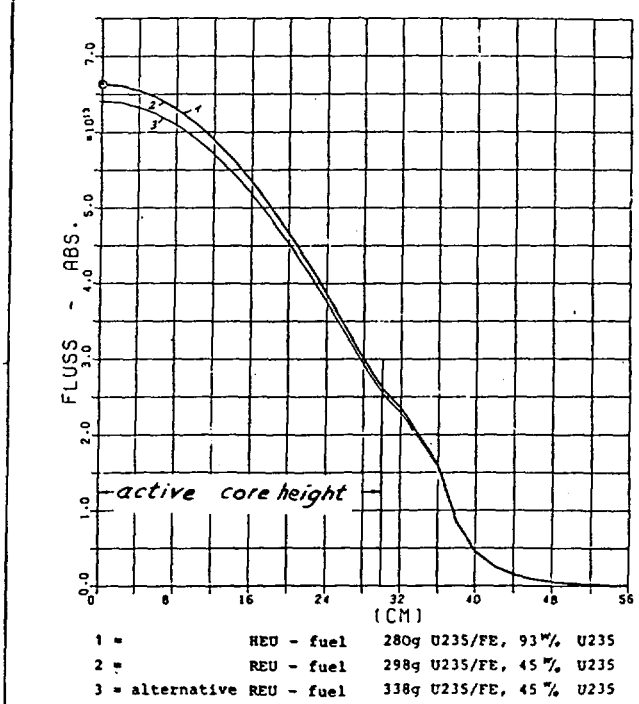

10MW-RZ-MODEL BOL XE-EQUILIBRIUM
FLUSS - VERTEILUNG 3.GRUPPE
SPALTE 1 (IRRADIATION CHANNEL)

ABB 2.1.9

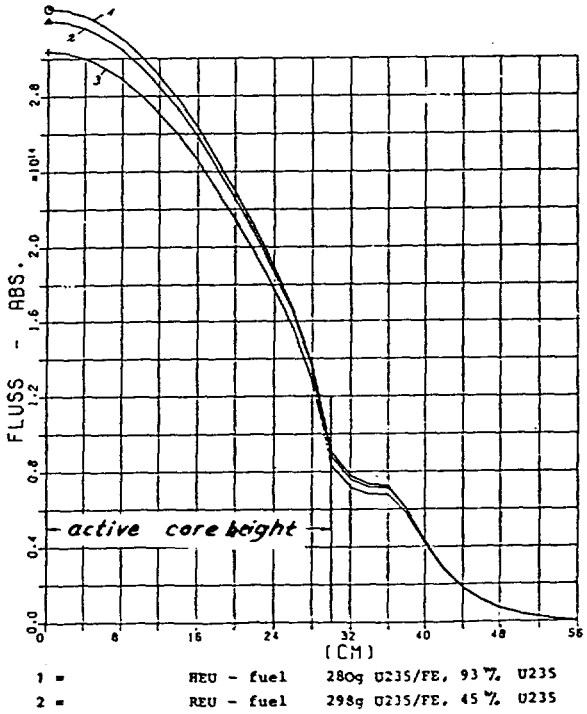

10MW-RZ-MODEL BOL XE-EQUILIBRIUM
FLUSS - VERTEILUNG 4.GRUPPE
SPALTE 1 (IRRADIATION CHANNEL)

ABB 2.1.10

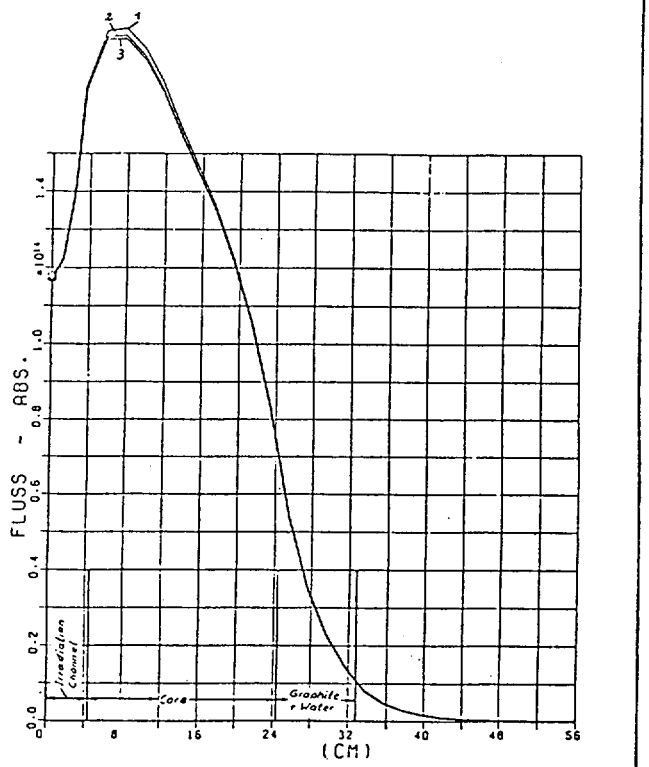

1 = HEU - fuel 280g U235/FE, 93 % U235
2 = REU - fuel 298g U235/FE, 45 % U235
3 = alternative REU - fuel 338g U235/FE, 45 % U235

10MW-RZ-MODEL EOL XE-EQUILIBRIUM
FLUSS - VERTEILUNG 1.GRUPPE
ZEILE 1

ABB 2.1.11

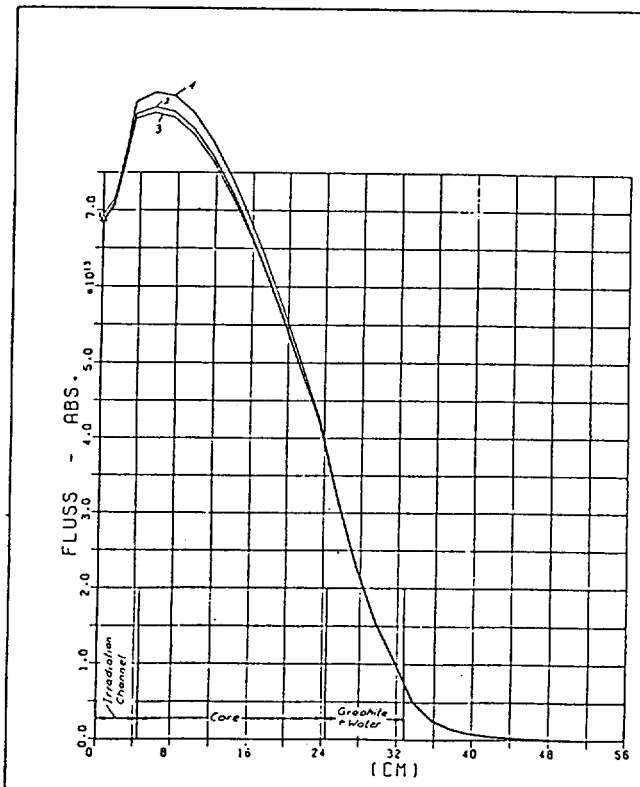

1 = HEU - fuel 280g U235/FE, 93 % U235
2 = REU - fuel 298g U235/FE, 45 % U235
3 = alternative REU - fuel 338g U235/FE, 45 % U235

10MW-RZ-MODEL EOL XE-EQUILIBRIUM
FLUSS - VERTEILUNG 3.GRUPPE
ZEILE 1

ABB 2.1.12

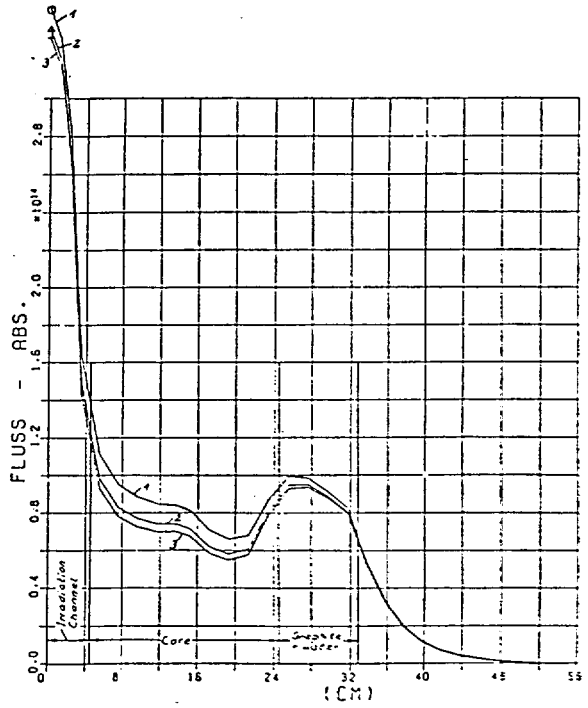

1 = HEU - fuel 280g U235/FE, 93 % U235
2 = REU - fuel 298g U235/FE, 45 % U235
3 = alternative REU - fuel 338g U235/FE, 45 % U235

10MW-RZ-MODEL EOL XE-EQUILIBRIUM
FLUSS - VERTEILUNG 4.GRUPPE
ZEILE 1

ABB 2.1.13

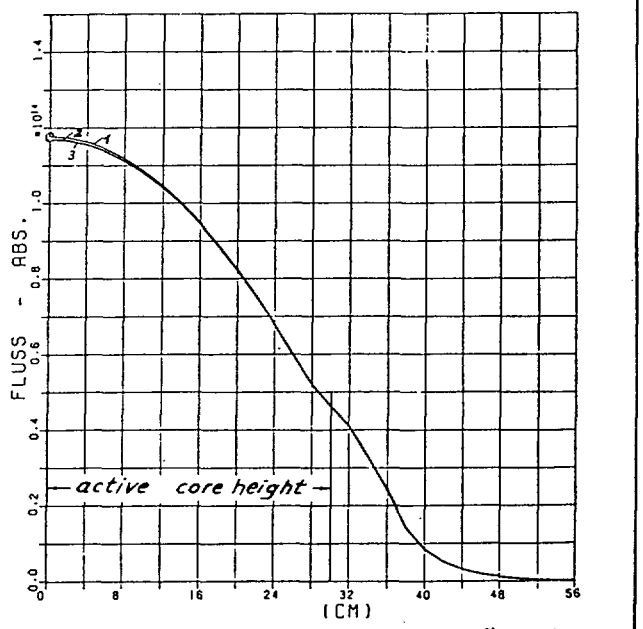

1 = REU - fuel 280g U235/FE, 93 % U235
2 = REU - fuel 298g U235/FE, 45 % U235
3 = alternative REU - fuel 338g U235/FE, 45 % U235

10MW-RZ-MODEL EOL XE-EQUILIBRIUM
FLUSS - VERTEILUNG 1.GRUPPE
SPALTE 1 (IRRADIATION CHANNEL)

ABB 2.1.14

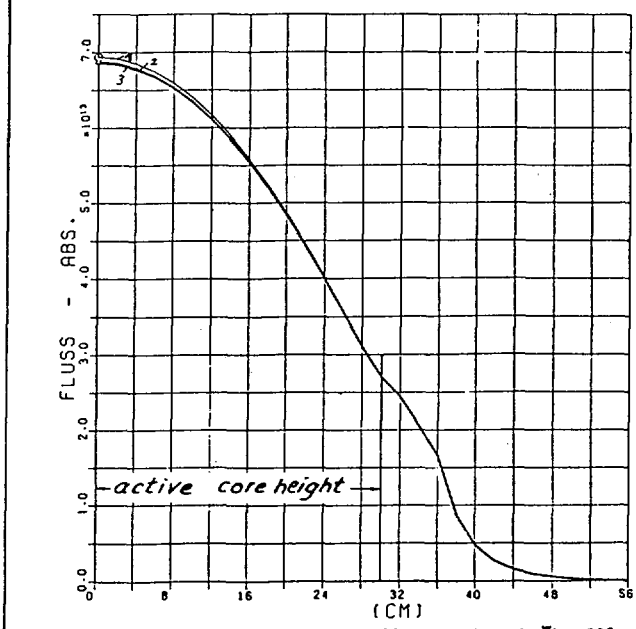

1 = REU - fuel 280g U235/FE, 93 % U235
2 = REU - fuel 298g U235/FE, 45 % U235
3 = alternative REU - fuel 338g U235/FE, 45 % U235

10MW-RZ-MODEL EOL XE-EQUILIBRIUM
FLUSS - VERTEILUNG 3.GRUPPE
SPALTE 1 (IRRADIATION CHANNEL)

ABB 2.1.15

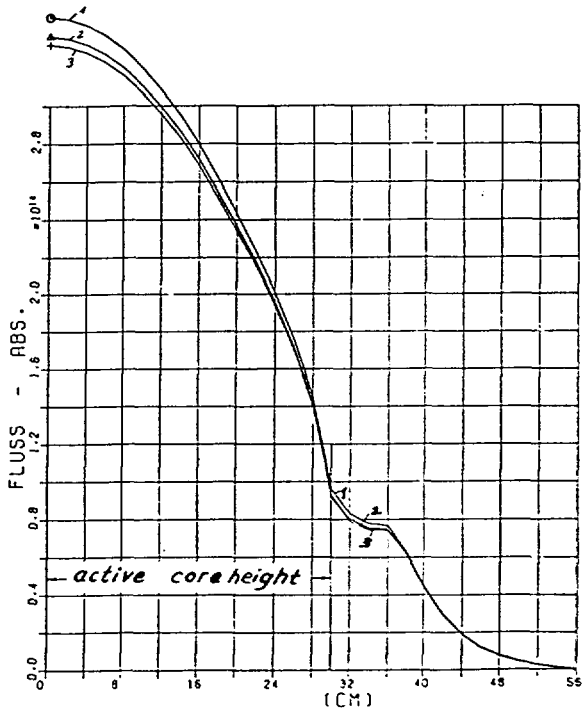

1 = REU - fuel 280g U235/FE, 93 % U235
2 = REU - fuel 298g U235/FE, 45 % U235
3 = alternative REU - fuel 338g U235/FE, 45 % U235

10MW-RZ-MODEL EOL XE-EQUILIBRIUM
FLUSS - VERTEILUNG 4.GRUPPE
SPALTE 1 (IRRADIATION CHANNEL)

ABB 2.1.16

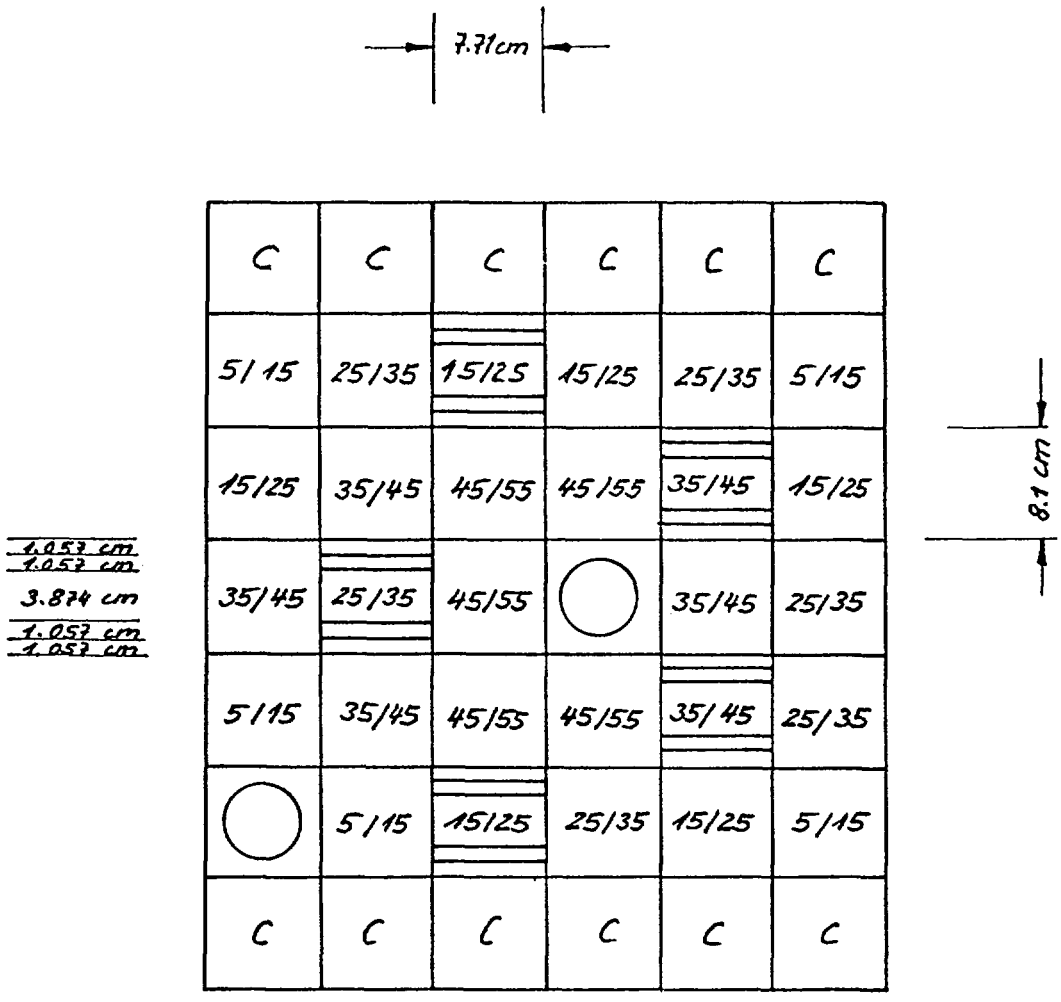

C = Graphite

W_i / W_f = Burnup at BOL / Burnup at EOL

10 MW - Core

XY-Model for Diffusion Calculations

2.1.17

- for both fuels, i. e. HEU as well as REU the pure calculation figures of the reactivity are reduced ($\Delta\rho \approx 2.5$ %) by the different shape of the core and the burnup distribution. This can be seen from the fig. 2.1.18 in comparison to fig. 2.1.4. Furthermore we checked the differences in reactivity comparing a calculation with homogeneous xenon to another using the heterogeneous xenon distribution as a function of the local power. The differences resulting are lower than 0.1 o/oo Δ k.

- the differences in fluxes are very similar to the results of the RZ-calculations and can be seen at the figures 2.1.19 to 2.1.26 (2.1.19 and 2.1.20 show two thermal flux traverses at BOL, 2.1.21-2.1.26 two flux traverses in three energy groups at EOL).

  Moreover these figures give a better impression of the flux shape across the core in the central cross section, taking into account the different burnup of the fuel elements and the irradiation channels and the control rods (fork absorber) at their real positions *).

  There is one fact to extract from the XY-results concerning the thermal fluxes within the reflector peak. Whereas one finds a small peak-difference of approx. 2 % in the case of water as a reflector material only when changing from 93 w/o U235 to 45 w/o U235 (fig. 2.1.19, 2.1.23) one gets up to 6 % reduction in the graphite reflector (fig. 2.1.26) (The maximal value of the thermal flux is outside the graphite area).

2.1.5 REU-Fuel using the BOL-criterion

Using the BOL excess reactivity matching criterion in the simplified RZ model only (because its validity for determination of REU-fuel is proven in Chapter 2.1.4) a different REU-fuel results.

*) It must be mentioned here again that the XY-flux results are axially averaged.

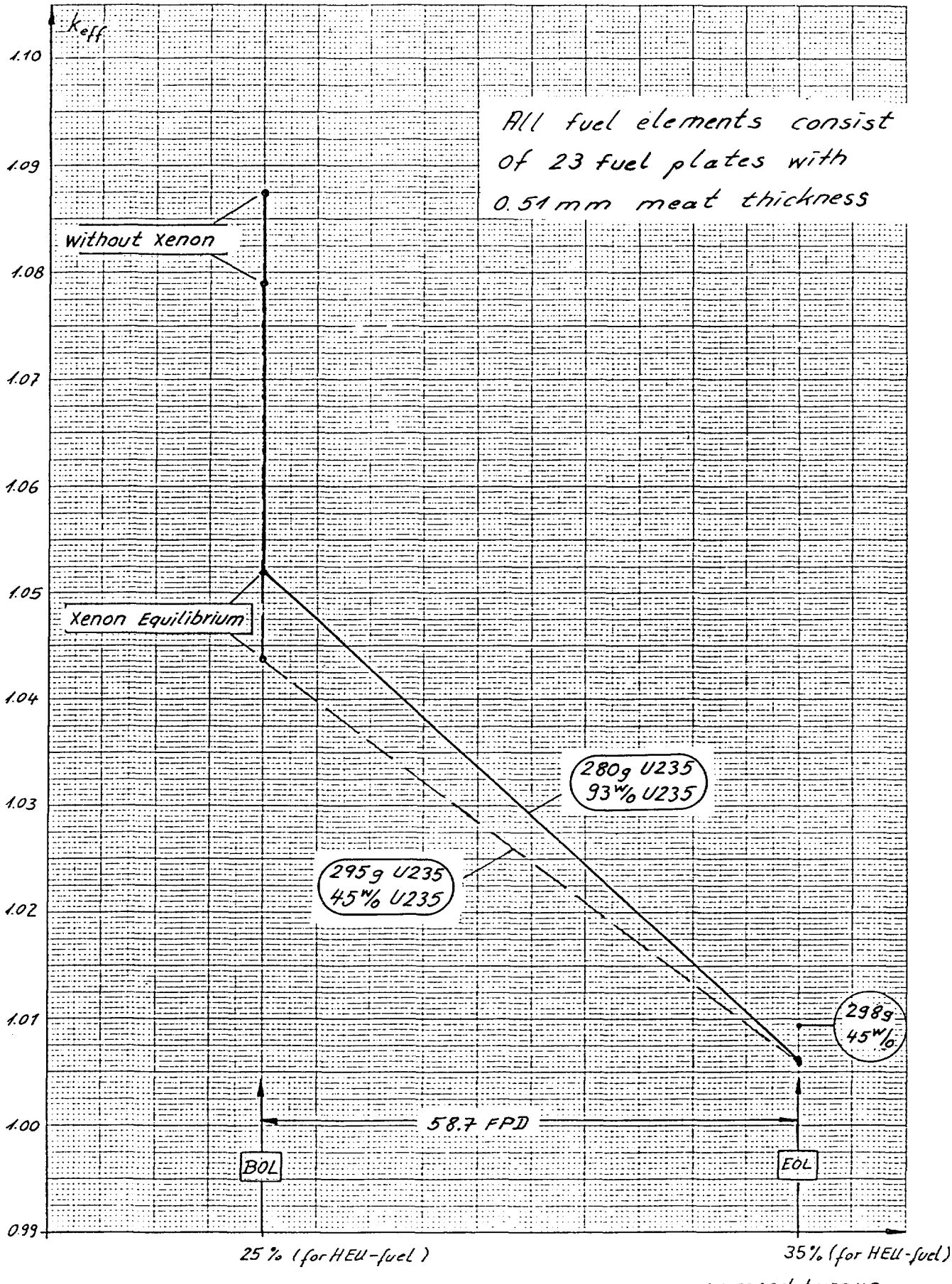

1o MW - Reactor Conversion EOL-Criterion
Determination of REU-Fuel with 45 w/o U235 using the XY-Calculation Model

2.1.18

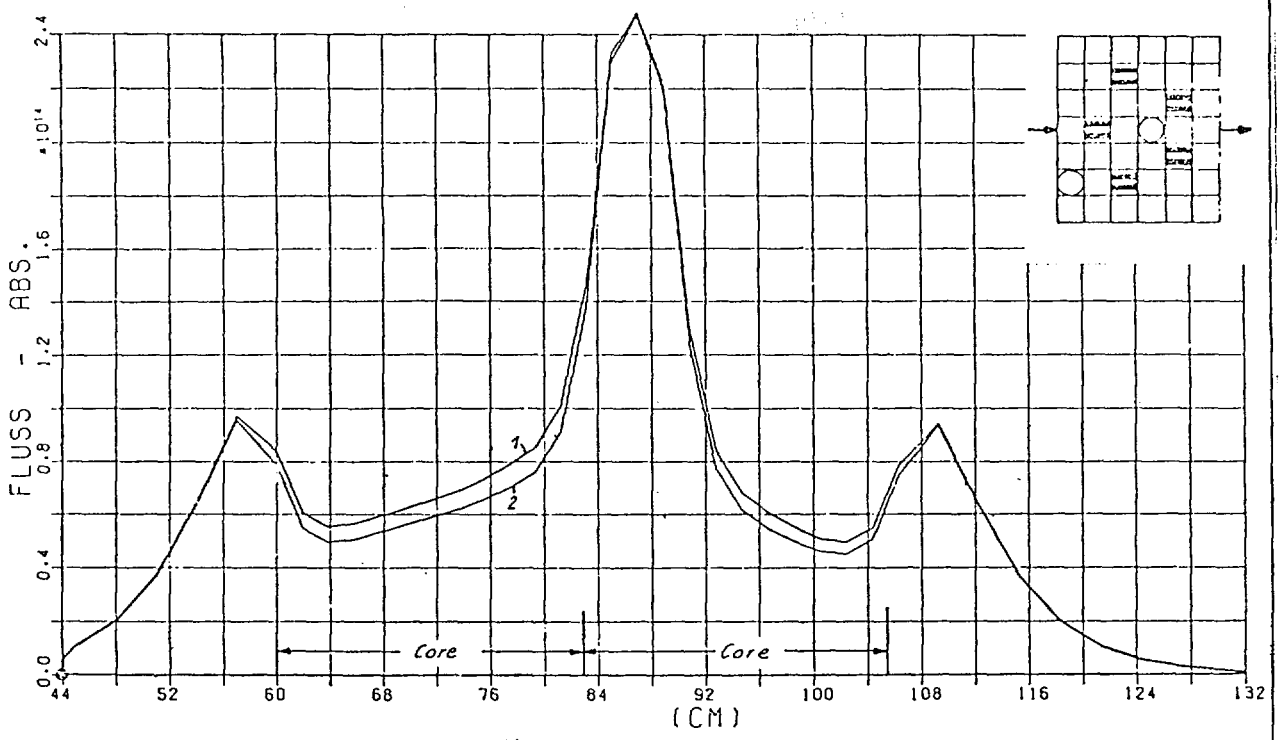

1 = HEU - fuel 280g-U235/FE 93 % -U235
2 = REU - fuel 295g-U235/FE 45 % -U235

10MW-XY-MODEL BOL XE-EQUILIBRIUM
FLUSS - VERTEILUNG 4.GRUPPE

ABB 2.1.19

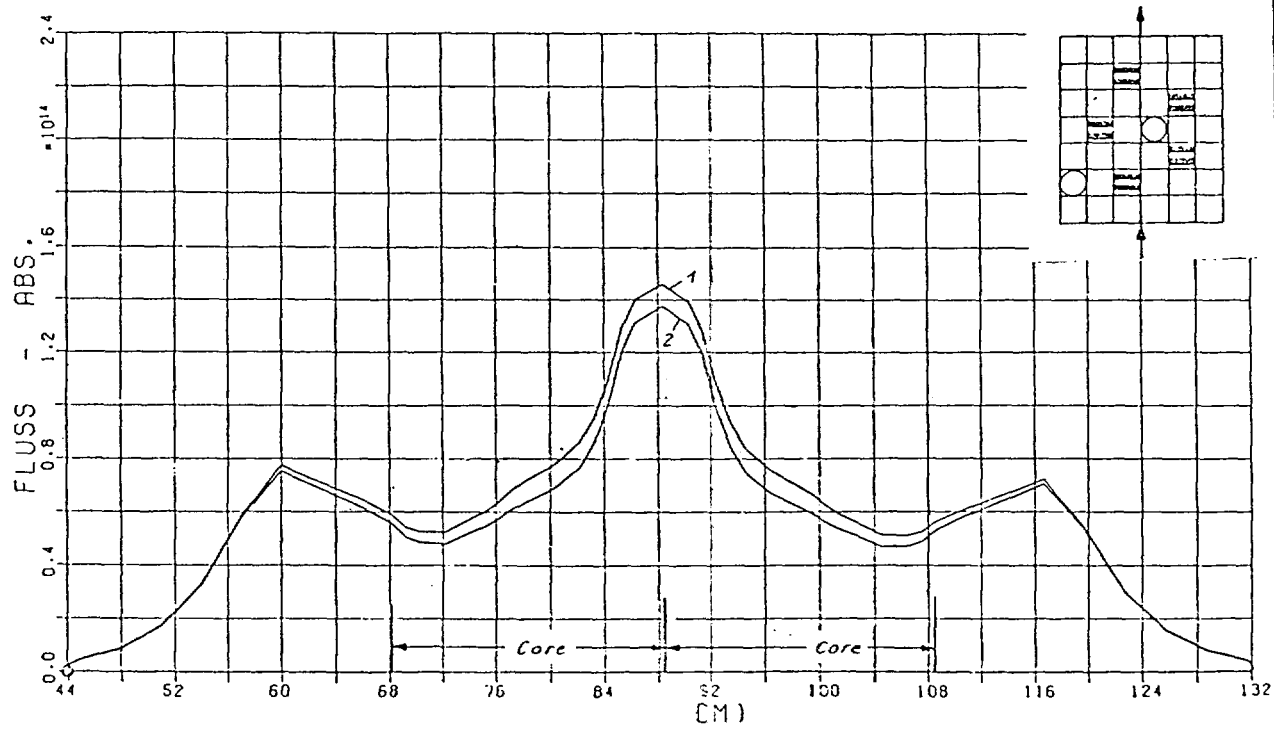

1 = HEU - fuel 280g-U235/FE 93 % -U235
2 = REU - fuel 295g-U235/FE 45 % -U235

10MW-XY-MODEL BOL XE-EQUILIBRIUM
FLUSS - VERTEILUNG 4.GRUPPE

ABB 2.1.20

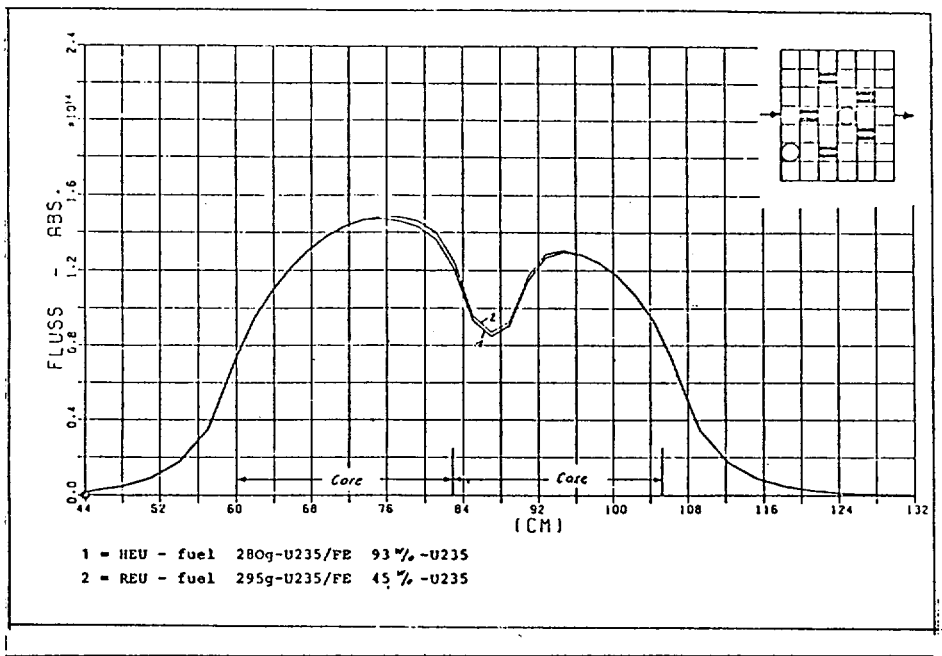

ABB 2.1.21

10MW-XY-MODEL EOL XE-EQUILIBRIUM
FLUSS - VERTEILUNG 1.GRUPPE

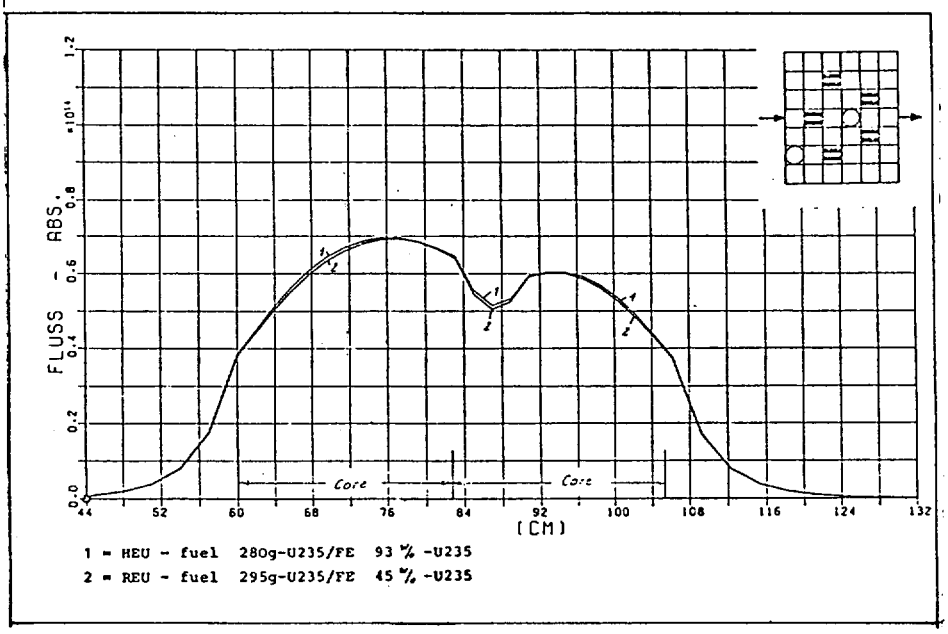

ABB 2.1.22

10MW-XY-MODEL EOL XE-EQUILIBRIUM
FLUSS - VERTEILUNG 3.GRUPPE

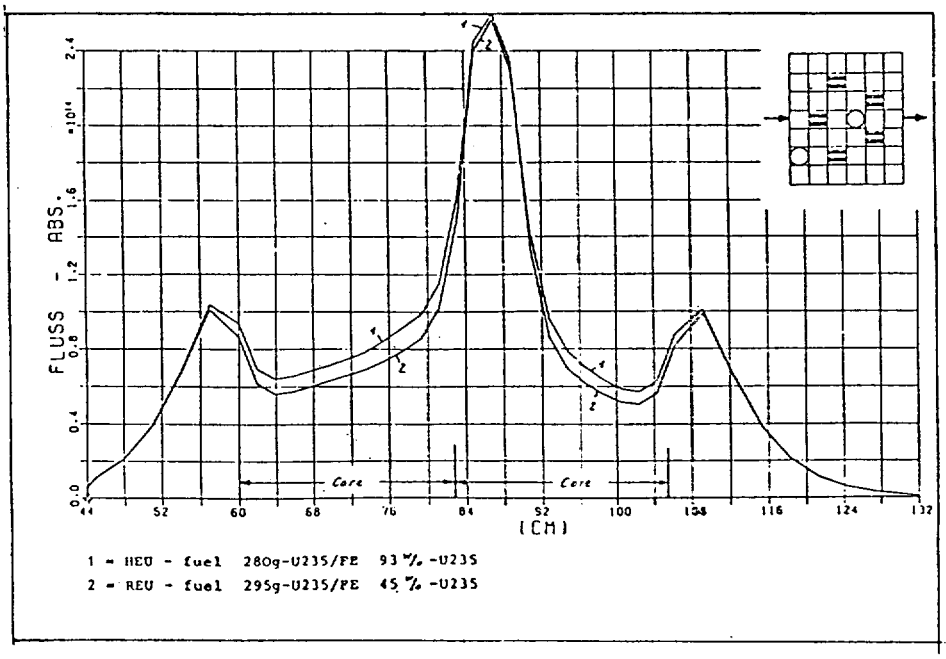

ABB 2.1.23

10MW-XY-MODEL EOL XE-EQUILIBRIUM
FLUSS - VERTEILUNG 4.GRUPPE

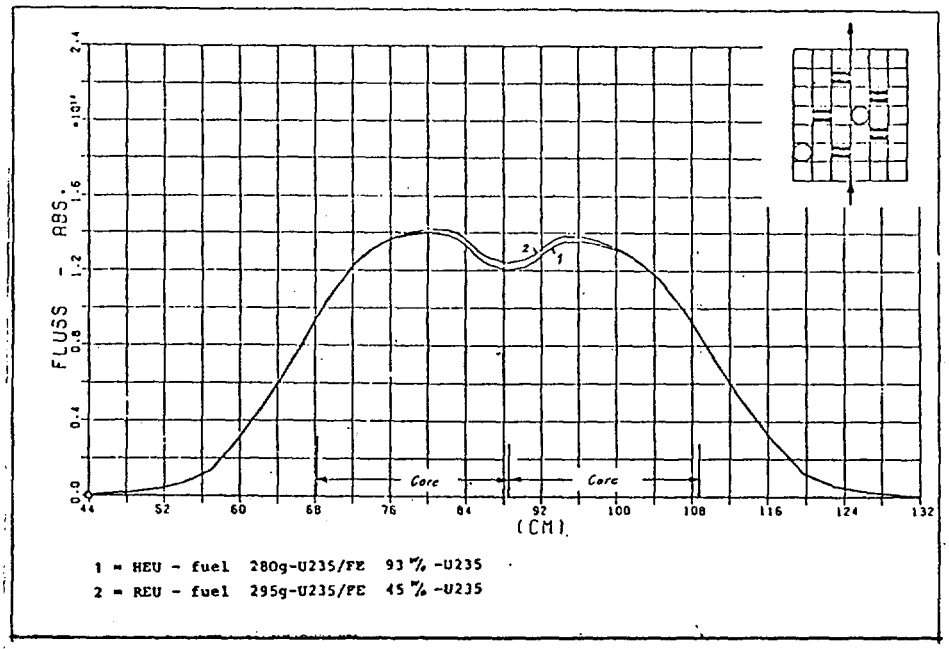

ABB 2.1.24

10MW-XY-MODEL EOL XE-EQUILIBRIUM
FLUSS - VERTEILUNG 1.GRUPPE

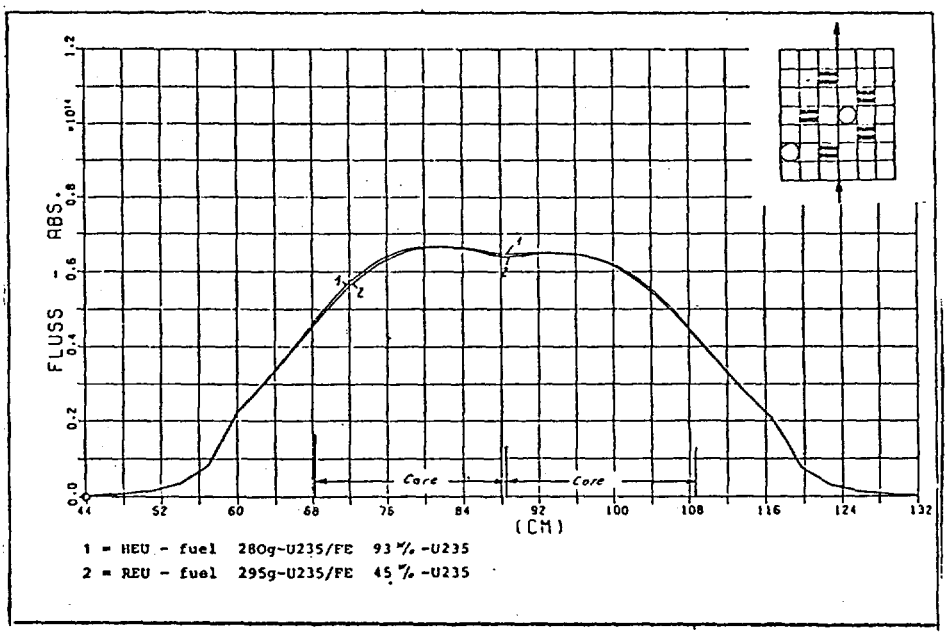

ABB 2.1.25

10MW-XY-MODEL EOL XE-EQUILIBRIUM
FLUSS - VERTEILUNG 3.GRUPPE

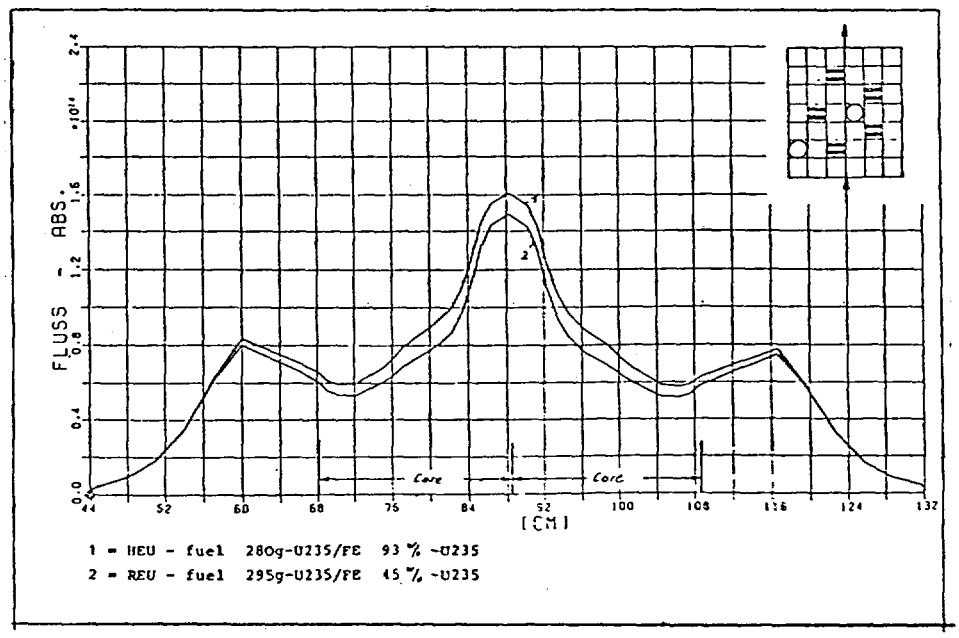

ABB 2.1.26

10MW-XY-MODEL EOL XE-EQUILIBRIUM
FLUSS - VERTEILUNG 4.GRUPPE

What is found out is an U235-loading of 307 g (figure 2.1.3, right ordinate). The fuel used is specified within table 2.1.1. This loading leads of course to an increased burnup-period if the same excess reactivity at EOL as in the previous calculation should be matched. The results are represented at figure 2.1.27 for the reactivity behaviour and they are to compare with the results of the EOL-criterion at fig. 2.1.4. The burnup period is enlarged by 25 %. The loss of shutdown reactivity may cause some problems at BOL. A separate flux interpretation of the calculations are omitted since the effect of a further enlargement of the uranium loading is shown more drastically by the alternative REU-fuel got from the fuel availability criterion (see chapter 2.1.6).

2.1.6 REU-fuel using the fuel availability limits

Moreover an operator of a research reactor can go even a step further using the maximum uranium-density available. This figure isn't exactly fixed and depends on the manufacturer as well as on the point of time when the fuel should be available. For the investigations reported here we chose the density stated by the German NUKEM company for near term availability which is 1.7 gU/cm³*, just to show the principle effect of this alternative REU-fuel, as we call it.

With this fuel the user is given on hand a potential of improving his core-design, especially to come to high burnup values at the discharge of the spent fuel, provided that the reactivity control measures at the plant will match the requirements of this fuel. The results of these calculations are presented at figure 2.1.28 as far as the reactivity behaviour and the irradiation period is concerned.

The fuel specifications of this alternative REU-fuel are given within table 2.1.1, whereat the uranium density of 1.7 g U/cm³ leads to a U235-loading of 338 g U235 per fuel element, 40 g more than in the case of the EOL-criterion.

From fig. 2.1.28 one extracts further the fact, that by this alternative fuel the irradiation period is more than doubled (121.9 full power days instead of the previous 58.7 full power days). On the other hand the reactivity at BOL goes up by $\Delta\rho \simeq 1.8$ % causing higher requirement to the reduced effectiveness of the shutdown system. By that a shortened burnup period has to be recommended.

---

* This value also represents the first step in the German Fuel Development Program.

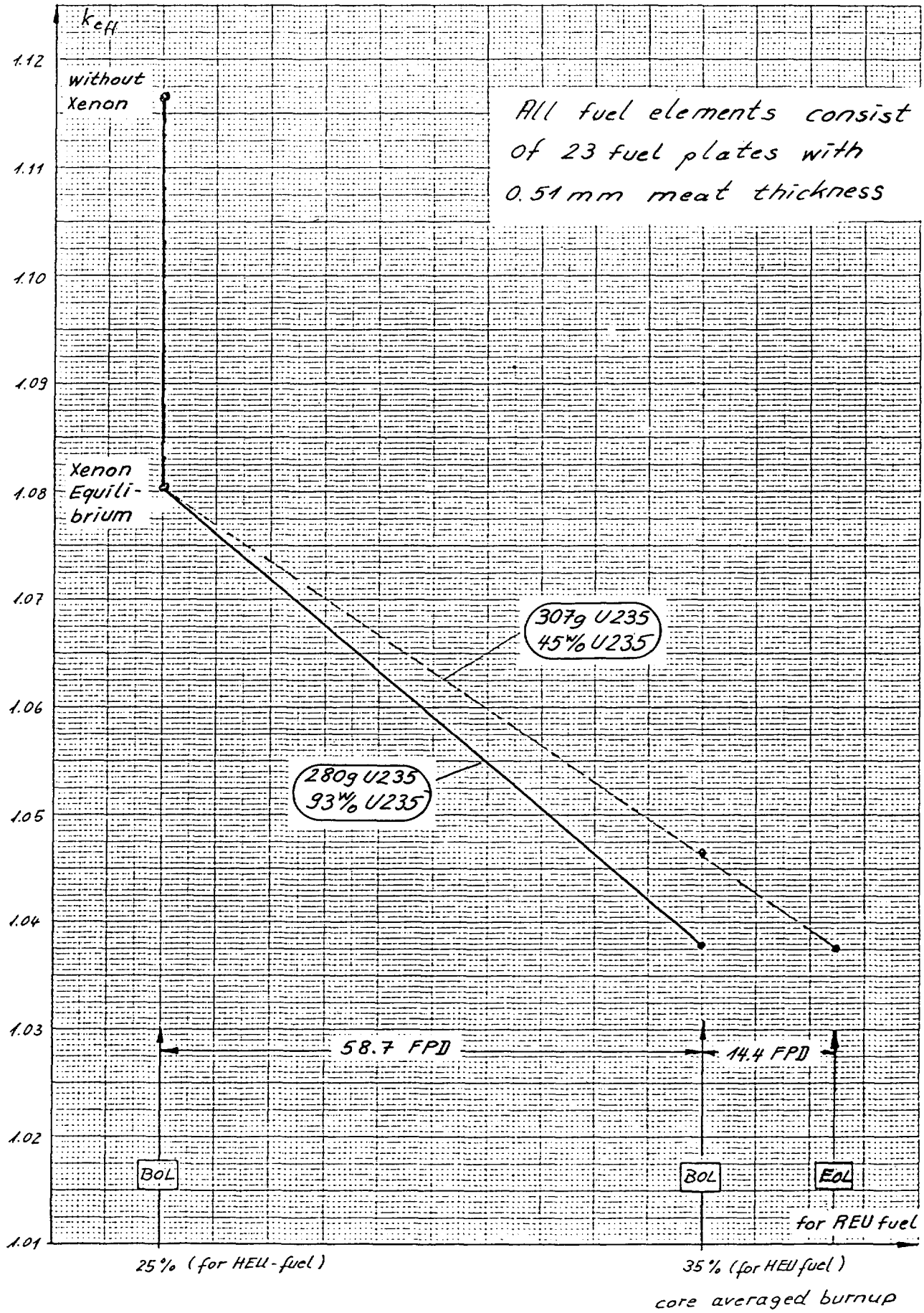

1o MW - Reactor Conversion BOL-Criterion
Determination of REU-Fuel with 45 w/o U235 using the simplified RZ-Calculation

2.1.27

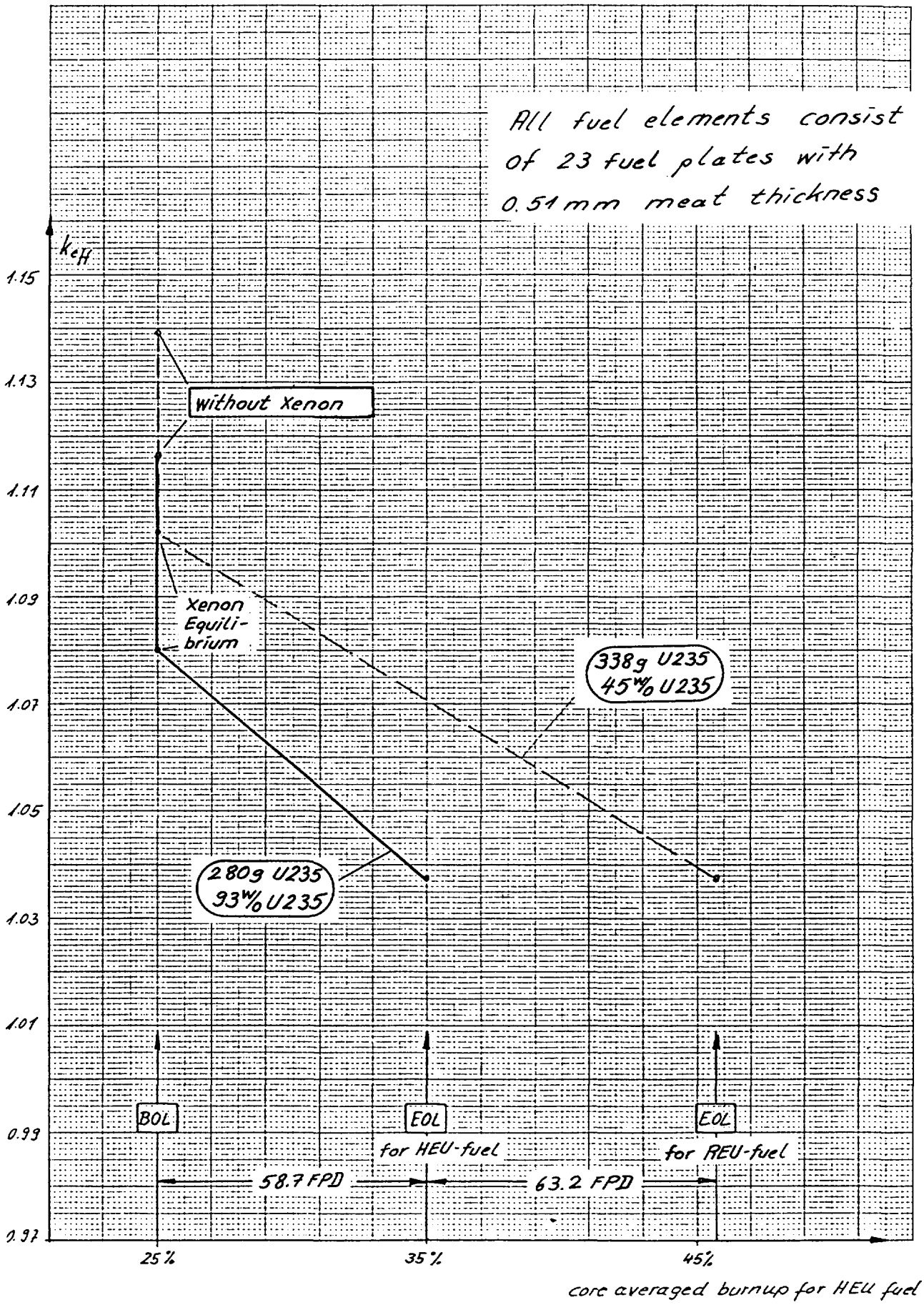

10 MW - Reactor Conversion Fuel Availability Criterion
Determination of REU-Fuel with U-Density 1.7 g/cm³ Meat
using the simplified RZ-Model

2.1.28

To demonstrate the effect of this high uranium loading to the flux levels the resulting fluxes are included within the figures 2.1.5 to 2.1.16 for the different core states and core traverses.

2.1.7 First Core Problems

From our point of view the first core states no specific problem within the conversion to reduced enriched fuel.

Nevertheless we made some investigations concerning the first core just to give the operators a feeling of what is to be expected. Disregarding the effect that core conversions will run by implementing the new fuel with reduced enrichment into the old core step by step in most of the cases, we tried to find out the size, i. e. the number of fuel assemblies necessary for a total fresh core, in comparison to the first core with the HEU-fuel. Using the simplified RZ-model for this calculation oncemore, we found the results presented at figure 2.1.29. Whereas the first core with the HEU-fuel is made up of 13 fuel elements and additional 5 control elements (CE) matching therewith nearly the excess reactivity of the working core with the HEU-fuel, in the case of the REU-fuel 14 fuel elements instead of 13 are necessary to match the BOL-excess reactivity resulting from the EOL-criterion. 15 fuel elements together with the 5 control elements will even fit the BOL-criterion.* This one or two additional fuel assemblies can be inserted into the grid plate without any problem. To demonstrate the influence to the flux level at figures 2.1.30, 31 only the relative values of the thermal flux of the first core with the HEU-fuel are compared to the first core containing 14 fuel elements made out of the REU-fuel (for the nomenclature of these figures see table 2.1.2).

2.1.8 REU-Fuel with unchanged U235-loading

As stated previously there was an early approach to the definition of REU-fuels. This approach kept the U235-loading per fuel assembly unchanged when reducing the fuel enrichment. Obviously the reactivity of this fuel must be reduced by the enlargment of the U238-content. From fig. 2.1.3 in connection with fig. 2.1.27

---

* It should be mentioned here, that at figure 2.1.29 the scaling at the abscissa is done in percentage of U235-loss as a measure of burnup for both the HEU- and the REU-fuel, which gives a different view compared to figure 2.1.4.

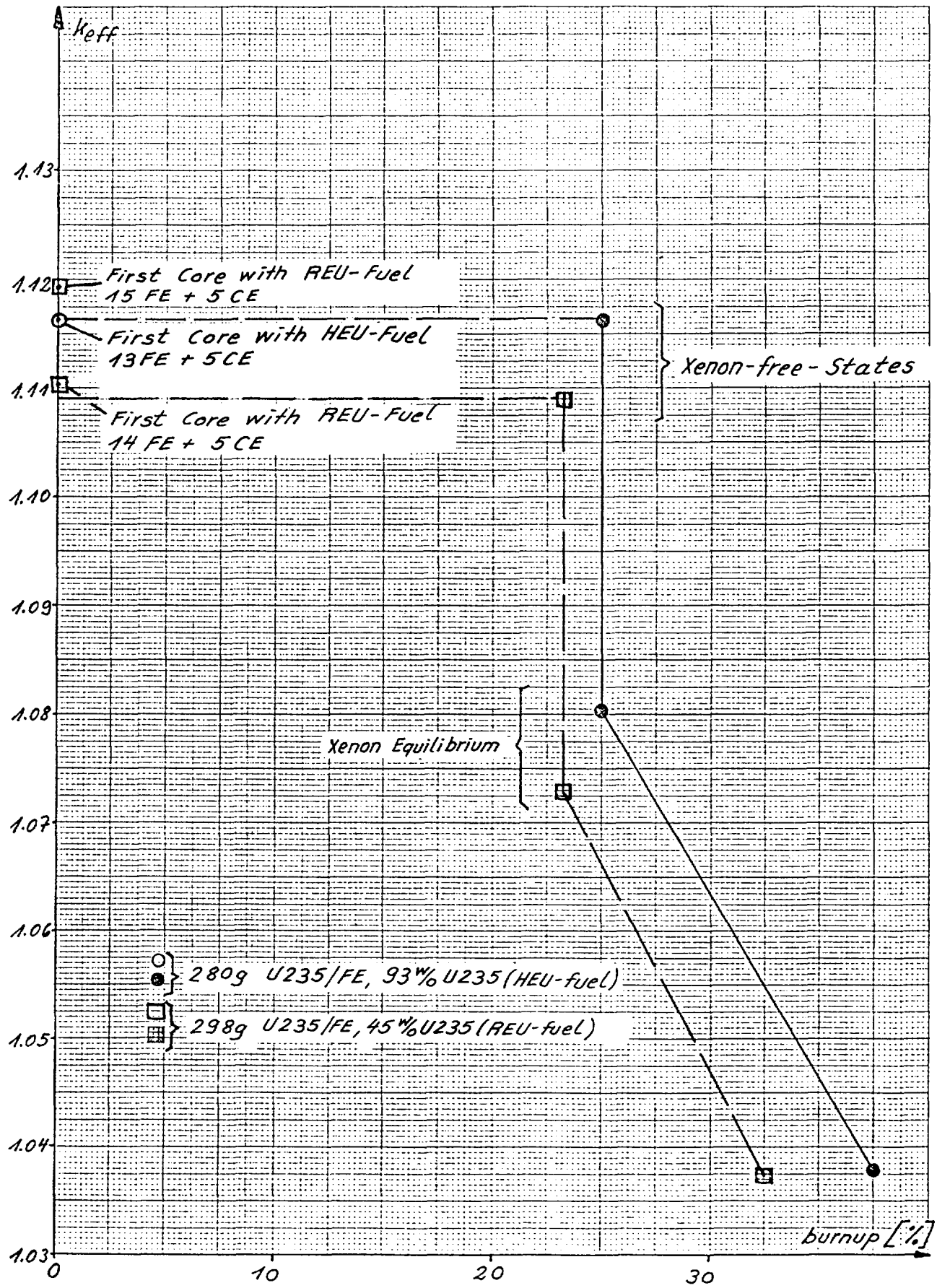

10 MW Reactor Conversion
Determination of Core Loading for the First Core using the simplified RZ-Calculation

2.1.29

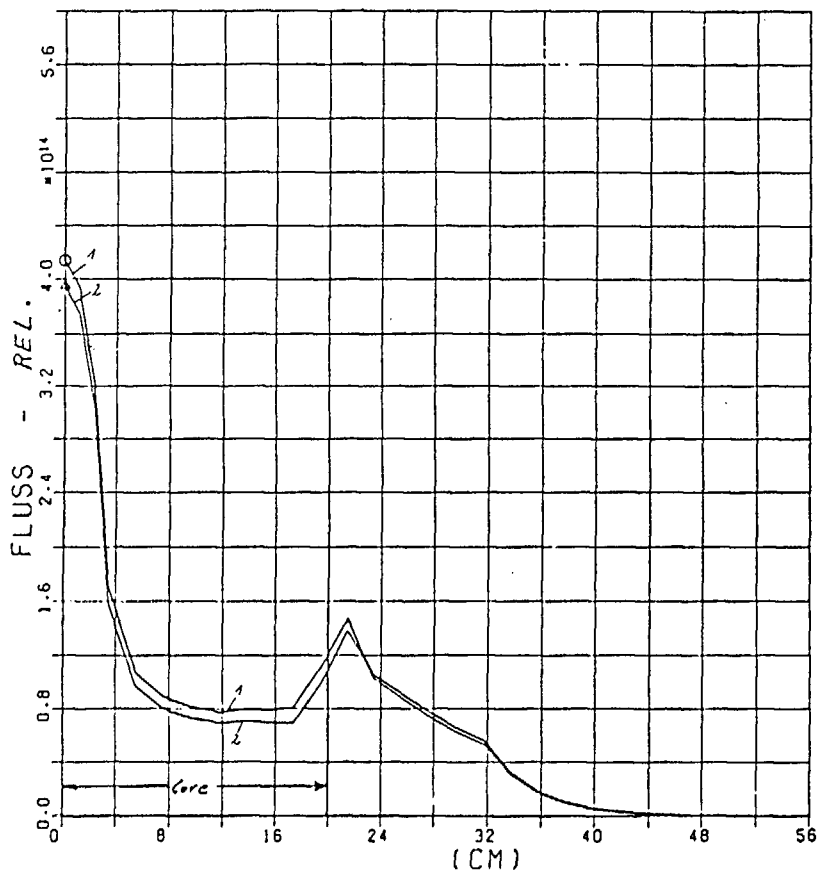

1 = HEU - fuel 280g U235/ FE, 93 % U235, 13 FE + 5 CE

2 = REU - fuel 298g U235/ FE, 45 % U235, 14 FE + 5 CE

10MW-RZ-MODEL FIRST CORE BOL XE-FREE
FLUSS - VERTEILUNG 4.GRUPPE
ZEILE 1

ABB 2.1.30

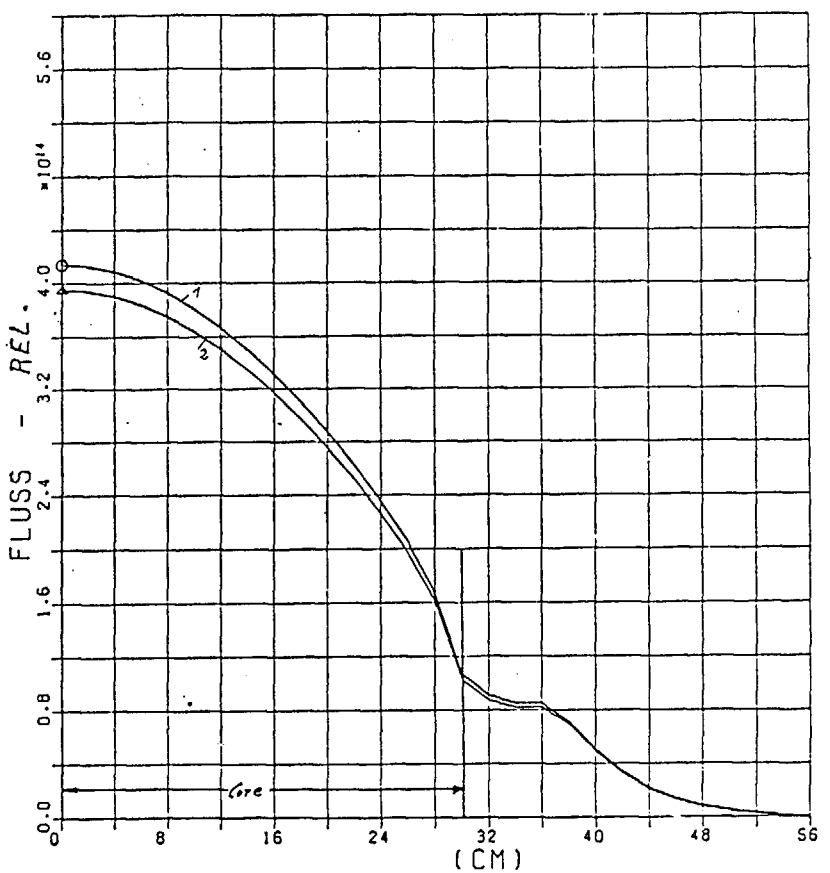

1 = HEU - fuel 280g U235/ FE, 93 % U235, 13 FE + 5 CE

2 = REU - fuel 298g U235/ FE, 45 % U235, 14 FE + 5 CE

10MW-RZ-MODEL FIRST CORE BOL XE-FREE
FLUSS - VERTEILUNG 4.GRUPPE
SPALTE 1 (IRRADIATION CHANNEL)

ABB 2.1.31

one extrapolates that in this case (280 g U235 with 45 w/o U235) a remaining excess reactivity of ca. 1.4 % $\Delta\varrho$ exists only. This leads to a cycle length of ca. 12 full power days, i. e. only 20 % of the basic cycle length. So it is not necessary to invest exact calculations to this kind of REU-fuel.

2.1.9 Isotopic composition of disloaded fuel

The main aspect of the reduction of the enrichment of MTR-fuel is the proliferation aspect. So it is suitable to filter out the basic data of weapongrade material for the REU-fuels. The isotopes of some importance are the two fissionable isotopes of plutonium, Pu239 and Pu241. Their content in the fuel with reduced enrichment (here 45 weight % U235) is of course much higher than it was for the HEU-fuel. Therefore figure 2.1.32 and 2.1.33 show the plutonium-content and the fissionable plutonium content plottet versus the burnup of the fuel in percentage. For the disloaded fuel (55 % burnup for the basic fuel) this content is approximately 1 % for the total plutonium and nearly 8.5 ‰ for the fissionable plutonium. This is to compare with the 3.8 °/₀₀ and 3.2 °/₀₀, resp. for the HEU-fuel. The total amount per fuel element is approximately 5 g of total plutonium (ca. 0.5 g for the HEU-fuel).

2.1.10 Reactivity Feedbacks

The calculated fuel temperature coefficient is very small for MTR-fuel. The calculated value for $C_D = - 1/k\ dk/dT$ is approximately $10^{-6}\ K^{-1}$ for the HEU-fuel, whereas the REU-fuel produces a value higher by a factor of 10 due to the high U238-content. The calculated moderator temperature coefficient is of the same order but higher by a factor of 2.5 than the fuel temperature coefficient. Of some importance is the void coefficient. We calculated it by changing the water density in one fuel element at different positions in the core by - 1 %. This density reduction leads to a reactivity reduction between $\Delta\varrho$ = - 1.3 o/oo and $\Delta\varrho$ = - 0.8 o/oo. Using the same burnup in % for the different fuels with the water density changed these changes in the void coefficient are lower than 10 % relatively.

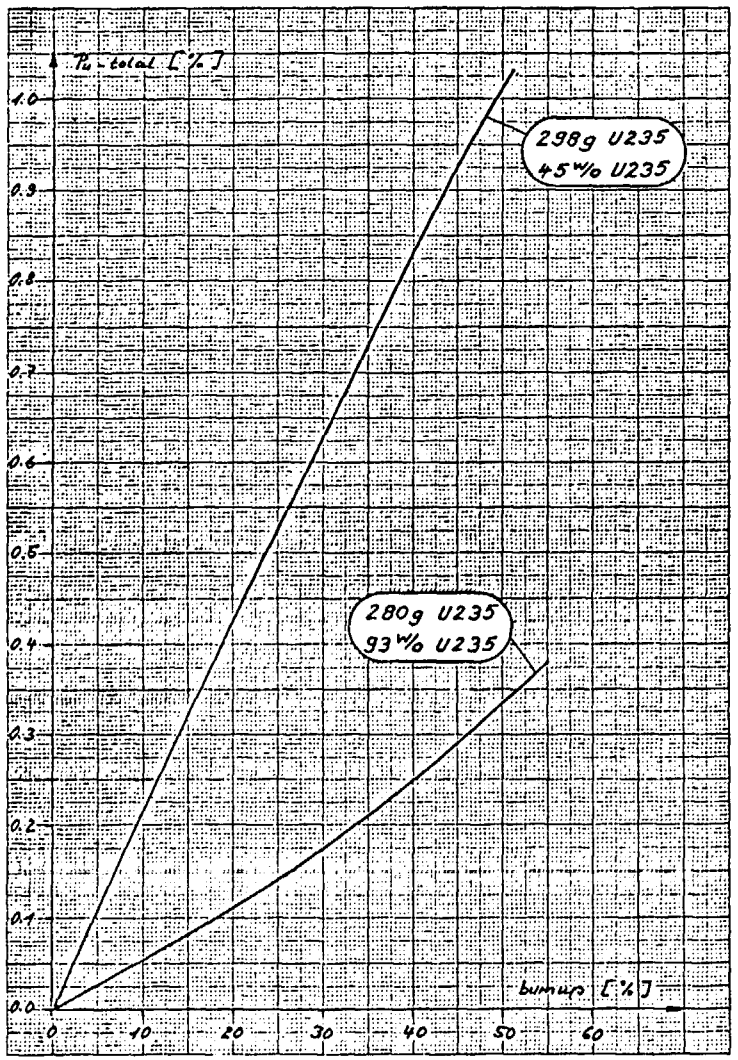

Total Plutonium Content (in Percentage of the total Heavy Metal Content) versus Burnup (in Percentage of the Loss of U235)

2.1.32

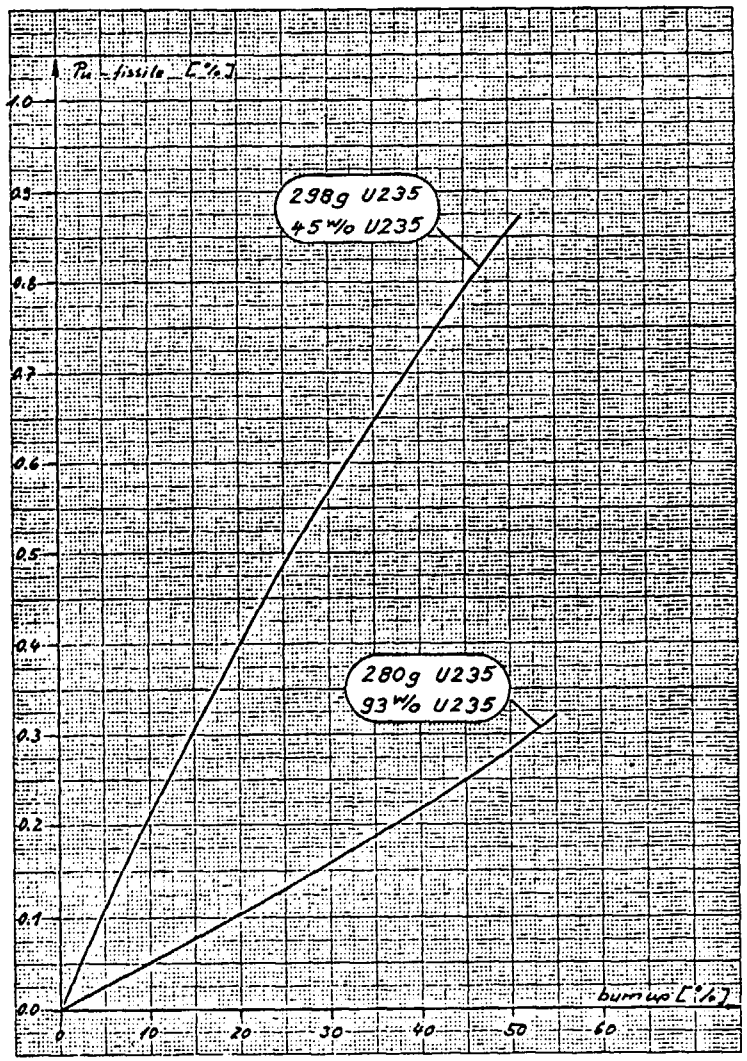

Fissile Plutonium Content (in Percentage of the total Heavy Metal Content) versus Burnup (in Percentage of the Loss of U235)

2.1.33

2.1.11 Conclusions

As demonstrated there exist a lot of possible ways to use REU-fuel instead of HEU. The different prerequisites of a real research reactor plant will determine the way how to specify the REU-fuel. A decisive limit will be the requirement to the reactivity control mechanism very often. A determination of the REU fuel using the specified EOL-criterion will weaken this point nearly totally. If there is some shutdown reactivity in reserve the BOL-criterion would be suitable. Thereby an enlargement of the cycle length of approximately 25 % seems to be possible. Keeping the cycle length unchanged to avoid the enlarged requirements to the shutdown reactivity even with a U235-loading resulting from the BOL-criterion or from the fuel availability limits one will get a remarkable enlargement of the total burnup of the REU-fuel measured in MWd compared to the results with the HEU-fuel. This fact will compensate some of the costs resulting from the higher U235-loading of this fuel.

2.2 The 2 MW-Reactor

2.2.1 Prerequisites

Compared to the 10 MW-reactor the conversion of the fuel of the 2 MW-core is more complicated. The boundary condition to keep the geometry of the basic fuel unchanged does not hold here owing to the lower power level. So it seems necessary to take different numbers of fuel plates with different meat thicknesses into account. A reduction of the number of fuel plates corresponds to a reduction of heated surface the consequences of which have to be checked from thermal-hydraulic sight. On the other hand that reduction offers the possibility to enlarge the meat thickness and the meat volume. Thereby the enlargment in the uranium-density can be limited to values available. Since a meat thickness of 1 mm is within the fabrication range of MTR-fuel, we limited ourselves within these calculations to this meat thickness only to show the principle aspects of the change of the meat thickness when using REU-fuels.

Furthermore it seems necessary to prove the thermal-hydraulic conditions for the different fuels under consideration.

2.2.2 Fuel elements

Starting from the basic fuel with 19 fuel plates per fuel element and the meat thickness of 0.51 mm (see fig. 2.2.1) we tried to find out the best REU-fuel matching the different criteria by using three different fuel element geometries. Their specifications are listed within table 2.2.1; the main differences are

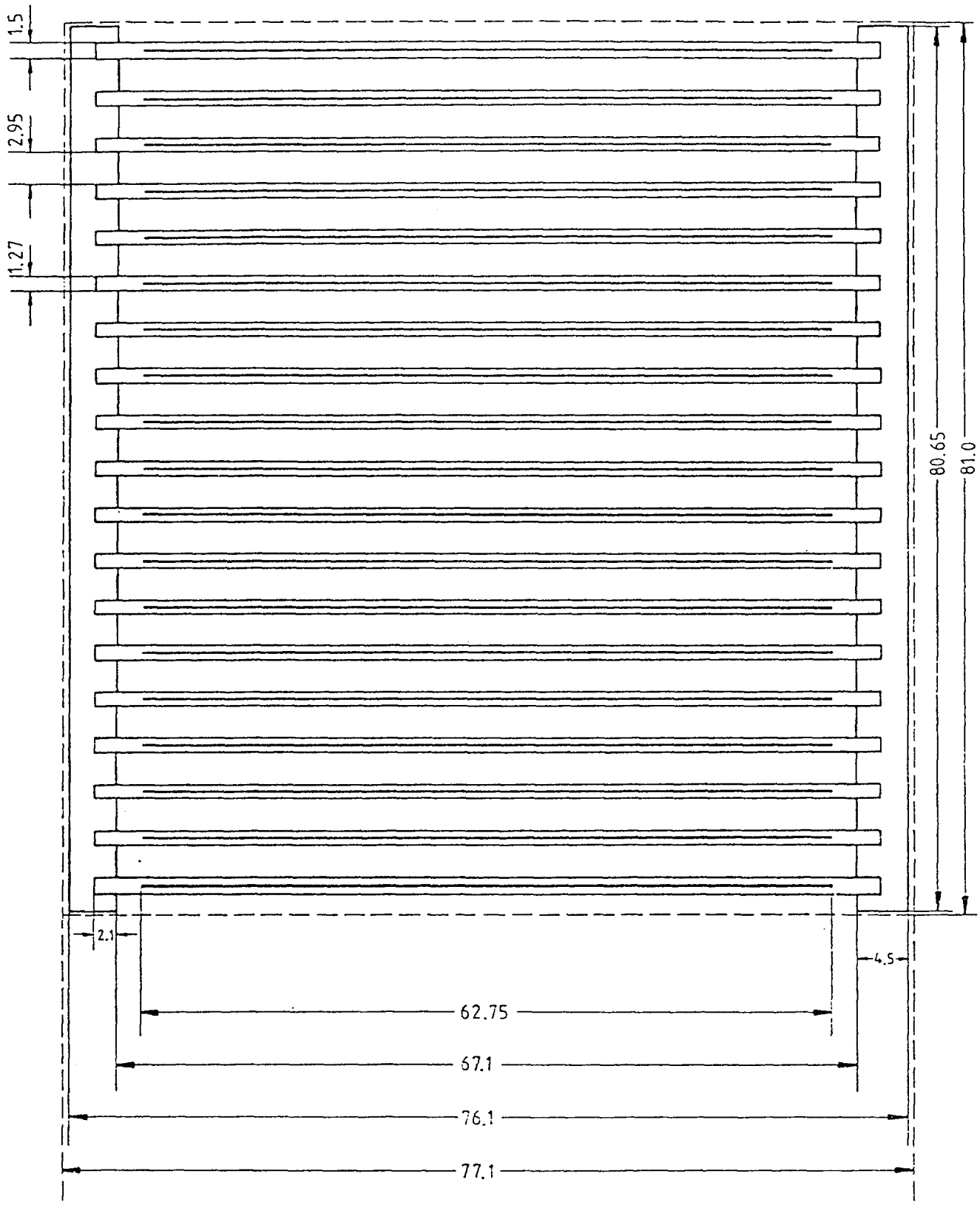

all dimensions in mm

2 MW - CORE
FUEL ELEMENT GEOMETRY
(HORIZONTAL CROSS SECTION)

2.2.1

- 19 fuel plates, 0.51 mm meat thickness
- 17 fuel plates, 1.00 mm meat thickness
- 15 fuel plates, 1.00 mm meat thickness

The frist of those three fuels is calculated only to demonstrate the effects if keeping the fuel assembly-geometry of the HEU-fuel unchanged, since this fuel leads to high uranium-density and therefore it is not a good choice of a REU-fuel.

2.2.3 REU-Fuel Determination by RZ-Calculations

The cross section sets for the different core calculations have been presented by their k_∞ versus burnup-behaviour in fig. 2.04 and 2.05. The simplified RZ-model used for diffusion calculations and being very similar to the analogous model of the 10 MW-core is shown by fig. 2.2.2. It is used to get the reactivities and flux distributions

- for the state BOL without xenon
- for the state BOL with xenon-equilibrium
- for the state EOL with xenon-equilibrium.

Starting with the HEU-fuel (180 g U235 per fuel element with 93 weight % U235 in 19 fuel plates per fuel element) we tried to find out the U235-loading per fuel element of 3 different REU-fuels using the EOL criterion. All the resulting REU-fuels are specified within table 2.2.1 together with the HEU-fuel. The way we determined the REU-fuel, i. e. how we found out the EOL-reactivity matching U235-loading of the different REU-fuels is shown at fig. 2.2.3.

The main results are

- HEU-fuel
  180 g 235 with 93 w/o U235
  (19 plate-fuel element with .51 mm meat thickness)
- REU-fuel
  207 g U235 with 20 w/o U235
  (19 plate-fuel element with 0.51 mm meat thickness)
- REU-fuel
  232 g U235 with 20 w/o U235
  (17 plate-fuel element with 1.0 mm meat thickness)
- REU-fuel
  216 g U235 with 20 w/o U235
  (15 plate-fuel element with 1.0 mm meat thickness)

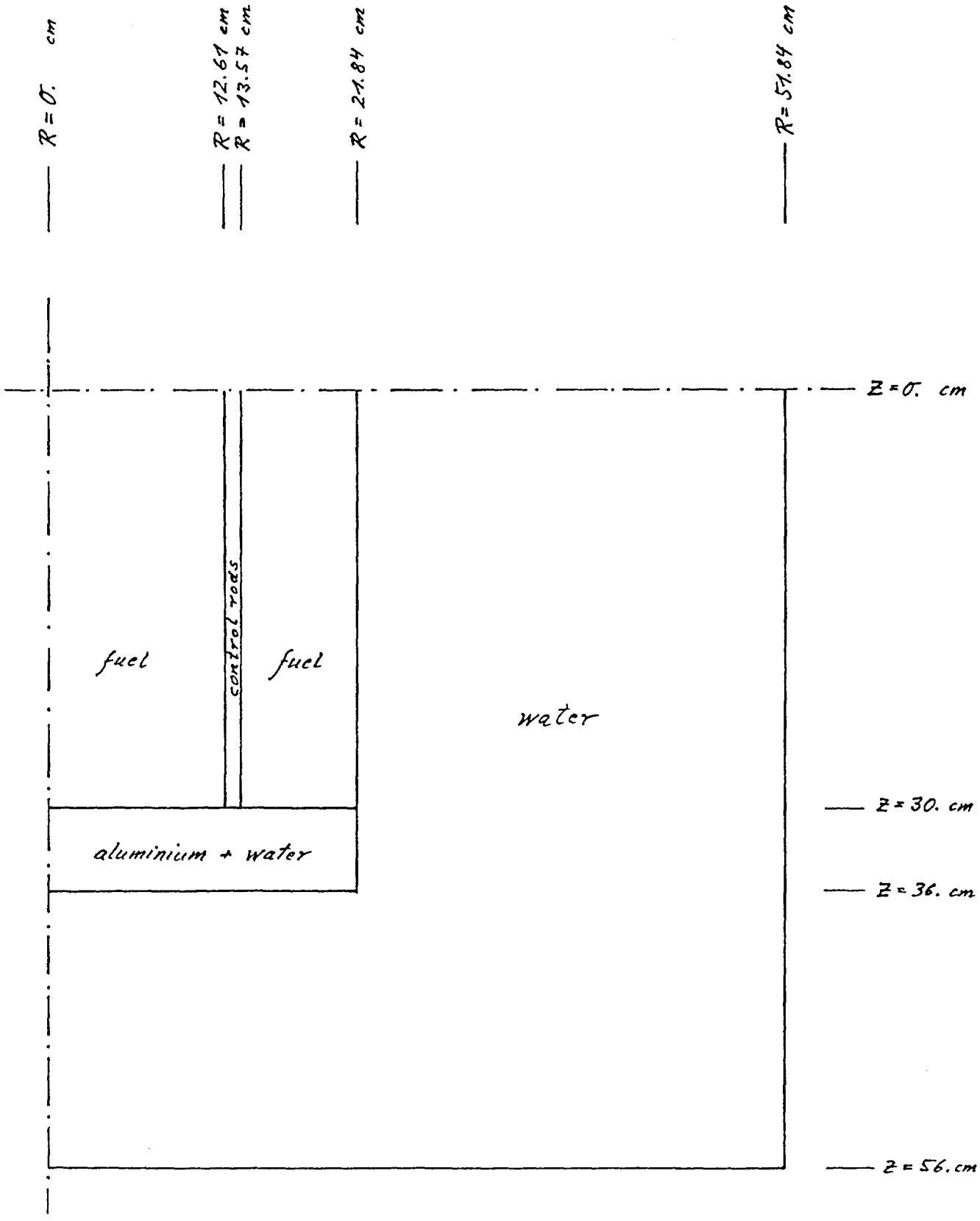

2 MW - Core
RZ-Model for Diffusion Calculations

2.2.2

Table 2.2.1 Fuel specifications / 2 MW case

	HEU-fuel	LEU-fuels using the EOL-criterion			alternative LEU-fuels using the uranium density 3.0 g/cm³ *)	
number of fuel plates	19	15	17	19	15	17
meat volume/FE	364.83 cm³	564.75 cm³	640.05 cm³	364.829 cm³	564.75 m³	640.05 cm
inner water gap width	.295 cm	.360 cm	.295 cm	.295 cm	.360 cm	.295 cm
grid space per FE	8.1cmx7.71cm x60cm	8.1cmx7.71cm x60cm	8.1cmx7.71cm x60cm	8.1cmx7.71cm x60cm	8.1cmx7.71cm x60cm	8.1cmx7.71cm x60cm
uranium thickness	0.051 cm	0.1 cm	0.1 cm	0.051 cm	0.1 cm	0.1 cm
U235 loading/FE	180 g U235	216 g U235	232 g U235**)	207 g U235	339 g U235	384 g U235
enrichment	93 w/o U235	20 w/o U235	20 w/o U235	20 w/o U235	20 w/o U235	20 w/o U235
uranium loading/fuel plate	10.187 gU	72.0 gU	68.235 gU	54.474 gU	113 gU	112.94 gU
uranium density	.531 g/cm³	1.912 gU/cm³ ***)	1.812 gU/cm³ ***)	2.837 gU/cm³	3.0 gU/cm³	3.0 gU/cm³
weight percentage/ meat	16.9 w/o U	44.8 w/o U	43.2 w/o U	57.3 w/o U	59.4 w/o U	59.4 w/o U
moderation ratio at BOL averaged burnup (15 % for basic fuel)	394	306	264	334	186	143

*) this value was chosen because it is a long term gain of the German fuel development program

**) result of RZ-calculation; XY calculations show 235 g U235 instead of 232 g U235

***) these uranium-densities are somewhat higher than the near term availibility of 1.7 g U/cm³ based on UAl_x-Al-fuel as far as the German NUKEM company is concerned. On the other hand it is simple to exchange this type of fuel with U_3O_8-fuel the near term availability of which is 2.6 g/cm³.

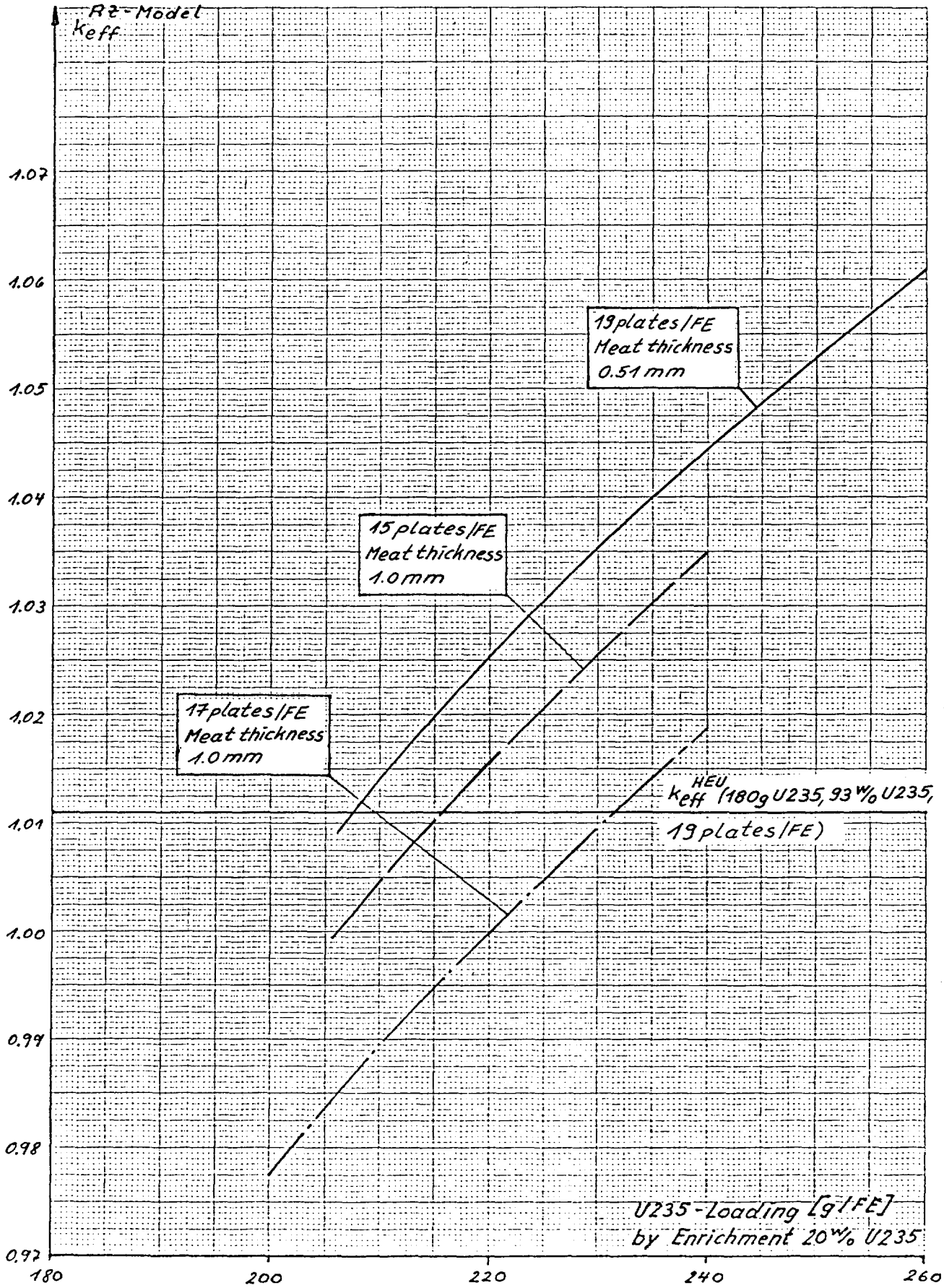

2 MW Reactor Conversion
EOL-Excess Reactivity Matching Criterion
Determination of Uranium Loading for Conversion

2.2.3

With these U235-loadings fixed we are able to calculate the BOL-states to get an overview of the reactivity behaviour of the REU-fuels in comparison to the HEU-fuel. Fig. 2.2.4 demonstrates the results of a thinkable conversion with unchanged fuel element-geometry whereas fig. 2.2.5 shows the results of the realistic REU-fuels with 1 mm meat thickness and 15 and 17 fuel plates per element, resp. Both figures are given in the way of a k_{eff} versus burnup-plot (for the abscissas used within these figures see paragraph 2.1.3).

The expected reduction of the excess reactivity turns out be at BOL with fresh fuel using the EOL-reactivity matching-criterion

- $\Delta\rho \approx$ 6.2 °/₀₀ for the 19 plates-REU-fuel
- $\Delta\rho \approx$ 6.5 °/₀₀ for the 17 plates-REU-fuel
- $\Delta\rho \approx$ 7.9 °/₀₀ for the 15 plates-REU-fuel.

BOL with xenon-equilibrium these reductions are roughly 1 °/₀₀ lower. The same flattened burnup behaviour appears as in the 10 MW-case with its corresponding advantage in view to reactivity compensation during the irradiation period.

Passing over to the second important result of these calculations we found the flux distribution as shown within the figures 2.2.6 to 2.2.17 for the axial and the radial traverse through the core center at BOL and at EOL, resp. These figures again use the nomenclature given by table 2.1.2. Each figure compares the flux shape resulting from the usage of the HEU-fuel with those of the three fuels which are alternatives for conversion.

From figure 2.2.8 containing the thermal flux behaviour in radial direction one extracts relatively large reductions of the fluxes especially in the center of the core:

- 18 % remaining with 19 plates/FE loaded with 207 g U235 (.51 mm meat)
- 22 % passing over to 15 plates/FE loaded with 216 g U235 (1.0 mm meat)
- 30 % passing over to 17 plates/FE loaded with 232 g U235 (1.0 mm meat),

which of course are not of great importance for the user and therefore merely illustrativ whereas at the reflector peak the differences are reduced to approximately 4 % for the different REU-fuels only.
Further relationships can be extracted from the figures directly.

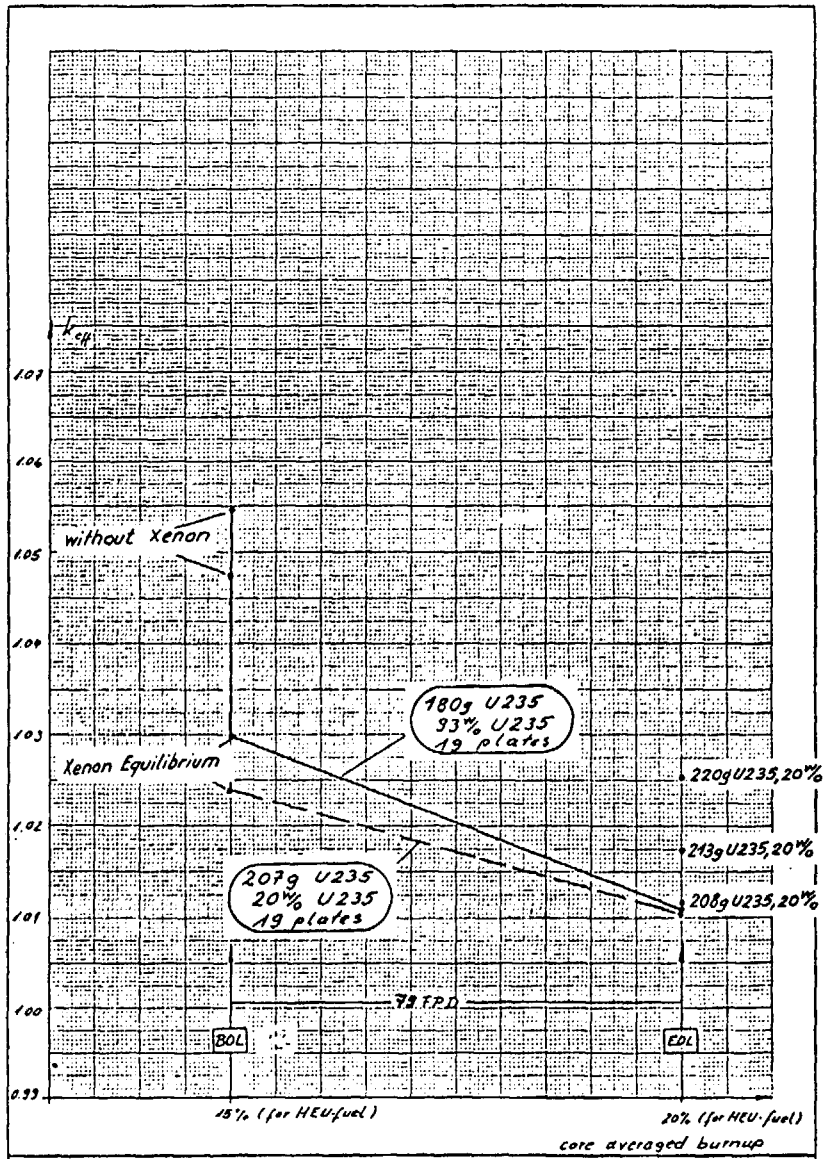

2 MW - Reactor Conversion EOL -Criterion
Determination of REU-Fuel with 2o w/o U235 with constant Fuel Element Geometry using the simplified RZ-Calculation

2.2.4

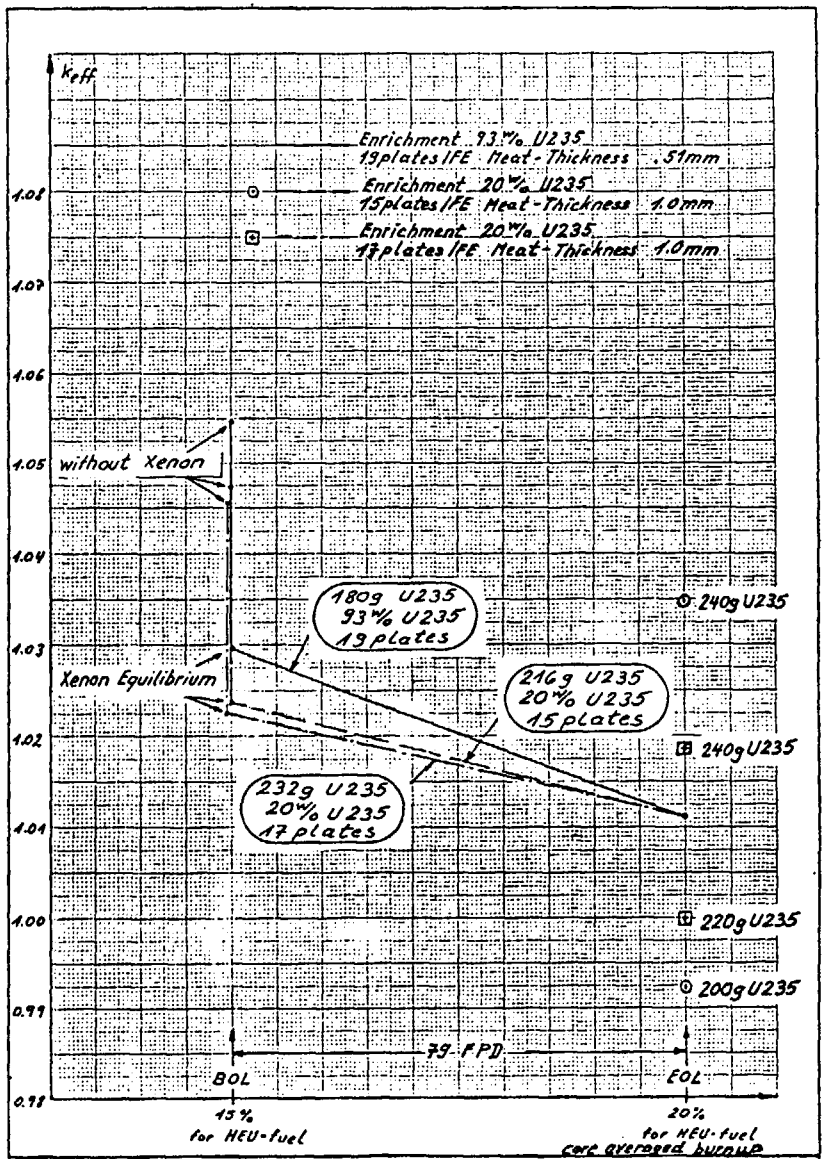

2 MW - Reactor Conversion EOL-Criterion
Determination of REU-Fuels with 2o w/o U235 and with Change in the Fuel Element Geometry using the simplified RZ-Calculation

2.2.5

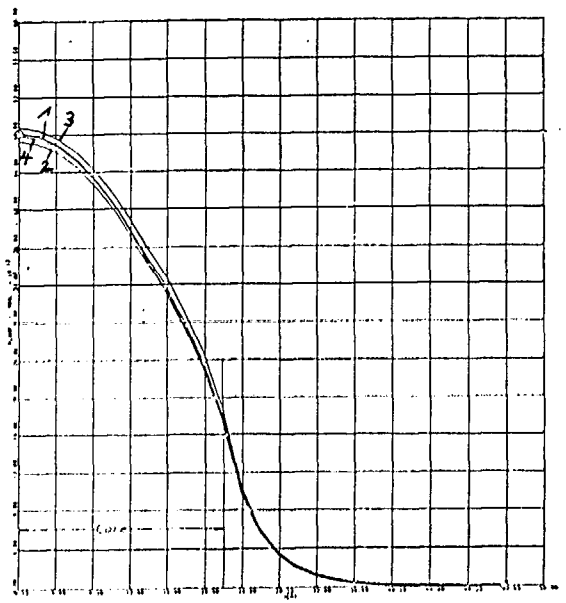

1 = HEU - fuel 18og-U235 93 % -U235 19plates/FE .51mm meat
2 = REU - fuel 2o7g-U235 2o % -U235 19plates/FE .51mm meat
3 = REU - fuel 232g-U235 2o % -U235 17plates/FE 1.oomm meat
4 = REU - fuel 216g-U235 2o % -U235 15plates/FE 1.oomm meat

2MW-RZ-MODEL BOL XE-EQUILIBRIUM
FLUSS - VERTEILUNG 1.GRUPPE
ZEILE 1

ABB 2.2.6

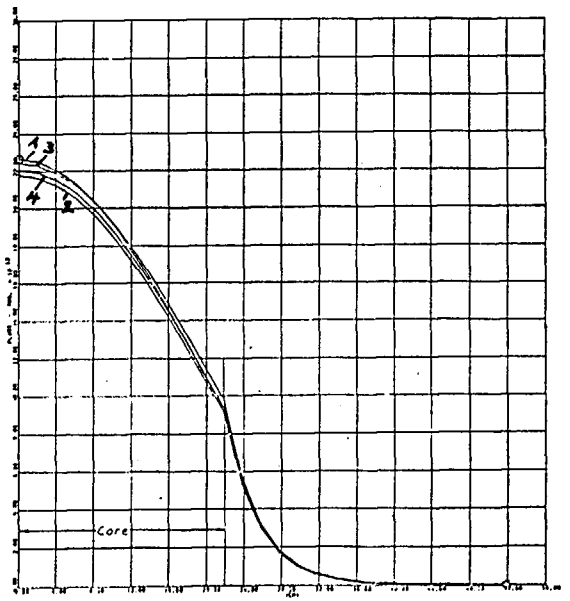

1 = HEU - fuel 18og-U235 93 % -U235 19plates/FE .51mm meat
2 = REU - fuel 2o7g-U235 2o % -U235 19plates/FE .51mm meat
3 = REU - fuel 232g-U235 2o % -U235 17plates/FE 1.oomm meat
4 = REU - fuel 216g-U235 2o % -U235 15plates/FE 1.oomm meat

2MW-RZ-MODEL BOL XE-EQUILIBRIUM
FLUSS - VERTEILUNG 3.GRUPPE
ZEILE 1

ABB 2.2.7

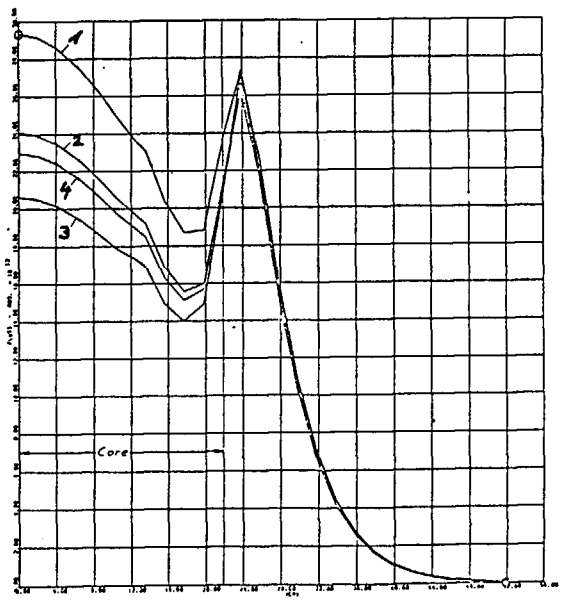

1 = HEU - fuel 18og-U235 93 % -U235 19plates/FE .51mm meat
2 = REU - fuel 2o7g-U235 2o % -U235 19plates/FE .51mm meat
3 = REU - fuel 232g-U235 2o % -U235 17plates/FE 1.oomm meat
4 = REU - fuel 216g-U235 2o % -U235 15plates/FE 1.oomm meat

2MW-RZ-MODEL BOL XE-EQUILIBRIUM
FLUSS - VERTEILUNG 4.GRUPPE
ZEILE 1

ABB 2.2.8

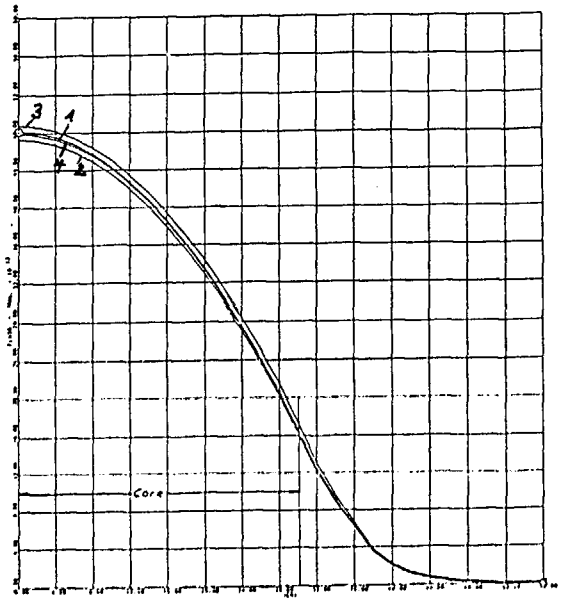

1 = HEU - fuel 18og-U235 93 % -U235 19plates/FE .51mm meat
2 = REU - fuel 2o7g-U235 2o % -U235 19plates/FE .51mm meat
3 = REU - fuel 232g-U235 2o % -U235 17plates/FE 1.oomm meat
4 = REU - fuel 216g-U235 2o % -U235 15plates/FE 1.oomm meat

2MW-RZ-MODEL BOL XE-EQUILIBRIUM
FLUSS - VERTEILUNG 1.GRUPPE
SPALTE 1

ABB 2.2.9

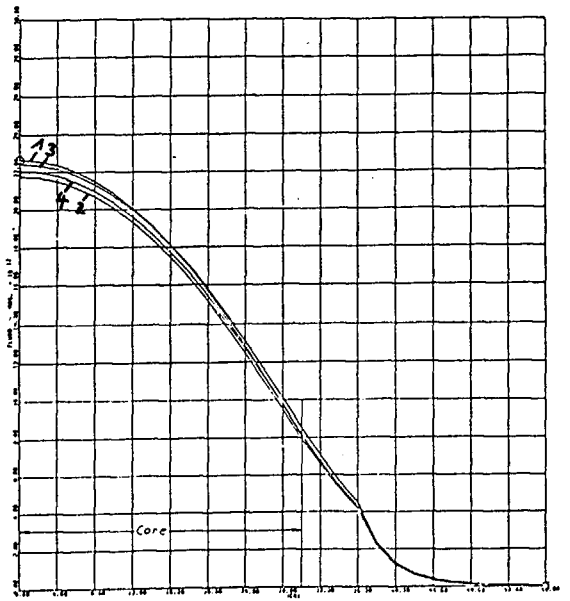

1 = HEU - fuel 18og-U235 93 % -U235 19plates/FE .51mm meat
2 = REU - fuel 2o7g-U235 2o % -U235 19plates/FE .51mm meat
3 = REU - fuel 232g-U235 2o % -U235 17plates/FE 1.oomm meat
4 = REU - fuel 216g-U235 2o % -U235 15plates/FE 1.oomm meat

2MW-RZ-MODEL BOL XE-EQUILIBRIUM
FLUSS - VERTEILUNG 3.GRUPPE
SPALTE 1

ABB 2.2.10

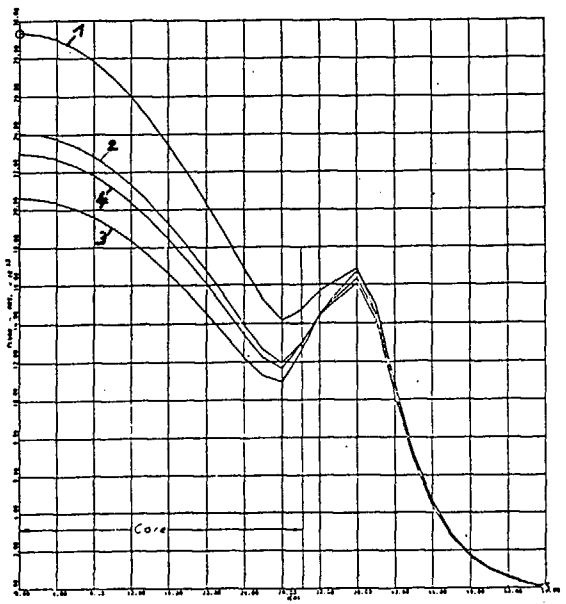

1 = HEU - fuel 18og-U235 93 % -U235 19plates/FE .51mm meat
2 = REU - fuel 2o7g-U235 2o % -U235 19plates/FE .51mm meat
3 = REU - fuel 232g-U235 2o % -U235 17plates/FE 1.oomm meat
4 = REU - fuel 216g-U235 2o % -U235 15plates/FE 1.oomm meat

2MW-RZ-MODEL BOL XE-EQUILIBRIUM
FLUSS - VERTEILUNG 4.GRUPPE
SPALTE 1

ABB 2.2.11

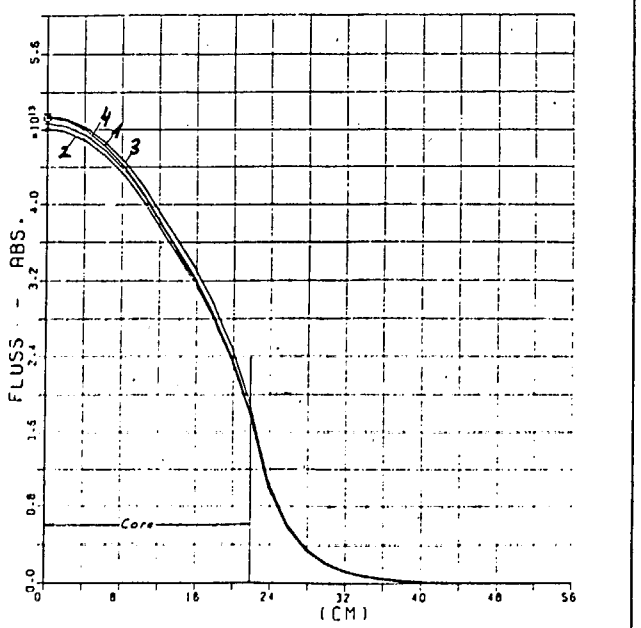

2MW-RZ-MODEL EOL XE-EQUILIBRIUM
FLUSS - VERTEILUNG 1.GRUPPE
ZEILE 1

ABB 2.2.12

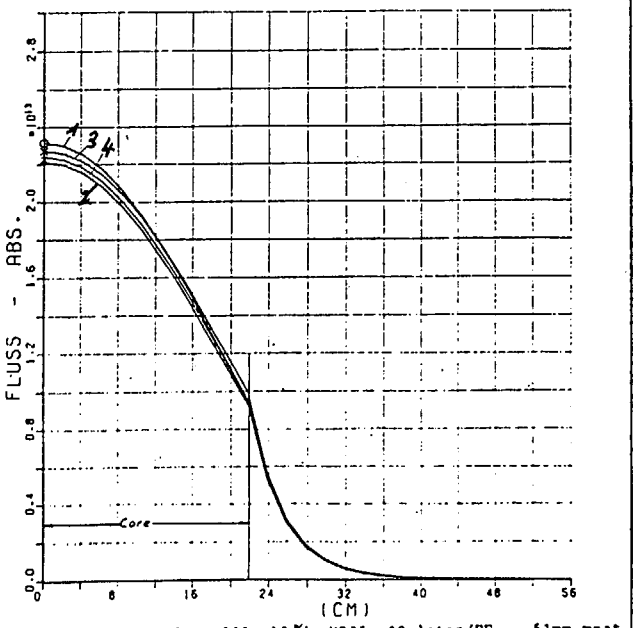

2MW-RZ-MODEL EOL XE-EQUILIBRIUM
FLUSS - VERTEILUNG 3.GRUPPE
ZEILE 1

ABB 2.2.13

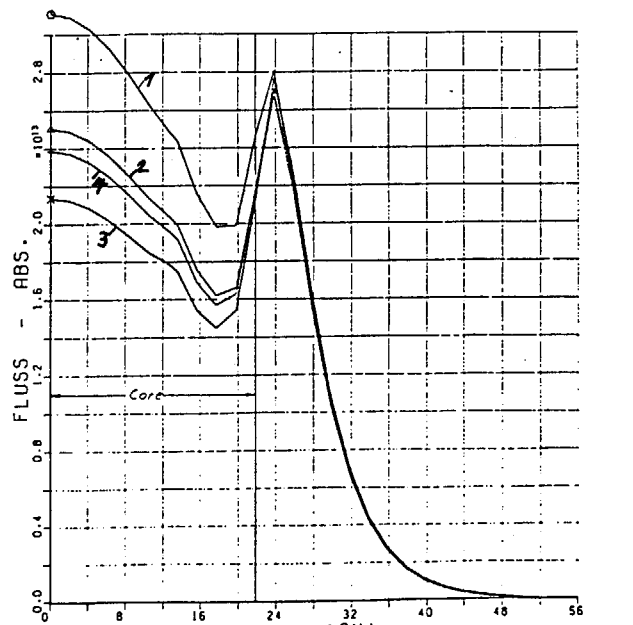

2MW-RZ-MODEL EOL XE-EQUILIBRIUM
FLUSS - VERTEILUNG 4.GRUPPE
ZEILE 1

ABB 2.2.14

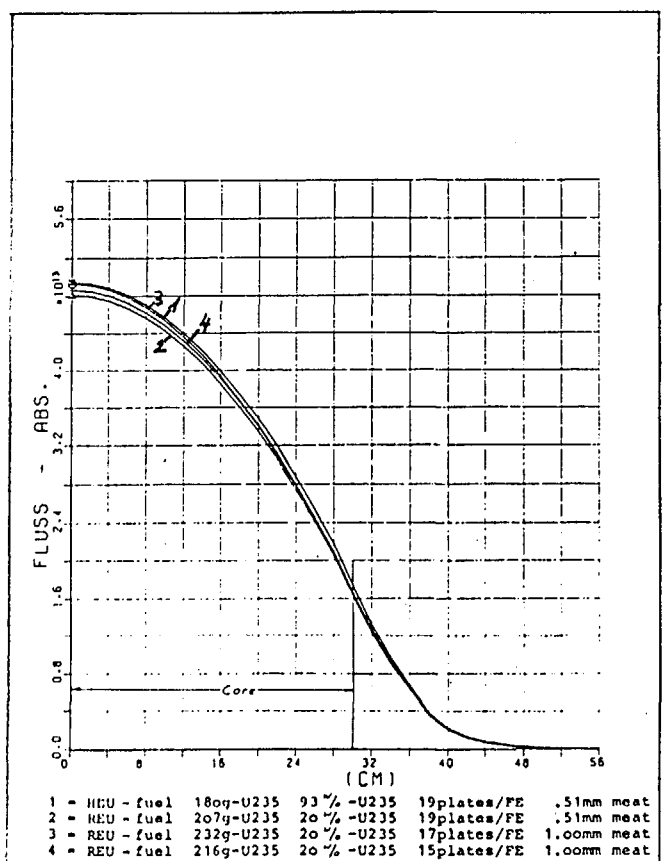

2MW-RZ-MODEL EOL XE-EQUILIBRIUM
FLUSS - VERTEILUNG 1.GRUPPE
SPALTE 1

ABB 2.2.15

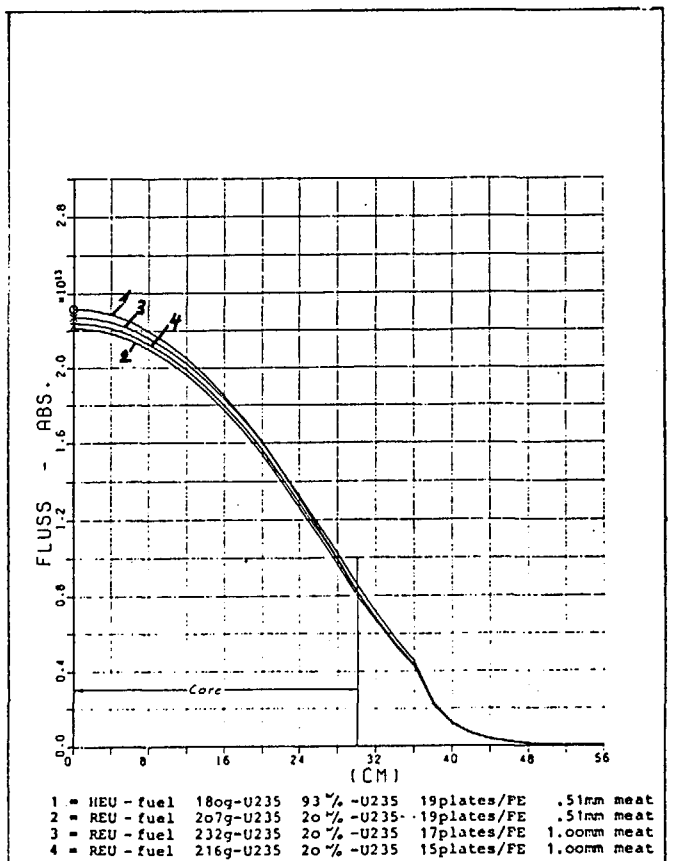

2MW-RZ-MODEL EOL XE-EQUILIBRIUM
FLUSS - VERTEILUNG 3.GRUPPE
SPALTE 1

ABB 2.2.16

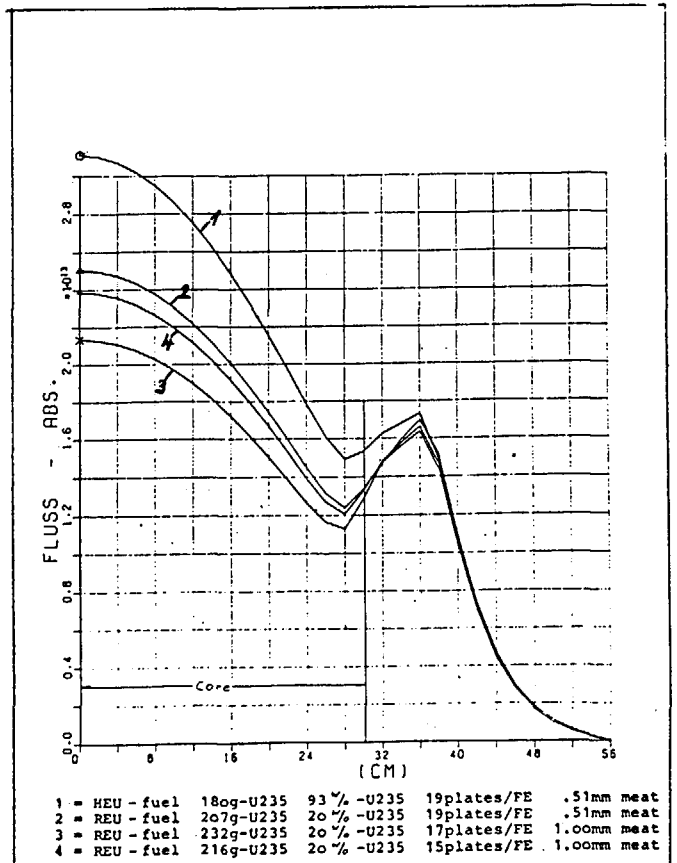

2MW-RZ-MODEL EOL XE-EQUILIBRIUM
FLUSS - VERTEILUNG 4.GRUPPE
SPALTE 1

ABB 2.2.17

As in the 10 MW-case one can discuss the aspect of the reduction of the control rod effectiveness. Starting from the reduction in thermal flux at the area of the control rods (fig. 2.2.20)

- approx. 20 % for the fuel with 15 plates/FE
- approx. 28 % for the fuel with 17 plates/FE

and provided that the reduction of the control rod-effectiveness is of the same percentage one has to compare that with the parallel reduction of control demands. Here one finds (fig. 2.2.5)

- approx. 16 % reduction for 15 plates/FE
- approx. 20 % reduction for 17 plates/FE.

Therefore the major part of the loss of control effectiveness is compensated by the reduction of control demands. Nevertheless there remains a small part of loss uncompensated. So a recalculation of this effect in a case by case study is unavoidable.

2.2.4 Prove of the RZ-Results by XY-Calculations

As in the 10 MW-case we made a prove wether the results of the simplified RZ-calculations may by affected by the simplifications of the model. The XY-model used is given in figure 2.2.18 including the burnup distribution of the HEU-fuel at BOL and EOL, resp.
This model is in agreement with the results of the Vienna-meeting, 29. Nov. to 2. Dez. 78. The presented working cores of fig. 2.2.18 corresponds in its averaged burnup to the burnup used in the RZ-calculations; the burnup distribution is chosen so that the fresh fuel is loaded into the mid of the core. We limited this prove to the 15 plate- and the 17 plate-fuel element.

The main results of the XY-calculations are:

- In the case of 17 fuel plates per element the U235 loading differs by 3 g U235 from the previous RZ-result. The sign of this figure is opposite to the analogous result at the 10 MW-case. This may result from the different way of loading the two cores (fresh fuel into the mid of the core here instead of fresh fuel to the outer core positions in the 10 MW-case). The exact figures for the U235-loadings

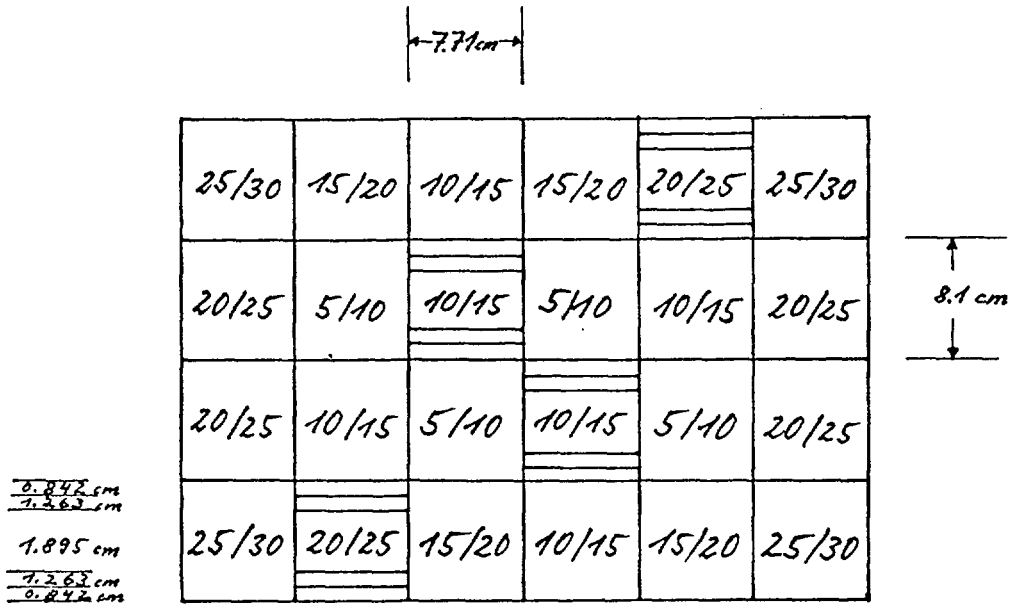

W_i / W_f = Burnup at BOL / Burnup at EOL

2 MW - Core
XY - Model for Diffusion Calculations

2.2.18

is 235 g U235 per fuel element. In the case of the 15 fuel plates per element the U235-loading resulting from RZ-calculations is nearly unchanged by the XY-calculations. (A small enlargement of the U235-loading of 1 g has been assessed. A real recalculation with this loading has been omitted (see fig. 2.2.19)). Again we found by this prove a good agreement with the results based on the RZ-model.

- the pure calculation figures of the reactivity are reduced again compared to the RZ-model. This can be seen by comparing fig. 2.2.19 with 2.2.5. Figure 2.2.19 composes the reactivity behaviour versus burnup of the two calculated REU-fuels in comparison to the behaviour of the HEU-fuel.

- the differences in fluxes are shown within figures 2.2.20 to 2.2.27 for 3 energy groups, two traverses through the core cross section perpendicular to each other, and two states of the core (BOL and EOL). These flux traverses again give a good impression of the flux shaping across the core taking into account the different burnup and the positions of the control rods *).

2.2.5 REU-Fuel using the BOL-Criterion

Using the BOL-excess reactivity matching criterion in the RZ-model, we found U235-loadings as follows(fig.2.2.28)

- 213g U235 if one remains with the element consisting out of 19 fuel plates
- 242g U235 if one passes over to a fuel element with 17 fuel plates
- 223g U235 if one chooses a fuel element with 15 fuel plates.

The fuel specifications are given within table 2.2.2. The results of this calculations in the way of effective reactivity versus length of the burnup period are shown in figure 2.2.29 and 2.2.30 for the fuel with unchanged fuel element geometry and for the fuel with changed geometry, resp.

*) All absolute fluxes are axially averaged within XY-plots

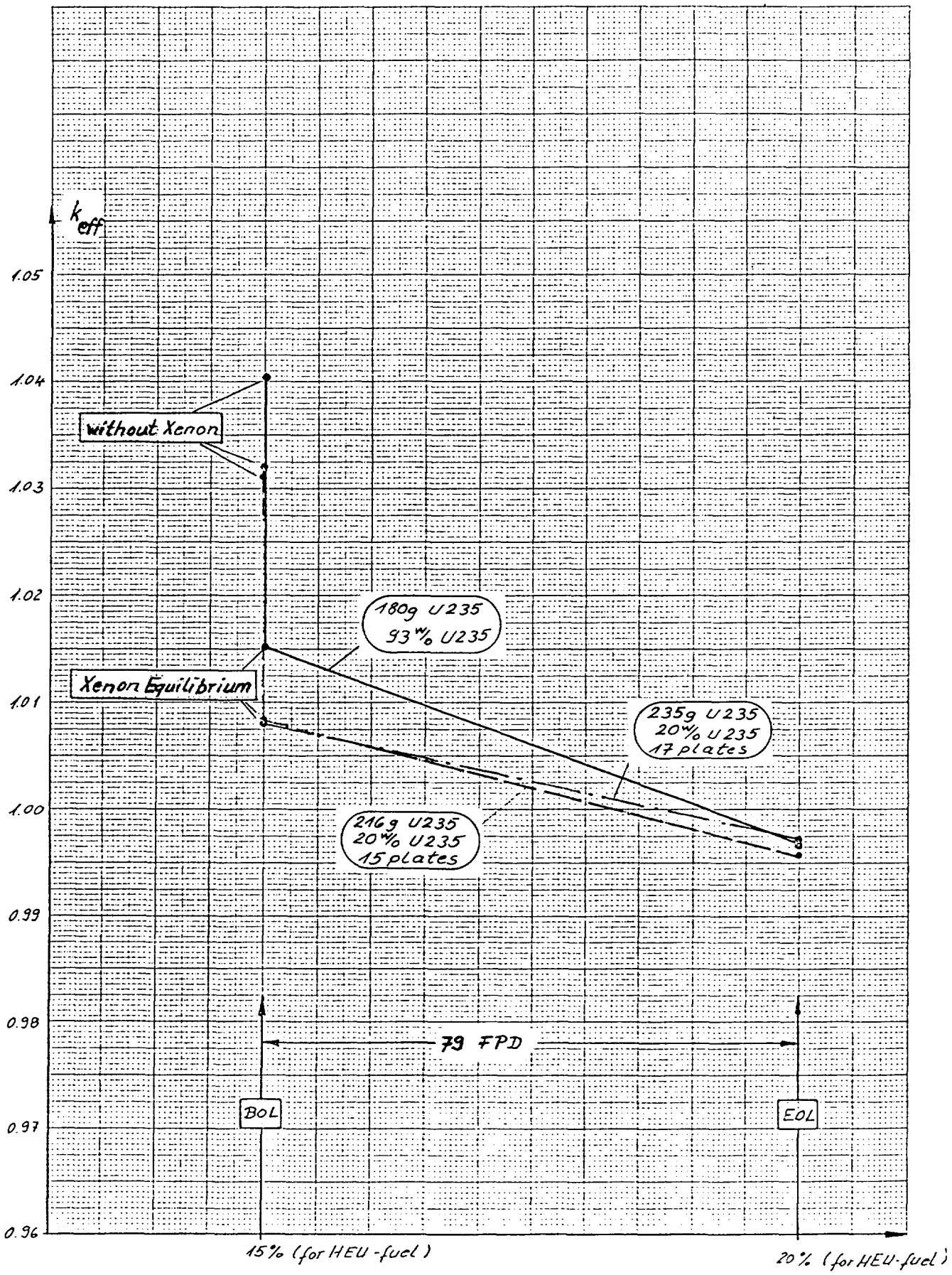

2 MW - Reactor Conversion EOL-Criterion
Determination of REU-Fuels with 2o w/o U235 using the XY-Calculation

2.2.19

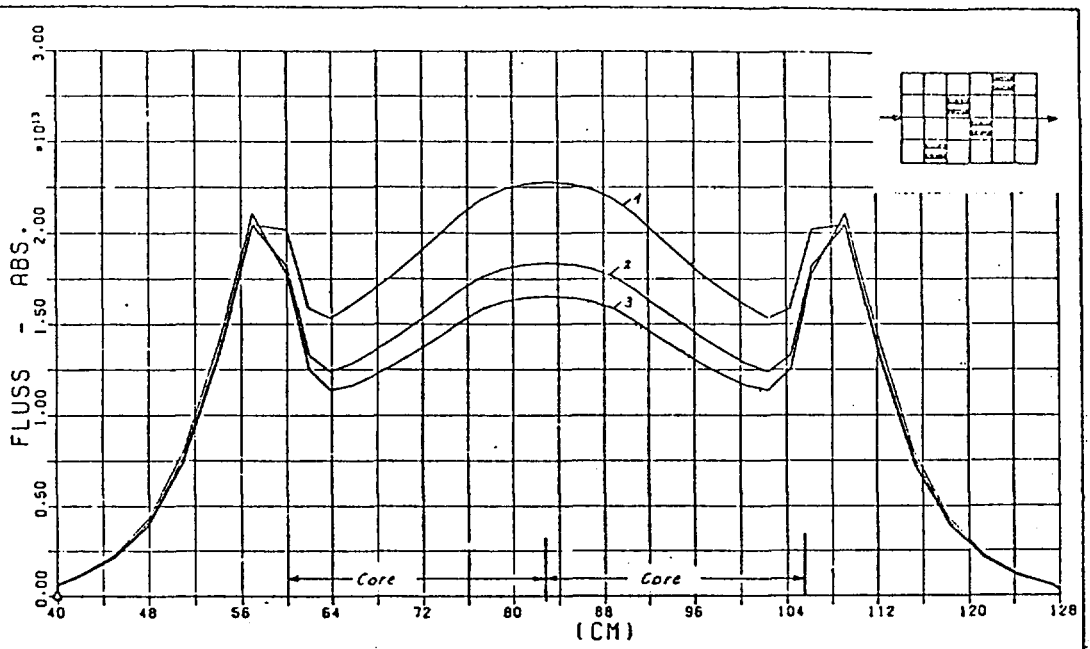

1 = HEU - fuel 180g-U235 93 %-U235 19plates/FE .51mm meat
2 = REU - fuel 216g-U235 20 %-U235 15plates/FE 1.0mm meat
3 = REU - fuel 235g-U235 20 %-U235 17plates/FE 1.0mm meat

2MW-XY-MODEL BOL XE-EQUILIBRIUM
FLUSS - VERTEILUNG 4.GRUPPE

ABB 2.2.20

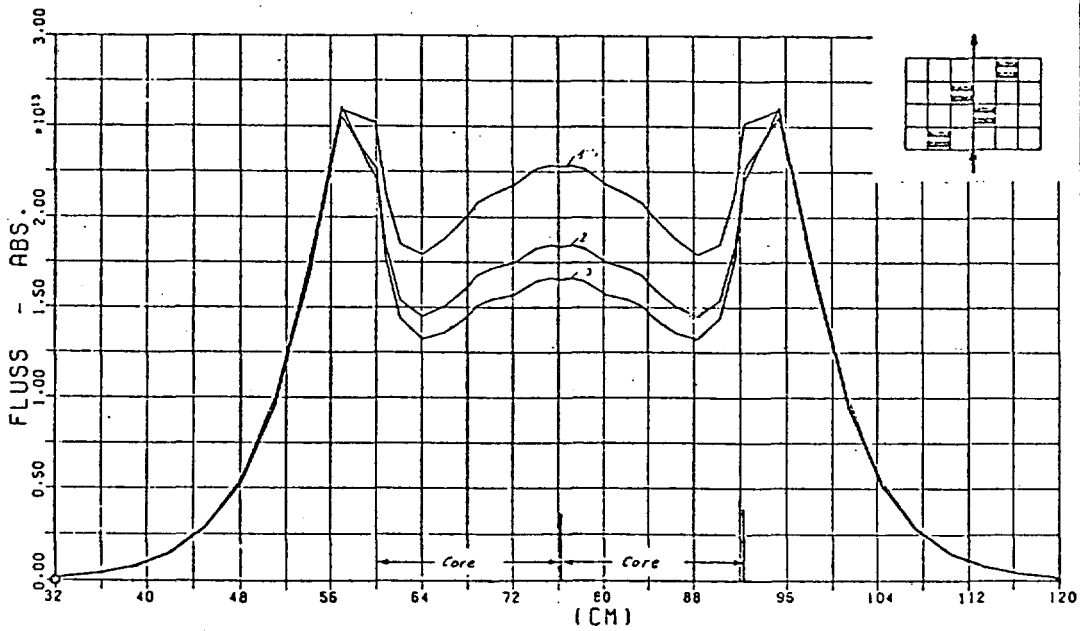

1 = HEU - fuel 180g-U235 93 %-U235 19plates/FE .51mm meat
2 = REU - fuel 216g-U235 20 %-U235 15plates/FE 1.0mm meat
3 = REU - fuel 235g-U235 20 %-U235 17plates/FE 1.0mm meat

2MW-XY-MODEL BOL XE-EQUILIBRIUM
FLUSS - VERTEILUNG 4.GRUPPE

ABB 2.2.21

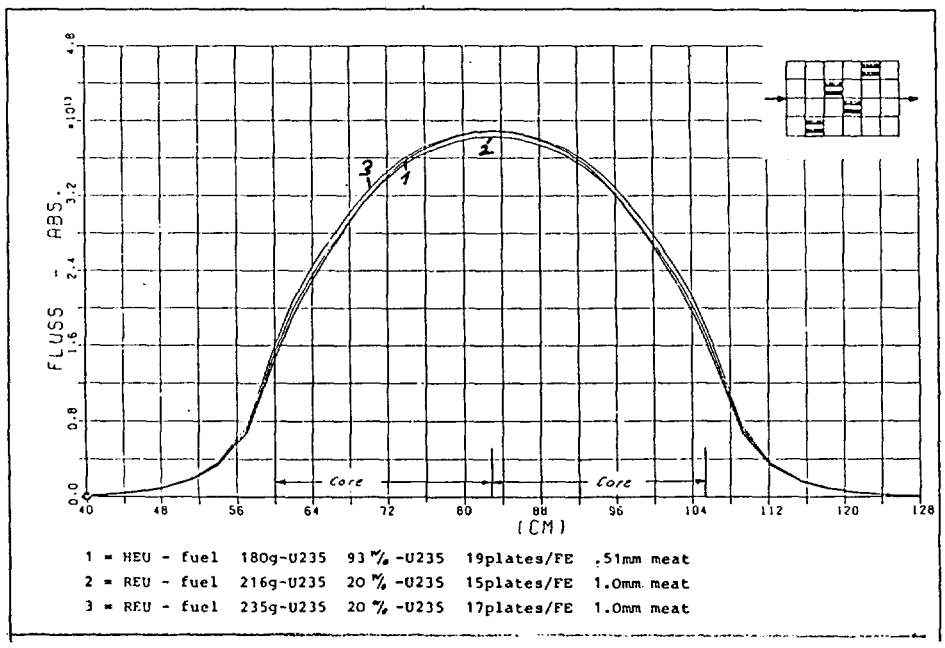

ABB 2.2.22

2MW-XY-MODEL EOL XE-EQUILIBRIUM
FLUSS - VERTEILUNG 1.GRUPPE

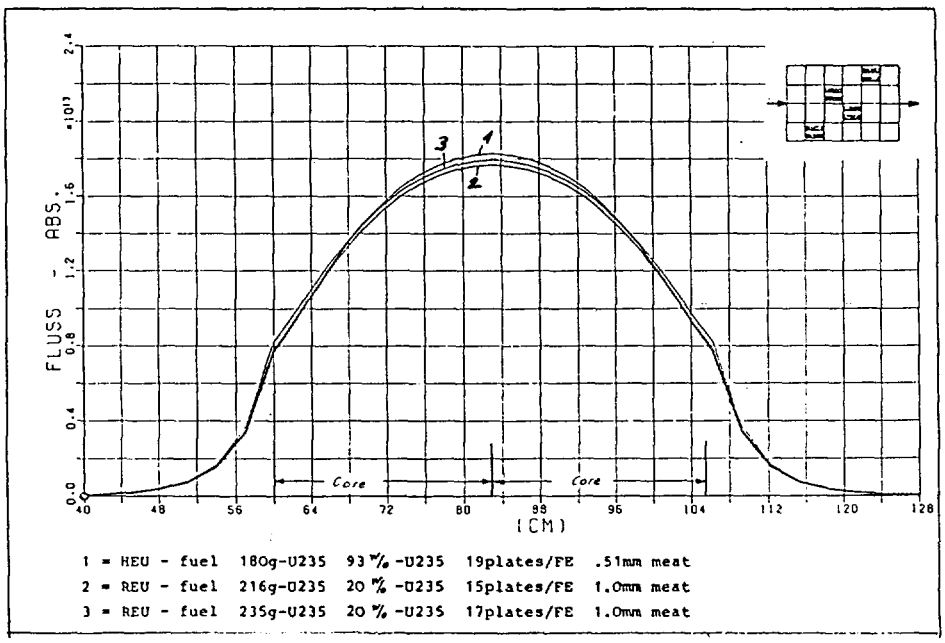

ABB 2.2.23

2MW-XY-MODEL EOL XE-EQUILIBRIUM
FLUSS - VERTEILUNG 3.GRUPPE

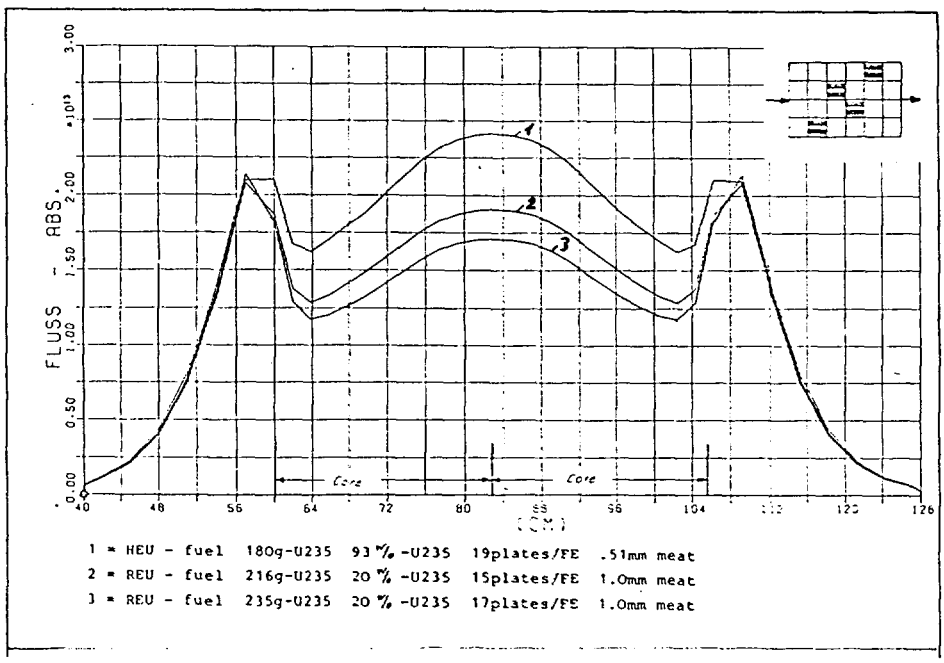

ABB 2.2.24

2MW-XY-MODEL EOL XE-EQUILIBRIUM
FLUSS - VERTEILUNG 4.GRUPPE

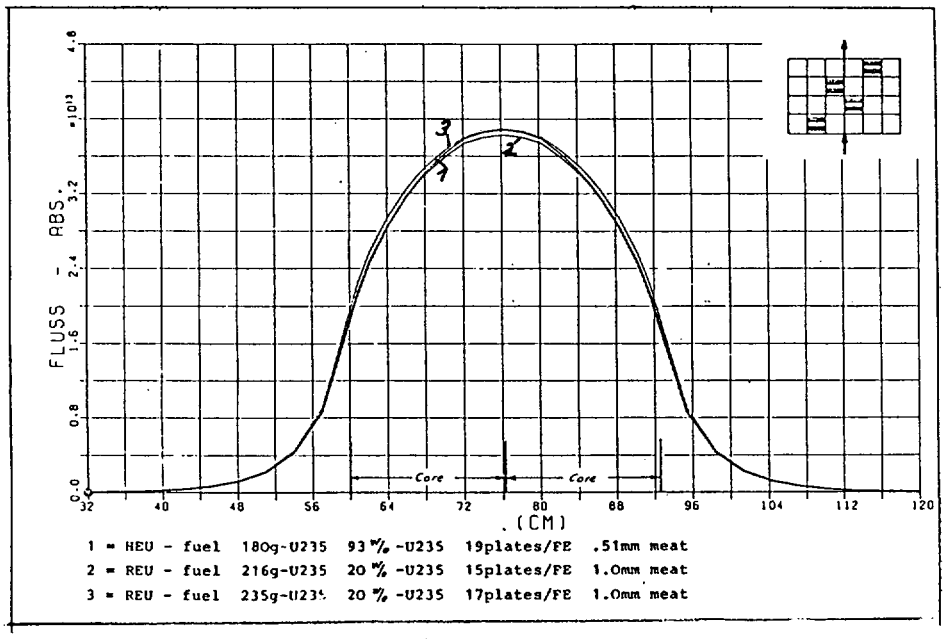

ABB 2.2.25

2MW-XY-MODEL EOL XE-EQUILIBRIUM
FLUSS - VERTEILUNG 1.GRUPPE

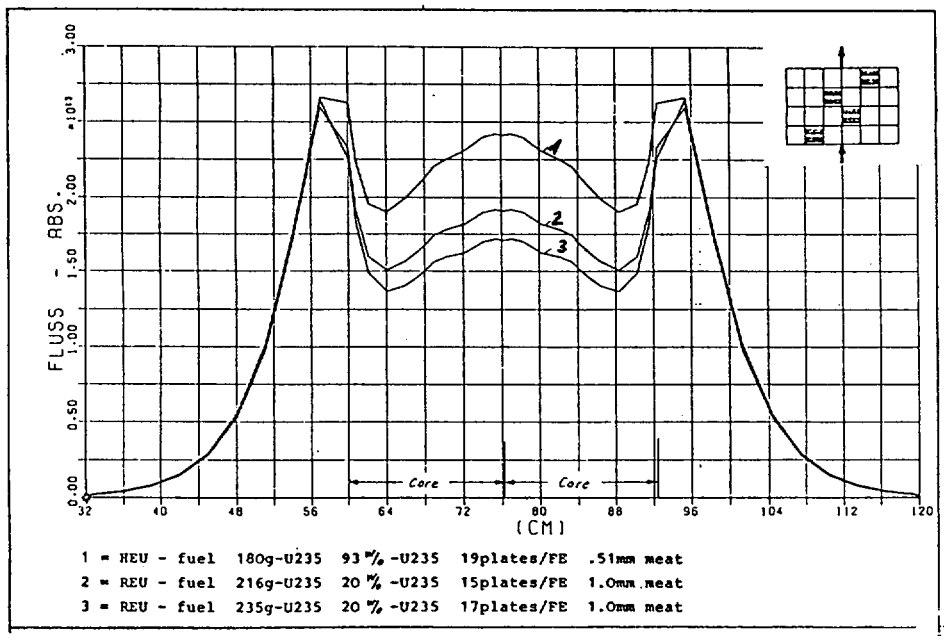

ABB 2.2.27

2MW-XY-MODEL EOL XE-EQUILIBRIUM
FLUSS - VERTEILUNG 4.GRUPPE

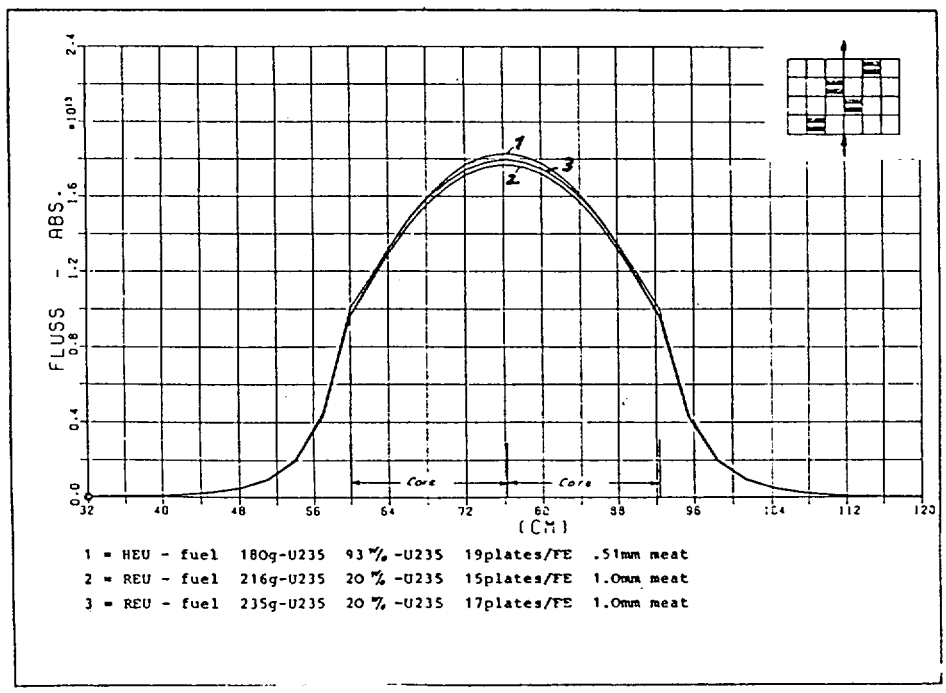

ABB 2.2.26

2MW-XY-MODEL EOL XE-EQUILIBRIUM
FLUSS. - VERTEILUNG 3.GRUPPE

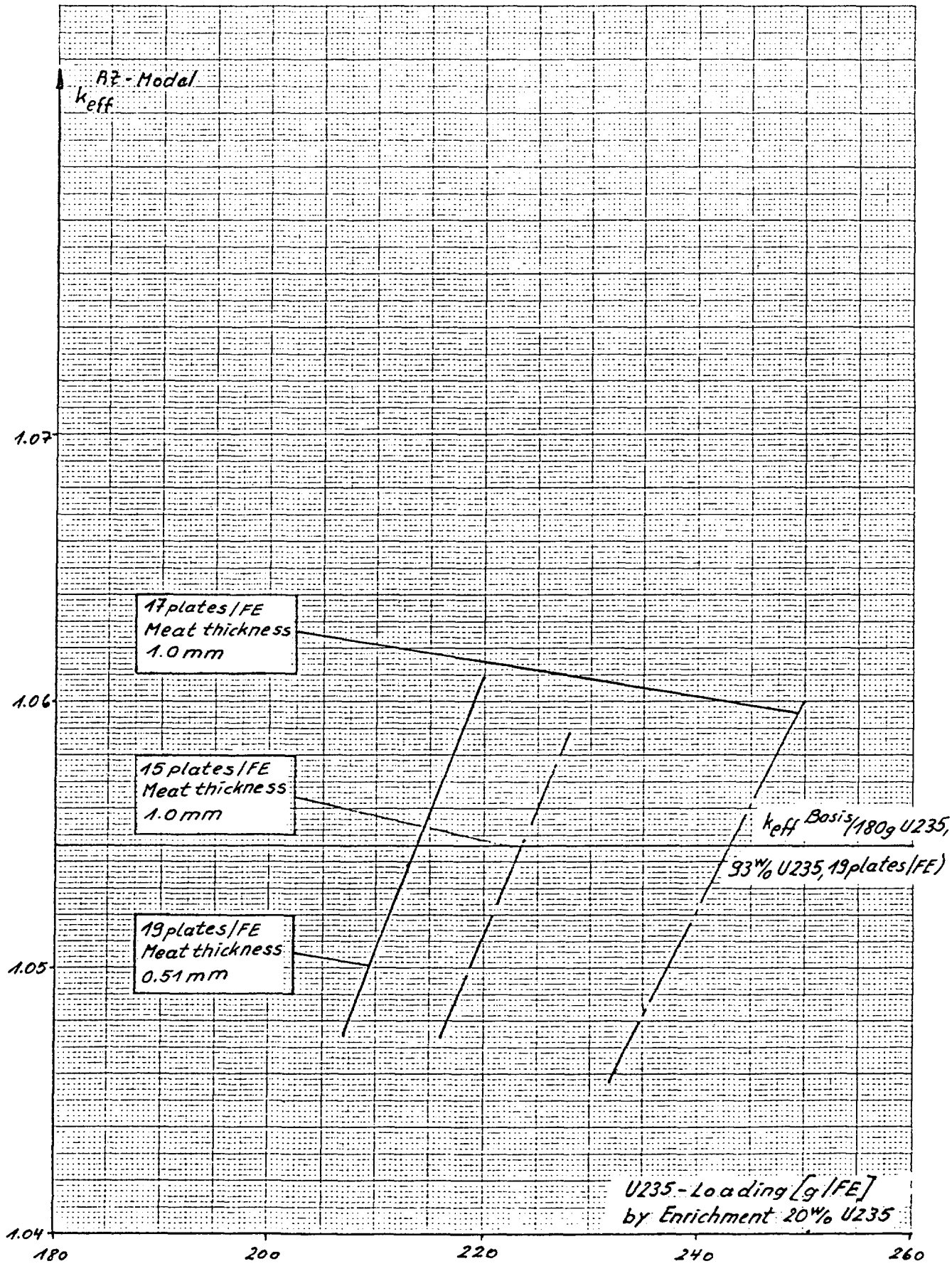

2 MW - Reactor Conversion
BOL-Excess-Reactivity Matching Criterion
Determination of Uranium Loading for Conversion

2.2.28

Table 2.2.2 Fuel specifications / 2 MW case

	HEU-fuel	LEU-fuels using the BOL criterion		
number of fuel plates	19	15	17	19
meat volume/FE	364.83 cm^3	564.75 cm^3	640.05 cm^3	364.829 cm^3
inner water gap width	.295 cm	.360 cm	.295 cm	.295 cm
grid space per FE	8.1cmx7.71cm x60cm	8.1xm.7.71cm x60cm	8.1cmx7.71cm x60cm	8.1cmx7.71cm x60cm
uranium thickness	0.051 cm	0.1 cm	0.1 cm	0.051 cm
U235-loading/FE	180 g U235	223 g U235	242 g U235	213 g U235
enrichment	93 w/o U235	20 w/o U235	20 w/o U235	20 w/o U235
uranium loading/fuel plate	10.187 gU	74.33 gU	71.18 gU	56.05 gU
uranium density	.531 gU/cm^3	1.974 U/cm^3	1.891 gU/cm^3	2.919 gU/cm^3
weight percentage/ meat	16.9 w/oU	45.8 w/o U	44.5 w/o U	58.3 w/o U
moderation ratio at BOL averaged burnup (15 % for HEU-fuel)	394	296	252	323

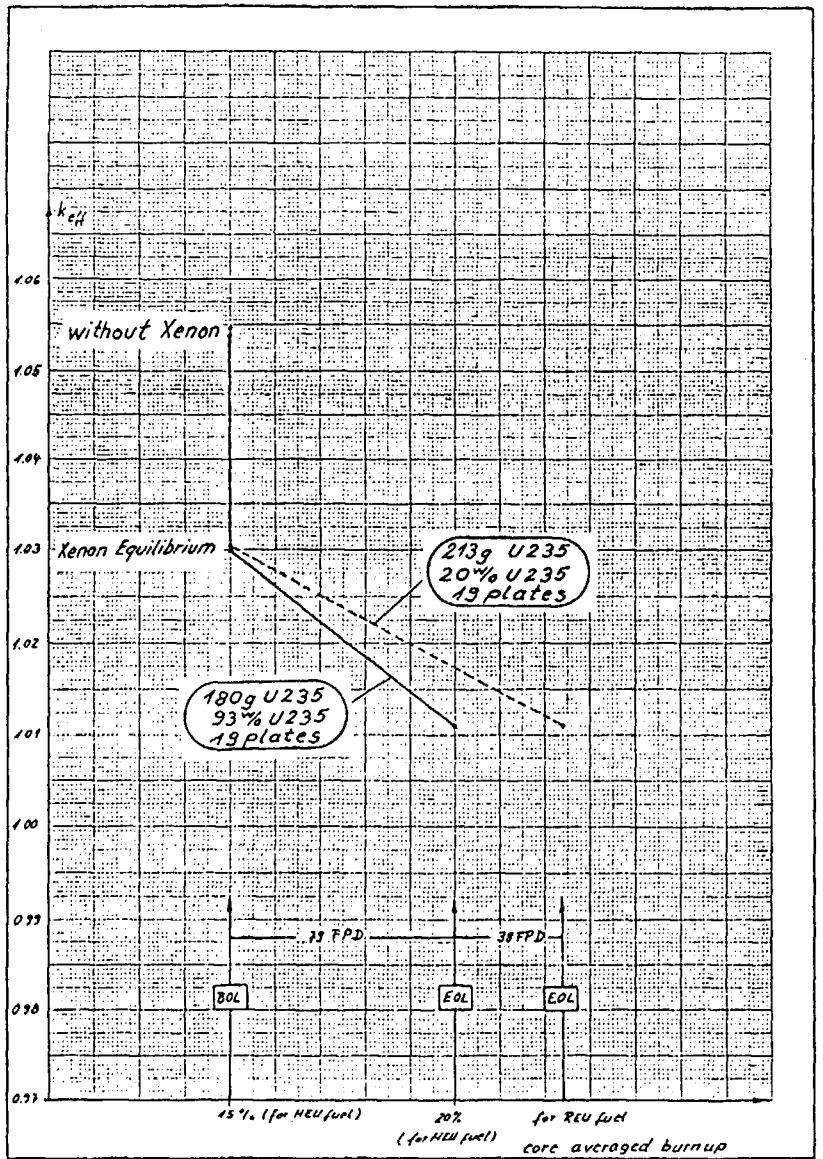

2 MW - Reactor Conversion BOL-Criterion
Determination of REU-Fuel with 2o w/o U235 and constant Fuel Fuel Element Geometry using the Simplified RZ - Calculation

2.2.29

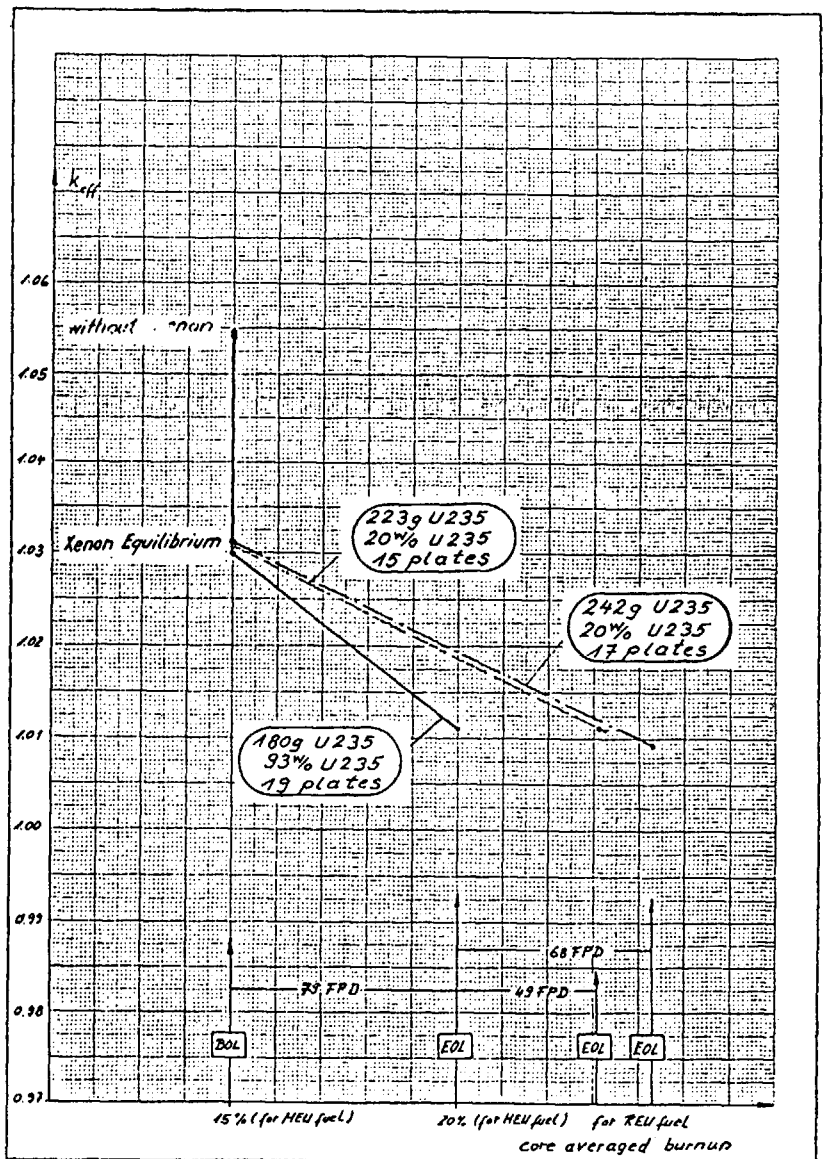

2 MW - Reactor Conversion BOL-Criterion
Determination of REU-Fuel with 2o w/o U235 and with Change in the Fuel Element Geometry using the simplified RZ-Calculation

2.2.3o

2.2.6 REU-Fuel using the Fuel Availability Limits

The uranium-densities in the meats of the different REU-fuels for the 2 MW-core are higher than 1.7 g U/cm³ (see table 2.2.1). So to use the fuel availability-criterion one can pass over to the higher limit of 3.0 g U/cm³ for long term-availability only. The REU-fuel herewith is not very realistic in our specific example. The only intension of the calculations done with this uranium-density is to show the potential that exists for fuels. The 3.0 g U/cm³ are chosen because they are stated by the German NUKEM company and they are as well the second step in the German Fuel Development Program. A wide potential for improving the core design is placed at a user's disposal by this high density fuel. This potential is demonstrated by figure 2.2.31 for the 15 - and 17-plate fuel element. In the case of 19 fuel plates per element there exists nearly no such potential since the density of this fuel is near to the limit of 3.0 g/cm³ even in the case of using the EOL-criterion.

The hypothetical enlargement of the burnup period when using these potential REU-fuels is more than a factor of 10 (see fig. 2.2.31). If one looks at this the other way round the statement is: there exists a wide potential of possibilities within these fuels with 1 mm - meat thickness even for higher total power of cores than 2 MW, if the thermal-hydraulic prerequisites will fit with the reduction of fuel plates per element necessary. This will be discussed within the next chapter.

2.2.7 REU-Fuel using the unchanged U235-content

As done in the 10 MW case we assessed the core behaviour in the case when the U235 content per fuel assembly is kept unchanged. Only the U238-content is enlarged to get the 20 w/o-enrichment for the fuel. This fuel is specified by 180 g U235/FE, 20 w/o-U235.
Varying in this case the number of fuel plates per assembly and the meat thickness as done for the previous criteria we assessed the following results:

- with 17 plates per fuel assembly the BOL-reactivity even without xenon is lower than the EOL-value of the HEU-fuel so that there is no possibility to use the core in the way provided for

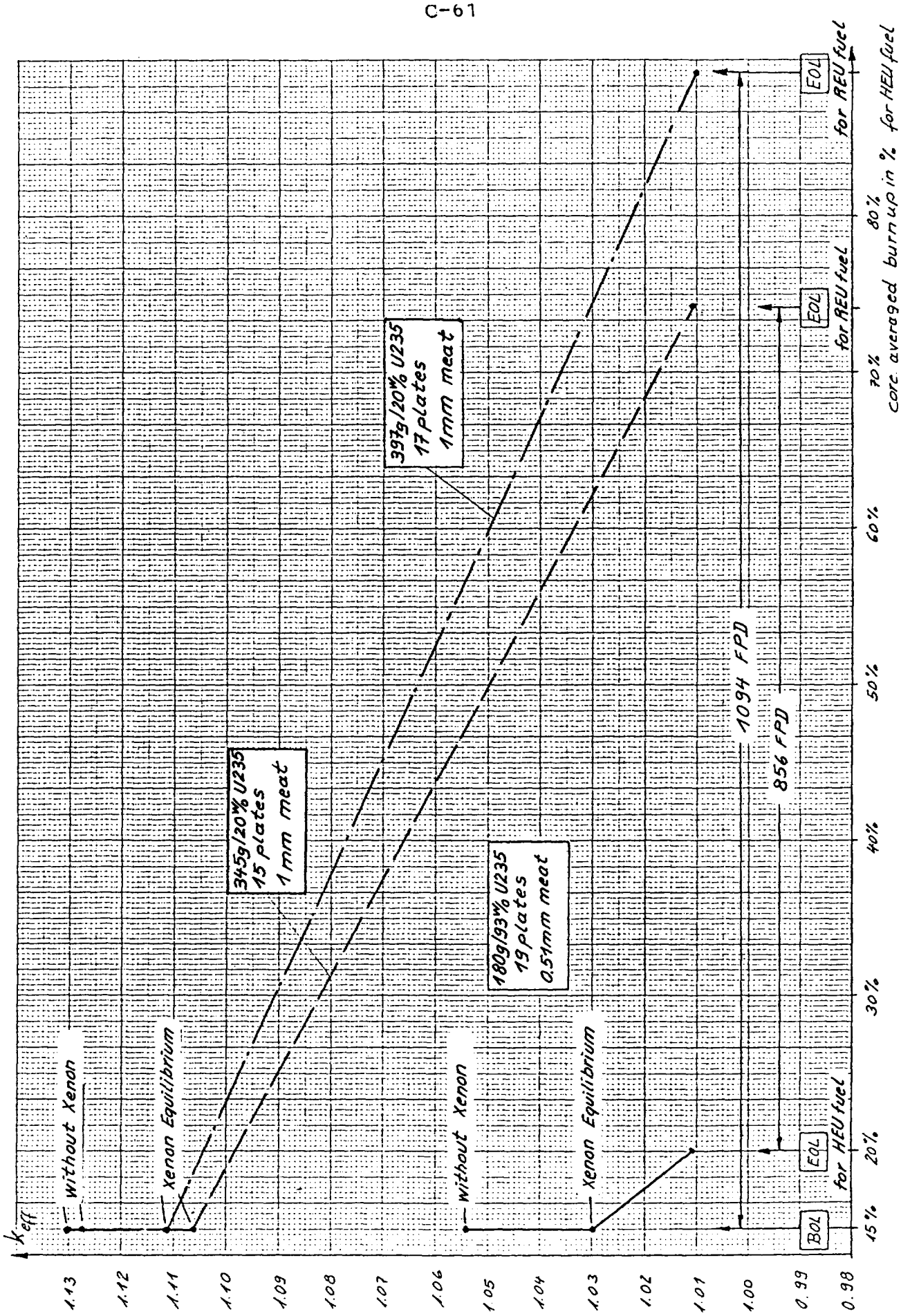

2 MW - Reactor Conversion Fuel Availability Criterion
Assessment of the Potential of REU-Fuels with U-Density
3.0 g/cm³ using the simplified RZ-Model

2.2.31

- with 15 plates there exist a small excess reactivity of ca. 3 o/oo $\Delta\rho$ starting without xenon. But taking into account the 2.2 % $\Delta\rho$ of the xenon equilibrium this excess reactivity is comperatively small and a real load cycle is not possible.

In consequence of these facts there exists no possibility for using fuel with the U235-content unchanged.

2.2.8 Thermal-hydraulic analysis

The consequences of a reduction of the number of fuel plates per assembly from 19 (reference case) to 17 or 15 on the thermal-hydraulic performance of the core have been analysed.

Fuel plate and fuel assembly geometry data are summarized in Table 2.2.3, which also gives the nuclear hot channel factors. Fig. 2.2.32 shows the axial power distribution, it is assumed to be the same for the three fuel assembly types.

The core thermal power was taken to be 2 MW. Two different core flow rates were used, i. e. 150 m^3/h and 300 m^3/h. The specific flow rate is thus 75 $m^3/(h.MW)$ and 150 $m^3/(h.MW)$. The lower value is typical for a number of MTR-cores.

The thermal-hydraulic performance of the three types of fuel assemblies has been evaluated on the basis of calculations for the cooling channel with the highest power input. Because no detailed specifications are currently available this investigation had to be based on nominal conditions for fuel assembly geometry, fuel loading, flow distribution etc. The power distributions correspond to worst case conditions.

Table 2.2.4 and 2.2.5 present the results of these preliminary analyses for the two flow rates.

Since the lower flow rate results in reduced margins against DNB and flow stability limits only this case will be discussed further.

As can be seen from Table 2.2.5 the DNB-ratios are very high even under the conservative assumption that no subcooling exists. These ratios would increase by a factor of about 2.5 if the actual subcooling would be used.

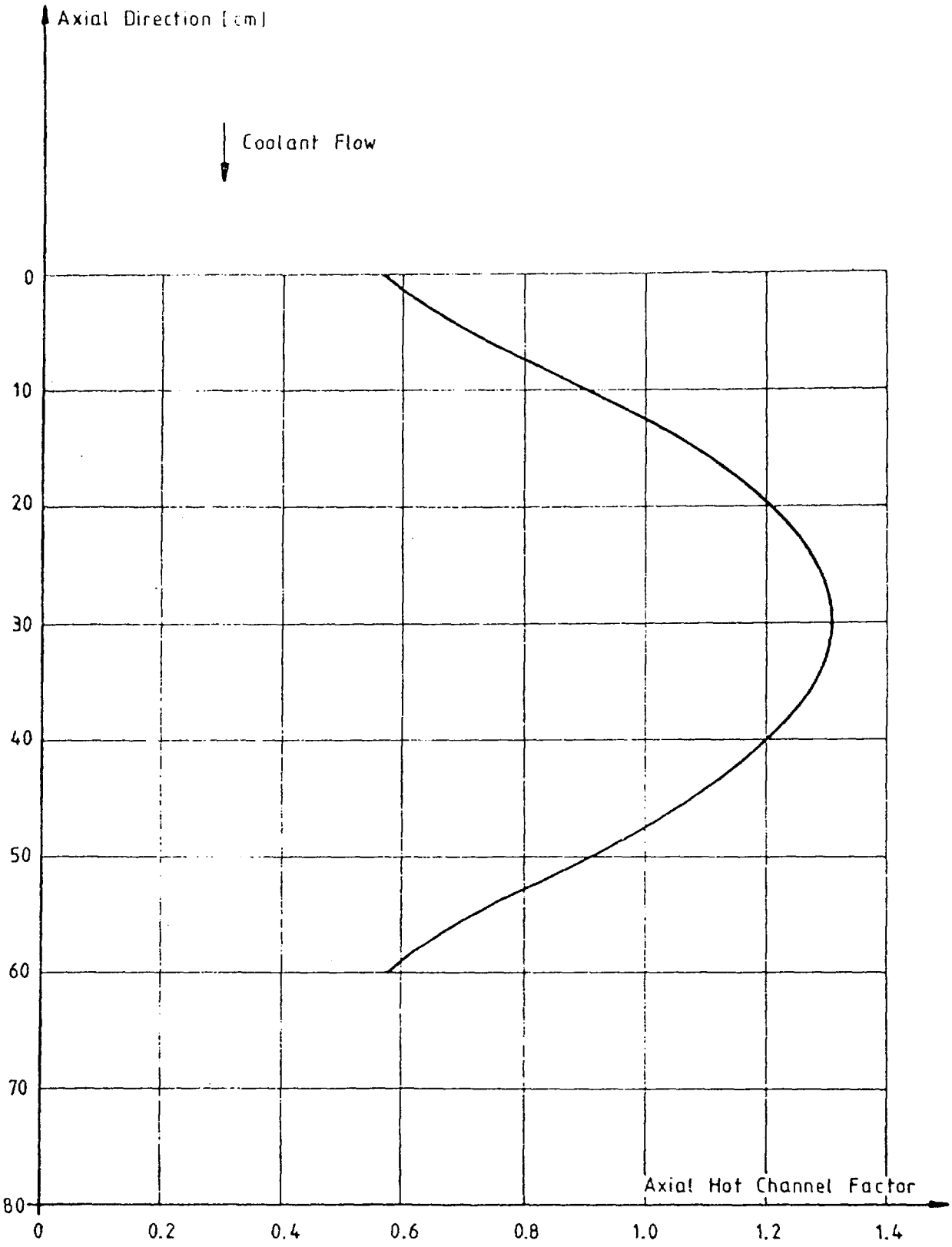

2 MW-CORE
AXIAL POWER DISTRIBUTION
(BASED ON A CALCULATION USING THE HEU-FUEL)

2.2.32

Table 2.2.3: Geometry data and nuclear hot channel factors

Fuel plates/assembly	19	17	15
Channel length, cm	62.5	62.5	62.5
Heated channel length, cm	60.0	60.0	60.0
Channel thickness, cm (inner channel)	0.295	0.295	0.360
Channel width, cm	6.71	6.71	6.71
Meat width, cm	6.275	6.275	6.275
Hydraulic diameter, cm	0.5652	0.5652	0.6833
Number of fuel assemblies	24	24	24
Number of fuel plates	432	386	341
Total heat transfer area, cm^2	$32.53.10^4$	$29.11.10^4$	$25.68.10^4$
Fuel assembly pitch, cm	7.71x8.1	7.71x8.1	7.71x8.1
Core flow area, cm^2	908.4	814.9	871.6
Radial hot channel factor	1.465	1.37	1.40
Axial hot channel factor	1.308	1.308	1.308
Uncertainty of radial hot channel factor, %	10	10	10
Uncertainty of axial hot channel factor, %	10	10	10

Table 2.2.4 Thermal-hydraulic parameters at a flow rate of 300 m^3/h

Fuel plates/assembly	19	17	15
Average heat flux, W/cm^2	6.15	6.87	7.79
Maximum heat flux, W/cm^2	14.26	14.90	17.26
Coolant velocity, cm/s	91.7	102.3	95.6
Heat transfer coefficient, $W/(cm^2.K)$	0.518	0.592	0.540
Core pressure drop, bar	0.0169	0.0209	0.0151
Pressure at core exit, bar	1.961	1.961	1.961
Saturation temperature, °C	119.2	119.2	119.2
Core inlet temperature, °C	38.0	38.0	38.0
Temperature rise across core, K	5.8	5.8	5.8
Temperature rise across hot channel, K	9.3	8.7	8.9
Maximum plate surface temperature, °C	70.2	67.5	74.4
Plate surface temperature with boiling heat transfer, °C	130	130	130
DNB-ratio (Labuntsov-correlation, zero subcooling)	16.1	15.9	13.4

Table 2.2.5: Thermal-hydraulic parameters at a flow rate of 150 m^3/h

Fuel plates/assembly	19	17	15
Average heat flux, W/cm^2	6.15	6.87	7.79
Maximum heat flux, W/cm^2	14.26	14.90	17.26
Coolant velocity, cm/s	45.9	51.1	47.8
Heat transfer coefficient, $W/(cm^2.K)$	0.312	0.341	0.311
Core pressure drop, bar	0.0047	0.0058	0.0042
Pressure at core exit, bar	1.961	1.961	1.961
Saturation temperature, °C	119.2	119.2	119.2
Core inlet temperature, °C	38.0	38.0	38.0
Temperature rise across core, K	11.6	11.6	11.6
Temperature rise across hot channel, K	18.6	17.4	17.8
Maximum plate surface temperature, °C	93.0	90.4	102.5
Plate surface temperature with boiling heat transfer, °C	130	130	130
DNB-ratio (Labuntsov-correlation, zero subcooling)	13.7	13.3	11.4

Various experimental investigations for heated narrow rectangular cooling channels at low system pressure have shown, however, that the pressure drop vs. channel flow curve goes through a minimum, the location of which depends on the power supplied to the channel. If the operating point of the cooling channel coincides with the minimum of the pressure drop vs. flow curve a small increase in channel power results in a sudden flow excursion with a significant reduction in channel flow. The channel power must therefore be limited to a value which guarantees a stable operating point at the imposed core pressure drop. The experiments have shown, that the flow is stable as long as no steam bubbles detach from the heated wall.

On the basis of this criterion the limiting channel power was determined to be higher than the actual maximum channel power by a factor of about 3.8 for the assembly with 19 fuel plates, the factors for the two other assembly types being slightly higher. At this power level the DNB-ratios would still be at least around 3 assuming zero subcooling.

An other frequently used criterion is the requirement, that no fully developped subcooled boiling should occur or that the maximum wall surface temperatur should not exceed the saturation temperature. These criteria are considerably more conservative than the flow stability criterion.

Summarizing the results of this preliminary analysis of the thermal-hydraulic performance of the three fuel assemblies it is concluded that both the 17 plate assembly and the 15 plate assembly are comparable to the performance of the 19 plate reference assembly. At a later stage a detailed hot channel analysis has to be carried out in order to determine the actual margins against DNB, flow stability threshold and void formation.

2.2.9 First Core Problems

Investigations concerning the fresh first core setups with the different REU-fuels are not carried out in the 2 MW-case. But the problems and the results of such investigations should be very similar to those described within chapter 2.1.7.

2.2.10 Isotopic Composition of Disloaded Fuel

An evaluation of the different fuels under consideration here under the prolifiration aspect had been carried out in the way that the amount and the composition of plutonium produced during burnup were compiled within figure 2.2.33 and 2.2.34. These figures show the total and the fissionable plutonium content plottet versus the burnup of the fuel in percentage.
The disloaded fuel contains at 30 % (for the HEU-fuel) approximately

- 4.1/4.4 (3.7/4.0)g
  of total (fissile) plutonium per fuel element
  for the REU-fuels with 15/17 plates/FE compared to

- 0.24 (0.21) g
  of total (fissile) plutonium per fuel element
  for the HEU-fuel with 19 plates/FE.

2.2.11 Conclusions

For the low power MTR-cores the main problem was to specify the REU-fuel most suitable to exchange the existing HEU-fuel.
The range within the geometry of the fuel assembly can be changed is relatively wide due to the low thermal-hydraulic requirements. Within this range an optimization of the meat thickness and the moderation ratio should be part of the calculation process. This contribution fulfills this demand only partially by giving examples out of that range. Nevertheless the results demonstrate the spectrum of possibilities using three different types of fuel assemblies (15, 17, 19 plates per FE) with REU-fuel each with respect to the three criteria stated. The REU-fuels resulting from the application of these criteria can be used in the different ways stated in chapter 2.1.11. This conclusion is limited to the 15- and 17-plates-assemblies with 1 mm meat thickness.

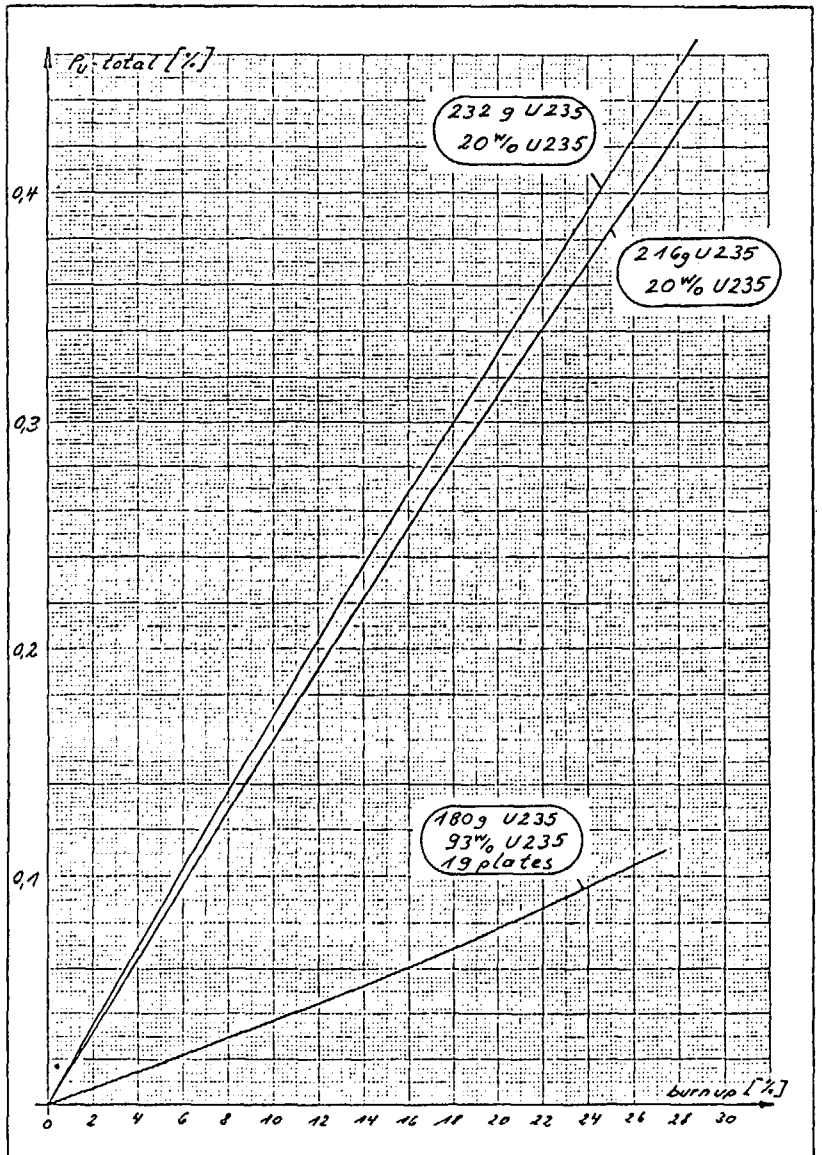

Total Plutonium Content (in Percentage of the total Heavy Metal Content) versus Burnup (in Percentage of the loss of U235)

2.2.33

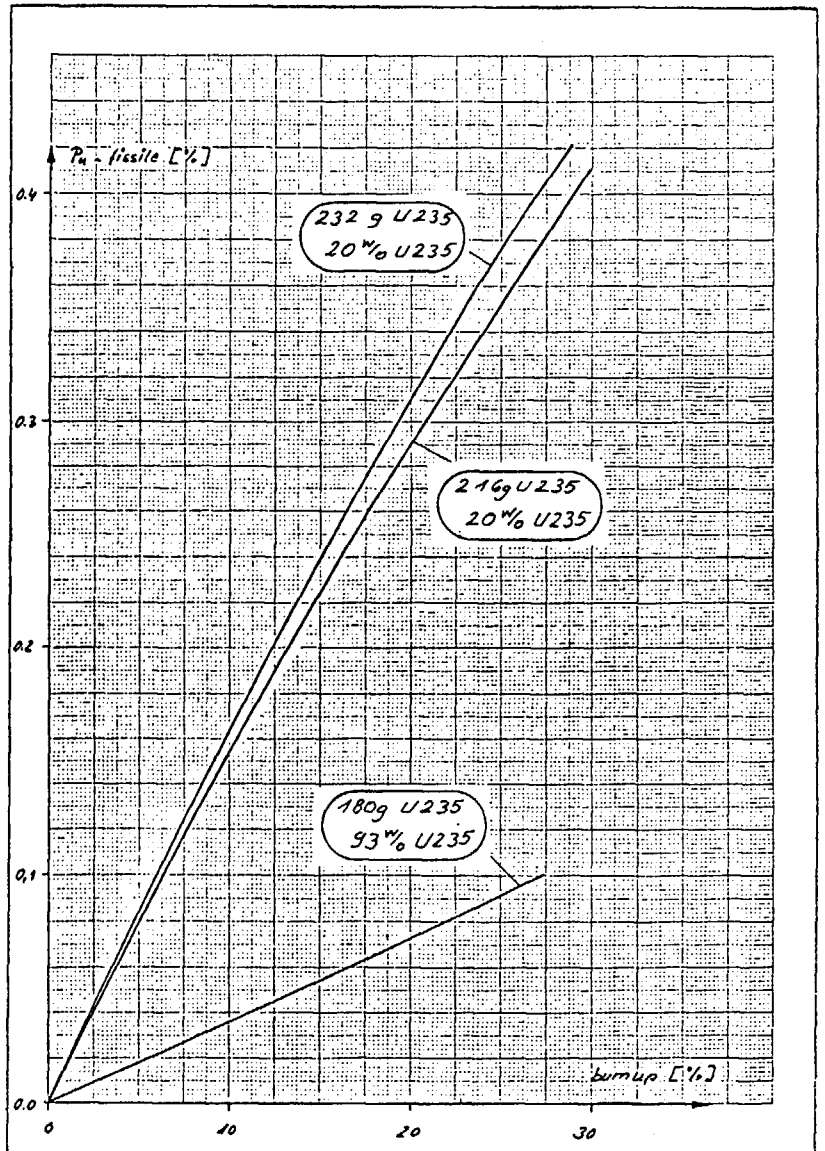

Fissile Plutonium Content (in Percentage) of the total Heavy Metal Content) versus Burnup (in Percentage of the Loss of U235)

2.2.34

For the 19 plates-assembly with .51 mm meat thickness the limits given by the fuel availability prevent its use within this range.

2.3 Methods

2.3.1 Nuclear Methods and Cross Section Data

For the numerical calculation of the different aspects of MTR-cores the standard set of INTERATOM's program system for calculating thermal reactors is used. This system is backed by the experience gained with the first and second core of the FDR of the nuclear merchant ship "Otto Hahn" as well as by different calculations to special problems for other power reactors of the KWU. Furthermore nuclear computations concerning the two main fuel-types of research reactors (TRIGA, MTR) were carried out for example on the BERII-Reactor at Berlin and the TRIGA MK1 at the German Cancer Research Center at Heidelberg.

A short review of these methods is put together here. The most frequently used programs are the INTERATOM-burnup program MONSTRA calculating group constants in dependency of burnup and a lot of other parameters for the fuel elements and the INTERATOM 2 dimensional core code IAMADY, a diffusion program usable in RZ- and XY-geometry in up to 4 energy groups.

MONSTRA itself consists in its first part of a MUFT-type routine for the fast and epithermal energy region (20 energy groups, 0.625 eV to 10 MeV) and of a multigroup SN-routine for the thermal energy region (25 energy groups). Included is the code INGAMM3 for the calculation of the resonance absorption by intermediate resonance approximation in dependence of the fuel-temperature. The combination of the different cell calculations within that first part is done by material dependent flux weighing in a XY-diffusion code. Moreover the MONSTRA-cycle contains a burnup-routine to recalculate the isotopic composition. The total MONSTRA-cycle is automatically rerun for each burnup-step. Averaging routines deliver homogenized group constants (macroscopic cross sections) for different areas. These group constants including their dependencies are the input for the diffusion calculations by IAMADY.

IAMADY is a coupled sample of programs containing a group constant interpolation modul, a two dimensional (RZ-, XY-geometry) diffusion modul or alternatively a three dimensinal coarse mesh-code, two different thermohydraulic codes (DYNAMIT and COBRA3C), an averaging routine for the resulting power distribution, and moduls for burnup in different core zones in dependence on local power as well as on heterogeneous xenon content in the different core zones. Different xenon-states can be calculated, xenon-free, xenon equilibrium with or without taking into account the power distribution, and xenon override. Similarily the samarium poisoning is to be handled. By using a suitable group constant sample as an input to IAMADY different reactivity effects can be calculated in a full core model.

To check the results of the MONSTRA-code by independent computations a chain of programs is used as

- INGAMM3-HOBBI-IANSN
  whereas the 1 dimensional multigroup S_n-code IANSN is used in the thermal and the fast region separately. HOBBI is a spectral code in 54 groups for the fast energy region based on MUFT IV. All input data to this chain are based on ENDFB IV.

The results of this check show a difference in k_∞ of the order of 1.4 %, i. e. a difference in of lower than 0.5 %.

Reflector group constants for the different materials surrounding the core or for fuel free parts of the core are calculated by the IANSN-code as well as by the MONSTRA-code.

Furthermore calculations for different reactivity effects such as the Doppler- or the moderator-density effect etc. are done with the INGAMM3-HOBBI-IANSN-chain as well as with the MONSTRA-code, the latter especially if burnup dependency of the effects has to be taken into account.

It must be stated that this short review shows only a limited selection of the total amount of codes, limited to the programs been used really for the calculation described within this contribution. Among the programs not mentioned here are the transports codes normally used for absorber calculations. By calculating the absorption rate within the transport code and similarily by a diffusion code the diffusion cross sections are adjusted to equal absorption rates.

2.3.2 Thermal-hydraulic Methods

A typical thermal-hydraulic analysis of a MTR-type reactor core at steady state operation may be performed in the following way:

1. Evaluation of the available core flow rate based on the primary pump characteristics and the combined hydraulic resistances of the primary cooling system.

2. Analysis of the core flow distribution taking into account variations in fuel assembly geometry, power generation, fuel assembly location etc.

3. Detailed calculation of the thermal-hydraulic parameters in the limiting cooling channel assuming nominal values and worst case tolerances for cooling channels and fuel plates, fissile material, inlet flow distribution etc. The maximum power of the hot channel may be limited by different criteria, for example by a flow stability criterion or a burnout criterion.

Very often step 1 is not required, since the core flow rate is already known from calculation for previous core loadings and the new core has approximately the same pressure drop vs. flow characteristics.

Step 2 and 3 will be performed by means of the computer program DYNAMIT. This code considers a core to be made up of a number of parallel cooling channels connected to the same inlet and exit plenium. There is no transverse coupling between the cooling channels, i. e. no heat and/or mass exchange between adjacent channels takes place.

Several options for the inlet and exit boundaries are available:

- total flow rate for the channel arrangement is specified
- flow rate through a single channel is specified
- the pressure drop across a single channel is imposed

The program can handle single phase flow, subcooled boiling flow and net boiling flow. Apart from generally accepted empirical correlations for BWR- and PWR-application of the code correlations covering the low pressure range typical for MTR-type of cores are provided. Whenever possible empirical correlations are used which were derived from experiments on rectangular channel test sections or have been checked against such experiments.

The most important empirical correlations are:

- heat transfer coefficient for forced convection single phase flow, subcooled boiling flow, and net boiling flow
- friction and acceleration pressure drop for single phase flow, subcooled boiling flow, and net boiling flow
- Void fraction for subcooled boiling flow and net boiling flow
- burnout correlation

Experimental work in these areas has been done for example at CEA in France, at GKSS in the Federal Republic of Germany, at Harwell in England and at other institutions.

For transient analyses of the reactor core the widely used thermal-hydraulic program COBRA-IIIC will be applied. In order to avoid inconsistencies between DYNAMIT- and COBRA-IIIC-results the same set of empirical correlations as in DYNAMIT is used.

2.3.3 Test of the Methods

To check whether the calculation methods and/or the cross section data sets produce reasonable results in comparison to measured core setups, for the MTR-type fuel we recalculated setups of the Berlin-MTR BER II of the Hahn-Meitner-Institut. Above all this recalculation was done to find out the differences in the absolute reactivity between calculation and corresponding experiment. A lack of most of such calculations is the impossibility to take into account all the details of the specific core configuration, i. e. detailed description of the top- and the bottom-reflector, radiation tubes, effect of the control rods withdrawn into their upper positions, etc.

Nevertheless our calculations so far show good agreement with the reactivity values measured within $\pm$ 1.5 %. Furthermore the methods and cross section sets are checked by calculating TRIGA-type reactor setups as well as critical experiments for the nuclear ship "Otto Hahn" and a lot of power reactors such as the KWU-types KWO and BIBLIS and the FDR-Ship Reactor, all within good agreement to measured values.

APPENDIX D

Generic Enrichment Reduction Calculations

performed by

CEA

CEN - SACLAY

B.P.2

91190 Gif-Sur-Yvette

FRANCE

ABSTRACT

Methods and results of calculations for the conversion of 2 and 10 MW cores from HEU to LEU fuel are described. Results are shown for the conversion using classical dispersed plate type fuels and UO_2-Zr Caramel fuels. Details are given also on the thermalhydraulic methods used in calculating safety margins for converted cores.

INTRODUCTION

As presented in this report the French Reduction Enrichment Program is based on two differents technological ways : the implementation of the plate type UO_2-Zr Caramel fuels and the development of MTR type UAl_x/U_3O_8-Al fuels.

The evaluations made to assess the core conversion capabilities are connected with both types of fuel. One considers first the Caramel fuel implementation, then the MTR fuels. The neutronic calculation methods are the same, they have been used in the benchmark problem (appendix F 5), where they are described. The thermohydraulic methods and safety criteria must be presented before entering the details of the evaluations.

Part 1: THERMALHYDRAULICS

THERMALHYDRAULIC ANALYSIS AND SAFETY CRITERIA

It is very important to establish clearly the assumptions on which the cooling characteristics requirements are based. For all the thermohydraulics analysis performed by the CEA, the safety criteria taken into account are the present criteria required by the French Safety Authorities, presently used for the reactors either under construction or being converted to low enrichment fuel.

Of course some reactors are not operating under the last safety hypothesis. But as far as the fuel assembly geometry is modified, or may be sometimes if the materials are changed, the overall safety analysis has to be reevaluated. In many cases this conversion to REU may be the opportunity to upgrade the safety conditions to the present ones.

This is why it was thought important to perform this work under realistic conditions. These were of two kinds :

- first during the steady state operation under nominal conditions to avoid nucleate boiling.
- second during the most severe transient conditions due to a defect in the cooling conditions to avoid the flow instability and blocage. This is a conservative criteria, for it occurs before the dry out of the channel and then before any damage to the clad integrity.

In fact the second criteria is more severe, and in most cases it covers the first situation.

The calculations have been performed taking into account the different kinds of uncertainties which must be considered :

- the uncertainties about the measurements of the true operation conditions of the core :
  - power
  - flow rate - flow rate distribution amongst assemblies
  - inlet temperature
  - pressure
  - power peaking
- the uncertainties due to the fabrication tolerances
  - uranium loading
  - uranium homogeneity in the fuel plate
  - water gap thickness
- the uncertainties coming from the experimental correlations used in the calculations
  - double phase flow pressure drop
  - heat exchange coefficient

Furthermore we have assumed realistic conditions on the numerous parameters which influence the safety limits such as :

- temperature reactivity coefficient for fuel and water
- reactivity insertion of the rods vs time
- delay time to rods shut-down after reaching the thresholds
- pumps slowing down vs time with and without flywheels
- values of the safety threshold

The results for the typical lattices of the 10 and 2 MW reactors are gathered in the fig. I.1-I.2. They have been drawn in a relative shape so that they can be used easily in a differential mode, to compare the necessary cooling requirements in flow rate and loss of pressure of a converted core to the original one.

For instance we can withdraw from this figure the characteristics of the Caramel core.

	10 MW	
	93 % or 20 % UAl_x-Al	Caramel UO_2-Zr
lattice water gap	23 plates 1.27 mm 2.12 mm	16 plates 2.25 mm 2.75 mm
water velocity	1.8 m/s	2 m/s
flow rate	600 m^3/h	630 m^3/h
pressure frop	0.1 bar	0.1 bar

This table shows the possibility to convert HEU core with thin plates to REU core with thick plates without any apparent problem. Of course for more accurate features this shall be investigated on a case by case basis.

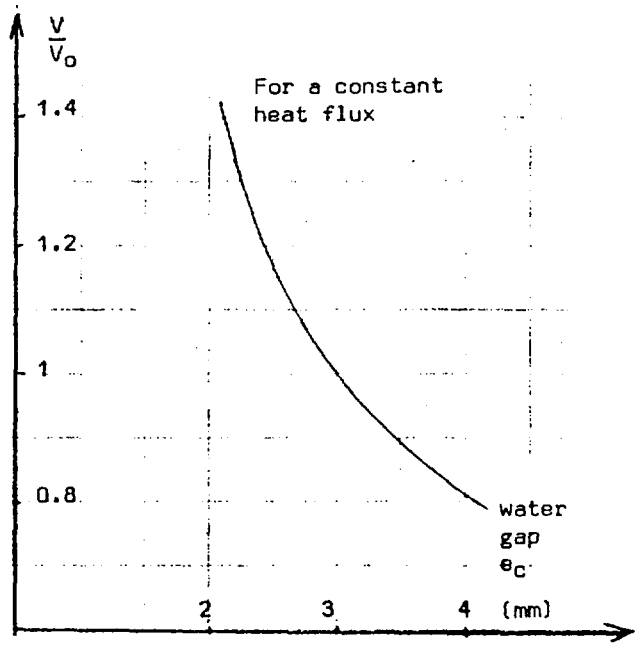

Fig. I.1

Relative variations of water velocity for various plate type assembly geometry.

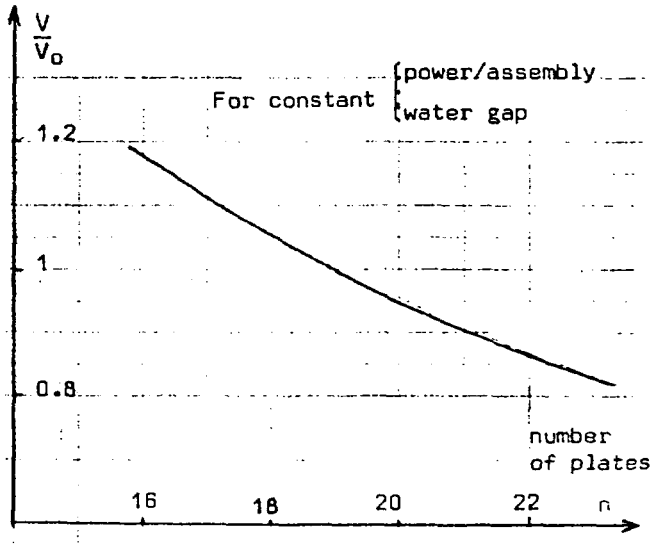

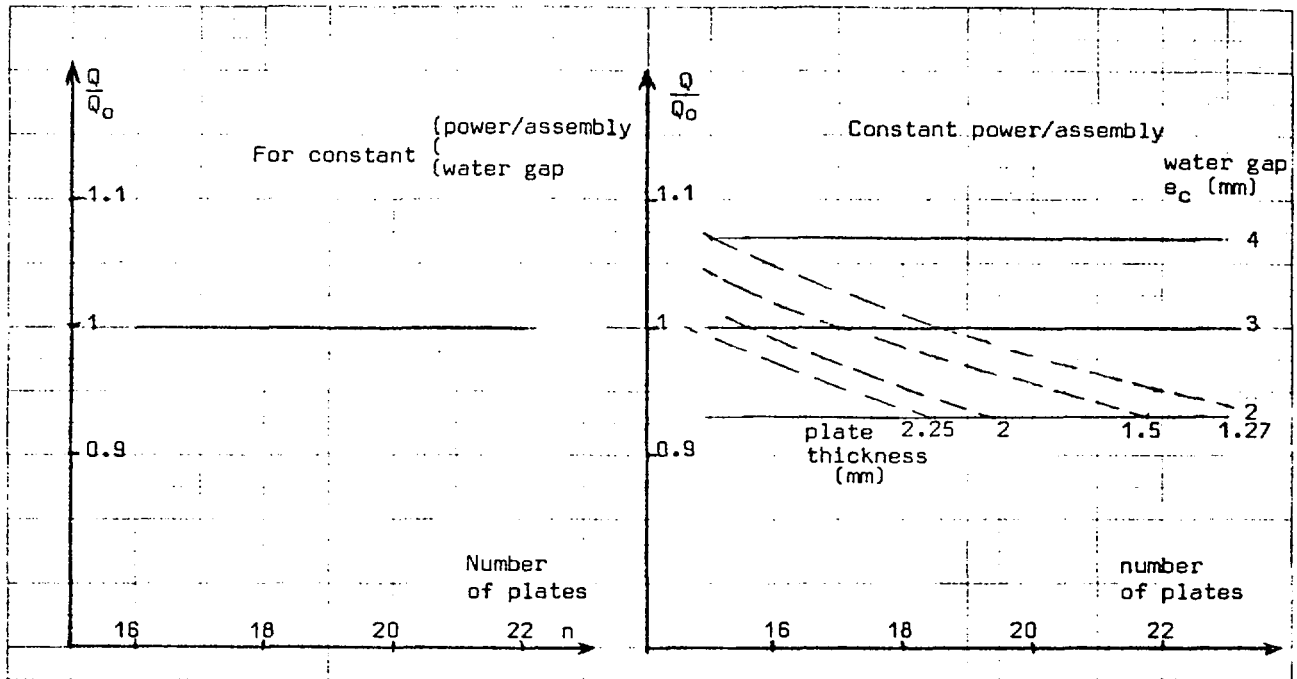

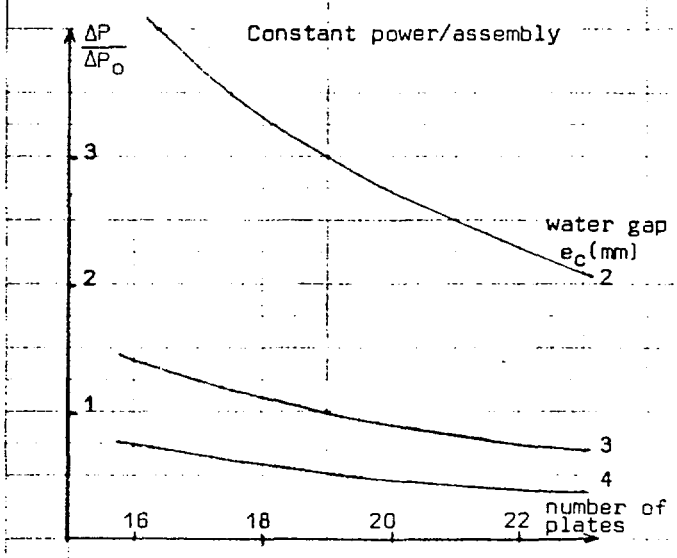

Fig. I.2

Relative variations of flow rate and pressure drop for various plate type assembly geometry.

Typical data

of the core conversion
Generic studies 93 % U_5 basis

	10 MW	2 MW
	23 plates 1.27 mm per standard assembly	19 plates 1.27mm
water velocity V	1.8 m/s	0.5 m/s
flow rate Q	600 m^3/h	150 m^3/h
pressure drop ΔP	0.1 bar	0.01 bar

THERMALHYDRAULIC METHODS

We present the background used in the thermohydraulic calculations [1]; the formula and data necessary for these evaluations are gathered, they show how to estimate with enough precision the operating conditions and the margin from the critical heat flux occurence.

Determination of the operating conditions in steady state

These conditions depend on four parameters :

- heat flux
- coolant velocity
- inlet water temperature
- pressure

The wall temperature T_w at a fixed point of the fuel plate is

$$T_w = T + \frac{\varphi}{h}$$

T water temperature

φ heat flux

h heat transfer coefficient

This wall temperature will be compared to T_{sat} water ebullition temperature in these pressure conditions. So that we need to estimate the local pressure and the heat transfer coefficient.

Pressure

The pressure drop in the core is due to

- the acceleration along the channel
- the friction loss in the fuel channel
- the change in height
- the inlet and outlet pressure losses

Friction pressure losses

Most of the pressure drop in research reactors comes from the friction loss in the fuel channel :

$$\frac{\partial F}{\partial Z} = \frac{\Lambda}{D} \rho \frac{V^2}{2}$$

for a channel with constant geometry (hydraulic diameter) the friction losses for a whole channel are :

$$\Delta F = \Lambda \frac{L}{D} \rho \frac{V^2}{2}$$

D hydraulic diameter

$D = \frac{4\,S}{B}$ S water channel cross section area

B wet perimeter of the channel

ρ specific mass of the fluid

W water velocity

Λ Darcy number

- *without heating*

$\Lambda = \Lambda_o = 0.00560 + 0.5\ Re^{-0.32}$ KOO formula

for a smooth wall and for a Reynolds number between 3 000 and 300 000

$Re = \rho \frac{V\,D}{\mu}$ μ dynamic viscosity

for Re < 2 000 $\Lambda_o = \frac{K}{Re}$ K = 96 for rectangular channels

for 2 000 < Re < 3 000 an intermediate value is adopted

- *with heating*

$\Lambda = R\ \Lambda_o$ R results form experimental measurements [2]

$R = 1 - 0.5\ (1+Y)^b\ \log_{10}(1+Y) + 0.04$

$$Y = \left(\frac{\mu}{\mu_w} - 1\right) \left(\frac{\mu}{\mu_w}\right)^{0.17}$$

$$b = 0.17 - 2.10^{-6}\ Re + \frac{1\,800}{Re}$$

μ dynamic viscosity at water temperature T

μ_w dynamic viscosity at wall temperature T_w

This correlation is valid for circular and rectangular channels.

An approximation is given by

$$R = 1 - (0.0047 - 0.000033\ T)\ (T_w - T) \qquad [3]\quad T\ °C$$

The influence of others parameters (see § 1.2.2.) especially the plate corrugations must be considered.

Entrance and exit pressure losses

The pressure drop comes from

- the variation of dynamic pressure, positive at the entrance, negative at the exit,
- the energy loss $k\ \rho \frac{V^2}{2}$, $\rho \frac{V^2}{2}$ from the channel

k being at the inlet $k_i = \left(\frac{1}{\beta} - 1\right)^2 + 0.05 \qquad \beta = 0.63 + 0.37 \left(\frac{s}{S}\right)^2$

at the outlet $k_o = \left(1 - \frac{s}{S}\right)^2 + 0.05$

s the small cross section area

Heat transfer coefficient h

The most recent data used come from [4]. The results are represented by the correlation

$$M_s = 0.0092\ \ Re^{-0.12}\ \ Pr^{-0.5} \left(\frac{\mu}{\mu_w}\right)^{0.14}$$

M_s Margoulis number $\frac{h}{\rho\ CV}$ (C water specific heat capacity)

P_r Prandlt number at temperature T $\frac{\mu\ C}{\lambda}$ (λ water heat conductivity)

R_e Reynolds number at temperature T

The total maximal uncertainty to be taken on this correlation is 15 % in a wide range of rectangular channels operating conditions

φ	10	to	210	W cm^{-2}
V	2	to	11	m s^{-1}
T	20	to	85	°C

Onset of nucleate boiling (ONB)

The ONB is taken as a limit in steady state conditions. It does not correspond to any critical event but it is considered as a conservative statement.

The nucleate boiling occurs at a wall temperature over T_{sat} by a quantity $T_w - T_{sat} = \Delta T_{sat}$ which depends on the heat flux and the local pressure [6]

$$T_w - T_{sat} = 4.57\ \varphi^{0.35}\ p^{-0.23}$$

T_w	and T_{sat}	being expressed	in	°C
	heat flux	"	"	W cm^{-2}
p	pressure	"	"	bar

Others parameters

Some others parameters influence the local conditions. The proportion of gas dissolved in the water - When the wall temperature reaches T_{sat} the gas is starting to be released, and it is important when T_{wall} reaches $T_{sat} + \Delta T_{sat}$. It leads to an increase in the heat transfer coefficient, which is beneficial, without sensitive modification of the pressure drop. As a first approach we can evaluate T_{wall} for ONB neglecting the effect of the degasing.

We have assumed the plates smooth which is not true. The plates have natural corrugations. In fact for the fuel plates commonly used we do not take into account the effect of these corrugations on the heat transfer coefficient, but it has to be considered to evaluate the friction coefficient which determines the friction pressure losses. This is being done by the calculation of the Λ factor versus Re and ε, relative corrugations factor (a good example of this dependence is given by the Colebrook curves).

The lateral conduction reduces the hot spot conditions due either to a point defect or to the conduction along the boundary between the fuel itself and the frame. These have to be estimated for a more detailed evaluation.

Determination of the ebullition crisis (or DNB)

A cooling defect or an overpower leads to the water boiling, the increase of the steam volume causes a flow blockage of the channel cooling with a strong plate temperature increase, burn-out and eventual plate melting.

The purpose of the safety analysis is to keep the cladding as a healthy barrier against the radio-activ products release. Conservatively we assume the flow blockage or flow instability to be the critical phenomenon we have to avoid.

The safety thermohydraulic criterion is defined as a no flow instability occurence for the most severe accidental cooling transient. The most severe cooling transient usually considered is one pump blockage, with all the uncertainties taken into account; these are of three types :

- uncertainties on the operating parameters of the reactor, including the necessary power variation due to the control capability and the reactor operating caracteristics measurements.

- uncertainties on the fuel assemblies parameters corresponding to the fabrication tolerances, water gap width, fuel content, fuel homogeneity ---

- uncertainties on the experimental correlations used in the calculations, and on the calculations themselves (evaluation of the power peaking for instance).

The evaluation of the flow instability is described in details in [1]. We give here a formula which is an approximation precise enough for a first rough estimate of the power which can be extracted in a particular reactor. The flow instability occurs with the following conditions :

$$R = \frac{1}{1 + 3.15 \frac{D}{L} G^{0.29}}$$

$$R = \frac{(T_{outlet} - T_{inlet})\ \text{water heating}}{(T_{sat_{outlet}} - T_{inlet})\ \text{water under saturation}}$$

D	hydraulic diameter	(cm)
L	active length	(cm)
G	mass velocity	($g\ cm^{-2}.s^{-1}$)

For a first estimate one can admit that the mass flow rate when the flow instability occurs is 108 % of the flow rate without heating at about 25 °C.

Note

For the purpose of this study the calculations have been performed in a somehow more sophisticated way, using the code FLICA [5]. It takes into account all the parameters mentionned above and goes through a true transient calculation with representation of the neutronics effects (kinetic coefficients, water temperature and Doppler coefficient, rod insertion, delayed neutrons).

References

[1] FABREGA J.
"Le calcul thermique des réacteurs de recherche refroidis par eau
Rapport CEA-R-4114", Mars 1971, 106 pages

[2] LAFAY J.
"Mesure du coefficient de frottement avec transfert de chaleur en convection forcée dans un canal circulaire".
Rapport CEA-R-3896, Février 1970, 29 pages + 9 tableaux + 20 figures.

[3] COSTA J.
"Mesure du coefficient de frottement en écoulement turbulent simple phase avec transfert de chaleur, dans un canal rectangulaire".
Note CEA N 1142, Octobre 1969, 15 pages + 10 figures.

[4] LAFAY J.
"Mesure du coefficient d'échange thermique de l'eau en convection forcée dans un canal rectangulaire".
Note CEA N 1144, Octobre 1969, 49 pages + 25 figures.

[5] FAJEAU M.
"Programme FLICA - Etude thermodynamique d'un réacteur ou d'une boucle d'essai"
Rapport CEA R-3716, Janvier 1969, 64 pages.

[6] RICQUE R., SIBOUL R.
"Ebullition locale de l'eau en convection forcée"
Rapport CEA R-3894, Mai 1970, 45 pages + 47 figures

Part 2: NEUTRONIC STUDIES

INTRODUCTION

This paper illustrates the possibility of using low ^{235}U enrichment in experimental research reactor instead of high ^{235}U enrichment. This work was realized on two research reactors proposed by IAEA. These two reactors use MTR fuel elements with UAl plates and 93 % ^{235}U. Powers are respectively of 2 and 10 MW. U specific weight in meat are not very high compared to current values used in french reactors. They are respectively of 0,53 et 0,68 g/cm3 compared to 0,82 g/cm3 SILOE value.

In each case, we illustrate with two different fuel technologies :

- UAl fuel
- UO2 fuel or CARAMEL

With UAl fuel, the maximum U specific weight is 3 g/cm3. The value has to be still confirmed. Using UO_2 fuel, U specific weight are very higher (10.2 g/cm3). In the two reactors, the 20 % enrichment was used with UAl fuel. U specific weights are respectively 2.9 and 3.5 g/cm3 in 2 and 10 MW reactors. Let us take notice of this last value ; it is upper than the expected technological limit value of 3 g/cm3. These values have been selected only for matching cycle length.

Two kinds of fuel element were considered with UO_2-caramel. In the 2 MW reactor, standard element fuel has only five plates of 5 mm thick with a 4 mm meat thickness. The enrichment is 6 %.

Standard fuel element of the 10 MW reactor contains 16 plates of 2,25 mm with a 1,45 mm meat thickness. Control fuel element has the same plate, but there is only 13 plates. The enrichment is 7.5 %. Nevertheless, cycle lengths with these low values are longer here than using UAl fuel.

I) CALCULATION MODEL

Fuel element cross section and burn up calculations

The APOLLO code (*) was used to generate the cross sections as a function of burn up in a four group structure with energy as shown below :

Energy groups used in the calculation

Group	Energy	
1	10 Mev	0.9 Mev
2	0.9 Mev	5.50 kev
3	5.50 Kev	0.625 ev
4	0.625 ev	0

APOLLO calculates the space and energy dependent flux for a one dimensional geometry, in the multigroup approximation of the transport equation. For a one dimensional geometry refined collision probabilities have been used for the resolution of the integral form of the transport equation. APOLLO uses a library with 99 groups (52 fast and 47 thermal). This library contains all the isotopes of the UKNDL library and of the ENDF/BIV library. The fission products compilation of Cook have been added to the APOLLO library.

The self shielding of the heavy isotopes is treated by an accurate technics which preservesthe reaction rates of the fundamental fine structure.

APOLLO is designed to perform accurate depletion calculations. Any decay chain can be defined for heavy nuclides and fission products. The depletion calculation can be done separately for a few regions in the cell.

---

* A. HOFFMANN, F. JEAN PIERRE, A. KAVENOKY, M. LIVOLANT, H. LORRAIN : APOLLO. Code multigroupe de résolution de l'équation du transport pour les neutrons thermiques et rapides.
Note CEA N-1610

Calculations of cross sections are made in two steps.

In first step we consider the infinite-medium cell : which consists of the plate and the associated water channel. We calculate the self shielding of the heavy isotopes. We obtain the homogeneous equivalent cross section and the Bell factor for this exact geometry.

In a second step we consider the infinite-medium cell with extra-region. This latter region contains Al-structures and surrounding water. The first step calculations provides the self-shielding parameters. For more convenient calculations, standard and control fuel assemblies have the same cross sections. The extra water and the extra-al-structures cross sections of the large water channel of the control element are determined separately.

Depletion calculations are made untill fifty percent of ^{235}U is burned. The irradiation ratio α decreases from 1 to 0.5 by step of 0.05. A critical buckling is automatically adjusted at each step of irradiation.

REFLECTOR CROSS SECTION CALCULATIONS

Reflector and central water hole cross sections have been evaluated by 1D plane geometry APOLLO calculations where reflectors and homogeneized core are described. These calculations have been performed for each fuel enrichment.

CORE CALCULATIONS

We use the NEPTUNE modular scheme which has been developed to provide the design engineer with a single system of codes for the calculation of light water reactor. In this reactor phase, 2D diffusion calculations have been performed by the use of the finite element method. These 2D calculations are done by the BILAN module. We can use a large space mesh with this method and obtain an accurate calculation.

To evaluate the length of theequilibrium cycle the Haling* criterion was used. With this criterion the burn-up distribution was found which corresponds to a constant power distribution during each cycle. This criterion insures to reach the minimum power peaking. The 2 MW reactor contains 19 standard fuel elements and 4 control elements. At each cycle, a fresh standard fuel element is introduced. Fresh control elements are introduced one at a time, at approximately equal intervals. Each control element is burned during 19 cycles. In a equilibrium condition, only the twentieth cycle will be equivalent to the first cycle. Thus many cycles were computed to reach convergence.

The 10 MW reactor contains 23 standard fuel elements and 5 control elements. A fresh standard element is introduced at each cycle. Thus calculations similar to those run for the 2 MW reactor were undertaken.

XY geometry was used. The third dimension was represented by an axial buckling. This latter simulates axial neutron leakage and non-uniform axial burn up. When the equilibrium cycle was reached with the BILAN-HALING* module, BILAN calculations were made at beginning and end of cycle (BOC and EOC) to provide flux distributions.

* Haling, Rk.: Operating Strategy for Maintaining an Optimum Power Distribution throughout Life -ANS- Nuclear Performance of Power Reactors - San Francisco, 20-27 September 1963 - Conf 360-6

II) 2 MW REACTOR

- Core description

Calculations are based on 6 x 4 element core reflected by water. One water hole is inside the core. There are 19 standard and 4 control fuel elements.

- Fuel element

. UAl fuel. The MTR fuel elements were considered. The standard fuel element and the control fuel element respectively contain 19 and 15 identical fuel plates. Thickness of plates is 1.27 mm. Active height of the fuel is 600 mm. Fuel element cross section is 76 x 80 mm. In the control element, there are four plates of pure aluminium, each 1.27 mm thick, in the position of the first, the third, the seventeenth and the nineteenth standard plates. Thickness of the Al side plates is 4.75 mm. The pitch of the grid plate per fuel element is 77 x 81 mm. Meat dimensions are 63 x 0.51 x 600 mm. All characteristics are reported in table 2.1.

. UO_2 fuel. The standard and control fuel element contain 5 identical plates (figure 2.1). Thickness of the plate is 5 mm. Active height is 600 mm. Fuel element cross section is 76 x 80 mm. All structures material are ZR4. Meat dimensions are 65.4 x 4 x 600 mm. Thickness of ZR4-Side plates is 3 mm. All characteristics are reported in table 2.1.

Table 2.1

① Core and fuel element					
Power	MW	2	2	2	2
Fuel material		UAl_x	UAl_x	UO_2 with ZR separators	UO_2 with ZR separators
U 235 enrichment	%	93	20	6	4,5
Number of standard fuel elements		19	19	19	19
Number of control fuel elements		4	4	4	4
Number of experimental elements		1	1	1	1
Number of plates in standard fuel element		19	19	5	5
Number of plates in control fuel element		15	15	5	5
U 235 weight in standard fuel element	g	180	213	396	250
U 235 weight in control fuel element	g	142	168	396	250
Total uranium weight	g	4288	23 595	151 750	126 458
Uranium specific weight	g/cm3	0.528	2.907	8.407	8.407
U 235 specific weight	g/cm3	0.491	0.581	0.50	0,38
Active height	mm	600	600	600	500
Lattice pitch	mm x mm	77 x 81	77 x 81	77 x 81	77 x 81
Fuel element cross section	mm x mm	76 x 80	76 x 80	76 x 80	76 x 80
Material of the side plates		Al	Al	Zr	Zr
Thickness of the side plates	mm	4.75	4.75	3	3
② Plate					
Plate thickness	mm	1.27	1.27	5	5
Meat thickness	mm	0.51	0.51	4	4
Meat width	mm	63	63	65.4	65.4
U percentage	%	17.5	59	84.4	84.4
ρUAl or ρUZR	g/cm3	3.02	4.93	9.961	9.961
③ Water Temperature for neutronic calc.	°C	20	20	20	20
Effective uranium temperature	°C	20	20	20	20

- Core loading

Fresh standard element is introduced at each cycle at the center of the core near the central water hole. The discharged standard element is at the core periphery. The loading map and burn up fuel element distribution are given in figure 2.2, 2.3 and 2.4 for the three fuels (93 %, 20 % and 7.5 %). For UAl and UO_2 fuels we give in these figures U 235 weight by element at beginning and end of cycle. For UO_2 fuel we give the same information in megawatt day per ton too, which is the usual unit (fig. 2.5).

Results

Reactivity

Information about keff at Xe equilibrium for the studied cycle are given in table 2.2

Table 2.2

Keff	UAl 93 %	UAl 20 %	UO_2 6 %
BOC	1.02359	1.02313	1.03014
EOC	1.02119	1.02112	1.02120

Cycle length

Cycle lengths of the average cycles and cycles given in figure 2.2, 2.3, 2.4 are indicated below in table 2.3.

Table 2.3

Cycle length (days)	UAl 93 %	UAl 20 %	UO_2 6 %
Average cycle	9.8	10.3	110.5
Studied cycle	7.8	8.3	84.8

The UA1 20 % cycle length is 5 % greater than UA1 93 %. With caramel UO_2, the cycle length is longer.

Flux distributions

Thermal flux variations in reflector between UA1 93 % and the 2 other cases are given in table 2.4. These values are at beginning of cycle at maximum thermal flux position.

Table 2.4

Thermal flux variation in reflector - BOC

Case	$1 - \frac{\varphi_4}{\varphi_4\ (93\ \%)}$ (%)
UA1 20 %	- 3
UO_2 6 %	- 15

Maximum thermal flux in reflector, averaged on the active height is 2.54 10^{13} n/s/cm2 with UA1 93 % fuel.

In the central water hole, averaged fluxes at BOC with UA1 93 % at the center of the trap are :

φ_1 : 1.02 10^{13} n/s/cm2

φ_2 : 1.17 10^{13} n/s/cm2

φ_3 : 1.24 10^{13} n/s/cm2

φ_4 : 5.48 10^{13} n/s/cm2

STANDARD ELEMENT - CARAMEL UO_2 - 4mm THICK

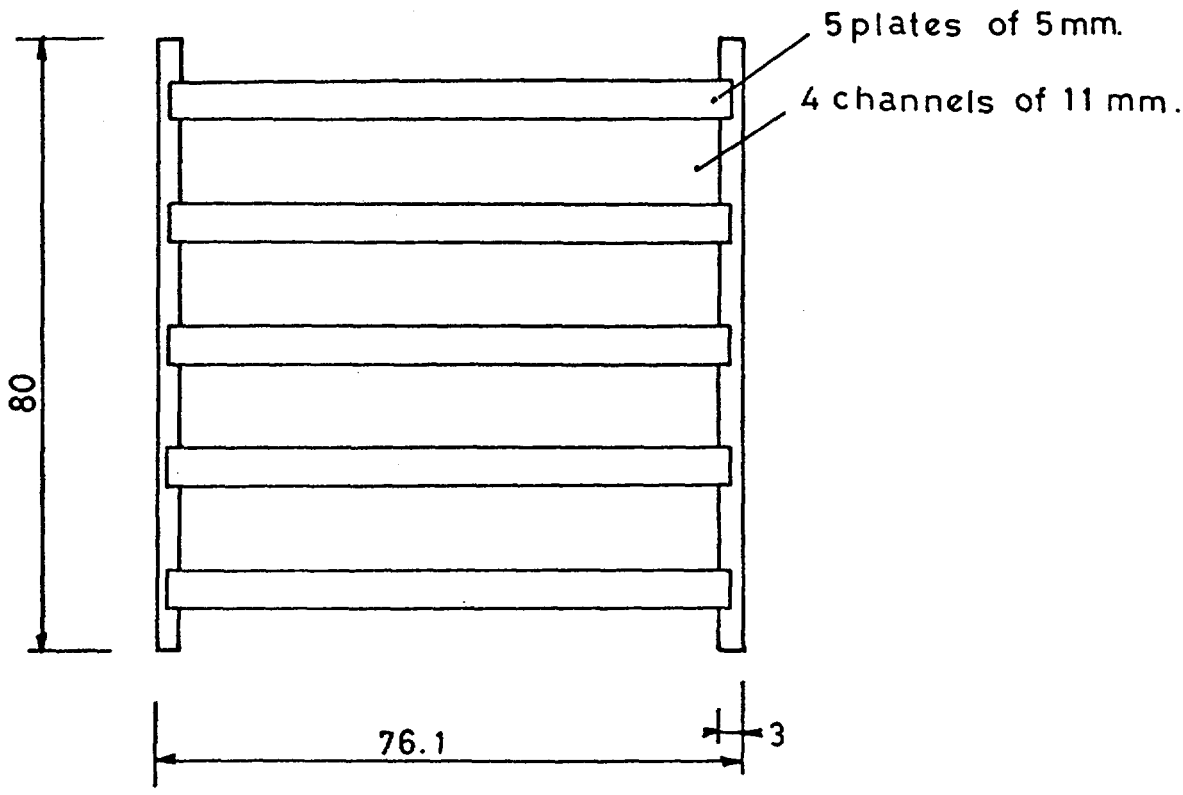

Figure 2.1

Figure 2.2 - 2 MW reactor - HEU 93 % Fuel
Beginning and end of equilibrium cycle distribution of ^{235}U

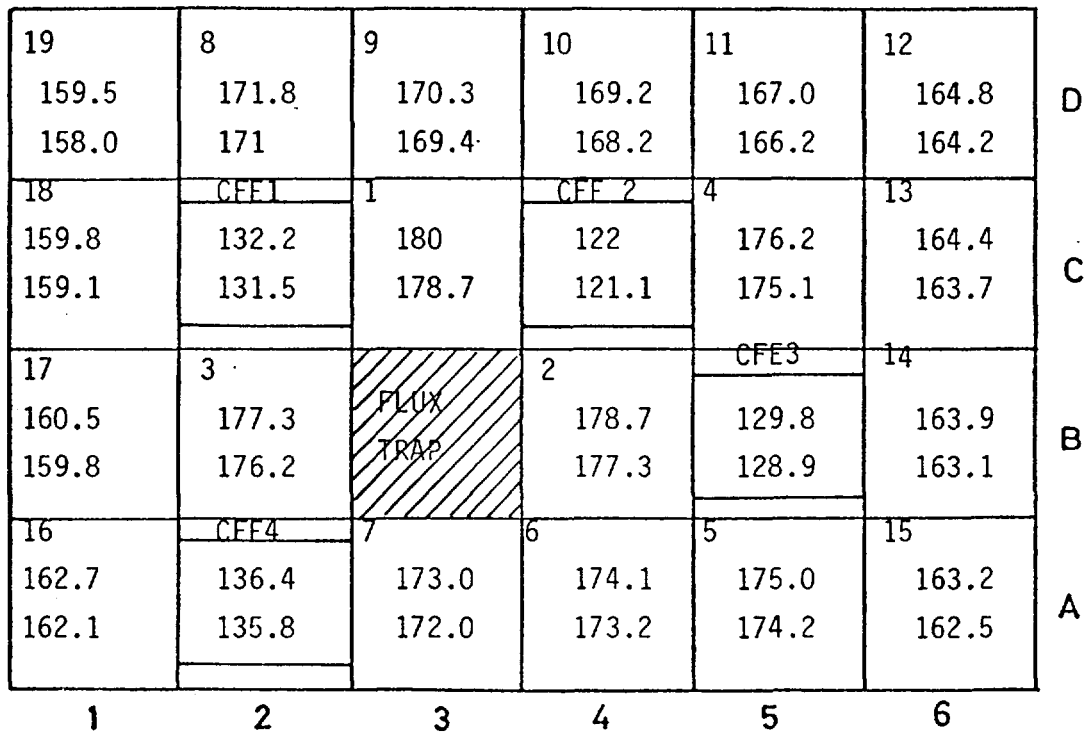

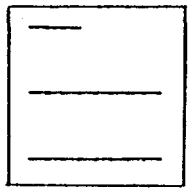

Fuel shuffling

^{235}U Weight at BOC by element (g)

^{235}U weight at EOC by element (g)

Cycle length ..... 7.8 days
Average cycle length .... 9.8 days
Keff (BOC) 1.0236
Keff (EOC) 1.0212

^{235}U weight in fresh standard fuel element : 180 g
^{235}U weight in fresh control fuel element : 142 g

Figure 2.3 - 2 MW reactor - LEU 20 % fuel
Beginning and end of equilibrium cycle distribution of ^{235}U

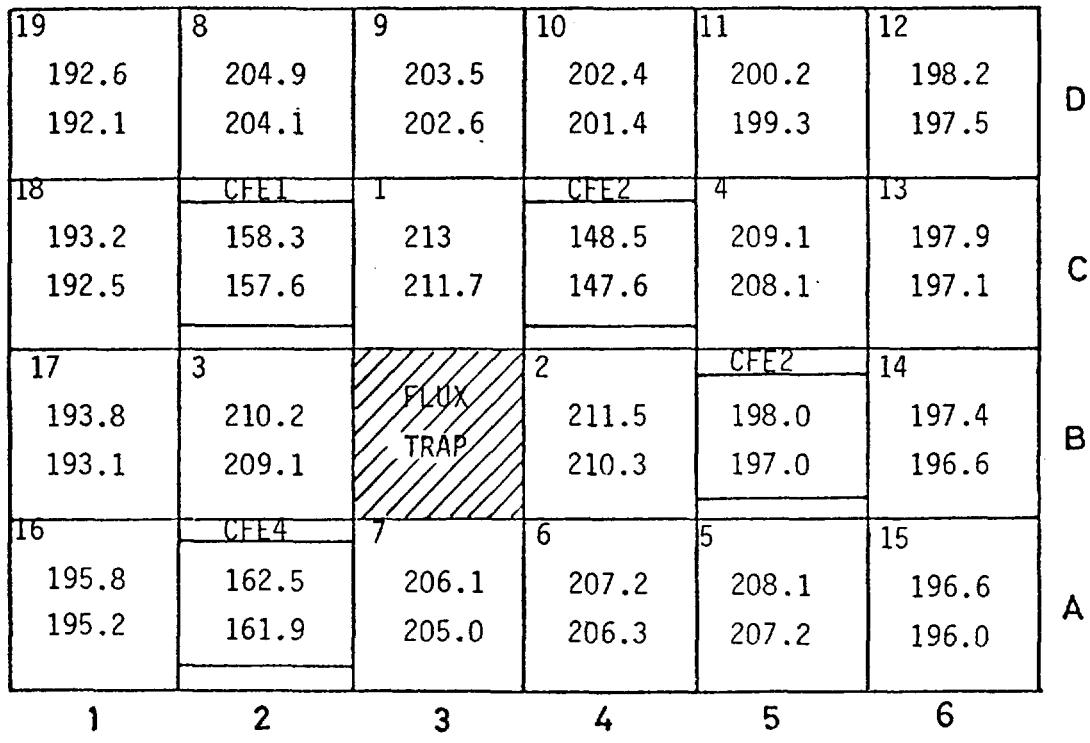

Fuel shuffling

^{235}U weight at BOC by element (g)

^{235}U weight at EOC by element (g)

Cycle length ..... 8.3 days
Average cycle length ..... 10.3 days
Keff (BOC) 1.02313
Keff (EOC) 1.02112

^{235}U weight in fresh standard fuel element : 213 g
^{235}U weight in fresh control fuel element : 168 g

Figure 2.4 - 2 MW reactor - Caramel fuel 6 %
Beginning and end of equilibrium cycle distribution of ^{235}U

19 199.9 195.9	8 303.0 295.5	9 287.6 279.4	10 277.0 268.5	11 256.6 250.1	12 238.3 233.7	D
18 198.75 193.7	CFE1 280.1 272.3	1 396. 379.6	CFE2 182.6 175.6	4 348.4 337.8	13 235.5 229.9	C
17 202.6 197.8	3 362.1 349.1		2 378.7 362.6	CFE3 253.4 245.7	14 233.9 228.1	B
16 225.1 220.5	CFE4 323.0 315.8	7 317.0 305.3	6 327.6 319.1	5 337.1 328.6	15 227.9 223.3	A
1	2	3	4	5	6	

Fuel shuffling

^{235}U weight at BOC by element (g)

^{235}U weight at EOC by element (g)

Cycle length ..... 84.8 days
Average cycle length ..... 110.5 days
Keff (BOC) 1.03014
Keff (EOC 1.02120
^{235}U weight in fresh standard fuel element : 396 g
^{235}U weight in fresh control fuel element : 396 g

Figure 2.5 - 2 MW reactor - caramel fuel 6 %
Beginning and end of equilibrium cycle distribution of burn up

19 27 400 28 020	8 12 190 13 240	9 14 340 15 500	10 15 830 17 050	11 18 780 19 720	12 21 490 22 180	D
18 27 590 28 380	CFE1 15 390 16 510	10 0. 2063	CFE2 30 200 31 340	4 6098 7482	13 21 910 22 750	C
17 26 970 27 720	3 4297 6007		2 2178 4239	CFE3 19 240 20 380	14 22 150 23 020	B
16 23 480 24 170	CFE4 9476 10 450	7 10 290 11 870	6 8853 10 070	5 7580 8719	15 23 050 23 750	A
1	2	3	4	5	6	

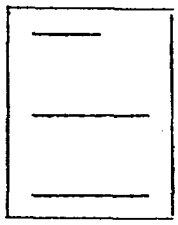

Fuel shuffling

Fuel burn up at BOC MWd/t

Fuel burn up at EOC MWd/t

Cycle length ..... 84.8 days
Average cycle length ..... 110.5 days
Keff (BOC) 1.03014
Keff (EOC) 1.02120

^{235}U weight in fresh standard fuel element : 396 g
^{235}U weight in fresh control fuel element : 396 g

2 MW reactor - flux in group 1 & 2 of UAl 20% and UO_2 6% fuels, normalized to UAl - 93% flux at BOC and EOC

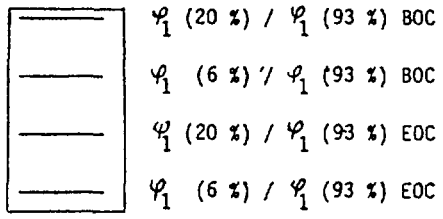

Fig. 2.6 - flux in group 1

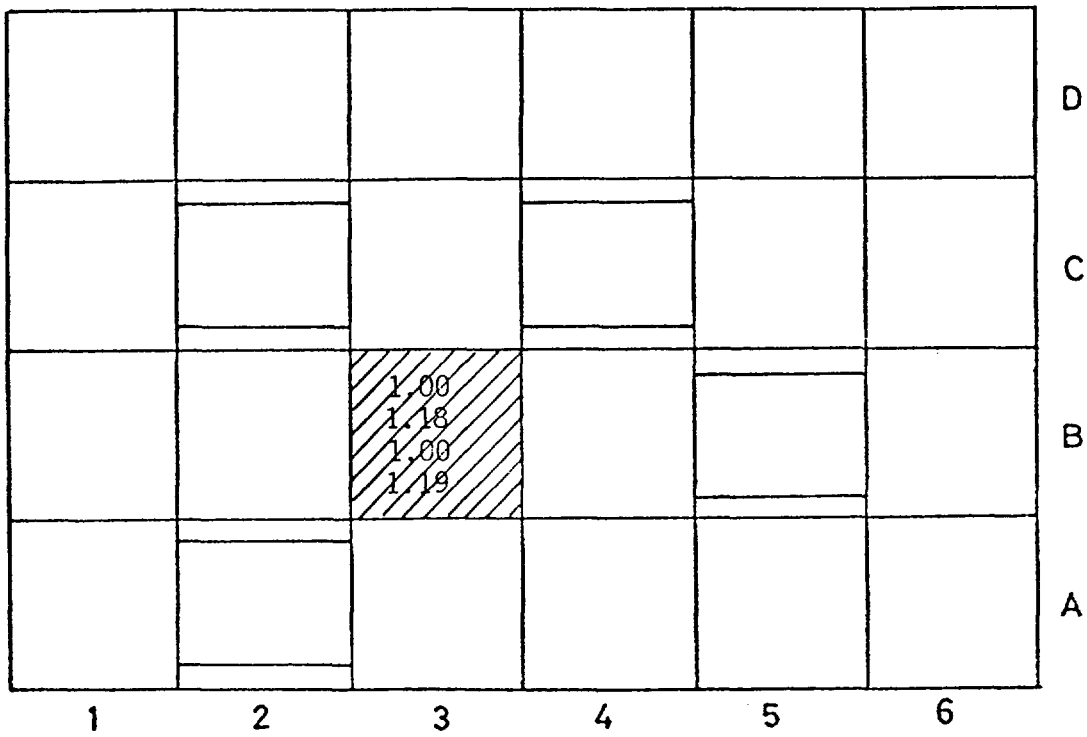

Fig. 2.7 - flux in group 2

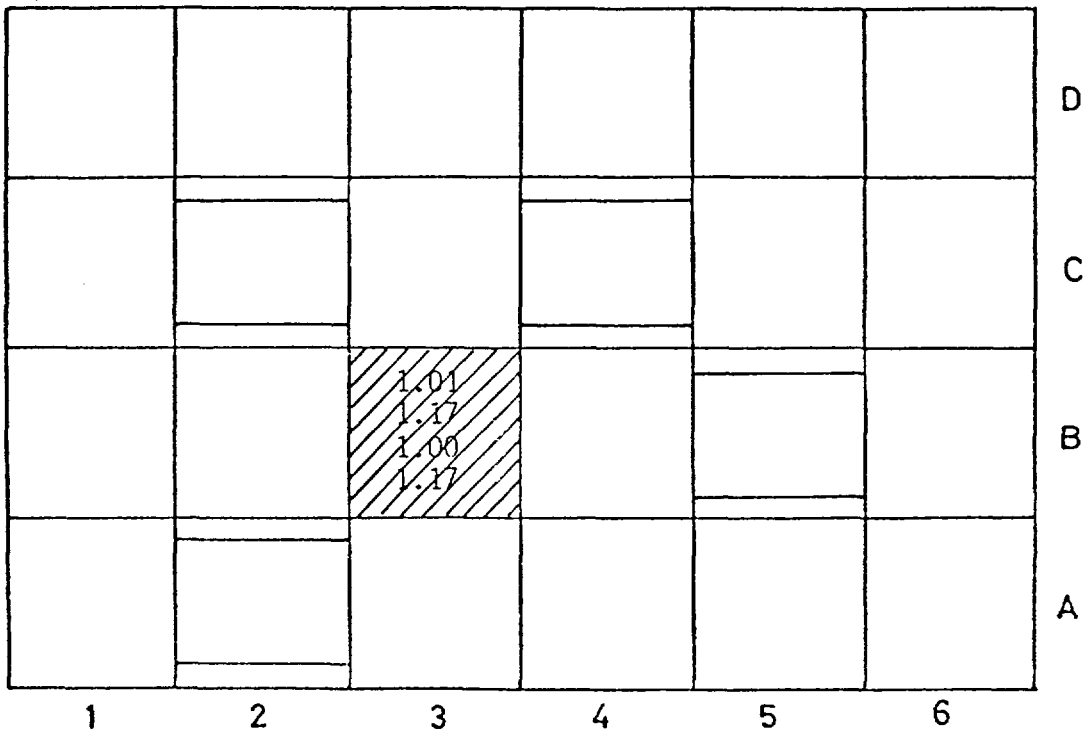

2 MW reactor - flux in group 3 and 4 of UAl 20% and UO_2 6% fuels normalized to UAl - 93% et BOC and EOC

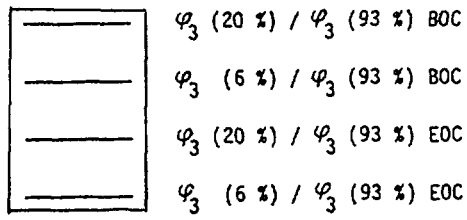

Fig. 2.8 - flux in group 3

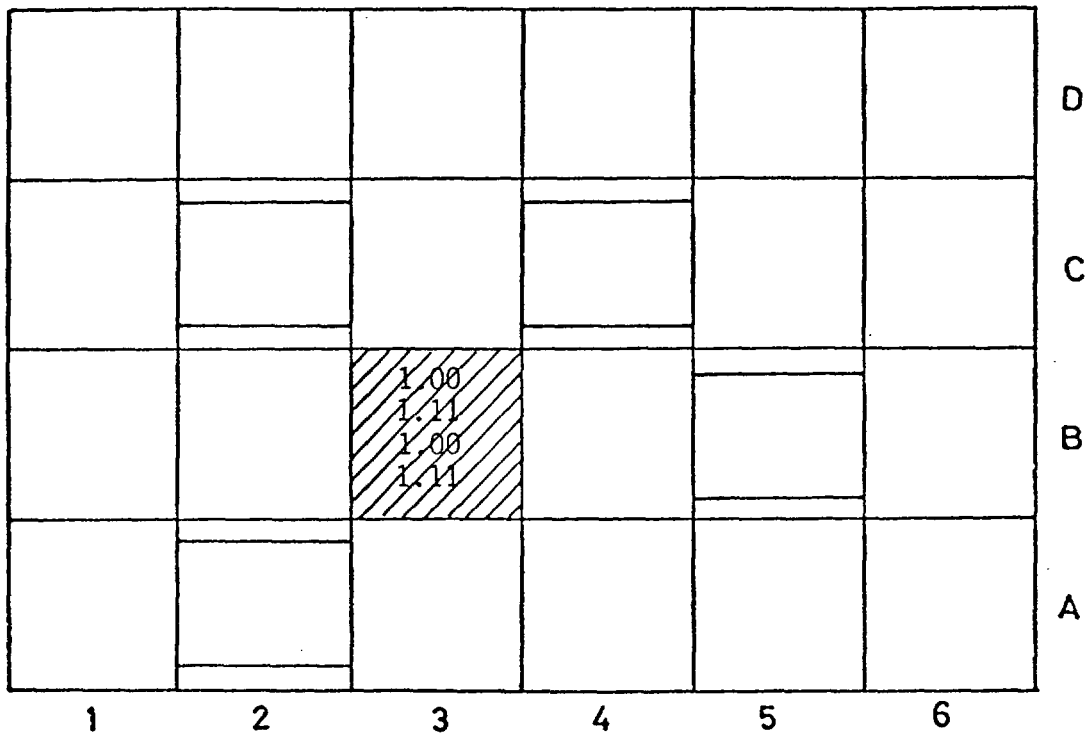

Fig. 2.9 - flux in group 4

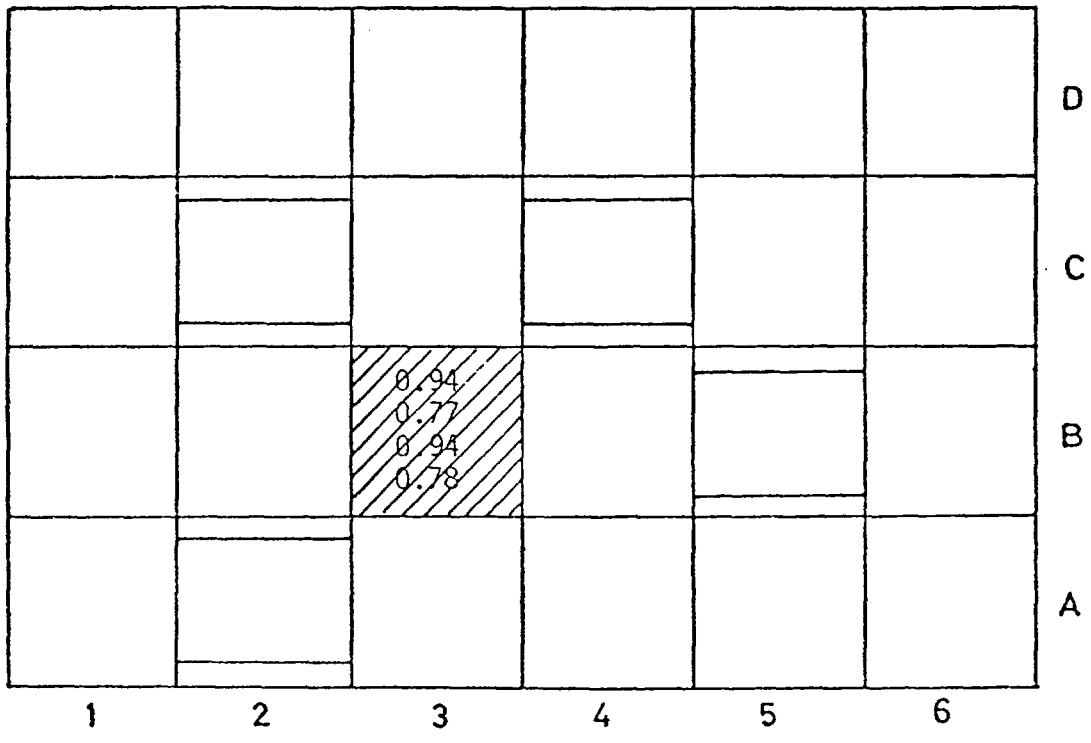

III) 10 MW REACTOR

- Core description

Calculations are based on 6 x 5 elements core reflected by a graphite row on two sides and surrounded by water. Two water holes are inside the core. There are 23 standard and 5 control fuel elements.

- Fuel element

. UAl fuel. The MTR fuel elements were considered. The standard fuel element and the control fuel element respectively contain 23 and 17 identical fuel plates. Thickness of plates is 1.27 mm. Active height of the fuel is 600 mm. Fuel element cross section is 76 x 80 mm. In the control elements, there are 4 plates of pure aluminium, each 1.27 mm thick, in the position of the first, the third, the twenty-first and the twenty-third standard plates.

Thickness of the Al-side plates is 4.75 mm. The pitch of the great plate per fuel element is 77 x 81 mm. Meat dimensions are 63 x 0.51 x 600 mm.

All characteristics are reported in table 3.1.

. UO_2 fuel. The standard fuel element and the control fuel element respectively contain 16 and 13 identical fuel plates (fig. 3.1 and 3.2). Thickness of plates is 2.25 mm. Active height of the fuel is 600 mm. Fuel element cross section is 76 x 80 mm. All structure materials are ZR4. Meat dimensions are 65.4 x 1.45 x 600 mm. Thickness of the ZR4-side plate is 3 mm. All characteristics are reported in table 3.1

Table 3.1

① Core and fuel element					
Power	MW	10	10	10	10
Fuel material		UAl_x	UAl_x	UO_2 with Zr separators	UO_2 with Zr separators
U 235 enrichment	%	93	20	7,5	6.5
Number of standard fuel elements		23	23	23	23
Number of control fuel elements		5	5	5	5
Number of experimental elements		2	2	2	2
Number of plates in standard fuel element		23	23	16	16
Number of plates in control fuel element		17	17	13	13
U 235 weight in standard fuel element	g	280	313	574.0	500
U 235 weight in control fuel element	g	207	231.3	466.4	406
Total uranium weight	g	8038	41 779	207 107	207 107
Uranium specific weight	g/cm3	0.679	3.52	8.407	8.407
U 235 specific weight	g/cm3	0.631	0.705	0.631	0.55
active height	mm	600	600	600	600
lattice pitch	mm x mm	77 x 81	77 x 81	77 x 81	77 x 81
fuel element cross section	mm x mm	76 x 80	76 x 80	76.1 x 80	76.1 x 80
material of the side plates		Al	Al	Zr	Zr
thickness of the side plates	mm	4.75	4.75	3	3
② Plate					
Plate thickness	mm	1.27	1.27	2.25	2.25
meat thickness	mm	0.51	0.51	1.45	1.45
meat width	mm	63	63	65.4	65.4
u percentage in UAl	%	22.0	65.7	84.4	84.4
pu al or u Zr	g/cm3	3.09	5.36	9.961	9.961
③ Water temperature for neutronic calc.	°C	20	20	35	35
Effective uranium temperature	°C	20	20	170	170

- Core loading

Fresh standard element is introduced at each cycle at the center of the core near the central water hole. The discharged standard element is at the core periphery near the graphite row. The loading map and burn up fuel element distribution are given in figure 3.3, 3.4 and 3.5 for the three fuels (93 %, 20 % and 7.5 %). For UAl and UO_2 fuels we give in these figures U 235 weight by element at beginning and end of cycle. For UO_2 fuel we give the same information in megawatt day per ton too, which is the usual unit (fig. 3.6).

- Results

. Reactivity. Informations about keff at Xe equilibrium are given in table 3.2

Table 3.2

Keff	UAl 93 %	UAl 20 %	UO_2 7.5 %
BOC	1.04304	1.03880	1.03970
EOC	1.02995	1.02996	1.02998

. Cycle length. Cycle lengths of the average cycles and the cycles given in figure 2.3, 2.4 and 2.5 are shown below in table 3.3.

Table 3.3

Cycle length (days)	UAl 93 %	UAl 20 %	UO_2 7.5 %
Average cycle	16.4	15.9	25.7
Studied cycle	14.1	13.7	22.7

The UAl 20 % cycle length is 3 % shorter than UAl 93 %. With caramel UO_2, the cycle length is 59 % longer.

. Flux distributions. Figures 3.7 to 3.10 compares flux distributions in water holes at beginning and end of cycle of the four groups.

Flux variations between UAl 93 % and the 2 other cases are given in table 3.4 on a vertical axis through the central water hole at maximum thermal flux points and at north and south positions. These values are at beginning of cycle. Maximum thermal flux in reflector, averaged on the active height is 2.77 10^{13} n/s/cm2 with UAl 93 % fuel.

Table 3.4

BOC - flux variations in reflector

$1 - \frac{\varphi_g}{\varphi_g(93\%)}$ % / case	Group							
	1		2		3		4	
	N	S	N	S	N	S	N	S
UAl 20 %	- 2	- 1	- 2	0	- 3	- 1	- 5	- 4
UO_2 7.5 %	- 2	+ 4	- 6	- 1	- 6	0	-14	- 9

N : North position

S : South position

The maximum thermal flux with UAl 93 % in water reflector, averaged on the active height is 1.04 10^{14} n/cm2/s. In the central water hole, averages fluxes with UAl 93 % at the center of the trap are :

φ_1 : 5.40 10^{13} n/cm2/s

φ_2 : 6.27 10^{13} n/cm2/s

φ_3 : 6.64 10^{13} n/cm2/s

φ_3 : 2.77 10^{14} n/cm2/s

Caramel UO_2 - 1.45 mm thick

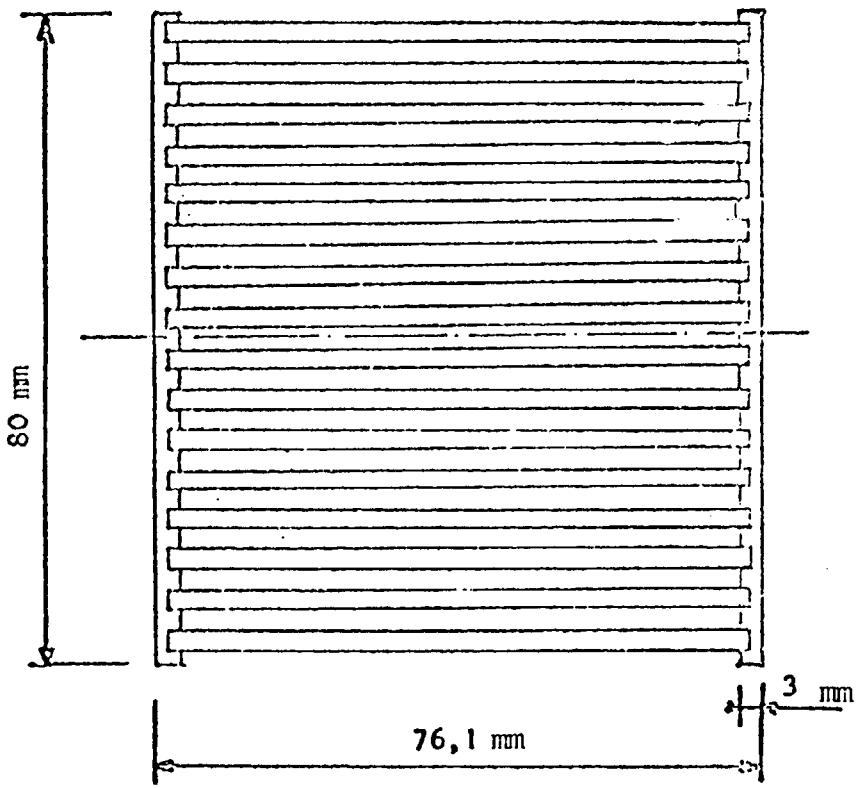

Fig. 3.1: Standard Element
15 channels of 2.75mm
16 plates of 2.25mm

Caramel UO_2 - 1.45 mm thick

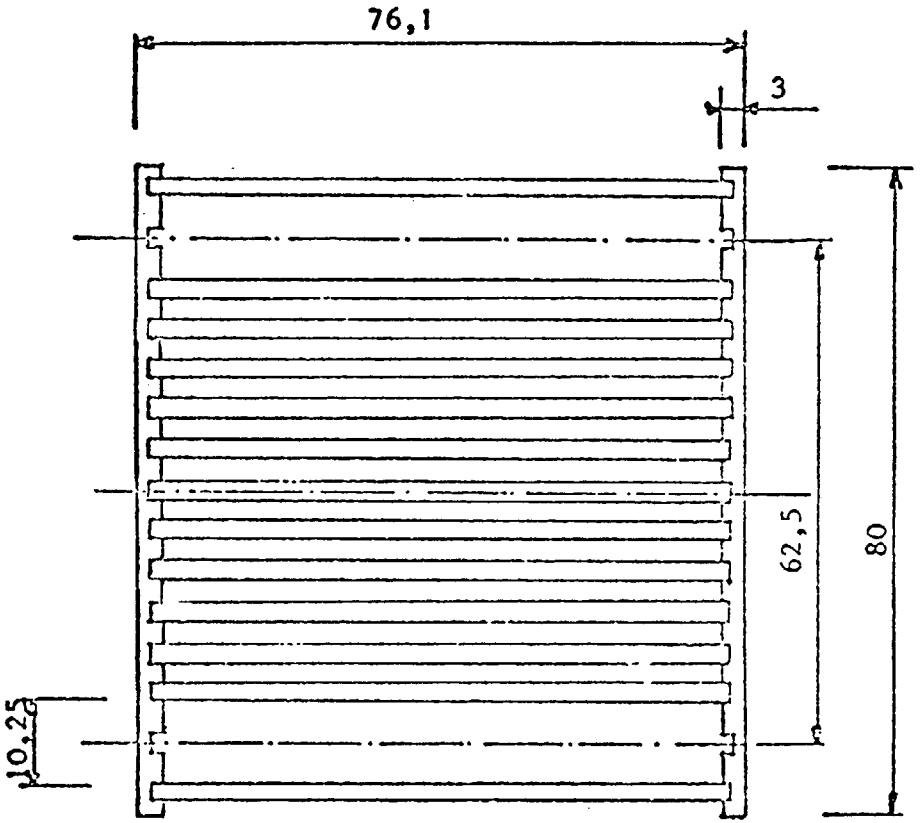

Fig. 3.2: Control Element
10 channels of 2.75mm
13 plates of 2.25mm

Figure 3.3 - 10 MW reactor - HEU 93 % fuel
Beginning and end of equilibrium cycle distribution of ^{235}U

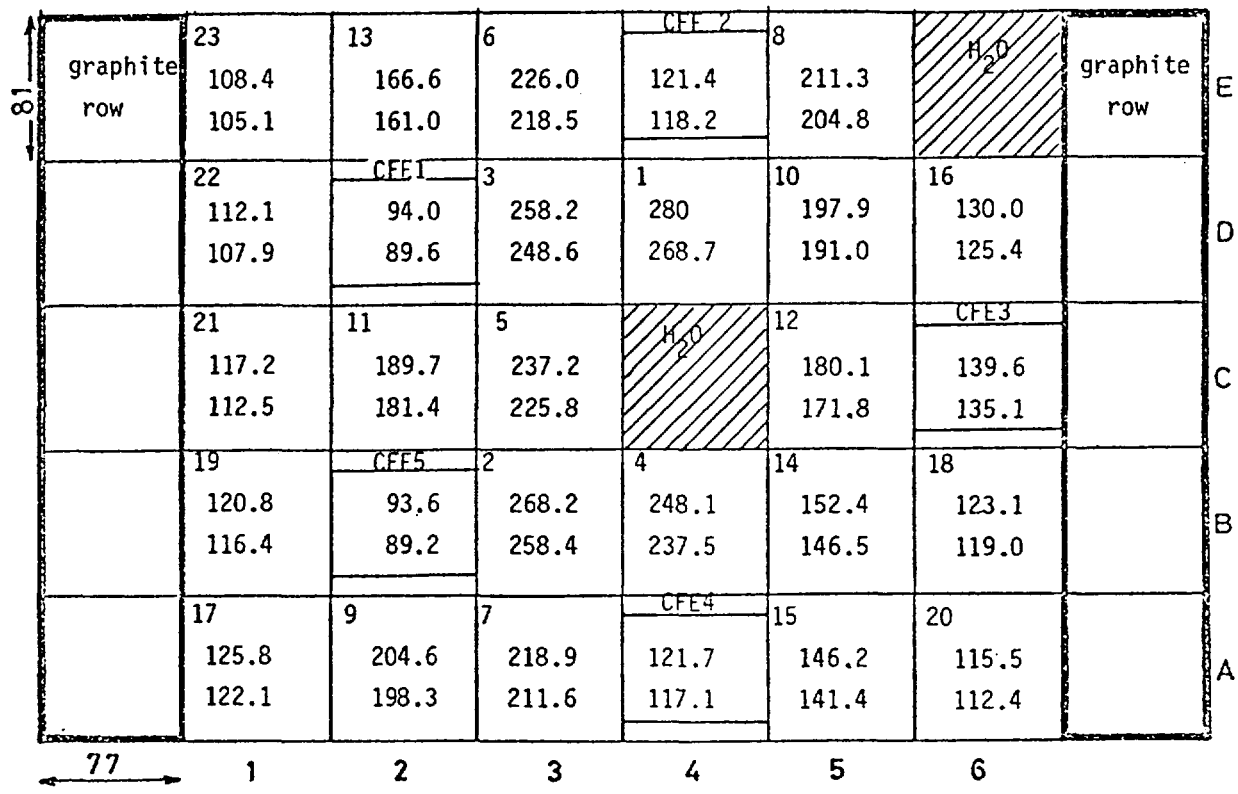

Fuel shuffling

^{235}U weight at BOC by element (g)

^{235}U weight at EOC by element (g)

Cycle length ..... 14.1 days
Average cycle length ..... 16.4 days
Keff EOC 1.0299

^{235}U weight in fresh standard fuel element : 280 g
^{235}U weight in fresh control fuel element : 207 g

Figure 3.4 - 10 MW reactor - LEU 20 % fuel UAl_x-Al
Beginning and end of equilibrium cycle distribution of ^{235}U

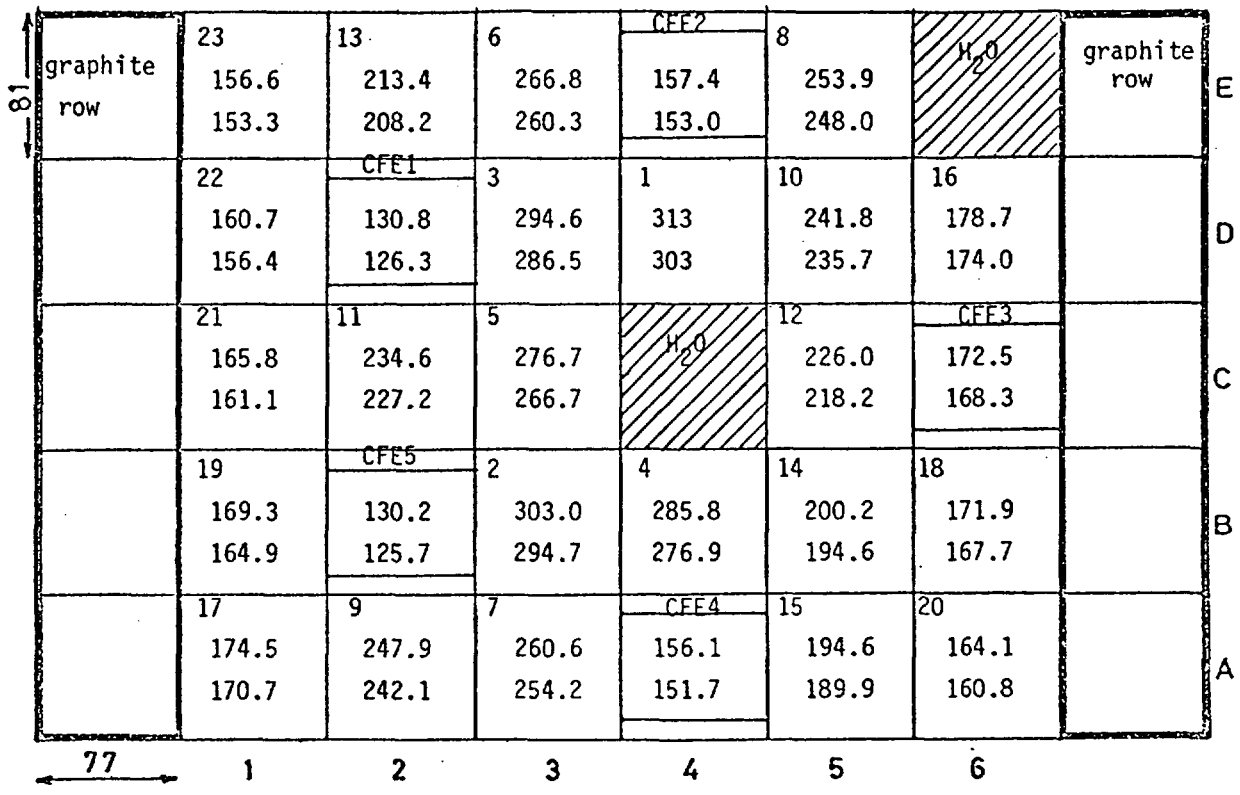

Fuel shuffling

^{235}U weight at BOC by element (g)

^{235}U weight at EOC by element (g)

Cycle length ..... 13.7 days
Average cycle length ..... 15.9 days
Keff (EOC) 1.0299

^{235}U weight in fresh standard fuel element : 313 g
^{235}U weight in fresh control fuel element : 231.3 g

Figure 3.5 - 10 MW reactor - Caramel fuel 7.5 %
Beginning and end of equilibrium cycle distribution of ^{235}U

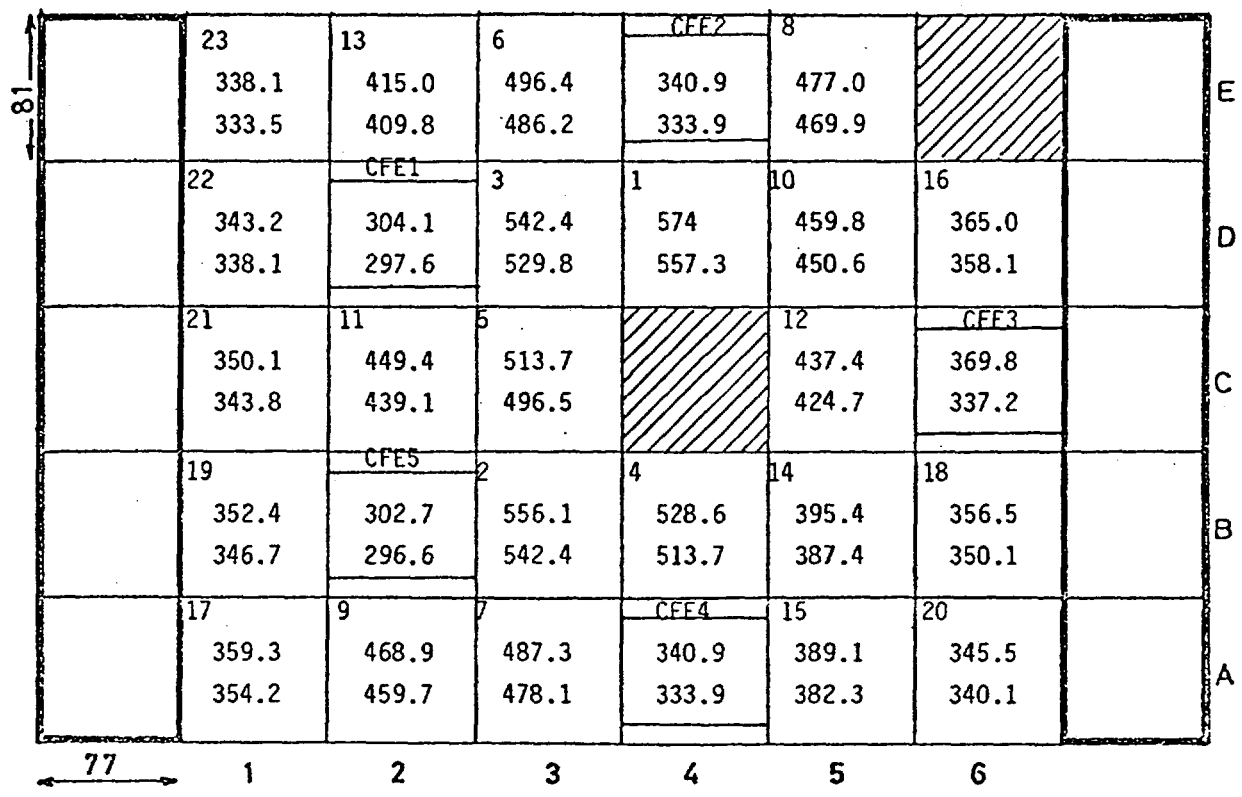

Fuel shuffling

^{235}U weight at BOC by element (g)

^{235}U weight at EOC by element (g)

Cycle length ..... 22.7 days
Average cycle length ..... 25.7 days
Keff (EOC) 1.0299

^{235}U weight in fresh standard fuel element : 574 g
^{235}U weight in fresh control fuel element : 466.4 g

Figure 3.6 - 10 MW reactor - Caramel fuel 7.5 %
Beginning and end of equilibrium cycle distribution of burn up

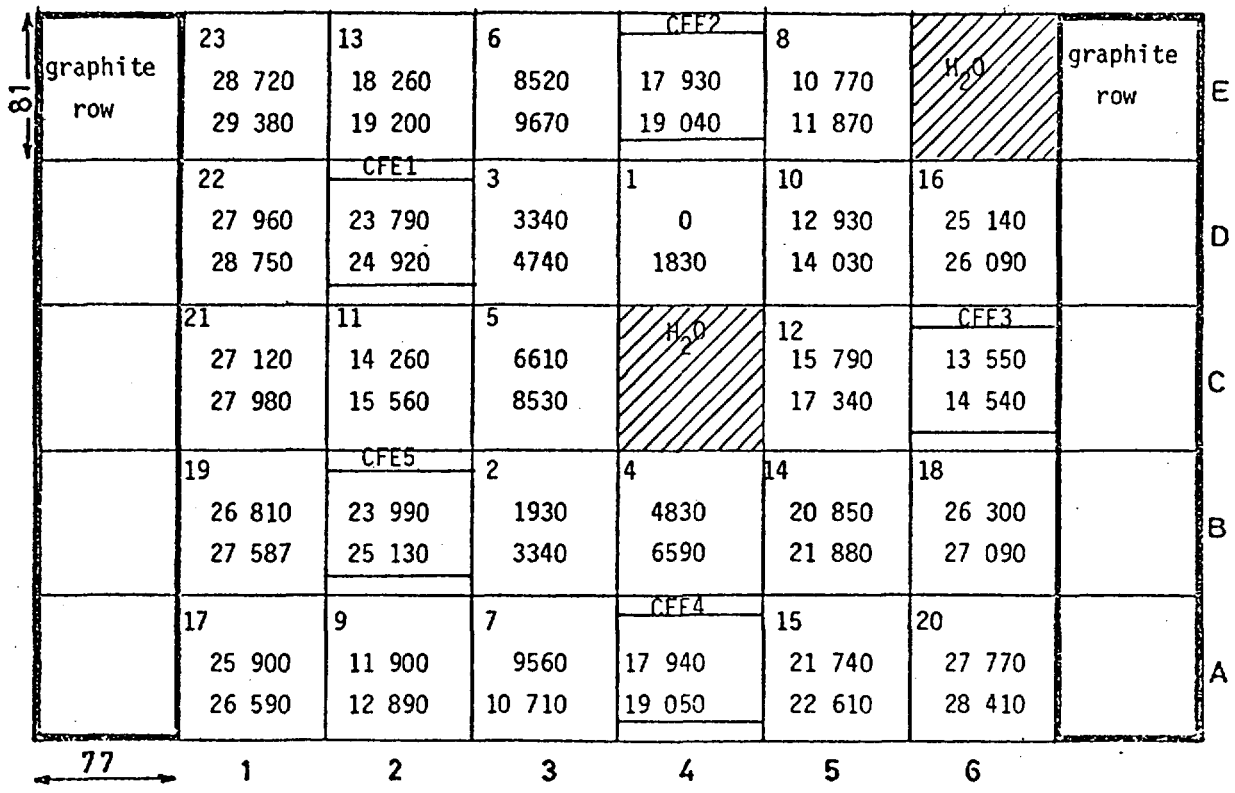

Fuel shuffling

Fuel burn up at BOC MWd/t

Fuel burn up at EOC MWd/t

Cycle length ..... 22.7 days
Average cycle length ..... 25.7 days
Keff (EOC) 1.0299

^{235}U weight in fresh standard fuel element : 574.0 g
^{235}U weight in fresh control fuel element : 466.4 g

Figure 3.7 - 10 MW reactor - Flux in group 1 of UAl 20 % and UO_2- 7.5 % fuels, normalised to UAl - 93 % flux at BOC and EOC

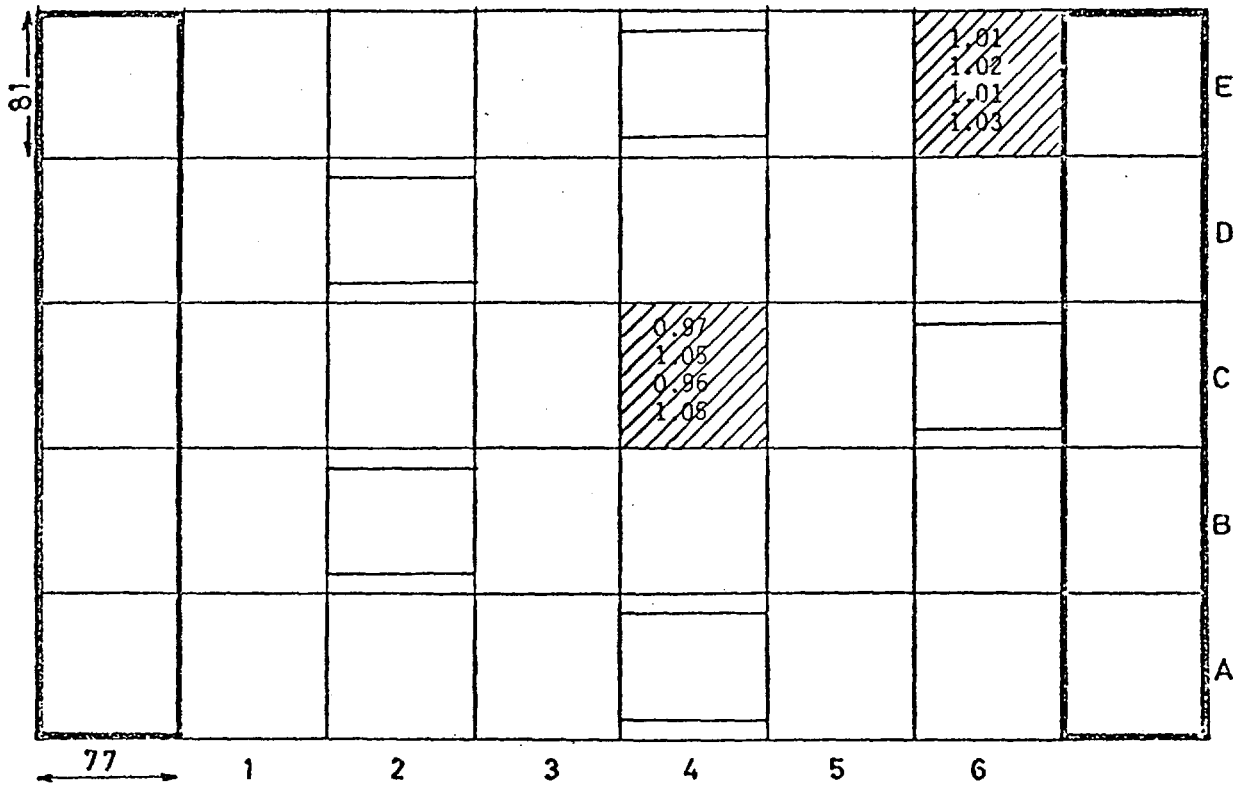

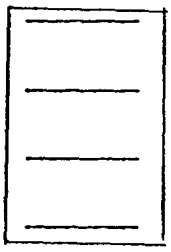

φ_1 (20 %) / φ_1 (93 %) BOC

φ_1 (7.5 %) / φ_1 (93 %) BOC

φ_1 (20 %) / φ_1 (93 %) EOC

φ_1 (7.5 %) / φ_1 (93 %) EOC

Figure 3.8 - 10 MW reactor - flux in group 2 of UAl 20 % and UO_2 - 7.5 % fuels, normalised to UAl - 93 % flux at BOC and EOC

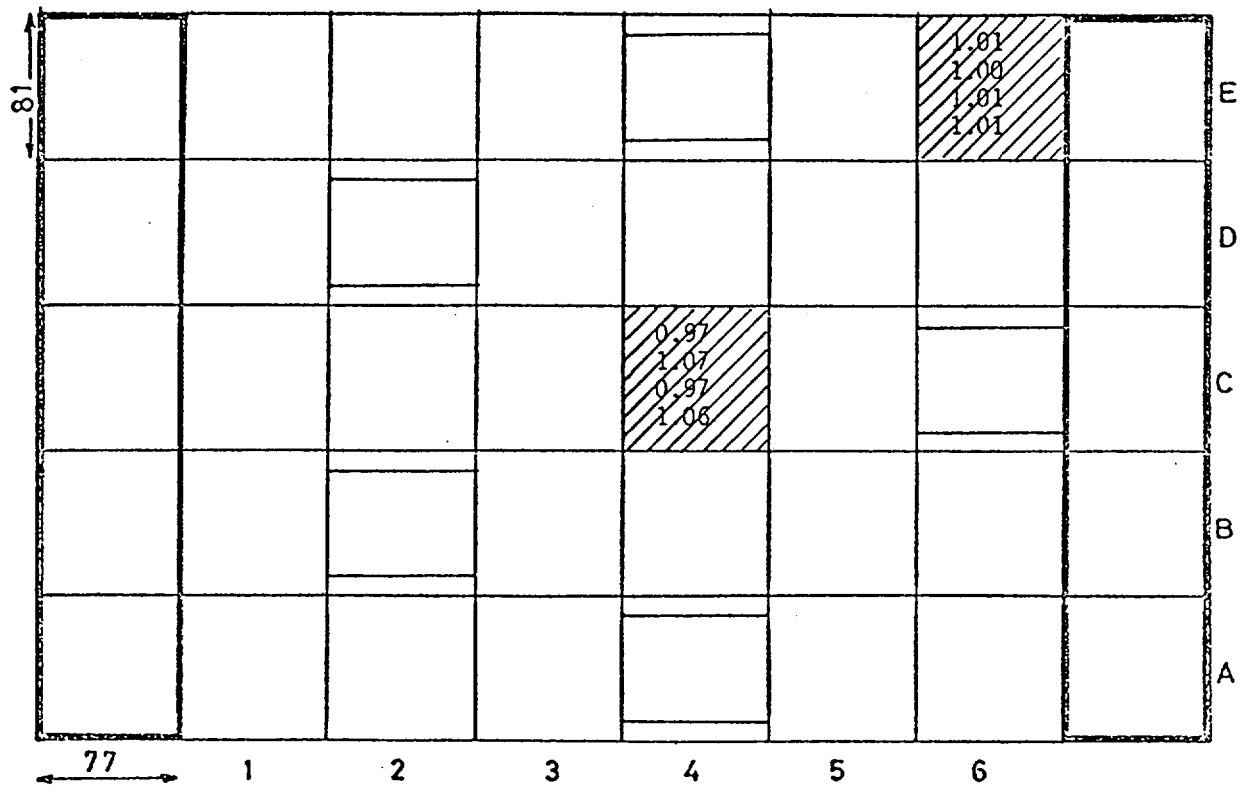

Figure 3.9 - 10 MW reactor - Flux in group 3 of UAl 20 % and UO_2 - 7.5 % fuels, normalised to UAl - 93 % flux at BOC and EOC

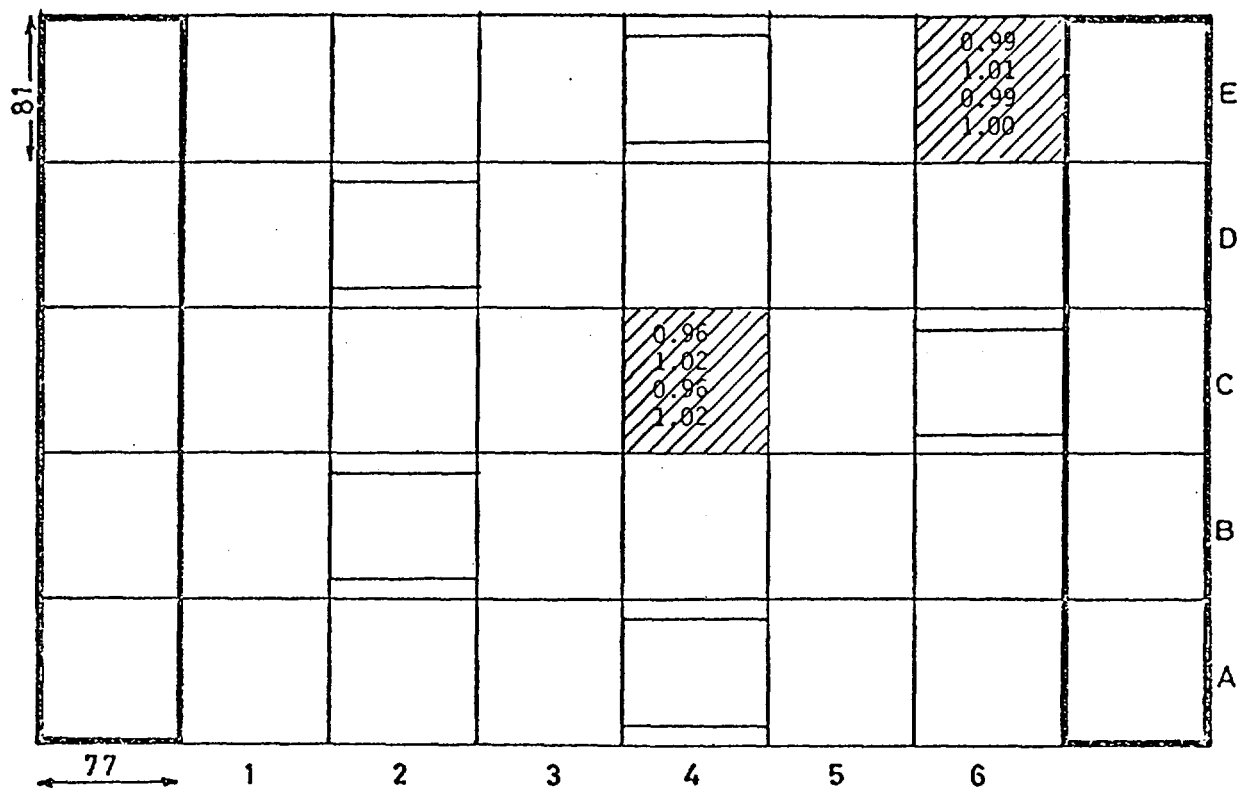

φ_3 (20 %) / φ_3 (93 %) BOC

φ_3 (7.5 %) / φ_3 (93 %) BOC

φ_3 (20 %) / φ_3 (93 %) EOC

φ_3 (7.5 %) / φ_3 (93 %) EOC

Figure 3.10 - 10 MW reactor - Flux in group 4 of UAl 20 % and UO_2 - 7.5 % fuels, normalised to UAl - 93 % flux at BOC and EOC

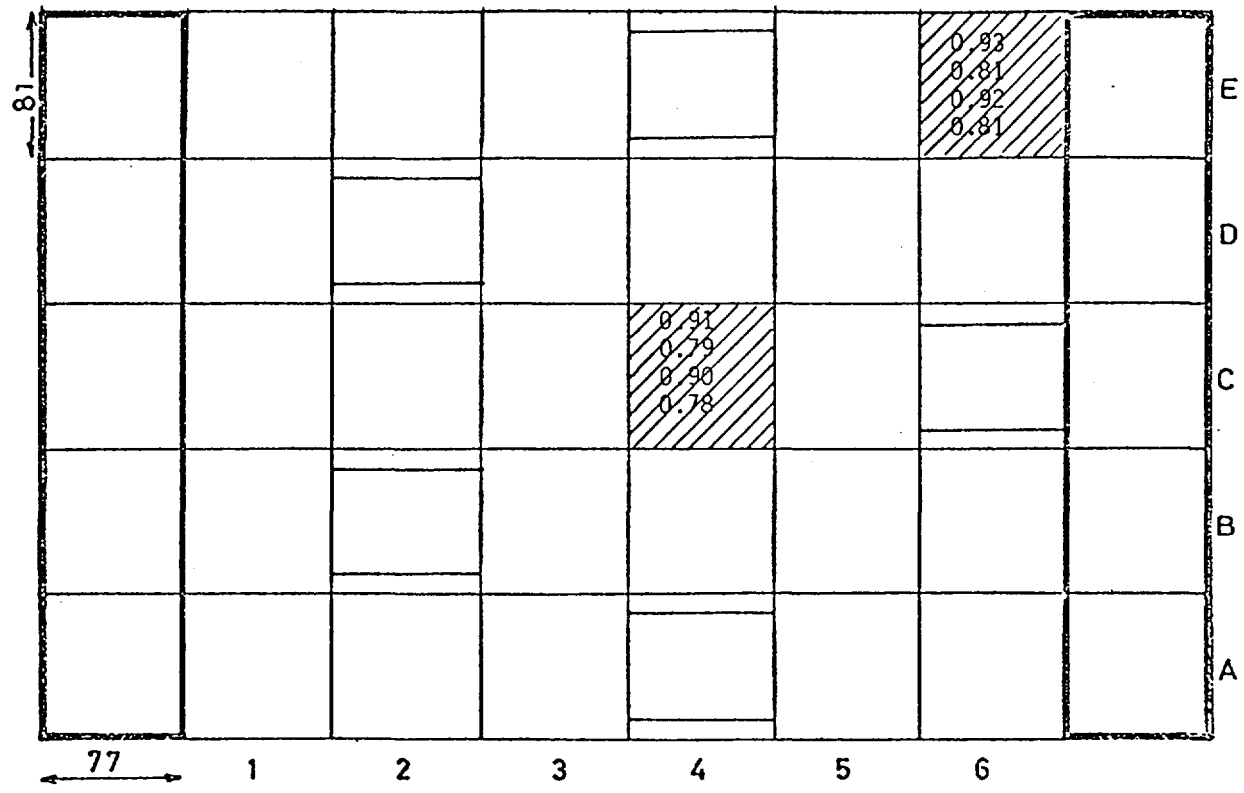

Conclusion

The studies performed by CEA on the possibilities to convert HEU cores to REU cores show rather clear conclusions :

- with Caramel fuel and enrichment down from 7 % to 4 % U_{235}, one reaches the same range of performances for the two cores studied. This conclusion can be extended to a wide range of cores and powers, demonstrating the capability of Caramel fuel to fulfil the requirements of their experimental and operational program.

- with classic MTR U-Al fuels 20 % enriched, the range of research reactors which could be right now be converted to LEU is not so wide; the technological limitations in the U meat density reduce the extension of its present uses. Experimental performances in fluxes are slightly decreased as far as the thermal flux is concerned.

- in the case when intermediate 45 % U_{235} enriched fuel is needed (for the upper range of the research reactors), the evaluations developed in the benchmark problem (Appendix E 5) are representative of the performances in fluxes : the experimental capability of the reactor is not really modified. The only problem is connected with the lifetime; it can be kept at the same value depending on the present characteristics of the lattice, and in some cases cannot fit the reactor requirements.

APPENDIX E-1

NEUTRON STUDIES ON THE CONVERSION OF THE RA-3 REACTOR TO LEU FUEL

performed by

J. Babino, M. Madariaga, J. Testoni

CNEA, Reactor Department

Buenos Aires

Avda, Del Libertador 8250

Argentina

ABSTRACT

Results of preliminary neutronic studies for conversion of the RA-3 reactor to LEU fuel are described.

1. THE RA-3 MAIN CHARACTERISTICS

The 7 MW*RA-3 reactor is operating in Buenos Aires, Argentina, since 1967. It is mainly used in the production of radioisotopes for applications.

The RA-3 utilizes standard MTR-type fuel elements (Fig. 1) containing 90 wt% enriched uranium. The fuel elements are composed of 19 plates of Al-U-Alloy with an uranium concentration of 18.7 wt%, being the corresponding uranium density of 0.59 g/cm^3.

The 0.52 mm meat plates are protected by an 0.39 mm Al cladding.

Normal cores consist of 25 standard fuel elements and 4 fuel fuel elements with control rods.

Typical final burn-ups are of about 40% consumed U-235 with a cycle length of around 20 days at 3 MW. At the end of each cycle one fuel element is replaced.

The medium thermal flux at 3 MW is of about 1.5×10^{13} neutrons/. cm^2 sec.

The thermohydraulic system allows a coolant flow of 900 m^3/hr, being the coolant temperature 45°C.

2. THE CONVERSION OF THE RA-3 TO LEU FUEL

The above mentioned coolant flow means heavy economical penalties, i.e. important changes in the primary circuit, if fuel elements have to suffer important geometry changes, i.e. diminution in the number of plates.

In this situation we must rely upon only two kinds of changes:

a) the increase of the uranium density in the meat,

b) minor geometric changes in the fuel elements, as changes in thickness and width in the meat or the cladding.

3. NEUTRONIC CALCULATIONS

We will now show some results of scoping neutronic calculations we have made in order to evaluate the effects on the RA-3 reactivity and burn-up of several kinds of geometric and composition changes.

In this first stage we have limited ourselves to cell calculations.

3.1 Calculation Methods

The calculations were performed using the WIMS-D cell code in the pin cell option with condensations from its 69 group library and the S4 option

*Operating at power level 3.5 MW

for the main transport calculation performed with the following four group structure.

1st group	10 Mev	-	0.821 Mev
2nd group	0,821 Mev	-	5.53 keV
3rd group	5.55 KeV	-	0.625 eV
4th group	0.62 eV	-	0. eV

In order to adapt the actual cell geometry to the WIMS code, the cell was assumed composed of three kinds of infinite layers (Fig. 2).

Fuel (Al + U)
Clad + lateral support material (Al)
Coolant (H_2O)

so that the following conditions are fulfilled:

a) the fuel plate thickness is conserved

b) the volume ratios of the different materials are conserved.

3.2 Results

3.2.1. Reference case

Evaluation was performed for the current geometry and composition of the fuel elements and also for a fuel element with the same geometry and a 20% enriched meat with uranium concentration of 60 wt% and uranium density of 2.8 g/cm^3.

As a reference in the next sections we will compare two parameters:

a) the reactivity of a typical cold and clean water reflected configuration ($B^2 = 0.0078\ cm^{-2}$)

b) the average burn-up corresponding to zero reactivity.

Looking at Fig. 3 we can point out as a first remark that, in this case, the reactivity (parameter a) decreases from 13600 pcm to 9900 pcm and that the burn-up (parameter b) decreases from 30% to 22%.

3.2.2 Uranium concentration changes

In Fig. 4 the variations of reactivity and burn-up with the uranium concentration for the present geometry are shown. As it can be seen these parameters suddenly get apart from the present values while lowering the uranium concentration.

In order to obtain the present reactivity a concentration of 65 wt% is required ($\rho_u = 3.32\ g/cm^3$). As a reference we can point out that an increase in the porosity factor from 0.84 to 0.95 means increases in reactivity that ranges from 1000 pcm to 3500 for 80 wt% concentration and 40 wt% concentration respectively.

3.2.3 Geometrical changes

In the following sections we will consider the effect on reactivity and burn-up of different geometrical changes in the 20% enriched fuel with uranium concentration of 60 wt%. Uranium loadings are always shown.

3.2.3.1 Variation of fuel thickness with constant can thickness.

Fig. 5 shows the incidence on reactivity and burn-up of the substitution of fuel volumes by moderator volumes. As it can be expected there is an optimal relation between fuel and moderator that, in our case, occurs for a fuel thickness of 0.72 mm.

Anyway, neither present reactivity nor burn-up are reached with this optimal thickness, a difference of 2200 pcm and 2.5% respectively being found.

3.2.3.2 Variations of the can thickness with constant moderator thickness.

In this case fuel is added at the expense of a lowering of the clad aluminum. This change is always positive from the neutronic point of view as it can be seen in Fig. 6.

It can also be observed that the present burn-up is reached decreasing the clad thickness in only 0.06 mm, while the present reactivity is achieved decreasing that thickness in 0.1 mm.

It must be pointed out, however, that the resulting clad thicknesses, remarkably in the second case, are not acceptable from the safety point of view.

3.2.3.3 Variations of the can thickness with constant fuel thickness (Fig. 7).

In this case, the clad thickness is diminished thanks to the moderator thickness, keeping the U-235 loading in 204 g. In this case too low values of clad thickness are necessary in order to reach the current reactivity and burn-up.

3.2.3.4 Variation of the plate number.

a) An alternative way of obtaining a similar result to that of the section 3.2.3.3 is to decrease the number of plates keeping the clad thickness, as well as the total fuel amount, constant.

   The effect produced by this modification is shown in Fig. 8. It may be observed that the present burn-up is achieved with 12 plates while the present reactivity is obtained with less than 10 plates.

   However it must be pointed out that, although the clad thickness is kept constant, a decrease in the number of plates leads to serious problems from the thermohydraulic point of view.

b) Finally, we studied the effects of geometrical variations, as changes in the volumes of materials in the cell. Such kind of changes normally imply changes in the fuel thickness and in the cell pitch.

As it is shown in Fig. 9 the effects of that kind of changes are negligible. We can conclude that reactivity and burn-up variations observed in the case a) of this section are mainly due to the interchange between aluminium and not to spatial disadvantage factors and the geometrical parameters used in the resonance calculations.

4. SUMMARY AND CONCLUSIONS

From the point of view of the conversion possibilities of RA-3 to 20% enriched fuel it is possible to define three regions for the parameter concentration of uranium in the meat:

1) High concentration region

$$65 \text{ wt\%} \leq C_u \leq 69 \text{ wt\%}$$

$$3.32 \text{ g/cm}^3 \leq \rho_u \leq 3.82 \text{ g/cm}^3$$

With this concentration the conversion without penalties would be direct with no modification in the gometry of the current fuel element.

2) Intermediate concentrations

$$C_u \approx 60 \text{ wt\%}$$

$$\rho_u \approx 2.8 \text{ g/cm}^3$$

in this region, and adequate combination of geometric modifications as described in section 3 make the conversion to 20% enrichment feasible without heavy penalties.

3) Low concentration region

$$C_u \approx 50\%$$

$$\rho u < 2 \text{ g/cm}^3$$

in this region the conversion would imply severe penalties on reactivity and burnup.

Finally, we can mention that calculations made for 45% enriched fuel show that almost direct conversion can be made with 38 wt% concentrations and uranium densities around 1.35 g/cm^3.

5. NEXT STEPS IN NEUTRONIC CALCULATION FOR THE RA-3 CONVERSION

Presently, we have finished a first draft containing the calculations made with our methods of the benchmark proposed by the Consultants Meeting held June 1975 in Vienna.

First comparisons show that our results are in good agreement with those obtained by other groups of work.

Soon we will perform shuffling calculations for different LEU fuel elements in order to obtain more accurate results than those we have outlined in this report.

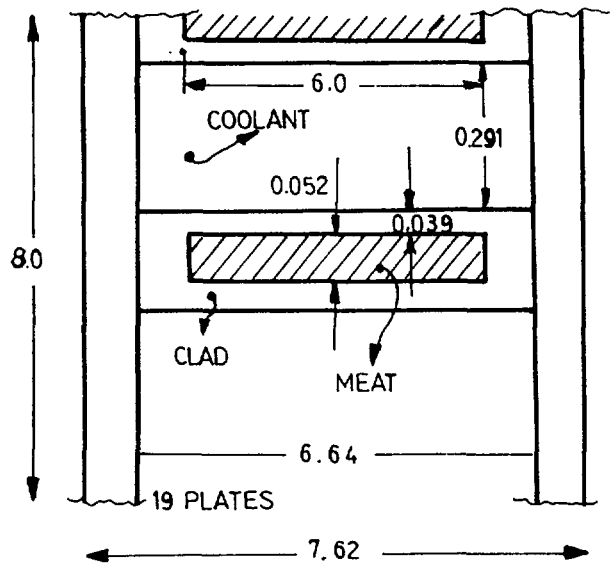

CURRENT FUEL ELEMENT

FIGURE 1

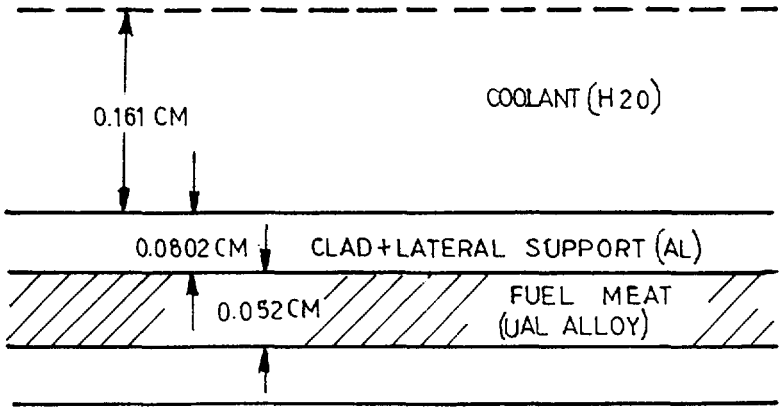

CURRENT FUEL ELEMENT REPRESENTATION IN WIMS

FIGURE 2

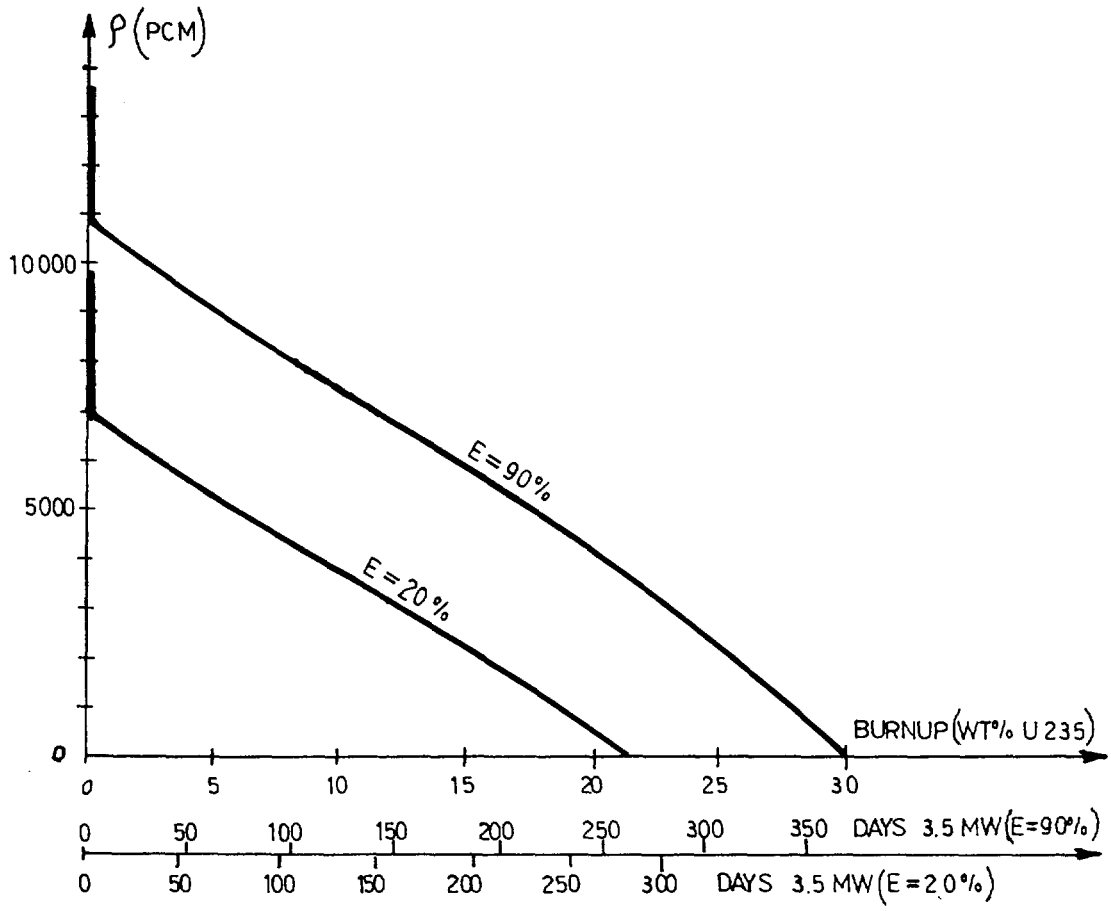
ρ (PCM)
10000
5000
0
E=90%
E=20%
BURNUP (WT% U 235)
0 5 10 15 20 25 30
0 50 100 150 200 250 300 350 DAYS 3.5 MW (E=90%)
0 50 100 150 200 250 300 DAYS 3.5 MW (E=20%)

FIGURE 3

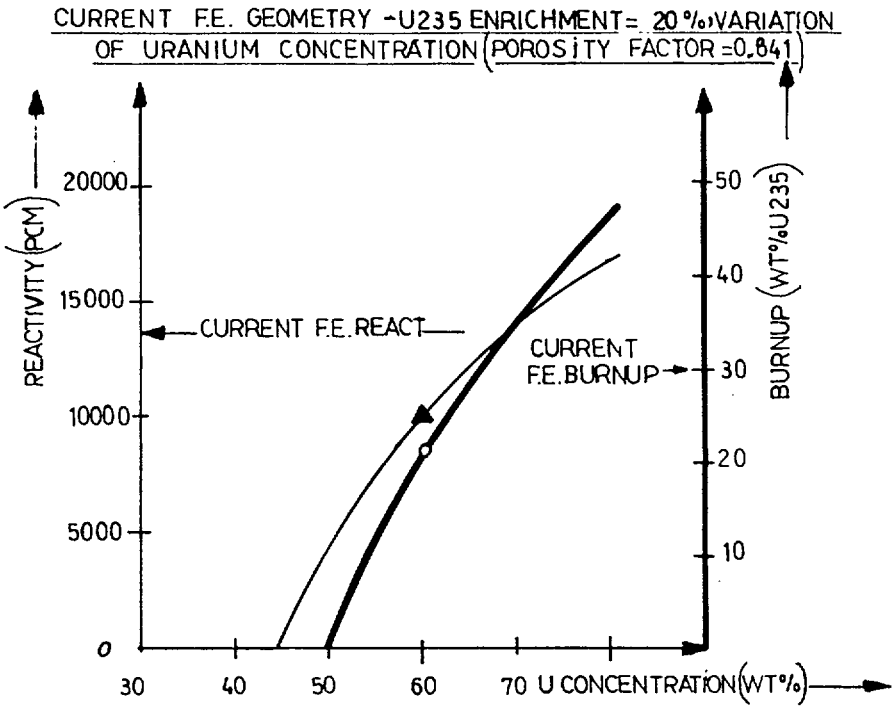

FIGURE 4

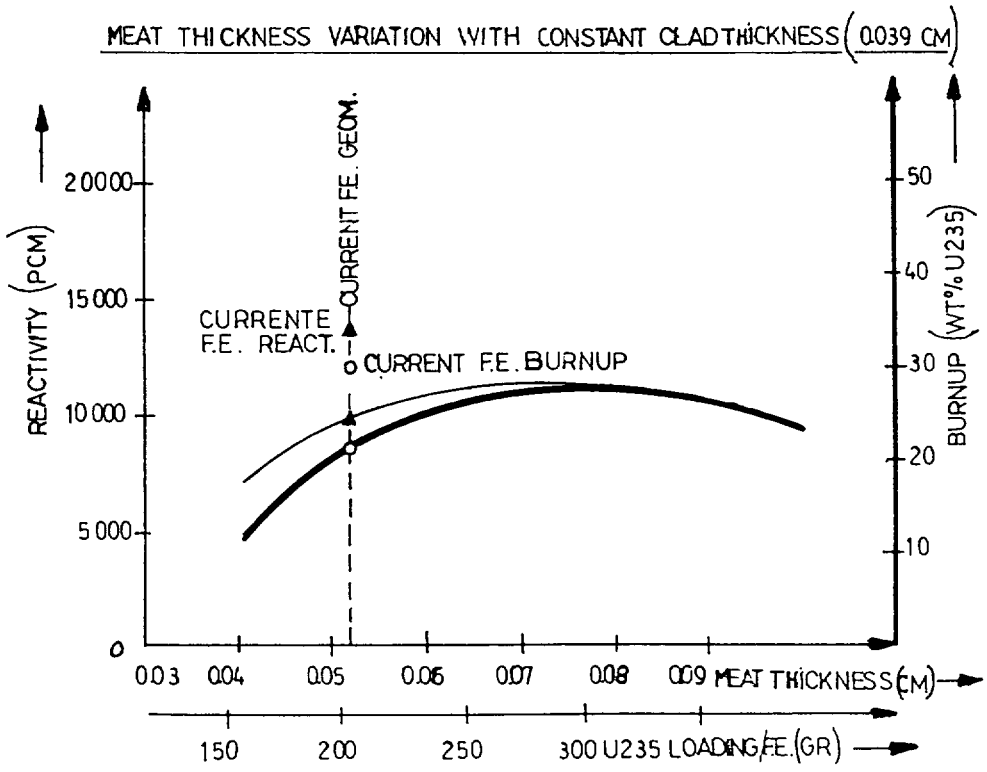

FIGURE 5

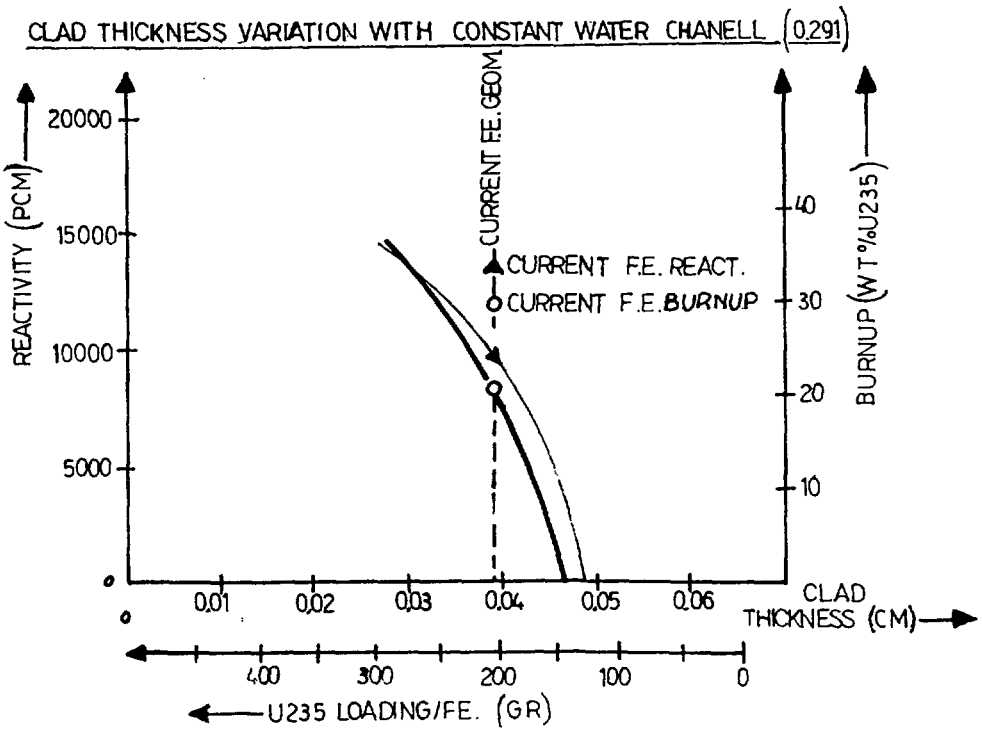

FIGURE 6

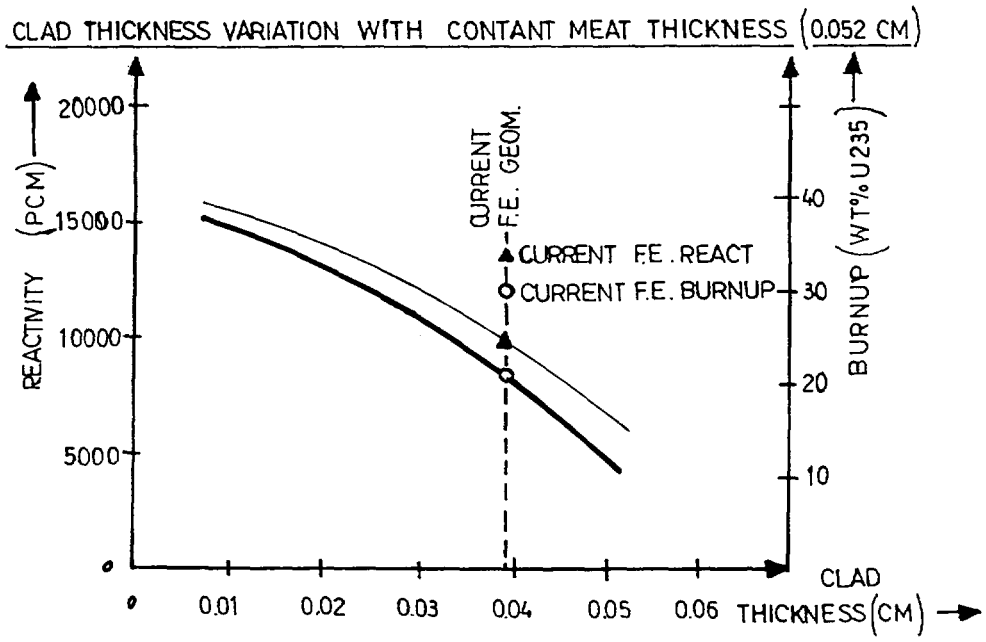

FIGURE 7

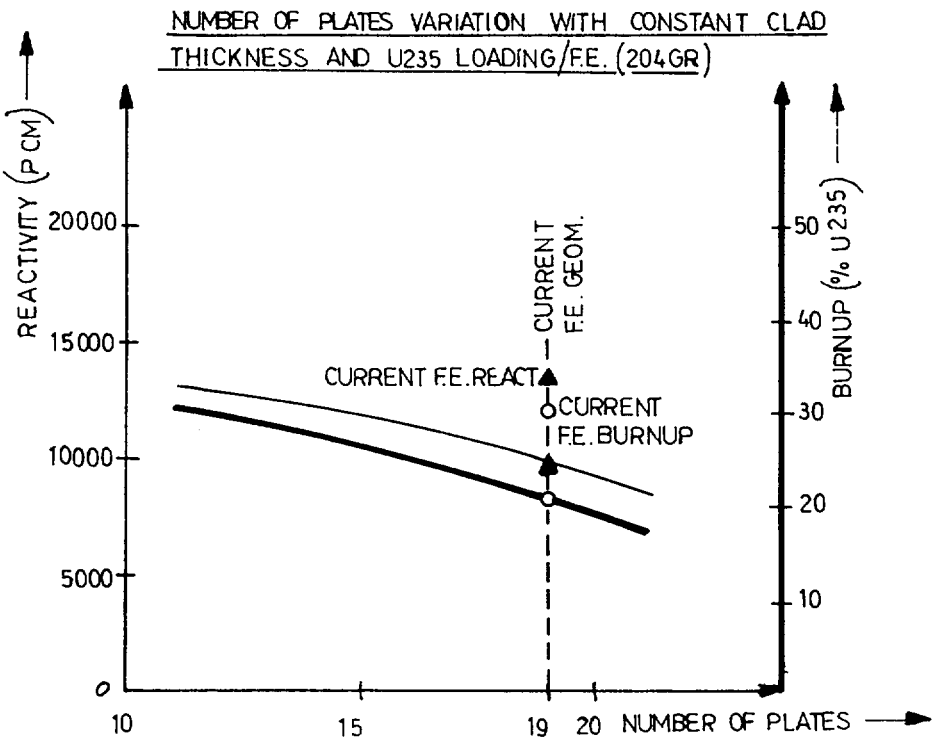

FIGURE 8

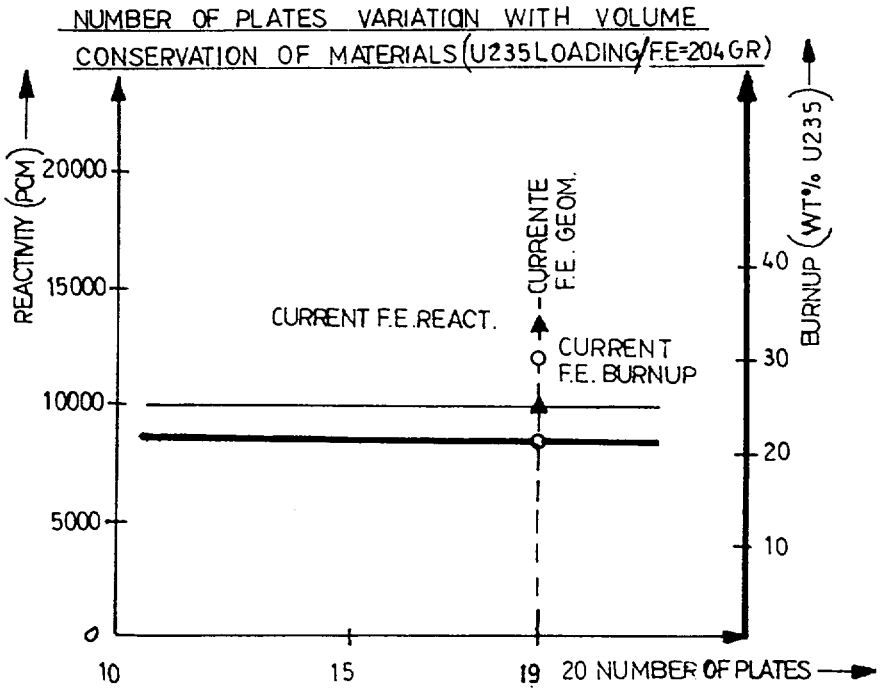

FIGURE 9

APPENDIX E-2

Methods of Generic Enrichment Reduction Calculations

Performed by

Japan Atomic Energy Research Institute (JAERI)
Tokai-mura, Ibaraki-ken
Japan

ABSTRACT

The outline of the computer code system of JAERI for analysing research reactors is presented and the results of check calculations to validate the code system are evaluated by the experimental data.

APPENDIX E

CONTENTS

E.1. Introduction

In this appendix E, firstly the outline of our computer code system* composed of multi-group nuclear constant library, SN code and three dimensional neutron diffusion code is presented for analysing the core performance of research reactors. Next, to validate the computer code system, the results of check calculations are compared with those by the Monte Carlo code. In the last section, for a demonstration of our computer code system, three-dimensional burn-up distributions are shown for the JMTR (Japan Material Test Reactor) Core.

E.2. Calculation Method

E.2.1 Outline of the computer code system for analysing research reactors at JAERI

A code system has been developed with KURRI (Kyoto University Research Reactor Institute) for analysing the core performances of research reactors. This code system consists of three parts. The first part is to obtain the multi-group nuclear constants library (MGCL) which is generated from the nuclear data file ENDF/B-4[1], and the 2nd part is to obtain burn-up dependent cell averaged few group constants table (FG-Table) by using the SN code ANISN-JR[2]. The third part is to calculate the burn-up dependent core performance using the three-dimensional neutron diffusion code FEDM or DIFFUSION-ACE-2[3]. In these diffusion codes a reactor is divided in several layers along the Z axis and in several channels across the x-y plane as shown in Fig.E.1. A region formed by a channel and a layer is named a block whose nuclear cross sections are obtained with the cell calculation. A one-dimensional neutron flux calculation is performed for each channel with the radial leakage coefficient. A two-dimensional neutron flux calculation is then made for each layer with the axial leakage determined from the one-dimensional calculation. The one- and two-dimensional leakages will be iterated until the consistency is attained between the two.

The computer codes used for this benchmark calculation are listed in Table E.1.

E.2.2 Generation of the multi-group nuclear constants library (MGCL)

The computer code system to produce the MGCL is shown in Fig.E.2. The production of temperature dependent ultra-fine cross sections (about 70,000 energy points data) is performed by the computer code RESEND-D which is an improved version of RESEND[4] developed at JAERI. To collapse the energy groups of the ultra fine data points, two kinds of neutron energy spectra for the weight function are applied. One is introduced from the following equation.

$$\phi(\varepsilon) = \frac{\sigma_o \phi_s}{\sigma_t^i + R^i \sigma_t^{238} + \sigma_o} \quad , \qquad (1)$$

---

* Main parts of this code system were developed by cooperative research with Kyoto University Research Reactor Institute.

where ϕ_s is a standard neutron energy spectrum which consists of three parts, that is, fission spectrum, 1/E and Maxwellian parts,

$$\sigma_o = \frac{1}{N^i} \left(\sum_{k \neq i, 238} N^k \sigma_t^k + \frac{aG}{l} f(r) \right) \quad ,$$

$$R^i = \frac{N^{238}}{N^i} \quad .$$

The other is obtained by solving the neutron slowing down equation with the code FINESPEC. For many nuclides, the first weight function (1) is used and only for important nuclides, the second weight function is applied to obtain multi-group constants. The energy group structure for the MGCL is the same as the standard 137 energy group structure at JAERI shown in Table E.2. By dividing effective multi-group constants (σ_{eff}) by the infinite multi-group constants (σ_∞), neutron shielding factors are obtained. These shielding factors are arranged in a shielding table.

The scattering matrices composed of 137 groups are obtained by using the computer codes SUPERTOG[5] and FLANGE[6] or PIXSE[7] as shown in Fig.E.2. In these matrices, the up-scattering is taken into consideration for energies below 1.855 eV (45 energy groups of 137 groups). The infinite dilution cross sections, shielding factors and scattering matrices are edited into the MGCL.

E.2.3 Generation of the few-group nuclear constants library (FG-Table) or cell calculation

The computer code system to produce the FG-Table is shown in Figs.E.3. and E.4. This system is sometimes called the cell calculation system. The cell calculation routines consist of two parts, one is a unit cell calculation with 137 energy group constants and the other is a super cell calculation with collapsed group constants obtained from the unit cell calculation. Using the neutron energy spectrum distribution in a super cell, the effective microscopic few group ($\simeq$3) cross sections are obtained and stored in FG-Table.

E.2.4 Whole core calculation

Using the FG-Table and atomic number densities, macroscopic cross sections are calculated by using the MACFIT code for each material block in the core (see Fig.E.5). The neutron flux and thermal power distributions are obtained by solving the neutron diffusion equation with three dimensional diffusion code FEDM or DIFFUSION-ACE-2. With these neutron flux, and collapsed microscopic cross sections to one group, the burn-up distribution and atomic number densities distribution in a core are calculated by the COREBURN code.

E.3. Check calculation

E.3.1 Check calculations of the TCA lattices for evaluating the MGCL

E.3.1.1 Purpose

In order to validate the multi-group constants library MGCL, Monte Carlo calculations were performed on many TCA critical Experiments[8].

E.3.1.2 Method

The Tank-type Critical Assembly (TCA) essentially consists of fuel rods, grid plates and a core tank (1.83 m in diam. and 2.08 m in height). The vertical cross-sectional view is shown in Fig.E.6.

The experimental lattices were built in the core tank. The moderator was light water. The reactor was operated by raising the water level from the bottom of the core tank by a feed water pump. No control rod was used for reactor operation. The maximum limitation of the power was 200 Watts. The fuel rods were made from 2.6 w/o enriched UO_2 or 3.0 w/o enriched PuO_2-natural UO_2. The fuel specifications are shown in Fig.7 and Table E.3. The water to fuel volume ratio in a lattice cell ranged from 1.50 to 3.00 for the UO_2 lattices or from 2.42 to 5.55 for the PuO_2-UO_2 lattices. The critical sizes were determined by measuring critical water level. The lattices were named by the water to fuel volume ratio and the fuel rod type. For example, the lattice name 1.50U corresponds to the UO_2 lattice of which water to fuel volume ratio is 1.50, and a lattice name 2.42Pu to the PuO_2-UO_2 lattice of which the water to fuel volume ratio is 2.42. A list of the lattice names is shown in Table E.4 with lattice pitches. Some examples of pattern of lattice configuration are shown in Fig.E.8. Atomic number densities of materials in the lattice are given in Table E.5.

To check the reliability of the MGCL used for following benchmark calculations, the many experimental data of TCA were analysed with the Monte Carlo code KENO-4[9] varying the lattice pitch and the number of fuel rods.

In these calculations, the number of neutron histories was selected to 30,000. To check the effect of the number of histories, recalculations with 60,000 histories were performed for UO_2 lattices of TCA.

E.3.1.3 Results

The computed results by the KENO-4 with the MGCL are shown in Figs.E.9 and E.10. The comparison between the computed results with 30,000 histories and 60,000 histories, shows that the standard deviation of the mean effective multiplication factor (k_{eff}) for 60,000 histories becomes smaller than that for 30,000 histories and the mean effective multiplication factors in both cases are almost the same.

The computed mean multiplication factors in UO_2 and PuO_2-UO_2 lattices are 0.99265 and 0.99412, respectively. That is, the computed values with the MGCL are about 0.7% $\Delta k/k$ smaller than the experimental one.

E.3.1.4 Discussion

Using our multi-group cross section library MGCL, computed multiplication factors for light water moderator lattices with low enriched fuel rods show smaller by about 0.7% than the measured ones. It is considered that this discrepancy comes from the estimation error of the neutron shielding factor of ^{238}U. We intend to correct the shielding factor using more precise neutron energy spectrum.

E.3.2 Check calculations of the TCA lattices for evaluating the core calculation method

E.3.2.1 Purpose

As shown in Figs.E.3, E.4 and E.5, the cell calculations were performed with the ANISN code and the core calculation was carried out with the diffusion code.

In order to validate the present cell calculation method, the computed

results by the ANISN code were compared with those by the KENO-4 code for the several unit cells of TCA whose cell structure is shown in Fig.E.11 for an example.

The effective multiplication factors of the ANL benchmark problems were computed by the diffusion code ADC[10] with the cell group constants obtained by the ANISN code. The computed results by the ADC were, therefore, compared with those by the KENO-4 code for the previously mentioned TCA lattices. The most important point of this study is to evaluate the diffusion coefficients obtained by the ANISN code.

E.3.2.2 Method

The 137 group constants library for the ANISN code and the KENO code was produced from the MGCL by the MAIL code. Using the same library, the effective multiplication factors in a unit cell of TCA were calculated by the ANISN code and the KENO code, to compare the results with each other. The effective multiplication factors in TCA lattices were also obtained by two-dimensional diffusion calculation (ADC) and compared with those by the KENO code. A core model for diffusion calculation is shown in Fig.E.12. To estimate perpendicularly directional neutron leakage, the vertical neutron flux buckling was obtained using the measured reflector saving shown in Table E.6. The number of energy groups for the ADC is three, whose energy structure is shown in Table E.7. The diffusion coefficients for the ADC were obtained from $D = 1/3\ \Sigma_{tr}$, where the Σ_{tr} was computed by the ANISN code.

E.3.2.3 Results

The computed results on several unit cell by the ANISN and the KENO are given in Table E.8, which shows a good agreement with each other. The computed results on TCA lattices by the ADC and the KENO code are shown in Table E.9, which shows again a nice agreement with each other.

E.3.2.4 Discussion

One of the most difficult problems on diffusion calculations is how to estimate the diffusion coefficients. The diffusion coefficients used in our calculation seems to be relevant.

E.3.3 Three-dimensional burn-up distribution in JMTR core

E.3.3.1 Purpose

Our calculation scheme differs from those of other countries. The differences in the method between JAERI and ANL are as follows:

i) Our scheme contains the super cell calculation.
ii) Our cut-off energies for few group constants differ from those of ANL.
iii) Burn-up dependent atomic number densities of fissile materials are obtained not by cell code but by core performance calculation code.
iv) Burn-up distribution in the core is calculated not by two-dimensional diffusion code but by three-dimensional code.

Figure 13 shows a ratio of ^{238}U capture to ^{235}U fission in the IAEA 10MW benchmark MTR-type reactor, which predicts space dependency of neutron energy spectrum. This is the reasion why we do not compute the burn-up dependent atom density distribution at the stage of cell calculation but of full core calculation.

In this section, we will show computed results by our computer system.

The JMTR (Japan Material Test Reactor) was chosen for an example to show the three-dimensional burn-up distribution in the core.

E.3.3.2 Method

The calculational scheme is quite the same as shown in Figs.E.3, E.4 and E.5. The JMTR design parameters are given in Table E.10. The unit cell and the super cell configurations are shown in Figs.E.14 to E.19. The core configuration and mesh specification are shown in Figs.E.20, E.21 and E.22. In addition, atomic number densities of the fresh fuel are given in Table E.11. The three-dimensional core burn-up calculation was performed by the computer codes FEDM and COREBURN.

Mixed method of the finite difference and the finite element method is adopted in the FEDM code. The two-dimensional x-y calculation is performed by the finite element method for each layer and the one-dimensional calculation along the Z axis is performed by the finite difference method for each channel. Atomic number densities in each burn-up block in the core are calculated with microscopic cross sections stored in the FG-Table and with computed neutron flux by the FEDM. The burn-up dependent macroscopic cross sections in each calculational block are produced using the atomic number densities and their microscopic cross sections.

E.3.3.3 Results

The results of the demonstration calculation are shown in Table E.12 for the three-dimensional isotope distribution in a No.7 channel of JMTR.

E.4. Conclusion

Several check calculations were performed and the following conclusions were attained.

i) Using our multi-group cross section library MGCL, the computed multiplication factors in light water moderator lattices with low enriched fuel rods are about 0.7% smaller than the measured values.

ii) The computed results on several unit cells by the ANISN and the KENO show a good agreement with each other.

iii) The computed results on TCA lattices by the diffusion code ADC and the Monte Carlo code KENO show a nice agreement with each other. The results of the above two check calculations justify for us to use Sn code for cell calculations and diffusion code for core calculations.

References

1. M.K. DRAKE, "Data Formats and Porcedures for the ENDF Neutron Cross Section Library", BNL 50274, (1970)

2. K. KOYAMA et al., "ANISN-JR, A One-Dimensional Discrete Ordinates, Code for Neutron And Gamma-Ray Transport Calculations" JAERI-M 6954, (1977)

3. Y. NAITO et al., "A Three-Dimensional Neutron Diffusion Calculation Code: DIFFUSION-ACE", JAERI 1262, (1979)

4. O. OZER, "Program RESEND", BNL 17134, (1972)

5. R.Q. WRIGHT et al., "SUPERTOG: A Program to Generate Group Constants and Pn Scattering Marices from ENDF/B", ORNL-TM-2679 (1969)

6. H.C. HONECK and D.R. FINCH, "FLANGE II : A Code to Procee Thermal Neutron Data from an ENDF/B Tape", DP-2179 (1971)

7. J.D. MACDOUGALL, "PIXSE", AEEW-M318 (1963)

8. H. TSURUTA et al., "Critical Sizes of Light-Water Moderated UO_2 and PuO_2-UO_2 Lattice", JAERI 1254, (1978)

9. L.M. PERTIE and N.F. CROSS, "KENO IV-An improved Monte Carlo Criticality Program", ORNL 4938 (1975)

10. M. AKIMOTO and Y. NAITO, "A General Dimensional Neutron Diffusion Calculation Code: ADC", JAERI-1260 (1978)

Table E.1 Computer Codes Used in the Benchmark Calculation at JAERI

Name	Comments
Cross Section Generation	
RESEND-D	to produce temperature dependent ultra fine point data from an ENDF/B - tape
FINESPEC	to calculate ultra fine neutron energy spectrum
SUPERTOG	to generate fine group constants and Pn scattering matrices from ENDF/B
FLANGE	to process thermal neutron data from an ENDF/B
PIXSE	to process thermal neutron data
MAIL	to produce cross section library for ANISN and KENO-4
Transport Codes	
ANISN	one-dimensional discrete ordinate transport code
KENO-4	improved Monte Carlo criticality program
Diffusion Codes	
ADC	general dimensional neutron diffusion calculation code
DIFFUSION-ACE	three dimensional neutron diffusion calculation code with leakage iterative method
FEDM	mixed method of two-dimensional finite element and finite difference method

Table E.2 Standard energy group structure at JAERI

	Group NO.	Upper Energy Boundary	Lethergy width ΔU		Group NO.	Upper Energy Boundary	Lethergy width ΔU
	1	16.487 Mev	0.125		37	183.16 Kev	0.125
	2	14.550	0.125		38	161.63	0.125
	3	12.840	0.125		39	142.64	0.125
	4	11.331	0.125		40	125.88	0.125
	5	10.000	0.125		41	111.09	0.125
	6	8.825	0.125		42	98.037	0.125
	7	7.788	0.125		43	86.517	0.125
	8	6.8729	0.125		44	76.351	0.125
	9	6.0653	0.125		45	67.379	0.125
	10	5.3526	0.125		46	59.462	0.125
	11	4.7237	0.125		47	52.475	0.125
	12	4.1686	0.125		48	46.309	0.125
	13	3.6788	0.125		49	40.868	0.125
	14	3.2465	0.125		50	36.066	0.125
	15	2.8650	0.125		51	31.828	0.125
	16	2.5284	0.125		52	28.088	0.125
	17	2.2313	0.125		53	24.788	0.125
	18	1.9691	0.125		54	21.875	0.125
	19	1.7377	0.125		55	19.305	0.125
	20	1.5335	0.125		56	17.036	0.125
	21	1.3533	0.125		57	15.034	0.25
	22	1.1943	0.125		58	11.709	0.25
	23	1.0540	0.125		59	9.1188	0.25
	24	930.14 Kev	0.125		60	7.1017	0.25
	25	820.85	0.125		61	5.5308	0.25
	26	724.40	0.125		62	4.3075	0.25
	27	639.28	0.125		63	3.3546	0.25
	28	564.16	0.125		64	2.6126	0.25
	29	497.87	0.125		65	2.0347	0.25
	30	439.37	0.125		66	1.5846	0.25
	31	387.74	0.125		67	1.2341	0.25
	32	342.18	0.125		68	961.12 ev	0.25
	33	301.97	0.125		69	748.52	0.25
	34	266.49	0.125		70	582.95	0.25
	35	235.18	0.125		71	454.00	0.25
	36	207.54	0.125		72	353.58	0.25

Table E.2 (Continued)

	Group NO.	Upper Energy Boundary	Lethergy width ΔU		Group NO.	Upper Energy Boundary	Lethergy width ΔV
	73	275.36 ev	0.25	18	110	0.29792 ev	270 m/sec
	74	214.45	0.25	19	111	0.27699	270
	75	167.02	0.25	20	112	0.25683	270
	76	130.07	0.25	21	113	0.23742	270
	77	101.30	0.25	22	114	0.21878	270
	78	78.893	0.25	23	115	0.20090	270
	79	61.442	0.25	24	116	0.18378	270
	80	47.851	0.25	25	117	0.16743	270
	81	37.267	0.25	26	118	0.15183	270
	82	29.023	0.25	27	119	0.13700	270
	83	22.603	0.25	28	120	0.12293	270
	84	17.603	0.25	29	121	0.10962	270
	85	13.710	0.25	30	122	0.09708	270
	86	10.677	0.25	31	123	0.085295	270
	87	8.3153	0.25	32	124	0.074274	270
	88	6.4760	0.25	33	125	0.064015	270
	89	5.0435	0.25	34	126	0.054518	270
Thermal Group NO.	90	3.9279	0.25	35	127	0.045783	270
	91	3.0590	0.25	36	128	0.037811	270
	92	2.3824	0.25	37	129	0.030600	270
1	93	1.8554	0.125	38	130	0.024152	270
2	94	1.6374	0.125	39	131	0.018465	270
3	95	1.4450	0.125	40	132	0.013541	270
4	96	1.2752	0.125	41	133	0.009379	270
5	97	1.1254	0.125	42	134	0.005979	270
6	98	0.99312	0.125	43	135	0.003341	270
7	99	0.87642	0.125	44	136	0.001466	270
8	100	0.77344	0.125	45	137	0.000352	270
9	101	0.68256	0.125			0.000033	270
10	102	0.60236	0.125				
11	103	0.53158	0.125				
12	104	0.46912	0.125				
13	105	0.41399	270 m/sec				
14	106	0.38925	270				
15	107	0.36528	270				
16	108	0.34206	270				
17	109	0.31961	270				

Table E.3 Fuel specification of TCA

	UO_2	PuO_2-UO_2
Fuel		
Enrichment, w/o	2.596, ^{235}U	3.01 ± 0.05, $\frac{PuO_2}{(PuO_2+UO_2)}$
Isotope ratio, w/o		
Uranium		Natural
^{235}U	2.596	
^{238}U	97.404	
Plutonium		
^{238}Pu	—	0.494 (1971-8-19)*
^{239}Pu	—	68.18 (1971-8-19)
^{240}Pu	—	22.02 (1971-8-19)
^{241}Pu	—	7.26 (1971-8-19)
^{242}Pu	—	2.04 (1971-8-19)
Americium		
^{241}Am	—	530 ppm (1971-8-16) in PuO_2
Impurity content	—	$0.90^{+0.09}_{-0.12}$ ppm equivalent boron concentration in PuO_2-UO_2
O/M	2.04	2.07
Pellet		
Fabrication method	Sintered	Mechanically blended and pre-sintered
Diameter, mm	12.50	10.65
Density, g/cm^3	10.40	6.056 ± 0.076
Stack length, mm	1441.5 ± 3	706 ± 3
Cladding		
Material	Al	Zircaloy-2
Inner diameter, mm	12.65	10.83 ± 0.06
Thickness, mm	0.76	0.70 ± 0.07

* Date of assaying.

Table E.4 Name of TCA lattice

Lattice name	H/U or H/Pu	Lattice pitch (cm)
1.50U	4.33	1.849
1.83U	5.28	1.956
2.48U	7.16	2.150
3.00U	8.65	2.293
2.42PU	402	1.825
2.98PU	494	1.956
4.24PU	703	2.225
5.55PU	921	2.474

Table E.5.1 Atomic number densities

Region	Material	Atomic number density at 20℃ ($\times 10^{24}$ atoms/cm^3)	
		2.6 w/o UO_2	3.0 w/o PuO_2–UO_2
Fuel	^{234}U	—	7.436×10^{-7}
	^{235}U	6.086×10^{-4}	9.393×10^{-5}
	^{238}U	2.255×10^{-2}	1.295×10^{-2}
	^{238}Pu	—	2.000×10^{-6}
	^{239}Pu	—	2.749×10^{-4}
	^{240}Pu	—	8.843×10^{-5}
	^{241}Pu	—	2.903×10^{-5}*)
	^{242}Pu	—	8.124×10^{-6}
	^{241}Am	—	2.121×10^{-7}*)
	O	4.725×10^{-2}	2.784×10^{-2}
Cladding (with air gap)	Aluminum	5.587×10^{-2}	—
	Zircaloy-2	—	3.840×10^{-2}
Moderator	H_2O	3.338×10^{-2}	
	B		
	72 ppm	4.024×10^{-6}	
	147 〃	8.155×10^{-6}	
	345 〃	1.919×10^{-5}	
	554 〃	3.082×10^{-5}	

*) Date of assaying; on 1971-8-16.

Table E.5.2 Atomic number densities of ^{241}Pu and ^{241}Am as a function of time

Date	Elapsed time (days)	Atomic number density ($\times 10^{24}$ atoms/cm^3)	
		^{241}Pu	^{241}Am
1971-8-19	0	2.903×10^{-5}	2.121×10^{-7}
1972-4-1	226	2.819	1.059×10^{-6}
1973-4-1	591	2.687	2.374
1974-4-1	956	2.562	3.629
1975-4-1	1321	2.442	4.824
1976-4-1	1686	2.328	5.964
1977-4-1	2051	2.219	7.051

Table E.6 Reflector savings

Lattice name	Vertical (cm)	Horizontal (cm)
1.50U	12.6±0.3	17.0±0.8
1.83U	12.2±0.3	13.9±0.8
2.48U	11.3±0.2	13.7±0.5
3.00U	11.1±0.5	14.0±0.8
2.42PU	12.5±0.2	14.6±0.3
2.98PU	12.0±0.2	14.1±0.3
4.24PU	11.6±0.2	13.4±0.2
5.55PU	11.3±0.2	13.1±0.2

Table E.7 Energy Groups Used in the Calculation

Group	E_U, eV	E_L, eV
1	1.6487×10^7	1.8316×10^5
2	1.8316×10^5	0.68256
3	0.68256	0.0

Table E.8 Comparison of infinite multiplication factors in TCA cells calculated by ANISN-JR with those by KENO-4

K∞

	ANISN - JR	KENŌ - IV
1.50 U	1.3554	1.3541 ± 0.00306
1.83 U	1.3703	1.3699 ± 0.00274
2.48 U	1.3695	1.3651 ± 0.00275
3.00 U	1.3540	1.3438 ± 0.00293

K∞ in 1972

	ANISN - JR	KENŌ - IV
2.42 Pu	1.3542	1.3505 ± 0.00297
2.98 Pu	1.3481	1.3511 ± 0.00310
4.24 Pu	1.3046	1.3081 ± 0.00275
5.55 Pu	1.2469	

K∞ in 1973

	ANISN - JR	KENŌ - IV
2.42 Pu	1.3499	1.3531 ± 0.00318
2.98 Pu	1.3439	1.3441 ± 0.00307
4.24 Pu	1.3005	1.3041 ± 0.00269
5.55 Pu	1.2430	

K∞ in 1974

	ANISN - JR	KENŌ - IV
2.42 Pu	1.3435	
2.98 Pu	1.3398	1.3402 ± 0.00290
4.24 Pu	1.2966	1.3018 ± 0.00298
5.55 Pu	1.2392	

K∞ in 1975

	ANISN - JR	KENŌ - IV
2.42 Pu	1.3419	1.3479 ± 0.00313
2.98 Pu	1.3360	1.3358 ± 0.00293
4.24 Pu	1.2929	1.2979 ± 0.00268
5.55 Pu	1.2356	

Table E.9 Comparison of effective multiplication factors in TCA Lattices calculated by ANISN-ADC with those by KEWO-4

Pattern	Fuel Rod Array	Critical Water Level(cm)	ANISN-JR ADC K_{eff}	KENO-4 K_{eff}
	Lattice Name 1.50 U			
18	19 × 19	99.45	0.99334	0.99463 ± 0.00463
24	22 × 22	53.23	0.99543	0.99450 ± 0.00401
29	25 × 25	40.89	0.99473	0.98707 ± 0.00390
Average K_{eff}			0.99450	0.99207 ± 0.00418
	Lattice Name 1.83 U			
3	14 × 24	85.36	0.99224	0.98910 ± 0.00416
6	15 × 19	139.72	0.99205	0.99062 ± 0.00421
18	19 × 19	60.38	0.99387	0.99738 ± 0.00544
Average K_{eff}			0.99272	0.99237 ± 0.00460
	Lattice Name 2.48 U			
11	16 × 16	78.67	0.99107	0.99057 ± 0.00429
13	17 × 17	59.96	0.99150	0.98829 ± 0.00422
18	19 × 19	44.55	0.99160	0.99030 ± 0.00422
Average K_{eff}			0.99139	0.98972 ± 0.00424
	Lattice Name 3.00 U			
5	16 × 16	90.75	0.99034	0.98783 ± 0.00435
13	17 × 17	52.87	0.99128	0.98311 ± 0.00375
18	19 × 19	41.54	0.99125	0.99319 ± 0.00392
Average K_{eff}			0.99096	0.98804 ± 0.00401
Average K_{eff} of UO_2 System			0.99239	0.99055 to 12 cases 0.99265 to 40 cases

Table E.9 (Continued)

Pattern	Fuel Rod Array	Date	Critical Water Level(cm)	ANISN-JR ADC K_{eff}	KENO-4 K_{eff}
Lattice Name 2.42 Pu					
26	23 × 23	72-6- 7	59.55	0.99271	0.99699 ± 0.00438
26	23 × 23	75-5-16	66.46	0.99494	0.99302 ± 0.00408
28	24 × 24	72-6- 7	53.30	0.99220	0.99635 ± 0.00445
28	24 × 24	74-5-14	56.68	0.99429	0.99346 ± 0.00419
28	24 × 24	75-5-16	58.36	0.99429	1.00145 ± 0.00445
Average K_{eff}				0.99369	0.99625 ± 0.00431
Lattice Name 2.98 Pu					
21	20 × 21	72-5-18	67.10	0.99361	0.98949 ± 0.00390
22	21 × 21	72-5-18	61.50	0.99249	0.99847 ± 0.00419
22	21 × 21	73-5-22	64.39	0.99400	0.98760 ± 0.00424
22	21 × 21	74-5-28	66.87	0.99460	0.99403 ± 0.00416
23	21 × 22	72-5-18	57.38	0.99206	0.98698 ± 0.00377
23	21 × 22	75-5-21	63.88	0.99461	0.99417 ± 0.00439
26	23 × 23	74-5-28	51.94	0.99378	0.99538 ± 0.00419
28	24 × 24	75-5-21	48.68	0.99363	0.99445 ± 0.00436
Average K_{eff}				0.99360	0.99257 ± 0.00415
Lattice Name 4.24 Pu					
20	20 × 20	72-4-13	60.32	0.99332	0.99182 ± 0.00405
20	20 × 20	75-5-28	68.18	0.99607	0.99635 ± 0.00445
22	21 × 21	75-5-28	59.05	0.99576	0.99634 ± 0.00411
24	22 × 22	74-6- 6	51.74	0.99512	0.99219 ± 0.00404
28	24 × 24	75-5-28	45.62	0.99493	0.99931 ± 0.00421
Average K_{eff}				0.99504	0.99520 ± 0.00417
Lattice Name 5.55 Pu					
22	21 × 21	72-4-28	62.05	0.99532	0.99246 ± 0.00374
23	21 × 22	72-4-26	58.73	0.99494	0.98709 ± 0.00388
23	21 × 22	73-6- 6	61.10	0.99601	0.99709 ± 0.00368
24	22 × 22	73-6- 6	58.08	0.99593	0.99620 ± 0.00391
Average K_{eff}				0.99555	0.99321 ± 0.00380
Average K_{eff} of PuO_2 System				0.99430	0.99412

Table E.10 JMTR-Description of Design Parameters Used in Demonstration Calculations

Reactor Design Description

Reactor Type	Tank-Type MTR
Steady-State Power Level	50 MW
Number of Standard Fuel Element	27
Irradiation Channels	8 at Core Center
Core Geometry	5 × 7 Arrangement
Grid Plate	12 × 12
^{235}U Content/Core	7657 g (Case 1) 8632 g (Case 2)
Active Core Volume	116 ℓ
Average Volumetric Power Density	43.1 KW/ℓ
Specific Power	6637 KW/kg ^{235}U (Case 1) 5888 KW/kg ^{235}U (Case 2)
Moderator, Coolant	Water
Reflector	Beryllium and Aluminium on All Four Sides

Fuel Element Design Description

Type	MTR, Straight Plates
Uranium Enrichment	93% (Case 1) 45% (Case 2)
Lattice Pitch	77.2 × 77.2 mm
Fuel Element Dimensions	76.2 × 76.2 × 750 mm
Plate Thickness	1.27 mm
Water Channel Thickness	2.604 mm
Plate/Standard Fuel Element	19
Fuel Meat	U-Aℓ Alloy (21.5 wt·%U) (Case 1) U-Aℓ Alloy (40 wt·%U) (Case 2)
Meat Dimensions	0.51 × 59.5 × 750 mm
Clad Thickness (Aℓ)	0.38 mm
^{235}U Density in Fuel Meat	0.6414 g/cm^3 (Case 1) 1.1933 g/cm^3 (Case 2)
^{235}U/Standard Fuel Element	283.6 g (Case 1) 319.7 g (Case 2)
Coolant Flow Rate	6000 m^3/h
Core Inlet Temperature	47 °C
Burnup Status of Core	Equilibrium Core

Table E.11 Atomic Number Density in Fresh Core

Material			Atomic Number Density ($\times 10^{-24}$ cm^{-3})	
1	Fuel Element		93 %	45 %
	Fuel :	U-235	0.001681	0.001895
		U-238	0.0001884	0.002287
		Aℓ	0.05698	0.05502
	Clad :	Aℓ	0.060299	0.060299
	H_2O	O	0.032973	0.032973
		H	0.065946	0.065946
	Extra :	Aℓ	0.03534	0.03534
		O	0.01365	0.01365
		H	0.02729	0.02729
2	Beryllium Reflector			
		Be	0.1118	0.1118
		O	0.002979	0.002979
		H	0.005957	0.005957
3	Aluminium Reflector (1)			
		Aℓ	0.05221	0.05221
		O	0.004421	0.004421
		H	0.008842	0.008842
4	Aluminium Reflector (2)			
		Aℓ	0.05637	0.05637
		O	0.002149	0.002149
		H	0.004298	0.004298
5	Zirconium Gamma Ray Shielding Plate			
		Zr	0.03636	0.03636
		O	0.004781	0.004781
		H	0.009562	0.009562
6	H_2O			
		O	0.03297	0.03297
		H	0.06595	0.06595

Table E.12-1 Axial distribution of nuclide number densities in a NO.7 channel of JMTR

****
AFTER STEP 3 TOTAL TIME 21.000 DAYS BURN-UP 262.50 MWD
****

NUCLIDE NUMBER DENSITIES FOR EACH BURN-UP BLOCK

*** CHANNEL 7 ***

	BURN-UP BLOCK				
NUCLIDE	1	2	3	4	5
	11	12			
U-235	1.6538E-04	1.5644E-04	1.4972E-04	1.4524E-04	1.4305E-04
	1.6407E-04	1.7079E-04			
U-236	2.9196E-06	4.3542E-06	5.4270E-06	6.1392E-06	6.4865E-06
	3.1293E-06	2.0426E-06			
U-238	2.1983E-04	2.1911E-04	2.1855E-04	2.1817E-04	2.1798E-04
	2.1973E-04	2.2027E-04			
PU-239	1.2421E-06	1.7782E-06	2.1555E-06	2.3925E-06	2.5039E-06
	1.3190E-06	8.8726E-07			
PU-240	3.8604E-08	8.3024E-08	1.2607E-07	1.5861E-07	1.7567E-07
	4.3964E-08	1.9188E-08			
PU-241	3.3039E-09	1.0630E-08	2.0227E-08	2.8891E-08	3.3856E-08
	4.0248E-09	1.1440E-09			
PU-242	5.0430E-11	2.5505E-10	6.2987E-10	1.0454E-09	1.3122E-09
	6.6329E-11	1.1846E-11			
F.P.	1.5105E-05	2.2682E-05	2.8405E-05	3.2235E-05	3.4111E-05
	1.6214E-05	1.0530E-05			
XE-135	1.7832E-09	1.7411E-09	1.6913E-09	1.6537E-09	1.6343E-09
	1.7801E-09	1.7747E-09			
SM-149	1.8886E-08	1.7963E-08	1.7274E-08	1.6815E-08	1.6588E-08
	1.8745E-08	1.9437E-08			

NUCLIDE	6	7	8	9	10
U-235	1.4318E-04	1.4551E-04	1.4887E-04	1.5310E-04	1.5817E-04
U-236	6.4647E-06	6.0974E-06	5.5643E-06	4.8899E-06	4.0775E-06
U-238	2.1799E-04	2.1819E-04	2.1847E-04	2.1883E-04	2.1925E-04
PU-239	2.4976E-06	2.3846E-06	2.2080E-06	1.9747E-06	1.6791E-06
PU-240	1.7460E-07	1.5677E-07	1.3212E-07	1.0351E-07	7.3195E-08
PU-241	3.3540E-08	2.8419E-08	2.1814E-08	1.4968E-08	8.7775E-09
PU-242	1.2945E-09	1.0188E-09	6.9888E-10	4.1068E-10	1.9499E-10
F.P.	3.3993E-05	3.2001E-05	2.9133E-05	2.5525E-05	2.1212E-05
XE-135	1.6356E-09	1.6565E-09	1.6850E-09	1.7183E-09	1.7526E-09
SM-149	1.6603E-08	1.6848E-08	1.7195E-08	1.7630E-08	1.8145E-08

Table E.12-2 Three dimensional power distribution in JMTR

*** JMTR 93 ENRICHMENT 50 MW 3 STEP BURN-UP CALCULATION ***

BURN-UP BLOCK RELATIVE POWER

	CHANNEL				
BURN-UP BLOCK	1	2	3	4	5
1	8.1371E-01	7.4150E-01	5.9362E-01	7.8061E-01	4.9701E-01
2	1.2086E+00	1.1175E+00	8.9902E-01	1.1734E+00	7.5816E-01
3	1.4883E+00	1.4032E+00	1.1255E+00	1.4711E+00	9.5186E-01
4	1.6603E+00	1.5894E+00	1.2688E+00	1.6655E+00	1.0741E+00
5	1.7692E+00	1.6584E+00	1.3330E+00	1.7413E+00	1.1295E+00
6	1.7902E+00	1.6012E+00	1.3157E+00	1.6890E+00	1.1159E+00
7	3.5633E-26	1.3993E+00	1.2283E+00	1.4862E+00	1.0403E+00
8	2.8628E-26	1.2300E+00	1.1073E+00	1.3148E+00	9.3910E-01
9	2.2414E-26	1.0636E+00	9.6444E-01	1.1413E+00	8.1953E-01
10	1.6166E-26	8.9440E-01	8.0238E-01	9.5941E-01	6.8329E-01
11	1.0392E-26	6.9050E-01	6.1169E-01	7.4110E-01	5.2110E-01
12	5.4347E-27	4.4995E-01	3.9374E-01	4.8429E-01	3.3366E-01

BURN-UP BLOCK	6	7	8	9	10
1	7.3974E-01	6.2887E-01	6.7262E-01	6.0073E-01	4.7009E-01
2	1.1080E+00	9.4600E-01	1.0173E+00	9.0982E-01	7.2341E-01
3	1.3834E+00	1.1836E+00	1.2738E+00	1.1406E+00	9.1076E-01
4	1.5634E+00	1.3383E+00	1.4387E+00	1.2898E+00	1.0272E+00
5	1.6514E+00	1.4140E+00	1.5272E+00	1.3698E+00	1.0897E+00
6	1.6460E+00	1.4084E+00	1.5372E+00	1.3789E+00	1.0952E+00
7	1.5561E+00	1.3260E+00	1.4741E+00	1.3228E+00	1.0475E+00
8	1.4213E+00	1.2091E+00	1.3605E+00	1.2201E+00	9.6400E-01
9	1.2494E+00	1.0620E+00	1.2033E+00	1.0782E+00	8.5107E-01
10	1.0425E+00	8.8605E-01	1.0083E+00	9.0216E-01	7.1340E-01
11	7.9937E-01	6.7874E-01	7.7248E-01	6.9047E-01	5.4436E-01
12	5.2100E-01	4.4139E-01	4.9965E-01	4.4617E-01	3.4662E-01

Table E.12-3 Axial distribution of uranium and pultonium quantities in a NO.7 channel of JMTR

*** JMTR 93 ENRICHMENT 50 MW 3 STEP BURN-UP CALCULATION ***

CHANNEL NO. 7

TOTAL

9.082E-03	-----	BURN-UP	(MWD/CC)
2.679E+02	-----	U-235	(GRAM)
6.630E+02	-----	U-TOTAL	(GRAM)
3.626E+00	-----	PU-TOTAL	(GRAM)

BLOCK 1	BLOCK 2	BLOCK 3	BLOCK 4	BLOCK 5	BLOCK 6
5.384E-03	8.158E-03	1.029E-02	1.174E-02	1.245E-02	1.240E-02
2.404E+01	2.274E+01	2.176E+01	2.111E+01	2.079E+01	2.081E+01
5.682E+01	5.563E+01	5.473E+01	5.412E+01	5.383E+01	5.384E+01
1.898E-01	2.768E-01	3.405E-01	3.817E-01	4.015E-01	4.003E-01

BLOCK 7	BLOCK 8	BLOCK 9	BLOCK 10	BLOCK 11	BLOCK 12
1.165E-02	1.056E-02	9.213E-03	7.616E-03	5.786E-03	3.733E-03
2.115E+01	2.164E+01	2.225E+01	2.299E+01	2.385E+01	2.482E+01
5.416E+01	5.461E+01	5.518E+01	5.586E+01	5.665E+01	5.755E+01
3.801E-01	3.494E-01	3.096E-01	2.604E-01	2.021E-01	1.342E-01

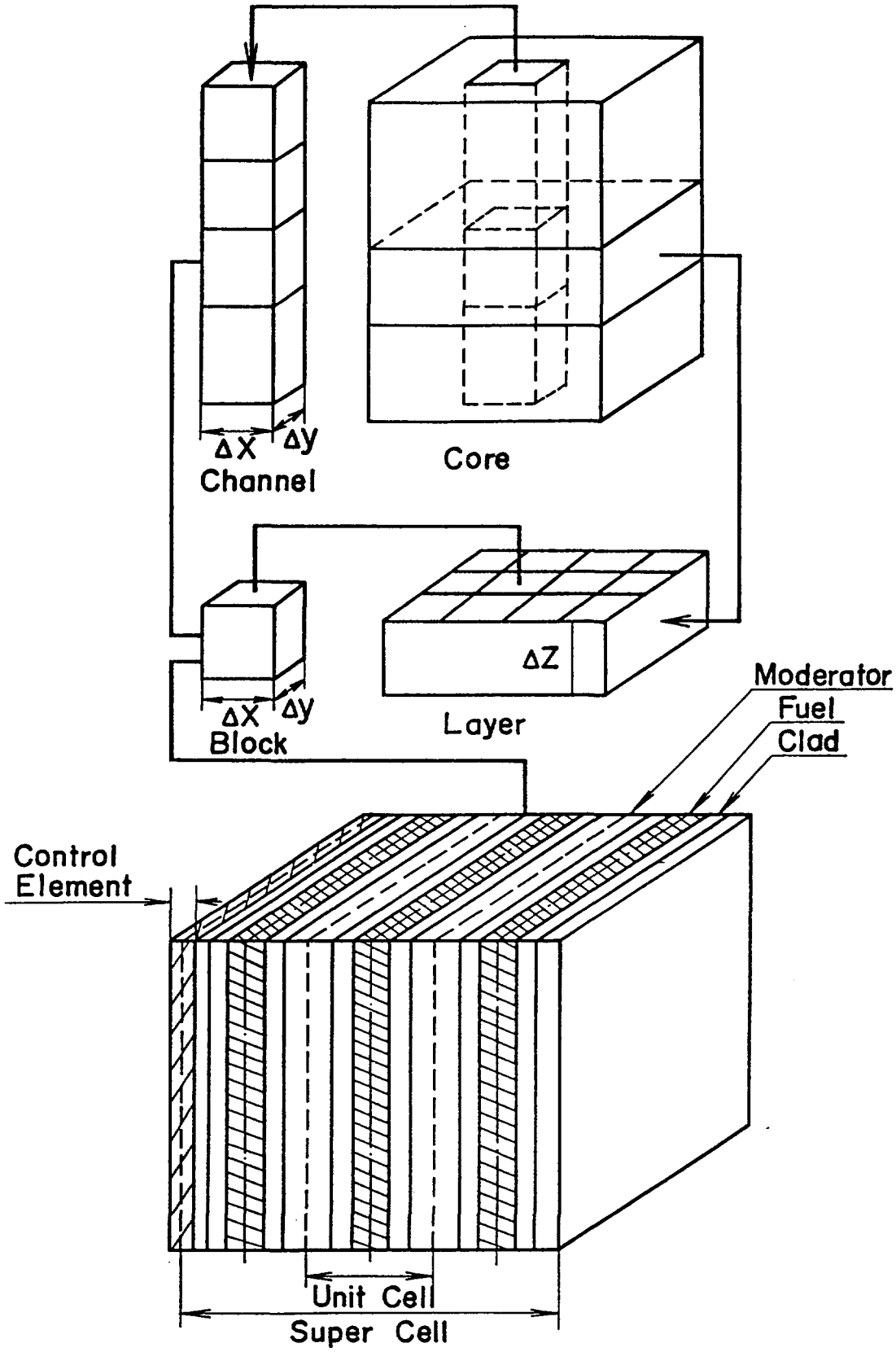

Fig.E.1 Configuration of channels, layers, block and super cell

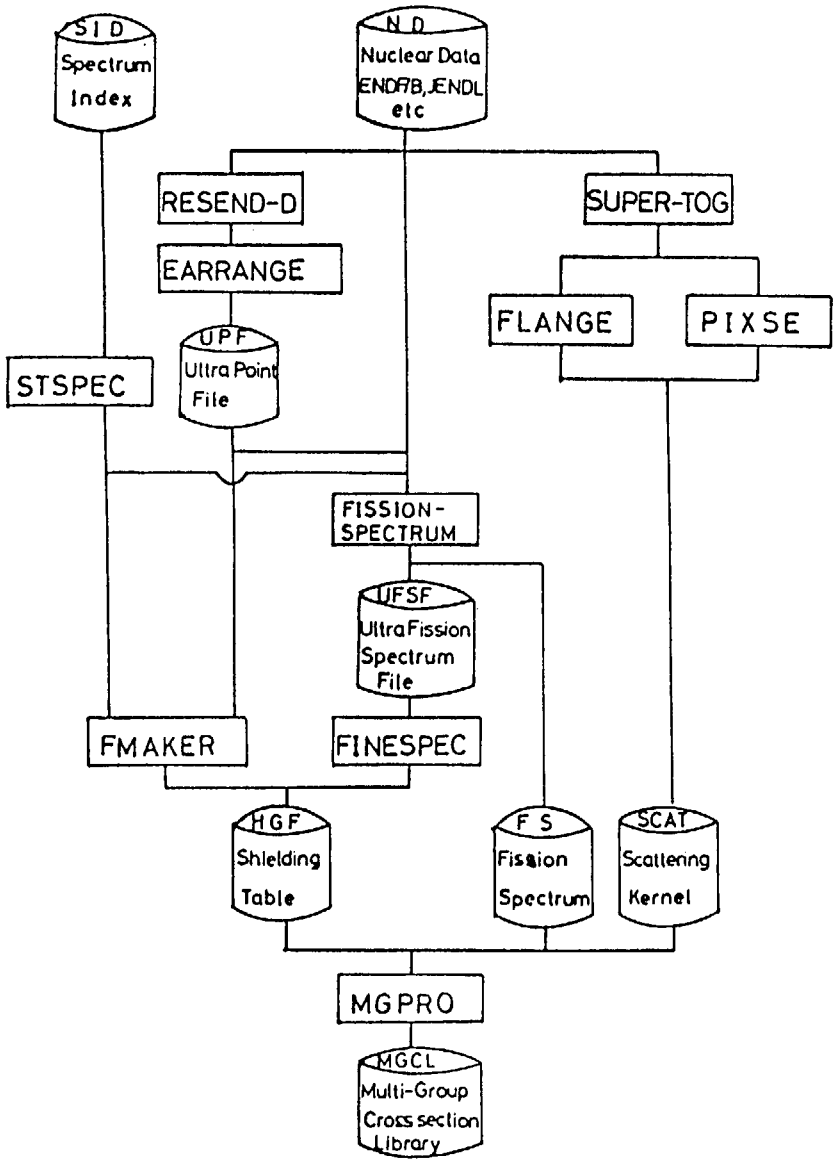

Fig. E.2 Flow diagram for MGCL

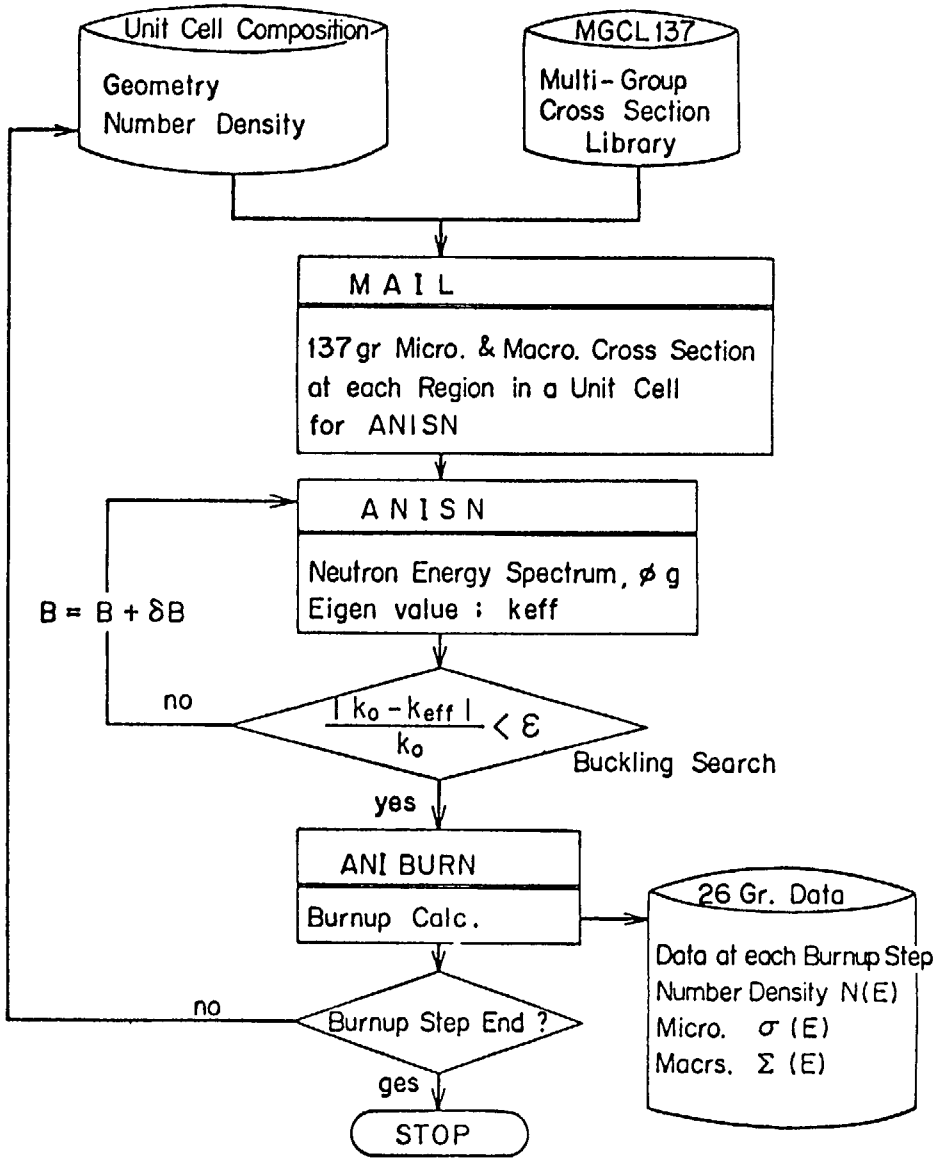

Fig. E.3 Flow diagram for unit cell calculation

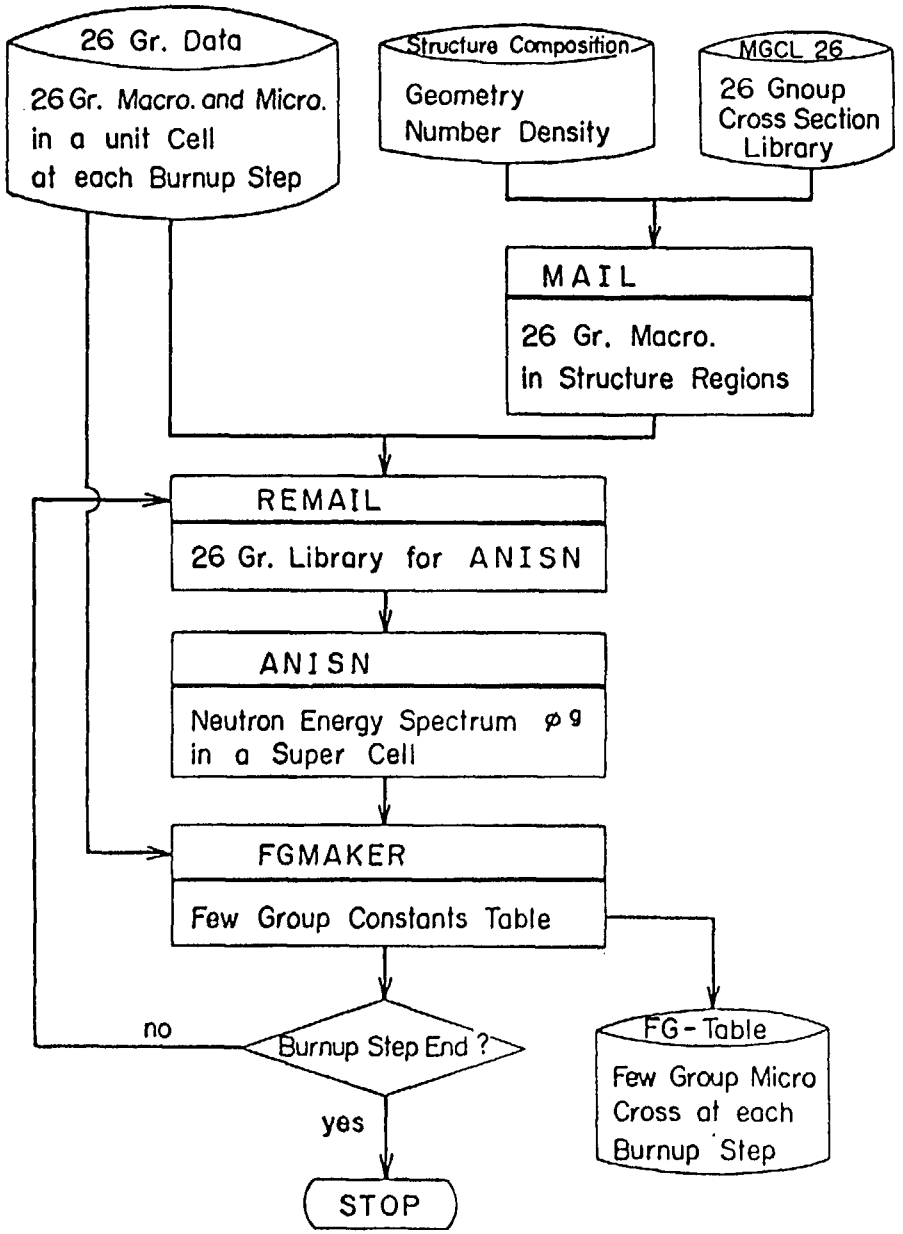

Fig. E.4 Flow diagram for super cell calculation

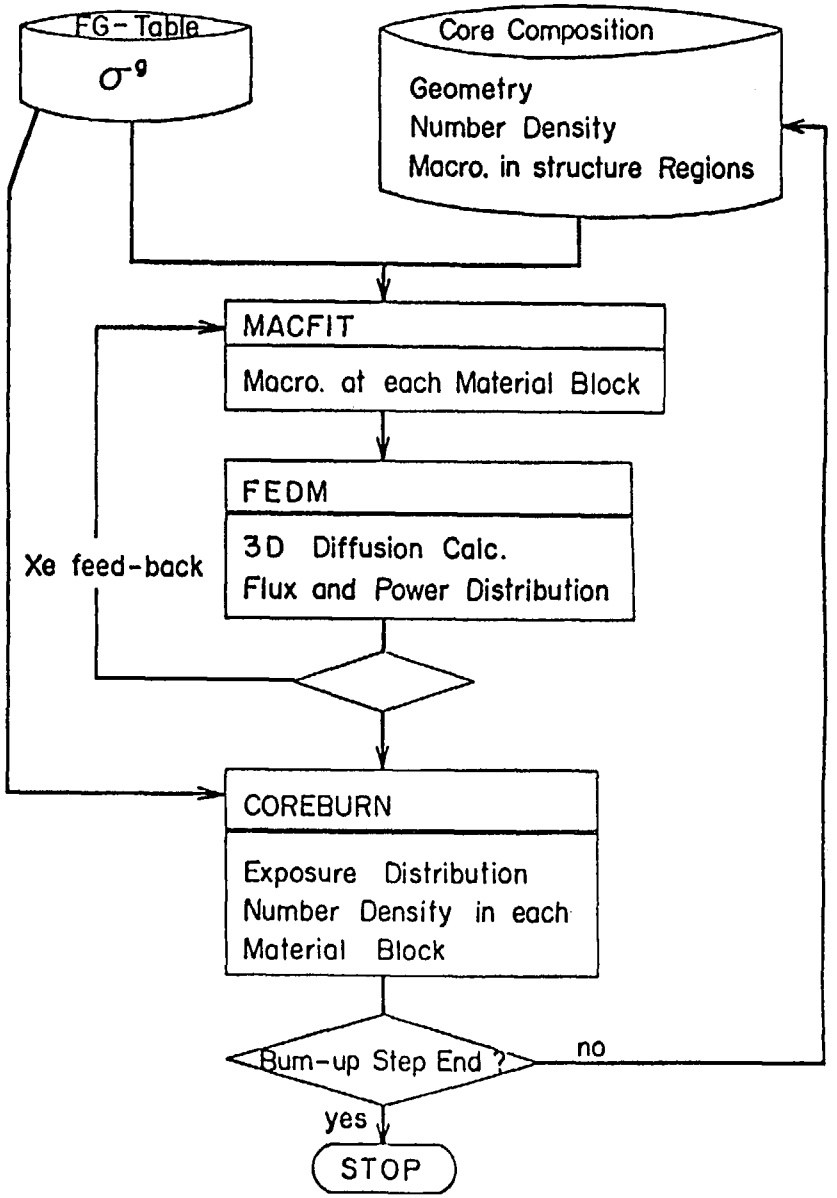

Fig. E.5 Flow diagram for whole core calculation

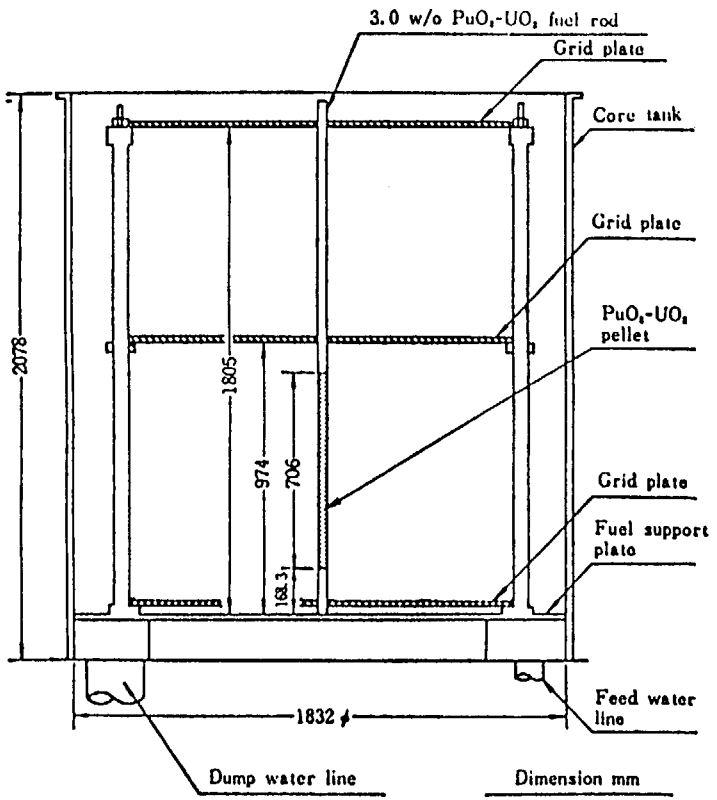

Fig. E.6 Vertical cross-sectional view of core

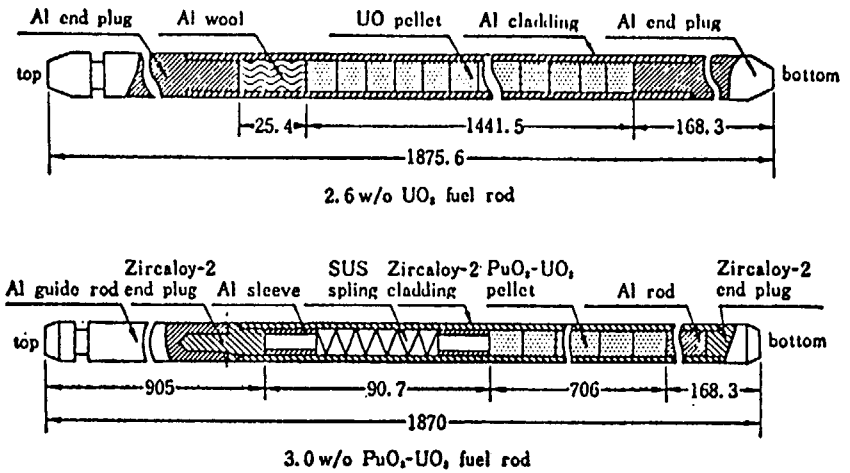

Fig. E.7 2.6w/o UO_2 and 3.0w/o PuO_2-natural UO_2 fuel rods

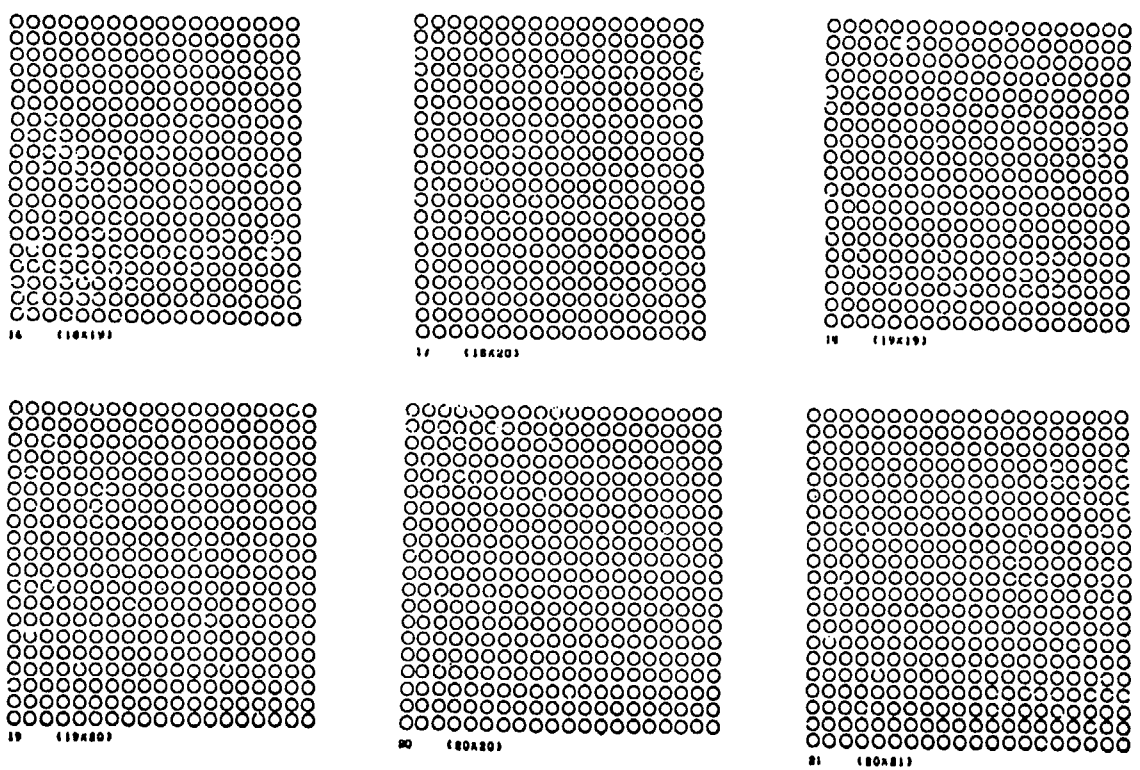

Fig. E.8 Patterns of lattice configurations

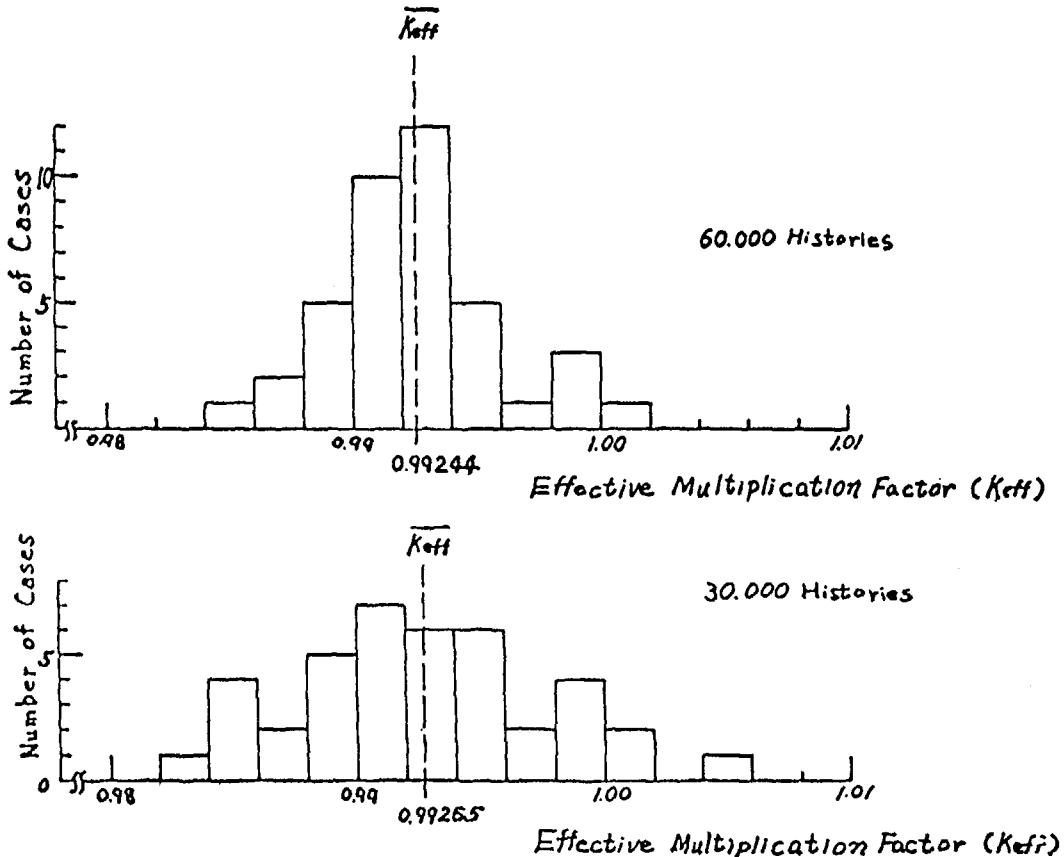

Fig. E.9 Histograms of the number of cases computed with 60000 and 30000 histories in UO_2 system

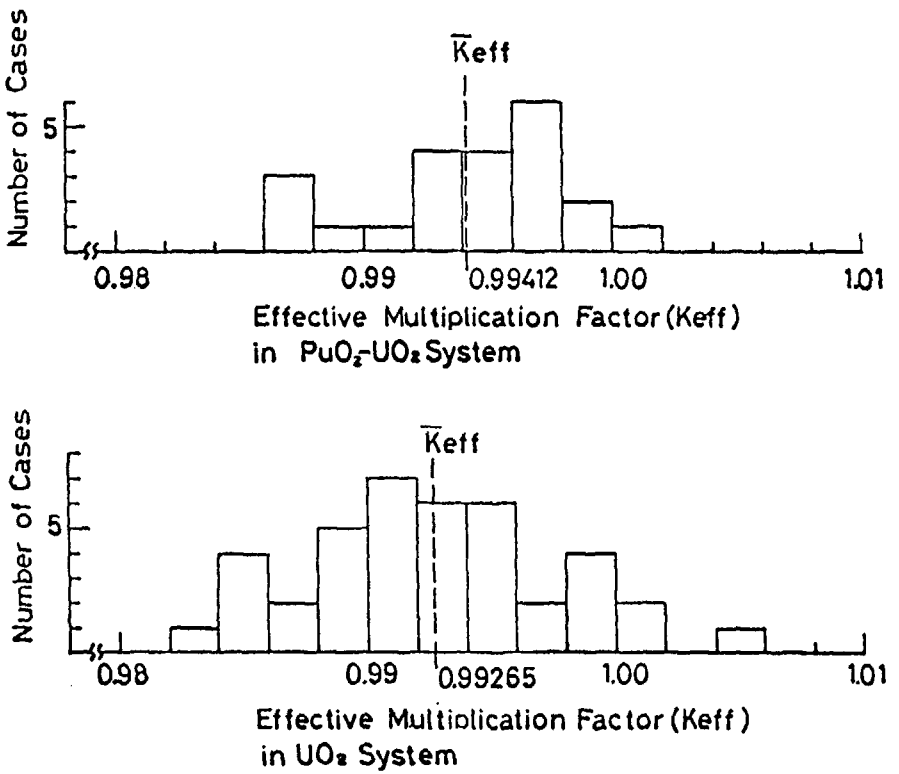

Fig. E.10 Histograms of the number of cases in PuO_2-UO_2 systems

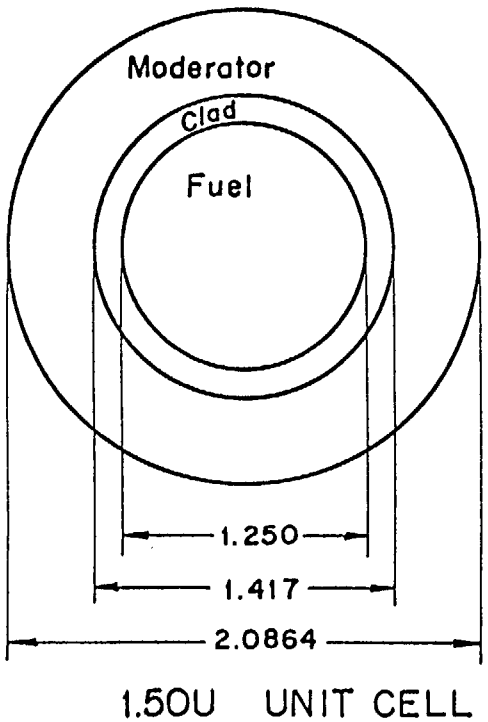

Fig. E.11 1.50U unit cell of TCA
(all dimension in Cm)

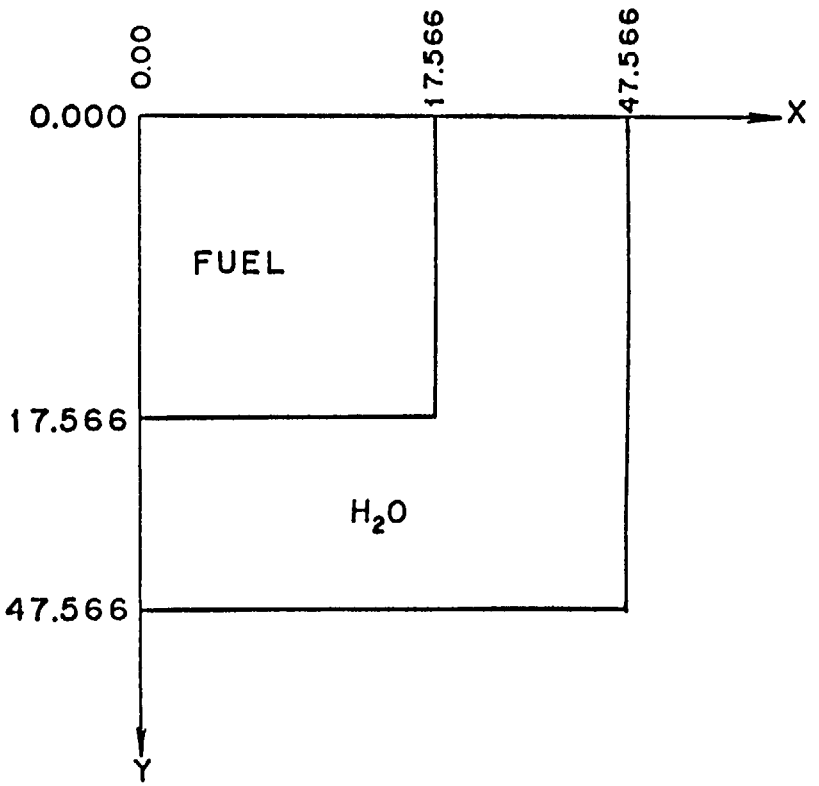

Fig. E.12 X-Y model on TCA for two-dimensional calculation
(all dimension in Cm)

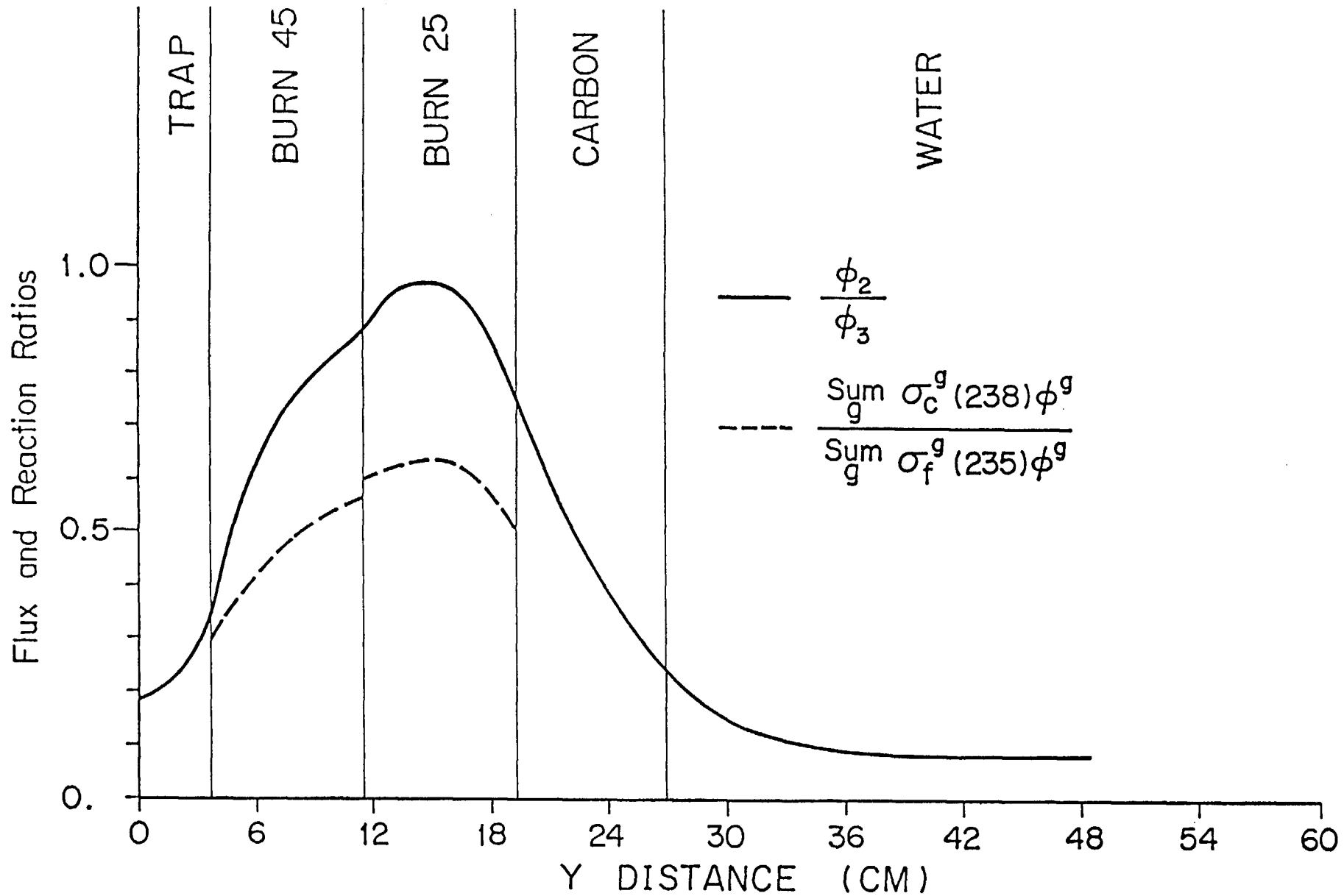

Fig. E.13 ^{238}U capture to ^{235}U fission ratio and thermal to epi-thermal flux ratio IAEA 10 MW Benchmark 93 % U-235 BOL

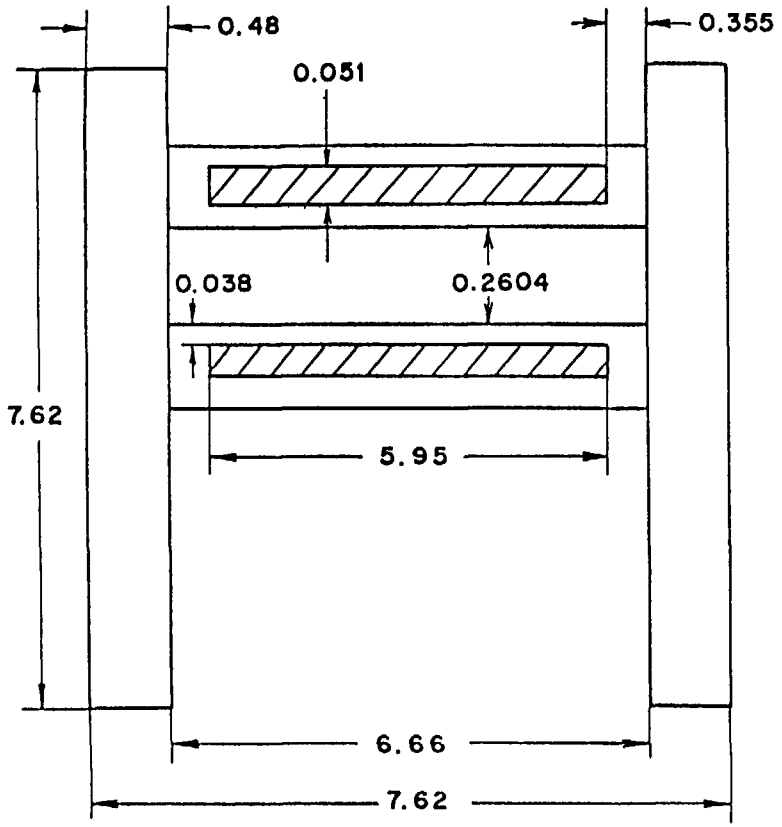

(all dimension in Cm)

Including a 0.5 mm water channel surrounding each element

Volume Fractions

Fuel	Meat	0.0967
Al		0.2844
H_2O		0.6189

Fig. E.14 JMTR-standard fuel element

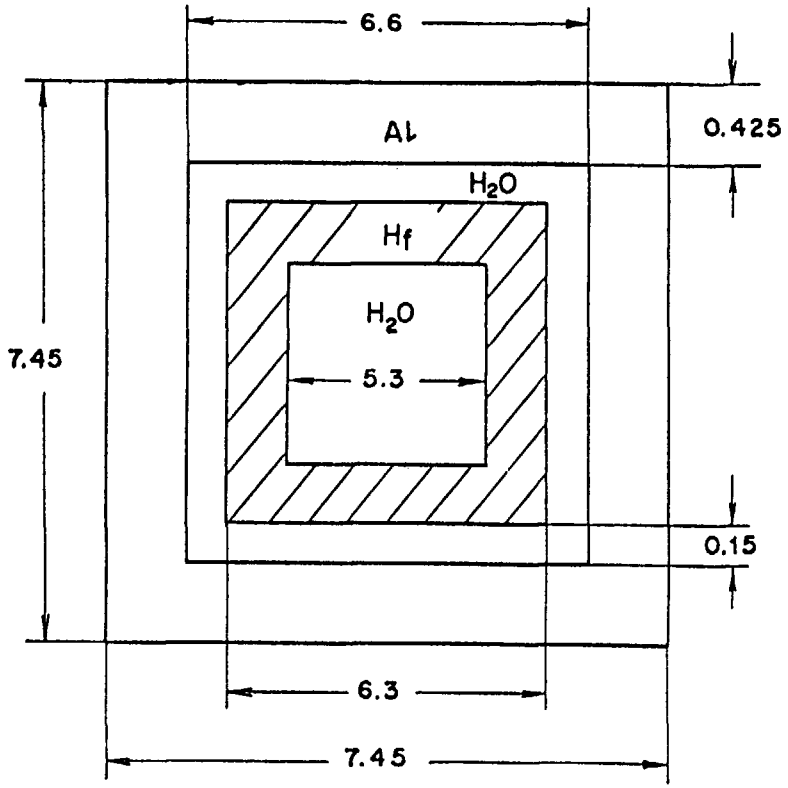

(all dimension in Cm)

Including a 1.35mm water channel surrounding element

Volume Fraction

H_f	0.1946
Al	0.2004
H_2O	0.6050

Fig. E.15 JMTR-control element

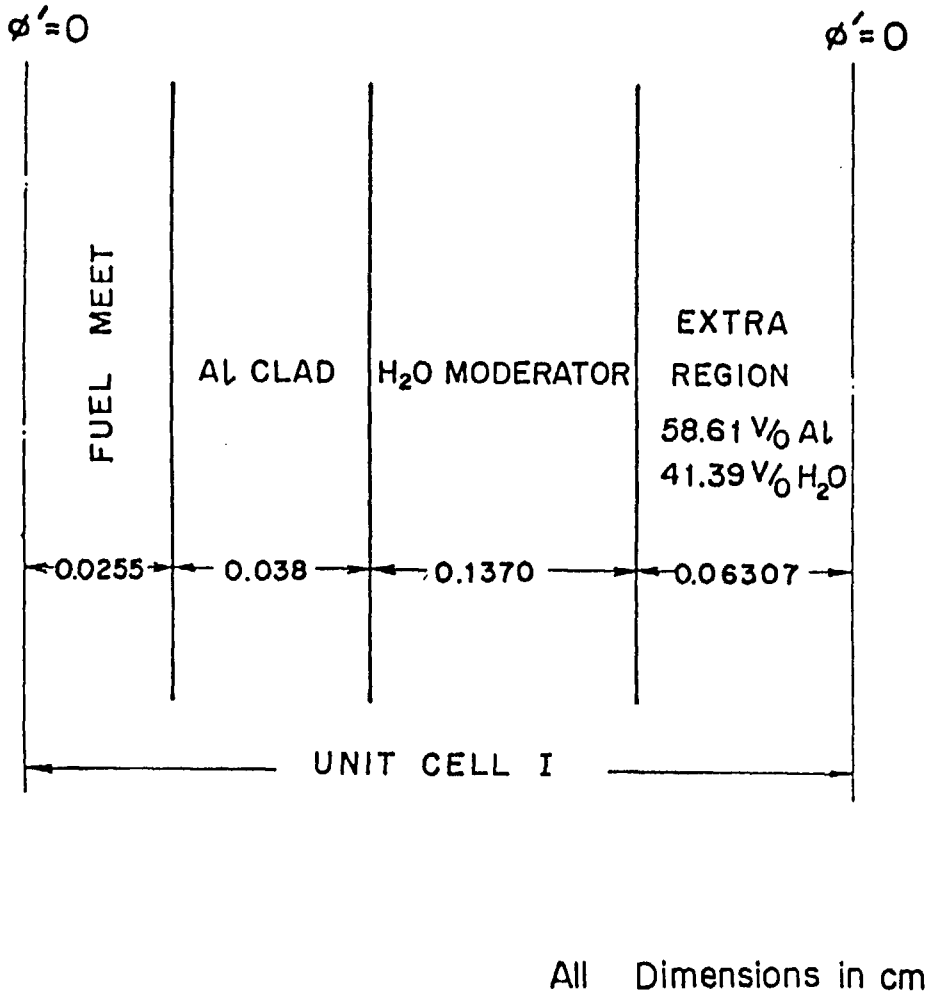

Fig. E.16 Slab geometry of unit cell I (fuel element)

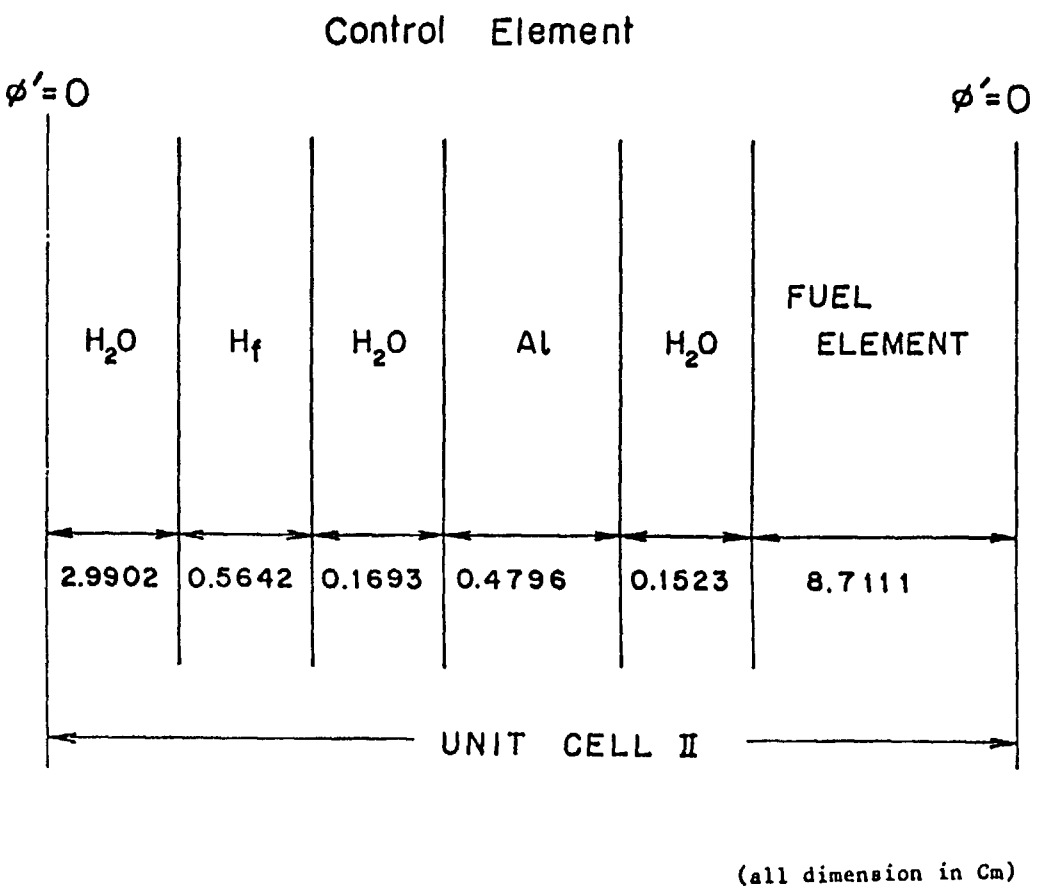

Fig. E.17 Slab geometry of unit cell II (control element)

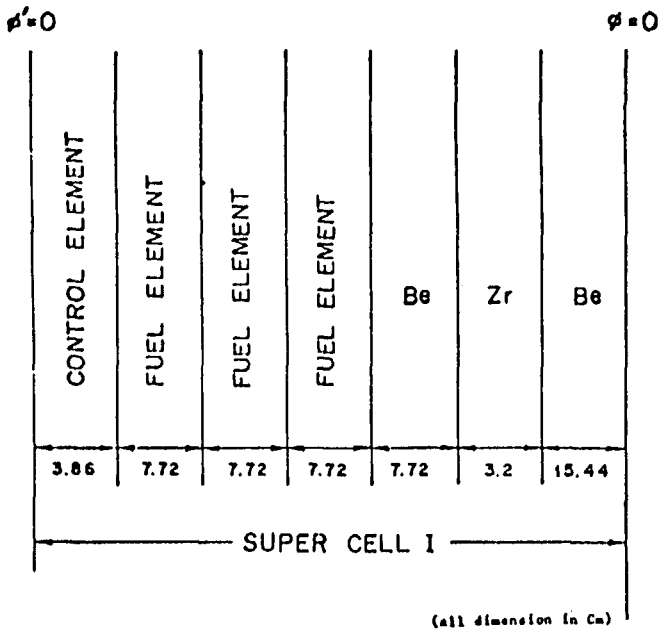

Fig. E.18 Slab geometry of super cell I

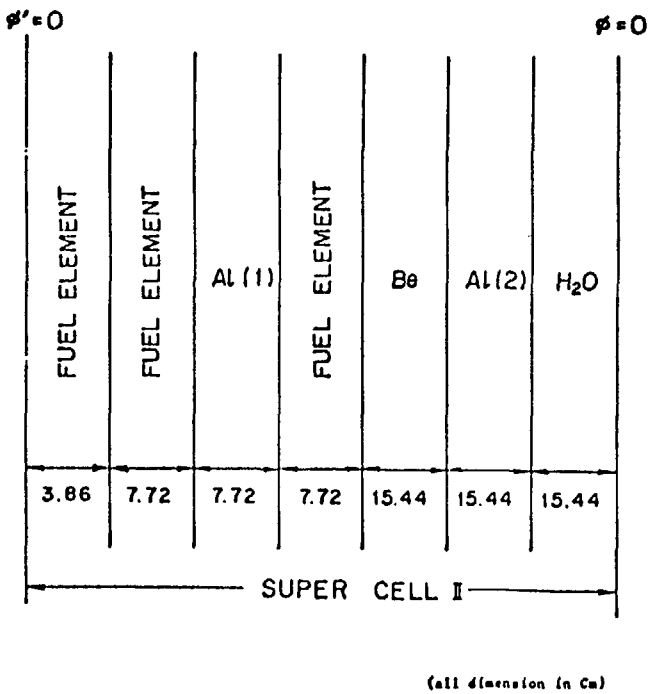

Fig. E.19 Slab geometry of super cell II

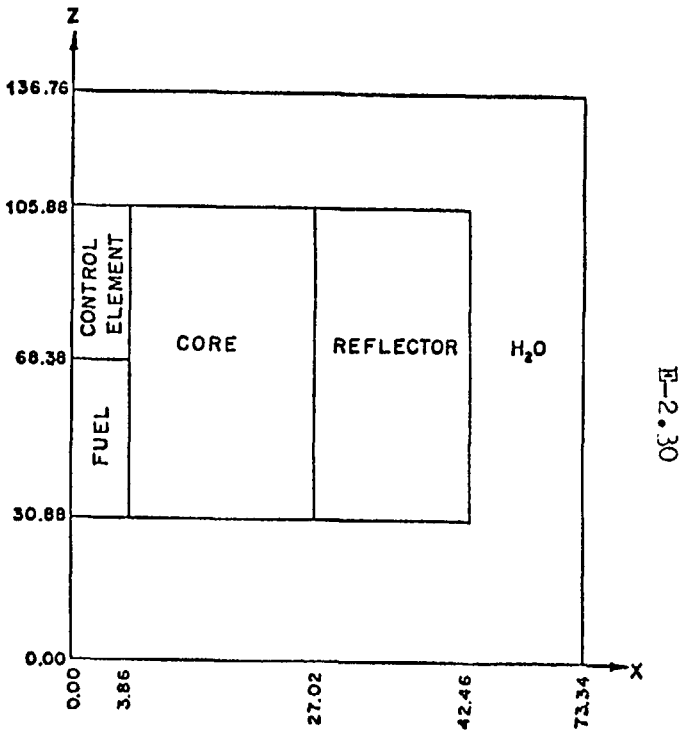

Fig. E.20 X-Z model on JMTR

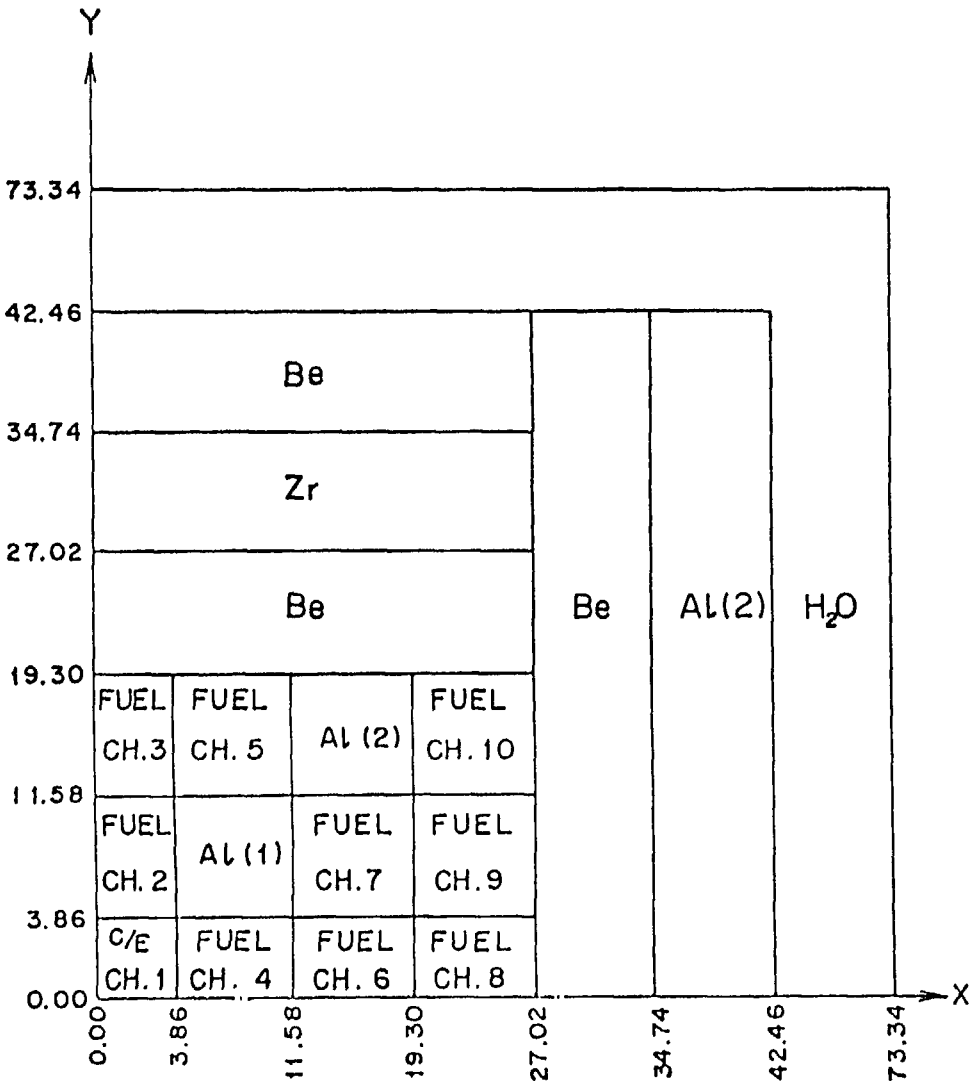

C/E — Control Element
FUEL — Fuel Element
Al(1) Al(2) - Aluminium
Be — Beryllium
Zr — Zriconium

Fig. E.21 X-Y model on JMTR

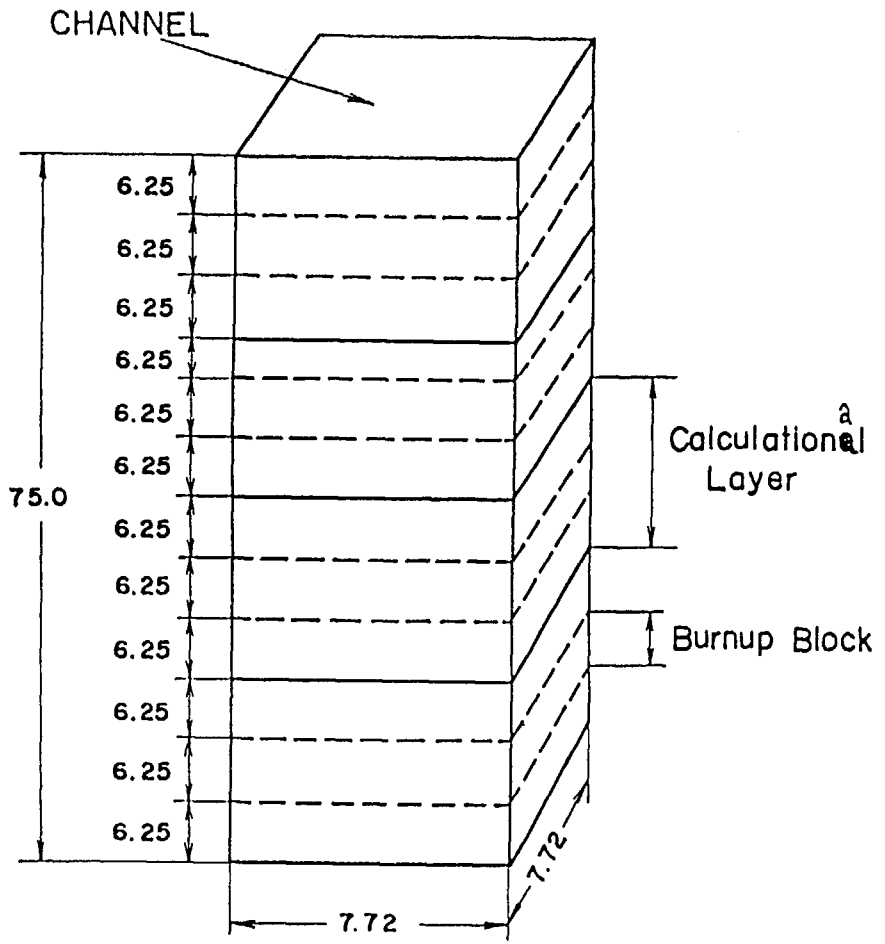

(all dimension in Cm)

Fig. E.22 Mesh specification of a channel for three-dimensional burn-up calculation

APPENDIX F

Benchmark Calculations

F-0 Specifications

The benchmark calculations were performed by the following organizations:

F-1 ANL (USA)

F-2 INTERATOM (FRG)

F-3 EIR (Switzerland)

F-4 ÖSGAE (Austria)

F-5 CEA (France)

F-6 JAERI (Japan)

F-7 CNEA (Argentina)

ABSTRACT

Benchmark calculations were performed to compare the computational methods of various organizations. The methods and results of neutronics calculations for the specified core are described in Appendices F-1 to F-7. Only limited conclusions for actual core conversions from HEU fuel to LEU fuel should be drawn from these results.

APPENDIX F-O

Specifications

Aims: Comparison of the different calculation methods and cross-section data sets used in different laboratories, limited conclusions for real conversion problems.

Table 1 Specifications for the Methodical Benchmark-Problem

Data and Specifications Agreed Upon:

Active Core Height 600 mm
Extrapolation Length 80 mm (in 80 mm distance from the core, the cosine-shaped flux goes to zero)
X-Y Calculations only

Space at the grid plate per fuel element 77 mm x 81 mm

Fuel element cross-section
76 mm x 80.5 mm including support plate
76 mm x 80.0 m without support plate

Meat dimensions
63 mm x 0.51 mm x 600 mm

Aluminum-canning with $\rho_{Al} = 2.7\ g \cdot cm^{-3}$

Thickness of support plate 4.75 mm; $\rho_{Al} = 2.7\ g \cdot cm^{-3}$

Number of fuel plates per fuel element:
23 identical plates, each 1.27 mm thick

Number of fuel plates per control element:
17 identical plates, each 1.27 mm thick

Identification of the remaining plate positions of the control element:
4 plates of pure aluminum $\rho_{Al} = 1.7\ g \cdot cm^{-3}$, each 1.27 mm thick in the position of the first, the third, the twenty-first, and the twenty-third standard plate position; water gaps between the two sets of aluminum plates.

Specifications of the different fuels (UAl_x-Al Fuel) for HEU, MEU, LEU corresponding to the previous definitions:

HEU:
- Enrichment 93 w/o (weight %) U-235
- 280 g U-235 per fuel element, which corresponds to 12.174 g U-235 per each fuel plate
- 21 w/o of uranium in the UAl_x-Al
- only U-235 and U-238 in the fresh fuel

MEU:
- Enrichment 45 w/o U-235
- 320 g U-235 per fuel element (23 plates)
- 40 w/o of uranium in the UAl_x-Al
- only U-235 and U-238 in the fresh fuel

LEU:
- Enrichment 20 w/o U-235
- 390 g U-235 per fuel element (23 plates)
- 72 w/o of uranium in the UAl_x-Al
- only U-235 and U-238 in the fresh fuel

Total power: 10 MW_{th} (power buildup by 3.1×10^{10} fission/Joule)

Thermal hydraulic data:
Water temperature 20°C
Fuel temperature 20°C
Pressure at core height 1.7 bar

Xenon-State:
Homogeneous Xenon content corresponding to average-power-density

Results

k_{eff}; fluxes and flux ratios along the two symmetry-axes of the core in three groups and for begin of cycle (BOL) and end of cycle (EOL), respectively.

$\phi_{thermal}$ with $0\ eV < E_n < 0.625\ eV$

$\phi_{epithermal}$ with $0.625\ eV < E_n < 5.531\ keV$

ϕ_{fast} with $E_n > 5.531\ keV$

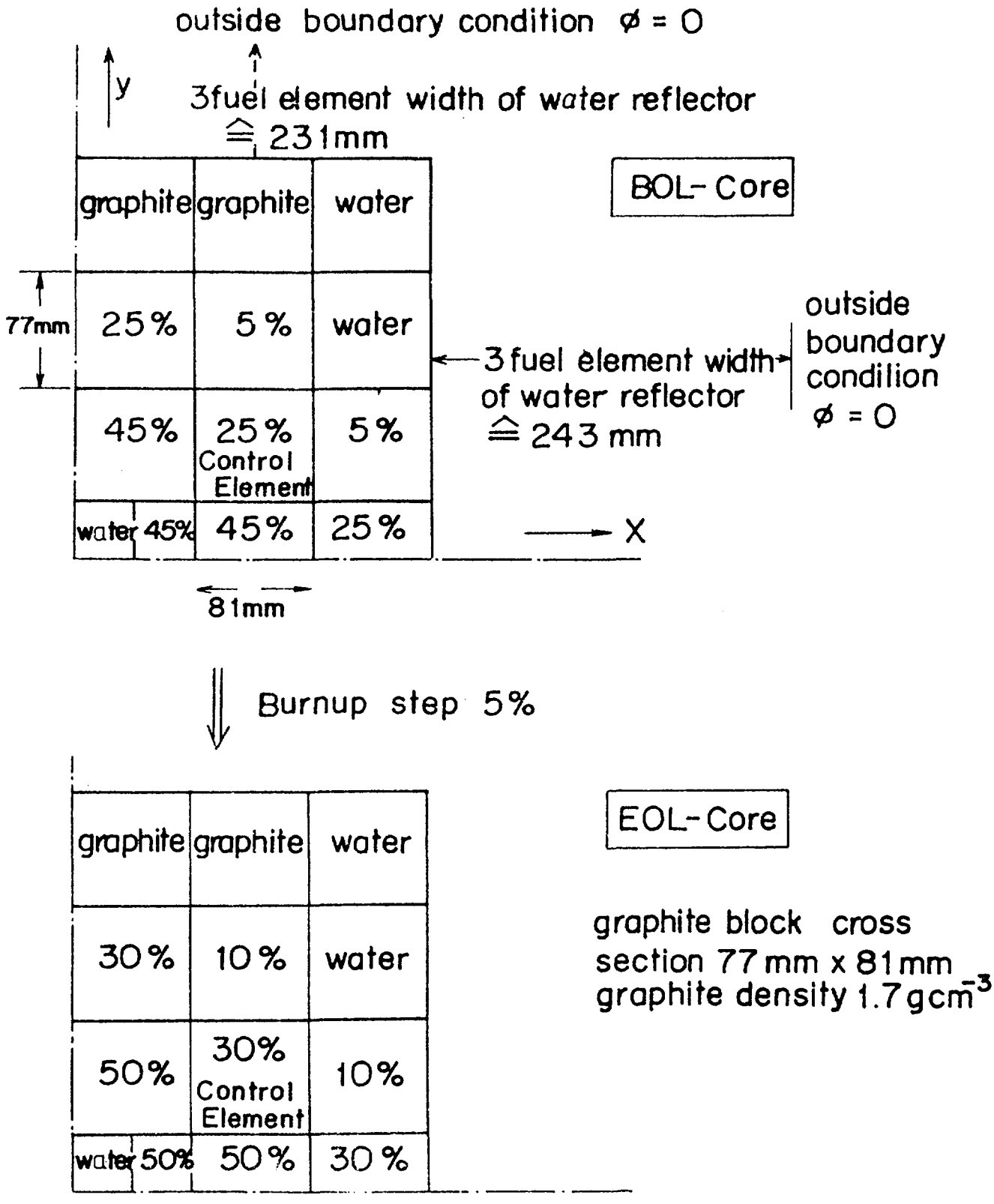

Burnup definition : (%) means the percentage of loss of the number of U 235 - Atoms

METHODICAL BENCHMARK
10 MW CASE
CORE CROSS SECTION

Fig. 1

APPENDIX F-1

Benchmark Calculations

Performed by the

Reduced EnrichmentResearch and Test Reactor

(RERTR) Program

Argonne National Laboratory

Argonne, Illinois 60439

U.S.A.

CALCULATIONS FOR THE BENCHMARK MTR-TYPE REACTORS WITH HIGH, MEDIUM AND LOW ENRICHMENTS

Introduction

In order to compare reactor physics calculational methods used in various research centers, benchmark problems were specified at the Consultants Meeting on "Preparation of a Programme on Research Reactor Core Conversions to Use LEU instead of HEU", IAEA, June 19-22, 1979 in Vienna, Austria.

Detailed specifications of these benchmarks are included in the App. I-0. Briefly, they correspond to a 10 MW, 6 x 5 element core in several stages of burnup. The core is reflected by graphite on two sides and surrounded by water. Uranium enrichments of 93%, 45%, and 20% are considered in standard MTR elements with 23 fuel plates containing 280, 320, and 390 grams U, respectively.

The models and results of both two-dimensional diffusion calculations are detailed, three-dimensional Monte Carlo calculations are described and compared.

1. DIFFUSION THEORY CALCULATIONS

1.1 Cross Section and Burnup Calculations

The EPRI-CELL code was used to generate the cross sections as a function of burnup. The code is esentially a combination of GAM-I for the non-thermal cross sections, THERMOS for the thermal cross sections, and CINDER for burnup. Modifications made at Argonne in the code as received from EPRI include the addition of an infinite slab cell capability, and the addition of ENDF/B-IV data to the library for the important reactor isotopes.

The fuel element and unit cell used in the calculations are shown in Figs. 1 and 2. The region marked XTRA includes the aluminum in the plates beyond the width of the meat, the aluminum side plates, the water beyond the width of the meat, and the water channels surrounding the fuel element. The buckling input to EPRI-CELL was 7.8367×10^{-3} cm^{-2}, and was derived as the geometric buckling of a cylinder of height 60 cm and radius 22.72 cm with reflector savings of 8 cm added to the top, bottom and radius of the reactor. The 22.72 cm radius corresponds to the same area as the fuelled region plus the central flux trap. The Dancoff factor used in EPRI-CELL in calculating an effective $_p$ for table-look-up in the resonance tables was input as $C = 2E_3(\cdot t) = 0.5349$ where $\cdot t$ is the potential scattering cross section times the thickness for the combination of clad, H_2O and XTRA regions. Also, fine group shielding factors over the resonance region were input to EPRI-CELL for the resonance materials. These were calculated for the unit cell of the EPRI-CELL calculations using integral transport theory over the resonance region with the MC^2-2 code and ENDF/B-IV data, and used in a scheme designed to improve the resonance cross sections determined in the EPRI-CELL code by table look-up. The importance of these shielding factors is mainly for ^{238}U. They make little difference in the 93% enriched case, since little ^{238}U is present, but in the 20% enriched case, the k is increased by about 0.004 when the shielding factors are included.

Cross sections were generated for the 93%, 45%, and 20% enrichment cases for ^{235}U burnup in 5% increments from 0 to 50% using a five-group structure with the energy boundaries shown in Table 1. The input power rating used for depletion of the ^{235}U was that of the average plate in the core.

Atom densities in the fuel meat for the EPRI-CELL calculations for the 93%, 45%, and 20% enriched fuel elements with various stages of burnup are shown in Tables 2, 3, and 4, respectively.Separate calculations were not done for the control fuel element since most of the fuel plates have nearly the same environment, whether in the standard or control elements. In Tables 2-4 the notations F.P.E. and F.P.T. refer to the epithermal and thermal lumped fission products (i.e., those other than ^{135}Xe and ^{149}Sm).

Microscopic cross sections are presented in a three group structure in Tables 5 - 7 for all three enrichments as a function of ^{235}U percent burnup for ^{235}U, ^{238}U and the two lumped fission products. The first two groups consist of combinations of groups 1 and 2, and groups 3 and 4 of Table 1, while the third group is group 5 of Table 1. These are the three groups for which plots are requested in the benchmark specifications. The cross sections for the lumped fission products are presented in order to make the corresponding atom densities in Tables 2 - 4 meaningful. Tables 5 - 7 show the decrease in the cross sections in group 3 of the 3-group structure as the spectrum in the thermal range gets harder. The large decrease in the ^{238}U absorption cross section in group 2, which includes the resonance region, in going from 93% to 45% to 20% enrichment is readily apparent. Resonance shielding in ^{238}U becomes very important as the enrichment is decreased and the ^{238}U concentration is correspondingly increased.

The ^{135}Xe and ^{149}Sm concentrations as a function of burnup for the three enrichments are plotted in Figs. 3 and 4. In order to display the relative importance to the neutron economy of the ^{135}Xe and ^{149}Sm, and the epithermal and thermal lumped fission products, their relative absorption rates for the 93% and 20% enriched cases as a function of burnup are shown in Figs. 5 and 6, respectively. The ^{135}Xe and ^{149}Sm absorption rates are essentially constant as a function of burnup. However, the absorption rate of ^{135}Xe is about five times that of ^{149}Sm. Absorption in the lumped thermal fission products increases with burnup to a value comparable with that of ^{135}Xe near 50% burnup. Absorption in the lumped epithermal fission products exceeds that of ^{149}Sm for burnups greater than about 20%. Thus, the accuracy of the treatment of the lumped fission products in generating cross sections can have a significant effect on calculated reactivities.

Table 8 presents the k_∞ computed by EPRI-CELL as a function of ^{235}U burnup at the 5% intervals from 0 to 5% for all three fuel enrichments.

Separate calculations were also run to generate cross sections for the water reflector and the flux trap, and for the graphite reflector by using a ^{235}U fission source distribution in each material. The resulting diffusion coefficients and macroscopic absorption cross sections for water and graphite in the 5-group and 3-group structures are shown in Table 9.

1.2 Results - Reactor Calculations

Two-dimensional diffusion theory calculations in x-y geometry were performed with the Argonne code DIF2D[2] using the geometry for one-quarter of the reactor as shown in the diagram in the Appendix. A total of 51 mesh intervals in the x-direction and 56 in the y-direction was used. The fluxes were normalized to a power of 2.5 MW in the quarter core, with an axial half height of 30 cm and reflector savings on one end of 8 cm producing a chopped cosine axial distribution of fluxes and power. Values of k_{eff} obtained for the six specified benchmark cases, as well as some extra cases are presented in Table 10.

In Table 10 the cases with fresh fuel in all fuel regions and the cases with no lumped fission products (i.e., F.P.E. and F.P.T) were run primarily for comparison with Monte Carlo calculations to be reported in Section 2. Cases with 45% and 20% enrichments were also run using the same timesteps as for the 93% enrichment case. Thus, they represent the same total power generation in MWd as in the 93% case, but with smaller percent burnups of ^{235}U. That is, in each region of these DIF2D problems, fuel with the same burnup in MWD as the 93% enrichment case rather than the same percent burnup was used.

Table 11 presents some fluxes from the DIF2D problems. The core region in this table refers to all regions containing fuel. Average fluxes are averaged both over the x-y plane and over the axial direction which has a copped cosine distribution. The notation ϕ_1 refers to the flux from 5.531 keV to 10 MeV, ϕ_2 refers to the flux from 0.625 eV to 5.531 keV, ϕ_f refers to the flux above 0.625 eV, and ϕ_{th} refers to the flux below 0.625 eV.

Neutron inventories for the benchmark 93% EOL and 20% EOL cases are presented in Table 12. Here the absorptions and fissions in all the fuel-containing regions are lumped together by material. Normalization is such that absorption plus leakage from the reactor is unity.

Plots of the fluxes from some of the DIF2D calculations are given in Figs. 7 - 18. Figures 7 - 10 present the required plots in three groups along the x- and y-axes at BOL and EOL for 93% enrichment. Note that the midplane fluxes are plotted; i.e., there has been no axial averaging over a chopped cosine. Figures 11 - 14 show the ratios of the 45% and 93% enrichment fast, epithermal, and thermal fluxes along the x- and y-axes for both BOL and EOL (based on equal burnup in MWd). Figures 15 - 18 show the corresponding flux ratios for 20% and 93% enrichment at BOL and EOL (again, based on equal burnup in MWd).

The results of the k_{eff} calculations for the BOL and EOL benchmarks should not be used to compare the merits of the various fuel enrichments. This is because the given burnup steps in % burnup of ^{235}U involve longer time steps for the 45% enriched case than for the 93% enriched case, and still longer timesteps for the 20% enriched case. In the EPRI-CELL problems the times for 50% ^{235}U burnup in the 45% and 20% enriched cases are 1.165 and 1.467 times longer than for 50% burnup in the 93% enriched case. This fact was the motivation for running problems with 45% and 20% enrichment with the same MWd power generation as for the 93% enrichment case.

2. MONTE CARLO CALCULATIONS

2.1 The Monte Carlo Model

This section deals with a sequence of high-statistics, three-dimensional Monte Carlo calculations based on the specifications in the Appendix. Monte Carlo methods[7] are relatively free of cross-section preparation problems and allow for three-dimensional, heterogeneous calculation in a straight-forward manner. These calculations are intended for comparison with some of the diffusion calculations reported above in order to provide an independent verification of the methods employed and the rsults obtained.

All fuel elements in the calculations have the same basic geometry as shown in Fig. 1. In addition, all fuel and graphite elements have a 15.0 cm Al-H_2O axial reflector at each end with 20% Al - 80% H_2O volume fractions. These Al-H_2O reflectors are in turn, followed by 15.0 cm of H_2O reflector. The following cases were calculated:

	Uranium Enrichment	
1.	93%	fresh core
2.	20%	fresh core
3.	93%	EOL (% Burnup)
4.	20%	EOL (% Burnup)
5.	20%	EOL (Equal MWd)

The burnup varies from element to element throughout the reactor according to the benchmark specifications. In the fresh cores all elements have zero burnup.

The resulting models consist of 222 unique geometric shapes (bodies) which combine to form 886 unique material regions for the fresh cores and 1326 unique material regions for the EOL cores. Fresh core atom densities are given in Table 13 and EOL fuel atom densities for the three stages of burnup are given in Table 14. It should be noted that only the fuel atom densities change from model to model.

Both the diffusion and Monte Carlo calculations reported here were run without lumped fission product absorber equivalents, but did include ^{135}Xe and ^{149}Sm. The Monte Carlo libraries do include a 1/v absorber to represent the thermal lumped fission products, but a "dummy" isotope is not currently available to represent the epithermal component. To provide a clean comparision without a "1/v thermal tail" extending into the epithermal range, the number densities of the lumped fission products were set to zero in both the Monte Carlo and diffusion calculations.

Results

Each Model Calculation consisted of 100,000 histories corresponding to a statistical uncertainity in the computed eigenvalue of about 1/3%.

The calculated eigenvalues are given in Table 15. The corresponding diffusion theory values are also given in this table and are compared with the Monte Carlo value in terms of difference and difference in units of statistical uncertainity (σ).

REFERENCES

1. EPRI-CELL code supplied to Argonne National Laboratory by Electric Power Research Institute, Palo-Alto, California (1977).

2. G. D. Joanou and J. S. Dudek, "GAM-I: A Constant P_1 Multigroup Code for the Calculation of Fast Neutron Spectra and Multigroup Constants," GA-1850, June 1961.

3. H. C. Honeck, "THERMOS, A Thermalization Transport Theory Code for Reactor Lattice Calculations," BNL-5826, September 1961.

4. T. R. England, "CINDER - A One-Point Depletion and Fission Product Program," WARD-TM-334 (Revised), June 1964.

5. H. Henryson II, B. J. Toppel and C. G. Stenberg, "MC^2-2: A Code to Calculate Fast Neutron Spectra and Multigroup Cross Sections," ANL-8144 (ENDF 239) June 1976.

6. T. A. Daley, G. K. Leaf and A. S. Kennedy, "The ARC System Two-Dimensional Diffusion Theory Capability, DARC2D," ANL-7716, May 1972.

7. R. E. Prael and L. J. Milton, "A User's Manual for the Monte Carlo Code VIM," FRA-TM-84, February 20, 1976.

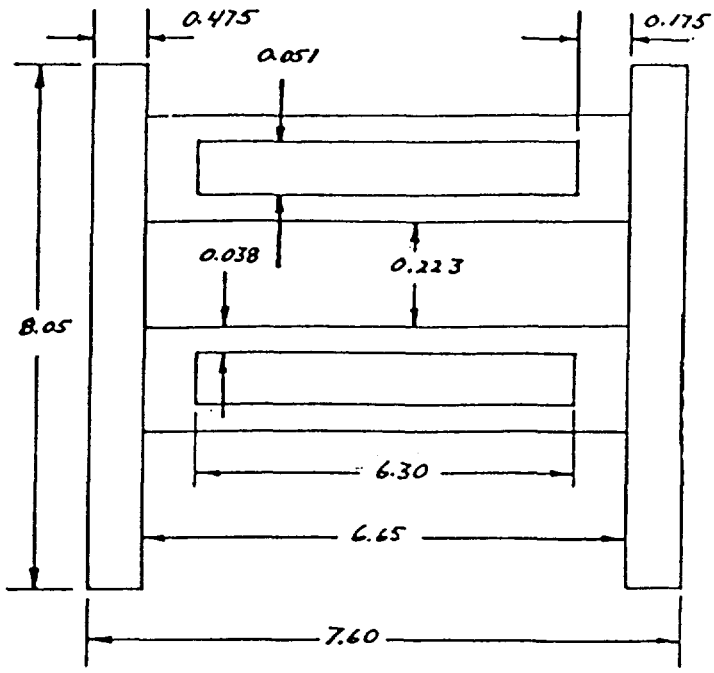

Fig. 1. Standard (23 Plates/Element) and Control (17 Plates/Element) Fuel Elements

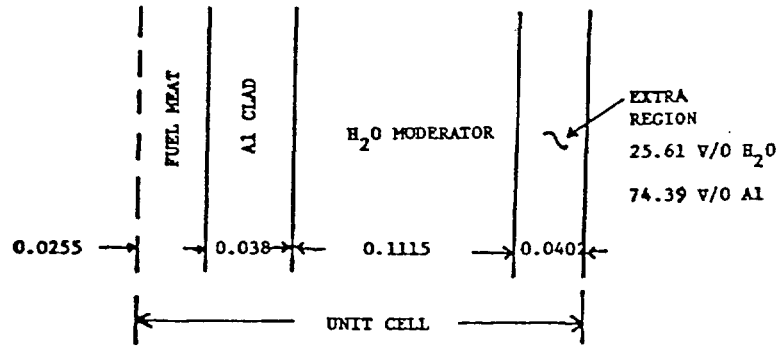

Fig. 2. Unit Cell used in EPRI-CELL

Table 1. Energy Groups used in the Calculations

Group	E_U, eV	E_L, eV
1	1.0×10^7	8.21×10^5
2	8.21×10^5	5.53×10^3
3	5.53×10^3	1.855
4	1.855	0.625
5	0.625	0.0

Table 2. Atom Densities in 93% Enriched Fuel Meat vs ^{235}U Burnup

Atom Densities ($cm^{-3} \times 10^{24}$)

Burnup (%)	Al	^{135}Xe	^{149}Sm	^{235}U	^{236}U	^{238}U
0	5.70110-2	0.0	0.0	1.61790-3	0.0	1.20200-4
5	5.70110-2	1.70943-8	1.33929-7	1.53701-3	1.34683-5	1.19729-4
10	5.70110-2	1.64155-8	1.28239-7	1.45612-3	2.68848-5	1.19231-4
25	5.70110-2	1.40338-8	1.07554-7	1.21342-3	6.62984-5	1.17682-4
30	5.70110-2	1.32194-8	1.00692-7	1.13254-3	7.91391-5	1.17146-4
45	5.70110-2	1.07091-8	8.01311-8	8.89845-4	1.16718-4	1.15456-4
50	5.70110-2	9.84972-9	7.32815-8	8.08949-4	1.28901-4	1.14857-4

Burnup (%)	^{239}Pu	^{240}Pu	^{241}Pu	^{242}Pu	F.P.E.	F.P.T.
0	0.0	0.0	0.0	0.0	0.0	0.0
5	4.37692-7	8.56897-9	3.77796-10	3.00945-12	1.05229-3	4.93857-3
10	8.47746-7	3.32473-8	2.99548-9	4.97504-10	2.29663-3	8.88099-3
25	1.80022-6	1.78887-7	3.99137-8	1.96792-9	6.22039-3	1.90982-2
30	2.03037-6	2.43571-7	6.46856-8	4.07045-9	7.51802-3	2.21936-2
45	2.47988-6	4.59669-7	1.76152-7	2.04908-8	1.12869-2	3.10182-2
50	2.55349-6	5.33805-7	2.23117-7	3.12422-8	1.24867-2	3.38111-2

Table 3. Atom Densities in 45% Enriched Fuel Meat vs ^{235}U Burnup

Atom Densities ($cm^{-3} \times 10^{24}$)

Burnup (%)	Al	^{135}Xe	^{149}Sm	^{235}U	^{236}U	^{238}U
0	5.36910-2	0.0	0.0	1.84900-3	0.0	2.23140-3
5	5.36910-2	1.92855-8	1.54248-7	1.75656-3	1.56065-5	2.22696-3
10	5.36910-2	1.86177-8	1.48533-7	1.66410-3	3.11550-5	2.22223-3
25	5.36910-2	1.61477-8	1.26291-7	1.38677-3	7.67712-5	2.20731-3
30	5.36910-2	1.52875-8	1.18791-7	1.29430-3	9.16201-5	2.20204-3
45	5.36910-2	1.25949-8	9.60313-8	1.01696-3	1.34960-4	2.18514-3
50	5.36910-2	1.16594-8	8.83635-8	9.24513-4	1.48972-4	2.17904-3

Burnup (%)	^{239}Pu	^{240}Pu	^{241}Pu	^{242}Pu	F.P.E.	F.P.T.
0	0.0	0.0	0.0	0.0	0.0	0.0
5	4.05564-6	8.20667-8	3.94347-9	3.16612-11	1.20940-3	5.66464-3
10	7.86305-6	3.17327-7	3.12326-8	5.22682-10	2.64533-3	1.03459-2
25	1.68459-5	1.69487-6	4.12891-7	2.05086-8	7.17151-3	2.25071-2
30	1.90757-5	2.30544-5	6.67231-7	4.23061-8	8.67832-3	2.62242-2
45	2.36481-5	4.35294-6	1.80034-6	2.10867-7	1.30909-2	3.69391-2
50	2.45028-5	5.06327-6	2.27452-6	3.20462-7	1.45124-2	4.03814-2

Table 4. Atom Densities in 20% Enriched Fuel Meat vs ^{235}U Burnup

Atom Densities ($cm^{-3} \times 10^{24}$)

Burnup (%)	Al	^{135}Xe	^{149}Sm	^{235}U	^{236}U	^{238}U
0	3.81710-2	0.0	0.0	2.25360-3	0.0	8.90050-3
5	3.81710-2	2.30226-8	1.91678-7	2.14092-3	1.94582-5	8.88775-3
10	3.81710-2	2.24095-8	1.86339-7	2.02823-3	3.88442-5	8.87411-3
25	3.81710-2	1.98787-8	1.61934-7	1.69020-3	9.56508-5	8.83036-3
30	3.81710-2	1.89700-8	1.53457-7	1.57752-3	1.14100-4	8.81469-3
45	3.81710-2	1.60514-8	1.27167-7	1.23952-3	1.67779-4	8.76349-3
50	3.81710-2	1.50123-8	1.18131-7	1.12691-3	1.85044-4	8.74467-3

Burnup (%)	^{239}Pu	^{240}Pu	^{241}Pu	^{242}Pu	F.P.E.	F.P.T.
0	0.0	0.0	0.0	0.0	0.0	0.0
5	1.13740-5	2.42263-7	1.32772-8	1.07946-10	1.49776-3	7.01035-3
10	2.20424-5	9.29571-7	1.04740-7	1.77419-9	3.27912-3	1.30600-2
25	4.74782-5	4.87965-6	1.35957-6	6.84154-8	8.90476-3	2.88592-2
30	5.39063-5	6.61161-6	2.18113-6	1.40153-7	1.07938-2	3.37596-2
45	6.75486-5	1.24109-5	5.76350-6	6.83703-7	1.64013-2	4.81703-2
50	7.03139-5	1.44336-5	7.23640-6	1.03141-6	1.82397-2	5.29133-2

Table 5.

EPRI-CELL Cross Sections vs ^{235}U Burnup for the 93% Enrichment Case

^{235}U		^{235}U		^{238}U		F.P.E.	F.P.T.
Burnup (%)	Group	σ_a	σ_f	σ_a	σ_f	σ_a	σ_a
0	1	1.72709	1.45346	0.345260	0.179966	0.0	0.0
	2	39.2357	25.9938	27.1369	6.17835-5	0.999092	0.0
	3	422.841	360.532	1.76920	0.0	0.0	0.647818
5	1	1.72712	1.45348	0.345266	0.179967	0.0	0.0
	2	39.3375	26.0492	27.1610	6.17277-5	0.999104	0.0
	3	422.092	359.877	1.76614	0.0	0.0	0.646653
10	1	1.72714	1.45350	0.345273	0.179968	0.0	0.0
	2	39.4375	26.1024	27.1873	6.16808-5	0.999116	0.0
	3	426.152	363.376	1.78135	0.0	0.0	0.652325
15	1	1.72717	1.45352	0.345280	0.179970	0.0	0.0
	2	39.5383	26.1558	27.2137	6.16347-5	0.999127	0.0
	3	430.477	367.104	1.79752	0.0	0.0	0.658356
20	1	1.72720	1.45354	0.345287	0.179971	0.0	0.0
	2	39.6399	26.2097	27.2406	6.15885-5	0.999138	0.0
	3	434.999	371.001	1.81442	0.0	0.0	0.664656
25	1	1.72723	1.45355	0.345294	0.179973	0.0	0.0
	2	39.7422	26.2640	27.2681	6.15421-5	0.999149	0.0
	3	439.696	375.049	1.83197	0.0	0.0	0.671197
30	1	1.72726	1.45357	0.345301	0.179974	0.0	0.0
	2	39.8452	26.3188	27.2962	6.14953-5	0.999160	0.0
	3	444.598	379.273	1.85028	0.0	0.0	0.678019
35	1	1.72729	1.45359	0.345309	0.179976	0.0	0.0
	2	39.9487	26.3740	27.3251	6.14480-5	0.999171	0.0
	3	449.716	383.683	1.86939	0.0	0.0	0.685136
40	1	1.72731	1.45361	0.345316	0.179978	0.0	0.0
	2	40.0523	26.4295	27.3548	6.14003-5	0.999181	0.0
	3	455.055	388.283	1.88931	0.0	0.0	0.692554
45	1	1.72734	1.45362	0.345323	0.179979	0.0	0.0
	2	40.1578	26.4871	27.3855	6.13521-5	0.999192	0.0
	3	460.633	393.090	1.91013	0.0	0.0	0.700300
50	1	1.72737	1.45364	0.345330	0.179981	0.0	0.0
	2	40.2632	26.5449	27.4174	6.13037-5	0.999203	0.0
	3	466.486	398.133	1.93195	0.0	0.0	0.708420

Table 6.

EPRI-CELL Cross Sections vs ^{235}U Burnup for the 45% Enrichment Case

^{235}U		^{235}U		^{238}U		F.P.E.	F.P.T.
Burnup (%)	Group	σ_a	σ_f	σ_a	σ_f	σ_a	σ_a
0	1	1.72774	1.45376	0.344980	0.179501	0.0	0.0
	2	38.6792	25.6777	11.1510	6.27663-5	0.999063	0.0
	3	411.051	350.372	1.72511	0.0	0.0	0.631360
5	1	1.72777	1.45378	0.344988	0.179509	0.0	0.0
	2	38.7871	25.7358	11.1660	6.27109-5	0.999073	0.0
	3	409.986	349.446	1.72086	0.0	0.0	0.629752
10	1	1.72780	1.45380	0.344997	0.179512	0.0	0.0
	2	38.8922	25.7904	11.1824	6.26654-5	0.999080	0.0
	3	413.868	352.793	1.73542	0.0	0.0	0.635189
15	1	1.72784	1.45382	0.345005	0.179514	0.0	0.0
	2	38.9971	25.8441	11.1995	6.26216-5	0.999082	0.0
	3	418.035	356.386	1.75104	0.0	0.0	0.641014
20	1	1.72787	1.45384	0.345013	0.179517	0.0	0.0
	2	39.1024	25.8976	11.2172	6.25783-5	0.999082	0.0
	3	422.412	360.159	1.76742	0.0	0.0	0.647126
25	1	1.72790	1.45386	0.345022	0.179520	0.0	0.0
	2	39.2084	25.9511	11.2355	6.25350-5	0.999079	0.0
	3	427.009	364.122	1.78462	0.0	0.0	0.653541
30	1	1.72793	1.45388	0.345031	0.179523	0.0	0.0
	2	39.3154	26.0049	11.2546	6.24912-5	0.999075	0.0
	3	431.823	368.271	1.80262	0.0	0.0	0.660253
35	1	1.72796	1.45390	0.345039	0.179526	0.0	0.0
	2	39.4234	26.0593	11.2744	6.24468-5	0.999071	0.0
	3	436.870	372.621	1.82149	0.0	0.0	0.667283
40	1	1.72799	1.45392	0.345048	0.179529	0.0	0.0
	2	39.5322	26.1143	11.2950	6.24015-5	0.999067	0.0
	3	442.167	377.186	1.84127	0.0	0.0	0.674655
45	1	1.72802	1.45393	0.345057	0.179533	0.0	0.0
	2	39.6417	26.1698	11.3165	6.23553-5	0.999063	0.0
	3	447.750	381.998	1.86212	0.0	0.0	0.682419
50	1	1.72804	1.45395	0.345066	0.179536	0.0	0.0
	2	39.7522	26.2268	11.3389	6.23079-5	0.999059	0.0
	3	453.623	387.058	1.88403	0.0	0.0	0.690578

Table 7.

EPRI-CELL Cross Sections vs ^{235}U Burnup for the 20% Enrichment Case

^{235}U		^{235}U		^{238}U		F.P.E.	F.P.T.
Burnup (%)	Group	σ_a	σ_f	σ_a	σ_f	σ_a	σ_a
0	1	1.72920	1.45441	0.343615	0.178505	0.0	0.0
	2	37.8447	25.2009	6.09503	6.38103-5	0.999003	0.0
	3	392.606	334.476	1.65603	0.0	0.0	0.605549
5	1	1.72923	1.45443	0.343627	0.178509	0.0	0.0
	2	37.9599	25.2617	6.10113	6.37600-5	0.999010	0.0
	3	391.023	333.106	1.64984	0.0	0.0	0.603221
10	1	1.72927	1.45445	0.343639	0.178514	0.0	0.0
	2	38.0696	25.3164	6.10816	6.37222-5	0.999006	0.0
	3	394.540	336.114	1.66310	0.0	0.0	0.608175
15	1	1.72930	1.45448	0.343652	0.178519	0.0	0.0
	2	38.1777	25.3683	6.11576	6.35878-5	0.998994	0.0
	3	398.363	339.443	1.67749	0.0	0.0	0.613547
20	1	1.72934	1.45450	0.343664	0.178524	0.0	0.0
	2	38.2855	25.4189	6.12389	6.36548-5	0.998975	0.0
	3	402.421	342.945	1.69274	0.0	0.0	0.619241
25	1	1.72937	1.45452	0.343677	0.178530	0.0	0.0
	2	38.3941	25.4691	6.13249	6.36221-5	0.998953	0.0
	3	406.711	346.645	1.70884	0.0	0.0	0.625252
30	1	1.72940	1.45454	0.343691	0.178536	0.0	0.0
	2	38.5044	25.5196	6.14153	6.35888-5	0.998928	0.0
	3	411.253	350.562	1.72586	0.0	0.0	0.631607
35	1	1.72944	1.45457	0.343704	0.178542	0.0	0.0
	2	38.6167	25.5711	6.15100	6.35542-5	0.998902	0.0
	3	416.045	354.694	1.74382	0.0	0.0	0.638306
40	1	1.72947	1.45459	0.343718	0.178548	0.0	0.0
	2	38.7315	25.6240	6.16090	6.35179-5	0.998875	0.0
	3	421.115	359.064	1.76279	0.0	0.0	0.645384
45	1	1.72950	1.45461	0.343732	0.178555	0.0	0.0
	2	38.8488	25.6786	6.17125	6.34795-5	0.998849	0.0
	3	426.484	363.692	1.78287	0.0	0.0	0.652872
50	1	1.72953	1.45463	0.343747	0.178563	0.0	0.0
	2	38.9683	25.7349	6.18209	6.34388-5	0.998825	0.0
	3	432.191	368.610	1.80409	0.0	0.0	0.660820

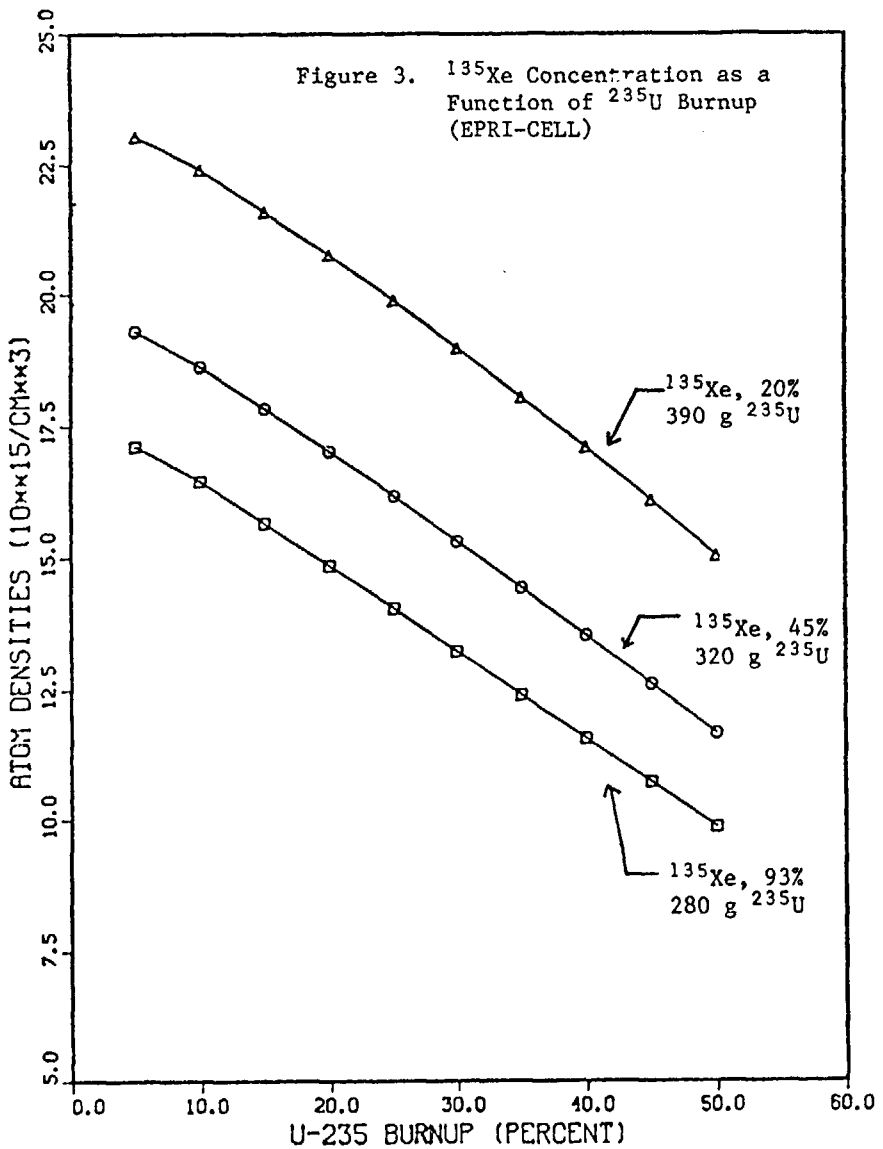

Figure 3. ^{135}Xe Concentration as a Function of ^{235}U Burnup (EPRI-CELL)

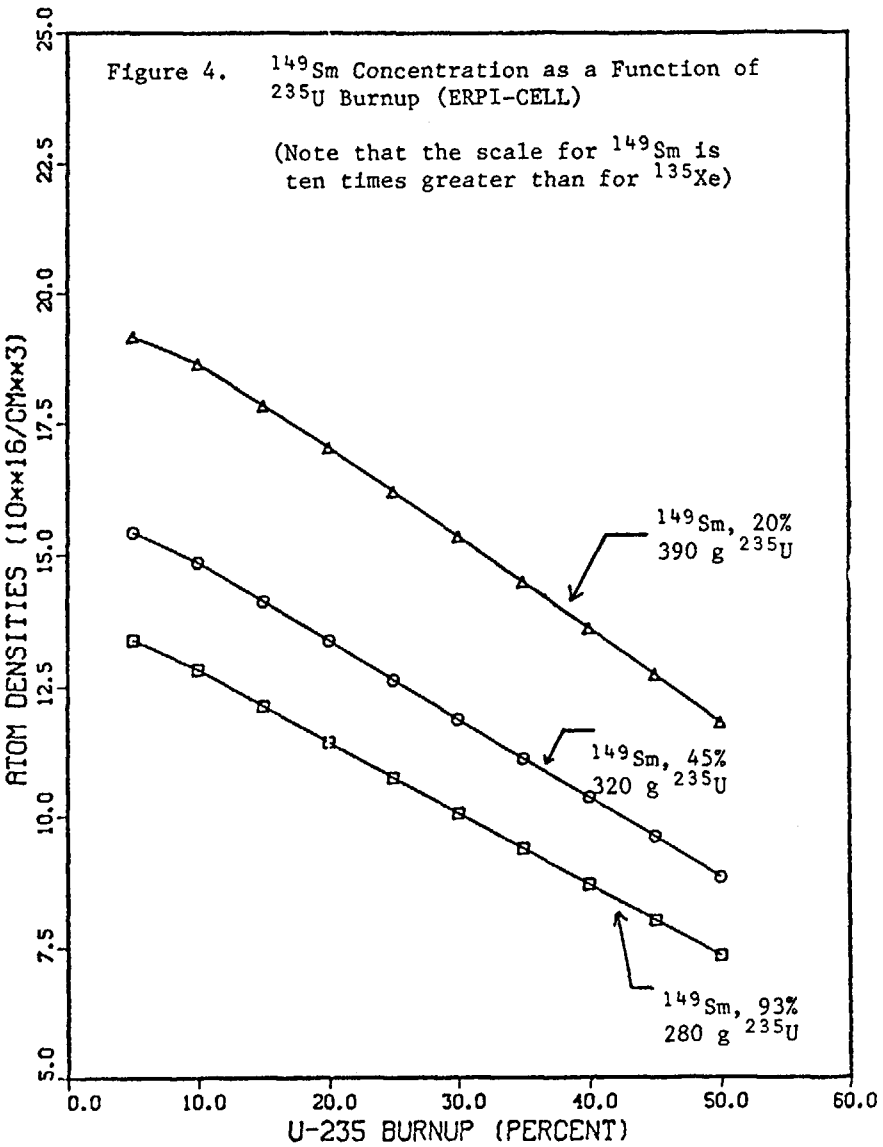

Figure 4. ^{149}Sm Concentration as a Function of ^{235}U Burnup (ERPI-CELL)

(Note that the scale for ^{149}Sm is ten times greater than for ^{135}Xe)

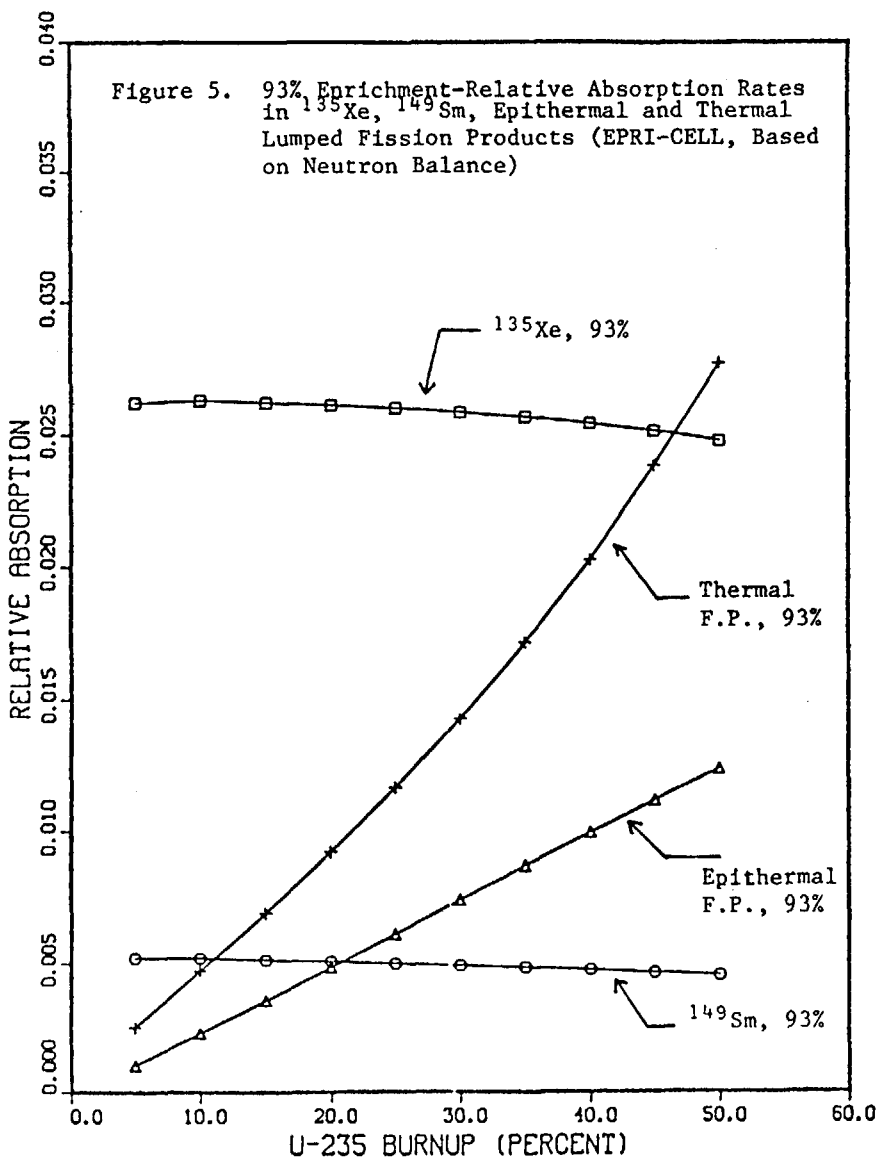

Figure 5. 93% Enrichment-Relative Absorption Rates in ^{135}Xe, ^{149}Sm, Epithermal and Thermal Lumped Fission Products (EPRI-CELL, Based on Neutron Balance)

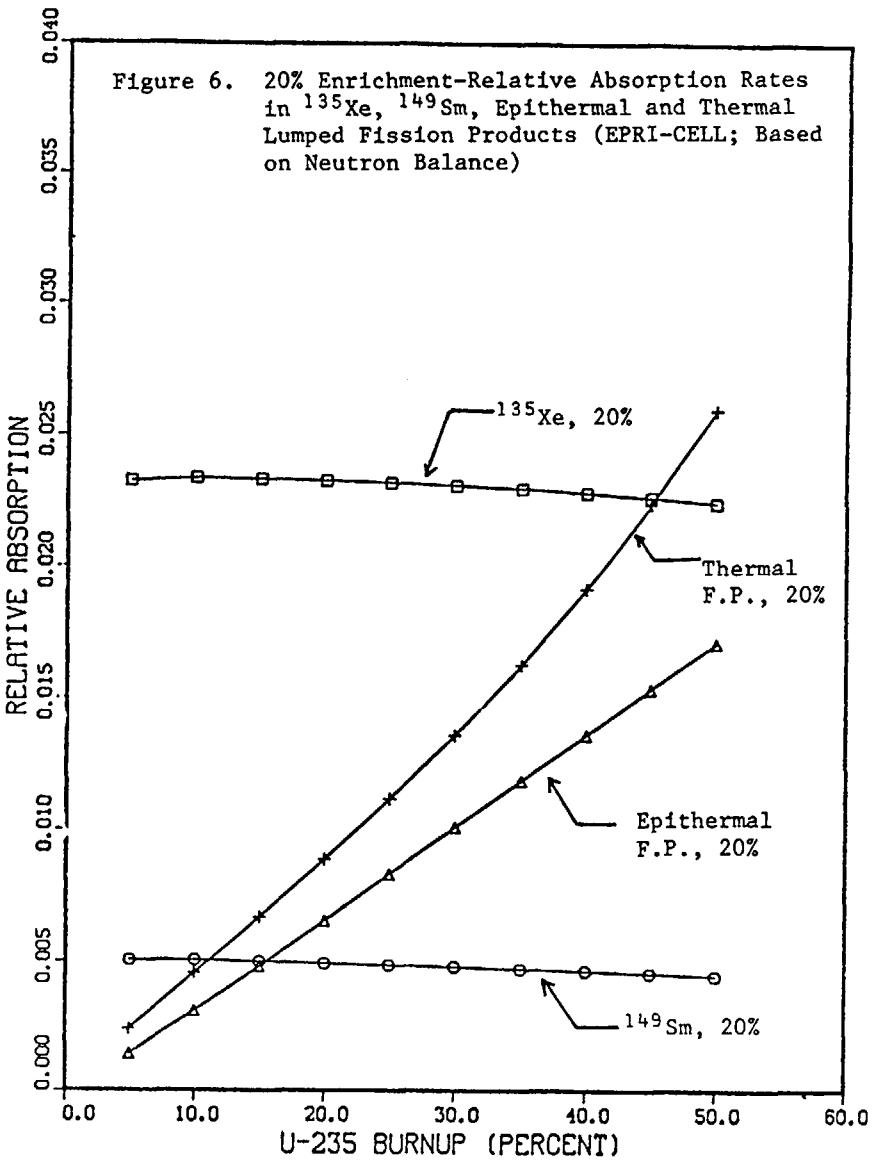

Figure 6. 20% Enrichment-Relative Absorption Rates in ^{135}Xe, ^{149}Sm, Epithermal and Thermal Lumped Fission Products (EPRI-CELL; Based on Neutron Balance)

Table 8. EPRI-CELL k_∞ vs. ^{235}U Burnup For Three Enrichments

	Enrichment		
Burnup(%)	93%	45%	20%
0	1.73698	1.70442	1.65475
5	1.63697	1.60817	1.56410
10	1.61653	1.58845	1.54447
15	1.59534	1.56803	1.52413
20	1.57275	1.54633	1.50257
25	1.54853	1.52312	1.47972
30	1.52227	1.49812	1.45544
35	1.49358	1.47106	1.42957
40	1.46199	1.44153	1.40183
45	1.42692	1.40907	1.37191
50	1.38761	1.37305	1.33935

Table 9. Water and Graphite Reflector Constants

	Water Reflector		Graphite Reflector	
Energy Group	D	Σ_a	D	Σ_a
1	2.847	4.361×10^{-4}	2.226	4.649×10^{-5}
2	0.955	9.691×10^{-6}	1.027	0.0
3	0.584	6.312×10^{-4}	0.877	8.239×10^{-6}
4	0.464	3.459×10^{-3}	0.875	4.504×10^{-5}
5	0.147	1.901×10^{-2}	0.842	2.510×10^{-4}
1	1.729	2.271×10^{-4}	1.334	1.160×10^{-5}
2	0.569	1.002×10^{-3}	0.876	1.297×10^{-5}
3	0.147	1.901×10^{-2}	0.842	2.510×10^{-4}

Table 10. Values of k_{eff} from X-Y Diffusion Theory Calculations

Enrichment	Description	k_{eff}
93%	Fresh Fuel	1.18343
93%	BOL	1.02333
93%	EOL	1.00038
93%	EOL with no Lumped F.P.	1.03366
45%	Fresh Fuel	1.17817
45%	BOL (% Burnup)	1.02471
45%	EOL (% Burnup)	1.00331
45%	BOL (Equal MWd)	1.04095
45%	EOL (Equal MWd)	1.02381
20%	Fresh Fuel	1.16830
20%	BOL (% Burnup)	1.02127
20%	EOL (% Burnup)	1.00142
20%	BOL (Equal MWd)	1.05399
20%	EOL (Equal MWd)	1.04187
20%	EOL (% Burnup) with no Lumped F.P.	1.03934
20%	EOL (Equal MWd) with no Lumped F.P.	1.06847

Table 11 Fluxes from the DIF2D Problems (n/cm^{2}sec)

	Core					Flux Trap	
	Average Fluxes				Average	Center Ave.	Center Midplane
Case	ϕ_1	ϕ_2	ϕ_f	ϕ_{th}	ϕ_{th}	ϕ_{th}	ϕ_{th}
93% BOL	1.1279+14	5.4807+13	1.6759+14	6.3296+13	2.1345+14	2.7518+14	3.6080+14
93% EOL	1.1512+14	5.5966+13	1.7109+14	6.7390+13	2.1999+14	2.8132+14	3.6885+14
45% BOL	1.1272+14	5.3932+13	1.6665+14	5.5091+13	2.0341+14	2.6793+14	3.5129+14
45% EOL	1.1497+14	5.5029+13	1.7000+14	5.8386+13	2.0915+14	2.7351+14	3.5861+14
20% BOL	1.1292+14	5.2788+13	1.6571+14	4.4719+13	1.9017+14	2.5852+14	3.3896+14
20% EOL	1.1514+14	5.3835+13	1.6897+14	4.7048+13	1.9498+14	2.6352+14	3.4551+14

Table 12. Neutron Inventories for the 93% and 20% Enriched EOL Benchmarks

93% EOL			20% EOL		
Material	Absorption	Fission	Material	Absorption	Fission
Al	3.73687-2	0.0	Al	2.32547-2	0.0
Xe-135	2.46285-2	0.0	Xe-135	2.27450-2	0.0
Sm-149	4.65275-3	0.0	Sm-149	4.68630-3	0.0
U-235	4.90298-1	4.11683-1	U-235	4.54620-1	3.79214-1
U-236	2.52904-3	4.60684-5	U-236	3.16149-3	6.55205-5
U-238	2.73423-3	3.33384-5	U-238	5.45721-2	2.47287-3
Pu-239	1.93913-3	1.31079-3	Pu-239	3.69074-2	2.46079-2
Pu-240	2.55588-4	5.00559-7	Pu-240	5.31994-3	1.31389-5
Pu-241	1.19989-4	8.94871-5	Pu-241	2.61142-3	1.95116-3
Pu-242	1.30515-6	1.58080-8	Pu-242	3.83182-5	5.22235-7
F.P.E.	6.10702-3	0.0	F.P.E.	8.45247-3	0.0
F.P.T.	1.50246-2	0.0	F.P.T.	1.47525-2	0.0
H	7.98324-2	0.0	H	5.32968-2	0.0
O	1.32246-3	0.0	O	1.30355-3	0.0
Total Fuel	0.666813	0.413163	Total Fuel	0.685722	0.408326
Total Non-Fuel H_2O	0.243356	0.0	Total Non-Fuel H_2O	0.228791	0.0
Total Graphite	0.000700	0.0	Total Graphite	0.000589	0.0
Reactor Total	0.910870	0.413163	Reactor Total	0.915101	0.408326
Reactor Leakage	0.089127		Reactor Leakage	0.084896	

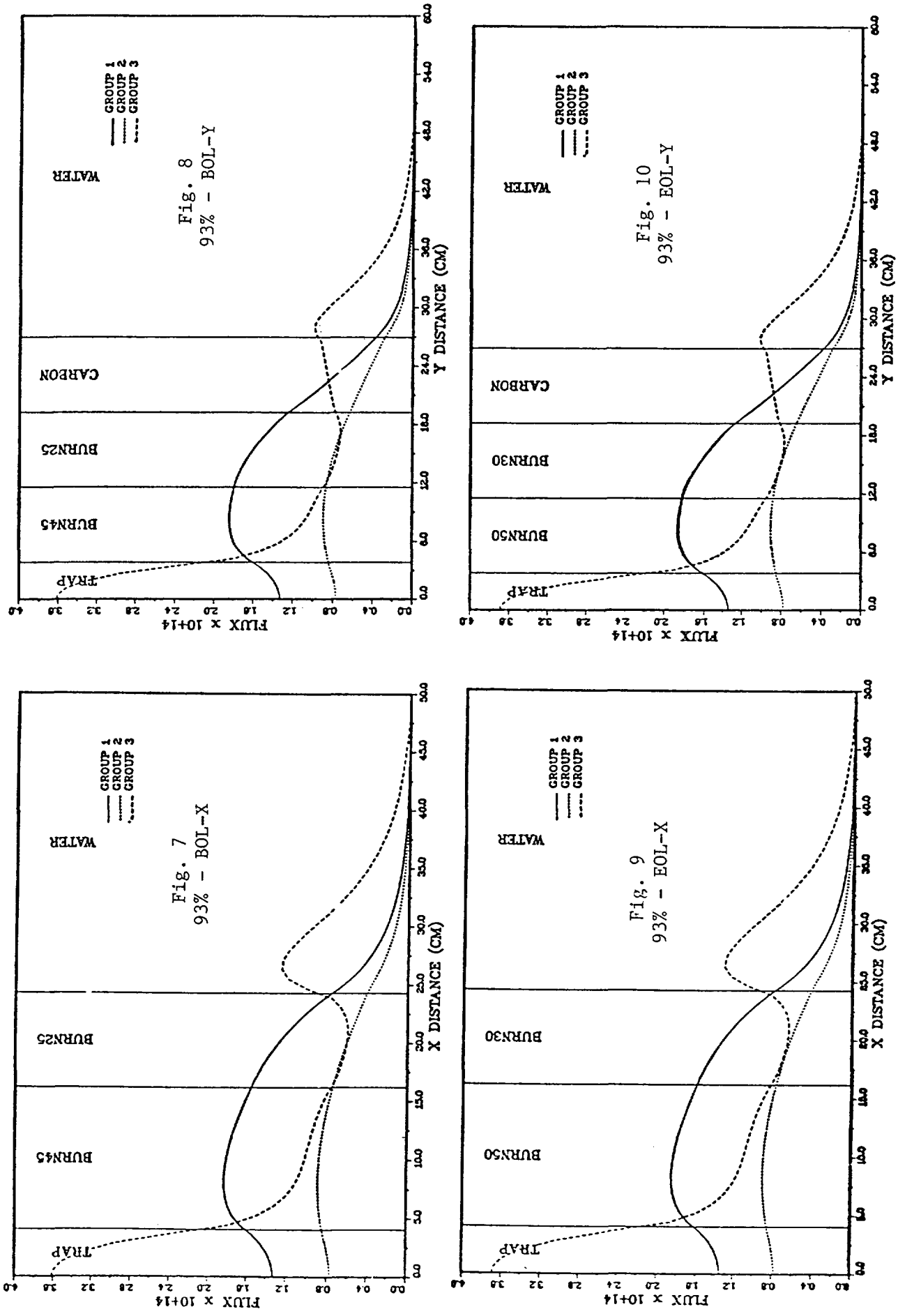

Figures 7 to 10. 10 MW Benchmark - 93% Enrichment Midplane Fluxes at BOL and EOL Along X-Axis and Y-Axis

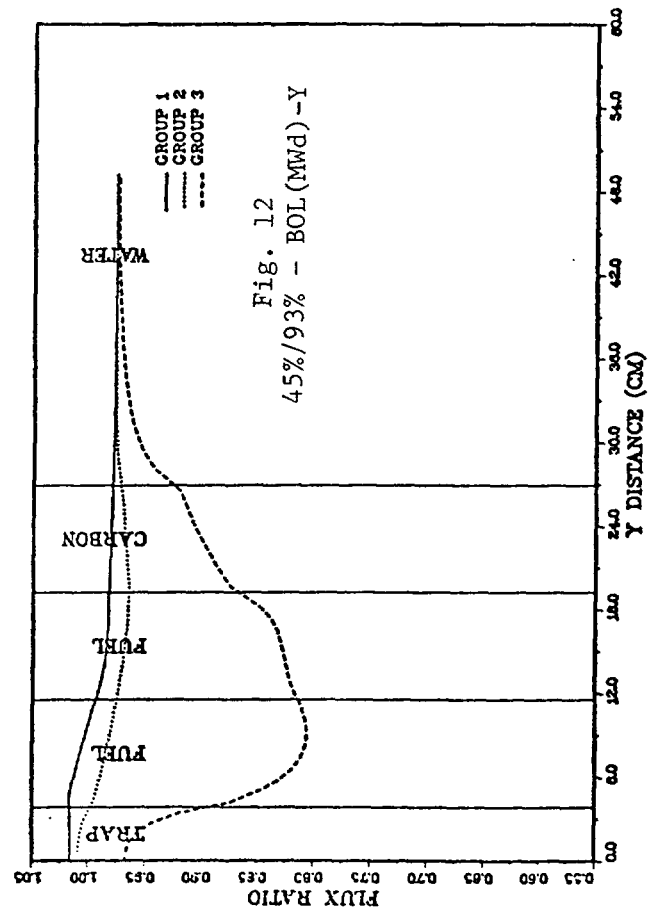

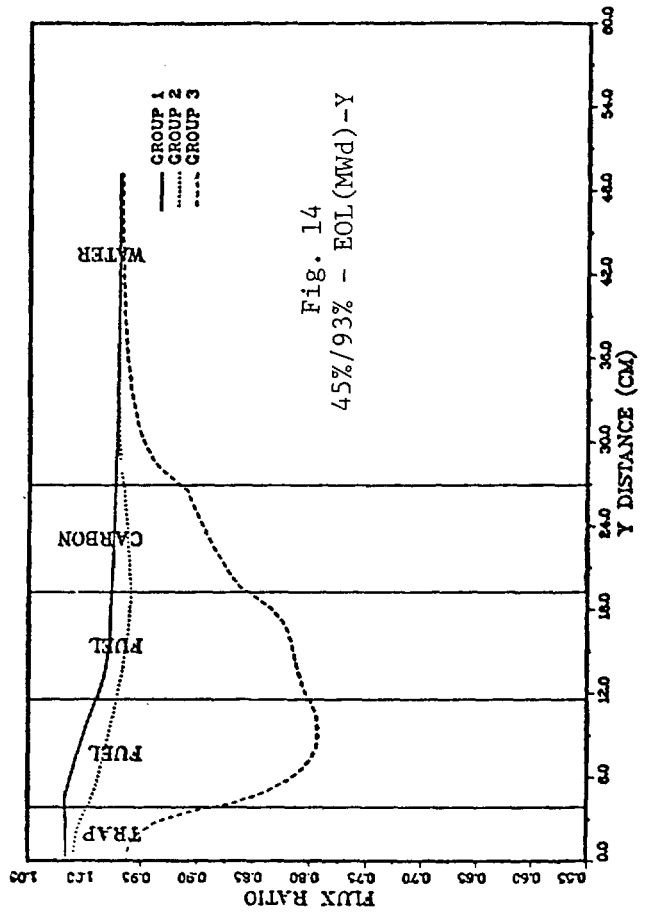

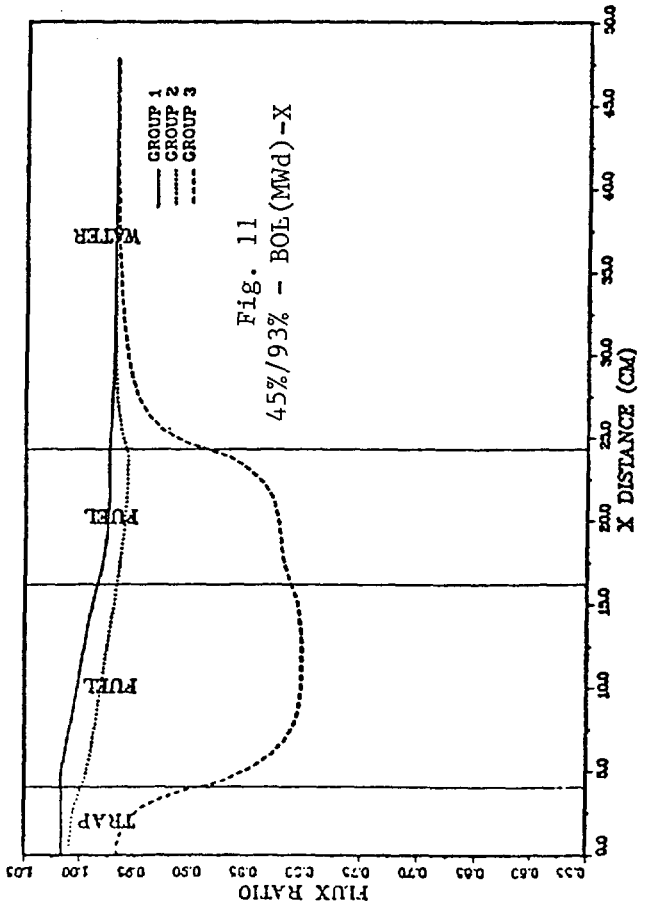

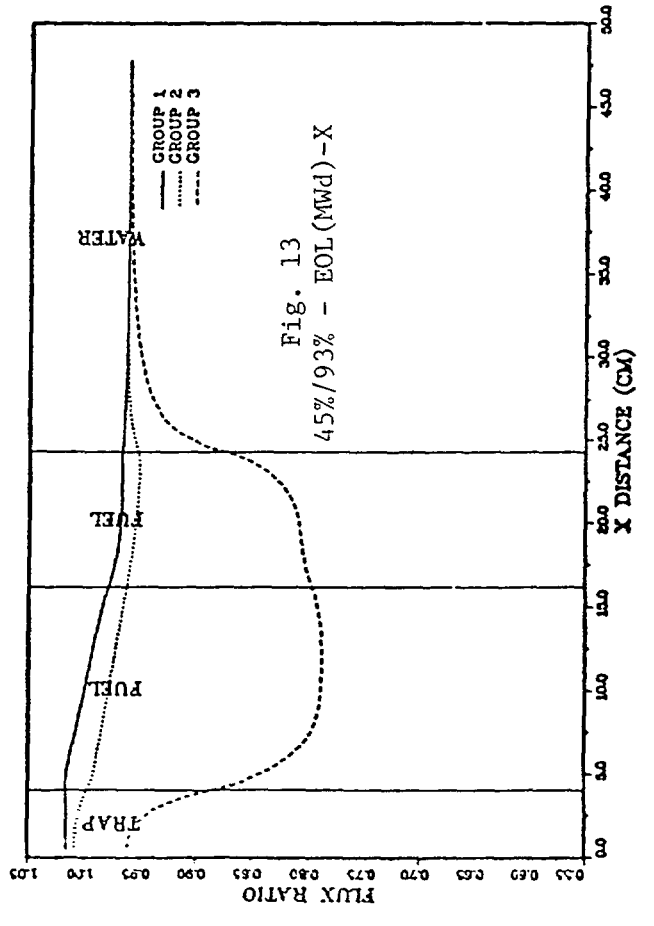

Figures 11 to 14. 10 MW Benchmark - 45%/93% Midplane Flux Ratios at BOL(MWd) and EOL(MWd) Along X-Axis and Y-Axis

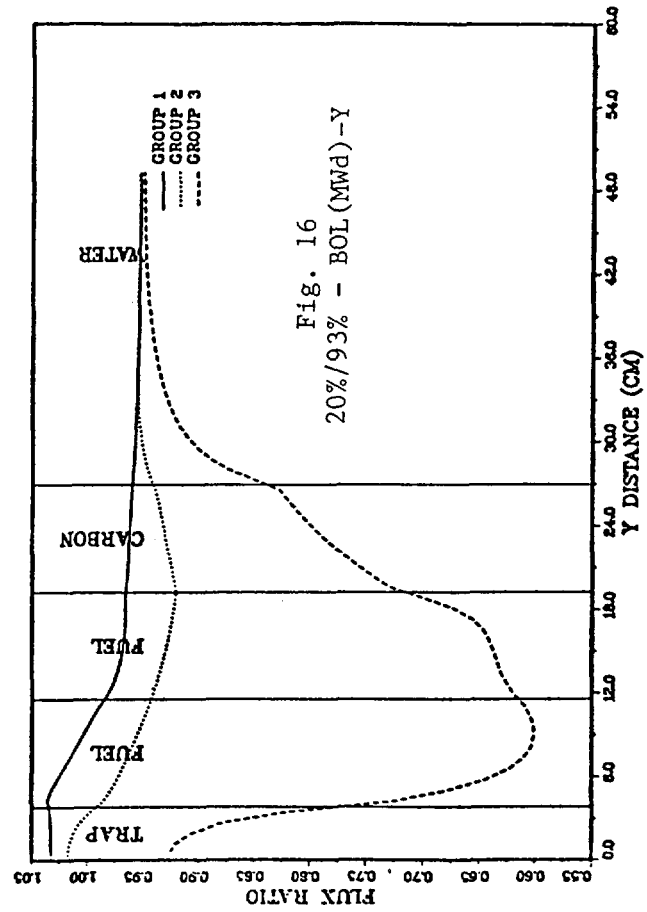

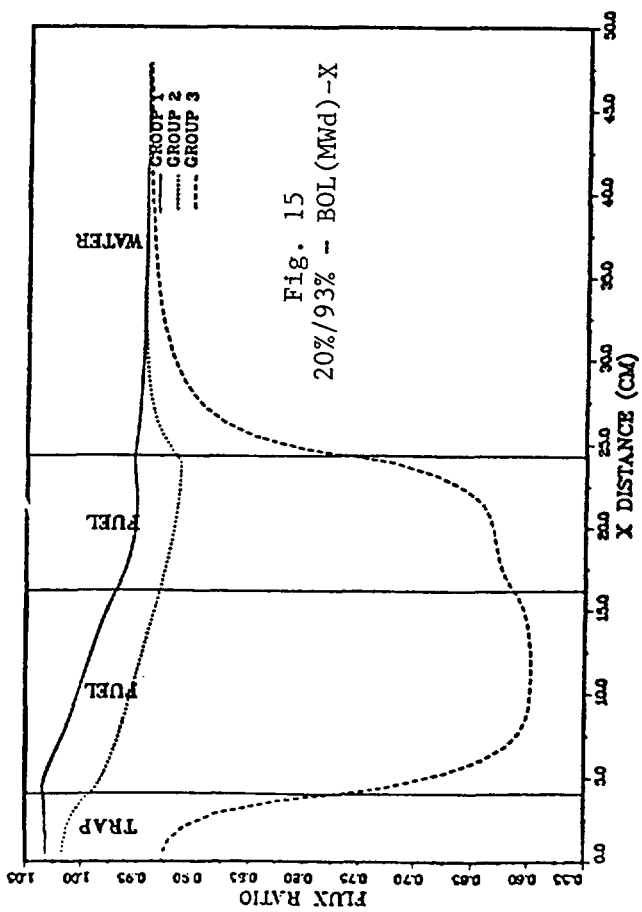

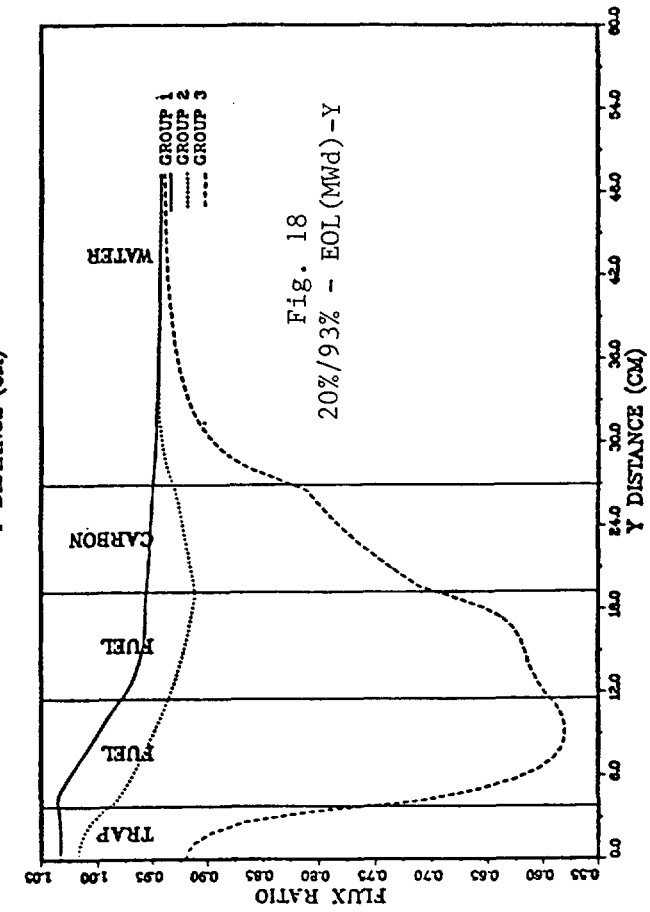

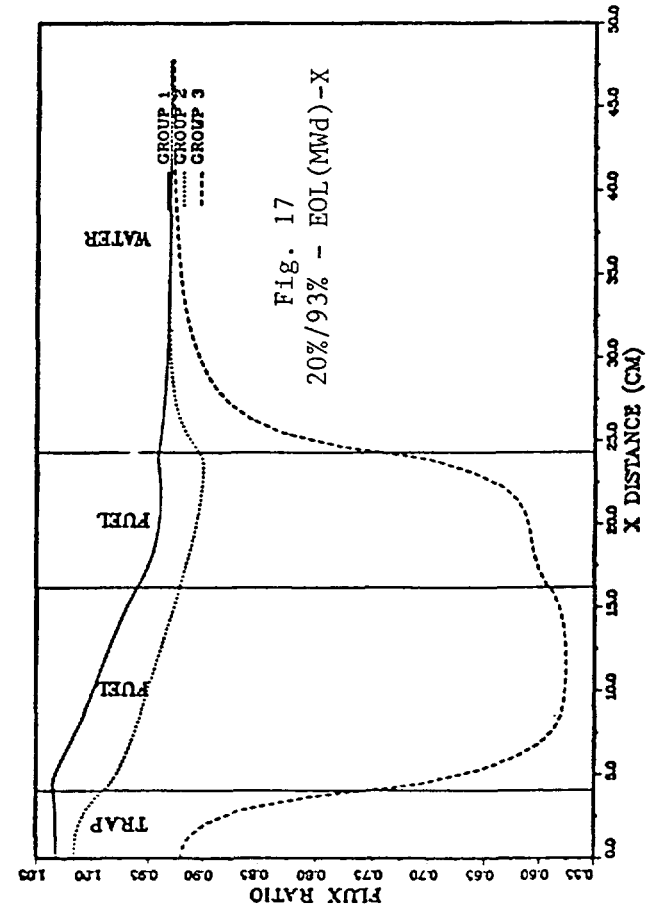

Figures 15 to 18. 10 MW Benchmark - 20%/93% Midplane Flux Ratios at BOL(MWd) and EOL(MWd) Along X-Axis and Y-Axis

Table 13. Fresh Core Atom Number Densities for 93% and 20% Fuel Enrichment

	93% (10^{24})	20% (10^{24})
Fuel:		
U-235	0.0016179	0.0022536
U-238	0.0001202	0.0089005
Al	0.057011	0.038171
Al Clad	0.060260	0.060260
Graphite	0.085234	0.085234
H_2O		
O	0.033428	0.033428
H	0.066856	0.066856
Axial Reflector (20% Al - 80% H_2O)		
Al	0.0120520	0.0120520
O	0.0267424	0.0267424
H	0.0534848	0.0534848

Table 14. End-of-Life Core Fuel Atom Number Densities for 93% and 20% Fuel Enrichment and 50%, 30%, 10% Burnup

	50% (10^{24})	30% (10^{24})	10% (10^{24})
EOL 93%			
Pu-240	0.533805-6	0.243571-6	0.332473-7
Pu-241	0.223117-6	0.646856-7	0.299548-8
U-235	0.808949-3	0.113254-2	0.145612-2
U-238	0.114857-3	0.117146-3	0.119231-3
Pu-239	0.255349-5	0.203037-5	0.847746-6
U-236	0.128901-3	0.791391-4	0.268848-4
Pu-242	0.312422-7	0.407045-8	0.497504-10
Al	0.570110-1	0.570110-1	0.570110-1
Sm-149	0.732815-7	0.100692-6	0.128239-6
Xe-135	0.984972-8	0.132194-7	0.164155-7
EOL 20%			
Pu-240	0.144336-4	0.661161-5	0.929571-6
Pu-241	0.723640-5	0.218113-5	0.104740-6
U-235	0.112691-2	0.157752-2	0.202823-2
U-238	0.874467-2	0.881469-2	0.887411-2
Pu-239	0.703139-4	0.539063-4	0.220424-4
U-236	0.185044-3	0.114100-3	0.388442-4
Pu-242	0.103141-5	0.140153-6	0.177419-8
Al	0.381710-1	0.381710-1	0.381710-1
Sm-149	0.118131-6	0.153457-6	0.186339-6
Xe-135	0.150123-7	0.189700-7	0.224095-7
EOL 20%*			
Pu-240	0.853998-5	0.371885-5	0.497299-6
Pu-241	0.322375-5	0.886782-6	0.401335-7
U-235	0.146015-2	0.177254-2	0.209134-2
U-238	0.879798-2	0.884152-2	0.888172-2
Pu-239	0.594141-4	0.420955-4	0.162748-4
U-236	0.133008-3	0.820098-4	0.280384-4
Pu-242	0.260852-6	0.365848-7	0.476623-9
Al	0.381710-1	0.381710-1	0.381710-1
Sm-149	0.143059-6	0.166796-6	0.189553-6
Xe-135	0.178552-7	0.204119-7	0.227615-7

*Burnup in MWD equivalent to 93% case.

Table 15. Comparison of Monte Carlo* and Diffusion Theory Eigenvalues

Core	Monte Carlo k	Diffusion k	$k_{mc} - k_d$	$(k_{mc} - k_d)/\sigma$
93% Fresh	1.189 ± .0033	1.18343	+.006	1.82
20% Fresh	1.168 ± .0033	1.16830	0.0	0
93% EOL**	1.045 ± .0036	1.03366	+.011	3.06
20% EOL**	1.048 ± .0034	1.03934	+.009	2.65
20% EQ MWD**	1.072 ± .0027	1.06847	+.004	1.48

*100,000 Histories per calculation.

**These calculations did not include lumped fission products.

APPENDIX F - 2

Benchmark Calculations

performed by

INTERATOM

Internationale Atomreaktorbau GmbH
9120 Kernauslegung Therm. Reaktoren
Postfach
5060 Bergisch Gladbach 1
Federal Republic of Germany

Summary

The benchmark agreed upon was calculated with the methods used at INTERATOM when designing research reactors. The same methods are used in the Appendix C.

The results are presented as reactivities with different dependencies, as absolute fluxes and/or flux ratios (REU/HEU), and as important fuel specific isotopic contents (Plutonium, Xenon).

All these results are in very good agreement with those obtained by other contributors as may be seen from comparisons done within chapter 2.4 of the main part.

FRG-Benchmark Calculations

This contribution describes the calculations concerning the methodical benchmarks agreed upon at Vienna, June 1979, 19.-21. The calculations have been run with the same computer codes and cross section libraries as our results presented in Appendix C. The results are presented mainly in graphs; they are all based on the core cross section fixed at Vienna and presented in fig. 1 of App. F-0. Fig. F.2.1 shows the reactivity behaviour during the burnup step for the 3 different fuels used:

- 280 g U235 per fuel element
  93 w/o U235 enrichment
  23 plates per fuel element
- 320 g U235 per fuel element
  45 w/o U235 enrichment
  23 plates per fuel element
- 390 g U235 per fuel element
  20 w/o U235 enrichment
  23 plates per fuel element

Fig. F.2.2 compares the behaviour of the k_∞ of the 3 different fuels agains their burnup/MWd/, including Xe-equilibrium for constant power level of 10 MW for the total core.

The next four figures (F.2.3 to F.2.6) give the absolute flux shapes resulting from the basic calculations with the 93 w/o enriched fuel of the core states BOL and EOL resp. as well as for the two axes of symmetry (X-direction and Y-direction of fig. 1 of App. F-0).

To give a good impression of the change in fluxes when reducing the enrichment from 93 w/o U235 to 45 w/o U235 and to 20 w/o U235, resp. fig. F.2.7 to fig. F.2.10 demonstrate the flux ratios for the three fluxes (fast epithermal, thermal) dividing the 45 w/o U235-results and the 20 w/o U235-results, resp. by the 93 w/o U235-results.

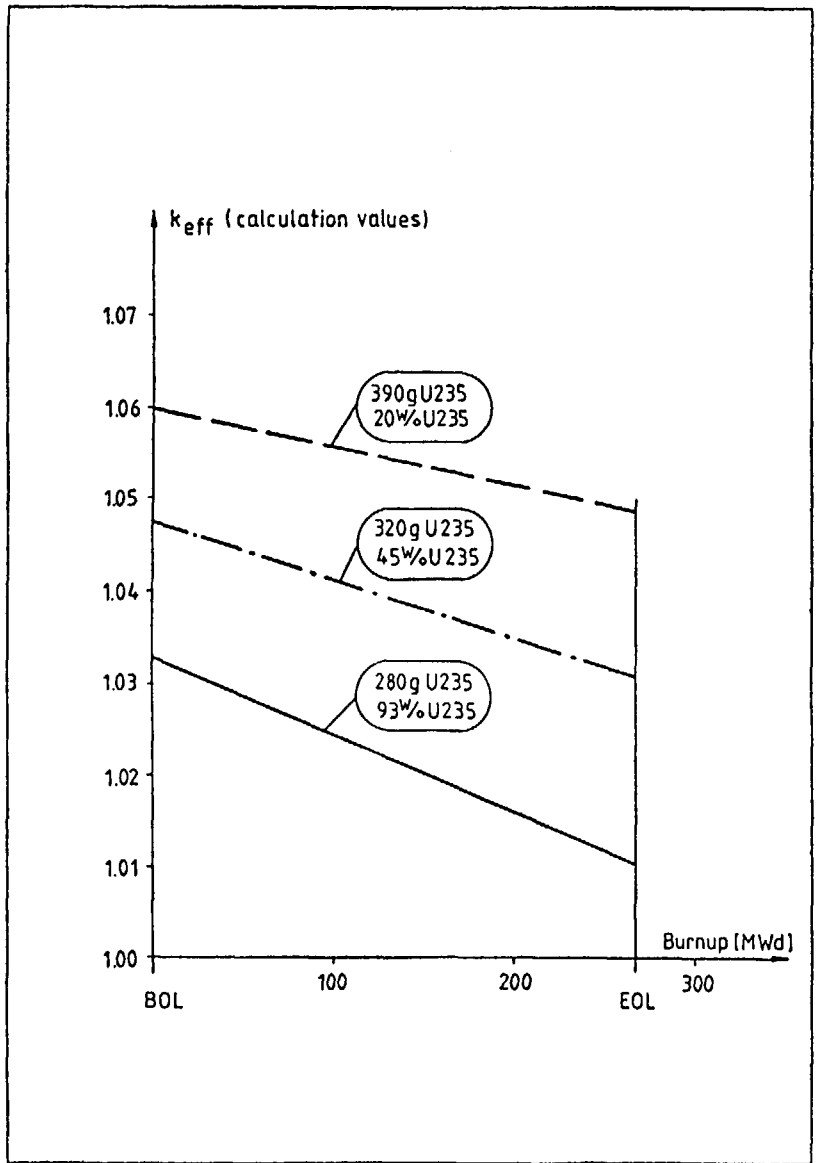

REACTIVITY VS. BURNUP

FIG. F. 2.1

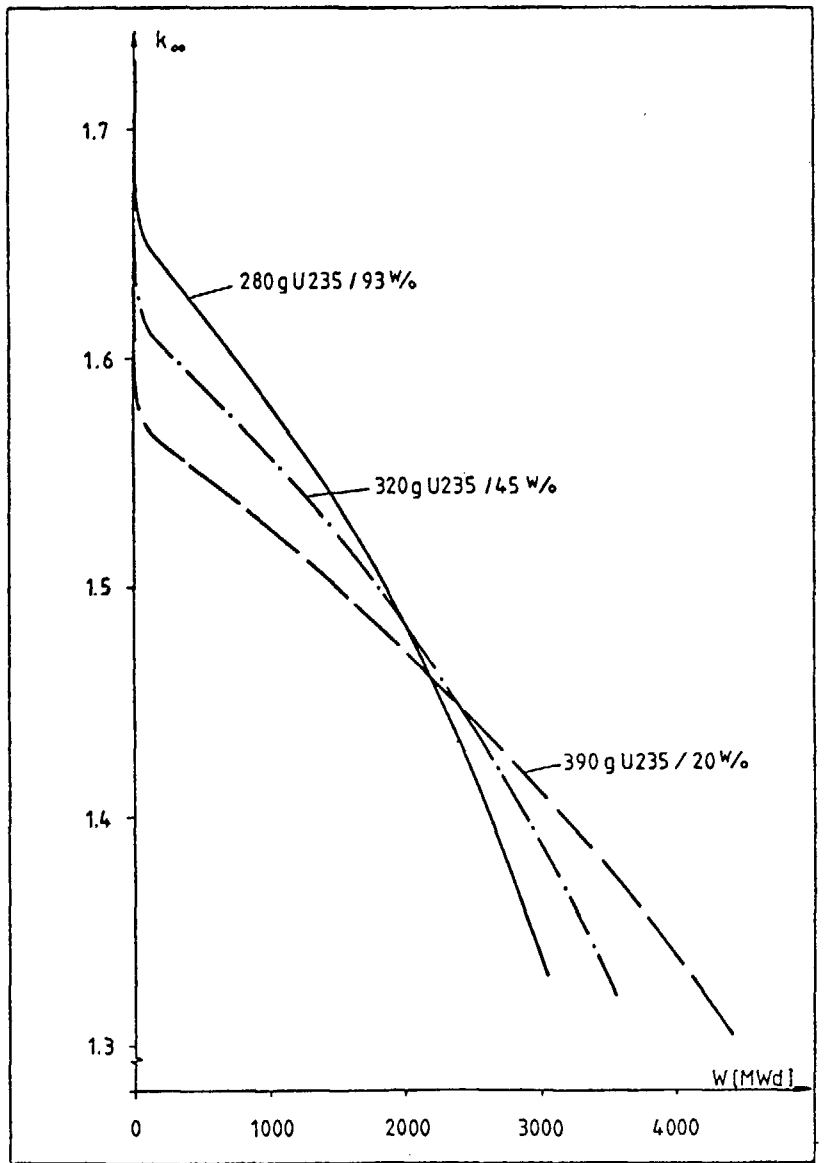

k_∞ AS A FUNCTION OF THE BURNUP W FOR THE THREE DIFFERENT FUELS

FIG. F. 2.2

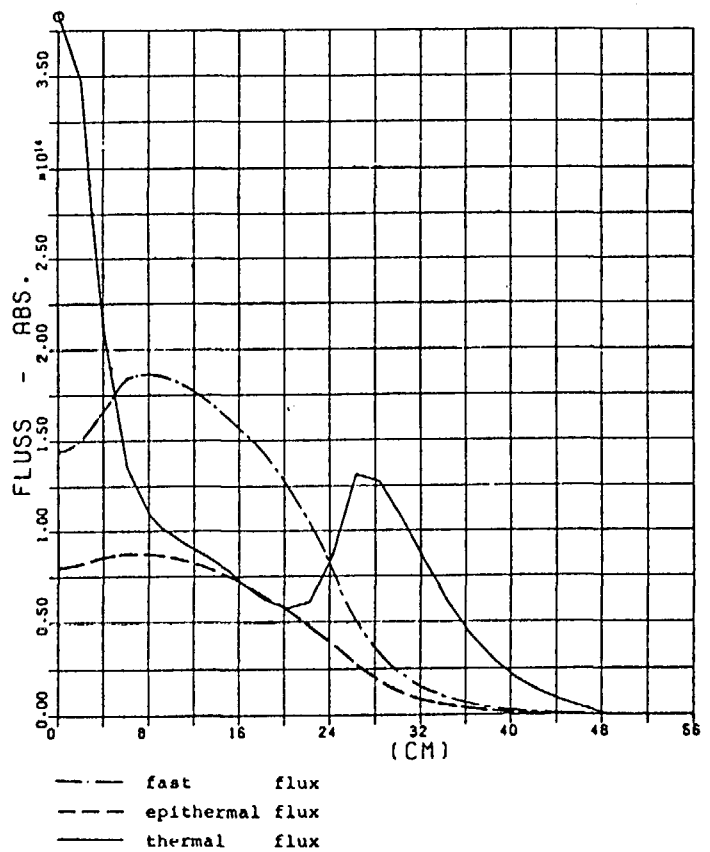

10 MW - Benchmark - core with HEU - Fuel
Absolute Fluxes along X - Direction
Core State BOL Xe - Equilibrium

Fig F.2.3

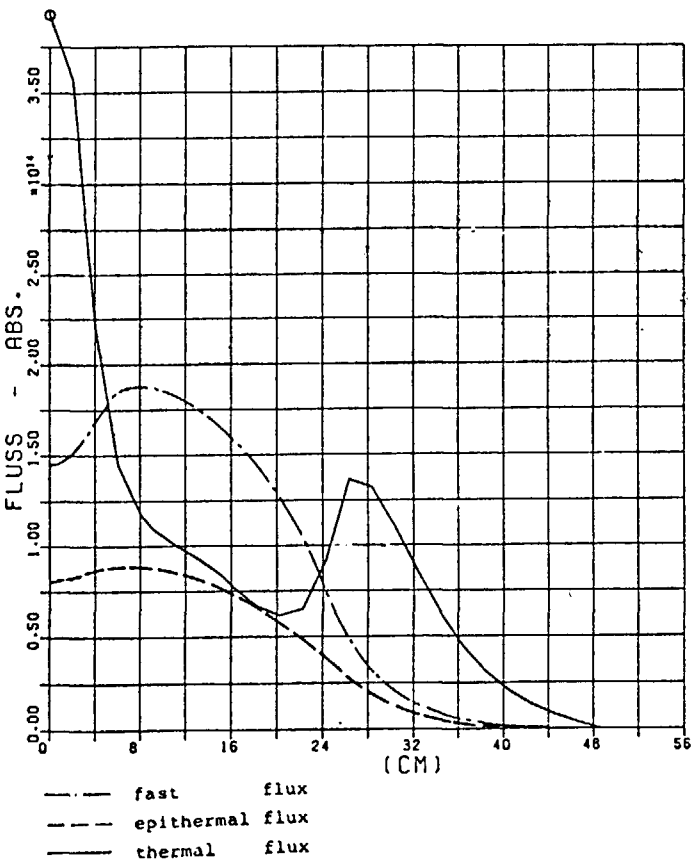

10 MW - Benchmark - core with HEU - Fuel
Absolute Fluxes along X - Direction
Core State EOL Xe - Equilibrium

Fig. F.2.4

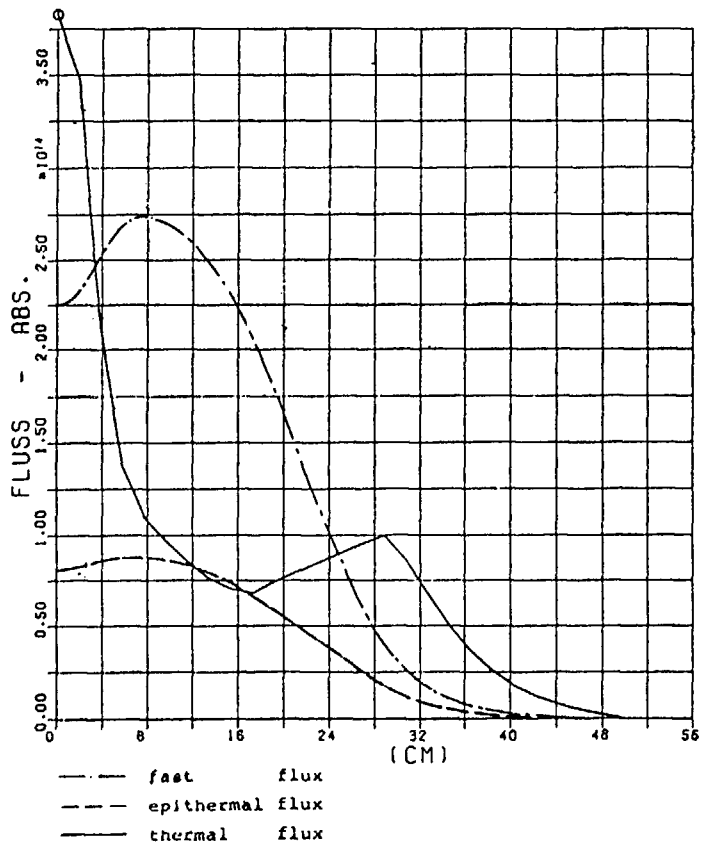

10 MW - Benchmark - Core with HEU - Fuel
Absolute Fluxes along Y- Direction
Core State BOL Xe - Equilibrium

Fig. F.2.5

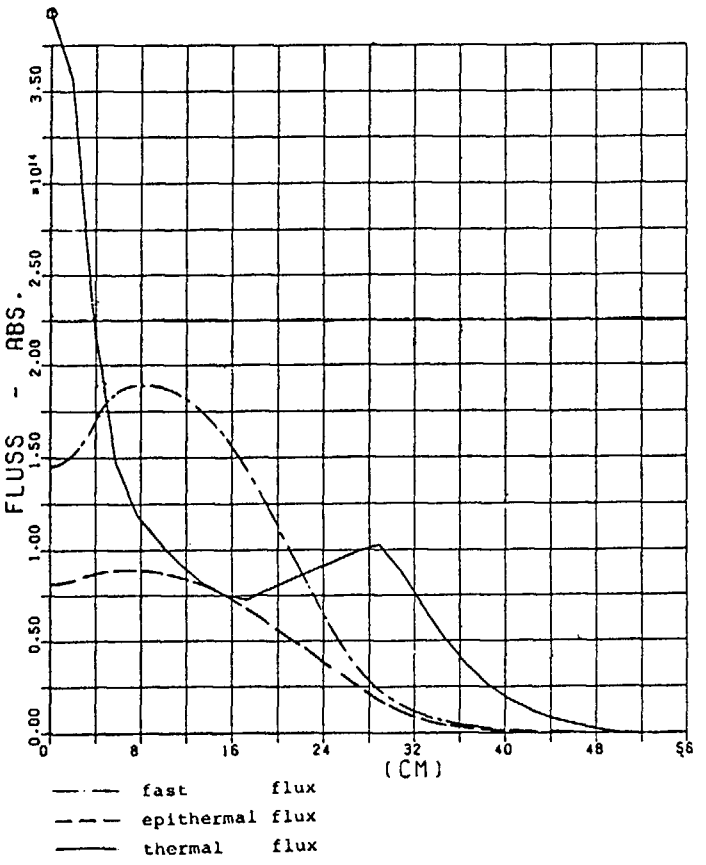

10 MW - Benchmark - Core with HEU - Fuel
Absolute Fluxes along Y- Direction
Core State EOL Xe - Equilibrium

Fig. F.2.6

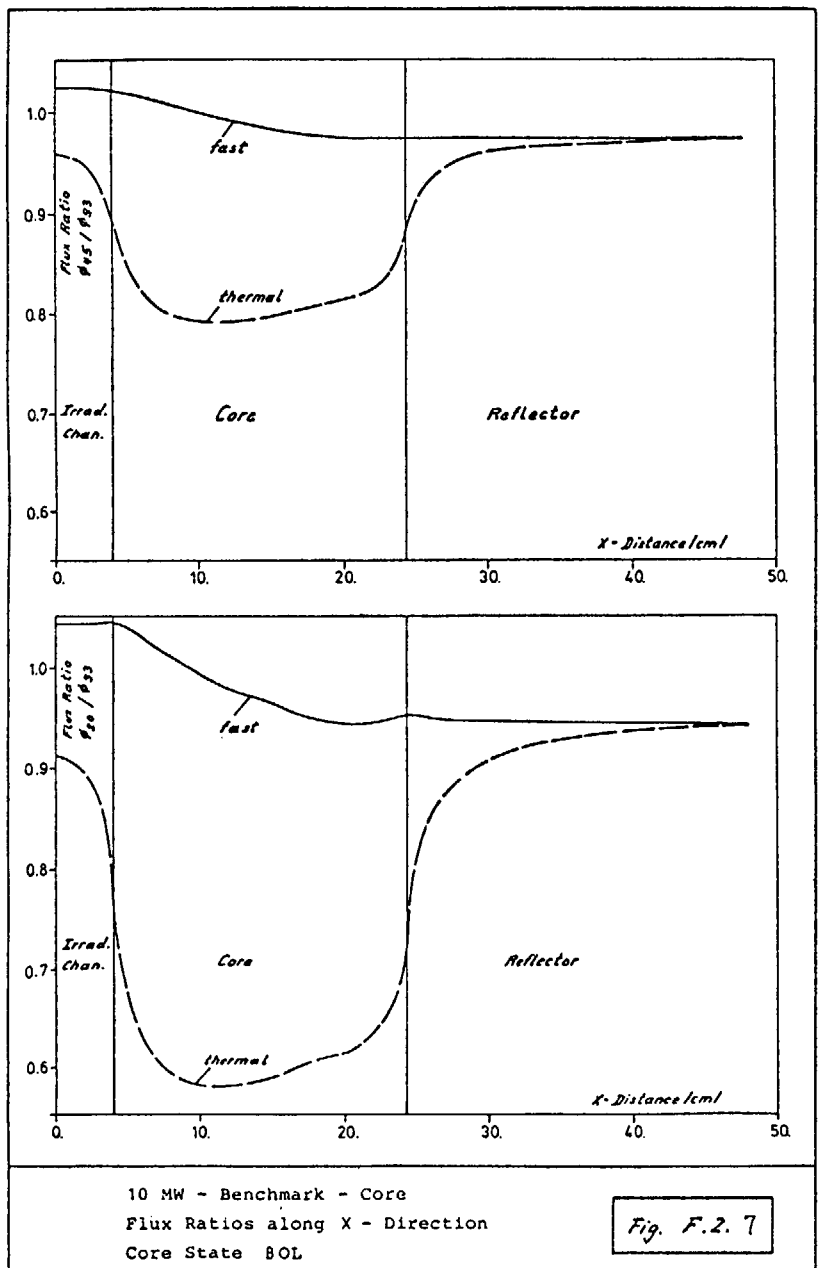

10 MW - Benchmark - Core
Flux Ratios along X - Direction
Core State BOL

Fig. F.2.7

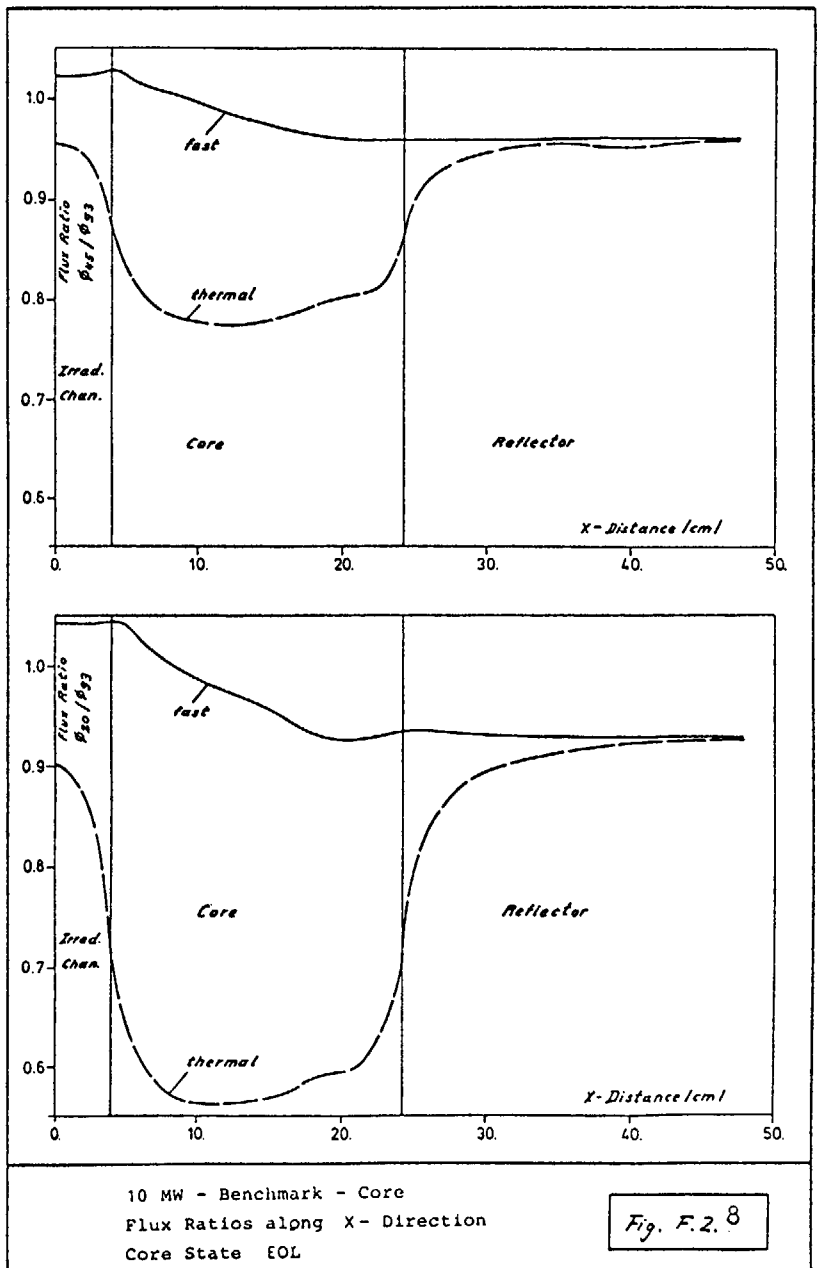

10 MW - Benchmark - Core
Flux Ratios along X- Direction
Core State EOL

Fig. F.2.8

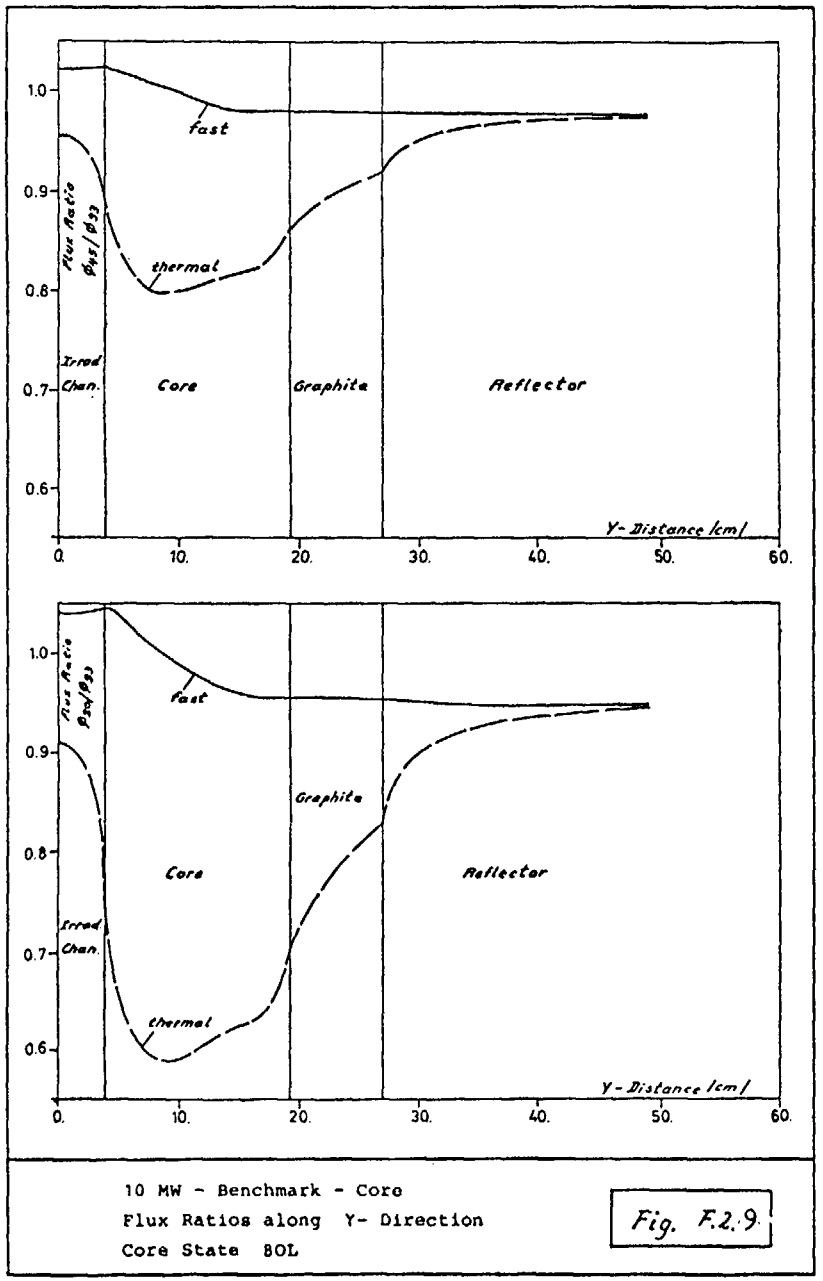

10 MW - Benchmark - Core
Flux Ratios along Y- Direction
Core State BOL

Fig. F.2.9

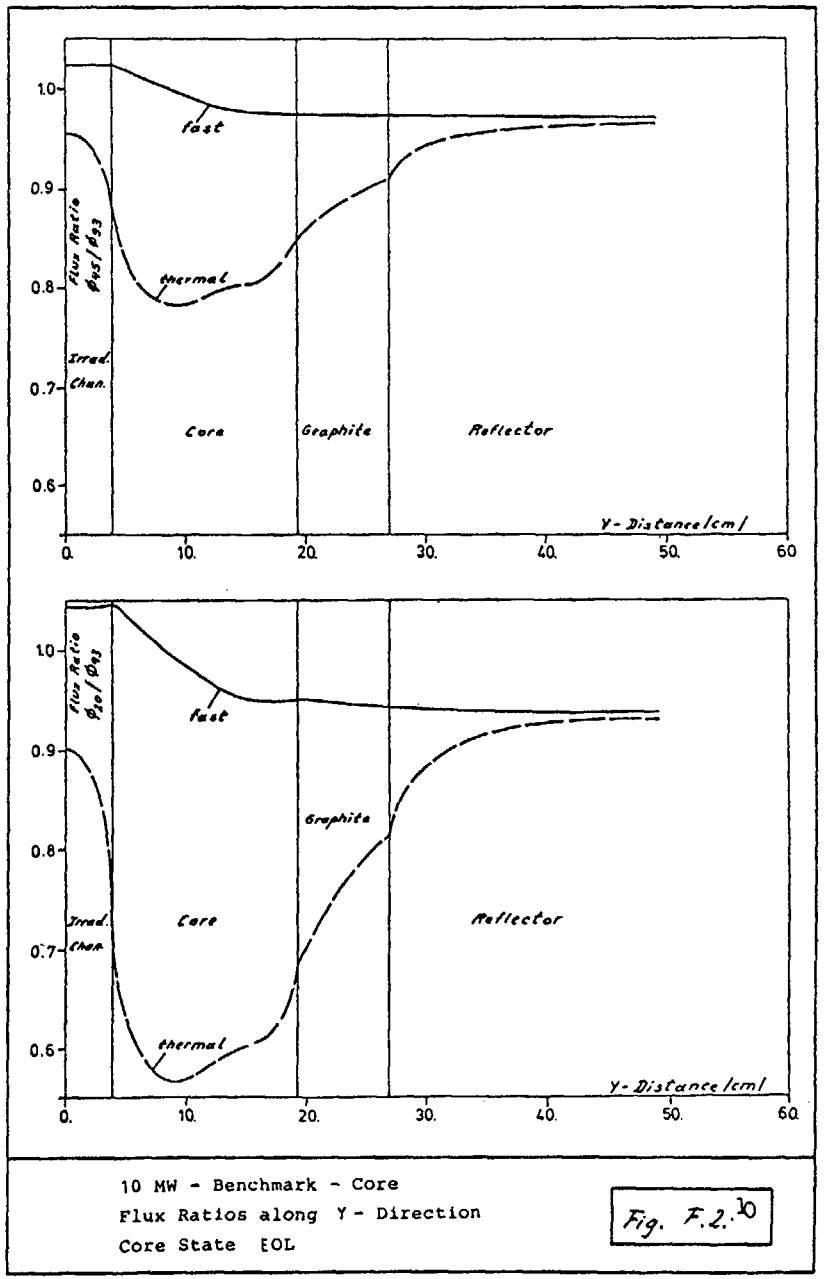

10 MW - Benchmark - Core
Flux Ratios along Y - Direction
Core State EOL

Fig. F.2.10

Each of the following figures compares the flux distributions at core midplane of the three fuels under consideration:

- Fig. F.2.11 to Fig. F.2.13 are the computer plotted flux distributions along the X-direction of the core at begin of life (BOL),

- Fig. F.2.14 to Fig. F.2.16 are the similarly plotted flux distributions along the Y-direction of Fig. 1 (App. F-0) at BOL,

- Fig. F.2.17 to Fig. F.2.22 repeat the whole information for the core state end of life (EOL).

A nomenclature of the figures is given by table F.2.1.

Because of the importance of the xenon content of the fuel for the calculation results Fig. F.2.23 demonstrates the xenon concentration (meat volume averaged) of the three fuels under consideration.

Moreover the plutonium present in a fuel element is given for the various enrichments at a burnup in MWd corresponding to the MWd at 50 % burnup for the high enriched fuel. These figures are

280 g U235/93 w/o U235	0.42 g Pu239/FA	0.54 g P_{tot}/FA
320 g U235/45 w/o U235	4.41 g Pu239/FA	5.44 g P_{tot}/FA
390 g U235/20 w/o U235	11.92g Pu239/FA	14.12g P_{tot}/FA

Table F.2.1
Nomenclature of Flux Figures

The flux figures show flux traverses (FLUSS-VERTEILUNG) of neutron fluxes in different energy groups.

These groups (Gruppen) are marked by numbers:

- 1. GRUPPE 10 MeV > E_n > 5.531 keV (fast flux)
  (this is a summing up of the 1. and 2. group calculated)

- 3. GRUPPE 5.531 keV > E_n > .625 eV (epithermal flux)

- 4. GRUPPE .625 eV > E_n (thermal flux)

All fluxes are given in absolute values based on a total power of 10 MW at core midplane.

The core state is described by

- End of Life or Begin of Life (EOL or BOL)
- Xenon-State (NO-XE = No Xenon, XE-EQUI = Xenon Equilibrium)
- Enrichment of the fuel (20 = 20 W/%-U5)

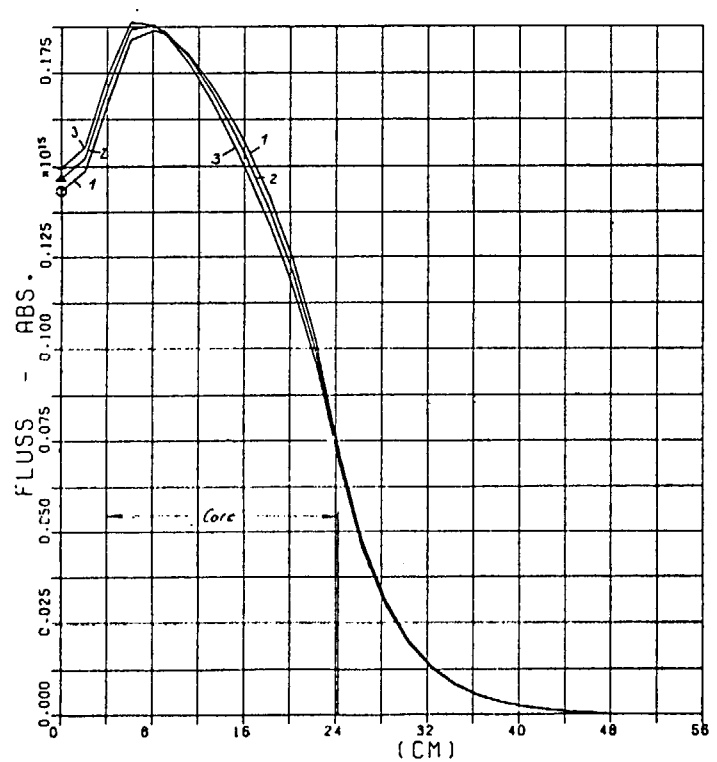

1 = HEU - fuel 280g U235/FE 93 % U235
2 = REU - fuel 1 320g U235/FE 45 % U235
3 = REU - fuel 2 390g U235/FE 20 % U235

IAEA-BENCHMARK 93-45-20 BOL-XE-EQUI
FLUX - DISTRIBUTION 1 . GRUPPE
10 MW - CASE X - DIRECTION

Fig. F.2.11

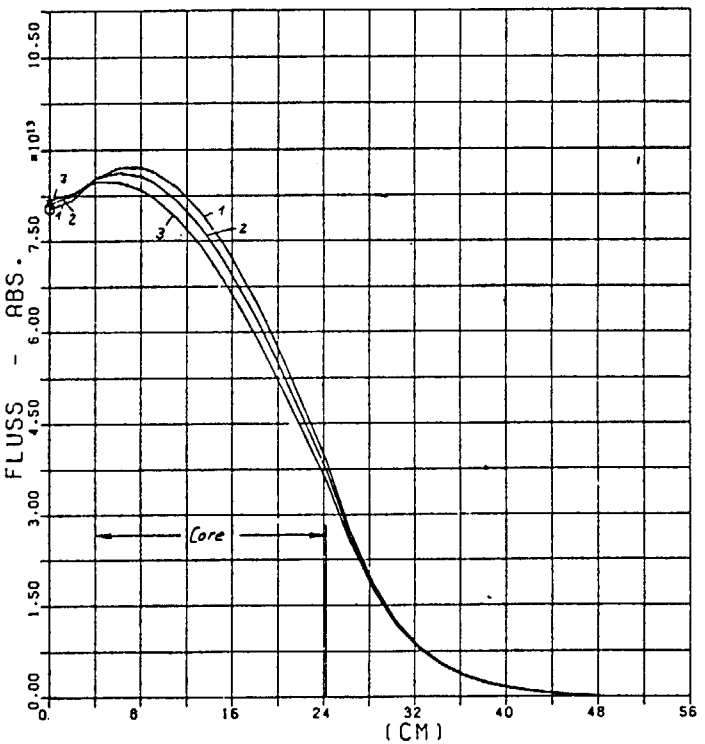

1 = HEU - fuel 280g U235/FE 93 % U235
2 = REU - fuel 1 320g U235/FE 45 % U235
3 = REU - fuel 2 390g U235/FE 20 % U235

IAEA-BENCHMARK 93-45-20 BOL-XE-EQUI
FLUX - DISTRIBUTION 3 . GRUPPE
10 MW - CASE X - DIRECTION

Fig. F.2.12

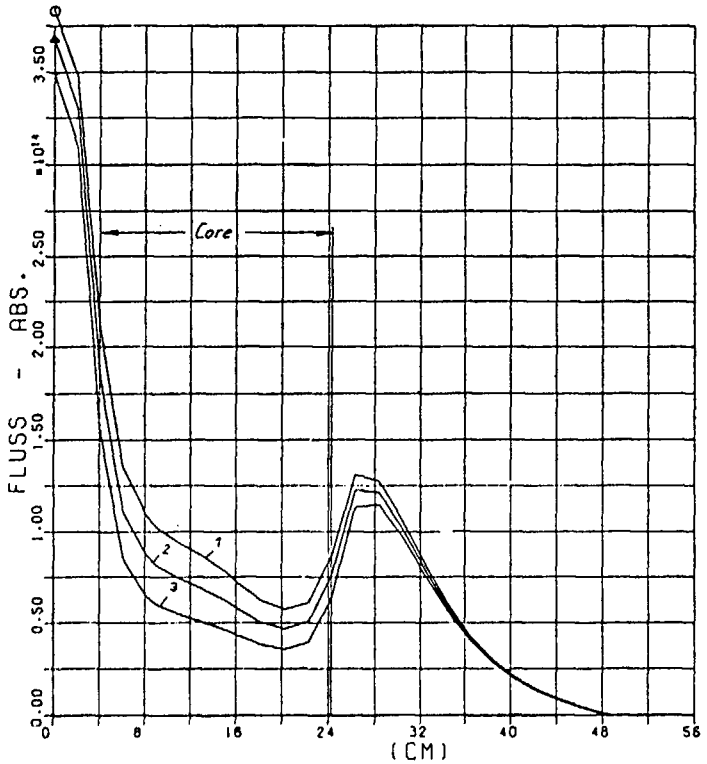

1 = HEU - fuel 280g U235/FE 93 % U235
2 = REU - fuel 1 320g U235/FE 45 % U235
3 = REU - fuel 2 390g U235/FE 20 % U235

IAEA-BENCHMARK 93-45-20 BOL-XE-EQUI
FLUX - DISTRIBUTION 4. GRUPPE
10 MW - CASE X - DIRECTION

Fig. F.2.13

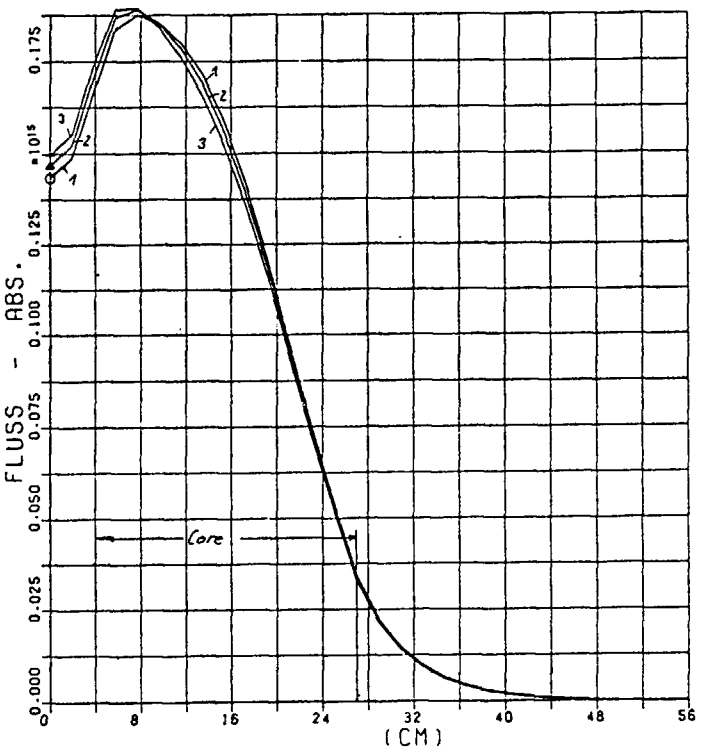

1 = HEU - fuel 280g U235/FE 93 % U235
2 = REU - fuel 1 320g U235/FE 45 % U235
3 = REU - fuel 2 390g U235/FE 20 % U235

IAEA-BENCHMARK 93-45-20 BOL-XE-EQUI
FLUX - DISTRIBUTION 1. GRUPPE
10 MW - CASE Y - DIRECTION

Fig. F.2.14

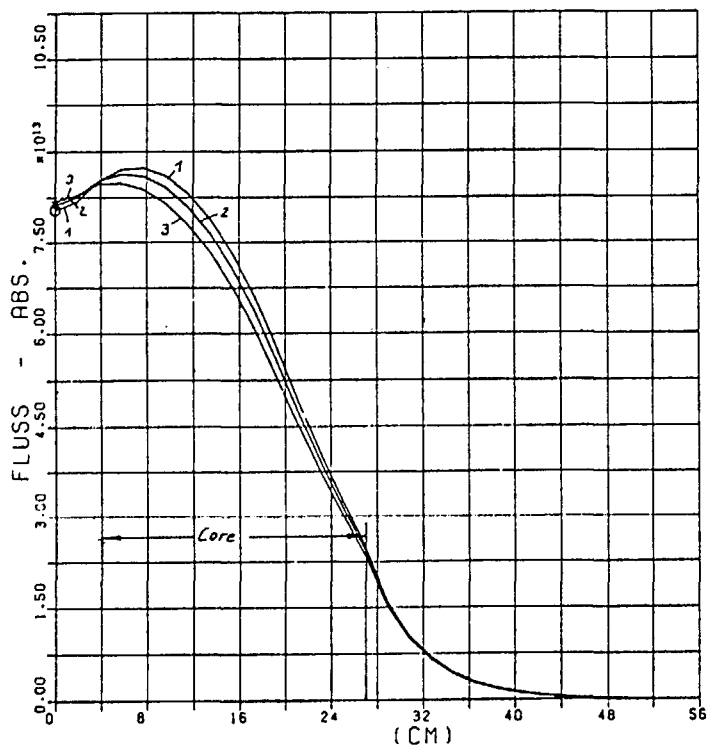

1 = HEU - fuel 280g U235/FE 93 % U235
2 = REU - fuel 1 320g U235/FE 45 % U235
3 = REU - fuel 2 390g U235/FE 20 % U235

IAEA-BENCHMARK 93-45-20 BOL-XE-EQUI
FLUX - DISTRIBUTION 3 . GRUPPE
10 MW - CASE y - DIRECTION

Fig. F.2.15

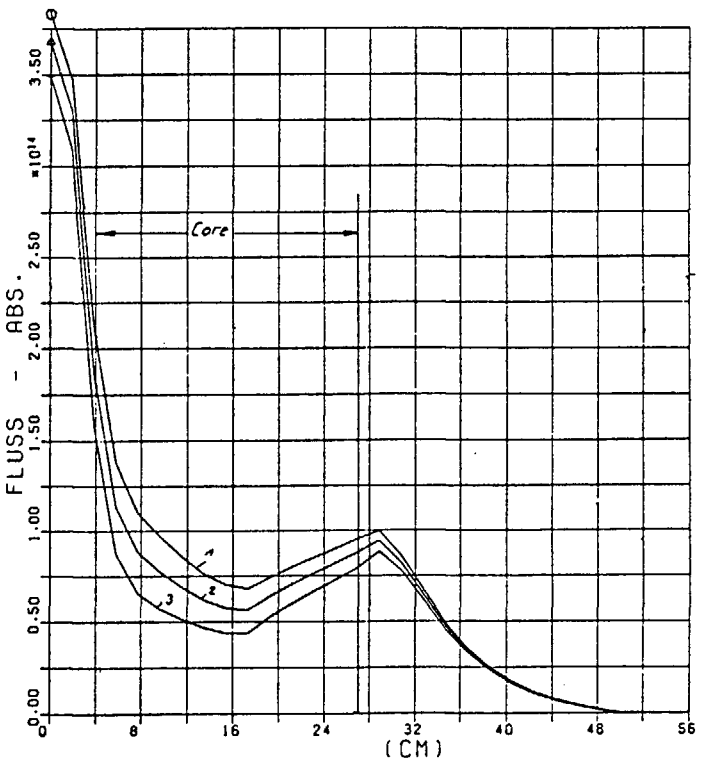

1 = HEU - fuel 280g U235/FE 93 % U235
2 = REU - fuel 1 320g U235/FE 45 % U235
3 = REU - fuel 2 390g U235/FE 20 % U235

IAEA-BENCHMARK 93-45-20 BOL-XE-EQUI
FLUX - DISTRIBUTION 4 . GRUPPE
10 MW - CASE y - DIRECTION

Fig. F.2.16

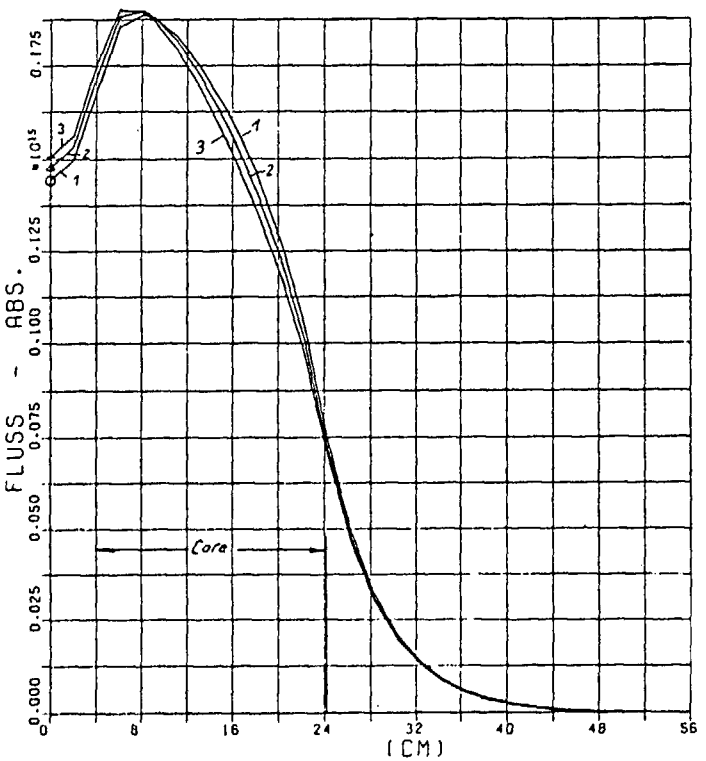

1 = HEU - fuel 280g U235/FE 93 % U235
2 = REU - fuel 1 320g U235/FE 45 % U235
3 = REU - fuel 2 390g U235/FE 20 % U235

IAEA-BENCHMARK 93-45-20 EOL-XE-EQUI
FLUX - DISTRIBUTION 1. GRUPPE
10 MW - CASE X - DIRECTION

Fig. F.2.17

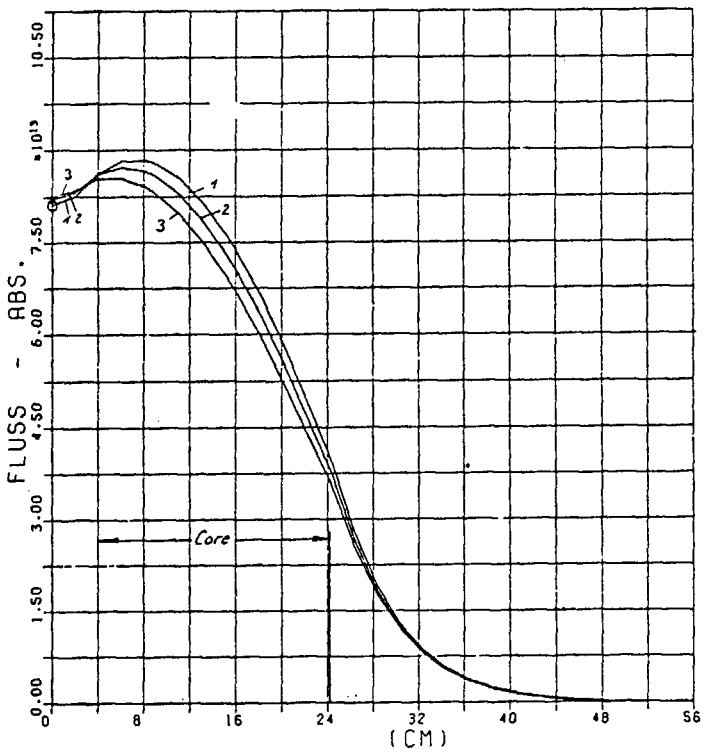

1 = HEU - fuel 280g U235/FE 93 % U235
2 = REU - fuel 1 320g U235/FE 45 % U235
3 = REU - fuel 2 390g U235/FE 20 % U235

IAEA-BENCHMARK 93-45-20 EOL-XE-EQUI
FLUX - DISTRIBUTION 3. GRUPPE
10 MW - CASE X - DIRECTION

Fig. F.2.18

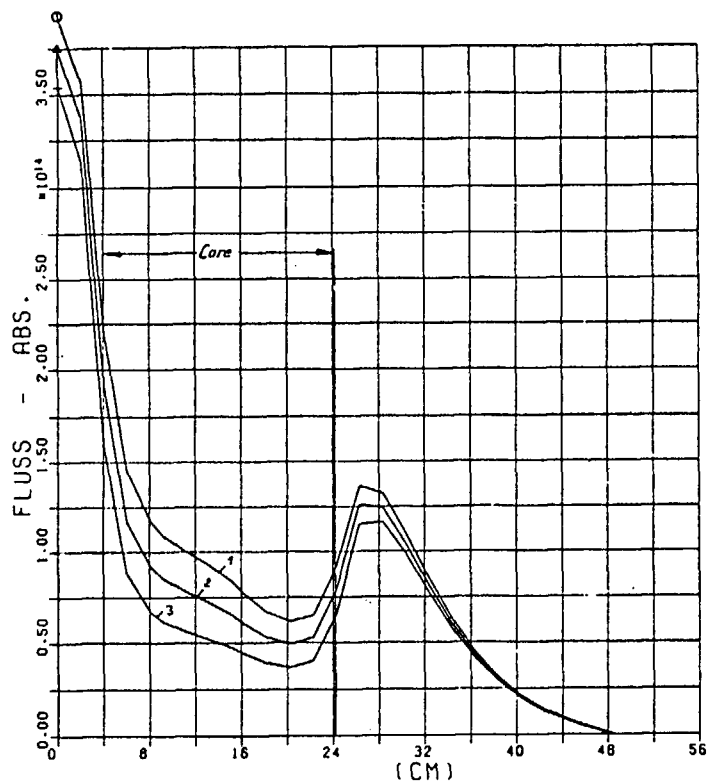

1 = HEU - fuel 280g U235/FE 93 % U235
2 = REU - fuel 1 320g U235/FE 45 % U235
3 = REU - fuel 2 390g U235/FE 20 % U235

IAEA-BENCHMARK 93-45-20 EOL-XE-EQUI
FLUX - DISTRIBUTION 4. GRUPPE
10 MW - CASE X - DIRECTION

Fig. F.2.19

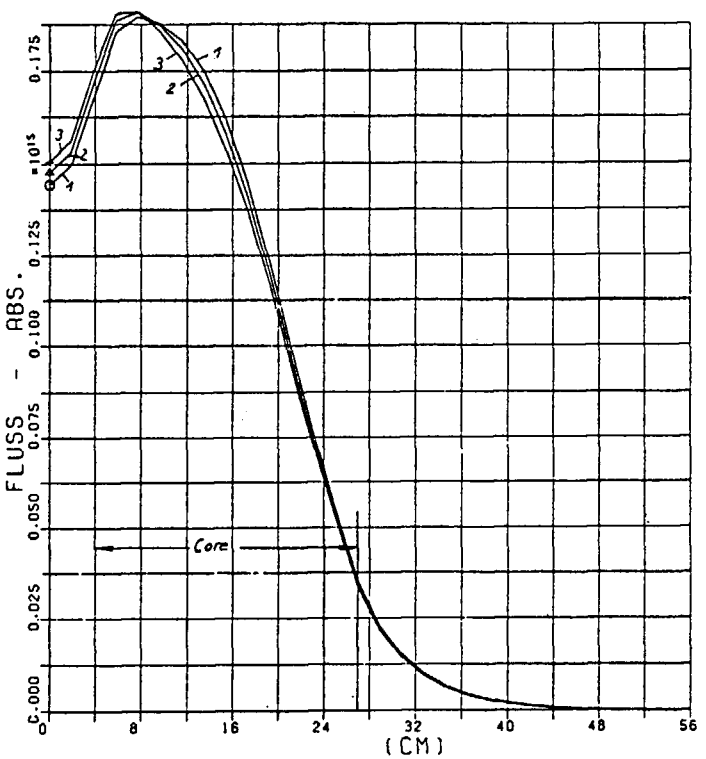

1 = HEU - fuel 280g U235/FE 93 % U235
2 = REU - fuel 1 320g U235/FE 45 % U235
3 = REU - fuel 2 390g U235/FE 20 % U235

IAEA-BENCHMARK 93-45-20 EOL-XE-EQUI
FLUX - DISTRIBUTION 1. GRUPPE
10 MW - CASE y - DIRECTION

Fig. F.2.20

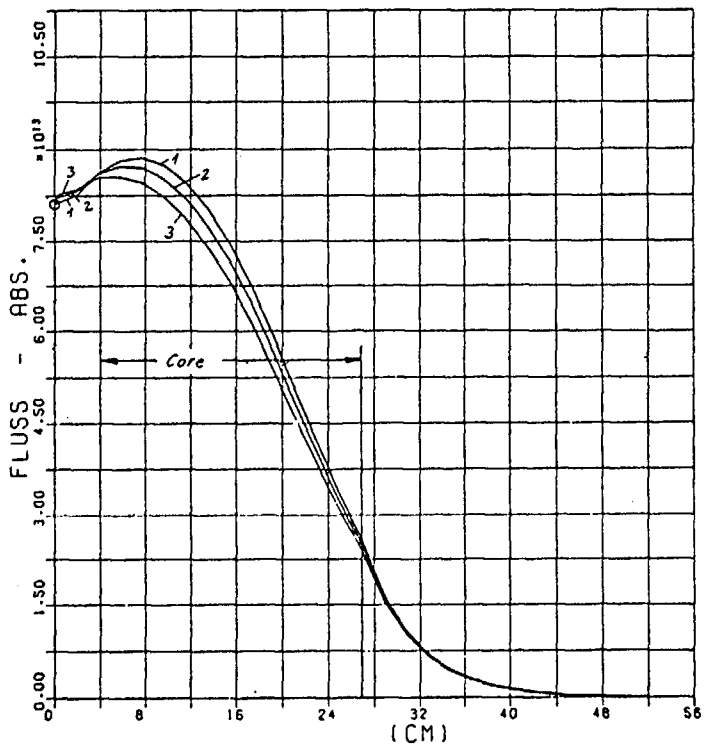

1 = HEU - fuel 280g U235/FE 93 % U235
2 = REU - fuel 1 320g U235/FE 45 % U235
3 = REU - fuel 2 390g U235/FE 20 % U235

IAEA-BENCHMARK 93-45-20 EOL-XE-EQUI
FLUX - DISTRIBUTION 3. GRUPPE
10 MW - CASE Y - DIRECTION

Fig. F.2.21

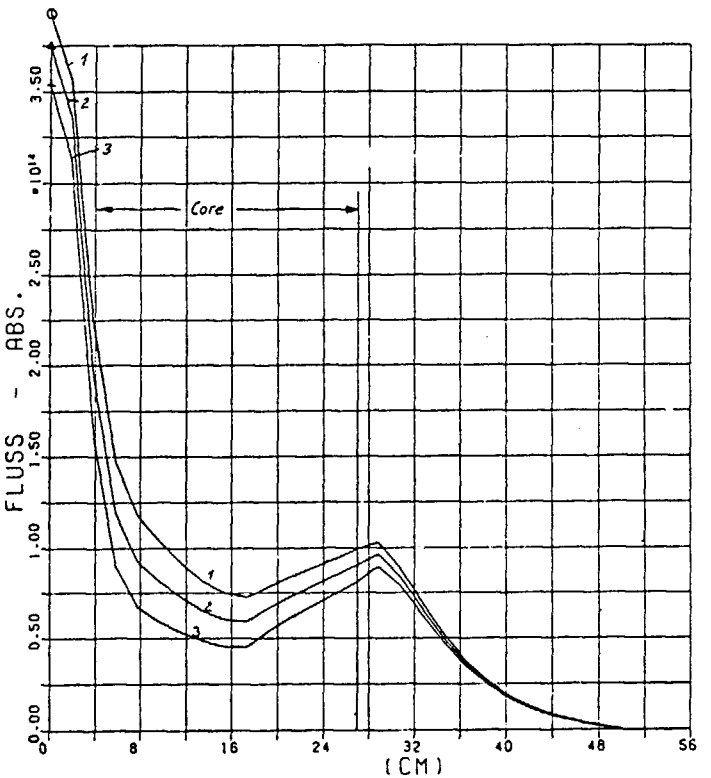

1 = HEU - fuel 280g U235/FE 93 % U235
2 = REU - fuel 1 320g U235/FE 45 % U235
3 = REU - fuel 2 390g U235/FE 20 % U235

IAEA-BENCHMARK 93-45-20 EOL-XE-EQUI
FLUX - DISTRIBUTION 4. GRUPPE
10 MW - CASE Y - DIRECTION

Fig. F.2.22

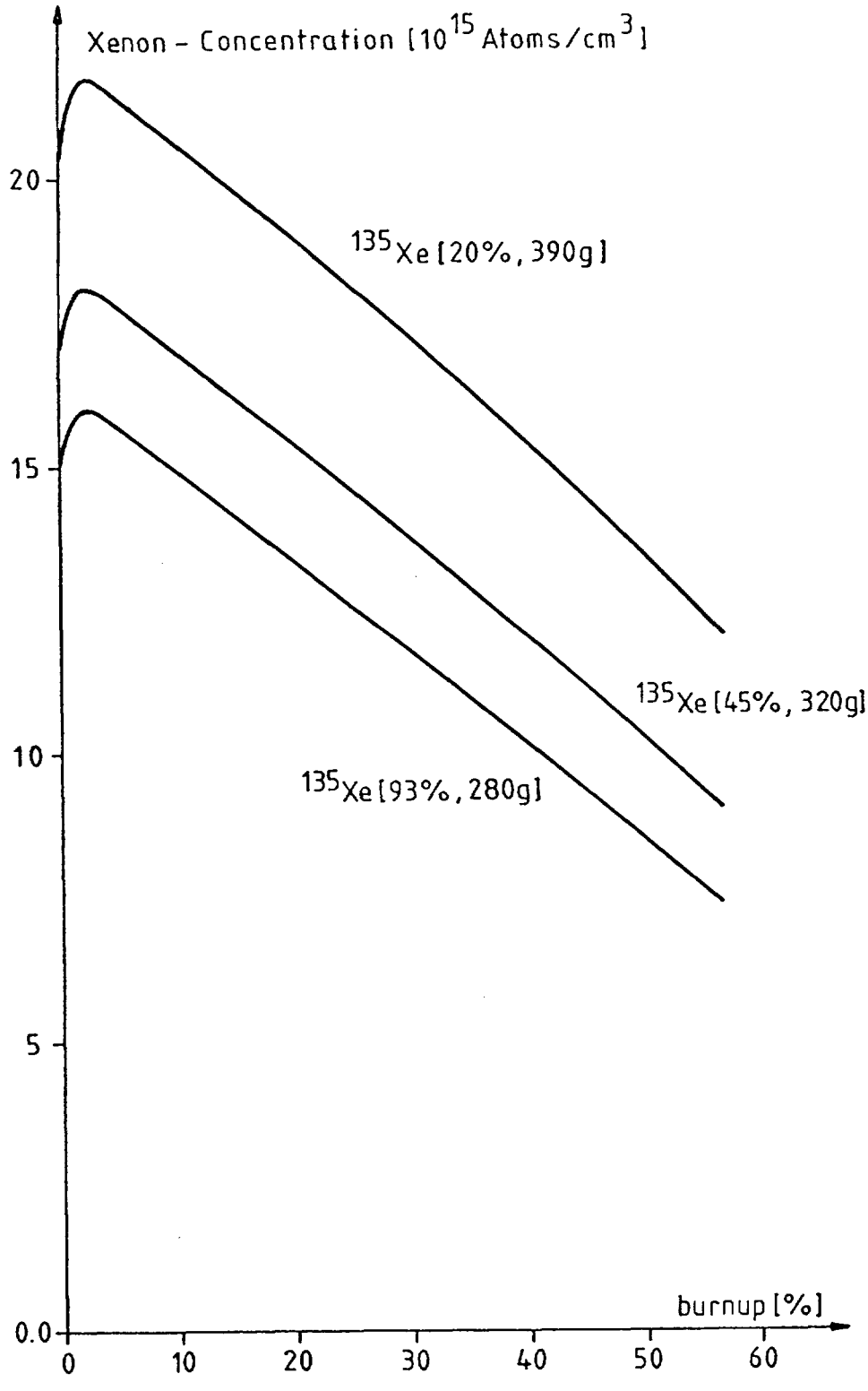

10 MW Benchmark Calculations
Xenon - Concentration vs. Burnup
normalized to the Meat-Volume of 441.635 cm^3

FIG.F.2.2.3

APPENDIX F-3

Benchmark-Calculations for MTR-Reactors

(Influence of Enrichment Reduction)

performed by

H. Winkler / J. Zeis

Department of SAPHIR

Eidg. Institut für Reaktorforschung
Würenlingen / Schweiz

January 1980

TABLE OF CONTENTS

1. INTRODUCTION

In order to compare the accuracy of the core calculations methods in different research centers, benchmark-problems were calculated with the methods used for the SAPHIR-reactor. The benchmark problems were specified during the Consultants Meeting on "Preparation of a Programme on Research Reactor Core Conversions to use LEU instead of HEU", IAEA, 19. ÷ 22. June 1979 in Vienna and are given in App. F-0.

This report describes the generation of the cross-section datas in funtion of burn up, the results of the two dimensional x-y diffusion calculations and some reactivity effects as void and Xe.

The main Core calculations are based on a 6 x 5 element core reflected by a graphite row on two side and surrounded by water. The standard-MTR-elements contain 23 fuel plates, value considered for enrichment were 93, 45 and 20% corresponding to a ^{235}U-content of 280, 320 g and 390 g respectively. The power was set at 10 MW. The main calculations were carried out with Xe-equilibrium at two thermal flux levels of 4,1 and $\sim 8{,}5 \cdot 10^{13} n \cdot cm^{-2} \cdot s^{-1}$. Various burn up conditions are considered as given in Appendix F-0 for the BOL and EOL cores.

2. CROSS SECTION DATA

The WIMS-D1 code (Ref. 1) was used to generate the cross section datas for the different enrichment (93, 45 and 20 %) in function of burn up in a 5 group condensation.

Spectrum version 2 has been used because it has been found to give better agreement between calculation and experiment.

The WIMS-Code uses 69 neutron energy groups to calculate the five groups cross sections, which energy ranges are given in Table 1.

A condensation to two groups constants is also available but this data can only be used for rough estimations. Earlier calculations executed for SAPHIR has shown that at least 4 neutron energy groups must be used to have an agreement between calculation and critical experiment.

The WIMS-Code calculates different geometries. A slab geometry (with symmetry) option was used. Fig. 1b shows the cell configuration.

2.1 Energy groups

For the calculation of the cross section 5 neutron energy groups were considered. Condensed 2 group data are also available. The energy groups are given in Table 1:

Table 1: Neutron energy range

1a) 5 Groups

Group	Energy range	WIMS-Groups
1	10 MeV ÷ 0,821 MeV	1 ÷ 5
2	821 keV ÷ 5,53 kEv	6 ÷ 15
3	5,53 keV ÷ 0,625 eV	16 ÷ 45
4	0,625 eV ÷ 0,14 eV	46 ÷ 55
5	0,14 eV ÷ 0 eV	56 ÷ 69

1b) 2 Groups

		> E <	
$\Phi_{1,2}$	fast	10 MeV ÷ 0,625 eV	1 ÷ 45
Φ_{th}	thermal	0,625 eV ÷ 0 eV	46 ÷ 69

1c) 3 Groups for flux condensation

$\Phi_{1,2}$	10 MeV ÷ 5,53 keV
Φ_3	5,53 keV ÷ 0,625 eV
Φ_{th}	0,625 eV ÷ 0 eV

2.2 Fuel cell and material concentration for standard 23-plate-element

In order to simplify the core calculations, the actual fuel plate has been modified to an artificial fuel cell with a meat zone homogenized over the entire width of the element.

As further simplification the side plate material (Aℓ) of the water gap with has been introduced homogeneously in the water gap.

The homogenizations of the fuel meat, which gives smaller Uranium concentrations, have to be taken into account if cross section values of different calculation methods are to be compared.

Fig. 1a shows the actual fuel cell and Fig. 1b the artificial homogenized cell.

Fig. 1a: Actual fuel cell

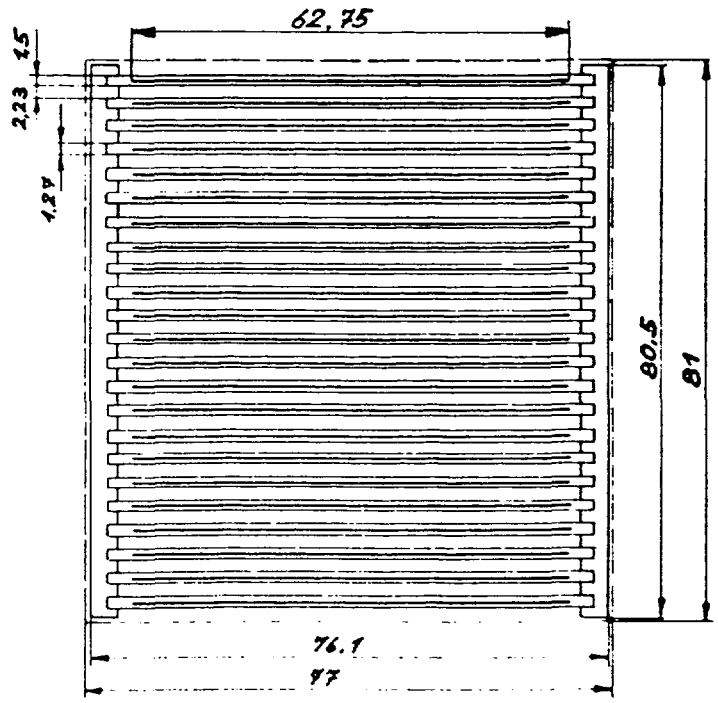

Fig. 1b: Homogenized fuel cell

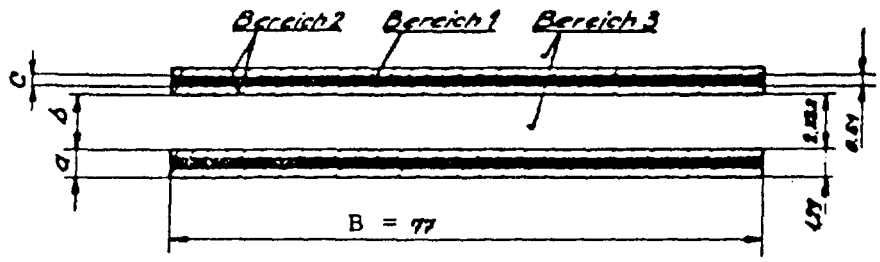

For the calculation of the weight portions of the different materials in the meatzone, the following relations are used:

$$U_{tot} = \frac{^{235}U}{\alpha}$$

$$^{238}U = U_{tot} - ^{235}U = ^{235}U \left(\frac{1}{\alpha} - 1\right)$$

$$Al_{tot} = U_{tot}\frac{(1-\beta)}{\beta} + 10{,}823\ g$$

α = enrichment
^{235}U = content per plate [g]

β = weight portion of U in the meat
10,823 g is the content of Al on outside of the meat

Densities:

$\rho_{H_2O} = 0{,}9982\ g \cdot cm^{-3}$

$\rho_{Al} = 2{,}70\ g \cdot cm^{-3}$

Atomic weights: $^{235}U = 235{,}0439\ g \cdot mol^{-1}$
$^{238}U = 238{,}0508\ g \cdot mol^{-1}$
$Al = 26{,}98154\ g \cdot mol^{-1}$
$A = 6{,}0248 \cdot 10^{23} mol^{-1}$

The considered volumes and material densities of the different zones of the fuel cell are given in Tables 2a & 2b for all three enrichments.

Table 2a: Material values of a fuel cell for different enrichments

Zone	Volume [cm³]	Material	Material densities [g·cm⁻³]			Material per plate [g]		
			93%	45%	20%	93%	45%	20%
Meat	(0,051x7,7x60) 23,562	^{235}U	0,5167	0,5905	0,7197	12,174	13,913	16,957
		^{238}U	0,0389	0,7771	2,8786	0,917	17,005	67,826
		Al	2,549	2,428	1,859	60,070	57,200	43,794
		U_{tot}	0,5556	1,3122	3,5983	13,091	30,918	84,783
Canning	(0,039x7,7x60) 18,018	Al	2,668			2 x 48,080		
Moderator	(0,2232x7,7x60) 103,118	Al	0,316			32,543		
		H_2O	0,870			89,699		

Table 2b: Atomic Concentration

Zone	^{235}U [g]	93/280	45/320	20/390
Meat	$A_{U^{35}}/cm^3$	1,3244E+21	1,5136E+21	1,8447E+21
	$A_{U^{38}}/cm^3$	9,8425E+19	1,8266E+21	7,2855E+21
	A_{Al}/cm^3	5,6927E+22	5,4208E+22	4,1510E+22
Canning	A_{Al/cm^3}:	5,960E+22		

Moderator	A_{Al/cm^3}	A_{H/cm^3}	A_{O/cm^3}	
	7,054E+21	5,884E+22	2,942E+22	

2.3 Control element

The layout of the control element is given in Fig. 2 and the homogenized fictive cell in a control element in Fig. 3.

Fig. 2: Control element

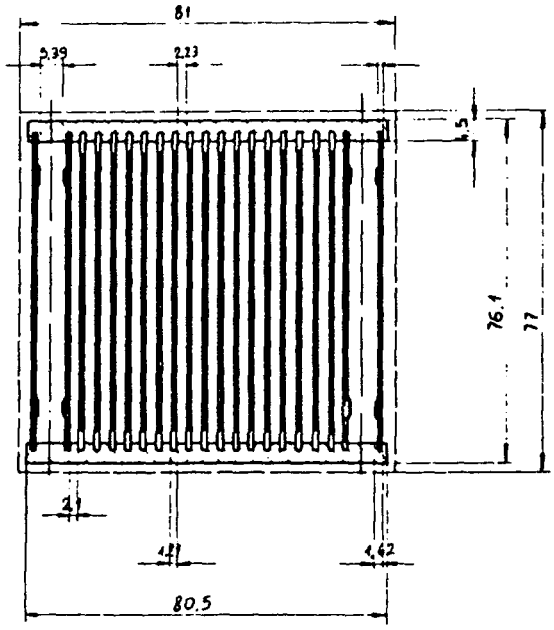

Fig. 3: Control element cell

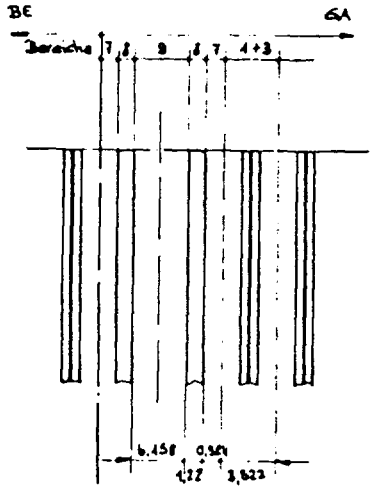

The material densities in the fuel plates are the same as in the standard element. Therefore only the material densities for the guide plates and the control rod gap are given in Table 3. For the calculation of the homogenized cross section one has chosen the half of a control element with centered control rod gap. The calculation has been done without control blade (control rod completely withdrawn).

Table 3: Material density (Control element)

Zone	Volume	Material	Densitiy [g·cm^{-3}]	Atoms/cm^3
Fuel plate	see Table 2a + b			
Guide plate		Aℓ	2,668	5,96 E+22
control rod		Aℓ	0,316	Aℓ: 7,054 E+21
gap		H_2O	0,879	H: 5,884 E+22
				O: 2,942 E+22

From these input data, the cross sections for the standard and control element is calculated for a burn up range from 0 to 55% of initial ^{235}U content in steps of ∿ 5%

2.4 Results of WIMS-Calculation

The WIMS cross-section calculations has been executed for two flux levels. In a first step a initial thermal flux of $7,1 \cdot 10^{13}$ corresponding to the max. flux in the fuel has been choosen. During WIMS-burn up calculation this flux rises to about $1,2 \cdot 10^{14}$.

A second WIMS calculation has been done with constant thermal flux during burn up of about $4,1 \cdot 10^{13}$ corresponding to the mean core flux of the 20% enriched case. As can be seen (Table 7) the differences due to Xe-poisoning of both flux values is small and is in the order of $\frac{\Delta K}{K}$ ∿ 0,4 ÷ 0,7% for the K_{eff} of the core reactivity.

2.5 Results of the WIMS-D1-cell calculation

From the burn up calculations with the code WIMS all influenced material densities, production of fission products including Xe and Sm, the transuranium as Pu as well as K_∞ and the cross section and scattering matrix for 5 and 2 neutron energy groups are obtained. Some of the results are given in the following tables and figures:

Table 4: Two group cross section for standard fuel cell
($\Phi \sim 4{,}1 \cdot 10^{13} n \cdot cm^{-2} \cdot s^{-1}$)

enrichment	burn up %	D	Σ_a	$\nu\Sigma_f$	Σ_s	K_∞
93 %	0	1,474+0 3,021-1	3,436-3 9,779-2	4,661-3 1,762-1	2,626-2	1,74966
	5,03	1,475+0 3,025-1	3,385-3 9,852-2	4,442-3 1,672-1	2,629-2	1,65295
	10,05	1,475+0 3,015-1	3,327-3 9,529-2	4,218-3 1,599-1	2,633-2	1,63160
	30,14	1,476+0 2,969-1	3,082-3 8,138-2	3,313-3 1,295-1	2,650-2	1,53674
	50,06	1,478+0 2,912-1	2,798-3 6,624-2	2,406-3 9,692-2	2,670-2	1,405618
45 %	0	1,464+0 3,043-1	4,894-3 1,076-1	5,268-3 1,960-1	2,515-2	1,700571
	5,00	1,464+0 3,048-1	4,848-3 1,090-1	5,040-3 1,870-1	2,518-2	1,607060
	9,97	1,465+0 3,083-1	4,802-3 1,060-1	4,811-3 1,800-1	2,521-2	1,586979
	29,77	1,466+0 2,994-1	4,627-3 9,255-2	3,866-3 1,499-1	2,531-2	1,498301
	49,52	1,468+0 2,939-1	4,425-3 7,704-2	2,894-3 1,162-1	2,543-2	1,380974
20 %	0	1,448+0 3,069-1	6,935-3 1,241-1	6,448-3 2,287-1	2,374-2	1,635652
	5,00	1,449+0 3,074-1	6,899-3 1,268-1	6,202-3 2,198-1	2,376-2	1,545050
	9,94	1,449+0 3,064-1	6,871-3 1,243-1	5,955-3 2,134-1	2,377-2	1,525530
	29,29	1,451+0 3,021-1	6,823-3 1,123-1	4,957-3 1,849-1	2,374-2	1,440267
	48,36	1,453+0 2,974-1	6,746-3 9,726-2	3,909-3 1,512-1	2,374-2	1,338159

Table 4.1: WIMS-five and two group reflector constants

Group	D	Σ_a	Scattering Matrix 2	3	4	5
Be-Metall						
1	1.5005E+0	-8.762E-03	6.743E-02	0	0	0
2	6.1076E-1	1.043E-07	0	1.8035E-02	0	0
3	4.8642E-1	3.288E-04	0	0	1.5964E-02	6.0361E-06
4	4.7663E-1	2.385E-04	0	1.2691E-03	0	8.3076E-02
5	4.4078E-1	6.307E-04	0	0	6.722E-03	0
1	77.028E-02	-20.302E-04		6.1550E-03		
2	44.790E-02	55.285E-05				
Graphite						
1	2.3405E+0	6.189E-06	2.1504E-02	0	0	0
2	1.1680E+0	3.733E-09	0	6.7808E-03	0	0
3	9.3549E-1	1.161E-05	0	0	6.1520E-03	5.5400E-06
4	9.2523E-1	8.483E-05	0	1.0298E-03	0	3.4275E-02
5	8.7538E-1	2.262E-04	0	0	3.7390E-03	0
1	1.4018E+0	5.857E-06	2.216E-02			
2	8.8595E-01	1.9624E-04				
H_2O						
1	2.2689E+0	4.5922E-04	1.099E-1	6.831E-04	0	0
2	7.7382E-1	2.2340E-07	0	1.546E-01	1.258E-05	2.588E-06
3	5.5922E-1	9.7135E-04	0	0	1.203E-01	2.394E-02
4	2.9027E-1	6.9856E-03	0	2.237E-03	0	7.262E-01
5	1.4807E-1	1.9285E-02	0	0	3.971E-02	0
1	11.518E-01	48.763E-05	5.1658E-02			
2	16.525E-02	17.799E-03				

Table 5 gives the values of K_∞ in function of burn up for the three enrichment and two thermal fluxes of $\Phi \tilde{=} 4{,}1 \cdot 10^{13}$ resp. $\sim 8{,}5 \cdot 10^{13}$ n $cm^{-2} \cdot s^{-1}$. These fluxes correspond approx. to the mean flux, resp. the maximum flux in the fuel region of the benchmark core configuration. For the given MWd-figures not only the burned ^{235}U is considered but also the burn up of the produced Pu-239 and Pu-241. In order to calculate the energy production in MWd a total of 23,956 standard elements (21 standard and 5 control-elements) and 1,25 g/MWd fissionable material is considered.

Table 5a: K_∞ in function of burn up and enrichment
($\Phi_{th} = 4{,}1 \cdot 10^{13}$ n·cm^{-2}·s^{-1})

93%			45%			20%		
% U^{35}	burn up MWd	K_∞	% U^{35}	burn up MWd	K_∞	% U^{35}	burn up MWd	K_∞
0	0	1,74966	0	0	1,70057	0	0	1,63565
5,03	270	1,65295	5,0	308	1,60706	5,0	379	1,54505
10,05	540	1,63160	9,97	617	1,58698	9,94	759	1,52553
15,08	810	1,61012	14,95	926	1,56640	14,83	1140	1,50518
20,11	1081	1,58678	19,89	1236	1,54459	19,67	1521	1,48411
25,13	1351	1,56347	24,85	1549	1,52286	24,50	1908	1,46322
30,14	1620	1,53674	29,77	1861	1,49830	29,29	2295	1,44027
35,14	1889	1,50935	34,74	2178	1,47370	34,13	2694	1,41806
40,12	2158	1,47767	39,66	2495	1,44509	38,90	3112	1,39245
45,09	2426	1,44457	44,6	2815	1,41523	43,60	3490	1,36581
50,06	2694	1,40562	49,52	3156	1,38097	48,36	3900	1,33859
						53,03	4310	1,30738

Table 5b: K_∞ in function of burn up and enrichment
($\Phi_{th} \sim 8{,}5 \cdot 10^{13}$ n·cm^{-2}·s^{-1})

93%			45%			20%		
% U^{35}	burn up MWd	K_∞	% U^{35}	burn up MWd	K_∞	% U^{35}	burn up MWd	K_∞
0	0	1,74966	0	0	1,70057	0	0	1,63565
5,03	270	1,64621	5,02	309	1,60010	5,2	394	1,53787
10,05	540	1,62515	10,0	617	1,58023	10,32	785	1,51773
15,06	809	1,60334	14,95	925	1,55965	15,37	1175	1,49683
20,07	1078	1,58039	19,87	1232	1,53817	20,36	1565	1,47512
25,07	1347	1,55594	24,76	1538	1,51567	25,27	1953	1,45265
30,05	1615	1,52967	29,60	1843	1,49165	30,11	2346	1,42932
35,03	1883	1,50118	34,42	2149	1,46614	34,88	2726	1,40508
39,99	2150	1,47003	39,25	2453	1,43879	39,57	3110	1,37983
44,94	2417	1,43565	43,95	2757	1,40928	44,20	3494	1,35351
49,88	2683	1,39739	48,65	3059	1,37724	48,74	3876	1,32580
54,81	2949	1,35434	53,32	3362	1,34226	53,20	4256	1,29645

Fig. 4 gives the dependence of K_∞ as function of burn up in % of the initial U.235 content, whereas Fig. 5 shows K_∞ as function of the MWd for the whole core (23.956 standard element).
Fig. 6 shows the Pu content in a standard fuel element whereas in Fig. 7a and 7b the Xe-concentration is given for the two flux values.
Table 6 gives some atom densities in the fuel meat of the homogenized fuel cell. A calculation error has been detected in the Aluminium density of the meat. A recalculation of K_{eff} with the correct Al density has given no significant differences in the result. The error of K_∞ is less than 0,003, and $\Delta K_{eff} < 0{,}15\%$.

Table 6: Atom densities in fuel meat vs. burn up

Atom densities $[cm^{-3} \cdot 10^{24}]$, $\Phi_{th} = 4,1 \cdot 10^{13} n \cdot cm^{-2} \cdot s^{-1}$

93 %	0 %	5,03%	10,05%	20,11%	30,14%	50,06%
Al-27 *	4,7114-2					4,7114-2
Xe-135	0	1,295-8	1,237-8	1,106-8	9,638-9	6,872-9
Sm-149	0	1,164-7	1,167-7	1,145-7	1,089-7	8,975-8
U-235	1,3244-3	1,258-3	1,191-3	1,058-3	9,252-4	6,615-4
U-236	0	1,136-5	2,261-5	4,481-5	6,646-5	1,079-4
U-238	9,8425-5	9,803-5	9,763-5	9,680-5	9,595-5	9,414-5
Pu-239	0	3,674-7	6,983-7	1,248-6	1,651-6	2,060-6
Pu-240	0	7,042-9	2,694-8	9,719-8	1,952-7	4,265-7
Pu-241	0	3,095-10	2,366-9	1,699-8	5,026-8	1,702-7
Pu-242	0	2,685-12	4,324-11	6,952-10	3,472-9	2,596-8
45 %	0 %	5,00%	9,97%	19,89%	29,77%	49,52%
Al-27 *	4,4397-2					4,4397-2
Xe-135	0	1,501-8	1,414-8	1,312-8	1,158-8	8,473-9
Sm-149	0	1,349-7	1,367-7	1,368-7	1,323-7	1,123-7
U-235	1,5136-3	1,438-3	1,363-3	1,213-3	1,063-3	7,639-4
U-236	0	1,311-5	2,604-5	5,144-5	7,618-5	1,238-4
U-238	1,8266-3	1,822-3	1,817-3	1,808-3	1,798-3	1,776-3
Pu-239	0	4,152-6	7,896-6	1,417-5	1,891-5	2,419-5
Pu-240	0	8,181-8	3,109-7	1,111-6	2,224-6	4,883-6
Pu-241	0	3,900-9	2,963-8	2,106-7	6,207-7	2,103-6
Pu-242	0	3,413-11	5,443-10	8,610-9	4,269-8	3,184-7
20 %	0%	5,00 %	9,94%	19,67%	29,29%	48,36%
Al-27 *	3,1692-2					3,1692-2
Xe-135	0	1,904-8	1,841-8	1,709-8	1,539-8	1,173-8
Sm-149	0	1,698-7	1,749-7	1,804-7	1,792-7	1,597-7
U-235	1,8447-3	1,752-3	1,661-3	1,482-3	1,304-3	9,526-4
U-236	0	1,639-5	3,243-5	6,356-5	9,365-5	1,509-4
U-238	7,2855-3	7,273-3	7,260-3	7,233-3	7,204-3	7,141-3
Pu-239	0	1,138-5	2,162-5	3,878-5	5,201-5	6,799-5
Pu-240	0	2,358-7	8,852-7	3,092-6	6,100-6	1,320-5
Pu-241	0	1,283-8	9,639-8	6,756-7	1,928-6	6,362-6
Pu-232	0	1,147-10	1,801-9	2,751-8	1,327-7	9,427-7

Meat volume: 23,562 cm^3

* This values should be higher according to Table 2b

3. CORE-CALCULATIONS

3.1 Configuration and code

For the reactor core configuration a two dimensional diffusion code CODIFF of the programme Boxer ([2]) is used. This code has been developed by the Swiss Federal Institut of Reactor Research for the calculation of light water reactors and is adapted to MTR-calculations. The calculation has been effected with 5 energy groups and the flux results condensed to two and three groups according to Table 1.

The calculated benchmark core configuration is shown in Fig. 8a (BOL) and 8b (EOL) for two different burn up states of the element. In Fig. 9 the typical CODIFF-calculation scheme for the core is given together with the dimensions of the mesh point distribution. In the x and y direction 42 and 46 respectively mesh points have been used. The reactor core, including graphite rows, is reflected on all sides by water with a thickness corresponding to three elements each.

The third dimension is given from the vertical buckling of $B_z^2 = 1{,}7087 \cdot 10^{-3} \cdot cm^{-2}$ corresponding to a reflector saving of 8,0 cm. ($H_{extr.}$ 76,0 cm).

3.2 Results of benchmark calculations

The CODIFF-calculations gives the effective multiplication factor (K_{eff}) of the core configuration, the horizontal mean power distribution (linear power in $W \cdot cm^{-3}$) and the corresponding flux distribution of the 5 neutron energy groups as well as the condensated 2 and 3 group fluxes for the choosen total power of 10 MW. The calculation is made in Xe-equilibrium for each burn up and two fluxes, corresponding to mean and maximum flux respectively in the fuel region. ($4{,}1 \cdot 10^{13}$ and $\sim 8{,}5 \cdot 10^{13} n \cdot cm^{-2} \cdot s^{-1}$).

3.2.1 K_{eff} of EOL and BOL core

A calculation of the fresh core without any burn up is given for comparison reasons only.
The calculated multiplication factor K_{eff} for the three enrichment and the different burn up states (BOL, EOL and fresh core) are given for both flux values in Table 7. The differences in K_{eff} is due to the different Xe and Sm content.
Fig. 10 shows the changement of K_{eff} in function of burn up in MWd. Linear extrapolation is used between the burn up states.

Table 7: Value of K_{eff} from two dimensional diffusion calculation

Enrichment	Core definition	Operation time MWd	K_{eff} ϕ=4,1·10¹³	K_{eff} ϕ=8,1÷8,9·10¹³
93 %	fresh core	) ∿ 1300	1.1939413	
	BOL	) 268	1,036826	1,032204
	EOL		1,013799	1,009607
	mean bu 30%		-	1,033061
45 %	fresh core	) ∿ 1460	1.179125	
	BOL	) 298	1,030593	1,026669
	EOL		1,009911	1,006831
	mean bu 30%		-	1,026824
20 %	fresh core	) ∿ 1800	1.15937	
	BOL	) 369	1,017854	1,010724
	EOL		0,999954	0,992637
	mean bu 30%		-	1,009895

BOL = Beginn Of Life definition, mean bu over core ∿ 24%

EOL = End Of Life definition, mean bu over core ∿ 29%.

3.2.2 Flux of BOL and EOL core

Table 8 presents some fluxes from the CODIFF calculation. The fluxes in the fuel region are averaged both over the x-y plane and over the axial direction which has a chopped cosine distribution. The notation Φ_f refers to the flux from 0,625 eV to 10 MeV, Φ_{th} refers to the flux below 0,625 eV and Φ_3 from the flux from 0,625 eV to 5,53 keV.

The fluxes in the irradiation position (flux trap) are averaged over the same three dimensions in the water gap.

For the determination of the effective mid-plane flux or the flux in every vertical position, a normalized vertical flux distribution is given in Fig. 11. This curves has been calculated for several control rod positions with stuck rod operation (^{6}). The flux distribution has been normalized to:

$$\varphi(z) = \frac{\Phi(z)}{\Phi_{max}} \cdot \beta$$

where

$$\beta = \frac{P_{max}(z)}{\bar{P}(z)}$$

$P(z)$ = vertical power distribution in fuel

The factor β depends on a non linear way from the control rod position, mainly if stuck rod operation is used.

Fig. 12 to 15 shows the flux distribution (vertical average) for the x and y axis for the BOL and EOL core for 93% enrichment. Finally figures 16 to 23 shows the ratios of the 45% (20% resp.) and 93% enrichment fast, epithermal and thermal fluxes along the two axis. In Table 8.1 and 8.2 the corresponding flux ratios are given for x-direction.

For the graphical flux representation the condensation of neutron groupes has been choosen as discussed in the Vienna meeting of September 10, 1979 of the IAEA advisory group for conversion of research reactors. The fluxes $\Phi_{1,2}$, Φ_3, Φ_{th} have the following neutron energy limits:

$\Phi_{1,2}$ 10 MeV > E > 5,531 keV

Φ_3 5,53 keV > E > 0,625 eV

Φ_{th} 0,625 eV > E > 0.

Table 8: Fluxes from CODIFF calculations
$(n \cdot cm^{-2} \cdot s^{-1})$

Case	Core average fluxes (fuel)			Flux trap average			Flux trap center average	
	Φ_f	Φ_3	Φ_{th}	Φ_f	Φ_3	Φ_{th}	Φ_f	Φ_{th}
93% BOL	1,683+14	5,357+13	5,922+13	1,694+14	6,159+13	2,220+14	1,566+14	2,637+14
93% EOL	1,720+14	5,504+13	6,326+13	1,714+14	6,237+13	2,285+14	1,583+14	2,700+14
45% BOL	1,680+14	5,292+13	5,071+13	1,716+14	6,193+13	2,135+14	1,587+14	2,573+14
45% EOL	1,713+14	5,400+13	5,378+13	1,734+14	6,267+13	2,188+14	1,604+14	2,627+14
20% BOL	1,678+14	5,181+13	4,026+13	1,743+14	6,237+13	2,025+14	1,615+14	2,492+14
20% EOL	1,707+14	5,268+13	4,224+13	1,763+14	6,313+13	2,068+14	1,633+14	2,537+14

For mid plane flux multiply Φ-values with 1,29 (see Fig. 11)

Φ_f 10 MeV > E > 0,625 keV
Φ_3 5,53 keV > E > 0,625 eV
Φ_{th} 0,625 eV > E > 0

Table 8.1: Flux ratios in x-Direction for 45% enrichtment

Pos.	Distance [cm]	BOL - Core $\frac{\Phi_{1,2}^{45}}{\Phi_{1,2}^{93}}$	BOL - Core $\frac{\Phi_{3}^{45}}{\Phi_{3}^{93}}$	BOL - Core $\frac{\Phi_{th}^{45}}{\Phi_{th}^{93}}$	EOL - Core $\frac{\Phi_{1,2}^{45}}{\Phi_{1,2}^{93}}$	EOL - Core $\frac{\Phi_{3}^{45}}{\Phi_{3}^{93}}$	EOL - Core $\frac{\Phi_{th}^{45}}{\Phi_{th}^{93}}$
0	0						
1	4,05	1.0001E+00	1.0000E+00	9.9848E-01	9.9703E-01	9.9699E-01	9.9528E-01
2	8,10	1.0000E+00	9.9996E-01	9.9787E-01	9.9702E-01	9.9694E-01	9.9471E-01
3	12,15	1.0000E+00	9.9981E-01	9.9662E-01	9.9701E-01	9.9680E-01	9.9347E-01
4	14,175	1.0000E+00	9.9949E-01	9.9466E-01	9.9703E-01	9.9650E-01	9.9146E-01
5	16,20	1.0001E+00	9.9910E-01	9.9291E-01	9.9707E-01	9.9612E-01	9.8965E-01
6	18,225	1.0001E+00	9.9839E-01	9.9018E-01	9.9715E-01	9.9543E-01	9.8682E-01
7	20,25	1.0003E+00	9.9709E-01	9.8581E-01	9.9730E-01	9.9416E-01	9.8227E-01
8	22,275	1.0005E+00	9.9468E-01	9.7788E-01	9.9757E-01	9.9179E-01	9.7398E-01
9	24,30	1.0009E+00	9.8989E-01	9.5886E-01	9.9802E-01	9.8706E-01	9.5411E-01
10	26,325	1.0026E+00	9.8276E-01	8.7546E-01	9.9975E-01	9.8002E-01	8.6920E-01
11	28,25	1.0004E+00	9.8223E-01	8.4928E-01	9.9756E-01	9.7957E-01	8.4238E-01
12	30,375	9.9974E-01	9.8247E-01	8.4411E-01	9.9709E-01	9.7995E-01	8.3692E-01
13	32,40	1.0008E+00	9.8344E-01	8.4126E-01	9.9841E-01	9.8113E-01	8.3420E-01
14	34,425	1.0039E+00	9.8499E-01	8.3693E-01	1.0020E+00	9.8294E-01	8.3064E-01
15	36,45	1.0061E+00	9.8667E-01	8.3466E-01	1.0046E+00	9.8489E-01	8.2855E-01
16	38,475	1.0081E+00	9.8845E-01	8.3372E-01	1.0070E+00	9.8693E-01	8.2773E-01
17	40,50	1.0106E+00	9.9048E-01	8.3429E-01	1.0097E+00	9.8921E-01	8.2851E-01
18	42,525	1.0139E+00	9.9303E-01	8.4160E-01	1.0134E+00	9.9198E-01	8.3630E-01
19	44,55	1.0180E+00	9.9667E-01	8.7368E-01	1.0177E+00	9.9579E-01	8.6866E-01
20	46,575	1.0167E+00	1.0055E+00	9.5998E-01	1.0163E+00	1.0045E+00	9.5632E-01
21	48,60	1.0165E+00	1.0089E+00	9.7576E-01	1.0162E+00	1.0083E+00	9.7291E-01
22	50,625	1.0165E+00	1.0089E+00	9.7576E-01	1.0162E+00	1.0083E+00	9.7292E-01
23	52,65	1.0167E+00	1.0055E+00	9.5998E-01	1.0163E+00	1.0045E+00	9.5632E-01
24	54,675	1.0180E+00	9.9668E-01	8.7368E-01	1.0177E+00	9.9579E-01	8.6869E-01
25	56,70	1.0139E+00	9.9304E-01	8.4161E-01	1.0134E+00	9.9199E-01	8.3631E-01
26	58,725	1.0106E+00	9.9048E-01	8.3429E-01	1.0097E+00	9.8922E-01	8.2852E-01
27	60,75	1.0081E+00	9.8845E-01	8.3373E-01	1.0070E+00	9.8695E-01	8.2774E-01
28	62,775	1.0061E+00	9.8667E-01	8.3466E-01	1.0046E+00	9.8491E-01	8.2857E-01
29	64,80	1.0039E+00	9.8499E-01	8.3693E-01	1.0020E+00	9.8296E-01	8.3066E-01
30	66,825	1.0008E+00	9.8344E-01	8.4126E-01	9.9843E-01	9.8115E-01	8.3421E-01
31	68,85	9.9974E-01	9.8247E-01	8.4411E-01	9.9707E-01	9.7997E-01	8.3694E-01
32	70,875	1.0004E+00	9.8223E-01	8.4928E-01	9.9759E-01	9.7959E-01	8.4240E-01
33	72,90	1.0026E+00	9.8277E-01	8.7546E-01	9.9977E-01	9.8004E-01	8.6922E-01
34	74,925	1.0009E+00	9.8990E-01	9.5886E-01	9.9804E-01	9.8708E-01	9.5414E-01
35	76,95	1.0005E+00	9.9468E-01	9.7788E-01	9.9759E-01	9.9181E-01	9.7400E-01
36	78,975	1.0003E+00	9.9710E-01	9.8582E-01	9.9732E-01	9.9418E-01	9.8229E-01
37	81,00	1.0001E+00	9.9839E-01	9.9018E-01	9.9717E-01	9.9545E-01	9.8684E-01
38	83,025	1.0001E+00	9.9910E-01	9.9291E-01	9.9706E-01	9.9614E-01	9.8967E-01
39	85,05	1.0000E+00	9.9949E-01	9.9466E-01	9.9704E-01	9.9651E-01	9.9149E-01
40	89,10	1.0000E+00	9.9981E-01	9.9662E-01	9.9703E-01	9.9682E-01	9.9349E-01
41	93,15	1.0000E+00	9.9996E-01	9.9786E-01	9.9704E-01	9.9696E-01	9.9474E-01
42	97,20	1.0001E+00	1.0000E+00	9.9847E-01	9.9704E-01	9.9701E-01	9.9531E-01

Table 8.2: Flux ratios in x-Direction for 20% enrichment

Pos.	Distance [cm]	BOL - Core $\frac{\Phi_{1,2}^{20}}{\Phi_{1,2}^{93}}$	BOL - Core $\frac{\Phi_{3}^{20}}{\Phi_{3}^{93}}$	BOL - Core $\frac{\Phi_{th}^{20}}{\Phi_{th}^{93}}$	EOL - Core $\frac{\Phi_{1,2}^{20}}{\Phi_{1,2}^{93}}$	EOL - Core $\frac{\Phi_{3}^{20}}{\Phi_{3}^{93}}$	EOL - Core $\frac{\Phi_{th}^{20}}{\Phi_{th}^{93}}$
0	0						
1	4,05	1.0026E+00	1.0026E+00	9.9898E-01	9.9553E-01	9.9551E-01	9.9163E-01
2	8,10	1.0025E+00	1.0024E+00	9.9770E-01	9.9549E-01	9.9542E-01	9.9051E-01
3	12,15	1.0025E+00	1.0022E+00	9.9495E-01	9.9545E-01	9.9515E-01	9.8769E-01
4	14,175	1.0025E+00	1.0015E+00	9.9054E-01	9.9550E-01	9.9453E-01	9.8316E-01
5	16,20	1.0026E+00	1.0007E+00	9.8653E-01	9.9561E-01	9.9372E-01	9.7903E-01
6	18,225	1.0028E+00	9.9904E-01	9.8030E-01	9.9584E-01	9.9216E-01	9.7260E-01
7	20,25	1.0032E+00	9.9600E-01	9.7028E-01	9.9628E-01	9.8919E-01	9.6224E-01
8	22,275	1.0038E+00	9.9016E-01	9.5214E-01	9.9705E-01	9.8346E-01	9.4339E-01
9	24,30	1.0050E+00	9.7834E-01	9.0897E-01	9.9832E-01	9.7182E-01	8.9855E-01
10	26,325	1.0090E+00	9.6090E-01	7.2000E-01	1.0024E+00	9.5462E-01	7.0724E-01
11	28,35	1.0030E+00	9.5972E-01	6.6678E-01	9.9653E-01	9.5369E-01	6.5312E-01
12	30,375	1.0010E+00	9.6004E-01	6.5771E-01	9.9492E-01	9.5443E-01	6.4365E-01
13	32,40	1.0030E+00	9.6186E-01	6.5151E-01	9.9770E-01	9.5687E-01	6.3780E-01
14	34,425	1.0098E+00	9.6489E-01	6.3911E-01	1.0058E+00	9.6068E-01	6.2707E-01
15	36,45	1.0143E+00	9.6825E-01	6.3370E-01	1.0114E+00	9.6480E-01	6.2209E-01
16	38,475	1.0184E+00	9.7191E-01	6.3136E-01	1.0165E+00	9.6920E-01	6.2000E-01
17	40,50	1.0237E+00	9.7630E-01	6.3151E-01	1.0227E+00	9.7427E-01	6.2059E-01
18	42,525	1.0316E+00	9.8212E-01	6.4434E-01	1.0314E+00	9.8069E-01	6.3433E-01
19	44,55	1.0420E+00	9.9084E-01	7.1052E-01	1.0425E+00	9.8988E-01	7.0137E-01
20	44,575	1.0383E+00	1.0125E+00	9.0886E-01	1.0388E+00	1.0121E+00	9.0185E-01
21	48,60	1.0378E+00	1.0205E+00	9.4484E-01	1.0383E+00	1.0203E+00	9.3961E-01
22	50,625	1.0378E+00	1.0205E+00	9.4484E-01	1.0383E+00	1.0203E+00	9.3962E-01
23	52,65	1.0383E+00	1.0125E+00	9.0887E-01	1.0388E+00	1.0121E+00	9.0185E-01
24	54,675	1.0420E+00	9.9085E-01	7.1053E-01	1.0425E+00	9.8989E-01	7.0138E-01
25	56,70	1.0316E+00	9.8213E-01	6.4434E-01	1.0315E+00	9.8071E-01	6.3434E-01
26	58.725	1.0237E+00	9.7631E-01	6.3151E-01	1.0227E+00	9.7428E-01	6.2060E-01
27	60,75	1.0185E+00	9.7192E-01	6.3137E-01	1.0165E+00	9.6921E-01	6.2001E-01
28	62,775	1.0143E+00	9.6826E-01	6.3370E-01	1.0114E+00	9.6482E-01	6.2210E-01
29	64,80	1.0098E+00	9.6491E-01	6.3912E-01	1.0058E+00	9.6069E-01	6.2708E-01
30	66,825	1.0030E+00	9.6187E-01	6.5152E-01	9.9772E-01	9.5688E-01	6.3781E-01
31	68,85	1.0019E+00	9.6005E-01	6.5772E-01	9.9494E-01	9.5445E-01	6.4366E-01
32	70,875	1.0030E+00	9.5973E-01	6.6679E-01	9.9655E-01	9.5371E-01	6.5314E-01
33	72,90	1.0090E+00	9.6091E-01	7.2001E-01	1.0024E+00	9.5464E-01	7.0725E-01
34	74,925	1.0050E+00	9.7835E-01	9.0899E-01	9.9834E-01	9.7184E-01	8.9857E-01
35	76,95	1.0039E+00	9.9017E-01	9.5216E-01	9.9707E-01	9.8349E-01	9.4342E-01
36	78,975	1.0032E+00	9.9601E-01	9.7030E-01	9.9630E-01	9.8921E-01	9.6226E-01
37	81,00	1.0028E+00	9.9906E-01	9.8032E-01	9.9586E-01	9.9218E-01	9.7263E-01
38	83,025	1.0026E+00	1.0007E+00	9.8655E-01	9.9563E-01	9.9374E-01	9.7906E-01
39	85,05	1.0025E+00	1.0015E+00	9.9056E-01	9.9552E-01	9.9455E-01	9.8315E-01
40	89,10	1.0025E+00	1.0022E+00	9.9497E-01	9.9548E-01	9.9518E-01	9.8772E-01
41	93,15	1.0025E+00	1.0025E+00	9.9772E-01	9.9551E-01	9.9544E-01	9.9054E-01
42	97,20	1.0026E+00	1.0026E+00	9.9901E-01	9.9555E-01	9.9554E-01	9.9185E-01

4. XENON POISONING

The effect of Xe-poisoning is calculated by setting the ^{135}Xe-concentration zero for each considered burn up and recalculating the cross sections with WIMS. In order to simplifiy the calculations a core with uniform burn up (BU) of 30%, corresponding approx. to the mean burn up of the EOL-Core has been choosen. This configuration which has been denominated EOL* is given in Fig. 8c.

Table 9: Xenon poisoning of core
($\Phi_{th} \sim 8{,}5 \cdot 10^{13}$)

Enrichment		K_{eff} with Xenon	K_{eff} without Xenon	ΔK %	$\Delta\rho_{Xe}$ [$]
93%	BOL	1,009607	1,047399	3,78	4,47
	EOL*	1,033061	1,072299	3,92	4,43
45%	EOL*	1,026824	1,070415	4,36	4,96
20%	EOL*	1,009895	1,049812	3,99	4,71

(β_{eff} = 10,8%)

The resulting reactivity difference is given in Table 9 for the EOL* core configurations and for the BOL-93% case. The thermal neutron flux in this calculations corresponds to the maximum flux in the fuel, e.a. $\Phi_{th} \sim 8{,}5\ 10^{13} n \cdot cm^{-2} \cdot s^{-1}$.

5. VOID COEFFICIENT

To investigate the effect of the different enrichments on the void coefficient the EOL* core configuration, with a uniform mean burn up of 30%, is calculated for different void fractions in the moderator zone. For this purpose the water density in the element water gap is reduced by 5 and 10% and new cell calculations with WIMS are carried out. For this calculations the Xe-concentration has been put to zero.

The investigated core configuration is given in Fig. 8c. The void coefficient is determined in one element at a central position (position A) for all enrichments. The results which are in good agreement with experiments and earlier calculations ([3])are given in Table 10 and in Fig. 24.

Table 10: Void coefficient

Enrichment	Void fract. %	Void at position A K_{eff}	Core reactivity ρ_E[$]	$\Delta\rho$ [¢]	linear void coefficient [¢·cm^{-1}]
93%	0	1,072299	8,428	0	0,081
	5	1,071508	8,342	8,6	
	10	1,070691	8,253	17,5	
45%	0	1,070415	8,223	0	0,086
	5	1,069584	8,132	9,1	
	10	1,068727	8,038	18,4	
20%	0	1,049812	5,931	0	0,094
	5	1,048941	5,832	9,9	
	10	1,048059	5,732	19,9	

β = 0,8%

6. BERYLLIUM-REFLECTOR

The reactivity of a core configuration can be increased if Beryllium is used as reflector material instead of graphite or water. In order to show the influence of the enrichment on such improvements,different reflected benchmark core configurations have been calculated.

In a first step the graphite reflector rows on both side of the EOL core have been replaced by metallic Beryllium reflector elements with the dimensions of a standard element (7.7 x 8,1 x 60 cm); a second calculation gives the results for a complete Beryllium-reflected core with 1 row of Beryllium elements on each side. In this configuration, four additional irradiation positions in each corner of the core with H_2O reflector are considered. The configuration is given in Fig. 8d and 8c as EOL-Be_{2S} and EOL-Be_{4S}.

Table 11: K_{eff} for Be-reflected cores.

Enrichm. %	EOL K_{eff}	EOL-Be_{2S} K_{eff}	EOL-Be_{2S} $\Delta\rho_2$ [\$]	EOL-Be_{4S} K_{eff}	EOL-Be_{4S} $\Delta\rho_4$ [\$]	$\Delta\rho_4 - \Delta\rho_2$ [\$]
93	1,013799	1.046417	3,85	1,096756	9,326	5,483
45	1,009911	1,041374	3,74	1,090344	9,131	5,391
20	0,999954	1,029619	3,61	1,076537	8,893	5,291

The calculated multiplication factors are given in Table 11 and some flux values in Table 12.

Table 12: Flux in Be-reflected cores

Case	Core average Flux fuel $\Phi_{1,2}$	Core average Flux fuel Φ_{th}	Flux trap center average $\Phi_{1,2}$	Flux trap center average Φ_{th}
EOL-Be-2S				
93%	1,690+14	6,295+13	1,507+14	2,584+14
45%	1,685+14	5,354+13	1,527+14	2,513+14
20%	1,680+14	4,210+13	1,555+14	2,427+14
EOL-Be-4S				
93%	1,666+14	6,228+13	1,365+14	2,356+14
45%	1,662+14	5,302+13	1,383+14	2,290+14
20%	1,658+14	4,174+13	1,407+14	2,208+14

In Fig. 25 to Fig. 30 the flux ratios (R) are given between the Beryllium reflected and the Graphite reflected, 93% enriched EOL-Core.

$$R = \frac{\Phi_{EOL\text{-}Be}}{\Phi_{EOL\text{-}C\text{-}93}}$$

The graphs are given for the 2 and 4 side reflected case in the y-direction only. In Table 13 the corresponding flux rations in the x-direction are given.

In order to show the influence of the Beryllium reflector on the corner irradiation positions, the thermal flux distribution along the y-line through the corner irradiation position (row 11) is given in Fig. 31. The flux ratios compared to the graphite moderated core are given in Fig. 32 and 33.

Conclusions for Beryllium reflected cores

The calculations shows that a considerable gain in reactivity is obtained with a Beryllium reflector, and that this gain is not appreciably influenced by the enrichment.

Otherwise the flux distribution will be changed so that the flux in the center irradiation position is lowered up to 15%, but in the corner irradiation position a flux gain of 15% to 20% ist obtained for the all side reflected case. For the replacement of the Graphite by Beryllium only a reduction in Flux of 10 - 15 % has to be accepted.

The influence on the flux rations $\frac{\Phi_x}{\Phi_{93}}$ for different enrichments is about the same as with the standard benchmark core.

Table 13: Flux ratios for Beryllium reflected core in X-direction
(EOL-Be-4S, 4-side reflected)

Pos.	Distance [cm]	$\frac{\Phi_{1,2}^{45}Be}{\Phi_{1,2}^{93}C}$	$\frac{\Phi_{3}^{45}Be}{\Phi_{3}^{93}C}$	$\frac{\Phi_{th}^{45}Be}{\Phi_{th}^{93}C}$	$\frac{\Phi_{1,2}^{20}Be}{\Phi_{1,2}^{93}C}$	$\frac{\Phi_{3}^{20}Be}{\Phi_{3}^{93}C}$	$\frac{\Phi_{th}^{20}Be}{\Phi_{th}^{93}C}$
0	0						
1	4,05	1.1830E+00	1.4525E+00	1.6792E+00	1.1849E+00	1.4547E+00	1.6680E+00
2	8,10	1.2327E+00	1.6097E+00	1.7486E+00	1.2348E+00	1.6119E+00	1.7329E+00
3	12,15	1.3569E+00	1.9260E+00	1.8153E+00	1.3595E+00	1.9274E+00	1.7899E+00
4	14,175	1.5900E+00	2.3200E+00	1.7481E+00	1.5937E+00	2.3181E+00	1.7070E+00
5	16,20	1.8232E+00	2.5159E+00	1.5693E+00	1.8279E+00	2.5390E+00	1.5143E+00
6	18,225	2.3550E+00	2.6422E+00	1.1534E+00	2.3620E+00	2.6240E+00	1.0901E+00
7	20,25	2.3737E+00	2.3820E+00	8.6465E-01	2.3813E+00	2.3584E+00	8.0637E-01
8	22,275	2.0768E+00	1.9574E+00	6.8626E-01	2.0839E+00	1.9310E+00	6.2788E-01
9	24,30	1.6725E+00	1.5521E+00	6.3177E-01	1.6791E+00	1.5231E+00	5.6015E-01
10	26,325	1.2551E+00	1.3030E+00	8.9600E-01	1.2612E+00	1.2723E+00	7.2267E-01
11	28,35	1.1110E+00	1.1616E+00	9.3127E-01	1.1134E+00	1.1330E+00	7.2520E-01
12	30,375	1.0316E+00	1.0657E+00	8.9736E-01	1.0325E+00	1.0391E+00	6.9259E-01
13	32,40	9.8056E-01	1.0009E+00	8.5024E-01	9.8224E-01	9.7675E-01	6.5111E-01
14	34,425	9.4632E-01	9.5660E-01	8.1079E-01	9.5160E-01	9.3508E-01	6.1226E-01
15	36,45	9.2015E-01	9.2536E-01	7.8247E-01	9.2762E-01	9.0637E-01	5.8714E-01
16	38,475	9.0067E-01	9.0325E-01	7.6179E-01	9.1008E-01	8.8669E-01	5.6996E-01
17	40,50	8.8692E-01	8.8797E-01	7.4742E-01	8.9886E-01	8.7400E-01	5.5898E-01
18	42,525	8.7844E-01	8.7819E-01	7.4301E-01	8.9432E-01	8.6743E-01	5.6241E-01
19	44,55	8.7485E-01	8.7332E-01	7.6376E-01	8.9606E-01	8.6721E-01	6.1507E-01
20	46,575	8.7337E-01	8.7452E-01	8.3531E-01	8.9260E-01	8.8008E-01	7.8634E-01
21	48,60	8.7275E-01	8.7465E-01	8.4796E-01	8.9164E-01	8.8449E-01	8.1772E-01
22	50,625	8.7276E-01	8.7465E-01	8.4796E-01	8.9164E-01	8.8450E-01	8.1773E-01
23	52,65	8.7339E-01	8.7454E-01	8.3532E-01	8.9261E-01	8.8009E-01	7.8635E-01
24	54,675	8.7487E-01	8.7333E-01	7.6377E-01	8.9609E-01	8.6724E-01	6.1509E-01
25	56,70	8.7847E-01	8.7821E-01	7.4302E-01	8.9435E-01	8.6746E-01	5.6243E-01
26	58,725	8.8695E-01	8.8800E-01	7.4744E-01	8.9890E-01	8.7404E-01	5.5900E-01
27	60,75	9.0070E-01	9.0329E-01	7.6182E-01	9.1013E-01	8.8673E-01	5.6999E-01
28	62,775	9.2020E-01	9.2540E-01	7.8251E-01	9.2769E-01	9.0643E-01	5.8717E-01
29	64,80	9.4638E-01	9.5665E-01	8.1083E-01	9.5168E-01	9.3515E-01	6.1230E-01
30	66,825	9.8063E-01	1.0010E+00	8.5030E-01	9.8233E-01	9.7683E-01	6.5116E-01
31	68,85	1.0317E+00	1.0658E+00	8.9743E-01	1.0326E+00	1.0392E+00	6.9265E-01
32	70,875	1.1111E+00	1.1617E+00	9.3135E-01	1.1135E+00	1.1331E+00	7.2527E-01
33	72,90	1.2552E+00	1.3031E+00	8.9608E-01	1.2613E+00	1.2725E+00	7.2275E-01
34	74,925	1.6727E+00	1.5522E+00	6.3183E-01	1.6793E+00	1.5233E+00	5.6021E-01
35	76,95	2.0770E+00	1.9576E+00	6.8634E-01	2.0842E+00	1.9312E+00	6.2795E-01
36	78,975	2.3740E+00	2.3822E+00	8.6475E-01	2.3815E+00	2.3586E+00	8.0646E-01
37	81,00	2.3553E+00	2.6424E+00	1.1536E+00	2.3623E+00	2.6243E+00	1.0903E+00
38	83,025	1.8234E+00	2.5162E+00	1.5695E+00	1.8282E+00	2.5093E+00	1.5145E+00
39	85,05	1.5903E+00	2.3202E+00	1.7484E+00	1.5939E+00	2.3184E+00	1.7072E+00
40	89,10	1.3571E+00	1.9263E+00	1.8156E+00	1.3597E+00	1.9276E+00	1.7901E+00
41	93,15	1.2329E+00	1.6099E+00	1.7488E+00	1.2349E+00	1.6121E+00	1.7331E+00
42	97,20	1.1832E+00	1.4526E+00	1.6795E+00	1.1851E+00	1.4549E+00	1.6682E+00

Table 13.1: Flux ratios für Beryllium reflected core in X-direction
(EOL-Be-2S, 2-side reflected)

Pos.	Distance [cm]	$\frac{\Phi_{1,2}^{45}Be}{\Phi_{1,2}^{93}C}$	$\frac{\Phi_{3}^{45}Be}{\Phi_{3}^{93}C}$	$\frac{\Phi_{th}^{45}Be}{\Phi_{th}^{93}C}$	$\frac{\Phi_{1,2}^{20}Be}{\Phi_{1,2}^{93}C}$	$\frac{\Phi_{3}^{20}Be}{\Phi_{3}^{93}C}$	$\frac{\Phi_{th}^{20}Be}{\Phi_{th}^{93}C}$
0	0						
1	4,05	9.1468E-01	9.1476E-01	9.1418E-01	9.1509E-01	9.1518E-01	9.1287E-01
2	8,10	9.1447E-01	9.1457E-01	9.1362E-01	9.1485E-01	9.1495E-01	9.1159E-01
3	12,15	9.1409E-01	9.1421E-01	9.1245E-01	9.1443E-01	9.1446E-01	9.0890E-01
4	14,175	9.1363E-01	9.1372E-01	9.1064E-01	9.1399E-01	9.1366E-01	9.0469E-01
5	16,20	9.1334E-01	9.1331E-01	9.0904E-01	9.1376E-01	9.1283E-01	9.0091E-01
6	18,225	9.1303E-01	9.1270E-01	9.0658E-01	9.1358E-01	9.1137E-01	8.9507E-01
7	20,25	9.1273E-01	9.1172E-01	9.0262E-01	9.1353E-01	9.0877E-01	8.8567E-01
8	22,275	9.1250E-01	9.1004E-01	8.9539E-01	9.1374E-01	9.0392E-01	8.6860E-01
9	24,30	9.1241E-01	9.0683E-01	8.7784E-01	9.1439E-01	8.9420E-01	8.2783E-01
10	26,325	9.1350E-01	9.0268E-01	8.0144E-01	9.1762E-01	8.8049E-01	6.5279E-01
11	28,35	9.1399E-01	9.0481E-01	7.7935E-01	9.1475E-01	8.8209E-01	6.0484E-01
12	30,375	9.1684E-01	9.0840E-01	7.7752E-01	9.1657E-01	8.8588E-01	5.9848E-01
13	32,40	9.2185E-01	9.1319E-01	7.7851E-01	9.2281E-01	8.9166E-01	5.9563E-01
14	34,425	9.2931E-01	9.1982E-01	7.7873E-01	9.3430E-01	8.9895E-01	5.8818E-01
15	36,45	9.3569E-01	9.2459E-01	7.8011E-01	9.4334E-01	9.0653E-01	5.8593E-01
16	38,475	9.4158E-01	9.3027E-01	7.8256E-01	9.5168E-01	9.1420E-01	5.8628E-01
17	40,50	9.4748E-01	9.3586E-01	7.8636E-01	9.6067E-01	9.2221E-01	5.8902E-01
18	42,525	9.5383E-01	9.4150E-01	7.9653E-01	9.7168E-01	9.3113E-01	6.0409E-01
19	44,55	9.6049E-01	9.4749E-01	8.2966E-01	9.8459E-01	9.4211E-01	6.6962E-01
20	46,575	9.6333E-01	9.5770E-01	9.1412E-01	9.8517E-01	9.6481E-01	8.6191E-01
21	48,60	9.6590E-01	9.6271E-01	9.3083E-01	9.8735E-01	9.7436E-01	8.9877E-01
22	50,625	9.6590E-01	9.6272E-01	9.3083E-01	9.8736E-01	9.7436E-01	8.9877E-01
23	52,65	9.6334E-01	9.5771E-01	9.1414E-01	9.8519E-01	9.6483E-01	8.6193E-01
24	54,675	9.6052E-01	9.4752E-01	8.2963E-01	9.8462E-01	9.4213E-01	6.6964E-01
25	56,70	9.5386E-01	9.4153E-01	7.9655E-01	9.7172E-01	9.3116E-01	6.0410E-01
26	58,725	9.4751E-01	9.3590E-01	7.8638E-01	9.6071E-01	9.2225E-01	5.8904E-01
27	60,75	9.4162E-01	9.3039E-01	7.8259E-01	9.5172E-01	9.1424E-01	5.8630E-01
28	62,775	9.3573E-01	9.2463E-01	7.8015E-01	9.4339E-01	9.0658E-01	5.8595E-01
29	64,80	9.2936E-01	9.1886E-01	7.7877E-01	9.3434E-01	8.9900E-01	5.8821E-01
30	66,825	9.2191E-01	9.1323E-01	7.7855E-01	9.2286E-01	8.9171E-01	5.9566E-01
31	68,85	9.1689E-01	9.0844E-01	7.7756E-01	9.1662E-01	8.8593E-01	5.9851E-01
32	70,875	9.1403E-01	9.0486E-01	7.7939E-01	9.1480E-01	8.8214E-01	6.0487E-01
33	72,90	9.1355E-01	9.0272E-01	8.0148E-01	9.1767E-01	8.8054E-01	6.5283E-01
34	74,925	9.1246E-01	9.0598E-01	8.7789E-01	9.1445E-01	8.9425E-01	8.2787E-01
35	76,95	9.1255E-01	9.1008E-01	8.9544E-01	9.1380E-01	9.0397E-01	8.6864E-01
36	78,975	9.1278E-01	9.1177E-01	9.0267E-01	9.1359E-01	9.0982E-01	8.8572E-01
37	81,00	9.1308E-01	9.1274E-01	9.0662E-01	9.1363E-01	9.1142E-01	8.9511E-01
38	83,025	9.1339E-01	9.1336E-01	9.0909E-01	9.1381E-01	9.1288E-01	9.0096E-01
39	75,05	9.1368E-01	9.1377E-01	9.1069E-01	9.1405E-01	9.1371E-01	9.0474E-01
40	89,10	9.1414E-01	9.1426E-01	9.1249E-01	9.1448E-01	9.1451E-01	9.0894E-01
41	93,15	9.1452E-01	9.1462E-01	9.1366E-01	9.1490E-01	9.1499E-01	9.1162E-01
42	97,20	9.1473E-01	9.1481E-01	9.1422E-01	9.1513E-01	9.1523E-01	9.1291E-01

7. CONCLUSIONS

The calculations show that an enrichment reduction to 45% for the European 23 plate standard element gives no significant alteration of the physical behaviour. This of course is valid only, if the ^{235}U-content can be increased to ∿ 320 g per element. Earlier calculations (4) have showed that maintaining the ^{235}U-content at 280 g will give significant loss in nuclear characteristics.

Rough estimations indicate that also the thermohydraulic behaviour should be acceptable. For these demonstration of course, experiments with real elements must be executed. This is necessary also in order to demonstrate that the technical fabrication of the new fuel is adequate enough.

As soon as the enrichment is reduced to values lower than 45%, the physical characteristics will be noticeable influenced. The calculations show that even with the high loading of 390 g U^{235} per element, which is not obtainable today from the metallurgical standpoint, a high loss of reactivity must be taken into account. The penalty of the thermal flux in an incore irradiation position for pure water is small, but as soon as material such as the Aluminium is introduced the flux will be lowered by 40% or more. This reduction is not acceptable for a 5 to 10 MW research reactor.

It is shown that all nuclear parameters will be influenced accordingly. This shows clearly that the element construction must be changed, if LEU has to be used instead of HEU or MEU.

On the other hand, earlier calculations made at the EIR for a 20 plate element (5) have showed that this alteration of the construction gives also worse physical characteristics, and additionally less safety margin for most of the research reactors.

In order to reduce the enrichment below 45%, it is thus necessary to carry out optimalisation calculations for the fuel element layout, and accordingly developments of fabrication technique.

Furthermore the reliability of such elements must be demonstrated experimentally by irradiation test under real conditions.

REFERENCES

([1]) a) J.R. Askew, et. al.
A general description of the lattice code WIMS.
J.B.N.E.S. Oct. 1966 p. 564

b) M.J. Roth, J.D. Macdougall, P.B. Kemshell, 1967
AEEW-R-538:
The preparation of input data for WIMS

c) M.J. Roth, 1969
AEEW-M-845:
The WIMS-Multigroup scheme
status and difference between versions

([2]) J.M. Paratte, EIR-Würenlingen
DIFFUS - un programme basé sur la théorie de diffusion pour le calcul à deux dimensions des flux neutroniques
EIR-Bericht Nr. 237 - Mai 1973

C. Maeder, J.M. Paratte, EIR-Würenlingen
Calculation of LWR fuel elements containing burnable poisons and plutonium
TANS-20, p. 359 (1975)

J.M. Paratte, EIR-Würenlingen
DEFINE: Programme d'input du cote de calcul des boîtes de réacteurs à eau légère
TM-PH-471 (15.6.1973)

C. Maeder, EIR-Würenlingen
Programm MICOND: Energetische und räumliche Kondensation von Wirkungsquerschnitten
(TM-PH-590) (15.3.1976)

([3]) H. Winkler / J. Zeis, EIR-Würenlingen
Der Blasenkoeffizient am Reaktor SAPHIR
TM-SR-108 (15.8.1977)

([4]) H. Winkler, EIR-Würenlingen
Calculation of 10 MW MTR-Core (benchmark-Problem)
Draft for IAEA-Consultant-Meeting
"Preparation to use LEU instead of HEU",
(June 19. - 21. Vienna)

([5]) H. Winkler / J. Zeis, EIR-Würenlingen
Einfluss des Anreicherungsgrades auf die Reaktivität bei MTR-Brennelementen
TM-SR-112 (21.9.1978)

([6]) H. Winkler / J. Zeis, EIR-Würenlingen
Vertikales Buckling für SAPHIR-Betriebsladungen
TM-SR-111 (20.6.1978)

Multiplication factor K_∞
($\Phi \sim 8{,}5 \cdot 10^{13} n \cdot cm^{-2} \cdot s^{-1}$)

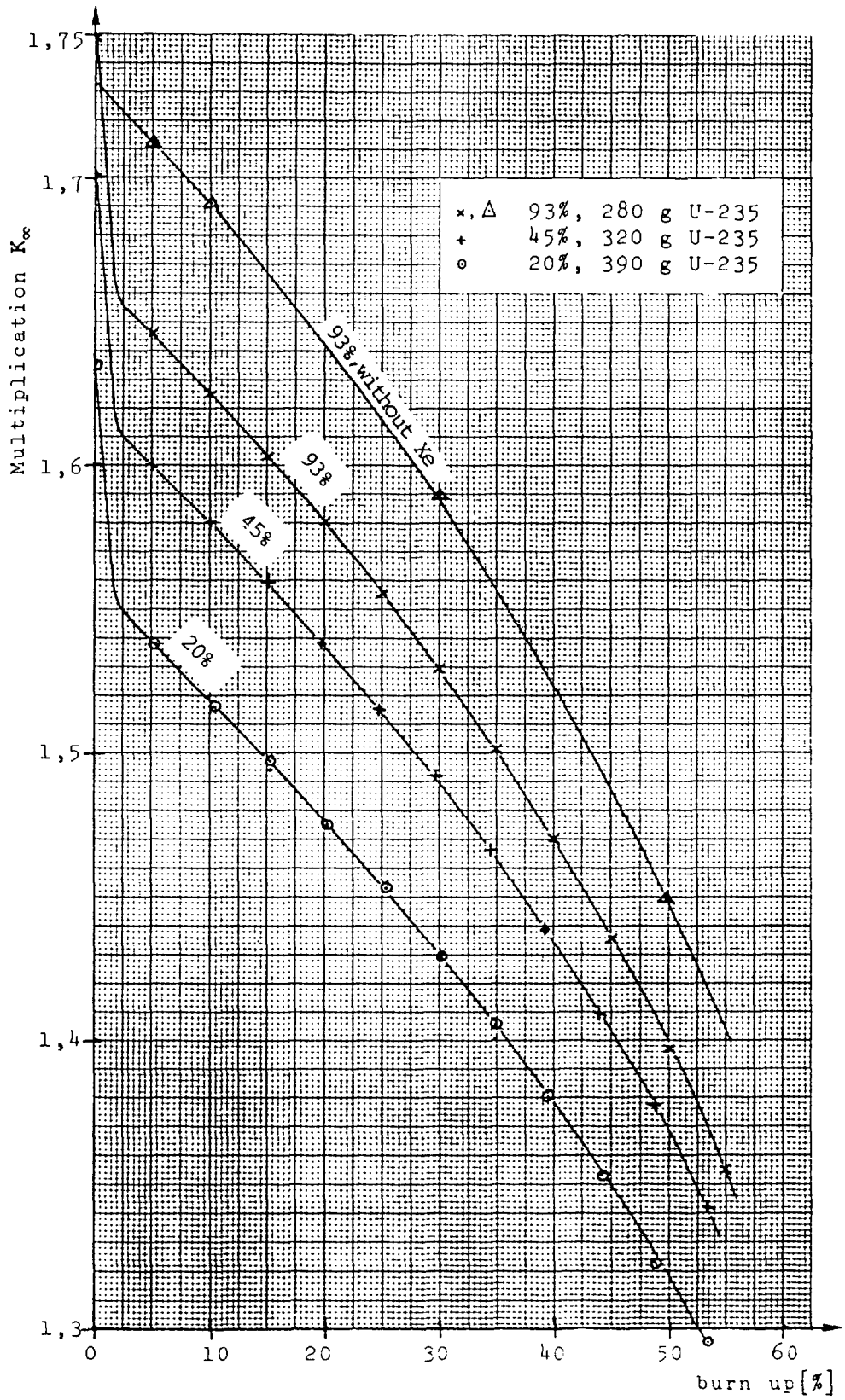

Fig. 4

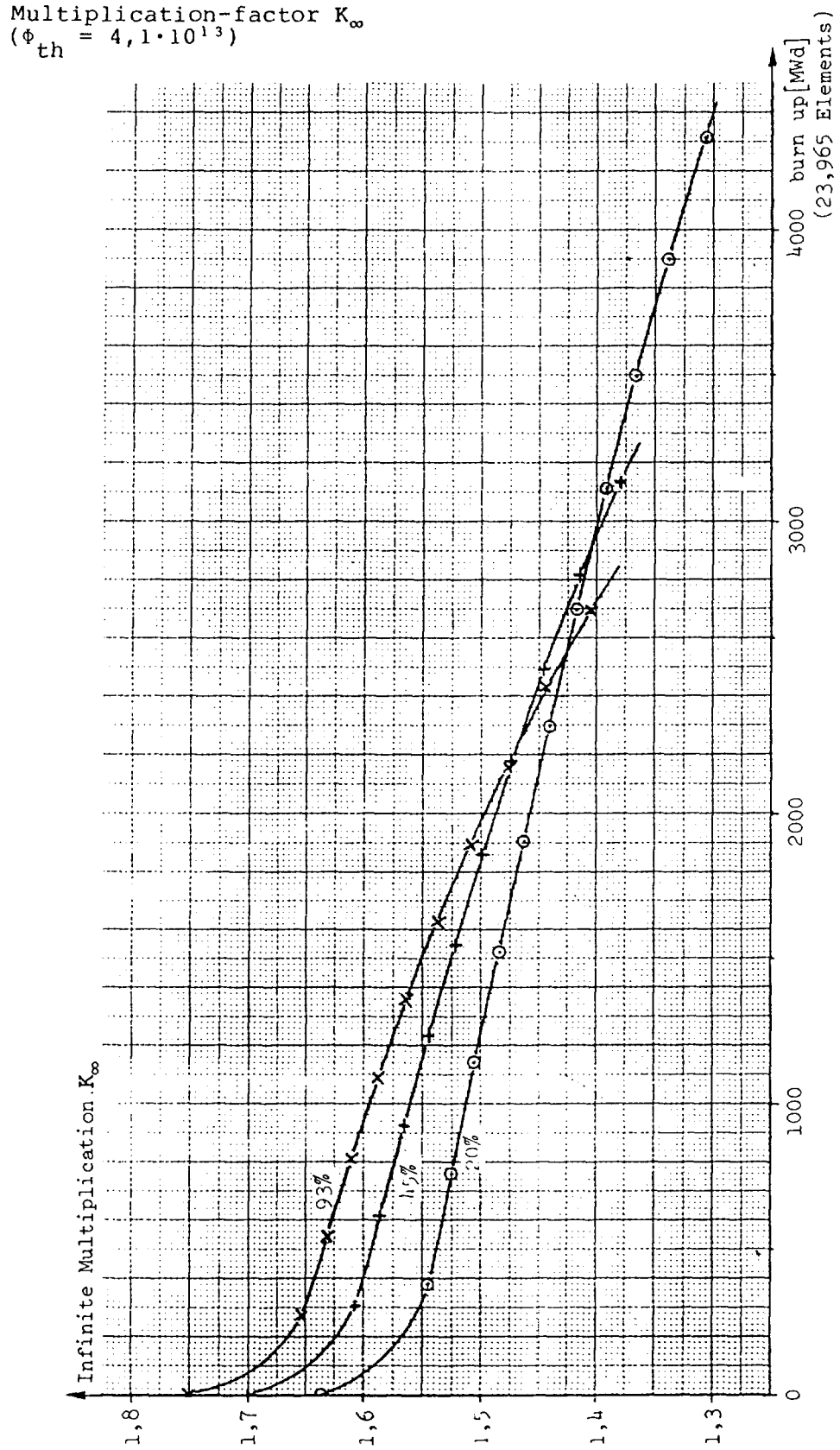
Multiplication-factor K_∞
($\Phi_{th} = 4,1 \cdot 10^{13}$)
Infinite Multiplication K_∞
1,8
1,7
1,6
1,5
1,4
1,3
0
1000
2000
3000
4000 burn up [MWd]
(23,965 Elements)
93%
1,5%
2,0%

Fig. 5

Pu-239 content per Element

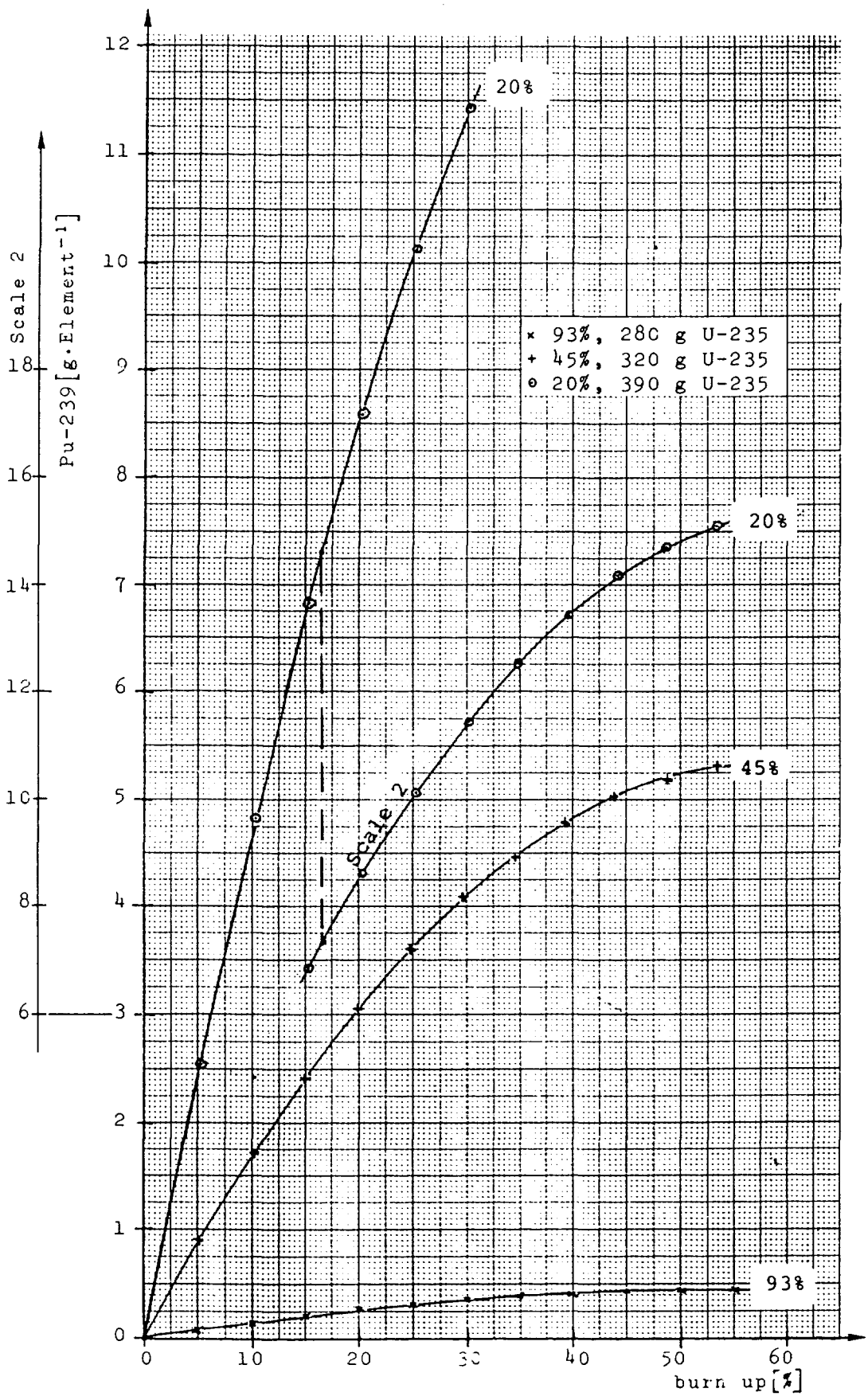

Fig. 6

^{135}Xe-Concentration, thermal flux

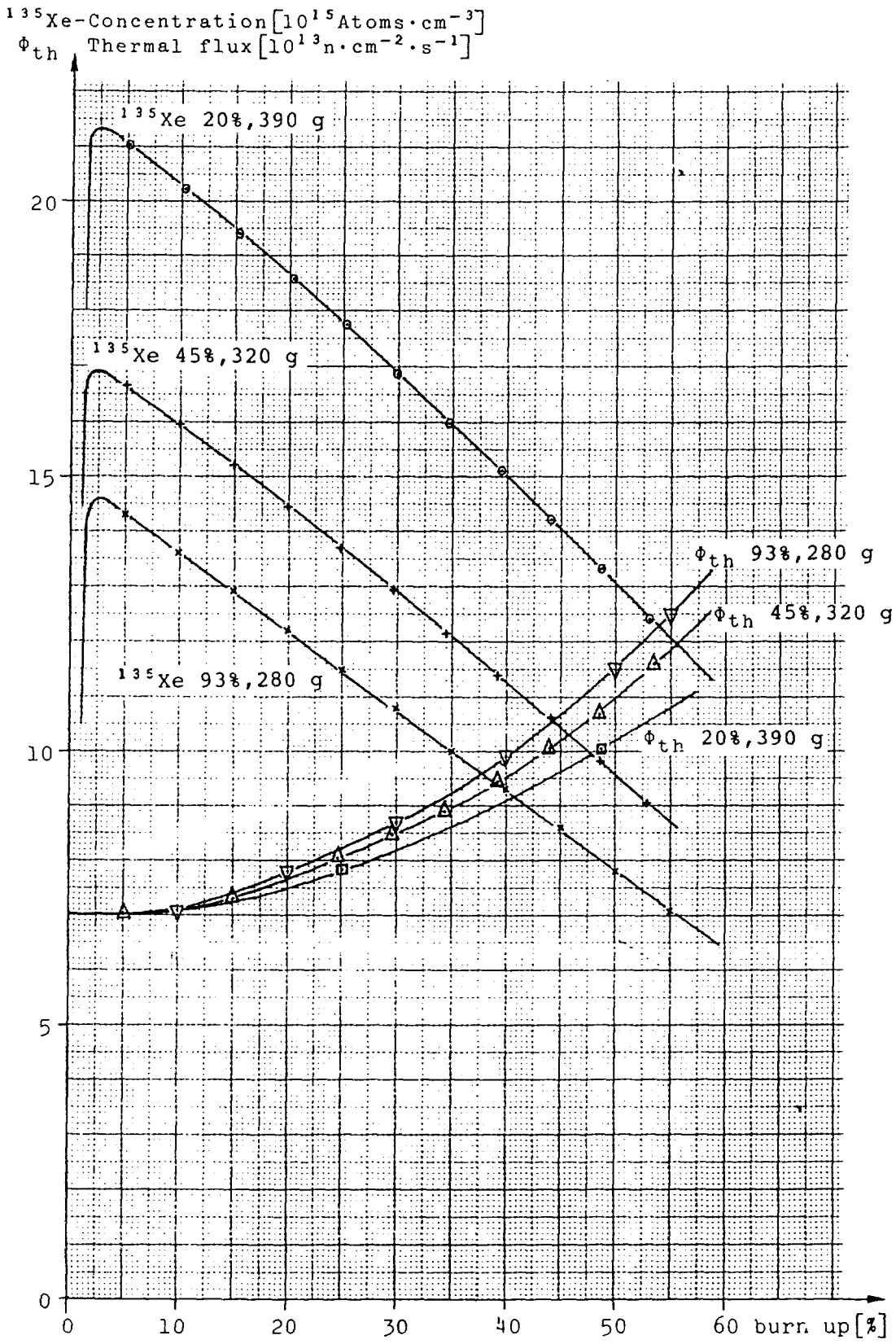

Fig. 7a

^{135}Xe-Concentration (Φ_{th} = 4,1·10^{13}n·cm^{-2}·s^{-1})

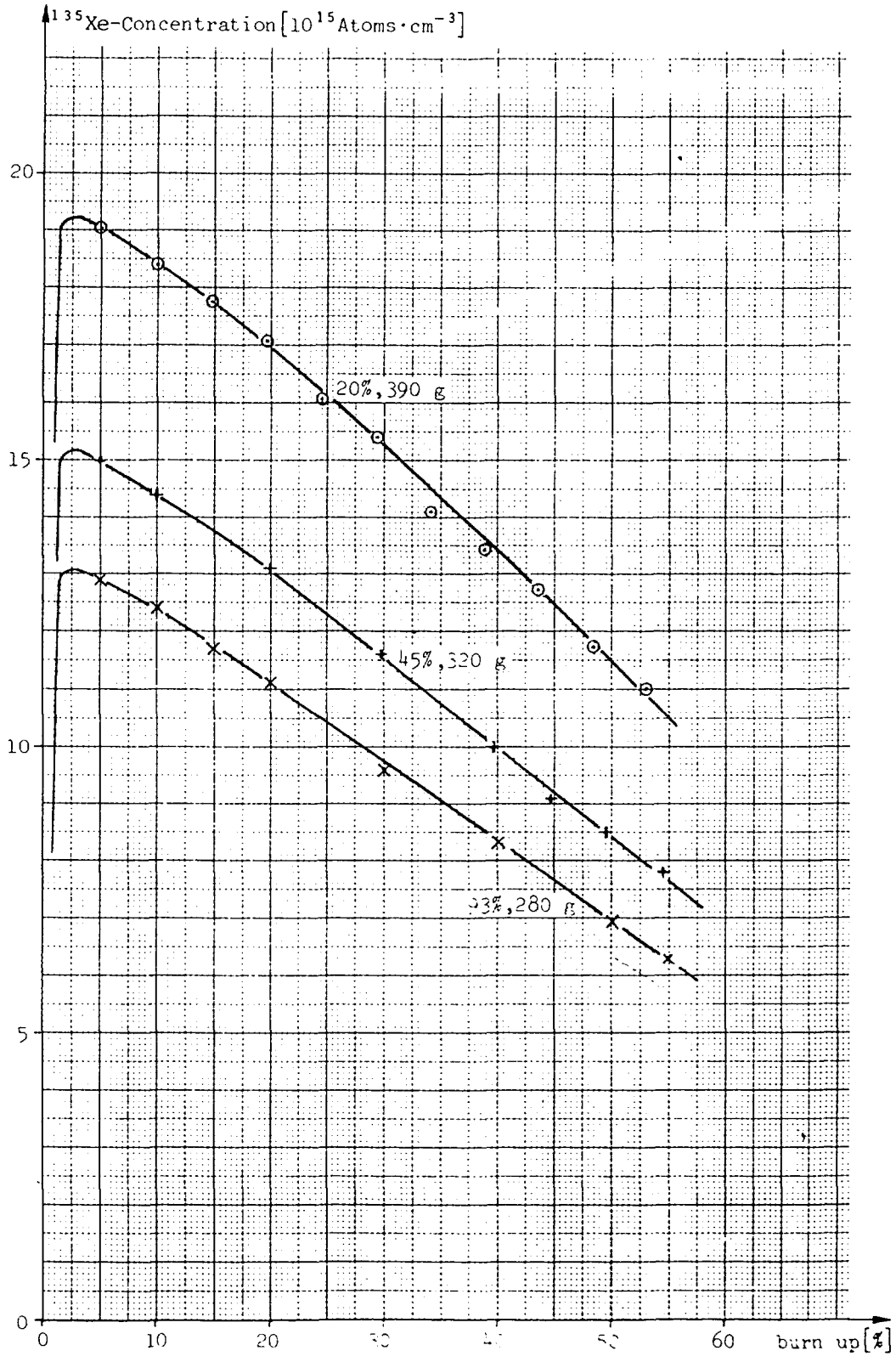

Fig. 7 b

Datenblatt für LADUNG - Nr. Benchmark MTR P_{max} nom.: 10 MW

Ladung für: _____ VA-Nr.: _____

LADUNGSANORDNUNG 8a — BOL

BU	Normalelement	1
Nr.	Kontrollelement	2
BU	GA-Kontrollelement	3
C	Reflektorelement Graphite	4
Q	Neutronenquelle	5
25	burn up % of initial U-235	6
		7
		8
		9

Bemerkungen:

BU = Burn Up in %

	1	2	3	4	5	6	7	8	9
11			3 Element Water						
	Water			5	25	5			Water
	Element	C	5	25	45	25	5	C	Element
	Element	C	25	45	45 / H_2O / 45	45	25	C	Element
	3	C	25	45		45	25	C	3
		C	5	25	45	25	5	C	
				5	25	5			
			3 Element Water						
91									99

LADUNGSANORDNUNG 8b — EOL

BU	Normalelement	1
Nr.	Kontrollelement	2
BU	GA-Kontrollelement	3
C	Reflektorelement Graphite	4
Q	Neutronenquelle	5
50	burn up % of initial U-235	6
		7
		8
		9

Bemerkungen:

	1	2	3	4	5	6	7	8	9
11									
				10	30	10			
		C	10	30	50	30	10	C	
		C	30	50	50 / H_2O / 50	50	30	C	
		C	30	50		50	30	C	
		C	10	30	50	30	10	C	
				10	30	10			
91									99

LADUNGSANORDNUNG 8c

BU	Normalelement	1
Nr.	Kontrollelement	2
BU	GA-Kontrollelement	3
C	Reflektorelement Graphite	4
Q	Neutronenquelle	5
30	burn up % of initial U-235	6
		7
		8
		9

Bemerkungen:

	1	2	3	4	5	6	7	8	9
11									
				30	30	30			
		C	30	30	30	30	30	C	
		C	30	30	30 / H_2O / 30	30	30	C	
		C	30	30		30	30	C	
		C	30	30	30^A	30	30	C	
				30	30	30^B			
91									99

Fig. 8: Core-Configuration

Datenblatt für LADUNG - Nr. Benchmark / MTR P_{max}nom.: 10 MW

Ladung für: _____ VA-Nr.: _____

LADUNGSANORDNUNG 8d

Nr.	Normalelement
Nr.	Kontrollelement
Nr.	GA-Kontrollelement
Be	Reflektorelement
Q	Neutronenquelle
50	Burn up %of initial U^{235}

Bemerkungen:

EOL-Be-2S

Row 11 → 21 →

	1	2	3	4	5	6	7	8	9
1	"								
2				10	30	10			
3		Be	10	30	50	30	10	Be	
4		Be	30	50	50 / H_2O	50	30	Be	
5		Be	30	50	50	50	30	Be	
6		Be	10	30	50	30	10	Be	
7				10	30	10			
8									
9	01								00

LADUNGSANORDNUNG 8e

Nr.	Normalelement
Nr.	Kontrollelement
Nr.	GA-Kontrollelement
Be	Reflektorelement
Q	Neutronenquelle
50	Burn up % of initial U^{235}

Bemerkungen:

EOL-Be-4S

Row 11 → 21 →

	1	2	3	4	5	6	7	8	9
1	"	Be	Be	Be	Be	Be	Be	Be	
2		Be		10	30	10		Be	
3		Be	10	30	50	30	10	Be	
4		Be	30	50	50 / H_2O	50	30	Be	
5		Be	30	50	50	50	30	Be	
6		Be	10	30	50	30	10	Be	
7		Be		10	30	10		Be	
8		Be	Be	Be	Be	Be	Be	Be	
9	01								00

LADUNGSANORDNUNG

Nr.	Normalelement
Nr.	Kontrollelement
Nr.	GA-Kontrollelement
Be	Reflektorelement
Q	Neutronenquelle

Bemerkungen:

	1	2	3	4	5	6	7	8	9
1	"								
2									
3									
4									
5									
6									
7									
8									
9	01								00

Fig. 8d; e Core configuration

Codiff-calculation scheme

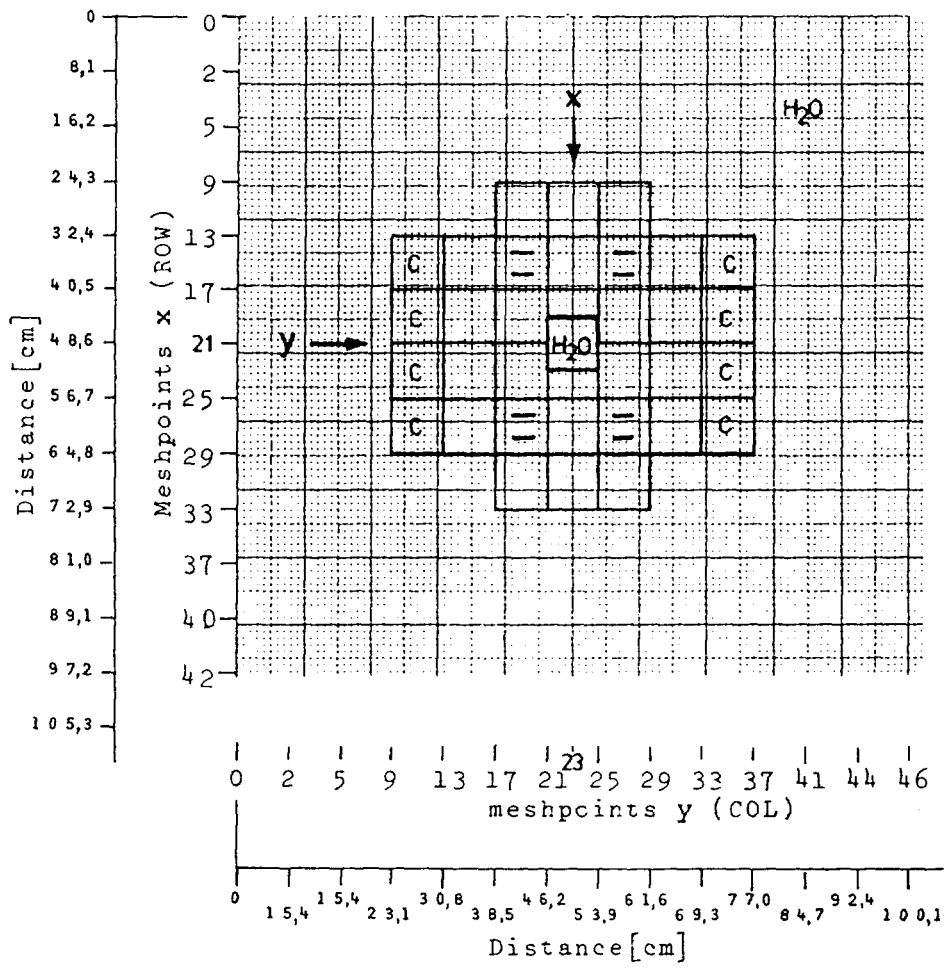

Fig. 9

K_{eff} of Benchmarkcore as function of burn up
($\Phi_{th} = 4{,}1 \cdot 10^{13} n \cdot cm^{-2} \cdot s^{-1}$)

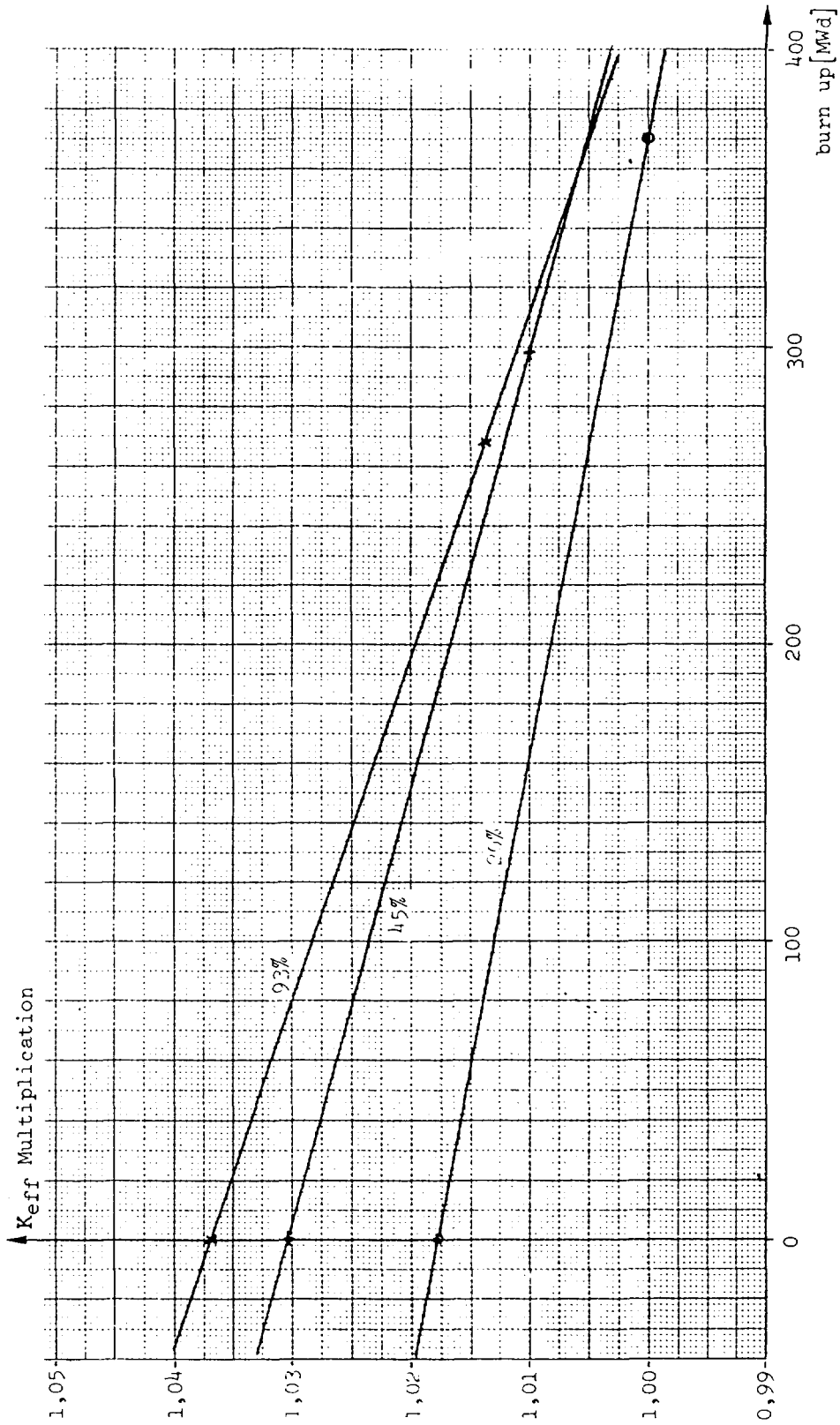

Fig. 10

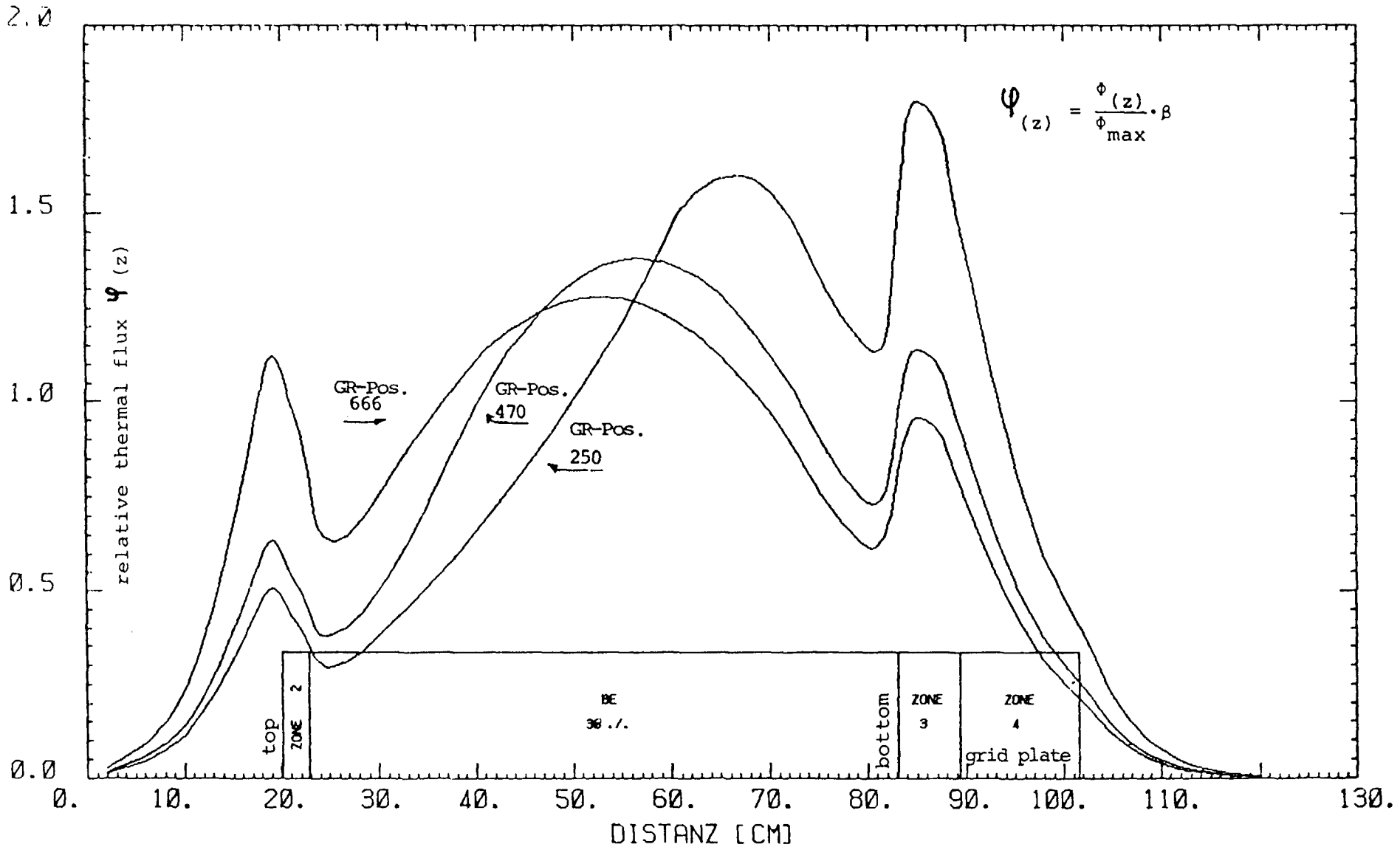

FIG. 11: VERTICAL FLUX DISTRIBUTION FOR 3 CONTROL ROD POSITION

(NORMALIZED)

Fig. 11

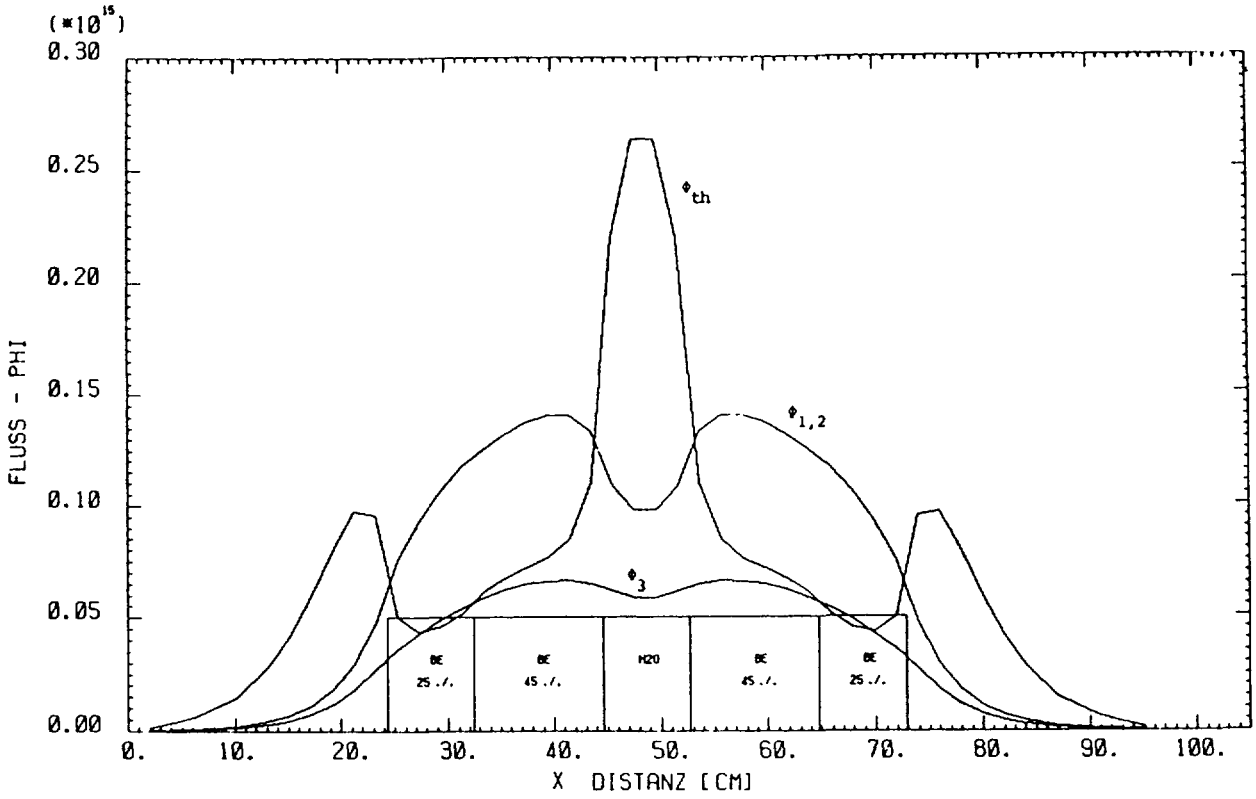

FIG. 12 FLUX BOL-93(4E13) [COL. 23]

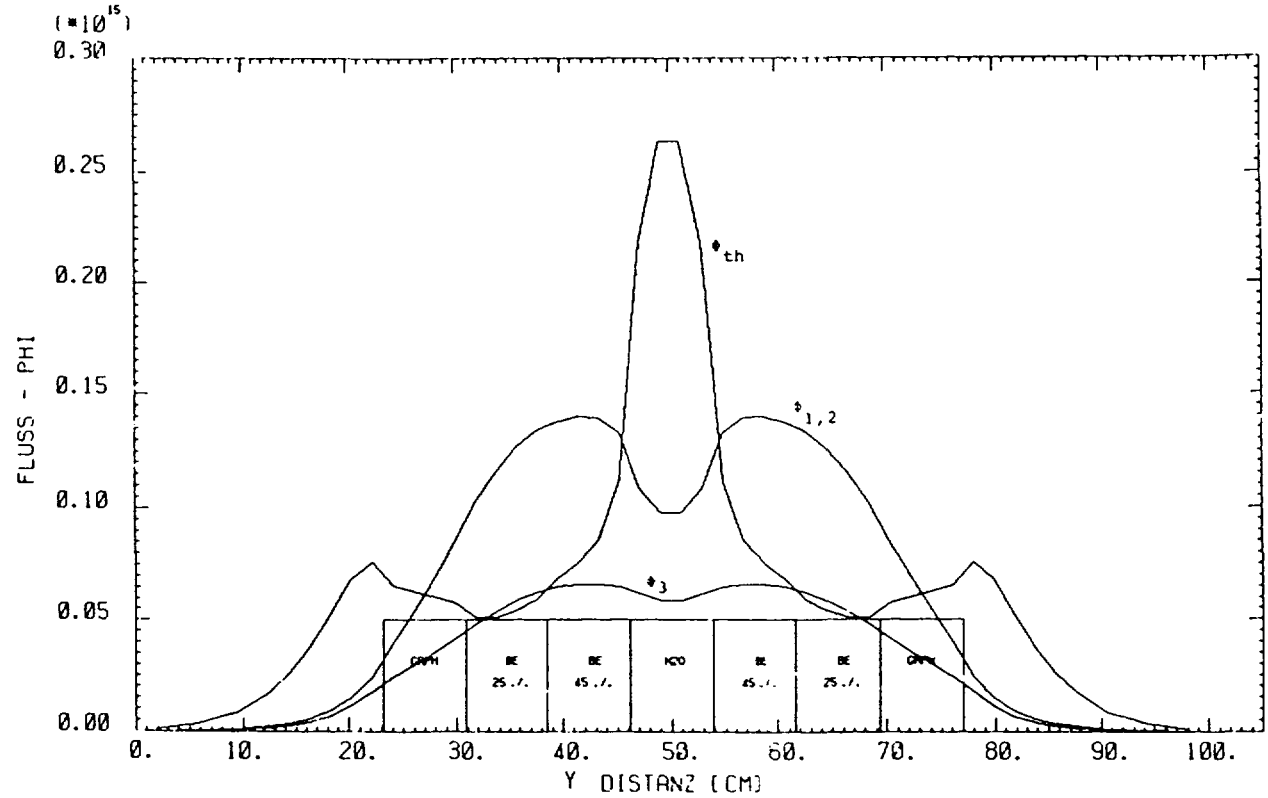

FIG.13 FLUX BOL-93(4E13) [ROW 21]

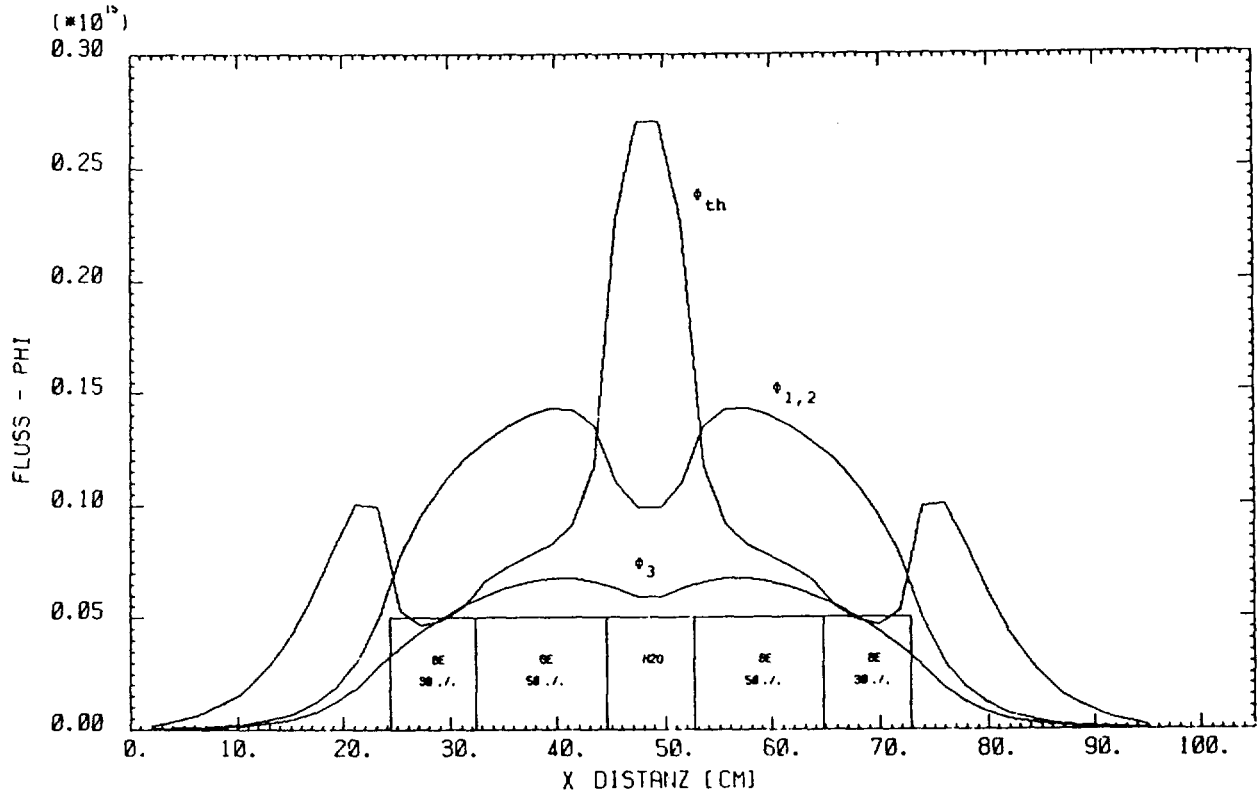

FIG. 14 FLUX EOL-93(4E13) [COL. 23]

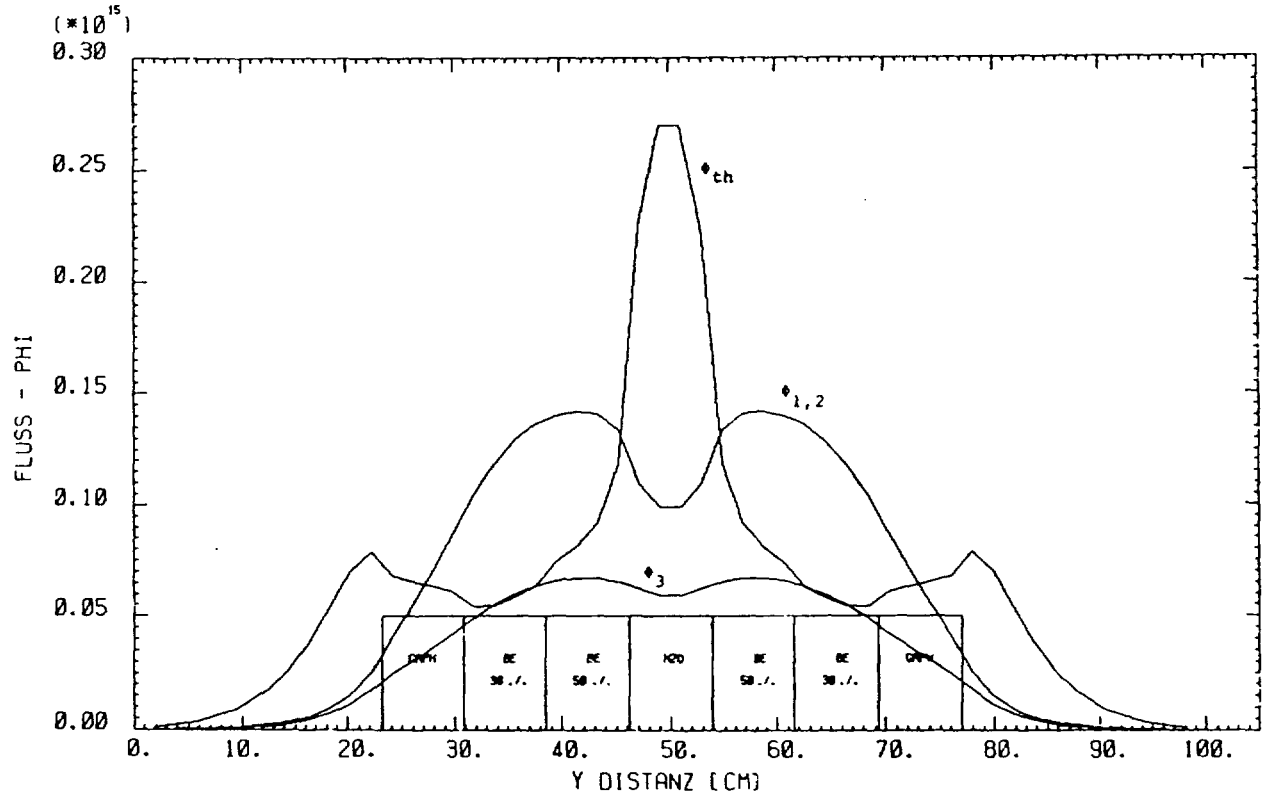

FIG. 15 FLUX EOL-93(4E13) [ROW 21]

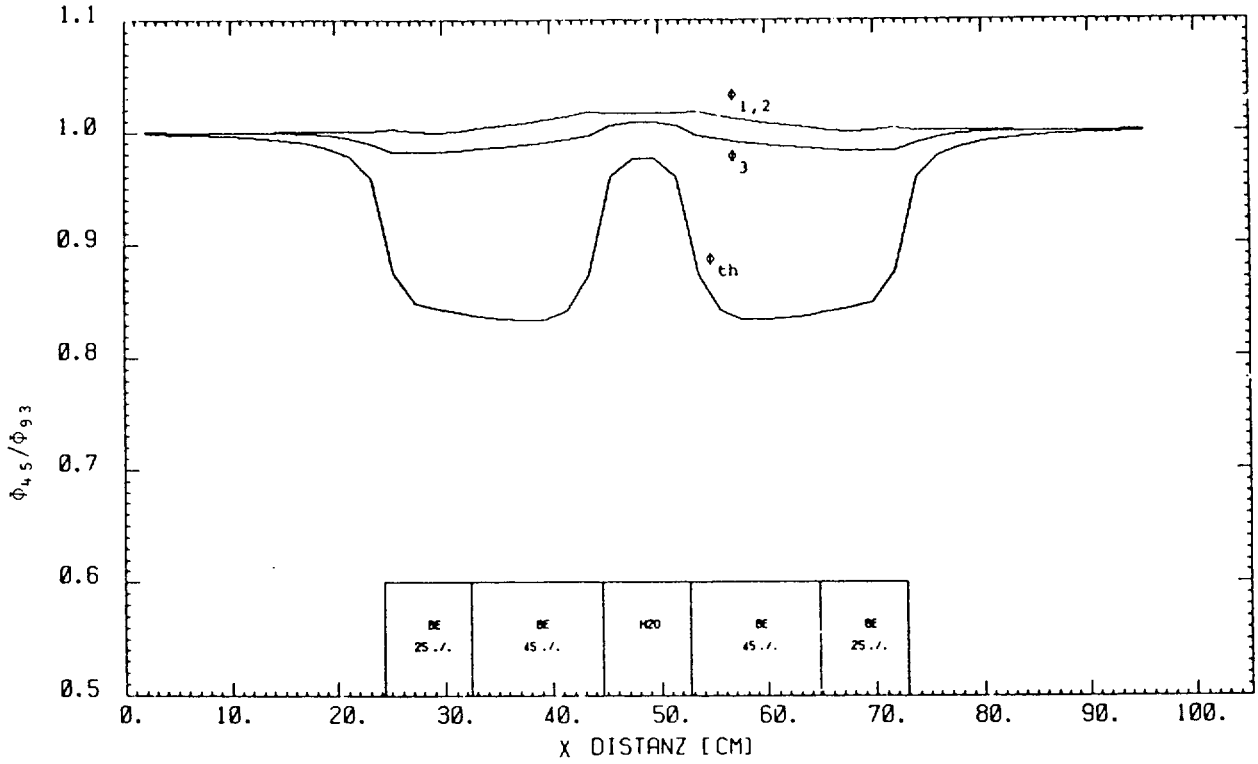

FIG. 16 QUOTIENT BOL 45(4E13) / BOL 93(4E13) [COL. 23]

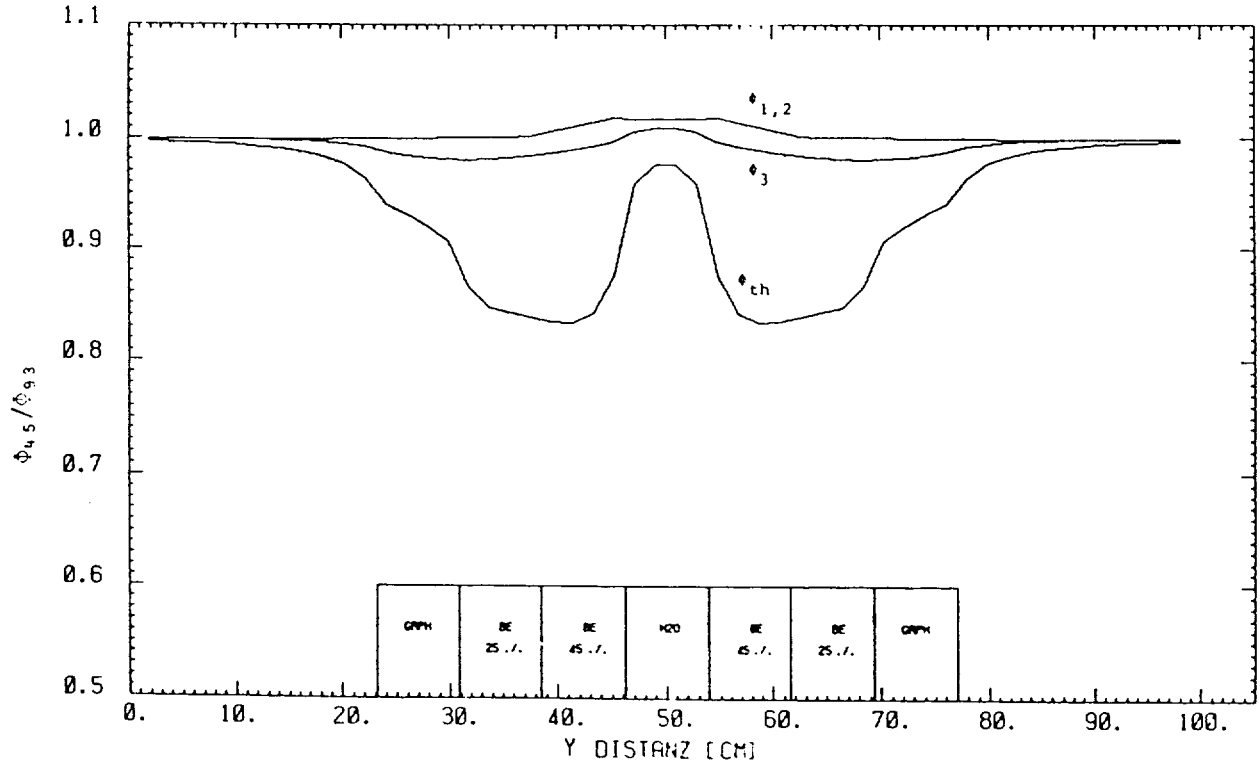

FIG. 17 QUOTIENT BOL 45(4E13) / BOL 93(4E13) [ROW 21]

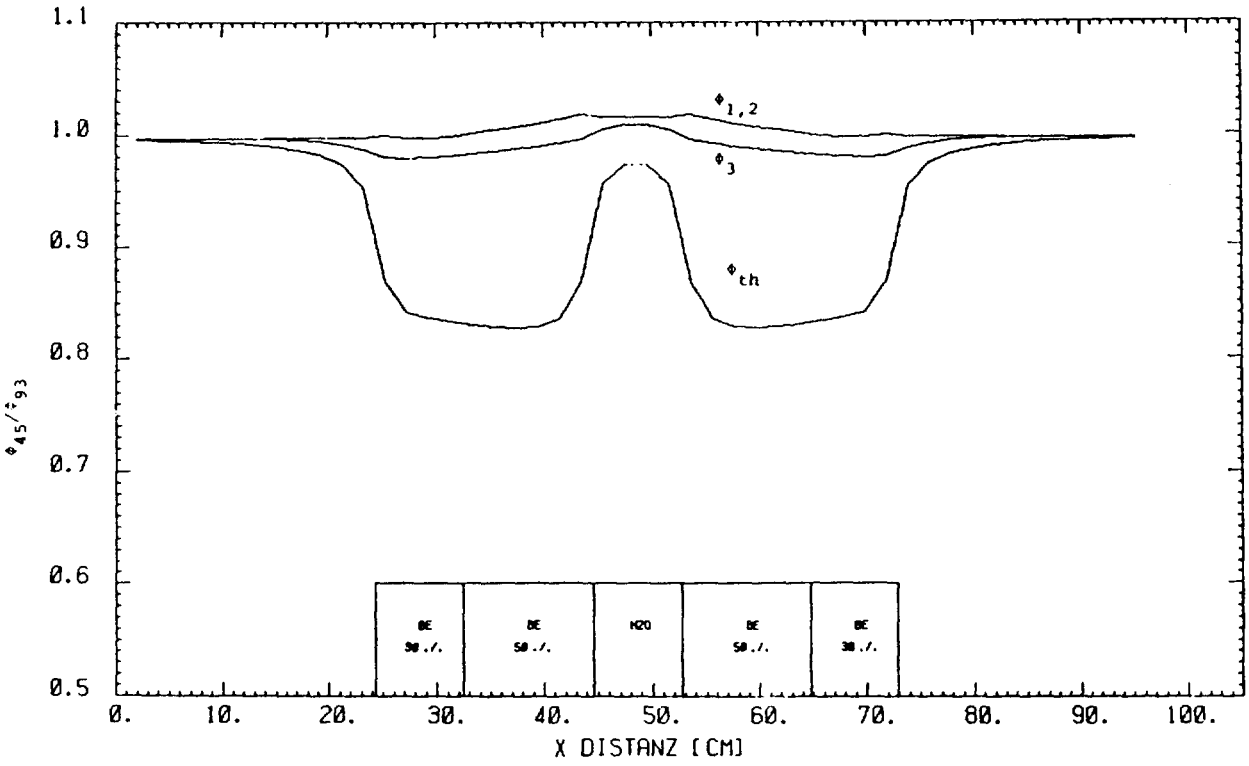

FIG. 18 QUOTIENT EOL 45(4E13) / EOL 93(4E13) [COL. 23]

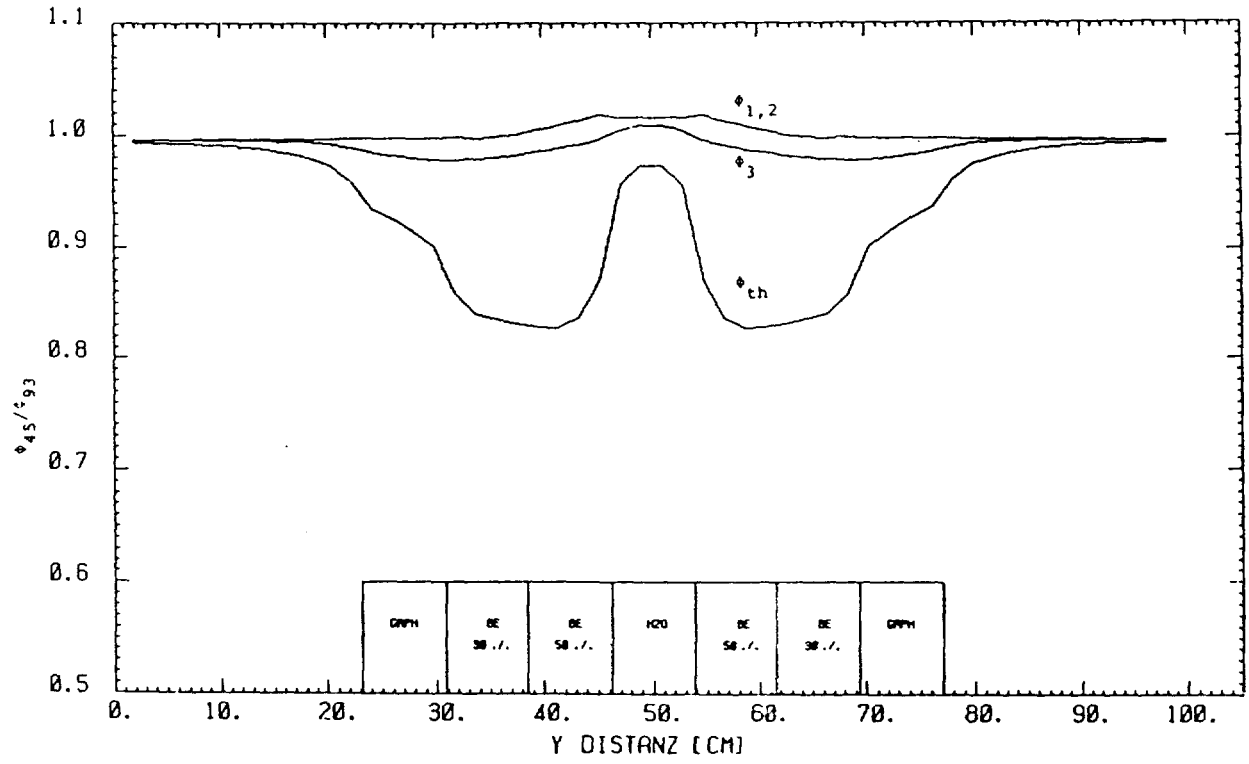

FIG. 19 QUOTIENT EOL 45(4E13) / EOL 93(4E13) [ROW 21]

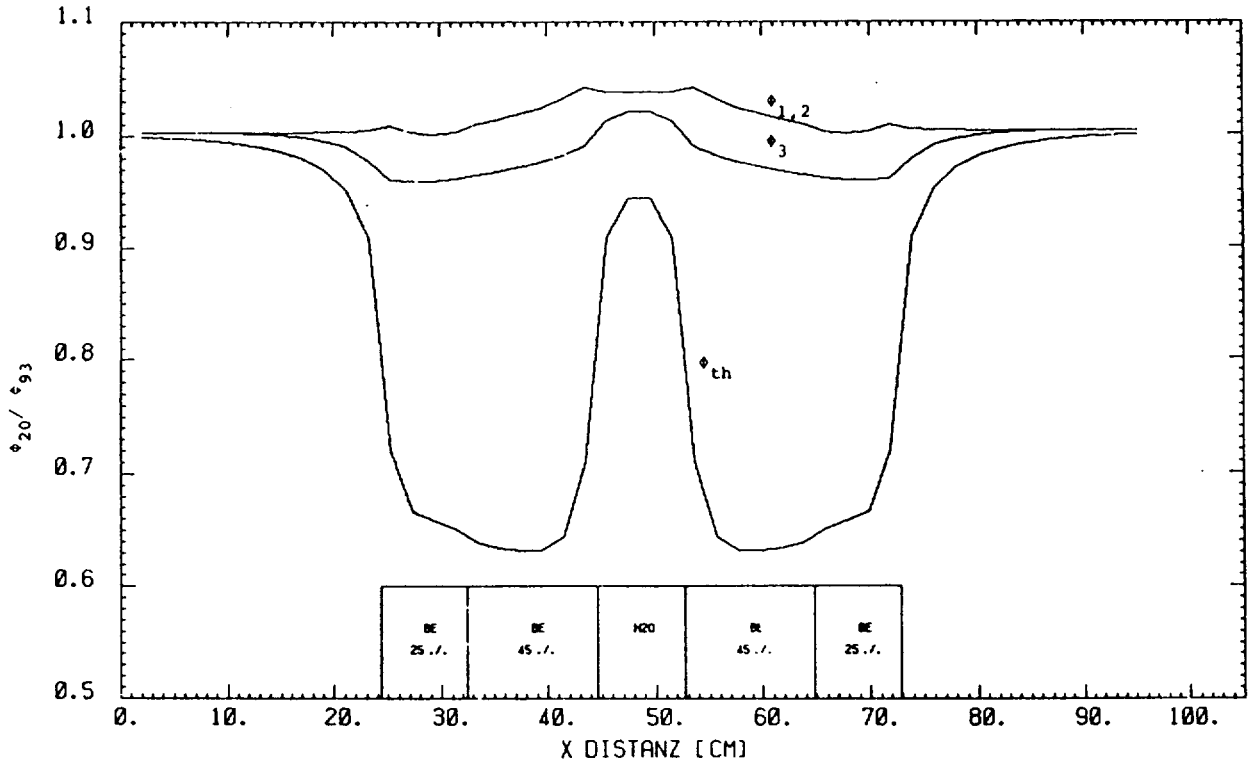

FIG. 20 QUOTIENT BOL 20(4E13) / BOL 93(4E13) [COL. 23]

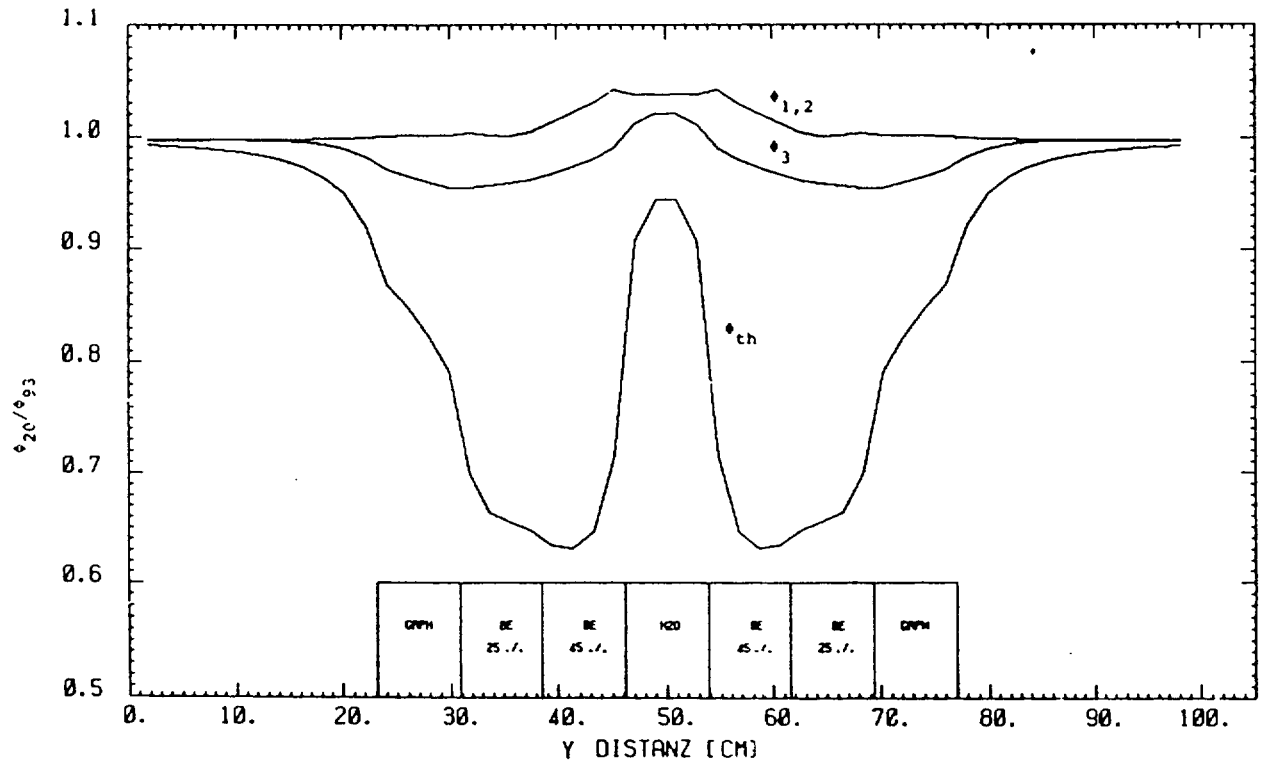

FIG. 21 QUOTIENT BOL 20(4E13) / BOL 93(4E13) [ROW 21]

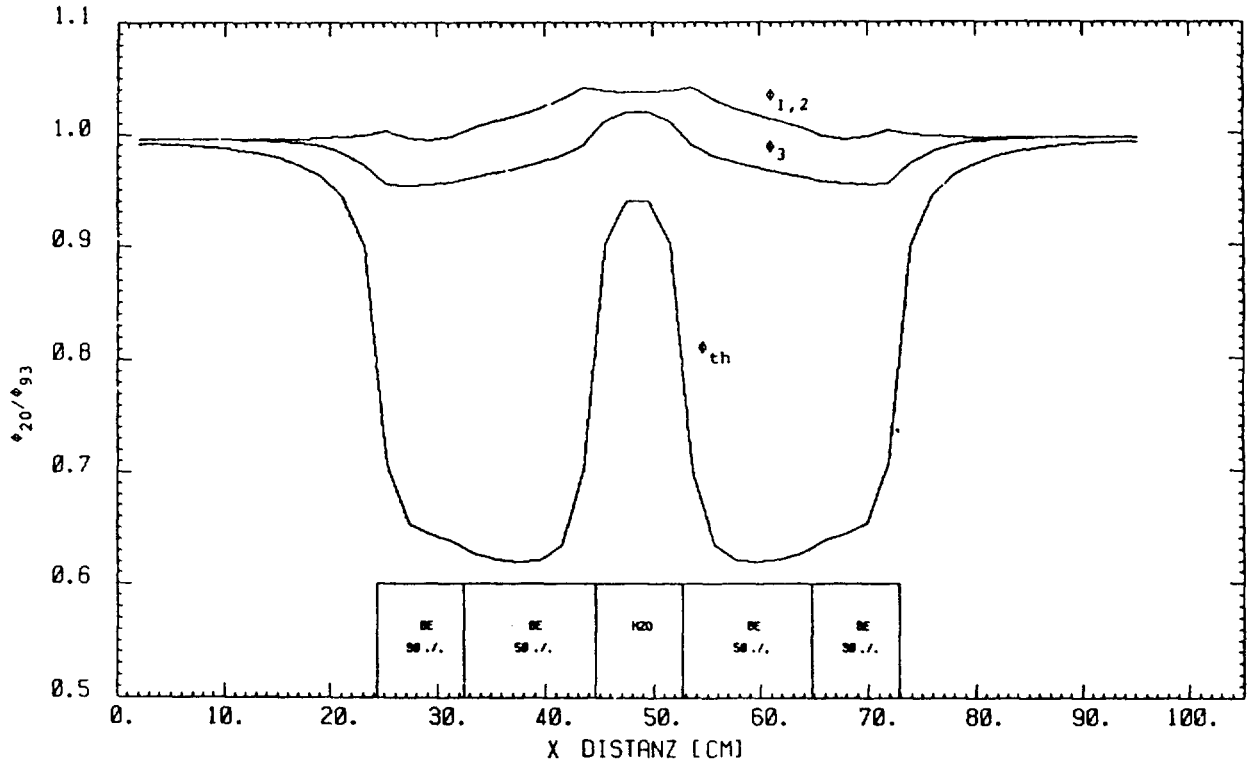

FIG. 22 QUOTIENT EOL 20(4E13) / EOL 93(4E13) [COL. 23]

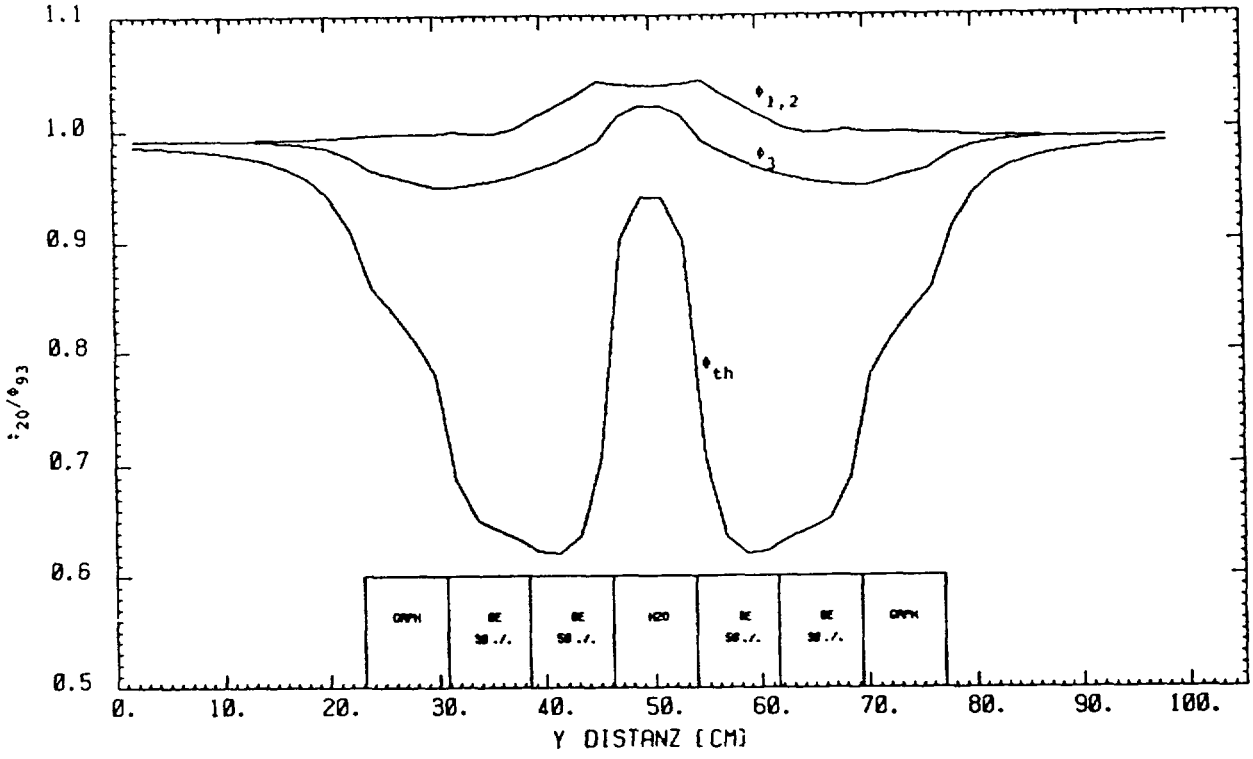

FIG. 23 QUOTIENT EOL 20(4E13) / EOL 93(4E13) [ROW 21]

Void effect at central element

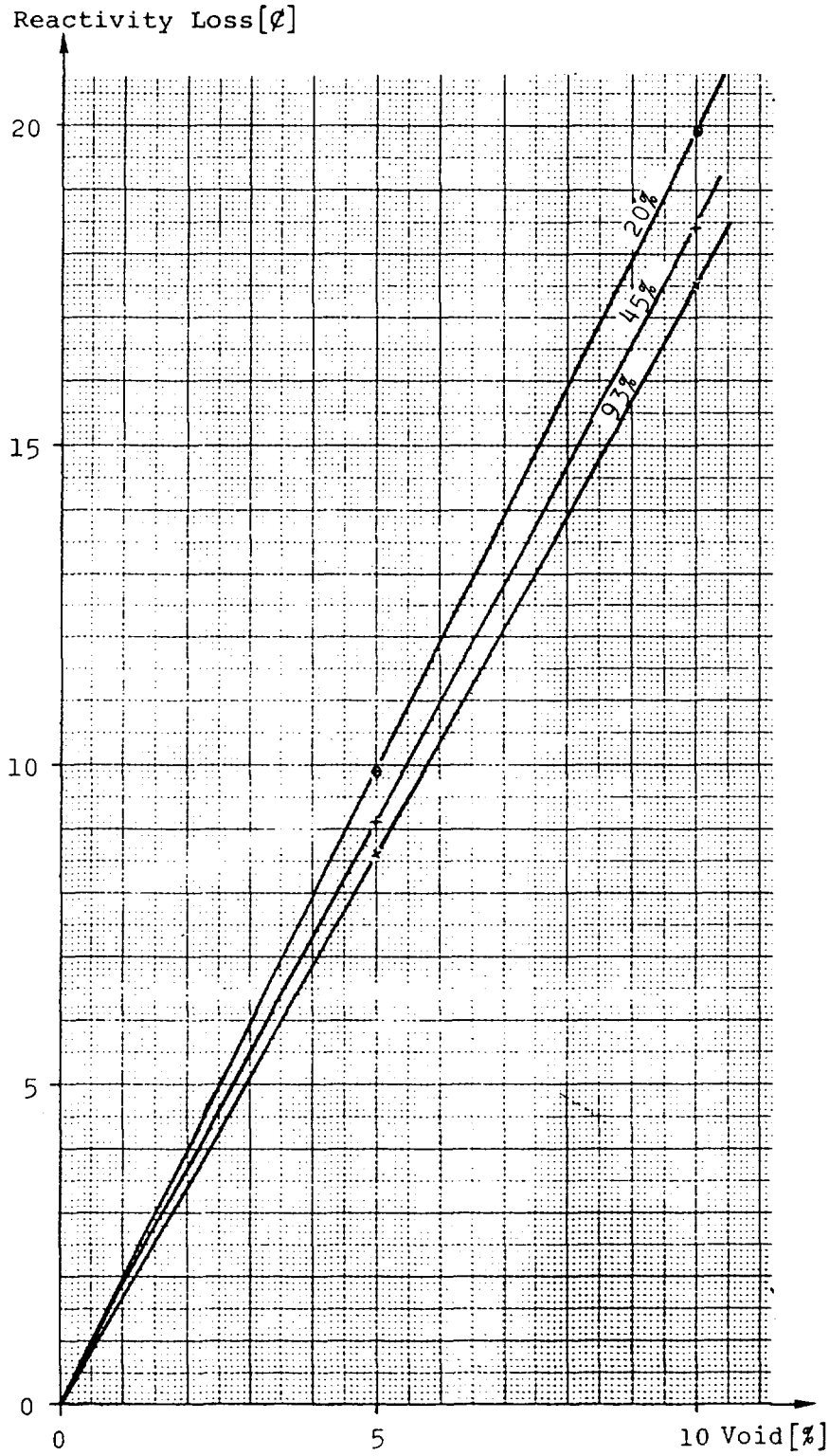

Fig. 24

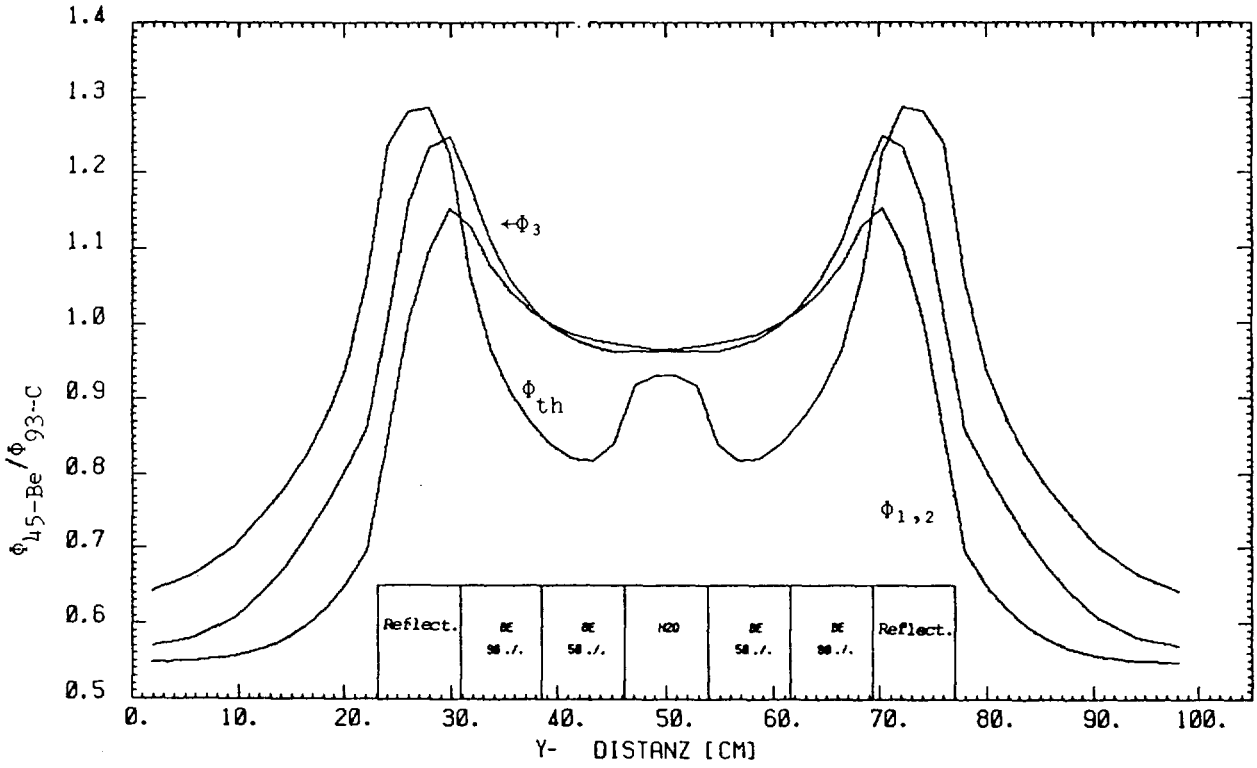

FIG. 25 QUOTIENT EOL45-4E13/93-4E13 , BE-M.2S/GRPH. [ROW 21]

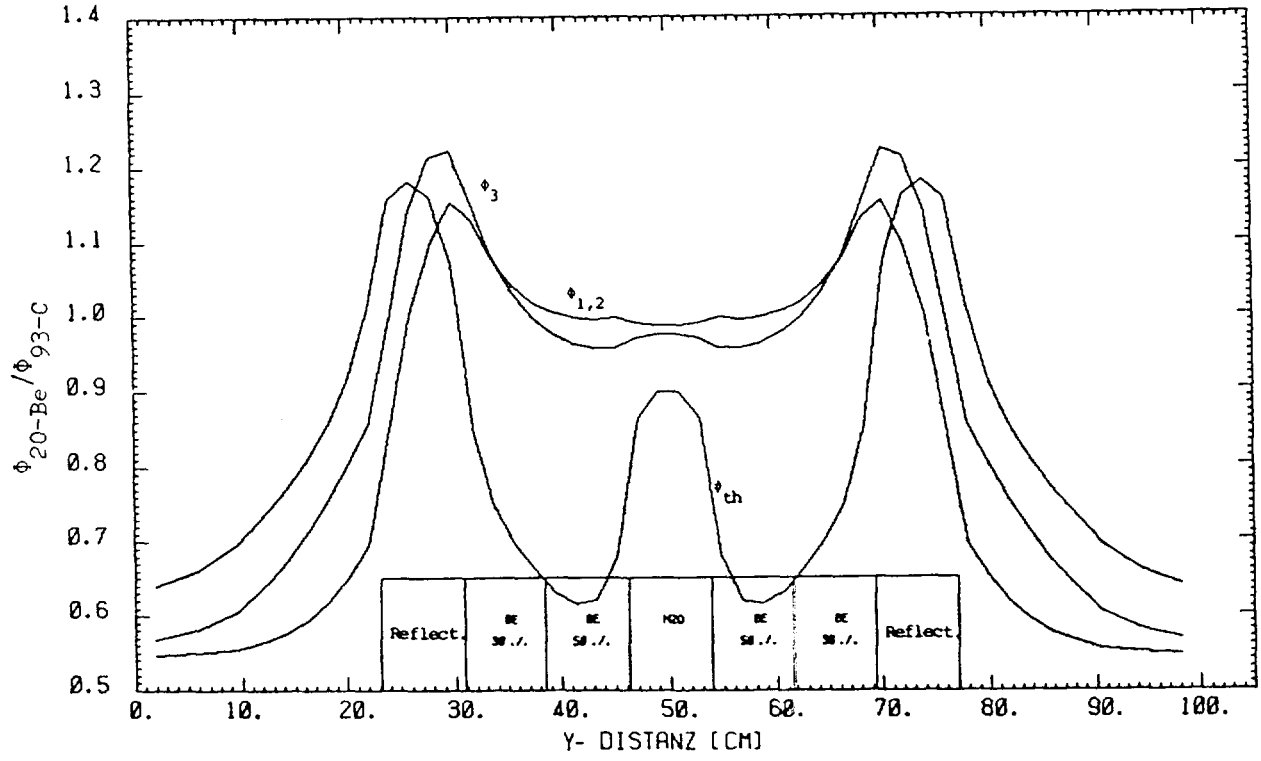

FIG. 26 QUOTIENT EOL20-4E13/93-4E13 , BE-M.2S/GRPH. [ROW 21]

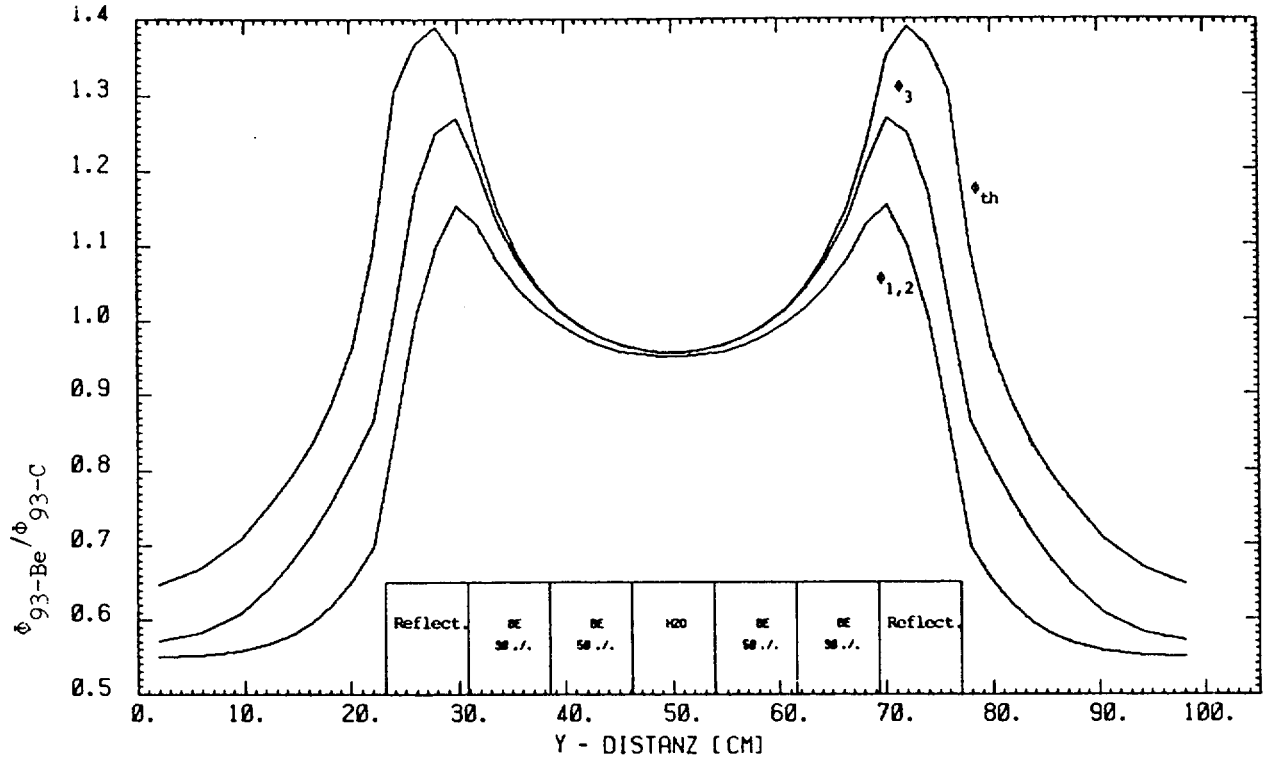

FIG. 27 QUOTIENT EOL93-4E13/93-4E13 , BE-M.2S/GRPH. [ROW 21]

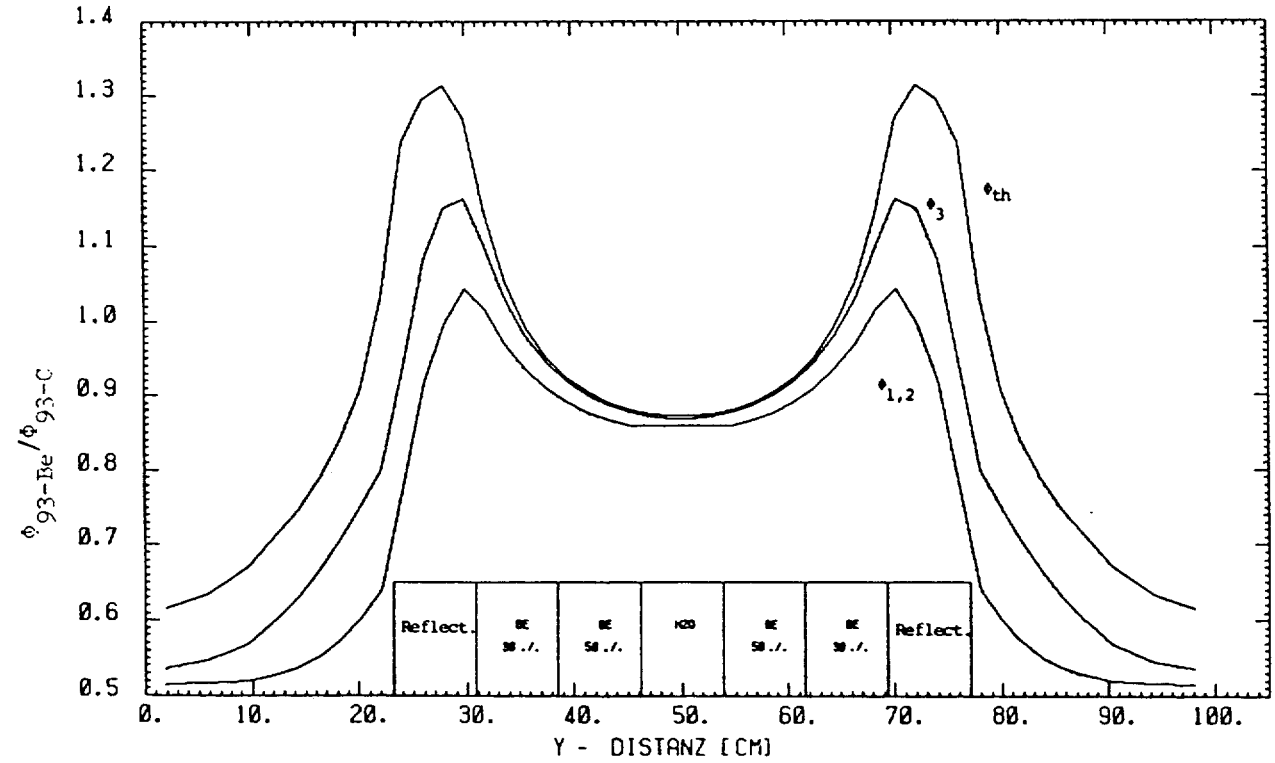

FIG. 28 QUOTIENT EOL93-4E13/93-4E13 , BE-M.4S/GRPH. [ROW 21]

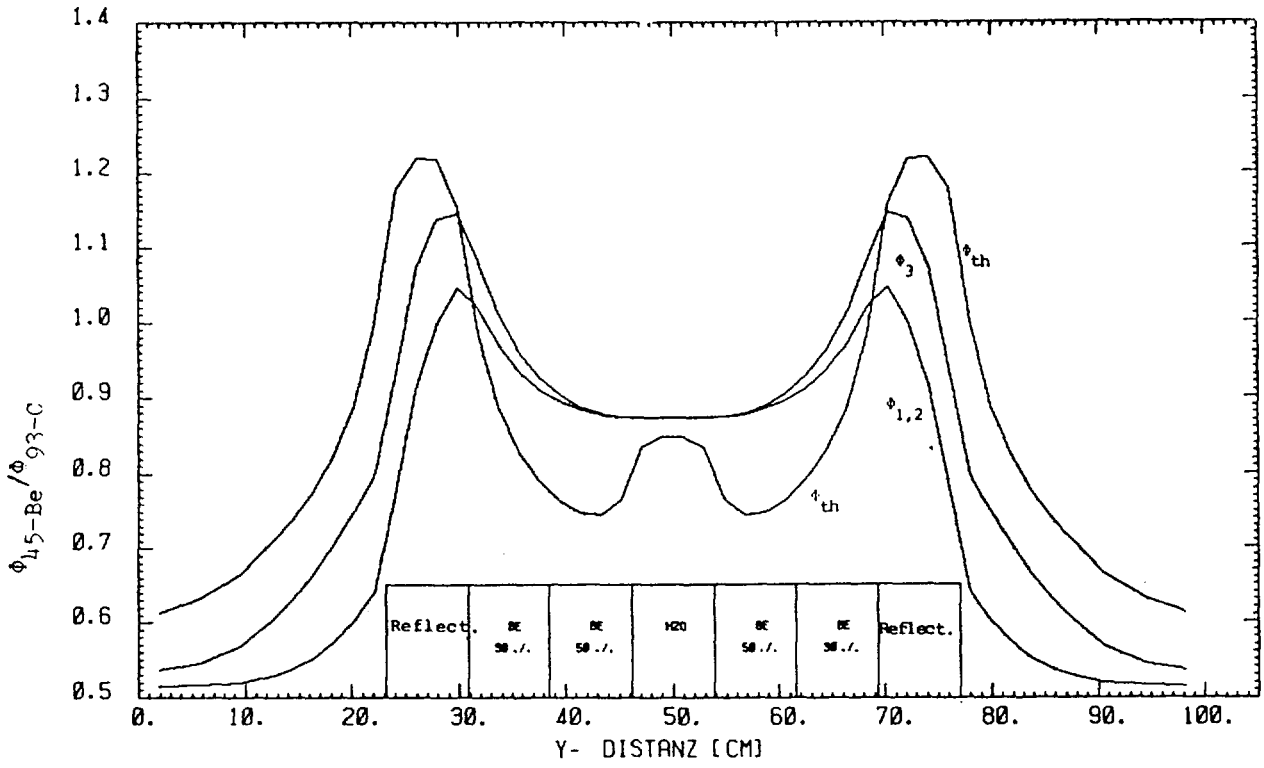

FIG. 29 QUOTIENT EOL45-4E13/93-4E13 , BE-M.4S/GRPH. [ROW 21]

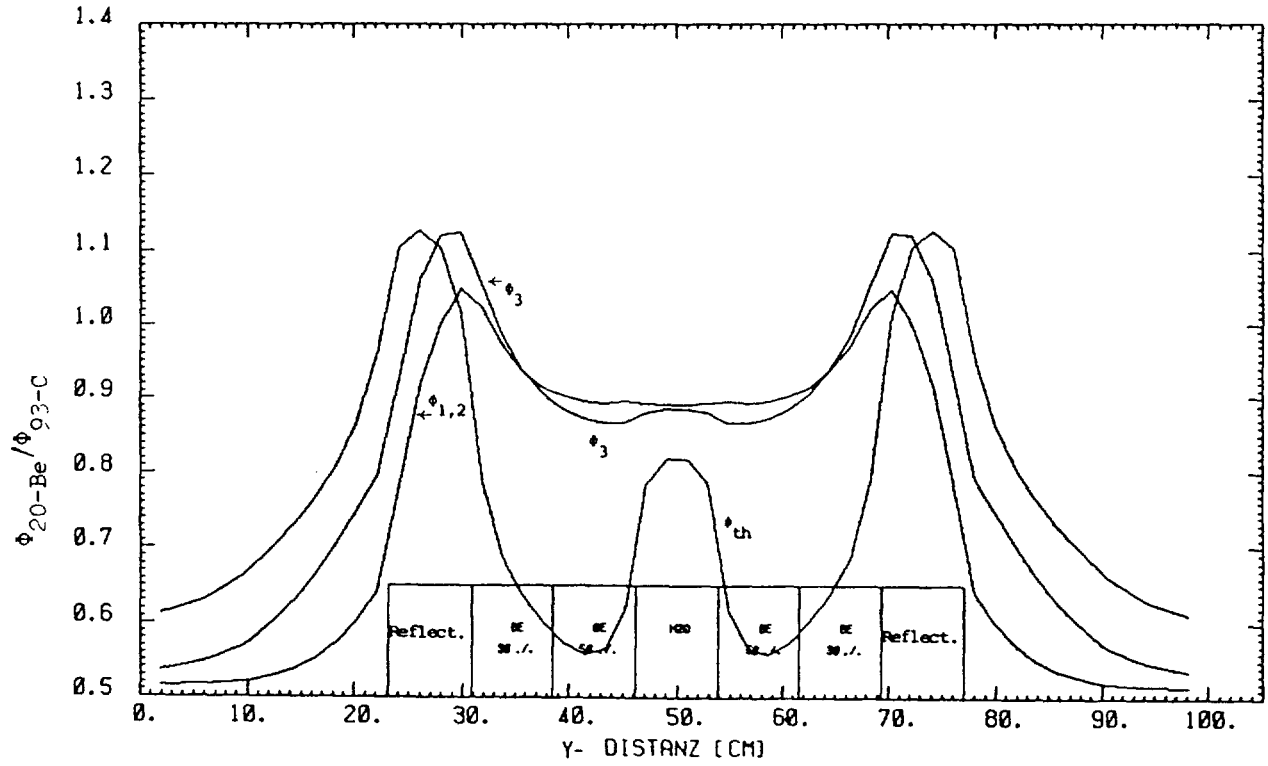

FIG. 30 QUOTIENT EOL20-4E13/93-4E13 , BE-M.4S/GRPH. [ROW 21]

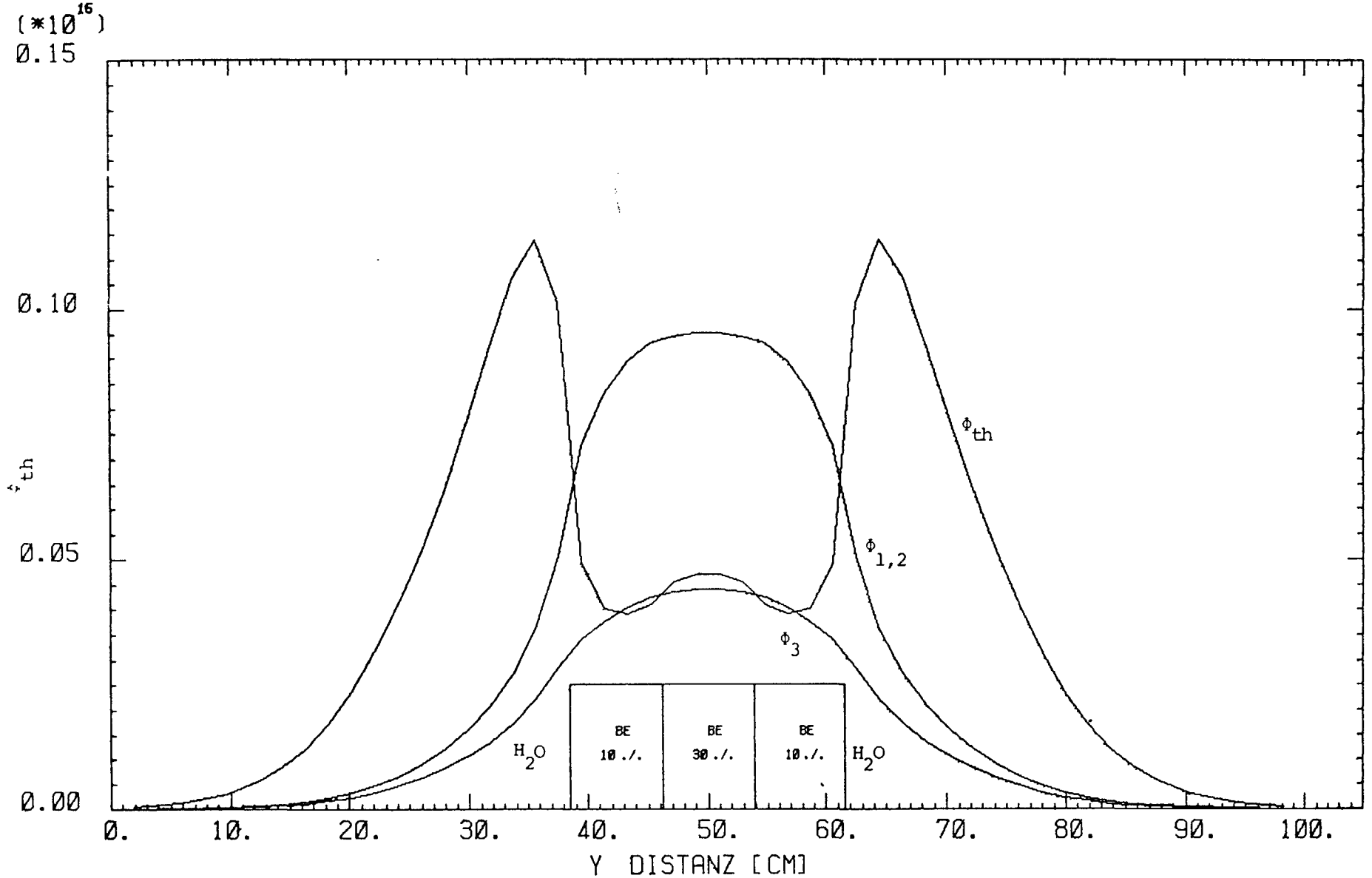

FIG. 31 FLUX EOL-93(4E13) GRPH. [ROW 11] Φ_{th}

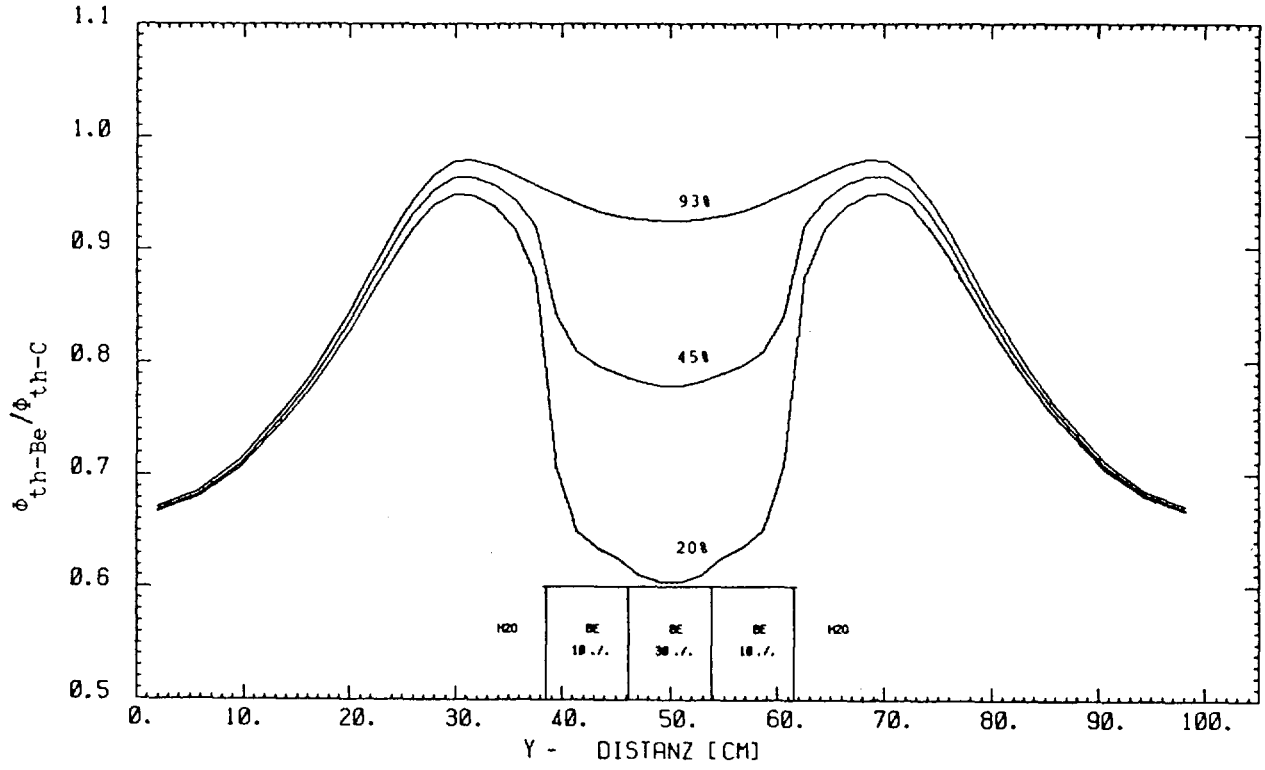

FIG. 32 QUOTIENT EOL-PHICD Φ_{th} : BE-M.2S / GRPH. [ROW 11]

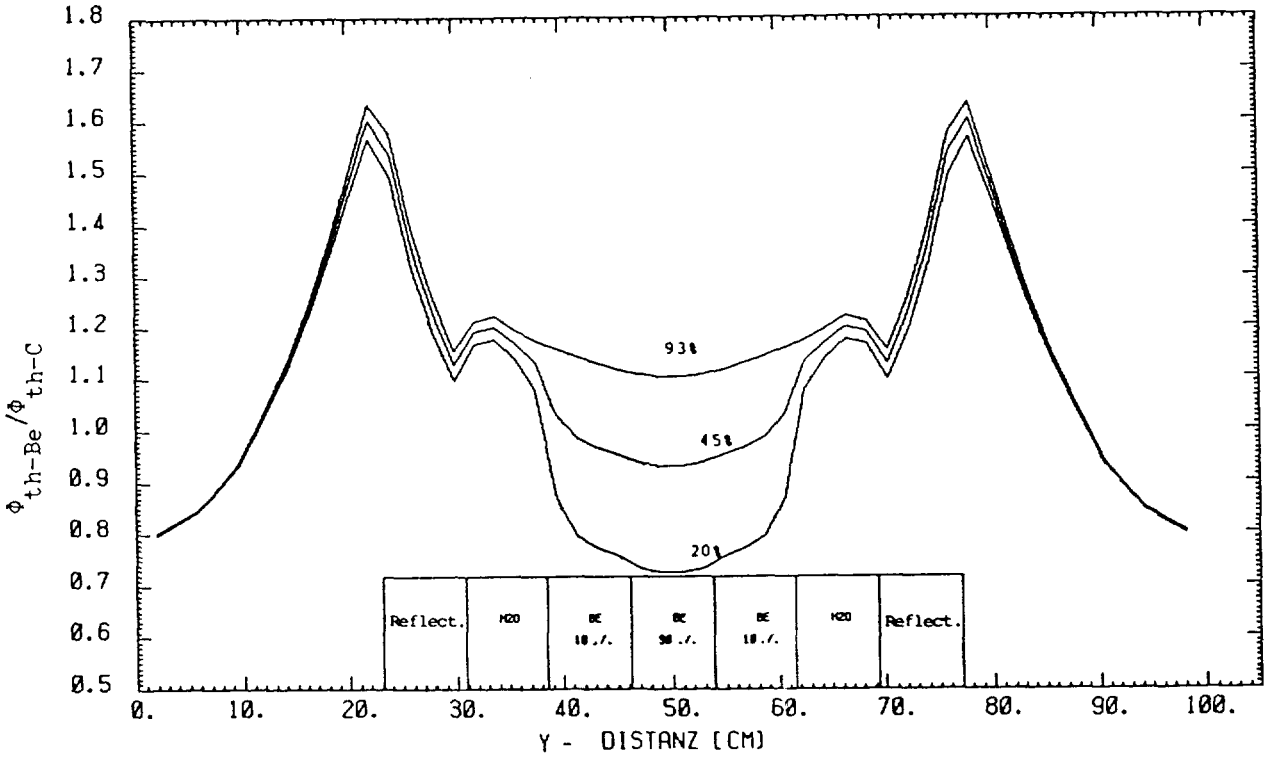

FIG. 33 QUOTIENT EOL-PHICD Φ_{th} BE-M.4S / GRPH. [ROW 11]

APPENDIX F-4

Benchmark-Core-Calculations for the Research Reactor Core Conversion to Lower Enrichments

performed by

A. Burtscher

F. Woloch

Österreichische
Studiengesellschaft fur Atomenergie
Ges.m.b.H.

Forschungszentrum Seibersdorf

ASTRA-Reaktor-Institut
Institut für Reaktorsicherheit

REX 142 revised edition

February 1980

BENCHMARK-CORE-CALCULATIONS FOR THE RESEARCH REACTOR CORE CONVERSION TO LOWER ENRICHMENTS

1. Indroduction

In view of the efforts to reduce the high enrichment of uranium for research reactors the Consultants Meeting held in June in Vienna has agreed upon a specification for benchmark calculations of a 1o MW core (see App. F-0). The core contains 21 standard fuel and 4 control elements. The aim of the calculations is a comparison of methods and data used by the different research centres as a first step towards preparing a programme on research reactor core conversion to use lower enrichments of uranium. For this final version of the report fresh cores have been studied in addition to the BOL (begin of life) and EOL (end of life) cores of the three enrichment cases, HEU (93 %), MEU (45 %) and LEU (2o %).

2. Method of calculation and results

The method chosen for the benchmark calculations was the WIMS-D code (Ref. 1) in conjunction with the diffusion code EXTERMINATOR (Ref. 2).

The WIMS-D code performs cell burn up calculations using as a data base a 69 group nuclear data library (Ref. 3). It contains resonance tables which are applied in transport theory calculations and are based on the equivalence principle of resounance absorption. The burn up calculation contains 33 explicit fission products and a single lumped fission product.

The macroscopic neutron cross sections gained from the burn up calculations were interpolated for the burn up needed in different regions of the core and

fed to EXTERMINATOR. This is a neutron diffusion code using 2 dimensional geometry. Although the problem defined represents only a quarter of a core, its modelling with 2400 mesh points and five groups has taken many hours of computer time on the CYBER 74 of the Technical University in Vienna.

2.1 Cell definition

The problem of modelling the fuel cell of the MTR type standard element into a one dimensional unit was solved by using laterally only the fuelled width of the element. All material from the unfuelled width was collected in an extra region. The fuel cell arrived at contains the 23rd part of the total fuel element with small water gaps included between the fuel elements. These gaps are generated by the pitch of element positions on the grid plate. To save the cell modelling and extra burn up calculations for the control element, the relevant material regions in EXTERMINATOR were filled with neutron cross sections for the standard element and two sets of water-aluminium mixtures.

2.2 Burn up and transport calculations

During the burn up of the standard fuel element cell transport calculations in 22 groups (Table 1) recalculated the neutron spectrum after 12 progressive burn up steps of 5 % including Xenon equilibrium. The smeared and condensed macroscopic neutron cross sections formed a working library for the EXTERMINATOR input. Table 1 also shows the five edit groups for this energy condensation to be applied to the neutron cross sections.

Table 1 Energy partition for cell transport and diffusion theory

Groups for transport theory	Upper Boundaries	Groups for diffusion theory
1	1o MeV	1
2	6.o7 MeV	1
3	3.68 MeV	1
4	2.23 MeV	1
5	1.35 MeV	1
6	0.82 MeV	2
7	0.183 MeV	2
8	4o.85 keV	2
9	5.53 keV	3
1o	48.o5 eV	3
11	15.97 eV	3
12	9.88 eV	3
13	4.oo eV	3
14	1.o7 eV	3
15	0.625	4
16	0.3oo eV	4
17	0.14o eV	5
18	0.o67 eV	5
19	0.o5o eV	5
2o	0.o35 eV	5
21	0.o25 eV	5
22	0.o15	5

Table 2 contains macroscopic absorption and production cross sections of the standard element for the energy range between 0. and 0.625 eV at the burn up stages needed in the input. Table 3 shows along with Fig. 1 and 2 the k_{∞} values for all three enrichment cases vs burn up (%) and MWd. Special calculations were needed for the regions containing water, graphite and aluminium water mixtures.

Fig. 3 gives the Pu^{239} amount in g per standard element for the cases studied.

Table 2

Thermal Neutron Cross Sections of the Standard Fuel Element for the Benchmark Problem at 1o MW including Xenon Equilibrium

% BU	HEU		MEU		LEU	
	Absorption	Production	Absorption	Production	Absorption	Production
5	0.o985	0.1657	0.1o87	0.1852	0.1259	0.2173
1o	0.o954	0.1587	0.1o56	0.1781	0.1231	0.21o4
25	0.o853	0.1363	0.o955	0.1553	0.1135	0.1876
3o	0.o817	0.1286	0.o919	0.1473	0.1o99	0.1794
45	0.o7o7	0.1o48	0.o8o4	0.1221	0.o982	0.1528
5o	0.o669	0.o966	0.o763	0.1131	0.o939	0.1432

2.3 Diffusion Calculations

The basic pitches of the grid plate are 7.7 and 8.1 cm. The area of a standard element including water gaps was represented at least by 64 mesh points in the calculation. A summary of the results of the calculations for fresh BOL and EOL cores of all considered enrichments is given in Table 4. Since all diffusion calculations were performed in 2 dimensional geometry the fluxes obtained represent axial averages. To compare them with centre plane values a factor of 1.31 is applied, assuming a cosine distribution with an extrapolated core height of 76 cm.

Figures 4 to 7 show the three group fluxes for MEU and LEU related to the corresponding LEU case against the x and y coordinates starting from the core centre. Only the BOL cases have been drawn since the EOL cases are only

Table 3

BENCHMARK CALCULATION: 1o MW CORE

k_{oo}-values for Xenon-Equilibrium

H E U			M E U			L E U		
BURN UP		k_{oo}	BURN UP		k_{oo}	BURN UP		k_{oo}
% U-235	MWd		% U-235	MWd		% U-235	MWd	
	0	(1.743)	0	0	(1.7o7)	0	0	(1.657)
0	0	1.669	0	0	1.637	0	0	1.593
5	272	1.641	5	3o6	1.61o	5	375	1.565
1o	532	1.621	1o	612	1.59	1o	749	1.546
15	8o4	1.598	15	93o	1.568	15	1135	1.525
2o	1o76	1.575	2o	1236	1.547	2o	1526	1.5o4
25	1348	1.55o	25	1554	1.523	25	1917	1.481
3o	162o	1.524	3o	1871	1.498	3o	2314	1.457
35	1891	1.495	35	2189	1.471	35	271o	1.432
4o	2163	1.463	4o	25o6	1.442	4o	3118	1.4o5
45	2435	1.428	45	2836	1.4o9	45	3537	1.375
5o	27o7	1.39o	5o	3166	1.373	5o	3955	1.344
55	2992	1.344	55	3495	1.333	55	4385	1.3o8
6o	3276	1.293	6o	3837	1.287	6o	4815	1.27o

( ) k_{oo}-values without Xenon

Table 4

Summary of Results of Benchmark Calculations

Case		HEU	MEU	LEU
enrichment %		93	45	2o
U-235 content in g				
	standard fuel element	28o	32o	39o
	fresh core	67o8	7666	9343
	equilibrium core (24,2 % BU)	5o87	5814	7o85
	burn up core (29,2 % BU)	4752	543o	6618
	burn up step of 5 %, g U-235	335	384	467
MWd of 5 % step		268	3o7	374
k_{eff} fresh core		1.1966	1.1896	1.1813
k_{eff} BOL core		1.o32o	1.o334	1.o32o
k_{eff} EOL core		1.oo9o	1.o116	1.o12o
Δk	%	2.3o	2.18	2.o
Δk/1oo MWd	%	0.86	0.71	0.53
g Pu^{239} in S.E. at 5o % BU		0.42	4.34	12.3o
ϕ_{th} (0 - 0.625 eV) centre hole in $1o^{14}$ n/cm^{2}s		2.56	2.49	2.38
ϕ_{th} centre hole	x 1.31	3.36	3.26	3.12
ϕ_{th} core edge hole in $1o^{14}$ n/cm^{2}s		0.6o	0.59	0.57
ϕ_{th} core edge hole	x 1.31	0.79	0.77	0.75

Table 5

Energy Partition of Flux Plot

Group	Flux	Energy Boundaries
1 + 2	fast	5.531 keV - 1o MeV
3	epithermal	0.625 eV - 5,531 keV
4 + 5	thermal	0 - 0.625 eV

marginally different. Figures 8 - 1o show the three group fluxes themselves with the group partitions of table 5.

3.) Discussion and Outlook

The method chosen is characterized by a rather large number of neutron energies used in the WIMS-D code in the resonance region in order to take into account the resonance absorption in the U-238 especially for the MEU- and LEU-fuels. Therefore, these calculations are also expected to give a good estimate of the Plutonium produced in the elements containing fuel with reduced enrichments.

Although this method of calculation was applied the first time at the ASTRA reactor institute for cores containing MTR fuel elements with different burn up values the k_{eff}-values agree well with the results obtained at other research institutions. Therefore the method can be considered capable to study the actual conversion of the ASTRA core to lower enriched fuels. Preliminary calculations in 2 dimensions have shown that there is an overprediction of reactivity for realistic ASTRA cores. A part of this overestimation could be attributed to the omission of axial burn up effects. Furthermore the situation is different in the ASTRA core from the assumptions used in the benchmark calculations, since beryllium elements with central-channels are used for irradiations in the core and a beryllium reflector is used instead of the graphite reflector. Finally the fuel element with 23 fuel plates will not be suitable for 2o % enriched fuel in a realistic study because of the larger amounts of uranium to be accommodated in the plates.

4.) References

1) J.R.ASKEW et al, A General Description of the lattice code WIMS JENES Oct. 1966 p 564
2) T.B. FOWLER, M.L. TOBIAS, D.R. VONDY, EXTERMINATOR-2 A Fortran IV Code for Solving Multigroup Neutron Diffusion Equations in Two Dimensions ORNL 4o78, April 1967
3) C.J. TAUBMANN, The WIMS 69-Group Library Tape 166259, AEEW-M 1234, 1975

Table 6/1

Ø MEU/ Ø HEU: x-direction

x /cm/	GROUP 1 + 2		GROUP 3		GROUP 4 + 5	
	BOL	EOL	BOL	EOL	BOL	EOL
0.003	1.006	1.007	1.000	1.001	0.970	0.969
2.03	1.006	1.007	0.999	0.999	0.963	0.961
4.050	1.007		0.992		0.912	
6.075	1.004		0.988		0.861	
8.10	1.000	1.000	0.985	0.985	0.847	0.844
8.804	0.999		0.984		0.846	
10.653	0.996		0.982		0.845	
13.65	0.994	0.993	0.979	0.979	0.847	0.843
15.495	0.993		0.979		0.849	
16.200	0.992		0.978		0.850	
18.225	0.991		0.978		0.852	
20.250	0.991		0.978		0.854	
22.28	0.993	0.991	0.978	0.977	0.863	0.858
24.300	0.996		0.980		0.910	
26.33	0.995	0.993	0.988	0.986	0.963	0.960
28.350	0.995		0.991		0.977	
30.375	0.995		0.993		0.983	
32.40	0.995	0.992	0.993	0.992	0.987	0.985
34.425	0.996		0.993		0.990	
36.45	0.997	0.991	0.995	0.992	0.991	0.988
38.475	0.995		0.997		0.993	
40.500	0.992		0.994		0.992	
44.550	0.995	0.996	0.992	1.000	0.993	1.000

Table 6/2

Ø LEU/ Ø HEU: x-direction

x /cm/	GROUP 1 + 2 BOL	GROUP 1 + 2 EOL	GROUP 3 BOL	GROUP 3 EOL	GROUP 4 + 5 BOL	GROUP 4 + 5 EOL
0.003	1.013	1.013	1.000	1.000	0.929	0.926
2.025	1.013	1.014	0.997	0.996	0.913	0.908
4.050	1.015		0.982		0.796	
6.075	1.007		0.971		0.684	
8.10	0.997	0.997	0.964	0.963	0.658	0.650
8.804	0.995		0.962		0.656	
10.653	0.990		0.958		0.656	
13.65	0.984	0.982	0.953	0.950	0.659	0.651
15.495	0.981		0.951		0.665	
16.200	0.980		0.950		0.666	
18.225	0.977		0.948		0.671	
20.250	0.978		0.949		0.674	
22.28	0.983	0.979	0.950	0.946	0.690	0.682
24.300	0.989		0.952		0.793	
26.33	0.988	0.984	0.970	0.967	0.914	0.908
28.350	0.987		0.979		0.946	
30.375	0.987		0.982		0.961	
32.40	0.986	0.983	0.985	0.981	0.969	0.964
34.425	0.988		0.986		0.975	
36.46	0.987	0.982	0.989	0.981	0.979	0.974
38.475	0.985		0.991		0.981	
40.500	0.984		0.986		0.982	
44.55	0.986	0.982	0.984	0,992	0.986	1.000

Table 6/3

Ø MEU/ Ø HEU: y-direction

y	GROUP 1 + 2		GROUP 3		GROUP 4 + 5	
/cm/	BOL	EOL	BOL	EOL	BOL	EOL
0.003	1.006	1.007	1.000	1.001	0.970	0.969
1.925	1.006	1.007	0.999	0.999	0.962	0.961
3.850	1.007		0.992		0.913	
5.775	1.004		0.987		0.863	
7.700	1.000	1.000	0.984	0.985	0.848	0.845
9.625	0.997		0.982		0.846	
11.550	0.994		0.980		0.848	
13.475	0.992	0.992	0.978	0.978	0.851	0.847
15.400	0.992		0.978		0.854	
17.325	0.993		0.978		0.862	
19.250	0.994	0.992	0.977	0.976	0.895	0.891
21.175	0.994		0.979		0.912	
23.100	0.994	0.992	0.981	0.980	0.925	0.921
25.025	0.993		0.984		0.935	
26.950	0.994	0.992	0.986	0.985	0.944	0.941
28.875	0.994		0.989		0.967	
30.800	0.994		0.992		0.977	
32.725	0.994	0.991	0.992	0.992	0.982	0.980
34.650	0.994		0.995		0.985	
36.575	0.991		0.995		0.988	
38.500	0.993		0.993		0.988	
40.425	0.993		0.992		0.990	
42.350	0.993	0.982	0.995	0.991	0.990	0.988

Table 6/4

Ø LEU/ Ø HEU: y-direction

y	GROUP 1 + 2		GROUP 3		GROUP 4 + 5	
/cm/	BOL	EOL	BOL	EOL	BOL	EOL
0.003	1.013	1.013	1.000	1.000	0.929	0.926
1.925	1.013	1.014	0.997	0.996	0.912	0.908
3.850	1.015		0.982		0.798	
5.775	1.007		0.971		0.688	
7.700	0.997	0.997	0.963	0.962	0.659	0.651
9.625	0.990		0.958		0.658	
11.550	0.984		0.953		0.664	
13.475	0.980	0.977	0.950	0.948	0.670	0.661
15.400	0.979		0.948		0.675	
17.325	0.982		0.947		0.689	
19.250	0.985	0.982	0.945	0.942	0.760	0.752
21.175	0.984		0.950		0.798	
23.100	0.984	0.981	0.955	0.952	0.828	0.820
25.025	0.984		0.960		0.852	
26.950	0.984	0.981	0.966	0.963	0.871	0.864
28.875	0.983		0.973		0.924	
30.800	0.983		0.979		0.945	
32.725	0.983	0.980	0.981	0.979	0.957	0.952
34.650	0.985		0.982		0.964	
36.575	0.981		0.980		0.968	
38.500	0.985		0.982		0.973	
40.425	0.983		0.981		0.974	
42.350	0.982	0.965	0.983	0.979	0.977	0.973

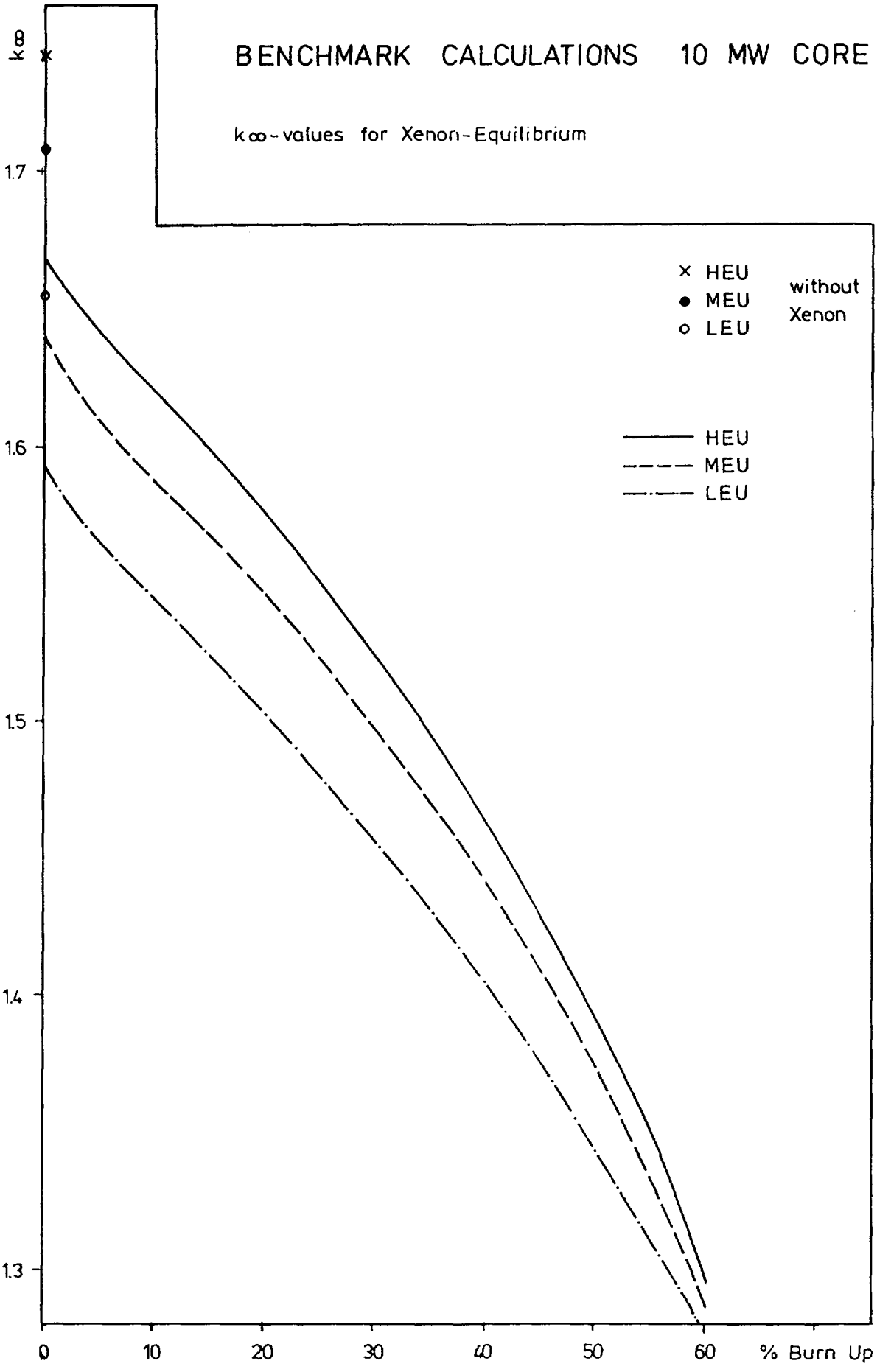
BENCHMARK CALCULATIONS 10 MW CORE
k∞-values for Xenon-Equilibrium
k∞
1.7
1.6
1.5
1.4
1.3
× HEU
● MEU
○ LEU
without Xenon
HEU
MEU
LEU
0
10
20
30
40
50
60
% Burn Up

Fig.: 1

BENCHMARK CALCULATIONS 10 MW CORE Fig.: 2

$k\infty$ - values for Xenon-Equilibrium

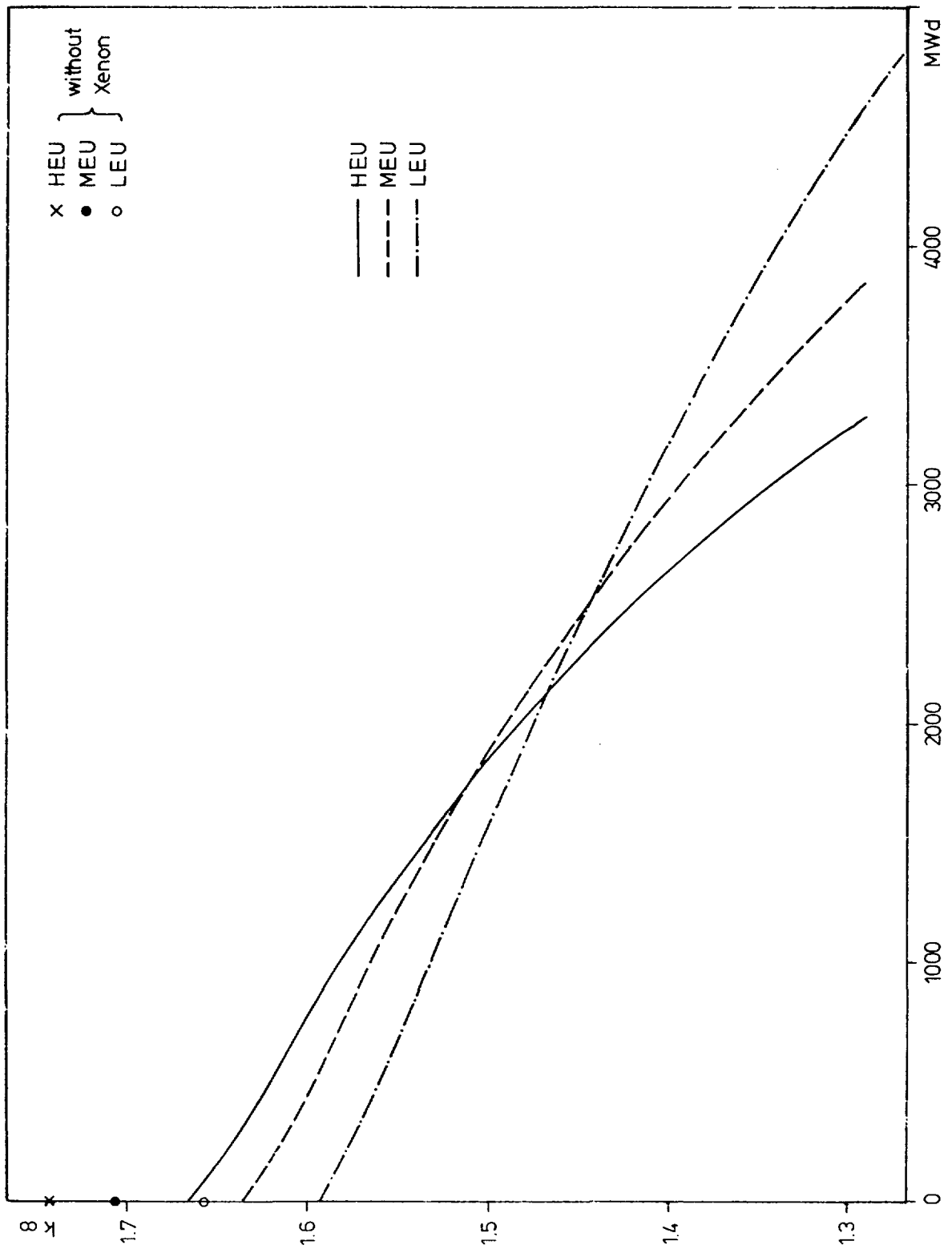

BENCHMARK CALCULATIONS 10 MW CORE

Pu-Production in Standard Fuel Element

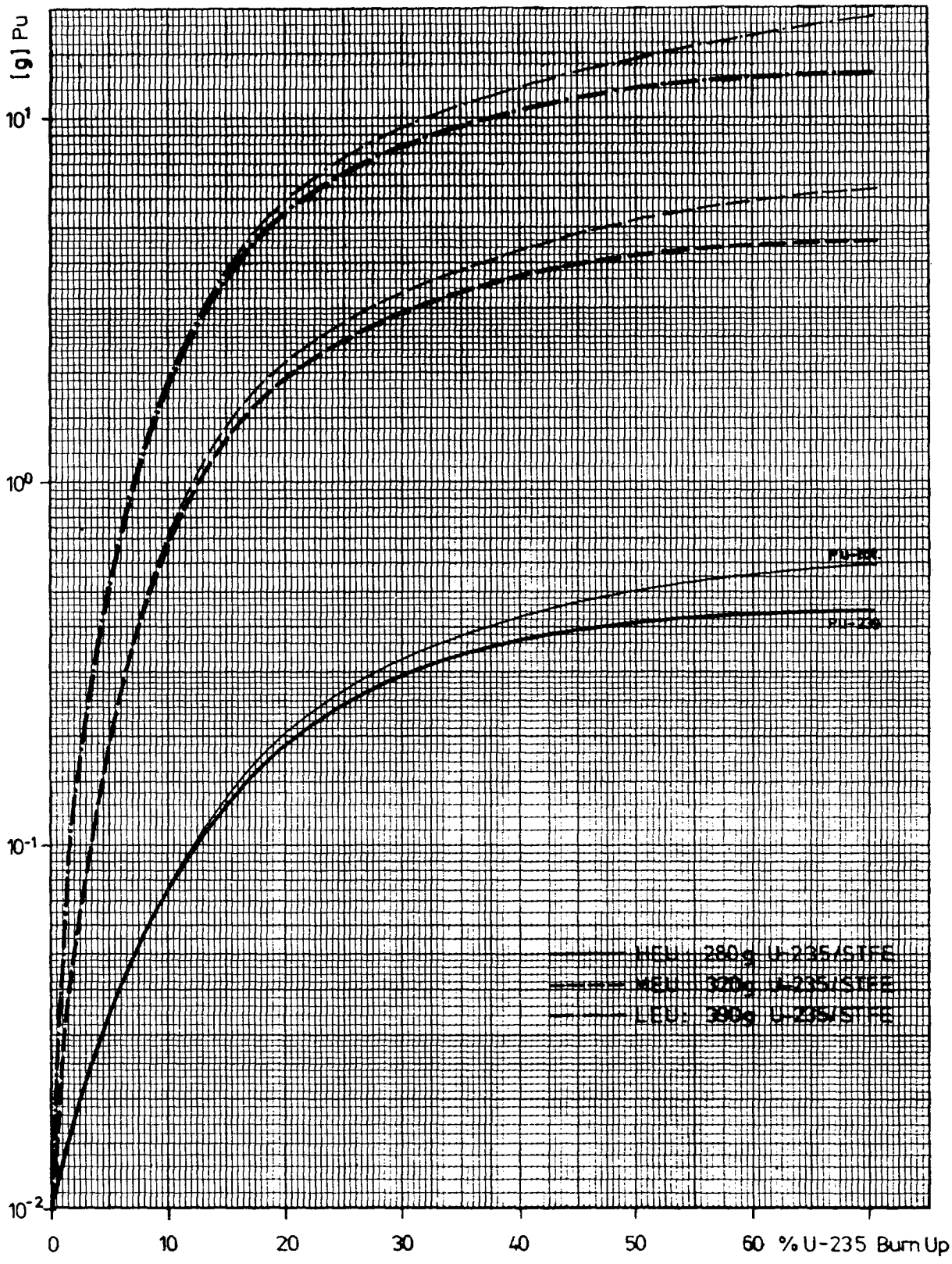

Fig.: 3

BENCHMARK CALCULATIONS, 10 MW CORE

45% enriched Uranium

Ratio of flux-values in the core center-line :
BOL, Xenon-Equilibrium
Φ MEU/ΦHEU, x-direction

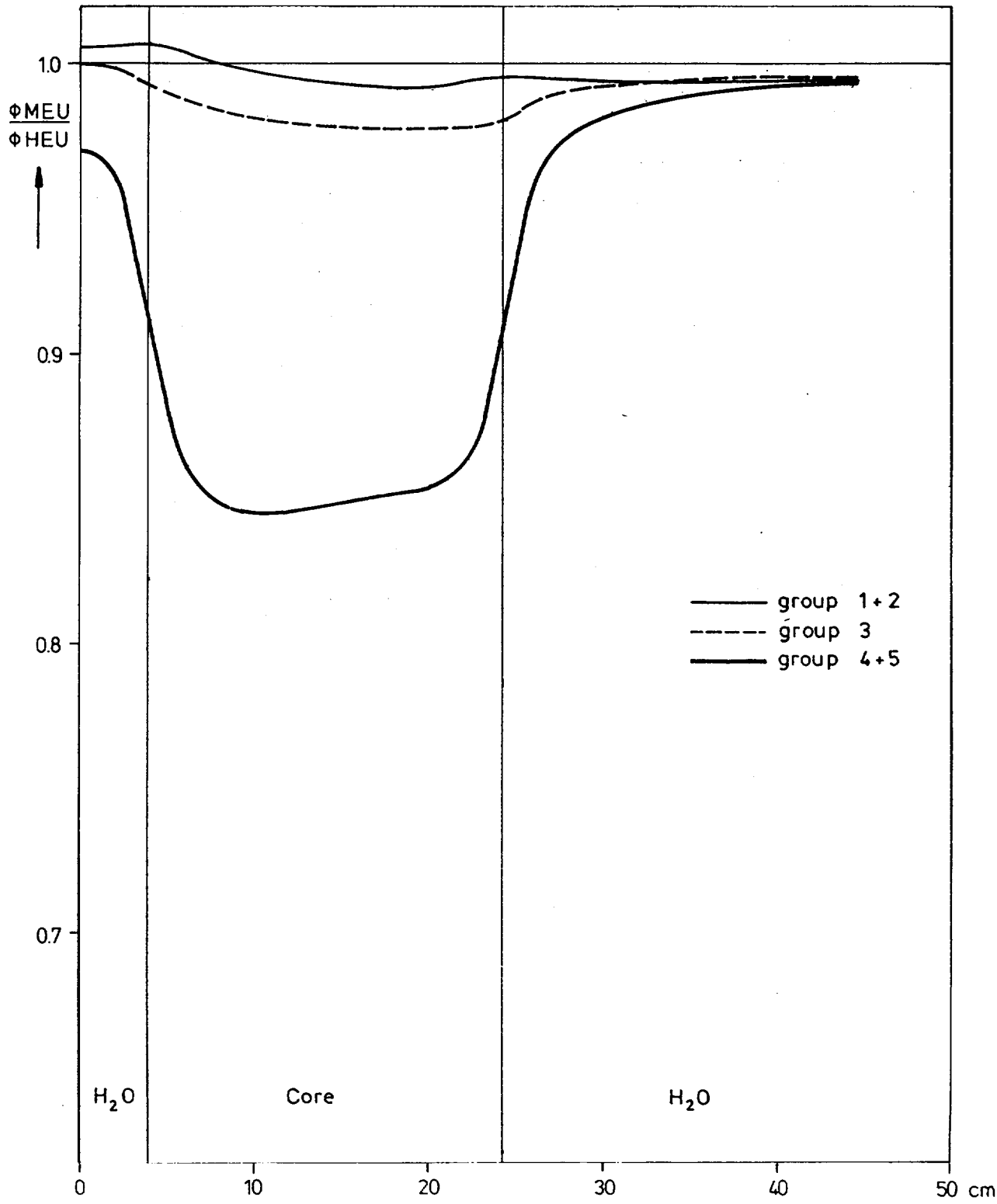

Fig.: 4

BENCHMARK CALCULATIONS, 10 MW CORE

45% enriched Uranium

Ratio of flux-values in the core center-line :
BOL, Xenon-Equilibrium
Φ MEU/ΦHEU, y-direction

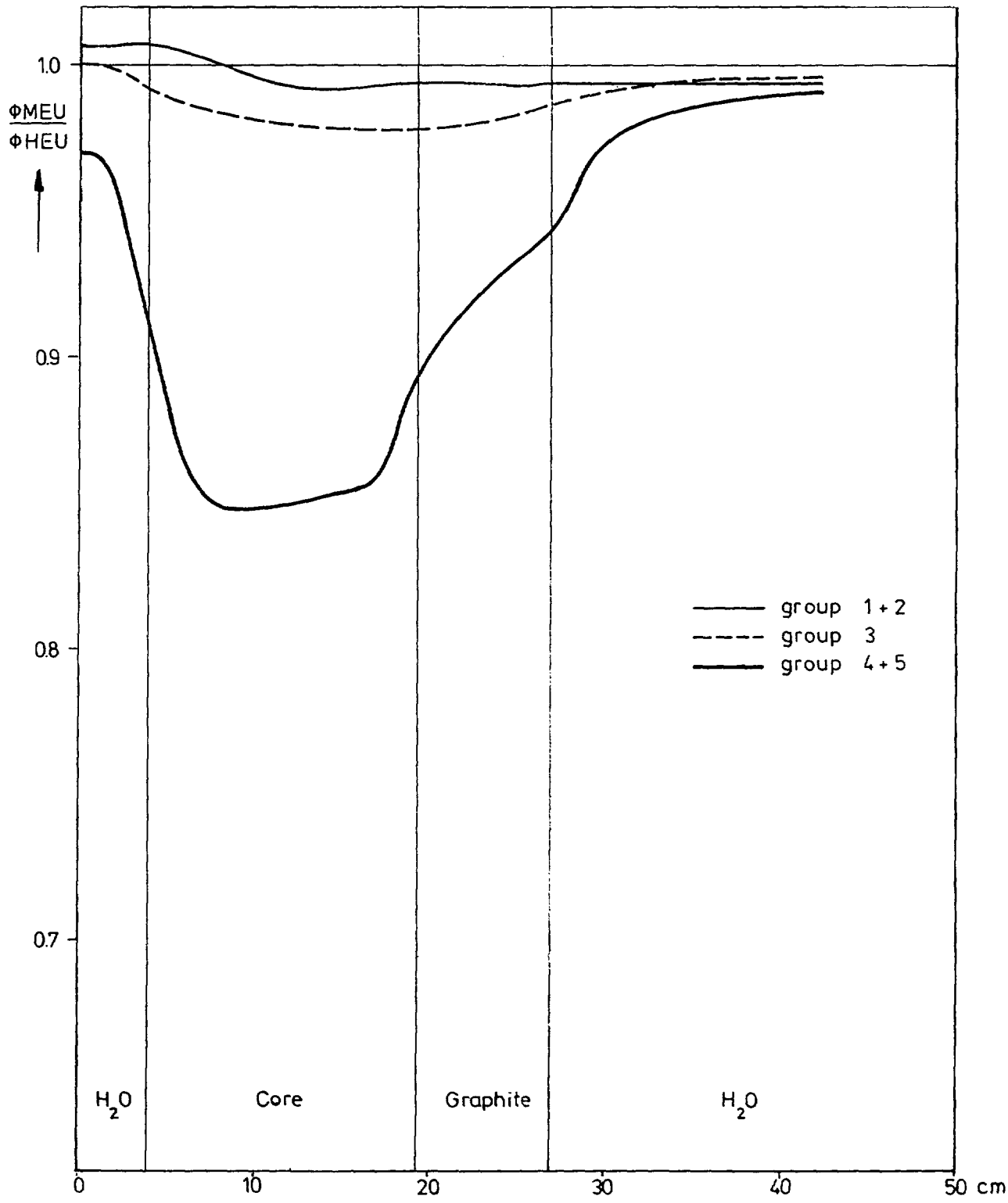

Fig.: 5

BENCHMARK CALCULATIONS,. 10 MW CORE

20% enriched Uranium

Ratio of flux-values in the core center-line :
BOL, Xenon-Equilibrium
ΦLEU/ΦHEU, x-direction

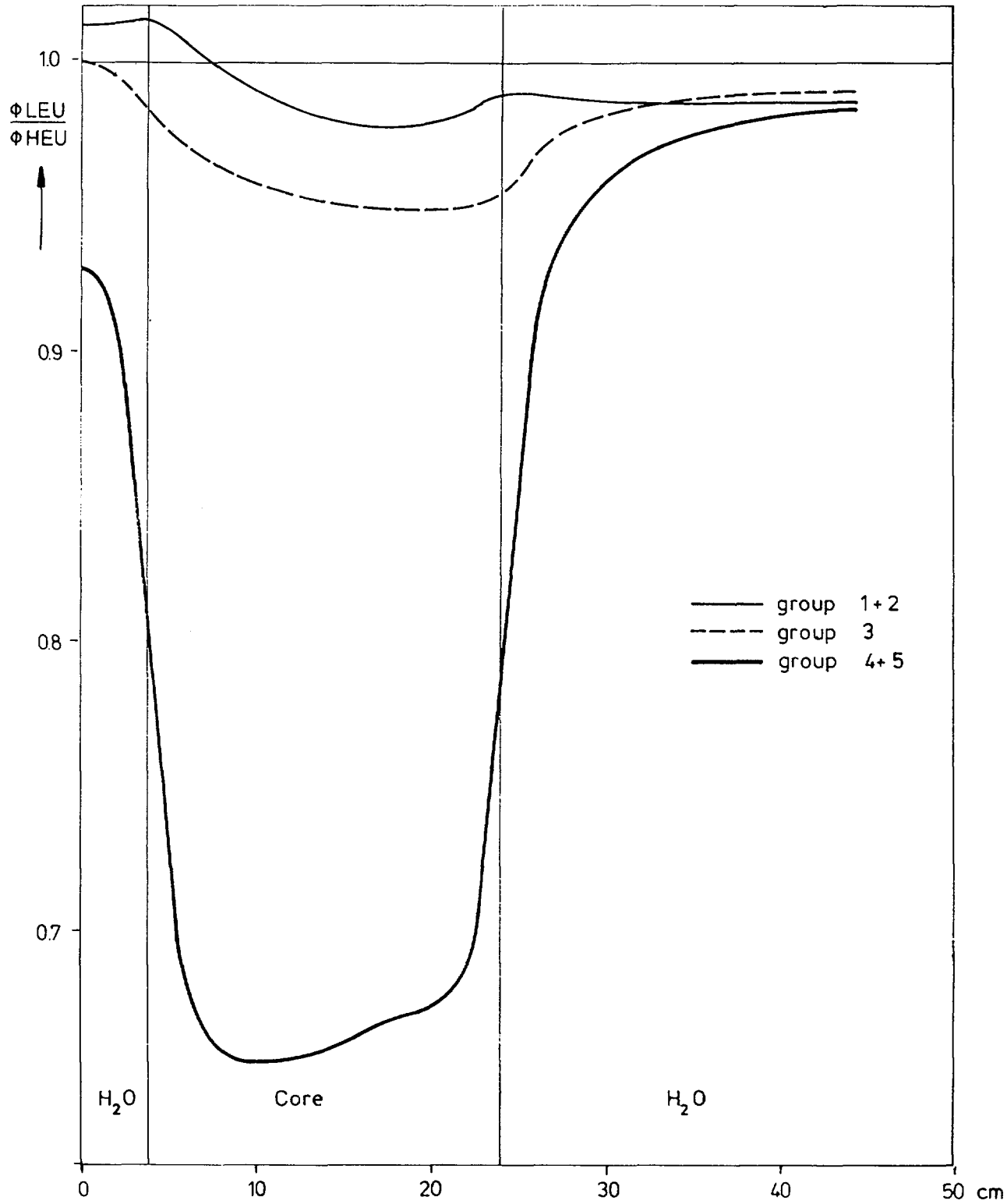

Fig.: 6

BENCHMARK CALCULATIONS, 10 MW CORE

20% enriched Uranium

Ratio of flux-values in the core center line :
BOL, Xenon-Equilibrium
Φ LEU/ΦHEU, y-direction

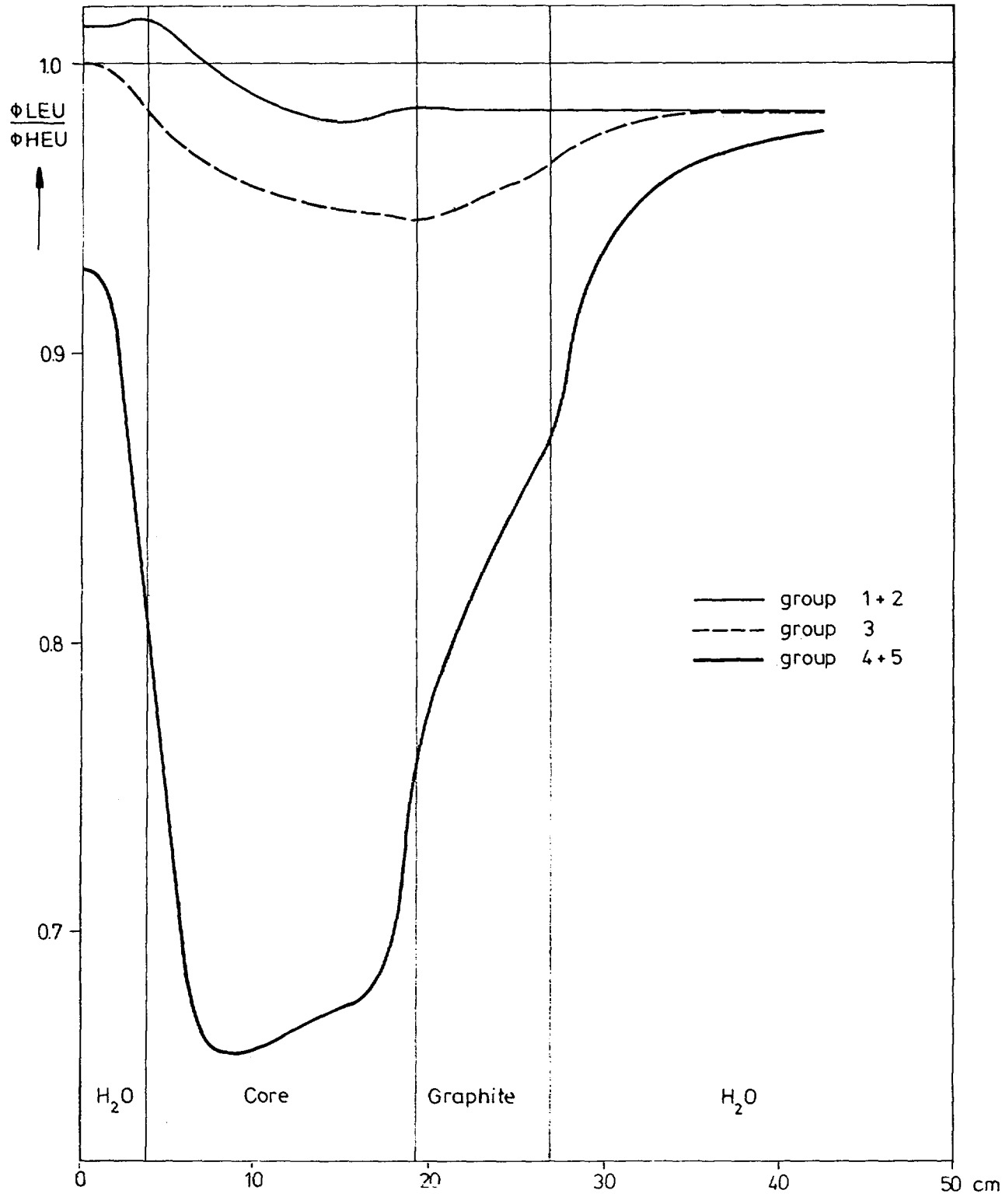

Fig.: 7

BENCHMARK CALCULATIONS. 10 MW CORE

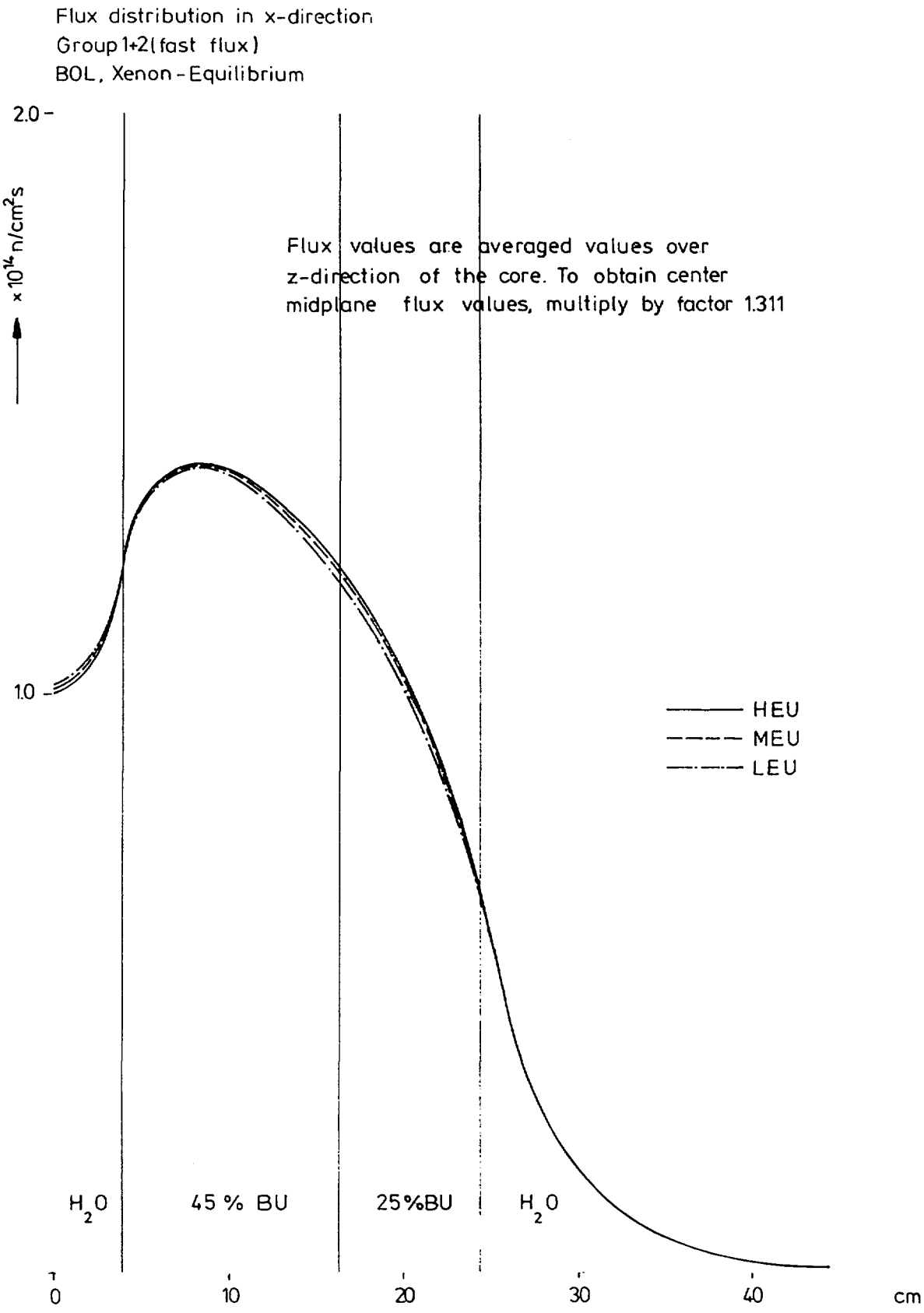

Fig.: 8

BENCHMARK CALCULATIONS, 10 MW CORE

Flux distribution in x-direction
Group 3 (epithermal flux)
BOL, Xenon-Equilibrium

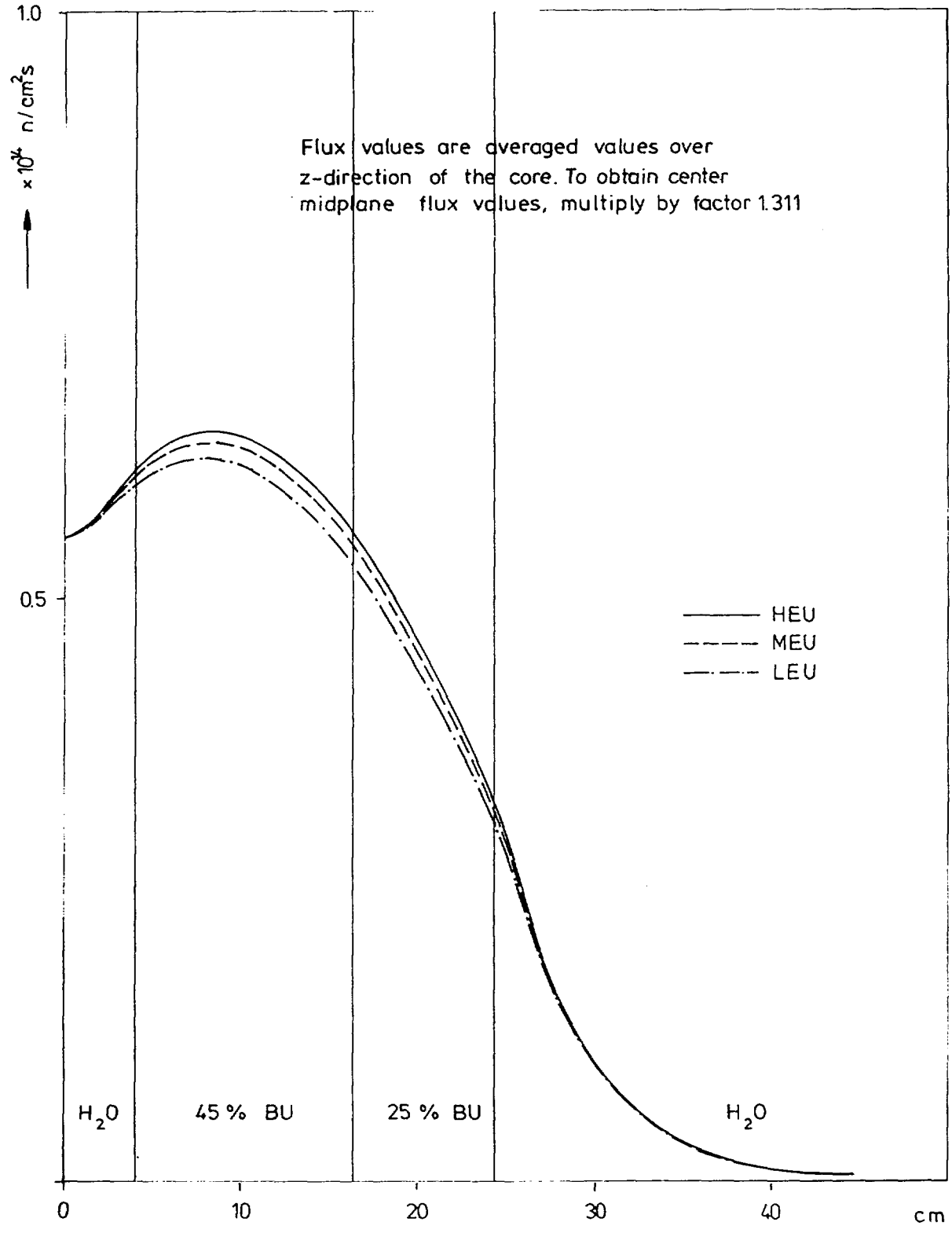

Fig.: 9

BENCHMARK CALCULATIONS, 10 MW CORE

Fig.: 10

Flux distribution in x-direction
Group 4+5(thermal flux)
BOL, Xenon-Equilibrium

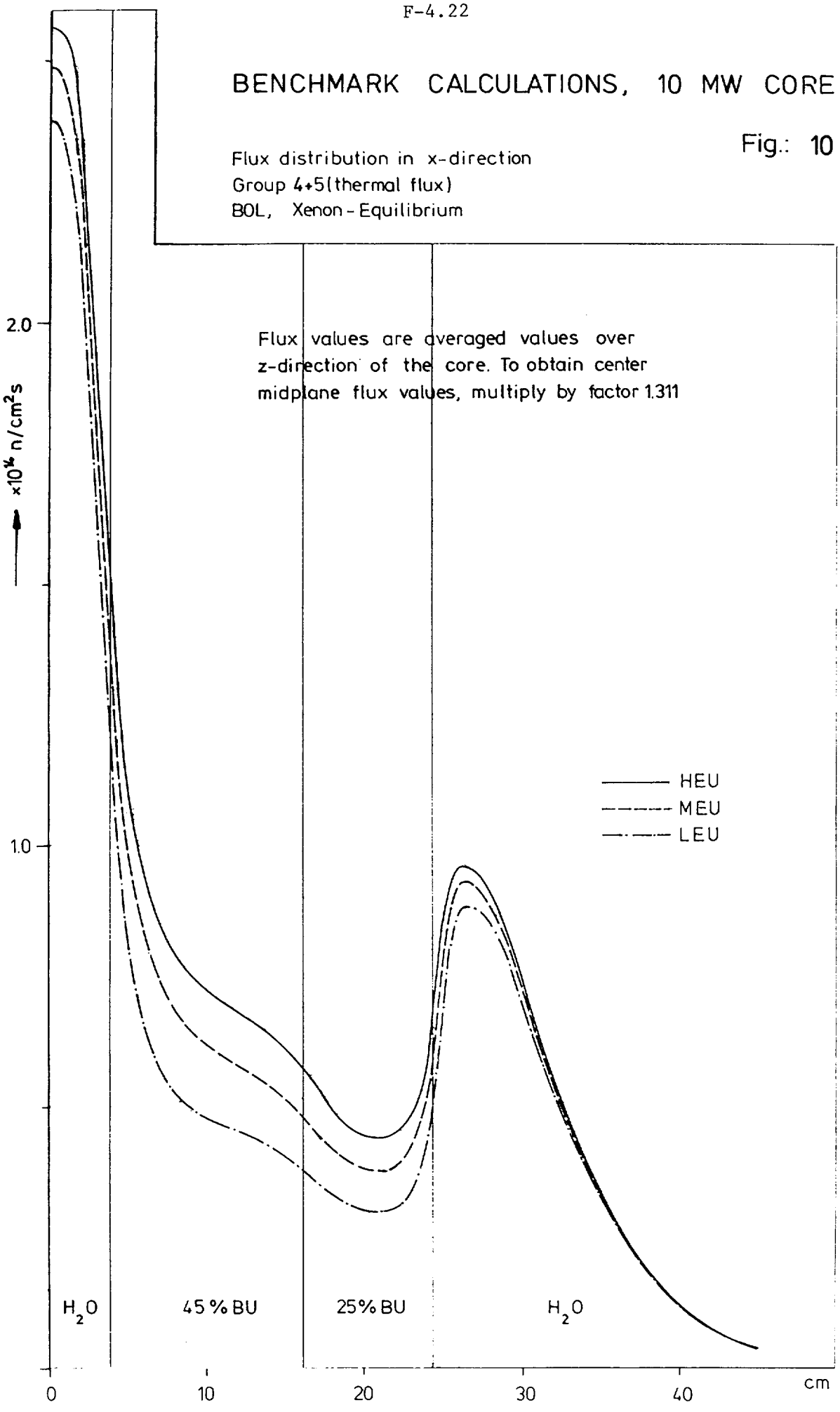

APPENDIX F-5

Benchmark Calculations for MTR type Reactors with High, Medium and Low Enrichment

performed by

Commissariat à l'Énergie Atomique, CEA

France

BENCHMARK CALCULATION FOR MTR TYPE REACTOR WITH HIGH, MEDIUM AND LOW ENRICHMENT

INTRODUCTION

In order to compare the accuracy of the research reactors calculations methods, benchmark problems were calculated with the methods developped at the Commissariat à l'Energie Atomique. The benchmark problems were specified at Vienne, June 19-22.

FUEL ELEMENT

The MTR fuel elements were considered. The standard fuel element and the control fuel element respectively contain 23 and 17 identical fuel plates. Thickness of plates is 1.27 mm. Active height of the fuel is 600 mm. Fuel element cross section is 76 x 80 mm. In the control elements there are 4 plates of pure aluminium, each 1.27 mm thick, in the position of the first, the third, the twenty-first and the twenty-third standard plates.

Thickness of the Al-side plates is 4.75 mm.

The pitch of the grid plate per fuel element is 77 x 81 mm.

FUEL PLATES

Meat dimensions are 63 x 0,51 x 600 mm.

Three cases were considered. Their caracteristics are reported in table 1.

Table 1

Case	Number of plates	U 235 by element (g)	U 235 by plate (g)	U 235 enrich-ment %	U percentage in UAl %	U specific weight (g/cm3)	UAl meat specific weight (g/cm3)
HEU	23	280	12:174	93	21	0,679	3.233
MEU	23	320	13.913	45	40	1,604	4.009
LEU	23	390	16.956	20	72	4.398	6.108

CORE CONFIGURATION

Calculations are based on 6 x 5 element core reflected, by a graphite row on two sides and surrounded by water. Two states of fuel irradiation were considered. Core configuration and burn up element are reported in figure 1.

WORKING DATA

- power ..... 10 MW
- water temperature ..... 20 °C
- fuel temperature ..... 20 °C
- pressure at core height ..... 1.7 bar
- xénon state : local equilibrium xenon corresponding to local power density

CALCULATION MODEL

Fuel element cross section and burn up calculations

The APOLLO code (*) was used to generate the cross sections as a function of burn up in a four group structure with energy as shown below :

Energy groups used in the calculation

Group	Energy	
1	10 Mev	0.9 Mev
2	0.9 Mev	5.50 kev
3	5.50 Kev	0.625 ev
4	0.625 ev	0

APOLLO calculates the space and energy dependent flux for a one dimensional geometry, in the multigroup approximation of the transport equation. For a one dimensional geometry refined collision probabilities have been used for the resolution of the integral form of the transport equation. APOLLO uses a library with 99 groups (52 fast and 47 thermal). This library contains all the isotopes of the UKNDL library and of the ENDF/BIV library. The fission products compilation of Cook have been added to the APOLLO library.

The self shielding of the heavy isotopes is treated by an accurate technics which preservesthe reaction rates of the fundamental fine structure.

APOLLO is designed to perform accurate depletion calculations. Any decay chain can be defined for heavy nuclides and fission products. The depletion calculation can be done separately for a few regions in the cell.

---

* A. HOFFMANN, F. JEAN PIERRE, A. KAVENOKY, M. LIVOLANT, H. LORRAIN : APOLLO. Code multigroupe de résolution de l'équation du transport pour les neutrons thermiques et rapides.
Note CEA N-1610

Calculations of cross sections are made in tow steps.

In first step we consider the infinite-medium cell : which consists of the plate and the associated water channel. We calculate the self shielding of the heavy isotopes. We obtain the homogeneous equivalent cross section and the Bell factor for this exact geometry.

In a second step we consider the infinite-medium cell with extra-region. This latter region contains Al-structures and surrounding water. The first step calculations provides the self-shielding parameters. For more convenient calculations, standard and control fuel assemblies have the same cross sections. The extra water and the extra-al-structures cross sections of the large water channel of the control element are determined separately.

Depletion calculations are made untill fifty percent of ^{235}U is burned. The irradiation ratio α decreases from 1 to 0.5 by step of 0.05. A critical buckling is automatically adjusted at each step of irradiation.

REFLECTOR CROSS SECTION CALCULATIONS

Reflector and central water hole cross sections have been evaluated by 1D plane geometry APOLLO calculations where reflectors and homogeneized core are described. These calculations have been performed for each fuel enrichment.

CORE CALCULATIONS

We use the NEPTUNE modular scheme which has been developed to provide the design engineer with a single system of codes for the calculation of light water reactor. In this reactor phase, 2D diffusion calculations have been performed by the use of the finite element method. These 2D calculations are done by the BILAN module. We can use a large space mesh with this method and obtain an accurate calculation.

We used an uniform axial geometric buckling with 80 mm extrapolation length. Equilibrium xenon concentrations were calculated with local flux.

RESULTS

Reactivity

Figure 2 compares the behaviour of the k_∞ of the 3 different fuels against their burn up/MWd, including Xe-equilibrium for constant power level of 10 MW for the total core.

In table 2 we give the keff of the 3 different cores at BOL and EOL.

Table 2

Enrichment %	93	45	20
BOL keff (0 Xe)	1.07797	1.07819	1.0758
BOL keff (eq Xe)	1.04041	1.04077	1.0394
BOL Xenon effect %	3.55	3.53	3.47
EOL keff (0 Xe)	1.05337	1.05530	1.05468
EOL keff (eq Xe)	1.01703	1.01896	1.01913
EOL Xenon effect %	3.51	3.50	3.43
Reactivity decrease between BOL and EOL eq Xe %	2.27	2.12	1.97
Fresh keff (0 Xe) core	1.202	1.195	1.187

Flux distributions

. Figures 3 to 6 compares flux distributions along the horizontal symmetry axis of the core at beginningof life for the 4 groups of the 3 different fuels.

. Figures 7 to 10 compares flux distributions along the vertical symmetry axis of the core at begening of life.

. Figures 11 to 14 compares flux distributions along the horizontal symmetry axis of the core at end of life for the 4 groups of the 3 different fuels.

. Figures 15 to 18 compares flux distributions along the vertical symmetry axis of the core at end of life.

. Figure 19 shows flux distributions along the horizontal symmetry axis, normalised to 93 % enrichment-flux. That has only been done for group 4 at beginning of life. The EOL results are verry similar and have not been represented.

In tables 3 to 6, flux along the horizontal symmetry axis normalised to 93 % enrichment flux are reported for each group at BOL and EOL.

Figure 1

Core configuration

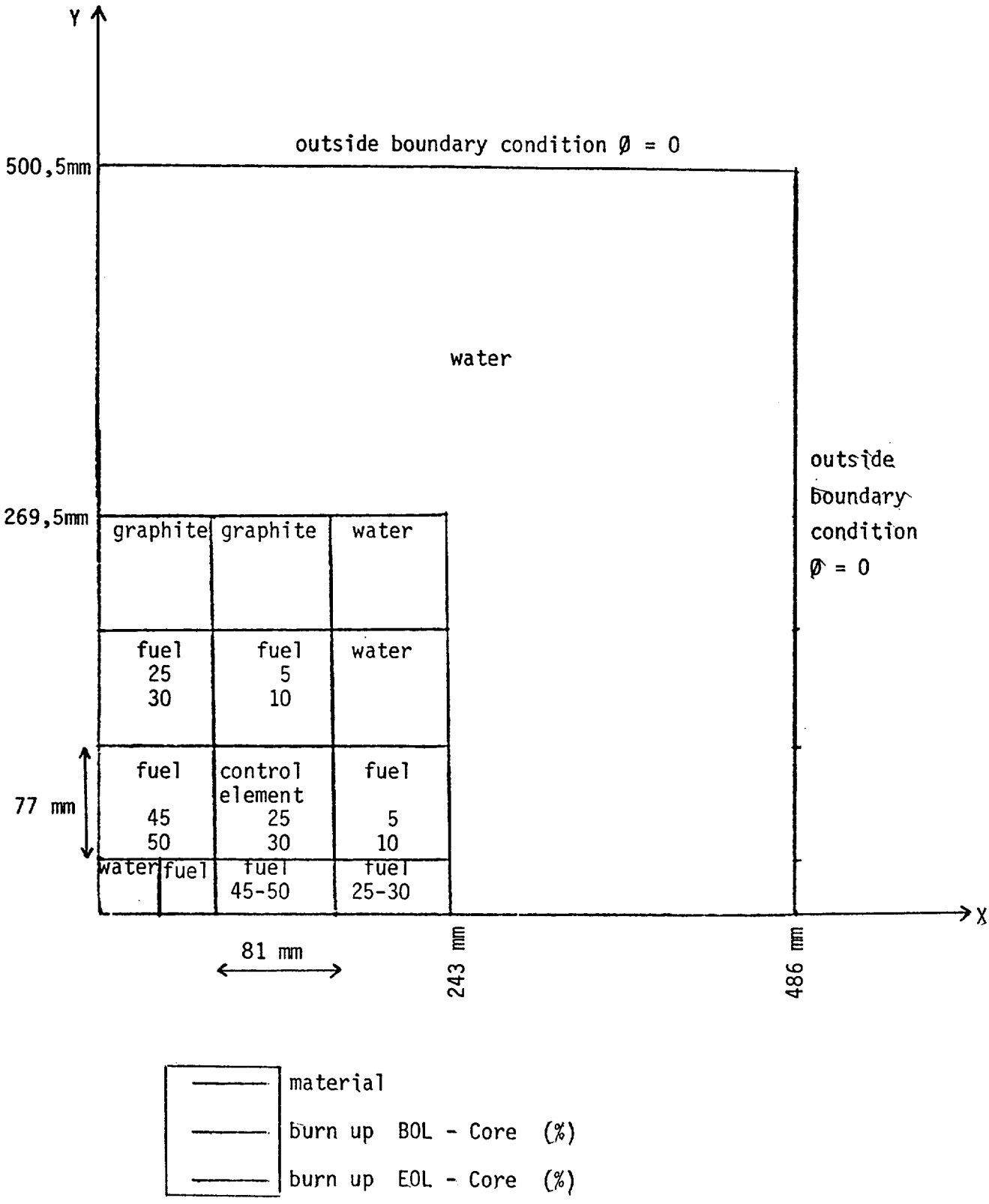

Burn up definition : it is the percentage of loss of U 235-atoms

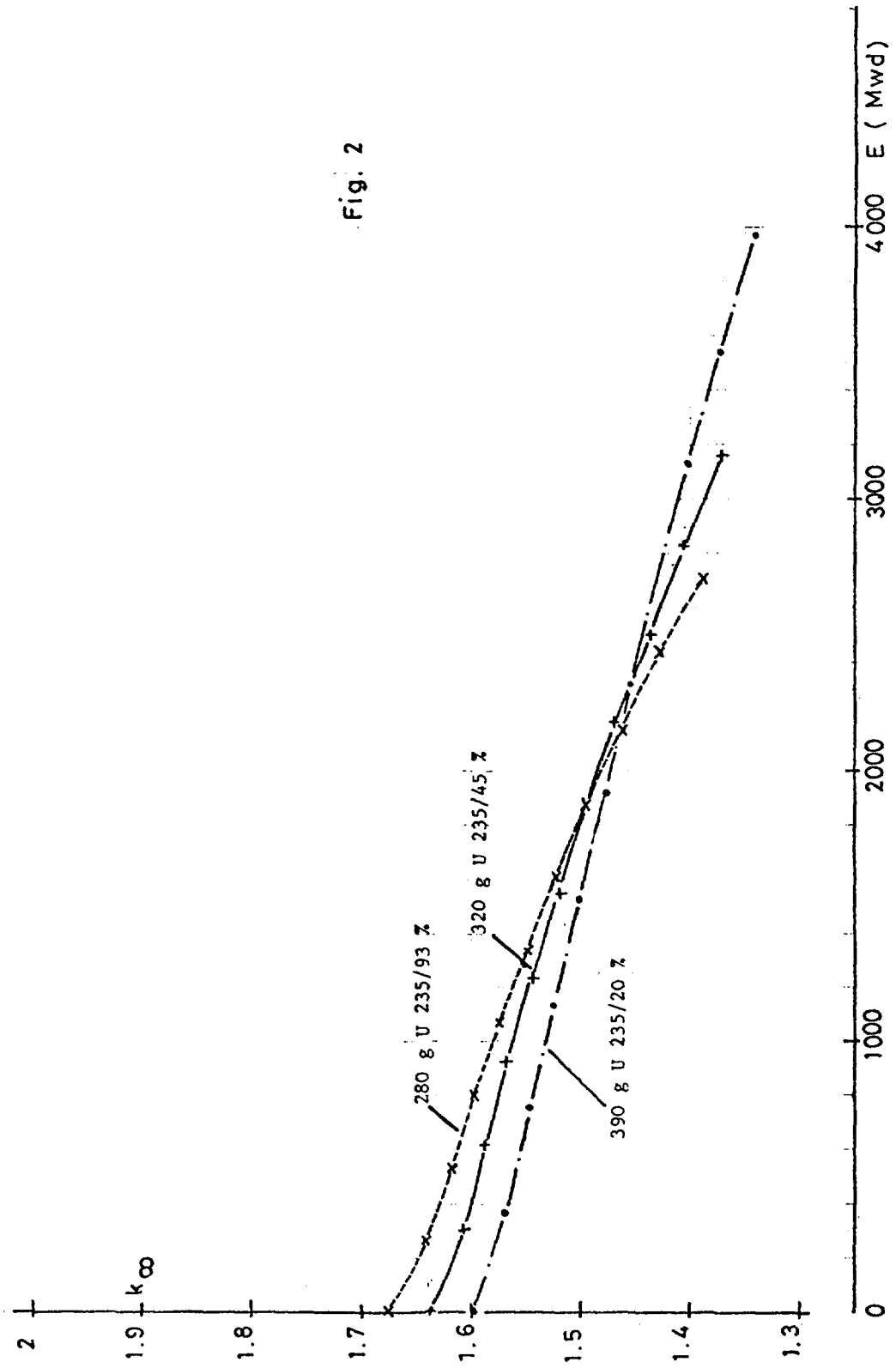
k∞
2
1.9
1.8
1.7
1.6
1.5
1.4
1.3
0
1000
2000
3000
4000
E (Mwd)
280 g U 235/93 %
320 g U 235/45 %
390 g U 235/20 %

Fig. 2

Fig. 3

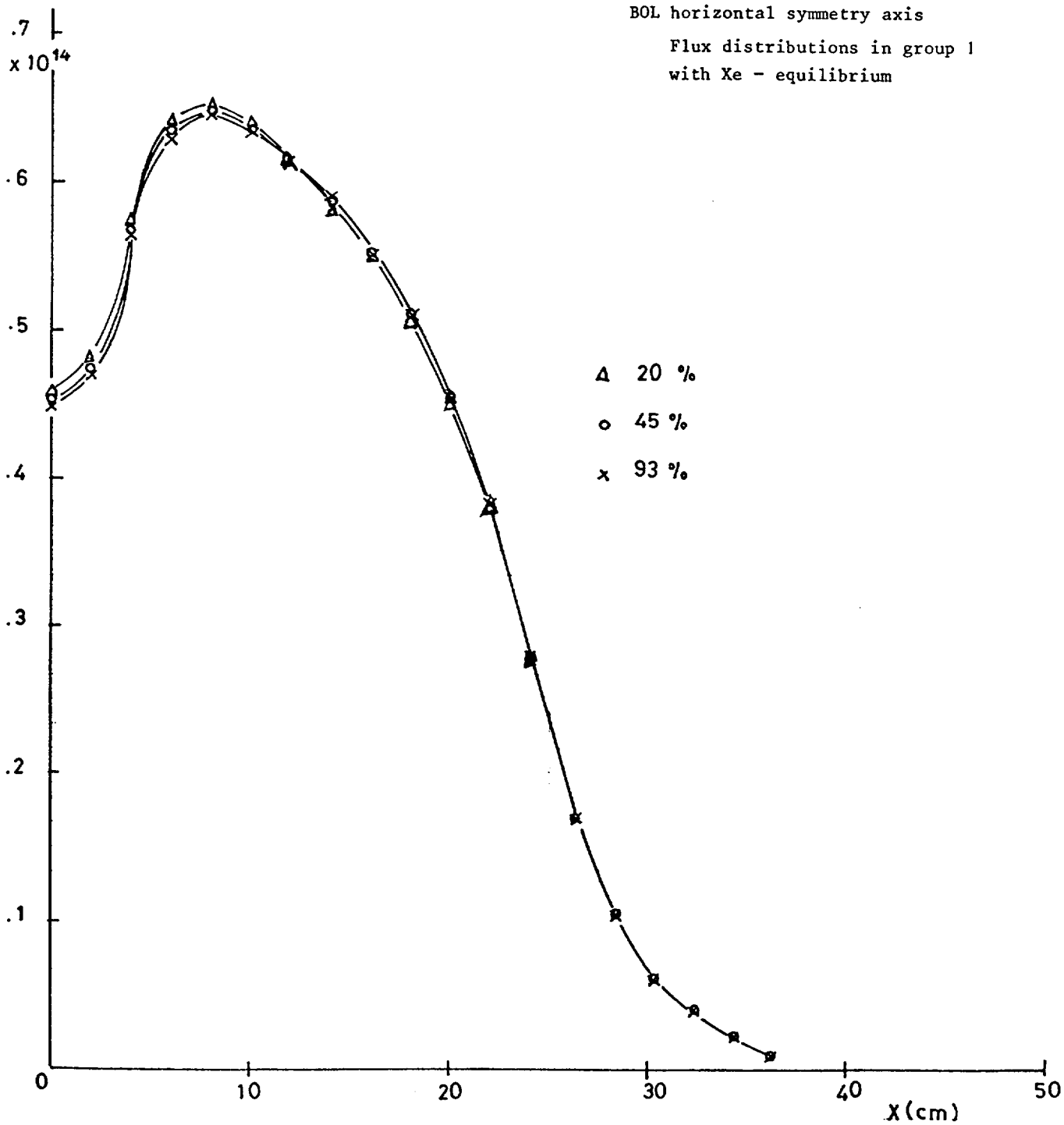
BOL horizontal symmetry axis
Flux distributions in group 1
with Xe - equilibrium
.7
x 10^14
.6
.5
.4
.3
.2
.1
0
10
20
30
40
50
X (cm)
Δ 20 %
o 45 %
x 93 %

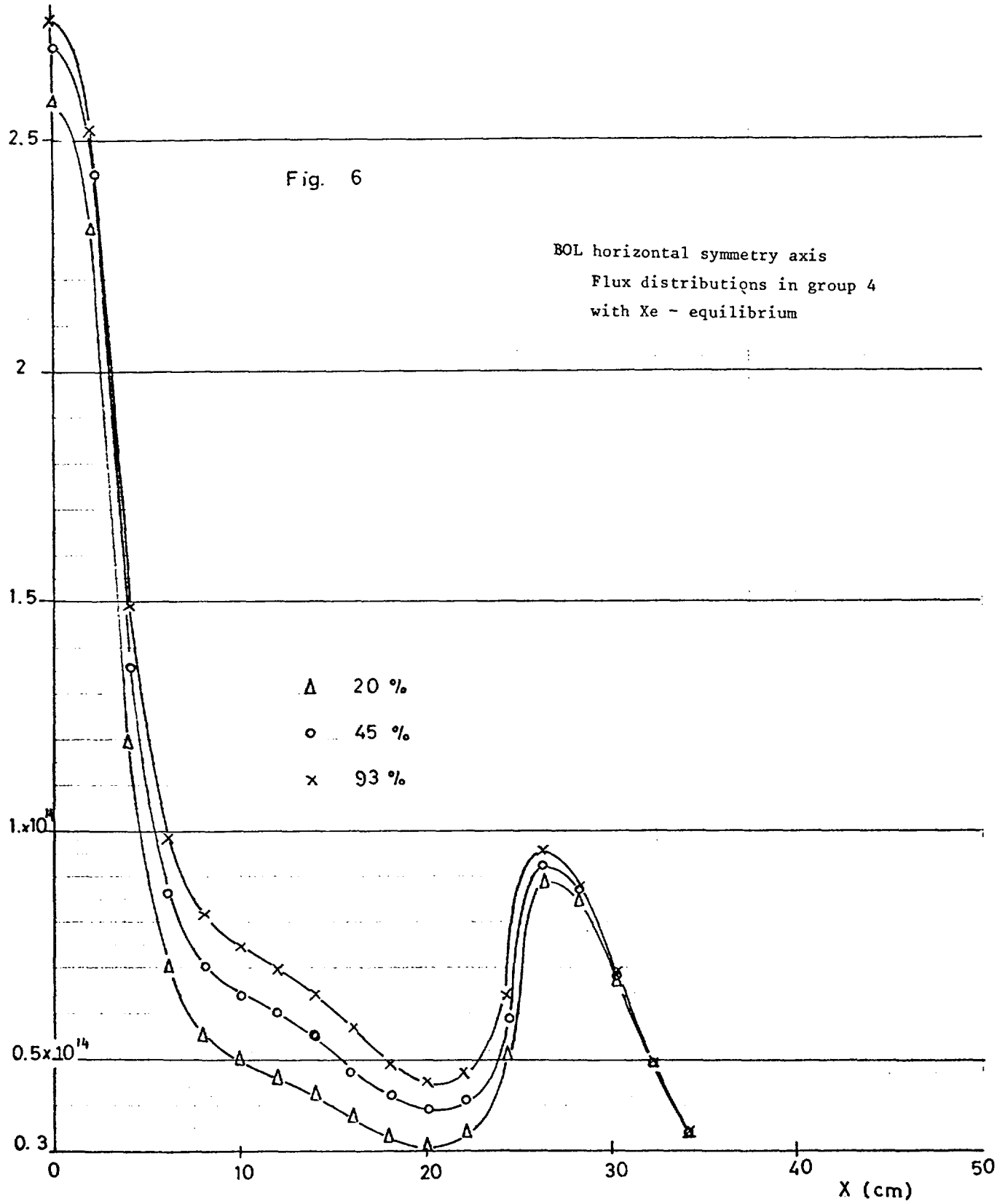

Fig. 6

BOL horizontal symmetry axis
Flux distributions in group 4
with Xe - equilibrium

Fig 7

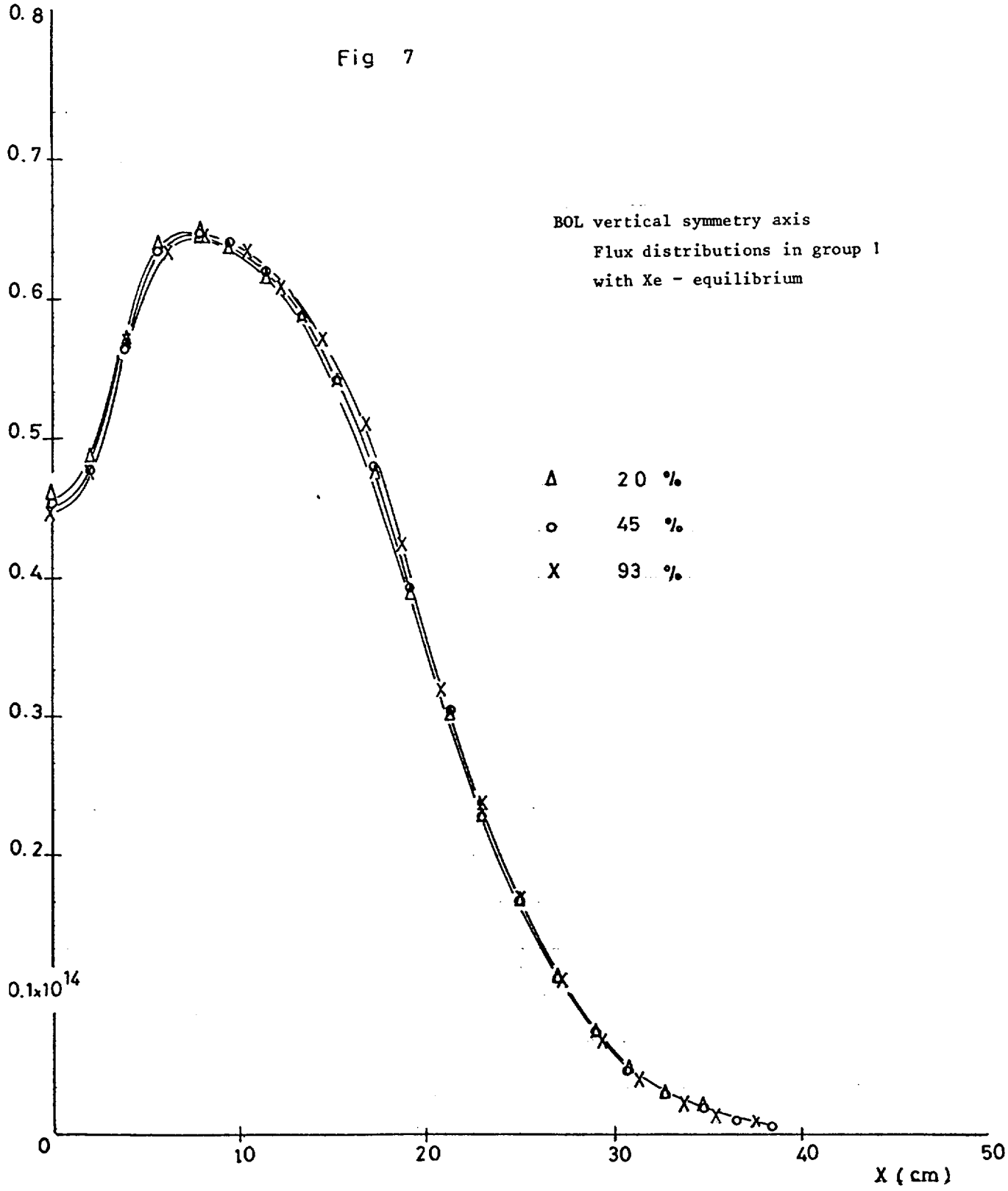
0.8
0.7
0.6
0.5
0.4
0.3
0.2
0.1x10^14
0
10
20
30
40
50
X (cm)
BOL vertical symmetry axis
Flux distributions in group 1
with Xe - equilibrium
Δ 20 %
o 45 %
X 93 %

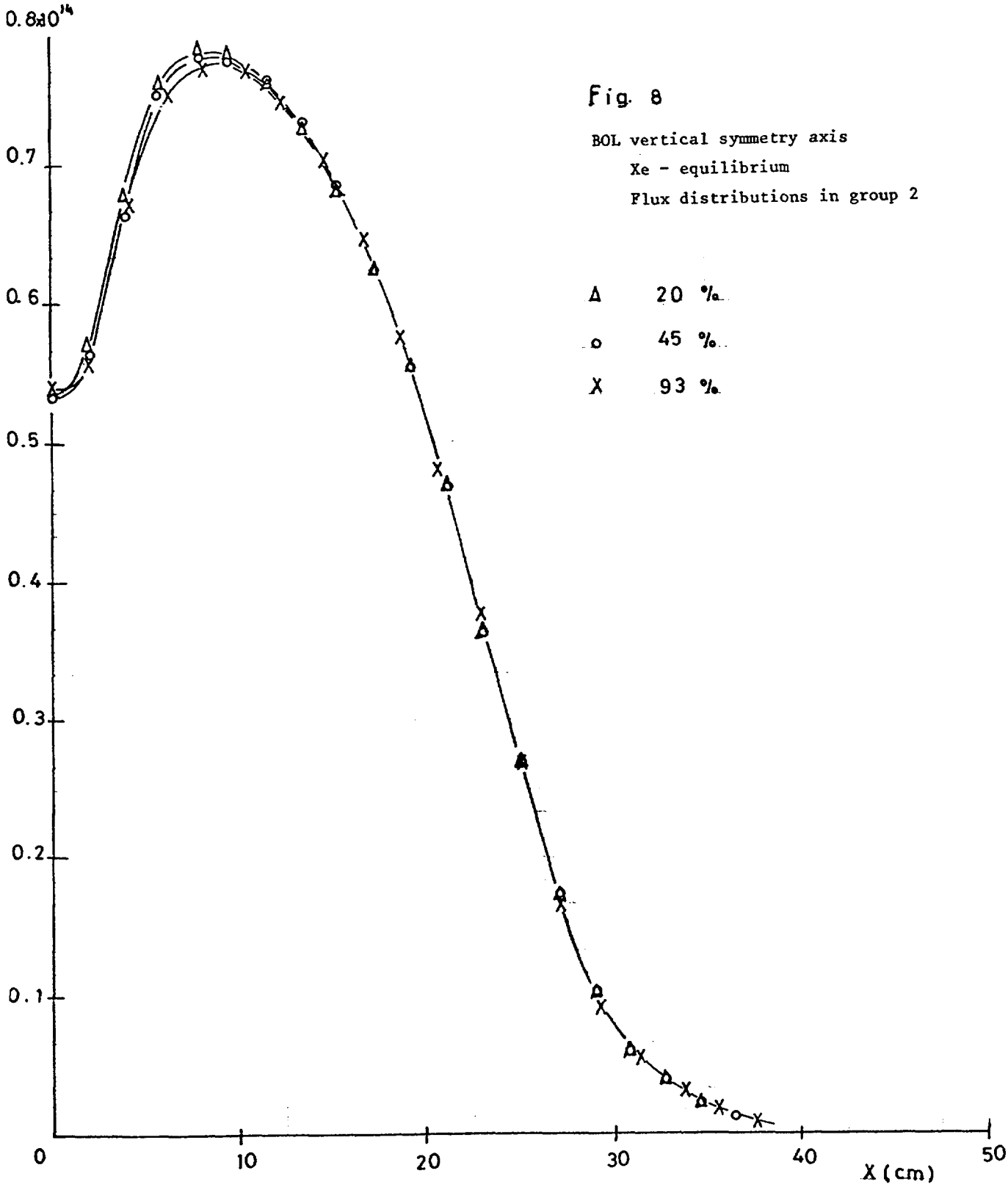

Fig. 8

BOL vertical symmetry axis
Xe - equilibrium
Flux distributions in group 2

Δ 20 %
o 45 %
X 93 %

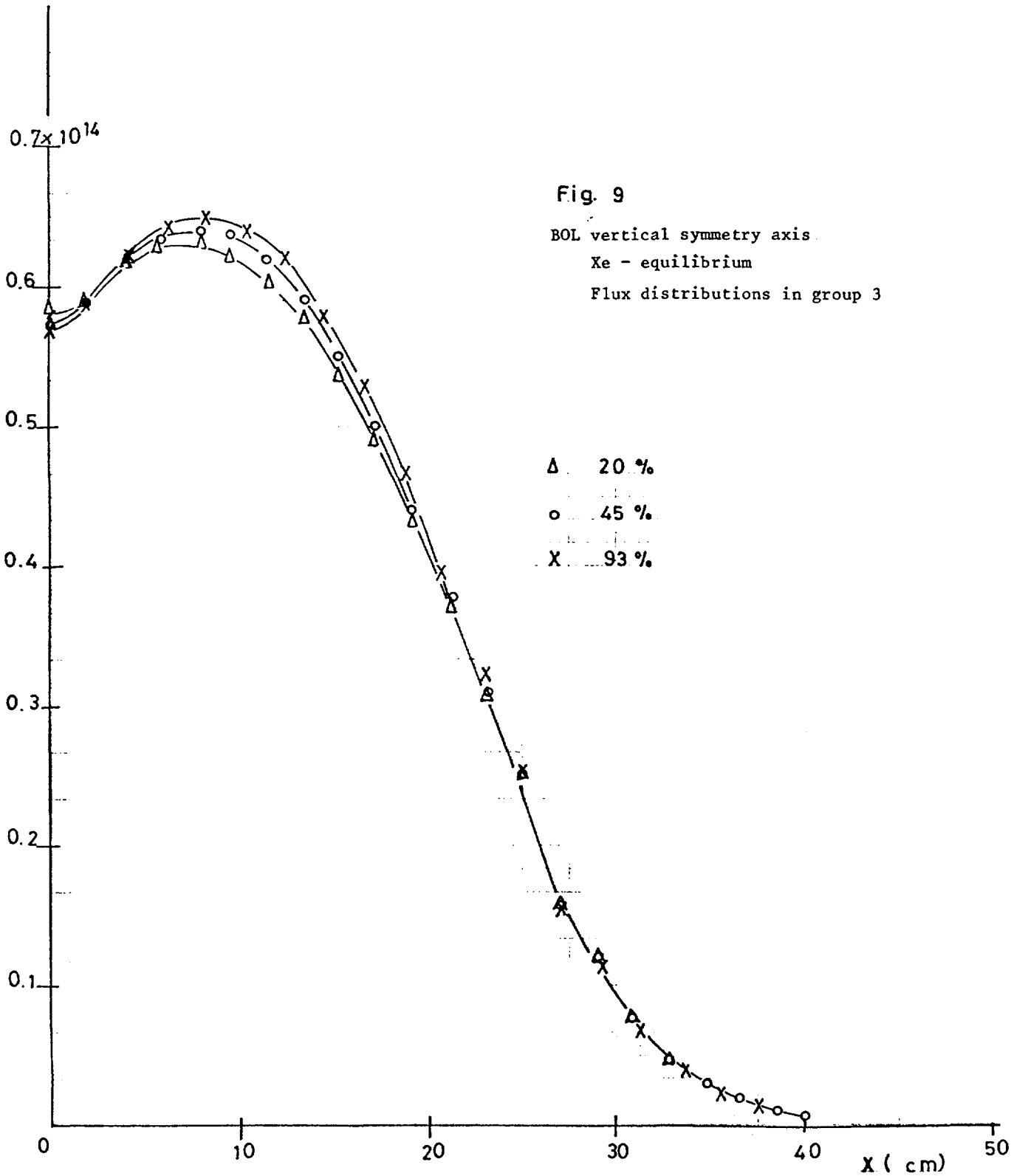

Fig. 9

BOL vertical symmetry axis
Xe - equilibrium
Flux distributions in group 3

Fig 10

BOL vertical symmetry axis
Xe equilibrium
Flux distributions in group 4

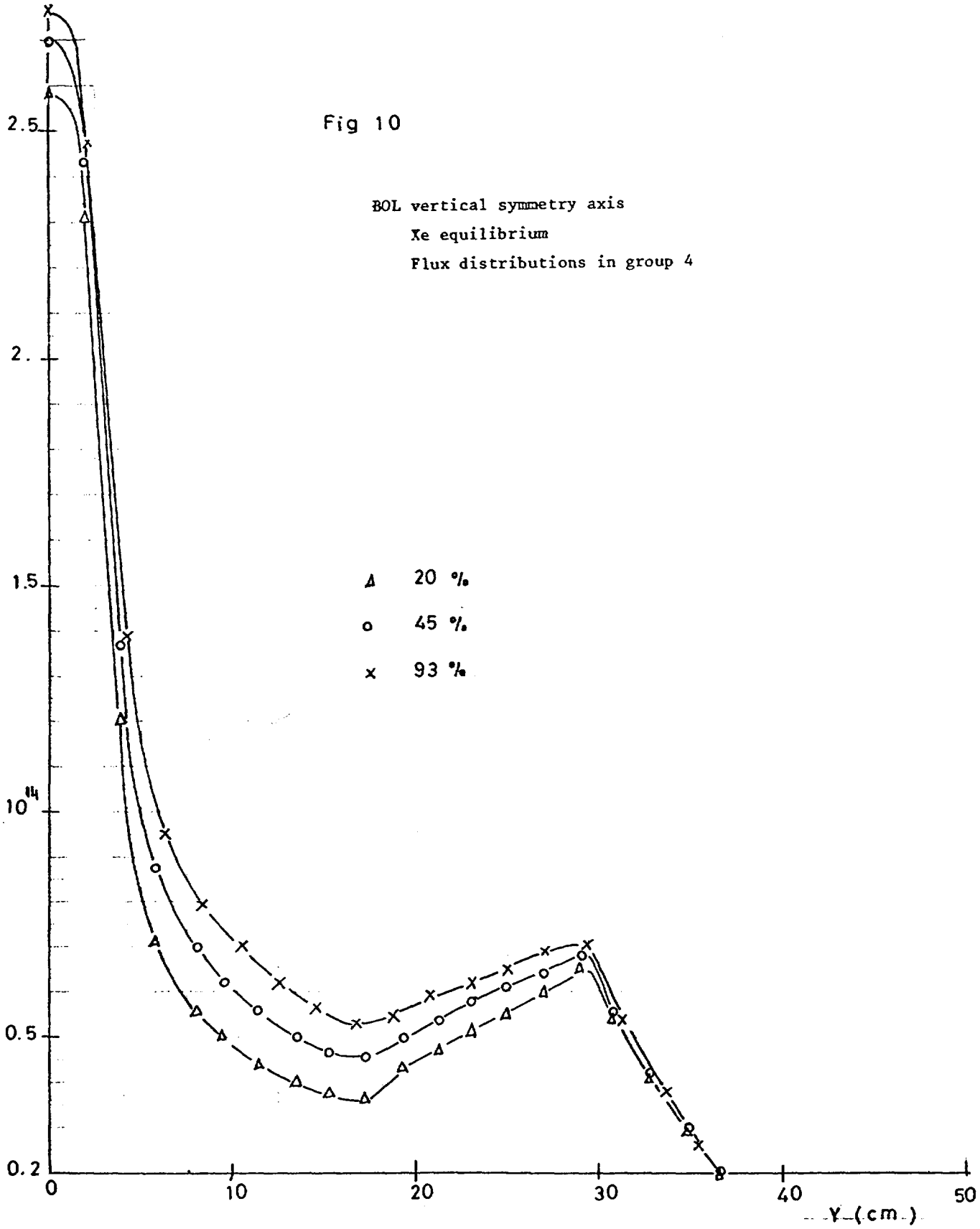

Fig. 11

EOL horizontal symmetry axis
Xe - equilibrium
Flux distributions in group 1

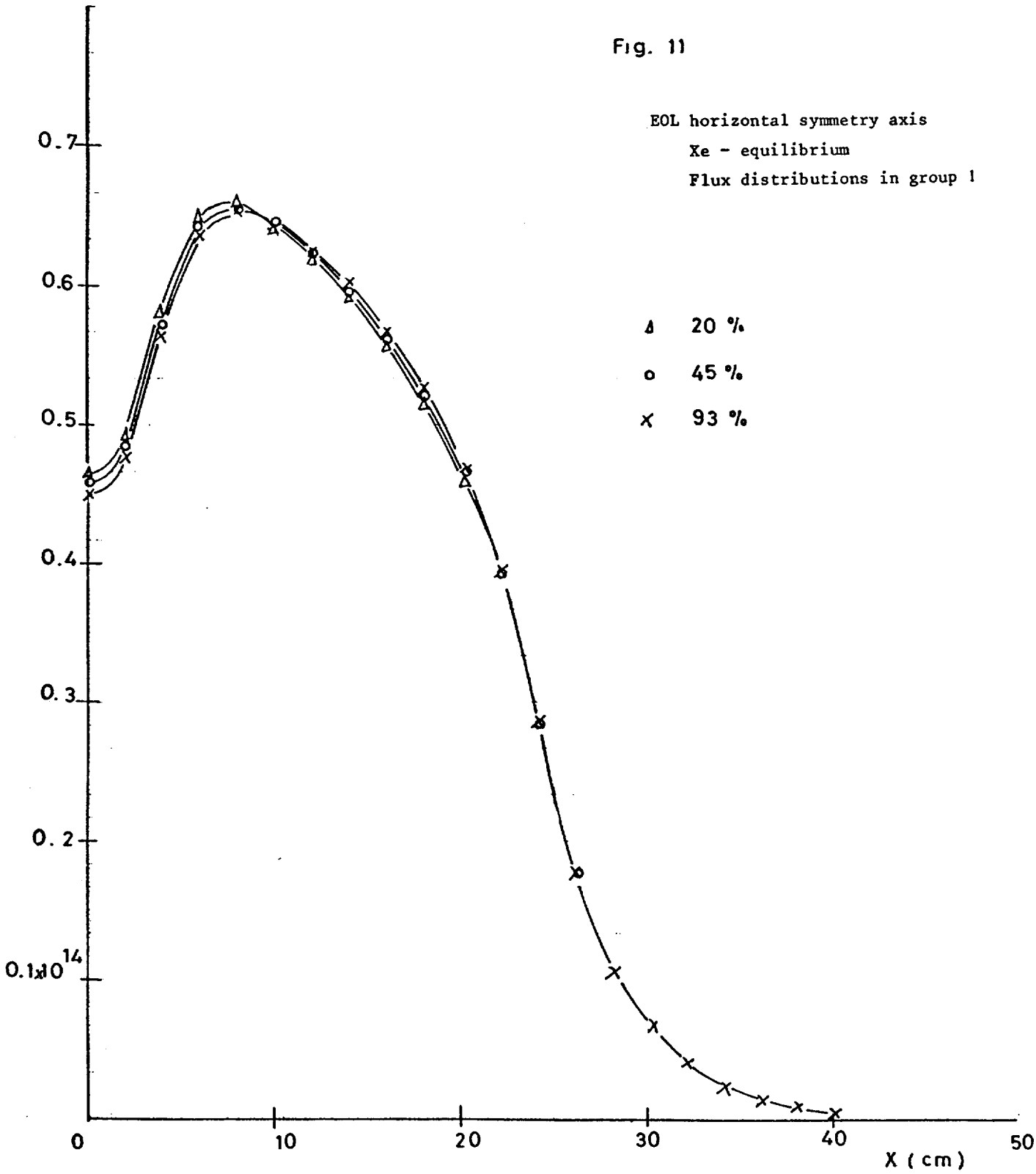

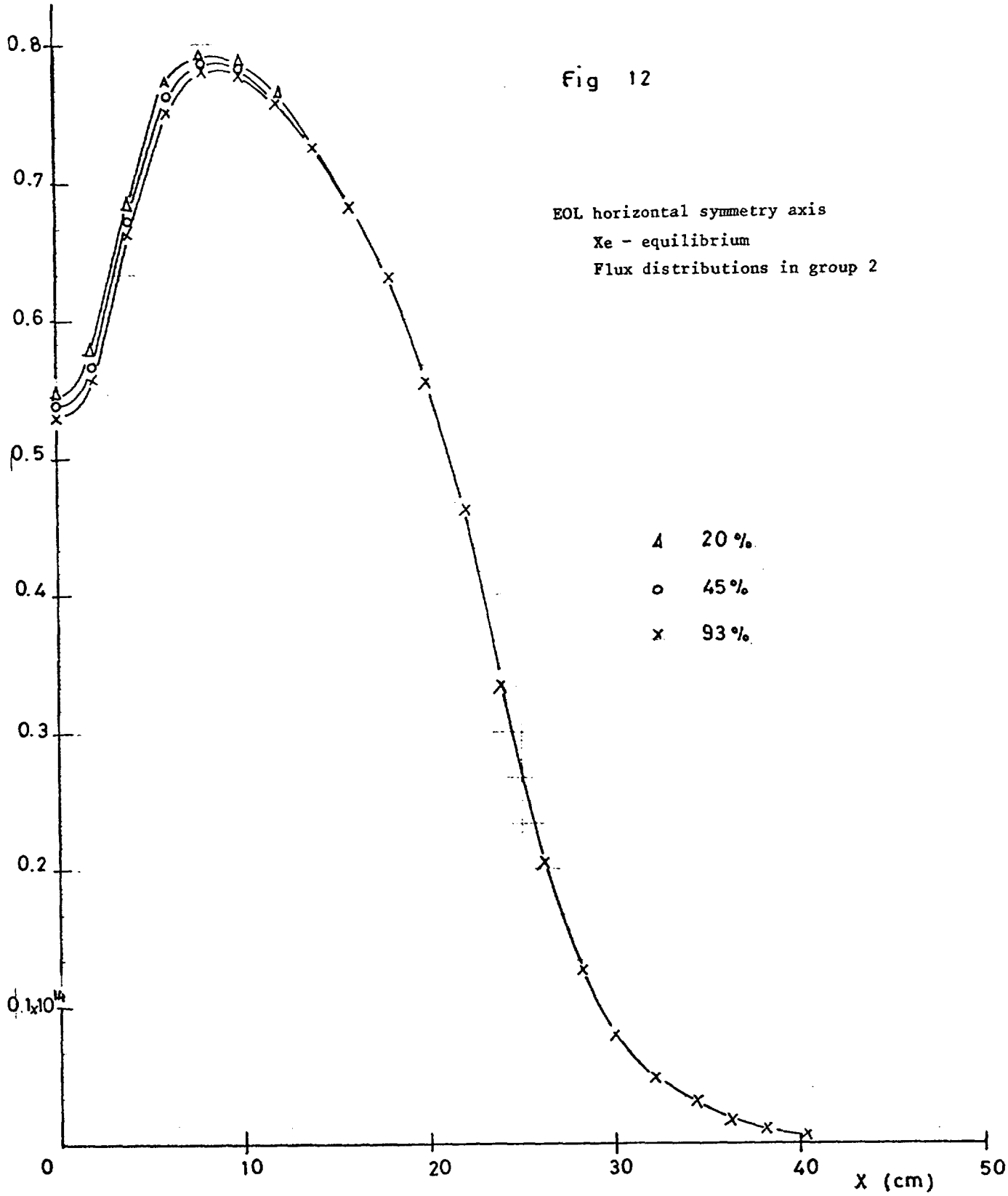

Fig 12

EOL horizontal symmetry axis
Xe - equilibrium
Flux distributions in group 2

Fig 13

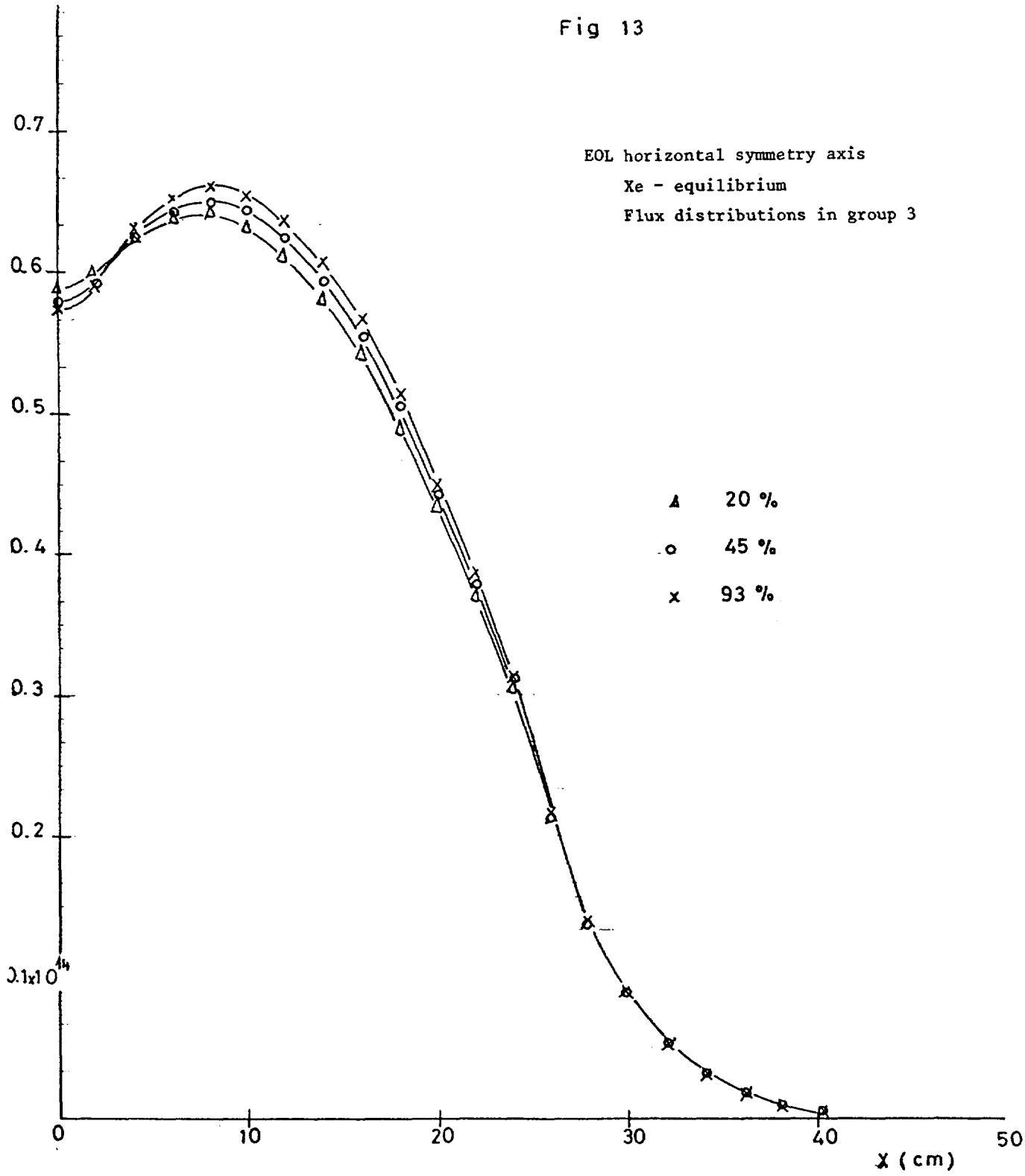
EOL horizontal symmetry axis
Xe - equilibrium
Flux distributions in group 3
20 %
45 %
93 %
0.7
0.6
0.5
0.4
0.3
0.2
0.1x10 14
0
10
20
30
40
50
X (cm)

Fig 14

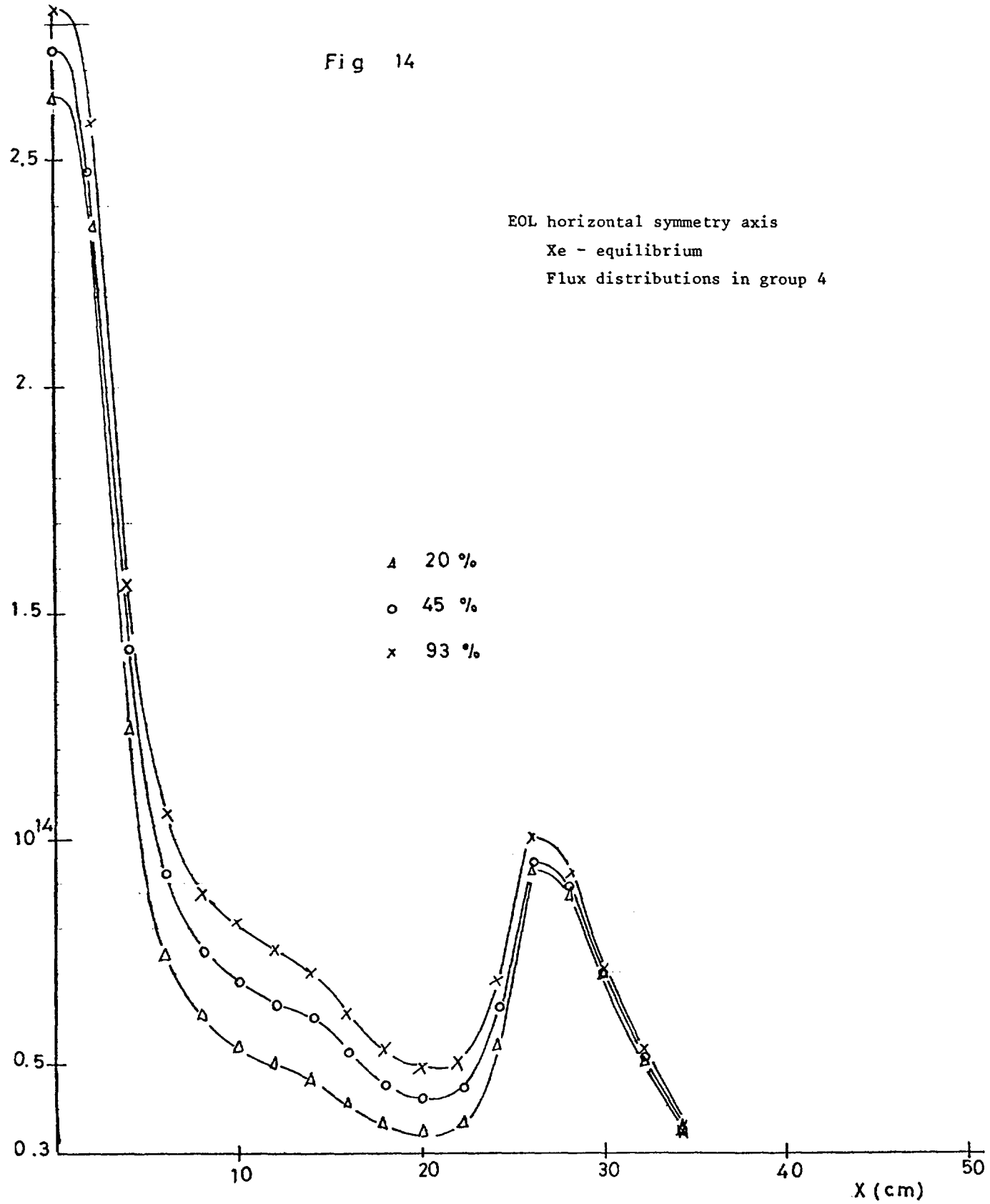
EOL horizontal symmetry axis
Xe - equilibrium
Flux distributions in group 4
Δ 20 %
o 45 %
x 93 %
2.5
2.
1.5
10^{14}
0.5
0.3
10
20
30
40
50
X (cm)

Fig 15

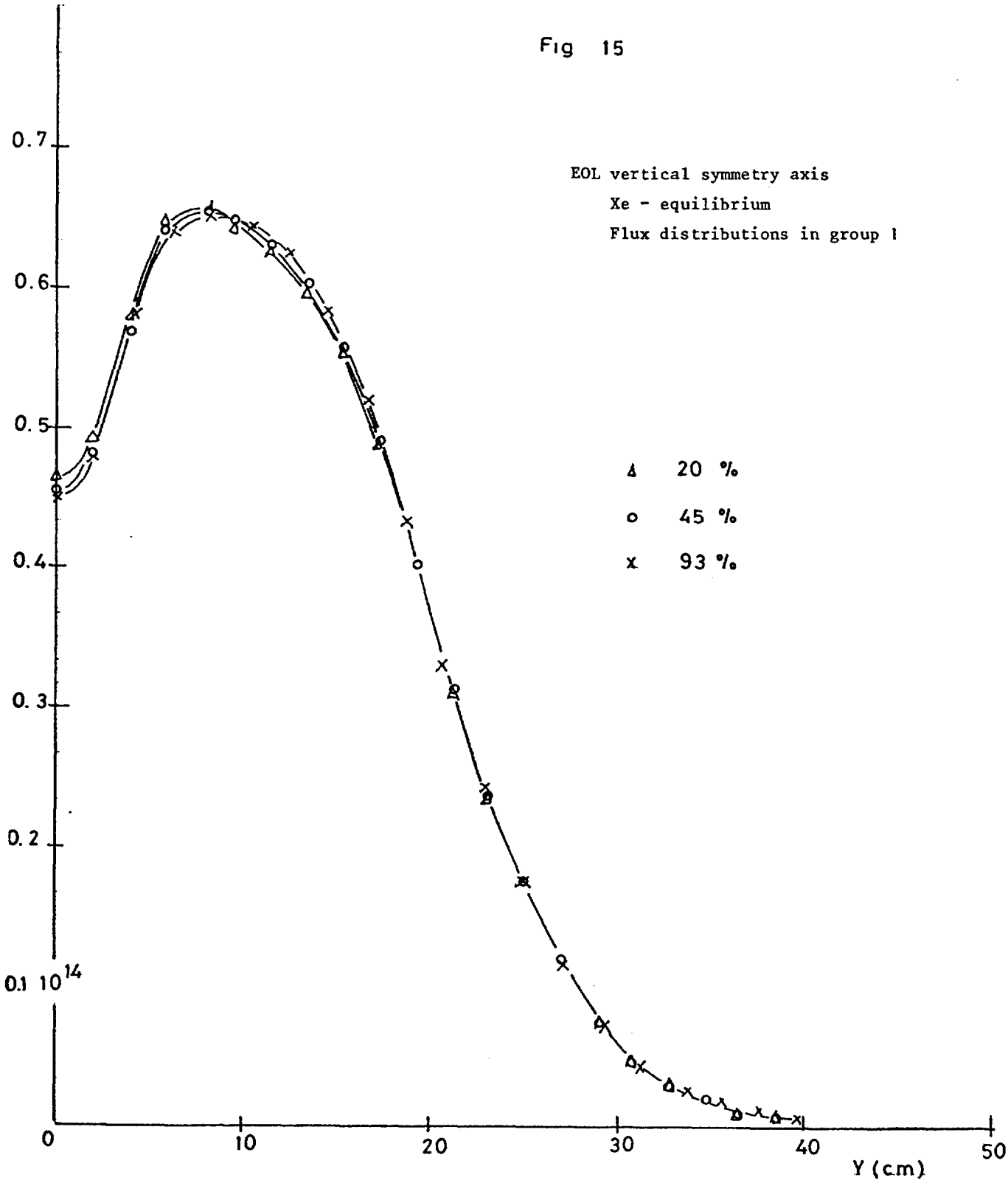
EOL vertical symmetry axis
Xe - equilibrium
Flux distributions in group 1
Δ 20 %
o 45 %
x 93 %
0.7
0.6
0.5
0.4
0.3
0.2
0.1 10^14
0
10
20
30
40
50
Y (cm)

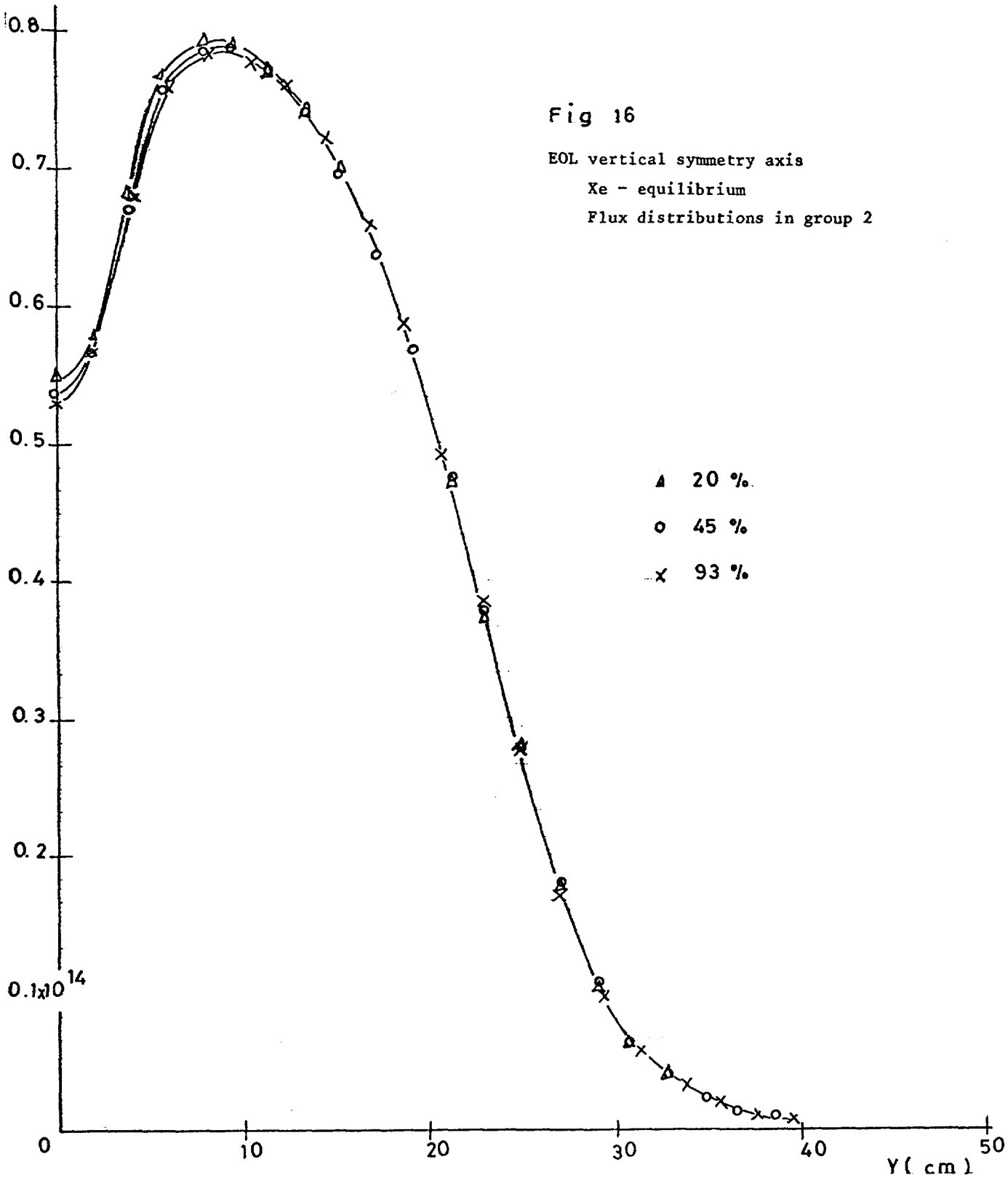

Fig 16

EOL vertical symmetry axis

Xe - equilibrium

Flux distributions in group 2

Fig 17

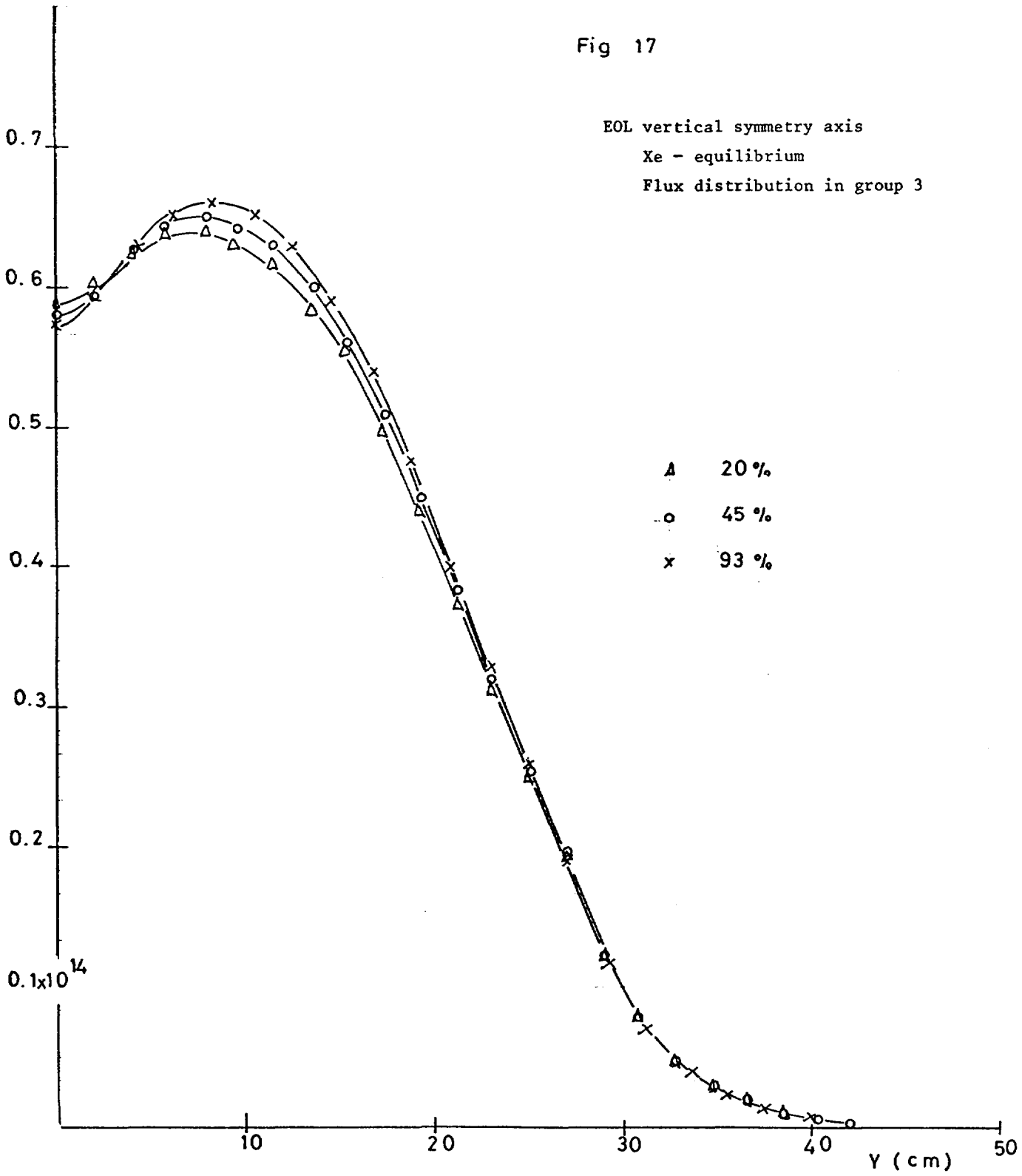
EOL vertical symmetry axis
Xe - equilibrium
Flux distribution in group 3
Δ 20 %
o 45 %
x 93 %
0.7
0.6
0.5
0.4
0.3
0.2
0.1x10^14
10
20
30
40
50
Y (cm)

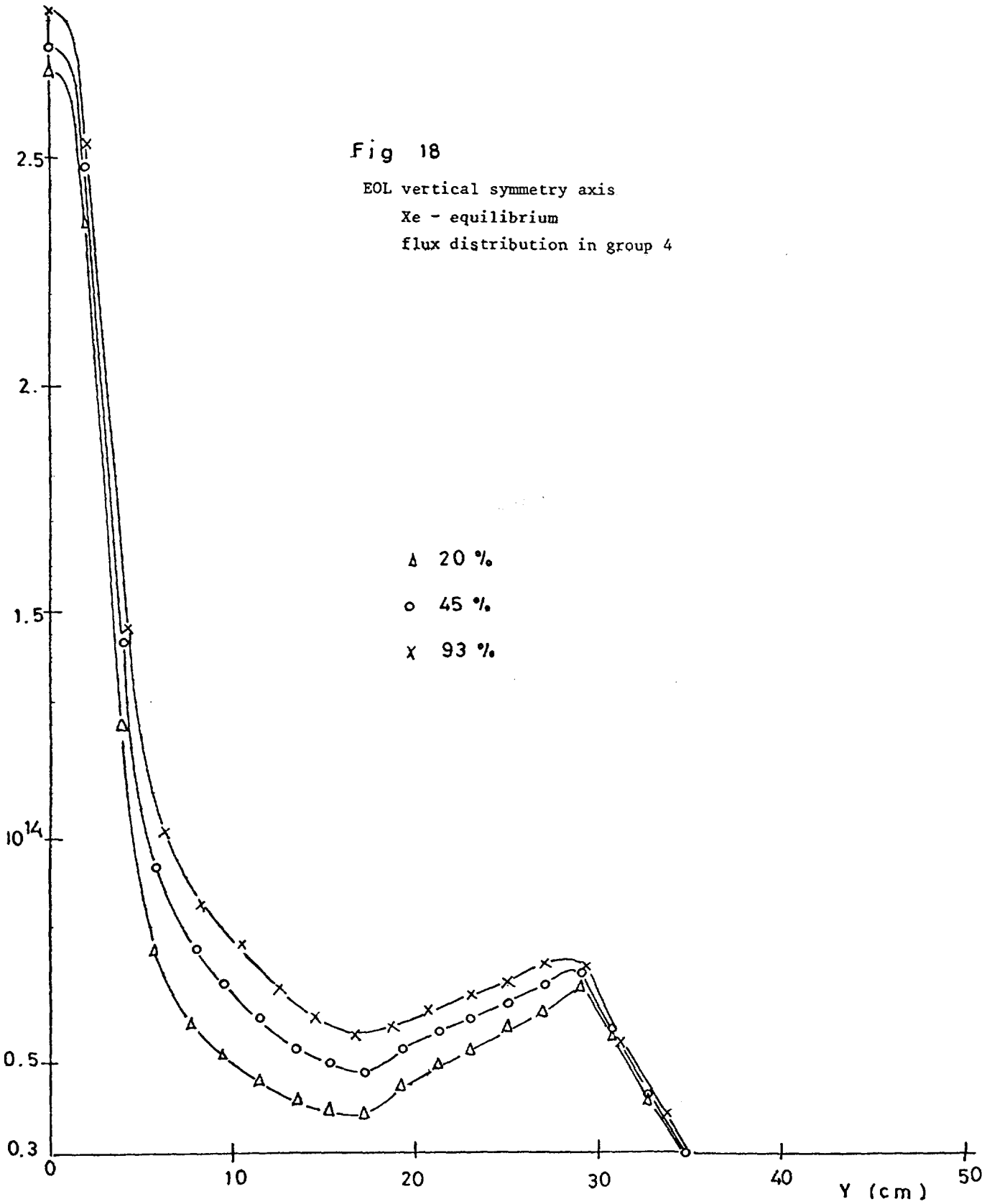

Fig 18

EOL vertical symmetry axis
Xe - equilibrium
flux distribution in group 4

Fig 19

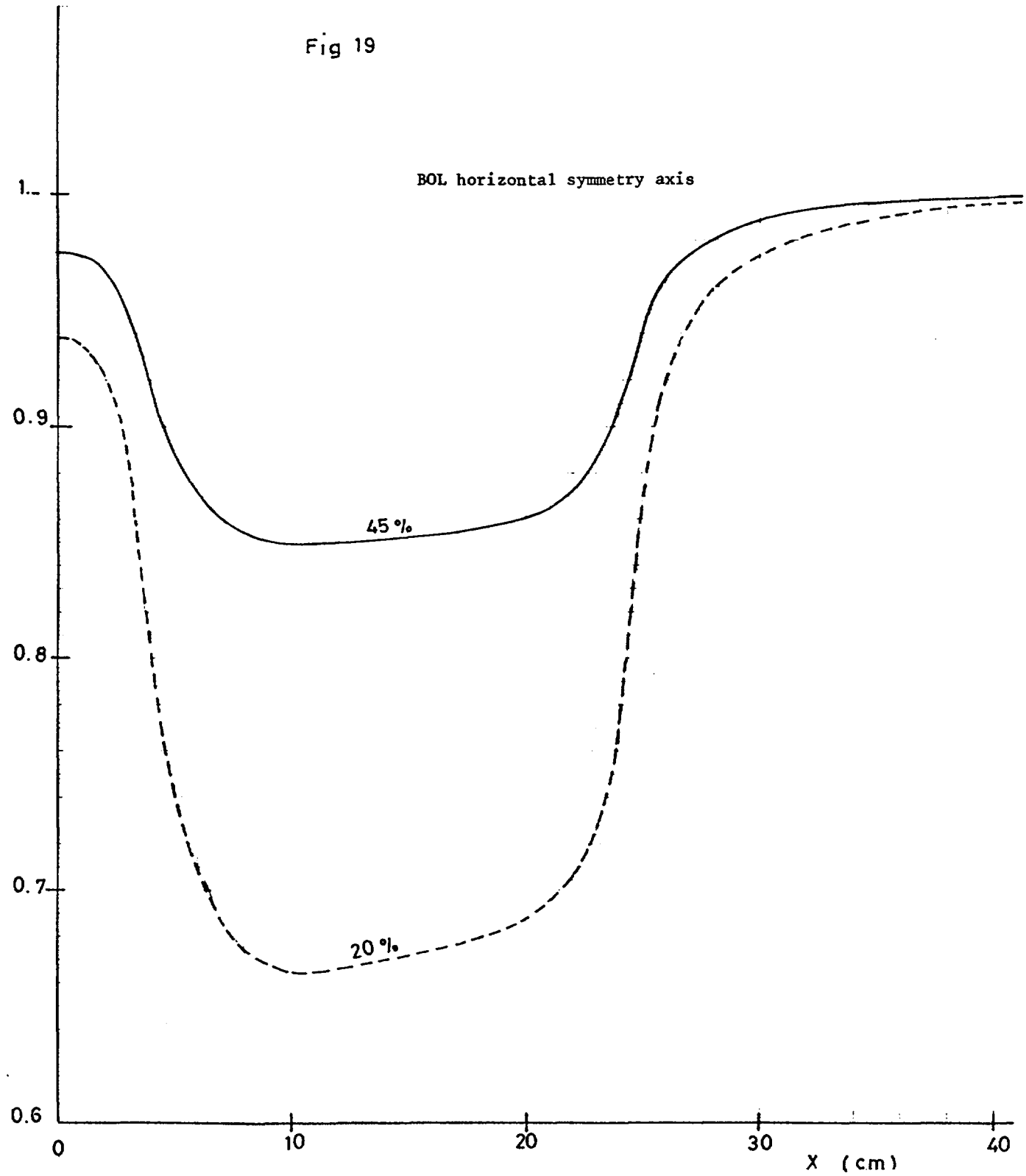
BOL horizontal symmetry axis
1.
0.9
0.8
0.7
0.6
45 %
20 %
0
10
20
30
40
X (cm)

Table 3 - φ_{45} % BOC with Xe/φ_{93}

X cm	φ_{1/ϕ_1}	φ_{2/ϕ_2}	φ_{3/ϕ_3}	φ_{4/ϕ_4}
0.0	1.0124	1.0128	1.0096	0.9728
2.025	1.0126	1.0126	1.0074	0.9656
4.05	1.0131	1.0129	0.9987	0.9137
6.075	1.0097	1.0106	0.9921	0.8700
8.10	1.0049	1.0072	0.9883	0.8535
10.125	1.0012	1.0042	0.9856	0.8497
12.15	0.9985	1.0020	0.9835	0.8496
14.175	0.9966	1.0001	0.9817	0.8511
16.20	0.9943	0.9982	0.9807	0.8539
18.2249	0.9928	0.9970	0.9798	0.8567
20.24998	0.9936	0.9971	0.9800	0.8604
22.27499	0.9964	0.9987	0.9813	0.8740
24.29999	0.9993	1	0.9854	0.9142
26.3249	0.9994	1	0.9949	0.9675
28.34999	1	1	0.9993	0.9817
30.37498	1	1	1.0022	0.9886
32.39999	1	1	1.0036	0.9926
34.42499	1	1	1.0029	0.9959
36.44998	1	1	1.0096	0.9973
38.47499	1	1	1.0079	0.9986
40.49998	1	1	1.0131	1
42.52498	1	1	1	1
44.54999	1	1	1	1
46.57498	1	1	1	1
48.59999	/	/	/	/

Table 4 - φ_{20} % BOL with Xe/φ_{93}

X cm	φ_1/ϕ_1	φ_2/ϕ_2	φ_3/ϕ_3	φ_4/ϕ_4
0.0	1.0245	1.0274	1.0196	0.9353
2.025		1.0274	1.0149	0.9186
4.05	1.0260	1.0289	0.9944	0.7992
6.075	1.0168	1.0237	0.9791	0.7038
8.10	1.0050	1.0155	0.9702	0.6711
10.125	0.9966	1.0090	0.9644	0.6650
12.15	0.9912	1.0042	0.9601	0.6657
14.175	0.9871	1.0005	0.9568	0.6694
16.20	0.9825	0.9971	0.9552	0.6758
18.2249	0.9795	0.9946	0.9538	0.6821
20.24998	0.9819	0.9957	0.9545	0.6894
22.27499	0.9901	1	0.9585	0.7167
24.29999	0.9982	1.0036	0.9666	0.8039
26.3249	0.9983	1.0019	0.9893	0.9263
28.34999	0.9981	1.0016	1.0007	0.9590
30.37498	0.9985	1.0013	1.0068	0.9747
32.39999	0.9975	1.0021	1.0091	0.9841
34.42499	0.9959	1.0035	1.0088	0.9903
36.44998	1	1	1.0145	0.9947
38.47499	1	1	1.0139	0.9972
40.49998	1	1	1.0131	1
42.52498	1	1	1.0213	1
44.54999	1	1	1	1
46.57498	1	1	1	1
48.59999	/	/	/	/

Table 5 - φ_{45} % EOL with Xe/φ_{93}

X cm	φ_{1/ϕ_1}	φ_{2/ϕ_2}	φ_{3/ϕ_3}	φ_{4/ϕ_4}
0.0	1.0107	1.0119	1.0272	0.9715
2.025	1.0114	1.0120	1.0072	0.9640
4.05	1.0120	1.0124	0.9985	0.9110
6.075	1.0085	1.0105	0.9920	0.8670
8.10	1.0040	1.0071	0.9884	0.8501
10.125	1.0006	1.00451	0.9858	0.8460
12.15	0.9982	1.0023	0.9840	0.8459
14.175	0.9964	1.0008	0.9825	0.8470
16.20	0.9946	0.9992	0.9818	0.8494
18.2249	0.9934	0.9982	0.9811	0.8518
20.24998	0.9941	0.9985	0.9815	0.8557
22.27499	0.9971	1.0002	0.9827	0.8700
24.29999	1	1.0012	0.9866	0.9106
26.3249	1	1.0015	0.9962	0.9651
28.34999	1	1.0016	1.0007	0.9798
30.37498	1	1.0013	1.0035	0.9870
32.39999	1	1	1.0056	0.9912
34.42499	1	1	1.0061	0.9943
36.44998	1	1	1.0099	0.9961
38.47499	1	1	1	0.9973
40.49998	1	1	1	0.9979
42.52498	1	1	1	0.9983
44.54999	1	1	1	1
46.57498	1	1	1	1
48.59999	/	/	/	/

Table 6 - φ_{20} % EOL with Xe/φ_{93}

X cm	φ_1/ϕ_1	φ_2/ϕ_2	φ_3/ϕ_3	φ_4/ϕ_4
0.0	1.0212	1.0254	1.0365	0.9327
2.025	1.0220	1.0257	1.0137	0.9153
4.05	1.0232	1.0272	0.9935	0.7937
6.075	1.0142	1.0226	0.9785	0.6977
8.10	1.0031	1.0149	0.9701	0.6770
10.125	0.9954	1.0090	0.9644	0.6575
12.15	0.9906	1.0049	0.9606	0.6582
14.175	0.9870	1.0018	0.9579	0.6614
16.20	0.9834	0.9988	0.9565	0.6673
18.2249	0.9813	0.9969	0.9559	0.6732
20.24998	0.9838	0.9981	0.9569	0.6803
22.27499	0.9919	1.0027	0.9603	0.7082
24.29999	1.0003	1.0058	0.9690	0.7966
26.3249	1	1.0050	0.9919	0.9215
28.34999	1	1.0016	1.0029	0.9551
30.37498	1	1.0040	1.0081	0.9714
32.39999	1	1.0022	1.0131	0.9811
34.42499	1	1.0036	1.0129	0.9878
36.44998	1	1	1.0149	0.9923
38.47499	1	1	1.0081	0.4953
40.49998	1	1	1.0135	0.9968
42.52498	1	1	1	0.9983
44.54999	1	1	1	1
46.57498	1	1	1	1
48.59999	/	/	/	/

APPENDIX F-6

Benchmark Calculations

Performed by

Japan Atomic Energy Research Institute

Tokai-mura, Ibaraki-ken, Japan

1. Calculations for the Benchmark MTR-Type Reactors with High, Medium and Low Enrichments

1.1 Purpose

In order to compare our calculational methods and the results with those of various research centers, some of the benchmark problems proposed by IAEA were analysed using our code system. As shown in Appendix E, calculation method and thermal and epithermal cut-off energies used by JAERI differs from those of ANL. For benchmark problems, therefore, we modefied our method and cut-off energies to be able to compare our results with those of ANL. Variation of atomic number densities and 3 group constants versus burn-up steps were especially compared with each other.

1.2 Method

The burn-up dependent unit cell calculation code (see Fig.E.3) was used to generate the cross sections and atomic number densities of fissile material in the cell (Fig.F.6.1) were calculated as a function of burn-up steps. Three energy group structure was selected to compare the computed results with those of ANL (Table F.6.1).

The two-dimensional X-Y geometry diffusion theory calculations were performed with the JAERI code ADC using the core composition and mesh specifications shown in Figs.F.6.2 and F.6.3.

1.3 Results and discussion

The computed results of cell burn-up calculation are shown in Figs.F.6.4, F.6.5, F.6.6, F.6.7, and F.6.8 and Tables F.6.2, F.6.3, F.6.4.

Figure F.6.4 shows the comparison of infinite multiplication factors k_∞ calculated by ANISN (JAERI) and EPRI-CELL (ANL). The values of k_∞ by JAERI decrease more slowly versus ^{235}U burn-up than those by ANL. Table F.6.4 shows the variation of atomic number densities versus ^{235}U burn-up. Plutonium isotopes are produced more in the case of ANL than that of JAERI. This reason comes from the discrepancy between the computed results of ^{238}U epithermal absorption cross section by JAERI and by ANL as shown in Tables F.6.2, and F.6.3 and Fig.F.6.5.

The computed effective multiplication factors k_{eff}'s by the two-dimensional diffusion calculations are shown in Table F.6.5. For 93% enriched cases with all fresh fuel loaded core, the effective multiplication factor k_{eff} calculated by JAERI is almost coincide with the value by ANL. But for the other cases, the computed k_{eff}'s by JAERI are larger than those by ANL. These come from the same reasons menthioned above, that is, slowly variation of k_∞ versus ^{235}U burn-up and smaller ^{238}U epithermal absorption cross section.

Figures F.6.6, F.6.7, F.6.8 and F.6.9 show neutron flux distributions in the core. Figure F.6.10 shows a ratio of ^{238}U capture to ^{235}U fission which predicts space dependency of neutron energy spectrum. This is the reason why we do not compute the burn-up dependent atom density distribution at the stage of cell calculation but of full core calculation.

The difference of computed results by JAERI from those by ANL, comes from the different estimation of absorption rate of a lumped fission product as shown in Fig.F.6.11 and the different estimation of ^{238}U epithermal absorption cross section. These two estimations are the most important ones for studies of reactor conversion from HEU to LEU fuel.

2. Studies of ^{235}U Loading with Uranium Enrichments of 45% and 20% to Match Infinite Excess Reactivity of 93% Enriched Reference Core

2.1 Purpose

The uranium densities in the fuel meat with uranium enrichments of 45% and 20% were estimated by ANL to match the excess reactivity of 93% enriched reference core. Using the uranium densities, we calculated the excess reactivity of 93%, 45% and 20% enriched core and compared the results with those of ANL.

2.2 Method

The excess reactivity was calculated by the three dimensional diffusion code DIFFUSION-ACE-2. The calculation system for the DIFFUSION-ACE-2 is shown in Fig.F.6.12. Three energy group diffusion parameters for DIFFUSION-ACE-2 were obtained by cell calculations using the ANISN code. The cell configuration and atomic number densities are shown in Fig.F.6.13 and Table F.6.6. In our calculations, three dimensional diffusion code was used, so that it was not necessary to estimate the vertical neutron flux buckling.

2.3 Results and Discussion

The computed results by the DIFFUSION-ACE-2 code are shown in Table F.6.7 together with those computed by ANL.

The values of k_{eff} calculated by JAERI become larger than those by ANL as the enrichment goes down. This tendency is explained from the difference of ^{238}U epithermal absorption cross section obtained by JAERI from that by ANL.

In this three-dimensional calculation, computing time was less than 100 sec CPU for FACOM-230-75 computer.

3. Studies of 2 MW Reactor Conversion from HEU to LEU Fuel

3.1 Purpose

The purpose of these studies was to provide an indication of (1) what type of reactor conversion could be feasible for reactors of this type either with current technology or with technology under development, (2) what performance and characteristics could be expected from the converted core, and (3) what methods could be followed to evaluate the conversion.

As shown in Appendix E, the burn-up dependent core performance calculation method of JAERI differs from the ANL's one. Therefore, for these benchmark problems, we modefined our calculational scheme to be able to compare our results with those described in the ANL report. Effective multiplication factors and produced plutonium of BOL and EOL were compared.

3.2 Method

Firstly, cell burn-up calculation was carried out to express burn-up dependent macroscopic cross sections as a function of ^{235}U depletion. With the cell averaged macroscopic cross section of each region in the core, three-dimensional diffusion calculations were performed with the DIFFUSION-ACE code to evaluate the effective multiplication factor of the core. The cell and core geometry and mesh specification for this computation are shown in Figs.F.6.14, F.6.15, F.6.16 and F.6.17. The atomic number densities in the cell are given in Table F.6.8.

3.3 Results and discussion

The computed results by JAERI are compared with those by ANL in Figs.F.6.18 and F.6.19. The amount of produced plutonium calculated by JAERI is less than that by ANL, and reactivity change from BOL to EOL is also less than that by ANL. This tendency comes from the same reason described in the previous sections.

Table F.6.1 Energy Groups Used in the Calculations

Group	E_U, eV	E_L, eV
1	16.487×10^6	5.5308×10^3
2	5.5308×10^3	0.68256
3	0.68256	0.000033

Table F.6.2-1 Cross Section vs. ^{235}U Burnup for 93% Enrichment Case

Burnup (%)	Group	^{235}U		^{238}U		^{239}Pu	
		σ_a	σ_f	σ_a	σ_f	σ_a	σ_f
0	1	1.7198	1.4669	0.38927	0.23491	1.9475	1.7721
	2	39.025	25.759	24.534	6.6775-5	46.280	27.325
	3	431.85	368.36	1.8176	9.9968-9	1059.4	711.67
5	1	1.7202	1.4671	0.38931	0.23488	1.9477	1.7721
	2	39.155	25.835	24.563	6.6648-5	46.316	27.350
	3	431.70	368.22	1.8166	1.0032-8	1061.3	712.72
10	1	1.7199	1.4669	0.38925	0.23488	1.9476	1.7721
	2	39.267	25.897	24.583	6.6620-5	46.334	27.361
	3	435.63	371.61	1.8311	9.8526-9	1057.5	711.37
15	1	1.7199	1.4669	0.38925	0.23487	1.9476	1.7721
	2	39.393	25.969	24.609	6.6530-5	46.363	27.381
	3	439.69	375.11	1.8460	9.6681-9	1053.5	710.01
20	1	1.7203	1.4672	0.38929	0.23482	1.9477	1.7721
	2	39.53	26.048	24.639	6.6397-5	46.402	27.408
	3	443.86	378.71	1.8614	9.4794-9	1049.5	708.63
25	1	1.7203	1.4672	0.38928	0.23480	1.9477	1.7721
	2	39.663	26.124	24.666	6.6299-5	46.435	27.430
	3	448.19	382.45	1.8773	9.2851-9	1045.3	702.21
30	1	1.7200	1.4670	0.38924	0.23483	1.9476	1.7721
	2	39.787	26.193	24.688	6.6253-5	46.456	27.444
	3	452.67	386.30	1.8937	9.0861-9	1041.1	705.76
35	1	1.7201	1.4670	0.38925	0.23482	1.9476	1.7721
	2	39.926	26.272	24.716	6.6150-5	46.488	27.466
	3	457.29	390.29	1.9106	8.8812-9	1036.7	704.27
40	1	1.7205	1.4673	0.38926	0.23474	1.9477	1.7721
	2	40.074	26.357	24.747	6.6017-5	46.528	27.493
	3	462.09	394.43	1.9282	8.6695-9	1032.2	702.74
45	1	1.7202	1.4671	0.38923	0.23478	1.9476	1.7721
	2	40.217	26.439	24.771	6.5958-5	46.552	27.509
	3	467.10	398.74	1.9464	8.4523-9	1027.5	701.18
50	1	1.7206	1.4673	0.38924	0.23471	1.9478	1.7720
	2	40.380	26.533	24.804	6.5816-5	46.593	27.537
	3	477.24	403.17	1.9652	8.2280-9	1022.7	699.58

Table F.6.2-2 Cross Section vs. ^{235}U Burnup for 45% Enrichment Case

Burnup (%)	Group	^{235}U		^{238}U		^{239}Pu	
		σ_a	σ_f	σ_a	σ_f	σ_a	σ_f
0	1	1.7204	1.4672	0.38893	0.23439	1.9475	1.7718
	2	38.529	25.463	9.1977	6.7958-5	45.904	27.074
	3	421.15	359.14	1.7781	1.0491-8	1069.7	715.21
5	1	1.7205	1.4672	0.38891	0.23436	1.9475	1.7718
	2	38.653	25.533	9.2043	6.7885-5	45.929	27.091
	3	420.80	358.83	1.7763	1.0539-8	1071.8	716.30
10	1	1.7206	1.4672	0.38889	0.23432	1.9476	1.7718
	2	38.781	25.605	9.2112	6.7800-5	45.959	27.110
	3	424.71	362.2	1.7907	1.0360-8	1067.7	714.84
15	1	1.7206	1.4672	0.38891	0.23434	1.9476	1.7718
	2	38.913	25.679	9.2186	6.7704-5	45.991	27.132
	3	428.76	365.7	1.8057	1.0174-8	1063.6	713.37
20	1	1.7206	1.4673	0.38891	0.23431	1.9476	1.7718
	2	39.047	25.754	9.2261	6.7607-5	46.024	27.154
	3	433.0	369.35	1.8213	9.9805-9	1059.3	711.85
25	1	1.7207	1.4673	0.38890	0.23429	1.9476	1.7718
	2	39.183	25.831	9.2334	6.7511-5	46.056	27.175
	3	437.38	373.13	1.8374	9.7821-9	1055.0	710.33
30	1	1.7207	1.4673	0.38888	0.23425	1.9476	1.7718
	2	39.320	25.907	9.2406	6.7426-5	46.087	27.195
	3	441.96	377.07	1.8542	9.5760-9	1050.5	708.78
35	1	1.7208	1.4673	0.38887	0.23423	1.9476	1.7718
	2	39.464	25.987	9.2486	6.7321-5	46.121	27.218
	3	446.71	381.17	1.8716	9.3632-9	1045.9	707.20
40	1	1.7208	1.4674	0.38886	0.23421	1.9476	1.7717
	2	39.610	26.068	9.2566	6.7218-5	46.156	27.241
	3	451.66	385.44	1.8897	9.1427-9	1041.2	705.58
45	1	1.7212	1.4676	0.38888	0.23415	1.9477	1.7717
	2	39.769	26.157	9.2663	6.7071-5	46.200	27.270
	3	456.81	389.88	1.9086	8.9143-9	1036.3	703.93
50	1	1.7212	1.4676	0.38888	0.23415	1.9478	1.7717
	2	39.929	26.249	9.2747	6.6964-5	46.235	27.294
	3	462.22	394.54	1.9283	8.6785-9	1031.3	702.25

Table F.6.2-3 Cross Section vs. ^{235}U Burnup for 20% Enrichment Case

Burnup (%)	Group	^{235}U		^{238}U		^{239}Pu	
		σ_a	σ_f	σ_a	σ_f	σ_a	σ_f
0	1	1.7221	1.4680	0.38828	0.23330	1.9477	1.7712
	2	37.840	25.051	4.6925	6.9305-5	45.478	26.786
	3	404.09	344.43	1.7148	1.1296-8	1086.4	720.98
5	1	1.7222	1.4680	0.38826	0.23327	1.9477	1.7712
	2	37.972	25.125	4.6946	6.9235-5	45.504	26.802
	3	403.36	343.80	1.7116	1.1371-8	1088.7	722.10
10	1	1.7222	1.4680	0.38826	0.23326	1.9477	1.7712
	2	38.111	25.203	4.6971	6.9136-5	45.537	26.824
	3	407.15	347.07	1.7256	1.1195-8	1084.2	720.39
15	1	1.7223	1.468	0.38826	0.23324	1.9477	1.7714
	2	38.25	25.279	4.6997	6.9042-5	45.570	26.846
	3	411.17	350.54	1.7405	1.1008-8	1079.7	718.65
20	1	1.7226	1.4683	0.38828	0.23319	1.9478	1.7712
	2	38.398	25.361	4.7030	6.8907-5	45.609	26.873
	3	415.34	354.14	1.7559	1.0815-8	1075.1	716.96
25	1	1.7224	1.4681	0.38825	0.23320	1.9477	1.7712
	2	38.534	25.433	4.7051	6.885-5	45.424	26.782
	3	419.76	357.95	1.7722	1.0612-8	1069.7	714.86
30	1	1.7225	1.4681	0.38821	0.23313	1.9477	1.7711
	2	38.681	25.513	4.7081	6.8745-5	45.432	26.791
	3	424.37	361.92	1.7891	1.0401-8	1064.7	712.97
35	1	1.7225	1.4682	0.38822	0.23315	1.9477	1.7712
	2	38.833	25.595	4.7104	6.8638-5	45.445	2.6802
	3	429.19	366.08	1.8069	1.0181-8	1059.8	711.22
40	1	1.7225	1.4682	0.38821	0.23312	1.9478	1.7711
	2	38.987	25.677	4.7134	6.8536-5	45.460	26.815
	3	434.25	370.44	1.8255	9.9516-9	1054.8	709.46
45	1	1.7226	1.4682	0.38821	0.23310	1.9478	1.7711
	2	39.147	25.764	4.7166	6.8424-5	45.483	26.831
	3	439.58	375.04	1.8450	9.7107-9	1049.6	707.66
50	1	1.7227	1.4683	0.38821	0.23308	1.9478	1.7711
	2	39.315	25.855	4.7201	6.8296-5	45.513	26.852
	3	445.16	379.84	1.8654	9.4615-9	1044.3	705.88

Table F.6.3 Comparison of absorption cross sections calculated by JAERI with those by ANL

0% ^{235}U Burn-up

Nuclide	^{235}U Enrichment	Energy Group	JAERI	ANL
^{235}U	93%	1	1.7198	1.7271
		2	39.025	39.235
		3	431.83	422.84
	45%	1	1.7204	1.7277
		2	38.529	38.679
		3	421.15	411.05
	20%	1	1.7221	1.7292
		2	37.840	37.845
		3	404.09	392.61
^{238}U	93%	1	0.38927	0.34526
		2	24.534	27.137
		3	1.8176	1.7692
	45%	1	0.38893	0.34498
		2	9.1977	11.151
		3	1.7781	1.7251
	20%	1	0.38828	0.34362
		2	4.6925	6.0950
		3	1.7148	1.6560

Table F.6.4-1 Atom Densities in 93% Enriched Fuel Meat vs. ^{235}U Burnup
Atomic Number Density (burn·cm)$^{-1}$

Burnup(%)	Al	^{135}Xe	^{149}Sm	^{235}U	^{236}U	^{238}U
0	5.7011-2	0.0	0.0	1.6179-3	0.0	1.2020-4
5	5.7011-2	1.4633-8	1.6931-7	1.5370-3	1.3335-5	1.1980-4
10	5.7011-2	1.4022-8	1.6089-7	1.4561-3	2.6603-5	1.1938-4
15	5.7011-2	1.3326-8	1.5189-7	1.3752-3	3.9738-5	1.1895-4
20	5.7011-2	1.2619-8	1.4288-7	1.2943-3	5.2753-5	1.1851-4
25	5.7011-2	1.1904-8	1.3389-7	1.2134-3	6.5637-5	1.1807-4
30	5.7011-2	1.1180-8	1.2493-7	1.1325-3	7.8388-5	1.1762-4
35	5.7011-2	1.0449-8	1.1600-7	1.0516-3	9.1006-5	1.1716-4
40	5.7011-2	9.7073-9	1.0708-7	9.7074-4	1.0348-4	1.1669-4
45	5.7011-2	8.9558-9	9.8161-8	8.8985-4	1.1581-4	1.1621-4
50	5.7011-2	8.1964-9	8.9277-8	8.0895-4	1.2800-4	1.1571-4
				7.2806-4		

Burnup(%)	^{239}Pu	^{240}Pu	^{241}Pu	^{242}Pu
0	0.0	0.0	0.0	0.0
5	3.7183-7	7.1357-9	3.3242-10	2.6409-12
10	7.1845-7	2.7539-8	2.6141-9	4.3352-11
15	1.0250-6	5.9034-8	8.3887-9	2.2090-10
20	1.2924-6	9.9461-8	1.8744-8	6.9709-10
25	1.5217-6	1.4689-7	3.4338-8	1.6944-9
30	1.7146-6	1.9958-7	5.5434-8	3.4945-9
35	1.8727-6	2.5600-7	8.1946-8	6.4380-9
40	1.9966-6	3.1475-7	1.1343-7	1.0926-8
45	2.0869-6	3.7462-7	1.4916-7	1.7430-8
50	2.1454-6	4.3445-7	1.8816-7	2.6502-8

Table F.6.4-2 Atom Densities in 45% Enriched Fuel Meat vs ^{235}U Burnup
Atomic Number Density (burn·cm)$^{-1}$

Burnup (%)	Al	^{135}Xe	^{149}Sm	^{235}U	^{236}U	^{238}U
0	5.3691-2	0.0	0.0	1.8490-3	0.0	2.2314-3
5	5.3691-2	1.6548-8	1.9532-7	1.7566-3	1.5442-5	2.2278-3
10	5.3691-2	1.5925-8	1.8633-7	1.6641-3	3.0818-5	2.2240-3
15	5.3691-2	1.5189-8	1.7641-7	1.5717-3	4.6023-5	2.2201-3
20	5.3691-2	1.4437-8	1.6645-7	1.4792-3	6.1085-5	2.2161-3
25	5.3691-2	1.3672-8	1.5646-7	1.3868-3	7.5970-5	2.2121-3
30	5.3691-2	1.2891-8	1.4645-7	1.2943-3	9.0707-5	2.2079-3
35	5.3691-2	1.2097-8	1.3642-7	1.2019-3	1.0526-4	2.2036-3
40	5.3691-2	1.1287-8	1.2635-7	1.1094-3	1.1966-4	2.1992-3
45	5.3691-2	1.0464-8	1.1628-7	1.0170-3	1.3387-4	2.1946-3
50	5.3691-2	9.6228-9	1.0616-7	9.245 -4	1.4790-4	2.1899-3

Burnup (%)	^{239}Pu	^{240}Pu	^{241}Pu	^{242}Pu
0	0.0	0.0	0.0	0.0
5	3.2201-6	6.3783-8	3.2482-9	2.5994-11
10	6.2287-6	2.4536-7	2.5531-8	4.2672-10
15	8.8990-6	5.2369-7	8.1695-8	2.1672-9
20	1.1249-5	8.7952-7	1.8226-7	6.8265-9
25	1.3285-5	1.2946-6	3.3307-7	1.6546-8
30	1.5023-5	1.7546-6	5.3676-7	3.4058-8
35	1.6470-5	2.2451-6	7.9164-7	6.5284-8
40	1.7638-5	2.7556-6	1.0940-6	1.0866-7
45	1.8534-5	3.2746-6	1.4360-6	1.7131-7
50	1.9163-5	3.7944-6	1.8085-6	2.5854-7

Table F.6.4-3 Atom Densities in 20% Enriched Fuel Meat vs ^{235}U Burnup
Atomic Number Density $(burn \cdot cm)^{-1}$

Burnup(%)	Al	^{135}Xe	^{149}Sm	^{235}U	^{236}U	^{238}U
0	3.8170-2	0	0	2.2536-3	0	8.9005-3
5	3.8170-2	1.9840-8	2.4291-7	2.1409-3	1.9245-5	8.8904-3
10	3.8170-2	1.9220-8	2.3317-7	2.0282-3	3.8390-5	8.8797-3
15	3.8170-2	1.8432-8	2.2173-7	1.9156-3	5.7319-5	8.8689-3
20	3.8170-2	1.7617-8	2.1013-7	1.8029-3	7.6050-5	8.8570-3
25	3.8170-2	1.6779-8	1.9839-7	1.6902-3	9.4562-5	8.8459-3
30	3.8170-2	1.5918-8	1.8657-7	1.5775-3	1.1285-4	8.8339-3
35	3.8170-2	1.5032-8	1.7464-7	1.4648-3	1.3091-4	8.8241-3
40	3.8170-2	1.4123-8	1.6262-7	1.3522-3	1.4872-4	8.8112-3
45	3.8170-2	1.3187-8	1.5050-7	1.2395-3	1.6630-4	8.7977-3
50	3.8170-2	1.2226-8	1.3828-7	1.1268-3	1.8362-4	8.7835-3

Burnup(%)	^{239}Pu	^{240}Pu	^{241}Pu	^{242}Pu
0	0	0	0	0
5	8.6929-6	1.8097-7	1.0564-8	8.5611-11
10	1.6795-5	6.9003-7	8.2624-8	1.3976-9
15	2.4013-5	1.4613-6	2.6329-7	7.0665-9
20	3.0391-5	2.4358-6	5.8450-7	2.2153-8
25	3.5955-5	3.5613-6	1.0637-6	5.3744-8
30	4.0753-5	4.7919-6	1.7053-6	1.0950-7
35	4.4807-5	6.0925-6	2.5029-6	2.0026-7
40	4.8141-5	7.4311-6	3.4399-6	3.3723-7
45	5.0786-5	8.7839-6	4.4939-6	5.3397-7
50	5.2759-5	1.0128-5	5.6322-6	8.0562-7

Table F.6.5 Values of k_{eff} from X-Y Diffusion Theory Calculations

Enrichment	Description	keff	
		JAERI	ANL
93%	BOL Benchmark	1.04199	1.02333
93%	EOL Benchmark	1.02195	1.00038
93%	Fresh Fuel in All Fuel Regions	1.18104	1.18343
45%	BOL Benchmark	1.04893	1.02471
45%	EOL Benchmark	1.03058	1.00331
45%	Fresh Fuel in All Fuel Regions	1.18107	1.17817
20%	BOL Benchmark	1.05782	1.02127
20%	EOL Benchmark	1.04122	1.00142
20%	Fresh Fuel in All Fuel Regions	1.18339	1.16830

Table F.6.6 Survey of ^{235}U Loading with Uranium Enrichment of 20%, 45% and 93% - Atom Number Density ($\times 10^{-24}$)

93% Enrichment U-Aℓ Alloy

^{235}U/Element, g	140	180	220	260	300
U-235	9.7906×10^{-4}	1.2584×10^{-3}	1.5404×10^{-3}	1.8197×10^{-3}	2.0991×10^{-3}
U-238	7.3389×10^{-5}	9.3635×10^{-5}	1.1388×10^{-4}	1.3413×10^{-4}	1.5690×10^{-4}
Aℓ	5.5855×10^{-2}	5.5526×10^{-2}	5.5206×10^{-2}	5.4796×10^{-2}	5.4509×10^{-2}

45% Enrichment $UAℓ_x$-Aℓ

^{235}U/Element, g	150	197	247	300	357
U-235	1.0483×10^{-3}	1.3789×10^{-3}	1.7274×10^{-3}	2.1016×10^{-3}	2.5051×10^{-3}
U-238	1.2628×10^{-3}	1.6652×10^{-3}	2.0853×10^{-3}	2.5357×10^{-3}	3.0191×10^{-3}
Aℓ	5.2605×10^{-2}	5.1560×10^{-2}	5.0334×10^{-2}	4.9078×10^{-2}	4.7808×10^{-2}

20% Enrichment $UAℓ_x$-Aℓ

^{235}U/Element, g	163	221	289	371	475
U-235	1.1380×10^{-3}	1.5480×10^{-3}	2.0248×10^{-3}	2.5963×10^{-3}	3.3216×10^{-3}
U-238	4.4945×10^{-3}	6.1141×10^{-3}	7.9969×10^{-3}	1.0254×10^{-2}	1.3119×10^{-2}
Aℓ	4.7771×10^{-2}	4.4725×10^{-2}	4.1275×10^{-3}	3.7062×10^{-2}	3.1731×10^{-2}

Aℓ Clad and H_2O Moderator

Aℓ	6.0260×10^{-2}
O	3.3428×10^{-2}
H	6.6856×10^{-2}

Table F.6.7 Survey of ^{235}U Loading with Uranium Enrichment of 20%, 45% and 93% - Excess Reactivity

93% Enrichment U-Aℓ Alloy

^{235}U/Element,g	140	180	220	260	300
k_{eff}(by ANL)	0.9869	1.0521	1.0983	1.1327	1.1592
k_{eff}(by JAERI)	0.9920	1.0558	1.1012	1.1345	1.1601

45% Enrichment $UAℓ_x$-Aℓ

^{235}U/Element,g	150	197	247	300	357
k_{eff}(by ANL)	0.9869	1.0521	1.0983	1.1327	1.1592
k_{eff}(by JAERI)	0.9969	1.0558	1.1063	1.1404	1.1667

20% Enrichment $UAℓ_x$-Aℓ

^{235}U/Element,g	163	221	289	371	475
k_{eff}(by ANL)	0.9869	1.0521	1.0983	1.1327	1.1592
k_{eff}(by JAERI)	1.0008	1.0662	1.1133	1.1487	1.1771

Table F.6.8 2 MW and 10 MW Atom Number Densities for 93% and 20% Fuel Enrichment (Standard Fuel Element and Control Fuel Element)

2 MW Reactor

	93% (10^{-24})		20% (10^{-24})	
	SFE	CFE	SFE	CFE
U-235	1.2584×10^{-3}	9.9444×10^{-4}	1.4917×10^{-3}	1.1764×10^{-3}
U-238	9.3635×10^{-5}	7.3389×10^{-5}	5.8914×10^{-3}	4.6488×10^{-3}
Aℓ	5.5526×10^{-2}	5.5885×10^{-2}	4.5110×10^{-2}	4.7445×10^{-2}

10 MW Reactor

	93% (10^{-24})		20% (10^{-24})	
	SFE	CFE	SFE	CFE
U-235	1.9606×10^{-3}	1.4481×10^{-3}	2.1913×10^{-3}	1.6352×10^{-3}
U-238	1.468×10^{-4}	1.0882×10^{-4}	8.6524×10^{-3}	6.3798×10^{-3}
Aℓ	5.4778×10^{-2}	5.5319×10^{-2}	4.009×10^{-2}	4.4208×10^{-2}

Aℓ Clad	6.0260×10^{-2}
O	3.3428×10^{-2}
H	6.6856×10^{-2}

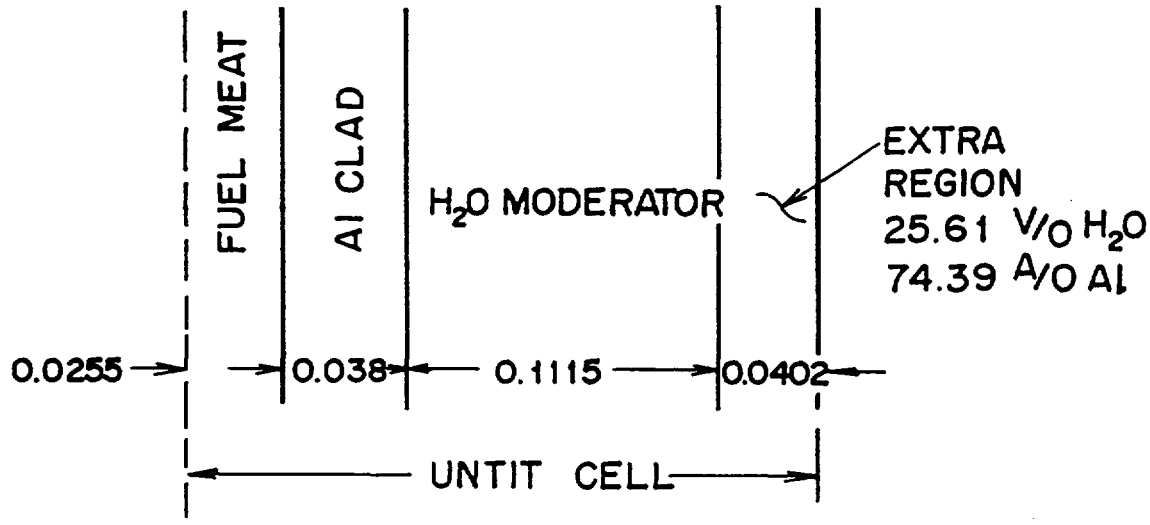

Standard Fuel Elment

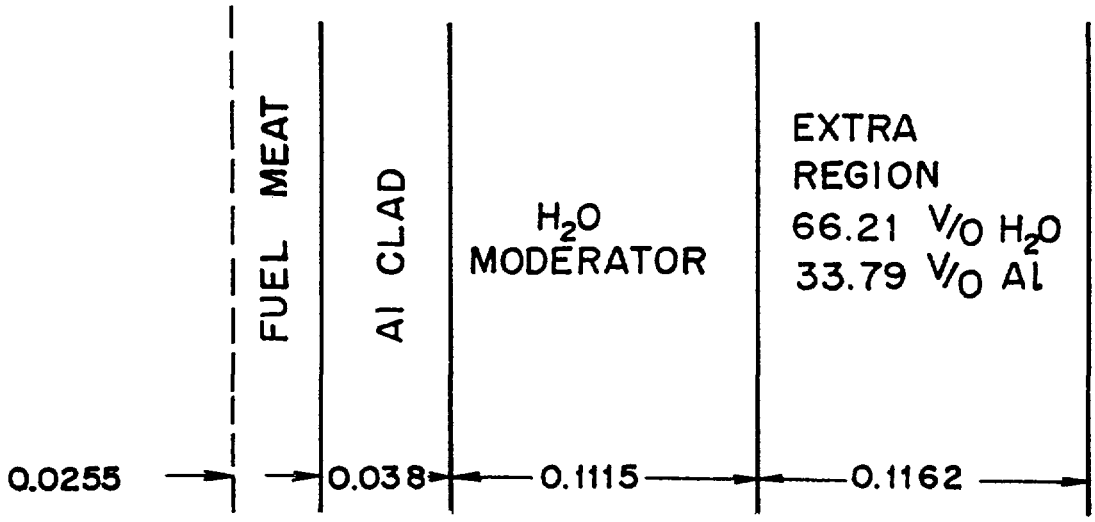

Control Fuel Element

Fig. F.6.1 Slab geometry of unit cell in MTR type reactor

(all dimension in Cm)

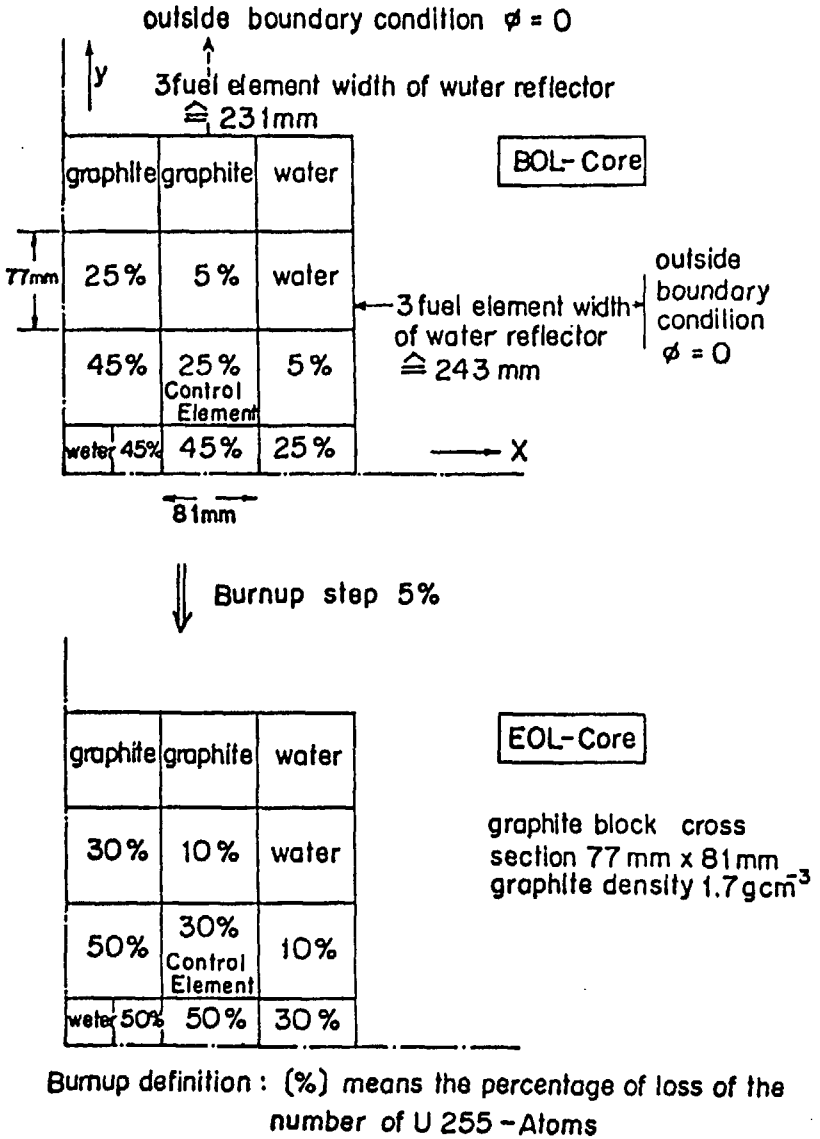

Burnup definition : (%) means the percentage of loss of the number of U 255 - Atoms

Fig. F.6.2 Core composition for the methodical benchmark problem

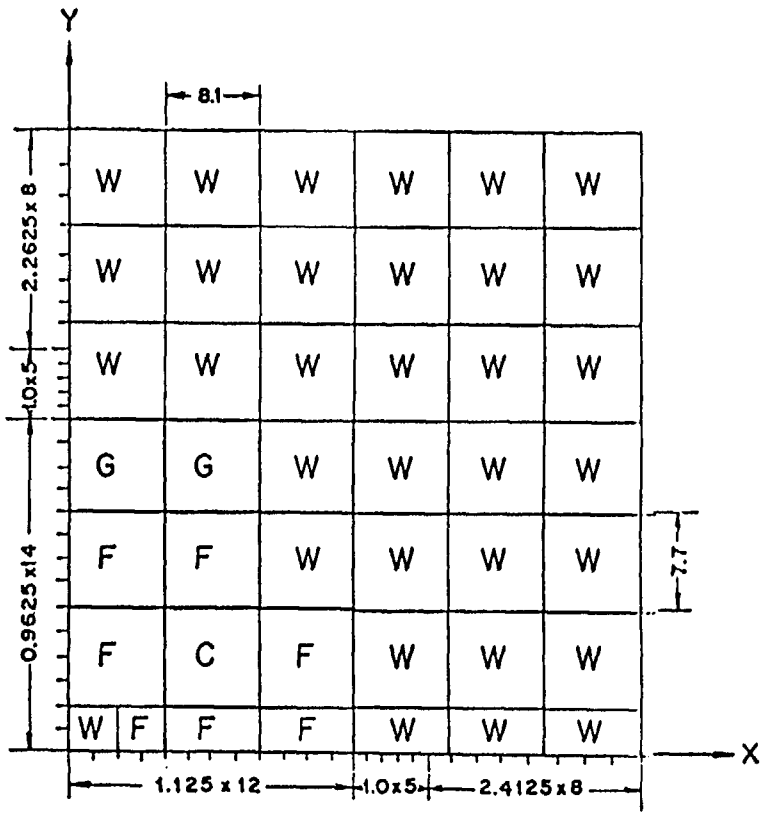

F : Standard Fuel Element
C : Control. Fuel Element
G : Graphite.
W : Water.

Fig. F.6.3 X-Y model on MTR type reactor for two-dimensional calculation
(all dimension in Cm)

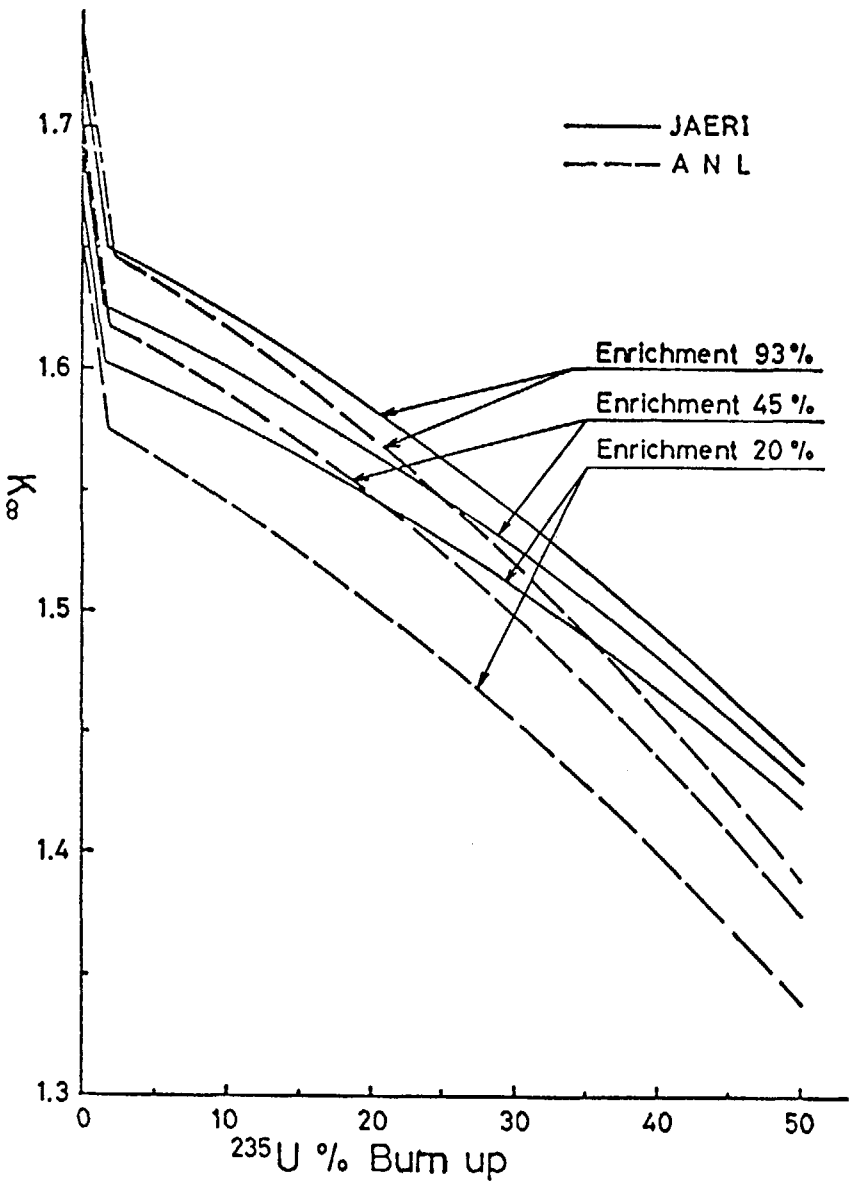

Fig. F.6.4 K_∞ vs. ^{235}U burnup as a parameter of enrichments

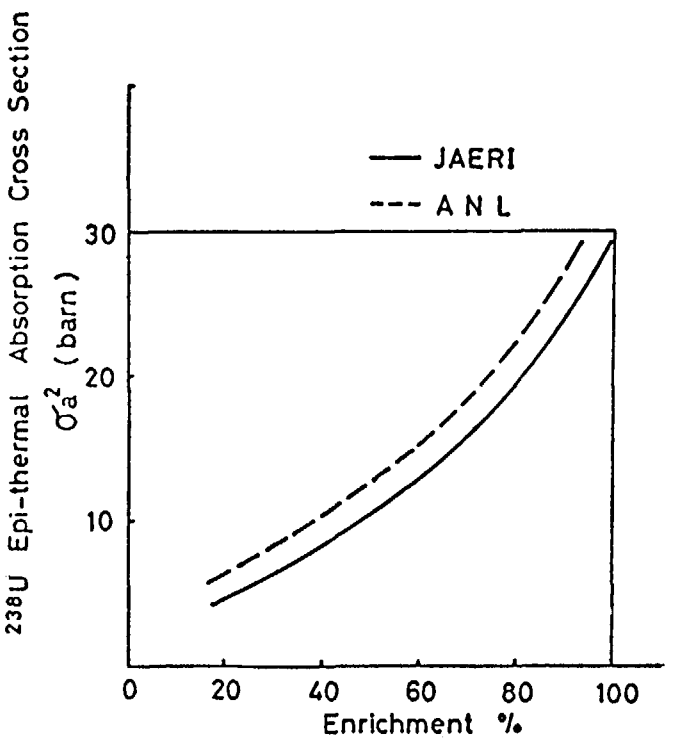

Fig. F.6.5 Variation of ^{238}U epithermal absorption cross section vs, ^{235}U enrichment

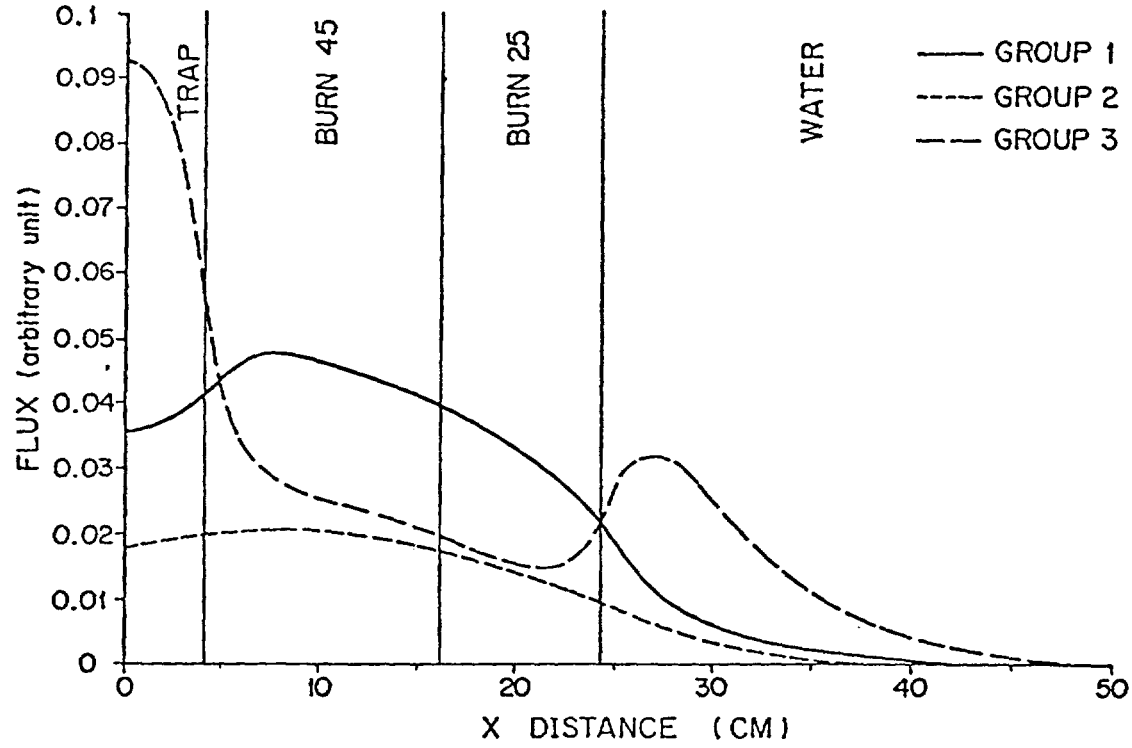

Fig.F.6.6 Fluxes at midplane along X-axis
IAEA 10 MW Benchmark 93% U-235 BOL

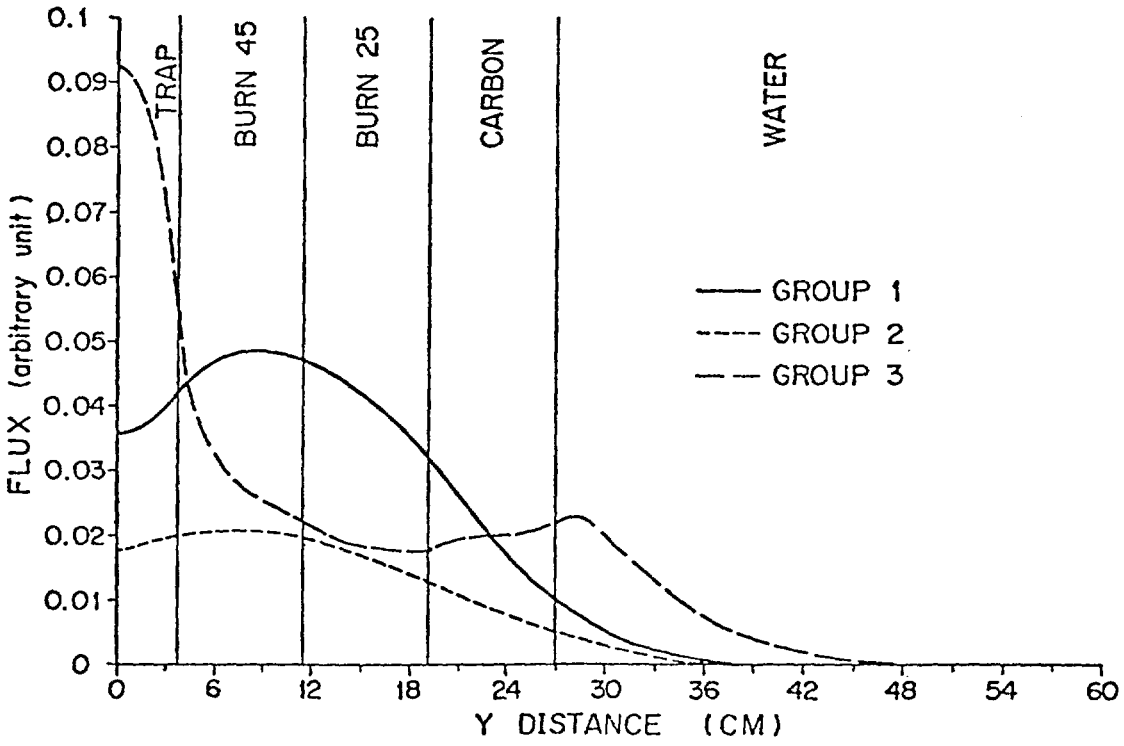

Fig.F.6.7 Fluxes at midplane along Y-axis
IAEA 10 MW Benchmark 93% U-235 BOL

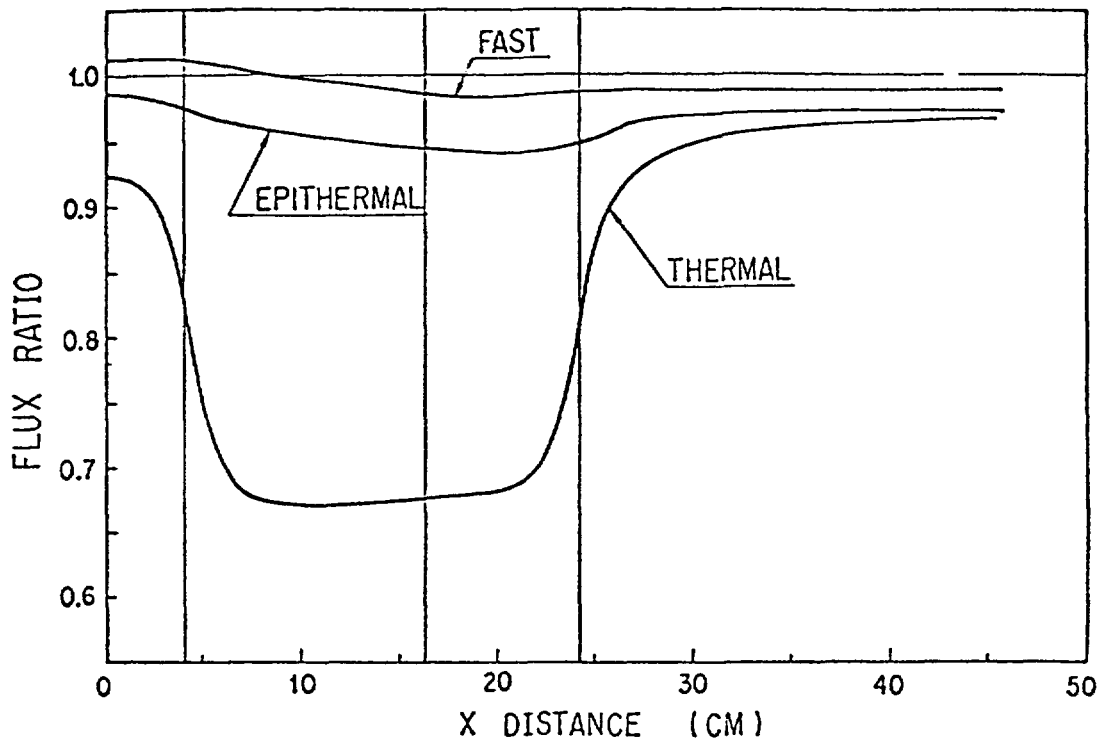

Fig.F.6.8 10 MW-BENCHMARK
FLUX RATIO AGAINST X-DISTANCE
20 w/o U235 / 93 w/o U235

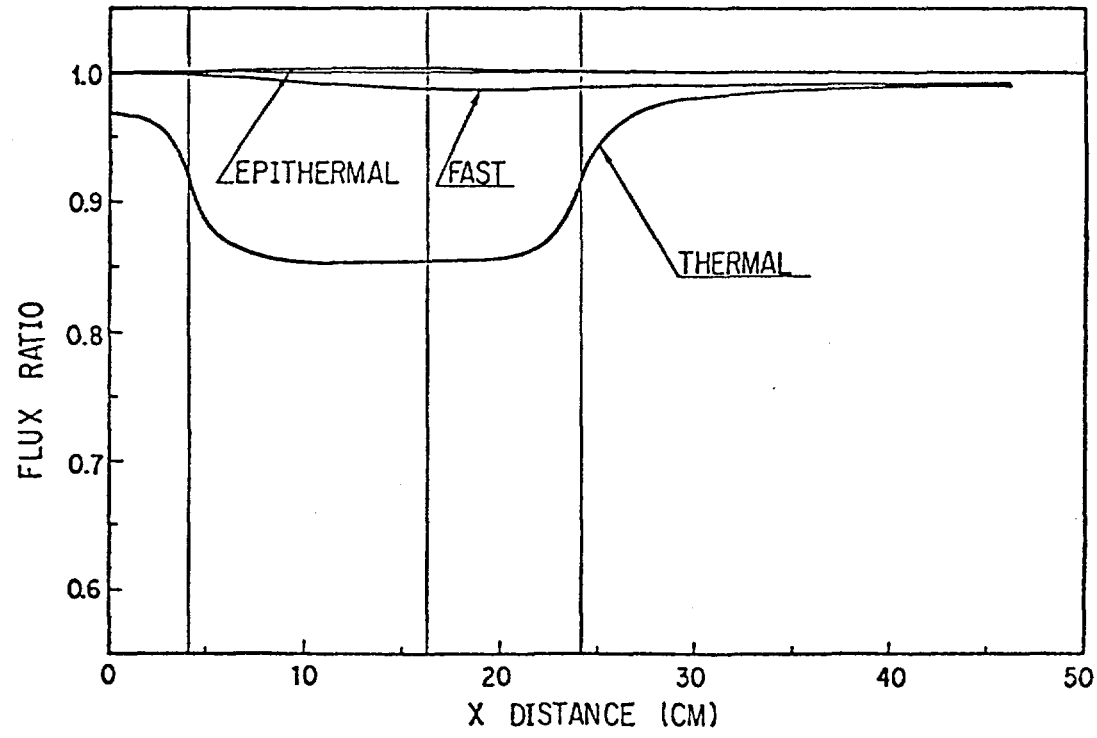

Fig.F.6.9 10 MW-BENCHMARK
FLUX RATIO AGAINST X DISTANCE
45 w/o U235 / 93 w/o U235

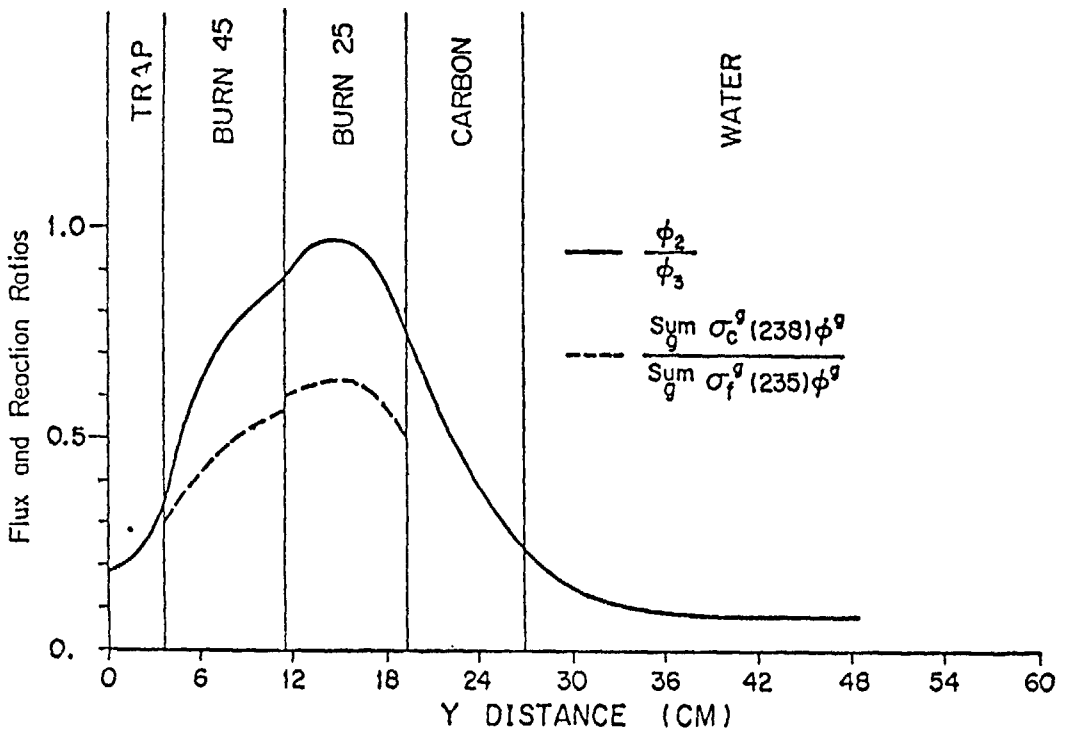

Fig.F.6.10 ^{238}U capture to ^{235}U fission ratio and thermal to epi-thermal flux ratio IAEA 10 MW Benchmark 93 % U-235 BOL

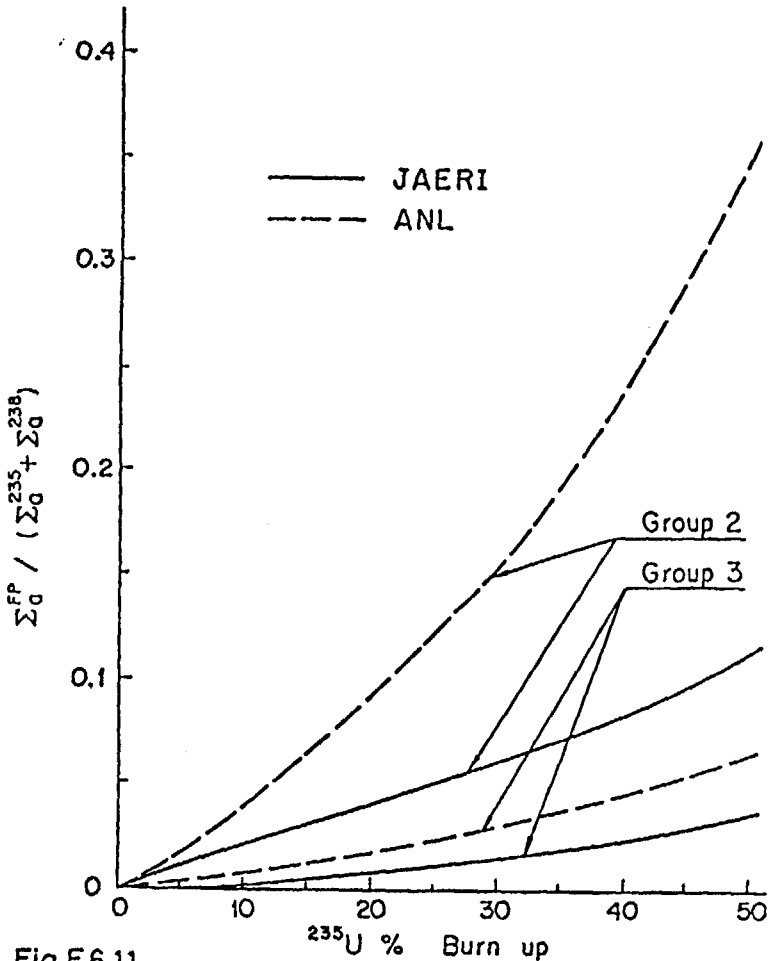

Fig.F.6.11 Variation of absorption rate of lumped fission product to ^{235}U and ^{238}U absorption vs. ^{235}U % burn-up

F-6.21

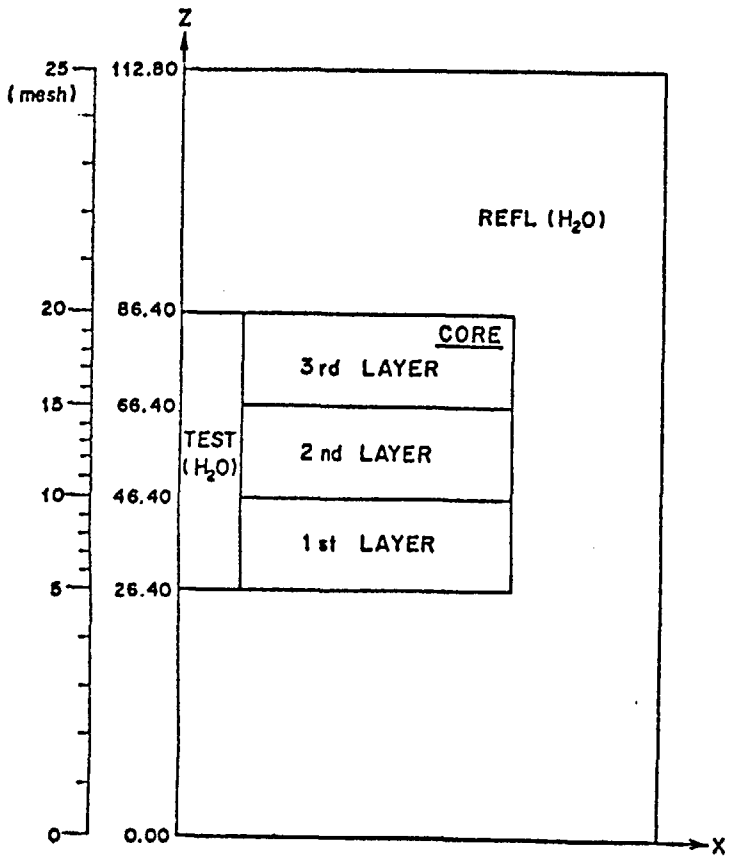

Fig. F.6.12-1 X-Z mode on 2 MW reactor for three-dimentional calculation (all dimension in Cm)

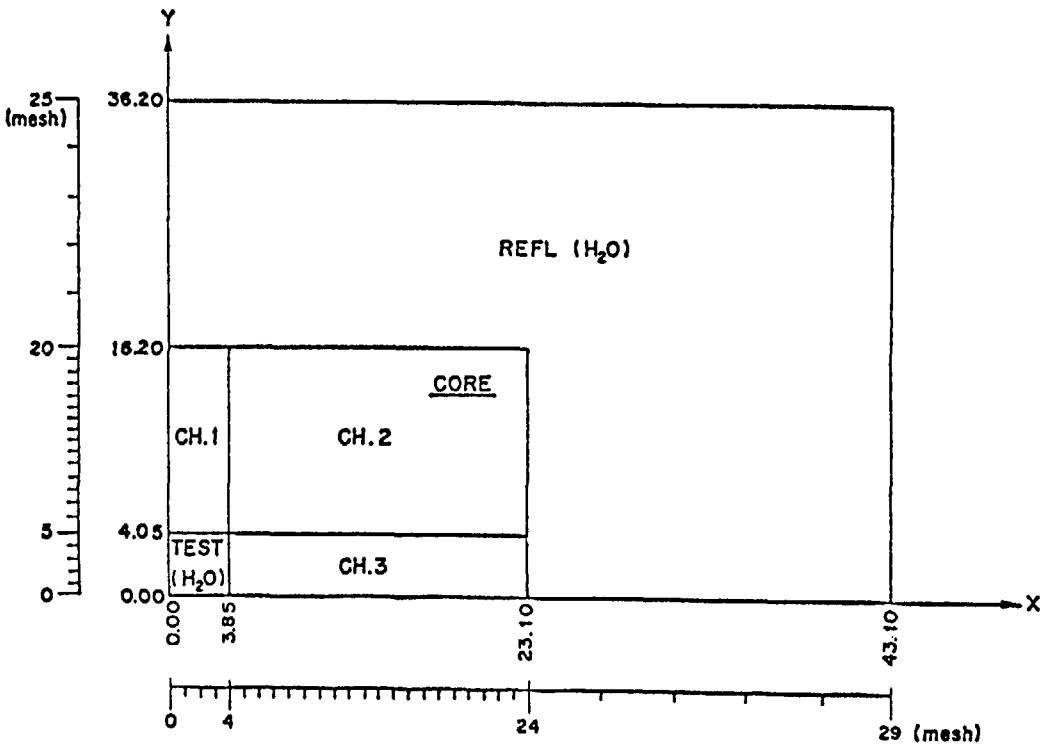

Fig. F.6.12-2 X-Y model on 2 MW reactor for three dimentional calculation (all dimension in Cm)

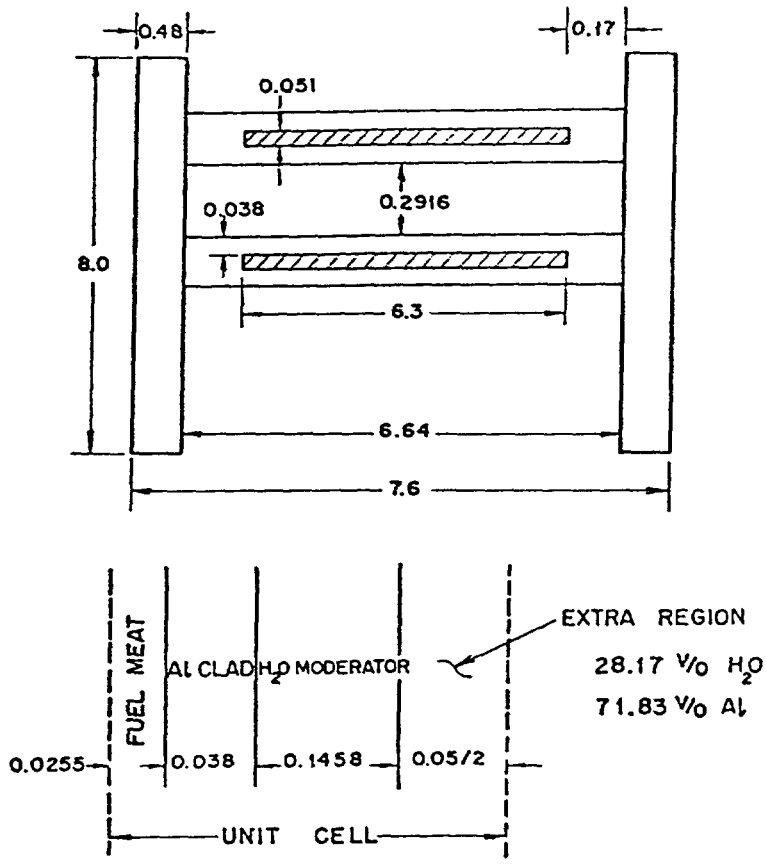

Fig. F.6.13 2 MW reactor-fuel element and unit cell
(all dimension in Cm)

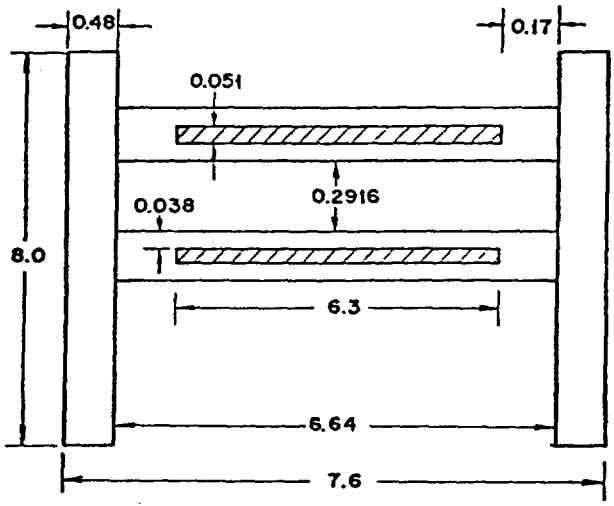

Fig. F.6.14

2 MW reactor-standard (19 plates/element)

and control (15 plates/element) fuel element
(all dimension in Cm)

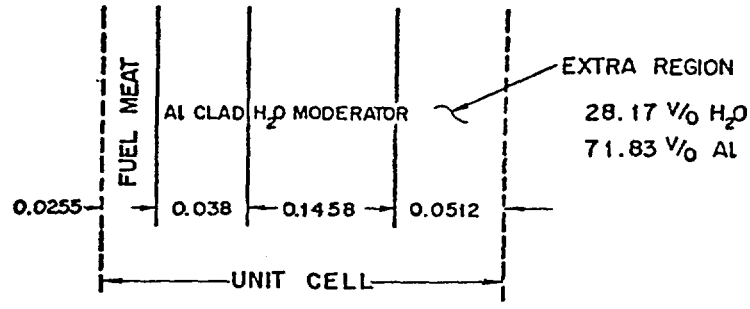

standard fuel element

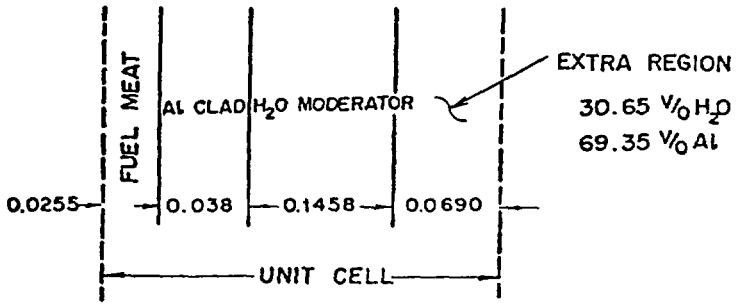

control fuel element

Fig. F.6.15 Slab geometry of unit cell in 2 MW reactor
(all dimension in Cm)

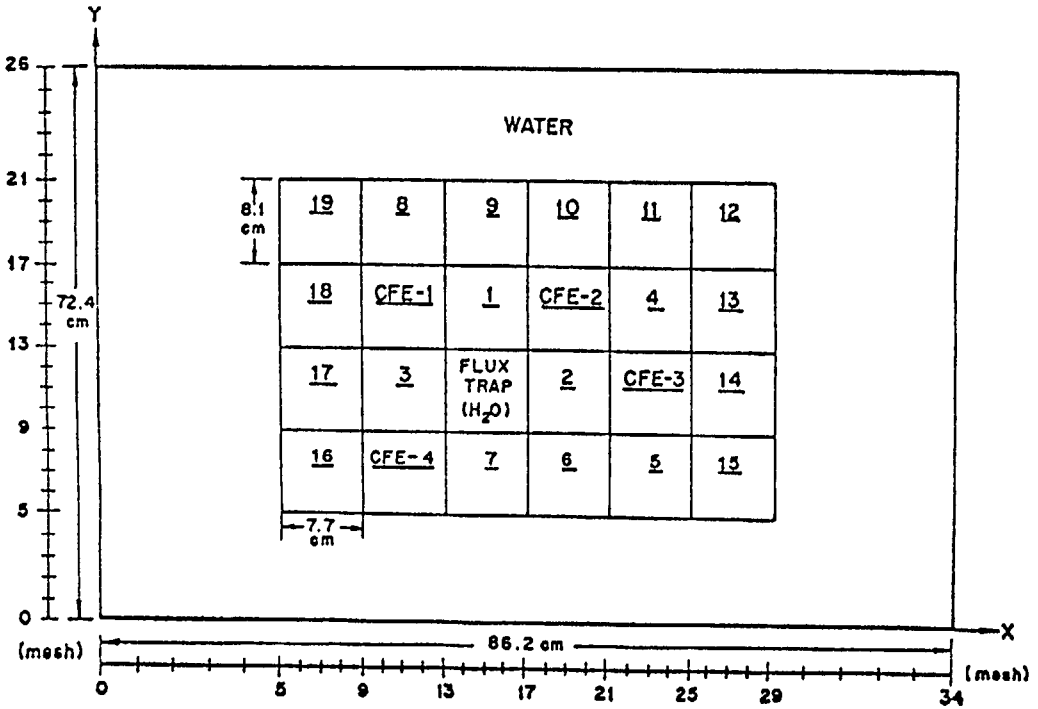

Fig. F.6.16 X-Y model on 2 MW reactor for burnup studies

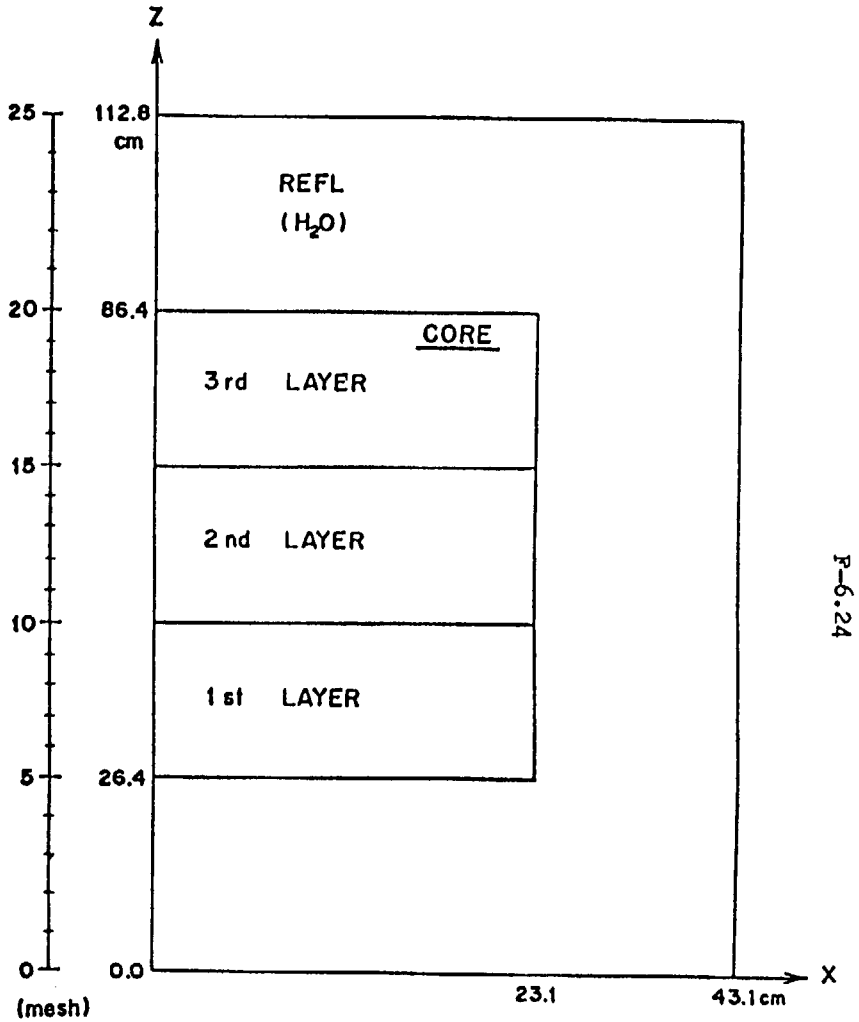

F-6.24

Fig. F.6.17 X-Y model on 2 MW reactor for three-dimensional calculation

U Enrichment : 93 %
U Density : 0.528 g/cm³
Fresh Fuel. Loading : 180 g

BOC Keff
JAERI : 1.0029
ANL : 1.0059
EOC Keff
JAERI : 0.9994
ANL : 1.0000

Channel NO.
235U Weight
Pu JAERI (ANL)

BOC

19 159.9 g 0.064 g (0.06 g)	8 170.5 0.031 (0.03)	9 169.5 0.034 (0.03)	10 168.3 0.038 (0.04)	11 167.0 0.042 (0.04)	12 165.9 0.047 (0.05)
18 160.8 0.062 (0.06)	CFE-1 132.4 0.022 (0.03)	1 180.0 0.0 (0.0)	CFE-2 130.1 0.027 (0.04)	4 175.3 0.018 (0.02)	13 165.1 0.049 (0.05)
17 161.7 0.059 (0.06)	3 176.8 0.015 (0.01)	FLUX TRAP (H_2O)	2 178.3 0.011 (0.01)	CFE-3 131.7 0.024 (0.03)	14 164.1 0.052 (0.05)
16 162.3 0.058 (0.06)	CFE-4 134.5 0.017 (0.02)	7 171.7 0.027 (0.03)	6 172.9 0.024 (0.02)	5 173.9 0.017 (0.02)	15 163.1 0.055 (0.05)

EOC

19 159.2 0.066 (0.07)	8 169.5 0.034 (0.03)	9 168.3 0.038 (0.04)	10 167.0 0.042 (0.04)	11 165.9 0.047 (0.05)	12 165.1 0.049 (0.05)
18 159.9 0.064 (0.06)	CFE-1 131.3 0.025 (0.03)	1 178.3 0.011 (0.01)	CFE-2 128.8 0.028 (0.04)	4 173.9 0.017 (0.02)	13 164.1 0.052 (0.05)
17 160.8 0.062 (0.06)	3 175.3 0.018 (0.02)	FLUX TRAP (H_2O)	2 176.6 0.015 (0.01)	CFE-3 130.6 0.026 (0.04)	14 163.1 0.055 (0.05)
16 161.7 0.059 (0.06)	CFE-4 133.9 0.019 (0.02)	7 170.5 0.031 (0.03)	6 171.7 0.027 (0.03)	5 172.9 0.024 (0.02)	15 162.3 0.058 (0.06)

Fig. F.6.18 2 MW reactor-HEU (93%) fuel

U Enrichment : 20 %
U Density : 2.91 g/cm³
Fresh Fuel Loading : 213 g.

BOC Keff
JAERI : 1.0069
ANL : 1.0050
EOC Keff
JAERI : 1.0032
ANL : 0.9999

CHANNEL NO
235U Weight
Pu JAERI (ANL)

19 193.2 g 1.20 g (1.36 g)	8 203.7 0.61 (0.67)	9 202.7 0.68 (0.74)	10 201.5 0.76 (0.82)	11 200.2 0.83 (0.91)	12 199.2 0.90 (0.98)
18 194.1 1.18 (1.30)	CFE-1 158.6 0.47 (0.68)	1 213.1 0.0 (0.0)	CFE-2 156.4 0.57 (0.83)	4 208.4 0.30 (0.33)	13 198.4 0.95 (1.03)
17 195.0 1.12 (1.25)	3 209.8 0.21 (0.24)	FLUX TRAP (H_2O)	2 211.4 0.12 (0.12)	CFE-3 158.1 0.47 (0.73)	14 197.4 1.00 (1.10)
16 195.8 1.10 (1.21)	CFE-4 160.7 0.36 (0.47)	7 204.9 0.53 (0.59)	6 206.1 0.45 (0.51)	5 207.1 0.30 (0.44)	15 196.4 1.05 (1.16)

19 192.5 g 1.22 (1.40)	8 202.7 0.68 (0.74)	9 201.5 0.76 (0.82)	10 200.2 0.83 (0.91)	11 199.2 0.90 (0.98)	12 198.4 0.95 (1.03)
18 193.2 1.20 (1.36)	CFE-1 157.5 0.51 (0.75)	1 211.4 0.12 (0.12)	CFE-2 155.1 0.59 (0.91)	4 207.1 0.38 (0.44)	13 197.4 1.00 (1.10)
17 194.1 1.18 (1.30)	3 208.4 0.30 (0.33)	FLUX TRAP (H_2O)	2 209.8 0.21 (0.24)	CFE-3 156.9 0.54 (0.81)	14 196.4 1.05 (1.16)
16 195.0 1.12 (1.25)	CFE-4 159.9 0.40 (0.53)	7 203.7 0.61 (0.67)	6 204.9 0.53 (0.59)	5 206.1 0.45 (0.51)	15 195.6 1.10 (1.21)

Fig. F.6.19 2MW reactor-LEU (20%) fuel

APPENDIX F-7

BENCHMARK CORE CALCULATIONS

performed by

J. Babino, M. Madariaga, J. Testoni

CNEA - Departmento de Reactores

Buenos Aires

Argentina

1. INTRODUCTION

In order to compare reactor physics calculational methods used in various research centers we have calculated the benchmark problems proposed by the Consultants Meeting on "Preparation of a Programme on Research Reactor Conversions to LEU Instead of HEU", IAEA, June 1979 in Vienna using our current methods.

In this preliminary report we describe the generation of cross sections, burn-up and x-y diffusion calculations.

2. CROSS SECTIONS

Cell cross sections for burn-up at 10 MW were obtained up to 50% of consumed U-235 in steps of 5% for 93% and 20% enrichment cases.

The WIMS-D code /1/ and its 69 group library were used in the pin cell option with condensation to the five energy groups of Table I.

The main transport calculation was performed with the S4 option in the above mentioned group structure. The actual cell geometry has been adapted to the code assuming the cell composed of three kinds of infinite layers (Fig. 9).

Fuel (Al + U)
Clad + Lateral Support (Al)
Coolant (H_2O)

so that

a) the volume ratios of the different materials are conserved.

b) option 1): the cell pitch is conserved (see Fig. 9.1)
option 2): the meat thickness is conserved (see Fig. 9.2).

A buckling of 0.008 cm^{-2} corresponding to a cylinder with a fuel volume equivalent to that of the benchmark configurations was used.

Three group cross sections for water and carbon reflectors were obtained by condensation of the 200 groups GCTC-ENEL /2/ library with a slowing down U-235 fission spectrum in water. The cross sections for the trap were those obtained for the coolant in the cell calculation. The control rod channels were represented by a weighted mixture of coolant and clad cross sections.

Tables II and III give the atomic densities in the fuel meat for the 93% and 20% enriched fuel elements with various stages of burn-up.

Table IV shows the k_∞ obtained for the different burn-ups.

Tables II to IV correspond to the option 1) in the cell transformation, i.e. pitch conservation.

Tables II' to IV' correspond to the option 2) i.e. meat thickness conservation.

3. REACTOR CALCULATIONS

The two dimensional three group (see Table 1), x-y diffusion calculation was performed with EXTERMINATOR-II code /3/ using one quarter reactor geometry.

A total of 48 and 52 mesh intervals was used in the x and y directions respectively.

The fluxes were normalized to 10 MW in the whole core. The axial buckling of 1.709×10^{-3} cm^{-2} corresponds to a chopped cosine axial flux distribution with a 8 cm reflector savings.

The control rod channels were represented as H_2O + Al zones at both sides of the corresponding fuel elements.

In Table V the k_{eff} values for fresh-fuels, BOL and EOL situations for 93% and 20% enrichments are shown. Table V refers to cross sections obtained with pitch conservation in the transformed cell (option 1), Table V" refers to the meat thickness conservation (option 2).

Table VI presents fluxes in different regions of the reactor (with option 1). Average fluxes were averaged both over x-y plane and along the axial direction which has a chopped cosine distribution.

Plots of the fluxes in midplanes along the x and y-axis for the 93% BOL and EOL cases are shown in Fig. 1 to 4.

Flux ratios of the 20% and 93% cases are shown in Fig. 5 to 8.

4. FINAL REMARKS

The present report is a first draft useful for preliminary comparisons. More detailed descriptions of methods, microscopic and macroscopic cross sections and general discussions will be included in a final report.

REFERENCE

/1/ M. J. ROTH, J. D. MAC'DOUGALL, P. B. KEMSHELL, "The preparation of input data for WIMS" AEEW-R-538,

/2/ O. CHIOVATO, F. DI PASQUANTONIO. "GGTC - ENEL", CNA - CPL, 1977.

/3/ T. B. FOWLER et al, "EXTERMINATOR-II a FORTRAN 4 code for solving multigroup neutron diffusion equations in two dimensions", ORNL - 4078, 1967.

TABLE I: Energy Groups Used in the cell calculations.

Five-group structure	Three-group structure	E_U (eV)	E_L (eV)
1	1	1.000+07	8.210+05
2		8.210+05	5.530+03
3	2	5.530+03	1.500+00
4		1.500+00	0.625+00
5	3	0.625+00	0.

TABLE II: Atom Densities in 93% Enriched Fuel Meat vs ^{235}U Burnup.
Atom Densities (cm^{-3} x 10^{24}) (Pitch conservation).

Burnup (%)	Al	^{135}Xe	^{149}Sm	^{235}U	^{236}U	^{238}U
0	5.7013-02	0.0	0.0	1.6180-03	0.0	1.2025-04
5	5.7013-02	1.6313-08	1.4041-07	1.5371-03	1.3750-05	1.1977-04
10	5.7013-02	1.5569-08	1.4175-07	1.4562-03	2.7395-05	1.1929-04
15	5.7013-02	1.4812-08	1.4150-07	1.3753-03	4.0903-05	1.1880-04
20	5.7013-02	1.4043-08	1.4040-07	1.2944-03	5.4269-05	1.1830-04
25	5.7012-02	1.3263-08	1.3848-07	1.2135-03	6.7506-05	1.1779-04
30	5.7013-02	1.2472-08	1.3578-07	1.1326-03	8.0613-05	1.1728-04
35	5.7013-02	1.1669-08	1.3235-07	1.0517-03	9.3565-05	1.1675-04
40	5.7013-02	1.0854-08	1.2822-07	9.7091-04	1.0636-04	1.1621-04
45	5.7013-02	1.0028-08	1.2342-07	8.9015-04	1.1899-04	1.1565-04
50	5.7013-02	9.1899-09	1.1799-07	8.0947-04	1.3144-04	1.1508-04

Burnup (%)	^{239}Pu	^{240}Pu	^{241}Pu	^{242}Pu
0	0.0	0.0	0.0	0.0
5	4.3948-07	8.3958-09	3.6393-10	3.1461-12
10	8.3459-07	3.2001-08	2.7710-09	5.0353-11
15	1.1846-06	6.8361-08	8.8647-09	2.5478-10
20	1.4910-06	1.1519-07	1.9835-08	8.0297-10
25	1.7555-06	1.7046-07	3.6461-08	1.9538-09
30	1.9793-06	2.3230-07	5.9118-08	4.0370-09
35	2.1633-06	2.9887-07	8.7761-08	7.4488-09
40	2.3089-06	3.6863-07	1.2205-07	1.2663-08
45	2.4170-06	4.4012-07	1.6129-07	2.0232-08
50	2.4887-06	5.1196-07	2.0448-07	3.0798-08

TABLE II': Atom Densities in 93% Enriched Fuel Meat vs ^{235}U Burn-up.
Atom Densities ($cm^{-3} \times 10^{24}$) (Meat thickness conservation).

Burnup (%)	Al	^{135}Xe	^{149}Sm	^{235}U	^{236}U	^{238}U
0						
5	5.7013-02	1.6298-08	1.4017-07	1.5370-03	1.3755-05	1.1977-04
10	5.7013-02	1.5554-08	1.4150-07	1.4560-03	2.7405-05	1.1929-04
15	5.7013-02	1.4796-08	1.4125-07	1.3751-03	4.0918-05	1.1880-04
20	5.7013-02	1.4028-08	1.4014-07	1.2941-03	5.4290-05	1.1831-04
25	5.7013-02	1.3248-08	1.3822-07	1.2132-03	6.7533-05	1.1780-04
30	5.7013-02	1.2456-08	1.3552-07	1.1322-03	8.0646-05	1.1729-04
35	5.7013-02	1.1653-08	1.3209-07	1.0512-03	9.3604-05	1.1676-04
40	5.7013-02	1.0839-08	1.2797-07	9.7032-04	1.0641-04	1.1622-04
45	5.7013-02	1.0012-08	1.2317-07	8.8949-04	1.1905-04	1.1567-04
50	5.7013-02	9.1745-09	1.1775-07	8.0873-04	1.3152-04	1.1510-04

Burnup (%)	^{239}Pu	^{240}Pu	^{241}Pu	^{242}Pu
0				
5	4.3802-07	8.3692-09	3.6284-10	3.1390-12
10	8.3181-07	3.1902-08	2.7628-09	5.0242-11
15	1.1807-06	6.8151-08	8.8390-09	2.5424-10
20	1.4860-06	1.1484-07	1.9778-08	8.0138-10
25	1.7495-06	1.6996-07	3.6358-08	1.9501-09
30	1.9724-06	2.3162-07	5.8952-08	4.0299-09
35	2.1557-06	2.9801-07	8.7518-08	7.4366-09
40	2.3006-06	3.6759-07	1.2171-07	1.2643-08
45	2.4082-06	4.3889-07	1.6084-07	2.0202-08
50	2.4793-06	5.1054-07	2.0390-07	3.0756-08

TABLE III: Atom Densities in 20% Enriched Fuel Meat vs ^{235}U Burnup
Atom Densities (cm^{-3} x 10^{24}). (Pitch conservation).

Burnup(%)	Al	^{135}Xe	^{149}Sm	^{235}U	^{236}U	^{238}U
0	3.8177-02	0.0	0.0	2.2539-03	0.0	8.9016-03
5	3.8177-02	2.2146-08	2.0380-07	2.1412-03	1.9932-05	8.8872-03
10	3.8177-02	2.1415-08	2.0983-07	2.0286-03	3.9690-05	8.8729-03
15	3.8177-02	2.0643-08	2.1289-07	1.9158-03	5.9253-05	8.8582-03
20	3.8177-02	1.9837-08	2.1434-07	1.8031-03	7.8576-05	8.8430-03
25	3.8177-02	1.8999-08	2.1424-07	1.6904-03	9.7683-05	8.8272-03
30	3.8177-02	1.8113-08	2.1268-07	1.5777-03	1.1655-04	8.8109-03
35	3.8177-02	1.7208-08	2.0970-07	1.4650-03	1.3519-04	8.7939-03
40	3.8177-02	1.6270-08	2.0538-07	1.3523-03	1.5358-04	8.7762-03
45	3.8177-02	1.5298-08	1.9977-07	1.2396-03	1.7170-04	8.7577-03
50	3.8177-02	1.4276-08	1.9290-07	1.1270-03	1.8953-04	8.7382-03

Burnup (%)	^{239}Pu	^{240}Pu	^{241}Pu	^{242}Pu
0	0.0	0.0	0.0	0.0
5	1.2153-05	2.5179-07	1.3570-08	1.2152-10
10	2.3173-05	9.5224-07	1.0321-07	1.9461-09
15	3.3067-05	2.0205-06	3.2904-07	9.8268-09
20	4.1854-05	3.3816-06	7.3116-07	3.0777-08
25	4.9587-05	4.9748-06	1.3330-06	7.4305-08
30	5.6293-05	6.7463-06	2.1418-06	1.5219-07
35	6.2008-05	8.6513-06	3.1521-06	2.7845-07
40	6.6756-05	1.0650-05	4.3464-06	4.6935-07
45	7.0559-05	1.2708-05	5.6966-06	7.4325-07
50	7.3439-05	1.4793-05	7.1669-06	1.1214-06

TABLE III': Atom Densities in 20% Enriched Fuel Meat Vs ^{235}U Burnup.
Atom Densities ($cm^{-3} \times 10^{24}$) (Meat thickness conservation).

Burnup (%)	Al	^{135}Xe	^{149}Sm	^{235}U	^{236}U	^{238}U
0						
5	3.8177-02	2.2118-08	2.0338-07	2.1411-03	1.9936-05	8.8877-03
10	3.8177-02	2.1382-08	2.0929-07	2.0283-03	3.9701-05	8.8737-03
15	3.8177-02	2.0603-08	2.1225-07	1.9154-03	5.9276-05	8.8593-03
20	3.8177-02	1.9792-08	2.1361-07	1.8026-03	7.8614-05	8.8443-03
25	3.8177-02	1.8948-08	2.1342-07	1.6896-03	9.7741-05	8.8289-03
30	3.8177-02	1.8057-08	2.1177-07	1.5767-03	1.1663-04	8.8129-03
35	3.8177-02	1.7147-08	2.0872-07	1.4637-03	1.3530-04	8.7962-03
40	3.8177-02	1.6204-08	2.0433-07	1.3507-03	1.5373-04	8.7788-03
45	3.8177-02	1.5226-08	1.9864-07	1.2377-03	1.7189-04	8.7606-03
50	3.8177-02	1.4199-08	1.9171-07	1.1248-03	1.8976-04	8.7415-03

Burnup (%)	^{239}Pu	^{240}Pu	^{241}Pu	^{242}Pu
0				
5	1.1899-05	2.4643-07	1.3280-08	1.1898-10
10	2.2689-05	9.3212-07	1.0102-07	1.9060-09
15	3.2376-05	1.9782-06	3.2205-07	9.6273-09
20	4.0980-05	3.3115-06	7.1564-07	3.0160-08
25	4.8549-05	4.8730-06	1.3047-06	7.2838-08
30	5.5113-05	6.6101-06	2.0962-06	1.4922-07
35	6.0703-05	8.4791-06	3.0849-06	2.7311-07
40	6.5344-05	1.0442-05	4.2536-06	4.6049-07
45	6.9058-05	1.2463-05	5.5745-06	7.2949-07
50	7.1865-05	1.4513-05	7.0127-06	1.1011-06

TABLE IV: WIMS K_∞ vs. ^{235}U Burnup for 93% and 20% Enrichments. (Pitch conservation).

	Enrichment	
Burnup (%)	93%	20%
0	1.74221	1.65257
5	1.64377	1.56348
10	1.62233	1.54330
15	1.60020	1.52226
20	1.57691	1.50026
25	1.55212	1.47710
30	1.52541	1.45276
35	1.49643	1.42701
40	1.46476	1.39954
45	1.42983	1.37008
50	1.39089	1.33820

TABLE V: Values of Keff from X - Y Diffusion Theory Calculations. (Pitch conservation).

Enrichment	Description	Keff
93%	BOL Benchmark	1.03765
93%	EOL Benchmark	1.01425
93%	Fresh Fuel in All Fuel Regions	1.20018
20%	BOL Benchmark	1.03316
20%	EOL Benchmark	1.01300
20%	Fresh Fuel in All Fuel Regions	1.18150

TABLE IV': WIMS k_∞ vs. ^{235}U Burnup For 93% and 20 % Enrichments
Enrichment (Meat thickness conservation).

Burnup (%)	93%	20%
0		
5	1.64231	1.56537
10	1.62085	1.54515
15	1.59870	1.52409
20	1.57540	1.50205
25	1.55058	1.47884
30	1.52384	1.45446
35	1.49480	1.42861
40	1.46313	1.40101
45	1.42817	1.37137
50	1.38916	1.33926

TABLE V': Values of k_{eff} from X-Y Difussion theory Calculations.

Enrichment	Description	k_{eff}
93%	BOL Benchmark	1.03620
93%	EOL Benchmark	1.01278
93%	Fresh fuel in all fuel regions	
20%	BOL Benchmark	1.03334
20%	EOL Benchmark	1.01348
20%	Fresh fuel in all fuel regions	

TABLE VI: Fluxes from the DIF2D Problems (n/cm^2 sec). (Pitch conservation).

	Core Average Fluxes				Flux Trap Average	Flux Trap Center Ave.	Flux Trap Center Midplane
Case	ϕ_1	ϕ_2	ϕ_f	ϕ_{th}	ϕ_{th}	ϕ_{th}	ϕ_{th}
93% BOL	1.1403+14	5.2846+13	1.6688+14	5.9785+13	1.9813+14	2.5734+14	3.3743+14
93% EOL	1.1655+14	5.4041+13	1.7059+14	6.3787+13	2.0507+14	2.6409+14	3.4627+14
20% BOL	1.1332+14	5.0669+13	1.6399+14	4.1533+13	1.7220+14	2.3668+14	3.1033+14
20% EOL	1.1550+14	5.1662+13	1.6716+14	4.3701+13	1.7691+14	2.4156+14	3.1673+14

FIG. 1: IAEA 10 Mw. BENCHMARK 93% U-235 BOL
FLUXES AT MIDPLANE ALONG X - AXIS.

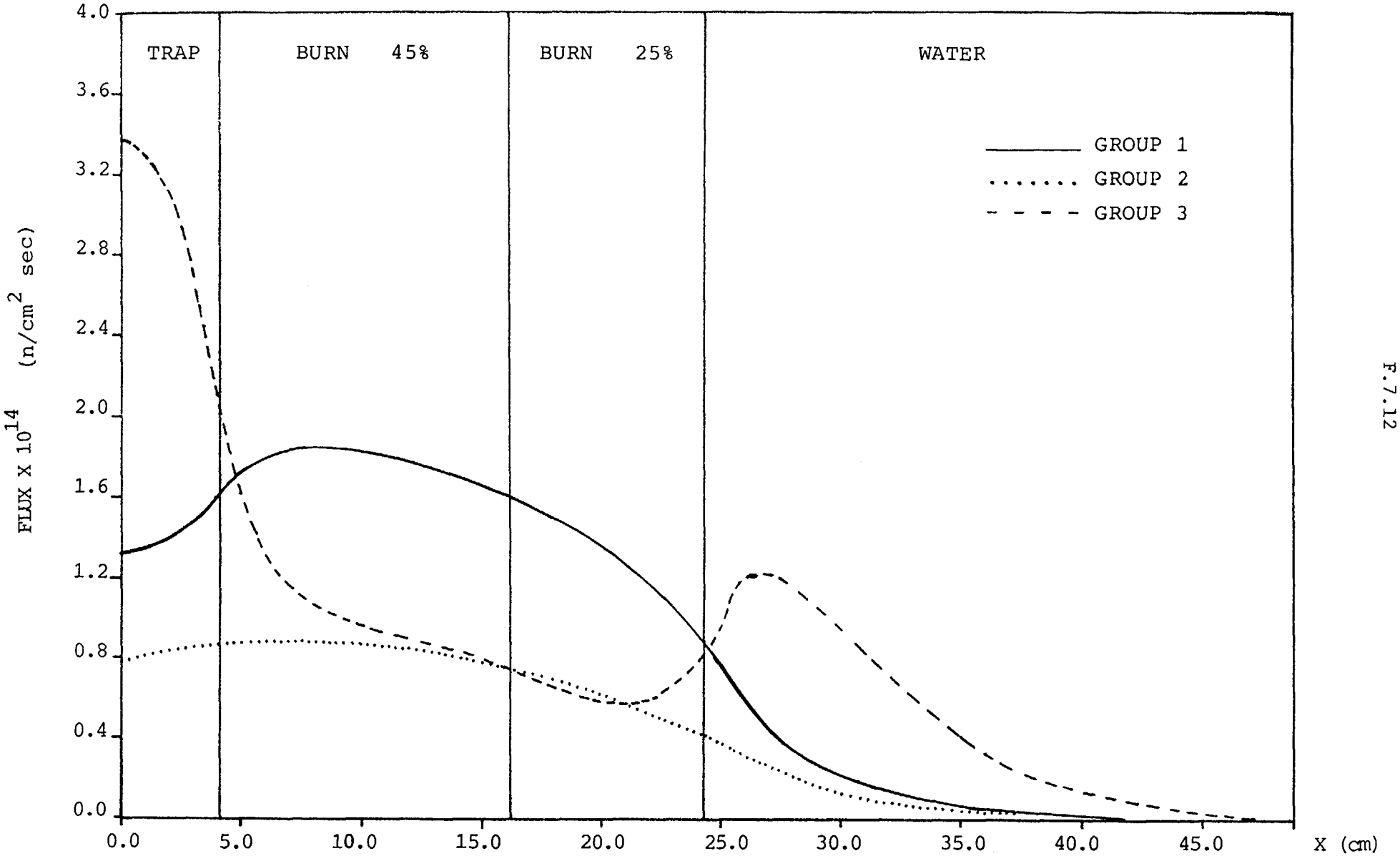

FIG. 2: IAEA 10 Mw BENCHMARK 93% U-235 BOL
FLUXES AT MIDPLANE ALONG Y - AXIS

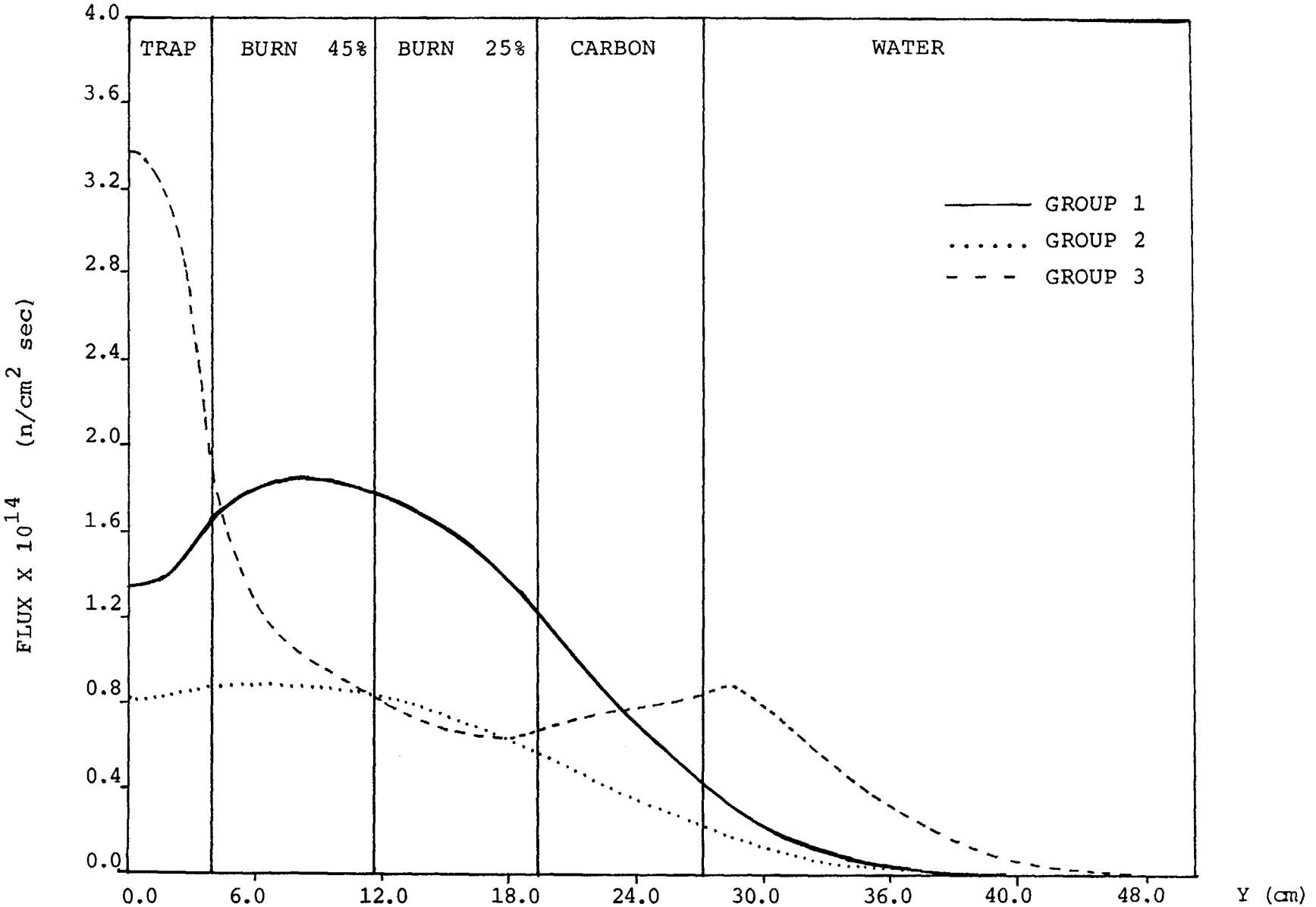

FIG. 3: IAEA 10 Mw BENCHMARK 93% U-235 EOL
FLUXES AT MIDPLANE ALONG X-AXIS.

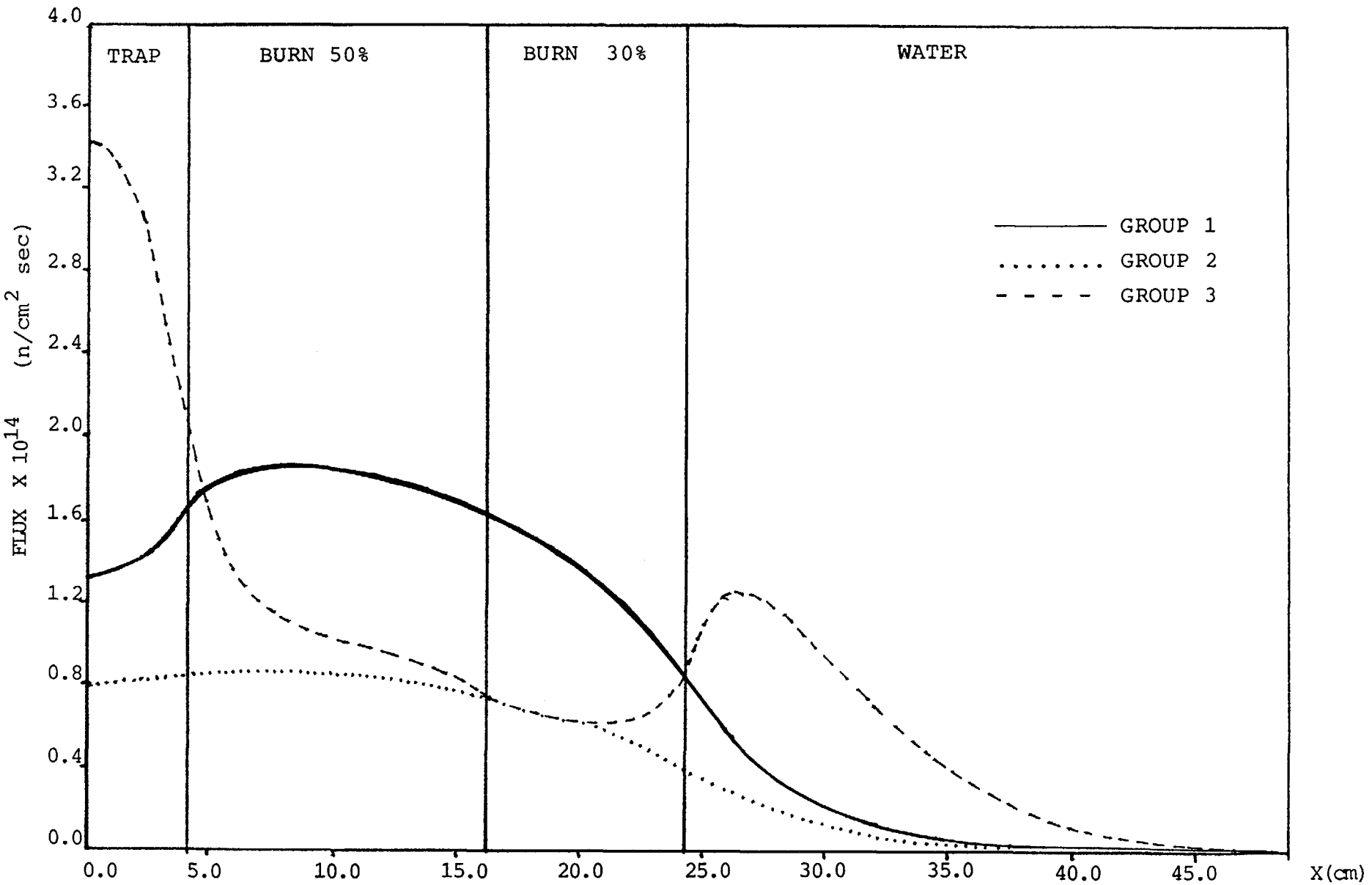

FIG. 4: IAEA BENCHMARK 93% U-235 EOL
FLUXES AT MIDPLANE ALONG Y-AXIS

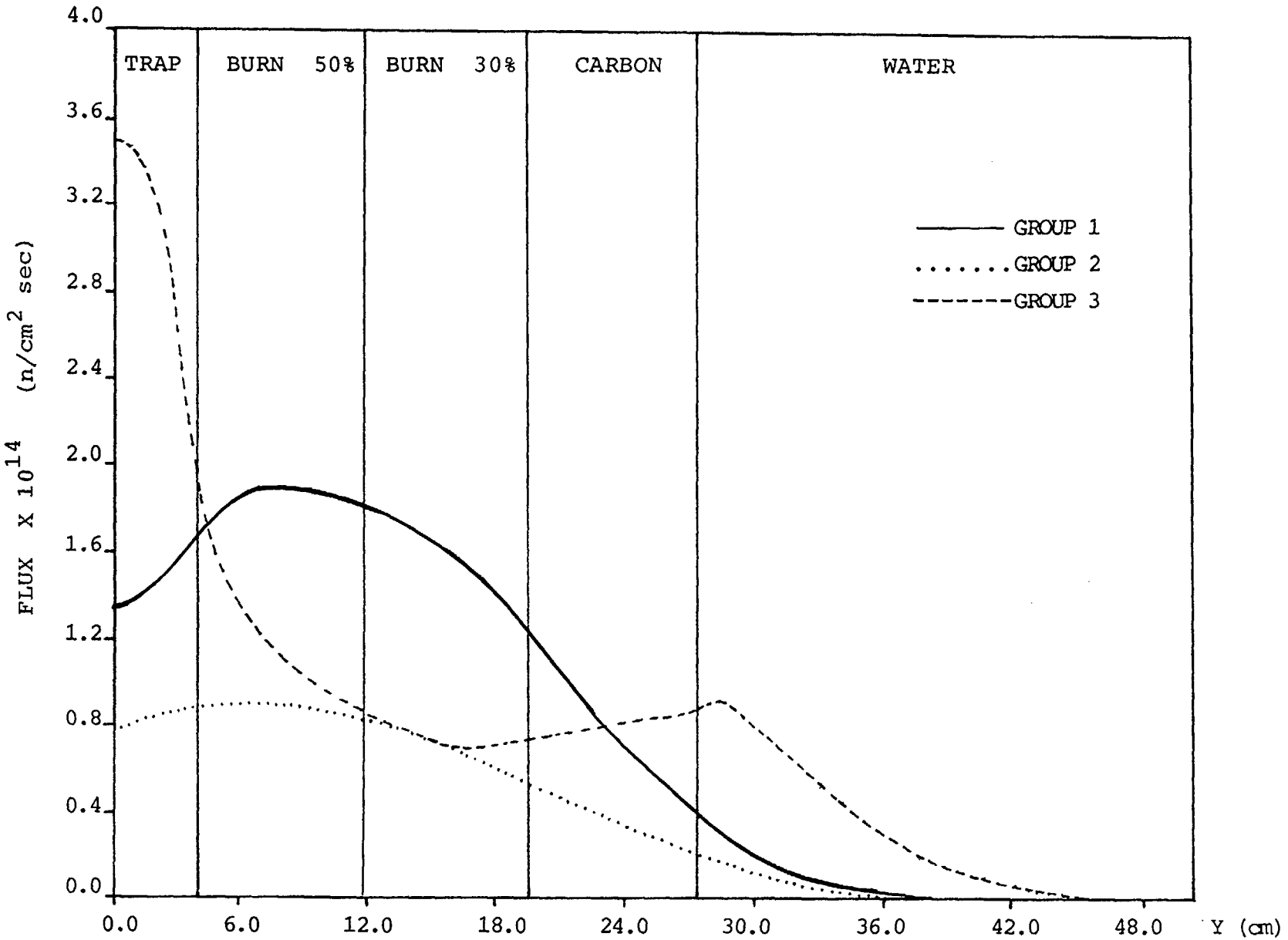

FIG. 5: FLUX RATIOS FOR 20% U-235 / 95% U-235 BOL
MIDPLANE ALONG X-AXIS.

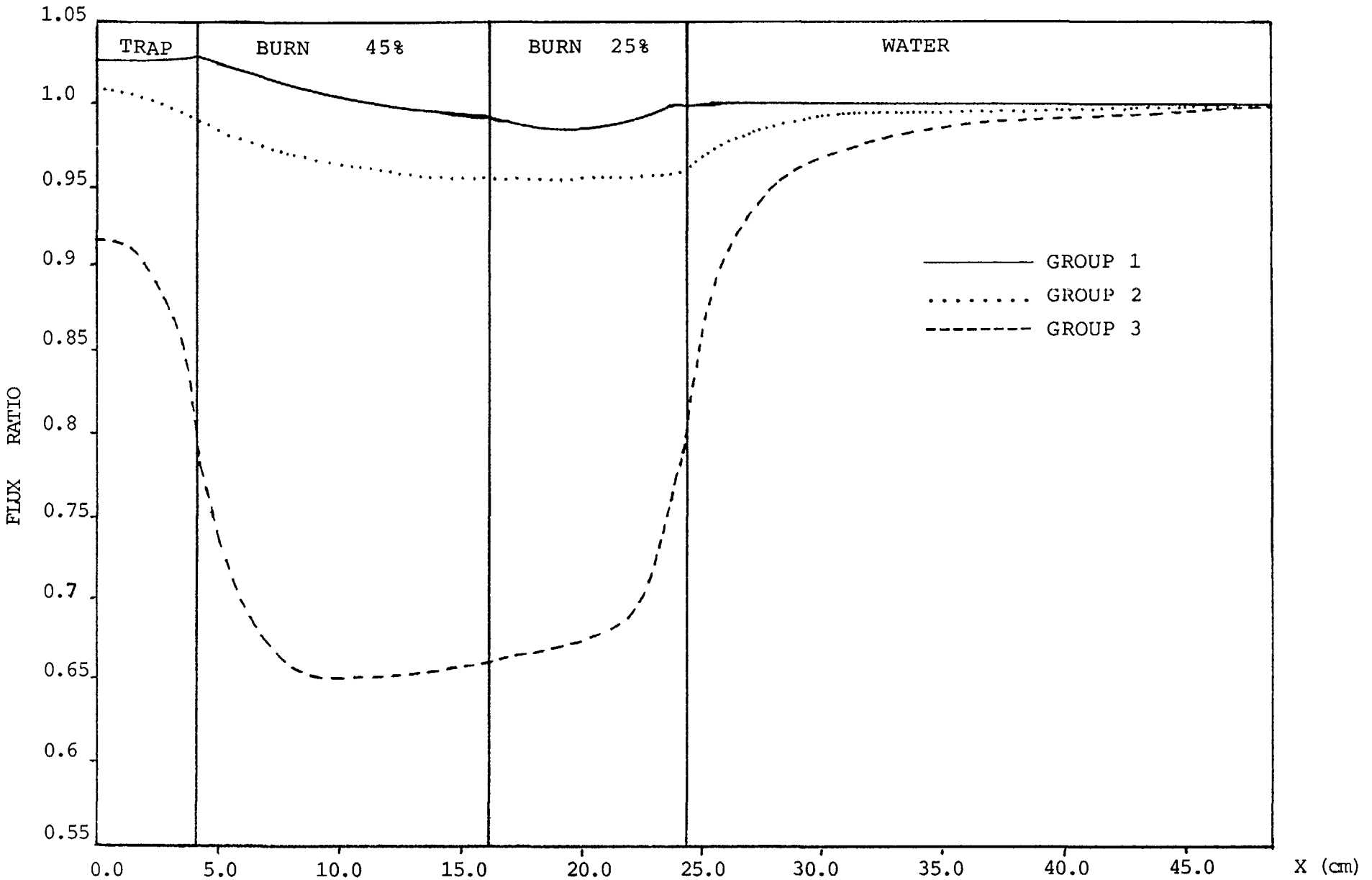

FIG. 6: FLUX RATIOS FOR 20% U-235 / 93% U-235 BOL MIDPLANE ALONG Y-AXIS.

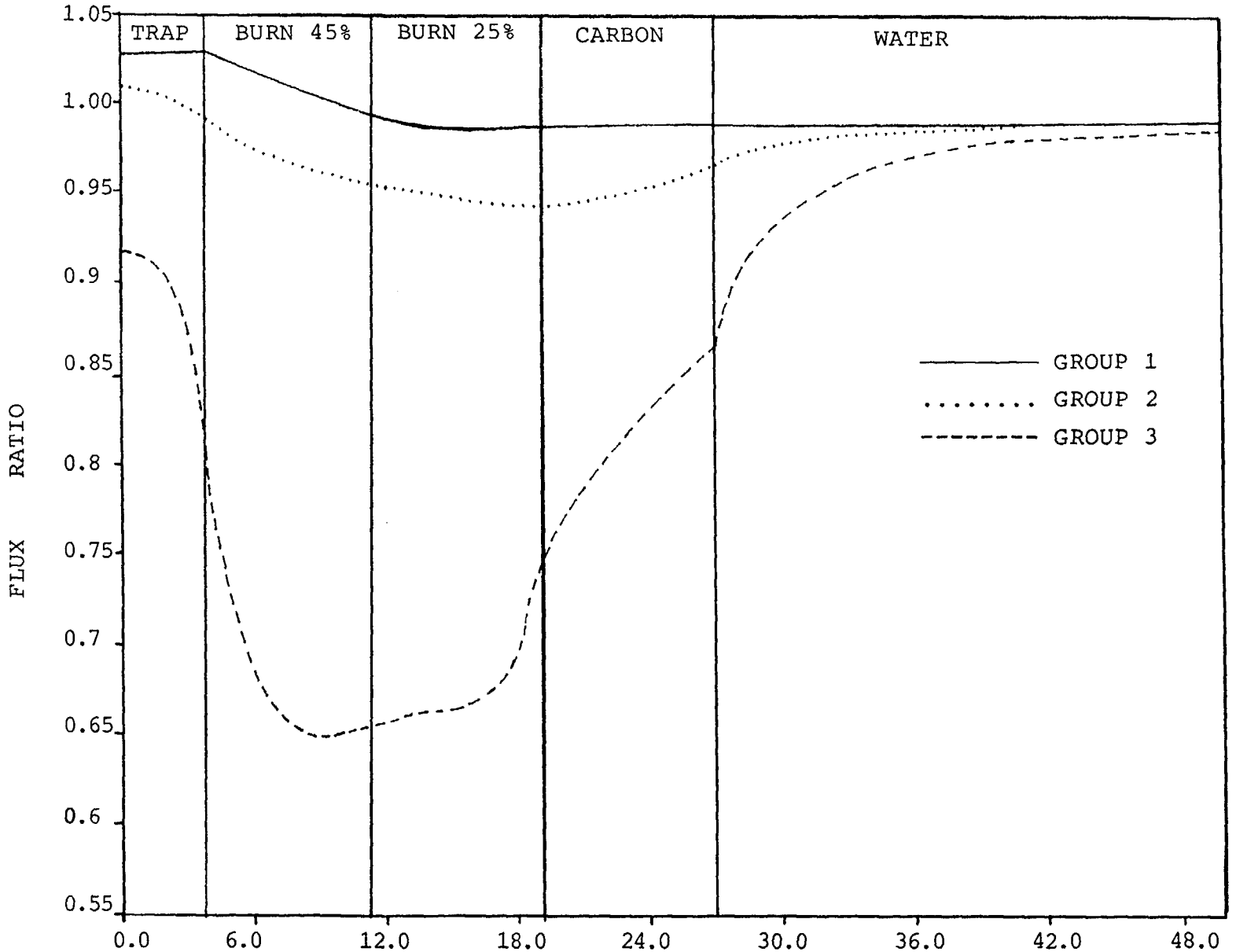

FIG. 7: FLUX RATIOS FOR 20% U-235 / 93% U-235 EOL
MIDPLANE ALONG X-AXIS.

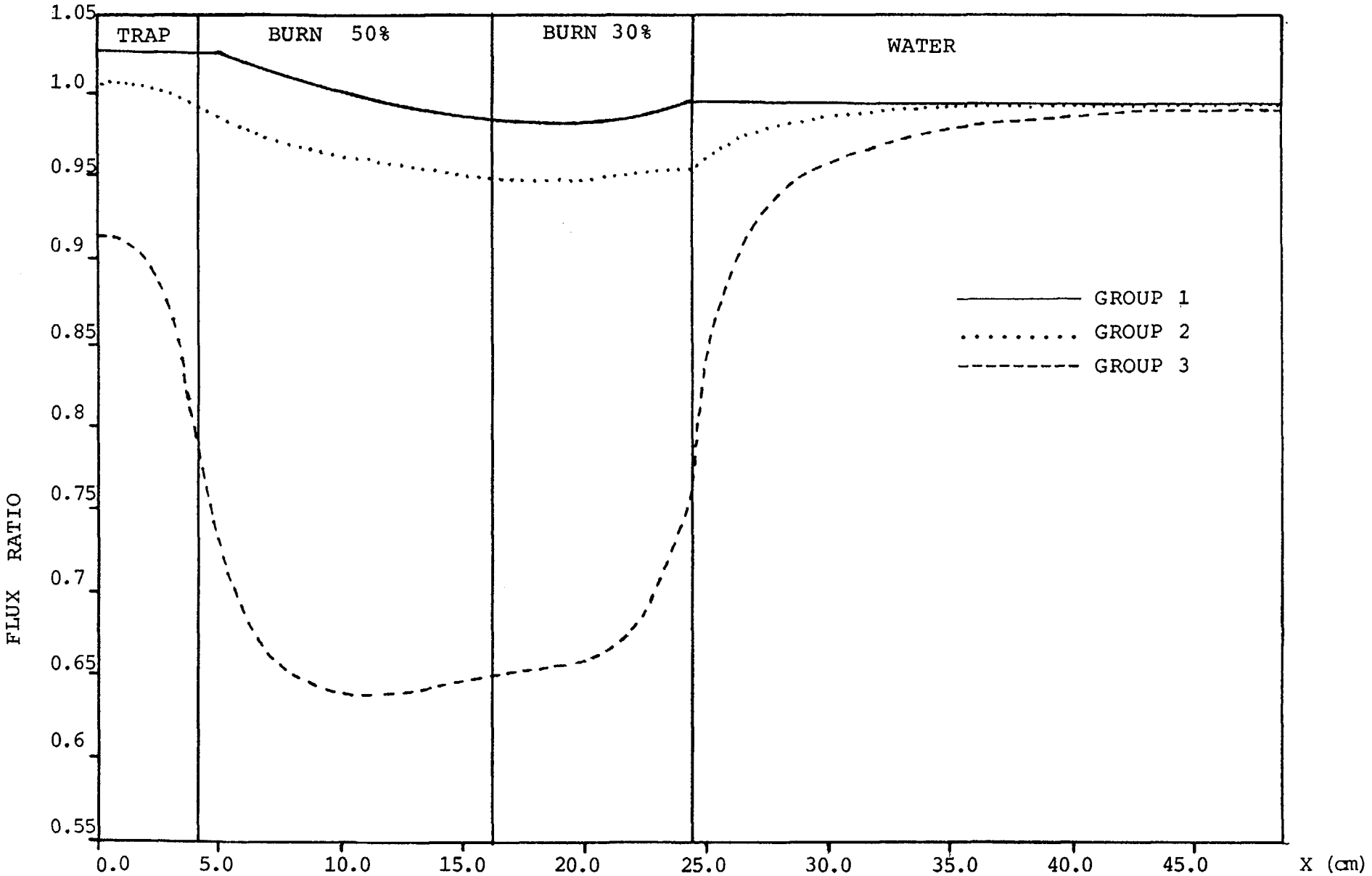

FIG. 8: FLUX RATIOS FOR 20% U-235 / 93% U-235 EOL FOR MIDPLANE ALONG Y-AXIS.

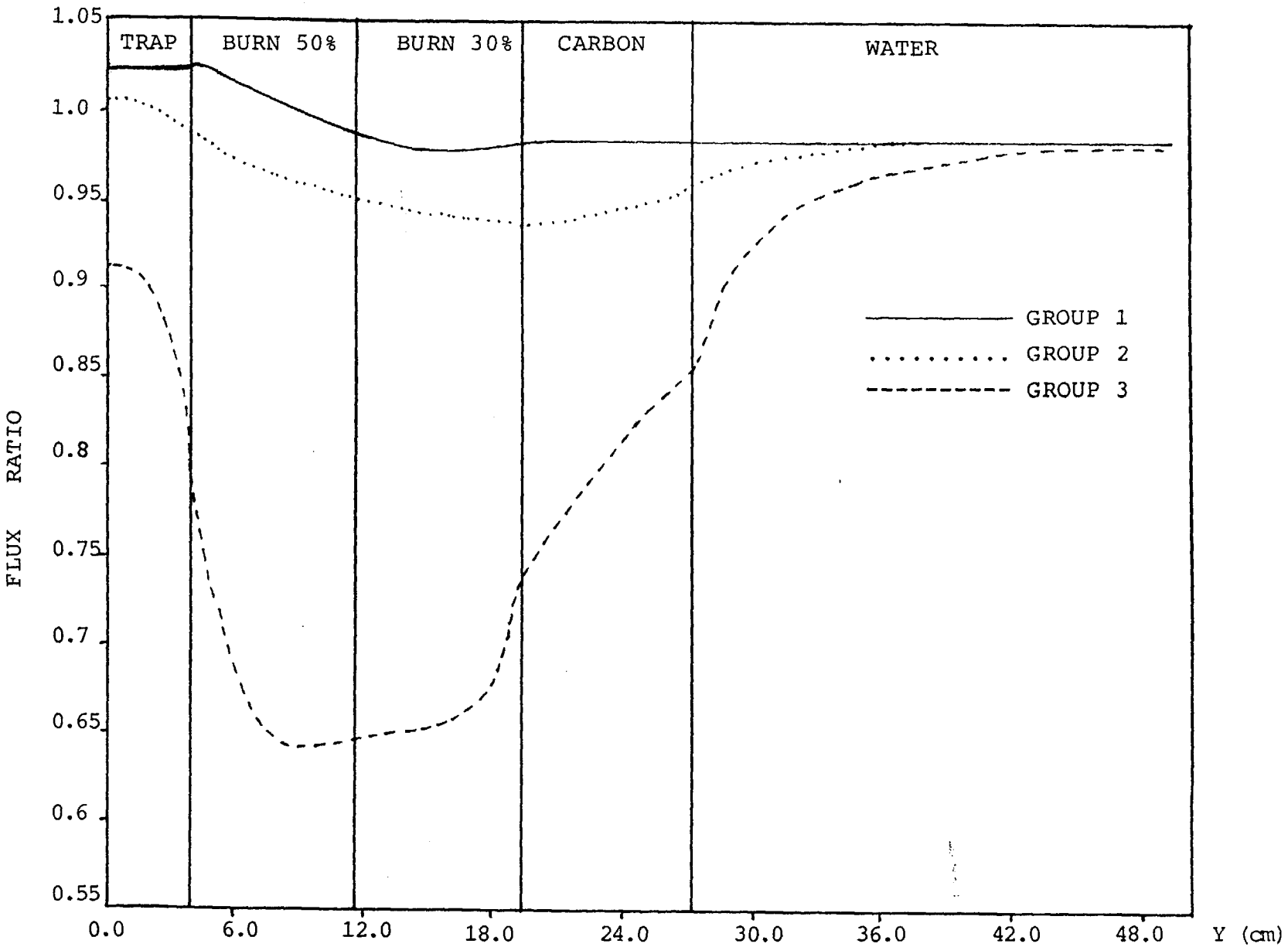

FIGURE 9: SLAB GEOMETRY USED IN WIMS

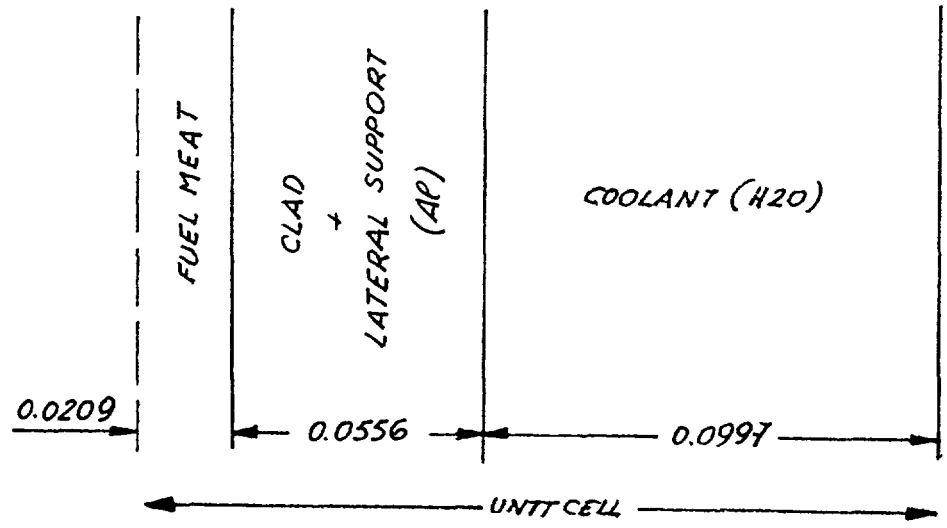

1) WITH PITCH CONSERVATION

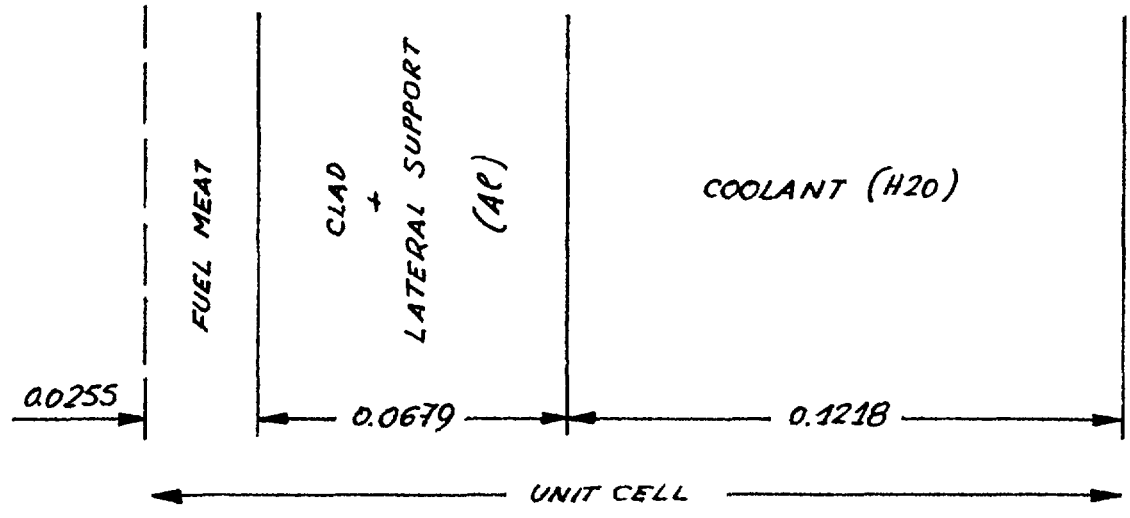

2) WITH MEAT THICKNESS CONSERVATION

APPENDIX G

Typical Research Reactor Data Needed for Enrichment Reduction Conversion Studies

Provided by

Österreichische Studiengesellschaft
für Atomenergie, GmbH
Research Reactor Seibersdorf
Austria

ABSTRACT

Typical data needed for a core conversion study are shown for the ASTRA reactor as an example. Using a questionnaire, data are provided on the reactor in general, and on its fuel, fuel cycle, thermal-hydraulics, neutronics, operating experience, safeguards, modifications, experimental facilities and utilization.

OPERATING REACTORS
RESEARCH, TRAINING, AND TEST REACTOR DIRECTORY
QUESTIONNAIRE

1. GENERAL

1.1	Reactor Name (Acronym)	ASTRA
1.2	License Number	
1.3	Docket Number	
1.4	Reactor Address	Research Center Seibersdorf 2444 Seibersdorf
1.5	Reactor Telephone	02254/80-2350
1.6	Reactor Telex	
1.7	Reactor Owner	Österr. Studiengesellschaft für Atomenergie, Ges.m.b.H.
1.8	Reactor Operator	Austrian Atomic Energy Research Organisation Ltd.
1.9	Reactor Administrators	Reactor owner
1.10	Reactor Facility Staff	
	a. Scientific/Technical	10/20
	b. Operations	18
	c. Support	∿10
	d. Normal Number of Personnel in Reactor Containment/ Confinement	5 - 10
1.11	Operations Staff Annual Salary Range	
	a. Chief Reactor Operator (Operations Supervisor)	
	b. Shift Supervisor	

	c. Senior Reactor Operator	
	d. Reactor Operator	
1.12	Reactor Architect/ Engineer	
1.13	Reactor Constructor	AMF (American Machine and Foundry Corp.)
1.14	Organization/Country Supplying Nuclear Technology	USA
1.15	Reactor Setting	
1.16	Reactor Operating Status	
	a. Initial Criticality Date	Sept. 24, 1960
	b. Full Power Date	May 1962
	c. Operating Cycle	5 days/week
	d. Full Power Hours/Year	2600 - 2800 hours/year
	e. Pulses/Year, Average Energy	
1.17	Reactor Facility Cost	US $ 3.50 Millions (basis 1960)
1.18	Annual Operating Budget	US $ 1.35 Million/year incl. overhead charges and costs for energy, wastewater treatment and environmental monitoring
1.19	Facility Insurance	
	a. Coverage	
	b. Annual Premium	

2. REACTOR

2.1	Reactor Type	Swimming Pool Pool-type reactor

2.2	Reactor Vessel		
	a.	Configuration	See attached drawing
	b.	Overall Dimensions	
	c.	Material	Aluminium liner
	d.	Normal Operating Pressure	atmospheric
	e.	Normal Operating Temperature	approx. $50^{o}C$
2.3	Core		
	a.	Volume	approx. 81 dm^3
	b.	Overall Dimensions	approx. 31 x 57 x 60 cm

c.	Lattice Configuration	rectangular 7.7 x 8.1 cm
d.	Number of Elements	
1.	Standard	18 El
2.	Control	4 El
e.	Maximum Number of Grid Locations that can be used for Fuel	6 x 9 positions
f.	Subdivided Core	
1.	Number of Subdivisions	-
2.	Subdivision Differentiating Characteristics	-
3.	Number of Elements per Subdivision	-
2.4	Containment	
a.	Type	Negative pressure, cylindrical
b.	Volume	approx. 10 000 m^3
c.	Material	reinforced concrete
2.5	Moderator	H_2O
2.6	Blanket Gas	
2.7	Reflectors	Metallic Be-Elements and H_2O
2.8	Thermal Shield	water, lead, 3.8 cm
2.9	Biological Shield	water, heavy concrete, 2 m
a.	External Radiation Levels	0.1 mr/h outside shielding 1 mr/h at top of reactor
2.10	Power Level	
a.	Normal Steady State	8 MW
b.	Pulsing	-

2.11	Normal Average Thermal Power Density	
	a. Volumetric (2.10.a/2.3.a)	100 kW/liter
	b. Linear (2.10.a/(Number of Plates/ Pins X Plate/ Pin Length))	8 000 kW/(23.18 + 17.4).60 cm = 276 W/cm
2.12	Normal Specific Power (2.10.a/2.3.f)	2 200 kW/kg U-235
2.13	Reactor Control	
	a. Safety Rods	
	1. Number	4
	2. Shape and Dimensions	fork type (double blade), blade similiar to fuel plate
	3. Material and Loading	Ag-In-Cd
	4. Normal Withdrawal/ Insertion Speed	6 cm/min
	5. Scram Insertion Speed	1.2m/sec.
	6. Total Reactivity	approx. 14 % Δk/k
	7. Normal Average Reactivity Addition Rate	$0.030\%^{\Delta k}/k$ per sec.
	8. Scram Mechanism	Dropping rods by de-energizing electro-magnets
	b. Regulating Rods	
	1. Number	Identical with Safety Rods
	2. Shape and Dimensions	
	3. Material and Loading	
	4. Normal Withdrawal/ Insertion Speed	
	5. Total Reactivity	
	6. Normal Average Reactivity Addition Rate	$0.01\%^{\Delta k}/k$ per sec.

c. Chemical Shim Control

1. Chemical — Not applicable
2. Loading
3. Control Mechanism
4. Total Reactivity

d. Burnable Poison

1. Isotopes Utilized
2. Location
3. Loading
4. Total Reactivity

3. FUEL

3.1 Standard Fuel Element

a. Configuration — MTR-type fuel elements (See attached figure)

b. Element Dimensions — 7.6 x 8.1 x 90 (150) cm

c. Overall Plate/Pin Dimensions — 7.075 x 0.127 x 62.5 cm

d. Number of Plates/Pins per Element — 23 plates/standard el., 17 plates/control

e. Distance between Plate/Pin Centerlines — 0.3 35 cm

f. Active Portion of Fuel Plate/Pin

1. Dimensions — 0.05 x 6.3 x 60 cm
2. Composition — Al/U
3. U-235 Enrichment — 93%
4. Fissile Material Density — 0.64 g/cm^3

g. Reflector Portion of Fuel Plate/ Pin

1. Composition

2. Dimensions

h. Clad

1. Composition: Al

2. Thickness: 0.038 cm

i. Side Plate

1. Composition

2. Thickness

j. Structural Material: Al

3.2 Control Rod Fuel Element

a. Specify Differences from Standard Fuel Elements: C-element is longer (providing guidance for control rod) and has 2 gaps (instead of 4 fuel plates) for insertion of absorber plates. Otherwise identical with standard element.

3.3 Fuel Cycle

a. Criteria for Refueling: reactivity balance

b. Frequency of Refueling: 5 - 6/year

c. Normal Element Lifetime: 3,5 years

d. Burnup

1. Average U-235 Burnup: 60%

2. Peak U-235 Burnup: ~75%

3. Maximum Allowed U-235 Burnup: -

e. Number of Elements Replaced During Typical Refueling: 1 element

f. Spent Fuel

1. Minimum Cooling Time: 3 months

2. Maximum Amount in Storage: 30 storage positions in reactor pool, additional storage capacity in separate storage pool in the hot cell building.

g. Disposition of Spent Fuel: Until 1974: reprocessing of spent fuel elements at Eurochemie/MOL/Belgium

h.	Spent Fuel Shipping Cask	2 Casks for 13 fuel elements each from Transnuclear/Hanau/FRG; 13 Tonnes/cask
i.	Spent Fuel Handling	loading in reactor pool.
j.	Fuel Failure Detection	Sipping of fuel elements in the reactor core during low power opeation

3.4 Fuel Inventory

a.	Current Fissile Material Inventory Status	
1.	New Fuel In-Process	
2.	New Fuel On Hand	1,734 kg U-235/1,863 kg U-total
3.	Fuel In-Core	3,68 kg U-235/4,62 kg U-total
4.	Spent Fuel In Storage	2,442 kg U-235/3,753 kg U-total
5.	Spent Fuel Being Reprocessed	-
6.	Non-fuel Special Nuclear Material	0,283 kg U-235/7,13 kg U-total
b.	Fissile Material Inventory Needed to Assure Continuity of Operations	
1.	New Fuel In-Process	∿2,0 kg U-235
2.	New Fuel On Hand	∿2,0 kg U-235
3.	Fuel In-Core	3,68 kg U-235 (irrad.), 5,75 kg U-235 in unirrad. fuel elements.

3.5 Fuel Source

a.	Fuel Fabricator	NUKEM Ges.m.b.H; Hanau/FRG, CERCA, S.A; Paris/France
b.	Fuel Supplier	USA; DOE

c.	Fissile Material Origin	USA
d.	Enrichment Supplier	USA
e.	Method of Fabrication	MTR-plates: U-Al-alloy as meat material
f.	Fuel Element Cost	US $ 4 000,-/element fabrications cost (including conversion and transport)

4. HEAT TRANSFER DATA

4.1	Fuel Element Heat Transfer Area (Number of Plates/Pins X Active Plate/Pin Surface in Contact with Coolant)	1.656 m^2 (Standard fuel element)
4.2	Fuel Element Flow Area	34.2 cm^2
4.3	Fuel Element Wetted Perimeter	331 cm
4.4	Fuel Meat Thermal Resistivity	
4.5	Clad-Coolant Heat Transfer Coefficient (at Hot Spot)	1,95 $W/cm^2\ ^oC$
4.6	Heat Flux at Plate Surface	
	a. Normal Average Heat Flux	23,5W/cm^2
	b. Peak Heat Flux	
	1. Without Hot Channel Factors	58,7 W/cm^2
	2. With Hot Channel Factors	
	c. Axial Peaking Factor in Hot Channel (from Axial Fission Rate Distribution)	
	1. Without Hot Channel Factors	1.4
	2. With Hot Channel Factors	
	d. Hot Spot Location	10 cm below horizontal centraline

4.7	Peak Operating Fuel Plate/Pin Temperature	
	a. At Plate/Pin Surface	
	1. Without Hot Channel Factors	85,4 °C
	2. With Hot Channel Factors	94°C
	b. Inside Fuel Meat	
	1. Without Hot Channel Factors	
	2. With Hot Channel Factors	
4.8	Primary Coolant	H_2O
4.9	Coolant Flow	
	a. Flow Direction	downward
	b. Flow Induced by	force of gravity
	c. Normal Flow Rate	230 l/min
	d. Maximum Flow Rate	230 l/min
	e. Mean Core Flow Velocity	2.7 m/sec.
	f. Normal Core Inlet Temperature	38°C
	g. Normal Core Temperature Rise (ΔT)	8°C
	h. Peak Coolant Temperature Rise (ΔT) at Hot Spot	
	1. Without Hot Channel Factors	16,3°C
	2. With Hot Channel Factors	19,7°C
	i. Coolant Pressure at Core Outlet (Absolute)	1,545 at
	j. Coolant Pressure at Hot Spot (Absolute)	
	1. Without Hot Channel Factors	1,64 at
	2. With Hot Channel Factors	

4.10	Hot Channel Factors (Including Only Effects Other than Nuclear Peaking; Specify Breakdowns)	
	a. For Coolant Temperature Rise	1.21
	b. For Film Temperature Rise	1.20
	c. Others	$T^{x}_{sat} = T_{sat} - 0,5^{o}C$ $(T_{boiling} - T_{sat})^{x} = 0.79\ (T_{boil} - T_{sat})$
4.11	Core Heat Dissipation System	Heat exchanger Cooling tower
4.12	Shutdown Heat Removal System	Reactor Pool
	a. Worst Case Elapsed Time from Shutdown to Coolant Independence Without Fuel Distortion	loss of forced coolant flow: 0,5 min total loss of coolant: ∿10 days
4.13	Emergency Core Cooling System	1. Automatic spray nozzle system 2. Additional manually operated spray nozzle system.

5. NUCLEAR DATA

5.1	Fuel Loading	
	a. Minimum Critical Mass	∿1.5 kg U-235
	b. Normal Core Loading (Beginning of Cycle at Rated Power)	3,68 kg U-235 (irrad. fuel)

c. Maximum K_{excess} components

1.	Temperature	0,22% Δk/k
2.	Equilibrium Xenon	3,2%
3.	Equilibrium Samarium	1,0%
4.	Xenon Override	
5.	Burnup (Including Burnable Poison)	1,8%
6.	Experimental Sample	0,5%
7.	Others	
8.	Total	6,7% Δk/k

d. Shutdown Margin — 7,3% Δk/k

5.2 Reactivity Coefficients

a. Temperature

1.	Moderator	
2.	Doppler	-0.011% Δk/k/°C
3.	Fuel Expansion	
4.	Burnable Poisons	

b. Void — -0,2% Δk/k/% void in moderator

5.3 Neutron Flux Densities

a.	Steady State Average Thermal	$6.0\ 10^{13}$ n/cm^2/sec.
b.	Steady State Peak Thermal	$1.1\ 10^{14}$ n/cm^2/sec.
c.	Steady State Average Fast	$9.1\ 10^{13}$ n/cm^2/sec.
d.	Steady State Peak Fast	$1.8\ 10^{14}$ n/cm^2/sec.
e.	Peak Pulsing Power	
f.	Pulse Integrated Power	

5.4 Pulsing Characteristics

a.	Pulse Period	
b.	Full Width at Half Maximum	-

	c. Maximum Frequency of Pulses	-
5.5	Fission Density	
	a. Normal Average	2.4 10^{13} fissions/cm^3/sec.
	b. Peak	5.0 10^{13} fissions/cm^3/sec.
	c. Axial Peak/Average Ratio for Typical Element	1.4
5.6	Maximum Fission Product Inventory	$\sim 10^8$ Ci

6. OPERATING EXPERIENCE

6.1	Forced Outages in the Past Five Years	
	a. Equipment Malfunction	
	b. Personnel Error	
	c. Full Power Operating Hours	

7. SAFEGUARDS

7.1	Agency Responsible for Regulatory Jurisdiction	IAEA

8. PAST MODIFICATIONS AND FUTURE PLANS

8.1	Past Major Modifications	
	a. Power Increase	5 → 8 MW; fork type absorber plates,
	b. Fuel Conversion	16 → 23 plate type fuel elements
	c. Other	Be - refl. elements
	d. Date	1969
8.2	Future Major Modifications	
	a. Power Increase	

b. Fuel Conversion _____

c. Decommissioning _____

d. Other _____

e. Date _____

8.3 Future Reactors

a. Type _____

b. Date _____

9.1 REACTOR, LABORATORY, AND EXPERIMENTAL FACILITIES

Irradiation Facilities	Description	Dimensions	Neutron flux (n/cm^2/sec) Thermal	Neutron flux (n/cm^2/sec) Fast	Gamma flux (rad/hr)
Beamports	see attached figure		2.10^{13}		
Converter Blocks					
Irradiation Racks					
Pneumatic Tubes	2	2.10^{13}			
Neutron Source					
Reactor Core	14 irrad. channels		3.10^{13}-10^{14}	2.10^{13}-8.10^{13}	2 - 5.10^{8}
Reactor Pool	1 seed irrad. facility		1.10^{8}	5.10^{8}	10^{3}
Thermal Column	1		5.10^{10}		

9.1 REACTOR, LABORATORY, AND EXPERIMENTAL FACILITIES (CONT'D)

Laboratory Facilities	Description
Accelerator	
Critical Assemblies	
Gamma Sources	one 20 kCi Gamma source (Co-60) several 1 Kci Gamma sources (Co-60)
Hot Cells	7 hot cells for 50 kCi Co-60)
Neutron Activation Analysis	several laboratories (biology, agriculture, chemistry physics, ASTRA) are fully equipped for neutron activation analysis.
Neutron Generator	1 Neutron Generator for 14 meV neutrons
Neutron Radiograph	
Neutron Spectrometer	two three-axis-neutron spectrometers one position sensitive diffractometer
Radioisotope Laboratories	Molybdenum-Technecium laboratory Ir-192 production in the Hot Cells

10. RESEARCH AND TECHNICAL PROGRAM AND REACTOR UTILIZATION SUMMARY

10.1 Research, Technical, and Training Program

Investigation of condensed matter by neutron spectrometry

1) Solidstate physics (collaboration with ILL, Grenoble, Saclay, Paris, Harwell)

a) Phase transitions: mechanism of the NaCl - CsCl lattice transition of RbJ

b) Structure of hydrogen loaded metals e.g. Nb, La...

c) Texture measurements for materials science.

d) Anharmonicity of interaction potentials via phonon frequency shifts under pressure.

e) Related theory.

2) Liquid state:

a) Structure determinations of metals with high melting temperature: Al, Cu, Ni over temperature ranges.

b) Investigation of the dynamics of liquid metals (Al)

c) Related theory...

3) Development of apparatus for above research program:

a) Neutron diffractometers with position sensitive detectors.

b) High temperature and high pressure equipment.

c) Electronics and software for control of spectrometers and goniometers.

Nuclear physics

a) Investigation of weak interaction forces via free neutron decay.

b) Development of related equipment (high vacuum pumps, ion sources),

Training. Research program is carried out by scientists and Ph-D students

10.2 Principal Isotopes Produced

Mo-99-Tc-99 m : 500 Ci/year for nuclear medicine

Tc-99 m labelled pharmaceuticals

Na-24, K-42, Cu-64, F-18 for medical use (in vitro diagnosis)

Y-90 for therapeutical use

Ir-192. 5000 Ci/year sealed sources for radiography

Co-60: 1 Ci/year sealed sources for industrial use

11. COMPUTER CODES UTILIZED IN DESIGN

11.1 Neutronics

11.2 Structural Design

a. Reactor Vessel

b. Fuel

c. Containment

11.3 Heat Transfer

12. FACILITY DESIGN AND OPERATION REFERENCE DOCUMENTS

ASTRA Reactor Safety Report

Directory of Nuclear Reactors, Vol. VI,

Research, Test and Experimental Reactors

IAEA, Vienna, 1966, ST1/PUB 125

(AUSTRIA) **ASTRA**

ADAPTED SWIMMING POOL TYPE REACTOR AUSTRIA

PURPOSE: Research

DATE OF INFORMATION: August 1976

GENERAL

1. Reactor type	Pool type, fully enriched (>90%) uranium, light water moderated and cooled, graphite and water reflected	5. Owner and operator	Oesterreichische Studiengesellschaft fuer Atomenergie
2. Nominal reactor power	8 MW, convertible to 12 MW	6. Designer and builder	AMF Atomics, division of the American Machine and Foundry Co.
3. Purpose	Research in neutron physics, isotope production and engineering tests	7. Present status & construction schedule	In operation Start of construction Nov. 1958 Reactor critical Sep. 1960
4. Location	Seibersdorf, Niederoesterreich, Austria		

REACTOR PHYSICS

8. Neutron energy and lifetime	Thermal 0.031 eV Lifetime 5.3×10^{-5} sec	10. Neutron flux	Thermal av. 4.3×10^{13} n/cm² sec Thermal max. 1.1×10^{14} n/cm² sec Fast av. 9.1×10^{13} n/cm² sec Fast max. 1.8×10^{14} n/cm² sec
9. Core parameters	$\eta = 2.072$ $f = 0.852$ $k_{\infty} = 1.766$ $L^2(cm^2) = 2.834 \tau(cm^2) = 53.2$ $K_{eff} = 1.0$ $p = 1.0$ $\epsilon = 1.0$	11. Reactivity balance	Max. built in (cold, clean) 8.59% To compensate for temperature 0.22% Xe and Sm 4.17% burn-up 0.80% experiments 1.50% beam tubes 1.90%

CORE

12. Shape and dimensions	Parallelepiped approx. 31 × 60 cm, 63 cm high	18. Average power density in core	86 kW/liter
		19. Burnup	Average: 30% Maximum: 60%
13. No. of channels & subassemblies	Grid plate with 6 × 9 positions Initial operating core of 14 fuel elements	20. Fuel loading and unloading	Manual
14. Lattice	Rectangular 7.7 × 8.1 cm	21. Irradiated fuel storage	Storage racks for 30 fuel elements
15. Critical mass	3.20 kg 235U for water reflected core 2.285 kg 235U for water and graphite core 1.5 kg 235U for water and beryllium reflected core	22. Moderator	Demineralized light water in the pool
16. Core loading at rated power	3.6 kg 235U (average burn up: 30%)		
17. Average specific power in fuel	2200 kW/kg 235U	23. Blanket gas	None

FUEL ELEMENT

24. Form and composition	MTR type, curved plates Meat dimensions 0.05 × 6.2 × 60 cm	25. Cladding	0.38 mm aluminium inner plates 0.50 mm aluminium outer plates
		26. Subassemblies	23 plates per standard fuel element 17 plates per control rod element

CORE HEAT TRANSFER

27. Heat transfer area	$46.5 m^2$	32. Coolant mass flow rate	233 kg/sec
28. Heat flux	Av. 17.2 W/cm^2	33. Coolant pressures & temperatures	Inlet 37.8° C, atmospheric Outlet 45.0° C, atmospheric
29. Fuel element temperatures	Max. cladding 100° C	34. Hot channel factors	1.75 for temperature drop through film 1.46 for temperature rise in coolant
30. Heat transfer coefficient	0.24 cal/cm² sec deg C		
31. Coolant flow area & velocity	Total for 20 standard fuel elements 826.7 cm^2 Velocity 2.8 m/sec.	35. Shut-down heat removal	Safety flapper in plenum chamber below grid plate

CONTROL

36. Control, regulating and safety rods	4 shim safety rods Ag, In, Cd Total worth of rods approx. 20% $\frac{\Delta k}{k}$	38. Scram time & mechanism	Delay time 30 msec Rod travel time 0.5 sec Magnets gravity
		39. Sensitivity of auto. control	±0.5%
		40. Temperature coefficients	0.011% $\frac{k}{k}/^{\circ}C$
		41. Burnable poison	None
		42. Other control, safety & shut-down provisions	None
37. Reactivity addition rate	Max. 0.07% $\frac{\Delta k}{k}$ /sec		

REACTOR VESSEL & OVERALL DIMENSIONS

43. Form, material and dimensions	Concrete pool, inside approx. 2.60 × 2.85 m	44. Working, design & test pressures	Atmospheric
		45. Reactor with shielding	7.01 x 11.63 m, 11.20 m high

REFLECTOR AND SHIELDING

46. Reflector	Beryllium (metal) elements similar to fuel elements	48. Shielding	Sides: 1.0 m water, 3.8 cm lead, 2.0 m barytes concrete Bottom: 0.35 m concrete + earth Top: 7.8 m water
47. Radiation levels	0.1 mr/hr at core level outside shielding 1.0 mr/hr at top of reactor		

CONTAINMENT

49. Type and material	Concrete cylinder, 25 cm wall thickness, 26 m diam., 23.5 m high Inside pressure — 30 mm H_2O Leakage rate 20 m^3/min	50. Surroundings	Sparsely populated rural area, nearest village at 2 km with 346 inhabitants, nearest residences at 1 km distance

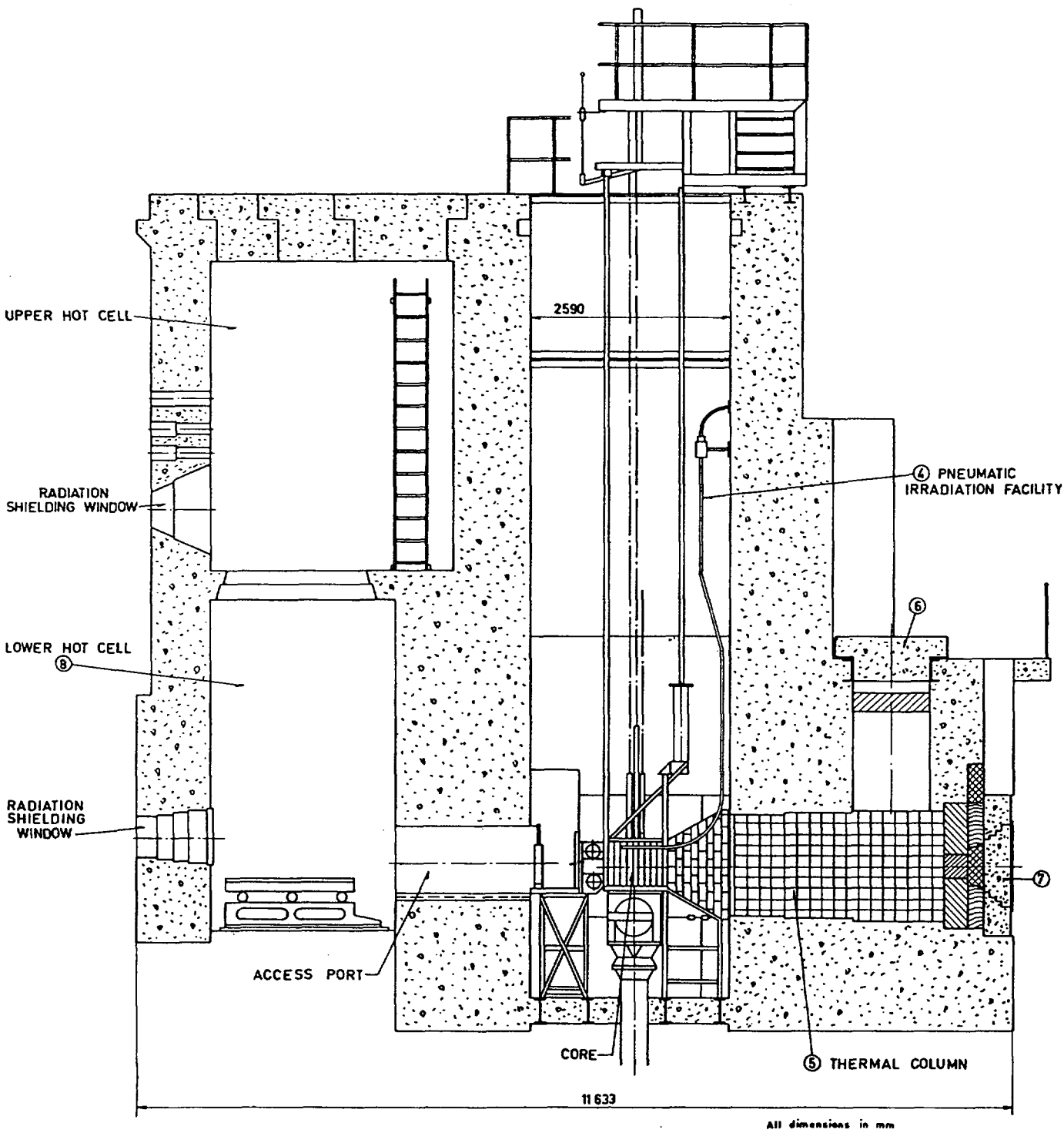

VERTICAL SECTION REACTOR ASTRA

RESEARCH FACILITIES

Designation	No.	Position	Useful dimensions (cm)	Neutron flux (n/cm²sec)	Remarks
Horizontal beam tubes reaching core	7	(1)	15 diam.	th. av. 2 10^{13} f. 10^{12}	
reaching reflector	1	(2)	30 × 30		
going through	2	(3)	15 diam.		
Isotope production holes			3.5 diam.	th. 10^{13} to 10^{14}	
in graphite reflector elements			5.2 diam. 6.0 diam.	f. 10^{12} to 3×10^{13}	
Pneumatic rabbits	2	(4)	5 diam.	th. 5×10^{12} to 3×10^{13}	
Hydraulic rabbits	1		5 diam.	f. 5×10^{11} to 3×10^{12}	
Thermal column	1	(5)	120 × 120	th. max. 10^{11}	
Vertical access to thermal column	1	(6)	100 diam.	th. max. 10^{11}	
Horizontal access to thermal column (rabbit system)	1	(7)	—	th. max. 4.10^{10}	
Engineering test facility	1		30 × 30	th. 2×10^{13} f. 4×10^{12}	
Seed Neutron Irradiation facility					10^{5} rad/hr

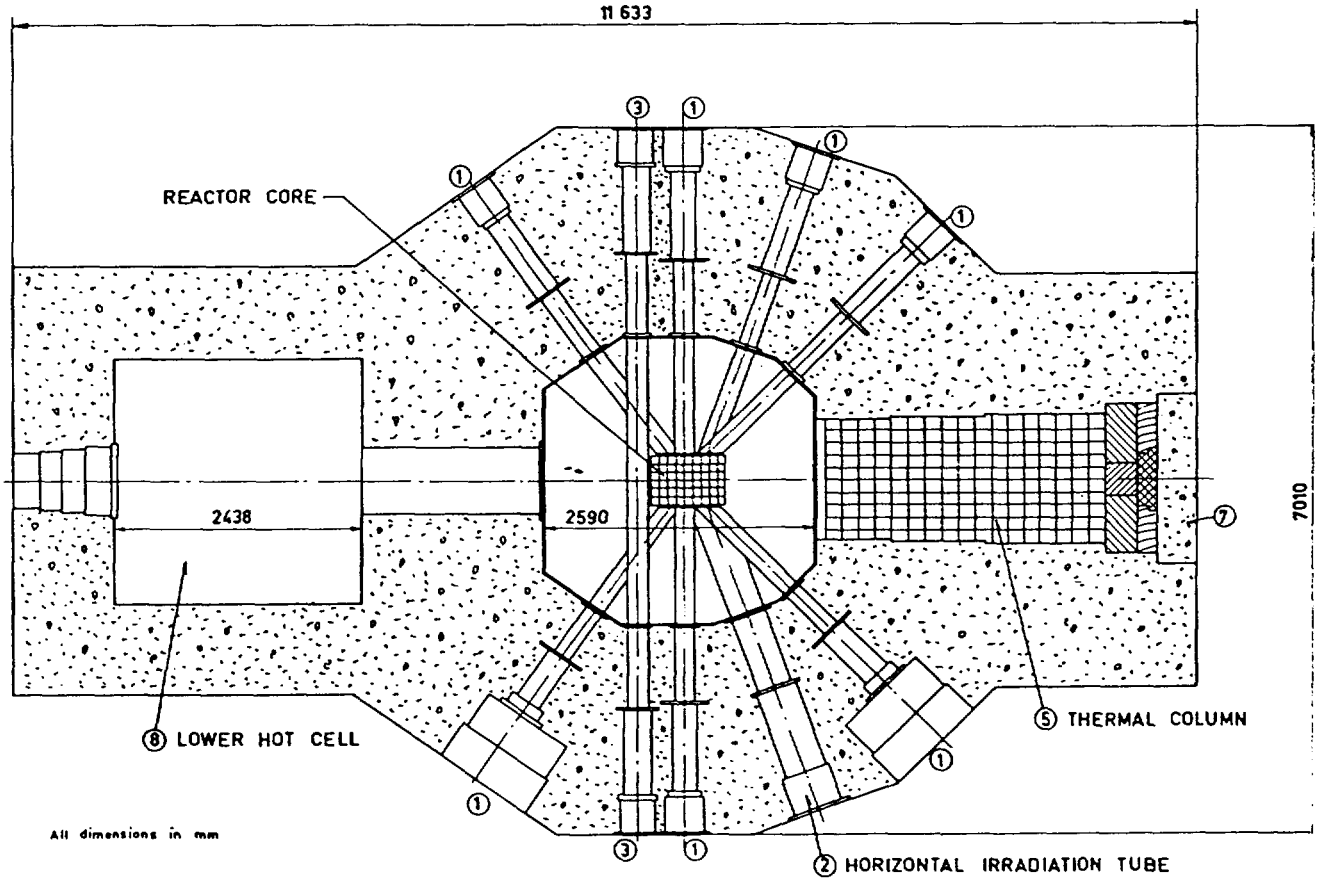

HORIZONTAL SECTION REACTOR ASTRA

RESEARCH CENTER
SEIBERSDORF
ASTRA REACTOR

Standard Brennelement

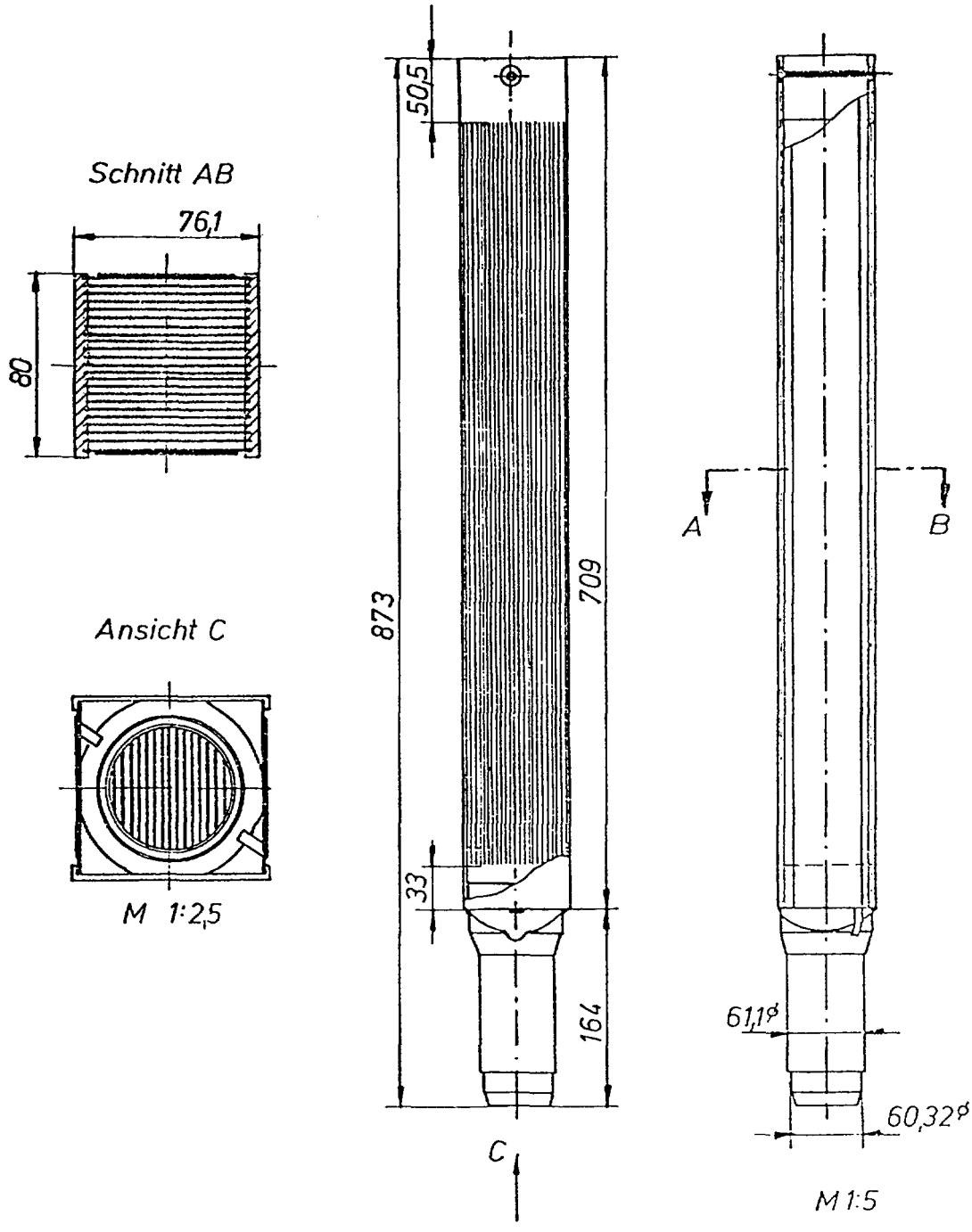

Abb. F- 1a

RESEARCH CENTER
SEIBERSDORF
ASTRA REACTOR

Partielles Element

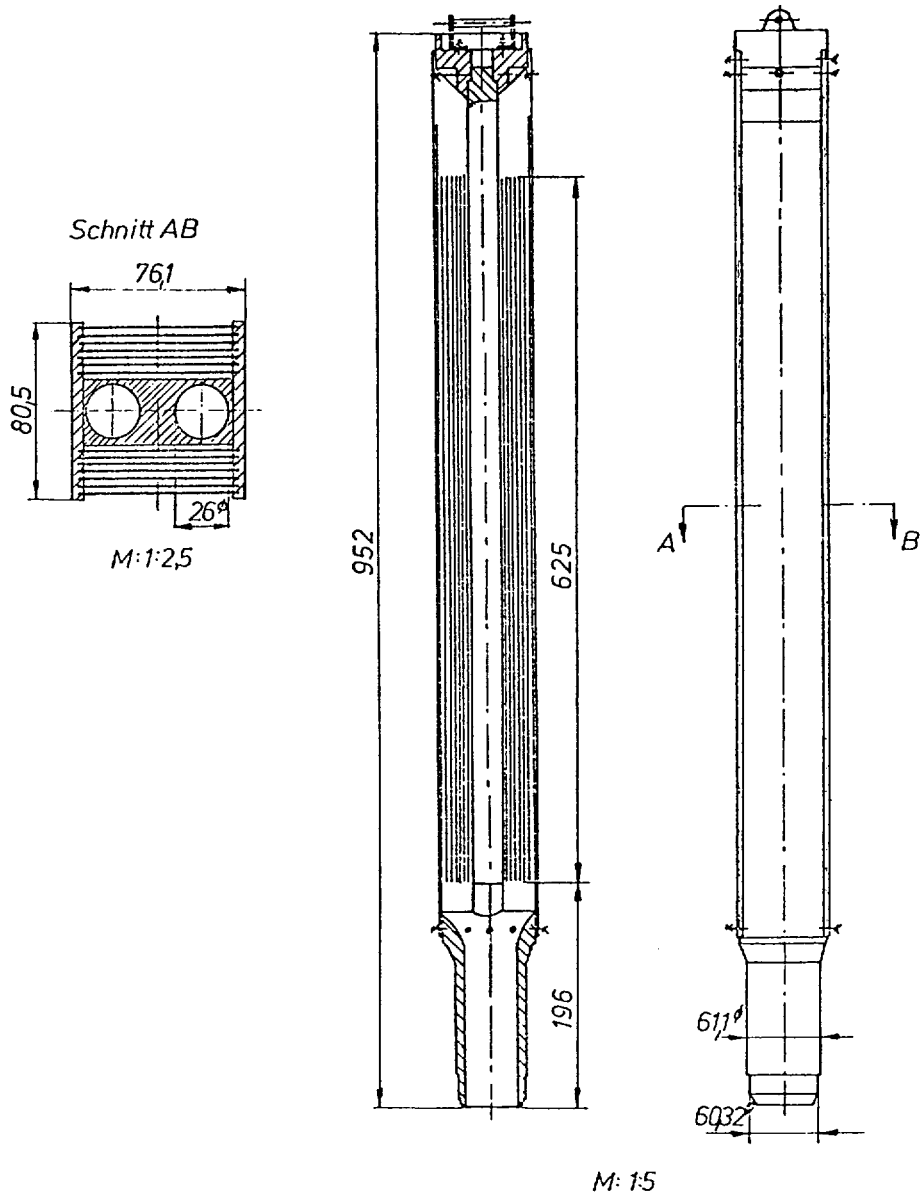

Abb. F-1b

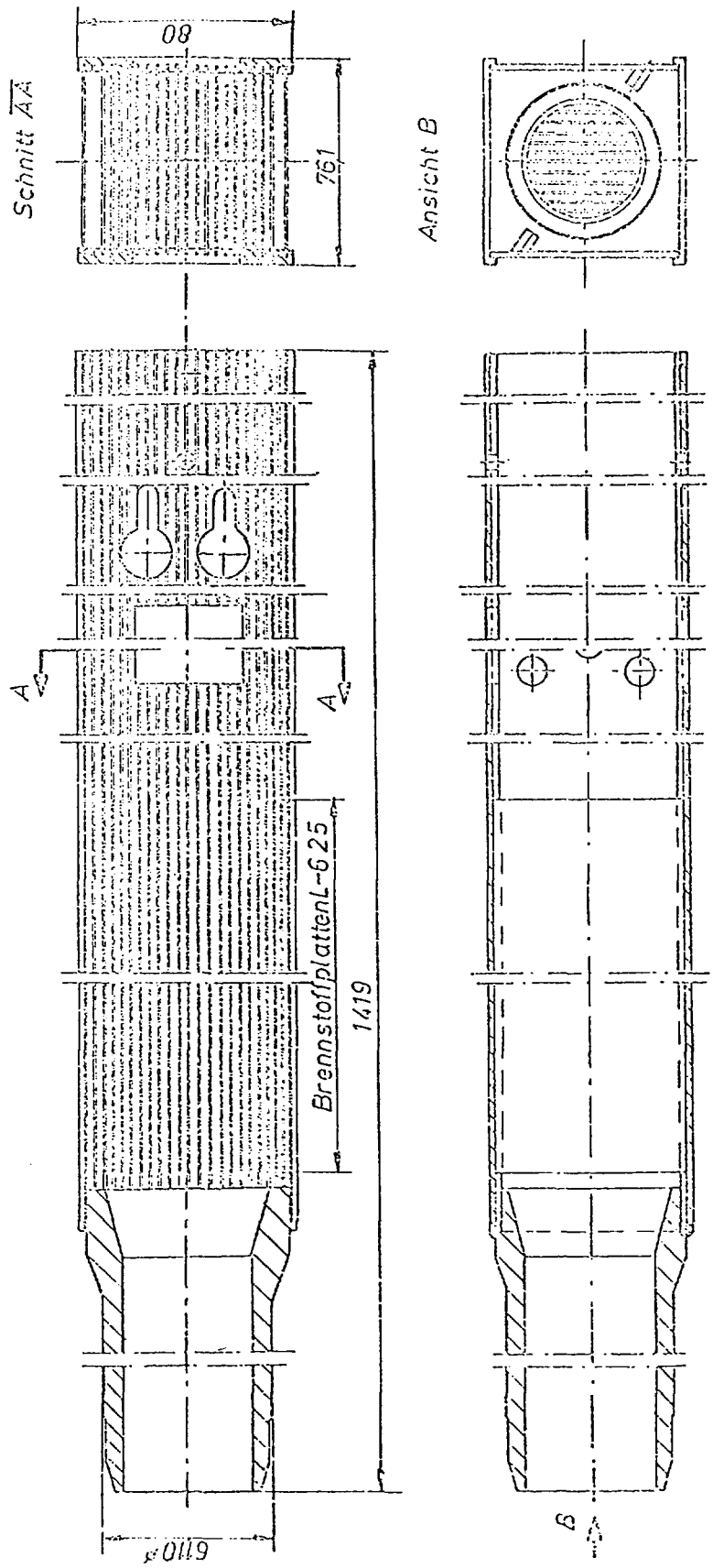
Schnitt AA
Ansicht B
Kontroll-Element
RESEARCH CENTER
SEIBERSDORF
ASTRA REACTOR
08
761
A
A
Brennstoffplatten L-625
1419
ø110
B

Abb. F-2a

RESEARCH CENTER
SEIBERSDORF
ASTRA REACTOR

Gabelförmiger Absorberstab

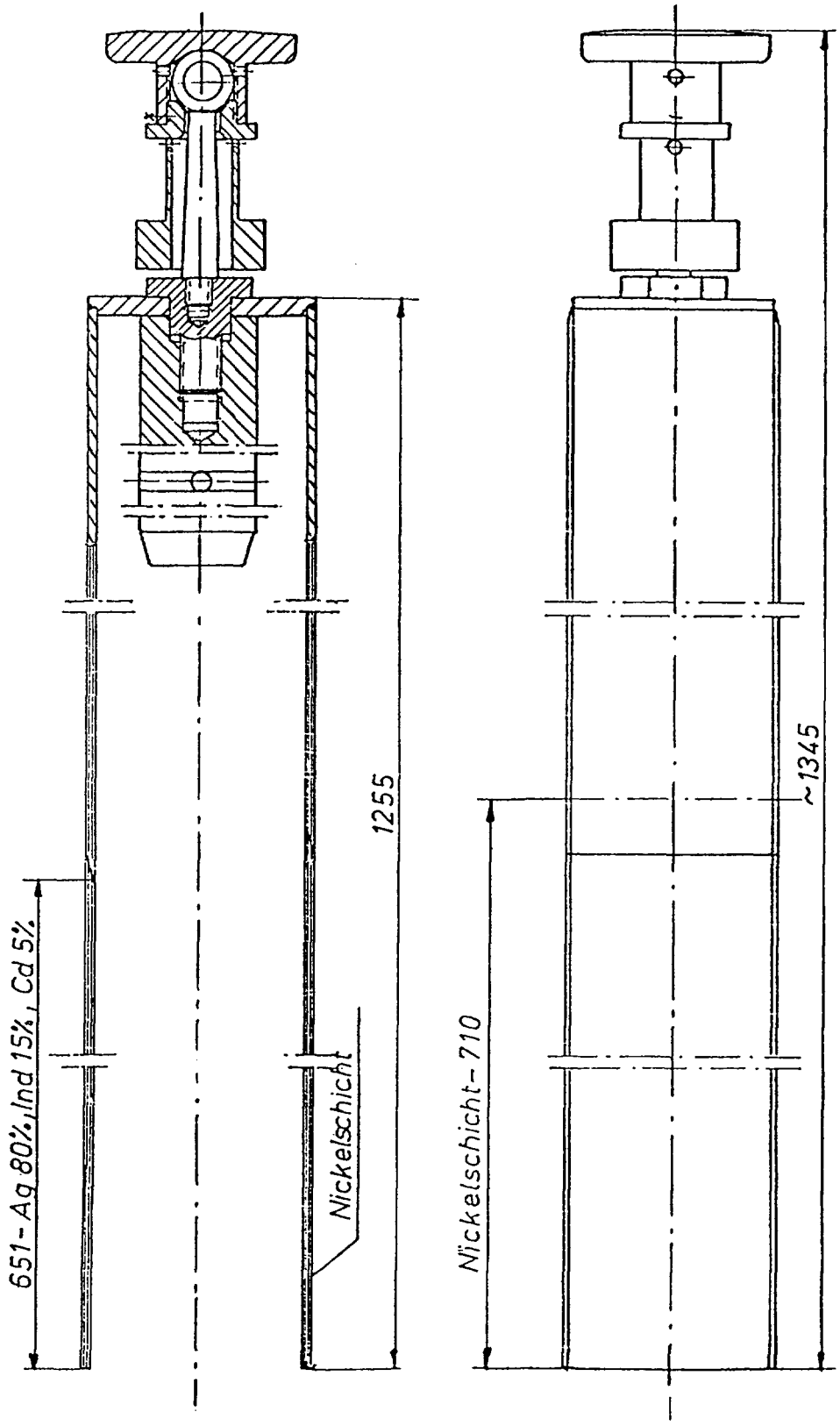

Abb. F-2b

Research Center Seibersdorf
ASTRA REACTOR

ASTRA REACTOR

FUEL AND CORE PARAMETERS

TYPE: Pool Type Reactor
POWER LEVEL: 8 MW
OPERATION TIME: ~3ooo h/a
FUEL TYPE: MTR-Fuel Elements
STANDARD FUEL ELEMENTS:
23 Plates/EL
U-content: 283 g U-235/EL
93 % enriched
CONTROL FUEL ELEMENTS:
17 Plates/EL
U-content: 21o g U-235/EL
93 % enriched
PARTIAL FUEL ELEMENTS:
14 Plates/EL
U-content: 172 g U-235/EL
93 % enriched
2 irradiation channels/Element
WATER CHANNEL: 2,12 (2,23) mm

ABSORBER ELEMENTS: 4 fork-type absorber elements
absorber material: Ag (8o %), In (15 %), Cd (8 %)

REACTOR REFLECTOR: 24 beryllium metalreflector elements

REACTOR CORE: 17 Standard fuel elements
4 Control fuel elements
1 Partial fuel element

Fuel burn up (U-235) : ~ 6o % at time of unloading

Fuel consumption/year: ~ 2 kg/year, uranium, 93 % enriched

RESEARCH CENTER SEIBERSDORF
ASTRA REACTOR

FUEL PLATE DIMENSIONS

TYPE:	FLAT FUEL PLATE
LENGTH:	INNER PLATE: 625,o ± 0,2 mm OUTER PLATE: 693,5 ± 0,2 mm
WIDTH:	7o,75 ± 0,15 mm
PLATE-THICKNESS:	INNER PLATE: 1,27 ± 0,o4 mm OUTER PLATE: 1,5 ± 0,o4 mm
MEAT-THICKNESS:	0,51 ± 0,o5 mm
CLADDING-THICKNESS:	INNER PLATE: 0,38 mm OUTER PLATE: 0,495 mm
MEAT LENGTH:	6oo ± 1o mm
MEAT WIDTH:	62,75 ± 2,4 mm
WATER CHANNEL WIDTH:	2,23 mm (NUKEM) 2,12 mm (CERCA)

RESEARCH CENTER SEIBERSDORF
ASTRA REACTOR

Technical Data of the ASTRA-Fuel-Elements

	Standard-	Control- Fuel Element	Partial-
Number of fuel plates	23	17	14
U-Content/plate	13,2 g	13,2 g	13,2 g
U-235 Content/plate	12,3 g	12,3 g	12,3 g
U-Content/Element	3o3,6 g	224,4 g	184,o g
U-235 Content/Element	282,9 g	2o9,1 g	172,2 g
Enrichment	93,2 %	93,2 %	93,2 %
Area of Element-cross-section	62,45 cm^2	62,45 cm^2	62,45 cm^2
Length of Fuel-zone	6o,o cm	6o,o cm	6o,o cm
Volume of Fuel-zone	3.747 cm^3	3.747 cm^3	3.747 cm^3
Metal-Water ratio			
H_2O	0,5699	0,5957	0,544o
Al	0,4259	0,4o14	0,4533
U	0,oo42	0,oo29	0,oo27

Physical Data of ASTRA-Standard-Elements

Enrichment	93 %	45 %		
U-235 Content (g)	28o	28o	32o	36o
U-total (g)	3o2	622	711	8oo
η	2.o72	2.o72	2.o72	2.o72
Thermal utilization f	0.869	0.865o	0.8794	0.891o
Resonance esc.prob.p.	0.988	0.958o	0.9545	0.951o
Fast fission fact. ε	1.ooo	1.oo15	1.oo17	1.oo2o
koo	1.78o	1.72o	1.742	1.759

APPENDIX H

Notes on the Status and Development Potential of Research and Test Reactor Fuels

prepared by

Argonne National Laboratory, USA
with contributions from
CEA, CERCA, GA, and NUKEM

ABSTRACT

The current status and the potential for development of all the major types of fuels which can be considered for use in research and test reactors are discussed, with special emphasis on the application of these fuels in reactor core conversions from HEU to LEU fuels.

For plate-type geometry, the fuel materials examined include U-Al alloys, UAl_x-Al dispersions, U_3O_8-Al dispersions, UO_2-Zr, and new fuel types such as U_3Si-Al dispersions. For rod-type geometry, the fuel materials examined include UZrH and UO_2-Zr.

It is concluded that the fuel development efforts now underway are likely to provide the technical means for converting research and test reactors to the use of LEU fuels. Extensions of currently utilized fuels should allow the conversion of low and high power reactors and the new high density fuels should allow the conversion of very high power reactors.

THE STATUS AND DEVELOPMENT POTENTIAL OF RESEARCH AND TEST REACTOR FUELS

TABLE OF CONTENTS

THE STATUS AND DEVELOPMENT POTENTIAL OF RESEARCH AND TEST REACTOR FUELS

The concern about the proliferation potential of HEU fuels and about anticipated restrictions on HEU supplies has stimlated development programs on fuels with higher uranium content which would allow the use of uranium of lower enrichment. Fuel development programs are underway in the U.S., Canada, France, the Federal Republic of Germany, Japan, and Argentina.

The fundamental objective of these fuel development programs is to develop existing and new research and test reactor fuels of both plate-type and rod-type to their maximum feasible uranium loading, with the intent of improving the performance of reduced-enrichment reactors.

H.1 PLATE-TYPE FUELS

A variety of fuel element materials are under development for plate-type fuels. Some of these materials correspond to extensions of materials which are in current use, while others are entirely new. The enrichment reduction potential of the current and new fuels are shown in Table H1. It is evident from the table that extensions of currently utilized fuels will permit enrichment reductions to <20% enriched fuel in low and high power research and test reactors, but that only the new fuels will permit such reductions for very high power reactors. It is also evident from the table that enrichment reduction to <20% for low power reactors fuels could be accomplished with existing technology.

In the following sections, the presently utilized fuels and the new fuels are characterized as to uranium content and performance, and the limits of uranium loading of these fuels for plate-type reactors are estimated.

Table H1. Uranium Density and Enrichment Reduction Potential of Candidate Fuels for Research and Test Reactors with Plate-Type Fuels

Fuel Type	Current Uranium Loading, g/cm^3	Near-Term Uranium Loading, g/cm^3	Long-Term Uranium Loading, g/cm^3	Current/Near-Term/Long-Term Enrichment Reduction Potential,%		
				Low-Power Reactors	High-Power Reactors	Very High-Power Reactors
U-Al Alloy	1.1	1.3	~1.6	<20	70/45/45	93
UAl_x-Al	1.7	2.2-2.6	2.6-2.8	<20	45/20/20	93/45/45
U_3O_8-Al	1.7	2.2-3.3	3.3-3.8	<20	45/20/20	93/45/45
UO_2 Caramel	9.1[a]	-	-	<20	<20	<20[b]
U_3Si-Al	-	4.2-6.0	7.0-8.0	<20	93/20/20	93/45/20
U_3Si (bulk)	-	-	~11	<20	93/93/20	93/93/20

[a]8.7 if the zircaloy spacers are smeared within the fuel meat. The density of the UO_2 is 10.3 g/cm^3.

[b]For very high-power reactors, UO_2 would have to be fabricated in very thin sections to provide proper heat removal.

H.1.1 Uranium-Aluminum Alloy Fuel

H.1.1.1 Introduction

Alloys of uranium and aluminum with uranium densities up to about 1.1 g/cm^3 can be easily fabricated by melting and casting techniques to yield uniform uranium distribution, in the form of UAl_3 and UAl_4 precipitates in an essentially uranium-free aluminum matrix. By proper casting and heat treating the amount of the more brittle UAl_4 phase can be reduced. However, with increasing uranium content, it becomes increasingly more difficult to achieve uranium uniformity and the ductility of the alloy decreases as well.[1,2]

The ductility may be increased by suppressing the formation of the brittle UAl_4 phase in favor of the more ductile UAl_3 phase by the use of certain ternary additions. Silicon has been successfully used as a suppressant. Additions of 0.8 and 3.0 wt% were found to completely suppress UAl_4 formation in uranium-aluminum alloys with uranium densities of about 0.6 g/cm^3 (20 wt% U) and 2.1 g/cm^3 (48 wt% U), respectively.[3] Other ternary additions which suppress UAl_4 formation are tin, germanium, zirconium, and titanium.[2] The ternary alloy additions, however, complicate the standard reprocessing schemes.[4] This difficulty coupled with the introduction of the aluminum dispersion fuels has curtailed further exploration of these systems.

H.1.1.2 Fuel Performance

Fuel assemblies containing fuel plates with U-Al alloy fuel meat with uranium densities between 0.55 and 0.70 g/cm^3 have been tested extensively in the MTR and ETR.[1] The average burnup of the fuel has exceeded 25% with peaks of 1.8×10^{21} fission/cm^3. Experimental assemblies have been run to 75% burnup with no deleterious effect.[5] Swelling appears to be linearly related to irradiation exposure with a value of 6.38% $\Delta V/V$ per 10^{21} fissions/cm^3. Unmodified U-Al fuels have performed well with uranium densities of 0.77 and 1.04 g/cm^3.

A good example of application of the U-Al alloy fuel with a uranium density of 1.06 g/cm^3 in the fuel meat[6] is provided by the GETR. The core contains 20 standard elements (each with 19 plates) and 6 control elements (each with 14 plates). The active height of the plates is 914 mm and their thickness is 1.27 mm. Each standard element contains 510 g of 93% enriched uranium. The power level of the GETR is 50 MW, corresponding to a core-averaged specific power of 4,084 w/cm^3 in the fuel meat. The average heat flux is 101 w/cm^2. The core average burnup limit is 50%, or 204 MWD/element, with a maximum of 2.0×10^{21} fissions/cm^3.[7].

Experimental irradiations were also performed with U-Al alloys containing ternary additions. Small plates containing fuel meat with 2.1 g/ U/cm^3 (48 wt% U) and 3 wt% Si were successfully irradiated to burnups of 83% (7.5×10^{20} fissions/cm^3).[8] Standard plates containing up to 2.25 g U/cm^3 with additions of silicon and tin were irradiated to large burnups (85% and 1.0×10^{21} fissions/cm^3) under MTR conditions without dimensional distortion.[9]

H.1.1.3 Development Potential

As noted above, U-Al alloy plates have been produced which contained up to 2.25 g U/cm^3 plus small ternary additions to suppress the formation of the brittle UAl_4 phase. Recent development activity at NUKEM and at SRL has been directed toward increasing the uranium density to 1.6 and to perhaps 1.9 g/cm^3 without ternary additions by proper casting and hot working techniques.[10,11] However, due to its limited potential as indicated in Table H1, U-Al alloy fuel was not included in the U.S. RERTR program, and for the same reasons has also been dropped from the NUKEM and SRL development programs.

H.1.2 Uranium Aluminide-Aluminum Dispersion Fuel

H.1.2.1 Introduction

As noted in Section H.1.1, the difficulty in achieving uniform fuel distribution in U-Al alloy fuels led to development of dispersion fuels in which fuel particles were dispersed in a metallic matrix. The dispersion approach provides a distinct separation of the fissile fuel particle and the metal matrix so that their desirable properties are retained. The metal matrix material must possess the following properties: good formability, good thermal conductivity, good corrosion and radiation resistance, and low thermal neutron cross section. Among others, alloys of Al, Be, Mg, Nb, Zr, and stainless steel have been employed as matrix materials.[12]

The fuel particles must possess good radiation resistance, high uranium density, and good corrosion resistance, and must be compatible with the matrix material. The particles should also possess some hot formability when high particle concentrations are used. The particle size should be large enough (>100 μm) so that fission product damage is concentrated in the particle. Particle spacing should be large enough so that damage zones, which surround the particles, do not link up. Porosity which is usually associated with the particles also provides some swelling accomodation. A number of fissile compounds are given in Table H2. The theoretical uranium content per unit volume of dispersed phase, its relation to the density of uranium metal, and the melting points of the compounds, which provide a relative indication of stability, have also been included in the table.

Table H2. Fissile Dispersants[a]

Compound	Melting Point, °C	Density, g/cm^3	Uranium Loading, g/cm^3	Relative Uranium Loading
U	1133	19.1	19.1	1.00
UAl_2	1590	8.1	6.6	0.35
UAl_3	1350	6.7	5.0	0.26
UAl_4	730	6.0	4.1	0.21
UBe_{13}	2000	4.37	2.9	0.15
UC	2500	13.6	13.0	0.68
UC_2	~2500	11.7	10.6	0.56
UO_2	2875	10.96	9.7	0.51
U_3O_8	-[b]	8.40	7.1	0.37
UN	2630	14.3	13.5	0.71
U_6Fe	815	17.7	17.0	0.89
UFe_2	1235	13.2	9.0	0.47
U_3Si	930[b]	15.6	15.0	0.79
U_3Si_2	1665	12.2	11.3	0.59

[a]From Ref. 13; [b]Decomposes

In addition to many tests on UO_2 and aluminum, U_3Si, U_3Si_2, UC, and UC_2 were evaluated at 620°C up to 48 hours for the potential for an exothermic "thermite" reaction between the components. No reaction occurred with UC_2; however U_3Si, U_3Si_2, and UC were found to react with aluminum, but at a slower rate than UO_2.[14] Of the aluminides, UAl_4 does not react with aluminum, UAl_3 reacts slowly, and UAl_2 reacts rapidly with aluminum to form the stable UAl_4.[15] A mixture of aluminides, designated UAl_x but compositionally close to UAl_3, does therefore react with aluminum in the reactor but at a very slow rate. The stable compound, UAl_4, is not used directly since it is very brittle and not easily formable with present plate-fuel technology.

H.1.2.2 Fuel Performance

Dispersions of UAl_x in aluminum have performed satisfactorily in the ETR and ATR with uranium densities of 0.68 and 1.6-1.7 g/cm^3, respectively.[1,16] Standard elements are exposed to average burnup levels of 30% (0.8×10^{21} fissions/cm^3) and peak levels of ~90% (~2.3×10^{21} fissions/cm^3).[16,17] Experimental plates have performed successfully after irradiation in the MTR,, ETR, HFIR, and FR2 (Karlsruhe) under a wide variety of conditions with the maximum burnup closely approaching total depletion of the uranium-235 (~2.8×10^{21} fissions/cm^3).[1,9,16,18]

Swelling rates are generally about one half that of U-Al alloy at about 3% $\Delta V/V$ per 10^{21} fissions/cm^3.[1] However, for the MTR experiments where slightly lower temperatures and water pressures exist, swelling rates were found to approach that of the U-Al alloy. It is postulated that at these conditions the process of in-pile densification, which reduces swelling, is impeded. For most irradiations, swelling was roughly linear with burnup to the maximum value tested. The exception was the FR2 (Karlsruhe) data which showed an increase in swelling to about 12% $\Delta V/V$ per 10^{21} fissions/cm^3 after a burnup of 40% (~1.5×10^{21} fissions/cm^3).[18]

A good example of application of the UAl_x-Al dispersion fuel with a uranium density of 1.6-1.7 g/cm^3 in the fuel meat is provided by the ATR. The core contains 40 elements, each with 19 plates. The active height of the plates is 121 mm and their thickness varies between 1.27 mm and 1.31 mm. Each element contains 510 g of 93% enriched uranium. The operating power level of the ATR is 275 MW, corresponding to a core-average specific power of 8,640 w/cm^3 in the fuel meat. The average heat flux is 185 w/cm^2. The average burnup is 32%, or 266 MWD/element.

H.1.2.3 Development Potential

Potential exists for increasing the uranium density in UAl_x-Al dispersion fuels. In the past, experimental loadings of only 1.8 g U/cm^3 were fabricated.[17] However, it is anticipated that a uranium density of 2.1 g/cm^3, equivalent to about 50 vol.% UAl_x, can be easily fabricated as part of a develpment program. This limit may possibly be extended to 2.5 g U/cm^3 ; however, careful control of fabrication parameters will be necessary to prevent dogboning and to maintain uniform meat thickness, width, and uranium distribution.

H.1.3 Uranium Oxide-Aluminum Dispersion Fuel

H.1.3.1 Introduction

Dispersions of uranium oxide (U_3O_8) in aluminum have received wide application in research and test reactor fuels. All the general considerations mentioned in Section H.1.2.1 and concerning dispersion fuels in general apply also to U_3O_8-Al dispersions.

The work on uranium oxide dispersions in aluminum began with UO_2 as the dispersed phase, because of its stability and high density of uranium. The 1955 Geneva Converence Reactor (GCR) used a UO_2-Al fuel. Great difficulty was experienced during manufacture of the GCR fuel elements because of abnormal dimensional growth during elevated temperature fabrication procedures. The growth of the fuel plates was traced to volume changes accompanying the reaction of UO_2 and aluminum. The reaction reached 90 to 100 percent completion in 10 hr at 600°C in plates with fuel meat containing about 1.9 g U/cm^3 (52 wt% UO_2).[15] Fortunately, experiments at ANL discovered that U_3O_8 was more stable than UO_2 with aluminum and recommended its use.[19] Later experiments at ORNL confirmed that the reaction of U_3O_8 with aluminum was much slower at the temperatures needed for fabrication.[20] It was shown that 3000 hr were required for complete reaction at 600°C.[21] Fuel plates could, therefore, be fabricated from U_3O_8 and aluminum with relatively little difficulty arising from dimensional changes due to a reaction between the components. This process, however, leads to a fuel element in which the potential for an exothermic "thermite" reaction between the components must be carefully evaluated.

H.1.2.1 Fuel Performance

Fuel plates with fuel meats consisting of a dispersion of uranium oxide (U_3O_8) in aluminum, and clad in aluminum, are used in High Flux Isotope Reactor (HFIR) at Oak Ridge National Laboratory. The maximum uranium density is about 1.2 g U/cm^3 (about 40 wt% U_3O_8) in the uranium-bearing-portion (meat) of a HFIR fuel plate. The core contains two coaxial cylindrically similar elements with involute-shaped fuel plates. The inner element holds 171 plates, and the outer element holds 369 plates. The thickness of the plates is 1.27 mm and their effective height is 508 mm. The inner and outer elements contain, respectively, 2791 and 7317 g of 93% enriched uranium. The operating power level of the HFIR is 100 MW, corresponding to a core-averaged specific power of ~15,300 W/cm^3 in the fuel meat. The average heat flux is 245 W/cm^2. The average burnup of the fissile atom is 31% (0.9×10^{21} fissions/cm^3), with peaks of 65% (~1.9×10^{21} fissions/cm^3).[22] Experimental plates have experienced burnups of ~75% (~2.1×10^{21} fissions/cm^3) without failure or gross dimensional change.

As part of the U_3O_8 dispersion fuel development for HFIR and the Puerto Rico Nuclear Center Reactor (PRNC), test samples were made, irradiated, and evaluated by the Oak Ridge National Laboratory.[8,23] The uranium density was about 2.3 g/cm^3 (64 wt% U_3O_8) in the fuel meat, which was about 610 μm (about 0.024 in.) in thickness. Short plate-type specimens were found to be dimensionally stable after a burnup of 7.7×10^{20} fissions/cm^3 (>90% ^{235}U depletion). A full size MTR-type element was found to be dimensionally stable after a burnup of ~4×10^{20} fissions/cm^3 (~50% ^{235}U depletion).[8] Thus, 2.3 g U/cm3 represents the present maximum uranium density in U_3O_8-Al dispersion-type plate fuel.

Related recent development activity at Savannah River Laboratory on U_3O_8-Al dispersion-fueled tubes has indicated that a uranium loading of about 1.9 g/cm^3 (58 wt% U_3O_8) has performed well after 141 irradiation days.[11]

H.1.3.3 Development Potential

The potential for develpment of higher uranium densities in U_3O_8 dispersion-type aluminum plate fuel does exist. As part of the U_3O_8 dispersion fuel development at ORNL for HFIR and at SRL, test samples were made that contained up to 5.6 g U/cm^3 (100 wt% U_3O_8) in the meat.[11,22] As expected, for uranium densities greater than about 2.8 g/cm^3 (about 70 wt% U_3O_8), depending on void content, the continuous phase of the dispersions changed from aluminum to U_3O_8. However, all cold-pressed U_3O_8 dispersions exhibited sufficient green strength after compacting to permit some handling without breaking. All of the plate fuel appeared to roll-clad satisfactorily, as was evident from the absence of internal cracks. However, for the tubular fuel elements, high extrusion ratios led to overheating which produced a thermite reaction between U_3O_8 and aluminum. Reductions in meat thickness and extrusion ratio are being made to eliminate this problem.[11]

In addition to the potential for a thermite reaction, the other technical issues which must be addressed to increase the uranium density beyond 2.3 g/cm^3 include: adequate control of cladding thickness, dogboning, a continuous aluminum phase in the meat, uranium homogeneity, and fuel behavior under long irradiation (i.e., unacceptable swelling and shrinking). Of perhaps critical importance is the need and maintenance of a continuous aluminum phase that will facilitate heat flow out of the meat. Based on simple geometric consideration, a uranium loading of about 60 vol% which is about 3.6 - 3.7 g U/cm^3 (about 80 wt% U_3O_8) would appear to be the theoretical limit to maintain the continuous aluminum phase in U_3O_8-Al dispersion with U_3O_8 spheres. Slightly higher loadings may be possible with particle size, shape, and size distribution control.

H.1.3.4 Thermite Reaction Concerns

As noted above, the potential exists for a thermite reaction which must be evaluated as part of the safety analysis. Both off-normal and transient effects must be considered. Fortunately, some data are available under both of these conditions.

Fleming and Johnson heated cold pressed pellets of mixtures of U_3O_8 and aluminum at 33°C/min.[24] Violent exothermic reactions occurred between 900 and 1100°C with the peak energy release of 1.2 Mw-sec/kg fuel at uranium densities in the range 2.3 - 3.0 g/cm^3 (65 - 75 wt% U_3O_8). This reaction was also studied by workers at ANL using various pretreatments, environments, and particle size distributions.[25,26] However, the slow heat-up rate (25°C/min) tests failed to duplicate the violent reactions of Fleming and Johnson. Only temperature excursions to a maximum of 1300°C were observed. Similar results were obtained for specimens inserted into a furnace at 1250°C. However, for specimens which were sintered at 600°C after pressing, violent reactions were observed with uranium densities of 3.0 and 4.0 g/cm^3 (75 and 85 wt% U_3O_8). Thus, the reaction rate is strongly related to the preconditioning of the compacts.

Large scale full-size element tests were performed by SRL for U_3O_8-Al cores with $\leq$1.9 g U/cm^3 ($\leq$57 wt% U_3O_8).[11] It was found that the maximum fuel temperature was 1370°C, only 370°C above the furnace temperature. Thus the heat of reaction was not an important energy source for these fuel elements.

In-reactor (TREAT) transient experiments on U_3O_8-Al HFIR fuel were performed by ANL.[27] The tests simulated nuclear excursion accidents in a water-cooled reactor. Specimens of U-Al fuel were included for comparison. The major conclusions were that the U_3O_8-Al specimens retained their shape up to 1400°C (a significantly higher temperature than U-Al fuel) and that the exothermic reaction was not an important energy source. Confirmatory testing is underway at ORNL.

H.1.4 Uranium Oxide-Zirconium Fuel

Despite the poor thermal conductivity of UO_2, it has good thermal performance since it can be operated at steady state central temperatures approaching its melting point.[39] UO_2 was used as the fuel material for the first U.S. prototype power reactors - the Shippingport pressurized water reactor (PWR) and the Vallecitos boiling water reactor (BWR) - built in the late 1950s. However, metal fuels were utilized in the early experimental reactors: the STR, developed by ANL, Westinghouse, and the Naval Reactors Division - USAEC; and the EBWR, developed by ANL.[40] The shift to oxide fuel was made since the metal alloy fuel behavior was found to be inadequate.[39]

The reference fuel for both the PWR and the BWR is still UO_2 in the form of pellets of ~93% theoretical density. Satisfactory performance has been obtained at burnups of over 40,000 MWD/T.[41,42] This led to the consideration of oxide fuel for LMFBRs and to the development of an information data base on oxide fuels for this application.[43] A similar document is also available for LWR oxide fuel behavior.[44] UO_2 fuel rods have also been used in the PULSTAR reactors which contain ~5% enriched uranium.

More recently, the French have utilized UO_2 wafers (Caramels) in a compartmentalized zircaloy cladding arrangement for plate-type reactors.[45] The plates have performed well to a maximum burnup of 30,000 MWD/T. The French design is similar in concept to that employed in the second core of Shippingport, which utilized UO_2-ZrO_2 as fuel and UO_2 in the blanket. As part of the development of the UO_2 plates for the blanket, Westinghouse performed high-temperature irradiations to burnup as high as 140,000 MWD/T (4×10^{21} fission/cm^3).[46] However, plate failures occurred at as low a burnup as 20,000 MWD/T ($\sim 0.6 \times 10^{21}$ fission/cm^3) due to fission gas release.

H.1.5 New Fuel Types

H.1.5.1 Introduction

Although the development of increased uranium densities in current research reactor fuel types, if successful, will allow many research reactors to utilize lower-enrichment uranium in the fuel, there will still be several research and test reactors which cannot be converted to the use of low-enrichment uranium fuel. These are the reactors that are already operating with high uranium densities and highly-enriched fuel. Also, these are in general the more advanced (higher power-density) and more highly-utilized research reactors which are designed for extra-long core life.

Thus, for new research reactors, and for replacement fuels in the higher power-density research reactors, one option is to develop a different research reactor fuel specifically designed for high uranium densities. This option could allow the research reactor to convert to low-enrichment uranium fuel with a minimum impact on the core design or operation as compared with other options such as complete core modification or decommissioning. Developent of this fuel option also provides a backup if the planned developments based on current fuel do not work out.

Several advanced fuel types have been and are being studied. The properties of some of these fuels are shown in Table H3 (taken from Ref. 28). Not all of these are compatible with a water-cooled research reactor environment, but some are. The candidate fuel materials possess much higher densities than the currently utilized dispersion fuels which possess a uranium density of only 1.7 g/cm^3. The corrosion resistance, irradiation performance, and development potential of some of these fuel candidates is given in the following sections. These materials could be utilized alone or even as a dispersant since their densities, as listed in Table H3, are much greater than UAl_x or U_3O_8.

H.1.5.2 Corrosion Resistance

Metallic uranium alloys and compounds were extensively investigated, principally at ANL, Bettelle, KAPL, and Westinghouse in the uS. in the late 1940s and the 1950s as fuel for light water reactors. Several thorough reviews of the subject have been published.[29,30] These investigations focused on alloying to improve the poor corrosion resistance of uranium and to ameliorate the anisotropic growth problem inherent in pure uranium. In these early efforts, almost every metallic lement was alloyed with uranium in an attempt to produce a fuel which would be resistant to high temperature water. The alloys with good to moderate resistance fall structurally into two groups: metastable gamma alloys and distorted alpha alloys. The former are produced by quenching from 800-1000°C. Molybdenum and niobium compositions in the range of 7 to 15 wt%, respectively, have been studied. Corrosion resistance was highly dependent on heat treatment conditions with molybdenum being superior to niobium. The alpha alloy group consisted mainly of alloys with zirconum (up to 10 wt%), niobium (up to 6 wt%), and both zirconium and niobium in ternary alloys. However, when these alloys were heat treated or aged for maxium corrosion resistance, they exhibited poor dimensional stability under irradiation, and vice versa.

It is also possible to provide corrosion resistance by the formation of intermetallic compounds. U_3Si has been studied because it possesses reasonable ductility and moderately high melting point. With proper heat treatment, this compound provides nearly as good corrosion resistance as the best uranium-molybdenum alloy.[31] More recent work on this alloy system by the Atomic Energy of Canada Limited (AECL) has shown that the addition of 1 1/2% aluminum substantially increases the corrosion resistance of the fuel.[32]

Another approach to the problem of providing corrosion resistance was developed at the DuPont Savannah River Laboratory (SRL).[33] Corrosion resistance can be provided by a diffusion bond between an intermediate layer and both the fuel and cladding. The fuel was bonded to the aluminum cladding by utilizing an Al-Si dip-canning process on early fuel elements and an electro-plated nickel layer on later fuel elements. Both methods were followed by a hot die-sizing process to form the diffusion bond. This technique substantially reduces the exposure of the fuel to hot water in the event of a penetration in the cladding. A diffusion bond between a uranium-zirconium alloy and the zircaloy-2 cladding created by coextrusion was also found to provide excellent corrosion resistance.[30]

Of the ceramic compounds listed in Table H3, only UO_2 possesses chemical inertness and resistance to high temperature water.

Table H3. Properties of Fuels

	U	U-10% Mo	U_3Si	U-Fs[c]	UO_2	UC	UC_2
Melting point, °K	1405	1423	1203	1275	3138	2780 ± 25	2773
Density, g/cm^3	19.12	17.12	15.58	18	10.96	13.61	12.86
Heavy metal density, g/cm^3	19.12	16.38	14.91	17.5	9.65	12.97	11.68
Crystal structure	a	b	bct	bcc (>1000 K)	fcc (CaF_2)	fcc (NaCl)	fcc (CaF_2)
Thermal conductivity, W/cm-°K	0.35 (670 K)	0.29 (870 K)	0.2 (to 1170 K)	0.33 (820 K)	0.03 (1270 K)	0.216 (to 1270 K)	0.35 (to 1270 K)
Thermal expansion, 10^{-6}/°K	19 (to 920 K)	12.3 (to 670 K)	16 (to 1070 K)	17 (to 820 K)	10.1 (to 1270 K)	11.6 (to 1470 K)	18.1 (1970 K)
Electrical resistivity, ohm-cm	35×10^{-6} (298°K)		75×10^{-6} (to 1070 K)		1×10^3	40.3×10^{-6} (298 K)	
Specific heat, cal/g-°K	0.026 (to 773 K)	0.035 (to 773 K)	0.043 (to 773 K)		0.065 (700 K)	0.048 (298 K)	0.12 (298 K)
Heat of fusion, cal/mole	4760				16,000	11,700	
Vapor pressure, atm	5×10^{-6} (2300 K)	5×10^{-6} (2300 K)			8.5×10^{-8} (2000 K)	1.7×10^{-10} (2300 K)	2.5×10^{-11} (2300 K)
Debye temperature, °K	200 K				<600 K, 870 K	--	--
Free energy of formation, kcal/mole	-				-218 (1000 K)	-23.4 (298 K)	
Heat of formation, kcal/mole	-				-260 (to 1500 K)	-23.63 (298 K)	-23 (298 K)
Entropy, cal/mole-°K	-				18.6 (298 K)	14.15 (298 K)	16.2 (298 K)
Poisson ratio	0.21	0.35			0.3	0.284	
Modulus of rupture, MPa					80		
Modulus of elasticity, MPa	1.7×10^5	10^5		6×10^4	1.8×10^5	2×10^5	
Shear modulus, MPa	0.85×10^5	3×10^4			0.75×10^5	0.873×10^5	
Tensile strength, MPa	400	300	600	270	35		
Compressive strength, MPa			2000		1000	350	
Thermal neutron fission cross section, barns	4.18 (natural)	4.18 (natural)	0.159 (natural)		0.102 (natural)	0.137 (natural)	0.112 (natural)
Thermal neutron absorption cross section, barns	7.68 (natural)	6.68 (natural)	0.293 (natural)		0.187 (natural)	0.252 (natural)	0.207 (natural)
Eta (η)[d]	1.34	1.34	1.34	1.34	1.34	1.34	1.34

[a] Orthorhombic (<936°K), tetragonal (936-1043°K), body-centered cubic (>1043°K).

[b] Orthorhombic plus tetragonal (<838°K), body-centered cubic (>838°K).

[c] U containing 5% fissium (0.22% Zr + 2.5% Mo + 1.5% Ru + 0.3% Rh + 0.5% Pd). U-5% fissium is bcc above 1000°K, bcc + monoclinic U_2Ru between 825°K and 1000°K, and bcc + U_2Ru + tetragonal below 825°K.

[d] Number of fission neutrons released per neutron absorbed.

H.1.5.3 Fuel Performance

Uranium-molybdenum alloys generally exhibit satisfactory irradiation behavior. In early work, the U-10 wt% Mo alloy was shown to be stable to at least 5 at% burnup except for abnormal swelling for some samples operated at 335-390°C, possibly due to plastic flow effects near the alpha-beta transition temperature.[30] The corrosion resistance of these materials were relatively good since the gamma phase was stablized by the irradiation. Similar behavior was found in more recent work at SRL on lower Mo concentration alloys containing 0.1 wt% silicon.[34] Swelling rates of 2 - 4%/at% burnup were found after irradiations of 9000 and 12000 MWD/T up to 600°C maximum fuel temperature, again with the exception of abnormal swelling at ~400°C. The irradiation bebavior of uranium-niobium alloys was found to be similar to that or uranium-molybdenum.[30] However, additions of 4-6 wt% of zirconium to U-10 wt% Nb did raise the abnormal swelling temperature to above 450°C.

The irradiation behavior of uranium-zirconium and uranium-zirconium-niobium generally has not been good.[30,34] However, additions of carbon were found to greatly modify swelling behavior in low burnup tests.[30] Good irradiation stability has been obtained with a U-5% Fs alloy (where the fissium is made up of mixture of fission products expected in recycled fuel) to burnups exceeding 10 at% in the EBR-II.[35] However, these cast and heat treated rods are bonded to the cladding with sodium which provides volume for ~30% swelling up to about 4 at% burnup, after which the cladding can easily restrain the spongy fuel.

Ongoing experiments at SRL with very small additions of Cr, Al, Si, Fe, and Mo to uranium have produced interesting results.[34] Most of these alloys were quenched from 725°C then irradiated to 9000 and 13000 MWD/T at various temperatures ranging from 200 to 600°C. Swelling rates of 3-4%/at%-burnup were found for alloys containing 800-1150 ppm Al + Si at temperatures below the swelling threshold of 350°C. Alloys containing the above Al + Si concentrations were further improved by the addition of 250-350 ppm Fe, 200 ppm Cr, and 1000 ppm Mo was found to be stable to approximately 425°C.

The early irradiations of U_3Si fuel material produced maixed results. Extruded samples irradiated to 9.17 at% burnup by Westinghouse-APD were found to have increased in both length and diameter.[30] Several samples were bowed and all exhibited cracks, peculiar blister and bands. However, in tests performed by ANL, bit cast and extruded samples exhibited good irradiation stabilibity.[36] Recent irradiation experiments at AECL with U_3Si, and U_3Si modified by aluminum, have indicated that these fuels have excellent irradiation performance.[37,38] By utilizing annular fuel rods, diameter increases with U_3Si clad in zircaloy were less than 1% after 10,000 MWD/T and about 1.2% after 19,000 MWD/T at a maximum temperature of about 500-600°C. With the 1.5 and 2.4 wt% aluminum, diameter increases were reduced slghtly and, as noted earlier, the corrosion resistance of the alloy fuel was improved.

H.1.5.4 Development Potential

From the data presented in the foregoing sections, it was concluded that U_3Si, probably modified with aluminum, has the potential of providing the necessary uranium density and irradiation performance levels. Uranium-molybdenum alloys are thought to be the second best choice, with UO_2 third. UO_2 would have to be produced as very thin members due to its poor thermal conductivity. The French fuel development effort has also chosen U-Mo alloys as a backup to their UO_2 Caramel fuel.[46]

It is likely that U_3Si can be utilized as a dispersant in aluminum, provided that the positive volume change upon reaction to form UAl_3 can be reduced or slowed by alloy addition. As shown in Fig. H1, U_3Si provides a much higher uranium loading than does equal volumes of U_3O_8 or UAl_x. For example, an expected volume fraction range of 0.5-0.7 would yield uranium loadings of about 7.0-10.0 g/cm^3, as indicated in Fig. H1. Thus an alloy addition would not greatly reduce the uranium loading. The use of an aluminum dispersion would mean that present dispersion fuel meat technology could be utilized, rather than some advanced technology which might require cladding with zircaloy or other stiffer cladding material. However, the greater density difference between U_3Si and aluminum would require greater care in the blending of powders to maintain uniform fuel particle distribution.

One potential problem with U_3Si with regard to reprocessing must also be resolved. Silicon in some weight fraction ranges has been shown to interfere with phase separation in the extraction column.[47] However, a study is underway at ANL to determine whether the aqueous process can be successfully modified or whether a suitable non-aqueous method can be utilized to accomplish the reprocessing of plate-type fuels containing U_3Si.

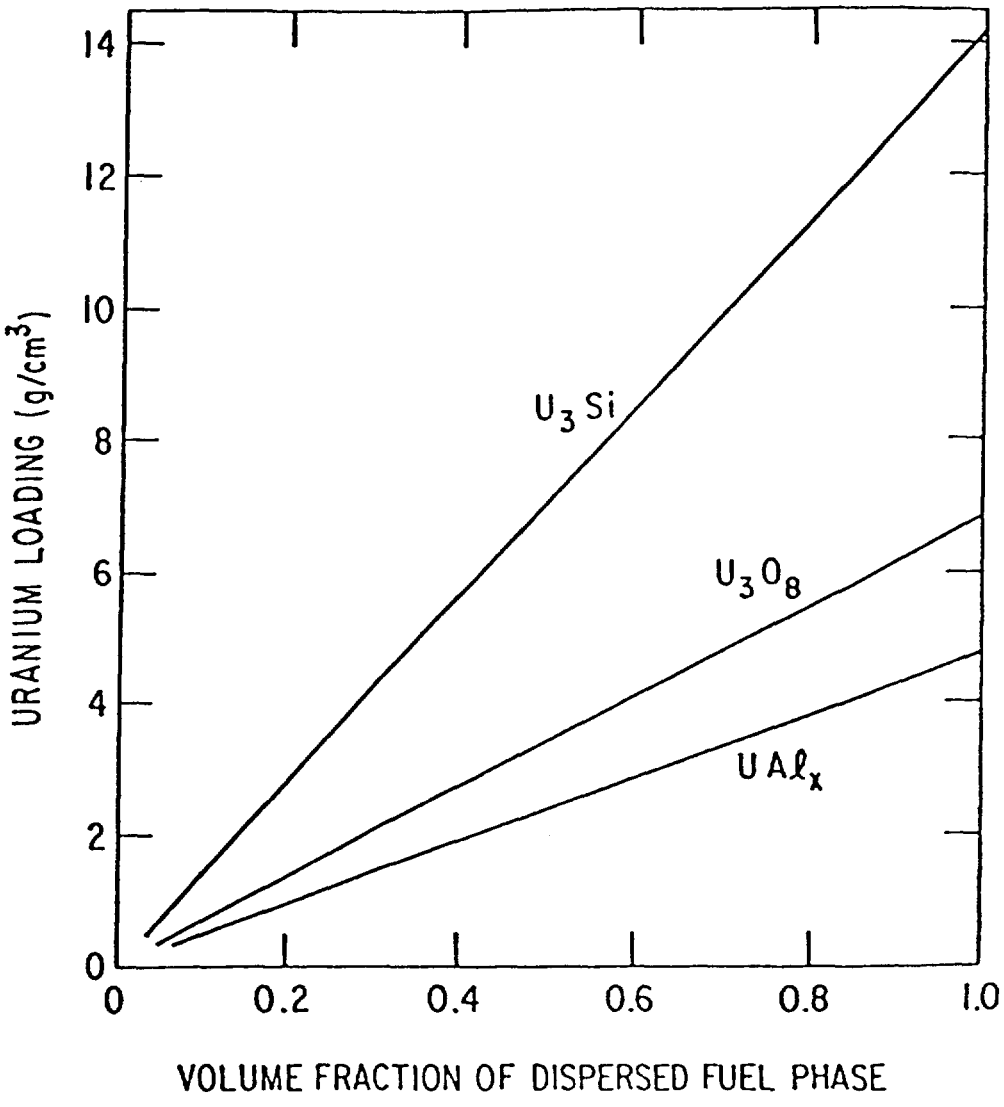

Figure H1. Relationships Between Uranium Density and Volume Fraction of Dispersed Fuel Phase for Uranium Dispersion Fuels.

H.2 ROD-TYPE FUELS

H.2.1 Up to 1.3 g U/cm^3 (20 wt% U)in UZrH Fuel

Sixty TRIGA reactors have been sold and the earliest of these are now passing twenty years of operation. All of these reactors use the uranium-zirconium hydride fuel (UZrH) which provides certain unique advantages arising out of its large prompt negative temperature coefficient, very low fission product release,[48] and high temperature capability. With only a few exceptions, TRIGA reactors have always used low-enriched uranium (LEU) fuel with an enrichment of 19.9%. The original standard TRIGA fuel has a uranium density of 0.5 g/cm^3 (8.5 wt% U) and is 20% enriched (nominal). Experience with TRIGA fuel includes over 650 reactor years of successful operation. TRIGA fuel with a uranium density of 0.75 g/cm^3 (12 wt% U) has been proved through successful reactor operation for over a decade. Previous work on UZrH fuels during the Space Nuclear Auxilliary Power (SNAP) reactor program[49,50] had developed the technology up to 1.3 g U/cm^3 (20 wt% U) and found no indication of this being a limit. Burnup of U-235 reached values of about 80% in SNAP program tests. The LEU development program at General Atomic has also included extensive tests with 1.3 g U/cm^3. Tests have shown fuel with greater than 1.3 g U/cm^3 to have essentially the same fission product retentivity as TRIGA fuel with 0.5 g U/cm^3.[51] On-going in-core tests with 1.3 g U/cm^3 fuel, started in April 1978, have been an unqualified success during pulsing and steady-state operation including over 1500 thermal cycles where the reactor has gone from shutdown to powers of 1 to 1.5 MW with 1.3 g U/cm^3 fuel.[52]

H.2.2 Up to 3.7 g U/cm^3 (45 wt% U) in UZrH Fuel

General Atomic undertook an LEU development program in early 1976. Laboratory and production tests of fuels containing up to 3.7 g U/cm^3 (45 wt% U) are complete. In-core tests of production elements for thermal cycling and pulsing tests have been under way since April of 1978. The extensive metallographic, electron microprobe and X-ray diffraction examinations have shown that the more highly loaded alloys contain no significant differences in structural characteristics when compared with the standard 0.5 and 0.75 g U/cm^3 fuels.[53] The phase distribution and homogeneity are excellent and these factors, coupled with the grain structure observed, support expectation of excellent long-term irradiation behavior. The measured fission product release[51] and physical properties[54] show very suitable characteristics up to 3.7 g U/cm^3. The fission product release experiments were conducted to temperatures up to 1100°C and showed very low release fractions, characteristic of the standard TRIGA fuels, where the temperature independent value to about 300°C is 1.5 x 10^{-5}. Test results on samples quenched from up to 1200°C can be characterized as showing remarkably benign response.[55] Some minor cracking, volume shrinkage, loss of hydrogen and surface oxidation occurred. Out-of-pile thermal cycling tests show that the ZrH matrix stabilizes the fuel material such that it is dimensionally stable when repeatedly cycled through the uranium phase change temperature of about 680°C.[53] Reactor testing of production elements includes 1.3 and 3.7 g U/cm^3 fuels being tested in the TRIGA Mark F reactor at General Atomic[52] both in the steady state and pulsing modes. The principal objective of these tests is to demonstrate the fuel stability for thermal cycling from ambient to operating temperatures. Nearly 2000 in-core cycles have been completed to date and no adverse conditions noted. An irradiation test of a standard 16-rod cluster configuration has been in progress in the 30 MW ORR since December, 1979.

Table H4. TRIGA LEU FUELS

1)	FUEL TYPE	U-Er-ZrH	U-Er-ZrH	U-Er-ZrH	U-Er-ZrH	U-Er-ZrH
	General Atomic Catalogue Number	624	622	620	626	618
	Wt% Uranium/Enrichment	45-20	45-20	30-20	20-20	20-20
2)	CONFIGURATION					
	Number of Fuel Clusters	30	30	~30	~25	25
	Rod/Cluster	25	16	9	4	4
	Rod Nom. OD (in./cm)	0.54/1.37	0.54/1.37	~0.7/1.78	~1.3/3.30	1.41/3.58
	Active Height (in./cm)	22/55.9	22/55.9	22/55.9	20/50.8	15/38.1
3)	POWER LEVEL (MW)	15	10	5	2	~1.5 (Natural Convection)
4)	SPECIFIC POWER (Avg. in Max. Rod) (watts/cc. of U-ZrH)	515	530	~270	~78	~69
	(Core Avg.)	270	280	~150	~49	~43
5)	HEAT FLUX (Core Avg.) (BTU/hr-ft2)	2.6×10^5	2.7×10^5	~1.9×10^5	~1.2×10^5	~1.1×10^5
6)	BURN UP (MWD)	7000	4100	~1200	~1300	~1000
7)	URANIUM CONTENT (gm/rod)	274	274	~264	~534	460
	(gm/cc of U)	3.7	3.7	2.1	1.3	1.3
			Also used at 5 MW with about 25 clusters	Also used at 3 MW with 25 to 30 clusters	Also used at 3 MW with 25 to 30 clusters	Cat.#604 (8.5-20) can also be used in this configuration

H.2.3 UO_2 in Zr Fuel

UO_2-Zr rod-type fuel elements are currently being used in France in the Cabri reactor. This experience has demonstrated the capability for such fuels to behave satisfactorily in research reactors.

H.3 SUMMARY AND CONCLUSIONS

The current emphasis on the conversion of research and test reactor fuel from fully-enriched uranium to less than 20% enrichment or to some intermediate enrichment, perhaps 45%, has stimulated the development of more highly uranium-loaded fuels. The development effort has been logically divided into two areas: the extension of currently utilized fuels to their maximum uranium loading; and the development of new high-density fuels.

The uranium density and enrichment reduction potential of current plate-type fuels was summarized in Table H1. It is anticipated that U-Al alloy fuel can be developed which contains 1.6 - 1.9 g U/cm^3; however, this loading will only permit reductions to less than 20% enrichment for low power reactors and reductions to intermediate enrichment for other reactors. Aluminide and U_3O_8 dispersion fuels could reach uranium densities as high as 2.8 and 3.7 g/cm^3, respectively, which would make possible the use of less than 20% enriched uranium in high power reactors. This assumes that dispersions containing 60 vol% of the dispersed fuel phase are possible. For both of these materials, fuel fabricators and developers have stated that ~55 vol% is the maximum loading possible as a result of development efforts during a round table discussion held at ANL as part of an International meeting.[56] If only 50 vol% dispersions are possible, which is a more likely outcome, then the aluminide dispersion might not permit the conversion of high power reactors without some modification to the fuel meat thickness and element geometry. This may be true for U_3O_8 dispersions as well. With these extensions of currently utilized fuels, there exists little or nor high-burnup experience; however, much positive experience exists for the lower uranium loadings. This suggests that if uniform dispersions of highly loaded fuel can be successfully fabricated there is a strong likelihood that they will exhibit satisfactory irradiation behavior.

For the new high density fuels, a somewhat opposite situation exists. There is very little low-temperature, high-burnup irradiation experience. For U_3Si and U-Mo alloys, the maximum burnup was less than 20,000 MWD/T, while for UO_2 plates, the maximum burnup was less than 30,000 MWD/T. As far as uranium loading is concerned, these materials are more than adequate, and dispersions may be utilized to take advantage of existing dispersion fuel technology. However, the compatibility of the fuel compound with the matrix must be assessed. U_3Si, for example, must be stablized so that its slow in-pile reaction with aluminum does not yield large volume increases. Such dispersions with 50 or more volume percent of dispersed fuel would allow conversion of even the very high power reactors.

For rod-type fuels, good irradiation experience is available for fuel containing up to 1.3 U/cm^3 in UZrH fuel clad in Incoloy and for UO_2 pellets with 9.1 g U/cm^3 clad in zircaloy and stainless steel. Reactor testing of UZrH production elements with both 1.3 and 3.7 g U/cm^3 is in progress in the TRIGA Mark F reactor at General Atomic, and a total of 600 cycles have been completed with positive results. An irradiation test of a standard 16-rod configuration is in progress in the ORR reactor. Extensive metallographic electron microprobe and X-ray diffraction examinations have shown that the structural characteristics of the more highly loaded alloys are essentially the same as those of standard TRIGA fuels. This supports the expectation of excellent long-term irradiation behavior.

Thus, it is likely that the fuel development effort now underway will provide the technical means of reducing enrichment in research and test reactors. Extensions of currently utilized fuels should allow the conversion of low and high power reactors and the new high density fuels should allow the conversion of very high power reactors.

REFERENCES

1. G. W. Gibson, "The Development of Powdered Uranium-Aluminide Compounds for Use as Nuclear Reactor Fuels," IN-1133, December 1967.

2. J. E. Cunningham, R. J. Beaver, W. C. Thurber, and R. C. Waugh, "Fuel Dispersions in Aluminum-base Elements for Research Reactors," Fuel Elements Conference, Paris, Nov. 1957, TID-7546 Bk. 1, pp. 269-297, March 1958.

3. R. O. Williams, "Metallurgy Division Quarterly Progress Report-Period Ending October 31, 1950," ORNL-910, pp. 9-11 (1951).

4. B. E. Paige, G. W. Gibson, and K. L. Rohde, "The Effect of Silicon on Fabrication and Reprocessing of Aluminum Alloy Reactor Fuels," IN-1194, November 1968.

5. J. R. Huffman, "Technical Quarterly Report-Fourth Quarter 1953," IDO-16153, pp. 27-28, February 1954.

6. GETR Safety Analysis Report, NEDO-12522, Vallecitos Nuclear Center, June 1977.

7. W. A. Erwin, General Electric, Nuclear Energy Division, Pleasanton, CA, Private Communication, March 1978.

8. A. E. Richt, C. F. Leitten, Jr., and R. J. Beaver, "Radiation Performance and Induced Transformations in Aluminum-Base Fuels," Research Reactor Fuel Element Conference, Sept. 1962, Gatlinburg, TN, TID-7642, Bk. 2, pp. 469-488.

9. W. C. Francis, G. W. Gibson, and W. P. Scarrah, "Some Results of Uranium Aluminum Irradiations at the MTR/ETR," Ibid., pp. 444-468.

10. H. W. Hassel, NUKEM GmbH, Hanau, Federal Republic of Germany, Private Communication, May 1978.

11. G. F. Merz, R. L. Frontroth, and J. R. Hester, Savannah River Laboratory, Aiken, SC, Private Communication, April 1978.

12. C. E. Weber and H. H. Hirsch, "Dispersion-Type Fuel Elements," Proc. Int'l. Conf. on Peaceful Uses of Atomic Energy," Geneva, Vol. 9, pp. 196-202 (1955).

REFERENCES (Cont.)

13. F. A. Rough and A. A. Bauer, "Constitution of Uranium and Thorium Alloys," BMI-1300, June 1958.

14. M. J. Graber, W. F. Zelezny, and G. W. Gibson, "Annual Progress Report on Reactor Fuels and Materials Development for FY 1964," IDO-17037, November 1964.

15. M. L. Picklesimer, "The Reaction of UO_2 with Aluminum," CF-56-8-135, August 1956.

16. "Safety Analysis-Utilization of Intermeatallic Uranium Aluminide and Uranium Oxide Cermet Fuel Cores in the Ford Nuclear Reactor," Univ. of Mich., Ann Arbor, License Submittal R-28, June 1977 (Rev. October 1977).

17. W. C. Francis, EG&G Idaho, Inc., Private Communication, June 1978.

18. W. Dienst, S. Nazare, and F. Thummler, "Irradiation Behavior of UAl_x-Al Dispersion Fuels for Thermal High Flux Reactors," J. Nucl. Mat'ls., 64, pp. 1-13 (1977).

19. J. H. Handwerk, R. A. Noland, and D. E. Walker, "Uranium-Oxide-Containing Fuel Element Composition and Method of Making Same," U.S. Patent 2,805,473, September 1957.

20. R. J. Beaver and J. E. Cunningham, "Recent Developments in Aluminum-Base Fuel Elements for Research Reactors," TID-7559, August 1959.

21. R. C. Waugh, J. E. Cunningham, and R. J. Beaver, "Aluminum-Uranium Oxide Reaction," in Uranium Oxide: Properties and Nuclear Applications, J. Belle (Ed.), USAEC, pp. 364-371, July 1961.

22. M. M. Martin, Oak Ridge National Laboratory, Oak Ridge, TN, Private Communication, April 1978.

23. M. M. Martin, A. E. Richt, and W. R. Martin, "Irradiation Behavior of Aluminum-Base Fuel Dispersions," ORNL-4856, May 1973.

24. J. D. Fleming and J. W. Johnson, "Aluminum-U_3O_8 Exothermic Reactions," Nucleonics 21(5), pp. 84-87 (1963).

25. L. Baker, J. D. Bingle, R. Warchal, and C. Barners, "Aluminum-U_3O_8 Thermite Reaction," ANL/CEN Semiannual Report July-December 1963, ANL-6800, pp. 390-402 (1964).

26. L. Baker and J. D. Bingle, "Aluminum-U_3O_8 Thermite Reaction," ANL/CEN Semiannual Report for January-June 1964, ANL-6900, pp. 298-303 (1964).

27. R. O. Ivins and F. J. Testa, "Studies with Aluminum-U_3O_8 Cermet Fuel in TREAT," Chemical Engineering Semiannual Report, July-December 1965.

28. M. T. Simnad and J. P. Howe, "Materials for Nuclear Fission Power Reactor Technology," GA-A14012, December 1976.

29. H. S. Kalish, et al., "Uranium Alloys," Reactor Handbook, Second Edition, Interscience Publ., New York, 1969, pp. 147-210.

REFERENCES (Cont.)

30. A. Boltax, "Behavior of Fissionable Material Under Irradiation," Nuclear Reactor Fuel Elements-Metallurgy and Fabrication, Interscience Publ., New York, pp. 292-361, (1962).

31. J. E. Draley, "Problems of Fuel Element Corrosion in Water," Nuclear Fuel Elements, Reinhold Publ., New York, pp. 314-328, (1959).

32. M. A. Feraday, et al., "Irradiation Behavior of Uranium-Silicide Fuels at High Power," Trans. Am. Nucl. Soc. 14(2), pp. 569-570 (1971).

33. W. R. McDonnel and E. F. Sturcken, "Development of High-Performance Uranium-Metal Fuels for Savannah River Reactors," Nuclear Tech., 26, pp. 420-429 (1975).

34. W. R. McDonnel and W. N. Rankin, "Swelling Resistance of Uranium Alloys at High Irradiation Exposures," DP-MS-71-1, Savannah River Laboratory, Proposed for Publ. in J. of Nucl Mat'ls.

35. B. R. Seidel and R. Einziger, "In-Reactor Cladding Breach of EBR-II Driver Fuel Elements," Int'l. Mtg. on Breeder Structural Mat'ls., Scottdale, AR, June 1977.

36. J. H. Kittel and K. F. Smith, "Effects of Irradiation on Some Corrosion - Resistant Fuel Alloys," ANL-5640, May 1960.

37. M. A. Feraday, et al., "The Irradiation Behavior of U_3Si Elements to High Burnup," AECL-4058, Chalk River Nuclear Laboratories, March 1974.

38. M. A. Feraday, et al., "Irradiation Behavior of a Corrosion Resistant U-Si-Al Fuel Alloy," AECL-5028, Chalk River Nuclear Laboratories, March 1975.

39. R. B. Holden, "Ceramic Fuel Elements," Gordon and Breach, New York (1966).

40. M. T. Simnad, "Fuel Element Experience in Nuclear Power Reactors," Gordon and Breach, New York (1971).

41. "Current Status and Future Technical and Economic Potential of Light Water Reactors," USAEC Report WASH-1082, March 1968.

42. "Operating Experience with Thermal Fuels," Proc. Joint Topical Meeting on Commercial Fuel Technology Today, Toronto, Canada, April 28-30, 1975.

43. Nuclear Systems Materials Handbook, TID-26666, Hanford Engineering Development Laboratory, Richland, Washington.

44. MATPRO-Version 09, A Handbook of Materials Properties for Use in the Analysis of Light Water Reactor Fuel Rod Behavior, TREE-NUREG-1005, EG&G, Idaho.

45. J. P. Schwartz, Uranium Dioxide Caramel Fuel, presented at Intl. Conf. on Nuclear Non-Proliferation and Safeguards, AIF, New York, Oct. 22-25, 1978.

46. T. D. Anderson, Effects of High Burnup on Bulk UO_2 Fuel Elements, Nucl. Saf. 6(2), 164-169 (1964).

REFERENCES (Cont.)

47. M. Rapin, CEA, France, personal communication (May 1978).

48. "Summary of TRIGA Fuel Fission Product Release Experiments," by F. C. Foushee and R. H. Peters, Gulf-EES-A10801 (1971).

49. "Review of UZr-Hydride Driver Fuel Elements for Thermionic Reactors," by M. T. Simnad, Gulf-GA-A11075, June 1972.

50. "An Empirical Study of SNAP Reactor Fuel Irradiation Behavior," by K. R. Birney NAA-SR-12284 (1967).

51. "Fission Product Release from TRIGA-LEU Reactor Fuels," by N. L. Baldwin, F. C. Foushee, and J. S. Greenwood, E117-830, to be published.

52. "Results of In-Core Tests on TRIGA-LEU Fuel Elements in the TRIGA Mark F. Reactor," by W. L. Whittemore, E117-835, to be published.

53. "The U-ZrH_x Alloy: Its Use in Standard and LEU TRIGA Fuel," by M. Simnad, E117-833, February 1980

54. "Physical Properties of TRIGA-LEU Fuel," by F. C. Foushee, E117-834, to be published.

55. "Low-Enriched TRIGA Fuel Water-Quench Safety Tests," by J. R. Lindgren and M. T. Simnad, GA-A15413, June 1979.

56. Proc. Intl. Mtg. of Research Reactor Fuel Designers, Developers, and Fabricators, Argonne National Laboratory, Nov. 9-10, 1978, in press.

APPENDIX I-1

Economic Aspects of Reactor Core Conversions for Classical Plate-Type Fuel

performed by A. Burtscher

Österreichische
Studiengesellschaft für Atomenergie
Ges.m.b.h.
Research Reactor Seibersdorf
Austria
February 1980

ABSTRACT

Fuel cycle costs for the 10 MW generic reactor are compared for HEU and LEU fuels using methods and assumptions based on the fuel cycle of the ASTRA reactor.

COMPARISON OF FUEL CYCLE COSTS FOR MTR-FUEL ELEMENTS WITH DIFFERENT ENRICHMENTS

1. Summary:

The fuel cycle cost components of a 1o MW Research Reactor, operated at a 4o % duty cycle, are compared for fuel elements with high (93 %), medium (45 %) and low enriched (2o %) uranium. The costs assessed are based on valid prices for uranium and reprocessing charges, on offers for HEU-fuel element fabrication and on price estimates from NUKEM for MEU- and LEU-fuel elements. The prices for shipment of fresh or irradiated fuel elements are based on recent offers and refer to the ASTRA, located near Vienna/Austria. The U-235 content of the fuel elements with MEU and LEU are based on or extrapolated from the "benchmark calculations".

Although some of the cost components assumed are valid only for the specific case assumed, the principal method of calculation can be applied to any research reactor. In order to generalize the results, some parametric studies were made, showing the influence of U-235 loading, fuel element fabrication price and burn up on the total fuel cycle costs.

The conversion of reseach reactor cores to MEU and LEU fuels increases most of the cost components of the fuel cycle, mainly due to the higher uranium content required for the fuel elements, the increased fuel element fabrication costs and to the increased reprocessing costs. The comparison of the different fuel cycle costs shows, that the cost increases can be compensated to a large extent, if the energy production per fuel element can be increased proportionally. The same costs/MWd as for HEU-fuel can also be obtained for MEU- and LEU-fuel, if the U-235 burn up is as high as in the reference HEU-fuel. For a given burn up fuel elements with higher U-235 loadings give lower cost per MWd. For 6o % burn up and under the assumptions made with respect to the required U-235 content of the MEU- and LEU-fuel elements one obtains a value of $ (16o $\pm$ 3)/MWd.

The influence of the uncertainties of the fuel element fabrication price for the MEU- and LEU-elements is small and remain in order of a few percent.

The burn up has the highest influence on the costs per MWd. Decreasing the U-235 burn up from 6o % to 5o % results in a cost increase of about 13 %. Keeping the burn up in terms of MWd's equal to the burn up of the HEU-reference fuel element, this results to lower percent burn up values and accordingly to higher fuel cycle costs per MWd.

The influence of the capital interest rate and escalation rate on the fuel cycle costs comparison can be considered from the results obtained as rather small. Assuming the capital interest rate 4 % higher than the escalation rate, one obtains by applying the "present money worth" method a 5 % reduction for the costs per MWd as compared with the generally used method in this paper, taking no time dependant factors into account.

2. Assumption made for the cost comparison

- Reactor Power: 1o MW
- Duty Cycle: 4o % (energy production/year: 146o MWd)
- Equilibrium Core: (core size 22 - 24 fuel elements).
  No specific assumption about core seize or core geometry is required for the cost comparison, exept that sufficient reactivity is available in order to achieve the specified burn up.
- Batch size of new fuel elements ordered:
  26 fuel elements (21 standard- and 5 control-fuel elements). This batch size was chosen with respect to the capacity of 26 elements of the two casks used for the shipment of spent fuel elements.
- HEU-Reference Fuel Element:
  23 plates standard element, 28o g U-235/el., 93,2 % enr.
  (control fuel element: 17 plates, 2o7 g U-235/el.)
- Burn up of Reference Fuel Element:
  6o % U-235 burn up, corresponding to 135 MWd/FE (1,25 g U-235/MWd)
- Fuel Loadings: The U-235 content for elements using MEU and LEU are derived from the "benchmark calculations" and from generic studies of core conversions to LEU by ANL.
  The following assumptions were made:
  MEU-Element: 32o g U-235 for 6o % burn up (ϱu = 1,6 g/cm^3)
  31o g U-235 for 135 MWd burn up (ϱu = 1,55 g/cm^3)

fuel element geometry: identical with
HEU-Reference Element (23 plates).

LEU-Element:

Different element designs have been assumed with respect to uranium loading, uranium density in the fuel meat and plate number. In order to obtain uranium densities which can be achieved in the near future ($\varrho < 3{,}0$ g/cm^3), the plate thichness was increased to 1,6o mm.

For 6o % U-235 burn up:

39o g U-235, 21 plates/FE, 2,9 g U/cm^3
35o g U-235, 21 plates/FE, 2,6 g U/cm^3
32o g U-235, 21 plates/FE, 2,4 g U/cm^3

For equal MWd burn up as HEU-Ref. FE (135 MWd):

35o g U-235, 21 plates, 2,6 g U/cm^3
32o g U-235, 19 plates, 2,62 gU/cm^3

- Fuel Element Weight: Calculated from fuel element geometry and fuel loading. Endfittings are assumed to be cut off before shipment to reprocessing plant.

HEU-Ref. FE (23 plates):		5,oo kg/FE
MEU-Ref. FE	:	5,4o kg/FE
LEU-FE: 39o g U-235,	21 plates:	6,65 kg/FE
35o g U-235,	21 plates:	6,5o kg/FE
32o g U-235,	21 plates:	6,35 kg/FE
	19 plates:	6,oo kg/FE

- Formula used: For the calculation of the uranium credit, the enrichment and the amount of the irradiated uranium is required. The following formulas were derived, assuming the ratio of $\sigma c/\sigma f = 0{,}17$ for U-235
Enrichment e(B) after burn up B:

$$e(B) = \frac{(1-B)\,e_o}{1-0{,}83\,B\,e_o}$$

e_o = original enrichment
B = burn up of U-235

- Remaining U-235 (B) after burn up B:

$$U_{235}(B) = U_{235}(O) \ (1 - B)$$

$U_{235}(O)$ .... Original amount of U-235

- Remaining $U_{total}(B)$ after burn up B:

$$U_{tot}(B) = U_{tot}(O) \quad (1 - 0{,}83\ B\ e_o)$$

(The production of Plutonium has been neglected)

- U-235 used per MWd:

1,25 g U-235/MWd

3. Fuel Cycle Cost Components

3.1 Total Uranium Costs

This cost component includes:

- Cost of enriched uranium according to presently valid prices for natural uranium and separative work units (see Table I).
- 2,5 % uranium losses during conversion and fuel element fabrication.
- Shipping costs of UF-6 from USA to Europe:
  costs assumed are based on the shipment of about 200 kg enr. uranium:
  $ 3000 + $ 550/kg U

3.2 Fuel Element Fabrication:

- Price for HEU-Reference fuel element:
  DM 12.000 ≅ US $ 6700
- Price for MEU-fuel element, 23 plates, (310 ± 10) g U-235
  NUKEM Estimate:
  1,15 x HEU Reference FE ≅ $ 7700
- Price for LEU-fuel element
  NUKEM Estimate:
  lower limit: 1,35 x HEU-Ref. FE ≅ $ 9000
  upper limit: 1,50 x HEU-Ref. FE ≅ $ 10000.
- Fresh Fuel Element Shipping Costs:
  $ 400/FE (based on offers)
- Total Fuel Element Fabrication Costs:
  FE Fabrication Costs + Shipping Costs

3.3 Shipping Costs for 26 Fuel Irradiated Elements:

$ 81.650 (based on offers)

(2 Casks for 13 elements each; Transport from ASTRA to reprocessing plant, Savanna River Plant/USA).

The shipping costs per fuel element are $ 3140; this value could be appreciably reduced, if the available crane and fuel storage facilities at the reactor station allow the use of larger and heavier casks.

3.4 Reprocessing Costs:

$ 400/kg U-Al

(based on current US-reprocessing prices including waste handling and storage: 41 Federal Register 36244,August 27, 1976).

3.5 Net Uranium Credit:

- Price for the uranium in the 26 irradiated fuel elements shipped to reprocessing plant, (Interpolation from Table I for different enrichments) reduced by the price of the uranium cost and by handling and shipping and conversion charges:
- Uranium losses during reprocessing and conversion: 2,5 %
- Conversion costs: $ 260/kg U
- Shipping charges to reprocessing plant: 2 % of uranium credit.

From the burn up values assumed, the following enrichments are obtained for the reprocessed uranium:

Fuel	Orig. enrichments	burn up	enrichment of the reprocessed uranium
HEU	93 %	60 %	69,14
MEU	45 %	60 %	23,10
	45 %	310 g U-235/FE 135 MWd ≙ 54,4 %	25,60
LEU	20 %	60 %	8,9
	20 %	350 g U-235/FE 135 MWd ≙ 48,2 %	11,3
	20 %	320 g U-235/FE 135 MWd ≙ 52,7 %	10,4

4. Comparison of Fuel Cycle Cost Components

The comparison of the 5 fuel cycle cost components listed above is summarized in Table II and Table III.

In Table II a U-235 burn up of 6o % was assumed; in Table III, the same burn up in terms of MWd as for the HEU-reference fuel elements (135 MWd/ standard FE and 1oo MWd for the control FE) was taken into account for the MEU and LEU elements.

In both tables, the time scale is indicated, when the different costs are incurred.

For this time table, the following assumption were made:
- Insertion of first fuel elements into the core: 12 months after uranium costs are incurred.
- Shipment Costs: 6 month after the last fuel element of the 26 elements batch has been removed from the core.
- Reprocessing Costs: 12 month after last fuel element removal.
- Net Uranium Credit: 18 month after last fuel element removal.

From the Tables II and III it can be seen, that the main cost components of the fuel cycle are the uranium and the fuel fabrication costs. They represent for the fuel cycle of the ASTRA under the assumptions made nearly the total fuel cycle costs. The remaining costs for shipment and reprocessing of the spent fuel are incurred about 3 - 4 years later and are nearly balanced by the net uranium credit. As a first approximation, no attempt was made for this comparison to refer all costs to the beginning of the fuel cycle (present money worth) or to introduce escalation factors, taking into account future incrases of the cost components. The influence of these factors is discussed later in this paper. The total fuel cycle costs shown in Tables II and III are therefore the sum of the cost components assumed.

It can be seen that the costs per MWd remain constant, if equal U-235 burn up as for the HEU-reference fuel can also be achieved for the MEU and LEU fuel. However, assuming equal energy production per element as for the HEU-reference element, the costs per MWd increase by 6 % and (22 $\pm$ 2 %) for the MEU and LEU fuel respectively.

In the last line of the Tables II and III an attempt was made to estimate the relative costs for the MEU and LEU fuel per unit fluence, assuming a value of 1oo for the HEU-reference fuel. From the "benchmark calculation" the following ratios of thermal neutron fluxes were assumed:

	central irradiation channel	edge of graphite reflector (beam tubes)
$\frac{\phi \text{ MEU}}{\phi \text{ HEU}}$	0,97	0,92
$\frac{\phi \text{ LEU}}{\phi \text{ HEU}}$	0,925	0,85

The main purpose of operating a research reactor is the production of neutrons for irradiation and for beam tube experiments. Therefore the cost per unit of neutron fluence as compared with the HEU core seem to be a proper measure to indicate the penalties obtained from a core conversion to MEU or LEU fuel.

The relative costs per fluence unit indicated in Table II represent a rough estimate only, because the flux values used were derived from the benchmark calculations and not from calculated flux distributions of a realistic research reactor core.

5. Parametric Calculations

The method of calculation outlined in Table I and II has been applied to fuel elements with different U-235 loadings and different burn up values. The results are shown graphically in the Figures 1 - 3.

In Fig. 1 and 2, the influence of the fuel element fabrication cost for LEU-fuel is shown as a function of the U-235 loading. From the "Benchmark Calculations" and the "ANL-Generic Calculations" one can assume the range from 35o g U-235/FE to 39o g U-235/FE as a realistic range for the U-235 loading required for LEU-fuel elements for a 1o MW reactor. Assuming further the range from $ 9ooo to $ 1oooo as the probable fabrication price for LEU-fuel elements, one obtains for a burn up value of 6o %

$$\$ \ (165 \pm 8)/\text{MWd}$$

as an estimate of the probable LEU-fuel cycle costs. Compared with $ 162/MWd for the HEU-reference fuel element, the difference can be considered as marginal.

In Fig. 3, the influence of the U-235 burn up on the fuel cycle costs is shown over a wide range of burn up values. The fuel cycle costs in terms of $/MWd are inversely proportional to the burn up B; therefore one expects a hyperbolic shape of the cost/MWd function. Due to the increasing uranium credit with decreasing burn up, the actual shape of the cost/MWd function increases slower with lower burn up values than the CONST/B curve.

The LEU-fuel element containing 39o g U-235 gives in the burn up range considered nearly the same fuel cycle costs as the HEU-reference element. For the lower U-235 loadings considered (35o g and 32o g U-235) the burn up would have to be increased by about 6 % and 1o % respectively to obtain the same costs/MWd. However, the maximum burn up will be limited by the available excess reactivity in the core which decreases with decreasing U-235 loading in the fuel element. The real costs as a function of fuel loading can only be calculated knowing the achievable burn up values of the fuel elements at the time of discharge from the reactor core. It can be concluded that the fuel cycle costs for LEU-fuel elements with lower loadings than 39o g U-235/FE increase faster than indicated by the intersection of the ordinate at a certain burn up value with the curves shown in Fig. 3.

In Fig. 4 the influence of the shipment costs for irradiated fuel elements is shown. Using larger and heavier casks, the shipping costs per fuel element can be reduced up to a factor of 2 as compared with the assumptions made for the ASTRA; however, a longer storage of the irradiated fuel elements is required.

6. Influence of Capital Costs and Escalation

The fuel cycle considered in Table II and III extent over several years depending on the reactor power and the duty cycle. During such long periods the costs of the fuel cycle components increase; on the other hand, costs wich are incurred after a few years are smaller in terms of the present money worth.

In order to compare costs which are due at different times as it is the case in the fuel cycle, one refers all cost components to the beginning of the cycle, by multiplying the cost component $K_i(ti)$ which will be due at the time ti by the factor

$$fp(ti) = \left(\frac{1}{1+p}\right)^{ti/12}$$

p : capital interest rate/year
ti: time in months

The fuel cycle cost component K_i (ti) due at the time ti can be obtained from the present costs K_i multiplied by the escalation factor fe(ti):

$$K_i(ti) = K_i \quad fe(ti) = K_i(1+e)^{ti/12}$$

e: escalation rate/year

The sum of the fuel cycle component costs referred to the beginning of the cycle is therefore obtained as follows:

$$K(O) = \sum_{i=1}^{n} K_i(O) = \sum_{i=1}^{n} K_i \quad fe(ti) \quad fp(ti) =$$

$$= \sum_{i=1}^{n} K_i \left(\frac{1+e}{1+p}\right)^{ti/12}$$

$K_i(O)$ stands for the fuel cycle component cost referred to the beginning of the cycle (ti = o)

For small values of e and p, the ratio $\frac{1+e}{1+p}$ can be approximated by 1-(p-e). Therefore, the influence of the capital interest rate and the escalation rate on the total fuel cycle costs essentially depends on the difference (p - e) and only to a very small part on the absolute value of p or e.

As an example, the total fuel cycle costs of two batches a 26 MTR fuel elements are calculated in Table IV for different values of (p - e). In the MTR-fuel cycle, the component cost for shipment and reprocessing of the irradiated fuel are essentielly covered by the uranium credit; therefore, the application of the present worth method has a negligible influence on the results obtained in the Tables II and III. Therefore, in order to demonstrate the present worth method including the effect of escalation, the MTR- fuel cycle was extended to 2 x 26 fuel elements. In Fig. 5 the results are shown as a function of (p-e). Shortening the cycle length by assuming a higher duty cycle or a higher reactor power reduces the influence of the capital interest and the escalation rate. In the calculation shown in the Tables II and III the influence of capital costs and escalation has not been considered; this can be interpreted as assuming the capital interest rate and escalation rate to be equal (p = e).

From the results shown in Fig. 5, one can conclude that the influence of (p - e) is small for the set of assumptions made and that the conclusions drawn from the simpler method applied in the Tables II and III have not to be changed.

ENRICHED URANIUM PRICES

Assumptions made:

Tails assay: o,2 %
Cost of Separative Work Unit (SWU): US $ 98.35/SWU (after Oct. 1979)
Cost of Natural Uranium after Conversion to UF-6, incl. o,5 Conversion losses: US $ 117.2/kg U_{nat}.

Enrichment	kg U_{nat} required	Costs for U_{nat} (S)	SWU	Costs for Enrichment	Price for 1 kg $U_{enr.}$	U-235
5 %	9,39	11oo,5	8,851	875,5o	1971,oo	3942o,o8
1o %	19,178	2247,66	2o,866	2o52,17	4299,83	42998,33
15 %	28,963	3394,46	33,228	3267,97	6662,44	44416,25
2o %	38,748	4541,27	45,752	4499,71	9o4o,98	452o4,87
3o %	58,317	6834,75	71,o71	6989,83	13824,59	46681,95
4o %	77,886	9128,24	96,616	95o2,18	1863o,42	46576,o6
45 %	87,671	1o275,o4	1o9,48	1o767,36	21o42,4o	4676o,89
5o %	97,456	11421,84	122,344	12o32,53	23454,38	469o8,75
6o %	117,o25	13715,33	148,25	1458o,39	28295,72	47159,53
7o %	136,595	16oo8,93	174,32	17144,37	33153,31	47361,87
8o %	156,164	183o2,42	2oo,624	19731,37	38o33,79	47542,24
9o %	175,734	2o596,o3	227,363	22361,15	42957,18	4773o,2o
93,2 %	181,996	21329,93	236,127	23223,o4	44552,98	478o3,62

Table I

COMPARISON OF FUEL CYCLE COSTS FOR MTR-FUEL ELEMENT WITH DIFFERENT ENRICHMENTS

Assumptions: Burn up of U-235: 6o %
Reaktor Power: 1o MW
Duty Cycle: 4o %

Cost Component of Fuel Cycle	HEU (93 %)		MEU (45 %)		LEU (2o %): 21 Plates/FE					
	Costs of Fuel Element Fabrication									
	Month	HEU Ref.FE $ 67oo	Month	1,15xHEU Ref.FE $ 77oo	Month	1,35xRef.FE $ 9ooo	1,5oxHEU Ref.FE $ 1o ooo	Month	1,35xRef.FE $ 9ooo	1,5oxHEU Ref.FE $ 1o ooo
U-235 Loading/FE [g]		28o		32o		39o	39o		35o	35o
Total Uranium Costs [$]	0	346 o83	0	396 263	0	474 o72	474 o72	0	425 682	425 682
FE-Fabrication [$]	9	184 6oo	9	21o 6oo	9	244 4oo	27o 4oo	9	244 4oo	27o 4oo
Subtotal: U + FE.Fabr.Costs [$]		53o 683		6o6 863		718 472	744 472		67o o82	696 o82
Shippment of Irr.FE [$]	45	81 65o	49	81 65o	56	81 65o	81 65o	52	81 65o	81 65o
Reprocessing Costs [$]	51	52 ooo	55	56 16o	62	69 oo4	69 oo4	58	67 6oo	67 6oo
Net Uranium Credit [$]	57	-124 o11	61	-133 942	68	-145 243	-145 243	64	-13o 172	-13o 172
Total Fuel Cycle Costs [$]		54o 322		61o 731		723 883	749 883		689 16o	715 16o
MWd Produced		3 335		3 794		4 6oo	4 6oo		4 128	4 128
$/MWd		162,o		161,o		157,4	163,o		167,o	173,3
Rel.Costs/Fluence Unit		1oo		1o3 -1o8		1o5- 114	1o9- 118		111 -121	116 -126

Tabel II

FUEL CYCLE COSTS FOR MTR-FUEL ELEMENTS WITH DIFFERENT ENRICHMENTS

Assumption: Burn up of Fuel: 3335 MWd (as HEU-Ref. Fuel)
Reactor Power: 1o MW
Duty Cycle: 4o %

Fuel Cycle Cost Components	Months	HEU (93 %)	MEU (45 %)	LEU (2o %): 21 Plates/FE		LEU (2o %): 19 Plates/FE	
		Costs of Fuel Element Fabrication					
		Ref. FE $ 67oo	1,15xHEU Ref.FE $ 77oo	1,35 x Ref. FE $ 9ooo	1,5o x HEU Ref.FE $ 1o ooo	1,35 x Ref.FE $ 9ooo	1,5o x HEU Ref.FE $ 1o ooo
U-235 Loading/FE		28o	31o	35o	35o	32o	32o
Total Uranium Costs [$]	o	346 o53	384 236	425 682	425 682	39o 77o	39o 77o
FE-Fabrication [$]	9	184 6oo	21o 6oo	244 4oo	27o 4oo	244 4oo	27o 4oo
Subtotal: U + FE-Fabr.Costs [$]		53o 683	594 836	67o o82	696 o82	635 171	661 17o
Shippment of Irr.FE [$]	45	81 65o	81 65o	81 65o	81 65o	81 65o	81 65o
Reprocessing Costs [$]	51	52 ooo	56 16o	67 6oo	67 6oo	62 4oo	62 4oo
Net Uranium Credit [$]	57	-124 o11	-148 486	-175 144	-175 144	-147 354	-147 354
Total Fuel Cycle Costs [$]		54o 322	584 16o	644 188	67o 188	636 349	657 866
MWd Produced		3 335	3 335	3 335	3 335	3 335	3 335
$/MWd		162,0	175,2	193,2	2o1,o	189,5	197,2
Rel.Costs/Fluence Unit		1oo	1oo - 115	13o -14o	135- 146	128 -138	133 -144

Table III

Total Fuel Cycle Costs of 2 x 26 MTR-Fuel Elements

Assumptions: Reactor Power: 1o MW; Duty Factor: 4o %

LEU-Fuel Element (39o g U-235; FE.Fabr. Costs: $ 1o.ooo)

Escalation rate: 8 %/year

Capital interest rate: 8 %, 1o %, 12 % 14 %; (p - e)= O%,2 %, 4 %, 6 %

$$f(ti) = fp(ti) \times fe(ti) = \left(\frac{1+e}{1+p}\right)^{ti/12}$$

Time ti /months/	Fuel Cycle Cost Component	p - e = O		p - e = 2 %		p - e = 4 %		p - e = 6 %	
		f(ti)	K /k$/	f(ti)	Kxf(ti) /k$/	f(ti)	Kxf(ti) /k$/	f(ti)	Kxf(ti) /k$/
O	Uranium + FE.Fabrication for 26 FE.	1,o	746	1,o	746,o	1,o	746,o	1,o	746,o
38	Uranium + FE.Fabrication for 26 FE.	1,o	746	O,9436	7o3,9	O,8912	664,9	O,8426	628,6
47	Shipment of 26 FE.	1,o	82	O,93o7	76,3	O,8672	71,1	O,8o92	66,4
53	Reprocessing of 26 FE.	1,o	68	O,9222	62,7	O,8516	57,9	O,7876	53,6
53	Net Uranium Credit for 26 FE.	1,o	- 145	O,9222	- 133,7	O,8516	- 123,5	O,7876	- 114,2
85	Shipment of 26 FE.	1,o	82	O,8781	72,o	O,7729	63,4	O,6818	55,9
91	Reprocessing of 26 FE.	1,o	68	O,87o1	59,2	O,759o	51,6	O,6636	45,1
91	Net Uranium Credit for 26 FE.	1,o	- 145	O,87o1	- 126,2	O,759o	- 11o,1	O,6636	- 96,2
	Total fuel cycle costs referred to time O		15o2		146o,2		1421,3		1385,2
	Cost/MWd $/MWd		163,2		158,7		154,5		15o,6

TABLE IV

LEU-FUEL CYCLE COSTS IN $/MWd VERSUS U-235 LOADING

PARAMETER: FUEL ELEMENT FABRICATION COSTS

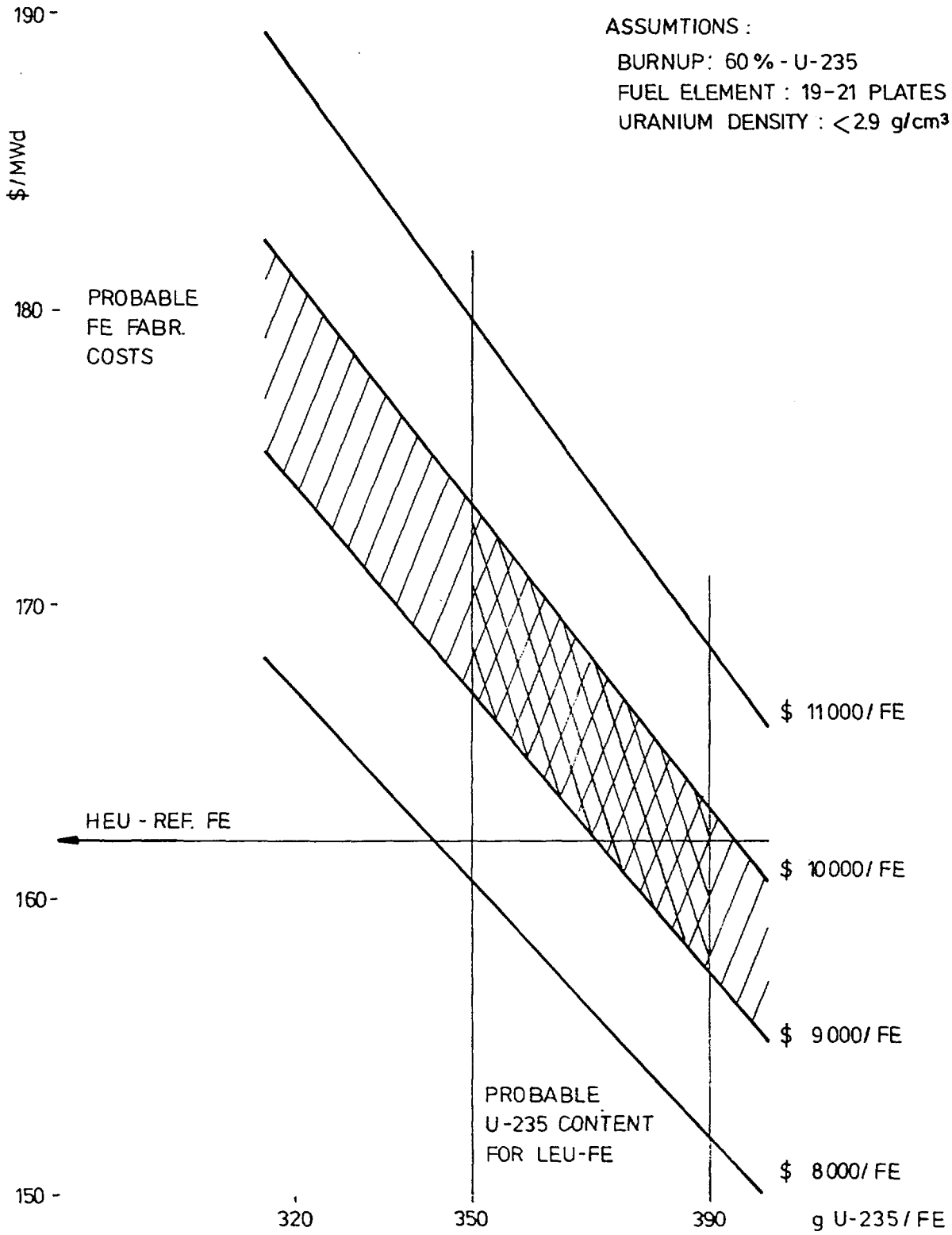

Fig.: 1

LEU-FUEL CYCLE COSTS IN $/MWd VERSUS FUEL ELEMENT FABRICATION COSTS

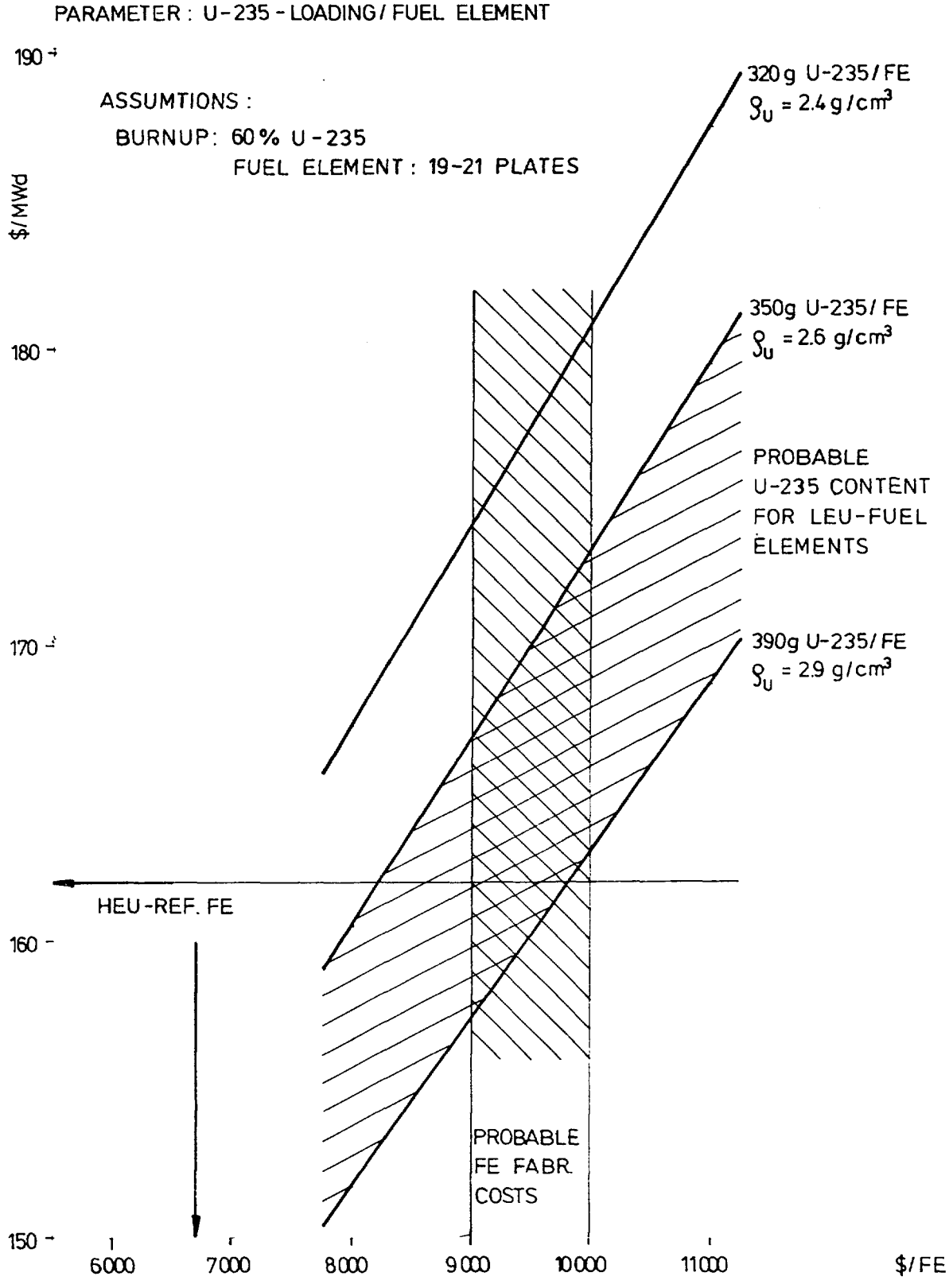

Fig.: 2

LEU-FUEL CYCLE COSTS IN $/MWd AS A FUNCTION OF U-235 BURNUP

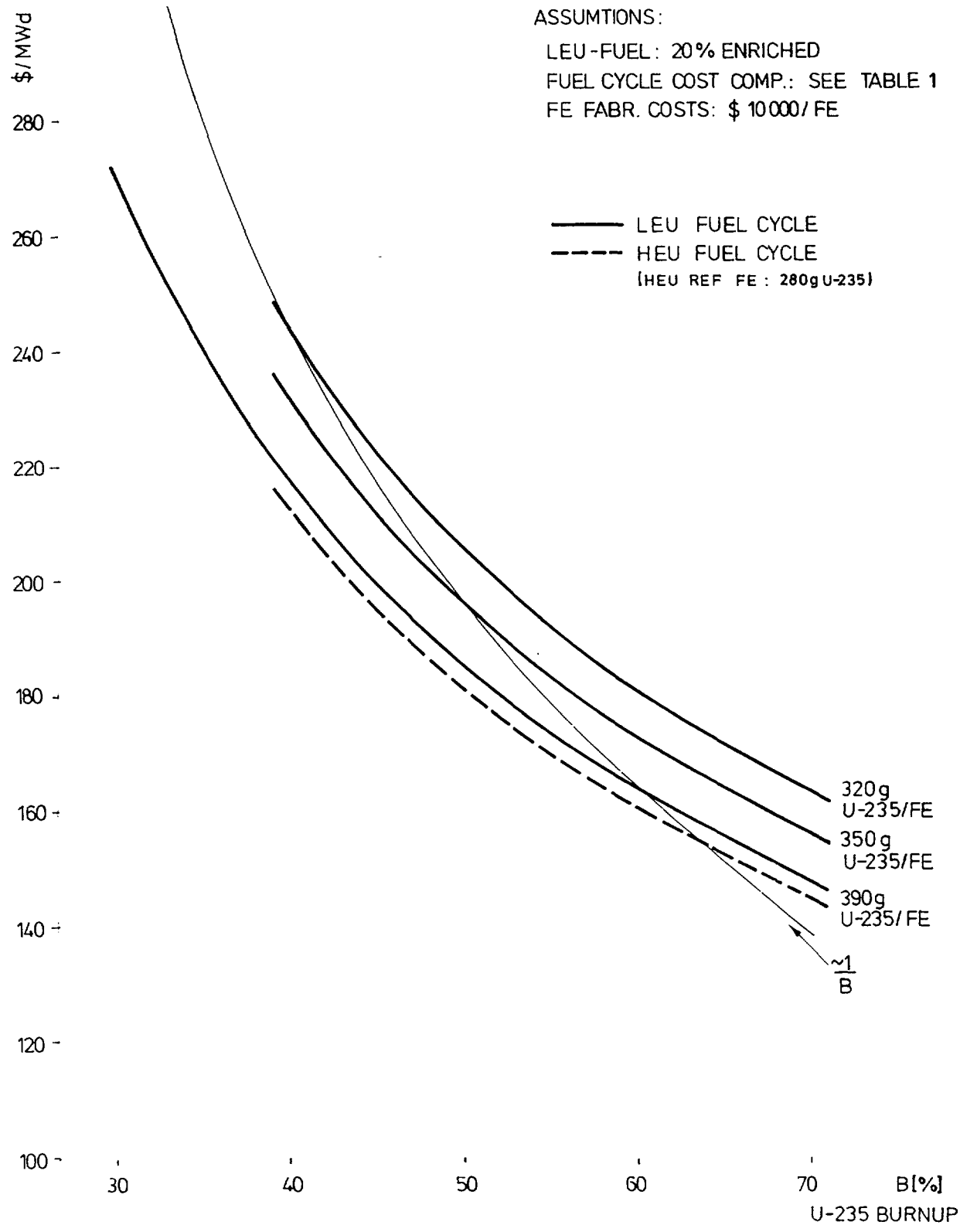

Fig.: 3

INFLUENCE OF SHIPMENT COST FOR IRRADIATED FUEL ON TOTAL FUEL CYCLE COSTS / MWd

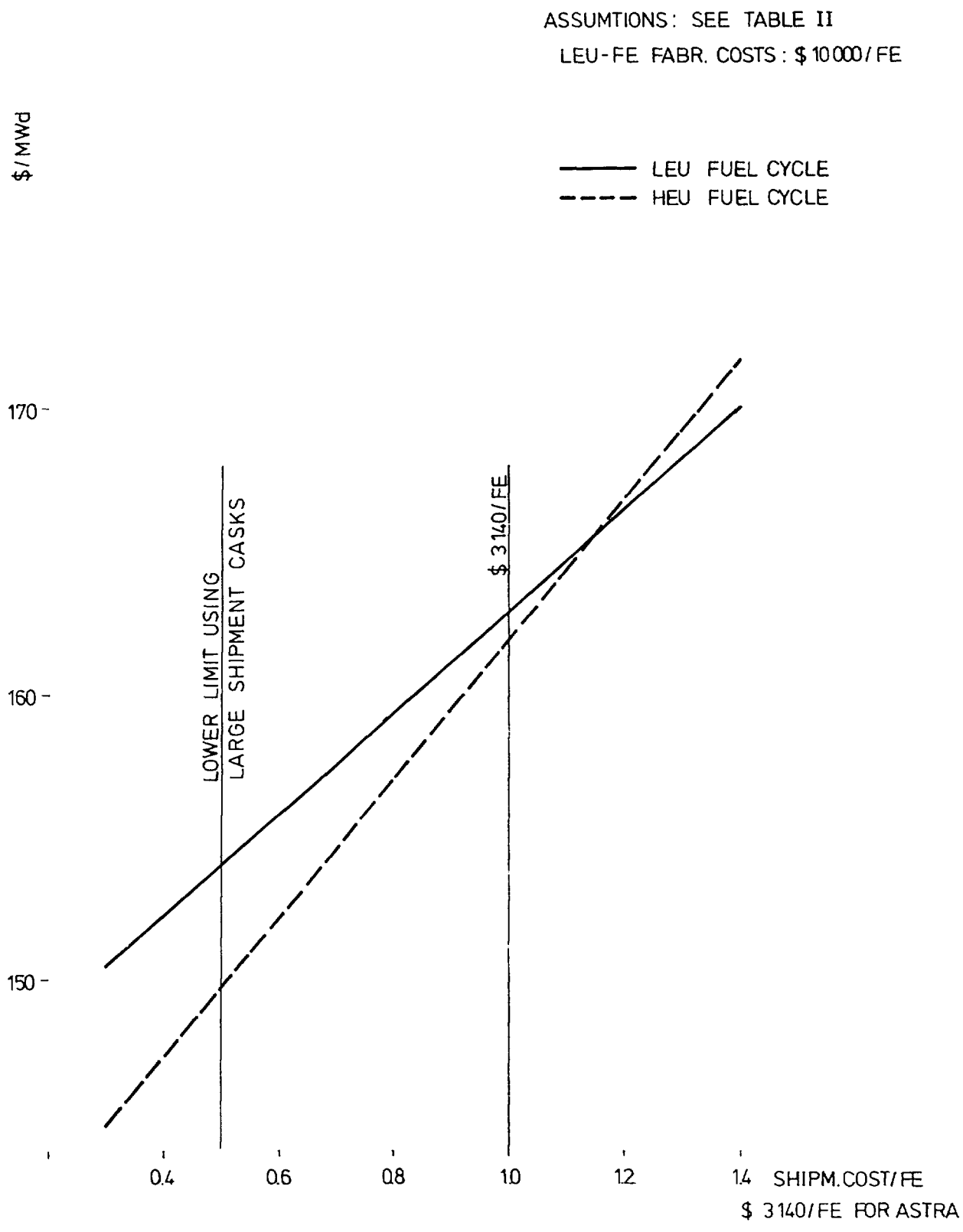

Fig.: 4

INFLUENCE OF CAPITAL INTEREST RATE AND ESCALATION RATE ON THE MTR FUEL CYCLE COSTS

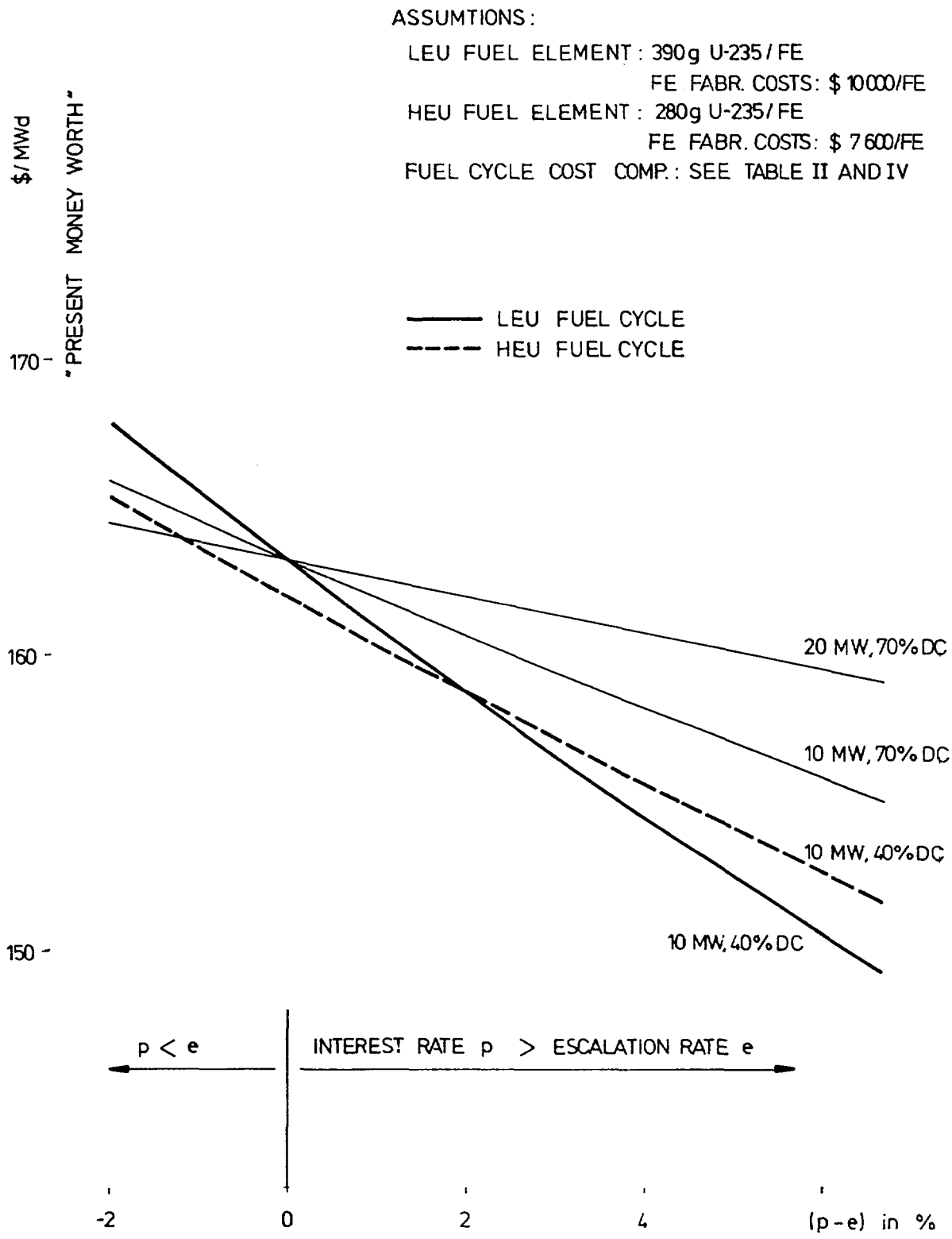

Fig.: 5

APPENDIX I-2

Economic Aspects of Reactor Core Conversions for TRIGA Fuel

performed by

General Atomic Company
P. O. Box 81608
San Diego, California 92138
U.S.A.

April 1980

ABSTRACT

Fuel cycle costs are presented for HEU and LEU TRIGA cores, and for HEU plate-type cores converted to LEU UZrH rod-type fuel. A simplified method for estimating fuel cycle costs for various types of cores is also presented.

INTRODUCTION

In addition to the technical and operational aspects that must be considered in reducing enrichment or in selecting a research reactor fuel, consideration must be given to the economics of the fuel cycle. The tendency to consider only the initial purchase price of the fuel elements can be very misleading. There are many other parameters which influence the overall fuel cycle cost and this cost can vary widely depending on the type of fuel used, its U-235 loading, core life, achievable burnup, cost escalation, shipping and reprocessing costs, etc.

Reactor users have various options in converting from highly enriched uranium (HEU) to low enriched uranium (LEU) fuel. TRIGA reactors which presently use HEU fuel can convert to low enriched, UZrH fuel which is currently available. MTR reactors can be converted to aluminide, U_3O_8, UO_2, or to other types of fuel in plate geometry which are under development, or they can convert to UZrH rod type elements which are currently available with low enrichment and are designed to directly replace MTR elements.

This section presents a simplified method for evaluating the fuel cycle costs for research and test reactors in order to compare alternative fuel types, and also presents calculated fuel cycle costs for the UZrH fuel using General Atomic's current catalog prices. The methods used are basically the same as used for the analysis presented in the previous section. General Atomic has computerized the analysis for ease in evaluating the effects of parameter variations.

1. SIMPLIFIED METHOD FOR ESTIMATING FUEL CYCLE COSTS

Rather than reproduce the equations used in the computer program a simplified method was developed which closely approximates the results of more detailed calculations. This equation is provided to allow reactor owners to estimate their fuel cycle costs for several different available fuel types. This method will also provide an estimate of anticipated costs and allow comparison of different reactor types for institutions evaluating a new reactor purchase.

For the purposes of this estimate it is assumed that a complete core is replaced when all of the fuel has achieved the same burnup as would be obtained by individual fuel elements. It is recognized that in an operating reactor a new fuel element is added when needed to provide the required excess reactivity. However, this method will provide a good approximation and the burnup fraction to be used is the average of that reached in spent elements which are removed.

The formula does not address cost escalation or the cost of invested capital. The results obtained will be the same as if these factors were included but with equal values. This is a good approximation for making an estimate. A detailed cost evaluation including parameters for a specific case should be made in conjunction with the fuel supplier.

The fuel Cycle Cost (FCC) in $/calendar year can be estimated as follows:

$$FCC = \frac{N\ (FF) + 51{,}500\ M_1 - 44{,}000\ M_2 + 120{,}000}{L}$$

where:

FF - the estimated Fuel Fabrication price of a fuel element in the year purchased (does not include the uranium value).

N - the total Number of fuel elements in the operating core for which the burnup specified is attained (typically 25 - 30).

M_1 - the Mass of U-235 in the initial core in Kg.

L - core Life in calendar years determined by the following formula:

$$L = \frac{BM_1}{0.00125\ (MWD)}$$

where B = Fraction of U-235 which has been consumed when the fuel element is removed (typically 0.2 to 0.5). The actual value depends on core size, fuel type, U-235 loading and operational conditions.

MWD = the number of Megawatt-Days the reactor is operated each year.

0.00125 = a constant that relates the burnup of U-235 to the energy produced, neglecting any plutonium contribution.

M_2 - the Mass of U-235 in Kgs remaining in the spent core, determined by:

$M_2 = M_1\ (1 - B)$

51,500 is the approximate cost of uranium ($/Kg of U-235) as of January 1, 1980. This value includes the U.S. Government charge for conversion of UF_6 to uranium metal and an allowance for production losses, waste and scrap recovery. The cost of U-235 is nearly independent of enrichment in the 4% to 93% enrichment range.

44,000 is the dollar value of the degraded-enrichment uranium recovered from the spent fuel as of January 1, 1980. This constant is a good from 8% to fully enriched. For fuel with an initial enrichment of less than 8%, this constant should be 35,000.

120,000 is the approximate dollar cost of shipping and reprocessing a 25-element core, as of January 1, 1980. Actual reprocessing costs depend upon an element's total metal weight and the residual uranium. Shipping costs will vary depending on distance to the reprocessor. However, these variations are small compared to the total fuel cycle cost estimate.

2. FUEL CYCLE COST EVALUATIONS

General Atomic has developed a computer program which enables investigation of the influence of each of the many variables on the overall fuel cycle cost for research reactors. This type of analysis is best applied on a case by case basis, however analyses of various parameters affecting the fuel cycle costs have been completed for UZrH fuel and the results are presented in this section.

The analyses include direct comparison of fuel cycle costs for converting an HEU-TRIGA to an LEU-TRIGA as the prices for these two types of elements are the same and are published. For the MTR conversions, the effects of a number of variables on the UZrH-LEU fuel cycle cost were investigated. These variables include power level, burnup, uranium loading, reprocessing costs, escalation, and present value factor. The reference cases assume equal values of escalation and present value factor. The effect of these two variables was investigated and is shown separately.

The effect of the enrichment reduction for a TRIGA reactor is shown in Table 1. For powers up to 15 MW the enrichment is reduced from 93% to 19.9% and the uranium content in the fuel is increased from 10 to 45 wt-%. The U-235 loading for the LEU case is slightly higher than for the HEU case, resulting in a longer lifetime and lower fuel cycle cost.

For the 2 MW case the enrichment is reduced from 70% (FLIP fuel) to 19.9% and the uranium content is increased from 8.5 to 20 wt-%. In this case the U-235 content for the LEU replacement is lower and results in a increase in the fuel cycle cost.

TABLE 1
TRIGA FUEL CYCLE COSTS (DOLLARS/MW-DAY)

	2 MW (40% burnup)	5-15 MW (60% burnup)
HEU	237	155
LEU	304	137

For conversion of MTR type reactors of 3-15 MW to low-enriched UZrH, General Atomic provides the 16-rod cluster described in Appendix B. The characteristics of principal importance to the economic evaluation is the very high U-235 loading (880 gms/element) which results in a very long core lifetime. This reduces the need for replacement fuel and also reduces fuel handling, shipping and reprocessing costs. Current prices for fabrication, uranium, shipping and processing result in a fuel cycle cost of $137/MW-Day for a burnup of 60%.

The average percent burnup of the U-235 achieved in the fuel removed from the reactor has an important impact on the overall fuel cycle cost as shown in Fig. 1.

One of the uncertainties in the fuel cycle cost analyses is the cost of reprocessing. The reference case value is that currently published by the U.S. government, i.e. $145/Kg for UZrH fuel. This is subject to change since the current published policy is valid only until December, 1982. In spite of the uncertainty in this parameter it is shown in Fig. 2 that the total fuel cycle costs are not changed substantially over a wide range in reprocessing costs. A change in reprocessing cost has less effect on UZrH fuel than on plate-type because the number of cores to be reprocessed with UZrH fuel is significantly less as a result of its longer lifetime.

The fuel cycle costs are affected by price escalation and the cost of invested capital, "the present value factor" (PVF). These numbers are subject to some uncertainty and will vary from time to time. Since the analysis presents all costs in terms of current dollars, the important parameter is the difference between the present value factor and the escalation rate. Fig. 3 shows the variation in fuel cycle cost for UZrH fuel with this difference. The value of this difference varies from time to time with economic conditions.

It is assumed in the analysis that the uranium prices escalate at the same rate as the fabrication cost; however, in recent years uranium price has escalated at a significantly higher rate. Since the spent UZrH fuel has a higher uranium content than the plate fuel, the escalation in the uranium price more than offsets the escalation in the fabrication and reprocessing cost, with some resultant benefit on fuel cycle cost.

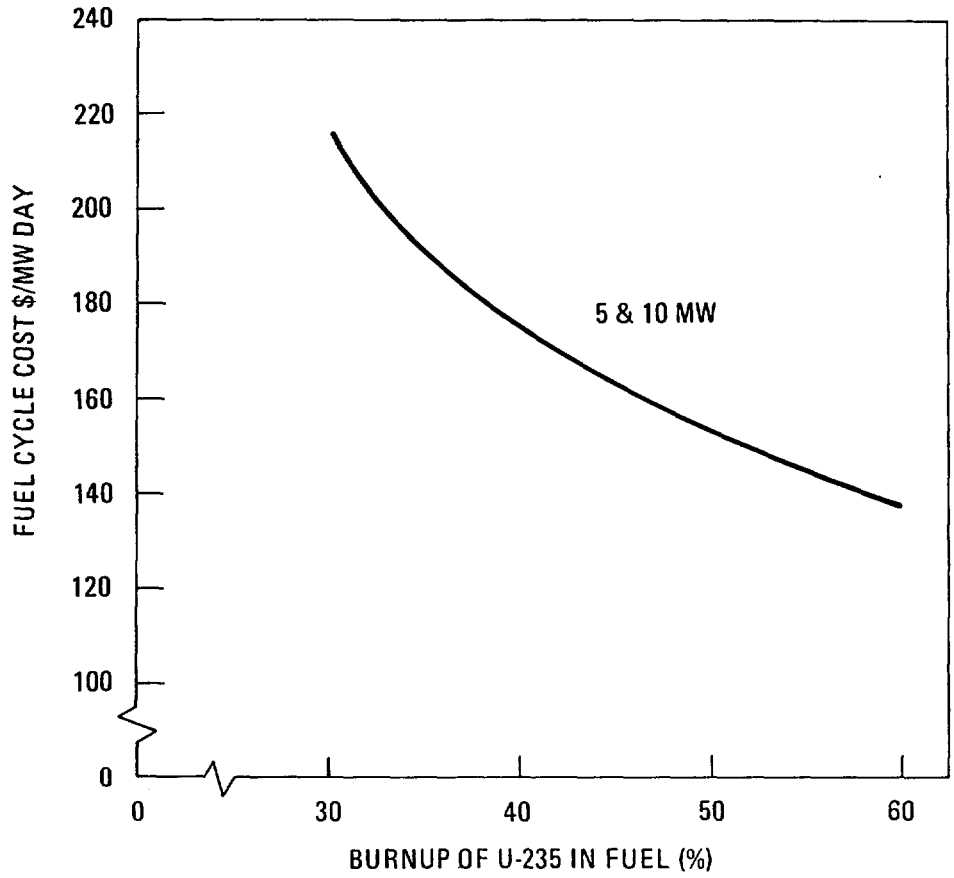

Fig. 1. Influence of Burnup on Fuel Cycle Cost

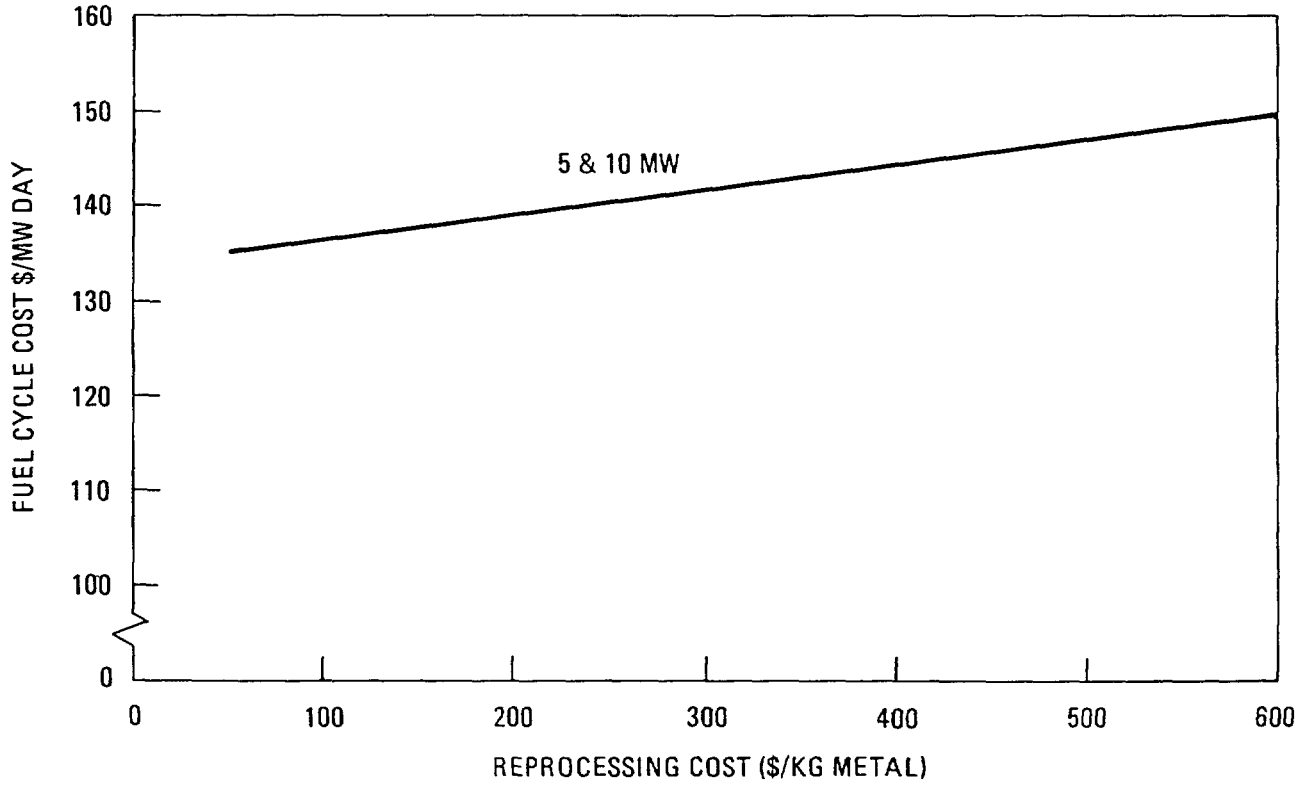

Fig. 2. Influence of Reprocessing Costs on Fuel Cycle Costs

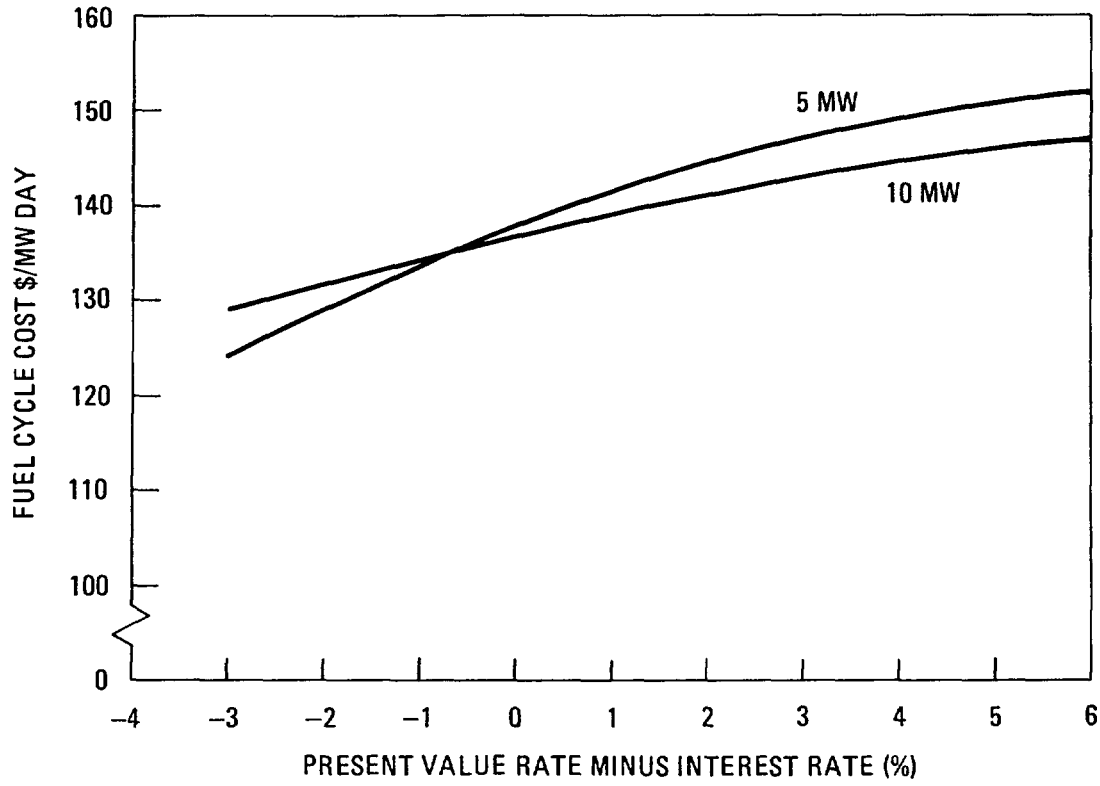

Fig. 3. Influence of the Difference in Escalation and Interest Rates on Fuel Cycle Cost

	1978	1979			1980	
	29Nov-01Dec.	19-21 June	10-12 Sept	10-11 Dec	11-12 March	17-23 April
FRANCE						
J. Doumerc CERCA 41 Avenue Montaigne 75008 Paris	x					
F. Joly CERCA 9-11 rue Georges Enesco 94000 Créteil		x	x	x	x	
B. Lerouge CEN Saclay B.P. no. 2 91190 Gir-sur-Yvette					x	
J. P. Schwartz CEN Saclay B.P. no 2 91190 Gif-sur-Yvette	x	x	x	x	x	x
GERMANY FED. REP.						
J. Benemann Interatom Friedrich-Ebert Strasse D-5060 Bergisch Gladbach 1	x	x	x	x		
H. W. Hassel NUKEM GmbH D-6450 Hanau 11	x	x	x	x	x	
M. Hrovat NUKEM GmbH D-6450 Hanau 11			x	x		
M. Kuechle Institut für Neutronenphysik und Reaktorphysik Kernforschungszentrum Karlsruhe (KFK)	x	x	x	x	x	
H. J. Roegler Interatom Friedrich-Ebert-Strasse D-5060 Bergisch Gladbach 1	x	x	x	x	x	
K. Wasserroth Hahn-Meitner-Institut für Kernforschung Berlin GmbH Glienicker Strasse 100 1000 Berlin 39					x	
GREECE						
N. G. Chrysochoides Reactor Division N.R.C. Demokritos Aghia Paraskevi, Athens	x			x		

	1978	1979			1980	
	29Nov-01Dec.	19-21 June	10-12 Sept	10-11 Dec	11-12 March	17-23 April
IRAN						
M. Sohrabpour Nuclear Research Centre Atomic Energy Organization of Iran PO Box 3327, North Amirabad Avenue Tehran	x					
JAPAN						
K. Kanda Research Reactor Institute Kyoto University Kumatori-cho, Sennan-gun Osaka 590-04				x	x	
S. Matsuura JAERI, Fukoku Seimei Bldg, 2-2, Uchisaiwai-cho 2 chome Chiyoda-ku, Tokyo 100					x	
Y. Naito Research and Development Office, Division of JPDR Tokai Research Establishment Tokai-mura, Naka-gun Ibaragi-ken 319-11				x		
PAKISTAN						
K. M. Akhtar Reactor Operation Group PINSTECH, Pakistan Atomic Energy Commission PO Box 1114, Islamabad	x					
POLAND						
W. Byzsewski Institute of Nuclear Research 05-400 Otwock	x					
ROMANIA						
N. Andreson Institute of Nuclear Power and Reactors BT 5203 Bucharest	x					
SWITZERLAND						
M. H. Winkler Institut féderal de recherches en matière de réacteurs 5303 Würnelingen		x	x	x	x	

	1978	1979			1980	
	29Nov-01Dec.	19-21 June	10-12 Sept	10-11 Dec	11-12 March	17-23 April
TURKEY						
D. Öner Reactor Operation Division Cekmece Nuclear Research and Training Centre Istanbul PK1, Havaalani	x					
U.K.						
C. J. Baglin GEC Reactor Equipment Ltd Cambridge Road, Whetstone Leicester LE8 3LH				x	x	
C. C. F. Bower GEC Reactor Equipment Ltd Cambridge Road, Whetstone Leicester LE8 3LH		x	x			
R. Panter Research Reactors Division Bld. 521, AERE Harwell Oxfordshire OX11 ORA			x	x	x	
U.S.A.						
S. Fraley Arms Control and Disarmament Agency Washington D.C.	x		x	x		
A. Gietzen TRIGA Division, General Atomic San Diego, CA 92138		x		x	x	x
H. Holm General Atomic Europe Weinbergstrasse 109 CH-8006 Zurich Switzerland	x	x	x	x		
R. Lewis Room 7282, OES/NET/EST U.S. State Department Washington D.C. 20520	x	x				
J Matos Argonne National Laboratory 9700 S. Cass Avenue Argonne, Illinois 60439				x	x	x
R. Peters General Atomic PO Box 81608 San Diego, CA 92138	x		x			
S. Ramos Nuclear Regulatory Commission Operating Reactors Branch 4 DOR, Washington D.C. 20555				x	x	

	1978	1979			1980	
	29Nov-01Dec.	19-21 June	10-12 Sept	10-11 Dec	11-12 March	17-23 April
U.S.A.						
J. Sheaks Department of State Arms Control and Disarmament Agency Washington D.C.20451					x	
A. Travelli Argonne National Laboratory 9700 S. Cass Avenue Argonne, Illinois 60439		x	x	x	x	x
IAEA						
Department of Research and Isotopes Division of Research and Laboratories Physics Section						
R. Ellis					x	
H. Reijonen	x	x	x			
U. Schütt			x	x	x	x

Pages 563, 564, 706 and 707
are missing in the original
IAEA-Tecdoc 233 document